

---

Kansas City  
Public Library



This Volume is for  
REFERENCE USE ONLY



From the collection of the



San Francisco, California  
2008







# THE BELL SYSTEM TECHNICAL JOURNAL

A JOURNAL DEVOTED TO THE  
SCIENTIFIC AND ENGINEERING  
ASPECTS OF ELECTRICAL  
COMMUNICATION

## *EDITORS*

R. W. KING

J. O. PERRINE

## *EDITORIAL BOARD*

C. F. CRAIG

H. S. OSBORNE

J. J. PILLIOD

O. E. BUCKLEY

M. J. KELLY

A. B. CLARK

F. J. FEELY

## TABLE OF CONTENTS AND INDEX

VOLUME XXVIII

1949

AMERICAN TELEPHONE AND TELEGRAPH COMPANY  
NEW YORK

PRINTED IN U. S. A.

THE BELL SYSTEM  
TECHNICAL JOURNAL

VOLUME XXVIII, 1949

Table of Contents

JANUARY, 1949

Propagation of $TE_{01}$ Waves in Curved Wave Guides— <i>W. J. Albersheim</i> .....	1
A New Type of High-Frequency Amplifier— <i>J. R. Pierce and W. B. Hebenstreit</i> .....	33
Experimental Observation of Amplification by Interaction Between Two Electron Streams— <i>A. V. Hollenberg</i> .....	52
The Synthesis of Two-Terminal Switching Circuits— <i>Claude E. Shannon</i> .....	59
A Method of Measuring Phase at Microwave Frequencies— <i>Sloan D. Robertson</i> .....	99
Reflection from Corners in Rectangular Wave Guides—Conformal Transformation— <i>S. O. Rice</i> .....	104
A Set of Second-Order Differential Equations Associated with Reflections in Rectangular Wave Guides—Application to Guide Connected to Horn— <i>S. O. Rice</i> .....	136

APRIL, 1949

A Carrier System for 8000-Cycle Program Transmission— <i>R. A. Leconte, D. B. Penick, C. W. Schramm and A. J. Wier</i> .....	165
Delay Equalization of Eight-Kilocycle Carrier Program Circuits— <i>C. H. Dagnall and P. W. Rounds</i> .....	181
Band Pass Filter, Band Elimination Filter and Phase Simulating Network for Carrier Program Systems— <i>F. S. Farkas, F. J. Hallenbeck and F. E. Stehlik</i> .....	196



A Precise Direct Reading Phase and Transmission Measuring System for Video Frequencies— <i>D. A. Alsberg and D. Leed</i> .....	221
Physical Principles Involved in Transistor Action— <i>J. Bardeen and W. H. Brattain</i> .....	239
Lightning Current Observations in Buried Cable— <i>H. M. Trueblood and E. D. Sunde</i> .....	278
The Electrostatic Field in Vacuum Tubes with Arbitrarily Spaced Elements— <i>W. R. Bennett and L. C. Peterson</i> .....	303
Transconductance as a Criterion of Electron Tube Performance— <i>T. Slonczewski</i> .....	315

## JULY, 1949

Editorial Note regarding Semiconductors.....	335
Hole Injection in Germanium—Quantitative Studies and Filamentary Transistors— <i>W. Shockley, G. L. Pearson and J. R. Haynes</i> .....	344
Some Circuit Aspects of the Transistor— <i>R. M. Ryder and R. J. Kircher</i> .....	367
Theory of Transient Phenomena in the Transport of Holes in an Excess Semiconductor— <i>Conyers Herring</i> .....	401
On the Theory of the A-C. Impedance of a Contact Rectifier— <i>J. Bardeen</i> .....	428
The Theory of p-n Junctions in Semiconductors and p-n Junction Transistors— <i>W. Shockley</i> .....	435
Band Width and Transmission Performance— <i>C. B. Feldman and W. R. Bennett</i> .....	490

## OCTOBER, 1949

Reactance Tube Modulation of Phase Shift Oscillators— <i>F. R. Dennis and E. P. Felch</i> .....	601
A Broad-Band Microwave Noise Source— <i>W. W. Mumford</i> .....	608
Electronic Admittances of Parallel-Plane Electron Tubes at 4000 Mega- cycles— <i>Sloan D. Robertson</i> .....	619
Passive Four-Pole Admittances of Microwave Triodes— <i>Sloan D. Robertson</i> .....	647
Communication Theory of Secrecy Systems— <i>C. E. Shannon</i> .....	656
The Design of Reactive Equalizers— <i>A. P. Brogle, Jr.</i> .....	716

## Index to Volume XXVIII

### A

- Admittances, Electronic, of Parallel-Plane Electron Tubes at 4000 Megacycles, *Sloan D. Robertson*, page 619.
- Admittances, Passive Four-Pole, of Microwave Triodes, *Sloan D. Robertson*, page 647.
- Albersheim, W. J.*, Propagation of  $TE_{01}$  Waves in Curved Wave Guides, page 1.
- Alsberg, D. A. and D. Leed*, A Precise Direct Reading Phase and Transmission Measuring System for Video Frequencies, page 221.
- Amplification by Interaction between Two Electron Streams, Experimental Observation of, *A. V. Hollenberg*, page 52.
- Amplifier, High-Frequency, A New Type of, *J. R. Pierce and W. B. Hebenstreit*, page 33.

### B

- Band Width and Transmission Performance, *C. B. Feldman and W. R. Bennett*, page 490.
- Bardeen, J.*, On the Theory of the A-C. Impedance of a Contact Rectifier, page 428.
- Bardeen, J. and W. H. Brattain*, Physical Principles Involved in Transistor Action, page 239.
- Bennett, W. R. and C. B. Feldman*, Band Width and Transmission Performance, page 490.
- Bennett, W. R. and L. C. Peterson*, The Electrostatic Field in Vacuum Tubes with Arbitrarily Spaced Elements, page 303.
- Brattain, W. H. and J. Bardeen*, Physical Principles Involved in Transistor Action, page 239.
- Broad-Band Microwave Noise Source, A, *W. W. Mumford*, page 608.
- Brogle, A. P. Jr.*, The Design of Reactive Equalizers, page 716.

### C

- Cable, Buried, Lightning Current Observations in, *H. M. Trueblood and E. D. Sunde*, page 278.
- Carrier Program Circuits, Eight-Kilocycle, Delay Equalization of, *C. H. Dagnall and P. W. Rounds*, page 181.
- Carrier Program Systems; Band Pass Filter, Band Elimination Filter and Phase Simulating Network for, *F. S. Farkas, F. J. Hallenbeck, and F. E. Stehlik*, page 196.
- Carrier System for 8000-Cycle Program Transmission, A, *R. A. Leconte, D. B. Penick, C. W. Schramm, and A. J. Wier*, page 165.
- Communication Theory of Secrecy Systems, *C. E. Shannon*, page 656.

### D

- Dagnall, C. H. and P. W. Rounds*, Delay Equalization of Eight-Kilocycle Carrier Program Circuits, page 181.
- Dennis, F. R. and E. P. Felch*, Reactance Tube Modulation of Phase Shift Oscillators, page 601.
- Differential Equations, A Set of Second-Order, Associated with Reflections in Rectangular Wave Guides—Application to Guide Connected to Horn, *S. O. Rice*, page 136.

### E

- Editorial Note regarding Semiconductors, page 335.
- Electron Streams, Two, Experimental Observation of Amplification by Interaction Between, *A. V. Hollenberg*, page 52.
- Electron Tube Performance, Transconductance as a Criterion of, *T. Slonczewski*, page 315.
- Electron Tubes, Parallel-Plane, at 4000 Megacycles, Electronic Admittances of, *Sloan D. Robertson*, page 619.

- Electrostatic Field, The, in Vacuum Tubes with Arbitrarily Spaced Elements, *W. R. Bennett and L. C. Peterson*, page 303.  
 Equalizers, Reactive, The Design of, *A. P. Brogle, Jr.*, page 716.  
 Equalization, Delay, of Eight-Kilocycle Carrier Program Circuits, *C. H. Dagnall and P. W. Rounds*, page 181.

## F

- Farkas, F. S., F. J. Hallenbeck, and F. E. Stehlik*, Band Pass Filter, Band Elimination Filter and Phase Simulating Network for Carrier Program Systems, page 196.  
*Felch, E. P. and F. R. Dennis*, Reactance Tube Modulation of Phase Shift Oscillators, page 601.  
*Feldman, C. B. and W. R. Bennett*, Band Width and Transmission Performance, page 490.  
 Filters: Band Pass Filter, Band Elimination Filter and Phase Simulating Network for Carrier Program Systems, *F. S. Farkas, F. J. Hallenbeck, and F. E. Stehlik*, page 196.

## G

- Germanium, Hole Injection in—Quantitative Studies and Filamentary Transistors, *W. Shockley, G. L. Pearson, and J. R. Haynes*, page 344.

## H

- Hallenbeck, F. J., F. E. Stehlik, and F. S. Farkas*, Band Pass Filter, Band Elimination Filter and Phase Simulating Network for Carrier Program Systems, page 196.  
*Haynes, J. R., W. Shockley, and G. L. Pearson*, Hole Injection in Germanium—Quantitative Studies and Filamentary Transistors, page 344.  
*Hebenstreit, W. B. and J. R. Pierce*, A New Type of High-Frequency Amplifier, page 33.  
*Herring, Conyers*, Theory of Transient Phenomena in the Transport of Holes in an Excess Semiconductor, page 401.  
 Hole Injection in Germanium—Quantitative Studies and Filamentary Transistors, *W. Shockley, G. L. Pearson, and J. R. Haynes*, page 344.  
 Holes in an Excess Semiconductor, Theory of Transient Phenomena in the Transport of, *Conyers Herring*, page 401.  
*Hollenberg, A. V.*, Experimental Observation of Amplification by Interaction between Two Electron Streams, page 52.

## I

- Impedance, A-C., of a Contact Rectifier, On the Theory of the, *J. Bardeen*, page 428.

## K

- Kircher, R. J. and R. M. Ryder*, Some Circuit Aspects of the Transistor, page 367.

## L

- Leconte, R. A., D. B. Penick, C. W. Schramm, and A. J. Wier*, A Carrier System for 8000-Cycle Program Transmission, page 165.  
*Leed, D. and D. A. Alsberg*, A Precise Direct Reading Phase and Transmission Measuring System for Video Frequencies, page 221.  
 Lightning Current Observations in Buried Cable, *H. M. Trueblood and E. D. Sunde*, page 278.

## M

- Microwave Frequencies, A Method of Measuring Phase at, *Sloan D. Robertson*, page 99.  
 Microwave Noise Source, A Broad-Band, *W. W. Mumford*, page 608.  
 Microwave Triodes, Passive Four-Pole Admittances of, *Sloan D. Robertson*, page 647.  
 Microwaves: Reflection from Corners in Rectangular Wave Guides—Conformal Transformation, *S. O. Rice*, page 104. A Set of Second-Order Differential Equations Associated with Reflections in Rectangular Wave Guides—Application to Guide Connected to Horn, *S. O. Rice*, page 136.  
 Modulation, Reactance Tube, of Phase Shift Oscillators, *F. R. Dennis and E. P. Felch*, page 601.  
*Mumford, W. W.*, A Broad-Band Microwave Noise Source, page 608.

## N

Noise Source, A Broad-Band Microwave, *W. W. Mumford*, page 608.

## O

Oscillators, Phase Shift, Reactance Tube Modulation of, *F. R. Dennis and E. P. Felch*, page 601.

## P

*Pearson, G. L., J. R. Haynes, and W. Shockley*, Hole Injection in Germanium—Quantitative Studies and Filamentary Transistors, page 344.

*Penick, D. B., C. W. Schramm, A. J. Wier and R. A. Leconte*, A Carrier System for 8000-Cycle Program Transmission, page 165.

*Peterson, L. C. and W. R. Bennett*, The Electrostatic Field in Vacuum Tubes with Arbitrarily Spaced Elements, page 303.

Phase at Microwave Frequencies, A Method of Measuring, *Sloan D. Robertson*, page 99.

Phase, A Precise Direct Reading; and Transmission Measuring System for Video Frequencies, *D. A. Alsberg and D. Leed*, page 221.

Phase Shift Oscillators, Reactance Tube Modulation of, *F. R. Dennis and E. P. Felch*, page 601.

*Pierce, J. R. and W. B. Hebenstreit*, A New Type of High-Frequency Amplifier, page 33.

Program Circuits, Eight-Kilocycle Carrier, Delay Equalization of, *C. H. Dagnall and P. W. Rounds*, page 181.

Program Systems, Carrier; Band Pass Filter, Band Elimination Filter and Phase Simulating Network for, *F. S. Farkas, F. J. Hallenbeck, and F. E. Stehlik*, page 196.

Program Transmission, 8000-Cycle, A Carrier System for, *R. A. Leconte, D. B. Penick, C. W. Schramm, and A. J. Wier*, page 165.

Propagation of  $TE_{01}$  Waves in Curved Wave Guides, *W. J. Albersheim*, page 1.

## R

Reactive Equalizers, The Design of, *A. P. Brogle, Jr.*, page 716.

Rectifier, Contact, On the Theory of the A-C. Impedance of a, *J. Bardeen*, page 428.

Reflection from Corners in Rectangular Wave Guides—Conformal Transformation, *S. O. Rice*, page 104.

*Rice, S. O.*, A Set of Second-Order Differential Equations Associated with Reflections in Rectangular Wave Guides—Application to Guide Connected to Horn, page 136.

Reflection from Corners in Rectangular Wave Guides—Conformal Transformation, page 104.

*Robertson, Sloan D.*, A Method of Measuring Phase at Microwave Frequencies, page 99.

Electronic Admittances of Parallel-Plane Electron Tubes at 4000 Megacycles, page 619.

Passive Four-Pole Admittances of Microwave Triodes, page 647.

*Rounds, P. W. and C. H. Dagnall*, Delay Equalization of Eight-Kilocycle Carrier Program Circuits, page 181.

*Ryder, R. M. and R. J. Kircher*, Some Circuit Aspects of the Transistor, page 367.

## S

*Schramm, C. W., A. J. Wier, R. A. Leconte, and D. B. Penick*, A Carrier System for 8000-Cycle Program Transmission, page 165.

Secrecy Systems, Communication Theory of, *C. E. Shannon*, page 656.

Semiconductor, Excess, Theory of Transient Phenomena in the Transport of Holes in an, *Conyers Herring*, page 401.

Semiconductors, Editorial Note regarding, page 335.

Semiconductors and p-n Junction Transistors, The Theory of p-n Junctions in, *W. Shockley*, page 435.

Semiconductors: On the Theory of the A-C. Impedance of a Contact Rectifier, *J. Bardeen*, page 428.

*Shannon, C. E.*, Communication Theory of Secrecy Systems, page 656. The Synthesis of Two-Terminal Switching Circuits, page 59.

*Shockley, W.*, The Theory of p-n Junctions in Semiconductors and p-n Junction Transistors, page 435.

- Shockley, W., G. L. Pearson, and J. R. Haynes*, Hole Injection in Germanium—Quantitative Studies and Filamentary Transistors, page 344.
- Slonczewski, T.*, Transconductance as a Criterion of Electron Tube Performance, page 315.
- Stehlik, F. E., F. S. Farkas, and F. J. Hallenbeck*, Band Pass Filter, Band Elimination Filter and Phase Simulating Network for Carrier Program Systems, page 196.
- Sunde, E. D. and H. M. Trueblood*, Lightning Current Observations in Buried Cable, page 278.
- Switching Circuits, Two-Terminal, The Synthesis of, *Claude E. Shannon*, page 59.

## T

- Transconductance as a Criterion of Electron Tube Performance, *T. Slonczewski*, page 315.
- Transformation, Conformal—Reflection from Corners in Rectangular Wave Guides, *S. O. Rice*, page 104.
- Transient Phenomena in the Transport of Holes in an Excess Semiconductor, Theory of, *Conyers Herring*, page 401.
- Transistor, Some Circuit Aspects of the, *R. M. Ryder and R. J. Kircher*, page 367.
- Transistor Action, Physical Principles Involved in, *J. Bardeen and W. H. Brattain*, page 239.
- Transistors: Editorial Note regarding Semiconductors, page 335. Theory of Transient Phenomena in the Transport of Holes in an Excess Semiconductor, *Conyers Herring*, page 401.
- Transistors, Filamentary, and Quantitative Studies—Hole Injection in Germanium, *W. Shockley, G. L. Pearson, and J. R. Haynes*, page 344.
- Transistors, p-n Junction, The Theory of p-n Junctions in Semiconductors and, *W. Shockley*, page 435.
- Transmission, 8000-Cycle Program, A Carrier System for, *R. A. Leconte, D. B. Penick, C. W. Schramm, and A. J. Wier*, page 165.
- Transmission Measuring System for Video Frequencies, A Precise Direct Reading Phase and, *D. A. Alsberg and D. Leed*, page 221.
- Transmission Performance, Band Width and, *C. B. Feldman and W. R. Bennett*, page 490.
- Triodes, Microwave, Passive Four-Pole Admittances of, *Sloan D. Robertson*, page 647.
- Trueblood, H. M. and E. D. Sunde*, Lightning Current Observations in Buried Cable, page 278.
- Tube Performance, Electron, Transconductance as a Criterion of, *T. Slonczewski*, page 315.
- Tubes, Parallel-Plane Electron, at 4000 Megacycles, Electronic Admittances of, *Sloan D. Robertson*, page 619.
- Tubes, Vacuum, with Arbitrarily Spaced Elements, The Electrostatic Field in, *W. R. Bennett and L. C. Peterson*, page 303.

## V

- Vacuum Tubes with Arbitrarily Spaced Elements, The Electrostatic Field in, *W. R. Bennett and L. C. Peterson*, page 303.
- Video Frequencies, A Precise Direct Reading Phase and Transmission Measuring System for, *D. A. Alsberg and D. Leed*, page 221.

## W

- Wave Guides, Curved, Propagation of  $TE_{01}$  Waves in, *W. J. Albersheim* page 1.
- Wave Guides, Rectangular, Reflection from Corners in—Conformal Transformation, *S. O. Rice*, page 104.
- Wave Guides, Rectangular, A Set of Second-Order Differential Equations Associated with Reflections in—Application to Guide Connected to Horn, *S. O. Rice*, page 136.
- Wier, A. J., R. A. Leconte, D. B. Penick, and C. W. Schramm*, A Carrier System for 8000-Cycle Program Transmission, page 165.

# THE BELL SYSTEM TECHNICAL JOURNAL

DEVOTED TO THE SCIENTIFIC AND ENGINEERING ASPECTS  
OF ELECTRICAL COMMUNICATION

Propagation of $TE_{01}$ Waves in Curved Wave Guides <i>W. J. Albersheim</i>	1
A New Type of High-Frequency Amplifier <i>J. R. Pierce and W. B. Hebenstreit</i>	33
Experimental Observation of Amplification by Interaction Between Two Electron Streams . . . <i>A. V. Hollenberg</i>	52
The Synthesis of Two-Terminal Switching Circuits <i>Claude E. Shannon</i>	59
A Method of Measuring Phase at Microwave Frequen- cies . . . . . <i>Sloan D. Robertson</i>	99
Reflection from Corners in Rectangular Wave Guides— Conformal Transformation . . . . . <i>S. O. Rice</i>	104
A Set of Second-Order Differential Equations Associated with Reflections in Rectangular Wave Guides—Ap- plication to Guide Connected to Horn . . . <i>S. O. Rice</i>	136
Abstracts of Technical Articles by Bell System Authors . . .	157
Contributors to this Issue . . . . .	162

AMERICAN TELEPHONE AND TELEGRAPH COMPANY  
NEW YORK

# THE BELL SYSTEM TECHNICAL JOURNAL

*Published quarterly by the  
American Telephone and Telegraph Company  
195 Broadway, New York, N. Y.*



## EDITORS

R. W. King

J. O. Perrine

## EDITORIAL BOARD

C. F. Craig

O. E. Buckley

O. B. Blackwell

M. J. Kelly

H. S. Osborne

A. B. Clark

J. J. Pilliod

F. J. Feely



## SUBSCRIPTIONS

Subscriptions are accepted at \$1.50 per year. Single copies are 50 cents each.  
The foreign postage is 35 cents per year or 9 cents per copy.



Copyright, 1949  
American Telephone and Telegraph Company

PRINTED IN U. S. A.



# The Bell System Technical Journal

Vol. XXVIII

January, 1949

No. 1

---

## Propagation of $TE_{01}$ Waves in Curved Wave Guides

By W. J. ALBERSHEIM

$TE_{01}$  waves transmitted through curve wave guides lose power by conversion to other modes, especially to  $TM_{11}$ .

This power transfer to coupled modes is explained by the theory of coupled transmission lines. It is shown that the power interchange between coupled lines and their propagation constants can be derived from a single coupling discriminant.

Earlier calculations of  $TE_{01}$  conversion loss in circular wave guide bends are confirmed and extended to S-shaped bends.

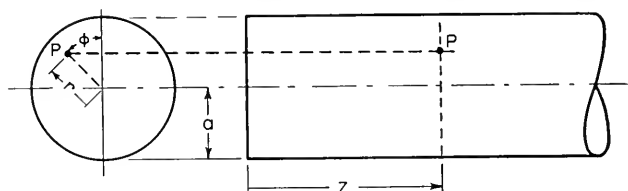
Tolerance limits for random deflections from an average straight course are given.

THE  $TE_{01}$  mode of propagation in circular wave guides has great potential value for the transmission of wide-band signals because its attenuation decreases with frequency. In order to take full advantage of this property one must use sufficiently large wave guides to operate well above the cutoff of the lowest transmitted frequency. The difficulty of this transmission method lies in the fact that  $TE_{01}$  is not the dominant mode and that energy may be lost by transfer to the many other modes capable of transmission in the wave guide. In an ideal wave guide, which is perfectly straight, perfectly circular and perfectly conducting, the propagation is undisturbed; but slight imperfections and especially a slight curvature of the wave guide axis may produce serious disturbances.

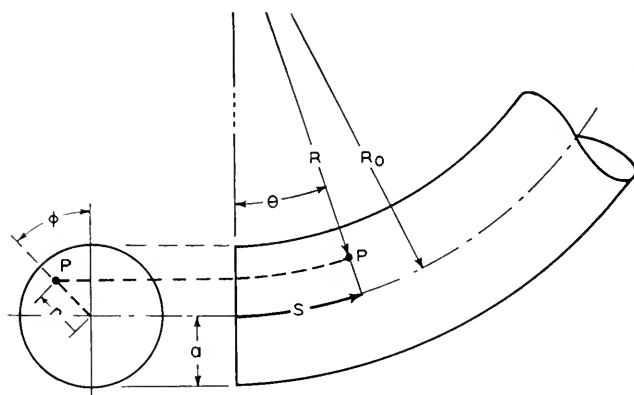
The character of these disturbances has been investigated in several publications by Prof. M. Jouguet<sup>1</sup> and in unpublished work by Mr. S. O. Rice of the Bell Telephone Laboratories. Both Jouguet and Rice use the method of perturbations, which is a form of calculus invented by astronomers to compute the deviations from the exact elliptical orbits of the planets which are caused by the disturbing influences of their fellow planets. Although the above-mentioned authors obtained valuable results, the interpretation of their solutions is difficult due to this rather abstract mathematical formulation. To most engineers the understanding of a physical problem is greatly helped if it is possible to use a method of analysis which is elementary in character and easily interpreted in familiar physical terms. The familiar concept on which the present treatment will be based is that of coupled circuits.

<sup>1</sup> See References 2 and 3, listed on page 7.

It has been stated by the earlier authors that the curvature of the wave guide produces a coupling between modes. Before going into a detailed analysis one may estimate by inspection the nature of this coupling and the kind of modes that are most strongly coupled to each other. Figure 1a shows the cross section and the longitudinal section of a straight cylindrical wave guide. The location of every point inside the wave guide is determined by three coordinates: the radial distance  $r$  from the cylinder axis; the azimuth angle  $\phi$  from an arbitrary 0 line and the axial distance  $z$  from the



a - CYLINDRICAL CO-ORDINATES IN STRAIGHT WAVEGUIDE



b - TOROIDAL CO-ORDINATES IN CURVED WAVEGUIDE

Fig. 1

origin. If the wave guide is bent as shown on Fig. 1b, but a wave front at right angles to the cylinder axis is to be maintained, the waves must be shortened at the inside of the bend and lengthened at the outside of the bend. Regarding compression as a positive and expansion as a negative deformation, one sees that the distortion of the wave shape is proportional to the curvature of the wave guide multiplied by the cosine of the azimuth angle. It is natural to assume that the coupling between modes is proportional to this distortion.

Now it is known that all modes of propagation in a circular wave guide

can be derived from functions  $J_n(\chi r) \cos n\varphi$ . In these functions,  $n$  is called the azimuthal index because it indicates the type of symmetry around the circumference of the wave guide. When these characteristic functions are multiplied by the distortion factor  $\cos \varphi$ , the resulting expressions are proportional to the sum of  $\cos (n + 1) \varphi$  and  $\cos (n - 1) \varphi$ . This means that the bending of the wave guide couples mainly those modes which differ by  $\pm 1$  in azimuthal index. Since the  $TE_{01}$  mode has the azimuthal index 0, it is coupled to all modes of the type  $TE_{1m}$  and  $TM_{1m}$ .

In the above qualitative discussion we have claimed that coupling exists without defining the physical coupling parameters and their effects. We must now supply this definition and show that the  $TE_{01}$  mode is particularly susceptible to coupling losses.

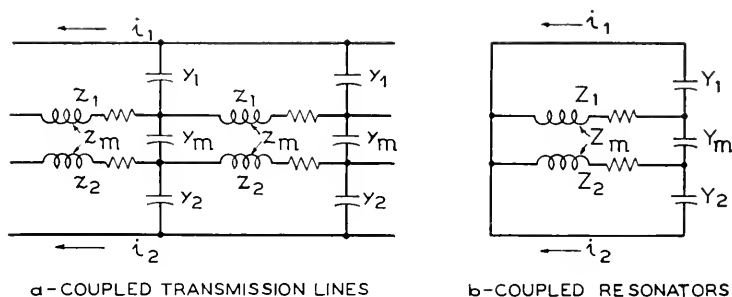


Fig. 2

Our investigation is guided by S. A. Schelkunoff's statement<sup>2</sup> that a wave guide mode has the same equation of propagation as a high-pass transmission line. Schelkunoff further points out<sup>3</sup> that the high-pass character of circular wave guide modes can be interpreted as the effect of interfering plane waves whose directions of propagation deviate from the wave guide axis by a constant slanting angle.

We therefore approach the problem of coupled wave guide modes by studying the behavior of two coupled transmission lines such as shown on Fig. 2a. Each transmission line is schematically shown as an array of small ladder sections. The series impedances per unit length of the lines are  $z_1$  and  $z_2$ ; their shunt admittances per unit length,  $y_1$  and  $y_2$ . The two lines are loosely coupled by small mutual series impedances per unit length ( $z_m$ ) and by small mutual shunt admittances per unit length ( $y_m$ ).

A network of coupled ladder sections is more tractable than a wave guide structure, but still somewhat complicated. Let us therefore carry the analogy one step further. Figure 2b shows two resonant circuits, each

<sup>2</sup> Ref. 4, pp. 378 and 381 of the book.

<sup>3</sup> Ref. 4, p. 410 of the book.

consisting of single capacity  $C$ , and an impedance  $Z$  which includes an inductance  $L$  and a damping resistance  $R$ . The resonators are coupled by a small mutual inductance  $Z_m$  and by a small mutual capacity  $Y_m$ .

The behavior of coupled resonators is very well known to radio engineers. They occur as tuned transformers in amplifier circuits, as band-pass filters and as "tank circuits" in radio transmitters. Even before the advent of radio, their acoustical equivalents were studied in the form of resonant tuning forks. The mathematical aspects of this problem were already clearly set forth in a paper by Wien written in 1897<sup>4</sup>. He showed that the interaction between the free vibrations of two tuned circuits depends on the coupling coefficient and on the ratio of their complex resonance frequencies. The closer the two frequencies are to each other, the less coupling is needed to transfer energy between the two circuits. The reason is that the individual free vibrations of two nearly synchronous circuits remain in step long enough to accumulate the small energy transfer impulses of many vibrations.

Now consider the two transmission lines of Fig. 2a and assume that a constant frequency signal is impressed upon the input of one or both of them. The signals are carried along the two lines as traveling waves. Again it is true that loosely coupled signals affect each other strongly if they remain in step. With traveling waves "remaining in step" means that they must travel with approximately equal phase velocities. We conclude that the phase velocities or phase constants of coupled transmission lines play a similar role as the resonant frequencies of coupled tuned circuits. This intuitive reasoning is confirmed by analysis (see Section 1 of the analytical part of this paper).

We thus find that we must expect trouble for  $TE_{01}$  wave guide transmission if a mode with an azimuth index 1 has a propagation constant close to that of the  $TE_{01}$ . It so happens that there exists one mode, the  $TM_{11}$ , which in an ideal wave guide has exactly the same propagation constant as the  $TE_{01}$ . This then should be the principal source of trouble—and from previous work it is known that such is the case.

Our discussion of coupled transmission lines has shown that the interaction effects are functions of their relative uncoupled propagation constants and of the coupling coefficient. The propagation constants of the  $TE_{01}$  and  $TM_{11}$  wave guide modes are known but their coupling coefficient remains to be found.

Since the energy of the transmission modes is located in the dielectric inside the wave guide, we consider first the coupling between the plane "slant wave" groups from which the modes are built up.

<sup>4</sup> Reference 5.

As shown in the analytical part, the coupling coefficient of these slant waves may be defined as the energy interchanged between the modes per unit length of line divided by the geometric mean of the energies per unit length stored up in each of the modes.

From the coupling coefficient of the slant waves the coupling coefficient of the wave guide modes is derived.

On the basis of the above physical interpretation the analysis is carried out and the properties of  $TE_{01}$  propagation through curved wave guides of various shapes are derived in the analytical part of this paper which is subdivided into the following nine sections:

Section 1 develops an approximate theory of loosely coupled, weakly damped circuits. The theory is first derived for coupled resonators which are familiar to communication engineers, and then applied in similar form to coupled transmission lines. It is shown that the important interaction properties of coupled lines are functions of a single coupling discriminant. The relative energy content of the two lines in each of the two possible coupled modes is plotted as a function of the coupling discriminant.

Section 2 contains the field equations of a straight circular wave guide and their modification by a toroidal bend.

Section 3 gives the solutions of the field equations for the uncoupled  $TE_{01}$  and  $TM_{11}$  modes in wave guides with infinite, and with small but finite conductivity.

Section 4 applies the coupling theory to the  $TE_{01}$  and  $TM_{11}$  modes in circular wave guide bends. The coupling coefficient, coupling discriminant and energy division between the two modes are derived as functions of the wave guide diameter bending radius and conductivity and of the signal frequency.

Section 5 derives the critical bending radius and the attenuation of  $TE_{01}$  waves in long wave guides of constant curvature. Two numerical examples are given.

Section 6 shows that in a curved section of wave guide which follows a long straight section or other source of pure  $TE_{01}$  the energy fluctuates back and forth between a condition of pure  $TE_{01}$  and of predominant  $TM_{11}$ . The length and magnitude of the fluctuations are derived.

Section 7 computes the increase in average attenuation caused by serpentine bends of regular shapes. Numerical examples are tabulated.

Section 8 shows that the results of Section 7 can be applied to helical bends and to small two-dimensional random deviations from a straight course.

Section 9 shows that for any given statistical distribution of random angular deviations the average attenuation is minimized by an optimum

wave guide radius for each signal wave length and by an optimum signal wave length for each wave guide radius.

Numerical examples are given for sinusoidal bends.

### *Summary of Results*

1. The energy loss of  $TE_{01}$  waves in curved wave guides by conversion into the  $TM_{11}$  mode is interpreted as a case of coupling between resonant transmission lines.
2. In a pair of coupled lines the energy cannot be confined entirely to a single line but travels through both in one or both of two possible combination modes.
3. All important properties of coupled circuits, including wave guide modes, are functions of a single discriminant.
4. When the discriminant is much smaller than one, most of the energy can be carried in one line or component mode.
5. When the discriminant is much larger than one, the energy flow is nearly equally divided between the two lines or component modes.
6. In wave guides of typical dimensions the coupling discriminant becomes one for a "critical" bending radius greater than a mile. For all sharper bends, that is for most practical installations, the discriminant is greater than one.
7. In a long wave guide section with more than critical curvature the average attenuation constant is the arithmetic mean between those of the  $TE_{01}$  and the  $TM_{11}$  modes.
8. If a wave guide region carrying pure  $TE_{01}$  is followed by a curved region, the energy in the curved region fluctuates back and forth between pure  $TE_{01}$  and predominant  $TM_{11}$ . The location of  $TE_{01}$  minima and maxima is a function of the signal frequency, the wave guide diameter and the total bending angle.
9. For highly supercritical curvatures the bending angles at which minima and maxima occur are nearly independent of the curvature and approach the limiting values previously computed by Jouguet and Rice. The minima approach zero. When the bending radius approaches or exceeds the critical value, the maxima and minima become shallower and their spacing is increased by a function of the coupling discriminant.
10. For regular serpentine bends or random angular deviations from an average straight course which are much smaller than the first extinction angle, the percentage increase in average attenuation is proportional to the square of the maximum deviation and to the fourth power of wave guide diameter and signal frequency.
11. Wave guide installations of practical dimensions for frequencies now

attainable are tolerant to random angular deviations of the order of 1 degree.

12. For any expected distribution of random angular deviations there exists an optimum wave guide radius for each signal wave length and an optimum signal wave length for each wave guide radius, which minimize the average attenuation.

#### REFERENCES

1. Jahnke & Emde, *Tables of Functions*, Dover Publications, New York, 1943.
2. M. Jouguet, Propagation dans les tuyaux courbés, *Comptes Rendus—Académie des Sciences, Paris*, Feb. 18, 1946, March 4, 1946 and Jan. 6, 1947.
3. M. Jouguet, Effets de la courbure dans un guide à section circulaire, *Cables & Transmission*, 1 No. 2, July 1947, pp. 133-153.
4. S. A. Schelkunoff, *Electromagnetic Waves*, D. Van Nostrand Company, Inc., New York, 1943.
5. M. Wien, Ueber die Rueckwirkung eines resonierenden Systems, *Ann. d. Physik*, 1897, Vol. 61, pp. 151-189.

#### ANALYSIS

##### 1. INTERACTION OF COUPLED CIRCUITS

###### 1.1 *Free Oscillations of Coupled Resonators (Fig. 1B)*

The circuits are coupled according to the following four equations:

$$e_1 = -Z_1 i_1 + Z_m i_2 \quad 1.1-1$$

$$i_1 = Y_1 e_1 + Y_m e_2 \quad 1.1-2$$

$$e_2 = -Z_2 i_2 + Z_m i_1 \quad 1.1-3$$

$$i_2 = Y_2 e_2 + Y_m e_1 \quad 1.1-4$$

where index <sub>1</sub> refers to circuit 1, index <sub>2</sub> to circuit 2 and index <sub>m</sub> to the mutual coupling impedance and admittance. The coupled oscillations have the solution:

$$e_1 = E_{1a} \epsilon^{p_a t} + E_{1b} \epsilon^{p_b t} \quad 1.1-5$$

$$e_2 = E_{2a} \epsilon^{p_a t} + E_{2b} \epsilon^{p_b t} \quad 1.1-6$$

In the limiting case of zero coupling ( $Y_m = 0, Z_m = 0$ ) the obvious solution shows independent oscillations in the two separate circuits:

$$e_{10} = K_1 i_{10} = E_{10} \epsilon^{p_1 t} \quad 1.1-7$$

$$e_{20} = K_2 i_{20} = E_{20} \epsilon^{p_2 t} \quad 1.1-8$$

The wave impedance  $K_1$  of the primary circuit is found by dividing equation 1.1-1 by 1.1-2

$$K_1 = \frac{e_1}{i_1} = \sqrt{\frac{Z_1}{Y_1}}$$



Similarly,

$$\kappa_2 = \frac{e_2}{i_2} = \sqrt{\frac{-Z_2}{Y_2}}$$

By multiplying equation 1.1-1 by 1.1-2 one finds

$$-Z_1 Y_1 = 1 \quad 1.1-9$$

from which one can compute the exponent  $p_1$ . In the specific circuits shown in Fig. 1b

$$Z_1 = L_1 p_1 + R_1 \quad \text{and} \quad 1.1-10$$

$$Y_1 = C_1 p_1 \quad 1.1-11$$

From 1.1-9, 10 and 11

$$p_1 = -\delta_1 + j\omega_1 = -\frac{R_1}{2L_1} + j\sqrt{\frac{1}{L_1 C_1} - \frac{R_1^2}{4L_1^2}} \quad 1.1-12$$

and by analogy

$$p_2 = -\delta_2 + j\omega_2 = -\frac{R_2}{2L_2} + j\sqrt{\frac{1}{L_2 C_2} - \frac{R_2^2}{4L_2^2}} \quad 1.1-13$$

In equations 1.1-7 and 1.1-8,  $E_{10}$  and  $E_{20}$  are amplitude constants determined by boundary conditions. In equations 1.1-12 and 1.1-13,  $\delta_1$  and  $\delta_2$  are the decay or damping constants,  $\omega_1$  and  $\omega_2$  the radian frequencies.

With finite but loose coupling and small damping the circuits can oscillate with either or both of the two frequencies.

$$p_a = \frac{p_1 + p_2}{2} + \frac{p_1 - p_2}{2} \sqrt{1 + \kappa^2} = p_1 + 0.5 p_2 (1 - \sqrt{1 + \kappa^2}) \quad 1.1-14$$

$$p_b = \frac{p_1 - p_2}{2} - \frac{p_1 - p_2}{2} \sqrt{1 + \kappa^2} = p_2 + 0.5 p_1 (1 - \sqrt{1 + \kappa^2}) \quad 1.1-15$$

In the last two equations, the symbol  $\kappa$ , defined by  $\kappa = \sqrt{\frac{p_1 p_2}{p_1 - p_2}} \cdot k$ , may

be called the coupling discriminant. The first term of the product on the right side of this expression is the reciprocal of the fractional difference between the uncoupled frequencies; the second term  $k$  is the "coupling coefficient."

When there is only one coupling impedance, the coupling coefficient is usually defined as the mutual circuit impedance divided by the geometric mean of the separate circuit impedances. A broader definition which applies to all combinations of mutual impedances and admittances is

$$k = \frac{P_{12}}{\sqrt{P_1 P_2}} = \frac{P_{21}}{\sqrt{P_1 P_2}} \quad 1.1-16$$

In this equation  $P_1$  is the energy stored in circuit 1,  $P_2$  the energy stored in circuit 2 and  $P_{12}$  is the energy transferred from one circuit to the other. One finds

$$P_1 = \frac{e_1^2}{2K} + \frac{i_1^2 K}{2} = \frac{e_1^2}{K_1} = i_1^2 K_1 \quad 1.1-17$$

$$P_2 = \frac{e_2^2}{K_2} = i_2^2 K_2 \quad 1.1-18$$

$$P_{12} = \frac{e_{12} e_2}{K_2} = i_{12} i_2 K_2 = \frac{e_{21} e_1}{K_1} + i_{21} i_1 K_1 \quad 1.1-19$$

Equations 1.1-5 and 1.1-6 contain four amplitude constants. Two of these, for instance  $E_{1a}$  and  $E_{2b}$ , can be adjusted to satisfy boundary conditions. The other two are fixed by the equation

$$\frac{E_{2a}^2 K_1}{E_{1a}^2 K_2} = \frac{p_a - p_1}{p_a - p_2} = \frac{p_b - p_2}{p_b - p_1} = \frac{E_{1b}^2 K_2}{E_{2b}^2 K_1}$$

The square root of this expression,

$$\frac{E_{2a}}{E_{1a}} \sqrt{\frac{K_1}{K_2}} = \frac{E_{1b}}{E_{2b}} \sqrt{\frac{K_2}{K_1}} = A$$

may be called the *normalized amplitude ratio*. It is a vector quantity denoting the amplitude ratio and phase relation of each oscillation frequency in the two circuits, assuming that they have been normalized to equal resistances by an ideal transformer. The absolute value

$$\left| \frac{E_{2a}^2 K_1}{E_{1a}^2 K_2} \right| = W_a = \frac{1}{W_b}$$

is the ratio of the energies stored in the two circuits oscillating at frequencies  $p_a$  and  $p_b$  respectively.

From 1.1-14, 15, 16 and 18

$$W_a = \left| \frac{\sqrt{1 + \kappa^2 - 1}}{\sqrt{1 + \kappa^2 + 1}} \right| = W$$

$$A_a = \sqrt{1 + \kappa^{-2} - \kappa^{-1}} = A$$

When the indexes are left off,  $W < 1$  and  $|A| < 1$  by definition. One sees that energy, amplitude and phase relations between the coupled circuits at each oscillating frequency are governed by the coupling discriminant. This also applies to the damping coefficients and frequencies

of the coupled oscillations. It can be shown by combining and transforming equations 1.1-14, 15, 19, that the coupled damping coefficients are

$$\delta_a = \frac{\delta_1 + \delta_2 W'}{1 + W'} = \delta_1 \frac{W'_{1a}}{W'_{total}} + \delta_2 \frac{W'_{2a}}{W'_{total}}$$

$$\delta_b = \frac{\delta_1 W' + \delta_2}{1 + W'} = \delta_1 \frac{W'_{1b}}{W'_{total}} + \delta_2 \frac{W'_{2b}}{W'_{total}}$$

The damping constants of two coupled resonances are found by combining the uncoupled damping constants in the same proportion as the energies oscillating in the two resonators.

The coupled frequencies are

$$\omega_a = \frac{\omega_1 - W_{\omega 2}}{1 - W} \text{ and}$$

$$\omega_b = \frac{\omega_2 - W_{\omega 1}}{1 - W}$$

## 1.2 Forced traveling waves in coupled transmission lines (Fig. 1A).

The two lines are coupled according to the four equations

$$\Gamma e_1 = z_1 i_1 + z_m i_2$$

$$\Gamma i_1 = y_1 e_1 + y_m e_2$$

$$\Gamma e_2 = z_2 i_2 + z_m i_1$$

$$\Gamma i_2 = y_2 e_2 + y_m e_1$$

which may be compared to the corresponding equations of section 1.1. There is a dimensional difference because in transmission lines the series impedances  $z$  are measured in ohm/meter and the shunt reactances  $y$  in mho/meter.  $\Gamma$  is the propagation constant of the wave traveling in the  $+s$  direction. If a sinusoidal signal with the radian frequency  $\omega$  is impressed upon the input of the lines, the coupled waves have the solution

$$e_1 = E_{1a} \epsilon^{j\omega t - \Gamma_a s} + E_{1b} \epsilon^{j\omega t - \Gamma_b s} \quad 1.2-1$$

$$e_2 = E_{2a} \epsilon^{j\omega t - \Gamma_a s} + E_{2b} \epsilon^{j\omega t - \Gamma_b s} \quad 1.2-2$$

For zero coupling one finds, in analogy to Section 1.1

$$e_{10} = K_1 i_1 = E_{10} \epsilon^{j\omega t - \Gamma_1 s}$$

$$e_{20} = K_2 i_2 = E_{20} \epsilon^{j\omega t - \Gamma_2 s}$$

it

$$K_1 = \sqrt{\frac{z_1}{y_1}}$$

$$K_2 = \sqrt{\frac{z_2}{y_2}}$$

and

$$\Gamma_1 = \sqrt{y_1 z_1}$$

$$\Gamma_2 = \sqrt{y_2 z_2}$$

$E_{10}$  and  $E_{20}$  are independent integration constants. For finite but loose coupling and small attenuation constants one finds in analogy to 1.1-14 and 1.1-15

$$\Gamma_a = \frac{\Gamma_1 + \Gamma_2}{2} + \frac{\Gamma_1 - \Gamma_2}{2} \sqrt{1 + \kappa^2} = \Gamma_1 + 0.5 \Gamma_2 (1 - \sqrt{1 + \kappa^2})$$

$$\Gamma_b = \frac{\Gamma_1 + \Gamma_2}{2} - \frac{\Gamma_1 - \Gamma_2}{2} \sqrt{1 + \kappa^2} = \Gamma_2 + 0.5 \Gamma_1 (1 - \sqrt{1 + \kappa^2})$$

where

$$\kappa = \frac{k}{\Gamma_1 - \Gamma_2} \sqrt{\Gamma_1 \Gamma_2} \quad 1.2-3$$

is the coupling discriminant. Just as in Section 1.1 the coupling coefficient  $k$  is defined by the equation

$$k = \frac{P_{12}}{\sqrt{P_1 P_2}} = \frac{P_{21}}{\sqrt{P_1 P_2}} \quad 1.2-4$$

$P_1$  is the energy per unit length stored in line 1;  $P_2$ , the energy per unit length stored in line 2, and  $P_{12} = P_{21}$ , the energy per unit length interchanged between the lines. The waves can travel in the coupled lines with either or both of two transmission constants. Two of the amplitude vectors in equations 1.2-1 and 1.2-2, for instance  $E_{1a}$  and  $E_{2b}$ , are free to satisfy boundary conditions; the other two are determined by the equation

$$\begin{aligned} \frac{E_{2a}^2 K_1}{E_{1a}^2 K_2} &= \frac{\Gamma_a - \Gamma_1}{\Gamma_a - \Gamma_2} = \frac{\Gamma_b - \Gamma_2}{\Gamma_b - \Gamma_1} = \frac{E_{1b}^2 K_2}{E_{2b}^2 K_1} \\ \frac{E_{2a}}{E_{1a}} \sqrt{\frac{K_1}{K_2}} &= \frac{E_{1b}}{E_{2b}} \sqrt{\frac{K_2}{K_1}} = A_a = -\frac{1}{A_b} \end{aligned} \quad 1.2-5$$

$A$  is the *normalized amplitude and phase ratio* for two lines transformed to equal wave impedances.

$$\begin{aligned} \left| \frac{E_{2a}^2 K_1}{E_{1a}^2 K_2} \right| &= W_a = \frac{1}{W_b} \\ W_a &= \left| \frac{\sqrt{1 + \kappa^2} - 1}{\sqrt{1 + \kappa^2} + 1} \right| = W \end{aligned}$$

is the ratio of energy flow in the two lines. At the propagation constant  $\Gamma_a$ ,

$$A_a = \sqrt{1 + \kappa^{-2}} - \kappa^{-1} = A \quad 1.2-6$$

When the indexes are left off,  $W < 1$  and  $|A| < 1$  by definition.

In a manner analogous to that of Section 1.1 it can be shown that the coupled attenuation constants are

$$\alpha_a = \frac{\alpha_1 + \alpha_2 W}{1 + W} = \alpha_1 \frac{W_{1a}}{W_{\text{total}}} + \alpha_2 \frac{W_{2a}}{W_{\text{total}}} \quad 1.2-7$$

$$\alpha_b = \frac{\alpha_2 + \alpha_1 W}{1 + W} = \alpha_1 \frac{W_{1b}}{W_{\text{total}}} + \alpha_2 \frac{W_{2b}}{W_{\text{total}}} \quad 1.2-8$$

The attenuation constants of the coupled waves are found by combining the uncoupled attenuation constants in the same proportion as the energies traveling in the two lines.

The coupled phase constants are

$$\beta_a = \frac{\beta_1 - W\beta_2}{1 - W} \text{ and} \quad 1.2-9a$$

$$\beta_b = \frac{\beta_2 - W\beta_1}{1 - W} \quad 1.2-9b$$

From equations 1.2-5 to 1.2-8 one sees that the coupled propagation constants are conveniently described in terms of the power ratio  $W$ .  $W$  itself is a known function of the complex coupling determinant  $\kappa$  which is shown on the attached Fig. 4 for the following three special cases:

*Case 1.*

The two lines have *equal phase constants* and *different attenuation constants*:  $\beta_2 = \beta_1$      $\alpha_2 \geq \alpha_1$

$\kappa$  is an imaginary number.

$W$  changes its character abruptly at the critical coupling.

$|\kappa \text{ critical}| = 1$

For  $|\kappa| < 1$

$$W < 1; \quad \alpha_b \geq \alpha_a; \quad \beta_b = \beta_a$$

For  $|\kappa| \geq 1$

$$W = 1; \quad \alpha_b = \alpha_a; \quad \beta_b \geq \beta_a$$

*Case 2.*

The lines have *different phase constants* and *equal attenuation constants*.

$\kappa$  is a real number

$W$  changes asymptotically from

$$W_0 = 0 \text{ to}$$

$$W_1 = 0.172 \text{ and to}$$

$$W_\infty = 1$$

Case 3.

The *phase* and *attenuation* constants *differ by equal amounts*. As shown below, in section 4, this case applies to the coupling between the  $TE_{01}$  and  $TM_{11}$  modes in curved circular wave guides with finite conductivity.

$\kappa^2$  is an imaginary number.

$W$  changes asymptotically from

$$W_0 = 0 \text{ to}$$

$$W_1 = 0.217 \text{ and}$$

$$W_\infty = 1$$

For  $\kappa \gg 1$  all three cases approach the limit

$$\begin{aligned} \beta_\infty &\doteq \frac{\beta_1 + \beta_2}{2} \left(1 + \frac{k}{2}\right) \\ \alpha_\infty &\doteq \frac{\alpha_1 + \alpha_2}{2} \left(1 + \frac{k}{2}\right) \doteq \frac{\alpha_1 + \alpha_2}{2} \end{aligned} \quad 1.2-10$$

## 2. DERIVATION OF FIELD EQUATIONS

Consider a straight circular cylinder with an inside radius such as shown on Fig. 1 A. Let the radial coordinate equal  $r$ , the azimuthal coordinate equal  $\varphi$  and the longitudinal coordinate equal  $z$ . Let the dielectric losses inside the cylinder be negligible.

The field equations inside the cylinder are<sup>5</sup>

$$\begin{aligned} \frac{\partial E_z}{r \partial \varphi} - \frac{\partial E_\varphi}{\partial z} &= -i\omega\mu H_r \\ \frac{\partial E_r}{\partial z} - \frac{\partial E_z}{\partial r} &= -i\omega\mu r H_\varphi \\ \frac{\partial(rE_\varphi)}{\partial r} - \frac{\partial E_r}{\partial \varphi} &= -j\omega\mu r H_z \end{aligned}$$

and

$$\begin{aligned} \frac{\partial H_z}{r \partial \varphi} - \frac{\partial H_\varphi}{\partial z} &= j\omega\epsilon E_r \\ \frac{\partial H_r}{\partial z} - \frac{\partial H_z}{\partial r} &= j\omega\epsilon E_\varphi \\ \frac{\partial(rH_\varphi)}{\partial r} - \frac{\partial H_r}{\partial \varphi} &= j\omega\epsilon r E_z \end{aligned}$$

<sup>5</sup> See Ref. 4, pg. 94 of the book.

The natural transmission modes which satisfy these equations have the form

$$E = f_n(r) \epsilon^{jn(\varphi + \varphi_0)} \cdot \epsilon^{j\omega t - \Gamma z} \quad 2-0$$

Each of these modes conforms to the same equations as a wave traveling in a transmission line with an impedance and phase velocity dependent upon the mode. In a straight cylinder with perfectly conducting walls, there exists no coupling between the different modes so that any and all can exist without interacting. If the conductivity of the walls in a straight circular cylinder is finite, it produces a resistive coupling between modes of equal azimuthal index ( $n$  in equation 2-0). In copper tubing and at the frequencies now obtainable ( $\omega < 10^{12}$ ) this coupling effect is negligible.

A stronger coupling may be caused by deviations of the wave guide from the shape of a straight circular cylinder. The deformation considered in the present analysis consists in a circular bend of the axis, as shown schematically on Fig. 1b.

In such a circular bend the longitudinal coordinate is replaced by the product of the bending radius  $R$  by the bending angle  $\theta$ :

$$z = R\theta$$

This transforms the first two component equations of curl  $E$  into

$$\begin{aligned} \frac{\partial(RE_\theta)}{Rr\partial\varphi} - \frac{\partial E_\varphi}{R\partial\theta} &= -j\omega\mu H_r \\ \frac{\partial E_r}{R\partial\theta} - \frac{\partial(RE_\theta)}{R\partial r} &= -j\omega\mu H_\varphi \end{aligned}$$

The variable  $R$  can be eliminated by the relation

$$R = R_0 - r \cos \varphi$$

where  $R_0$  is the bending radius of the cylinder axis. The coordinate  $\theta$  can be replaced by a longitudinal coordinate  $s$ , measured along the cylinder axis. Hence,

$$s = \theta R_0$$

The progressive modes which we investigate have the approximate form

$$E = f_n(r) \epsilon^{jn(\varphi + \varphi_0)} \epsilon^{j\omega t - \Gamma s}$$

Hence

$$\begin{aligned} \frac{\partial}{\partial\theta} &= R_0 \frac{\partial}{\partial s} = -R_0 \Gamma \\ \frac{\partial}{\partial\varphi} &= jn \quad \text{for all field components.} \end{aligned}$$



$\frac{\partial}{\partial r}$  may be expressed by a prime:

$$\frac{\partial F}{\partial r} = F'$$

Thus the equations with curl  $E$  become

$$\begin{aligned} \frac{jnE_s}{r} + \frac{E_s \sin \varphi}{R_0 - r \cos \varphi} + \frac{R_0 \Gamma E_\varphi}{R_0 - r \cos \varphi} &= -j\omega\mu H_r \\ \frac{-R_0 \Gamma E_r}{R_0 - r \cos \varphi} - E'_s + \frac{E_s \cos \varphi}{R_0 - r \cos \varphi} &= -j\omega\mu H_\varphi \\ E_\varphi + rE'_\varphi &= jnE_r = -j\omega\mu r H_s \end{aligned}$$

For gradual bends

$$R_0 \gg a > r$$

One may therefore approximate

$$\frac{R_0}{R_0 - r \cos \varphi} \doteq 1 + \frac{r}{R_0} \cos \varphi$$

It is convenient to introduce the symbol

$$c = \frac{a}{R_0}$$

which is proportional to the coupling coefficient. All powers of  $c$  greater than the first will be neglected. One can now write the approximate field equations in the curved cylinder:

$$\frac{jnE_s}{r} + \Gamma E_\varphi + \frac{c}{a} E_s \sin \varphi + c\Gamma \frac{r}{a} E_\varphi \cos \varphi = -j\omega\mu H_r \quad 2-1$$

$$-\Gamma E_r - E'_s - c\Gamma \frac{r}{a} E_r \cos \varphi + \frac{c}{a} E_s \cos \varphi = -j\omega\mu H_\varphi \quad 2-2$$

$$E_\varphi + rE'_\varphi - jnE_r = -j\omega\mu r H_s \quad 2-3$$

$$\frac{jnH_s}{r} + \Gamma H_\varphi + \frac{c}{a} H_s \sin \varphi + c\Gamma \frac{r}{a} H_\varphi \cos \varphi = j\omega\epsilon E_r \quad 2-4$$

$$-\Gamma H_r - H'_s - c\Gamma \frac{r}{a} H_r \cos \varphi + \frac{c}{a} H_s \cos \varphi = j\omega\epsilon E_\varphi \quad 2-5$$

$$H_\varphi + rH'_\varphi - jnH_r = j\omega\epsilon r E_s \quad 2-6$$

The coupling terms all contain the factor  $\cos \varphi$  or  $\sin \varphi$ . This means that every transmission mode is coupled only to modes with an azimuth index differing from its own by  $\pm 1$ .

3. CHARACTERISTIC EQUATIONS OF  $TE_{01}$  AND  $TM_{11}$  MODES

The mode which one desires to propagate through the wave guide is the  $TE_{01}$  mode. In a straight wave guide with perfectly conducting walls it is characterized by the following equations:

$$n = 0 \quad 3-1$$

$$E_{r1} = E_{z1} = H_{\phi 1} = 0 \quad 3-2$$

$$E_{\phi 1} = E_1 e^{j\omega t - \Gamma_1 z} J_1(y) = e_1 J_1(y) \quad 3-3$$

$$H_{r1} = -\frac{e_1 \Gamma_1}{j\beta_0 \eta} J_1(y) \quad 3-4$$

$$H_{z1} = -\frac{e_1 \chi}{j\beta_0 \eta} J_0(y) \quad 3-5$$

In these equations

$$\eta = \sqrt{\frac{\mu}{\epsilon}} = 377 \text{ ohm (intrinsic free space resistance)} \quad 3-6$$

$$\beta_0 = \omega \sqrt{\epsilon \mu} = \frac{2\pi}{\lambda_0} \quad 3-7$$

$$y = \chi r \quad 3-8$$

$$\Gamma_1 = \sqrt{\chi^2 - \beta_0^2} \quad 3-9$$

In a perfectly conducting wave guide

$$\chi_0 = \frac{3.832}{a} \quad 3-10$$

$$\nu = \frac{\chi_0}{\beta_0} = \frac{.61\lambda_0}{a} \text{ (cutoff factor)} \quad 3-11$$

$$\Gamma_1 = j\beta_0 \sqrt{1 - \nu^2} = j\beta_1 \quad 3-12$$

If the wave guide has the conductivity of  $g$  mho/m, its intrinsic high frequency impedance is

$$Z_i = (1 + j)R_i = (1 + j)34.4 \sqrt{\frac{\mu}{g\lambda_0}}^* \quad 3-13$$

This changes  $\chi$  to

$${}_1\chi \doteq \chi_0 - \frac{(1 - j)R_i \nu}{\eta a} \text{ and} \quad 3-14$$

$$\Gamma_1 \doteq j\beta_1 + \frac{\nu^2}{\sqrt{1 - \nu^2}} \frac{(1 + j)R_i \dagger}{a\eta} \quad 3-15$$

\* Ref. 4 pg. 83.

† Compare Ref. 4, pg. 390.

Due to the curvature of the guide, this desired mode is coupled to all modes which have the azimuthal index number 1.

However, for low curvatures, this coupling is very loose and only causes appreciable effects if it can act over a great length of wave guide without phase interference.

This means that the disturbing mode must have nearly the same phase velocity as the desired mode. It so happens that in a perfectly conducting circular cylinder there exists one mode, the  $TM_{11}$ , which has exactly the same velocity as the  $TE_{01}$ . Such a coincidence is called "degeneracy."

In the analysis of very gradual bends, only this  $TM_{11}$  mode need be considered. It is characterized in a straight guide by the following equations:

$$n = 1 \quad 3-16$$

$$E_{\varphi 2} = E_2 e^{j\omega\tau - \Gamma_2 z} \cdot \frac{J_1(y)}{y} \cos(\varphi + \varphi_0) = e_2 \frac{J_1(y)}{y} \cos \varphi \quad 3-17$$

The  $TM_{11}$  mode can be polarized in all directions. But since only the component directed toward

$$\varphi_0 = 0$$

is excited by the wave guide curvature,  $\varphi_0$  has been omitted in the last term of eq. (3-17).

$$E_{r2} = e_2 \frac{dJ_1(y)}{dy} \sin \varphi = e_2 j_1(y) \sin \varphi, \quad \text{where } j = \frac{dJ}{dy}$$

$$E_{z2} = \frac{-\chi_2 \ell_2}{\Gamma_2} J_1(y) \sin \varphi$$

$$H_{\varphi 2} = \frac{e_2 j \beta_0}{\eta \Gamma_2} j_1(y) \sin \varphi$$

$$H_{r2} = -\frac{e_2 j \beta_0}{\eta \Gamma_2} \frac{J_1(y)}{y} \cos \varphi$$

$$H_{z2} = 0$$

In a perfectly conducting wave guide the  $\chi$  defined by eq. 3-8 is

$$\chi = \chi_2 = \chi_0 \text{ and}$$

$$\Gamma_2 = \Gamma_1 = j\beta_1$$

In a wave guide with an intrinsic impedance per 3-13,

$$\chi_2 = \chi_0 - \frac{(1-j)R_i}{\eta a \nu} \quad \text{and} \quad 3-18$$

$$\Gamma_2 = j\beta_1 + \frac{(1+j)R_i}{\sqrt{1-\nu^2} a \eta} \quad 3-19$$

$$\text{From 3-15 and 3-19 one finds } \alpha_1 = \alpha_2 \nu^2 \quad 3-20$$

4. INTERACTION BETWEEN  $TE_{01}$  AND  $TM_{11}$  MODES

Since the separate modes of propagation behave like traveling waves in transmission lines<sup>2</sup>, their interaction can be derived from the coupling equations derived in Section 1 of this analysis.

The uncoupled propagation constants  $\Gamma_1$  and  $\Gamma_2$  are known (equations 3-15 and 3-19). In order to find the coupling discriminant one must derive the coupling coefficient from the field equations 2-1 to 2-6. The coupling coefficient is defined as

$$k = \frac{P_{12}}{\sqrt{P_1 P_2}} = \frac{P_{21}}{\sqrt{P_1 P_2}} \quad (\text{eq. 1.2-4})$$

In computing the coupling coefficient one may neglect the small attenuation constant. The energy stored by the  $TE_{01}$  wave per unit length is

$$P_1 = \int_0^a \frac{E_1^2}{\eta} \cdot 2\pi r \, dr = \int_0^a H_1^2 \eta \cdot 2\pi r \, dr \quad 4-1$$

This expression is not affected by the cutoff factor  $\nu$  because one may consider the field inside the guide as composed of slanting plane waves with the electric field strength  $E_1$ . The energy stored by the  $TM_{11}$  wave per unit length is

$$P_2 = \int_0^{2\pi} \int_0^a \frac{E_2^2}{\eta} r \, d\varphi \, dr = \int_0^{2\pi} \int_0^a H_2^2 \eta r \, d\varphi \, dr \quad \text{The inter-}$$

changed energy:

$$P_{21} = \int_0^{2\pi} \int_0^a \frac{E_{21} E_1}{\eta} d\varphi \, dr + \int_0^{2\pi} \int_0^a H_{21} H_1 \eta \, d\varphi \, dr$$

Combining equation (4-1) with 3-3, 3-8 and 3-10

$$P_1 = \frac{2\pi a^2 \epsilon_1^2}{3.832^2 \eta} \int_0^{3.832} y \delta_1^2 J_1(y) \, dy$$

From reference 1, page 146 of the book

$$\int_0^{3.832} y \delta_1^2 J_1(y) \, dy = \frac{3.832^2}{2} J_0(3.832)$$

Hence

$$P_1 = \frac{0.51 \epsilon_1^2 a^2}{\eta} \quad 4-2$$

In a similar manner one finds

$$P_2 = \frac{0.51 \epsilon_2^2 a^2}{2(1 - \nu^2) \eta} \quad 4-3$$

<sup>2</sup> Loc. cit.

and

$$P_{12} = P_{21} = \frac{0.51 c e_1 e_2 a^2}{3.832 \eta} \quad 4-4$$

Substituting the values of 4-2, 4-3 and 4-4 into 1.2-4 one finds for the coupling coefficient between the two groups of plane waves traveling at a slant to the wave guide axis

$$k_s = \frac{c \sqrt{2} \sqrt{1 - \nu^2}}{3.83} = \frac{0.369 a}{R_0} \sqrt{1 - \nu^2}$$

The coupling coefficient  $k$  between the  $TE_{01}$  and  $TM_{11}$  modes which are the resultants of their slant wave groups is greater than  $k_s$  according to the following reasoning:

From 1.2-10

$$\beta \doteq \beta_0(1 \pm 0.5 k_s)$$

This makes the cutoff factors of the coupled modes

$$\nu = \frac{x}{\beta} = \frac{\nu_0}{1 \pm 0.5 k_s}$$

and the coupled propagation constants

$$\Gamma = \beta \sqrt{1 - \nu^2} = \beta_0 \sqrt{(1 \pm 0.5 k_s)^2 - \nu_0^2}$$

For  $k_s \ll 1$

$$\Gamma \doteq \beta_0 \sqrt{1 - \nu_0^2} \left( 1 \pm \frac{0.5 k_s}{1 - \nu_0^2} \right) = \Gamma_0 (1 \pm 0.5 k)$$

Hence, in view of eq. 1.2-10, the effective coupling coefficient of the wave guide modes is

$$k = \frac{k_s}{1 - \nu^2} = \frac{0.369 a}{R_0 \sqrt{1 - \nu^2}} \quad 4-5$$

From equations 3-15 and 3-19

$$\Gamma_1 - \Gamma_2 = -\frac{1+j}{a\eta} R_i \sqrt{1 - \nu^2} \quad 4-6$$

$$\frac{\sqrt{\Gamma_1 \Gamma_2}}{\Gamma_1 - \Gamma_2} \doteq \frac{j \beta_0}{\Gamma_1 - \Gamma_2} \doteq \frac{-2\pi \eta a}{(1-j) R_i \lambda_0 \sqrt{1 - \nu^2}} \quad 4-7$$

From 1.2-3, 4-5 and 4-7 one obtains the coupling discriminant

$$\kappa = \frac{-0.369 \cdot 2\pi \cdot 377 a^2}{R_0 R_i \lambda_0 (1-j)(1 - \nu^2)}$$

Since

$$R_i = 0.00452 \lambda_0^{-0.5} \cdot \rho_r^* \quad 4-8$$

\* Loc. cit.

with the relative high frequency resistivity

$$\rho_r = \sqrt{\frac{\rho}{\rho_{\text{copper}}}}$$

$$\kappa = - \frac{9.65 \cdot 10^4 (1 + j) a^2 \lambda^{-0.5}}{R_0 \rho_r (1 - \nu^2)}$$

Its absolute value

$$|\kappa| = \frac{1.366 \cdot 10^5 a^2 \lambda^{-0.5}}{R_0 \rho_r (1 - \nu^2)}$$

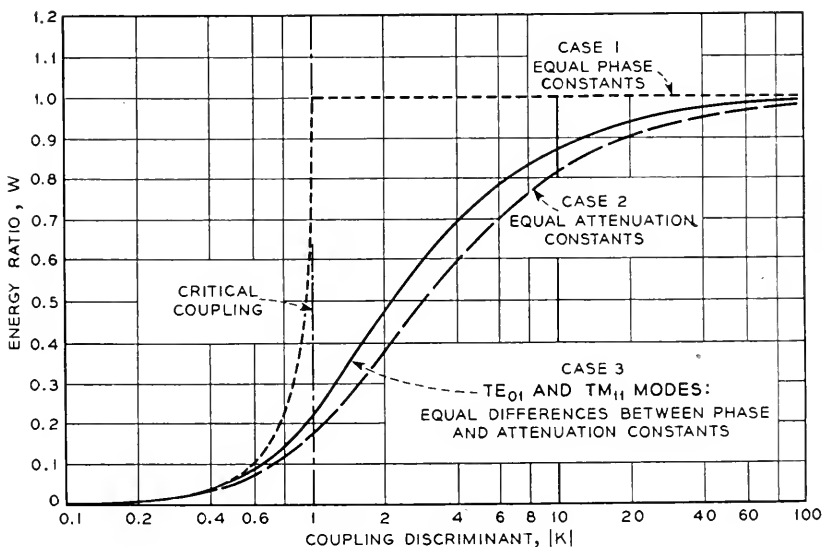


Fig. 3

As shown in equation 4-6, the differences between the propagation constants of the TM<sub>11</sub> and TE<sub>01</sub> waves are proportional to the intrinsic skin impedance  $R_i$  which contains the factor  $(1 + j)$ . This means that the phase and attenuation constants of the two waves differ by equal amounts in accordance with "Case 3" of Section 1. For this case the power ratio per 1.2-20 may be written

$$W = \left| \frac{\sqrt{1 + j|\kappa|^2} - 1}{\sqrt{1 + j|\kappa|^2} + 1} \right|$$

The numerical value of this function is plotted on Fig. 3. It can be computed conveniently by means of the following auxiliary parameters:

$$\sqrt{1 + j|\kappa|^2} = p + jq = \cosh x + j \sinh x \quad 4-9$$

$$\begin{aligned}
 p &= \sqrt{0.5 + 0.5\sqrt{1 + |\kappa|^4}} = \cosh x \\
 q &= \sqrt{-0.5 + 0.5\sqrt{1 + |\kappa|^4}} = \sinh x \\
 W &= \frac{p-1}{p} \tanh \frac{x}{2}
 \end{aligned}$$

In analogy to *Case 1* of Section 3, the condition of  $|\kappa| = 1$  may be called *critical coupling*. It occurs at the *critical radius of curvature*

$$R_{0\text{ cr}} = \frac{1.366 \cdot 10^5 a^2 \lambda^{-0.5}}{\rho_r (1 - \tau^2)} \text{ meters} \quad 4-10$$

For subcritical coupling ( $R_0 \gg R_{11}$ )  $W$  approaches

$$W_{\text{subcr.}} \doteq \frac{\kappa^2}{4} \longrightarrow 0$$

For supercritical coupling ( $R_0 \ll R_{\text{cr}}$ ),

$$W_{\text{supercr.}} \doteq 1 - \frac{\sqrt{2}}{|\kappa|} \longrightarrow 1$$

From the above results, it is possible to predict the behavior of waves originating either as  $\text{TE}_{01}$  or as  $\text{TM}_{11}$  modes, in any given wave guide configuration. This is done for some typical cases in the following sections.

## 5. PROPAGATION IN LONG WAVEGUIDES WITH CONSTANT CURVATURE

It has been shown in Section 3 that for each curvature there exist two modes of propagation.

In one,

$$W_a = \frac{P_{\text{TM}_{11}}}{P_{\text{TE}_{01}}} < 1 \quad 5-1$$

and the attenuation

$$\alpha_a < \frac{\alpha_{\text{TE}} + \alpha_{\text{TM}}}{2} \quad 5-2$$

In the other,

$$W_b = \frac{1}{W_a} > 1 \quad 5-3$$

and the attenuation

$$\alpha_b > \frac{\alpha_{\text{TE}} + \alpha_{\text{TM}}}{2} \quad 5-4$$

In a long wave guide the "b" mode will die down due to its greater attenuation, no matter how much of it was initially present, so that one need only consider the "a" mode.

This mode has a phase velocity slightly smaller than that of the uncoupled  $TE_{01}$  wave and an attenuation nearer to that of the  $TE_{01}$  than the  $TM_{11}$  wave.

The magnitude of the critical radius is illustrated by the two examples of Table I.

TABLE I  
CHARACTERISTIC VALUES

Parameter	Symbol	Equation	Example 1	Example 2
Wave guide radius	a		.05 m	.05 m
Free space wave length	$\lambda_0$		.03 m	.01 m
Cutoff ratio	$\nu$	3-11	.366	.122
Attenuation constant	$\alpha_{TE(cu)}$	3-15, 4-17	$2.04 \times 10^{-4}$ neper/m	$3.58 \times 10^{-5}$ neper/m
Attenuation constant	$\alpha_{TM(cu)}$	3-19	$1.53 \times 10^{-3}$ neper/m	$2.41 \times 10^{-3}$ neper/m
Critical Radius	$R_{crit}$	4-10	2.12 km.	3.44 km.

TABLE II  
RELATIVE ATTENUATION VERSUS RADIUS OF CURVATURE

General formulae				Example 1		Example 2	
$k$	$R_0/R_{cr}$	$H'$	$\alpha/\alpha_0$	$R_0/km$	$\alpha/\alpha_0$	$R_0/km$	$\alpha/\alpha_0$
0	$\infty$	0	1	$\infty$	1.00	$\infty$	1.00
0.1	10	0.0025	$1 + 0.0025 (\nu^{-2} - 1)$	19.7	1.02	34.15	1.17
0.2	5	0.01	$1 + 0.01$ "	9.85	1.06	17.08	1.66
0.5	2	0.06	$1 + 0.057$ "	3.84	1.38	6.83	4.45
1	1	0.22	$1 + 0.18$ "	1.97	2.16	3.42	12.94
2	0.5	0.48	$1 + 0.32$ "	0.98	3.11	1.71	22.2
5	0.2	0.75	$1 + 0.43$ "	0.38	3.83	0.68	26.6
10	0.1	0.87	$1 + 0.46$ "	0.20	4.05	0.34	27.9
$\infty$	0	1.00	$1 + 0.50$ "	0	4.30	0	34.1

The increase of attenuation in long wave guides with uniform curvature is shown on Table II, with numerical values for the same examples as in Table I.

#### 6. PROPAGATION IN A UNIFORMLY CURVED SECTION OF WAVE GUIDE FOLLOWING A LONG STRAIGHT SECTION. (FIG. 4)

No matter what mixture of modes may prevail at the beginning of the wave guide, all modes except the  $TE_{01}$  die down in the long straight section due to their higher attenuation, so that the wave form at the beginning of the curved section is pure  $TE_{01}$ .

Since it has been shown in Sections 1 and 4 that each of the two possible



modes of propagation in a curved wave guide consists of both  $TE_{01}$  and  $TM_{11}$  waves, it follows that both modes must be superimposed in such a manner that at the transition point the TM components cancel each other by interference.

Let the relative amplitudes of the two TE components equal  $a$  and  $b$ ; then the corresponding amplitudes of the TM modes are  $aA_a$  and  $bA_b$

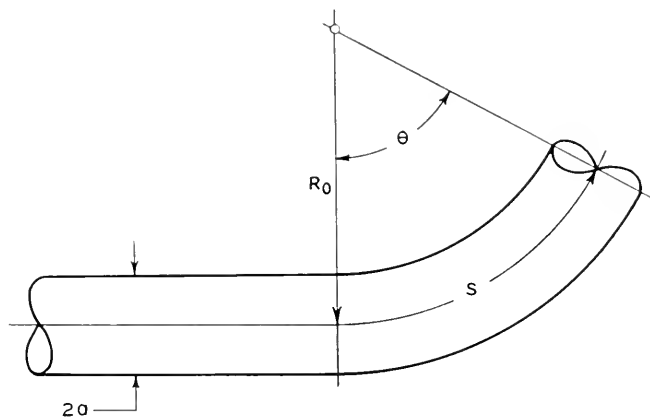


Fig. 4

respectively, where  $A_a$  and  $A_b$  are the normalized voltage ratios per 1.2-5. At the beginning of the curved section

$$a + b = 1 \quad (\text{TE amplitude})$$

$$aA_a + bA_b = aA_a - bA_a = 0 \quad (\text{TM amplitude})$$

Hence

$$a = \frac{1}{1 + A_a^2}$$

$$b = \frac{A_a^2}{1 + A_a^2}$$

$$\frac{b}{a} = A_a^2 = W$$

The two waves have different phase velocities and therefore interfere with each other. According to 1.2-9, the difference between the phase constants is

$$\beta_b - \beta_a = (\beta_2 - \beta_1) \frac{1 + W}{1 - W}$$

By means of equations 4-9, this can be transformed into

$$\beta_b - \beta_a = (\beta_2 - \beta_1)(p + q) \quad 6-1$$

The length of one complete interference cycle is

$$s_{2\pi} = \frac{2\pi}{(p+q)(\beta_2 - \beta_1)}$$

If both components had equal attenuation, the beats superimposed on the decaying envelope of the  $TE_{01}$  wave would correspond to an amplitude ratio

$$\frac{e_0 \max}{e_0 \min} = \frac{1 + H}{1 - H} = p + q$$

However, during the progress of the mixed wave through the curved section, the intensity of the fluctuations is reduced by the greater attenuation constant of the faster and weaker "b" component. In one complete interference cycle, the differential attenuation reduces the weaker component to

$$\frac{A_{2\pi}}{A_0} = e^{-(\alpha_2 - \alpha_1)s_{2\pi}} = e^{-(2\pi/p+q)}$$

#### *Approximation for Weak Coupling*

For  $|\kappa| \ll 1$

$$\beta_b - \beta_a \doteq (\beta_2 - \beta_1)(1 + 0.5 |\kappa|^2)$$

From 3-15 and 3-19

$$\begin{aligned} \beta_b - \beta_a &\doteq \frac{R_i}{a\eta} \sqrt{1 - \nu^2} \\ &\doteq \frac{1.2 \times 10^{-5}}{a} \sqrt{\frac{(1 - \nu^2)g_{cu}}{\lambda_0 g}} (1 + 0.5 |\kappa|^2) \text{ radian/m} \end{aligned}$$

For intermediate coupling, 6-1 may be transformed into

$$\beta_b - \beta_a = k\beta_1 f(\kappa)$$

$$\text{with } f_{(\kappa)} = \frac{p+q}{\sqrt{2}|\kappa|} = \frac{\sqrt{1 + \sqrt{1 + |\kappa|^4}} + \sqrt{-1 + \sqrt{1 + |\kappa|^4}}}{2|\kappa|}$$

#### *Approximation for Strong Coupling*

For  $|\kappa| \gg 1$

$$f_{(\kappa)} \doteq 1 + 0.125 |\kappa|^{-4} \quad \beta_b - \beta_a \doteq k\beta_1(1 + 0.125 |\kappa|^{-4})$$

Substituting the value of  $k$  from 4-13 and transforming,

$$\beta_b - \beta_a = \frac{2.32a}{\lambda_0 R_0} f_{(\kappa)} = \frac{2.32a}{\lambda_0 R_0} (1 + 0.125 |\kappa|^{-4}) \quad 6-2$$

The phase difference between the two components is

$$\Psi_{b-a} = \frac{2.32as}{\lambda_0 R_0} f_{(\kappa)} = \frac{2.32a\theta}{\lambda_0} f_{(\kappa)} = M\theta \quad 6-3$$

where  $\theta$  is the bending angle of the wave guide. The power carried by the  $TE_{01}$  wave is

$$P_{TE} = \cos^2 \frac{M\theta}{2}. \quad 6-4$$

Minima of  $TE_{01}$  occur when this phase difference is an odd multiple of  $\pi$ . Hence, the bending angles producing minima of  $TE_{01}$  amplitudes are:

$$\theta_{\min} \doteq (2n + 1) \cdot \frac{1.36\lambda_0}{a(1 + 0.125 |\kappa|^{-4})} \doteq \frac{(2n + 1)2.22\nu}{f(\kappa)} \quad 6-5$$

The initial fluctuation ratio approaches

$$\frac{e_{1\max}}{e_{1\min}} = p + q \doteq \sqrt{2} |\kappa|$$

which is a large value tending to infinity.

The relative attenuation of the slightly weaker component during one beat cycle is

$$\frac{A_{2\pi}}{A_0} = e^{-2\pi/p+q} = e^{-\sqrt{2}\pi/|\kappa|} \doteq 1 - \frac{4.44}{|\kappa|}$$

which is a small reduction tending to zero. Hence, the fluctuations persist through a large number of beats. The power is transformed back and forth between the  $TE_{01}$  and the  $TM_{11}$  modes.

In Section 5, it was shown that in a long, uniformly curved wave guide the attenuation is intermediate between that of the  $TE_{01}$  and  $TM_{11}$  modes. But from equations 1.2-7 and 8 it follows that the two modes contribute to the attenuation in proportion to their relative power flow. Since at the beginning of the bend the power of the  $TM_{11}$  component is zero, it is to be expected that the *initial* rate of attenuation equals that of the  $TE_{01}$  wave alone. This is proved by differentiating with regard to  $s$ . One finds for all values of  $\kappa$  that

$$\left. \frac{d}{ds} a e^{-\Gamma_a s} + b e^{-\Gamma_b s} \right|_{s=0} = -\alpha_1$$

### Discussion of Results

Equation 6-2 corresponds directly to an equation derived by S. O. Rice and, after allowing for the different choice of variables, to M. Jouguet's equation (75)<sup>6</sup>. It differs from the results of these earlier calculations by the factor  $f(\kappa) \doteq 1 + 0.125 |\kappa|^{-4}$  which is a reminder that the simplified form of the equations given by the earlier authors is an extrapolation to infinite conductivity or infinite curvature of the wave guide.

<sup>6</sup> Reference 3, pg. 150 of *Cables and Transmission*, July 1947.

From equations 6-3 and 6-4 it is seen that the  $TE_{01}$  wave is recovered by bends which are an even multiple of  $\theta_{min}$ . But such bends are efficient transmitters of  $TE_{01}$  waves only over a narrow frequency range since  $\theta_{min}$  varies with frequency.

If the circular bend is followed by a long straight section, the  $TE_{01}$  and  $TM_{11}$  components existing at the end of the bend are carried over into the straight section, but the  $TM_{11}$  component dies down due to its greater attenuation and constitutes a total loss.

#### *Numerical examples for first extinction angle.*

Using the same dimensions as in Table I of Section 5, one finds from eq. 6-5 for:

$$\text{Example 1: } \theta_{min} \doteq 0.816 \text{ Radians} \doteq 46.8^\circ$$

$$\text{Example 2: } \theta_{min} \doteq 0.272 \text{ Radians} \doteq 15.6^\circ$$

### 7. SERPENTINE BENDS

Sections 5 and 6 dealt with bends continued with uniform curvature over large angles. The present section considers the small random deviations from a straight course which are unavoidable in field installations.

Actual deviations are expected to be random both with regard to maximum deflection angle and to curvature; they are likely to approximate a sinusoidal shape. For purposes of computation, the following analysis assumes as a first case *circular S-bends* which consist of alternate regions of equal lengths and equal but opposite curvatures. An exaggerated schematic of such S-bends is shown on Fig. 5A.

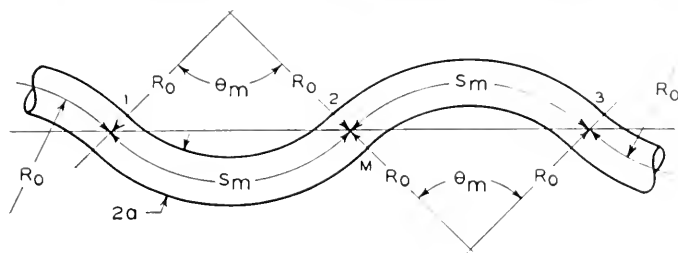
Each circular bend tends to produce a single mode with an attenuation per equation 1.2-7. However, the discontinuous reversals of curvature at the inflexion points produce mixed modes, and the initial part of each region reduces the amplitude of the TM components produced in the previous region.

Each region may be treated as a discrete 4-terminal section of a transmission network. Regardless of the wave composition at the input terminal, differential attenuation will establish in a long serpentine wave guide a steady state condition. In this steady state each region produces equal attenuation. This attenuation per region and the resulting average attenuation constant will now be derived.

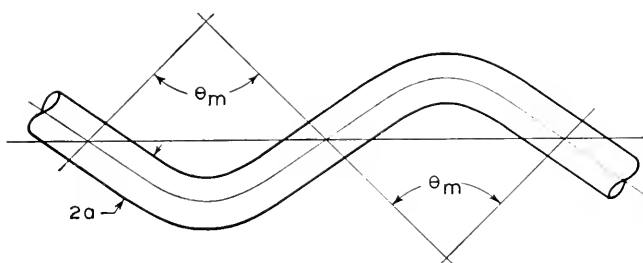
The  $TE_{01}$  and  $TM_{11}$  waves each consist of "a" and "b" components with separate amplitude ratios and propagation constants, as derived in Sections 1 and 4. In the first region (between points 1 and 2 of Fig. 5A)  $R_0$  is taken as positive, and

$$A = \sqrt{1 + \kappa^{-2}} - \kappa^{-1} \quad 1.2-6$$

In the second region, between points 2 and 3, the polarity of  $R_0$ , and consequently of  $\kappa$  and the ratio of TM to TE amplitudes, are reversed.



a - CIRCULAR 'S' BENDS



b - SINUSOIDAL BENDS

Fig. 5

Except for this change of polarity the amplitude ratios at points 1 and 2 are equal. Introducing the symbols

$$g = e^{-\Gamma_{sm}}$$

$$g_m = \frac{1}{2}(g_a + g_b)$$

$$g_d = \frac{1}{2}(g_b - g_a)$$

one can tabulate

point	$e_{TE}$	$e_{TM}$	
1	$a + b$	$aA - \frac{b}{A}$	7-1

2	$g_m \left( \frac{a}{g_d} + b g_d \right)$	$g_m \left( \frac{aA}{g_d} - \frac{b}{A} g_d \right)$	7-2
---	--	---	-----

Calling  $\frac{b}{a} = y$ , one finds

$$\frac{1 + y g_d^2}{1 + y} = \frac{-A^2 + y g_a^2}{A^2 - y} = \frac{g_d}{g_m} \cdot g_{\text{average}} = \frac{g_{\text{average}}}{g_a}$$

$$\Gamma_{\text{average}} = \Gamma_a + \frac{1}{s_m} \log \frac{1+y}{1+y g_d^2} \text{ with}$$

$$y = \frac{A}{2} \kappa^{-1} (1 + g_d^{-2}) + A \sqrt{g_d^{-2} + \frac{\kappa^{-2}}{4} (1 + g_d^{-2})^2}$$

This formal solution is hard to evaluate. It can be greatly simplified for the subcritical and supercritical cases.

### 1. Subcritical Curvature $|\kappa| \ll 1$

$$y \doteq \frac{\kappa^2}{2 + 2_d^2}$$

$$\Gamma_{\text{average}} = \Gamma_a \left( 1 + \frac{\kappa^2}{2} \frac{1 - g_d^2}{1 + g_d^2} \right) \doteq \Gamma_a \doteq \Gamma_1$$

For very low curvatures, the average attenuation approaches that of the "a" mode, and this in turn approaches that of the  $TE_{01}$  wave.

### 2. Supercritical Curvature. $|\kappa| \gg 1$

The differential attenuation constant is small compared to the differential phase constant.

$$|y| \doteq |A| \doteq 1$$

Substituting these values into 7-1 and 2, one finds

$$y \doteq e^{-0.5j\theta_m}$$

Expressed as a function of  $\theta$ :

$$y_\theta = \cos \psi + j \sin \psi \text{ with}$$

$$\psi = M(\theta - 0.5 \theta_m)$$

7-3

$M$  has the value per eq. 6-18.

The power ratio of the combined  $TM_{11}$  and  $TE_{01}$  waves is

$$W_\theta \doteq \tan^2 \psi / 2$$

In view of equation 1.2-7 the instantaneous rate of energy loss is

$$\alpha_\theta = \alpha_1 \cos^2 \frac{\psi}{2} + \alpha_2 \sin^2 \frac{\psi}{2} = \alpha_1 + (\alpha_2 - \alpha_1) \sin^2 \frac{\psi}{2} \quad 7-4$$

$$\alpha_{\text{average}} = \frac{1}{s_m} \int_0^{s_m} \alpha_s ds = \frac{1}{\theta_m} \int_0^{\theta_m} \alpha_\theta d\theta$$

$$\alpha_{\text{average}} = \alpha_1 + (\alpha_2 - \alpha_1) \left( \frac{1}{2} - \frac{\sin M\theta_m}{2M\theta_m} \right)$$

In view of 3-20

$$\alpha_{\text{average}} = \alpha_1 \left[ \frac{\nu^{-2} + 1}{2} - \frac{\nu^{-2} - 1}{2} \frac{\sin M\theta_m}{M\theta_m} \right]$$

For small deflection angles,  $M\theta_m \ll 2$

$$\alpha_{\text{average}} \doteq \alpha_1 \left[ 1 + \frac{\nu^{-2} - 1}{6} M^2 \theta_m^2 \right]$$

If a  $p\%$  increase in attenuation is the tolerance limit

$$\theta_m \leq \frac{1}{10M} \sqrt{\frac{6p}{\nu^{-2} - 1}}. \quad \text{Substituting the value of } M \text{ from 6-3,}$$

$$\theta_m = \frac{0.105 \sqrt{p} \nu \lambda_0}{a \sqrt{1 - \nu^2}}.$$

The maximum deflection equals

$$\Delta_\theta = 0.5 \theta_m. \quad \text{Hence, in view of 3-11}$$

$$\Delta_\theta \leq \frac{0.032 \sqrt{p} \lambda_0^2}{a^2 \sqrt{1 - \nu^2}} \text{ radians} = \frac{1.84 \lambda_0^2}{a^2} \sqrt{\frac{p}{1 - \nu^2}} \text{ degrees}$$

### 3. Sinusoidal Bends with Predominantly Supercritical Curvature.

Sinusoidal bends cannot be supercritically curved over their entire length because at the inflection points the curvature drops to zero. For sufficiently short bends, however, no great error is caused by treating the entire length as supercritical. In that case, equations 7-3 and 7-4 remain valid.  $\theta$  takes the new value

$$\theta = \frac{\theta_m}{2} + \frac{\theta_m}{2} \sin \frac{\pi(s - s_m)}{2s_m}$$

Hence

$$\psi = \frac{M\theta_m}{2} \sin \frac{\pi(s - s_m)}{2s_m}$$

$$\alpha_{\text{average}} = \alpha_1 + \frac{\alpha_2 - \alpha_1}{s_m} \int_0^{s_m} \sin^2 \left[ \frac{M\theta_m}{2} \sin \frac{\pi(s - s_m)}{2s_m} \right] ds$$

For small deflection angles,  $M\theta_m \ll 2$

$$\begin{aligned} \alpha_{\text{average}} &= \alpha_1 + \frac{\alpha_2 - \alpha_1}{s_m} \frac{M^2 \theta_m^2}{4} \int_0^{s_m} \sin^2 \frac{\pi(s - s_m)}{2s_m} ds \\ &= \alpha_1 + (\alpha_2 - \alpha_1) \frac{M^2 \theta_m^2}{4} = \alpha_1 \left[ 1 + \frac{\nu^{-2} - 1}{4} M^2 \theta_m^2 \right] \\ \Delta_\theta &= \frac{0.026 \lambda_0^2 \sqrt{p}}{a^2 \sqrt{1 - \nu^2}} \text{ radians} = \frac{1.49 \lambda_0^2}{a^2} \sqrt{\frac{p}{1 - \nu^2}} \text{ degrees} \end{aligned}$$

The tolerance limit for sinusoidal deflections is 20% smaller than for circular S bends.

The effect of supercritical but shallow circular and sinusoidal S bends is illustrated by the following *numerical examples*.

TABLE III  
INCREASE OF ATTENUATION IN S BENDS

Attenuation Increase $\delta\%$	Maximum deflection $\Delta\theta$ (in degrees)			
	Example 1 ( $\nu = .366$ )		Example 2 ( $\nu = .122$ )	
	Circular	Sinusoidal	Circular	Sinusoidal
10	2.25	1.82	0.23	0.19
20	3.18	2.58	0.33	0.27
30	3.89	3.15	0.41	0.33
40	4.50	3.64	0.47	0.38
50	5.03	4.07	0.52	0.42

### 8. HELICAL BENDS AND RANDOM TWO-DIMENSIONAL DEVIATIONS

A helical bend may be treated as a bend which has a constant absolute magnitude, but a changing direction of curvature. As indicated in eq. 3-17, the  $TM_{11}$  wave can be polarized in all directions. At any differential element of wave guide length, the  $TM_{11}$  component polarized in the local bending plane is coupled to the  $TE_{01}$  wave; the  $TM_{11}$  component polarized at right angles is not coupled and persists unchanged. By requiring that the absolute magnitude of the  $TM_{11}/TE_{11}$  amplitude ratio remain constant, a steady state solution can be found.

Shallow helical bends of small curvatures may be treated as the superposition of two sinusoidal bends offset by  $90^\circ$  in the longitudinal direction and in the bending plane. The increases in attenuation due to these two sinusoidal bends are computed from eq. 7-5 and added.

It is believed that random deviations from a straight course approach sinusoidal shape more closely than circular shape, hence equation 7-5 may be used to establish a tolerance limit for such random deviations. For quantitative results the statistical distribution of the squared deviation maxima must be taken into consideration.

### 9. OPTIMA OF WAVE GUIDE RADIUS, SIGNAL WAVE LENGTH AND ATTENUATION AS A FUNCTION OF ANGULAR DEVIATION

In a straight wave guide the attenuation decreases with wave guide radius and signal frequency. However, the deterioration due to wave guide curvature increases with wave guide radius and frequency. Hence, for a given tolerance limit to angular deviation from the straight course there exists an optimum radius for each wave length and an optimum wave length for each radius. This will be shown for the case of uniform sinusoidal bends, under the simplifying assumption that the cutoff ratio  $\nu \ll 1$ .



Solving 7-5 for  $p$  one obtains

$$p \doteq 0.45\Delta^2 a^4 \lambda^{-4} \quad 9-1$$

where  $p$  is the percentage increase in attenuation, and  $\Delta$  the deviation angle in degrees.

Hence the average attenuation

$$\alpha_{\Delta} = \alpha(1 + 0.01p) \quad 9-2$$

From 3-15 and 3-11

$$\alpha \doteq \frac{\nu^2 R_i}{a\eta_i} \doteq 10^{-3} R_i \lambda^2 a^{-3} \quad 9-3$$

Introducing the  $R_i$  value from 4-8

$$\alpha \doteq 4.5 \cdot 10^{-5} \rho_1 \lambda^{1.5} a^{-3} \quad 9-4$$

where  $\rho$  is the high-frequency resistance of the wave guide relative to copper. From 9-1, 2 and 4

$$\alpha_{\Delta} = 4.5 \cdot 10^{-6} \rho \lambda^{1.5} a^{-3} (1 + q \lambda^{-4} a^4) \quad 9-5$$

with

$$q = 4.5 \cdot 10^{-3} \Delta^2$$

The attenuation reaches a minimum when

$$f(\lambda, a) = \lambda^{1.5} a^{-3} + q \lambda^{-2.5} a = \text{minimum}$$

*Case 1.  $\lambda$  is given*

$$\delta f / \delta a = -3\lambda^{1.5} a^{-4} + q \lambda^{-2.5} = 0$$

$$a_{opt} = 1.32 \lambda q^{-0.25} = 5.2 \lambda \Delta^{-0.5}$$

From 9-5

$$\alpha_{\Delta opt} = 4\alpha = 1.29 \cdot 10^{-7} \rho \lambda^{-1.5} \Delta^{1.5}$$

*Case 2.  $a$  is given*

$$\delta f / \delta \lambda = 1.5 \lambda^{0.5} a^{-3} - 2.5 q \lambda^{-3.5} a = 0$$

$$\lambda_{opt} = 1.14 a q^{0.25} = 0.294 a \Delta^{0.5}$$

From 9-5

$$\alpha_{\Delta opt} = 1.6\alpha = 1.15 \cdot 10^{-6} \rho a^{-1.5} \Delta^{0.75}$$

*Numerical Example*

Let  $\Delta = 0.42^\circ$

$a = 0.05 \text{ m}$

$\lambda = 0.01 \text{ m}$

From Table III

$$\alpha_{\Delta} = 1.50 \alpha = 5.4 \cdot 10^{-5} \rho \text{ neper}/m$$

Case 1:  $\lambda$  fixed at 0.01  $m$

$$a_{opt} = 0.08 \text{ } m$$

$$\alpha_{opt} = 2.76 \cdot 10^{-5} \rho \text{ neper}/\text{meter}$$

Case 2:  $a$  fixed at 0.05  $m$

$$\lambda_{opt} = 0.0097 \text{ } m$$

$$\alpha_{opt} = 5.36 \cdot 10^{-5} \rho \text{ neper}/m$$

Assuming sinusoidal bends with a  $0.42^\circ$  maximum deviation, the attenuation of centimeter waves can be reduced to one half by increasing the wave guide radius from 5 to 8 cm. For a 5 cm wave guide radius, 1 centimeter wavelength is close to the optimum.

# A New Type of High-Frequency Amplifier

By J. R. PIERCE and W. B. HEBENSTREIT

This paper describes a new amplifier in which use is made of an electron flow consisting of two streams of electrons having different average velocities. When the currents or charge densities of the two streams are sufficient, the streams interact to give an increasing wave. Conditions for an increasing wave and the gain of the increasing wave are evaluated for a particular geometry of flow.

## 1. INTRODUCTION

**I**N CENTIMETER range amplifiers involving electromagnetic resonators or transmission circuits as, in klystrons and conventional traveling-wave tubes, it is desirable to have the electron flow very close to the metal circuit elements, where the radio-frequency field of the circuit is strong, in order to obtain satisfactory amplification. It is, however, difficult to confine the electron flow close to metal circuit elements without an interception of electrons, which entails both loss of efficiency and heating of the circuit elements. This latter may be extremely objectionable at very short wavelengths for which circuit elements are small and fragile.

In this paper the writers describe a new type of amplifier. In this amplifier the gain is not obtained through the interaction of electrons with the field of electromagnetic resonators, helices or other circuits. Instead, an electron flow consisting of two streams of electrons having different average velocities is used. When the currents or charge densities of the two streams are sufficient, the streams interact so as to give an increasing wave. Electromagnetic circuits may be used to impress a signal on the electron flow, or to produce an electromagnetic output by means of the amplified signal present in the electron flow. The amplification, however, takes place in the electron flow itself, and is the result of what may be termed an electromechanical interaction.<sup>1,2</sup>

While small magnetic fields are necessarily present because of the motions of the electrons, these do not play an important part in the amplification.

<sup>1</sup> Some electro-mechanical waves with a similar amplifying effect are described in "Possible Fluctuations in Electron Streams Due to Ions," J. R. Pierce, *Jour. App. Phys.*, Vol. 19, pp. 231-236, March 1948.

<sup>2</sup> While this paper was in preparation a classified report by Andrew V. Haefl entitled "The Electron Wave Tube—A Novel Method of Generation and Amplification of Microwave Energy" was received from the Naval Research Laboratory. Dr. Haefl's report (now declassified) contains a similar analysis of interaction of electron streams and in addition gives experimental data on the performance of amplifying tubes built in accordance with the new principle. We understand that similar work has been done at the RCA Laboratories.

The important factors in the interaction are the electric field, which stores energy and acts on the electrons, and the electrons themselves. The charge of the electrons produces the electric field; the mass of the electrons, and their kinetic energy, serve much as do inductance and stored magnetic energy in electromagnetic propagation.

By this sort of interaction, a traveling wave which increases as it travels, i.e., a traveling wave of negative attenuation, may be produced. To start such a wave, the electron flow may be made to pass through a resonator or a short length of helix excited by the input signal. Once initiated, the wave grows exponentially in amplitude until the electron flow is terminated or until non-linearities limit the amplitude. An amplified output can be obtained by allowing the electron flow to act on a resonator, helix or other output circuit at a point far enough removed from the input circuit to give the desired gain.

There are several advantages of such an amplifier. Because the electrons interact with one another, the electron flow need not pass extremely close to complicated circuit elements. This is particularly advantageous at very short wavelengths. Further, if we make the distance of electron flow between the input and output circuits long enough, amplification can be obtained even though the input and output circuits have very low impedance or poor coupling to the electron flow. Even though the region of amplification is long, there is no need to maintain a close synchronism between an electron velocity and a circuit wave velocity, as there is in the usual traveling-wave tube.

A companion paper by Dr. A. V. Hollenberg of these laboratories describes an experimental "double stream" amplifier tube consisting of two cathodes which produce concentric electron streams of somewhat different average velocity, and short helices serving as input and output circuits. No further physical description of double stream amplifiers will be given in this paper. Rather, a theoretical treatment of such devices will be presented.

## 2. SIMPLE THEORY

For simplicity we will assume that the flow consists of coincident streams of electrons of d-c. velocities  $u_1$  and  $u_2$  in the  $x$  direction. It will be assumed that there is no electron motion normal to the  $x$  direction. The treatment will be a small-signal or perturbation theory, in which products of a-c. quantities are neglected. M.K.S. units will be used. All quantities will be assumed to vary with time and distance  $\exp j(\omega t - \beta x)$ . The wavelength in the stream,  $\lambda_s$ , is then related to  $\beta$  by

$$\beta = 2\pi/\lambda_s \quad (1)$$

The following additional nomenclature will be used:

$\epsilon_0$	dielectric constant of vacuum $\epsilon_0 = 8.85 \times 10^{-12}$ farad/meter
$\eta$	charge-to-mass ratio of the electron $\eta = 1.76 \times 10^{11}$ coulomb/kilogram
$J_1, J_2$	d-c. current densities
$u_1, u_2$	d-c. velocities
$\rho_{01}, \rho_{02}$	d-c. charge densities $\rho_{01} = -J_1/u_1, \rho_{02} = -J_2/u_2$
$\rho_1, \rho_2$	a-c. charge densities
$v_1, v_2$	a-c. velocities
$V_1, V_2$	d-c. voltages with respect to the cathode
$V$	a-c. potential
$\beta_1 = \omega/u_1, \beta_2 = \omega/u_2$	

Although the small-signal equations relating charge density to voltage  $V$  have been derived many times, it seems well to present them for the sake of completeness. For one stream of electrons the first-order force equation is

$$\begin{aligned} \frac{dv_1}{dt} &= \frac{\partial v_1}{\partial t} + \frac{\partial v_1}{\partial x} u_1 = \eta \frac{\partial V}{\partial x} \\ (\omega - \beta u_1)v_1 &= -\eta \beta V \\ v_1 &= \frac{-\eta \beta V}{u_1(\beta_1 - \beta)} \end{aligned} \quad (2)$$

From the conservation of charge we obtain to the first order

$$\begin{aligned} \frac{\partial \rho_1}{\partial t} &= -\frac{\partial}{\partial x} (\rho_{01}v_1 + \rho_1u_1) \\ \omega \rho_1 &= \rho_{01}\beta v_1 + u_1\beta \rho_1 \\ \rho_1 &= \frac{\rho_{01}\beta v_1}{u_1(\beta_1 - \beta)} \\ \rho_1 &= -\frac{J_1\beta v_1}{u_1^2(\beta_1 - \beta)} \end{aligned} \quad (3)$$

From (2) and (3) we obtain

$$\rho_1 = \frac{\eta J_1 \beta^2 V}{u_1^3 (\beta_1 - \beta)^2} \quad (4)$$

We would find similarly

$$\rho_2 = \frac{\eta J_2 \beta^2 V}{u_2^3 (\beta_2 - \beta)^2} \quad (5)$$

It will be convenient to call the fractional velocity separation  $b$ , so that

$$b = \frac{2(u_1 - u_2)}{u_1 + u_2} \quad (6)$$

It will also be convenient to define a sort of mean velocity  $u_0$

$$u_0 = \frac{2u_1u_2}{u_1 + u_2} \quad (7)$$

We may also let  $V_0$  be the potential drop specifying a velocity  $u_0$ , so that

$$u_0 = \sqrt{2\eta V_0} \quad (8)$$

It is further convenient to define a phase constant based on  $u_0$

$$\beta_0 = \frac{\omega}{u_0} \quad (9)$$

We see from (6), (7) and (9) that

$$\beta_1 = \beta_0(1 - b/2) \quad (10)$$

$$\beta_2 = \beta_0(1 + b/2) \quad (11)$$

We shall treat only a special case, that in which

$$\frac{J_1}{u_1^3} = \frac{J_2}{u_2^3} = \frac{J_0}{u_0^3} \quad (12)$$

Here  $J_0$  is a sort of mean current which, together with  $u_0$ , specifies the ratios  $J_1/u_1^3$  and  $J_2/u_2^3$ , which appear in (4) and (5).

In terms of these new quantities, the expression for the total a-c. charge density  $\rho$  is, from (4) and (5) and (8)

$$\rho = \rho_1 + \rho_2 = \frac{J_0\beta^2}{2u_0V_0} \cdot \left[ \left[ \beta_0 \left( 1 - \frac{b}{2} \right) - \beta \right]^2 + \left[ \beta_0 \left( 1 + \frac{b}{2} \right) - \beta \right]^2 \right] V \quad (13)$$

Equation (13) is a *ballistical* equation telling what charge density  $\rho$  is produced when the flow is bunched by a voltage  $V$ . To solve our problem, that is, to solve for the phase constant  $\beta$ , we must associate (13) with a *circuit* equation which tells us what voltage  $V$  the charge density produces. We assume that the electron flow takes place in a tube too narrow to propagate a wave of the frequency considered. Further, we assume that the wave velocity is much smaller than the velocity of light. Under these circumstances the circuit problem is essentially an electrostatic problem. The a-c. voltage will be of the same sign as, and in phase with, the a-c. charge density  $\rho$ . In other words, the "circuit effect" is purely capacitive.

Let us assume at first that the electron stream is very narrow compared with the tube through which it flows, so that  $V$  may be assumed to be constant over its cross section. We can easily obtain the relation between

$V$  and  $\rho$  in two extreme cases. If the wavelength in the stream,  $\lambda_s$ , is very short ( $\beta$  large), so that transverse a-c. fields are negligible, then from Poisson's equation we have

$$\begin{aligned}\rho &= -\epsilon_0 \frac{\partial^2 V}{\partial x^2} \\ \rho &= \epsilon_0 \beta^2 V\end{aligned}\quad (14)$$

If, on the other hand, the wavelength is long compared with the tube radius ( $\beta$  small) so that the fields are chiefly transverse, the lines of force running from the beam outward to the surrounding tube, we may write

$$\rho = CV \quad (15)$$

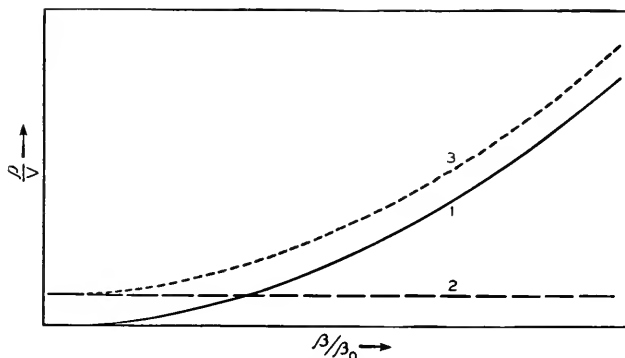


Fig. 1—A “circuit” curve for a narrow electron stream in a tube. The ratio of the a-c. charge density  $\rho$  to the a-c. voltage  $V$  produced by the charge density is plotted vs. a parameter  $\beta/\beta_0$ , which is inversely proportional to the wavelength  $\lambda_s$  in the flow. Curve 1 holds for very large values of  $\beta/\beta_0$ ; curve 2 holds for very small values of  $\beta/\beta_0$ , and curve 3 over-all shows approximately how  $\rho/V$  varies for intermediate values of  $\beta/\beta_0$ .

Here  $C$  is a constant expressing the capacitance per unit length between the region occupied by the electron flow and the tube wall.

We see from (14) and (15) that if at some particular frequency we plot  $\rho/V$  vs.  $\beta/\beta_0$  for real values of  $\beta$ ,  $\rho/V$  will be constant for small values of  $\beta$  and will rise as  $\beta^2$  for large values of  $\beta$ , approximately as shown in Fig. 1. For another frequency,  $\beta_0$  would be different and, as  $\rho/V$  is a function of  $\beta$ , the horizontal scale of the curve would be different.

Now, we have assumed that the charge is produced by the action of the voltage, according to the ballistical equation (10). This relation is plotted in Fig. 2, for a relatively large value of  $J_0/u_0V_0$  (curve 1) and for a smaller value of  $J_0/u_0V_0$  (curve 2). There are poles at  $\beta/\beta_0 = 1 \pm \frac{b}{2}$ , and a minimum between the poles. The height of the minimum increases as  $J_0/u_0V_0$  is increased.

A circuit curve similar to that of Fig. 1 is also plotted on Fig. 2. We see

that for the small-current case (curve 2) there are four intersections, giving *four real* values of  $\beta$  and hence *four unattenuated* waves. However, for the larger current (curve 1) there are only two intersections and hence two unattenuated waves. The two additional values of  $\beta$  satisfying both the circuit equation and the ballistical equation are complex conjugates, and represent waves traveling at the same speed, but with equal positive and negative attenuations.

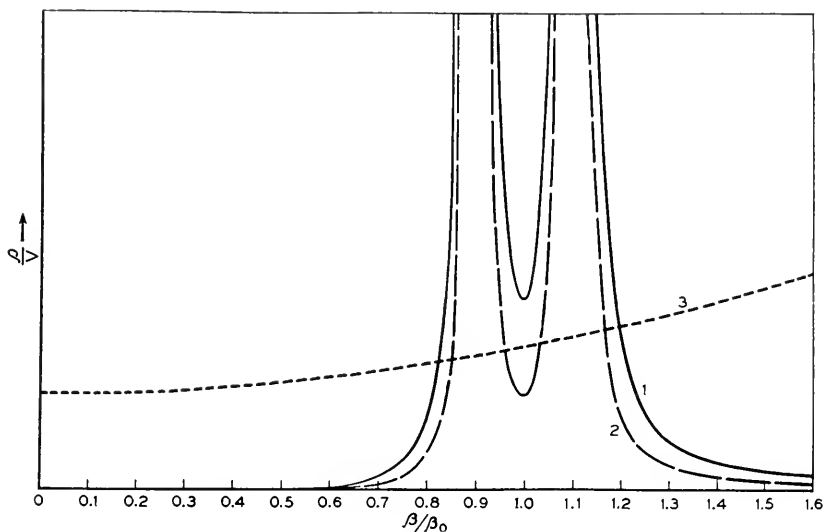


Fig. 2—Curve 3 is a circuit curve similar to that of Fig. 1. Curves 1 and 2 are based on a ballistical equation telling how much charge density  $\rho$  is produced when the voltage  $V$  acts to bunch a flow consisting of electrons of two velocities. The abscissa,  $\beta/\beta_0$ , is proportional to phase constant. Intersections of the circuit curve with a ballistical curve represent waves. Curve 2 is for a relatively small current. In this case intersections occur for four real values of  $\beta$ , so the four waves are unattenuated. For a larger current (curve 1) there are two intersections (two unattenuated waves). For the other two waves  $\beta$  is complex. There are an increasing and a decreasing wave.

Thus we deduce that, as the current densities in the electron streams are raised, a wave with negative attenuation appears for current densities above a certain critical value.

We can learn a little more about these waves by assuming an approximate expression for the circuit curve of Fig. 1. Let us merely assume that over the range of interest (near  $\beta/\beta_0 = 1$ ) we can use

$$\rho = \alpha^2 \epsilon_0 \beta^2 V \quad (16)$$

Here  $\alpha^2$  is a factor greater than unity, which merely expresses the fact that the charge density corresponding to a given voltage is somewhat greater



than if there were field in the  $x$  direction only and equation (11) were valid. Combining (16) with (13) we obtain

$$\left( \beta_0 \left( 1 - \frac{b}{2} \right) - \beta \right)^2 + \left( \beta_0 \left( 1 + \frac{b}{2} \right) - \beta \right)^2 = \beta_0^2 l^2 \quad (17)$$

where

$$l^2 = \frac{J_0}{2\alpha^2 \epsilon_0 \beta_0^2 u_0 V_0} \quad (18)$$

In solving (17) it is most convenient to represent  $\beta$  in terms of  $\beta_0$  and a new variable  $\delta$

$$\beta = \beta_0(1 + \delta) \quad (19)$$

Thus, (14) becomes

$$\left( \delta - \frac{b}{2} \right)^2 + \left( \delta + \frac{b}{2} \right)^2 = \frac{1}{l^2} \quad (20)$$

Solving for  $\delta$ , we obtain

$$\delta = \pm \left( \frac{b}{2} \right) \left[ \left( \frac{2U}{b} \right)^2 + 1 \pm \left( \frac{2U}{b} \right) \sqrt{\left( \frac{2U}{b} \right)^2 + 4} \right]^{1/2}. \quad (21)$$

The positive sign inside of the brackets always gives a real value of  $\delta$  and hence unattenuated waves. The negative sign inside the brackets gives unattenuated waves for small values of  $U/b$ . However, when

$$\left( \frac{U}{b} \right)^2 > \frac{1}{8} \quad (22)$$

there are two waves with a phase constant  $\beta_0$  and with equal and opposite attenuation constants.

Suppose we let  $U_M$  be the minimum value of  $U$  for which there is gain. From (22),

$$U_M^2 = b^2/8 \quad (23)$$

From (21) we have for the increasing wave

$$\delta = j \frac{b}{2} \left[ \frac{1}{2} \left( \frac{U}{U_M} \right)^2 \left( \sqrt{1 + 8 \left( \frac{U}{U_M} \right)^2} - 1 \right) - 1 \right]^{1/2} \quad (24)$$

The gain in db/wavelength is

$$\begin{aligned} \text{db/wavelength} &= 20(2\pi) \log_{10} e |\delta| \\ &= 54.6 |\delta| \end{aligned} \quad (25)$$

We see that by means of (24) and (25) we can plot db/wavelength per unit  $b$  vs.  $(U/U_M)^2$ . This is plotted in Fig. 3. Because  $U^2$  is proportional to current, the variable  $(U/U_M)^2$  is the ratio of the actual current to the current which will just give an increasing wave. If we know this ratio, we can obtain the gain in db/wavelength by multiplying the corresponding ordinate from Fig. 3 by  $b$ .

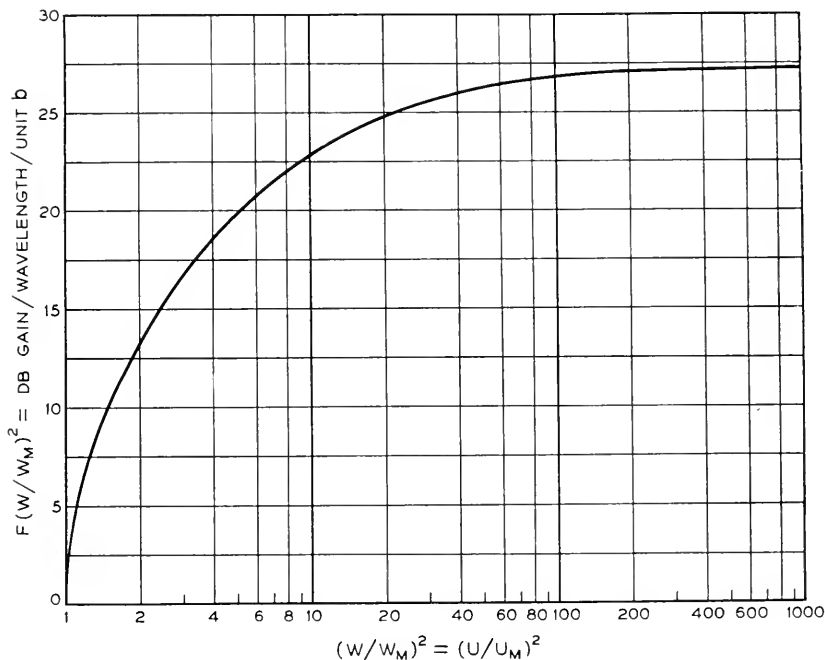


Fig. 3—The parameter  $(W/W_M)^2 = ((U/U_M)^2)$  is proportional to current. As the current is increased above a critical value for which  $(W/W_M)^2 = 1$ , there is an increasing wave of increasing gain. In this curve the gain per wavelength per unit  $b$ , called  $F(W/W_M)^2$ , is plotted vs.  $(W/W_M)^2$ . For large values of  $(W/W_M)^2$ ,  $F(W/W_M)^2$  approaches 27.3 and the gain per wavelength approaches 27.3  $b$ .

We see that, as the current is increased, the gain per wavelength at first rises rapidly and then rises more slowly, approaching a value of 27.3 $b$  db/wavelength for very large values of  $(U/U_M)^2$ .

We now have some idea of the variation of gain per wavelength with velocity separation  $b$  and with current  $(U/U_M)^2$ . A more complete theory would require the evaluation of the lower limiting current for gain (or of  $U_M^2$ ) in terms of physical dimensions and an investigation of the boundary conditions to show how strong an increasing wave is set up by a given input signal. The latter problem will not be considered in this paper; the former is dealt with in the third section and in the appendix.

## 3. DESIGN CURVES

It is proposed to present in this section material for actually evaluating the gain of the increasing wave for a particular geometry of electron flow. In this section there is some repetition from earlier sections, so that the material presented can be used without referring unduly to section 2. In order to avoid confusion, much of the mathematical work on which the section is based has been put in the appendix.

The flow considered is one in which electrons of two velocities,  $u_1$  and  $u_2$ , corresponding to accelerating voltages  $V_1$  and  $V_2$ , are intermingled, the corresponding current densities  $J_1$  and  $J_2$  being constant over the flow. The flow occupies a cylindrical space of radius  $a$ . It is assumed that the surrounding cylindrical conducting tube is so remote as to have negligible effect on the a-c. fields.

It will be assumed, according to (12), that the current densities and the voltages  $V_1$  and  $V_2$  are specified in terms of a "mean" current  $J_0$  and a "mean" voltage  $V_0$  corresponding to a velocity  $u_0$ , by

$$\frac{J_1}{V_1^{3/2}} = \frac{J_2}{V_2^{3/2}} = \frac{J_0}{V_0^{3/2}} \quad (12a)$$

The gain will depend on the beam radius, the free-space wavelength  $\lambda$ , and on  $J_0$  and  $V_0$ , and on the fractional velocity separation

$$b = \frac{2(u_1 - u_2)}{u_1 + u_2} \quad (6)$$

The wavelength in the beam,  $\lambda_s$ , which is associated with the voltage  $V_0$  is given by

$$\begin{aligned} \lambda_s &= \lambda \frac{u_0}{c} = \lambda \frac{\sqrt{2\eta V_0}}{c} \\ \lambda_s &= 1.98 \times 10^{-3} \lambda \sqrt{V_0} \end{aligned} \quad (26)$$

Here  $c$  is the velocity of light.

A dimensionless parameter  $W$  is defined to be

$$W^2 = \frac{\omega_e^2}{\omega^2} = \frac{J_0}{\epsilon_0 u_0 \omega^2} \quad (27)$$

$$W^2 = 8.52 \times 10^6 \frac{J_0}{f \sqrt{V_0}} \quad (28)$$

Here  $\omega_e$  is the electron plasma frequency associated with the average space charge density  $J_0/u_0$ , and  $\omega$  is the radian frequency corresponding to the wavelength  $\lambda$ . In (28), the constant is adjusted so that  $J_0$  is expressed in

amperes per square centimeter rather than in amperes per square meter, while  $f$  is expressed in megacycles.

Below a minimum value of  $H$ , which will be called  $H_M$ , there is no gain.  $H_M$  is a function of the velocity separation  $b$  and of the ratio of the beam radius  $a$  to the beam wavelength,  $\lambda_s$ . A plot of  $(H_M/b)^2$  as a function of  $(a/\lambda_s)$  is shown in Fig. 4.

The variation of gain in the interval,  $H_M \leq H < \infty$ , is shown in Fig. 3 where "Decibels gain wavelength/unit  $b$ " is plotted as a function of  $(H/H_M)^2$ . This is the same curve which was derived in section 2. The

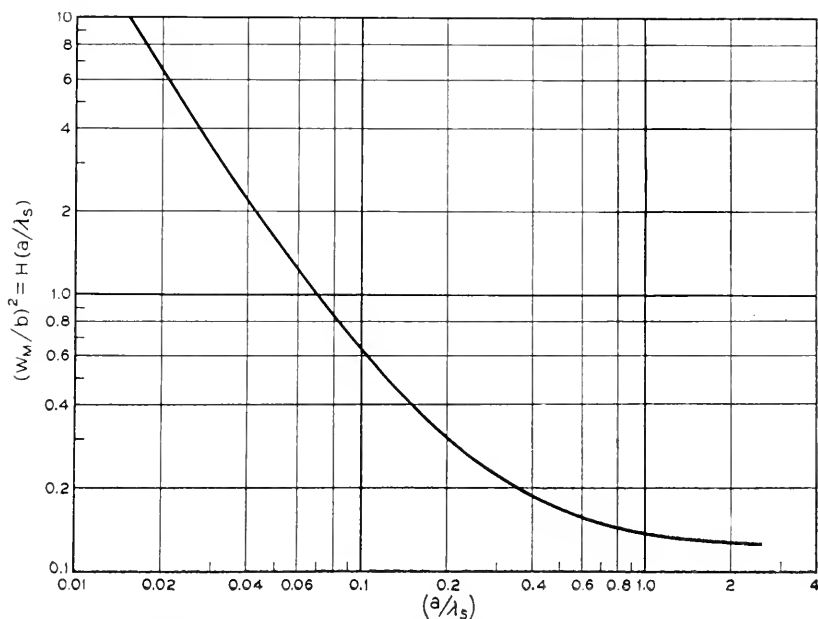


Fig. 4—As the ratio of beam radius  $a$  to wavelength in the beam,  $\lambda_s$ , is increased, the critical value of  $H$ ,  $H_M$ , decreases and less current is needed in order to obtain gain. Here  $(H_M/b)^2$ , which is called  $H(a/\lambda_s)$ , is plotted vs.  $(a/\lambda_s)$ .

ratio  $(H/H_M)^2$  is the same as the parameter  $(U/U_M)^2$  used there, although  $U$  and  $H$  are not the same.

The curve in Fig. 3 is useful in that it reduces the interdependence of a large number of parameters to a single curve. However, there are cases as, for example, when one is computing the bandwidth of an amplifier, in which it would be more convenient to have the curve in Fig. 3 broken up into a family of curves. We can do this by the following means:

We can write the gain in db/wavelength in the form

$$\text{db/wavelength} = bF(H/H_M)^2 \quad (29)$$

Here  $F(W/W_M)^2$  is the function plotted in Fig. 3. If  $\ell$  is the total length of the flow, the total gain in db,  $G$ , will thus be

$$G = \frac{\ell b}{\lambda_s} F(W/W_M)^2 \quad (30)$$

We will now express  $(W/W_M)^2$  in such a form as to indicate its dependence on wavelength in the beam,  $\lambda_s$ . We can write from (27)

$$W = \frac{\omega_e^2}{\omega^2} = \frac{\lambda_s^2}{\lambda_r^2} \quad (31)$$

Here  $\lambda_e$  is a "plasma wavelength," defined by the relation

$$\lambda_e = \frac{u_0}{(\omega_e/2\pi)} \quad (32)$$

We further have

$$W_M^2 = b^2 H(a/\lambda_s) \quad (33)$$

Here  $H(a/\lambda_s)$  is the function of  $(a/\lambda_s)$  which is plotted in Fig. 5.

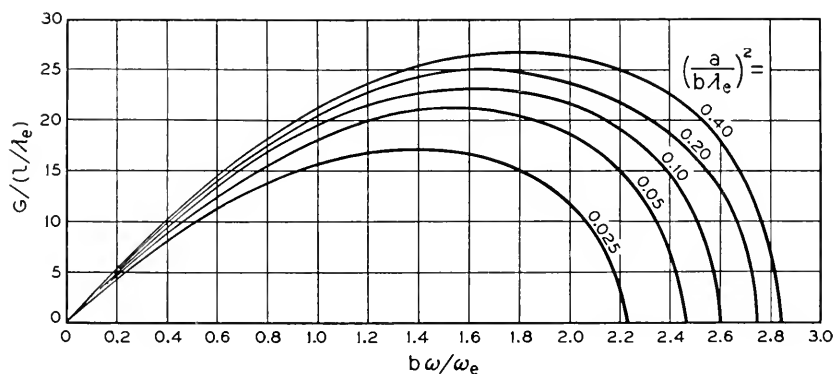


Fig. 5—In these curves the total gain in db,  $G$ , divided by the ratio of the length  $\ell$  to the plasma wavelength  $\lambda_e$ , is plotted vs.  $b\omega/\omega_e$ , which is proportional to frequency, for several values of the parameter  $(a/b\lambda_e)^2$ . Changing  $b$ , the velocity separation, changes both the parameter and the frequency scale.

Now, from (26), (27), and (29) we can write

$$G = \left(\frac{\ell}{\lambda_e}\right) \left(\frac{b\lambda_e}{a}\right) \left(\frac{a}{\lambda_s}\right) F \left[ \left(\frac{\lambda_s}{a}\right)^2 \left(\frac{a}{b\lambda_e}\right)^2 \frac{1}{H(a/\lambda_s)} \right] \quad (34)$$

For a given tube the parameters  $(\ell/\lambda_e)$  and  $(a/b\lambda_e)$  do not vary with frequency, while  $(a/\lambda_s)$  is proportional to frequency. Hence, we can construct universal frequency curves by plotting  $G/(\ell/\lambda_e)$  vs.  $(a/\lambda_s)$  for various values of the parameter  $(a/b\lambda_e)$ . It is more convenient, however, to use as an abscissa  $b\lambda_e/\lambda_s = b\omega/\omega_e$ , and this has been done in Fig. 5.

In order to use these curves it is necessary to express the parameters  $b\omega/\omega_e$ ,  $\lambda_e$  and  $(a/b\lambda_e)^2$  in terms of convenient physical quantities. We obtain

$$\begin{aligned} b\omega/\omega_e &= .545 \times 10^{-10} bV^{1/4} \omega/J_0^{1/2} \\ \lambda_e &= 2.04 \times 10^{-2} V_0^{3/4}/J_0^{1/2} \\ (a/b\lambda_e)^2 &= 767 I_0/b^2 V^{3/2} \end{aligned} \quad (35)$$

Here  $I_0$  is current in amperes and  $J_0$  is in amperes / cm.<sup>2</sup>

The broadness of the frequency response curves of Fig. 5 is comparable to that of curves for helix-type traveling-wave tubes.

It is interesting to note that the maximum value of  $G/(\ell/\lambda_e)$  varies little for a considerable range of the parameter  $a/b\lambda_e$ , approaching a constant for large values of the parameter. This means that, with a beam of given length, velocity and charge density, one can obtain almost the same optimum gain over a wide range of frequencies simply by adjusting the velocity-separation parameter  $b$ .

#### 4. CONCLUDING REMARKS

There is a great deal of room for extension of the theory of double-stream amplifiers. This paper has not dealt with the setting up of the increasing wave, nor with other geometries than that of a cylindrical beam in a very remote tube, nor with the effect of physical separation of the electron streams of two velocities nor with streams of many velocities or streams with continuous velocity distributions.

This last is an interesting subject in that it may provide a means for dealing with problems of noise in multivelocity electron streams. Indeed, it was while attempting such a treatment that the writers were distracted by the idea of double-stream amplification.

#### APPENDIX

##### DERIVATION OF RESULTS USED IN SECTION 3

Consider a double-stream electron beam whose axis coincides with the  $z$ -axis of a system of cylindrical coordinates  $(r, \varphi, z)$  and which is subject to an infinite, longitudinal, d-c. magnetic field. The radius of the beam is  $a$  and each of the streams is characterized by d-c. velocities,  $u_1$  and  $u_2$ , which are vectors in the positive  $z$  direction, and d-c. space charge densities,  $\rho_{01}$  and  $\rho_{02}$ . All d-c. quantities are assumed to be independent of the coordinates and time, except, of course, for the discontinuities at the surface of the beam. Small a-c. disturbances are superimposed upon these d-c. quantities and they are small enough so that their cross products can be neglected compared with the products of d-c. quantities and a-c. quantities. It is

further assumed that only those a-c. quantities are allowed which have no azimuthal variation, that is,  $\frac{\partial}{\partial \varphi} = 0$ . Fig. 6 shows the electron beam.

Outside the beam the appropriate Maxwell's equations are

$$\frac{1}{r} \frac{\partial}{\partial r} (r H_{\varphi}) = j \frac{k}{\eta_0} E_z \quad (\text{A-1})$$

$$\frac{\partial H_{\varphi}}{\partial z} = -j \frac{k}{\eta_0} E_r \quad (\text{A-2})$$

$$\frac{\partial E_z}{\partial r} - \frac{\partial E_r}{\partial z} = j k \eta_0 H_{\varphi} \quad (\text{A-3})$$

where

$$k = \frac{\omega}{c} \quad (\text{A-4})$$

$$\eta_0 = \sqrt{\frac{\mu_0}{\epsilon_0}} = 377 \text{ ohms} \quad (\text{A-5})$$

Inside the beam, equations (A-2) and (A-3) remain the same, but instead of equation (A-1) we have

$$\frac{1}{r} \frac{\partial}{\partial r} (r H_{\varphi}) = j \frac{k}{\eta_0} E_z + q_1 + q_2 \quad (\text{A-6})$$

where  $q_1$  and  $q_2$  are the first order a-c. convection current densities of the two streams. These quantities can be calculated from the force equation and the equation for the conservation of charge. Assuming that all a-c. quantities vary as  $\exp j(\omega t - \beta z)$ , the force equation is (for stream number one, say)

$$j\omega v_1 - j\beta u_1 v_1 = -(e/m)E_z \quad (\text{A-7})$$

and the equation for the conservation of charge is

$$j\beta \rho_{01} v_1 + j\beta u_1 \rho_1 = +j\omega \rho_1 \quad (\text{A-8})$$

Equations (A-7) and (A-8) can be solved for  $v_1$  and  $\rho_1$  :

$$v_1 = \frac{-(e/m)E_z}{j\omega \left(1 - \frac{\beta}{\beta_1}\right)} \quad (\text{A-7a})$$

$$\rho_1 = \frac{\beta \rho_{01}}{\omega \left(1 - \frac{\beta}{\beta_1}\right)} v_1 \quad (\text{A-8a})$$

where

$$\beta_1 = \frac{\omega}{u_1}$$

Combining equations (A-7a) and (A-8a) one has

$$\rho_1 = \frac{j\beta\rho_{01}(c/m)E_z}{\omega^2 \left(1 - \frac{\beta}{\beta_1}\right)^2} \quad (\text{A-9})$$

The first order a-c. convection current density is given by

$$q_1 = \rho_{01}v_1 + \rho_1u_1 \quad (\text{A-10})$$

which, by combining with (A-7a) and (A-8b), becomes

$$q_1 = \frac{j(k/\eta_0)(\rho_{01}/m\epsilon_0)E_z}{\omega^2 \left(1 - \frac{\beta}{\beta_1}\right)^2} \quad (\text{A-11})$$

Similarly

$$q_2 = \frac{j \frac{k}{\eta_0} \frac{\rho_{01}}{m\epsilon_0} \frac{c}{\omega} E_z}{\omega^2 \left(1 - \frac{\beta}{\beta_2}\right)^2} \quad (\text{A-12})$$

If we now define

$$\beta_0 = \frac{1}{2}(\beta_1 + \beta_2) \quad (\text{A-13})$$

$$B_1 = \frac{\beta_1}{\beta_0}; \quad B_2 = \frac{\beta_2}{\beta_0} \quad (\text{A-14})$$

and let

$$Z = \frac{\beta}{\beta_0} \quad (\text{A-15})$$

$$W_1 = \frac{\omega_{e1}}{\omega}; \quad W_2 = \frac{\omega_{e2}}{\omega} \quad (\text{A-16})$$

where  $\omega_e$ , the plasma-electron angular frequency given by

$$\omega_{e1}^2 = -\frac{c\rho_{01}}{m\epsilon_0}, \text{ etc.} \quad (\text{A-17})$$

Equations (11) and (12) become

$$q_1 = \frac{-j(k/\eta_0)W_1^2 B_1^2}{(Z - B_1)^2} E_z \quad (\text{A-18})$$

$$q_2 = \frac{-i(k/\eta_0)W_2^2 B_2^2}{(Z - B_2)^2} E_z \quad (\text{A-19})$$

Thus equation (A-6) becomes

$$\frac{1}{r} \frac{\partial}{\partial r} (rH_\varphi) = j \frac{k}{\eta_0} L E_z \quad (\text{A-6a})$$



where

$$L = 1 - \frac{W_1^2 B_1^2}{(Z - B_1)^2} - \frac{W_2^2 B_2^2}{(Z - B_2)^2} \quad (\text{A-20})$$

If we assume that the tube which surrounds the beam be taken as infinitely remote, the appropriate solutions outside the beam are

$$\hat{H}_{\varphi 0} = A_0 K_1(\gamma r) \quad (\text{A-21})$$

$$\hat{E}_{z0} = j \frac{\eta_0 \gamma}{k} A_0 K_0(\gamma r) \quad (\text{A-22})$$

and inside the beam

$$\hat{H}_{\varphi i} = A_i I_1(\xi r) \quad (\text{A-23})$$

$$\hat{E}_{zi} = -j \frac{\eta_0 \gamma}{\sqrt{L}} A_i I_0(\xi r) \quad (\text{A-24})$$

where

$$\begin{aligned} \gamma^2 &= \beta^2 - k^2 \approx \beta^2 \\ \xi^2 &= \gamma^2 L \end{aligned} \quad (\text{A-25})$$

The  $I$ 's and  $K$ 's in equations (A-21)–(A-24) are modified Bessel functions.<sup>3</sup> At the surface of the beam ( $r = a$ ), one has the following two independent boundary conditions

$$\hat{H}_{\varphi i} = \hat{H}_{\varphi 0} \quad (\text{A-26})$$

$$\hat{E}_{zi} = \hat{E}_{z0} \quad (\text{A-25a})$$

which, using equations (A-21)–(A-24), yield

$$\frac{I_0(\xi a)}{\sqrt{L} I_1(\xi a)} = -\frac{K_0(\gamma a)}{K_1(\gamma a)} \quad (\text{A-27})$$

From equations (A-13), (A-14), (A-15) and (A-24) one has

$$\xi a = Z\beta_0 a \sqrt{L} \quad (\text{A-28})$$

$$\gamma a = Z\beta_0 a \quad (\text{A-29})$$

If we now define a beam wavelength,  $\lambda_s$ , by the relations

$$\beta_0 = \frac{2\pi}{\lambda_s} \quad (\text{A-30})$$

and assume for the purpose of simplifying the calculation that in the expression for  $L$  in (A-20)

$$W_1^2 B_1^2 = W_2^2 B_2^2 = W^2 \quad (\text{A-31})$$

<sup>3</sup> See A Treatise on the Theory of Bessel Functions, G. N. Watson, Chapter 3.

We easily see that

$$W^2 = (\omega_e/\omega)^2 \quad (\text{A-32})$$

where

$$\omega_e = \frac{e}{m} J_0 / \epsilon_0 u_0 \quad (\text{A-33})$$

We obtain from (A-20), (A-28), (A-29) and (A-30)

$$\left[ \begin{array}{l} K_1 \left( \frac{2\pi a Z}{\lambda_s} \right) I_0 \left( \sqrt{L} \frac{2\pi a Z}{\lambda_s} \right) \\ K_0 \left( \frac{2\pi a Z}{\lambda_s} \right) I_1 \left( \sqrt{L} \frac{2\pi a Z}{\lambda_s} \right) \end{array} \right]^2 = L \quad (\text{A-34})$$

$$= 1 - \left[ \frac{W^2}{(Z - B_1)^2} + \frac{W^2}{(Z - B_2)^2} \right]$$

Equation (A-31) is equivalent to Equation (12) of the text or to

$$\frac{J_1}{V_1^{3/2}} = \frac{J_2}{V_2^{3/2}} \quad (\text{A-35})$$

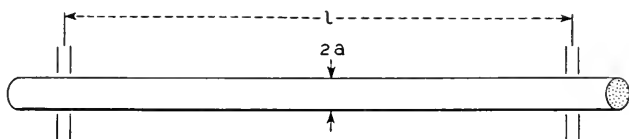


Fig. 6—The diameter of the electron flow considered is  $2a$ , and the length is  $\ell$ .

Letting  $Y = -L$  and making use of the following well known relations between the Bessel functions

$$\begin{aligned} I_0(jx) &= J_0(x) \\ I_1(jx) &= jJ_1(x) \end{aligned} \quad (\text{A-36})$$

Equation (A-34) becomes

$$Y = \left[ \begin{array}{l} K_1 \left( \frac{2\pi a}{\lambda_s} Z \right) J_0 \left( \sqrt{Y} \frac{2\pi a}{\lambda_s} Z \right) \\ K_0 \left( \frac{2\pi a}{\lambda_s} Z \right) J_1 \left( \sqrt{Y} \frac{2\pi a}{\lambda_s} Z \right) \end{array} \right]^2 \quad (\text{A-37})$$

$$= \frac{W^2}{(Z - B_1)^2} + \frac{W^2}{(Z - B_2)^2} - 1$$

Let the right-hand side of equation (A-37) be denoted by  $F_1(Z)$  and the middle of  $F_2(Z)$ . In order to find the real roots of equation (A-37) one can plot  $F_1$  and  $F_2$  as functions of  $Z$  on the same chart. The abscissae of the intersections of the two curves will then be the real roots. In Fig. 7,  $F_1$  is plotted as a function of  $Z$  for  $B_1 = 0.9$  and  $B_2 = 1.1$ .

In view of the definitions in equations (A-13) and (A-14), both  $B_1$  and  $B_2$  are uniquely defined by a single parameter, namely, the fractional velocity separation,  $b$ . That is

$$\begin{aligned} b &= 2(u_1 - u_2)/(u_1 + u_2) = 2(\beta_2 - \beta_1)/(\beta_2 + \beta_1) \\ &= B_2 - B_1 \end{aligned} \quad (\text{A-38})$$

and

$$\begin{aligned} B_1 &= 1 - (b/2) \\ B_2 &= 1 + (b/2) \end{aligned} \quad (\text{A-39})$$

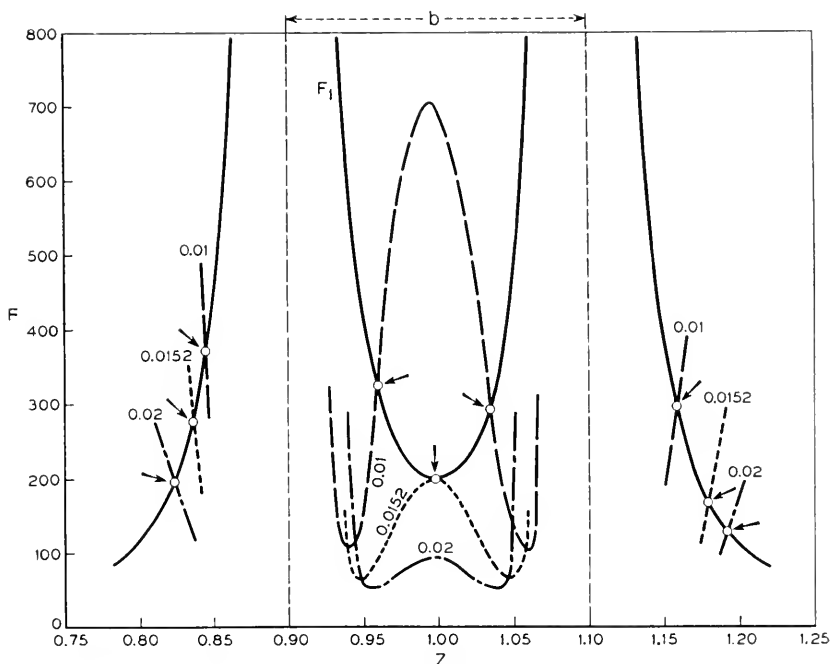


Fig. 7—A curve illustrating conditions giving rise to various types of roots.

A complete plot of  $F_2$ , for any value of the parameters  $W$  and  $(a/\lambda_s)$ , would show that equation (A-37) has an infinite number of real solutions. A real solution of equation (A-37) means an unattenuated wave. Thus there are an infinite number of unattenuated waves possible. The waves which will actually be excited in any given case, however, depend upon the boundary conditions at the input and output of the tube. Ordinarily only those waves will be excited which do not have a reversal in phase of the longitudinal  $E$  vector, say, as  $r$  varies from 0 to  $a$ . Attention, therefore,

will be given only to those waves for which  $E_z$  does not change sign over a cross-section of the beam. By inspection of equation (A-23), it is evident that this requirement is automatically satisfied if  $L > 0$ . On the other hand, if  $L$  is negative, one has

$$E_{zi} \sim J_0 \left( \sqrt{I} \frac{2\pi r}{\lambda_s} Z \right) \quad (\text{A-23a})$$

Thus attention will be limited to those roots which satisfy

$$\sqrt{I} \frac{2\pi a}{\lambda_s} Z < 2.405 \quad (\text{A-40})$$

where 2.405 is the first zero of the Bessel function in equation (A-21a).

Returning to Fig. 7, portions of three different  $F_2$  curves are plotted: one for  $W^2 = 0.01$ , one for  $W^2 = 0.0152$  and one for  $W^2 = 0.02$ . All three curves are for  $(a/\lambda_s) = 0.16$ . The intersections which represent roots which satisfy the inequality (A-40) are marked with arrows. Evidently there are either four real roots of this type or there are two real roots and a complex conjugate pair, the distinction being determined by the value of  $W$ . Thus there is a critical value of  $W^2$  (in this case it is 0.0152) for which two of the real roots are identical. This identical pair is indicated by two arrows near the minimum of the  $F_1$  curve at  $Z = 1$ .

A pair of conjugate complex roots means that there are an increasing wave and a decreasing wave. Thus for each value of  $b$  and  $(a/\lambda_s)$  there is a least value of  $W^2$  below which the tube will have no gain.

It can be shown that the critical tangency of the  $F_1$  and  $F_2$  curves occurs at a value of  $Z$  which is less than  $b^2$  away from unity. Very little error will be incurred, then, by assuming that this critical point occurs at  $Z = 1$  if  $b$  is small.

Letting  $Z = 1$  in equation (A-37), and using equations (A-39) one has

$$8(W_M/b)^2 - 1 = \left( \frac{K_1(2\pi a/\lambda_s)J_0(\sqrt{8(W_M/b)^2 - 1} 2\pi a/\lambda_s)}{K_0(2\pi a/\lambda_s)J_1(\sqrt{8(W_M/b)^2 - 1} 2\pi a/\lambda_s)} \right) \quad (\text{A-41})$$

where  $W_M$  is the critical value of  $W$ . Equation (A-41) determines  $(W_M/b)^2$  as a function of  $(a/\lambda_s)$ . This relationship is plotted in Fig. 4.

We will find that there will be an increasing wave in the range  $W_M \leq W < \infty$ . The calculation of the gain in this interval would be very laborious since Bessel functions of complex argument would be involved. However, a good approximation can be made when  $b$  is small. The real part of  $Z$  will always be near unity and the imaginary part will be found to be less than  $b/2$ . Therefore one can let  $Z = 1$  in equation (A-37) where it multiplies the factor  $(2\pi a/\lambda_s)$  in the argument of the Bessel functions and let  $Z - 1 = U$  in the right-hand side of Equation (A-37). With these

assumptions  $\Gamma$  can be determined as a function of  $(a/\lambda_s)$  and  $U$  can be determined as a function of  $\Gamma$ . We have from Equation (A-37)

$$\frac{1}{(U + b/2)^2} + \frac{1}{(U - b/2)^2} = \frac{1 + \Gamma}{W^2} \quad (\text{A-37a})$$

When  $U = 0$ ,  $W^2 = W_M^2 = W_M^2$ , so that

$$1 + \Gamma = 8(W_M/b)^2 \quad (\text{A-42})$$

and equation (A-37a) becomes

$$\frac{1}{(U + b/2)^2} + \frac{1}{(U - b/2)^2} = (8/b^2)(W_M/W)^2 \quad (\text{A-37b})$$

the solution of which, for the increasing wave, is

$$U = j(b/2)[(1/2)(W/W_M)^2(\sqrt{1 + 8(W_M/W)^2} - 1) - 1]^{\frac{1}{2}} \quad (\text{A-43})$$

and the gain will be given by

$$\text{Gain}/b = 27.3[(1/2)(W/W_M)^2(\sqrt{1 + 8(W_M/W)^2} - 1) - 1]^{\frac{1}{2}} \quad (\text{A-44})$$

db/wavelength/unit  $b$

“Decibels gain/wavelength/unit  $b$ ” is plotted against  $(W/W_M)^2$  in Fig. 3.

As  $(W/W_M)^2$  becomes very large, the gain per wavelength approaches 27.3  $b$  db.

# Experimental Observation of Amplification by Interaction Between Two Electron Streams

By A. V. HOLLENBERG

The construction and performance of an amplifier employing the interaction between two streams of electrons having different average velocities are described. Gain of 33 db at a center frequency of 255 Mc has been observed with bandwidth of 110 Mc between 3 db points.

## 1. INTRODUCTION

A NEW type of amplifier in which the gain is obtained by an interaction between streams of electrons of two or more average velocities is proposed in a companion paper by Pierce and Hebenstreit.<sup>1</sup> This amplifier contains input and output portions in which signals are impressed on and extracted from the electron flow by electromagnetic circuits and a central portion in which gain occurs purely by interaction between streams of electrons without any circuits being involved. A small signal theory for coincident electron streams of two d-c. velocities is presented in Pierce and Hebenstreit's paper.

In this paper a description of the construction and operation of an amplifier of this kind will be presented. Departures of the actual conditions in the amplifier from the assumptions of the theory limit the expectations of quantitative agreement. It is believed, however, that the evidence for gain arising from the interaction between two streams of electrons is clear, and that the broad frequency response predicted by the theory has been confirmed.

## 2. DESCRIPTION OF AMPLIFIER

The frequency range near 200 Mc was chosen for the first experimental test of the proposed method of amplification for reasons of convenience. The theory indicates that current density requirements increase with frequency, but that these requirements become severe only at the higher microwave frequencies. Availability of circuit parts and test equipment, rather than anticipated difficulties at higher frequencies, led to the choice that was made.

The essential features of one of the double-stream amplifier tubes which has been constructed and operated are represented in Fig. 1. The output helix was identical with the input helix in construction and connection

<sup>1</sup> A New Type of High Frequency Amplifier, J. R. Pierce and W. B. Hebenstreit, this issue of the *B. S. T. J.*

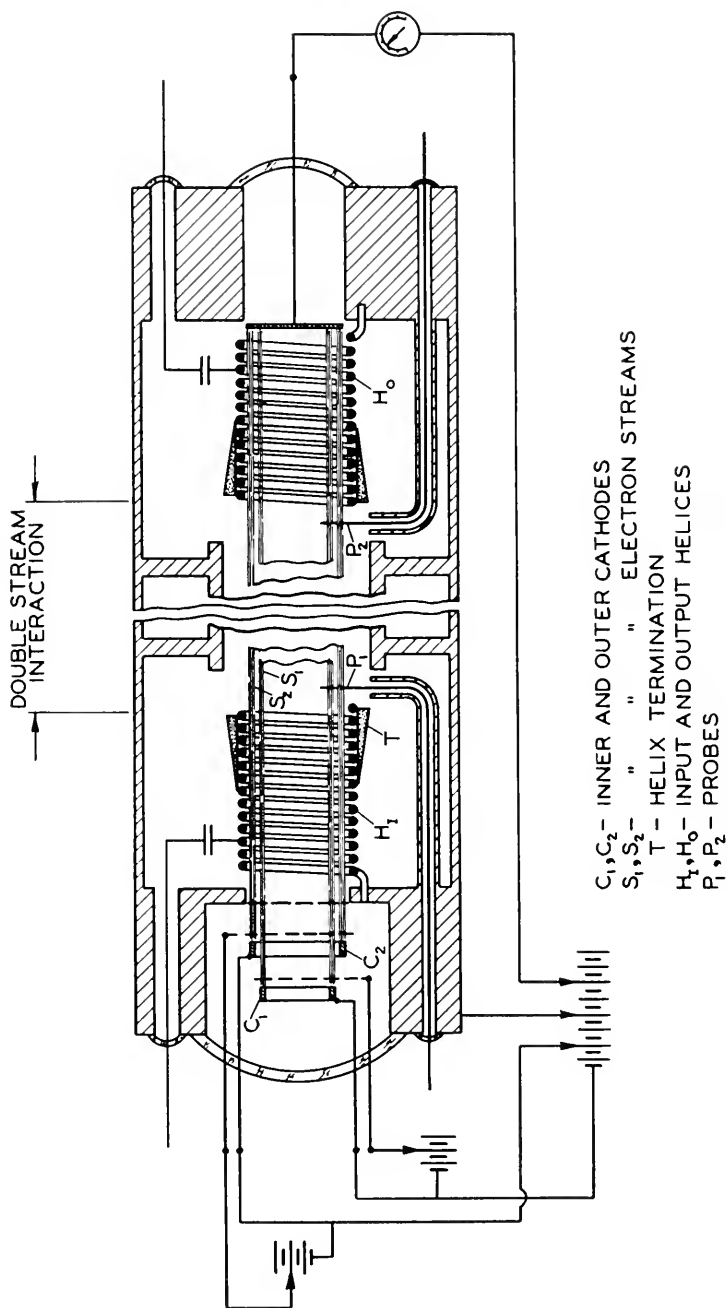


Fig. 1—Representation of double-stream amplifier with helix output.

to the coaxial line. The two identical probes  $p_1$ , and  $p_2$ , extending from coaxial lines into the two electron streams at the beginning and end of the central portion of the tube between the two helices were inserted for comparison of the signal amplitudes at the beginning and end of the region in which no circuit is present.

A similar tube containing an output gap in place of the output helix section is represented in Fig. 2.

In both cases concentric tubular electron streams originate at the ring-shaped emitting surfaces of the two cathodes at potentials  $V_1$  and  $V_2$ , pass through their respective control grids and through a common accelerating grid. An axial magnetic field of approximately 700 gauss is applied in order to maintain the definition of the beams. The outer and inner tubular beams

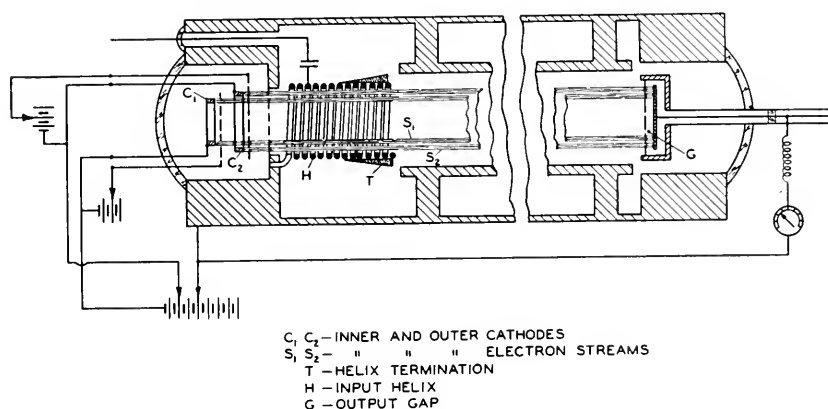


Fig. 2—Representation of double-stream amplifier with gap output.

have mean radii of 0.215" and 0.170" respectively and a wall thickness of 0.030" in each case.

The short sections of helix which are used for input and output are wound of 0.013" diameter molybdenum wire, 44 t.p.i., and mean diameter of 0.500". The axial velocity of signal propagation along this helix is equal to that of 54-volt electrons. The helix sections are each 2" long. Ceramic supporting rods on each helix section are sprayed with aquadag, over  $1\frac{1}{2}$ " of their length on the end nearest the center of the tube, for terminating purposes. The thickness of the spray coating increases toward the center of the tube. The distance between helices is 8.7".

The gain produced by the electronic interaction depends upon a difference in velocity between the two electron streams. The signal is impressed upon one of the streams by the helix when its velocity is that at which traveling wave amplifier interaction between the stream and the helix occurs. It



is required, therefore, for this helix that one of the streams travel at a velocity corresponding to a potential in the neighborhood of 54 volts. Useful interaction occurs from 50 to 60 volts. The inner stream is adjusted for helix interaction in this amplifier, and the outer stream travels at a lower velocity to bring about the interaction between the two streams. Operation about a mean voltage of about 50 volts was planned in designing the amplifier, and in estimating its expected performance. The amplifier is 16 wavelengths long in terms of the wavelength associated with a mean voltage of 50 volts and a frequency of 200 Mc. Eleven of these wavelengths are in the center portion between the helices.

The conditions in the amplifier tube differ from those assumed in the derivation of the theory of the double-stream interaction in the following significant ways:

1. The beams are separated in space and not completely intermingled. Calculations on the effect of this separation have been made. Numerical examples of the calculated magnitude of the effect on gain will be given below.
2. Hollow tubular beams are used, instead of "solid" beams of uniform current density over their cross-sectional area. The theory indicates that, for the beam dimensions and currents used here, the parameters which depend upon beam radius and total current in the beam are nearly the same whether the current is concentrated in an infinitely thin cylindrical shell or uniformly distributed over the cross-section of a cylinder of the same radius.
3. The metal wall surrounding the beams is not infinitely remote. Its diameter was chosen as a compromise between the requirements of preventing serious d-c. space charge depression of potential in the beam and of being far enough removed from the beam to prevent a large effect on the interaction due to its presence. Its proximity tends to increase the minimum current required for producing gain, and therefore to reduce the ratio of actual to critical current on which the gain depends.
4. The beams are not perfectly confined to hollow cylinders of the dimensions given. There is evidence that some spreading outside of these dimensions occurs. The currents reaching the collector can be measured and these are used as "beam currents" in the discussion to follow and in comparisons between theory and experiment. Somewhat larger currents than these were initially launched, and the lost fraction may have contributed to the interaction before striking the walls.

Although the assumptions of the theory are not fulfilled in the actual amplifier, estimates of its performance were first made without correction for the discrepancies. With voltages of 40 and 60 volts on the outer and

inner streams and currents of 0.5 and 0.8 milliampere, a gain of 40 db at 200 Mc due to the double-stream amplification was predicted, with bandwidth to 3 db points of 90 Mc, centered about 200 Mc. A later estimate, including the effect of the separation of the hollow beams in space, reduced the 40 db figure to 23 db.

Prediction of the performance of the device as a whole also requires an evaluation of the coupling of the helix sections to the electron stream. The length of the active portions of the helix sections was chosen to give gain of order unity as estimated from single-stream traveling wave amplifier considerations for the proposed operating current.

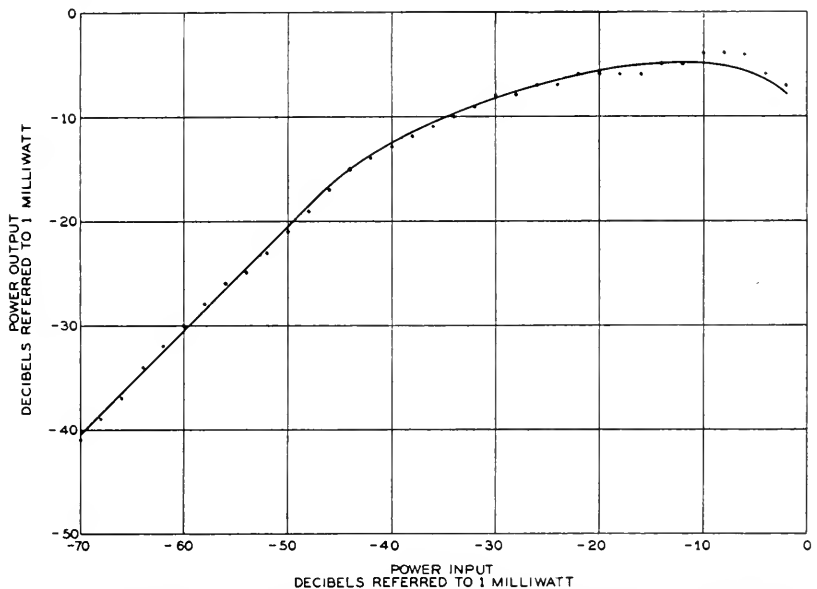


Fig. 3—Power output versus power input for double-stream amplifier at 200 Mc with beam potentials of 54 volts and 33 volts and 1.1 ma current in each beam.

### 3. EXPERIMENTAL OBSERVATIONS

The two beam potentials and the two beam currents were varied until good operating conditions were reached. In the amplifier tube with helix output, good operation with 29 db gain at 200 Mc was observed at low input signal levels with inner beam potential 54 volts, outer beam potential 33 volts, and 1.1 milliampere current in each beam. Measurements of output and input signal power are shown in Fig. 3, in which output power is plotted as a function of input power. The gain is seen to be constant at 29 db from low levels up to an output power of 0.03 milliwatts, at which point compression sets in. Maximum power output is 0.3 milliwatts.

The variation of gain with frequency under very nearly the same conditions as above is shown in Fig. 4. The input signal was in the linear region of Fig. 3. The figure shows a bandwidth of 110 Mc between points 3 db down from maximum. The center of the band is at approximately 255 Mc.

The currents required to realize the above results are some tenths of a milliamperere higher than those used in making estimates of performance of the amplifier, and the voltages for best performance are lower. The use of the actual operating values leads to a prediction of maximum gain at 240 Mc for the double-stream interaction in better agreement with the

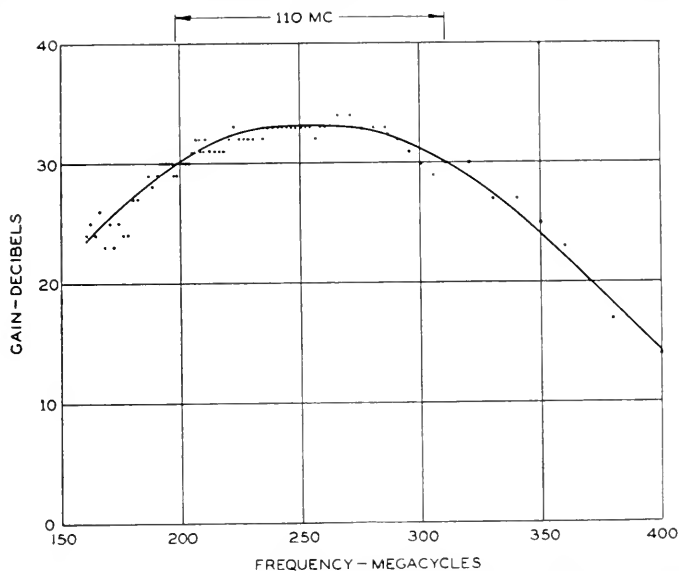


Fig. 4—Gain versus frequency for double-stream amplifier, operating in linear portion of Fig. 3.

observed maximum at 255 Mc than the value of 200 Mc originally estimated from the lower currents and higher voltages. Estimated double-stream gain at 240 Mc from theory for the separated hollow beams is 40 db.

Evidence that the gain of the amplifier resulted from the double-stream interaction was obtained in the following ways: by comparison of the transmission through the amplifier with both streams with that for each stream alone, and by comparison of signals obtained from the two identical probes in the electron streams at the ends of the central portion of the tube shown in Fig 1.

In a typical comparison of the first type, 1 db gain for the device was observed with the inner stream alone. This increased to 29 db when the outer stream was turned on. With the outer beam alone the loss in the

device was very large, for the velocity of the outer beam was far from that at which interaction with the helices occurs.

A signal from the probe at the end of the central portion of the tube 23 db greater than that from the probe at the beginning of this section was observed in a comparison of the second type. This can probably be taken as a measure of the increase in signal in this portion of the tube due to the double-stream interaction alone, although the probe arrangement may also be subject to some remaining complicating effects. Overall gain for the device in this measurement was 32 db. Further interaction of the same kind occurs in the portions of the tube outside of the space between the probes.

Measurements of the gain of an amplifier with helix output as a function of velocity separation between the streams have been made. For fixed mean voltage and current, theory predicts an increase in gain from zero db at zero separation to a maximum and then a decrease to zero as the velocity separation is further increased. A maximum gain was observed experimentally as velocity separation was varied, and in the neighborhood of the predicted optimum value of velocity separation for the current used.

In the amplifier tube with gap output it was possible to evaluate the a-c. component of current in the electron stream produced by the amplified signal since the impedance across the gap was known. The power output from this tube at saturation was 0.1 mw, a little less than the maximum shown in Fig. 3. For 75 ohm output impedance this power corresponds to 1.15 milliamperes r.m.s., or about one third of the total d-c. current to the collector in both streams. The output power, although relatively low, is thus of the right order of magnitude for the currents used.

#### ACKNOWLEDGMENT

The writer wishes to acknowledge his indebtedness to J. R. Pierce for valuable suggestions and discussion, and for supplying unpublished calculations concerning the relation between hollow and solid beams, the effect of the proximity of the conducting wall, and the effect of the separation of the beams in space.

Thanks are also due to A. R. Strnad for assistance in mechanical design and to R. E. Azud for construction of the amplifier tubes.

# The Synthesis of Two-Terminal Switching Circuits

By CLAUDE. E. SHANNON

## PART I: GENERAL THEORY

### 1. INTRODUCTION

THE theory of switching circuits may be divided into two major divisions, analysis and synthesis. The problem of analysis, determining the manner of operation of a given switching circuit, is comparatively simple. The inverse problem of finding a circuit satisfying certain given operating conditions, and in particular the *best* circuit is, in general, more difficult and more important from the practical standpoint. A basic part of the general synthesis problem is the design of a two-terminal network with given operating characteristics, and we shall consider some aspects of this problem.

Switching circuits can be studied by means of Boolean Algebra.<sup>1,2</sup> This is a branch of mathematics that was first investigated by George Boole in connection with the study of logic, and has since been applied in various other fields, such as an axiomatic formulation of Biology,<sup>3</sup> the study of neural networks in the nervous system,<sup>4</sup> the analysis of insurance policies,<sup>5</sup> probability and set theory, etc.

Perhaps the simplest interpretation of Boolean Algebra and the one closest to the application to switching circuits is in terms of propositions. A letter  $X$ , say, in the algebra corresponds to a logical proposition. The sum of two letters  $X + Y$  represents the proposition " $X$  or  $Y$ " and the product  $XY$  represents the proposition " $X$  and  $Y$ ". The symbol  $X'$  is used to represent the negation of proposition  $X$ , i.e. the proposition " $\text{not } X$ ". The constants 1 and 0 represent truth and falsity respectively. Thus  $X + Y = 1$  means  $X$  or  $Y$  is true, while  $X + YZ' = 0$  means  $X$  or ( $Y$  and the contradiction of  $Z$ ) is false.

The interpretation of Boolean Algebra in terms of switching circuits<sup>6,8,9,10</sup> is very similar. The symbol  $X$  in the algebra is interpreted to mean a make (front) contact on a relay or switch. The negation of  $X$ , written  $X'$ , represents a break (back) contact on the relay or switch. The constants 0 and 1 represent closed and open circuits respectively and the combining operations of addition and multiplication correspond to series and parallel connections of the switching elements involved. These conventions are shown in Fig. 1. With this identification it is possible to write an algebraic

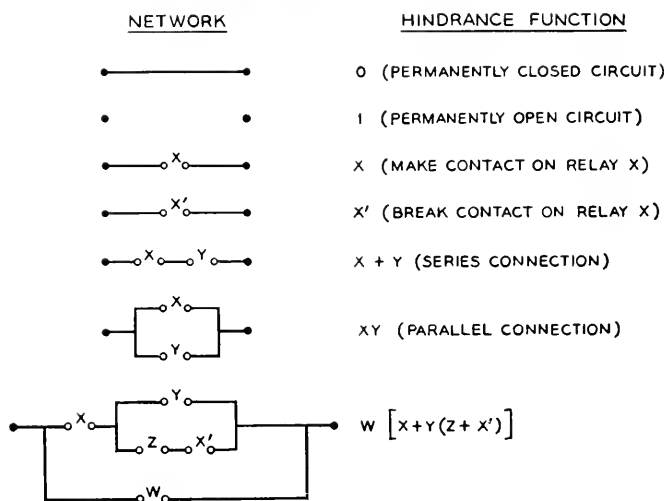


Fig. 1—Hindrane functions for simple circuits.

expression corresponding to a two-terminal network. This expression will involve the various relays whose contacts appear in the network and will be called the hindrance or hindrance function of the network. The last network in Fig. 1 is a simple example.

Boolean expressions can be manipulated in a manner very similar to ordinary algebraic expressions. Terms can be rearranged, multiplied out, factored and combined according to all the standard rules of numerical algebra. We have, for example, in Boolean Algebra the following identities:

$$0 + X = X$$

$$0 \cdot X = 0$$

$$1 \cdot X = X$$

$$X + Y = Y + X$$

$$XY = YX$$

$$X + (Y + Z) = (X + Y) + Z$$

$$X(YZ) = (XY)Z$$

$$X(Y + Z) = XY + XZ$$

The interpretation of some of these in terms of switching circuits is shown in Fig. 2.

There are a number of further rules in Boolean Algebra which allow

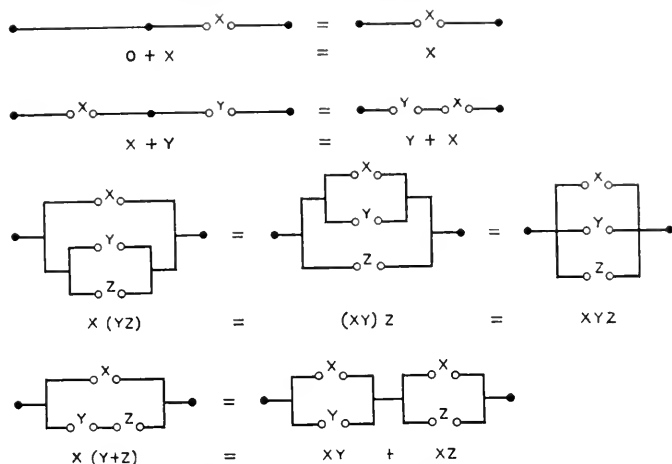


Fig. 2—Interpretation of some algebraic identities.

simplifications of expressions that are not possible in ordinary algebra. The more important of these are:

$$X = X + X = X + X + X = \text{etc.}$$

$$X = X \cdot X = X \cdot X \cdot X = \text{etc.}$$

$$X + 1 = 1$$

$$X + YZ = (X + Y)(X + Z)$$

$$X + X' = 1$$

$$X \cdot X' = 0$$

$$(X + Y)' = X'Y'$$

$$(XY)' = X' + Y'$$

The circuit interpretation of some of these is shown in Fig. 3. These rules make the manipulation of Boolean expressions considerably simpler than ordinary algebra. There is no need, for example, for numerical coefficients or for exponents, since  $nX = X^n = X$ .

By means of Boolean Algebra it is possible to find many circuits equivalent in operating characteristics to a given circuit. The hindrance of the given circuit is written down and manipulated according to the rules. Each different resulting expression represents a new circuit equivalent to the given one. In particular, expressions may be manipulated to eliminate elements which are unnecessary, resulting in simple circuits.

Any expression involving a number of variables  $X_1, X_2, \dots, X_n$  is

called a *function* of these variables and written in ordinary function notation,  $f(X_1, X_2, \dots, X_n)$ . Thus we might have  $f(X, Y, Z) = X + Y'Z + XZ'$ . In Boolean Algebra there are a number of important general theorems which hold for any function. It is possible to *expand* a function about one or more of its arguments as follows:

$$f(X_1, X_2, \dots, X_n) = X_1 f(1, X_2, \dots, X_n) + X'_1 f(0, X_2, \dots, X_n)$$

This is an expansion about  $X_1$ . The term  $f(1, X_2, \dots, X_n)$  is the function

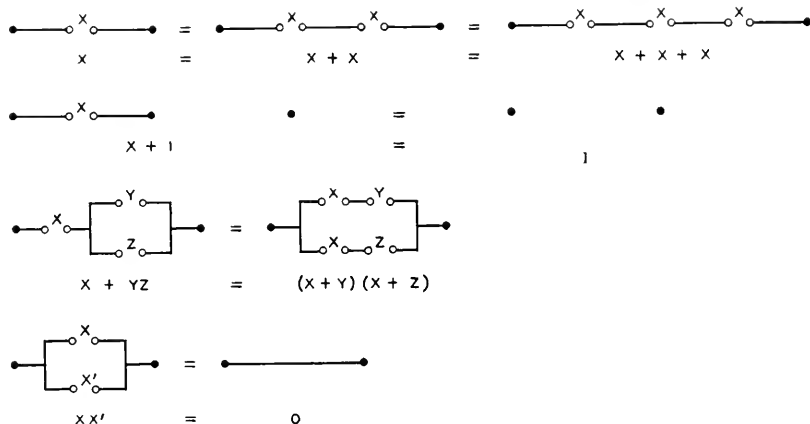


Fig. 3—Interpretation of some special Boolean identities.

$f(X_1, X_2, \dots, X_n)$  with 1 substituted for  $X$ , and 0 for  $X'$ , and conversely for the term  $f(0, X_2, \dots, X_n)$ . An expansion about  $X_1$  and  $X_2$  is:

$$f(X_1, X_2, \dots, X_n) = X_1 X_2 f(1, 1, X_3, \dots, X_n) + X_1 X'_2 f(1, 0, X_3, \dots, X_n) \\ + X'_1 X_2 f(0, 1, X_3, \dots, X_n) + X'_1 X'_2 f(0, 0, X_3, \dots, X_n)$$

This may be continued to give expansions about any number of variables. When carried out for all  $n$  variables,  $f$  is written as a sum of  $2^n$  products each with a coefficient which does not depend on any of the variables. Each coefficient is therefore a constant, either 0 or 1.

There is a similar expansion whereby  $f$  is expanded as a product:

$$f(X_1, X_2, \dots, X_n) \\ = [X_1 + f(0, X_2, \dots, X_n)] [X'_1 + f(1, X_2, \dots, X_n)] \\ = [X_1 + X_2 + f(0, 0, \dots, X_n)] [X_1 + X'_2 + f(0, 1, \dots, X_n)] \\ [X'_1 + X_2 + f(1, 0, \dots, X_n)] [X'_1 + X'_2 + f(1, 1, \dots, X_n)] \\ = \text{etc.}$$



The following are some further identities for general functions:

$$X + f(X, Y, Z, \dots) = X + f(0, Y, Z, \dots)$$

$$X' + f(X, Y, Z, \dots) = X' + f(1, Y, Z, \dots)$$

$$Xf(X, Y, Z, \dots) = Xf(1, Y, Z, \dots)$$

$$X'f(X, Y, Z, \dots) = X'f(0, Y, Z, \dots)$$

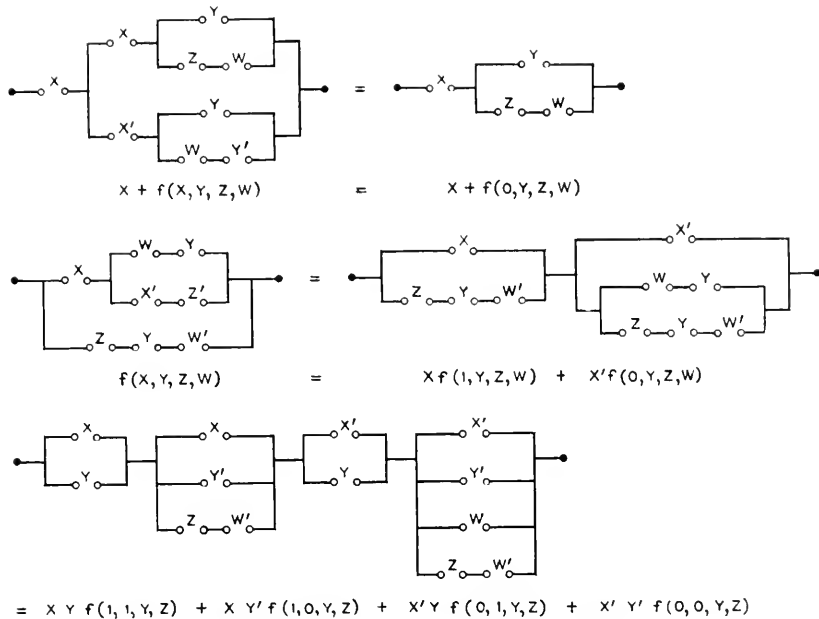


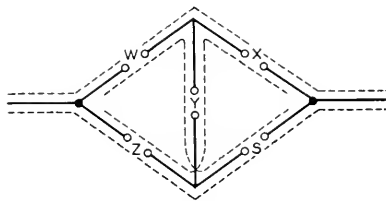
Fig. 4—Examples of some functional identities.

The network interpretations of some of these identities are shown in Fig. 4. A little thought will show that they are true, in general, for switching circuits.

The hindrance function associated with a two-terminal network describes the network completely from the external point of view. We can determine from it whether the circuit will be open or closed for any particular position of the relays. This is done by giving the variables corresponding to operated relays the value 0 (since the make contacts of these are then closed and the break contacts open) and unoperated relays the value 1. For example, with the function  $f = W[X + Y(Z + X')]$  suppose relays  $X$  and  $Y$  operated and  $Z$  and  $W$  not operated. Then  $f = 1[0 + 0(1 + 1)] = 0$  and in this condition the circuit is closed.

A hindrance function corresponds explicitly to a series-parallel type of circuit, i.e. a circuit containing only series and parallel connections. This is because the expression is made up of sum and product operations. There is however, a hindrance function representing the operating characteristics (conditions for open or closed circuits between the two terminals) for any network, series-parallel or not. The hindrance for non-series-parallel networks can be found by several methods of which one is indicated in Fig. 5 for a simple bridge circuit. The hindrance is written as the product of a set of factors. Each factor is the series hindrance of a possible path between the two terminals. Further details concerning the Boolean method for switching circuits may be found in the references cited above.

This paper is concerned with the problem of synthesizing a two-terminal circuit which represents a given hindrance function  $f(X_1, \dots, X_n)$ . Since any given function  $f$  can be realized in an unlimited number of different



$$f = (w+x)(z+s)(w+y+s)(z+y+x)$$

Fig. 5—Hindrance of a bridge circuit.

ways, the particular design chosen must depend upon other considerations. The most common of these determining criteria is that of economy of elements, which may be of several types, for example:

- (1) We may wish to realize our function with the least total number of switching elements, regardless of which variables they represent.
- (2) We may wish to find the circuit using the least total number of relay springs. This requirement sometimes leads to a solution different from (1), since contiguous make and break elements may be combined into transfer elements so that circuits which tend to group make and break contacts on the same relay into pairs will be advantageous for (2) but not necessarily for (1).
- (3) We may wish to distribute the spring loading on all the relays or on some subset of the relays as evenly as possible. Thus, we might try to find the circuit in which the most heavily loaded relay was as lightly loaded as possible. More generally, we might desire a circuit in which the loading on the relays is of some specified sort, or as near as possible to this given distribution. For example, if the relay  $X_1$

must operate very quickly, while  $X_2$  and  $X_3$  have no essential time limitations but are ordinary  $U$ -type relays, and  $X_4$  is a multicontact relay on which many contacts are available, we would probably try to design a circuit for  $f(X_1, X_2, X_3, X_4)$  in such a way as, first of all, to minimize the loading on  $X_1$ , next to equalize the loading on  $X_2$  and  $X_3$  keeping it at the same time as low as possible, and finally not to load  $X_4$  any more than necessary. Problems of this sort may be called *problems in spring-load distribution*.

Although all equivalent circuits representing a given function  $f$  which contain only series and parallel connections can be found with the aid of Boolean Algebra, the most economical circuit in any of the above senses will often not be of this type. The problem of synthesizing non-series-parallel circuits is exceedingly difficult. It is even more difficult to show that a circuit found in some way is the *most* economical one to realize a given function. The difficulty springs from the large number of essentially different networks available and more particularly from the lack of a simple mathematical idiom for representing these circuits.

We will describe a new design method whereby any function  $f(X_1, X_2, \dots, X_n)$  may be realized, and frequently with a considerable saving of elements over other methods, particularly when the number of variables  $n$  is large. The circuits obtained by this method will not, in general, be of the series-parallel type, and, in fact, they will usually not even be planar. This method is of interest theoretically as well as for practical design purposes, for it allows us to set new upper limits for certain numerical functions associated with relay circuits. Let us make the following definitions:

$\lambda(n)$  is defined as the least number such that any function of  $n$  variables can be realized with not more than  $\lambda(n)$  elements.\* Thus, any function of  $n$  variables can be realized with  $\lambda(n)$  elements and at least one function with no less.

$\mu(n)$  is defined as the least number such that given any function  $f$  of  $n$  variables, there is a two-terminal network having the hindrance  $f$  and using not more than  $\mu(n)$  elements on the most heavily loaded relay.

The first part of this paper deals with the general design method and the behaviour of  $\lambda(n)$ . The second part is concerned with the possibility of various types of spring load distribution, and in the third part we will study certain classes of functions that are especially easy to synthesize, and give some miscellaneous theorems on switching networks and functions.

## 2. FUNDAMENTAL DESIGN THEOREM

The method of design referred to above is based on a simple theorem dealing with the interconnection of two switching networks. We shall first

\* An *element* means a make or break contact on one relay. A *transfer element* means a make-and-break with a common spring, and contains two *elements*.

state and prove this theorem. Suppose that  $M$  and  $N$  (Fig. 6) are two  $(n + 1)$  terminal networks,  $M$  having the hindrance functions  $U_k$  ( $k = 1, 2, \dots, n$ ) between terminals  $a$  and  $k$ , and  $N$  having the functions  $V_k$  between  $b$  and  $k$ . Further, let  $M$  be such that  $U_{jk} = 1$  ( $j, k = 1, 2, \dots, n$ ). We will say, in this case, that  $M$  is a *disjunctive* network. Under these conditions we shall prove the following:

*Theorem 1: If the corresponding terminals 1, 2,  $\dots$ ,  $n$  of  $M$  and  $N$  are connected together, then*

$$U_{ab} = \prod_{k=1}^n (U_k + V_k) \quad (1)$$

where  $U_{ab}$  is the hindrance from terminal  $a$  to terminal  $b$ .

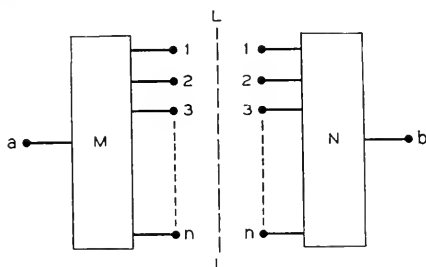


Fig. 6—Network for general design theorem.

Proof: It is known that the hindrance  $U_{ab}$  may be found by taking the product of the hindrances of all possible paths from  $a$  to  $b$  along the elements of the network.<sup>6</sup> We may divide these paths into those which cross the line  $L$  once, those which cross it three times, those which cross it five times, etc. Let the product of the hindrances in the first class be  $W_1$ , in the second class  $W_3$ , etc. Thus

$$U_{ab} = W_1 \cdot W_3 \cdot W_5 \cdots \quad (2)$$

Now clearly

$$W_1 = \prod_1^n (U_k + V_k)$$

and also

$$W_3 = W_5 = \cdots = 1$$

since each term in any of these must contain a summand of the type  $U_{jk}$  which we have assumed to be 1. Substituting in (2) we have the desired result.

The method of using this theorem to synthesize networks may be roughly

described as follows: The function to be realized is written in the form of a product of the type (1) in such a way that the functions  $U_k$  are the same for a large class of functions, the  $V_k$  determining the particular one under consideration. A basic disjunctive network  $M$  is constructed having the functions  $U_k$  between terminals  $a$  and  $k$ . A network  $N$  for obtaining the functions  $V_k$  is then found by inspection or according to certain general rules. We will now consider just how this can be done in various cases.

### 3. DESIGN OF NETWORKS FOR GENERAL FUNCTIONS—BEHAVIOR OF $\lambda(n)$ .

#### a. Functions of One, Two and Three Variables:

Functions of one or two variables may be dismissed easily since the number of such functions is so small. Thus, with one variable  $X$ , the possible functions are only:

$$0, 1, X, X'$$

and obviously  $\lambda(1) = 1$ ,  $\mu(1) = 1$ .

With two variables  $X$  and  $Y$  there are 16 possible functions:

$$\begin{array}{llllll} 0 & XY & XY' & X'Y & X'Y' & XY' + X'Y \\ 1 & X'Y' & X + Y & X + Y' & X' + Y & X' + Y' & XY + X'Y' \end{array}$$

so that  $\lambda(2) = 4$ ,  $\mu(2) = 2$ .

We will next show that any function of three variables  $f(X, Y, Z)$  can be realized with not more than eight elements and with not more than four from any one relay. Any function of three variables can be expanded in a product as follows:

$$\begin{aligned} f(X, Y, Z) = & [X + Y + f(0, 0, Z)][X + Y' + f(0, 1, Z)] \\ & [X' + Y + f(1, 0, Z)][X' + Y' + f(1, 1, Z)]. \end{aligned}$$

In the terminology of Theorem 1 we let

$$\begin{array}{ll} U_1 = X + Y & V_1 = f(0, 0, Z) \\ U_2 = X + Y' & V_2 = f(0, 1, Z) \\ U_3 = X' + Y & V_3 = f(1, 0, Z) \\ U_4 = X' + Y' & V_4 = f(1, 1, Z) \end{array}$$

so that

$$U_{ab} = f(X, Y, Z) = \prod_{k=1}^4 (U_k + V_k)$$

The above  $U_k$  functions are realized with the network  $M$  of Fig. 7 and it is

easily seen that  $U_{jk} = 1$  ( $j, k = 1, 2, 3, 4$ ). The problem now is to construct a second network  $N$  having the  $V_k$  functions  $V_1, V_2, V_3, V_4$ . Each of these is a function of the one variable  $Z$  and must, therefore, be one of the four possible functions of one variable:

$$0, 1, Z, Z'.$$

Consider the network  $N$  of Fig. 8. If any of the  $V$ 's are equal to 0, connect the corresponding terminals of  $M$  to the terminal of  $N$  marked 0; if any are equal to  $Z$ , connect these terminals of  $M$  to the terminal of  $N$  marked  $Z$ , etc. Those which are 1 are, of course, not connected to anything. It is clear from Theorem 1 that the network thus obtained will realize the function  $f(X, Y, Z)$ . In many cases some of the elements will be superfluous, e.g., if one of the  $V_i$  is equal to 1, the element of  $M$  connected to terminal  $i$  can

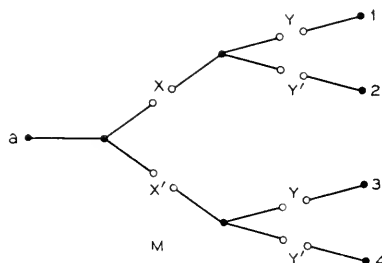


Fig. 7—Disjunctive tree with two bays.

be eliminated. At worst  $M$  contains six elements and  $N$  contains two. The variable  $X$  appears twice,  $Y$  four times and  $Z$  twice. Of course, it is completely arbitrary which variables we call  $X, Y$ , and  $Z$ . We have thus proved somewhat more than we stated above, namely,

*Theorem 2: Any function of three variables may be realized using not more than 2, 2, and 4 elements from the three variables in any desired order. Thus  $\lambda(3) \leq 8$ ,  $\mu(3) \leq 4$ . Further, since make and break elements appear in adjacent pairs we can obtain the distribution 1, 1, 2, in terms of transfer elements.*

The theorem gives only upper limits for  $\lambda(3)$  and  $\mu(3)$ . The question immediately arises as to whether by some other design method these limits could be lowered, i.e., can the  $\leq$  signs be replaced by  $<$  signs. It can be shown by a study of special cases that  $\lambda(3) = 8$ , the function

$$X \oplus Y \oplus Z = X(YZ + Y'Z') + X'(YZ' + Y'Z)$$

requiring eight elements in its most economical realization.  $\mu(3)$ , however, is actually 3.

It seems probable that, in general, the function

$$X_1 \oplus X_2 \oplus \cdots \oplus X_n$$

requires  $4(n - 1)$  elements, but no proof has been found. Proving that a certain function cannot be realized with a small number of elements is somewhat like proving a number transcendental; we will show later that almost all\* functions require a large number of elements, but it is difficult to show that a particular one does.

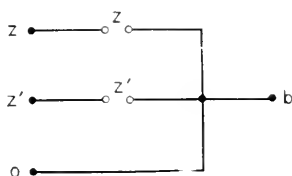


Fig. 8—Network giving all functions of one variable.

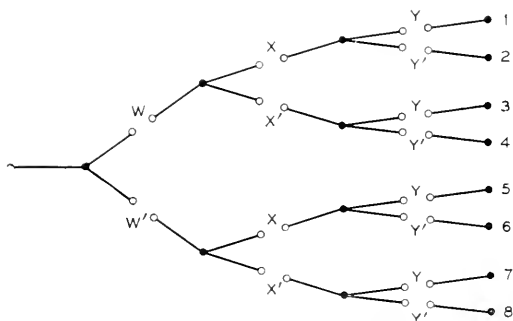


Fig. 9—Disjunctive tree with three bays.

#### b. Functions of Four Variables:

In synthesizing functions of four variables by the same method, two courses are open. First, we may expand the function as follows:

$$\begin{aligned} f(W, X, Y, Z) &= [W + X + Y + V_1(Z)] \cdot [W + X + Y' + V_2(Z)] \\ &\quad [W + X' + Y + V_3(Z)] \cdot [W + X' + Y' + V_4(Z)] \\ &\quad [W'' + X + Y + V_5(Z)] \cdot [W'' + X + Y' + V_6(Z)] \\ &\quad [W'' + X' + Y + V_7(Z)] \cdot [W'' + X' + Y' + V_8(Z)]. \end{aligned}$$

By this expansion we would let  $U_1 = W + X + Y$ ,  $U_2 = W + X + Y'$ ,  $\dots$ ,  $U_8 = W'' + X' + Y'$  and construct the  $M$  network in Fig. 9.  $N$  would

\* We use the expression "almost all" in the arithmetic sense: e.g., a property is true of almost all functions of  $n$  variables if the fraction of all functions of  $n$  variables for which it is not true  $\rightarrow 0$  as  $n \rightarrow \infty$ .

again be as in Fig. 8, and by the same type of reasoning it can be seen that  $\lambda(4) \leq 16$ .

Using a slightly more complicated method, however, it is possible to reduce this limit. Let the function be expanded in the following way:

$$f(W, X, Y, Z) = [W + X + V_1(Y, Z)] \cdot [W + X' + V_2(Y, Z)] \\ [W' + X + V_3(Y, Z)] \cdot [W' + X' + V_4(Y, Z)].$$

We may use a network of the type of Fig. 7 for  $M$ . The  $V$  functions are now functions of two variables  $Y$  and  $Z$  and may be any of the 16 functions:

$$\begin{array}{ccccc} A \begin{cases} 0 \\ 1 \end{cases} & B \begin{cases} Y \\ Y' \\ Z \\ Z' \end{cases} & C \begin{cases} YZ \\ Y'Z \\ YZ' \\ Y'Z' \end{cases} & D \begin{cases} Y + Z \\ Y + Z' \\ Y' + Z \\ Y' + Z' \end{cases} & E \begin{cases} Y'Z + YZ' \\ YZ + Y'Z' \end{cases} \end{array}$$

We have divided the functions into five groups,  $A$ ,  $B$ ,  $C$ ,  $D$  and  $E$  for later reference. We are going to show that any function of four variables can

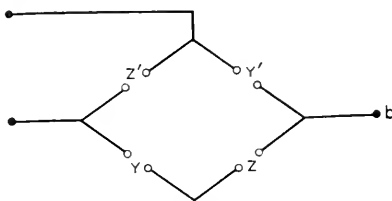


Fig. 10—Simplifying network.

be realized with not more than 14 elements. This means that we must construct a network  $N$  using not more than eight elements (since there are six in the  $M$  network) for any selection of four functions from those listed above. To prove this, a number of special cases must be considered and dealt with separately:

(1) If all four functions are from the groups,  $A$ ,  $B$ ,  $C$ , and  $D$ ,  $N$  will certainly not contain more than eight elements, since eight letters at most can appear in the four functions.

(2) We assume now that just one of the functions is from group  $E$ ; without loss of generality we may take it to be  $Y'Z' + Y'Z$ , for it is the other, replacing  $Y$  by  $Y'$  transforms it into this. If one or more of the remaining functions are from groups  $A$  or  $B$  the situation is satisfactory, for this function need require no elements. Obviously 0 and 1 require no elements and  $Y$ ,  $Y'$ ,  $Z$  or  $Z'$  may be "tapped off" from the circuit for  $Y'Z' + Y'Z$  by writing it as  $(Y + Z)(Y' + Z')$ . For example,  $Y'$  may be obtained with the circuit of Fig. 10. This leaves four elements, certainly a sufficient number for any two functions from  $A$ ,  $B$ ,  $C$ , or  $D$ .



(3) Now, still assuming we have one function,  $YZ' + Y'Z$ , from  $E$ , suppose at least two of the remaining are from  $D$ . Using a similar "tapping off" process we can save an element on each of these. For instance, if the functions are  $Y + Z$  and  $Y' + Z'$  the circuit would be as shown in Fig. 11.

(4) Under the same assumption, then, our worst case is when two of the functions are from  $C$  and one from  $D$ , or all three from  $C$ . This latter case is satisfactory since, then, at least one of the three must be a term of  $YZ' + Y'Z$  and can be "tapped off." The former case is bad only when the two functions from  $C$  are  $YZ$  and  $Y'Z'$ . It may be seen that the only

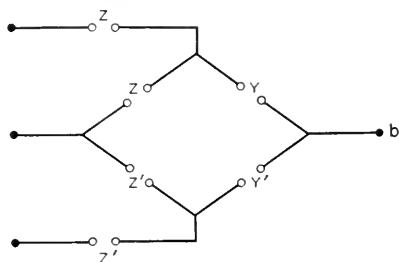


Fig. 11—Simplifying network.

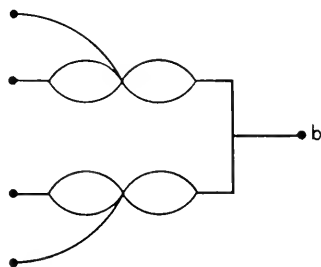


Fig. 12—Simplifying network.

essentially different choices for the function from  $D$  are  $Y + Z$  and  $Y' + Z$ . That the four types of functions  $f$  resulting may be realized with 14 elements can be shown by writing out typical functions and reducing by Boolean Algebra.

(5) We now consider the cases where two of the functions are from  $E$ . Using the circuit of Fig. 12, we can tap off functions or parts of functions from  $A$ ,  $B$  or  $D$ , and it will be seen that the only difficult cases are the following: (a) Two functions from  $C$ . In this case either the function  $f$  is symmetric in  $Y$  and  $Z$  or else both of the two functions may be obtained from the circuits for the  $E$  functions of Fig. 12. The symmetric case is handled in a later section. (b) One is from  $C$ , the other from  $D$ . There is only one unsymmetric case. We assume the four functions are  $Y \oplus Z$ ,  $Y \oplus Z'$ ,  $YZ$  and  $Y + Z'$ . This gives rise to four types of functions  $f$ , which can all be reduced by algebraic methods. This completes the proof.

*Theorem 3: Any function of four variables can be realized with not more than 14 elements.*

c. Functions of More Than Four Variables:

Any function of five variables may be written

$$f(X_1, \dots, X_5) = [X_5 + f_1(X_1, \dots, X_4)] \cdot [X_5' + f_2(X_1, \dots, X_4)]$$

and since, as we have just shown, the two functions of four variables can be realized with 14 elements each,  $f(X_1, \dots, X_5)$  can be realized with 30

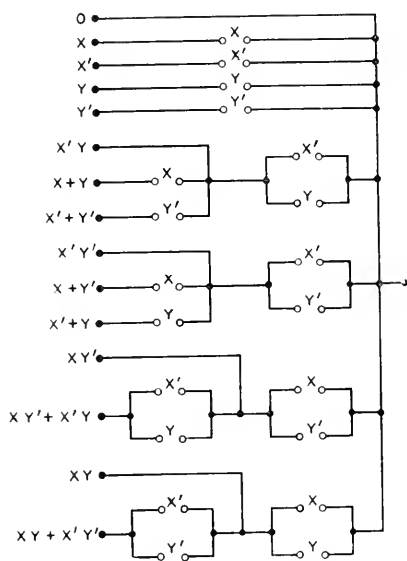


Fig. 13—Network giving all functions of two variables.

Now consider a function  $f(X_1, X_2, \dots, X_n)$  of  $n$  variables. For  $5 < n \leq 13$  we get the best limit by expanding about all but two variables.

$$f(X_1, X_2, \dots, X_n) = [X_1 + X_2 + \dots + X_{n-2} + V_1(X_{n-1}, X_n)] \cdot \dots \cdot [X_1' + X_2' + \dots + X_{n-2}' + V_s(X_{n-1}, X_n)] \quad (4)$$

The  $V$ 's are all functions of the variables  $X_{n-1}, X_n$  and may be obtained from the general  $N$  network of Fig. 13, in which *every* function of two variables appears. This network contains 20 elements which are grouped into five transfer elements for one variable and five for the other.\* The  $M$  network for (4), shown in Fig. 14, requires in general  $2^{n-1} - 2$  elements. Thus we have:

\* Several other networks with the same property as Fig. 13 have been found, but they all require 20 elements.

*Theorem 4.*  $\lambda(n) \leq 2^{n-1} + 18$

d. Upper Limits for  $\lambda(n)$  with Large  $n$ .

Of course, it is not often necessary to synthesize a function of more than say 10 variables, but it is of considerable theoretical interest to determine as closely as possible the behavior of  $\lambda(n)$  for large  $n$ .

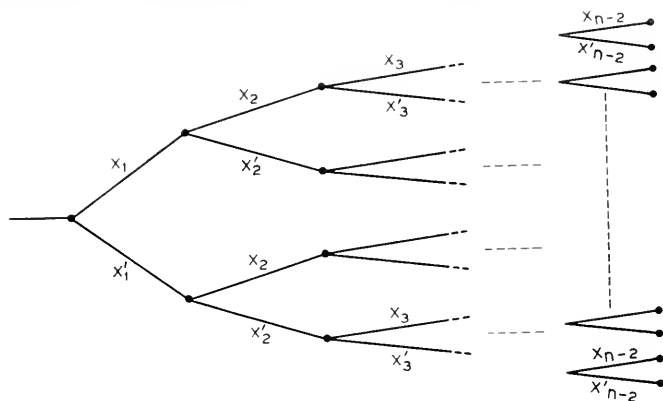


Fig. 14—Disjunctive tree with  $(n - 2)$  bays.

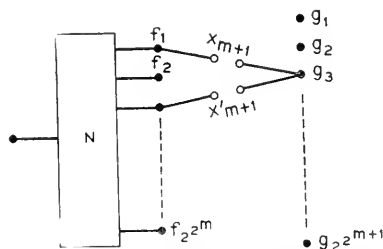


Fig. 15—Network giving all functions of  $(m + 1)$  variables constructed from one giving all functions of  $m$  variables.

We will first prove a theorem placing limits on the number of elements required in a network analogous to Fig. 13 but generalized for  $m$  variables.

*Theorem 5.* An  $N$  network realizing all  $2^{2^m}$  functions of  $m$  variables can be constructed using not more than  $2 \cdot 2^{2^m}$  elements, i.e., not more than two elements per function. Any network with this property uses at least  $(\frac{3}{2} - \epsilon)$  elements per function for any  $\epsilon > 0$  with  $n$  sufficiently large.

The first part will be proved by induction. We have seen it to be true for  $m = 1, 2$ . Suppose it is true for some  $m$  with the network  $N$  of Fig. 15. Any function of  $m + 1$  variables can be written

$$g = [X_{m+1} + f_a][X'_{m+1} + f_b]$$

where  $f_a$  and  $f_b$  involve only  $m$  variables. By connecting from  $g$  to the corresponding  $f_a$  and  $f_b$  terminals of the smaller network, as shown typically for  $g_3$ , we see from Theorem 1 that all the  $g$  functions can be obtained. Among these will be the  $2^{2^m} f$  functions and these can be obtained simply by connecting across to the  $f$  functions in question without any additional elements. Thus the entire network uses less than

$$(2^{2^{m+1}} - 2^{2^m})2 + 2 \cdot 2^{2^m}$$

elements, since the  $N$  network by assumption uses less than  $2 \cdot 2^{2^m}$  and the first term in this expression is the number of added elements.

The second statement of Theorem 7 can be proved as follows. Suppose we have a network, Fig. 16, with the required property. The terminals can be divided into three classes, those that have one or less elements di-

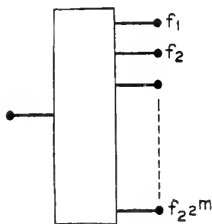


Fig. 16—Network giving all functions of  $m$  variables.

rectly connected, those with two, and those with three or more. The first set consists of the functions 0 and 1 and functions of the type

$$(X + f) = X + f_{x=0}$$

where  $X$  is some variable or primed variable. The number of such functions is not greater than  $2m \cdot 2^{2^{m-1}}$  for there are  $2m$  ways of selecting an " $X$ " and then  $2^{2^{m-1}}$  different functions  $f_{x=0}$  of the remaining  $m - 1$  variables. Hence the terminals in this class as a fraction of the total  $\rightarrow 0$  as  $m \rightarrow \infty$ . Functions of the second class have the form

$$g = (X + f_1)(Y + f_2)$$

In case  $X \neq Y'$  this may be written

$$XY + XY'g_{X=1, Y=0} + X'Yg_{X=0, Y=1} + X'Y'g_{X=0, Y=0}$$

and there are not more than  $(2m)(2m - 2)[2^{2^{m-2}}]^3$  such functions, again a vanishingly small fraction. In case  $X = Y'$  we have the situation shown in Fig. 17 and the  $XX'$  connection can never carry ground to another terminal since it is always open as a series combination. The inner ends of these elements can therefore be removed and connected to terminals

corresponding to functions of less than  $m$  variables according to the equation

$$g = (X + f_1)(X' + f_2) = (X + f_{1X=0})(X' + f_{2X=1})$$

if they are not already so connected. This means that all terminals of the second class are then connected to a vanishingly small fraction of the total terminals. We can then attribute two elements each to these terminals and at least one and one-half each to the terminals of the third group. As these two groups exhaust the terminals except for a fraction which  $\rightarrow 0$  as  $n \rightarrow \infty$ , the theorem follows.

If, in synthesizing a function of  $n$  variables, we break off the tree at the  $(n - m)$ th bay, the tree will contain  $2^{n-m+1} - 2$  elements, and we can find an  $N$  network with not more than  $2^{2^m} \cdot 2$  elements exhibiting every function of the remaining  $m$  variables. Hence

$$\lambda(n) \leq 2^{n-m+1} - 2 + 2 \cdot 2^{2^m} < 2^{n-m+1} + 2 \cdot 2^{2^m}$$

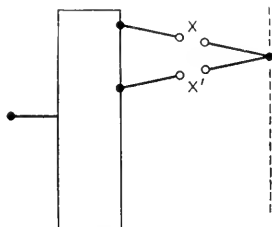


Fig. 17—Possible situation in Fig. 16.

for every integer  $m$ . We wish to find the integer  $M = M(n)$  minimizing this upper bound.

Considering  $m$  as a continuous variable and  $n$  fixed, the function

$$f(m) = 2^{n-m+1} + 2^{2^m} \cdot 2$$

clearly has just one minimum. This minimum must therefore lie between  $m_1$  and  $m_1 + 1$ , where

$$f(m_1) = f(m_1 + 1)$$

$$\text{i.e.,} \quad 2^{n-m_1+1} + 2^{2^{m_1}} \cdot 2 = 2^{n-m_1} + 2^{2^{m_1+1}} \cdot 2$$

$$\text{or} \quad 2^n = 2^{m_1+1}(2^{2^{m_1+1}} - 2^{2^{m_1}})$$

Now  $m_1$  cannot be an integer since the right-hand side is a power of two and the second term is less than half the first. It follows that to find the integer  $M$  making  $f(M)$  a minimum we must take for  $M$  the least integer satisfying

$$2^n \leq 2^{M+1} 2^{2^{M+1}}$$

Thus  $M$  satisfies:

$$M + 1 + 2^{M+1} \geq n > M + 2^M \quad (5)$$

This gives:

$n \leq 11$	$M = 2$
$11 < n \leq 20$	$M = 3$
$20 < n \leq 57$	$M = 4$
$57 < n \leq 70$	$M = 5$
$70 < n \leq 135$	$M = 6$
etc.	

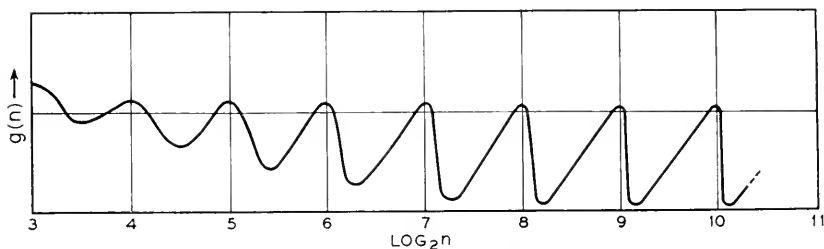


Fig. 18—Behaviour of  $g(n)$ .

Our upper bound for  $\lambda(n)$  behaves something like  $\frac{2^{n+1}}{n}$  with a superimposed saw-tooth oscillation as  $n$  varies between powers of two, due to the fact that  $m$  must be an integer. If we define  $g(n)$  by

$$2^{n-M+1} + 2^{2^M} 2 = g(n) \frac{2^{n+1}}{n},$$

$M$  being determined to minimize the function (i.e.,  $M$  satisfying (5)), then  $g(n)$  varies somewhat as shown in Fig. 18 when plotted against  $\log_2 n$ . The maxima occur just beyond powers of two, and closer and closer to them as  $n \rightarrow \infty$ . Also, the saw-tooth shape becomes more and more exact. The sudden drops occur just after we change from one value of  $M$  to the next. These facts lead to the following:

*Theorem 6. (a) For all  $n$*

$$\lambda(n) < \frac{2^{n+3}}{n}.$$

*(b) For almost all  $n$*

$$\lambda(n) < \frac{2^{n+2}}{n}.$$

(c) *There is an infinite sequence of  $n_i$  for which*

$$\lambda(n_i) < \frac{2^{n_i+1}}{n_i} (1 + \epsilon) \quad \epsilon > 0.$$

These results can be proved rigorously without much difficulty.

e. A Lower Limit for  $\lambda(n)$  with Large  $n$ .

Up to now most of our work has been toward the determination of upper limits for  $\lambda(n)$ . We have seen that for all  $n$

$$\lambda(n) < B \frac{2^n}{n}.$$

We now ask whether this function  $B \frac{2^n}{n}$  is anywhere near the true value of  $\lambda(n)$ , or may  $\lambda(n)$  be perhaps dominated by a smaller order of infinity, e.g.,  $n^p$ . It was thought for a time, in fact, that  $\lambda(n)$  might be limited by  $n^2$  for all  $n$ , arguing from the first few values: 1, 4, 8, 14. We will show that this is far from the truth, for actually  $\frac{2^n}{n}$  is the correct order of magnitude of  $\lambda(n)$ :

$$A \frac{2^n}{n} < \lambda(n) < B \frac{2^n}{n}$$

for all  $n$ . A closely associated question to which a partial answer will be given is the following: Suppose we define the "complexity" of a given function  $f$  of  $n$  variables as the ratio of the number of elements in the most economical realization of  $f$  to  $\lambda(n)$ . Then any function has a complexity lying between 0 and 1. Are most functions simple or complex?

*Theorem 7: For all sufficiently large  $n$ , all functions of  $n$  variables excepting a fraction  $\delta$  require at least  $(1 - \epsilon) \frac{2^n}{n}$  elements, where  $\epsilon$  and  $\delta$  are arbitrarily small positive numbers. Hence for large  $n$*

$$\lambda(n) > (1 - \epsilon) \frac{2^n}{n}$$

*and almost all functions have a complexity  $> \frac{1}{4}(1 - \epsilon)$ . For a certain sequence  $n_i$  almost all functions have a complexity  $> \frac{1}{2}(1 - \epsilon)$ .*

The proof of this theorem is rather interesting, for it is a pure existence proof. We do not show that any particular function or set of functions requires  $(1 - \epsilon) \frac{2^n}{n}$  elements, but rather that it is impossible for all functions

to require less. This will be done by showing that there are not enough networks with less than  $(1 - \epsilon) \frac{2^n}{n}$  branches to go around, i.e., to represent all the  $2^{2^n}$  functions of  $n$  variables, taking account, of course, of the different assignments of the variables to the branches of each network. This is only possible due to the extremely rapid increase of the function  $2^{2^n}$ . We require the following:

*Lemma: The number of two-terminal networks with  $K$  or less branches is less than  $(6K)^K$ .*

Any two-terminal network with  $K$  or less branches can be constructed as follows: First line up the  $K$  branches as below with the two terminals  $a$  and  $b$ .

$$\begin{array}{ll} \text{a.} & \begin{array}{l} 1-1' \\ 2-2' \\ 3-3' \\ 4-4' \\ \vdots \\ \vdots \end{array} \\ \text{b.} & K-K' \end{array}$$

We first connect the terminals  $a, b, 1, 2, \dots, K$  together in the desired way. The number of *different* ways we can do this is certainly limited by the number of partitions of  $K + 2$  which, in turn, is less than

$$2^{K+1}$$

for this is the number of ways we can put one or more division marks between the symbols  $a, 1, \dots, K, b$ . Now, assuming  $a, 1, 2, \dots, K, b$ , interconnected in the desired manner, we can connect  $1'$  either to one of these terminals or to an additional junction point, i.e.,  $1'$  has a choice of at most

$$K + 3$$

terminals,  $2'$  has a choice of at most  $K + 4$ , etc. Hence the number of networks is certainly less than

$$\begin{aligned} & 2^{K+1}(K + 3)(K + 4)(K + 5) \cdots (2K + 3) \\ & < (6K)^K \qquad K \geq 3 \end{aligned}$$

and the theorem is readily verified for  $K = 1, 2$ .

We now return to the proof of Theorem 7. The number of functions of  $n$  variables that can be realized with  $\frac{(1 - \epsilon)2^n}{n}$  elements is certainly less than the number of networks we can construct with this many branches multi-



plied by the number of assignments of the variables to the branches, i.e., it is less than

$$H = (2n)^{(1-\epsilon)(2^n/n)} \left[ 6(1-\epsilon) \frac{2^n}{n} \right]^{(1-\epsilon)(2^n/n)}$$

Hence

$$\begin{aligned} \log_2 H &= (1-\epsilon) \frac{2^n}{n} \log 2n + (1-\epsilon) \frac{2^n}{n} \log (1-\epsilon) \frac{2^n}{n} \cdot 6 \\ &= (1-\epsilon) 2^n + \text{terms dominated by this term for large } n. \end{aligned}$$

By choosing  $n$  so large that  $\frac{\epsilon}{2} 2^n$  dominates the other terms of  $\log H$  we arrive at the inequality

$$\begin{aligned} \log_2 H &< (1-\epsilon_1) 2^n \\ H &< 2^{(1-\epsilon_1)2^n} \end{aligned}$$

But there are  $S = 2^{2^n}$  functions of  $n$  variables and

$$\frac{H}{S} = \frac{2^{(1-\epsilon_1)2^n}}{2^{2^n}} \rightarrow 0 \quad \text{as } n \rightarrow \infty.$$

Hence almost all functions require more than  $(1-\epsilon_1)2^n$  elements.

Now, since for all  $n > N$  there is at least one function requiring more than (say)  $\frac{1}{2} \frac{2^n}{n}$  elements and since  $\lambda(n) > 0$  for  $n > 0$ , we can say that for all  $n$ ,

$$\lambda(n) > A \frac{2^n}{n}$$

for some constant  $A > 0$ , for we need only choose  $A$  to be the minimum number in the finite set:

$$\frac{1}{2}, \quad \frac{\lambda(1)}{2^1}, \quad \frac{\lambda(2)}{2^2}, \quad \frac{\lambda(3)}{2^3}, \quad \dots, \quad \frac{\lambda(N)}{2^N}$$

Thus  $\lambda(n)$  is of the order of magnitude of  $\frac{2^n}{n}$ . The other parts of Theorem 8 follow easily from what we have already shown.

The writer is of the opinion that almost all functions have a complexity nearly 1, i.e.,  $> 1 - \epsilon$ . This could be shown at least for an infinite sequence  $n_i$  if the Lemma could be improved to show that the number of networks is less than  $(6K)^{K/2}$  for large  $K$ . Although several methods have been used in counting the networks with  $K$  branches they all give the result  $(6K)^K$ .

It may be of interest to show that for large  $K$  the number of networks is greater than

$$(6K)^{K/4}$$

This may be done by an inversion of the above argument. Let  $f(K)$  be the number of networks with  $K$  branches. Now, since there are  $2^{2^n}$  functions of  $n$  variables and each can be realized with  $(1 + \epsilon) \frac{2^{n+2}}{n}$  elements ( $n$  sufficiently large),

$$f\left((1 + \epsilon) \frac{2^{n+2}}{n}\right) (2n)^{(1+\epsilon)(2^{n+2}/n)} > 2^{2^n}$$

for  $n$  large. But assuming  $f(K) < (6K)^{K/4}$  reverses the inequality, as is readily verified. Also, for an infinite sequence of  $K$ ,

$$f(K) > (6K)^{K/2}$$

Since there is no obvious reason why  $f(K)$  should be connected with powers of 2 it seems likely that this is true for all large  $K$ .

We may summarize what we have proved concerning the behavior of  $\lambda(n)$  for large  $n$  as follows.  $\lambda(n)$  varies somewhat as  $\frac{2^{n+1}}{n}$ ; if we let

$$\lambda(n) = A_n \frac{2^{n+1}}{n}$$

then, for large  $n$ ,  $A_n$  lies between  $\frac{1}{2} - \epsilon$  and  $(2 + \epsilon)$ , while, for an infinite sequence of  $n$ ,  $\frac{1}{2} - \epsilon < A_n < 1 + \epsilon$ .

We have proved, incidentally, that the new design method cannot, in a sense, be improved very much. With series-parallel circuits the best known limit\* for  $\lambda(n)$  is

$$\lambda(n) < 3 \cdot 2^{n-1} + 2$$

and almost all functions require  $(1 - \epsilon) \frac{2^n}{\log_2 n}$  elements.<sup>7</sup> We have lowered the order of infinity, dividing by at least  $\frac{n}{\log_2 n}$  and possibly by  $n$ . The best that can be done now is to divide by a constant factor  $\leq 4$ , and for some  $n$ ,  $\leq 2$ . The possibility of a design method which does this seems, however, quite unlikely. Of course, these remarks apply only to a perfectly general design method, i.e., one applicable to *any* function. Many special *classes* of functions can be realized by special methods with a great saving.

\* Mr. J. Riordan has pointed out an error in my reasoning in (6) leading to the statement that this limit is actually reached by the function  $X_1 \oplus X_2 \oplus \dots \oplus X_n$ , and has shown that this function and its negative can be realized with about  $n^2$  elements. The error occurs in Part IV after equation 19 and lies in the assumption that the factorization given is the best.

## PART II: CONTACT LOAD DISTRIBUTION

## 4. FUNDAMENTAL PRINCIPLES

We now consider the question of distributing the spring load on the relays as evenly as possible or, more generally, according to some preassigned scheme. It might be thought that an attempt to do this would usually result in an increase in the total number of elements over the most economical circuit. This is by no means true; we will show that in many cases (in fact, for almost all functions) a great many load distributions may be obtained (including a nearly uniform distribution) while keeping the total number of elements at the same minimum value. Incidentally this result has a bearing on the behavior of  $\mu(n)$ , for we may combine this result with

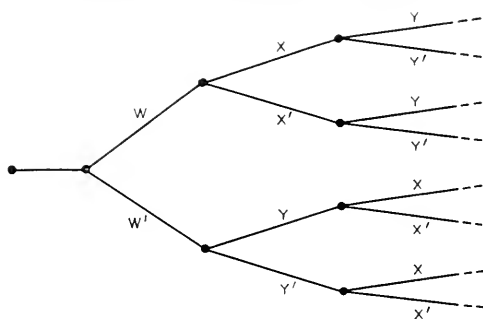


Fig. 19—Disjunctive tree with the contact distribution 1, 3, 3.

preceding theorems to show that  $\mu(n)$  is of the order of magnitude of  $\frac{2^{n+1}}{n^2}$  as  $n \rightarrow \infty$  and also to get a good evaluation of  $\mu(n)$  for small  $n$ .

The problem is rather interesting mathematically, for it involves additive number theory, a subject with few if any previous applications. Let us first consider a few simple cases. Suppose we are realizing a function with the tree of Fig. 9. The three variables appear as follows:

$W, X, Y$	appear
2, 4, 8	times, respectively.

or, in terms of transfer elements\*

1, 2, 4.

Now,  $W, X$ , and  $Y$  may be interchanged in any way without altering the operation of the tree. Also we can interchange  $X$  and  $Y$  in the lower branch of the tree only without altering its operation. This would give the distribution (Fig. 19)

1, 3, 3

\* In this section we shall always speak in terms of transfer elements.

A tree with four bays can be constructed with any of the following distributions

W	X	Y	Z
1,	2,	4,	8 = 1, 2, 4, + 1, 2, 4
1,	2,	5,	7 = 1, 2, 4 + 1, 3, 3
1,	2,	6,	6 = 1, 2, 4 + 1, 4, 2
1,	3,	3,	8 = 1, 2, 4 + 2, 1, 4
1,	3,	4,	7 = 1, 3, 3 + 2, 1, 4
1,	3,	5,	6 = 1, 4, 2 + 2, 1, 4
1,	4,	4,	6 = 1, 3, 3 + 3, 1, 3
1,	4,	5,	5 = 1, 4, 2 + 3, 1, 3

and the variables may be interchanged in any manner. The "sums" on the right show how these distributions are obtained. The first set of numbers represents the upper half of the tree and the second set the lower half. They are all reduced to the sum of sets 1, 2, 4 or 1, 3, 3 in some order, and these sets are obtainable for trees with 3 bays as we already noted. In general it is clear that if we can obtain the distributions

$$a_1, a_2, a_3, \dots, a_n$$

$$b_1, b_2, b_3, \dots, b_n$$

for a tree with  $n$  bays then we can obtain the distribution

$$1, a_1 + b_1, a_2 + b_2, \dots, a_n + b_n$$

for a tree with  $n + 1$  bays.

Now note that all the distributions shown have the following property: any one may be obtained from the first, 1, 2, 4, 8, by moving one or more units from a larger number to a smaller number, or by a succession of such operations, without moving any units to the number 1. Thus 1, 3, 3, 8 is obtained by moving a unit from 4 to 2. The set 1, 4, 5, 5 is obtained by first moving two units from the 8 to the 2, then one unit to the 4. Furthermore, every set that may be obtained from the set 1, 2, 4, 8 by this process appears as a possible distribution. This operation is somewhat analogous to heat flow—heat can only flow from a hotter body to a cooler one just as units can only be transferred from higher numbers to lower ones in the above.

These considerations suggest that a disjunctive tree with  $n$  bays can be constructed with any load distribution obtained by such a flow from the initial distribution

$$1, 2, 4, 8, \dots, 2^{n-1}$$

We will now show that this is actually the case.

First let us make the following definition: The symbol  $(a_1, a_2, \dots, a_n)$  represents any set of numbers  $b_1, b_2, \dots, b_n$  that may be obtained from the set  $a_1, a_2, \dots, a_n$  by the following operations:

1. Interchange of letters.

2. A flow from a larger number to a smaller one, no flow, however, being allowed to the number 1. Thus we would write

$$1, 2, 4, 8 = (1, 2, 4, 8)$$

$$4, 4, 1, 6 = (1, 2, 4, 8)$$

$$1, 3, 10, 3, 10 = (1, 2, 4, 8, 12)$$

but  $2, 2 \neq (1, 3)$ . It is possible to put the conditions that

$$b_1, b_2, \dots, b_n = (a_1, a_2, \dots, a_n) \quad (6)$$

into a more mathematical form. Let the  $a_i$  and the  $b_i$  be arranged as non-decreasing sequences. Then a necessary and sufficient condition for the relation (6) is that

$$(1) \quad \sum_{i=1}^s b_i \geq \sum_{i=1}^s a_i \quad s = 1, 2, \dots, n,$$

$$(2) \quad \sum_{i=1}^n b_i = \sum_{i=1}^n a_i, \quad \text{and}$$

(3) There are the same number of 1's among the  $a_i$  as among the  $b_i$ . The necessity of (2) and (3) is obvious. (1) follows from the fact that if  $a_i$  is non-decreasing, flow can only occur toward the left in the sequence

$$a_1, a_2, a_3, \dots, a_n$$

and the sum  $\sum_{i=1}^s a_i$  can only increase. Also it is easy to see the sufficiency of the condition, for if  $b_1, b_2, \dots, b_n$  satisfies (1), (2), and (3) we can get the  $b_i$  by first bringing  $a_1$  up to  $b_1$  by a flow from the  $a_i$  as close as possible to  $a_1$  (keeping the "entropy" low by a flow between elements of nearly the same value), then bringing  $a_2$  up to  $b_2$  (if necessary) etc. The details are fairly obvious.

Additive number theory, or the problem of decomposing a number into the sum of numbers satisfying certain conditions, (in our case this definition is generalized to "sets of numbers") enters through the following Lemma:

Lemma: If  $a_1, a_2, \dots, a_n = (2, 4, 8, \dots, 2^n)$  then we can decompose the  $a_i$  into the sum of two sets

$$a_i = b_i + c_i$$

such that

$$b_1, b_2, \dots, b_n = (1, 2, 4, \dots, 2^{n-1})$$

and

$$c_1, c_2, \dots, c_n = (1, 2, 4, \dots, 2^{n-1})$$

We may assume the  $a_i$  arranged in a non-decreasing sequence,  $a_1 \leq a_2 \leq a_3 \leq \dots \leq a_n$ . In case  $a_1 = 2$  the proof is easy. We have

$$\begin{array}{rcl} 1, 2, 4, \dots, 2^{n-1} & & B \\ 1, 2, 4, \dots, 2^{n-1} & & C \\ \hline 2, 4, 8, \dots, 2^n & & A \end{array}$$

and a flow has occurred in the set

$$4, 8, 16, \dots, 2^n$$

to give  $a_2, a_3, \dots, a_n$ . Now any permissible flow in C corresponds to a permissible flow in either A or B since if

$$c_j = a_j + b_j > c_i = a_i + b_i$$

then either

$$a_j > a_i \quad \text{or} \quad b_j > b_i$$

Thus at each flow in the sum we can make a corresponding flow in one or the other of the summands to keep the addition true.

Now suppose  $a_1 > 2$ . Since the  $a_i$  are non-decreasing

$$(n-1)a_2 \leq (2^{n+1} - 2) - a_1 \leq 2^{n+1} - 2 - 3$$

Hence

$$a_2 - 1 \leq \frac{2^{n+1} - 5}{n-1} - 1 \leq 2^{n-1}$$

the last inequality being obvious for  $n \geq 5$  and readily verified for  $n < 5$ . This shows that  $(a_1 - 1)$  and  $(a_2 - 1)$  lie between some powers of two in the set

$$1, 2, 4, \dots, 2^{n-1}$$

Suppose

$$2^{q-1} < (a_1 - 1) \leq 2^q$$

$$2^{p-1} < (a_2 - 1) \leq 2^p \quad q \leq p \leq (n-1).$$

Allow a flow between  $2^q$  and  $2^{q-1}$  until one of them reaches  $(a_1 - 1)$ , the other (say)  $R$ ; similarly for  $(a_2 - 1)$  the other reaching  $S$ . As the start toward our decomposition, then, we have the sets (after interchanges)

$$\begin{array}{ccccccc} & & L & & & & \\ (a_1 - 1) & 1 & 2, 4 \dots 2^{q-2} & R & 2^{q+1} \dots 2^{p-1} 2^p & 2^{p+1} \dots 2^{n-1} & \\ 1 & a_2 - 1 & 2, 4 \dots 2^{q-2} & 2^{q-1} & 2^q \dots 2^{p-2} S & 2^{p+1} \dots 2^{n-1} & \\ \hline a_1 & a_2 & 4, 8 \dots 2^{q-1} & \dots & & 2^{p+2} \dots 2^n & \\ & & L & & & & \end{array}$$

We must now adjust the values to the right of  $L - L$  to the values  $a_3, a_4, \dots, a_n$ . Let us denote the sequence

$$4, 8, \dots, 2^{q-1}, (2^{q-1} + R), 3 \cdot 2^q, 3 \cdot 2^{q+1}, \dots, (2^p + S), 2^{p+2}, \dots, 2^n$$

by  $\mu_1, \mu_2, \dots, \mu_{n-2}$ . Now since all the rows in the above addition are non-decreasing to the right of  $L - L$ , and no 1's appear, we will have proved the lemma if we can show that

$$\sum_{i=1}^i \mu_i \leq \sum_{i=3}^{i+3} a_i \quad i = 1, 2, \dots, (n-2)$$

since we have shown this to be a sufficient condition that

$$a_3, a_4, \dots, a_n = (\mu_1, \mu_n, \dots, \mu_{n-2})$$

and the decomposition proof we used for the first part will work. For  $i \leq q-2$ , i.e., before the term  $(2^{q-1} + R)$

$$\sum_{i=1}^i \mu_i = 4(2^i - 1)$$

and

$$\sum_3^{i+3} a_i \geq ia_2 \geq i2^{p-1} \geq i2^{q-1}$$

since

$$q \leq p$$

Hence

$$\sum_1^i u_i \leq \sum_3^{i+3} a_i \quad i \leq q-2$$

Next, for  $(q-1) \leq i \leq (p-3)$ , i.e., before the term  $(2^p + S)$

$$\begin{aligned} \sum_1^i \mu_i &= 4(2^{q-1} - 1) + R + 3 \cdot 2^q(2^{i-q+1} - 1) \\ &< 3 \cdot 2^{i+1} - 4 \leq 3 \cdot 2^{i+1} - 5 \end{aligned}$$

since

$$R < 2^q$$

also again

$$\sum_3^{i+3} a_i \geq i2^{p-1}$$

so that in this interval we also have the desired inequality. Finally for the last interval,

$$\sum_1^i \mu_i = 2^{i-1} - a_1 - a_2 \leq 2^{i+3} - a_1 - a_2 - 2$$

and

$$\sum_3^{i+3} a_i = \sum_1^{i+3} a_i - a_1 - a_2 \geq 2^{i+3} - a_1 - a_2 - 2$$

since

$$a_1, a_2, \dots, a_n = (2, 4, 8, \dots, 2^n)$$

This proves the lemma.

## 5. THE DISJUNCTIVE TREE

It is now easy to prove the following:

*Theorem 8: A disjunctive tree of  $n$  bays can be constructed with any distribution*

$$a_1, a_2, \dots, a_n = (1, 2, 4, \dots, 2^{n-1}).$$

We may prove this by induction. We have seen it to be true for  $n = 2, 3, 4$ . Assuming it for  $n$ , it must be true for  $n + 1$  since the Lemma shows that any

$$a_1, a_2, \dots, a_n = (2, 4, 8, \dots, 2^n)$$

can be decomposed into a sum which, by assumption, can be realized for the two branches of the tree.

It is clear that among the possible distributions

$$(1, 2, 4, \dots, 2^{n-1})$$

for the tree, an "almost uniform" one can be found for all the variables but one. That is, we can distribute the load on  $(n - 1)$  of them uniformly except at worst for one element. We get, in fact, for

$n = 1$	1
$n = 2$	1, 2
$n = 3$	1, 3, 3
$n = 4$	1, 4, 5, 5,
$n = 5$	1, 7, 7, 8, 8,
$n = 6$	1, 12, 12, 12, 13, 13
$n = 7$	1, 21, 21, 21, 21, 21, 21
	etc.

as nearly uniform distributions.

## 6. OTHER DISTRIBUTION PROBLEMS

Now let us consider the problem of load distribution in series-parallel circuits. We shall prove the following:



*Theorem 9: Any function  $f(X_1, X_2, \dots, X_n)$  may be realized with a series-parallel circuit with the following distribution:*

$$(1, 2, 4, \dots, 2^{n-2}), 2^{n-2}$$

*in terms of transfer elements.*

This we prove by induction. It is true for  $n = 3$ , since any function of three variables can be realized as follows:

$$f(X, Y, Z) = [X + f_1(Y, Z)][X' + f_2(Y, Z)]$$

and  $f_1(Y, Z)$  and  $f_2(Y, Z)$  can each be realized with one transfer on  $Y$  and one on  $Z$ . Thus  $f(X, Y, Z)$  can be realized with the distribution 1, 2, 2. Now assuming the theorem true for  $(n - 1)$  we have

$$f(X_1, X_2, \dots, X_n) = [X_n + f_1(X_1, X_2, \dots, X_{n-1})] \\ [X'_n + f_2(X_1, X_2, \dots, X_{n-1})]$$

and

$$\begin{array}{c} 2, 4, 8, \dots, 2^{n-3} \\ 2, 4, 8, \dots, 2^{n-3} \\ \hline 4, 8, 16, \dots, 2^{n-2} \end{array}$$

A simple application of the Lemma thus gives the desired result. Many distributions beside those given by Theorem 9 are possible but no simple criterion has yet been found for describing them. We cannot say any distribution

$$(1, 2, 4, 8, \dots, 2^{n-2}, 2^{n-2})$$

(at least from our analysis) since for example

$$3, 6, 6, 7 = (2, 4, 8, 8)$$

cannot be decomposed into two sets

$$a_1, a_2, a_3, a_4 = (1, 2, 4, 4)$$

and

$$b_1, b_2, b_3, b_4 = (1, 2, 4, 4)$$

It appears, however, that the almost uniform case is admissible.

As a final example in load distribution we will consider the case of a network in which a number of trees in the same variables are to be realized. A large number of such cases will be found later. The following is fairly obvious from what we have already proved.

*Theorem 10: It is possible to construct  $m$  different trees in the same  $n$  variables with the following distribution:*

$$a_1, a_2, \dots, a_n = (m, 2m, 4m, \dots, 2^{n-1}m)$$

It is interesting to note that under these conditions the bothersome 1 disappears for  $m > 1$ . We can equalize the load on all  $n$  of the variables, not just  $n - 1$  of them, to within, at worst, one transfer element.

## 7. THE FUNCTION $\mu(n)$

We are now in a position to study the behavior of the function  $\mu(n)$ . This will be done in conjunction with a treatment of the load distributions possible for the general function of  $n$  variables. We have already shown that any function of three variables can be realized with the distribution

$$1, 1, 2$$

in terms of transfer elements, and, consequently  $\mu(3) \leq 4$ .

Any function of four variables can be realized with the distribution

$$1, 1, (2, 4)$$

Hence  $\mu(4) \leq 6$ . For five variables we can get the distribution

$$1, 1, (2, 4, 8)$$

or alternatively

$$1, 5, 5, (2, 4)$$

so that  $\mu(5) \leq 10$ . With six variables we can get

$$1, 5, 5, (2, 4, 8) \text{ and } \mu(6) \leq 10$$

for seven,

$$1, 5, 5, (2, 4, 8, 16) \text{ and } \mu(7) \leq 16$$

etc. Also, since we can distribute uniformly on all the variables in a tree except one, it is possible to give a theorem analogous to Theorem 7 for the function  $\mu(n)$ :

*Theorem 11: For all  $n$*

$$\mu(n) \leq \frac{2^{n+3}}{n^2}$$

*For almost all  $n$*

$$\mu(n) \leq \frac{2^{n+2}}{n^2}$$

For an infinite number of  $n_i$ ,

$$\mu(n) \leq (1 + \epsilon) \frac{2^{n+1}}{n^2}$$

The proof is direct and will be omitted.

### PART III: SPECIAL FUNCTIONS

#### 8. FUNCTIONAL RELATIONS

We have seen that almost all functions require the order of

$$\frac{2^{n+1}}{n^2}$$

elements per relay for their realization. Yet a little experience with the circuits encountered in practice shows that this figure is much too large. In a sender, for example, where many functions are realized, some of them involving a large number of variables, the relays carry an average of perhaps 7 or 8 contacts. In fact, almost all relays encountered in practice have less than 20 elements. What is the reason for this paradox? The answer, of course, is that the functions encountered in practice are far from being a random selection. Again we have an analogue with transcendental numbers—although almost all numbers are transcendental, the chance of first encountering a transcendental number on opening a mathematics book at random is certainly much less than 1. The functions actually encountered are simpler than the general run of Boolean functions for at least two major reasons:

(1) A circuit designer has considerable freedom in the choice of functions to be realized in a given design problem, and can often choose fairly simple ones. For example, in designing translation circuits for telephone work it is common to use additive codes and also codes in which the same number of relays are operated for each possible digit. The fundamental logical simplicity of these codes reflects in a simplicity of the circuits necessary to handle them.

(2) Most of the things required of relay circuits are of a logically simple nature. The most important aspect of this simplicity is that most circuits can be broken down into a large number of small circuits. In place of realizing a function of a large number of variables, we realize many functions, each of a small number of variables, and then perhaps some function of these functions. To get an idea of the effectiveness of this consider the following example: Suppose we are to realize a function

$$f(X_1, X_2, \dots, X_{2n})$$

of  $2n$  variables. The best limit we can put on the total number of elements necessary is about  $\frac{2^{2n+1}}{2n}$ . However, if we know that  $f$  is a function of two functions  $f_1$  and  $f_2$ , each involving only  $n$  of the variables, i.e. if

$$f = g(f_1, f_2)$$

$$f_1 = f_1(X_1, X_2, \dots, X_n)$$

$$f_2 = f_2(X_{n+1}, X_{n+2}, \dots, X_{2n})$$

then we can realize  $f$  with about

$$4 \cdot \frac{2^{n+1}}{n}$$

elements, a much lower order of infinity than  $\frac{2^{2n+1}}{2n}$ . If  $g$  is one of the simpler functions of two variables; for example if  $g(f_1, f_2) = f_1 + f_2'$ , or in any case at the cost of two additional relays, we can do still better and realize  $f$  with about  $2 \frac{2^{n+1}}{n}$  elements. In general, the more we can decompose a synthesis problem into a combination of simple problems, the simpler the final circuits. The significant point here is that, due to the fact that  $f$  satisfies a certain functional relation

$$f = g(f_1, f_2),$$

we can find a simple circuit for it compared to the average function of the same number of variables.

This type of functional relation may be called functional separability. It is often easily detected in the circuit requirements and can always be used to reduce the limits on the number of elements required. We will now show that most functions are not functionally separable.

*Theorem 12: The fraction of all functions of  $n$  variables that can be written in the form*

$$f = g(h(X_1 \cdots X_s), X_{s+1}, \dots, X_n)$$

*where  $1 < s < n - 1$  approaches zero as  $n$  approaches  $\infty$ .*

We can select the  $s$  variables to appear in  $h$  in  $\binom{n}{s}$  ways; the function  $h$  then has  $2^{2^s}$  possibilities and  $g$  has  $2^{2^{n-s+1}}$  possibilities, since it has  $n - s + 1$  arguments. The total number of functionally separable functions is therefore dominated by

$$\sum_{s=2}^{n-2} \binom{n}{s} 2^{2^s} 2^{2^{n-s}+1}$$

$$\leq (n-3) \frac{n^2}{2} 2^{2^2} 2^{2^{n-1}}$$

and the ratio of this to  $2^{2^n} \rightarrow 0$  as  $n \rightarrow \infty$ .

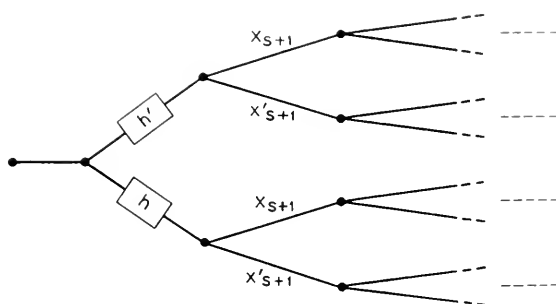


Fig. 20—Use of separability to reduce number of elements.

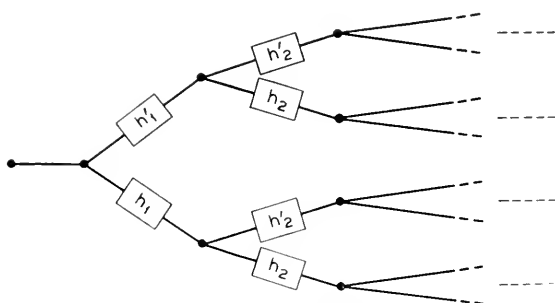


Fig. 21—Use of separability of two sets of variables.

In case such a functional separability occurs, the general design method described above can be used to advantage in many cases. This is typified by the circuit of Fig. 20. If the separability is more extensive, e.g.

$$f = g(h_1(X_1 \cdots X_s), h_2(X_{s+1} \cdots X_t), X_{t+1}, \cdots, X_n)$$

the circuit of Fig. 21 can be used, using for " $h_2$ " either  $h_1$  or  $h_2$ , whichever requires the least number of elements for realization together with its negative.

We will now consider a second type of functional relation which often occurs in practice and aids in economical realization. This type of relation may be called group invariance and a special case of it, functions symmetric

in all variables, has been considered in (6). A function  $f(X_1, \dots, X_n)$  will be said to be symmetric in  $X_1, X_2$  if it satisfies the relation

$$f(X_1, X_2, \dots, X_n) = f(X_2, X_1, \dots, X_n).$$

It is symmetric in  $X_1$  and  $X'_2$  if it satisfies the equation

$$f(X_1, X_2, \dots, X_n) = f(X'_2, X'_1, X_3, \dots, X_n)$$

These also are special cases of the type of functional relationships we will consider. Let us denote by

$N_{oo} \dots o = I$  the operation of leaving the variables in a function as they are,

$N_{1oo} \dots o$  the operation of negating the first variable (i.e. the one occupying the first position),

$N_{o1o} \dots o$  that of negating the second variable,

$N_{11o} \dots o$  that of negating the first two, etc.

So that  $N_{1o1}f(X, Y, Z) = f(X'YZ')$  etc.

The symbols  $Ni$  form an abelian group, with the important property that each element is its own inverse;  $NiNi = I$ . The product of two elements may be easily found — if  $N_iN_j = N_k$ ,  $k$  is the number found by adding  $i$  and  $j$  as though they were numbers in the base two but *without carrying*.

Note that there are  $2^n$  elements to this “negating” group. Now let  $S_{1,2,3,\dots,n} = I =$  the operation of leaving the variables of a function in the same order

$S_{2,1,3,\dots,n} =$  be that of interchanging the first two variables

$S_{3,2,1,4,\dots,n} =$  that of inverting the order of the first three, etc.

Thus

$$S_{312}f(X, Y, Z) = f(Z, X, Y)$$

$$S_{312}f(Z, X, Y) = S_{312}^2f(X, Y, Z) = f(Y, Z, X)$$

etc. The  $S_i$  also form a group, the famous “substitution” or “symmetric” group. It is of order  $n!$ . It does not, however, have the simple properties of the negating group—it is not abelian ( $n > 2$ ) nor does it have the self inverse property.\* The negating group is not cyclic if  $n > 2$ , the symmetric group is not if  $n > 3$ .

The outer product of these two groups forms a group  $G$  whose general element is of the form  $N_iS_j$  and since  $i$  may assume  $2^n$  values and  $j, n!$  values, the order of  $G$  is  $2^n n!$ .

It is easily seen that  $S_jN_i = N_kS_j$ , where  $k$  may be obtained by per-

\* This is redundant; the self inverse property implies commutativity for if  $XX = I$  then  $XY = (XY)^{-1} = Y^{-1}X^{-1} = YX$ .

forming on  $i$ , considered as an ordered sequence of zero's and one's, the permutation  $S_i$ . Thus

$$S_{2314} N_{1100} = N_{1010} S_{2314}.$$

By this rule any product such as  $N_i S_j N_k N_l S_m N_n S_p$  can be reduced to the form

$$N_i N_j \cdots N_n S_p S_q \cdots S_r$$

and this can then be reduced to the standard form  $N_i S_j$ .

A function  $f$  will be said to have a non-trivial group invariance if there are elements  $N_i S_j$  of  $G$  other than  $I$  such that identically in all variables

$$N_i S_i f = f.$$

It is evident that the set of all such elements,  $N_i S_j$ , for a given function, forms a subgroup  $G_1$  of  $G$ , since the product of two such elements is an element, the inverse of such an element is an element, and all functions are invariant under  $I$ .

A group operator leaving a function  $f$  invariant implies certain equalities among the terms appearing in the expanded form of  $f$ . To show this, consider a fixed  $X_i S_j$ , which changes in some way the variables (say)  $X_1, X_2, \dots, X_r$ . Let the function  $f(X_1, \dots, X_n)$  be expanded about  $X_1, \dots, X_r$ :

$$\begin{aligned} f = & [X_1 + X_2 + \cdots + X_r + f_1(X_{r+1}, \cdots, X_n)] \\ & [X'_1 + X_2 + \cdots + X_r + f_2(X_{r+1}, \cdots, X_n)] \\ & \dots \dots \dots \\ & [X'_1 + X'_2 + \cdots + X'_r + f_r(X_{r+1}, \cdots, X_n)] \end{aligned}$$

If  $f$  satisfies  $N_i S_j f = f$  we will show that there are at least  $\frac{1}{4} 2^r$  equalities between the functions  $f_1, f_2, \dots, f_{2^r}$ . Thus the number of functions satisfying this relation is

$$< (2^{2n-r})^{\frac{2r}{4}} = 2^{\frac{2rn}{4}}$$

since each independent  $f_i$  can be any of just  $2^{2^{n-r}}$  functions, and there are at most  $\frac{3}{4} 2^r$  independent ones. Suppose  $N_i S_i$  changes

$$X_1, X_2, \dots, X_r \quad A$$

into

$$X_{a_1}^*, X_{a_2}^*, \dots, X_{a_r}^* \quad \text{B}$$

where the  $*$ 's may be either primes or non primes, but no  $X_{a_i}^* = X_i$ . Give

$X_1$  the value 0. This fixes some element in B namely,  $X_{a_i}$  where  $a_i = 1$ . There are two cases:

(1) If this element is the first term,  $a_1 = 1$ , then we have

$$\begin{aligned} 0 X_2, \dots, X_r \\ 1 X_{a_1}, \dots, X_{a_r} \end{aligned}$$

Letting  $X_2, \dots, X_r$  range through their  $2^{r-1}$  possible sets of values gives  $2^{r-1}$  equalities between different functions of the set  $f_i$  since these are really

$$f(X_1, X_2, \dots, X_r, X_{r+1}, \dots, X_n)$$

with  $X_1, X_2, \dots, X_r$  fixed at a definite set of values.

(2) If the element in question is another term, say  $X_{a_2}$ , we then give  $X_2$  in line A the opposite value,  $X_2 = (X_{a_2}^*)' = (X_2^*)'$ . Now proceeding as before with the remaining  $r - 2$  variables we establish  $2^{r-2}$  equalities between the  $f_i$ .

Now there are not more\* than  $2^n n!$  relations

$$N_i S_j f = f$$

of the group invariant type that a function could satisfy, so that the number of functions satisfying any non-trivial relation

$$\leq 2^n n! 2^{2^n}.$$

Since

$$2^n n! 2^{2^n} / 2^{2^n} \rightarrow 0 \quad \text{as } n \rightarrow \infty$$

we have:

*Theorem 13: Almost all functions have no non-trivial group invariance.*

It appears from Theorems 12 and 13 and from other results that almost all functions are of an extremely chaotic nature, exhibiting no symmetries or functional relations of any kind. This result might be anticipated from the fact that such relations generally lead to a considerable reduction in the number of elements required, and we have seen that almost all functions are fairly high in "complexity".

If we are synthesizing a function by the disjunctive tree method and the function has a group invariance involving the variables

$$X_1, X_2, \dots, X_r$$

at least  $2^{r-2}$  of the terminals in the corresponding tree can be connected to

\* Our factor is really less than this because, first, we must exclude  $N_i S_j = I$ ; and second, except for self inverse elements, one relation of this type implies others, viz. the powers  $(N_i S_j)^p f = f$ .



other ones, since at least this many equalities exist between the functions to be joined to these terminals. This will, in general, produce a considerable reduction in the contact requirements on the remaining variables. Also an economy can usually be achieved in the  $M$  network. In order to apply this

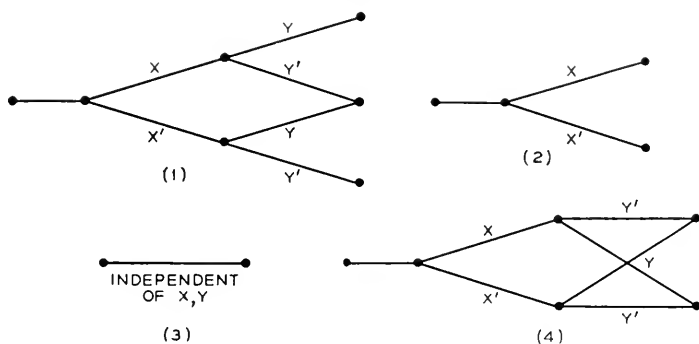


Fig. 22—Networks for group invariance in two variables.

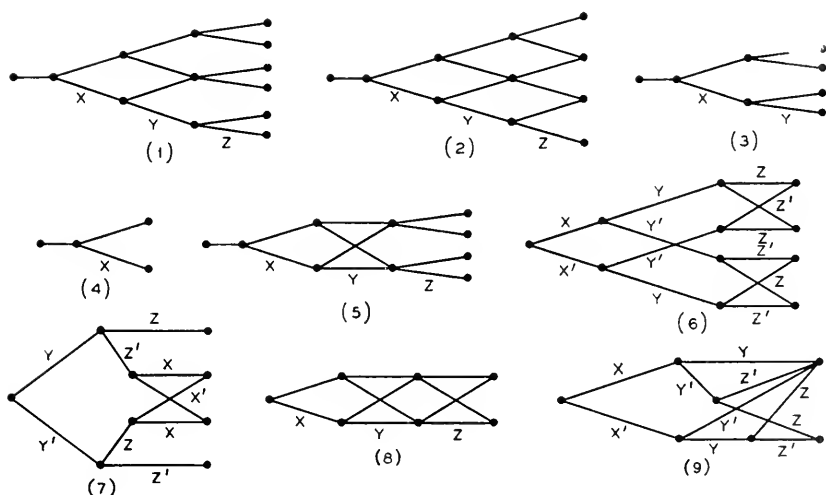


Fig. 23—Networks for group invariance in three variables.

method of design, however, it is essential that we have a method of determining which, if any, of the  $N_i S_j$  leave a function unchanged. The following theorem, although not all that might be hoped for, shows that we don't need to evaluate  $N_i S_j f$  for all  $N_i S_j$  but only the  $N_i f$  and  $S_j f$ .

*Theorem 14: A necessary and sufficient condition that  $N_i S_j f = f$  is that  $N_i f = S_j f$ .*

This follows immediately from the self inverse property of the  $N_i$ . Of

course, group invariance can often be recognized directly from circuit requirements in a design problem.

Tables I and II have been constructed for cases where a relation exists involving two or three variables. To illustrate their use, suppose we have a function such that

$$N_{111}S_{312}f = f$$

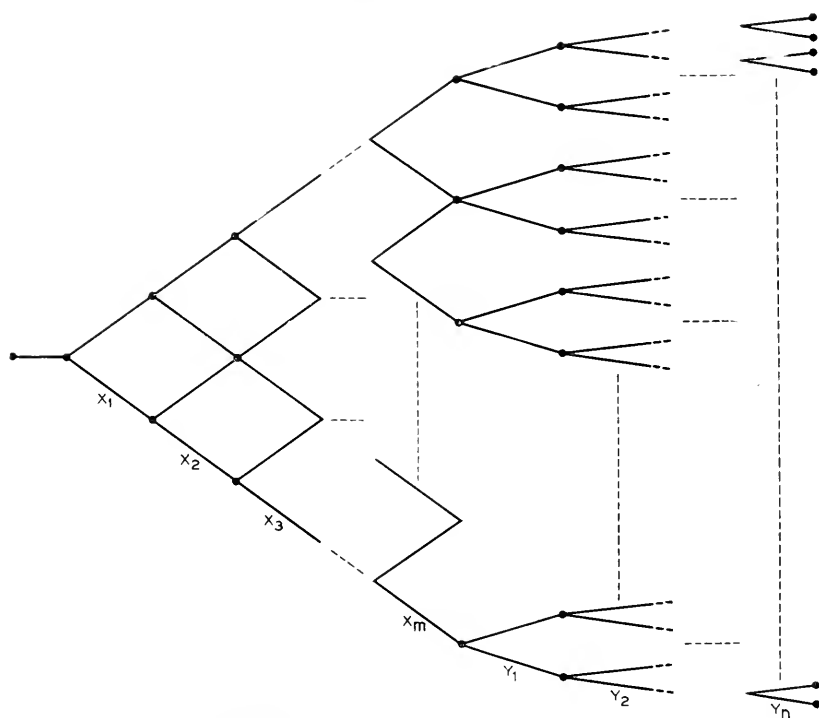


Fig. 24— $M$  network for partially symmetric functions.

The corresponding entry  $Z'Y'X$  in the group table refers us to circuit 9 of Fig. 23. The asterisk shows that the circuit may be used directly; if there is no asterisk an interchange of variables is required. We expand  $f$  about  $X, Y, Z$  and only two different functions will appear in the factors. These two functions are realized with two trees extending from the terminals of the network 9. Any such function  $f$  can be realized with (using just one variable in the  $N$  network)

$$\begin{aligned} & 9 + 2(2^{n-4} - 2) + 2 \\ & = 2^{n-3} + 7 \quad \text{elements,} \end{aligned}$$



and  $S_k(X_1, X_2, \dots, X_m)$  is the symmetric function of  $X_1, X_2, \dots, X_n$  with  $k$  for its only  $a$ -number.

This theorem follows from the fact that since  $f$  is symmetric in  $X_1, X_2, \dots, X_m$  the value of  $f$  depends only on the number of  $X$ 's that are zero and the values of the  $Y$ 's. If exactly  $K$  of the  $X$ 's are zero the value of  $f$  is therefore  $f_K$ , but the right-hand side of (6) reduces to  $f_K$  in this case, since then  $S_j(X_1, X_2, \dots, X_m) = 1, j \neq K$ , and  $S_K = 0$ .

The expansion (6) is of a form suitable for our design method. We can realize the disjunctive functions  $S_K(X_1, X_2, \dots, X_m)$  with the symmetric function lattice and continue with the general tree network as in Fig. 24, one tree from each level of the symmetric function network. Stopping the trees at  $Y_{n-1}$ , it is clear that the entire network is disjunctive and a second application of Theorem 1 allows us to complete the function  $f$  with two elements from  $Y_n$ . Thus we have

*Theorem 16.* Any function of  $m + n$  variables symmetric in  $m$  of them can be realized with not more than the smaller of

$$(m + 1)(\lambda(n) + m) \text{ or } (m + 1)(2^n + m - 2) + 2$$

elements. In particular a function of  $n$  variables symmetric in  $n - 2$  or more of them can be realized with not more than

$$n^2 - n + 2$$

elements.

If the function is symmetric in  $X_1, X_2, \dots, X_m$ , and also in  $Y_1, Y_2, \dots, Y_r$ , and not in  $Z_1, Z_2, \dots, Z_n$  it may be realized by the same method, using symmetric function networks in place of trees for the  $Y$  variables. It should be expanded first about the  $X$ 's (assuming  $m < r$ ) then about the  $Y$ 's and finally the  $Z$ 's. The  $Z$  part will be a set of  $(m + 1)(r + 1)$  trees.

#### REFERENCES

1. G. Birkhoff and S. MacLane, "A Survey of Modern Algebra," Macmillan, 1941.
2. L. Couturat, "The Algebra of Logic," Open Court, 1914.
3. J. H. Woodger, "The Axiomatic Method in Biology," Cambridge, 1937.
4. W. S. McCulloch and W. Pitts, "A Logical Calculus of the Ideas Immanent in Nervous Activity," *Bull. Math. Biophysics*, V. 5, p. 115, 1943.
5. E. C. Berkeley, "Boolean Algebra and Applications to Insurance," *Record (American Institute of Actuaries)*, V. 26, p. 373, 1947.
6. C. E. Shannon, "A Symbolic Analysis of Relay and Switching Circuits," *Trans. A. I. E. E.*, V. 57, p. 713, 1938.
7. J. Riordan and C. E. Shannon, "The Number of Two-Terminal Series Parallel Networks," *Journal of Mathematics and Physics*, V. 21, No. 2, p. 83, 1942.
8. A. Nakashima, Various papers in *Nippon Electrical Communication Engineering*, April, Sept., Nov., Dec., 1938.
9. H. Piesch, Papers in Archiv. from *Electrotechnik* XXXIII, p. 692 and p. 733, 1939.
10. G. A. Montgomerie, "Sketch for an Algebra of Relay and Contactor Circuits," *Jour. I. of E. E.*, V. 95, Part III, No. 36, July 1948, p. 303.
11. G. Pólya, "Sur Les Types des Propositions Composées," *Journal of Symbolic Logic*, V. 5, No. 3, p. 98, 1940.

## A Method of Measuring Phase at Microwave Frequencies

By SLOAN D. ROBERTSON

A method of measuring microwave phase differences is described in which it is unnecessary to compensate for amplitude inequalities between the signals whose phases are being compared. The apparatus described is also suited for the measurement of the magnitude of a transfer impedance as well as the phase.

WITH the increasing interest in wide-band amplifiers and circuits for microwave communication systems the measurement of the transfer phases of such components has become a necessary procedure. A commonly used technique for measuring phase at microwave frequencies is to sample the signal at the input and output of the device to be measured and to obtain a null balance between the two signals by varying the phase of one signal by a known amount. If the two samples are not of nearly equal amplitudes, it is necessary to attenuate the larger one with an attenuator of known phase shift. The latter operation presents difficulties.

A method of phase measurement has been developed which overcomes these difficulties by permitting measurements to be made with samples of unequal amplitudes. The method uses the homodyne detection principle and operates in the following manner: The output energy of a signal oscillator is divided into two portions. One portion is applied to a balanced modulator where it is modulated by an audio-frequency signal. The suppressed-carrier, double-sideband signal from the modulator is applied to the device to be measured. As before, means are available for sampling the signal at both the input and output of the device. The other portion of the oscillator power is fed through a calibrated phase shifter and is applied to a crystal detector in the manner of a local oscillator in a double-detection receiver. The signal samples are then alternately applied to the crystal detector where they are demodulated by the action of the homodyne carrier. In each case the phase shifter is adjusted so that the audio signal is a minimum in the detector output. This occurs when the phase of the homodyne carrier is in quadrature with the signal sidebands. The difference in phase between the two adjustments of the phase shifter is equal to the phase difference between the two samples.

Figure 1 shows the apparatus used for measuring phase in this manner. Radio frequency power from a suitable oscillator is applied to the H-plane branch of an hybrid junction<sup>1</sup> where it divides and emerges in equal portions

<sup>1</sup> W. A. Tyrrell, "Hybrid Circuits for Microwaves," *Proc. I. R. E.*, Vol. 35, No. 11, pp. 1294-1306; November 1947.

from the two lateral branches. The portion applied to the calibrated variable phase shifter at the top of the figure becomes the homodyne carrier. The remaining portion is applied to a balanced crystal modulator<sup>2</sup> through a second variable phase shifter which need not be calibrated. The latter was introduced in order that the phase of any modulated power reflected due to an imperfect balance in the modulator could be shifted so that it would be in quadrature with the homodyne carrier and would, therefore, not produce an audible signal in the detector.

The portion of the power which enters the modulator is modulated by a signal derived from an audio-frequency oscillator. The suppressed-carrier, double-sideband signal which leaves the modulator is applied, after a certain amount of attenuation, to the input of the device to be measured. Probes are provided at the input and output of the latter for sampling the signal. Provision is made for connecting either probe to a crystal detector of the type used for detecting an amplitude-modulated signal.

The homodyne carrier emerging from the calibrated phase shifter is attenuated to a level of about one milliwatt and is applied to the crystal detector. The output of the detector is connected to an audio-frequency amplifier terminated by a pair of headphones or an output meter. An attenuator may be placed between the amplifier and the detector as an aid in measuring the magnitude of a transfer impedance.

The procedure for adjusting the apparatus and measuring phase is as follows:

With both sampling probes disconnected from the detector the variable phase shifter between the oscillator and modulator is adjusted until the output of the detector is zero. This balances out the effect of any signal reflected by the modulator. The input probe is then connected to the detector and the calibrated phase shifter is adjusted until the signal disappears in the audio output. When this occurs the homodyne carrier is in quadrature with the signal sidebands, and the resultant signal applied to the detector is equivalent to a phase-modulated wave having a low modulation index, and consequently is not demodulated by a detector of the type used here.

The input probe is then disconnected from the detector and the output probe connected. The phase shifter is again adjusted for a null in the audio output. The difference in phase between the two adjustments of the phase shifter is equal to the phase shift between the input and output of the device. If the probes are not located exactly at the input and output terminals of the unknown it may be necessary to make a correction in the meas-

<sup>2</sup> C. F. Edwards, "Microwave Converters," *Proc. I. R. E.*, Vol. 35, No. 11, pp. 1181-1191; November 1947.

ured phase by allowing for the known phase shift in the line between the probes and the actual terminals of the unknown.

So much for the general method. Certain precautions are necessary in order to avoid errors in measurement. In practice the carrier is not completely suppressed in the output of the balanced modulator. It may be at a

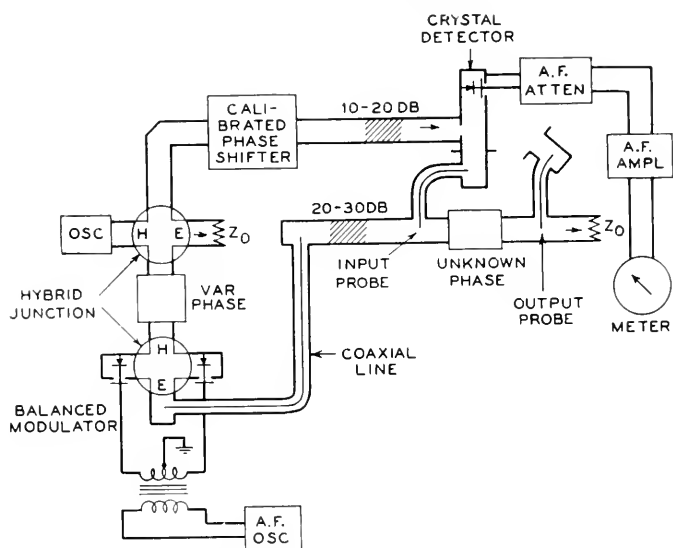


Fig. 1—Schematic circuit for microwave phase measurement.

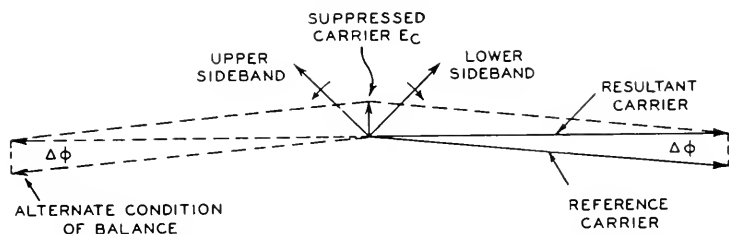


Fig. 2—Vector diagram of balanced condition with the resultant carrier in quadrature with the signal sideband.

level of the order of 10 to 20 decibels below the sidebands. Since the residual carrier will be added to the homodyne carrier in the detector, and since the null adjustment will be reached when the *resultant* carrier is in quadrature with the sidebands, it is desirable that the residual carrier be low in level compared with the homodyne carrier. The error in phase  $\Delta\phi$  introduced by the residual carrier is shown in the vector diagram of Fig. 2. A difference in level of about 40 decibels between the homodyne and residual carriers will give an error of not more than half a degree in phase. The

homodyne method of detection has all the conversion efficiency of the usual double-detection arrangements and, in addition, has the advantage in this particular application of having a very low noise level due to the relatively narrow band required for the audio signals. The 40-decibel level difference mentioned above is accordingly not a serious handicap.

Other precautions must be observed. The homodyne carrier can be brought in quadrature with the signal for two different phases  $180^\circ$  apart. This is illustrated in Fig. 2. In many applications, where only the variation

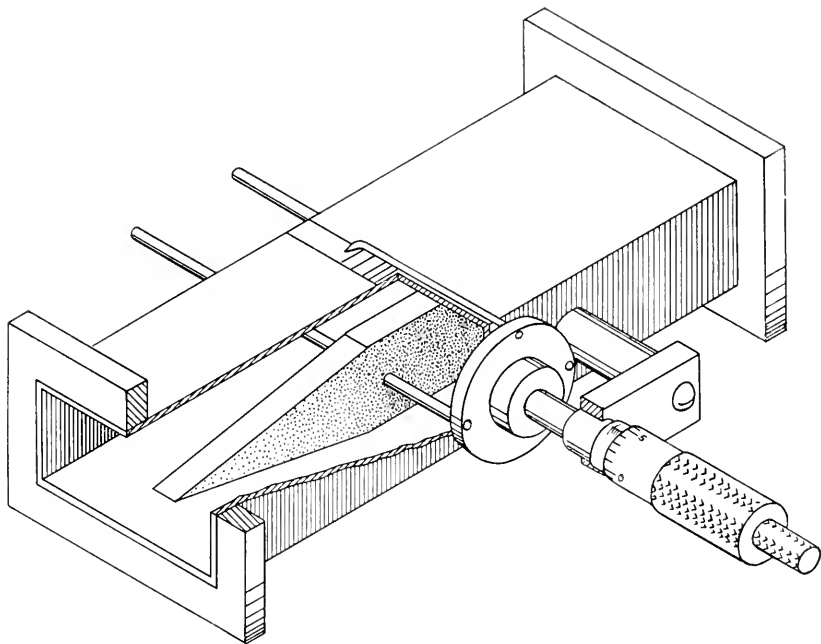


Fig. 3—Variable phase shifter using a polystyrene vane.

in phase difference is of importance, this uncertainty of  $180^\circ$  can be ignored. The correct setting of the homodyne carrier phase can, however, be determined very easily. Assume that the input probe is connected to the receiver and that the phase has been adjusted for a balance. Then disconnect the audio frequency drive from one of the crystals in the balanced modulator. The residual carrier will now no longer be suppressed and the error angle  $\Delta\phi$  of Fig. 2 will become larger. Whether the homodyne carrier is lagging or leading the signal carrier can be determined by observing whether more or less phase shift, respectively, must be introduced to restore balance. A similar test performed with the output probe will indicate whether or not it is necessary to add  $180^\circ$  to the measured phase difference. If either probe



test indicates a lead, whereas the other probe indicates a lag, then the addition of  $180^\circ$  is indicated.

In microwave circuits it frequently happens that the transfer phase varies quite rapidly with the frequency, particularly if some part of the circuit is at or near resonance. In measuring the phase characteristics of a circuit of this type over a band of frequencies it is necessary, therefore, to take the points of measurement close enough together to avoid phase errors corresponding to multiples of  $360^\circ$ .

When a balance has been established so that the signal is minimized in the detector output, one may observe the presence of the second harmonic of the audio tone. This harmonic is a distortion term generated in the detector. If it is objectionable, it can be eliminated either by a low-pass filter in the audio output, or by using a balanced detector.

In measuring transfer impedances it is desirable to know the ratio of the magnitudes of an output voltage and an input voltage as well as the phase difference. The equipment described here can be used for measuring amplitudes by adjusting the phase shifter for a maximum signal in the audio output. Maximum signal levels can then be compared with the aid of an audio-frequency attenuator and output meter connected as shown in Fig. 1.

The apparatus was assembled with standard 4000-megacycle waveguide components. A satisfactory phase shifter was made of an ordinary vane-type variable attenuator by replacing the resistance strip with a vane of quarter-inch thick polystyrene six inches in length. This phase shifter gave a total shift of about  $100^\circ$ . Constructional details of this phase shifter are shown in Fig. 3. Other phase shifters could have been used with equally satisfactory results. It is desirable, however, that the phase shifter be impedance matched to the line in which it is located in order that reaction back on the oscillator shall be a minimum. In the shifter of Fig. 3 the ends of the polystyrene vane have been tapered two inches at each end to accomplish this result.

The phase shifter can be readily calibrated by using a standing wave detector fitted with a sliding probe as a standard of phase. The standing wave detector is terminated on one end and connected to the modulated signal source on the other. The signal picked up by the sliding probe is applied to the crystal detector. Knowing the guide wavelength in the standing wave detector, known phase shifts can be introduced by sliding the probe along the guide. By adjusting the phase shifter in the homodyne carrier path for balance, calibration points can be established.

The measuring procedure described above has been tested experimentally at 4000 megacycles with very satisfactory results. With ordinary care it was possible to measure phase differences with an accuracy of better than half a degree.

# Reflection from Corners in Rectangular Wave Guides— Conformal Transformation\*

By S. O. RICE

A conformal transformation method is used to obtain approximate expressions for the reflection coefficients of sharp corners in rectangular wave guides. The transformation carries the bent guide over into a straight guide filled with a non-uniform medium. The reflection coefficient of the transformed system can be expressed in terms of the solution of an integral equation which may be solved approximately by successive substitutions. When the corner angle is small and the corner is not truncated the required integrations may be performed and an explicit expression obtained for the reflection coefficient. Although applied here only to corners, the method has an additional interest in that it is applicable to other types of irregularities in rectangular wave guides.

## INTRODUCTION

THE propagation of electromagnetic waves around a rectangular corner has been studied in two recent papers, one by Poritsky and Blewett<sup>1</sup> and the other by Miles<sup>2</sup>. Poritsky and Blewett make use of Schwarz' "alternating procedure" in which a sequence of approximations is obtained by going back and forth between two overlapping regions. Miles derives an equivalent circuit by using solutions of the wave equation in rectangular coordinates. Several papers giving experimental results have been published. Of these, we mention one due to Elson<sup>3</sup> who gives values of reflection coefficients for various types of corners.

Here we shall deal with the more general type of corner shown in Fig. 1 by transforming, conformally, the bent guide (in which the propagation "constant" of the dielectric is constant) into a straight guide in which the propagation "constant" is a function of position—its greatest deviation from the original value being in the vicinity of points corresponding to the corner. This type of corner has been chosen for our example because it possesses a number of features common to problems which may be treated by the transformation method.

The essentials of the procedure used are due to Routh<sup>4</sup> who studied the vibration of a membrane of irregular shape by transforming it into a rectangle. After the transformation the density (analogous to the propagation constant in the guide) was no longer constant but this disadvantage was more than offset by the simplification in shape.

Until this paper was presented at the Symposium I was unaware of any

\* Presented at the Second Symposium on Applied Mathematics, Cambridge, Mass., July 29, 1948.

<sup>1</sup> See list of references at end of paper.

other wave guide work based on conformal transformations (as described above) except that of Krasnooshkin<sup>5</sup>. At the meeting I learned that the transformation method had also been discovered (but not yet published) by Levine and by Piloty independently of each other. Levine has studied the same corner, see Fig. 1, as is done here. However, his method of approach is quite different in that he obtains expressions for the elements in the equivalent  $\pi$  network representing the corner, whereas here the reflection coefficient is considered directly. This is discussed in more detail at the beginning of Section 6. Piloty's work is closely related to the material presented in a companion paper<sup>6</sup> and is discussed in its introduction.

In this paper the partial differential equation resulting from the transformation, together with the boundary conditions, is converted into a rather complicated integral equation. Numerical work indicates that satisfactory values of the reflection coefficient, in which we are primarily interested, may be obtained by solving this integral equation by the method of successive substitutions. However, the question of convergence is not investigated.

Although they are here applied only to corners, the equations of Sections 3, 4 and 5 are quite general. In order to test their generality they were used to check the expression<sup>7</sup> for the reflection coefficient of a gentle circular bend in a rectangular wave guide,  $E$  being in the plane of the bend. The work has been omitted because of its length. It was found that the essential parts of the transformation may be obtained by regarding the inner and outer walls of the guide system as the two plates of a condenser, solving the corresponding electrostatic problem (using series of the Fourier type), and utilizing the relation between two-dimensional potentials and the theory of conformal mapping.

When the angle of the corner is small we may obtain the series (7-5) and (7-11) for the reflection coefficients corresponding to simple (i.e. not truncated)  $E$  and  $H$  corners, respectively (a corner having the electric intensity  $E$  in the plane of the bend will be called an  $E$  corner or an electric corner.  $H$  corners are defined in a similar manner). When the angle of the general  $E$  corner shown in Fig. 1 is small we may use the series (7-18).

The series (7-5) and (7-11) giving the reflection from small angle corners are related to the series giving the reflection coefficients for gentle circular bends. In fact, if the radii of curvature of the latter be held constant while the angle of bend is made small, the series for the circular bends reduce to those for the corners.

As for the limitations of the method, note first that it can be used only for wave guide systems in which the dimension normal to the plane of transformation is constant throughout. Moreover, the integral equations of the present paper, except for the work of Appendix III, are derived on the assumption that the dimensions of the guide approach constant

values at minus infinity and the same values at plus infinity. When this assumption is not met, a conformal transformation may still be used to carry the system into a straight guide. However, there appears to be some doubt as to the best way of dealing with the resulting partial differential equation. One method, discussed in the companion paper<sup>6</sup>, leads to an infinite set of ordinary linear differential equations of the second order. Again, possibly the Green's functions appearing in Sections 3 and 5 may be replaced by suitable approximations.

### 1. Representation of Field for Corner or Bend in Rectangular Guide

Quite often waves in rectangular wave guides are classed as "transverse electric" or "transverse magnetic". However, for our purposes it is more convenient to class them as "electrically oriented" or "magnetically oriented" waves.<sup>8,9</sup> Thus, the electric and magnetic intensities are obtained by multiplying

$$\begin{aligned} E_x &= \frac{1}{i\omega\epsilon} \frac{\partial^2 A}{\partial x \partial \zeta} - \frac{\partial B}{\partial y} & H_x &= \frac{\partial A}{\partial y} + \frac{1}{i\omega\mu} \frac{\partial^2 B}{\partial x \partial \zeta} \\ E_y &= \frac{1}{i\omega\epsilon} \frac{\partial^2 A}{\partial y \partial \zeta} + \frac{\partial B}{\partial x} & H_y &= -\frac{\partial A}{\partial x} + \frac{1}{i\omega\mu} \frac{\partial^2 B}{\partial y \partial \zeta} \\ E_\zeta &= -i\omega\mu A + \frac{1}{i\omega\epsilon} \frac{\partial^2 A}{\partial \zeta^2} & H_\zeta &= -i\omega\epsilon B + \frac{1}{i\omega\mu} \frac{\partial^2 B}{\partial \zeta^2} \end{aligned} \quad (1-1)$$

by  $e^{i\omega t}$  and taking the real part. Here  $\omega$ ,  $\mu$ , and  $\epsilon$  are the radian frequency, the permeability of the medium filling the guide ( $\mu = 1.257 \times 10^{-6}$  henries per meter for air), and the dielectric constant of the same ( $\epsilon = 8.854 \times 10^{-12}$  farads per meter for air), respectively.  $x$ ,  $y$ , and  $\zeta$  constitute a right-handed set of rectangular coordinates in which the  $\zeta$  axis is normal to the plane of the bend. Equations (1-1) may be verified by substituting them in Maxwell's equations.

The potentials  $A$  and  $B$  satisfy the wave equation

$$\begin{aligned} \frac{\partial^2 A}{\partial x^2} + \frac{\partial^2 A}{\partial y^2} + \frac{\partial^2 A}{\partial \zeta^2} &= \sigma^2 A \\ \sigma &= i\omega\sqrt{\mu\epsilon} = i2\pi/\lambda_0 \end{aligned} \quad (1-2)$$

where  $\lambda_0$  is the wave length in free space corresponding to the radian frequency  $\omega$ .

When the electric vector lies in the plane of the bend, as shown in Fig. 1, and the incident wave contains only the dominant mode we set

$$A = 0, \quad B = Q \sin(\pi\zeta/a) \quad (1-3)$$

where  $a$  is the wide dimension of the rectangular cross-section, the guide walls normal to the  $\zeta$  axis are at  $\zeta = 0$  and  $\zeta = a$ , and  $Q$  is a function of  $x$  and  $y$  such that

$$\frac{\partial^2 Q}{\partial x^2} + \frac{\partial^2 Q}{\partial y^2} - \Gamma_{10}^2 Q = 0 \quad (1-4)$$

$$\Gamma_{10} = i2\pi\lambda_0^{-1}(1 - \lambda_0^2 a^{-2}/4)^{1/2}$$

The guide walls are assumed to be perfect conductors and hence the tangential component of  $E$  must vanish at the walls. This requires the normal derivative of  $Q$  to vanish at those walls which are perpendicular to the plane of the bend:

$$\frac{\partial Q}{\partial n} = 0. \quad (1-5)$$

When the magnetic vector lies in the plane of the bend and the incident wave consists of the dominant mode, we set

$$A = P, \quad B = 0 \quad (1-6)$$

where  $P$  is a function of  $x$  and  $y$  such that

$$\frac{\partial^2 P}{\partial x^2} + \frac{\partial^2 P}{\partial y^2} - \Gamma_{00}^2 P = 0, \quad \Gamma_{00} = i2\pi/\lambda_0 \quad (1-7)$$

and

$$P = 0 \quad (1-8)$$

at the walls perpendicular to the plane of the bend. In this case the guide walls parallel to the plane of the bend are at  $\zeta = 0$  and  $\zeta = b$ .

## 2. Electric Vector in Plane of Bend

Figure 1 shows a section of the bend taken parallel to the electric vector.  $b$  is the narrow dimension of the guide. Let the frequency and the wide dimension  $a$  of the guide (measured normal to the plane of Fig. 1) be such that only the dominant mode is freely propagated. The position of any point in this section is specified by the complex number  $z = x + iy$  where the origin and the orientation of the axes have been chosen somewhat arbitrarily.

The constant  $k$  and related propagation constants which appear in the formulas dealing with  $Q$  and electric bends are given by

$$k = (2b/\lambda_0) [1 - (\lambda_0/2a)^2]^{1/2} = -i\Gamma_{10}b/\pi$$

$$\gamma_m^2 = m^2 - k^2; \quad m = 0, 1, 2, \dots; \quad \gamma_0 = ik \quad (2-1)$$

$$\lambda_0 = \text{free space wavelength}$$

Since, by assumption, only the dominant mode is freely propagated,  $k$  and  $\gamma_m$  for  $m > 0$  are real and positive.

We imagine an incident wave of unit amplitude coming down from  $z_5$  in the upper left portion of Fig. 1. What are the amplitudes of the reflected wave traveling back toward  $z_5$  and the transmitted wave traveling outward to the right towards  $z_3$ ? Our task is to find a  $Q(x, y)$ , satisfying the wave equation (1-4) and the boundary condition (1-5), which represents a disturbance of the assumed type.

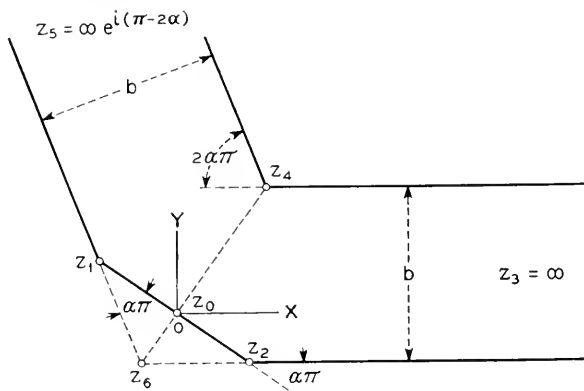


FIG. 1

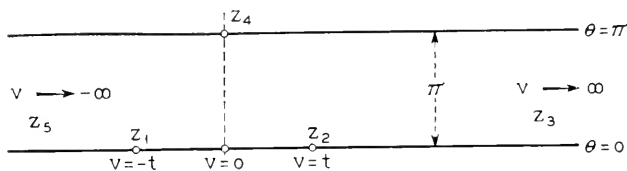


FIG. 2

The first step is to find the conformal transformation

$$z = x + iy = f(v + i\theta) = f(\bar{v}) \quad (2-2)$$

which carries the bent guide (shown in Fig. 1) in the  $(x, y)$  plane over into the straight guide (shown in Fig. 2) in the  $(v, \theta)$  plane. This may be done by the Schwarz-Christoffel method discussed in Appendix I. This transformation carries the wave equation (1-4) and the boundary condition (1-5) into

$$\frac{\partial^2 Q}{\partial \tau^2} + \frac{\partial^2 Q}{\partial \theta^2} + [1 + g(v, \theta)]k^2 Q = 0, \quad (2-3)$$

$$\frac{\partial Q}{\partial \theta} = 0 \text{ at } \theta = 0 \text{ and } \theta = \pi \quad (2-4)$$

where the upper and lower guide walls are carried into  $\theta = 0$  and  $\theta = \pi$ , respectively, and  $g(v, \theta)$  is given by

$$1 + g(v, \theta) = |f'(v + i\theta)|^2 \pi^2 / b^2 \quad (2-5)$$

$$g(v, \theta) = \frac{[ch v + \cos \theta]^{2\alpha}}{[ch(v-t) - \cos \theta]^\alpha [ch(v+t) - \cos \theta]^\alpha} - 1 \quad (2-6)$$

Here  $ch$  denotes the hyperbolic cosine,  $f'(v + i\theta)$  denotes the first derivative of  $f(w)$ , and from Appendix I,  $2\pi\alpha$  is the total angle of the bend.  $t$  is a parameter which depends upon  $\alpha$  and the ratio  $d/d_0$  where  $d = |z_1 - z_0|$  and  $d_0 = |z_4 - z_0|$  in Fig. 1. A table giving values of  $t$  for a  $90^\circ$  bend ( $\alpha = 1/4$ ) appears in Appendix I.

That the propagation constant is no longer uniform in the transformed guide shows up through the fact that the coefficient of  $k^2 Q$  in (2-3) is now a function of the coordinates  $(v, \theta)$ .  $g(v, \theta)$  measures the deviation of the propagation constant from its value at  $v = -\infty$ . For example, if we consider a wave front coming down from  $z_3$  we expect it to get past  $z_4$  before it reaches  $z_0$ . In Fig. 2 the same wave front is tilted forward corresponding to a high phase-velocity (or small propagation constant) at  $z_4$  where  $v = 0$  and  $\theta = \pi$ . This is in line with the fact that the coefficient of  $k^2 Q$  in (2-3) vanishes at  $z_4$  by virtue of (2-6). Similar considerations hold at  $z_1$  and  $z_2$ .

What is our reflection problem in terms of the transformed guide? In addition to satisfying the two equations (2-3) and (2-4)  $Q$  must behave properly at infinity. For large negative values of  $v$ ,  $Q$  must represent an incident wave plus a reflected wave. The incident wave is of unit amplitude and the reflected wave is of the, as yet, unknown value  $R_E$ . For large positive values of  $v$   $Q$  must represent an outgoing wave. Thus  $Q$  must also satisfy the two equations

$$Q = e^{-ikv} + R_E e^{ikv}, \quad v \rightarrow -\infty \quad (2-7)$$

$$Q = T_E e^{-ikv}, \quad v \rightarrow \infty \quad (2-8)$$

where the subscript  $E$  appears on the "reflection coefficient"  $R_E$  and the "transmission coefficient"  $T_E$  to indicate that here we are dealing with an electric corner.

Our problem is now to take the four equations (2-3, 4, 7, 8) and somehow or other obtain the value of  $R_E$ . We are not so much interested in  $T_E$  because it does not have the practical importance of the reflection coefficient. There are at least two different ways we may proceed from here. One is to transform the differential equation plus the boundary conditions into an integral equation which may be solved approximately by iteration. Another way is to assume  $Q$  to be a Fourier cosine series in  $\theta$  whose coefficients are functions of  $v$ . Substitution of the assumed series in the

differential equation (2-3) gives rise to a set of ordinary differential equations having  $v$  as the independent variable and the coefficients as the dependent variables. The integral equation method is used in this paper. The second method is discussed in the companion paper.<sup>6</sup>

### 3. Conversion of Differential Equation into an Integral Equation

The differential equation (2-3) may be converted into an integral equation by using the appropriate Green's function in the conventional manner. The only modifications necessary are essentially those given by Poritsky and Blewett<sup>1</sup> in a similar procedure.

The conversion is based upon Green's theorem in the form

$$\int \left( Q \frac{\partial G}{\partial n} - G \frac{\partial Q}{\partial n} \right) ds = \iint (Q \nabla^2 G - G \nabla^2 Q) dv d\theta \quad (3-1)$$

where the integration on the right extends over the rectangular region  $v_1 < v < v_2$ ,  $0 < \theta < \pi$  (inside the straight guide associated with  $(v, \theta)$ , i.e. the guide of Fig. 2) except for a very small circle surrounding the point  $(v_0, \theta_0)$ .  $G \equiv G(v_0, \theta_0; v, \theta)$  is the Green's function corresponding to

$$\frac{\partial^2 V}{\partial v^2} + \frac{\partial^2 V}{\partial \theta^2} + k^2 V = 0 \quad (3-2)$$

in the region  $-\infty < v < \infty$ ,  $0 < \theta < \pi$  subject to the boundary condition  $\partial V / \partial n = 0$  on the walls ( $\partial V / \partial \theta = 0$  at  $\theta = 0$  and  $\theta = \pi$ ).  $G$  becomes infinite as  $-\log r$  when  $r \rightarrow 0$ ,  $r$  being the distance between the variable point  $(v, \theta)$  and the fixed point  $(v_0, \theta_0)$ . Poritsky and Blewett\* have shown that, in the notation (2-1),

$$G = \sum_{m=0}^{\infty} \epsilon_m \gamma_m^{-1} \cos m\theta_0 \cos m\theta \epsilon^{-|v-v_0|\gamma_m} \quad (3-3)$$

$$\epsilon_0 = 1, \epsilon_m = 2 \quad \text{for } m = 1, 2, 3 \dots$$

Equation (3-1) leads to

$$\begin{aligned} 2\pi Q(v_0, \theta_0) + \int_0^\pi \left[ -Q \frac{\partial G}{\partial v} + G \frac{\partial Q}{\partial v} \right]_{v_1} d\theta + \int_0^\pi \left[ Q \frac{\partial G}{\partial v} - G \frac{\partial Q}{\partial v} \right]_{v_2} d\theta \\ = k^2 \int_{v_1}^{v_2} dv \int_0^\pi d\theta g(v, \theta) QG \end{aligned} \quad (3-4)$$

from which the required integral equation for  $Q$  is found to be  $Q(v_0, \theta_0) =$

$$e^{-ikv_0} + \frac{k^2}{2\pi} \int_{-\infty}^{\infty} dv \int_0^\pi d\theta g(v, \theta) Q(v, \theta) \sum_{m=0}^{\infty} \epsilon_m \gamma_m^{-1} \cos m\theta_0 \cos m\theta \epsilon^{-|v-v_0|\gamma_m} \quad (3-5)$$

\* We have replaced their  $i$  by  $-i$  since here we assume the time to enter through the factor  $e^{i\omega t}$  instead of  $e^{-i\omega t}$ .



where  $\gamma_m$  is given by (2-1). The term  $e^{-ikv_0}$  comes from the first integral on the left side of (3-4) as  $v_1 \rightarrow -\infty$ . Equation (3-5) is a general equation which may be applied to a number of wave guide problems by choosing a suitable function  $g(v, \theta)$ . For the corner of Fig. 1  $g(v, \theta)$  is given by (2-6).

If  $g(v, \theta)$  approaches zero when  $|v|$  becomes large, as it does for the corner, expressions for the reflection coefficient  $R_E$  and the amplitude  $T_E$  of the transmitted wave may be obtained by letting  $v_0 \rightarrow \pm\infty$  in (3-5). For very large values of  $|v_0|$  the contributions of all the terms in the summation except the first ( $m=0$ ) vanish. Comparison of the resulting expression for  $Q(v_0, \theta_0)$  with the limiting forms (2-7) and (2-8) defining  $R_E$  and  $T_E$  gives

$$R_E = -\frac{ik}{2\pi} \int_{-\infty}^{\infty} dv \int_0^{\pi} d\theta g(v, \theta) Q(v, \theta) e^{-ikv} \quad (3-6)$$

$$T_E = 1 - \frac{ik}{2\pi} \int_{-\infty}^{\infty} dv \int_0^{\pi} d\theta g(v, \theta) Q(v, \theta) e^{ikv} \quad (3-7)$$

Since the integrands involve the as yet unknown  $Q(v, \theta)$  these expressions are not immediately applicable. In fact, if we knew  $Q(v, \theta)$  it would not be necessary to use these integrals for  $R_E$  and  $T_E$ —we could simply let  $v \rightarrow \pm\infty$  and use (2-7) and (2-8). Nevertheless, (3-6) and (3-7) are useful in obtaining approximations to  $R_E$  and  $T_E$  when approximations to  $Q$  are known.

In Appendix IV it is shown that  $R_E$  is the stationary value, with respect to variations of the function  $Q$ , of an expression made up of integrals containing  $Q$  in their integrands. From the integral equation it follows that when  $k \rightarrow 0$ , i.e., when the frequency decreases toward the cut-off frequency of the dominant mode,  $Q$  becomes approximately  $\exp(-ikv)$ . Furthermore,  $R_E$  approaches zero. This is in contrast to the apparent behavior of  $R_H$  which, according to the discussion given in Section 5, may possibly approach  $-1$  under the same circumstances. Thus reflections from the two types of corners, or more generally, irregularities in the  $E$  plane and in the  $H$  plane, appear to behave quite differently as the cut-off frequency is approached.

$R_E$  and  $T_E$  are not independent. Since the energy in the incident wave is equal to the sum of the energies in the reflected and transmitted waves we expect

$$R_E R_E^* + T_E T_E^* = 1, \quad (3-8)$$

where the asterisk denotes the conjugate complex quantity. In addition, there is a relation between  $R_E$  and  $T_E$  which for a symmetrical irregularity, i.e. for  $g(v, \theta)$  an even function of  $v$ , states that the phase of  $R_E$  differs from that  $T_E$  by  $\pm\pi/2$ . In this special case  $T_E$  is determined to within a plus or

minus sign when  $R_E$  is given. These relations may be proved by substituting various solutions of equation (2-3) for  $Q$  and  $\hat{Q}$  in the equation

$$\left[ Q \frac{\partial \hat{Q}}{\partial v} - \hat{Q} \frac{\partial Q}{\partial v} \right]_{v_1} = \left[ Q \frac{\partial \hat{Q}}{\partial v} - \hat{Q} \frac{\partial Q}{\partial v} \right]_{v_2} \quad (3-9)$$

where  $v_1$  and  $v_2$  are large enough ( $v_1$  negative and  $v_2$  positive) to ensure that  $Q$  and  $\hat{Q}$  have reduced to exponential functions of  $v$ . Equation (3-9) follows from Green's theorem. When  $Q$  is taken to be the solution for which (2-7) and (2-8) holds and  $\hat{Q}$  its conjugate complex  $Q^*$ , equation (3-8) is obtained. Keeping the same solution for  $Q$  but now letting  $\hat{Q}$  denote the solution corresponding to an incident wave of unit amplitude coming in from the right:

$$\begin{aligned} Q_1 &= e^{ikv} + R_1 e^{-ikv}, & v \rightarrow \infty \\ Q_1 &= T_1 e^{ikv}, & v \rightarrow -\infty \end{aligned}$$

gives  $T = T_1$  where we have dropped the subscript  $E$  and have assumed that  $g(v, \theta)$  may be unsymmetrical. Taking  $\hat{Q}$  to be  $Q_1^*$  gives

$$RT_1^* + R_1^* T = 0$$

which is the relation sought. In the symmetrical case  $R = R_1$ ,  $R/T + R^*/T^*$  is zero and hence  $R/T$  is purely imaginary as was mentioned above. The same relations hold for  $R_H$  and  $T_H$ . These results are special cases of a more general result which states that the "scattering matrix" is symmetrical and unitary for a lossless junction.<sup>10</sup>

#### 4. Approximate Solution of Integral Equation

A first approximation to the solution of the integral equation (3-5) is obtained when we assume that the non-uniformity of the propagation constant has no effect on  $Q$ . Thus we put

$$Q^{(1)}(v, \theta) = e^{-ikv} \quad (4-1)$$

in the integral on the right and obtain an expression for the second approximation  $Q^{(2)}(v, \theta)$ , and so on. Here we shall not go beyond  $Q^{(2)}(v, \theta)$ .

It is convenient to expand  $g(v, \theta)$  in a Fourier cosine series

$$\begin{aligned} g(v, \theta) &= \sum_{n=0}^{\infty} a_n(v) \cos n\theta \\ a_n(v) &= \frac{\epsilon_n}{\pi} \int_0^{\pi} g(v, \theta) \cos n\theta \, d\theta, \quad \epsilon_0 = 1; \epsilon_n = 2, n > 0. \end{aligned} \quad (4-2)$$

The second approximation, obtained by substituting (4-1) in (3-5), may then be written as

$$Q^{(2)}(\tau_0, \theta_0) = e^{-ikv_0} + k^2 2^{-1} \sum_{m=0}^{\infty} \gamma_m^{-1} \cos m\theta_0 \cdot \int_{-\infty}^{\infty} a_m(v) e^{-ikv - |v - v_0| \gamma_m} dv. \quad (4-3)$$

The  $n$ th approximation  $R_E^{(n)}$  to the reflection coefficient (when the electric vector lies in the plane of the bend) is defined in terms of  $Q^{(n)}$  by

$$\lim_{v \rightarrow -\infty} Q^{(n)}(v, \theta) = e^{-ikv} + R_E^{(n)} e^{ikv} \quad (4-4)$$

$R_E^{(n)}$  is also equal to the integral obtained by replacing  $Q$  in (3-6) by  $Q^{(n-1)}$ . We have

$$R_E^{(1)} = 0, \quad R_E^{(2)} = -ik 2^{-1} \int_{-\infty}^{\infty} a_0(v) e^{-2ikv} dv, \\ R_E^{(3)} = R_E^{(2)} - ik^3 \sum_{m=0}^{\infty} (4\gamma_m \epsilon_m)^{-1} \cdot \int_{-\infty}^{\infty} d\tau_0 a_m(\tau_0) \int_{-\infty}^{\infty} dv a_m(v) e^{-ik(v + \tau_0) - |v - \tau_0| \gamma_m} \quad (4-5)$$

where  $\gamma_m$  is given by (2-1).

The results of this section have the same generality as the integral equation (3-5) in that they are not restricted to corners.

### 5. Truncated Corner—Magnetic Vector in Plane of Bend

When the magnetic vector lies in the plane of the bend the reflection may be calculated by a similar procedure. The wide dimension  $a$  of the wave guide now replaces the narrow dimension  $b$  in Fig. 1. We shall call the result of making this change the "modified Fig. 1". We again assume the frequency to be such that only the dominant mode is propagated without attenuation. In place of equations (1-3, 4, 5) involving  $Q$  we have those of (1-6, 7, 8) involving  $P$ .

The conformal transformation which carries the modified Fig. 1 into Fig. 2 leads to

$$\frac{\partial^2 P}{\partial \tau^2} + \frac{\partial^2 P}{\partial \theta^2} + [1 + g(\tau, \theta)] \kappa^2 P = 0 \quad (5-1) \\ P = 0 \quad \text{at} \quad \theta = 0 \quad \text{and} \quad \theta = \pi$$

where

$$\begin{aligned}\kappa &= 2a/\lambda_0 = -i\Gamma_{00}a/\pi, & c &= (\kappa^2 - 1)^{1/2} = ak/b \\ \delta_m^2 &= m^2 - 1 - c^2 = m^2 - \kappa^2, & \delta_1 &= ic\end{aligned}\quad (5-2)$$

$$\lambda_0 = \text{free space wave length}, \quad m = 1, 2, 3 \dots$$

and

$$|f'_{\text{mod}}(v + i\theta)|^2 \pi^2/a^2 = 1 + g(v, \theta). \quad (5-3)$$

Here  $f_{\text{mod}}(w)$  pertains to the modified Fig. 1. Since the expression for  $f'(w)$  given in Appendix I is proportional to  $b$  and since the modified transformation contains  $a$  in place of  $b$ , it follows that  $g(v, \theta)$  for the magnetic corner is exactly the same function, given by (2-6), as for the electric corner.

It is again assumed that the incident wave coming down from the left in the modified Fig. 1 is of unit amplitude and of the dominant mode. At large distances from the corner

$$\begin{aligned}P &= [e^{-icv} + R_H e^{icv}] \sin \theta, & v &\rightarrow -\infty \\ P &= T_H e^{-icv} \sin \theta, & v &\rightarrow +\infty\end{aligned}\quad (5-4)$$

which serve to define the coefficients of reflection and transmission. The subscript  $H$  on the reflection and transmission coefficients indicate that here we are dealing with a magnetic corner.

The conversion of the differential equation into the integral equation now employs the Green's function

$$G = 2 \sum_{m=1}^{\infty} \delta_m^{-1} \sin m\theta_0 \sin m\theta e^{-|v-v_0|\delta_m} \quad (5-5)$$

which corresponds to

$$\frac{\partial^2 V}{\partial v^2} + \frac{\partial^2 V}{\partial \theta^2} + \kappa^2 V = 0$$

$$V = 0 \quad \text{at} \quad \theta = 0 \quad \text{and} \quad \theta = \pi$$

The integral equation for  $P$  is found to be

$$\begin{aligned}P(v_0, \theta_0) &= e^{-icv_0} \sin \theta_0 \\ &+ \frac{\kappa^2}{2\pi} \int_{-\infty}^{+\infty} dv \int_0^\pi d\theta g(v, \theta) P(v, \theta) \sum_{m=1}^{\infty} 2\delta_m^{-1} \sin m\theta_0 \sin m\theta e^{-|v-v_0|\delta_m}\end{aligned}\quad (5-6)$$

where the parameters are given by (5-2). This is a general equation. For the corner of the modified Fig. 1  $g(v, \theta)$  is given by (2-6).

By letting  $v_0 \rightarrow -\infty$  we obtain the exact expression

$$R_H = -\frac{i\kappa^2}{\pi c} \int_{-\infty}^{\infty} dv \int_0^{\pi} d\theta g(v, \theta) P(v, \theta) e^{-icv} \sin \theta \quad (5-7)$$

When dealing with the electric corner we saw that  $R_E \rightarrow 0$  as  $k \rightarrow 0$ . The presence of  $c$  in the denominator of (5-7) suggests the possibility that  $R_H \rightarrow -1$  as  $c \rightarrow 0$ . For  $R_H$  must remain finite and this may perhaps come about through  $P(v, \theta) \rightarrow 0$  in the region, say around  $v = 0$ , where  $g(v, \theta)$  is appreciably different from zero. This and the fact that  $P(v, \theta)$  must contain a unit incident wave suggest that for  $v < 0$  the dominant portion of  $P(v, \theta)$  is  $2i \sin cv$  which gives  $R_H = -1$ . Incidentally, it is apparent that the approximations for  $P(v, \theta)$  given below in (5-8) and (5-10) (and therefore also the approximations (5-11) for  $R_H$ ) fail when  $c$  becomes small.

The first approximation to the solution of the integral equation (5-6) is

$$P^{(1)}(v, \theta) = e^{-icv} \sin \theta \quad (5-8)$$

When we introduce the coefficients

$$b_n(v) = \frac{2}{\pi} \int_0^{\pi} g(v, \theta) \sin \theta \sin n\theta d\theta$$

$$\sin \theta g(v, \theta) = \sum_{n=1}^{\infty} b_n(v) \sin n\theta \quad (5-9)$$

$$b_1(v) = a_0(v) - a_2(v)/2, \quad b_n(v) = [a_{n-1}(v) - a_{n+1}(v)]/2, \quad n > 1$$

we find that the second approximation is

$$P^{(2)}(v_0, \theta_0) = e^{-icv_0} \sin \theta_0 + \kappa^2 2^{-1} \sum_{m=1}^{\infty} \delta_m^{-1} \sin m\theta_0$$

$$\cdot \int_{-\infty}^{\infty} b_m(v) e^{-icv - |v - v_0| \delta_m} dv. \quad (5-10)$$

The successive approximations to the reflection coefficient are

$$R_H^{(1)} = 0, \quad R_H^{(2)} = -\frac{i\kappa^2}{2c} \int_{-\infty}^{+\infty} dv b_1(v) e^{-2icv}$$

$$R_H^{(3)} = R_H^{(2)} - i\kappa^4 \sum_{m=1}^{\infty} (4c\delta_m)^{-1} \int_{-\infty}^{+\infty} dv_0 b_m(v_0)$$

$$\cdot \int_{-\infty}^{+\infty} dv b_m(v_0) e^{-ic(v+v_0) - |v - v_0| \delta_m}. \quad (5-11)$$

### 6. Series for $R^{(2)}$ When Corner Has No Truncation

The integrals which appear in the approximations for the reflection coefficients are difficult to evaluate in general. This section serves to put on record several expressions which have been obtained for  $R^{(2)}$  when the corner is not truncated. Corresponding evaluations of  $R^{(3)}$  would be welcome since the work of Section 7 for small angle corners indicates that  $R^{(3)} - R^{(2)}$  is of the same order as  $R^{(2)}$ . However, I have been unable to go much beyond the results shown here.

As mentioned in the introduction, H. Levine has studied the effect of a corner in a wave guide by representing it as an equivalent pi network having an inductance for the series element and two equal condensers for the shunt elements. Early in 1947 he derived the following expressions (in our notation) for the elements corresponding to a simple  $E$  corner:\*

$$B_a/Y_0 = k \left[ \Psi \left( \frac{\beta - 1}{2} \right) - \Psi \left( -\frac{1}{2} \right) \right]$$

$$B_b/Y_0 = (k\pi)^{-1} \cot (\beta\pi/2)$$

where  $Y_0$  is the characteristic admittance of the straight guide,  $iB_a$  the admittance of one of the two equal shunt condensers,  $-iB_b$  the admittance of the series inductance,  $\Psi(x)$  the logarithmic derivative of  $\Gamma(x + 1)$ , and  $\beta\pi$  is the total angle of the simple corner (for no truncation we set  $\beta = 2\alpha$ ).

When the reflection coefficient for the corner is computed from the equivalent network for the case  $\beta \rightarrow 0$  it is found to lie between the approximate value  $R_E^{(2)}$  given by (7-3) and the considerably more accurate value  $R_E^{(3)}$  given by (7-5). All three approximations are of the form  $A\beta^2 + O(\beta^3)$  where  $A$  differs from approximation to approximation but is independent of  $\beta$ , and  $O(\beta^3)$  denotes correction terms of order  $\beta^3$ . Since  $R_E^{(3)}$  gives the exact value of  $A$ , it may be regarded as the standard when the three approximations are compared. If this comparison be taken as a guide, it suggests that the rather cumbersome expressions (6-2) and (6-5) for  $R_E^{(2)}$  given below are not as accurate as the simpler expressions resulting from Levine's work. Dr. Levine has also obtained corresponding results for the general  $E$ -corner of Fig. 1. It is hoped that his work will be published soon.

When the corner is not truncated it is convenient, as mentioned above, to replace  $2\alpha$  by  $\beta$  so that  $\beta\pi$  is the total angle of the bend. For no truncation  $t = 0$  and (2-6) becomes

$$g(\tau, \theta) = \left[ \frac{chv + \cos \theta}{chv - \cos \theta} \right]^3 - 1. \quad (6-1)$$

\* I am indebted to Dr. Levine for communicating these expressions to me.

From (4-2) and (4-5), or from (3-6),

$$\begin{aligned} R_E^{(2)} &= -\frac{ik}{2\pi} \int_{-\infty}^{\infty} dz \int_0^{\pi} d\theta_{\infty}(z, \theta) e^{-2ikz} \\ &= -ik \sum_{n=1}^{\infty} \frac{\Gamma(n-ik)\Gamma(n+ik)}{n!(n-1)!2} \sum_{m=0}^n \frac{(-2\beta)_{2m}(\beta)_{n-m}}{(2m)!(n-m)!} \end{aligned} \quad (6-2)$$

where we have expanded  $g(z, \theta)$  as given by (6-1) in powers of  $\cos \theta_{\infty} e^{ikz}$  and integrated termwise. The notation is  $(\alpha)_0 = 1$ ,  $(\alpha)_n = \alpha(\alpha+1) \cdots (\alpha+n-1)$ .

For a right angle corner  $\beta = 1/2$ , and a more rapidly convergent series may be obtained by subtracting the sum of the series corresponding to  $k = 0$ , namely

$$\log_e 2 = \sum_{n=1}^{\infty} \frac{(1/2)_n}{n! 2n} \quad (6-3)$$

Thus for  $\beta = 1/2$

$$\begin{aligned} R_E^{(2)} &= -ik \left[ \log_e 2 - \sum_{n=1}^{\infty} \frac{(1/2)_n}{n! 2n} (1 - A_n) \right], \\ A_1 &= \pi k / \sinh \pi k, \quad A_n = A_1 \prod_{m=1}^{n-1} (1 + k^2 m^{-2}), \quad n > 1 \end{aligned} \quad (6-4)$$

The rate of convergence of the more general series (6-2) may be increased in a somewhat similar way. It is found that

$$\begin{aligned} R_E^{(2)} &= -\frac{ik}{2} \left[ J - 2\beta^2(1 - A_1) - \frac{\beta^2}{3}(2 + \beta^2)(1 - A_2) \right. \\ &\quad \left. - \frac{2\beta^2}{135}(23 + 20\beta^2 + 2\beta^4)(1 - A_3) - \cdots \right] \\ J &= K + L \end{aligned} \quad (6-5)$$

$$\begin{aligned} K &= \sum_{n=1}^{\infty} \frac{(\beta)_n}{n! n} = \frac{1}{1-\beta} - \Psi(1-\beta) = .5772 \\ L &= \sum_{m=1}^{\infty} \frac{(-2\beta)_{2m}}{(2m)!} \sum_{n=m}^{\infty} \frac{(\beta)_{n-m}}{(n-m)! n} = -\beta \sum_{m=1}^{\infty} \frac{(1/2 - \beta)_m}{(1/2)_m m(m-\beta)} \end{aligned}$$

where .5772  $\cdots$  is Euler's constant,  $\Psi(x)$  is the logarithmic derivative of  $\Gamma(x) = \Gamma(x+1)$ , and  $A_n$  is given by (6-4).

The results corresponding to  $R_H^{(2)}$  are quite similar. When the corner is not truncated

$$\begin{aligned}
 R_H^{(2)} &= -i\kappa^2 \sum_{n=1}^{\infty} \frac{\Gamma(n-ic)\Gamma(n+ic)}{(n+1)!(n-1)!2c} \sum_{m=0}^n \frac{(-2\beta)_{2m}(\beta)_{n-m}}{(2m)!(n-m)!} \\
 &= -\frac{i\kappa^2}{2c} \left[ \hat{J} - \beta^2(1 - \hat{A}_1) - \frac{\beta^2}{3}(2 + \beta^2)(1 - \hat{A}_2) \right. \\
 &\quad \left. - \frac{\beta^2}{270}(23 + 20\beta^2 + 2\beta^4)(1 - \hat{A}_3) - \dots \right] \quad (6-6)
 \end{aligned}$$

$$\hat{J} = 1 - \Psi(1 - \beta) = .5772$$

$$- \beta(1 - \beta) \sum_{m=1}^{\infty} \frac{(1/2 - \beta)_m}{(1/2)_m m(m - \beta)(m - \beta + 1)}$$

in which  $\hat{A}_n$  is obtained by replacing  $c$  by  $k$  in the expression (6-4) for  $A_n$ .

The evaluation of the integrals for  $R_E^{(2)}$  and  $R_H^{(2)}$  for general values of  $l$  appears to be difficult although it is possible to obtain approximate expressions for the case when  $l$  is large.

### 7. Reflection from Small Angle Corners

The expressions for  $R^{(2)}$  and  $R^{(3)}$  may be evaluated approximately when the angle of the corner is small. It turns out that, for  $l = 0$ , they are of the same order of magnitude and both of them must be considered. Moreover  $R^{(n)}$  for  $n > 3$  differs from  $R^{(3)}$  by terms of the same order as those neglected in our approximations so that there is no point in going to the higher values of  $n$ .

We first obtain the approximation for  $R_E$  for a corner with no truncation having the total angle  $\pi\beta$ . Since  $\beta$  is very small (6-1) may be written as

$$\begin{aligned}
 g(v, \theta) &= \exp[\beta\varphi] - 1 = \beta\varphi + \beta^2\varphi^2/2! + O(\beta^3) \\
 \varphi &= \log(chv + \cos \theta) - \log(chv - \cos \theta) \quad (7-1)
 \end{aligned}$$

where  $O(\beta^3)$  denotes terms of order  $\beta^3$ . The expression  $\varphi$  becomes very large near the two points  $(0, 0)$  and  $(0, \pi)$  (the coordinates being  $(v, \theta)$ ). The following considerations indicate that this does not invalidate our procedure. The remainder, denoted by  $O(\beta^3)$ , in (7-1) is less than  $|\beta\varphi|^3 \exp|\beta\varphi|$ . Near  $(0, 0)$   $\varphi$  is approximately equal to  $2\log(2/r)$  where  $r^2 = v^2 + \theta^2$ . Consequently the remainder is less than  $(2\beta \log 2/r)^3 (2/r)^{2\beta}$ . When the expression (7-1) for  $g(v, \theta)$  is set in the integral equation it is seen that all terms, and in particular the remainder term (by virtue of the inequality just stated), of the double integral converge at  $(0, 0)$ . Hence the contribution of the remainder term is of order  $\beta^3$  even in the worst case when the



Green's function is replaced by  $-\log r$ . A similar result holds for the other point in question, namely  $(0, \pi)$ .

Integrating (7-1) from  $\theta = 0$  to  $\theta = \pi$  and using equations (A2-1, 3) of Appendix II gives

$$\begin{aligned} a_0(v) &= \beta^2[I_1(v, v) - I_2(v, v)] + O(\beta^3) \\ &= 4\beta^2 \sum_{n=1,3,5,\dots}^{\infty} n^{-2} e^{-2nv} + O(\beta^3) \end{aligned} \quad (7-2)$$

where  $v > 0$ . We consider only positive values of  $v$  since  $g(v, \theta)$  and the  $a_n(v)$ 's are even functions of  $v$ . Thus (4-5) yields

$$R_E^{(2)} = -ik2\beta^2 \sum_{n=1,3,5,\dots} n^{-1}(n^2 + k^2)^{-1} + O(\beta^3) \quad (7-3)$$

This is an approximation to the exact value given by the double series in (6-2). Comparison of (6-5) and (7-3) when  $\beta$  and  $k$  approach zero gives, incidentally,

$$\sum_{m=1}^{\infty} m^{-2} \sum_{n=1}^m (n - 1/2)^{-1} = 7 \sum_{m=1}^{\infty} m^{-3}.$$

From (4-2), (7-1) and the expansions (A2-2) of  $\log(chv \pm \cos \theta)$  it follows that

$$\begin{aligned} a_m(v) &= 4\beta m^{-1} e^{-m|v|} + O(\beta^2), & m &= 1, 3, 5, \dots \\ a_m(v) &= O(\beta^2), & m &= 0, 2, 4, 6, \dots \end{aligned} \quad (7-4)$$

Equations (4-5), (A2-4), the relation  $\gamma_m^2 = m^2 - k^2$ , and (A2-8) give us the answer we seek:

$$\begin{aligned} R_E^{(3)} &= R_E^{(2)} - ik^3 2\beta^2 \sum_{m=1,3,5,\dots} \gamma_m^{-1} m^{-2} J(m, m, k, \gamma_m, 0, 0) + O(\beta^3) \\ &= -ik2\beta^2 \sum_{m=1,3,5,\dots} \gamma_m^{-1} m^{-2} + O(\beta^3) \end{aligned} \quad (7-5)$$

It is not necessary to go to  $R_E^{(4)}$  because it differs from  $R_E^{(3)}$  by only  $O(\beta^3)$ .

When  $H$  lies in the plane of the bend the reflection from a small angle corner with no truncation may be obtained by much the same procedure. For brevity we shall not write down the order of magnitude of the remainder terms. From (5-9), (A2-1), and (A2-3)

$$\begin{aligned} b_1(v) &= a_0(v) - a_2(v)/2 \\ &= \beta^2[I_1 - I_2 - (I_3 - I_4)/2] \\ &= \beta^2[2e^{-2v} + 4 \sum_{n=3,5,\dots} n^{-2} e^{-2nv} - 4 \sum_{n=2,4,\dots} (n^2 - 1)^{-1} e^{-2nv}] \end{aligned} \quad (7-6)$$

where we have written  $I_m$  for  $I_m(v, v)$  and assumed  $v > 0$ . Then, using (5-11),

$$R_H^{(2)} = -i\kappa^2 c^{-1} \beta^2 [\kappa^{-2} + 2 \sum_{n=3,5,\dots} n^{-1} (n^2 + c^2)^{-1} - 2 \sum_{n=2,4,\dots} n (n^2 - 1)^{-1} (n^2 + c^2)^{-1}] \quad (7-7)$$

When we put

$$b_n(v) = [a_{n-1}(v) - a_{n+1}(v)]/2, \quad n > 1 \quad (7-8)$$

$$b_n(v) = 2\beta[(n-1)^{-1}e^{-(n-1)|v|} - (n+1)^{-1}e^{-(n+1)|v|}], \quad n = 2, 4, 6, \dots$$

$$b_n(v) = 0(\beta^2), \quad n = 1, 3, 5, \dots$$

in (5-11) and use the results of Appendix II we obtain

$$\begin{aligned} R_H^{(3)} = R_H^{(2)} - i\kappa^4 c^{-1} \beta^2 \sum_{n=2,4,6,\dots} \delta_n^{-1} [(n-1)^{-2} J(n-1, n-1, \delta_n, 0, 0) \\ + (n+1)^{-2} J(n+1, n+1, c, \delta_n, 0, 0) \\ - 2(n^2 - 1)^{-1} J(n-1, n+1, c, \delta_n, 0, 0)] \end{aligned} \quad (7-9)$$

The values of the first two  $J$ 's, obtained by setting  $m = n \pm 1$  in (A2-7), may be simplified by using

$$c^2 + (n \pm 1 + \delta)^2 = 2(n \pm 1)(n + \delta)$$

where we have dropped the subscript  $n$  from  $\delta_n$ . In order to eliminate  $\delta$  from the denominator we multiply both numerator and denominator by  $n - \delta$  and use

$$(n - \delta)(\delta + 2n \pm 2) = (n \pm 1)^2 + c^2 - \delta(n \pm 2)$$

$$n^2 - \delta^2 = 1 + c^2 = \kappa^2$$

Setting in the value, given by (A2-9), of the last  $J$  and separating the terms (into those which contain the first power of  $\delta$  and those which do not) enable us to write the term within the square brackets in (7-9) as

$$\begin{aligned} \frac{4n^2}{\kappa^4(n^2 - 1)^2} - \frac{\delta_n}{\kappa^2} \left[ \frac{(n-1) - 1}{(n-1)^2 \{c^2 + (n-1)^2\}} + \frac{(n+1) + 1}{(n+1)^2 \{c^2 + (n+1)^2\}} \right. \\ \left. + \frac{2n \{2(n^2 + c^2) - \kappa^2(n^2 - 1)\}}{\kappa^2(n^2 - 1)^2(n^2 + c^2)} \right] \end{aligned} \quad (7-10)$$

It is found that when (7-10) is put in (7-9), the contribution of the first two terms within the square bracket of (7-10) exactly cancels the summation

which is taken over 3, 5, 7 ... in the expression (7-7) for  $R_H^{(2)}$ . Moreover, if we make use of

$$\sum_{n=2,4,6,\dots} 4n(n^2 - 1)^{-2} = 1$$

we see that the contribution of the last term within the square brackets of (7-10) cancels the remaining terms in  $R_H^{(2)}$ . Only the contribution of the first term in (7-10) remains and it gives

$$R_H^{(3)} = -i4\beta^2 c^{-1} \sum_{n=2,4,6,\dots} n^2 (n^2 - 1)^{-2} \delta_n^{-1} + O(\beta^3) \quad (7-11)$$

The relative simplicity of this result indicates that there may be another method of derivation which avoids the lengthy algebra of our method.

Recently approximate expressions for the reflection coefficient of gentle circular bends have been published<sup>7</sup>. In our present notation these may be written as

$$R_E \approx -i b^2 \rho_1^{-2} \left[ \frac{\sin u}{24} - 4k \sum_{m=1,3,5,\dots} \frac{\cos u - e^{-u\gamma_m/k}}{\pi^4 m^4 \gamma_m} \right]$$

$$R_H \approx -i a^2 \rho_1^{-2} \left[ \frac{\sin u}{8\pi^2 c^2} - 8 \sum_{n=2,4,6,\dots} \frac{\cos u - e^{-u\delta_n/c}}{\pi^4 c \delta_n} \frac{n^2}{(n^2 - 1)^3} \right]$$

where  $\beta\pi$  is the angle of the bend,  $\rho_1$  is the radius of curvature of the center line of the guide and  $u$  is  $2\pi$  times the length of the center line in the bend divided by the wavelength in the guide:

$$u = \beta\pi^2 k \rho_1 / b = \beta\pi^2 c \rho_1 / a$$

The first expression for  $u$  is to be used in  $R_E$  and the second in  $R_H$ . If we now let  $\beta \rightarrow 0$ , keeping  $\rho_1$  fixed, then  $u \rightarrow 0$ . The trigonometric and exponential terms may be approximated by the first few terms in their power series expansions, and part of the series which make their appearance may be replaced by their sums given, for example, by equations (4.1-7) and (4.1-8) of reference<sup>7</sup>. After some cancellation, the above expression for  $R_E$  and  $R_H$ , which hold for gentle circular bends, reduce to (7-5) and (7-11), respectively, which hold for the sharp corners. In other words, the reflection coefficients for both the sharp and the circular bends approach zero as  $\beta \rightarrow 0$ , and furthermore their ratio approaches unity.

We shall merely outline the derivation of the approximation  $R_E^{(3)}$  for a truncated corner. Instead of (7-1) we have from (2-6),

$$g(v, \theta) = \exp[\alpha\varphi] - 1 = \alpha\varphi + \alpha^2\varphi^2/2! + O(\alpha^3), \quad (7-12)$$

$$\varphi = 2 \log[chv + \cos \theta] - \log[ch(v-t) - \cos \theta] - \log[ch(v+t) - \cos \theta]$$

The Fourier coefficients of  $g(v, \theta)$  may be obtained by using the results of Appendix II. Assuming  $v > 0$ ,  $m > 0$ ,

$$\begin{aligned} a_0(v) &= 2\alpha(v-t)\psi(v) + 2^{-1}\alpha^2\{4I_1(v, v) + I_1(v-t, v-t) \\ &\quad + I_1(v+t, v+t) - 4I_2(v-t, v) - 4I_2(v+t, v) + 2I_1(v-t, v+t)\}, \\ a_m(v) &= 2\alpha m^{-1}[-2(-)^m e^{-m|v|} + e^{-m|v-t|} + e^{-m|v+t|}] \end{aligned} \quad (7-13)$$

where  $\psi(v) = 1$  when  $0 < v < t$  and  $\psi(v) = 0$  when  $v > t$ . Substitution of the values (A2-3) for  $I_1$  and  $I_2$  gives

$$\begin{aligned} a_0(v) &= [2\alpha(v-t) + 2\alpha^2(v-t)^2]\psi(v) \\ &\quad + \alpha^2 \sum_{n=1}^{\infty} n^{-2} [4e^{-2nv} + e^{-2n v-2nt} - 4(-)^n e^{-2n v-n t} \\ &\quad + e^{-2n|v-t|} + 2e^{-n|v-t|-n|v+t|} - 4(-)^n e^{-n|v-t|-nv}] \end{aligned} \quad (7-14)$$

The second approximation to the reflection coefficient is

$$\begin{aligned} R_E^{(2)} &= i\alpha k^{-1} \sin^2 kt - i\alpha^2 k^{-2} 2^{-1} (2kt - \sin 2kt) \\ &\quad - i k \alpha^2 \sum_{n=1}^{\infty} n^{-1} (n^2 + k^2)^{-1} \{ 2 - (-)^n 2e^{-nt} \\ &\quad + [1 - 2(-)^n e^{-nt} + e^{-2nt}] \cos 2kt \\ &\quad + nk^{-1} [e^{-2nt} - (-)^n 2e^{-nt}] \sin 2kt \} \end{aligned} \quad (7-15)$$

The typical term in the summation (4-5) for  $R_E^{(3)}$  is

$$- \frac{ik^3}{4\gamma_m \epsilon_m} \int_{-\infty}^{+\infty} dv_0 a_m(v_0) \int_{-\infty}^{+\infty} dv a_m(v) e^{-ik(v+v_0)-|v-v_0|\gamma_m} \quad (7-16)$$

When  $m = 0$ ,  $\epsilon_0 = 1$ ,  $\gamma_0 = ik$ , and  $a_0(v)$  is  $2\alpha(v-t) + 0(\alpha^2)$  for  $0 < v < t$  and is  $0(\alpha^2)$  for  $v > t$ . The integral may then be approximated by replacing the upper limit  $\infty$  in (A2-14) by  $t$ . The value of (7-16) for  $m = 0$  is found to be, to within  $0(\alpha^2)$ ,

$$2^{-1}\alpha^2 t^2 (e^{-2ikt} - 1) - (3/4)i\alpha^2 k^{-2} (\sin 2kt - 2kt) \quad (7-17)$$

When  $m > 0$ ,  $\epsilon_m = 2$ ,  $\gamma_m^2 = m^2 - k^2$ , and the substitution of the value (7-13) for  $a_m(v)$  enables us to express (7-16) as the sum of six  $J$ 's where  $J$  is defined by (A2-4). The  $J$ 's may be evaluated with the help of (A2-7) and (A2-8). Substitution of this value of (7-16) and the value (7-17) for  $m = 0$ , together with  $R_E^{(2)}$  given by (7-15), in the expression (4-5) for  $R_E^{(3)}$  gives our final result

$$\begin{aligned} R_E^{(3)} &= i\alpha k^{-1} \sin^2 kt + \alpha^2 t^2 2^{-1} (e^{-2ikt} - 1) \\ &\quad + i\alpha^2 [4^{-1} k^{-2} (2kt - \sin 2kt) - B \sin 2kt + k \sum_{n=1}^{\infty} n^{-2} \gamma_n^{-1} A_n] \end{aligned} \quad (7-18)$$

where

$$B = \sum_{n=1}^{\infty} n^{-2} [e^{-2nt} - 2(-)^n e^{-nt}]$$

$$A_n = \cos 2kt - [2\cos kt - (-)^n e^{-\gamma_n t}]^2$$

Equation (7-18) is an approximation, to within terms of order  $\alpha^2$ , for the reflection coefficient of a truncated corner which turns through a small angle  $2\pi\alpha$ . The electric vector lies in the plane of the bend. When  $t = 0$ , (7-18) reduces to (7-5) by virtue of  $2\alpha = \beta$ .

## APPENDIX I

### CONFORMAL TRANSFORMATION OF TRUNCATED CORNER

We shall use a Schwarz-Christoffel transformation\* to carry the guide of Fig. 1 into the straight guide of Fig. 2. The first step is to transform the interior of Fig. 1 into the upper half of an auxiliary complex plane which we shall denote by  $\zeta$ . Let the points  $z_1, z_2, z_3, z_4, z_5$  in Fig. 1 correspond to the points  $-h, h, 1, \infty, -1$  in the  $\zeta$  plane. A suitable transformation is then

$$z = D + E \int_0^{\zeta} (\tau + h)^{-\alpha} (\tau - h)^{-\alpha} (\tau - 1)^{-1} (\tau + 1)^{-1} d\tau \quad (\text{A1-1})$$

where  $D, E$  and  $h$  are to be determined from the geometry of Fig. 1. Because of the symmetry of our transformation about the line joining  $z_0$  and  $z_4$  it follows that  $z = z_0$  corresponds to  $\zeta = 0$ . Hence  $D = z_0$ . As  $\zeta$  travels from  $1 - \epsilon$  to  $1 + \epsilon$ ,  $\epsilon$  being very small and positive, along a semicircular indentation above  $\zeta = 1$ ,  $z$  as given by (A1-1) increases by

$$E(1 - h^2)^{-\alpha} 2^{-1} \int_{1-\epsilon}^{1+\epsilon} (\tau - 1)^{-1} d\tau = \frac{-iE\pi}{2} (1 - h^2)^{-\alpha}$$

while, according to Fig. 1, it increases from  $z + i0$  to  $z + ib$ . Hence we set the real part of  $E$  equal to  $-2b\pi^{-1}(1 - h^2)^{\alpha}$ . We have tacitly assumed the factors in (A1-1) to have their principal values at  $\tau = 1 + \epsilon$  and also that  $0 < h < 1$ . As  $z$  goes from  $z_1$  to  $z_2$ ,  $\zeta$  goes from  $-h$  to  $+h$ . In this range  $\arg(\tau + h) = 0$  and  $\arg(\tau - h) = \pi$ .

Consequently, if  $|z_2 - z_1| = \ell$ , then

$$z_2 - z_1 = \ell e^{-i\alpha\pi} = -E e^{-i\alpha\pi} \int_{-h}^h (h^2 - \tau^2)^{-\alpha} (1 - \tau^2)^{-1} d\tau$$

\* See, for example, S. A. Schelkunoff, *Electromagnetic Waves*, New York (1943) pp. 184-187.

and we see that  $E$  is purely real. Hence

$$\ell = 2b\pi^{-1}(1 - h^2)^\alpha \int_{-h}^h (h^2 - \tau^2)^{-\alpha} (1 - \tau^2)^{-1} d\tau$$

is an equation from which  $h$  may be determined as a function of  $\ell$ . Setting  $\tau^2 = h^2 x$ , expanding  $(1 - h^2 x)^{-1}$  in powers of  $h^2$  and integrating termwise leads to

$$\begin{aligned} \frac{\ell}{2b} &= \frac{\pi^{-\frac{1}{2}} \Gamma(1 - \alpha)}{\Gamma(\frac{3}{2} - \alpha)} (1 - h^2)^\alpha h^{1-2\alpha} F(1, \frac{1}{2}; \frac{3}{2} - \alpha; h^2) \\ &= \frac{\pi^{-\frac{1}{2}} \Gamma(1 - \alpha)}{\Gamma(\frac{3}{2} - \alpha)} h^{1-2\alpha} F(\frac{1}{2} - \alpha, 1 - \alpha; \frac{3}{2} - \alpha; h^2) \\ &= \frac{1}{\sin \pi \alpha} + \frac{\pi^{-\frac{1}{2}} \Gamma(-\alpha)}{\Gamma(\frac{1}{2} - \alpha)} h^{1-2\alpha} (1 - h^2)^\alpha F(1, \frac{1}{2}; 1 + \alpha; 1 - h^2) \end{aligned} \quad (\text{A1-2})$$

where we have used relations from the theory of hypergeometric functions. The term  $1/\sin \pi \alpha$  is the reduced form of an original term containing a hypergeometric function which has been evaluated by the binomial theorem. The second and third expressions are suited to calculation when  $h^2 < 1/2$  and  $h^2 > 1/2$  respectively.

Now that the guide of Fig. 1 has been transformed into the upper half of the  $\zeta$  plane, the next step is to transform this upper half into the straight guide of Fig. 2. We want  $\zeta = -1$ , i.e.  $z_5$ , to go into  $v = -\infty$  and  $\zeta = 1$ , i.e.  $z_3$ , to go into  $v = +\infty$ . Again using the Schwarz-Christoffel formula with  $w = v + i\theta$  (the exterior angles at  $v = \pm\infty$  are equal to  $\pi$ )

$$w = D_1 + E_1 \int_0^\zeta (\tau + 1)^{-1} (\tau - 1)^{-1} d\tau \quad (\text{A1-3})$$

We take the point  $z_0$  in Fig. 1 to correspond to  $v = 0$ ,  $\theta = 0$  in Fig. 2. Since this corresponds to  $\zeta = 0$ ,  $D_1$  must be zero. Also  $d\bar{w}/d\zeta$  is real because  $w$  traverses the walls of the guide of Fig. 2 as  $\zeta$  moves along the real axis in the  $\zeta$  plane. Hence  $E_1$  is real. As  $\zeta$  goes from  $1 - \epsilon$  to  $1 + \epsilon$  around a small circular indentation above  $\zeta = 1$ ,  $w$  changes from  $\infty$  to  $\infty + i\pi$ . Thus

$$i\pi = E_1 2^{-1}(-i\pi) \quad \text{or} \quad E_1 = -2 \quad (\text{A1-4})$$

When (A1-3) is integrated, (A1-4) inserted, and the result solved for  $\zeta$  we obtain

$$\zeta = \tanh w/2 \quad (\text{A1-5})$$

The function we require is obtained by differentiating (A1-1) and (A1-3):

$$\begin{aligned}
 f'(v + i\theta) &= f'(w) = \frac{dz}{dw} = \frac{dz}{d\xi} \bigg/ \frac{dw}{d\xi} \\
 &= E(\xi^2 - h^2)^{-\alpha} (\xi^2 - 1)^{-1} E_1^{-1} (\xi^2 - 1) \\
 &= (1 - h^2)^\alpha (\xi^2 - h^2)^{-\alpha} b / \pi \\
 &= \frac{b}{\pi} \left[ \frac{ch^2 w / 2}{sh \frac{1}{2}(w - t) sh \frac{1}{2}(w + t)} \right]^\alpha \\
 &= \frac{b}{\pi} \left[ \frac{(e^w + 1)^2}{(e^{w-t} - 1)(e^{w+t} - 1)} \right]^\alpha
 \end{aligned} \tag{A1-6}$$

where

$$h = \tanh t/2 \tag{A1-7}$$

For a 90 degree corner  $\alpha = 1/4$  and

$$\frac{\ell}{2b} = 2^{1/2} (1 - d/d_0) \tag{A1-8}$$

where, in Fig. 1,  $d = |z_4 - z_0|$  and  $d_0 = |z_4 - z_6|$ . In order to obtain the relation between  $t$ , defined by (A1-7), and  $d/d_0$  various values of  $h^2$  were picked and the corresponding values of  $t$  and  $d/d_0$  (using (A1-2) and (A1-8)) computed. Representative values are given in the following table.

$d/d_0$	$t$	$d/d_0$	$t$
1.000	0	.5796	1.2302
.9041	.0633	.5385	1.4910
.8565	.1417	.5000	1.7594
.8292	.2007	.4615	2.0634
.7745	.3500	.3727	2.8872
.7196	.5421	.2804	4.0096
.6919	.6549	.1708	5.987
.6273	.9624	.0959	8.294

## APPENDIX II

### INTEGRALS ASSOCIATED WITH CORNERS OF SMALL ANGLE

The derivation of the integrals encountered in Sections 7 and 8 will be outlined here. The first ones are

$$I_1(u, v) = \frac{1}{\pi} \int_0^\pi \log(ch u - \cos \theta) \log(ch v - \cos \theta) d\theta$$

$$I_2(u, v) = \frac{1}{\pi} \int_0^\pi \log(ch u - \cos \theta) \log(ch v + \cos \theta) d\theta \quad (\text{A2-1})$$

$$I_3(u, v) = \frac{2}{\pi} \int_0^\pi \cos 2\theta \log(ch u - \cos \theta) \log(ch v - \cos \theta) d\theta$$

$$I_4(u, v) = \frac{2}{\pi} \int_0^\pi \cos 2\theta \log(ch u - \cos \theta) \log(ch v + \cos \theta) d\theta$$

Assuming  $u$  and  $v$  to be positive and using the expansions

$$\begin{aligned} \log(ch u - \cos \theta) &= \log(e^u/2) - 2 \sum_{n=1}^{\infty} n^{-1} e^{-nu} \cos n\theta \\ \log(ch u + \cos \theta) &= \log(e^u/2) - 2 \sum_{n=1}^{\infty} (-)^n n^{-1} e^{-nu} \cos n\theta \end{aligned} \quad (\text{A2-2})$$

leads to

$$\begin{aligned} I_1(u, v) &= \log(e^u/2) \log(e^v/2) + 2 \sum_{n=1}^{\infty} n^{-2} e^{-nu-nv} \\ I_2(u, v) &= \log(e^u/2) \log(e^v/2) + 2 \sum_{n=1}^{\infty} (-)^n n^{-2} e^{-nu-nv} \\ I_3(u, v) &= -e^{-2u} \log(e^v/2) - e^{-2v} \log(e^u/2) + 2e^{-u-v} \\ &\quad + 2 \sum_{n=1}^{\infty} n^{-1} (n+2)^{-1} e^{-nu-nv} (e^{-2u} + e^{-2v}) \\ I_4(u, v) &= -e^{-2u} \log(e^v/2) - e^{-2v} \log(e^u/2) - 2e^{-v-u} \\ &\quad + 2 \sum_{n=1}^{\infty} (-)^n n^{-1} (n+2)^{-1} e^{-nu-nv} (e^{-2u} + e^{-2v}) \end{aligned} \quad (\text{A2-3})$$

When  $u$  or  $v$  are negative they are to be replaced by their absolute values in the expressions (A2-2, 3).

Now we consider the double integral

$$J(\mu, m, c, \delta; r, s) = \int_{-\infty}^{+\infty} d\tau_0 \int_{-\infty}^{+\infty} d\tau \quad (\text{A2-4})$$

$$\cdot \exp [-\mu |\tau_0 - r| - m |\tau - s| - ic(\tau + \tau_0) - \delta |\tau - \tau_0|]$$

in which  $\mu, m, c, \delta$  are real and positive and  $r$  and  $s$  are real. The double integral may be reduced to a single integral by substituting

$$e^{-\delta |\tau - \tau_0|} = \frac{\delta}{\pi} \int_{-\infty}^{+\infty} (\delta^2 + x^2)^{-1} e^{ix(\tau - \tau_0)} dx, \quad (\text{A2-5})$$



interchanging the order of integration, and integrating with respect to  $x$  and  $v_0$ . Assuming  $s - r \geq 0$ , the integral is then evaluated by closing the path of integration by an infinite semicircle in the upper half plane and calculating the residues of the integrand at the poles  $i\delta$ ,  $c + im$ ,  $-c + i\mu$ :

$$\begin{aligned} J(\mu, m, c, \delta; r, s) &= \int_{-\infty}^{\infty} \frac{4\delta\mu m e^{ix(s-r) - ic(r+s)} dx}{\pi(\delta^2 + x^2)[\mu^2 + (x+c)^2][m^2 + (x-c)^2]} \\ &= 4\delta\mu m \left[ \frac{e^{-(\delta+ic)s + (\delta-ic)r}}{\delta[\mu^2 + (c+i\delta)^2][m^2 + (c-i\delta)^2]} \right. \\ &\quad + \frac{e^{-ms + (m-2ic)r}}{m[\delta^2 + (c+im)^2][\mu^2 + (2c+im)^2]} \\ &\quad \left. + \frac{e^{\mu r - (\mu+2ic)s}}{\mu[\delta^2 + (c-i\mu)^2][m^2 + (2c-i\mu)^2]} \right] \end{aligned} \quad (\text{A2-6})$$

Substituting special values for the parameters gives the results required in the text. Thus,

$$\begin{aligned} J(m, m, k, \gamma; l, l) &= e^{-2ikt} J(m, m, k, \gamma; 0, 0) \\ J(m, m, k, \gamma; -l, l) &= e^{2ikt} J(m, m, k, \gamma; 0, 2l) \\ J(m, m, k, \gamma; -l, 0) &= e^{2ikt} J(m, m, k, \gamma; 0, l) \\ J(m, m, c, \delta; 0, 0) &= \frac{2m(\delta + 2m)}{(c^2 + m^2)[c^2 + (m + \delta)^2]} \end{aligned} \quad (\text{A2-7})$$

which hold irrespective of any relations between the parameters. The derivation of the last result is simplified by setting  $\alpha = c + im$ ,  $\bar{\alpha} = c - im$  and factoring the denominators in (A2-6) so as to obtain terms of the form  $\bar{\alpha} \pm i\delta$ ,  $\alpha \pm i\delta$ .

When  $\gamma^2 = m^2 - k^2$  considerable simplification is possible and we obtain

$$\begin{aligned} J(m, m, k, \gamma; 0, 0) &= \frac{\gamma}{k^2} \left[ \frac{1}{\gamma} - \frac{m}{m^2 + k^2} \right] \\ J(m, m, k; \gamma, 0, l) &= \frac{\gamma e^{-ikt}}{k^2} \left[ \frac{e^{-\gamma l}}{\gamma} - \frac{e^{-ml}(m \cos kl - k \sin kl)}{m^2 + k^2} \right] \end{aligned} \quad (\text{A2-8})$$

If we put  $\mu = n - 1$ ,  $m = n + 1$ , and set  $\delta^2 = n^2 - 1 - c^2 = n^2 - \kappa^2$  where  $\kappa^2 = 1 + c^2$ , (A2-6) yields, after some reduction,

$$\begin{aligned} J(n-1, n+1, c, \delta; 0, 0) &= \frac{n^2 - 1}{(cn + i\delta)^2} + \frac{(n-1)\delta}{2(n+1)(1-ic)^2(n-ic)} \\ &\quad + \frac{(n+1)\delta}{2(n-1)(1-ic)^2(n+ic)} \\ &= \frac{c^2 n^2 - \delta^2}{\kappa^4(n^2 - 1)} + \frac{n\delta[2(n^2 + c^2) - \kappa^2(n^2 - 1)]}{\kappa^4(n^2 - 1)(n^2 + c^2)} \end{aligned} \quad (\text{A2-9})$$

The form of the final expression has been chosen so as to be suited to the use we shall make of it.

Another double integral which appears in our work is

$$I(k, \gamma) = \int_{-\infty}^{+\infty} dv_0 a(v_0) \cdot \int_{-\infty}^{\infty} dv a(v) \exp [-ik(v + v_0) - \gamma |v - v_0|] \quad (\text{A2-10})$$

where  $a(v)$  is an even function of  $v$  and is such that all of the integrals encountered converge. We begin our transformation by dividing the interval of integration  $(-\infty, \infty)$  for  $v_0$  into  $(-\infty, 0)$  and  $(0, \infty)$ . Making the change of variable  $v_0 = -v'_0$ ,  $v = -v'$  in the first interval, dropping the primes and using  $a(-v) = a(v)$  leads to

$$I(k, \gamma) = 2 \int_0^{\infty} dv_0 a(v_0) \int_{-\infty}^{\infty} dv a(v) e^{-\gamma |v - v_0|} \cos k(v + v_0) \quad (\text{A2-11})$$

We now split the interval of integration of  $v$  in (A2-11) into the intervals  $(-\infty, 0)$ ,  $(0, v_0)$ ,  $(v_0, \infty)$ . In  $(-\infty, 0)$  we change the variable from  $v$  to  $-v'$ , drop the prime, and use  $a(-v) = a(v)$ . By paying attention to the sign of  $v - v_0$  we may remove the absolute value sign. By changing the order of integration in the double integral arising from the third interval (in which  $0 \leq v_0 \leq \infty$ ,  $v_0 \leq v \leq \infty$ ) we may show that it is equal to the double integral arising from the second interval. Thus

$$I(k, \gamma) = 2 \int_0^{\infty} dv_0 a(v_0) \int_0^{\infty} dv a(v) e^{-\gamma v - \gamma v_0} \cos k(v_0 - v) \\ + 4 \int_0^{\infty} dv_0 a(v_0) \int_0^{v_0} dv a(v) e^{-\gamma v_0 + \gamma v} \cos k(v_0 + v) \quad (\text{A2-12})$$

When  $a(v)$ ,  $\gamma$  and  $k$  are real we may write (A2-12) as

$$I(k, \gamma) = 2 \left| \int_0^{\infty} dv a(v) e^{-\gamma v - ikv} \right|^2 \\ + 4 \text{Real} \int_0^{\infty} dv_0 a(v_0) e^{-\gamma v_0 + ikv_0} \int_0^{v_0} dv a(v) e^{\gamma v + ikv} \quad (\text{A2-13})$$

and when  $\gamma = ik$  we have

$$I(k, ik) = 2 \int_0^{\infty} dv_0 a(v_0) \int_0^{\infty} dv a(v) e^{-2ikv} \\ + 2 \int_0^{\infty} dv_0 a(v_0) \int_0^{v_0} dv a(v) [e^{2ikv} + e^{-2ikv_0}]. \quad (\text{A2-14})$$

## APPENDIX III

INTEGRAL EQUATION WHEN GUIDES ENTERING AND LEAVING IRREGULARITY  
ARE OF DIFFERENT SIZES

Here we shall indicate how the integral equation method may be extended to cover the case mentioned in the above title. It is supposed that only the dominant mode is propagated freely in both guides.

*E in Plane of Irregularity*

Let the notation for the guide carrying the incident wave be the same as for the *E*-corner.  $b$  denotes the narrow dimension of the guide and the quantities  $k$  and  $\gamma_m$  are given by (2-1). Both guides have the same wide

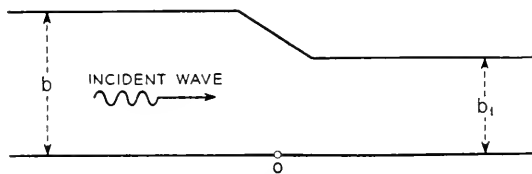


FIG. 3

dimension  $a$ . The narrow dimension of the guide shown on the right of Fig. 3 is  $b_1$ . We introduce the new quantity

$$k_1 = [(2b_1/\lambda_0)^2 - (b_1/a)^2]^{1/2} \quad (\text{A3-1})$$

to correspond to  $k$ . Since, by assumption, only the dominant mode is freely propagated in both guides both  $k$  and  $k_1$  are real positive quantities less than unity.

Let  $z = f(w)$  carry the system of Fig. 3 into a straight guide of width  $\pi$  in the  $w = v + i\theta$  plane (see Fig. 2), and let  $g(v, \theta)$  be defined by

$$1 + g(v, \theta) = |f'(w)|^2.$$

The behavior of  $g(v, \theta)$  at infinity is shown by the table

$v$	$dz/dw$	$g(v, \theta)$
$-\infty$	$b/\pi$	0
$+\infty$	$b_1/\pi$	$k_1^2 k^{-2} - 1$

where  $b_1/b = k_1/k$  has been used. It is convenient to introduce the approximation  $\hat{g}(v)$  to  $g(v, \theta)$ .  $\hat{g}(v)$  may be chosen at our convenience subject only to the conditions that it be differentiable,  $\hat{g}(-\infty) = 0$ , and  $\hat{g}(\infty) = k_1^2 k^{-2} - 1$ .

When we define  $G$  by equation (3-3) so that, as before, it is the Green's

function corresponding to a guide of width  $b$ , we may use equation (3-4) to derive the new integral equation

$$Q(v_0, \theta_0) = e^{-ikv_0} + \frac{k^2}{2\pi} \int_{-\infty}^{\infty} dv \int_0^{\pi} d\theta \cdot \{g(v, \theta)Q(v, \theta) - \hat{g}(v)T_B e^{-ik_1 v}\} G(v_0, \theta_0; v, \theta) + T_B F(v_0) \quad (\text{A3-2})$$

in which

$$\begin{aligned} F(v_0) &= e^{-ik_1 v_0} \hat{g}(v_0)/\hat{g}(\infty) - e^{-ikv_0} N^-(v_0) - e^{ikv_0} N^+(v_0) \\ N^-(v_0) &= 2^{-1} k(k_1 - k)^{-1} \int_{-\infty}^{v_0} \hat{g}'(v) e^{-i(k_1 - k)v} dv \\ N^+(v_0) &= 2^{-1} k(k_1 + k)^{-1} \int_{v_0}^{\infty} \hat{g}'(v) e^{-i(k_1 + k)v} dv \end{aligned} \quad (\text{A3-3})$$

Here  $\hat{g}'(v)$  denotes  $d\hat{g}(v)/dv$ . Equation (A3-2) and

$$\lim_{v \rightarrow \infty} Q(v, \theta) = T_B e^{-ik_1 v} \quad (\text{A3-4})$$

are to be solved for the unknown function  $Q(v, \theta)$  and the unknown quantity  $T_B$ . The method of successive approximations may be used in somewhat the same fashion as in the simpler case but we shall not give a general discussion.

The first approximations are found to be

$$T_B^{(1)} = 1/N^-(\infty), \quad R_B^{(1)} = -N^+(-\infty)/N^-(\infty) \quad (\text{A3-5})$$

where the  $N$ 's may be obtained by setting  $v_0 = \pm \infty$  in equations (A3-3).

One of the simplest choices for  $\hat{g}(v)$  is to let it be zero for negative values of  $v$  and to have the value  $\hat{g}(\infty) = k_1^2 k^{-2} - 1$  for positive values of  $v$ . Then

$$T_B^{(1)} = 2k(k_1 + k)^{-1}, \quad R_B^{(1)} = (k - k_1)(k + k_1)^{-1} \quad (\text{A3-6})$$

These are quite similar to the corresponding expressions for a transmission line which have been used extensively in wave guide work.

In working with these formulas, when  $k$  is small, it is sometimes convenient to use the result

$$\int_{v_1}^{v_2} dv \int_0^{\pi} d\theta g(v, \theta) = \pi^2 b^{-2} \int_{v_1}^{v_2} dv \int_0^{\pi} d\theta |f'(w)|^2 = (v_2 - v_1)\pi \quad (\text{A3-7})$$

where the evaluation of the double integral on the right is made easier by the fact that it represents the area in the original guide (in the  $(x, y)$  plane) enclosed by the lines corresponding to  $v = v_1$  and  $v = v_2$ .  $v_2$  and  $v_1$  are

chosen to be moderately large positive and negative numbers, respectively. It turns out that, when  $k_1$  and  $k$  are very small, this is related to the "excess capacity" localized at the irregularity whose effect must be added to that of the mismatch, indicated by (A3-6).

When the entering and leaving guides are of the same size it is still possible to use the formulas of this appendix.  $N^-(v_0)$  may be replaced by an expression which now has for its limiting value

$$N^-(\infty) = 1 + i(k/2) \int_{-\infty}^{\infty} g(v) dv \quad (\text{A3-8})$$

### *H in Plane of Irregularity*

Let the figure corresponding to the irregularity be Fig. 3 with  $b$  and  $b_1$  replaced by  $a$  and  $a_1$ , respectively. In addition to the quantities  $c$  and  $\kappa$  defined by equations (5-2) we define

$$\kappa_1 = 2a_1/\lambda_0, \quad c_1 = (\kappa_1^2 - 1)^{1/2} \quad (\text{A3-9})$$

where we assume  $\kappa$  and  $\kappa_1$  to lie between 1 and 2. At  $v = -\infty$   $P(v, \theta)$  still consists of the unit incident wave plus the reflected wave given by the first of equations (5-4) and  $g(v, \theta)$  is still zero. However, now, at  $v = \infty$ ,

$$\begin{aligned} P(v, \theta) &= T_H e^{-ic_1 v} \sin \theta \\ g(\infty) &= \kappa_1^2 \kappa^{-2} - 1 = \kappa^{-2}(c_1^2 - c^2) \end{aligned} \quad (\text{A3-10})$$

The integral equation for  $P(v, \theta)$  and  $T_H$  is

$$\begin{aligned} P(v_0, \theta_0) &= e^{-icv_0} \sin \theta_0 + \frac{\kappa^2}{2\pi} \int_{-\infty}^{\infty} dv \int_0^\pi \\ &\cdot d\theta \{ g(v, \theta) P(v, \theta) - g(v) T_H e^{*ic_1 v} \sin \theta \} G(v_0, \theta_0; v, \theta) \\ &+ T_H \sin \theta_0 F_H(v_0) \end{aligned} \quad (\text{A3-11})$$

in which

$$\begin{aligned} F_H(v_0) &= e^{-ic_1 v_0} g(v_0)/g(\infty) - e^{-icv_0} M^-(v_0) - e^{icv_0} M^+(v_0) \\ M^-(v_0) &= \kappa^2(2c)^{-1}(c_1 - c)^{-1} \int_{-\infty}^{v_0} g'(v) e^{-i(c_1 - c)v} dv \\ M^+(v_0) &= \kappa^2(2c)^{-1}(c + c_1)^{-1} \int_{v_0}^{\infty} g'(v) e^{-i(c_1 + c)v} dv \end{aligned} \quad (\text{A3-12})$$

First approximations are

$$T_H^{(1)} = 1/M^-(\infty), \quad R_H^{(1)} = -M^+(-\infty)/M^-(\infty) \quad (\text{A3-13})$$

which, when we choose  $\hat{g}(v)$  to be zero for  $v < 0$  and  $\kappa_1^2 \kappa^{-2} - 1$  for  $v > 0$ , become

$$T_H^{(1)} = 2c(c_1 + c)^{-1}, \quad R_H^{(1)} = (c - c_1)(c_1 + c)^{-1} \quad (\text{A3-14})$$

which again agrees with results obtained from transmission line considerations. When the entering and leaving guides are the same size we may use

$$M^-(\infty) = 1 + i\kappa^2(2c)^{-1} \int_{-\infty}^{\infty} \hat{g}(v) dv \quad (\text{A3-15})$$

It seems difficult to give any general rules for the choice of  $\hat{g}(v)$ . Since for  $R_H$  and  $T_H$ , the factor  $\sin \theta$  reduces the effect of the singularities on the walls of the transformed guide, the choice  $\hat{g}(v) = g(v, \pi/2)$  suggests itself. The factor  $\sin \theta$  is not present in the formulas for  $R_E$  and  $T_E$  and regions near the walls are more important. In this case the selection

$$\hat{g}(v) = \pi^{-1} \int_0^{\pi} g(v, \theta) d\theta$$

may be useful, especially since it allows us to use the result (A3-7) when  $k$  and  $k_1$  become small.

## APPENDIX IV

### VARIATIONAL EXPRESSIONS FOR REFLECTION COEFFICIENTS

The reflection coefficients are proportional to the stationary values of certain forms associated with the integral equations. In order to obtain these forms we proceed as follows. It is readily seen that the values of  $x_1$  and  $x_2$  which satisfy the symmetrical set of equations

$$\begin{aligned} a_{11}x_1 + a_{12}x_2 &= b_1 \\ a_{12}x_1 + a_{22}x_2 &= b_2 \end{aligned} \quad (\text{A4-1})$$

are the ones which make

$$J = a_{11}x_1^2 + 2a_{12}x_1x_2 + a_{22}x_2^2 - 2b_1x_1 - 2b_2x_2 \quad (\text{A4-2})$$

stationary when  $x_1$  and  $x_2$  are given small arbitrary increments. This stationary value of  $J$  is

$$J_s = -b_1x_1 - b_2x_2$$

If we take the integral equation to be the analogue of the set of linear equations, the reflection coefficient turns out to be proportional to  $J_s$ . In order to set down the actual expressions it is convenient to write  $r$  for

$(v, \theta)$  and  $dS$  for the element of area  $d\tau d\theta$  so that the integral equation (3-5) for  $Q(v, \theta)$  may be written as

$$Q(r_0) = e^{-ikv_0} + k^2(2\pi)^{-1} \int g(r)Q(r)G(r_0, r) dS \quad (\text{A4-3})$$

where the integration extends over the interior of the guide and  $G(r_0, r)$  denotes the Green's function (3-3).

If the number of equations in the set (A4-1) were increased from two to a large number  $N$ , the set of  $x$ 's would correspond, say, to the values of  $Q(r)$  or of  $g(r)Q(r)$ , and the  $b$ 's would correspond to the values of  $\exp(-ikv_0)$ . In any event, we take the analogue of  $J$  to be

$$\begin{aligned} J_E &= \int g(r)Q(r)[Q(r) - 2e^{-ikv}] dS \\ &= k^2(2\pi)^{-1} \iint g(r)Q(r)g(r_0)Q(r_0)G(r_0, r) dS_0 dS \end{aligned} \quad (\text{A4-4})$$

where the subscript  $E$  indicates that we are dealing with an electric corner. It may be verified,\* by giving  $Q(r)$  a small variation  $\delta Q(r)$ , that the function  $Q(r)$  which makes  $J_E$  stationary is the one which satisfies the integral equation (A4-3). Furthermore, when we assume  $Q(r)$  to satisfy the integral equation, the expression for  $J_E$  reduces to an integral which is proportional to the integral (3-6) for the reflection coefficient  $R_E$ . More precisely,  $R_E$  is given by

$$R_E = \frac{ik}{2\pi} [\text{Stationary value of } J_E] \quad (\text{A4-5})$$

It follows that if, by some means, we have obtained a fairly good approximation to  $Q$ , we may obtain a better approximation to  $R_E$  by computing  $J_E$  and using the formula

$$R_E \approx ik(2\pi)^{-1}J_E$$

When we use the first approximation  $\exp(-ikv)$  for  $Q$  to compute  $J_E$  it turns out that the above formula gives the third approximation,  $R_E^{(3)}$ , to the reflection coefficient.

The magnetic corner may be treated in much the same way. The integral equation (5-6) for  $P(v, \theta)$  becomes, in the notation of this appendix,

$$P(r_0) = e^{-icv_0} \sin \theta_0 + \kappa^2(2\pi)^{-1} \int g(r)P(r)G(r_0, r) dS \quad (\text{A4-6})$$

in which the  $v$  in  $dS = d\tau d\theta$  is integrated from  $-\infty$  to  $+\infty$  and  $\theta$  from 0 to  $\pi$ ,

\* See Courant and Hilbert, *Methoden der Mathematischen Physik*, Julius Springer, Berlin (1931), page 176, where a similar problem is treated.

as before, and  $G(r_0, r)$  now denotes the Green's function (5-5). We define  $J_H$  by

$$J_H = \int g(r)P(r)[P(r) - 2e^{-icr} \sin \theta]dS \\ - \kappa^2(2\pi)^{-1} \iint g(r)P(r)g(r_0)P(r_0)G(r_0, r) dS_0 dS. \quad (A4-7)$$

$J_H$  is stationary with respect to small variations in  $P(r)$  when  $P(r)$  satisfies the integral equation (A4-6). Furthermore, from the integral (5-7) for  $R_H$ ,

$$R_H = i\kappa^2(\pi c)^{-1} [\text{Stationary value of } J_H] \quad (A4-8)$$

which may be used in the same way as equation (A4-5) for  $R_E$ .

J. Schwinger has used variational methods with considerable success to deal with obstacles in wave guides.\* However, his variational equations differ somewhat from those given here. Some light on the relation between Schwinger's equations and the present one may be obtained by returning to the simple algebraic equations (A4-1) and (A4-2). A rough analogue of the expression required to be stationary in Schwinger's theory is

$$(a_{11}x_1^2 + 2a_{12}x_1x_2 + a_{22}x_2^2)/(b_1x_1 + b_2x_2)^2 \quad (A4-9)$$

The essential point here is that the stationary value of the expression corresponding to (A4-9) gives the value of an impedance or combination of impedances appearing in some equivalent circuit. Expression (A4-9) may be obtained by expressing  $J$ , defined by (A4-2), as a function of  $x_1$  and  $y = x_2/x_1$ .  $J$  is still to be made stationary but now it is a function of  $x_1$  and  $y$ . Solving  $\partial J/\partial x_1 = 0$  for  $x_1$  and setting this value of  $x_1$  in  $J$  gives the following function of  $y$

$$-(b_1 + b_2y)^2 (a_{11} + 2a_{12}y + a_{22}y^2)^{-1},$$

which is the stationary value of  $J$  with respect to variations in  $x_1$  when  $y$  is held constant. This function is still required to be stationary with respect to  $y$ . The same is true of its reciprocal which becomes (A4-9) when both numerator and denominator are multiplied by  $x_1^2$  and the definition of  $y$  used. When (A4-1) is replaced by a larger number of equations similar considerations lead to a generalized form of (A4-9). The expression required to be stationary by Schwinger is obtained when the sums in the generalized form are replaced by integrals.

\* An account of the method together with applications is given in "Notes on Lectures by Julian Schwinger: Discontinuities in Waveguides" by David S. Saxon. An account is also given by John W. Miles.<sup>11</sup>



## REFERENCES

1. Poritsky and Blewett, A Method of Solution of Field Problems by Means of Overlapping Regions, *Quart. Jl. Appl. Math.*, 3, 336-347 (1946).
2. J. W. Miles, The Equivalent Circuit of a Corner Bend in a Rectangular Wave Guide, *Proc. I. R. E.*, 35, 1313-1317 (1947).
3. N. Elson, Rectangular Wave Guide Systems, Bends, Twists and Junctions, *Wireless Engineer*, 24, 44-54 (1947).
4. E. J. Routh, Advanced Rigid Dynamics, 6th edition, pp. 461-467, London (1905).
5. P. Krasnooshkin, Acoustic and Electromagnetic Wave Guides of Complicated Shape, *Jl. of Physics (Acad. Sci. U.S.S.R.)*, 10, 434-445 (1946).
6. S. O. Rice, A Set of Second-Order Differential Equations Associated with Reflections in Rectangular Wave Guides—Application to Guide Connected to Horn, this issue of the B. S. T. J.
7. S. O. Rice, Reflections from Circular Bends in Rectangular Wave Guides—Matrix Theory, *B. S. T. J.*, 27, 305-349 (1948). In addition to the earlier work of R. E. Marshak referred to there, the interesting, but as yet unpublished, work of H. Levine should be mentioned. He uses variational methods to obtain the values of the impedances appearing in the equivalent network for the bend.
8. S. A. Schelkunoff, On Waves in Bent Pipes, *Quart. Jl. Appl. Math.*, 2, 171-172 (1944).
9. H. Buchholz, Der Einfluss der Krümmung von rechteckigen Hohlleitern auf das Phasenmass ultrakurzer Wellen, *E.N.T.*, 16, 73-85 (1939).
10. Montgomery, Dicke, and Purcell, Principles of Microwave Circuits, McGraw-Hill (1948), page 149.
11. J. W. Miles, The Equivalent Circuit for a Plane Discontinuity in a Cylindrical Wave Guide, *Proc. I.R.E.*, 34, 728-742 (1946).

## A Set of Second-Order Differential Equations Associated with Reflections in Rectangular Wave Guides—Application to Guide Connected to Horn\*

By S. O. RICE

In dealing with corners and similar irregularities in rectangular wave guides it is sometimes helpful to transform the system, conformally, into a straight guide. Propagation in the straight guide may then be studied by an integral equation method, as is done in a companion paper, or by a more general method based upon a certain set of ordinary differential equations. Here the second method is developed and applied to determine the reflection produced at the junction of a straight guide and a sectoral horn—a problem the first method is unable to handle. The *WKB* approximation for a single second-order differential equation is extended to a set of equations and approximate expressions for the reflection coefficient are derived.

**I**N A companion paper<sup>1</sup> the disturbance produced by a corner in a rectangular wave guide is examined by transforming the system, conformally, into a straight guide. Although the medium in the straight guide is no longer uniform, an integral equation may be set up and approximate solutions obtained.

In that paper the wave guide is assumed to have the same cross-section at  $+\infty$  as at  $-\infty$ . When this is not so, a conformal transformation may still be used to transform the system into a straight guide provided one dimension of the original cross-section is constant. However, now some advantage appears to be gained by replacing the integral equation by a set of differential equations. Since two cases appear, corresponding to *E* and *H* corners, there are two sets of equations to be considered.

These two sets of equations are studied in the present paper. After their derivation in Sections 1 and 2 several remarks are made in Section 3 concerning their solution, special emphasis being laid on the problem of determining the reflection coefficient. In the remainder of the paper the general theory is applied to a system formed by joining a rectangular wave guide to a horn (with plane sides) flared in one direction. The reflection coefficients for sectoral horns flared in the planes of the electric and magnetic intensity, respectively, are given approximately by equations (6-1) and (7-1). These approximations assume the angle of flare to be small so that, as it turns out, only the first equations of the respective sets need be considered.

As was mentioned in the companion paper, Robert Piloty has recently made use of conformal transformations in wave guide problems. In his

\* Presented at the Second Symposium on Applied Mathematics, Cambridge, Mass., July 29, 1948.

<sup>1</sup>See list of references at end of paper.

method the propagation function  $g(v, \theta)$  is derived graphically from the geometry of the wave guide irregularities and the result used in one or the other of two sets of differential equations which are equivalent to those derived below. Piloty's work is scheduled to appear soon in the *Zeitschrift für angewandte Physik* under the title "Ausbreitung el.-magn. Wellen in inhomogenen Rechteckrohren."

#### 1. Differential Equations when Electric Vector is in $(x, y)$ Plane

The partial differential equation to be solved is, from equation (2-3) of the companion paper<sup>1</sup>,

$$\frac{\partial^2 Q}{\partial v^2} + \frac{\partial^2 Q}{\partial \theta^2} + [1 + g(v, \theta)]k^2 Q = 0 \quad (1-1)$$

where

$$\frac{\partial Q}{\partial \theta} = 0 \text{ at } \theta = 0 \text{ and } \theta = \pi$$

$$1 + g(v, \theta) = 1 + \sum_{n=0}^{\infty} a_n \cos n\theta = |f'(v + i\theta)|^2 \pi^2 / b^2 \quad (1-2)$$

$$k = [(2b/\lambda_0)^2 - (b/a)^2]^{\frac{1}{2}}, \quad \lambda_0 = \text{free space wavelength}$$

In (1-2),  $z = x + iy = f(v + i\theta)$  is the transformation which carries the wave guide system in the  $(x, y)$  plane into the straight guide of width  $\theta = \pi$  in the  $(v, \theta)$  plane. For the sake of simplicity we shall always assume that far to the left the system becomes a straight wave guide of dimensions  $a, b$  ( $b < a$ ) such that only the dominant mode is propagated without attenuation. This insures that the  $a_n$ 's (which are functions of  $v$ ) will approach zero as  $v \rightarrow -\infty$ . The dimension (of our system) normal to the  $(x, y)$  plane is  $a$  throughout.

Since the normal derivative of  $Q$  vanishes on the walls at  $\theta = 0$  and  $\theta = \pi$  we assume

$$Q = F_0 + F_1 \cos \theta + F_2 \cos 2\theta + \dots, \quad (1-3)$$

where  $F_1, F_2, \dots$  are functions of  $v$ , and substitute it together with the Fourier series (1-2) for  $1 + g(v, \theta)$  in (1-1).

The equations obtained by setting the coefficients of the resulting cosine series to zero are

$$F_0'' + (1 + a_0)k^2 F_0 + \frac{k^2}{2} \sum_{n=1}^{\infty} a_n F_n = 0 \quad (1-4)$$

$$F_m'' + [(1 + a_0 + a_{2m}/2)k^2 - m^2]F_m + a_m k^2 F_0 + \frac{k^2}{2} \sum_{n=1}^{\infty} (a_{|n-m|} + a_{n+m})F_n = 0 \quad (1-5)$$

where  $m = 1, 2, 3, \dots$ ,  $F_m'' = d^2 F_m / dv^2$ , and the prime on  $\Sigma$  indicates that the term  $n = m$  is to be omitted. In grouping the terms we have assumed that  $F_0$  is the major part of  $Q$ .

The principal problem is to solve equations (1-4) and (1-5) when the fundamental mode  $F_0$  is of the form

$$\begin{aligned} F_0 &= e^{-ikv} + R_E e^{ikv}, & v \rightarrow -\infty \\ F_0 &= T_E(v), & v \rightarrow +\infty \end{aligned} \quad (1-6)$$

in which  $R_E$  is a constant and  $T_E(v)$  represents a wave traveling towards  $v = \infty$ . At  $v = \pm \infty$   $F_1, F_2, \dots$  have the form of waves traveling (or being attenuated) away from the region around  $v = 0$ . As before, we shall be mainly interested in determining the reflection coefficient  $R$ .

It is assumed that only the dominant mode is propagated without attenuation in the straight wave guide far to the left and hence  $F_1, F_2, \dots$  all become zero as  $v \rightarrow -\infty$ .

## 2. Differential Equations when Magnetic Vector is in $(x, y)$ Plane

The partial differential equation is now given by equation (5-1) of the companion paper<sup>1</sup>

$$\frac{\partial^2 P}{\partial v^2} + \frac{\partial^2 P}{\partial \theta^2} + [1 + g(v, \theta)] \kappa^2 P = 0 \quad (2-1)$$

where the dimension of the system normal to the  $(x, y)$  plane is now  $b$ ,  $a$  is the dimension (in the  $(x, y)$  plane) of the straight guide at the far left and

$$P = 0 \text{ at } \theta = 0 \text{ and } \theta = \pi$$

$$1 + g(v, \theta) = 1 + \sum_{n=1}^{\infty} a_n \cos n\theta \quad (2-2)$$

$$\kappa = 2a/\lambda_0, \lambda_0 = \text{free space wavelength}$$

$$c = (\kappa^2 - 1)^{1/2}$$

Since  $P = 0$  at  $\theta = 0$  and  $\theta = \pi$  we assume

$$P = \sum_{n=1}^{\infty} F_n \sin n\theta \quad (2-3)$$

where the  $F$ 's are functions of  $v$  to be determined by the equations

$$F_1'' + [\kappa^2(1 + a_0 - a_2/2) - 1]F_1 + \frac{\kappa^2}{2} \sum_{n=2}^{\infty} (a_{n-1} - a_{n+1})F_n = 0 \quad (2-4)$$

$$\begin{aligned} F_m'' + [\kappa^2(1 + a_0 - a_{2m}/2) - m^2]F_m + \frac{\kappa^2}{2} (a_{m-1} - a_{m+1})F_1 \\ + \frac{\kappa^2}{2} \sum_{n=2}^{\infty} (a_{|m-n|} - a_{m+n})F_n = 0 \end{aligned} \quad (2-5)$$

in which  $m = 2, 3, 4, \dots$  and the primes on  $F_m$  and  $\sum$  have the same significance as in (1-4) and (1-5).

The principal problem here is to solve equations (2-4) and (2-5) simultaneously subject to

$$\begin{aligned} F_1 &= e^{-icv} + R_H e^{icv}, & v &\rightarrow -\infty \\ F_1 &= T_H(v), & v &\rightarrow +\infty \end{aligned} \quad (2-6)$$

which again corresponds to a unit wave in the dominant mode incident from the left.  $T_H(v)$  and the remaining  $F$ 's correspond to outward traveling waves as before.  $F_2, F_3, \dots$  all approach zero as  $v \rightarrow -\infty$ .

### 3. Remarks on Solving the Equations of Sections 1 and 2 for the Reflection Coefficient

Suppose that we have a system in which the wave propagation is governed by the single differential equation

$$\frac{d^2 y}{dv^2} - h^2 y = 0 \quad (3-1)$$

where  $h \equiv h(v)$  is a positive imaginary function of  $v$ , twice differentiable and such that  $h \rightarrow ic$ ,  $c$  being a constant; as  $v \rightarrow -\infty$ . We desire the solution of (3-1) which, together with its first derivative, is continuous everywhere and at  $\pm\infty$  satisfies the conditions

$$y = e^{-icv} + R e^{icv}, \quad v \rightarrow -\infty \quad (3-2)$$

$$y' + (h + h'/(2h))y \rightarrow 0, \quad v \rightarrow \infty \quad (3-3)$$

The constant  $R$  (the reflection coefficient) is to be determined. Condition (3-3), in which the primes denote differentiation with respect to  $v$ , is suggested by the fact that we want  $y$  to represent a wave traveling in the positive  $v$  direction (the factor  $\exp(i\omega t)$  is suppressed). In writing (3-3) we have assumed that  $h$  is such that for large values of  $v$  the two solutions of (3-1) are asymptotically proportional to\*

$$y = h^{-1/2} e^{\pm \xi}, \quad (3-4)$$

$$\xi \equiv \xi(v) = icv + \int_{-\infty}^v (h - ic) dv. \quad (3-5)$$

Physical considerations suggest that solutions satisfying (3-2) and (3-3) exist in most cases of practical importance. However, if the function  $h$  is picked arbitrarily the corresponding solutions may be incapable of satisfying

\* S. A. Schelkunoff<sup>2</sup> mentions that this approximation, sometimes designated by "WKB", goes back to Liouville. The ideas we shall use are quite similar to those in Schelkunoff's paper.

the conditions. For example, if  $h = ic/(1 + \exp v)$  then  $h \rightarrow ic \exp(-v)$  as  $v \rightarrow \infty$ , and the solutions of (3-1) behave like Bessel functions of order zero and argument  $c \exp(-v)$ . It may be verified that these solutions do not satisfy (3-3). Again, condition (3-3) may be satisfied without  $y$  having much resemblance to an outgoing wave at  $v = \infty$ . Thus if  $h \rightarrow ia/v$  as  $v \rightarrow \infty$ ,  $y$  increases like  $v^n$  where  $n^2 - n - a^2 = 0$ . When  $0 < a < 1/2$  both values of  $n$  lie between 0 and 1, and both solutions satisfy (3-3). Despite these shortcomings it still seems best to retain (3-3) to specify the behavior of  $y$  at  $v = \infty$ .

It should be mentioned that P. S. Epstein<sup>3</sup> has obtained the reflected wave by transforming the hypergeometric differential equation into the form (3-1). This method has been extended by K. Rawer<sup>4</sup> who gives a number of references in which the approximation (3-4) is used to study propagation in a medium having a variable dielectric "constant". An interesting paper on the general subject of reflection in non-uniform transmission lines has been written by L. R. Walker and N. Wax<sup>5</sup>.

1. When most of the reflection occurs in a short interval, say near  $v = 0$   $R$  may be obtained by numerical integration of (3-1). One method is to start at  $v = 0$  with the initial conditions  $y = 1$ ,  $y' = 0$  and work outwards in both directions. Let  $\Gamma_a(v)$  denote this solution and  $\Gamma_b(v)$  the solution obtained by starting with  $y = 0$ ,  $y' = 1$ . The general solution is

$$y = C_1 \Gamma_a(v) + C_2 \Gamma_b(v). \quad (3-6)$$

$C_1$  and  $C_2$  are to be determined by the conditions

$$y = (\text{constant}) h^{-1/2} e^{-\xi} \quad , \quad v > v_2 \quad (3-7)$$

$$y = (ic/h)^{1/2} [e^{-\xi} + R e^{\xi}] \quad , \quad v < v_1 \quad (3-8)$$

where  $v_1$  and  $v_2$  are large negative and positive values, respectively, of  $v$ . These conditions lead to equations for  $C_1$ ,  $C_2$ ,  $R$ :

$$\begin{aligned} [y' + \theta^+ y]_{v=v_2} &= 0 \\ [y' - \theta^- y + 2(ich)^{1/2} e^{-\xi}]_{v=v_1} &= 0 \\ [y' + \theta^+ y - 2(ich)^{1/2} R e^{\xi}]_{v=v_1} &= 0 \end{aligned} \quad (3-9)$$

in which  $\xi$  is given by (3-5) and

$$\theta^{\pm} = h \pm h'/(2h). \quad (3-10)$$

The required value of  $R$  is obtained by letting  $v_1 \rightarrow -\infty$ ,  $v_2 \rightarrow \infty$  in the expressions, which follow from (3-9),

$$\begin{aligned}\gamma &= C_2/C_1 = -[(Y'_a + \theta^+ Y'_b)/(Y'_b + \theta^+ Y'_a)]_{v=v_2} \\ \Gamma &= [y'/y]_{v=v_1} = [(Y'_a + \gamma Y'_b)/(Y'_a + \gamma Y'_b)]_{v=v_1}\end{aligned}\quad (3-11)$$

$$R = [(\theta^+ + \Gamma)/(\theta^- - \Gamma)]_{v=v_1} \exp \left[ -2icv_1 - 2 \int_{-\infty}^{v_1} (h - ic) dv \right]$$

where the arguments of  $Y_a(v)$  and  $Y_b(v)$  have been omitted for brevity.

If  $h$  should change from a positive imaginary quantity to a positive real quantity in  $(v_1, v_2)$  and remain greater than some fixed positive number for  $v > v_2$  it may be shown that  $|R| = 1$  ( $\gamma$  and  $\Gamma$  are real and  $\text{Im } \theta^+ = \text{Im } \theta^-$ ,  $\text{Real } \theta^+ = -\text{Real } \theta^-$  at  $v = v_1$ ). This complete reflection is to be expected from physical consideration.

2. An exact expression for the reflection coefficient which holds when  $h$  satisfies the conditions following (3-1) (in particular it must not pass through zero anywhere in  $-\infty < v < \infty$ ) is

$$R = \frac{1}{2}(ic)^{-\frac{1}{2}} \int_{-\infty}^{\infty} e^{-\xi} y(v) \frac{d^2}{dv^2} h^{-\frac{1}{2}} dv \quad (3-12)$$

where  $\xi$  is given by (3-5). Before this integral for  $R$  may be evaluated  $y(v)$ , and hence  $R$  itself, must be known. Nevertheless, when  $R$  is small a useful approximation may be obtained by using the WKB approximation

$$y(v) \approx (ic/h)^{1/2} e^{-\xi} \quad (3-13)$$

Thus

$$\begin{aligned}R &\approx \frac{1}{2} \int_{-\infty}^{\infty} e^{-2\xi} h^{-\frac{1}{2}} \frac{d^2}{dv^2} h^{-\frac{1}{2}} dv \\ &= \frac{1}{2i} \int_{-\infty}^{\infty} e^{-2\xi} \left[ \frac{5}{16} K^{-5/2} \left( \frac{dK}{dv} \right)^2 - \frac{1}{4} K^{-3/2} \frac{d^2 K}{dv^2} \right] dv\end{aligned}\quad (3-14)$$

in which  $K = -h^2$ .

The expression (3-12) for  $R$  is obtained by letting  $v_0 \rightarrow -\infty$  in the integral equation

$$\begin{aligned}y(v_0) &= (ic/h_0)^{\frac{1}{2}} e^{-\xi_0} - \int_{-\infty}^{+\infty} G_a(v_0, v) y(v) h^{\frac{1}{2}} \frac{d^2}{dv^2} h^{-\frac{1}{2}} dv, \\ G_a(v_0, v) &= -\frac{1}{2} h_0^{-\frac{1}{2}} h^{-\frac{1}{2}} \begin{cases} e^{\xi - \xi_0}, & v < v_0 \\ e^{\xi_0 - \xi}, & v > v_0 \end{cases} \\ \xi_0 - \xi &= \int_v^{v_0} h dv, \quad h_0 \equiv h(v_0), \quad \xi_0 \equiv \xi(v_0).\end{aligned}\quad (3-15)$$

$G_a(v_0, v)$  is the approximate Green's function suggested by (3-13). The

integral equation may be obtained from the differential equation (3-1) and the boundary conditions (3-2) and (3-3) by the one-dimensional analogue of the method used in Section 3 of the companion paper<sup>1</sup>. If we multiply both sides of

$$\frac{d^2 y}{d\tau^2} - h^2 y = s(\tau) \quad (3-16)$$

(where  $s(\tau)$  has been added for generality) by  $G_a(\tau_0, \tau)$ , integrate twice by parts over the intervals  $(\tau_1, \tau_0 - \epsilon)$ ,  $(\tau_0 + \epsilon, \tau_2)$  with  $\epsilon > 0$  and  $\tau_1 < \tau_0 < \tau_2$ , and finally let  $\epsilon \rightarrow 0$  we obtain

$$y(\tau_0) = \int_{\tau_1}^{\tau_2} G_a(\tau_0, \tau) \left[ s(\tau) - y(\tau) h^2 \frac{d^2}{d\tau^2} h^{-\frac{1}{2}} \right] d\tau \\ + G_a(\tau_0, \tau_1) [y' - \theta^- y]_{\tau=\tau_1} - G_a(\tau_0, \tau_2) [y' + \theta^+ y]_{\tau=\tau_2}. \quad (3-17)$$

Equation (3-15) follows when we put  $s(\tau) = 0$  and let  $\tau_1 \rightarrow -\infty$ ,  $\tau_2 \rightarrow \infty$ . It will be recognized that (3-17) and (3-15) are closely related to integral equations occurring in the work of R. E. Langer<sup>6</sup> and E. C. Titchmarsh<sup>9</sup>.

When  $h$  has, for example, one or more simple zeros in  $-\infty < \tau < \infty$  the integral in (3-15) contains a factor which becomes infinite and the integral equation fails. However, we shall not concern ourselves with this case beyond remarking that it involves results obtained by H. Jeffreys<sup>10</sup>, Langer<sup>7</sup>, Furry<sup>11</sup> and others.

3. So far we have been considering the solution of only one equation whereas we really require the solution of a set of equations. If it is apparent that most of the disturbance is given by the first equation of the set it may be possible to proceed by successive approximations, each of the remaining equations being of the form (3-16) with  $s(\tau)$  determined by the solution of the first equation.

Another method of dealing with a system of  $N$  equations is that of numerical integration. As a contribution towards obtaining the boundary conditions at large positive and negative values of  $\tau$  we shall state a generalized form of the WKB solution. Although this solution is related to the general results obtained by Birkhoff<sup>12</sup>, Langer<sup>8</sup>, and Newell<sup>13</sup> concerning the asymptotic forms assumed by the solutions of a system of ordinary linear differential equations of the first order, it is worth mentioning explicitly.

Let the  $m$ th equation of the set be

$$\ddot{y}_m = \sum_{n=1}^N A_{mn} y_n, \quad m = 1, 2, \dots, N \quad (3-18)$$

where the  $A_{mn}$ 's are relatively slowly varying functions of  $\tau$  (see equations



(3-22) for a more precise statement of the assumptions) and the dots denote differentiation with respect to  $\tau$ . We shall reserve primes to denote transposition of matrices. It is supposed that  $A_{mn} = A_{nm}$  (equations (2-4) plus (2-5) satisfy this condition and (1-4) plus (1-5) may be made to do so by setting  $\tilde{F}_0 = 2^{1/2}F_0$ ).

The solution of (3-18) is approximately

$$y_m \approx \sum_{\ell=1}^N S_{m\ell} [e^{\xi_{\ell}} d_{\ell}^{-} + e^{-\xi_{\ell}} d_{\ell}^{+}] \quad (3-19)$$

where the  $d_{\ell}^{\pm}$  are the  $2N$  constants of integration and

$$\begin{aligned} \varphi_{\ell}^2 S_{m\ell} &= \sum_{n=1}^N A_{mn} S_{n\ell} \\ \varphi_{\ell} \sum_{n=1}^N S_{n\ell}^2 &= 1 \end{aligned} \quad (3-20)$$

$$\xi_{\ell} = \int_{v_{3\ell}}^v \varphi_{\ell} dv$$

serve to determine  $\varphi_{\ell}$ ,  $\xi_{\ell}$ , and  $S_{m\ell}$  (the last to within a plus or minus sign). We assume the  $N$  roots  $\varphi_1^2, \varphi_2^2, \dots, \varphi_N^2$  of the determinantal equation arising from the first of equations (3-20) to be unequal, and denote by  $\varphi_{\ell}$  that square root of  $\varphi_{\ell}^2$  which has a positive real part or, if the real part be zero, which has a positive imaginary part.  $v_{3\ell}$  is any convenient constant.

The approximation (3-19) may be obtained by setting the assumed form

$$y_m = g_m e^{\pm \xi}, \quad \xi = \int_{v_3}^v \varphi dv$$

in (3-18). The result is a set of  $N$  equations of which the  $m$ th is

$$\ddot{g}_m \pm 2\dot{g}_m \varphi \pm g_m \dot{\varphi} + g_m \varphi^2 = \sum_n A_{mn} g_n. \quad (3-21)$$

We also assume

$$|\dot{\varphi}| \ll |\varphi^2|, \quad |\ddot{g}_m| \ll |\dot{g}_m \varphi| \ll |g_m \varphi^2| \quad (3-22)$$

$$g_m = g_{m0} + g_{m1} + g_{m2} + \dots$$

where  $g_{mr}$  and its first two derivatives satisfy inequalities of the type

$$|g_{m0}| \gg |g_{m1}| \gg |g_{m2}| \dots$$

The first and second order terms in (3-21) give, respectively,

$$g_{m0} \varphi^2 - \sum_n A_{mn} g_{n0} = 0 \quad (3-23)$$

$$g_{m1} \varphi^2 - \sum_n A_{mn} g_{n1} = \mp 2 \dot{g}_{m0} \varphi \mp g_{m0} \dot{\varphi}. \quad (3-24)$$

The vanishing of the determinant of the coefficients of the  $g_{n0}$ 's in (3-23) determines  $N$  values of  $\varphi^2$ , the  $\ell$ th being  $\varphi_\ell^2$ . Once  $\varphi^2$  is selected the  $g_{n0}$ 's are determined to within a common multiplying factor (which may depend upon  $v$ ). This factor is then fixed to within a multiplying constant by the necessary and sufficient condition that (3-24) be consistent<sup>14</sup>, namely,

$$\sum_m h_m (2 \dot{g}_{m0} \varphi + g_{m0} \dot{\varphi}) = 0 \quad (3-25)$$

where  $h_m$  is any solution of the transposed system

$$h_m \varphi^2 - \sum_n A_{nm} h_n = 0.$$

Because  $A_{nm} = A_{mn}$  we may take  $h_n$  to be  $g_{m0}$ . Equation (3-25) may then be integrated and leads to the second of equations (3-20) when we set the constant of integration equal to unity and identify  $\varphi$  and  $g_{m0}$  with  $\varphi_\ell$  and  $S_{m\ell}$ , respectively. The first equation in (3-20) follows directly from (3-23).

Since equations (3-20) do not completely satisfy (3-24) ( $g_{m1}$  remains to be determined) our *WKB* solution for a set of equations is not, in a sense, as good an approximation as it is for a single equation. Nevertheless it still represents, just as in the case  $N = 1$ , the leading part of the asymptotic form approached as the  $A_{mn}$ 's vary more and more slowly with  $v$ .

In matrix form, the *WKB* approximation to the solution of

$$\dot{y} = Ay \quad (3-26)$$

is

$$y = Se^{\Xi} d^- + Se^{-\Xi} d^+ \quad (3-27)$$

where  $y$  and  $d^\pm$  are column matrices,  $A$  and  $S$  square matrices, and  $\exp(\pm \Xi)$  a diagonal matrix having  $\exp(\pm \xi_\ell)$  as the  $\ell$ th term in its principal diagonal. The element in the  $m$ th row and  $\ell$ th column of  $S$  is  $S_{m\ell}$  whence, from (3-20),

$$\begin{aligned} S\Phi^2 &= AS \\ S'S\Phi &= S\Phi S' = I \\ \dot{\Xi} &= \Phi \end{aligned} \quad (3-28)$$

where the primes denote transposition of elements,  $I$  is the unit matrix of order  $N$  and  $\Phi$  is the diagonal matrix having  $\varphi_\ell$  as the  $\ell$ th term in its principal diagonal. That the non-diagonal terms of  $S'S$  are zero follows from the first of equations (3-20) and from  $\varphi_\ell \neq \varphi_k$  if  $\ell \neq k$ .

Because of the second of equations (3-20), at least one of the  $S_{n\ell}$ 's becomes infinite as  $\varphi_\ell$  passes through zero. Hence we expect the approximate solutions to be valid only over intervals in which none of the  $\varphi_\ell$ 's become zero. When we hold fast to a given solution  $y_1, y_2, \dots, y_n$  of (3-18) as  $v$  passes through a value which makes one of the  $\varphi_\ell$ 's zero, we expect the set of constants  $d_\ell^\pm$  to be replaced by a new set (Stokes phenomenon). What is the relation between the new set and the old set? It may possibly be much the same as for the case  $N = 1$  (see Jeffreys<sup>10</sup>, Langer<sup>6</sup> and Furry<sup>11</sup>).

4. When the matrix  $A$  is such that the approximation (3-27) remains valid over the entire interval  $-\infty < v < \infty$  (unfortunately this restriction prevents us from applying the following results to the horn of Section 4) the matrix analogue of (3-15) is the integral equation

$$y(v_0) = S_0 e^{-\Xi_0} f^+ + \frac{1}{2} S_0 \int_{-\infty}^{v_0} e^{\Xi - \Xi_0} [\ddot{S}' + 2\Phi \dot{S}' + \dot{\Phi} S'] y(v) dv \quad (3-29)$$

$$+ \frac{1}{2} S_0 \int_{v_0}^{\infty} e^{\Xi_0 - \Xi} [\ddot{S}' - 2\Phi \dot{S}' - \dot{\Phi} S'] y(v) dv$$

where the subscript zero on  $S$  and  $\Xi$  indicates that they are to be evaluated at  $v = v_0$ . The column matrix  $y(v)$  giving the solution of (3-29) is that solution of  $\ddot{y} = Ay$  which satisfies the conditions

$$y = S e^{-\Xi} f^+ + S e^{\Xi} f^-, \quad v \rightarrow -\infty \quad (3-30)$$

$$y = S e^{-\Xi} g^+, \quad v \rightarrow \infty \quad (3-31)$$

where the column matrix  $f^+$  (corresponding to the incident wave) is given and  $f^-$  (corresponding to reflected wave) and  $g^+$  (corresponding to the transmitted wave) are to be determined. The elements of  $f^+$ ,  $f^-$ , and  $g^+$  are constants. It is further supposed that  $S$  satisfies the conditions

$$\dot{S}' S - S' \dot{S} = 0, \quad v \rightarrow \pm \infty$$

which are certainly met if the elements of  $A$  approach constants at  $\pm \infty$ . In the wave guide problem we assume  $\varphi_\ell$  to approach the limit  $\delta_\ell$  as  $v$  approaches  $-\infty$ . For this case it is convenient to define the  $\ell$ th element in the diagonal matrix  $\Xi$  as

$$\xi_\ell = \delta_\ell v + \int_{-\infty}^v (\varphi_\ell - \delta_\ell) dv$$

In any event we have

$$\Xi - \Xi_0 = \int_{v_0}^v \Phi dv$$

Although the *WKB* approximation has the same form as (3-30) in the region where  $v$  is finite, we regard (3-30) and (3-31) as being the exact limiting forms of  $y$ . Hence,  $g^+$  may differ from  $f^+$ .

Letting  $v_0 \rightarrow -\infty$  in (3-29) and comparing the result with (3-30) gives the exact result

$$f^- = \frac{1}{2} \int_{-\infty}^{\infty} e^{-\Xi} [\dot{S}' - 2\Phi\dot{S}' - \dot{\Phi}S']y(\tau) d\tau \quad (3-32)$$

which leads to an approximation for the reflected wave when  $y(\tau)$  is known approximately.

The integral equation (3-29) may be obtained by premultiplying both sides of  $\dot{y} = Ay$  by the transpose of the approximate Green's matrix

$$G_a(v_0, v) = \begin{cases} -\frac{1}{2}Se^{\Xi-\Xi_0}S'_0, & v < v_0 \\ -\frac{1}{2}Se^{\Xi_0-\Xi}S'_0, & v > v_0. \end{cases}$$

and integrating by parts twice. It is seen that each column of  $G_a(v_0, v)$  is an approximate solution of  $\dot{y} = Ay$ , in which the columnar constants of integration are the columns of  $S'_0$ , and represents a wave traveling away from  $v_0$  in both directions.  $G_a(v_0, v)$  is continuous at  $v = v_0$  and

$$\left[ \frac{\partial}{\partial v} G_a(v_0, v) \right]_{v=v_0+0} - \left[ \frac{\partial}{\partial v} G_a(v_0, v) \right]_{v=v_0-0} = S_0\Phi_0S'_0 = I$$

Thus the  $n$ th column of  $G_a(v_0, v)$  gives the approximate values of  $y_1(v)$ ,  $y_2(v)$ ,  $\dots$ ,  $y_n(v)$ , subject to the conditions that all these and all of their first derivatives are continuous at  $v = v_0$  except  $\dot{y}_n(v)$  which has the jump  $\dot{y}_n(v_0+0) - \dot{y}_n(v_0-0) = 1$ .

The presence of

$$\begin{aligned} 2\Phi\dot{S}' + \dot{\Phi}S' &= \Phi\dot{S}' - \Phi S'\dot{S}S^{-1} \\ &= \Phi(\dot{S}'S - S'\dot{S})S^{-1} \end{aligned}$$

in (3-29) and (3-32) makes the  $N$  variable case somewhat different from the case  $N = 1$ .

5. When  $Z_{mn}$  and  $\Gamma_{mn}$  are slowly varying functions of  $v$  the approximate solution of the transmission line equations

$$\begin{aligned} \frac{dV_m}{dv} &= - \sum_{n=1}^N Z_{mn} J_n \\ \frac{dJ_m}{dv} &= - \sum_{n=1}^N \Gamma_{mn} V_n \end{aligned} \quad (3-32)$$

where  $Z_{mn} = Z_{nm}$  and  $\Gamma_{mn} = \Gamma_{nm}$  is, as in (3-19),

$$\begin{aligned} V_m &\approx \sum_{\ell=1}^N S_{m\ell} [e^{\xi_\ell} d_\ell^- + e^{-\xi_\ell} d_\ell^+] \\ J_m &\approx \sum_{\ell=1}^N T_{m\ell} [e^{\xi_\ell} d_\ell^- - e^{-\xi_\ell} d_\ell^+]. \end{aligned} \quad (3-33)$$

Here  $\xi_\ell$  is the integral of  $\varphi_\ell$  as given by (3-20), and  $\varphi_\ell$  is determined by setting the determinant of the matrix  $\varphi^2 I - Z\Gamma$  to zero. When  $\varphi_\ell$  is known,  $S_{m\ell}$  and  $T_{m\ell}$  are determined (to within a plus or minus sign which may be absorbed by the constants  $d_\ell^\pm$  of integration) by the relations

$$\begin{aligned} \varphi_\ell S_{m\ell} &= - \sum_{n=1}^N Z_{mn} T_{n\ell} \\ \varphi_\ell T_{m\ell} &= - \sum_{n=1}^N \Gamma_{mn} S_{n\ell} \\ \sum_{n=1}^N S_{m\ell} T_{n\ell} &= 1 \end{aligned} \quad (3-34)$$

The last condition, which arises from the condition that the equations for the second-order terms be consistent, may be regarded as a generalization of Slater's<sup>15</sup> result for the case  $N = 1$ .

#### 4. Transformation for Wave Guide Plus Horn

The system to which we shall apply some of the preceding equations consists of a straight wave guide starting at  $x = -\infty$  and running to  $x = 0$  where it is connected to a sectoral horn. The horn is flared in the  $(x, y)$  plane only. The dimension of the system normal to the  $(x, y)$  plane is constant and equal to  $a$  or  $b$  according to whether the electric or magnetic vector is in the plane of the horn.

One might expect that the field in this system may also (in addition to our method) be determined by an alternating procedure of the type described by Poritsky and Blewett<sup>16</sup> using the equations obtained by Barrow and Chu<sup>17</sup> for transmission in the horn. However, we shall not investigate this possibility as we are primarily interested in using the system as an example to which we may apply the foregoing equations.

If the total angle of the horn is  $2\alpha\pi$ , and if the sides of the straight guide are at  $y = 0$  and  $y = b$ , (assuming the electric vector to be in the plane of the horn), the equation of the lower side, i.e., the continuation of the side  $y = 0$ , of the horn is  $y = -x \tan \alpha\pi$  and that of the upper side is  $y = b + x \tan \alpha\pi$ . If  $z = x + iy$  and  $w = v + i\theta$  then the Schwarz-Christoffel transformation

$z = f(w)$  which carries the guide plus horn in the  $z$  plane into the straight guide with walls at  $\theta = 0$ ,  $\theta = \pi$  in the  $w$  plane may be obtained from

$$\frac{dz}{dw} = (1 - e^{2w})^\alpha b/\pi \quad (4-1)$$

This gives, upon setting

$$\left| \frac{dz}{d\tau} \right|^2 = |f'(\tau + i\theta)|^2 = [1 - 2e^{2v} \cos 2\theta + e^{4v}]^\alpha b^2/\pi^2, \quad (4-2)$$

the relation

$$1 + g(v, \theta) = [1 - 2e^{2v} \cos 2\theta + e^{4v}]^\alpha$$

from which the  $a_n$ 's may be obtained in accordance with (1-2).

### 5. Expressions for the $a_n$ 's for Horn

The Fourier coefficients of  $1 + g(v, \theta)$  appearing in (1-2) and (2-2) are the same. It may be shown from (4-2) that

$$1 + a_0 = \begin{cases} e^{4\alpha v} F(-\alpha, -\alpha; 1; e^{-4v}) & , \quad v > 0 \\ \Gamma(1 + 2\alpha)/\Gamma^2(1 + \alpha) & , \quad v = 0 \\ F(-\alpha, -\alpha; 1; e^{4v}) & , \quad v < 0 \end{cases} \quad (5-1)$$

and

$$a_{2r} = \begin{cases} 2e^{4\alpha v - 2rv} (-\alpha)_r F(-\alpha, r - \alpha; r + 1; e^{-4v})/r! & , \quad v > 0 \\ 2(-\alpha)_r (1 + a_0)_{v=0}/(1 + \alpha)_r & , \quad v = 0 \\ 2e^{2rv} (-\alpha)_r F(-\alpha, r - \alpha; r + 1; e^{4v})/r! & , \quad v < 0 \end{cases} \quad (5-2)$$

where the  $F$ 's denote hypergeometric functions,  $r = 1, 2, \dots$  and we have used the notation

$$(\beta)_0 = 1, (\beta)_r = \beta(\beta + 1) \cdots (\beta + r - 1) \quad (5-3)$$

When  $n$  is odd,  $a_n = 0$  because of symmetry about  $\theta = \pi/2$ . The expressions for  $v > 0$  in (5-1) and (5-2) may be verified by expanding the two factors in

$$1 + g(v, \theta) = e^{4\alpha v} (1 - e^{2i\theta - 2v})^\alpha (1 - e^{-2i\theta - 2v})^\alpha$$

by the binomial theorem and picking out the terms containing  $e^{2ri\theta}$ . When  $v < 0$  we use the relation  $1 + g(v, \theta) = e^{4\alpha v} [1 + g(-v, \theta)]$ , and when  $v = 0$  we may sum the hypergeometric series.

Differentiation of (5-1) and (5-2) leads to

$$\frac{d}{dv} (1 + a_0) = \begin{cases} 4\alpha e^{4\alpha v} F(-\alpha, 1 - \alpha; 1; e^{-4v}) & , \quad v > 0 \\ 2\alpha(1 + a_0)_{v=0} & , \quad v = 0 \\ 4\alpha^2 e^{4v} F(1 - \alpha, 1 - \alpha; 2; e^{4v}) & , \quad v < 0 \end{cases} \quad (5-4)$$

$$\frac{d^2}{dv^2}(1 + a_0) = \begin{cases} 16\alpha^2 e^{4\alpha v} (1 - e^{-4v})^{2\alpha-1} F(\alpha, \alpha; 1; e^{-4v}), & v > 0 \\ 16\alpha^2 e^{4v} (1 - e^{4v})^{2\alpha-1} F(\alpha, \alpha; 1; e^{4v}), & v < 0 \end{cases} \quad (5-5)$$

where in obtaining (5-5) use was made of Euler's transformation

$$F(a, b; c; x) = (1 - x)^{c-a-b} F(c - a, c - b; c; x)$$

It is seen that  $d(1 + a_0)/dv$  is continuous at  $v = 0$  but the second derivative becomes infinite as  $v^{2\alpha-1}$ .

When  $1 + a_0$  and  $a_2$  are expressed as the customary integrals defining the Fourier coefficients it is seen that one of the coefficients occurring in equation (2-4) for  $F_1$  is given by

$$\begin{aligned} 1 + a_0 - a_2/2 &= \frac{2}{\pi} \int_0^\pi (1 - 2e^{2v} \cos 2\theta + e^{4v})^\alpha \sin^2 \theta d\theta \\ &= (e^{2v} + 1)^{2\alpha} F(-\alpha, \frac{1}{2}; 2; \operatorname{sech}^2 v) \end{aligned} \quad (5-6)$$

At  $v = 0$ ,  $1 + a_0 - a_2/2$  and its first and second derivatives are continuous, their values being

$$\begin{aligned} &\frac{\Gamma(2 + 2\alpha)}{\Gamma(1 + \alpha)\Gamma(2 + \alpha)}, \quad \frac{2\alpha\Gamma(2 + 2\alpha)}{\Gamma(1 + \alpha)\Gamma(2 + \alpha)}, \\ &\frac{4\alpha(2\alpha^2 + 2\alpha + 1)\Gamma(1 + 2\alpha)}{\Gamma(1 + \alpha)\Gamma(2 + \alpha)}, \end{aligned} \quad (5-7)$$

respectively. These may be obtained by differentiating the integral in (5-6) and setting  $v = 0$ .

A second expression for  $1 + a_0 - a_2/2$  follows from (5-1) and (5-2):

$$1 + a_0 - a_2/2 = \begin{cases} e^{4\alpha v} [F(-\alpha, -\alpha; 1; e^{-4v}) + \alpha e^{-2v} F(-\alpha, 1 - \alpha; 2; e^{-4v})], & v > 0 \\ F(-\alpha, -\alpha; 1; e^{4v}) + \alpha e^{2v} F(-\alpha, 1 - \alpha; 2; e^{4v}), & v < 0. \end{cases} \quad (5-8)$$

## 6. Approximation to Reflection Coefficient of Horn, Electric Vector in $(x, y)$ Plane

When the flare angle  $2\alpha\pi$  of the horn is very small the reflection coefficient may be shown to be

$$R_E = \frac{i\alpha}{2k} + 0(\alpha^2) \quad (6-1)$$

where  $0(\alpha^2)$  denotes correction terms of the order  $\alpha^2$ . This result is based upon the fact that when terms of order  $\alpha^2$  are neglected the set of differential equations (1-4) and (1-5) reduce to the single equation

$$F_0'' + (1 + a_0)k^2 F_0 = 0 \quad (6-2)$$

where, from (5-1, 4, 5),

$$\begin{array}{lll} v > 0 & & v < 0 \\ 1 + a_0 & e^{4\alpha v} & 1 \\ \frac{d}{dv}(1 + a_0) & 4\alpha e^{4\alpha v} & 0 \\ \frac{d^2}{dv^2}(1 + a_0) & 16\alpha^2 e^{4\alpha v}(1 - e^{-4v})^{2\alpha-1} & 16\alpha^2 e^{4v}(1 - e^{4v})^{2\alpha-1} \end{array}$$

The reflection coefficient (6-1) is the one corresponding to the differential equation (6-2) and may be computed by setting

$$(1 + a_0)k^2 = -h^2 = K \quad (6-3)$$

in the integrals (3-14).

The expression (6-1) for  $R_E$  may be obtained quickly (but the procedure is not trustworthy) by assuming that the principal contribution to the first integral in (3-14) comes from the region close to  $v = 0$ , say in  $-\epsilon < v < \epsilon$ , where the second derivative of  $h^{-1/2}$  is infinite but integrable. When the integration is performed approximately by replacing the second derivative by the first, (3-14) gives

$$\begin{aligned} R_E &\approx \frac{1}{2} \left[ h^{-\frac{1}{2}} \frac{d}{dv} h^{-\frac{1}{2}} \right]_{-\epsilon}^{+\epsilon} \\ &\approx \frac{1}{2ik} \left[ \frac{d}{dv} (1 + a_0)^{-\frac{1}{4}} \right]_{-\epsilon}^{\epsilon} = \frac{i\alpha}{2k} \end{aligned} \quad (6-4)$$

where  $\epsilon$  is assumed to be so small that  $1 + a_0$  is effectively unity and  $d(1 + a_0)/dv$  changes from 0 at  $-\epsilon$  to  $4\alpha$  at  $+\epsilon$ .

A more careful investigation based on the second integral in (3-14) also leads to the value (6-1) for  $R_E$ . It further suggests that possibly most of the correction term, denoted by  $0(\alpha^2)$  in (6-1), is given by

$$\frac{\alpha^2}{2ik} \int_0^\infty e^{-2\xi - 2\alpha v} dv = \frac{1}{4i\alpha} + \frac{e^{ix}}{4i} [Si(x) - \pi/2 + iCi(x)] \quad (6-5)$$

with  $x = k'\alpha$  and  $2\xi = ix[\exp(2\alpha v) - 1]$ .  $Si(x)$  and  $Ci(x)$  denote the integral sine and cosine functions. Incidentally, the rather curious result



$$\sum_{n=1}^{\infty} \sum_{m=1}^{\infty} \frac{1}{mn(m+n)} = 2 \sum_{n=1}^{\infty} \frac{1}{n^3}$$

turned up in the investigation of the orders of magnitude of the various terms.

### 7. Approximation to Reflection Coefficient of Horn, Magnetic Vector in $(x, y)$ Plane

The work of this section is quite similar to that in Section 6 except that here we enter into more of the details. We shall show that when  $\alpha$  is small the reflection coefficient appearing in equation (2-6) is

$$R_H = \frac{i\alpha}{2c^3} + O(\alpha^2). \quad (7-1)$$

From (2-4) the analogue of the differential equation (3-1) is

$$F_1'' + [\kappa^2(1 + a_0 - a_2/2) - 1]F_1 = 0 \quad (7-2)$$

and the  $K$  appearing in the second of equations (3-14) is now

$$K = -h^2 = \kappa^2(1 + a_0 - a_2/2) - 1 \quad (7-3)$$

The largest terms in the expression (5-8) for  $1 + a_0 - a_2/2$  yield, to within terms of  $O(\alpha)$ ,

$$\begin{aligned} K &= \kappa^2(e^{4\alpha v} + \alpha e^{-2v}) - 1, \quad v > 0 \\ \dot{K} &= \kappa^2(4\alpha e^{4\alpha v} - 2\alpha e^{-2v}) \end{aligned} \quad (7-4)$$

$$\ddot{K} = \kappa^2(16\alpha^2 e^{4\alpha v} + 4\alpha e^{-2v})$$

$$K = \kappa^2(1 + \alpha e^{2v}) - 1 = c^2 + \kappa^2 \alpha e^{2v}, \quad v < 0$$

$$\dot{K} = 2\alpha \kappa^2 e^{2v} \quad (7-5)$$

$$\ddot{K} = 4\alpha \kappa^2 e^{2v}$$

where the dots denote differentiation with respect to  $v$  and  $c^2 = \kappa^2 - 1$ . We have retained the  $\alpha^2$  in  $\ddot{K}$  as given by (7-4) because at this stage we do not know whether it may be neglected or not.

When  $v < 0$ , the definition (3-5) of  $\xi$  and (7-5) yield

$$\begin{aligned} \xi &= icv + i \int_{-\infty}^v (K^{\frac{1}{2}} - c) dv \\ &= icv + ic \int_{-\infty}^v [(1 + \kappa^2 c^{-2} \alpha e^{2v})^{\frac{1}{2}} - 1] dv = icv + O(\alpha) \end{aligned} \quad (7-6)$$

and we have

$$\begin{aligned}\int_{-\infty}^0 e^{-2\xi} K^{-5/2} \dot{K}^2 dv &= \int_{-\infty}^0 e^{-2icv} c^{-5} 4\alpha^2 \kappa^4 e^{4v} dv \\ &= 0(\alpha^2)\end{aligned}\quad (7-7)$$

which may be neglected. The other integral suggested by (3-14) is

$$\begin{aligned}\int_{-\infty}^0 e^{-2\xi} K^{-3/2} \dot{K} dv &= \int_{-\infty}^0 e^{-2icv} c^{-3} 4\alpha \kappa^2 e^{2v} dv \\ &= 2\alpha \kappa^2 c^{-3}/(1 - ic)\end{aligned}\quad (7-8)$$

When  $v > 0$ ,

$$\begin{aligned}\xi &= \xi_{v=0} + i \int_0^v [\kappa^2(e^{4\alpha v} + \alpha e^{-2v}) - 1]^{\frac{1}{2}} dv \\ &= i \int_0^v (\kappa^2 e^{4\alpha v} - 1)^{\frac{1}{2}} dv + 0(\alpha), \\ &= \frac{i}{2\alpha} [x - \tan^{-1} x - c + \tan^{-1} c] + 0(\alpha), \\ x &= (\kappa^2 e^{4\alpha v} - 1)^{\frac{1}{2}}, \quad 2\alpha dv = x(1 + x^2)^{-1} dx\end{aligned}\quad (7-9)$$

In the integrals containing  $\exp(-2v)$  as a factor,  $\xi$  may be taken to be  $icv$  since the integrand becomes negligibly small by the time  $icv$  differs significantly from (7-9). We have

$$\begin{aligned}\int_0^\infty e^{-2\xi} K^{-5/2} \dot{K}^2 dv &= \int_0^\infty e^{-2\xi} (\kappa^2 e^{4\alpha v} - 1)^{-\frac{1}{2}} \kappa^4 \alpha^2 (4e^{4\alpha v} - 2e^{-2v})^2 dv \\ &= \int_0^\infty e^{-2\xi} x^{-5} \kappa^4 \alpha^2 16e^{8\alpha v} dv \\ &= 8\alpha \int_c^\infty e^{-i[x - \tan^{-1} x - c + \tan^{-1} c]/\alpha} (x^{-4} + x^{-2}) dx\end{aligned}\quad (7-10)$$

where the integrals containing  $e^{-2v}$  and  $e^{-4v}$  have been neglected since their contribution is  $0(\alpha^2)$ . When  $\alpha$  becomes exceedingly small the exponential term oscillates rapidly and the last line of (7-10) is likewise  $0(\alpha^2)$ . This may be verified by integrating by parts, starting with

$$\begin{aligned}\exp \Gamma dx &= i\alpha x^{-2}(1 + x^2)d(\exp \Gamma), \\ \Gamma &= -i(x - \tan^{-1}x)/\alpha\end{aligned}$$

The last integral which must be considered is

$$\begin{aligned}
\int_0^\infty e^{-2\xi} K^{-3/2} \dot{K} dv &= \int_0^\infty e^{-2\xi} (\kappa^2 e^{4\alpha v} - 1)^{-1/2} \kappa^2 [16\alpha^2 e^{4\alpha v} + 4\alpha e^{-2v}] dv \\
&= 16\kappa^2 \alpha^2 \int_0^\infty e^{-2\xi} x^{-3} e^{4\alpha v} dv \\
&\quad + \int_0^\infty e^{-2icv-2v} c^{-3} \kappa^2 4\alpha dv \quad (7-11) \\
&= 8\alpha \int_c^\infty e^{-i[x-\tan^{-1}x-c+\tan^{-1}c]/\alpha} x^{-2} dx + 2\alpha\kappa^2 c^{-3}/(1+ic) \\
&= 0(\alpha^2) + 2\alpha\kappa^2 c^{-3}/(1+ic).
\end{aligned}$$

That the integral having  $x$  as the variable of integration is  $0(\alpha^2)$  may be shown as in (7-10).

When we combine our results in accordance with (3-14) we obtain

$$\begin{aligned}
R_H &= \frac{1}{2i} \int_{-\infty}^\infty e^{-2\xi} [\frac{5}{16} K^{-5/2} \dot{K} - \frac{1}{4} K^{-3/2} \dot{K}] dv \\
&= -\frac{\alpha\kappa^2 c^{-3}}{4i} \left[ \frac{1}{1-ic} + \frac{1}{1+ic} \right] + 0(\alpha^2) \quad (7-12) \\
&= i\alpha/(2c^3) + 0(\alpha^2)
\end{aligned}$$

which is (7-1).

If, instead of discarding (7-10) because it is  $0(\alpha^2)$ , we retain it and the corresponding integral in (7-11) (in the hope that they represent most of the difference between the approximate value (7-1) for  $R_H$  and the true value) we obtain the approximation

$$R_H = \frac{i\alpha}{2c^3} - \frac{i\alpha}{4} \int_c^\infty e^{-i(x-\tan^{-1}x-c+\tan^{-1}c)/\alpha} (5x^{-4} + x^{-2}) dx \quad (7-13)$$

in which the integral may be evaluated by numerical integration.

The approximations (6-1) and (7-1) for the reflection coefficients may also be obtained from an equation given by N. H. Frank.<sup>18</sup> However, care must be taken to suitably define the wave guide characteristic impedance which appears in his expression.

#### 8. Speculation on the Reflection Obtained from Horn Flared in Both Directions

All the work from Section 4 onward applies only to a horn flared in one plane. Nevertheless, it is interesting to speculate on how close an estimate of the reflection from a three-dimensional horn may be obtained by superposing the two reflection coefficients (6-1) and (7-1). It must be kept in mind that the flare angles (the  $\alpha$ 's) may be different in the two directions,

that  $k$  is given by (1-2) and  $c$  by (2-2), and finally the difference (not the sum) of  $R_E$  and  $R_H$  must be taken. In (6-1)  $R_E$  is the reflection coefficient of the component of the magnetic vector normal to the  $(x, y)$  plane (which is proportional to  $Q$ ), while in (7-1)  $R_H$  is the reflection coefficient of the transverse electric vector (which is proportional to  $P$ ) and there is a difference in sign just as in the case of voltage and current reflection coefficients. If  $a > b$  and  $\lambda_0$  is the wavelength in free space, the superposition gives the following expression for the reflection coefficient of the electric vector:

$$\begin{aligned} R &= R_H - R_E \\ &= \frac{i}{2} [(2a/\lambda_0)^2 - 1]^{-\frac{1}{2}} (\alpha_H / [(2a/\lambda_0)^2 - 1] - a\alpha_E/b) \end{aligned} \quad (8-1)$$

where  $2\pi\alpha_H$  and  $2\pi\alpha_E$  are the total horn angles in the planes of  $H$  and  $E$ , respectively. Of course this approximation can be expected to hold only when  $\alpha_H$  and  $\alpha_E$  are small.

### 9. Numerical Calculations— $R_H$ for $60^\circ$ Horn

The value of  $R_H$ , the reflection coefficient when the magnetic vector lies in the plane of the flare, was computed on the assumption that only the dominant mode need be considered.\* Thus, instead of the system of equations (2-4) and (2-5), only their simplified version, namely the single second order differential equation (7-2), was used. This equation may be written as

$$\frac{d^2 F_1}{dv^2} + K F_1 = 0 \quad (9-1)$$

where, according to (5-6),

$$\begin{aligned} K &= -h^2 = \kappa^2(1 + a_0 - a_2/2) - 1 \\ 1 + a_0 - a_2/2 &= (e^{2v} + 1)^{2\alpha} F(-\alpha, 1/2; 2; \operatorname{sech}^2 v). \end{aligned} \quad (9-2)$$

The problem was to obtain the  $R_H$  appearing in that solution  $F_1$  of (9-1) which satisfies the boundary conditions (2-6).

No computations for  $R_E$  were made.

In the first method of calculation the integrals in the approximation (3-14), namely

$$\begin{aligned} R_H &= \frac{1}{2i} \int_{-\infty}^{\infty} e^{-2\xi} K^{-1/4} \frac{d^2}{dv^2} K^{-1/4} dv \\ 2\xi &= 2icv + 2i \int_{-\infty}^v (K^{\frac{1}{2}} - c) dv, \end{aligned} \quad (9-3)$$

\* I am indebted to Miss M. Darville for carrying out the computations of this section.

were evaluated by Simpson's rule. The second derivative of  $K^{-1/4}$  was computed from the even order central differences of  $K^{-1/4}$ .<sup>19</sup> For  $\alpha = 1.6$ , corresponding to an angle of  $\pi/3$  between the two sides of the horn, calculations at two representative wave lengths led to the table

$\lambda_0$	$c$	$\kappa^2 = 1+c^2$	$R_H$	(9-4)
1.549a	.8173	1.6680	$-.0420 + i.0724$	
1.610a	.7376	1.5441	$-.0551 + i.0878$	

An idea of the variation of  $K$  may be obtained from its values at  $-\infty$ ,  $-.6$ ,  $0$ ,  $.6$ ,  $1.8$ ,  $3.6$  which are approximately  $.67$ ,  $.76$ ,  $.98$ ,  $1.62$ ,  $4.56$ ,  $17.4$ , respectively. The range of integration was  $-3 \leq v \leq 4.4$ .

The second method of computation used the formulas (3-11) with  $F_1$  playing the role of  $y$ . The differential equation (9-1) was integrated by the Kutta-Runge method, the interval between successive values of  $v$  being  $0.2$ . For  $c = .8173$  the values obtained were

$v_1$	$v_2$	$\gamma$	$\Gamma$	$R_H$	(9-5)
$-.6$	$.6$	$-.202 - i.981$	$-.142 - i.794$	$-.0167 + i.0658$	
$-1.2$	$1.2$	$-.218 - i1.004$	$-.049 - i.696$	$-.0525 + i.0754$	
$-1.8$	$1.8$	$-.225 - i.989$	$+.086 - i.716$	$-.0512 + i.0753$	
$-2.4$	$2.4$	$-.220 - i1.000$	$.136 - i.842$	$-.0424 + i.0722$	

In order to gain an idea of the meaning of these values of  $v$  it should be recalled that  $w = v + i\theta$  and the walls of the guide are at  $\theta = 0$  and  $\theta = \pi$ . An interval of length  $\pi = 3.14 \dots$  in the  $v$  direction therefore corresponds roughly to a distance equal to the width of the guide. The above table indicates that, loosely speaking, most of the reflection occurs close to the junction of the horn and wave guide.

The last value of  $R_H$  in (9-5) agrees quite well with the value  $-.0420 + i.0724$  obtained from the approximate expression (9-3). It appears that the method leading to (9-5) is superior to the one based on (9-3) since, in theory, it may be made as accurate (insofar as the single equation (9-1) may replace the set of equations (2-4, 5)) as desired. Moreover, less actual work seems to be required.

The approximation (7-1) yields, for  $c = .8173$ ,

$$R_H = \frac{i\alpha}{2c^3} = \frac{i(\frac{1}{6})}{2(.8173)^3} = i.153$$

which is considerably in error, as we might expect, since  $\alpha = 1.6$  is not small. However, if we use the approximation (7-13) and evaluate the integral by Simpson's rule we obtain

$$\begin{aligned}
 R_H &= i.153 - (.061 + i.077) \\
 &= -.061 + i.076
 \end{aligned}$$

which is in better agreement with the earlier values of  $R_H$ .

No similar computations have been made to test the corresponding approximation for  $R_E$  obtained when the correction term (6-5) is added to the leading term in (6-1). However, it appears that for  $\alpha = 1/6$  and the representative value  $k = .38$ , (6-5) is only about one sixth as large as  $i\alpha/(2k)$  and hence is relatively unimportant.

#### REFERENCES

1. S. O. Rice, Reflection from Corners in Rectangular Wave Guides—Conformal Transformation, this issue of the *B. S. T. J.*
2. S. A. Schelkunoff, Solution of Linear and Slightly Non-linear Differential Equations, *Quart. Jl. Appl. Math.*, **3**, 348-360 (1946).
3. P. S. Epstein, Reflection of Waves in an Inhomogeneous Absorbing Medium, *Proc. Natl. Acad. Sci.*, **16**, 627-637 (1930).
4. K. Rawer, Elektrische Wellen in einem geschichteten Medium, *Ann. der Physik*, **35**, 385-416 (1939).
5. L. R. Walker and N. Wax, Non-Uniform Transmission Lines and Reflection Coefficients, *Jl. Appl. Phys.*, **17**, 1043-1045 (1946).
6. R. E. Langer, The Asymptotic Solutions of Ordinary Linear Differential Equations of the Second Order, with Special Reference to the Stokes Phenomenon, *Bull. Amer. Math. Soc.*, **40**, 545-582 (1934). Many references to the earlier work are given.
7. R. E. Langer, On the Connection Formulas and the Solutions of the Wave Equation, *Phys. Rev.*, **51**, 669-676 (1937).
8. R. E. Langer, The Boundary Problem of an Ordinary Linear Differential System in the Complex Domain, *Trans. Am. Math. Soc.*, **46**, 151-190 (1939).
9. E. C. Titchmarsh, Eigen-function Transformations, Oxford (1946).
10. H. Jeffreys, On Certain Approximate Solutions of Linear Differential Equations of the Second Order, *Proc. London Math. Soc.*, (2), **23**, 428-436 (1924).
11. W. H. Furry, Two Notes on Phase Integral Methods, *Phys. Rev.*, **71**, 360-371 (1947).
12. G. D. Birkhoff and R. E. Langer, The Boundary Problems and Developments Associated with a System of Ordinary Linear Differential Equations of the First Order, *Proc. Amer. Acad. Arts and Sci.*, **58**, 49-128 (1923).
13. H. E. Newell, The Asymptotic Forms of the Solutions of an Ordinary Linear Matrix Differential Equation in the Complex Domain, *Duke Math. Jl.*, **9**, 245-258 (1942) and **10**, 705-709 (1943).
14. See, for example, Frank and von Mises, *Differential und Integralgleichungen*, Vol. 1, page 56, Braunschweig (1930).
15. J. C. Slater, *Microwave Transmission*, page 74, McGraw-Hill (1942).
16. Poritsky and Blewett, A Method of Solution of Field Problems by Means of Overlapping Regions, *Quart. Jl. Appl. Math.* **3**, 336-347 (1946).
17. Barrow and Chu, Theory of the Electromagnetic Horn, *Proc. I.R.E.*, **27**, 51-64 (1939).
18. N. H. Frank, Reflections from Sections of Tapered Transmission Lines and Wave Guides, *Radiation Lab. Rep.* 43-17, Jan. 6, 1943.
19. Whittaker and Robinson, *Calculus of Observations*, page 64, Blackie (1926).

## Abstracts of Technical Articles by Bell System Authors

*Pulse Echo Measurements on Telephone and Television Facilities.*<sup>1</sup> L. G. ABRAHAM, A. W. LEBERT, J. B. MAGGIO, and J. T. SCHOTT. Pulse echo measurements have been used on telephone and television facilities since 1940 to locate impedance irregularities and control quality in manufacture and installation. These sets send a pulse into a line and observe on an oscilloscope the echoes returned from irregularities. The shape and width of the pulse, the rate at which it is repeated and the pulse magnitude are important in determining the accuracy of the results and the requirements of the measuring apparatus. The "coaxial pulse echo set" is used for factory and field testing of coaxial cables. The "Lookator" was developed for use on much narrower band systems such as spiral-four field cable and open wire lines.

*Television Network Facilities.*<sup>2</sup> L. G. ABRAHAM and H. I. ROMNES. This paper describes television network facilities which are needed to connect studios and other pickup points to transmitters in the same and in distant cities, and discusses their transmission characteristics. Short-haul television circuits may be by microwave radio or over wire circuits. Long-haul television connections may be by radio relay or over coaxial systems of the type originally developed for carrier telephone circuits. Transmission requirements include adequate frequency band, accurate gain and phase equalization, and freedom from interference resulting from excessive noise, crosstalk, or modulation. Radio and wire systems are under development to provide extensive high-quality television networks.

*A Carrier Telephone System for Rural Service.*<sup>3</sup> J. M. BARSTOW. The M1 carrier telephone system was designed for the purpose of extending telephone service into areas served by rural power lines, but not served by co-existing rural telephone lines. To the local office operator and to a carrier subscriber the service provided is the same, so far as procedures involved in establishing a connection are concerned, as a voice-frequency line.

At the office end of the system a telephone wire line extends from the office to a point near the power line. Here is located a converter (called common terminal) which converts the voice-frequency signal to be transmitted to the subscriber to an amplitude-modulated double-sideband carrier signal. This signal is coupled to the power line through a coupling unit

<sup>1</sup> *Trans., A. I. E. E.*, vol. 66, 1947 (pp. 541-548).

<sup>2</sup> *Transactions, A. I. E. E.*, vol. 66, 1947 (pp. 459-464).

<sup>3</sup> *Trans. A. I. E. E.*, vol. 66, 1947 (pp. 501-507).

and high-voltage capacitor. At the subscriber's location the signal is taken off by similar means and led by separate wires to the subscriber premises, where it is reconverted to voice frequency by means of a subscriber terminal. A signal transmitted from the subscriber to the central office goes through similar conversions.

The usual number of parties per two-way channel may be assigned according to local custom, and divided-code or full-code ringing is provided. Equipment is available for five two-way channels over a single-power line employing frequencies in the range 150 to 425 kilocycles. A sixth channel has been discontinued because of radio interference.

A description is given of the manner in which the power line should be treated in order to reduce reflection effects. The power line treatment does not affect its capabilities in regard to power transmission.

*Application of Rural Carrier Telephone System.*<sup>4</sup> E. H. B. BARTELINK, L. E. COOK, F. A. COWAN,\* and G. R. MESSMER. This paper deals with the application of a carrier system developed primarily for providing rural telephone service over power distribution circuits in areas where this means of extending telephone service may be more attractive than other available methods. The modifications required in the power circuits to permit carrier frequency transmission are described, including the effect of these modifications on the operation of the power system. Construction features also are discussed. The use of the rural carrier telephone system over open wire telephone pairs is discussed briefly.

*An Improved Cable Carrier System.*<sup>5</sup> H. S. BLACK, F. A. BROOKS, A. J. WIER and I. G. WILSON. A new 12-channel cable carrier system is described which is suitable for transcontinental communications. Important features are negative feedback amplifiers of improved design, new arrangements for accurate equalization of the cable loss, and automatic thermistor regulators which continuously control the transmission of each system.

*Joint Use of Pole Lines for Rural Power and Telephone Services.*<sup>6</sup> J. W. CAMPBELL,\* L. W. HILL, L. M. MOORE, and H. J. SCHOLZ. The use of poles to carry both power and communication circuits is not new, having been employed before 1890. There are today more than 6,000,000 poles used jointly by power and telephone organizations in the United States. The great bulk of these poles are located in urban areas where the voltages of the power circuits concerned are generally less than 5,000 volts and the span lengths between poles generally do not exceed about 150 feet.

As power and telephone lines were extended into rural territory, new

<sup>4</sup> *Trans. A. I. E. E.*, vol. 66, 1947 (pp. 511-517).

<sup>5</sup> *Trans. A. I. E. E.*, vol. 66, 1947 (pp. 741-746).

<sup>6</sup> *Trans. A. I. E. E.*, vol. 66, 1947 (pp. 519-524).

\* Of Bell Tel. Labs.



problems were encountered in the application of joint construction because of the use of longer spans and higher voltages for the power circuits and the increased noise induction in the necessarily longer exposures. However, progress in the art through cooperation of the telephone industry with the Edison Electric Institute and the Rural Electrification Administration has brought about the developments reviewed in this paper which now make long span higher voltage rural joint use feasible where conditions are favorable.

*Atomic Energy.*<sup>7</sup> KARL K. DARROW. (*The 1947 Norman Wait Harris Lectures at Northwestern University.*) This little book, which reproduces four lectures substantially as they were given, is at once a very readable and a very accurate account of enough of the facts of nuclear physics to convey a good understanding of the atomic bomb and the possibilities of atomic power. The scientific accuracy of the presentation is instanced by the author's apologies for his title; he emphasizes that in reality his subject is *nuclear* energy, but that on the day of Hiroshima somebody wrote of an *atomic* bomb and the misuse spread like a chain reaction.

The role of electrons, protons and neutrons in atom building is told in a simple and entertaining style (but with a degree of ornamentation that may disturb some readers), and the discussion of rest mass and the Einstein relation between mass and energy is pointed up by well-chosen numerical illustrations beginning with the lightest composite nuclei. The role of fast-particle bombardment in increasing and decreasing the size of nuclei is also explained. The reader thus acquires a clear understanding of the basic phenomena for which nuclear fission is famed. The text is augmented by well-chosen cloud chamber photographs.

Though the author's treatment is accurate, his style and marshalling of facts are very readable. This is well illustrated by the closing paragraph of the third lecture, which follows immediately upon the author's development of the idea of the chain reaction:

Here is the climax of my lectures, and here is where you should be frightened; and if I had an orchestral accompaniment, here is where the orchestra would have mounted to a tumultuous fortissimo, with the drums rolling and the trumpets blaring and the tuba groaning and the strings in a frenzy, and whatever else a Richard Wagner could contrive to cause a sense of *Götterdämmerung*; for, let there be no doubt of it, this *is* something that could bring on the twilight of civilization. But at this crucial juncture I have only words to serve me, and all the words are spoiled. We speak of an awful headache, a dreadful cold, a frightful bore, and an appalling storm; and now when something comes along that is really awful and dreadful and frightful and appalling, all these words have been devaluated and have no terror in them. I have to fall back on the saying, of unknown origin and dubious value, that the strongest emphasis is understatement. Let then this picture, with its circles and its symbols and its numbers, be considered an emphatic understatement of the most terrific thing yet known to man.

<sup>7</sup> Published by John Wiley & Sons, Inc., New York, and Chapman & Hall, Ltd., London. 80 pages. \$2.00.

The book will be welcomed particularly by those who at one time or another have had a general acquaintance with radio-activity, cosmic rays and the results of cloud chamber research, but whose vocational activities have forced such special knowledge well into the nebulous regions of their memories.

*Network Theory Comes of Age.*<sup>8</sup> R. L. DIETZOLD. The third decade in the growth of modern network theory, the decade of maturity, is considered in this review of the advances in network theory evolved over the past ten years. New types of networks developed during the war are included.

*Thermistors as Components Open Product Design Horizons.*<sup>9</sup> K. P. DOWELL. These thermally sensitive resistors with high negative temperature coefficients have come a long way since they were laboratory curiosities and are now available in a wide range of types with diverse and stable characteristics. You may be able to transfer to your own problems some of the unusual design ideas described here.

*Gas Pressure for Telephone Cables.*<sup>10</sup> R. C. GIESE. Communication cables consist of a number of electric conductors insulated from one another and encased in a metal sheath. This encasement is subjected to numerous hazards, such as those caused by electrolysis, crystallization, various kinds of mechanical damage, and lightning burns. Any damage to the sheath which will permit water to enter the cable will decrease the effectiveness of the insulation material and thus cause an impairment or an interruption to the service. The entrance of moisture through small openings in the sheath can be materially retarded when the space inside the cable, not occupied by the conductors or insulation, is filled with a gas maintained under controlled conditions. Nitrogen is the gas usually used for this purpose because it is inert and does not combine chemically with the conductors or insulation. In addition the use of the gas provides a method of locating openings in the sheath by means of a pressure gradient, which is a material aid in cable maintenance.

*Rural Radiotelephone Experiment at Cheyenne Wells, Colo.*<sup>11</sup> J. HAROLD MOORE, PAUL K. SEYLER and S. B. WRIGHT. The first rural party-line telephone service by radio installations operating on the subscribers' premises was inaugurated August 20, 1946. This paper describes the equipment used, how it operates, and the results obtained during the preliminary testing and the initial period of regular operation. Radio is one of several new methods which the Bell System is exploring in its program for extension of telephone service in rural areas. It is expected that experience gained in

<sup>8</sup> *Electrical Engineering*, September 1948 (pp. 895-899).

<sup>9</sup> *Elec'l. Mfg.*, August 1948 (pp. 84-91).

<sup>10</sup> *Transactions, A. I. E. E.*, vol. 66, 1947 (pp. 471-478).

<sup>11</sup> *Trans. A. I. E. E.*, vol. 66, 1947 (pp. 525-528).

this experiment will aid in developing a standard rural radiotelephone system.

*Effect of Passive Modes in Traveling-Wave Tubes.*<sup>12</sup> J. R. PIERCE. As the beam current in a traveling-wave tube is increased, the local fields due to the bunched beam become appreciable compared with the fields propagating along the circuit. The effect is to reduce gain, to increase the electron speed for optimum gain, to introduce a lower limit to the range of electron speeds for which gain is obtained, and to change the initial loss.

*New Test Equipment and Testing Methods for Cable Carrier Systems.*<sup>13</sup> W. H. TIDD, S. ROSEN and H. A. WENK. Three portable test sets developed for the improved cable carrier telephone system are described: A high sensitivity selective transmission measuring set covering 10 to 150 kc, a decade oscillator for frequencies from 2 to 79 kc, and a tube test set.

*A New Microwave Television System.*<sup>14</sup> J. F. WENTZ and K. D. SMITH. A microwave point-to-point radio system is described which is designed for the transmission of television programs. This system is intended to supplement wire facilities for local distribution of television signals from pickup points to studios or from studios to broadcast transmitters and to long distance network terminals. The circuits and equipment are described in detail. Performance obtained in tests during 1946 is given.

<sup>12</sup> *Proc. I. R. E.*, August 1948 (pp. 993-997).

<sup>13</sup> *Trans. A. I. E. E.*, vol. 66, 1947 (pp. 726-730).

<sup>14</sup> *Transactions, A. I. E. E.*, vol. 66, 1947 (pp. 465-470).

## Contributors to this Issue

W. J. ALBERSHEIM, Technical Colleges, Aachen and Munich, Germany; B.Sc., Aachen, 1920; E.E., Aachen, 1922; Doctor of Engineering, Aachen, 1924; Professional Engineer, University of State of New York, 1937. Electrical Research Products, Inc., 1929-41; Bell Telephone Laboratories, 1941-. Dr. Albersheim was concerned with radar and jamming work during the war; he is now engaged in broadband FM transmission problems.

W. B. HEBENSTREIT, A.A., University of Chicago, 1935; B.S., California Institute of Technology, 1941. Bell Telephone Laboratories, 1941-47. While at the Bell Telephone Laboratories Mr. Hebenstreit worked on various microwave vacuum tubes including magnetrons, traveling wave tubes and the new double stream amplifier. He is now with the Hughes Aircraft Company.

A. V. HOLLENBERG, A.B., Willamette University, 1931; M.S., 1933, Ph.D., 1938, New York University; Instructor in Physics, Queens College, 1938-42. Columbia Radiation Laboratory, 1942-45; Bell Telephone Laboratories, 1946-. Dr. Hollenberg was engaged in research and development work on microwave magnetrons at the Columbia Radiation Laboratory. At Bell Telephone Laboratories he has been concerned with traveling wave amplifiers.

J. R. PIERCE, B.S. in Electrical Engineering, California Institute of Technology, 1933; Ph.D., 1936. Bell Telephone Laboratories, 1936-. Engaged in study of vacuum tubes.

S. O. RICE, B.S. in Electrical Engineering, Oregon State College, 1929; California Institute of Technology, 1929-30, 1934-35. Bell Telephone Laboratories, 1930-. Mr. Rice has been concerned with various theoretical investigations relating to telephone transmission theory.

SLOAN D. ROBERTSON, B.E.E., University of Dayton, 1936; M.Sc., Ohio State University, 1938, Ph.D., 1941; Instructor of Electrical Engineering, University of Dayton, 1940. Bell Telephone Laboratories, 1940-. Dr. Robertson was engaged in microwave radar work in the Radio Research Department during the war. He is now engaged in fundamental microwave radio research.

CLAUDE E. SHANNON, B.S. in Electrical Engineering, University of Michigan, 1936; S.M. in Electrical Engineering and Ph.D. in Mathematics, M.I.T., 1940. National Research Fellow, 1940. Bell Telephone Laboratories, 1941-. Dr. Shannon has been engaged in mathematical research principally in the use of Boolean Algebra in switching, the theory of communication, and cryptography.



# THE BELL SYSTEM TECHNICAL JOURNAL

DEVOTED TO THE SCIENTIFIC AND ENGINEERING ASPECTS  
OF ELECTRICAL COMMUNICATION

A Carrier System for 8000-Cycle Program Transmission  
*R. A. Leconte, D. B. Penick, C. W. Schramm, A. J. Wier* 165

Delay Equalization of Eight-Kilocycle Carrier Program  
Circuits.....*C. H. Dagnall and P. W. Rounds* 181

Band Pass Filter, Band Elimination Filter and Phase Simu-  
lating Network for Carrier Program Systems  
*F. S. Farkas, F. J. Hallenbeck, F. E. Stehlik* 196

A Precise Direct Reading Phase and Transmission Measur-  
ing System for Video Frequencies  
*D. A. Alsberg and D. Leed* 221

Physical Principles Involved in Transistor Action  
*J. Bardeen and W. H. Brattain* 239

Lightning Current Observations in Buried Cable  
*H. M. Trueblood and E. D. Sunde* 278

The Electrostatic Field in Vacuum Tubes with Arbitrarily  
Spaced Elements....*W. R. Bennett and L. C. Peterson* 303

Transconductance as a Criterion of Electron Tube  
Performance.....*T. Slonczewski* 315

Abstracts of Technical Articles by Bell System Authors.... 329

Contributors to this Issue..... 332

AMERICAN TELEPHONE AND TELEGRAPH COMPANY  
NEW YORK

# THE BELL SYSTEM TECHNICAL JOURNAL

*Published quarterly by the  
American Telephone and Telegraph Company  
195 Broadway, New York, N. Y.*

---

## EDITORS

R. W. King

J. O. Perrine

## EDITORIAL BOARD

C. F. Craig

O. E. Buckley

O. B. Blackwell

M. J. Kelly

H. S. Osborne

A. B. Clark

J. J. Pilliod

F. J. Feely

---

## SUBSCRIPTIONS

Subscriptions are accepted at \$1.50 per year. Single copies are 50 cents each.  
The foreign postage is 35 cents per year or 9 cents per copy.

---

Copyright, 1949

American Telephone and Telegraph Company

PRINTED IN U. S. A.



# The Bell System Technical Journal

Vol. XXVIII

April, 1949

No. 2

---

## A Carrier System for 8000-Cycle Program Transmission

By R. A. LECONTE, D. B. PENICK, C. W. SCHRAMM, A. J. WIER

With the rapid expansion of broad-band carrier telephone systems throughout the country, the use of these facilities for program transmission has become desirable. This paper describes a carrier program system capable of transmitting a band up to about 8000 cycles wide.

### INTRODUCTION

FROM the beginning of radio the Bell System has supplied the broadcasting industry the needed interconnecting links between broadcasting stations, studios, and other program originating points. For many years these facilities have been provided at audio frequency over loaded cable pairs,<sup>6</sup> or over open-wire lines.<sup>8</sup> Because present growth of message facilities over main traffic routes is predominantly in broad-band carrier telephone circuits, it has become desirable to adapt these new carrier facilities for the transmission of high-quality program material.

The carrier program system to be described operates in conjunction with message circuits and can be used to provide a band width of either 5000 or 8000 cycles. It can be applied to type K multipair cable,<sup>9</sup> type L coaxial cable,<sup>16</sup> and type J open-wire carrier systems.<sup>11</sup> Use of the 8000-cycle band of course requires more complete equalization than the 5000-cycle band, and requires the frequency space normally occupied by three message channels. It is expected that the 5000-cycle band can be accommodated by displacing two message channels. The carrier program system was developed by 1942 but, owing to the war, its first commercial application was not made until early in 1946 on the transcontinental type K route west of Omaha. It is now in use in all sections of the country, particularly the west and south, on type L as well as type K systems and has been successfully tested on type J. In general, a band width of 5000 cycles is used in these applications.

### OBJECTIVES

Existing audio-frequency program circuits may be as long as 7000 miles, may have 100 or more dropping or bridging points, any one of which may occasionally transmit to all of the others, and may be arranged for automatic reversal of the direction of transmission by means of a control signal.

In order to coordinate with these existing circuits and studio loops, a carrier program system must be capable of duplicating this flexibility while maintaining the desired standards of quality of transmission.

In setting an objective for the standards of transmission quality of this new system the trend towards wider band widths has been recognized. Most of the major networks now use a 100 to 5000-cycle band width. A large part of the present audio-frequency cable facilities, however, can be arranged to transmit a band from 50 to 8000 cycles. It was decided to match this grade of transmission in the design of the new carrier system. For the cases where still higher quality is desired, a 15-kilocycle carrier program system has been developed and is now available.

### DESIGN FEATURES

The 12-channel bank of message circuits forms the basic building block of the broad-band carrier telephone systems. In the channel bank, each of the 12 voice-frequency channels modulates one of 12 carriers spaced 4 kilocycles apart from 64 to 108 kilocycles. The lower sideband resulting from each modulation is selected by a band filter and combined with the other 11 lower sidebands to give a channel group occupying the frequency space from 60 kilocycles to 108 kilocycles. This channel group is then further modulated as a unit to its appropriate place on a broad-band spectrum for transmission over the line.

In order to arrange a channel bank for program transmission, message channels, 6, 7, and 8 are disabled, clearing a space from 76 kilocycles to 88 kilocycles in the group-frequency spectrum. In a program terminal separate from the channel bank, an audio frequency program modulates an 88-kilocycle carrier derived from the message channel carrier supply. Its lower sideband is selected by a band filter and, combined with the lower sidebands of message channels 1 to 5 and 9 to 12, gives a group-frequency spectrum shown diagrammatically in Fig. 1. This figure also shows the same spectrum after it has been modulated with a 120-kilocycle group carrier for transmission over a type K line. Other line-frequency spectra are similarly produced in type J and type L group modulators.

The reversing and control signal in an audio-frequency program circuit is a d-c. signal superimposed on the program pair. It may be applied at the studio which originates the program, and conditions all of the amplifiers along the line to transmit away from the originating studio. As long as the signal is applied, the direction of transmission is locked so that no other control station can inadvertently break the network. When the transmission from this studio ends, the signal is removed, and the next originating point applies it. This effects such reversals as are required for transmission and again locks all amplifiers. By this means it is possible to use

a single pair of wires and one set of amplifiers for transmission in either direction as required. The carrier system over which the carrier program channel is transmitted is constantly in operation in both directions simultaneously, and therefore requires no reversal. The program terminal itself, however, must be switched between transmitting and receiving lines if equipment is not to be needlessly duplicated for transmitting and receiving. In any case, a control signal must be carried through the carrier circuit and delivered to connecting audio-frequency circuits at the receiving end as a d-c. signal. This is accomplished by means of a 78-kilocycle control signal (42 kilocycles at K line frequencies) which is transmitted along

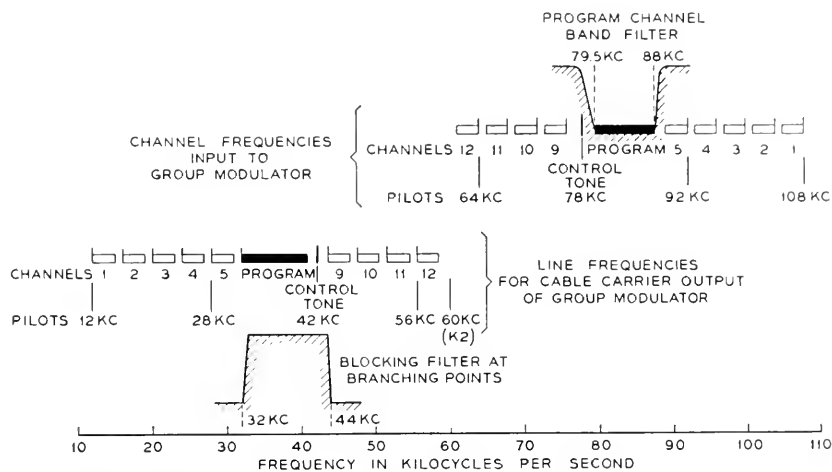


Fig. 1—Frequency allocation for one program channel and nine message channels in cable carrier systems.

with the program channel outside of its frequency band. This signal is generated in the transmitting program terminal whenever the d-c. signal is impressed from the transmitting audio-frequency circuit. At the receiving program terminal, the tone is converted into a d-c. signal which is impressed on the receiving voice-frequency facility. When there is no transmitted d-c. signal, there is no high-frequency signal and no received d-c. signal. Each program terminal, then, is ready either to receive d-c. from the voice circuit and send out 78 kilocycles to the carrier circuit or to receive 78 kilocycles from the carrier circuit and send out d-c. to the voice circuit. The program transmission path is maintained in the last established direction, regardless of the presence or absence of control, until a reversing signal is received.

The arrangement of the circuit elements in a carrier program terminal is shown in the block schematic of Fig. 2. The transmission circuit wiring is

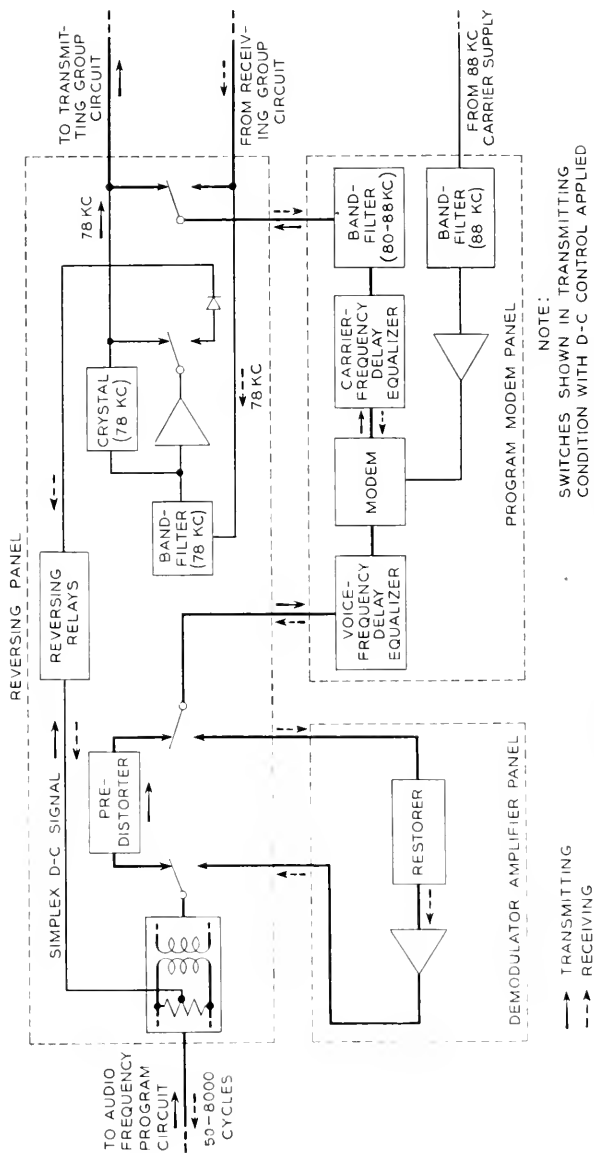


Fig. 2—Block schematic of carrier program terminal.

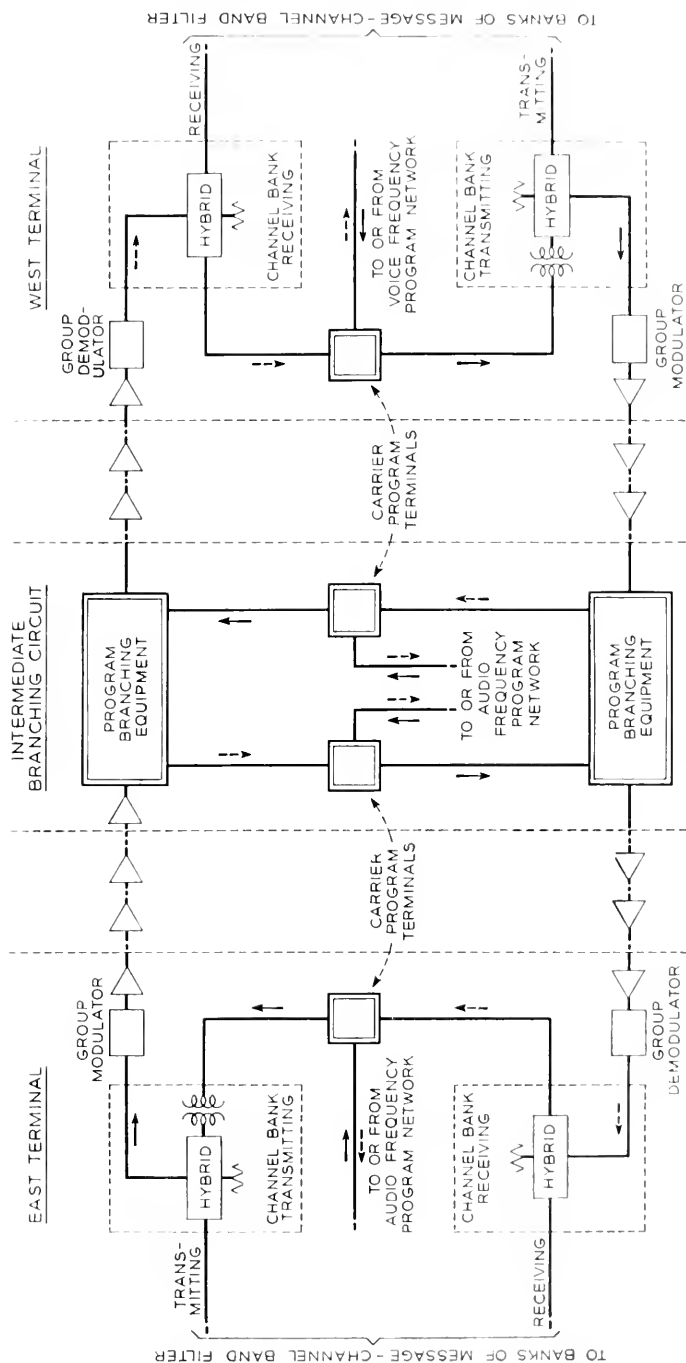


Fig. 3—Program link of cable carrier system with one intermediate branching point.

shown in heavy lines. The reversing and control circuits, indicated in light lines, are permanently connected to the external audio-frequency circuit and to the transmitting and receiving carrier line circuits regardless of the condition of the switching relays. Figure 3 shows a carrier program system including two terminals and a branching point as it is connected to a type K system. The program equipment is identified by double-line blocks. The carrier program terminals are connected into the networks in the same way as the audio-frequency facilities, through equalizers, amplifiers, bridges, and reversing circuits. Connected as one leg of a reversible bridge, a carrier program circuit may feed or be fed by any of the other legs, which may include cable, open-wire, studio loop, or other carrier circuits.

### TERMINAL CIRCUIT

As Fig. 2 indicates, a carrier program terminal consists of three elements: a modulator-demodulator or modem, a demodulator amplifier, and a reversing and control circuit. The heart of the terminal is the modem, which translates the program material from its original audio band to its desired position in the carrier-frequency spectrum or vice versa. It consists essentially of the non-linear varistor to which the carrier and program material are applied, and the band filter which selects the desired sideband from the modulation products. The varistor is connected in the double-balanced bridge arrangement in which the signal, carrier, and sideband circuits are each balanced against the other two. It is composed of copper-oxide elements and, in order to meet the conflicting requirements for high carrier-to-signal ratio and low transmitted carrier leak, a high degree of balance between the varistor bridge arms must be maintained. This is accomplished by building up each bridge arm of 16 copper-oxide elements connected in series-parallel. This modulator as compared to one using single-element bridge arms, has the same impedance, 12 decibels better carrier balance, 12 decibels greater carrier power capacity, and with the higher carrier power, 12 decibels lower non-linear distortion products. An amplifier provides the required power and a narrow-band filter gives additional suppression to carrier frequencies of other channels which are fed from the same carrier supply.

The band filter, which represents a major development in itself and is described in another paper,<sup>17</sup> introduces a considerable amount of delay distortion. This is corrected by delay equalizers incorporated in the modem circuit as shown in Fig. 2. Most of the delay correction is done in the audio-frequency branch of the circuit by a 31-section network which also includes equalization for the small residual attenuation distortion of the filter in its pass band. At the lower end of the audio-frequency band, however, attainment of the required phase characteristic with audio-frequency elements is

more difficult. Consequently, the delay correction for that portion of the band below 1000 cycles is actually done at sideband frequency, using quartz crystal elements. The design of these delay equalizers is described in another paper.<sup>13</sup> Transmission through the resulting modem unit is essentially constant in both attenuation and delay over the usable frequency range.

The demodulator amplifier is a conventional two-stage resistance-coupled amplifier. It is stabilized by 25 decibels of feedback to a nominal gain of 38 decibels, variable over a 12-decibel range by a potentiometer in the feedback circuit. The transmission characteristic is flat within 0.3 decibel over the 35 to 15,000-cycle frequency range. The output impedance is stabilized by the use of an output bridge for obtaining the feedback voltage. This amplifier feeds a  $-10$  vu point in the circuit and can deliver up to  $+18$  decibels above one milliwatt of output. Noise is kept to a minimum by operating the input stage vacuum tube at reduced voltages, mounting it and the magnetically shielded input transformer on a vibration-reducing suspension, and providing heavy filtering for the A and B battery circuits.

The limiting source of noise in any communication system is usually the transmission medium. In the carrier program system, the transmission medium is a carrier system which introduces noise energy equally distributed over the program band. The program energy being transmitted, however, is heavily concentrated at the lower frequencies. In order to increase the signal-to-noise ratio without an increase in total transmitted power, a predistorting network is introduced ahead of the modem, which attenuates the lower frequencies relative to the higher. The total discrimination is about 18 decibels, distributed symmetrically on a logarithmic frequency scale above and below 1500 cycles. A restoring network having an inverse characteristic is inserted in the receiving program path to return the program energy distribution to normal. The noise improvement thus obtained is about 7 decibels.

The reversing circuit consists of a set of five relays and a 78-kilocycle amplifier-oscillator. Two of these relays, as shown in Fig. 4, set up the transmission circuits for transmitting or receiving. The transmitting relay connects the predistorer in the audio-frequency circuit and connects the modem output to the transmitting high-frequency line. The receiving relay connects the modem to the receiving high-frequency line and inserts the restorer and demodulator amplifier in place of the predistorer. These relays are interlocked so that only one at a time can be operated. Their operation is supervised by two other relays, one transmitting and one receiving, which respond to the transmitting and receiving control signals respectively. The supervisory relays are similarly interlocked so that the control signal from only one direction at a time can be effective. They are

so connected to the transmission relays that, when no control signal is applied, both supervisory relays are released and the transmission relays maintain the circuit condition established at the last reversal.

A two-stage, tuned, feedback-stabilized amplifier is used to raise the level of the 78-kilocycle receiving control signal selected from the receiving high-frequency line by a narrow-band crystal filter. A copper-oxide rectifier converts the amplified signal to d-c. to operate a sensitive relay connected

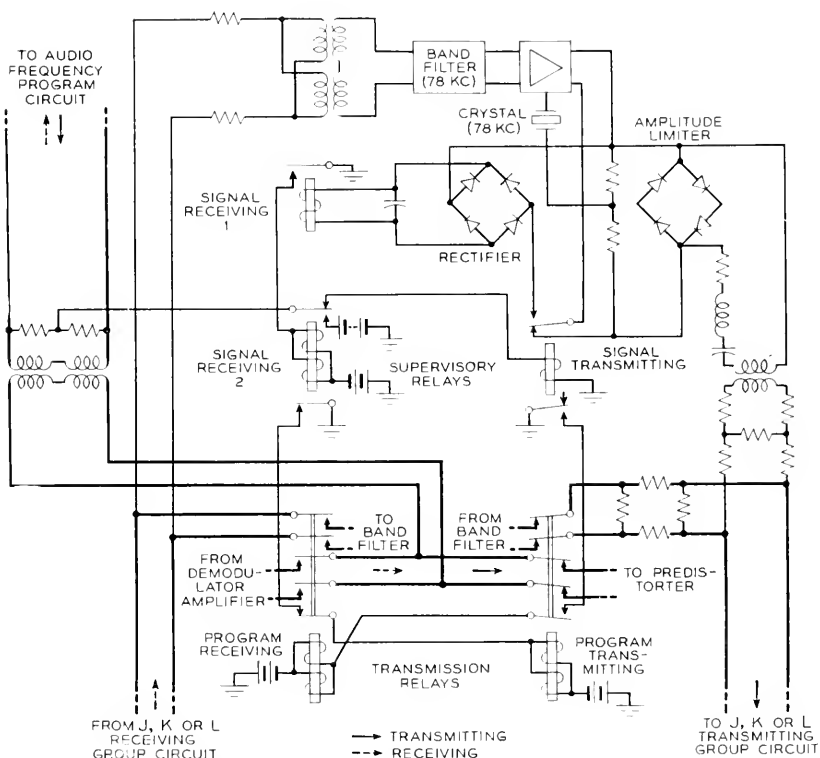


Fig. 4—Schematic of reversing and control circuit.

to the receiving supervisory relay. The supervisory relay, besides controlling the transmission circuits, also sends on a control signal as a d-c. simplex on the audio-frequency pair leaving the program terminal.

The same 78-kilocycle amplifier used for receiving the control signal is also used as an oscillator to generate the high-frequency control signal in the transmitting direction. The transmitting supervisory relay, under the control of a d-c. control signal coming in on the audio-frequency pair, disconnects the receiving control signal rectifier and connects instead a vari-



tor limiter across the output and a 78-kilocycle crystal from the output to the input, phased for positive feedback.

### TYPE K BRANCHING CIRCUIT

Because of the operating requirements of a radio broadcasting network there is need for complete switching flexibility. On a national network there may be scores of intermediate points, where the program must be tapped for local broadcasting and may originate in the case of special events. If, to obtain this flexibility, the network were made up of short carrier links, bringing the program down to audio frequencies at the end of each link, there would be in some cases, between the originating studio and the most distant broadcasting station, 50 to 100 or more links in tandem, involving double that number of band filters. Terminal phase and attenuation distortion, however, are proportional to the number of links. By means of advanced filter and equalizer designs, the present system has been made suitable for about 10 to 13 links in tandem. Additional arrangements therefore are needed at intermediate points to serve local broadcasters, without breaking in on the through program transmission. The branching circuit serves this need. End branching circuits which split off a program circuit from a carrier message route are needed for some network branches and are less elaborate than the through branching circuits which provide full switching service at intermediate points on a main trunk route.

The flexibility of the through branching circuit is illustrated in the following functions which it performs under remote control:

1. Provides a receiving leg on a reversible through program circuit.
2. Splits the network to provide independently reversible links in each direction with the same or different program material on each link.

These functions are performed with negligible reaction on the associated through-message circuits. A block schematic for one direction of transmission on a type K system is shown in Fig. 5.

For splitting the network a band elimination filter<sup>17</sup> blocks frequencies in the program assignment (32-44 kilocycles) while passing the remaining message frequencies. As network rearrangements are made during the program switching interval transmission may be rerouted through the phase simulating network<sup>17</sup> which is substituted for the BEF when the program is to go through instead of being blocked. The simulation of phase, which must be close in order to avoid disturbance of voice-frequency telegraph superimposed on any of the message channels, extends over all but the two channels adjacent to the program. The transfer from one transmission path to the other is accomplished by a chain of make-before-break relays in such a manner that transmission on the message channels is virtually unaffected.

Junctions of transmission circuits are made with resistance hybrid con-

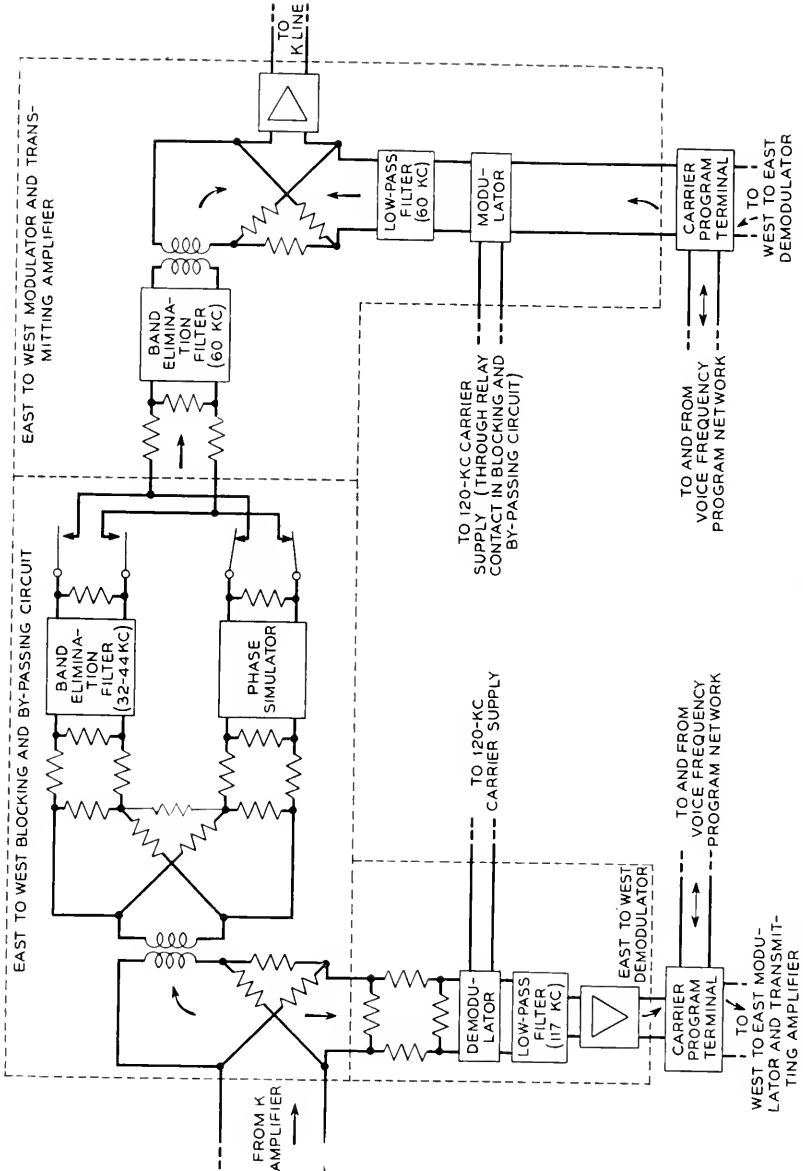


Fig. 5—Block schematic of type K branching circuit (one direction of transmission represented).

figurations to minimize transmission distortion and to give some directional discrimination.

Frequency translation from the 32–40 kilocycle range of the program on the line to the 80–88-kilocycle range of the program terminal is provided by modulating and demodulating circuits having 120-kilocycle carrier. It is of interest to note that the transmitting 120-kilocycle carrier is supplied through relay contacts which are normally open so that spurious noise and transmission will not interfere with the through program. The relay contacts are closed when the blocking filter is in circuit, thus permitting a local program origination only when the through circuit is cut off.

Relay control circuits have been arranged to coordinate with existing control practices and circuits so that reversibility may be under studio control and network splitting under local control.

Gain to offset circuit losses is supplied at the output by a transmitting amplifier so that the over-all loss of the through circuit is zero. Patching to spare circuits is thus facilitated.

In a K2 carrier system<sup>15</sup> the transmitting amplifier has unique properties in that it is self-oscillating at 60 kilocycles at an amplitude which complements the signal amplitude to produce a constant total output power. This feature is used as a carrier system line regulation control, and when a new program originates at the branching point it is necessary to generate another 60-kilocycle signal to complement the new total signal output, and to effectively block all 60-kilocycle received from the previous line section. A 60-kilocycle BEF is provided for that purpose.

These branching arrangements, developed for type K systems, have also been adapted for use with type L groups. Blocking and bridging functions are provided as they are for type K and in addition to the complete branching circuits, include simplified arrangements which make use of otherwise idle groups for carrier program circuits without message channels.

#### BRANCHING CIRCUIT PERFORMANCE

The performance characteristics of the blocking and by-passing circuits are shown in Fig. 6, which represents transmission vs. frequency over the type K range of line frequencies. The solid line gives the normal transmission characteristic for through transmission of the program and the nine message channels. The dotted line is the program blocking characteristic indicating 80-decibel minimum suppression over most of the 32–44-kilocycle frequency range. The dashed line is the characteristic effective during the brief interval in the switching process when both branches of the circuit are connected. Its similarity to the other two characteristics is a measure of the effectiveness of the phase simulation over most of the message channel spectrum. Its departure from the other characteristics in the channel 5

and channel 9 allocations marks the end of the region in which the phase of the blocking filter can be successfully simulated. Outside of this region, in parts of channels 5 and 9, the switching operation shifts both phase and amplitude of the transmission and precludes the use of these channels for voice-frequency telegraph or telephoto services.

### EQUIPMENT

As previously stated a carrier program terminal consists of a modem unit, a demodulator-amplifier panel, and a reversing panel. As shown in

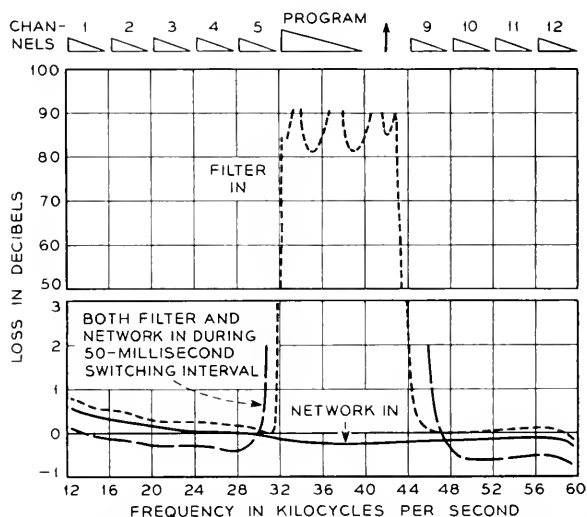


Fig. 6—Transmission characteristics of blocking and by-passing circuit under normal conditions and during switching.

Fig. 7 two such terminals, together with fuse panels for 24 and 130-volt battery supply for several bays, are mounted in one standard cable duct type bay 19" wide and 11'6" high. The equipment is mounted on the bay in a group, from top down, in the order mentioned. The front or wiring side of the equipment is provided with three separate covers which furnish the necessary electrical shielding as well as physical protection. Connections to carrier systems are made through carrier program high-frequency patching jacks on a 4-wire basis and to the program circuits through audio frequency testing jacks on a 2-wire basis from which point the carrier program channel is lined up for program service at the proper transmission levels for both directions of transmission.

A through branching circuit consists of two sets of line bridging equipment and two carrier program terminals mentioned above. As shown in



LINE BRANCH BAY (FRONT)    TERMINAL BAY (FRONT)

TERMINAL BAY (REAR)    LINE BRANCH BAY (REAR)

Fig. 7—Photograph of an early installation of carrier program terminals and associated type K branching circuits.

Fig. 7 the line bridging equipment is mounted in one standard cable duct type bay 19" wide and 11' 6" high. The equipment for each direction of transmission is mounted on the bay in a group consisting of a modulator and transmitting amplifier, blocking filter and by-passing network with switching relays, and demodulator and demodulator-amplifier. The rear or wiring side of this equipment is also provided with three separate covers. The apparatus or front side of two of the panels, modulator and demodulator-amplifiers, is equipped with parallel vacuum tube sockets so that the vacuum tubes can be removed from the circuit for testing purposes without

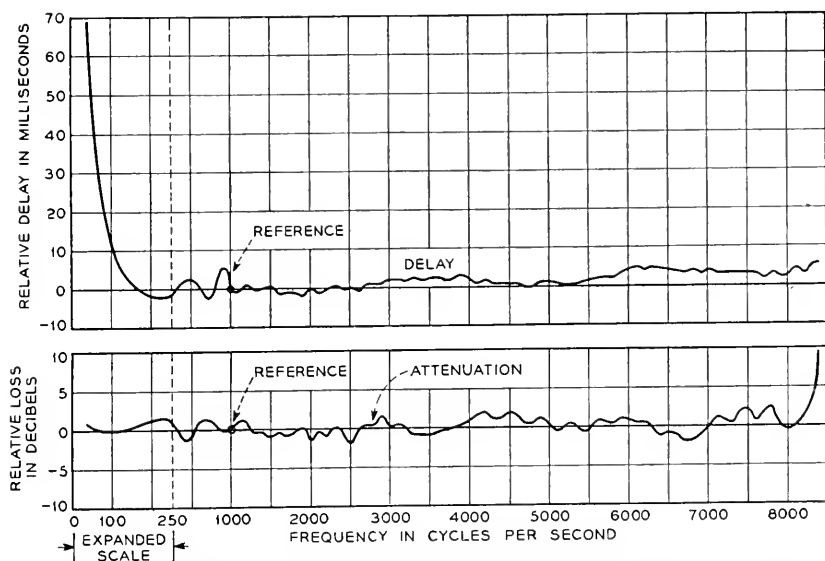


Fig. 8—Typical 10-link attenuation and delay distortion characteristics. The length of this circuit was 7300 miles.

interfering with service in the same manner as is done on K2 carrier telephone equipment.<sup>15</sup>

The necessary carrier supply for this equipment is obtained from regular standard carrier supply bays used for other broadband carrier equipment. The presence of undesired residual harmonics of 4-kilocycles from this carrier supply necessitates modification of the carrier circuits at several points to provide additional suppression to undesired components which would otherwise appear as 4 or 8-kilocycle tones in the program channel.

#### SYSTEM PERFORMANCE

The longest commercial network circuits now in operation are in the order of 7000 miles long, including the transcontinental backbone route

and feeder circuits along the Atlantic and Pacific coasts. On the assumption that these routes may some day be largely in carrier, exhaustive tests were made in 1947 of carrier program transmission applied to type K systems between Omaha and Los Angeles, looping back and forth as required to build up long circuits. Live program material transmitted around a 7300-mile loop consisting of 10 carrier links in tandem was judged to be of excellent quality by juries composed of experienced and critical observers. Attenuation and delay characteristics of this circuit relative to the 1000-cycle point are shown in Fig. 8 and indicate that design objectives are met with enough margin to justify practical operation over about 13 links in tandem. Background noise was about 53 decibels below the peak signal. Frequency shift due to differences in carrier frequency at the 20 terminals was less than 2 cycles. The time required for a complete reversal counting from the initial control signal release was 3 seconds. Shorter lengths will, of course, have even better performance. These characteristics, while they do not represent perfection in transmission quality, strike a balance between the various engineering limitations, which makes this system compare favorably with the best facilities previously available.

#### CONCLUSION

At the end of 1948, three years after the first installation, there were approximately 75,000 miles of carrier program circuits in service, about 70 per cent of them established full time. This is a substantial proportion of the total mileage of all grades of program service, which is in the order of 175,000 miles. The portions of the main transcontinental routes formerly carried by open-wire lines are now in carrier cables.

#### REFERENCES

1. "Use of Public Address System with Telephone Lines," W. H. Martin and A. B. Clark, *A. I. E. E. Journal*, April 1923, pp. 359-366.
2. "High-Quality Transmission and Reproduction of Speech and Music," W. H. Martin and H. Fletcher. *A. I. E. E. Journal*, March 1924, pp. 230-238.
3. "Telephone Circuits used as an adjunct to Radio Broadcasting," H. S. Foland and A. F. Rose. *Electrical Communication*, January 1925, pp. 194-202.
4. "Telephone Circuits for Program Transmission," F. A. Cowan. *A. I. E. E. Transactions*, 1929, pp. 1045-1049.
5. "Wire Line Systems for National Broadcasting," A. B. Clark. *Bell Sys. Tech. Jour.*, January 1930, pp. 141-149.
6. "Long Distance Cable Circuit for Program Transmission," A. B. Clark and C. W. Green. *Bell Sys. Tech. Jour.*, July 1930, pp. 567-594.
7. "Auditory Perspective" (A symposium), "Transmission Lines," H. A. Afel, R. W. Chesnut and R. H. Mills, *Electrical Engineering*, January 1934, pp. 9-32, 216-218.
8. "Wide Band Open-Wire Program System," H. S. Hamilton, *Electrical Engineering*, April 1934, pp. 550-562.
9. "A Carrier Telephone System for Toll Cables," C.W. Green and E. I. Green. *Bell Sys. Tech. Jour.*, January 1938, pp. 80-105.
10. "Cable Carrier Telephone Terminals," R. W. Chestnut, L. M. Ilgenfritz and A. Kenner. *Bell Sys. Tech. Jour.*, January 1938, pp. 106-124.
11. "A Twelve-Channel Carrier Telephone System for Open-Wire Lines," B. W. Kendall and H. A. Afel. *Bell Sys. Tech. Jour.*, January 1939, pp. 119-142.

12. "Engineering Requirements for Program Transmission Circuits," F. A. Cowan, R. G. McCurdy and I. E. Lattimer, *Electrical Engineering*, April 1941, pp. 142-147.
13. "Wide-Band Program Transmission Circuits," E. W. Baker, *Electrical Engineering*, March 1945, pp. 99-103.
14. "Transmission Networks for Frequency Modulation and Television," H. S. Osborne, *Electrical Engineering*, November 1945, pp. 392-397.
15. "An Improved Cable Carrier System," H. S. Black, F. A. Brooks, A. J. Wier and I. G. Wilson, *Electrical Engineering, A. I. E. E. Transactions*, 1947, Vol. 66, pp. 741-746.
16. "Frequency Division Techniques for a Coaxial Cable Network," R. E. Crane, J. T. Dixon and G. H. Huber, *A. I. E. E. Transactions*, 1947, Vol. 66, pp. 1451-1459.
17. "Band-pass Filter, Band Elimination Filter, and Phase Simulator Network for Carrier Program Systems." A companion paper by F. S. Farkas, F. J. Hallenbeck and F. E. Stehlik. This issue of *BSTJ*.
18. "Delay Equalization of 8-Kc Carrier Program Circuits," A companion paper by C. H. Dagnall and P. W. Rounds. This issue of *BSTJ*.



# Delay Equalization of Eight-Kilocycle Carrier Program Circuits

By C. H. DAGNALL and P. W. ROUNDS

This paper describes the equalization of delay in 8-ke program systems transmitted over broad-band carrier telephone facilities. Use is made of a condenser plate potential analog which provides a ready method for blocking out the basic design and arriving at the final equalizer constants. Most of the equalization is accomplished at audio frequencies, and the remainder at carrier frequencies with quartz-crystal equalizers.

**I**N TRANSMITTING programs for radio broadcasting over the United States, an extensive network of wire circuits has been established by the Bell System. Most of the additions to this network since the war have employed a single-sideband carrier system<sup>5</sup> applicable to broad-band carrier facilities. The selection of a single sideband requires sharp frequency discrimination, and when this discrimination is achieved with minimum-phase structures, it is of necessity accompanied by delay distortion.<sup>3</sup>

In one or two carrier links, each including a transmitting and receiving terminal, the delay distortion is sufficiently small so that no deterioration in the program is noticeable. However, flexibility of maintenance and operation of an extensive program network requires that the network be built up of a large number of links in tandem. When this is done, the effects of delay distortion become quite conspicuous and equalization of the delay is necessary. Furthermore, if the equalization is to be satisfactory between any two points in the network, each link must be independently equalized.

Most of the delay distortion arises in the carrier-frequency band-pass filter which selects the lower sideband, the small remaining portion being contributed by the amplifiers and repeating coils. Figure 1 illustrates the unequalized delay in one terminal. Equalizers have been added to each terminal to make the phase characteristic approach linearity and so permit at least ten links to be operated in tandem without excessive distortion.

## THEORY OF DESIGN

The equalization of delay distortion is accomplished through the use of all-pass networks which, in their most general form,<sup>2</sup> may be constructed as a tandem set of lattice sections of the type shown in Fig. 2. An electrostatic analogy, developed during the late thirties,<sup>4</sup> has been found to be of great assistance in visualizing the performance of these networks and in indicating a rational method of design.

Considering the single section shown in Fig. 2 as the basic building block, the loss and phase may be expressed in the form

$$e^{A+jB} = \frac{(p + k_n - j\omega_n)(p + k_n + j\omega_n)}{(p - k_n - j\omega_n)(p - k_n + j\omega_n)} \quad (1)$$

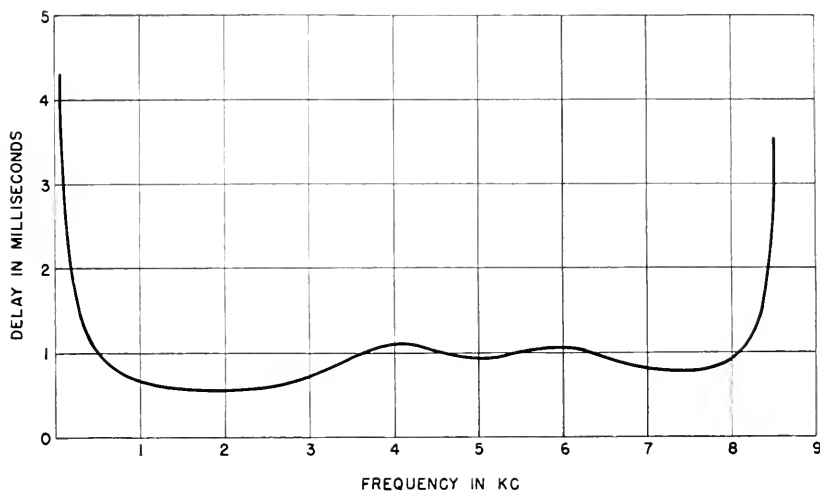


Fig. 1—Unequalized delay distortion of carrier program terminal.

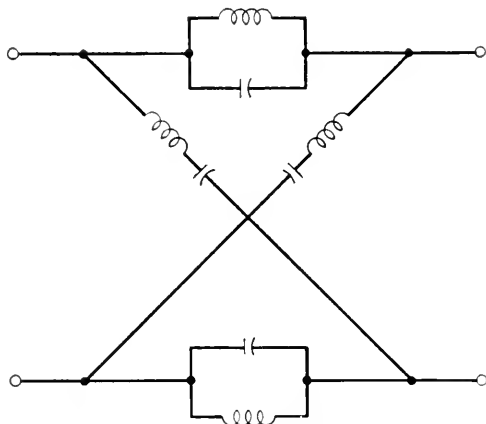


Fig. 2—Basic lattice delay section.

where

$A$  = insertion loss in nepers

$B$  = insertion phase in radians

$p = j\omega$

$\omega$  = frequency in radians per second

$k_n, \omega_n$  = real positive constants

An examination of equation (1) indicates that there are zeros at the two points:

$$p = -k_n + j\omega_n, \text{ and } p = -k_n - j\omega_n$$

and poles at the two points

$$p = +k_n + j\omega_n, \text{ and } p = +k_n - j\omega_n$$

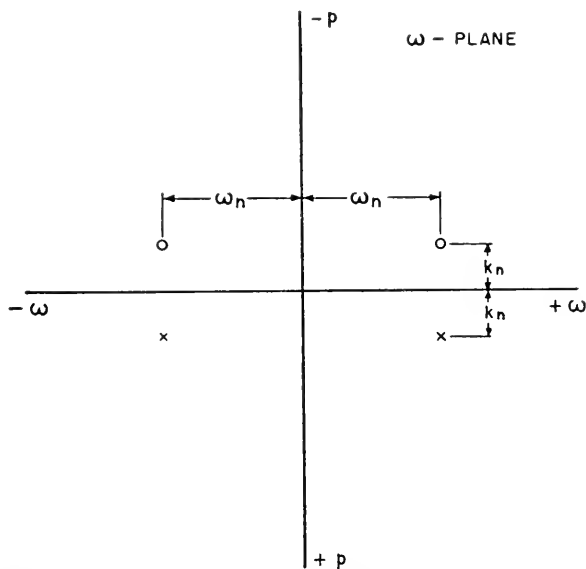


Fig. 3—Plot of zeros and poles of the network of Figure 2 on the complex-frequency plane.

The first zero in equation (1) contributes a delay (defined as the derivative of the phase with respect to frequency) of the form

$$T_1 = \frac{dB_1}{d\omega} = -\frac{1}{k_n \left[ 1 + \frac{(\omega - \omega_n)^2}{(k_n)^2} \right]} \quad (2)$$

Similar expressions may be obtained for the other zeros and poles, the total delay of the section then being equal to the sum of the delays contributed by each zero and pole.

The four zeros and poles of equation (1) may be plotted on the complex-frequency plane as shown in Fig. 3, where the circles indicate zeros and the crosses poles. The four points are seen to be symmetrically disposed with respect to the origin. With reference to this figure, it will be noted that, since  $\omega = -jp$ , positive real values of  $p$  correspond to negative imaginary

values of  $\omega$  and negative real values of  $p$  correspond to positive imaginary values of  $\omega$ . The axes of Fig. 3 have been labelled accordingly.

It is at this point that the electrostatic analogy begins to come into play. Assume that an infinite wire filament, positively charged throughout its length, is run through the zero  $p = -k_n + j\omega_n$  perpendicular to the plane of the paper and that a unit positive charge is placed at an arbitrary point,  $\omega$ , along the real frequency axis. The component of the force normal to the  $\omega$  axis exerted on the unit charge may be written in the form

$$F = \frac{1}{k_n \left[ 1 + \frac{(\omega - \omega_n)^2}{(k_n)^2} \right]} \quad (3)$$

When distances in equation (3) are identified with frequencies in equation (2), the two expressions are identical. A similar argument applies to the other zero, and also to the two poles provided that the filaments passing through the poles have charges of the opposite polarity. Thus we may say that the network of Fig. 2 will have a delay proportional to that component of the electric field intensity which is normal to the  $\omega$  axis, when a positive filament passes through each zero and a negative filament through each pole. Fig. 4 indicates the character of the delay as a function of frequency. Parenthetically we may note that the component of the field intensity parallel to the  $\omega$  axis is proportional to the derivative of the loss. Since this component is zero, the loss will be constant at all frequencies. In the case of the reactance networks with which we are dealing here, the loss is zero.

Although the usefulness of the electrostatic analogy lies principally in its application to more complex networks, several conclusions may be drawn from Fig. 4. The right-hand zero and pole, because of their symmetrical spacing and opposite charges, make equal contributions to the total delay. The same statement holds true for the left-hand zero and pole combination. As the zeros and poles approach the real-frequency axis, the delay peaks become sharper and higher because of the increased local field intensity. The figure also shows that the slope of the delay curve is zero at zero frequency and that, unless  $\omega_n$  is large compared to  $k_n$ , the delay at zero frequency is of appreciable magnitude. These isolated facts will be exploited later in considering more complex networks.

Assume, now, a tandem series of sections of the type shown in Fig. 2, in which the zeros and poles are so selected that they are evenly spaced at intervals,  $a$ , along straight lines parallel to the real-frequency axis as shown in Fig. 5. It was pointed out by H. W. Bode<sup>1</sup> that the resulting field intensity may be approximated by distributing the total of the discrete charges on the plates of an equivalent condenser passing through the zeros and poles and extending a distance of  $a/2$  beyond the extreme zeros and

poles. This approximation ignores the ripples caused by the granularity of the filament spacings, but it does permit the average delay to be determined in a particularly simple manner. The field intensity at any point,  $\omega$ ,

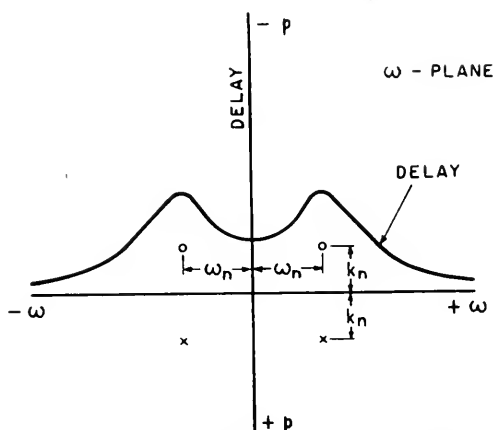


Fig. 4—Delay-frequency characteristic of the network of Fig. 2.

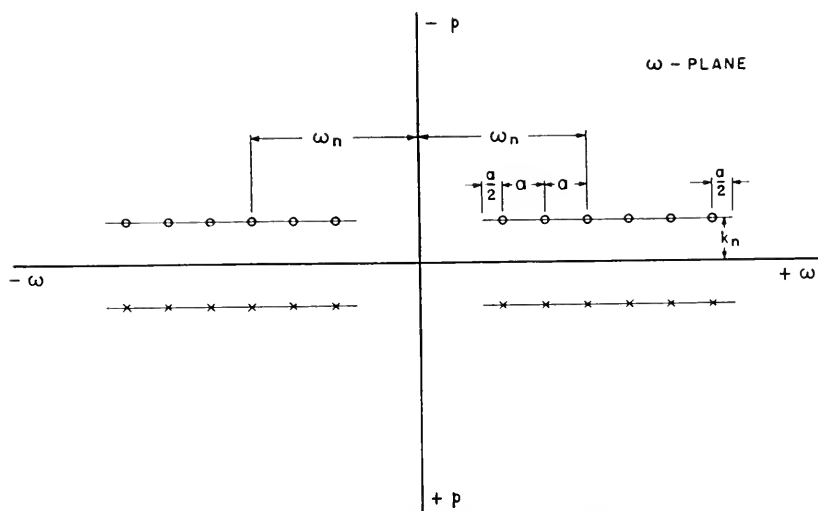


Fig. 5—Zeros and poles of a complex delay network based on the condenser-plate design.

resulting from the condenser charge is proportional to the angle subtended by the plates at that frequency. It is also proportional to the charge per unit length of plate or, in other words, to the density,  $1/a$ , of the filament spacings. The geometry is illustrated in Fig. 6, where  $2(c + d)$  is the

angle subtended by the plates at the frequency  $\omega$ . From this figure it may be seen that the field intensity in the region between the plates will have a fairly uniform value which falls off sharply as the edges are reached and becomes vanishingly small at frequencies remote from the plates.

Along with this simple determination of the average delay characteristic, D. F. Tuttle in an unpublished memorandum has derived expressions for the magnitude of the delay ripple. As shown in the appendix, the field

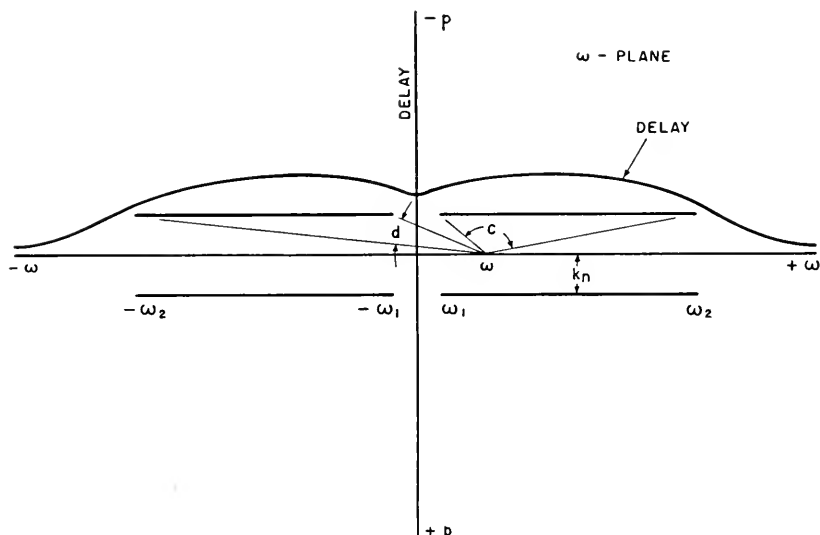


Fig. 6—Delay-frequency characteristic of the network of Fig. 5.

intensity or delay for an infinitely long set of charged filaments may be expressed in the form

$$T = \frac{2\pi}{a} \tanh \frac{2\pi k_n}{a} \left[ 1 - \left( \frac{\cos \frac{2\pi\omega}{a}}{\cosh \frac{2\pi k_n}{a}} \right) + \left( \frac{\cos \frac{2\pi\omega}{a}}{\cosh \frac{2\pi k_n}{a}} \right)^2 - \dots \right] \quad (4)$$

For reasonably large values of  $2\pi k_n/a$ , this relation may be replaced by the approximate expression

$$T \approx T_0 [1 - \delta \cos T_0 \omega] \quad (5)$$

where  $T_0 = 2\pi/a$  is the average delay and  $\delta = 2e^{-T_0 k_n}$  is the percentage ripple about the average value. The ratio  $k_n/a$  may thus be determined from the percentage delay ripple in accordance with the formula

$$\frac{k_n}{a} = \frac{1}{2\pi} \log_e \frac{2}{\delta} \quad (6)$$

To equalize the low-frequency and high-frequency filter delay shown in Fig. 1, a condenser plate of the form shown in Fig. 6 might be visualized. Although the high-frequency delay approximates that desired, the low-frequency delay shows insufficient shaping to be complementary to the filter characteristic because of the contribution of the negative-frequency plates. By bringing the plates closer to the frequency axis, that is by decreasing the ratio  $k_n/\omega_1$ , a sharper-breaking low-frequency characteristic could be obtained. However, to achieve a sufficiently small delay ripple, the spacing,  $a$ , as determined from equation (6) would then have to be decreased with the result that the number of sections would be correspondingly increased.

In attempting to reduce the total number of sections required, it was observed that a carrier-frequency delay equalizer would not be subject to

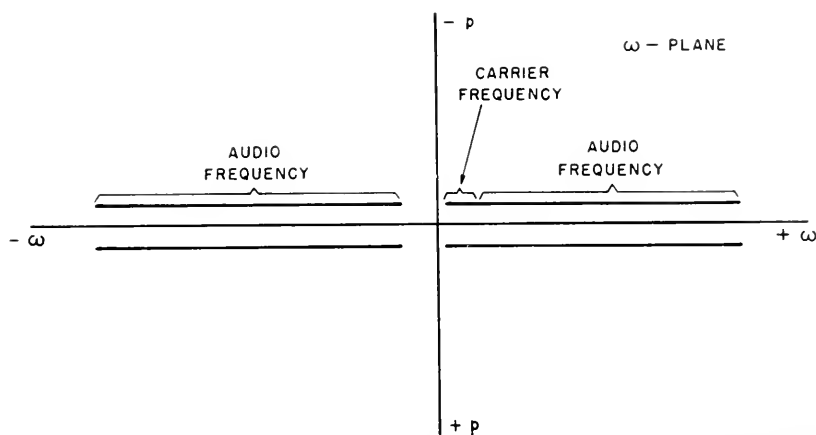


Fig. 7—Condenser-plate design for a combined carrier and audio-frequency delay equalizer.

the same low-frequency limitation, since the negative-frequency plates would be removed from the single-sideband signal by approximately twice the carrier frequency of 88 kc. However, since high-frequency delay sections are more expensive to construct than those operating at audio frequencies, a compromise is made in which the first few sections are built to operate at carrier frequencies and the remaining sections at audio frequencies. The equivalent condenser plates, referred to the audio-frequency signal, are shown in Fig. 7.

A condenser-plate design has thus been achieved which allows the low-frequency and high-frequency delay to be equalized at least approximately. Further modifications must be made in the design, particularly in the middle of the band, to shape the characteristic so that a more accurate complement of the filter delay may be obtained. The delay in a condenser-

plate design is directly proportional to the charge density along the plate. Up to now, this density has been assumed to be uniform. When the charge is located on discrete filaments, the restriction of uniform density is no longer necessary and it is possible to modify the delay characteristic as desired by changing the spacing of the filaments in inverse proportion to the desired change in delay.

The assumption of a flat plate is also useful in simplifying the analysis: in the actual design the equivalent plate is bowed out over the major portion of the frequency range to reduce the delay ripple. The final zeros and poles obtained are shown in Fig. 8, in which the carrier-frequency zeros and poles are plotted on an equivalent audio-frequency basis. A total of 29

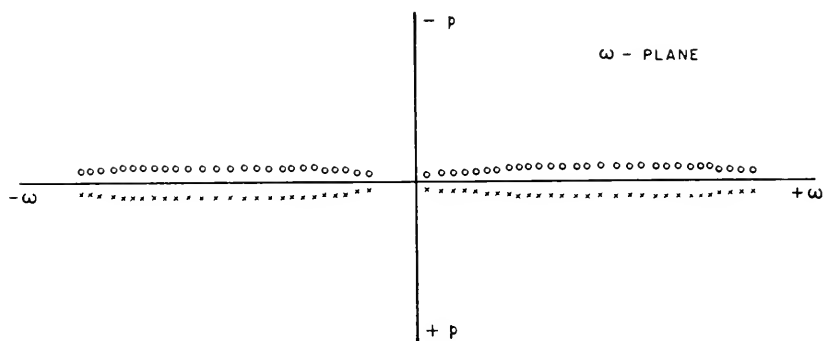


Fig. 8—Plot of the zeros and poles of the delay equalizer for 8-kc program terminals.

delay sections are required, of which three are assigned to the carrier-frequency equalizer and 26 to the audio-frequency equalizer.

#### AUDIO-FREQUENCY EQUALIZER

To complete the design of the audio-frequency equalizer some means must be found for absorbing the effects of dissipation in the coils and condensers so that the final dissipative network will exhibit the theoretical non-dissipative performance plus a loss which is constant with frequency. It can be shown that a non-dissipative all-pass section plus a flat-loss pad can be replaced with a dissipative all-pass section (of modified constants) in tandem with a minimum-phase loss equalizer as in Fig. 9. It would be uneconomical to associate a loss equalizer with every phase section; and it is in fact unnecessary, since any minimum-phase device accomplishing the same result will exhibit the same performance.<sup>3</sup> The problem is then reduced to equalizing the loss of the network composed of dissipative delay sections.



The dissipative loss of these sections may be determined from the approximate relation

$$\text{Dissipative Loss in nepers} \approx \frac{1}{2} \left( \frac{R}{L} + \frac{G}{C} \right) T \quad (7)$$

where

$\frac{R}{L}$  = resistance-inductance ratio of coils in ohms per henry

$\frac{G}{C}$  = conductance-capacitance ratio of condensers in micromhos per microfarad

$T$  = delay of network in seconds

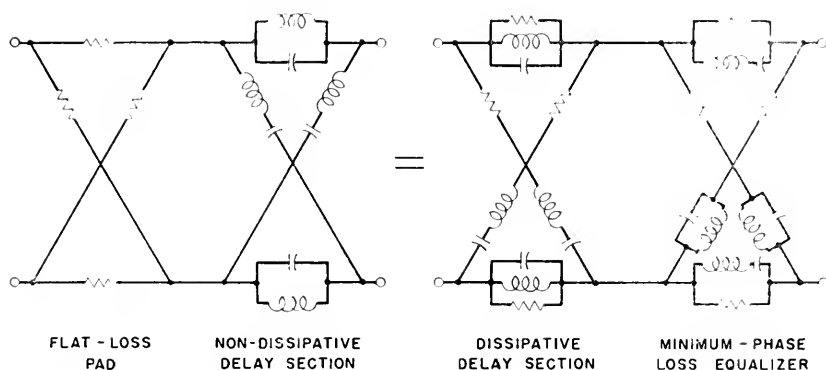


Fig. 9—Four-terminal equivalence showing the method of absorbing the effects of dissipation in the audio-frequency equalizer sections.

This expression indicates that, when the quantity  $(R/L + G/C)$  is nearly constant with frequency, the shape of the loss characteristic will be generally similar to that of the delay characteristic. The ripples in the delay characteristic have been made sufficiently small so that the corresponding loss ripples may be ignored and only the general trend considered. A schematic of the resulting equalizer is shown in Fig. 10. The attenuation equalizer sections, in tandem with the delay sections, produce a loss characteristic complementary to that of the band filter over the 8000-cycle program range. Resistors have been added to the crossarms of each lattice delay section to allow the dissipative losses to be adjusted to the nominal values assumed in the design. For manufacturing convenience, the sections are assembled in seven separate containers which are mounted on an  $8\frac{3}{4}$  inch by 19 inch relay-rack panel as illustrated in Fig. 11.

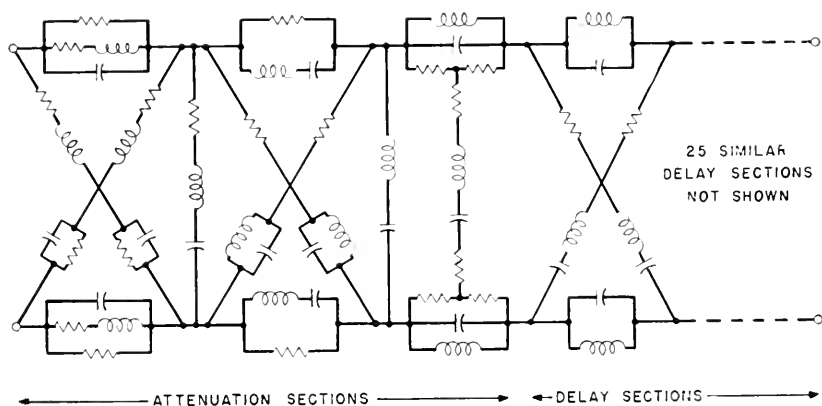


Fig. 10—Schematic of audio-frequency equalizer.

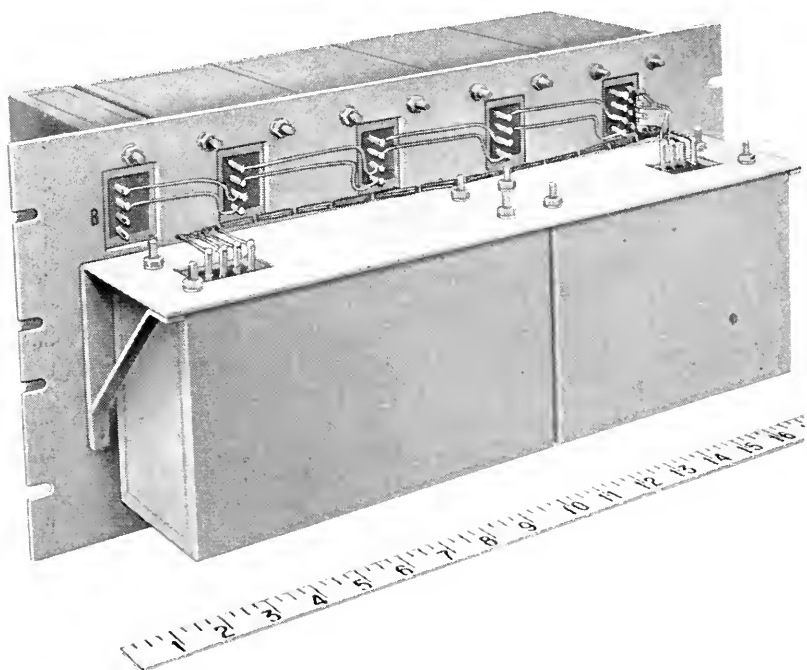


Fig. 11—Photograph of audio-frequency equalizer.

### CARRIER-FREQUENCY EQUALIZER

The critical frequencies of the carrier-frequency equalizer are located at 318, 610 and 890 cycles on an audio basis. Since the carrier is at 88 kc

and the lower sideband is transmitted, the corresponding carrier frequencies are 87682, 87390 and 87110 cycles, respectively.

The required change of phase per cycle is the same as at audio frequencies, but the percentage rate of change is eleven times that of the audio-frequency sections operating at 8000 cycles. This requires that the arms of the sections have proportionately stiffer reactances, higher  $Q$ 's, and greater tem-

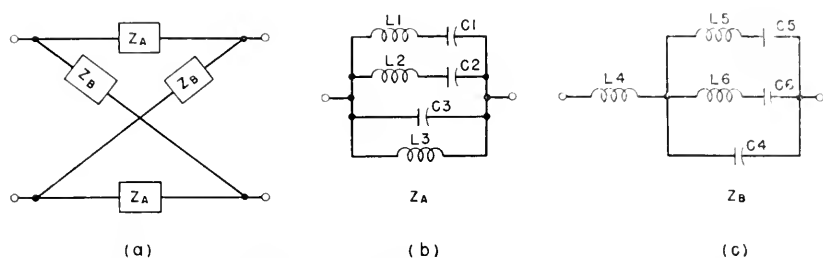


Fig. 12—Schematic of the lattice equivalent of three tandem sections of the type shown in Fig. 2.

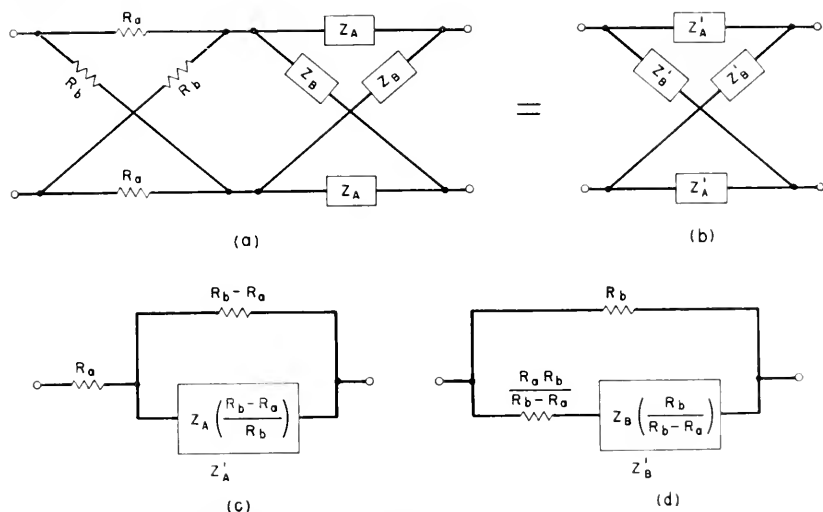


Fig. 13—Four-terminal equivalence showing the method of absorbing the effects of dissipation in the carrier-frequency equalizer.

perature stability. The only available elements meeting such requirements are piezo-electric crystals.

The approximate equivalent electrical circuit of a crystal is a capacitance in parallel with a series combination of an inductance and capacitance, and is not adaptable to the section of Fig. 2. However, when three such sections in tandem are combined into a single lattice, the configuration of

Fig. 12 is obtained. The stiffness of the reactances of arms  $Z_A$  and  $Z_B$  depends principally on the branches numbered 1, 2, 5 and 6. Each of these branches may be combined with a portion of  $C_3$  or  $C_4$  and replaced with a crystal.

One other restriction must be overcome before crystals can be used. Inductances  $L_1$  and  $L_2$  are in the order of 0.7 henry while  $L_5$  and  $L_6$  are in the order of 5000 henries, both inductance values being impractical for crystals. Two three-winding repeating coils are used to transform these inductances to values that may be provided by crystals. The two balanced windings of one repeating coil replace arms  $Z_B$  of Fig. 12(a), the third winding being connected to a reactance arm of the form of Fig. 12(c).

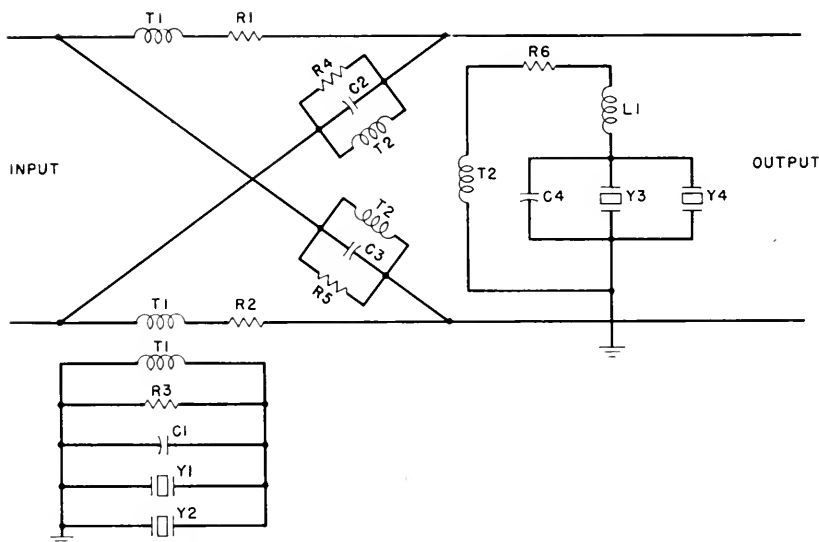


Fig. 14—Schematic of carrier-frequency equalizer.

The other repeating coil is similarly used for arms  $Z_A$ , the inductance  $L_3$  being provided by the repeating coil. The repeating coils unavoidably introduce parasitic inductances, a small one in series with  $Z_A$  and a larger one in parallel with  $Z_B$ , the effects of which are made negligible by the addition of a capacitance in parallel with  $Z_B$ .

Dissipation in the elements of the carrier-frequency equalizer is taken into account by making use of the equivalence of Fig. 13, in which (a) represents the non-dissipative equalizer in tandem with a pad and (b) a structure similar to the non-dissipative structure but with resistances added to its arms, as shown by (c) and (d). The dissipation in each coil, condenser or crystal can be associated to a close degree of approximation with

one of these resistances. Physical resistances are added to compensate for deficiencies in dissipation. The loss of the pad is made large enough to allow for manufacturing deviations.

The complete schematic is shown in Fig. 14, and the equalizer with the shield removed in Fig. 15. Below the panel in Fig. 15, from left to right are arranged the retardation coil  $L1$ , adjusting condensers  $C1$  and  $C4$ , the

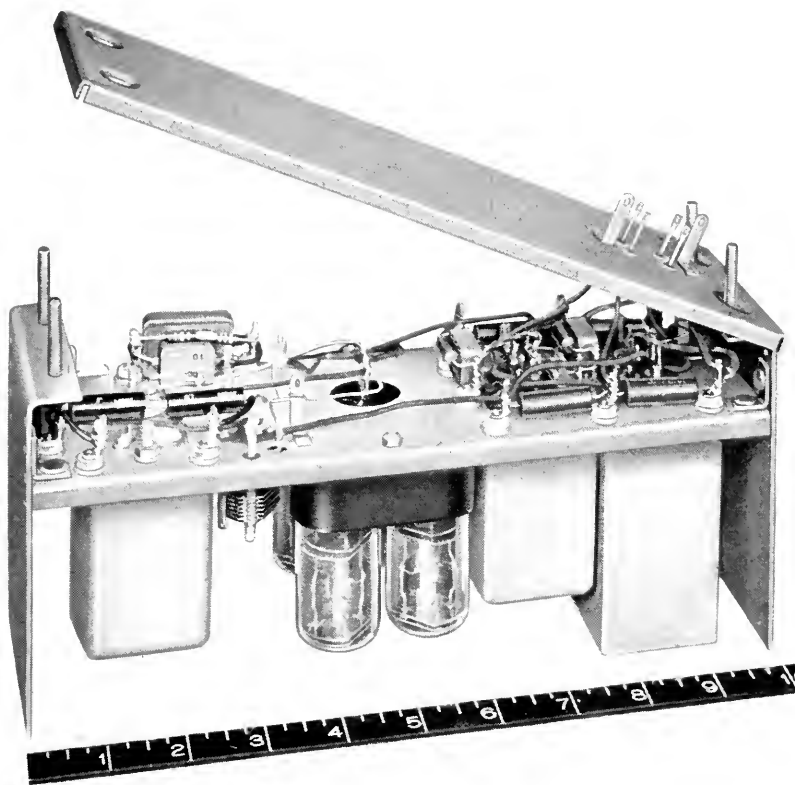


Fig. 15—Photograph of carrier-frequency equalizer.

crystals  $Y1$  to  $Y4$ , inclusive, and the repeating coils  $T1$  and  $T2$ . The fixed condensers and resistances are mounted above the panel.

### RESULTS

Curves *A* and *B* in Fig. 16 show the delay-frequency characteristics of the audio-frequency equalizer and the carrier-frequency equalizer, respectively. Curve *C* shows the equalized delay of one terminal, which is the sum of the delays of the equalizers added to the unequalized delay of Fig. 1.

Listening tests over ten carrier links in tandem indicate that the design objectives are sound and that a satisfactory reduction in delay distortion has been achieved.

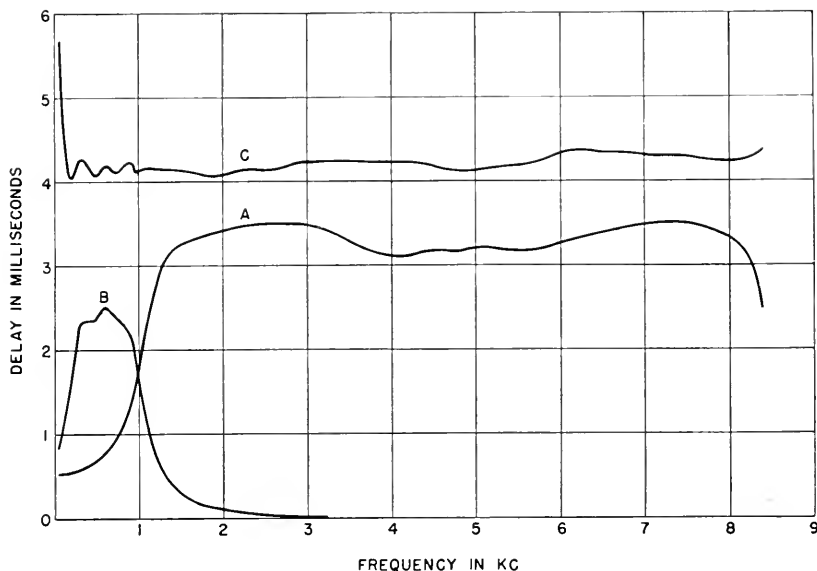


Fig. 16—Delay of audio and carrier-frequency equalizers and delay of equalized program terminal.

## APPENDIX

For an infinitely long set of charged filaments of the type shown in Fig. 3 and located at  $\omega = a/2, 3a/2, 5a/2$ , etc., the insertion loss and phase may be expressed by the infinite-product expansion of equation (1),

$$\begin{aligned}
 e^{A+jB} &= \prod_{n=1}^{\infty} \frac{[p + k_n - j(n - \frac{1}{2})a][p + k_n + j(n - \frac{1}{2})a]}{[p - k_n - j(n - \frac{1}{2})a][p - k_n + j(n - \frac{1}{2})a]} \\
 &= \prod_{n=1}^{\infty} \frac{1 - \left[ \frac{j2(p + k_n)\pi/a}{(2n - 1)\pi} \right]^2}{1 - \left[ \frac{j2(p - k_n)\pi/a}{(2n - 1)\pi} \right]^2}
 \end{aligned} \tag{8}$$

Expression (8) is a standard form of product expansion and may be written

$$e^{A+jB} = \frac{\cos j(p + k_n)\pi/a}{\cos j(p - k_n)\pi/a} \tag{9}$$

or

$$A + jB = \log \cos j(p + k_n)\pi/a - \log \cos j(p - k_n)\pi/a \tag{10}$$

Substituting  $j\omega$  for  $p$  and differentiating with respect to  $\omega$ , we obtain

$$\frac{dA}{d\omega} + j \frac{dB}{d\omega} = j \frac{2\pi}{a} \frac{\sinh 2\pi k_n/a}{\cosh 2\pi k_n/a + \cos 2\pi\omega/a} \quad (11)$$

from which  $dA/d\omega$  is zero. Equation (11) may be written

$$\frac{dB}{d\omega} = \frac{2\pi}{a} (\tanh 2\pi k_n/a) \left( \frac{1}{1 + \frac{\cos 2\pi\omega/a}{\cosh 2\pi k_n/a}} \right) \quad (12)$$

which, when expanded, gives equation (4).

#### REFERENCES

1. "Wave Transmission Network," H. W. Bode, *United States patent* 2,342, 638.
2. "Network Analysis and Feedback Amplifier Design" (book) Chapter 11, H. W. Bode, D. Van Nostrand Co., Inc., New York, N. Y., 1945.
3. Reference 2, Chapter 14.
4. "Network Theory Comes of Age," R. L. Dietzold, *Electrical Engineering*, Volume 67, Number 9, September 1948, page 898.
5. "A Carrier System for 8000-cycle Program Transmission," R. A. Leconte, D. B. Penick, C. W. Schramm, A. J. Wier. A companion paper. This issue of *BSTJ*.
6. "Band Pass Filter, Band Elimination Filter and Phase Simulating Network for Carrier Program Systems," F. S. Farkas, F. J. Hailenbeck, F. E. Stehlik. A companion paper. This issue of *BSTJ*.

# Band Pass Filter, Band Elimination Filter and Phase Simulating Network for Carrier Program Systems

By F. S. FARKAS, F. J. HALLENBECK, F. E. STEHLIK\*

A paper by Leconte, Penick, Schramm and Wier<sup>1</sup> discusses the system aspects of 8-kc program circuits over carrier facilities and outlines the functions of several filters and networks. This paper describes in detail two of the filters and one network. These are:

1. The channel selecting crystal band pass filter used at program terminals of all broad-band carrier systems,
2. The band elimination filter which blocks the program at branching points on type K carrier systems,
3. The network used at branching points on type K carrier systems to simulate the phase shift of the band elimination filter.

## CHANNEL SELECTING CRYSTAL BAND PASS FILTER

AN IMPORTANT component of the modulator-demodulator circuit at the carrier program terminal is the band pass filter which selects the lower side band resulting from modulation of the audio frequency program material with the 88-kc carrier. This step of modulation locates the program frequencies in their allotted position in the carrier frequency spectrum of the standard broad-band terminal.

System flexibility requires that long program circuits be established by tandem connections of carrier links. A link consists of a transmitting and a receiving carrier program terminal connected by the appropriate transmission medium. The original objectives were based on a ten-link carrier circuit. This means that each terminal must introduce no more than five per cent of the total allowable system distortion. Assuming the band filter introduces the major part of the terminal distortion it is seen that the requirements placed on each band filter are extremely severe.

One of the transmission objectives of the system is to transmit audio frequencies as low as 50 cps. Hence the band filter must transmit the wanted carrier frequency sideband to within 50 cps of the carrier and must suppress the unwanted sideband beginning at 50 cps above the carrier. This sharp cut-off and the need for low distortion in the pass band requires the use of filter elements with so little dissipation that the only possibility of realizing the desired performance is by the use of quartz crystal elements.

In addition to suppressing the unwanted sideband above the carrier the filter must also provide sufficient discrimination above and below the pass

\* Phase simulating network by F. S. Farkas.  
Band elimination filter by F. J. Hallenbeck.  
Band pass filter by F. E. Stehlik.



band to prevent crosstalk of the adjacent message channels into the program channel.

The necessity of using quartz crystal elements limits the maximum band width of filter which can be realized. This limitation is the result of the comparatively poor electromechanical coupling of quartz.<sup>2</sup> The resulting filter band width is 8.5 kc with the upper cut-off located near the 88-kc carrier. This is slightly greater than the 8-kc nominal band width of the system.

The crystal band pass filter designed for the single sideband program channel weighs approximately 30 lbs. and occupies 7 inches of mounting space on a standard 19 inch relay rack. A total of 44 filter components are required for its construction, half of which are balanced quartz crystal plates. The remaining components consist of eight adjustable air capacitors, three fixed mica capacitors, seven balanced retardation coils, three of which are adjustable, and four resistors. A schematic which shows the relative placement of these parts in the filter is given in Fig. 1.

The measured insertion loss characteristic of the filter between resistive terminations is shown in Fig. 2. The pass band and the vicinity of the upper cut-off are given in greater detail in the enlarged characteristics of Figs. 3 and 4. The extreme sharpness of the upper cut-off is evident in the latter figure. At 40 cps above the 88-kc carrier the discrimination has reached 20 db while the slope of the insertion loss versus frequency curve through this point is about 1 db per cps. Since at least two filters are connected in tandem in any program circuit a minimum of 40 db discrimination is provided to all frequencies in the unwanted sideband. The loss realized at frequencies outside the band also is shown in Fig. 2.

The delay distortion in the pass band of the filter, computed from the slope of its measured insertion phase characteristic, is given in Fig. 5. For short program systems, where no more than six filters are used in tandem, the delay distortion would not exceed the limits set for a high quality system. For longer systems it is necessary to equalize this delay distortion. The design and performance of the delay equalizers for this purpose are given in a separate paper.<sup>3</sup> These equalizers also include some attenuation equalization to correct for the systematic distortion of the filter.

Figure 6 shows an exterior view of the filter. On both sides of the mounting panel are metal containers which are provided with covers that can be soldered on to make a hermetic-sealed enclosure. In a corner of one can is a terminal box which contains the input and output terminals. These terminals are of the metal glass seal type which are vacuum tight. Mounted on brackets in each of the containers is a brass panel supporting the filter elements. One side of one of these panels is visible in Fig. 6, the other side is shown in Fig. 7.

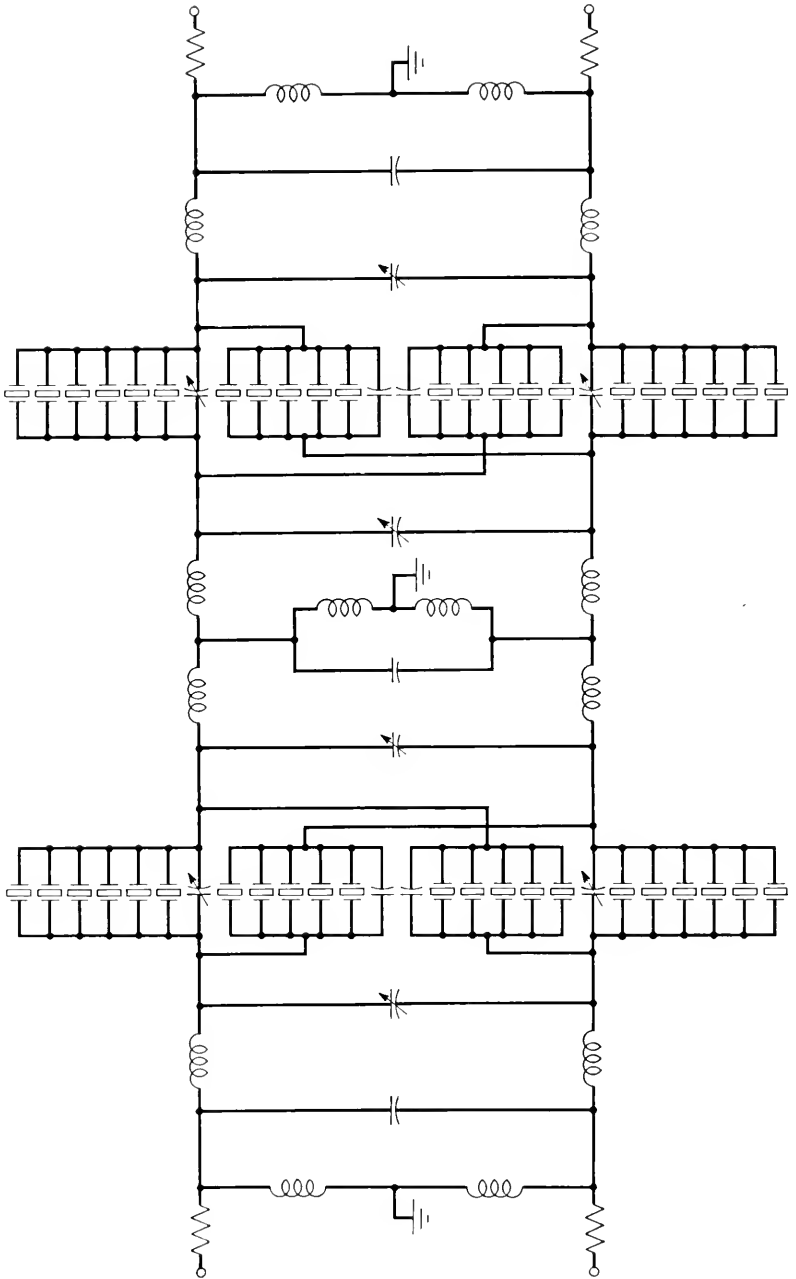


Fig. 1—Schematic of the channel selecting crystal band pass filter as constructed.

In Fig. 7 the two large cylindrical containers parallel to the panel house eleven of the balanced quartz crystal elements. The smaller cylindrical cans contain adjustable retardation coils while the rectangular cans house fixed coils. Adjustable air capacitors can be seen mounted on the hard rubber plate between the two crystal units.

The adjustment side of the brass panel is exposed in Fig. 6. Screwdriver adjustment of the retardation coils is possible through the circular holes at

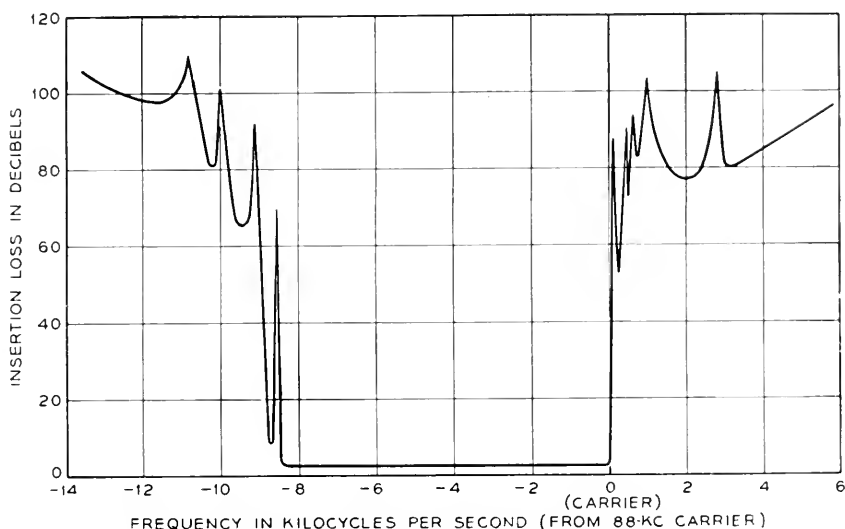


Fig. 2—The insertion loss-frequency characteristic of the filter.

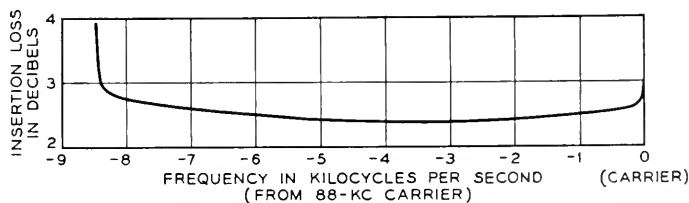


Fig. 3—Enlarged insertion loss-frequency characteristic of the filter pass band.

the top left and right of the panel. The rotors of three of the four air capacitors are visible inside the square cut-out in the panel. The panel in the lower half of the filter contains the remaining elements mounted and wired in a similar manner.

The schematic which was found to be most useful during the design of the filter is shown in Fig. 8. Thus the electrical circuit consists essentially of two complex lattice sections separated by one constant-k ladder section

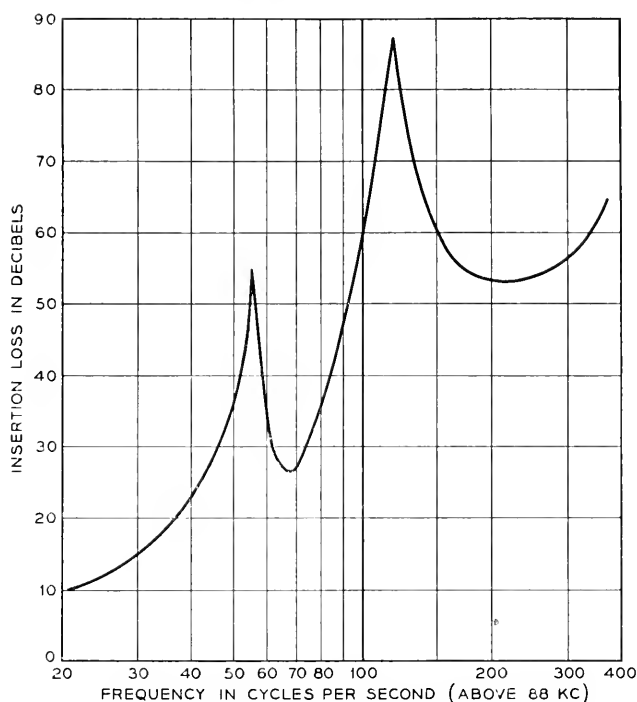


Fig. 4—The sharpness of the upper cut-off of the filter is shown in this enlarged loss characteristic.

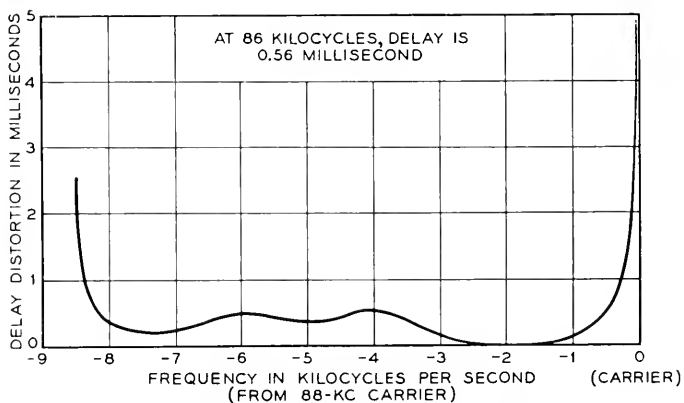


Fig. 5—Delay distortion in the pass band of the filter.

and terminated at each end by half-sections of the constant- $k$  ladder type. The performance of the filter results almost entirely from the lattice sections since they control the flatness of the pass band, the sharpness of the cut-off

and give practically all the discrimination required. It will be noted that the filter uses the equivalent of 130 electrical elements consisting of 63 inductors, 63 capacitors and 4 resistors.

The use of complex filter sections permits the realization of filter characteristics which have low distortion in the pass band and high discrimination outside the pass band with a more efficient utilization of elements than is possible with a larger number of simpler sections. Improved mathematical methods of network analysis developed in the past several years

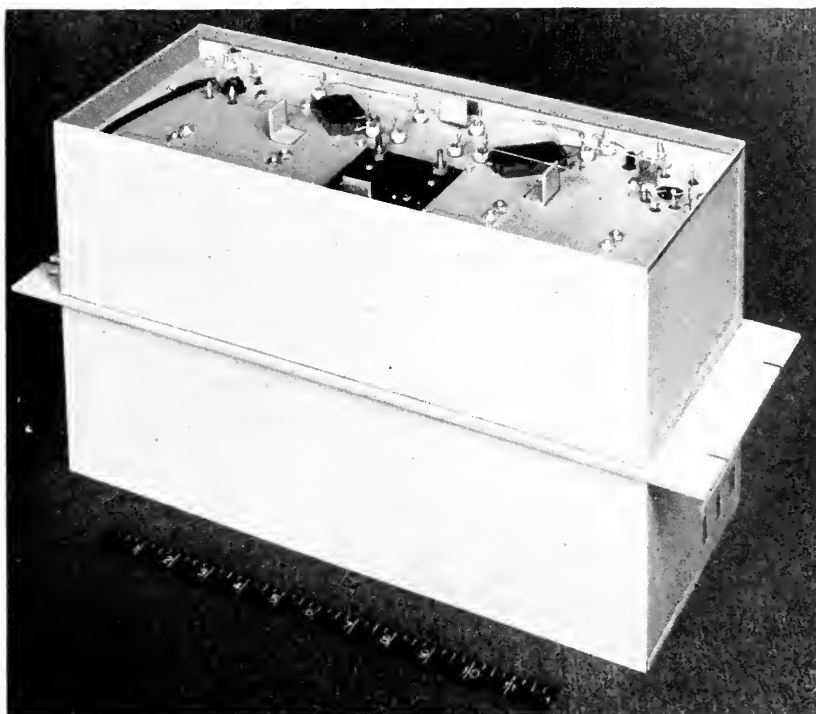


Fig. 6—Exterior view of the filter with one cover removed. After adjustments are completed the cover is soldered on to seal the assembly.

have made the design of such complex filter sections possible while recent developments of precise and stable filter elements and improved measuring circuits have made it possible to manufacture such filters.

It has been mentioned before that the use of quartz crystal elements restricts the filter band width which can be realized. In the frequency location selected for this filter (lower sideband of an 88-kc carrier frequency) a complex lattice section of the type shown in Fig. 8, when used alone, will permit the use of physical crystal elements for bands not over 7300 cps

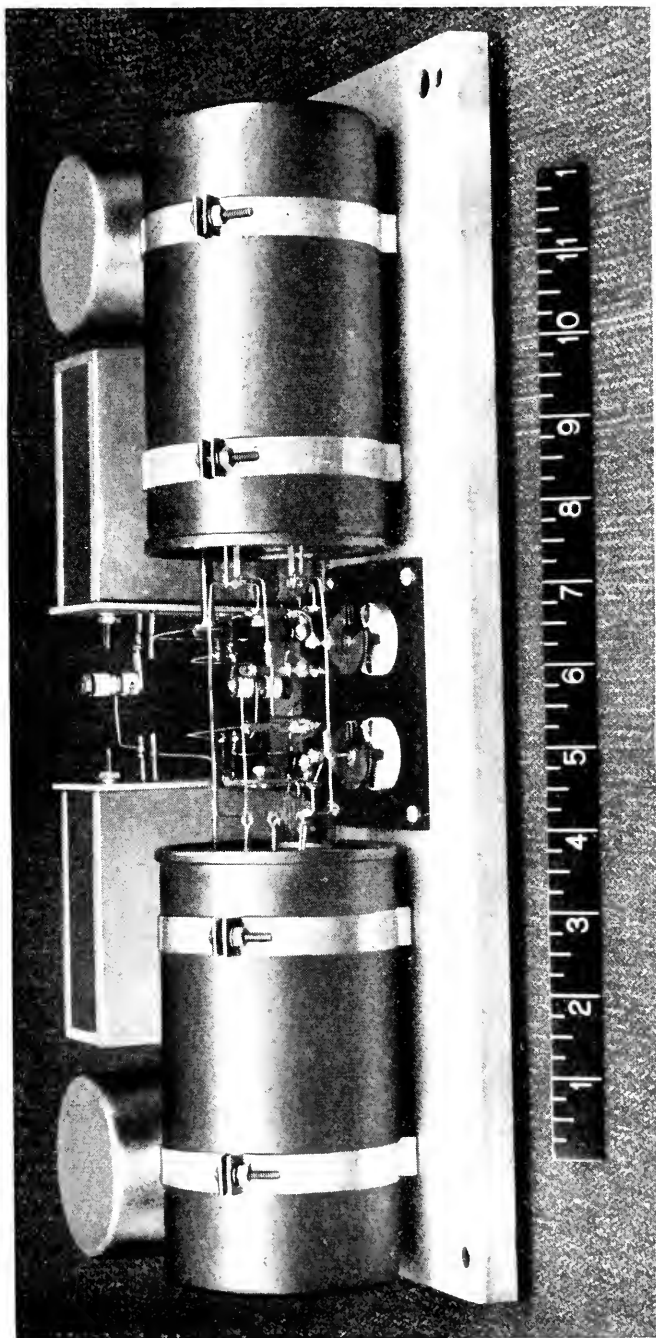


Fig. 7 Another view of one of the two panels which support the filter elements.

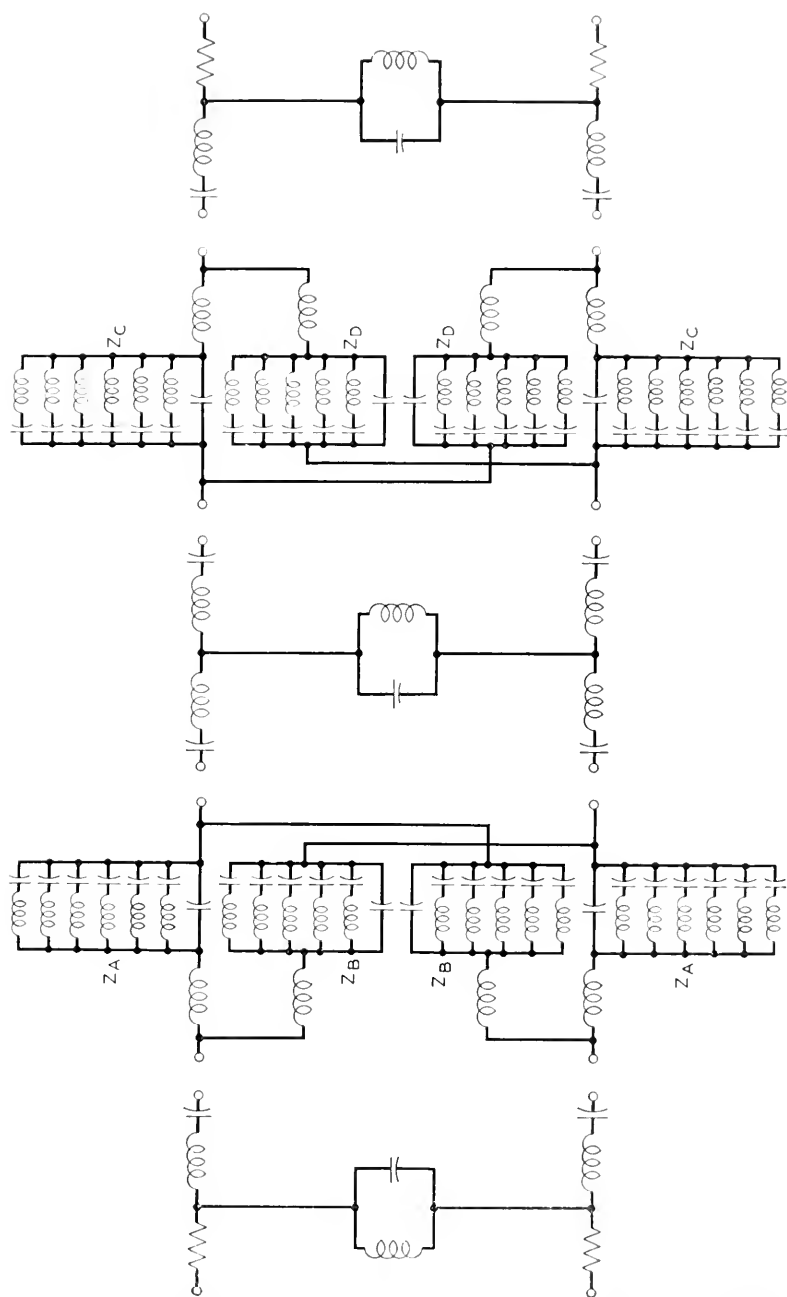


Fig. 8—The schematic used during the design of the filter contains 130 electrical elements.

wide. A wider band was obtained in this case by combining the complex lattice sections with ladder sections as shown in the figure. For this filter a combination of sections was designed which gave physically realizable crystal elements for a band width of 8.5 kc. This was the maximum band width possible without increasing the distortion in the band.

Summarizing, the filter design process consists of:

1. Design of wide band lattice sections which have quartz elements which cannot be realized in practice.
2. Design of electrical ladder sections of still wider band which introduce little distortion at the pass band frequencies of the lattice section. At this point the schematic is as shown in Fig. 8.
3. Combination of like elements, electrical transformations, and replacement of groups of elements consisting of an inductor and capacitor in series shunted by a second capacitor by their equivalent crystal elements. This gives the final schematic shown in Fig. 1, in which the crystal elements are physically realizable.

The general steps in the design of lattice filters<sup>2,4</sup> are as follows:

1. Choice of filter cut-offs.
2. Determination of number and location of impedance controlling frequencies to give a good match of image impedance to the termination.
3. Location of peaks of infinite attenuation to give the necessary transfer loss at frequencies removed from the pass band.
4. Determination of impedance level which gives the most reasonable element values.

Theoretically a filter could be designed which contains only one lattice section. The decision to split the filter into two sections was based on a desire to simplify the design to ease the manufacturing problems. The attenuation burdens of each section were reduced sufficiently to allow wider tolerances to be placed on the filter components. The last design steps are to determine the schematic of each section and to compute the theoretical element values in accordance with previously described methods.<sup>2,4</sup>

Although the filter elements computed were physically realizable they represented such extreme values as to introduce difficult problems. This was true especially of the crystal elements where the equivalent inductances of the eleven crystal elements in one section varied from 16 to 465 henries, a range of 1:29. A similar situation existed in the other section.

Crystal elements of the +5 degree X-cut type vibrating in their fundamental longitudinal mode are used in this filter. The equivalent inductance of such crystal elements varies directly with the thickness and inversely with the width of the plate. Therefore the high inductance plates are thick and narrow and the low inductance plates are thin and wide. In one section of the filter the dimensions of the plates required varied in width from



0.67 to 0.17 inch, in thickness from 0.119 to 0.012 inch and in length from 1.40 to 1.23 inches. The small variation in length is due to the fact that the length is determined primarily by the frequency of resonance of the plate and this change is small across the filter band. The temperature coefficient of the +5 degree X-cut quartz crystal element used in this filter is superior to the -18 degree X-cut longitudinal type which has been used in many other crystal filters but otherwise they are similar in use and in manufacture.

The filter attenuation distortion in the vicinity of the cut-offs is dependent on the dissipation in the elements which resonate there. In order to minimize this distortion, it has been found necessary to impose minimum  $Q$  requirements of 80,000 on the high-impedance crystal elements which resonate near the cut-offs. This high  $Q$  is realized by suspending the quartz crystal plates from fine wires<sup>5</sup> and operating them inside of evacuated containers. The low-impedance crystal elements which resonate at frequencies removed from the cut-offs require a minimum  $Q$  of 15,000. This comparatively low  $Q$  is realized by quartz crystal elements vibrating in air at atmospheric pressure.

In the equivalent electrical circuit of a quartz crystal element the large ratio of the shunt capacitance to the internal capacitance is a measure of the poor electromechanical coupling of quartz. For the +5 degree X-cut quartz crystal element this ratio of capacitances is about 140 for a plated blank before fabrication. It is obvious that fabrication, wiring and parasitic capacitances which may be in parallel with the quartz plate will make this ratio still higher and thus will reduce further the filter band width obtainable. For this reason it is important to keep to a minimum any capacitances which appear across any arms of the crystal lattices. One method used to minimize these capacitances was to assemble the eleven crystal elements required for each section in two containers instead of eleven separate ones. The five high-impedance elements requiring minimum  $Q$ 's of 80,000 are assembled in one evacuated metal container and the six low-inductance elements having the lower  $Q$ 's are assembled in another hermetic sealed container filled with dry air. A photograph showing the method of assembly used is given in Fig. 9.

A method was found to reduce the ratio of capacitances of the crystal elements. This method consists of dividing the plating on the surface of the quartz so that the driving voltage is removed from the end portions of the quartz plates. This plating division increases the equivalent inductance of the quartz plate but also decreases the direct capacitance between the plated surfaces. It has been found that the decrease in shunt capacitance with removal of plating is more rapid than the increase in equivalent inductance up to a certain point. If the plating is removed up to this optimum point it has been found possible to reduce the shunt capacitance about

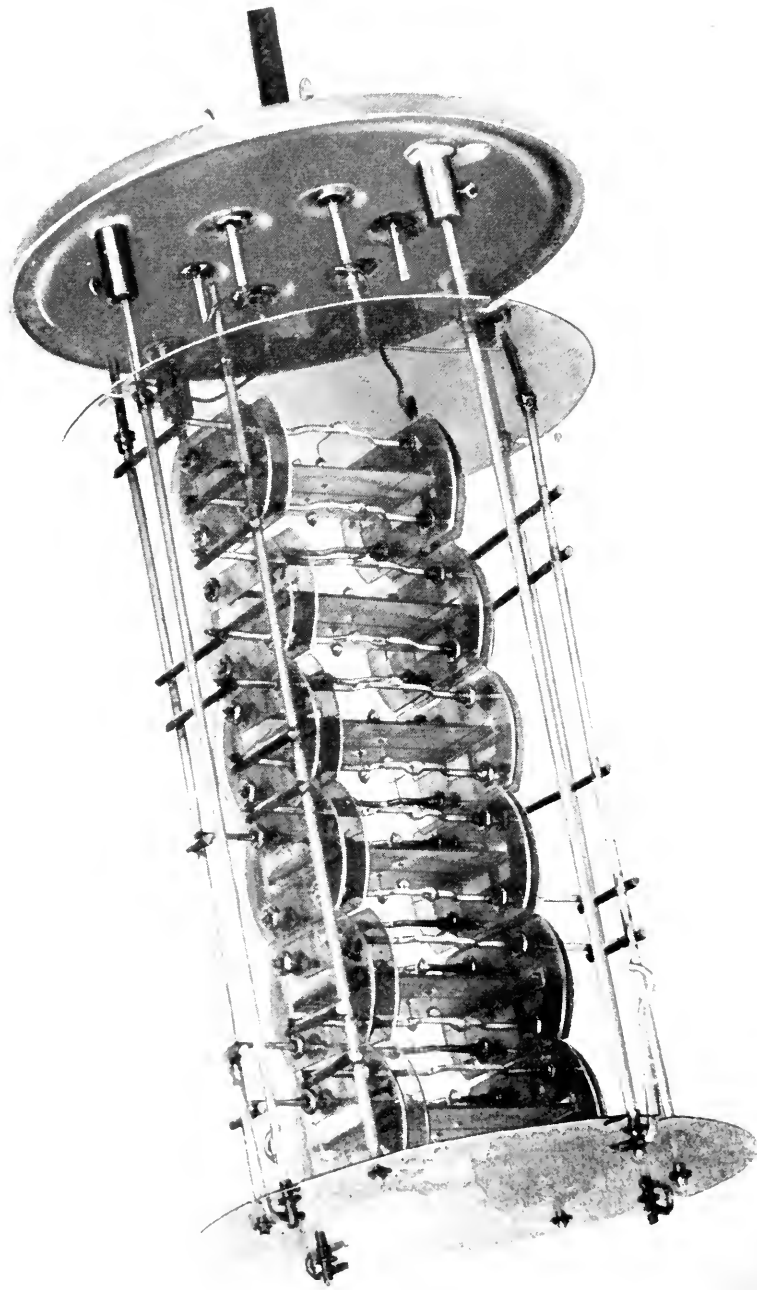


Fig. 9—Method of assembly of the quartz crystal elements.

17% below what it would be with a fully plated crystal element having the same inductance. This method of capacitance reduction was used on the six low-inductance crystal elements in each section. Another step in minimizing the unwanted capacitances was to design the retardation coils which connect to the terminal ends of each lattice to have as little capacitance as possible. Finally precautions were taken to keep the wiring capacitances to a minimum and the air condensers used inside the lattice for adjustment purposes are of special design having a minimum capacitance of only 0.5 mmf.

The resonant frequencies of each of the twenty-two crystal elements must be adjusted to the desired nominal frequencies within very close tolerances. On the ten high-impedance crystal elements the tolerance is  $\pm 2$  cps while on the 12 low-impedance crystal elements the tolerance is  $\pm 5$  cps. This precise frequency adjustment is accomplished by careful grinding of the length of the quartz plate.

The equivalent inductance of each of the 22 quartz crystal elements is required to be within two per cent of its nominal value. This specification is met primarily by close dimensional tolerances in the manufacture of the quartz plate. Any small adjustments which are necessary to meet this requirement are done by the aforementioned method of isolation of a small amount of plating from near the end of the quartz plate.

The four fixed retardation coils are adjusted to be within two per cent of their nominal inductance values. The variations from nominal are partially absorbed in the filter adjustment procedure where the coils are tuned with their associated variable capacitors to give the desired resonance frequency. The fixed mica capacitors are manufactured to be within 0.5 per cent of the desired nominal value. The three adjustable retardation coils are constructed to permit an inductance variation of five per cent on either side of their nominal values. This is done by moving a permalloy core in the field of the coil. Adjustment of these coils in the filter is accomplished by tuning them with their associated precision capacitor to give the desired resonance frequency within  $\pm 25$  cps. This type of adjustment procedure gives the correct  $LC$  product. The correct  $L/C$  quotient is obtained also since  $C$  is accurate to  $\pm 0.5$  per cent. The two resistors at each end of the filter compensate for the dissipation in the end retardation coils and thus restore the terminating impedance to the value required for optimum filter performance.

Each lattice of crystal elements and capacitors is a four-terminal bridge which is adjusted for maximum bridge balance at a particular frequency by means of the variable air capacitors in two of the arms. The precision of inductance adjustment of the crystal elements insures that the other peaks of attenuation will be sufficiently close to their nominal locations.

To obtain maximum loss at the filter peaks it is necessary to secure a conductance balance in each lattice section as well as a susceptance balance. This can be done if care is exercised in the choice of materials used in fabricating the crystal elements and capacitors which appear inside the lattice. In this case the crystal element insulators and dielectrics consist of glass, mica, quartz and clean dry air or vacuum while the air capacitors use glass, ceramic and air for their insulators and dielectrics. If these materials are clean and dry they have very low conductance and do not influence the bridge balance. A complete discussion of the effects of impedance unbalances on crystal lattice performance has been given in a recent paper by E. S. Willis.<sup>6</sup>

To further insure that dirt and moisture will not influence its performance the filter is adjusted, tested and hermetically sealed in an air conditioned room where the relative humidity does not exceed 40 per cent. Since manufacture started about the beginning of 1946 several hundred of these filters have been made and are functioning satisfactorily in the telephone plant.

#### BAND ELIMINATION FILTER AT BRANCHING POINTS

When broad-band carrier systems are equipped for the transmission of a carrier program channel, it is frequently necessary to provide between carrier terminals intermediate or branching points at which the program may also be received. If only receiving facilities are involved, rather simple bridging arrangements can be provided. However, program network needs often require a more flexible arrangement at the branching point so that a line may be cleared of the program originating at one terminal and a new program introduced for transmittal toward the next terminal.

To do this without affecting the message channels also being transmitted on the line, a filter has been developed to block the program channel already on the line while freely transmitting the message channels. With this filter in the circuit the high-frequency line between the branch point and the following terminal is free of program frequencies and the program originating at the branch point may be sent toward that terminal.

Since the program channel occupies frequency space near the center of the 12-channel message group, the remaining message channels appear above and below the program frequencies. Therefore the blocking filter at the branching points must be of the band elimination type. The circuit employing this filter may be designed to block either at line frequencies or at basic group frequencies. The latter method, of course, requires that a demodulation process be provided to translate line frequencies to basic group frequencies before the blocking filter is inserted in the circuit.

The band elimination filter described herein was developed for the type *K* carrier system (Carrier-on-Cable) for which the first option mentioned above was chosen. This filter operating at the line frequencies of the type *K* system is required to transmit frequencies from 12 to 31.6 kc and 44.2 to 60 kc while blocking those from 32 to 43.2 kc. Actually the filter will transmit frequencies below 12 kc and above 60 kc but these do not appear on the type *K* line and therefore there are no requirements in these ranges.

The filter which performs these functions is shown schematically in Fig. 10. Several factors made its design difficult. A high level of discrimination of the order of 75 db is required over a wide frequency range of about 12 kc. Also the allowable waste interval between wanted and unwanted frequencies is very small. The filter must transmit with a maximum distortion of 0.2 db to within 97.5% of the first unwanted frequencies at which a discrimination level of 75 db is required.

Because of the severe requirements the familiar image parameter design method was not employed. In this, as is well known, the composite filter first presented by Zobel<sup>7</sup> is made up of sections with matched image impedances but different transfer constants depending upon the attenuation requirements. Instead, it was felt that a design method proposed by Darlington<sup>8</sup> offered a better possibility of meeting the requirements with a reasonably sized filter. This procedure known as the *insertion loss* method is based upon the determination of a four-terminal transducer of reactances which, when inserted between definite resistance terminations, will produce a specified loss characteristic. A filter so designed has an advantage over image parameter filters in that the attenuation obtainable is greater for the same effective cut-off and an equal number of elements. *Effective cut-off* as used here means the last frequency of interest in the transmitted band. It is possible, therefore, with an *insertion loss* filter to use fewer elements for a given attenuation, or to obtain a wider transmission band with the same number of elements.

The advantage inherent in the newer design method is not derived from a difference in structure. In configuration there is no way to distinguish such a filter from one of conventional image design. The difference lies solely in the element values. A simple way to visualize how the *insertion loss* design varies from image design is to consider that the newer method removes an arbitrary restriction placed upon the image theory to simplify the mechanics of design. The restriction is that the nondissipative image attenuation must be identically zero over continuous frequency ranges including the transmitted bands and other than zero everywhere else. This leads to the familiar ladder image filter composed of matched sections, or the lattice filter with coincident critical frequencies.



Analysis of an *insertion loss* ladder filter shows that it may be considered a composite of image sections which are not matched in image impedance. As a composite filter this means that the effective pass band has been split into a number of pass bands each separated by a small attenuation region. Darlington has formulated the process by which these bands can be so arranged that advantage can be taken of the fact that the image attenuations in these bands for small mismatch are comparable to the terminal effects and that reflection gains up to 6 db are possible in the same regions. The combination of these effects, which can be controlled up to and including the cut-off, gives the *insertion loss* filter its improved performance since the *effective* and *theoretical* cut-offs can be made identical, with no

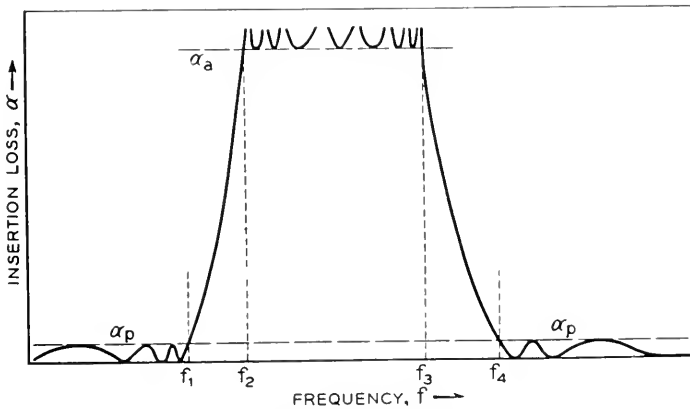


Fig. 11—Non-dissipative filter characteristic obtained by use of Tchebycheff parameters in pass bands and attenuation band.

frequency space needed for the rounding due to the terminal effects in image filters.

In general the mathematical steps required to design a filter by this method are as follows: An insertion loss frequency function is chosen which will satisfy the filter requirements and will lead to a structure economical of elements. From this are found the open and short circuit impedances of the proposed network which is normally of the standard lattice or ladder forms. Finally from these expressions the element values are determined.

The particular form of *insertion loss* design employed for the filter described here is a special case of the general theory. The filter requirements lent themselves to the use of Tchebycheff parameters simultaneously in the pass bands and attenuation band. The application of these parameters was first described by Cauer.<sup>9</sup> The typical non-dissipative characteristic resulting from their use is shown on Fig. 11. It is seen that the

pass band characteristic is of the *ripple* type with equal maxima and equal minima. In the attenuation region the valleys of loss are of equal value.

The general form for the insertion power ratio to obtain the desired characteristic is:

$$e^{2\alpha} = \frac{4R_1 R_2}{(R_1 + R_2)^2} [1 + (e^{2\alpha_p} - 1) \cosh^2 \theta_I]$$

In this equation  $R_1$  and  $R_2$  are the resistive terminations and  $\alpha_p$  is the maximum ripple in the pass band as shown in Fig. 11.

$\theta_I$  represents a function of frequency so chosen that  $\cosh \theta_I$  is an odd or even rational function of frequency. Also  $\theta_I$  must be a pure imaginary throughout the passing band and must be of the form  $(\alpha_I + n\pi i)$  in the attenuation region. The term  $\alpha_I$  is real at all attenuation frequencies becoming infinite at those required by the specification of minimum  $\alpha_a$  in Fig. 11.

Darlington further showed that  $\theta_I$  closely conforms with the image transfer constant of an image parameter filter if the effective pass band of the insertion loss filter coincides with the theoretical pass band of the image filter. Based on this conclusion a design method was formulated which permits a reference filter derived from image parameters to be used as the basis of the *insertion loss* filter. There is, of course, no correspondence between the elements of the reference image filter and the insertion filter. This reference filter is not a requisite to the development of the insertion theory but it does offer a convenient and well known transfer constant which is the right functional form for use in the insertion power ratio stated above.

Referring again to Fig. 11, the approximate minimum loss,  $\alpha_a$ , determines the number of peak sections required in the reference filter from the relationship:

$$\alpha_a = 20 \log (e^{2\alpha_p} - 1) - 10(2m + 1) \log q - 18$$

where " $m$ " is the number of peaks required and  $\alpha_p$  is the band ripple function as before. The new term introduced here is " $q$ " which is directly tied up with the selectivity demanded of the filter, i.e., the amount of frequency space available between the last useful frequency or *effective* cut-off and the first frequency at which attenuation equal to  $\alpha_a$  is needed. The relationships are as follows:

$$q = \frac{1}{2} \left[ \frac{1 - \sqrt{K'}}{1 + \sqrt{K'}} \right] + \frac{1}{16} \left[ \frac{1 - \sqrt{K'}}{1 + \sqrt{K'}} \right]^5$$

where  $K' = \sqrt{1 - K^2}$

and  $K = \frac{f_3 - f_2}{f_4 - f_1}$



The filter described here actually consists of two filters connected in tandem, each derived from a different power ratio. This step was taken because of the relatively low dissipation factor realizable with coils of reasonable size. By dividing the total attenuation between two power ratios, lower overall distortion due to dissipation was achieved. The distortion represented by the non-dissipative ripple " $\alpha_p$ " was minimized by so assigning the frequencies of infinite attenuation to the two functions that phasing in of the ripples was avoided as far as possible.

The two power ratios selected are:

$$e^{2\alpha_1} = 1 + (e^{2\alpha_p} - 1) \cosh^2 \theta_{I_1}$$

$$e^{2\alpha_2} = \frac{4R_1 R_2}{(R_1 + R_2)^2} [1 + (e^{2\alpha_p} - 1) \cosh^2 \theta_{I_2}]$$

For these the peak frequencies were assigned on an alternate basis as follows:

To  $\theta_{I_1}$  :  $m_1$ ,  $m_3$ ,  $m_5$  and  $m_7$

To  $\theta_{I_2}$  :  $m_1$ ,  $m_2$ ,  $m_4$  and  $m_6$

with the value of " $m$ " decreasing from  $m_1$  to  $m_7$  and  $m_1 = 1$ . The parameter " $m$ " has the same meaning as in image filter theory.

The next step in the process is the finding of the roots of the two power ratios. These may be obtained from the following expansions:

For  $e^{2\alpha_1}$  representing a reference filter of  $3\frac{1}{2}$  sections:

$$(m_3 + x)^2(m_5 + x)^2(m_7 + x)^2(1 + x) + \left( \frac{e^{\alpha_p} - 1}{e^{\alpha_p} + 1} \right) (m_3 - x)^2(m_5 - x)^2(m_7 - x)^2(1 - x) = 0$$

which is expressed in the form

$$K_1[x^7 + a_1x^6 + a_2x^5 + a_3x^4 + a_4x^3 + a_5x^2 + a_6x + a_7 = 0]$$

For  $e^{2\alpha_2}$  representing a reference filter of 4 sections:

$$(m_2 + x)(m_4 + x)(m_6 + x)(1 + x) + i \sqrt{\frac{e^{\alpha_p} - 1}{e^{\alpha_p} + 1}} (m_2 - x)(m_4 - x)(m_6 - x)(1 - x) = 0$$

which is expressed by

$$K_2[x^4 + a_8x^3 + a_9x^2 + a_{10}x + a_{11} = 0]$$

In the above expressions  $x = \sqrt{1 + \frac{1}{p^2}}$  where  $p = i\omega$  and  $\alpha_p$  for the filter

discussed here is 0.1 db. From the roots obtained from the above equations of 7th degree and 4th degree complexity, the open and short-circuit impedances are determined which in turn lead to the element values. The complete development of the process resulted in the filter portion of the network shown on Fig. 10.

The remainder of the schematic shows the equalizer which corrects the rounding of the filter characteristic near the cut-offs due to dissipation. The equalizer is of conventional bridged "T" design with constant "R" impedance in tandem with a simple series section.

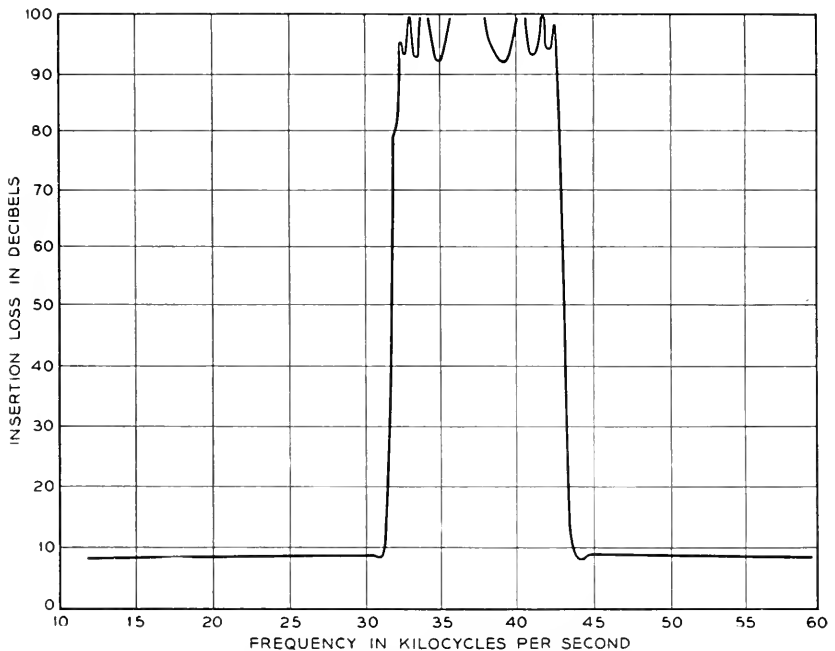


Fig. 12—Insertion loss-frequency characteristic of the band elimination filter.

Repeating coils are required as shown because the filter was designed at a 600-ohm level to give commercial elements whereas it is required to operate between 135 ohm resistances. In the schematic a resistance will be noted in series with one termination. This is needed because the "insertion" design with inverse impedance terminations as shown here requires unequal terminations to produce the specified loss characteristic. Usually this would be taken care of by proper design of the repeating coil but, in this case, economic reasons dictated the use of the same repeating coil at both ends of the structure. The termination was therefore built out with a

physical resistance. This of course introduces a flat loss but in this case enough gain was available in the circuit to permit it.

On Fig. 12 is shown a typical transmission characteristic when the filter is operating between 135-ohm resistances. A variety of component parts are required to give this performance. The filter portion employs mica condensers throughout and a mixture of molybdenum permalloy and air-core retard coils. As many permalloy coils are used as possible in order

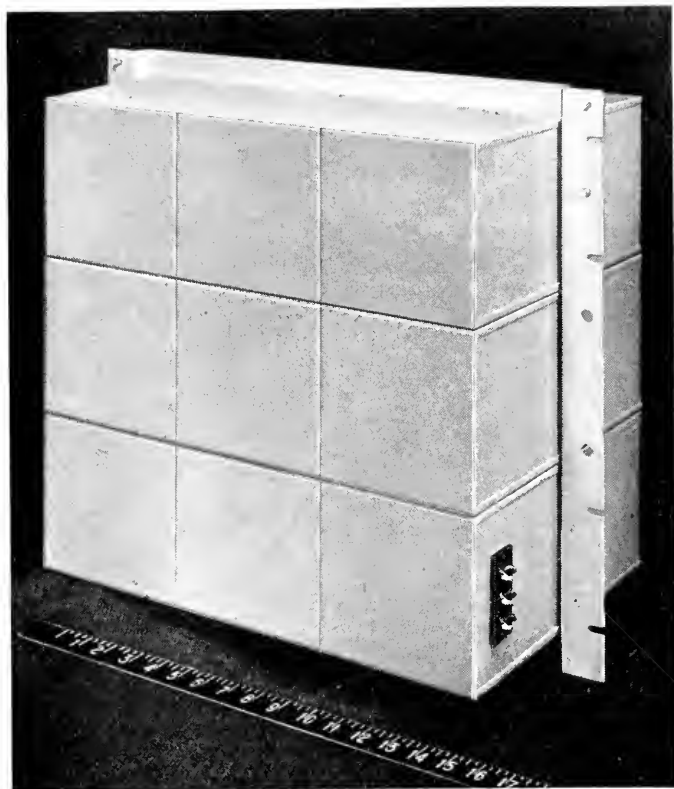


Fig. 13—Exterior view of the band elimination filter.

to obtain high " $Q$ ". The air-core coils, of an adjustable type, are used in those arms which control the peak frequencies near the pass band. These arms must be adjusted very accurately for resonance in order to maintain the steep slope of loss in the cut-off region. The equalizer sections employ duolaterally wound air core coils also adjustable in order to set the pass band losses accurately. Mica and paper condensers are used in the equalizer, the latter being used where capacity values make mica condensers extremely expensive.

A completed filter is shown in the photograph of Fig. 13, while the internal arrangements of one portion of the assembly are shown on Fig. 14.

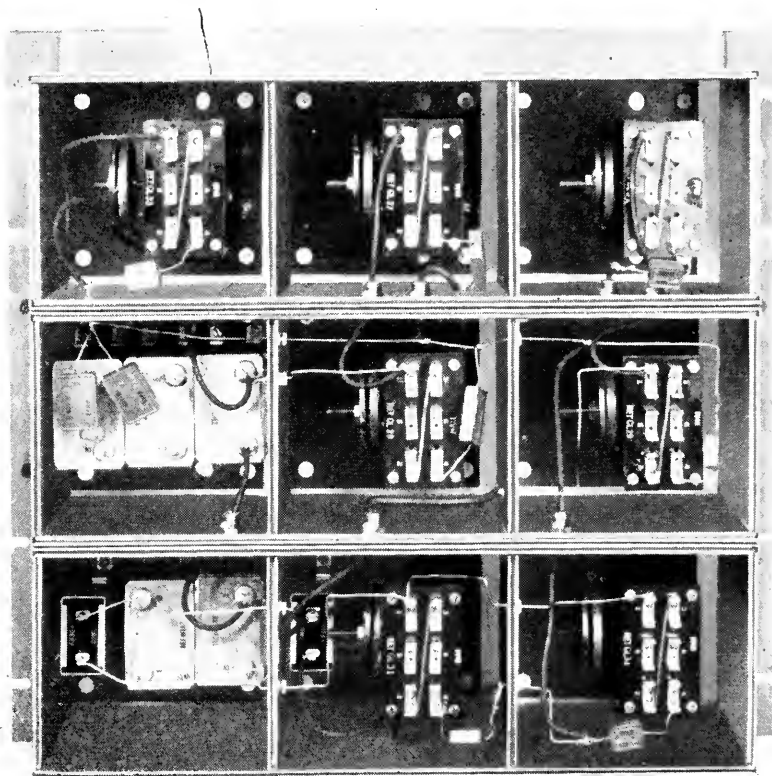


Fig. 14—Interior view of one portion of the assembly of the band elimination filter.

#### PHASE SIMULATING NETWORK

When program rearrangements at a branching point are required, the band elimination filter must be switched into or out of the through transmission path. This transfer is accomplished without opening the through path. Thus, for a brief time during the switching interval, message channels are transmitted simultaneously through the filter and the non-blocked circuit. A large phase difference between the two parallel paths is introduced by the filter which, in the absence of phase correction in the through circuit, could cause errors in the transmission of voice frequency telegraph signals. Therefore a network having phase shift similar to that of the filter over most of the message range is provided in the through circuit.

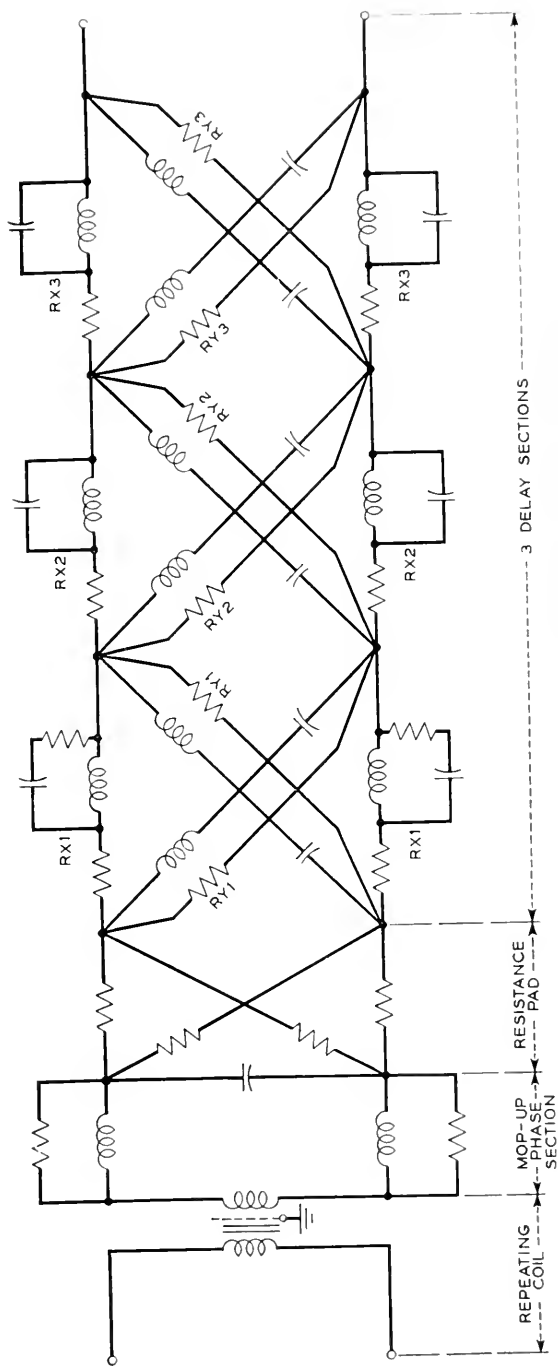


Fig. 15—Schematic of the phase simulating network showing the component sections.

The phase simulating network is shown in schematic form in Fig. 15.

The network is a balanced structure and consists of the following pieces of apparatus connected in tandem:

1. An input repeating coil to improve the longitudinal balance at the sending end,
2. A half-section high-frequency cut-off low-pass filter to mop up the phase shift introduced by two repeating coils of the band elimination filter,

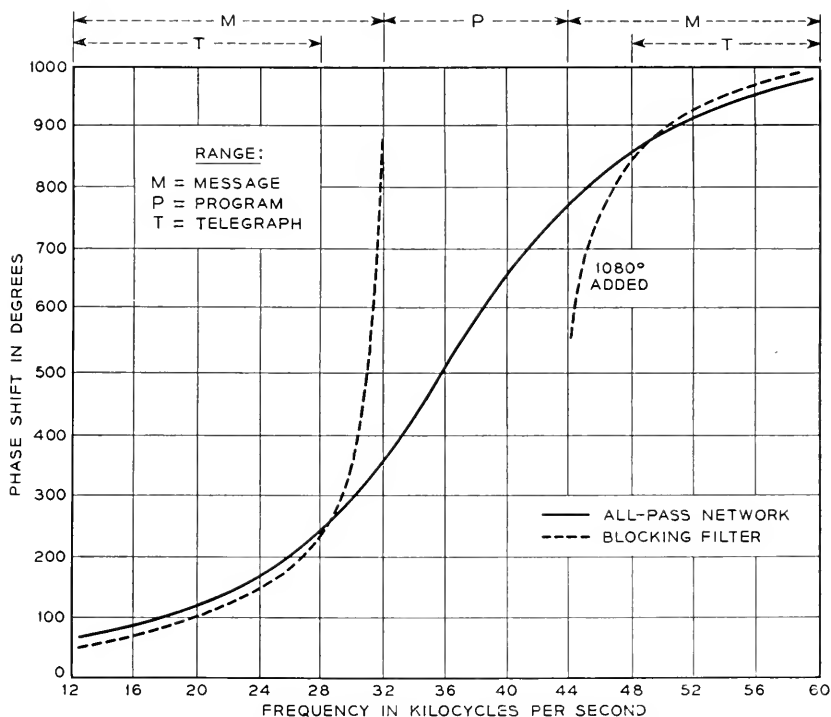


Fig. 16—Phase shift-frequency characteristic of the phase simulating network.

3. A resistance pad to equalize the over-all loss level of the all pass network to within  $\pm 0.1$  db of the pass band loss of the band elimination filter, and
4. Three delay sections, self equalized for loss,<sup>10</sup> for simulating the phase shift of the band elimination filter.

The network simulates the phase shift of the band elimination filter over the frequency ranges covered by message channels 1 to 4 and 10 to 12 to within 20 electrical degrees as shown in Fig. 16. As phase simulation is

incomplete in the frequency ranges occupied by channels 5 and 9 due to the steep phase shift slope of the band elimination filter near its cut-off points, no telegraph channel are assigned to these channels of type "K" carrier circuits equipped with branching points.

The phase shift of the band elimination filter is discontinuous between its cut-off frequencies and has a positive slope with frequency in its pass bands. As the phase shift of a delay section increases continuously with frequency, it is impossible to provide the exact counterpart of the filter in a delay network. However, the addition of any multiple of  $2\pi$  radians does not change the transmission characteristic. Hence  $6\pi$  radians (3

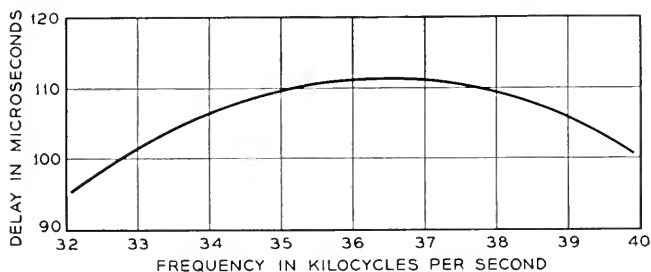


Fig. 17—Delay of the phase simulating network at program frequencies.

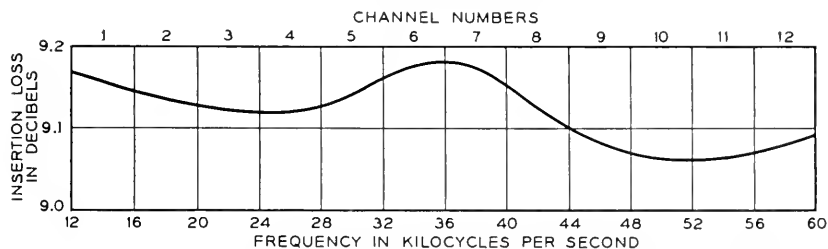


Fig. 18—Insertion loss-frequency characteristic of the phase simulating network.

revolutions) are added to the phase shift of the elimination filter above the upper cut-off to simulate its phase characteristic in the 10 to 12 message channel range, as well as to provide an almost linear phase slope in the 32 to 40 kc program channel range resulting in minimum delay distortion.

The delay distortion of the network over the program channel is approximately 16 microseconds as shown in Fig. 17. The loss distortion over the program channel is approximately 0.05 db and over any one message channel it is less than 0.05 db as shown in Fig. 18.

The self loss equalizing feature of a delay section is evaluated at zero frequency in the form of a resistance pad by making the pad loss approximate the insertion loss at the critical frequency of the delay section. The

resistance  $R_z$  located in the series branch may be evaluated from the expression

$$R_z = R \frac{\epsilon^\theta - 1}{\epsilon^\theta + 1} - R_{DC}$$

in which  $\epsilon^\theta$  is the transfer loss in nepers at the critical frequency,  $R$  is the 135 ohm resistance termination and  $R_{DC}$  is the DC resistance of the inductance coil. The resistance  $R_y$  located in parallel with the series resonant branch may be evaluated from the expression  $R_y = \frac{R^2}{R_z}$ .

By changing the loss,  $\epsilon^\theta$ , of the derived resistance pad at zero frequency slightly from the measured loss at the critical frequency of the delay section, a suitable loss compensation may be realized to produce an optimum loss equalization over the message and program channel ranges. It is satisfactory to follow this technique when the condenser  $Q$  factor is much greater than the coil  $Q$  factor. When this condition exists, the insertion loss about the critical frequency becomes geometrically dissymmetrical, that is, the loss falls off more rapidly for frequencies above the critical frequency because of the controlling condenser  $Q$  factor.

#### REFERENCES

1. "A Carrier System for 8000-Cycle Program Transmission," R. A. Leconte, D. B. Penick, C. W. Schramm, A. J. Wier., a companion paper. This issue of *BSTJ*.
2. "Electromechanical Transducers and Wave Filters" (book), W. P. Mason, D. Van Nostrand Co., New York, N. Y., 1942.
3. "Delay Equalization of 8-kc Carrier Program Circuits," C. H. Dagnall and P. W. Rounds, a companion paper. This issue of *BSTJ*.
4. "Communication Networks," Vol. II (book), E. A. Guillemin, John Wiley & Sons, New York, N. Y., 1935.
5. "The Mounting and Fabrication of Plated Quartz Crystal Units," R. M. C. Greenidge, *Bell Sys. Tech. Jour.*, Vol. 23, July 1944, page 234.
6. "A New Crystal Channel Filter for Broad Band Carrier Systems," E. S. Willis, *Elec. Eng.*, Vol. 65, March 1946, Page 134.
7. "Theory and Design of Uniform and Composite Electric Wave Filters," O. J. Zobel, *Bell Sys. Tech. Jour.*, Vol. 2, 1923, Pages 1-46.
8. "Synthesis of Reactance 4-Poles which Produce Prescribed Insertion Loss Characteristics," S. Darlington, *Journal of Mathematics and Physics*, Vol. 18, No. 4, Sept. 1939.
9. "Ein Interpolationsproblem mit Funktionen mit Positiven Realteil," W. Cauer, *Mathematische Zeitschrift*, 38, 1-44, 1933.
10. "Distortion Correction in Electrical Circuits with Constant Resistance Recurrent Networks," O. J. Zobel, *Bell Sys. Tech. Jour.*, Vol. 7, July 1928, Pages 438-534.



## A Precise Direct Reading Phase and Transmission Measuring System for Video Frequencies

By D. A. ALSBERG and D. LEED

THE evolution of transmission networks for communications systems progresses through three fairly well-defined phases—design, synthesis and final adjustment. The design phase ordinarily involves no problem of measurement. In the synthesis stage, during which the physical model is constructed from the paper design, precise equipment is often needed for measuring the magnitude of the various components comprising the network. The adjustment stage, in which the network is actually tested as an element in a transmission circuit, generally requires the most complex instrumentation. In the latter category we may include insertion loss, gain, and phase measurement systems.

Television and broad-band carrier facilities, such as the New York-Midwest video cable link, employ vast numbers of transmission networks. These include, for example, filters, equalizers, and repeaters. The final adjustment of these networks requires a large number of precise insertion phase and transmission measurements during both development and manufacturing stages. Consequently, the measurement equipment must combine laboratory accuracy with speed of measurement suitable for use in production testing.

The quantities measured are defined in Fig. 1. Conforming with current usage, the term *Transmission* is used herein to designate insertion loss and gain.

The performance of the system with respect to frequency range, measurement range and accuracy is as follows:

*Frequency Range:* 50–3600 kilocycles

*Generator and Network Termination Impedance:* 75  $\Omega$

*Transmission Range:* +40 db to –40 db; Accuracy  $\pm 0.05$  db  
–40 db to –60 db; reduced accuracy.

*Insertion Phase Shift Range:* 0–360°; Accuracy  $\pm 0.25$  degree (+40 db to –40 db)

The measuring circuit is based on the heterodyne principle whereby the phase and transmission of the *unknown* are translated from the variable frequency to a constant intermediate frequency at which the phase and transmission standards operate. Accurate phase-shifters and variable attenuators with negligible phase shifts are constructed readily for fixed

frequency operation. This advantage more than offsets resulting problems of modulator design and automatic frequency control.

Conforming with the definitions of insertion phase and transmission, the measurement system compares, with respect to phase and amplitude, the outputs of two transmission channels energized from the measurement frequency source, one of which serves as a standard or reference channel, while the other contains the apparatus under test. This is illustrated by the block drawing in Fig. 2.

For loss measurements the range attenuator *I* (Fig. 2) is set at 0 db. Measurement frequency *F* from the master oscillator is applied to both standard "S" and unknown "X" channels through splitting pad *I*. The voltages at "S" and "X" modulator inputs, points *A* and *B* respectively

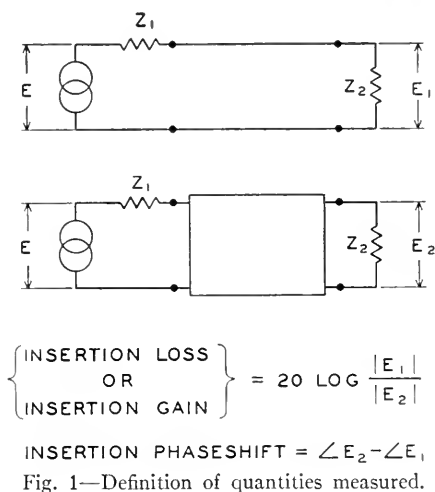
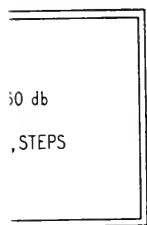


Fig. 1—Definition of quantities measured.

in Fig. 2, differ with respect to phase and amplitude because of the transmission differential introduced between the two channels by the apparatus under test. By frequency conversion in the "S" and "X" modulators these amplitude and phase differences at frequency *F* are translated at points *C* and *D* to a constant intermediate frequency, 31 kc. The second input to the "S" and "X" modulators, of frequency *F* + 31 kc, is supplied by the slave oscillator which automatically tracks at constant 31 kc difference with respect to the master oscillator. By selective filtering, only the difference frequency appears at the modulator outputs *C* and *D*. 31 kc has been chosen as the intermediate frequency, primarily on the basis of filtering requirements in the modulators. The detector (Fig. 2) compares the voltages of the "X" and "S" channels at *K* and *L* as to magnitude

ATTENUATOR



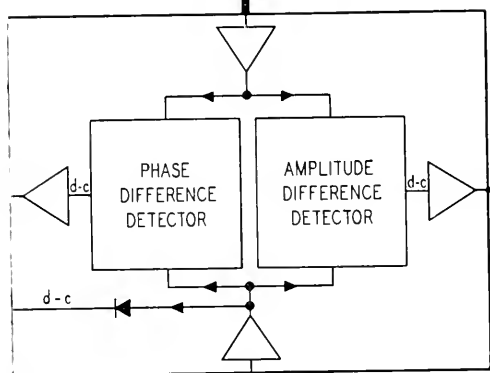
31 kc

"X"

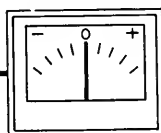
31 kc

L

DETECTOR



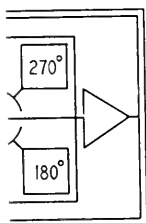
TRANSMISSION  
INDICATOR



K

"S"

31 kc



31 kc

PHASE SHIFTER  
RANGE 0°-360°

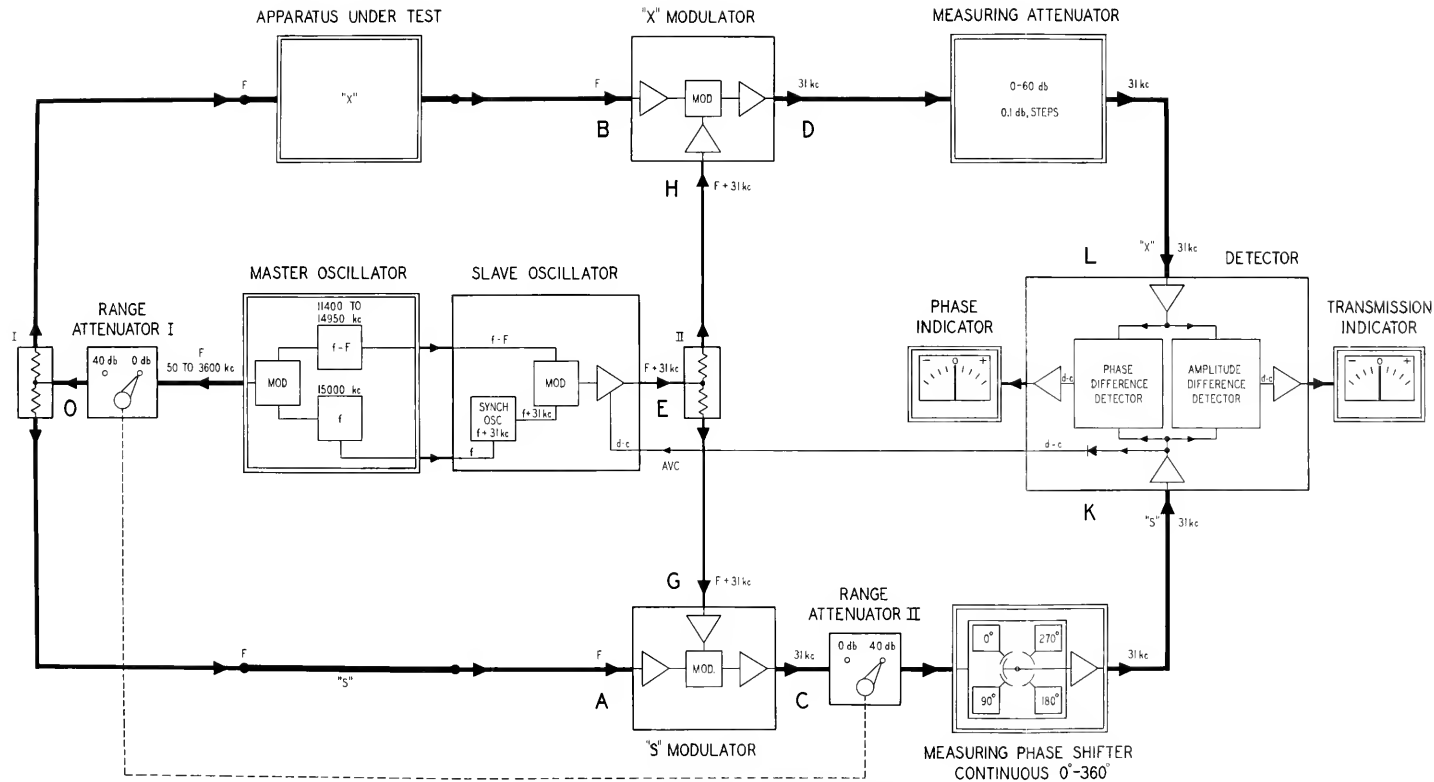


Fig. 2—Block schematic of the phase and transmission measurement system.

and phase, and indicates their difference on the direct reading scales of the indicator meters.

If the measuring attenuator is set at 60 db loss, and the range attenuator *II* at 40 db loss, "S" and "X" channels are in balance when the *apparatus under test* is replaced by a *zero loss* strap. The phase-shifter has, by design, 20 db loss; so that under these conditions "S" and "X" channels are nominally in balance, except for small residual phase and transmission differentials which may be *zeroed-out* by initial adjustment of the phase-shifter and of the relative gain between "S" and "X" channel amplifiers within the detector. Null readings on the phase and transmission difference indicating meters tell when exact phase and transmission balance between the two channels has been established. The phase-shifter and attenuator dials are arranged to read zero after this initial balance has been made. To measure apparatus transmission and phase, the strap is replaced by the *apparatus under test* and the balance restored by adjustment of the phase-shifter and the measuring attenuator. The insertion phase and transmission of the apparatus under test are then read directly from the calibrated dials of the phase shifter and attenuator.

When measuring loss, attenuation in the measuring attenuator is reduced by the amount of attenuation introduced in the high-frequency portion of "X" channel by the "apparatus under test." In measuring gain, the attenuation through the measuring attenuator must be increased by the amount of apparatus gain. To insure that "S" and "X" channel modulators are not overloaded by excessive input, range attenuator *I* is set to 40 db loss during gain measurements. This attenuator is common to both channels and therefore introduces no phase differential. Simultaneously and automatically, the range attenuator *II* immediately following the "S" modulator, is operated, removing 40 db loss from the 31 kc standard channel.

The measuring attenuator is self-computing and indicates directly in illuminated figures the gain or loss of the apparatus under test. A simple switching arrangement automatically controls the dial-lighting circuit of the measuring attenuator. When measuring gain the dial indications increase in one direction, and when measuring loss the indications increase in the opposite direction (Fig. 3).

In addition to the null-balance method, a deflection method of measurement using direct reading scales of the phase and transmission difference indicating meters is also possible. An automatic volume control circuit assures invariance of the indicator scale factors with either the modulator frequency-transmission characteristic, or input voltage variation at the "S" modulator caused by reflections from apparatus under test. The automatic volume control circuit regulates the output voltage of the slave oscillator to maintain the amplitude of the "S" channel input to the dif-



and phase, and indicates their difference on the direct reading scales of the indicator meters.

If the measuring attenuator is set at 60 db loss, and the range attenuator *II* at 40 db loss, "S" and "X" channels are in balance when the *apparatus under test* is replaced by a *zero loss* strap. The phase-shifter has, by design, 20 db loss; so that under these conditions "S" and "X" channels are nominally in balance, except for small residual phase and transmission differentials which may be *zeroed-out* by initial adjustment of the phase-shifter and of the relative gain between "S" and "X" channel amplifiers within the detector. Null readings on the phase and transmission difference indicating meters tell when exact phase and transmission balance between the two channels has been established. The phase-shifter and attenuator dials are arranged to read zero after this initial balance has been made. To measure apparatus transmission and phase, the strap is replaced by the *apparatus under test* and the balance restored by adjustment of the phase-shifter and the measuring attenuator. The insertion phase and transmission of the apparatus under test are then read directly from the calibrated dials of the phase shifter and attenuator.

When measuring loss, attenuation in the measuring attenuator is reduced by the amount of attenuation introduced in the high-frequency portion of "X" channel by the "apparatus under test." In measuring gain, the attenuation through the measuring attenuator must be increased by the amount of apparatus gain. To insure that "S" and "X" channel modulators are not overloaded by excessive input, range attenuator *I* is set to 40 db loss during gain measurements. This attenuator is common to both channels and therefore introduces no phase differential. Simultaneously and automatically, the range attenuator *II* immediately following the "S" modulator, is operated, removing 40 db loss from the 31 kc standard channel.

The measuring attenuator is self-computing and indicates directly in illuminated figures the gain or loss of the apparatus under test. A simple switching arrangement automatically controls the dial-lighting circuit of the measuring attenuator. When measuring gain the dial indications increase in one direction, and when measuring loss the indications increase in the opposite direction (Fig. 3).

In addition to the null-balance method, a deflection method of measurement using direct reading scales of the phase and transmission difference indicating meters is also possible. An automatic volume control circuit assures invariance of the indicator scale factors with either the modulator frequency-transmission characteristic, or input voltage variation at the "S" modulator caused by reflections from apparatus under test. The automatic volume control circuit regulates the output voltage of the slave oscillator to maintain the amplitude of the "S" channel input to the dif-

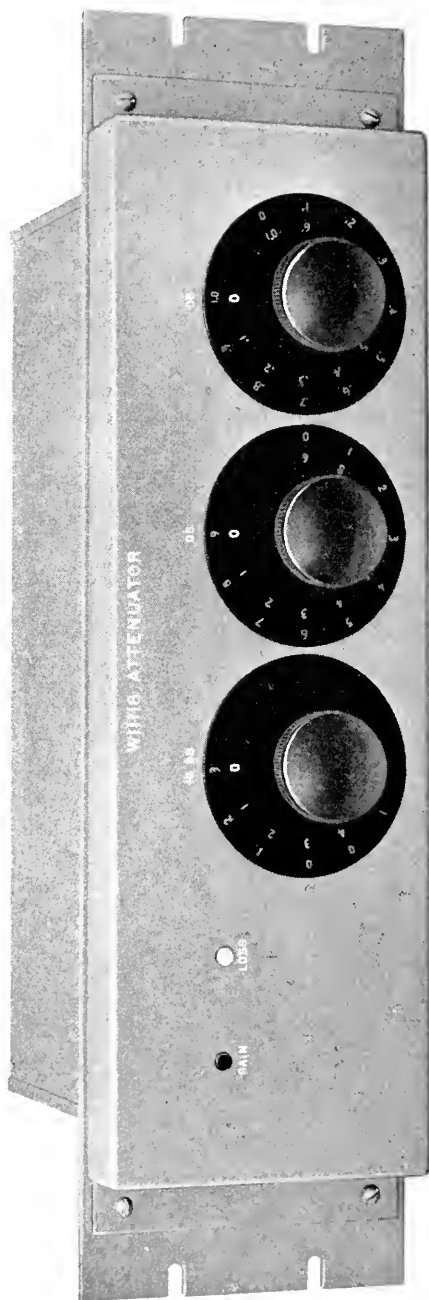


Fig. 3—Measuring attenuator with computing dials.



ferential detector constant. As the control action simultaneously affects both "S" and "X" modulators uniformly, the system zero is undisturbed.

Careful attention has been given to the problem of obtaining an electrical match between "S" and "X" modulators and coaxial cable lengths in the high-frequency channels. (RG 6/U cable contributes a phase shift of  $0.2^\circ$ /inch at 3600 kc.) Consequently, with the apparatus under test replaced by a *coaxial strap*, a balance indication on the phase and transmission difference indicators may be obtained which shifts less than 0.1 degree in phase and 0.02 db in transmission when the master oscillator frequency is varied over its entire band.

Because of the frequency independence of the system zero and the automatic frequency control of the slave oscillator, the master oscillator may be swept through the entire frequency band for rapid appraisal of the network performance by observation of the phase and transmission difference indicators.

The component chassis of the set are mounted in a specially designed console, shown in Fig. 4, which places all controls within easy reach of the operator. This console houses as much apparatus as three 6-foot relay racks within a floor space equal to that occupied by a 5-foot laboratory bench. Though not visible, a full bay of apparatus is mounted behind the central meter panel. Easily movable partitions and covers permit accessibility to all units, thus expediting maintenance.

Some of the significant design considerations are discussed separately under the following headings:

- (1) Master Oscillator
- (2) Slave Oscillator
- (3) Modulators
- (4) Phase and Transmission Detector
- (5) Phase-shifter

#### MASTER OSCILLATOR

As indicated in Fig. 2 and Fig. 5C, the master oscillator is of the heterodyne type. It employs 15,000 and 11,400-14,950 kc local oscillators. A high degree of frequency stability has been achieved through special oscillator circuit design. A motion picture film type scale, 300 inches in length, calibrated every 10 kc, and further subdivided every 2 kc, covers the entire frequency range 50-3600 kc without band-switching. A 0-10 kc interpolation dial with 100-cycle divisions, which operates on the fixed local oscillator frequency, is used to interpolate between adjacent 2 kc graduations on the main film scale. By oscilloscopic comparison with a 10 kc standard of frequency, the oscillator can be set within 50 cycles of any desired fre-

quency in its band. An A.V.C. circuit maintains the output power at six db above one milliwatt.

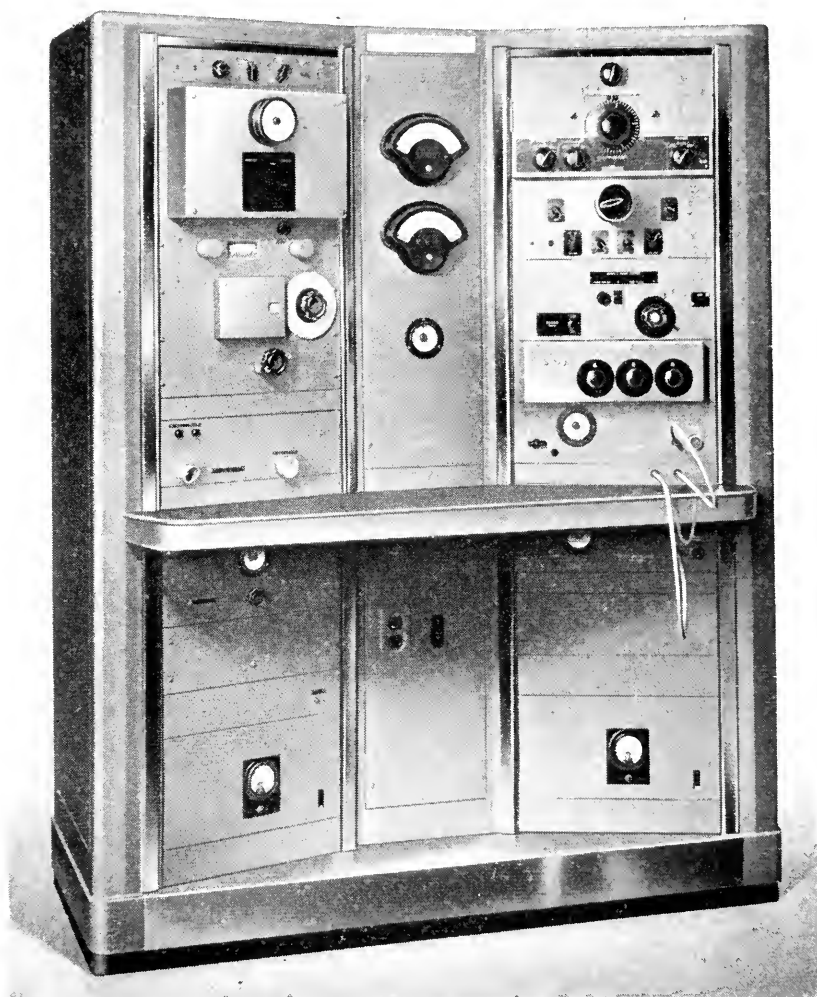


Fig. 4—The assembled phase and transmission measuring system.

#### SLAVE OSCILLATOR

To make possible the operation of the measuring attenuator, phase-shifter, and phase and transmission difference detectors at constant frequency, the inputs to the "S" and "X" channel modulators from the master and slave

(A)



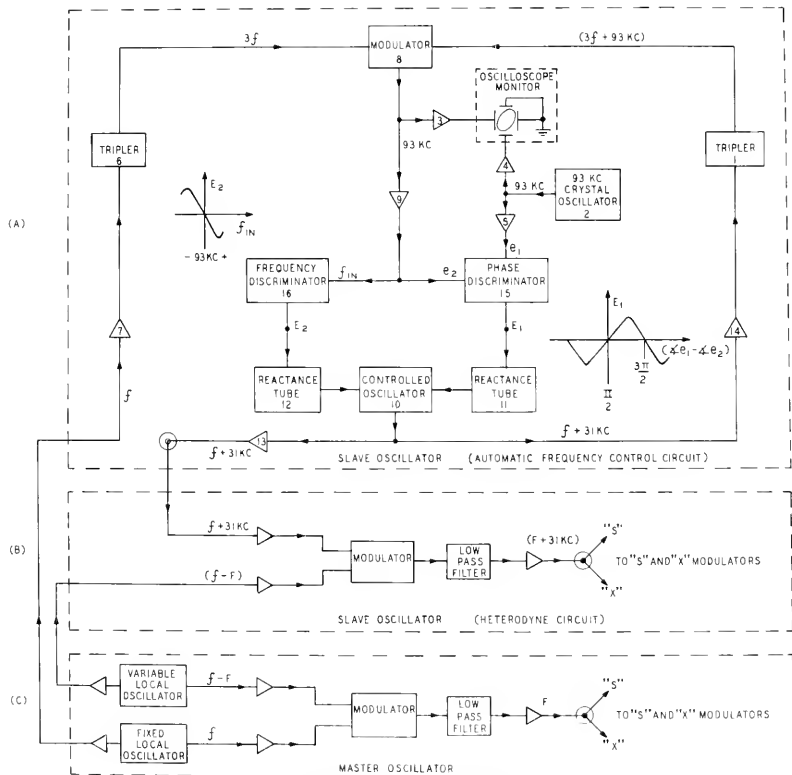


Fig. 5 Master and slave oscillators

oscillators must always differ in frequency by a constant amount. This difference is maintained at 31 kc by the control of the master oscillator over the slave oscillator frequency.

Very briefly, the scheme consists in applying the fixed local oscillator frequency,  $f$ , of the master oscillator, to an automatic frequency control circuit which produces an output frequency  $f + 31$  kc.  $f + 31$  kc is then modulated with variable local oscillator frequency,  $f - F$ , of the master oscillator, resulting in an output of frequency  $F + 31$  kc. Frequency  $F$ , formed by modulation of  $f$  and  $f - F$ , is the master oscillator frequency.

In the automatic control circuit, frequency  $f$  is compared with that of a controlled oscillator, by detecting their difference in a modulator. The nature of the control is such, that any deviation of this difference from 31 kc causes the frequency of the controlled oscillator to change in the direction which eliminates the deviation. While it is simpler to compare  $f$  and the controlled oscillator frequency directly, in the slave oscillator the comparison is made between the outputs of tripler circuits energized from the latter frequencies. In this way more complete isolation is realized between  $f$  and the controlled frequency than would be afforded with only buffer amplifiers. Because of the tripling, it follows that the oscillator must be controlled according to the departure of the difference between the tripler circuit frequencies from 93 kc. This, however, has the advantage of avoiding the generation of 31 kc anywhere in the automatic frequency control circuit, which could, by spurious modulation, cause the  $f + 31$  kc output to be contaminated with small traces of frequency  $f$ . The necessity for exceptional purity of  $f + 31$  kc output arises in the measurement of high losses where minute amounts of  $F$  at the  $F + 31$  kc input to "S" and "X" modulators may produce appreciable error.

Owing to phase tracking requirements between "S" and "X" intermediate frequency channels, and to the frequency dependence of the phase-shifter calibration, it is necessary to maintain the intermediate frequency as closely as possible to the precise value, 31,000 cycles. The permissible deviation from the correct value has been limited to  $\pm 1$  cycle. This precise control is maintained in the presence of 10 kc changes in  $f$ , which may occur when the setting of the 0-10 kc interpolation dial of the master oscillator is varied in the course of measurement.

Figures 5A and 5B illustrate the automatic frequency control and heterodyne circuits of the slave oscillator. The frequency of oscillator 10 in Fig. 5A is controlled by the reactance tubes 11 and 12. Reactance tube 12 is actuated by direct voltage from frequency discriminator 16, so that it controls oscillator 10 according to frequency error. Frequency error is the difference between the input frequency to discriminator 16 from amplifier 9, and 93 kc, the frequency of zero voltage output from the dis-



oscillators must always differ in frequency by a constant amount. This difference is maintained at 31 kc by the control of the master oscillator over the slave oscillator frequency.

Very briefly, the scheme consists in applying the fixed local oscillator frequency,  $f$ , of the master oscillator, to an automatic frequency control circuit which produces an output frequency  $f + 31$  kc.  $f + 31$  kc is then modulated with variable local oscillator frequency,  $f - F$ , of the master oscillator, resulting in an output of frequency  $F + 31$  kc. Frequency  $F$ , formed by modulation of  $f$  and  $f - F$ , is the master oscillator frequency.

In the automatic control circuit, frequency  $f$  is compared with that of a controlled oscillator, by detecting their difference in a modulator. The nature of the control is such, that any deviation of this difference from 31 kc causes the frequency of the controlled oscillator to change in the direction which eliminates the deviation. While it is simpler to compare  $f$  and the controlled oscillator frequency directly, in the slave oscillator the comparison is made between the outputs of tripler circuits energized from the latter frequencies. In this way more complete isolation is realized between  $f$  and the controlled frequency than would be afforded with only buffer amplifiers. Because of the tripling, it follows that the oscillator must be controlled according to the departure of the difference between the tripler circuit frequencies from 93 kc. This, however, has the advantage of avoiding the generation of 31 kc anywhere in the automatic frequency control circuit, which could, by spurious modulation, cause the  $f + 31$  kc output to be contaminated with small traces of frequency  $f$ . The necessity for exceptional purity of  $f + 31$  kc output arises in the measurement of high losses where minute amounts of  $F$  at the  $F + 31$  kc input to "S" and "X" modulators may produce appreciable error.

Owing to phase tracking requirements between "S" and "X" intermediate frequency channels, and to the frequency dependence of the phase-shifter calibration, it is necessary to maintain the intermediate frequency as closely as possible to the precise value, 31,000 cycles. The permissible deviation from the correct value has been limited to  $\pm 1$  cycle. This precise control is maintained in the presence of 10 kc changes in  $f$ , which may occur when the setting of the 0-10 kc interpolation dial of the master oscillator is varied in the course of measurement.

Figures 5A and 5B illustrate the automatic frequency control and heterodyne circuits of the slave oscillator. The frequency of oscillator 10 in Fig. 5A is controlled by the reactance tubes 11 and 12. Reactance tube 12 is actuated by direct voltage from frequency discriminator 16, so that it controls oscillator 10 according to frequency error. Frequency error is the difference between the input frequency to discriminator 16 from amplifier 9, and 93 kc, the frequency of zero voltage output from the dis-

criminator. The voltage from phase discriminator 15 controls oscillator 10 according to the difference of phase between the input from stage 9, and an input of reference phase from amplifier 5. This difference of phase is proportional to the time integral of the frequency error. The gross effect, therefore, is to control the oscillator 10 according to the controller law, *proportional to frequency error + time integral of frequency error*, or, in the terminology of feedback regulators, *proportional + integral control*<sup>1</sup>. When in equilibrium, the system operates with a static phase difference between the phase discriminator inputs, a condition which can exist only when these inputs are of equal frequency. The system is thus endowed with the property *zero frequency error*, and the frequency at the output of modulator 8 is maintained in exact equality with crystal oscillator 2 frequency. Consequently the intermediate frequency difference between input,  $f$ , and controlled oscillator 10 is held precisely at the value 31,000 cycles.

Automatic frequency control circuits of the phase sensitive type have been previously described<sup>2,3,4</sup>.

The system of combined phase and frequency sensitive control in the slave oscillator is superior to those which use only phase or frequency sensitive control. In a control circuit which uses only a phase discriminator and associated reactance tube, the controlled oscillator may lock-in at either of two sideband frequencies. These are  $f + 31$  kc, and  $f - 31$  kc. Operation is at upper sideband when control stabilizes on the positive slope of the phase discriminator output voltage curve in Fig. 5A, and at lower sideband if control is along the negative slope. Thus an ambiguity of sideband exists, though the attribute of *zero frequency error* is retained. When only a frequency discriminator and reactance tube are used, lock-in is possible at only one of the two sideband frequencies, determined by the poling of the frequency discriminator output voltage. A frequency error, however, is present.

The combination in Fig. 5 of the two systems operating jointly utilizes the phase sensitive discriminator to insure close control of oscillator frequency, and the polarizing property of the coarser frequency discriminator to eliminate the possibility of synchronization at the undesired sideband.

The joint system of phase and frequency sensitive automatic control has the further virtue of possessing a far greater degree of stability than is obtainable with the phase discriminator loop acting alone.

In the heterodyne circuit of Fig. 5B,  $f + 31$  kc from the automatic frequency control circuit is modulated with  $f - F$ , the variable local oscillator frequency of the master oscillator. The frequency at the output of the heterodyne circuit is  $F + 31$  kc, and this is modulated with frequency  $F$  in the "S" and "X" modulators to produce the constant intermediate frequency, 31 kc, in the measurement portion of the set.



## THE MODULATORS

The difficulties of precise measurement over a wide frequency band essentially are concentrated in the modulator. With the precision to which measurement must be made, effects ordinarily of small concern assume importance. The following discussion is valid for any modulator, though the specific example of the vacuum tube is used.

It is the function of the modulator to convert linearly changes in amplitude and phase from the input frequency  $F$  to the output frequency 31 kc. The linear range of conversion is limited by overload at the high-level limit and by noise at the low-level limit.

Let the input  $x$  to a modulator consist of two frequencies  $F_1$  and  $F_2$ . In the ideal square law modulator<sup>5</sup> perfect linearity results between changes in the input signal  $F_1$  and the output signal  $F_2 - F_1$ . The output filter rejects all frequencies but  $F_2 - F_1$ .

In actual tubes the plate current is

$$(1) \quad I_p = a_0 + a_1x + a_2x^2 + a_3x^3 + a_4x^4 + \dots$$

The effect of the term  $a_4x^4$  and higher even-order terms is to contribute output currents of frequency  $F_2 - F_1$  which do not vary linearly with the input.<sup>5</sup> In addition to this the effect of remodulation in plate, screen and suppressor circuits is that the coefficients  $a_2$ ,  $a_4$  etc. are not independent of the input  $x$  and so contribute to the distortion. Further, in presence of modulation of higher than second order, the d-c. term in even-order modulation will cause distortion if cathode bias is used. Removal of d-c. degeneration using fixed bias eliminates this effect.

The high-level limit may be defined as the signal value for which the total error due to overload equals the desired limits of modulator performance.

The lowest input level into the modulator which may be tolerated, and hence the lower limit of loss which can be measured, is determined by the effective signal-to-noise ratio at the modulator output. If no amplification exists preceding the modulator the input grid noise is usually limiting. The signal-to-noise ratio of the signal  $F_1$  and a noise band centered on  $F_1$  is unaffected by the modulation process as only the modulated portion of the noise band passes through the output filter. Yet for a noise band centered on the intermediate frequency  $F_2 - F_1$  for which the output filter is transparent the modulator acts as a straight amplifier; hence the effective signal-to-noise ratio is degraded approximately by the ratio of amplifier gain to conversion gain of the modulator.

The low-level limit may be defined as the signal value for which the error due to noise equals the desired modulator performance limit. For example for a noise error of 0.01 db, a signal-to-noise ratio of 1000 to 1 or 60 db is required.

To obtain maximum signal-to-noise ratio, a tube must be chosen to have the lowest product of *noise multiplied by the ratio of amplifier to conversion gain*, the latter requirement being in conflict to overload requirements. When inputs below the low-level limit are to be utilized a preamplifier ahead of the modulator tube is required. This amplifier also contains a noiseband centered on  $F_2 - F_1$ . If the amplifier is selective and rejects this noise band or if an  $F_2 - F_1$  rejection filter is inserted ahead of the modulator tube the resultant new low-level limit is determined by the signal-to-noise ratio of the preamplifier at the signal frequency  $F_1$  only.

Dynamic range is defined as the useful range of a modulator limited by the high-level limit on one end and by the low-level limit on the other. The dynamic range of a number of pentodes was determined. It was found experimentally that differences in dynamic range between pentodes of different power ratings, such as 6AK5, 6AC7, 6AG7, 6L6, 829B, are small. A dynamic range of 30–36 db can be realized with a 6AK5 for a .01 db linearity requirement. The 6AK5 was the most suitable tube of those investigated considering all other requirements of the circuit such as band width, available signal levels, etc.

Buffer amplifiers are required ahead of the modulator tube to prevent crosstalk between measuring and reference modulator through common paths. These buffer amplifiers are of conventional video amplifier design, with phase and gain characteristics closely controlled to the order of 0.01 db and 0.1 degree.

### THE PHASE AND TRANSMISSION DETECTOR

In the null type of phase measurement an initial *circuit zero* is made. When the circuit is rebalanced with the *apparatus under test* inserted, the phase detector must be able to verify that the same phase relationship has been reestablished as existed when the initial circuit zero balance was made. Bridge circuits yield high sensitivity and a high degree of independence of input voltage amplitudes. In Fig. 6 a four-arm resistance phase bridge is shown, which has two inputs  $E_1$  and  $E_2$ , and two outputs  $E_s$  and  $E_D$  corresponding to the vectorial sum and difference of the input voltages  $E_1$  and  $E_2$ .

As derived in the appendix, for the equal arm bridge, the amplitudes of the voltages  $E_s$  and  $E_D$  are equal for phase angles of  $\varphi = \pi/2 + n\pi$ , where  $n$  is any integer, regardless of the amplitudes of  $E_1$  and  $E_2$ . Thus equality of  $|E_s|$  and  $|E_D|$  is convenient to define the circuit phase zero. Equality of  $|E_s|$  and  $|E_D|$  by itself does not distinguish between  $90^\circ$  and  $270^\circ$  phase shifts. This ambiguity can be resolved with a detection circuit which responds to both the amount and the sign of the difference  $|E_s| - |E_D|$  and by making provision for the introduction of a small increase  $\Delta\varphi$

in phase angle  $\varphi$  of a known direction. From equation (11) in the appendix for equal amplitudes  $E_1$  and  $E_2$

$$(2) \quad |E_s| - |E_D| = |E_1| [\cos(\varphi/2) - \sin(\varphi/2)]$$

Substituting (a)  $\varphi = \pi/2 + \Delta\varphi$  and (b)  $\varphi = 3\pi/2 + \Delta\varphi$  into equation (2) it is evident that the sign of  $|E_s| - |E_D|$  in substitution (b) is the reverse of substitution (a).

$|E_s|$  and  $|E_D|$  are equal every  $180^\circ$  only if all arms of the phase bridge are exactly equal. If the arms are unequal, balance exists for all angles  $\varphi = \pi/2 + 2n\pi + \Delta\theta_1$  and  $\varphi = \pi/2 + (2n - 1)\pi + \Delta\theta_2$  where  $\Delta\theta$  may be called departure angle.

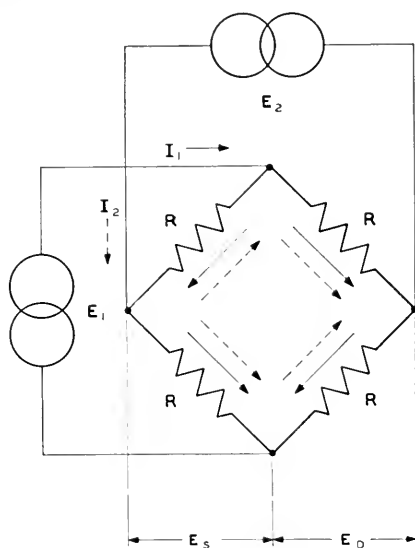


Fig. 6—The phase bridge.

The phase detector can also be used as a deflection bridge. If the phase indicating meter is calibrated according to equation (2), phase angle departures from  $\pi/2 + n\pi$  may be read directly on the indicator when  $|E_1| = |E_2|$  and the scale factor is adjusted for the amplitude of  $E_2$  which is maintained constant by the overall automatic volume control circuit. Equation (2) is almost a linear function and is plotted in Fig. 7.

In using the deflection on the indicator to measure phase shift, an error  $\Delta\psi$  is incurred if  $|E_1| \neq |E_2|$ . The maximum permissible ratio of  $|E_2|/|E_1|$  for a given error  $\Delta\psi$  is given by

$$(3) \quad |E_2|/|E_1| = \cos \varphi / \cos(\varphi + \Delta\psi) + \sqrt{[\cos \varphi / \cos(\varphi + \Delta\psi)]^2 - 1}$$

Equation (3) is derived in the appendix and plotted for several values  $\Delta\psi$  in Fig. 8.

The phase bridge essentially converts the measurement of phase into the measurement of voltage difference. Vacuum tube diodes are used as dif-

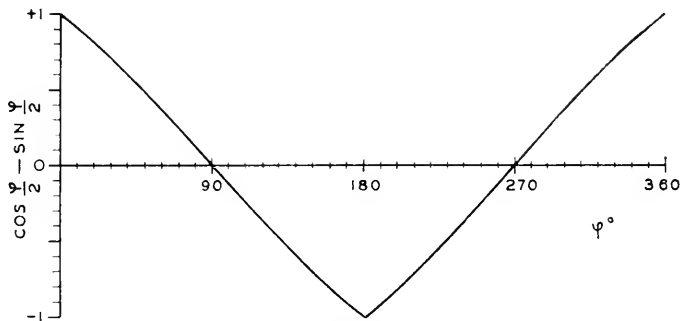


Fig. 7--Deflection response of the phase bridge.

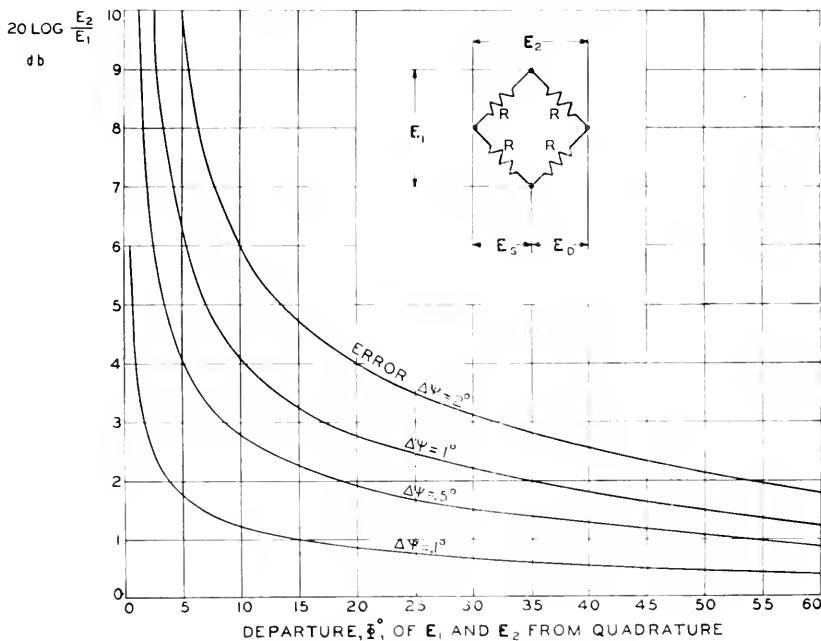


Fig. 8—Phase error  $\Delta\psi$  for unequal inputs.

ferential rectifiers with a high resistance load consisting of hermetically sealed carbon deposited resistors closely matched for value and temperature coefficient and specially mounted to minimize temperature differentials. The differential output of the rectifiers is amplified in a feedback stabilized

d-c. amplifier which has adjustable gain to adjust scale factors on the indicator. The phase detection circuit is energized from the output of the phase bridge and the almost identical transmission detection circuit is energized from the inputs to the phase bridge. Thus both phase and transmission are measured simultaneously.

Each indicator (Fig. 9) has three scales, *fine* ( $-5^\circ$  to  $+5^\circ$ ;  $-1$  db to  $+1$  db), *coarse* ( $-90^\circ$  to  $+90^\circ$ ;  $-10$  db to  $+3$  db), and *null balance*. The *fine* and *coarse* scales are linear while the *null balance* scale has maximum

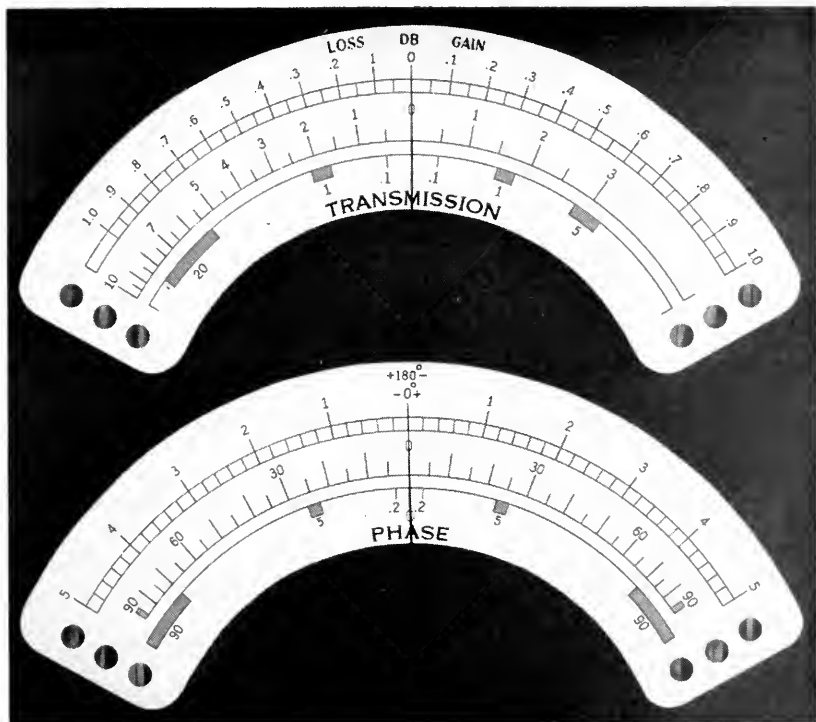


Fig. 9—Phase and transmission indicators.

sensitivity in the neighborhood of the center zero and greatly reduced sensitivity at each end. Varistor shunts across the indicators compress the null scale for large deflections. Colored pilot lights at the ends of the indicator scales, operated by the scale switch, indicate the scale in use directly.

#### THE PHASE SHIFTER

The phase-shifter employs a four-quadrant variable sine condenser. It has two linearly subdivided scales—*coarse*  $0$ – $360^\circ$  on a cylinder and *fine*

0-10° on a dial. The fine dial is connected through reduction gearing to the shaft of the sine condenser. The construction of a phase-shifter which has a sufficiently linear correspondence of electrical phase-shift and mechanical displacement of a shaft is not practical. Instead a movable index for the fine scale permits correction of the deviation from linearity. The index position is controlled by a corrector which is fastened to the condenser shaft. As the corrector is rigidly associated with the sine condenser position and not with the scales this permits shifting the linear scales inde-

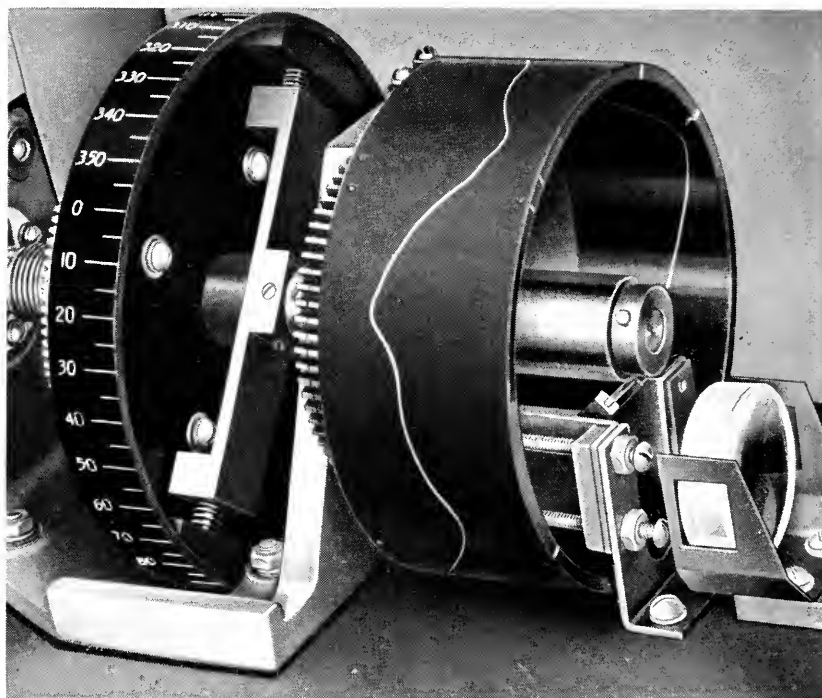


Fig. 10—Optical cam of phase shifter.

pendently without affecting the correction. The correction curve (Fig. 10) is printed on a photographic negative which is placed on a transparent lucite drum and projected optically as an index (Fig. 11) adjacent to the fine dial of the phase-shifter. The calibration curve is obtained by marking the correction at each calibrating point on a piece of cellulose acetate placed on the lucite drum. The correction point is projected on the screen adjacent to the fine scale during the calibration and problems arising from divergence or misalignment of the light beam are thus avoided. Since the index is projected upon a surface coplanar with the dial, no parallax exists.

The phase-shifter's deviation from linearity is sufficiently small that no correction is needed on the coarse scale.

Both dials can be moved with respect to their shafts by releasing friction clutches. Thus the measuring system phase zero can be established by an initial balance of the phase-shifter and restoration of the coarse and fine scales to zero. This is only possible because the scales are linear. Thus no zero readings have to be subtracted from the measurement readings and the need for a separate zero setting phase-shifter is avoided.

The phase-shifter is calibrated by a method of substitution. As discussed previously the phase-indicator indicates balance uniquely in mul-

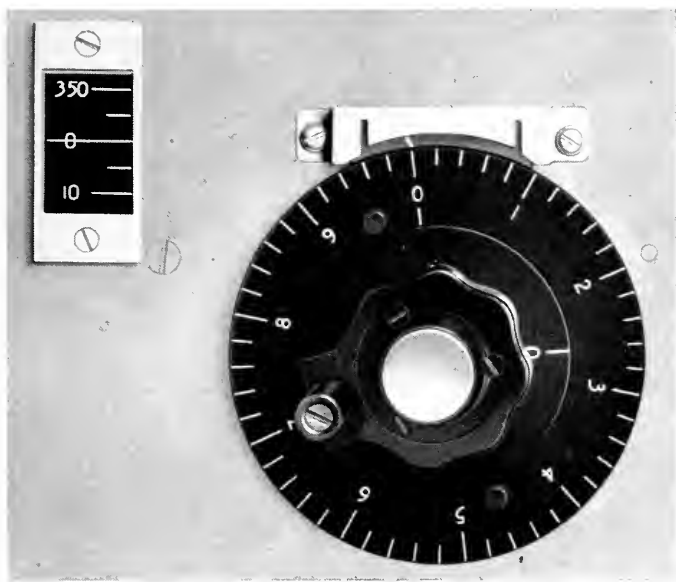


Fig. 11—Phase shifter scales and projected index.

tiples of  $360^\circ$  phase-shift. Exact sub-multiples of  $360^\circ$  can be generated and used to calibrate the phase-shifter.

For example (Fig. 12), to establish an exact  $180^\circ$  phase-shift the standard phase-shifter is set to an arbitrary starting point. With the switches in the position shown a null is obtained on the indicator by adjusting the auxiliary phase-shifter. The network of nominally  $180^\circ$  phase-shift is inserted and a null obtained on the indicator by adjusting the standard phase-shifter. Now the network is removed and the null reestablished by adjustment of the auxiliary phase-shifter. The  $180^\circ$  network again is inserted and a null obtained by adjustment of the standard phase-shifter, which now has been moved through twice the actual phase-shift of the

nominal  $180^\circ$  network. The amount the standard phase-shifter failed to return to the original starting point indicates the residual error of the  $180^\circ$  network. The  $180^\circ$  network is adjusted accordingly and the procedure repeated until an error is no longer discernible. Thus the  $180^\circ$  point on the phase-shifter scale can be determined. In similar fashion, by combination of the  $180^\circ$ ,  $90^\circ$  and  $60^\circ$  networks, calibration points in multiples of  $30^\circ$  are obtained. The equivalent of a  $10^\circ$  network is obtained by use of the  $\pm 5^\circ$  scale on the indicator and scale factor adjustment. Interpolation to  $1^\circ$  is then made using the scale divisions on the indicator. Calibration to an absolute accuracy of  $\pm 0.1^\circ$  was found adequate for use in the measuring system. Much higher accuracy could be obtained if the need arose. There appears to be no inherent frequency limitation in this calibration method.

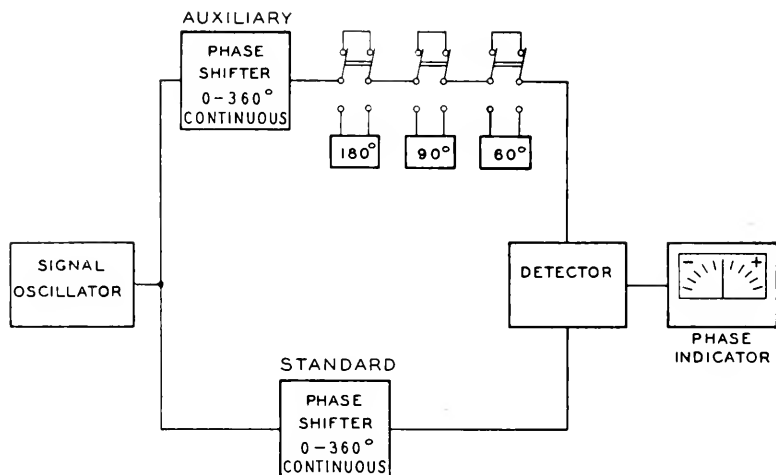


Fig. 12—Phase shifter calibration circuit.

### CONCLUSION

The design effort has been directed toward achieving laboratory precision in measurement and at the same time maintaining the speed necessary for production testing of transmission networks.

The measurement of phase-shift is unambiguous with respect to quadrants and the measurements of insertion phase-shift and loss or gain are independent of each other. The entire frequency range is covered without band switching by use of a heterodyne signal oscillator and the system zero is independent of measurement frequency. Detector tuning is eliminated through the use of frequency conversion, employing a beating oscillator automatically controlled in frequency by the signal oscillator. Phase-shift and transmission may be read directly, without auxiliary computations,



from the dials of the phase-shifter and attenuator or from the scales of the indicators.

#### ACKNOWLEDGMENT

Acknowledgment is due members of the groups supervised by Mr. E. P. Felch (electrical) and Mr. W. J. Means (mechanical) for contributions to the design.

#### APPENDIX

##### THE PHASE DISCRIMINATOR BRIDGE

The general phase relationship of the discriminator is shown in Fig. 13a.

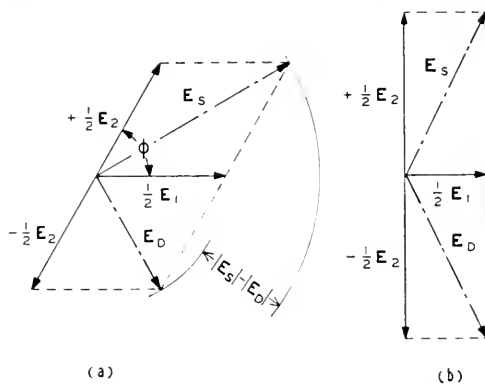


Fig. 13—Phase bridge vector relationships.

Using complex vectorial notation,

$$(4) \quad E_s = (1/2)(E_1 e^{j\varphi_1} + E_2 e^{j\varphi_2})$$

$$(5) \quad E_D = (1/2)(E_1 e^{j\varphi_1} - E_2 e^{j\varphi_2})$$

Hence for  $\varphi = \pi/2 + n\pi$  where  $\varphi = \varphi_1 - \varphi_2$  and  $n$  is an integer,

$$(6) \quad |E_s| = |E_D|$$

Stated in words: The amplitudes of  $E_s$  and  $E_D$  are equal if the relative phase angle  $\varphi$  is equal to  $90^\circ$ ,  $270^\circ$ ,  $450^\circ$ , etc., independently of the amplitudes of  $E_1$  and  $E_2$  (Fig. 13b).

Inequality of  $|E_s|$  and  $|E_D|$  can be utilized to measure phase departure from  $\varphi = \pi/2 + n\pi$

From (4) and (5),

$$(7) \quad |E_s|^2 = (1/4) \sqrt{|E_1|^2 + 2|E_1 E_2| \cos \varphi + |E_2|^2}$$

$$(8) \quad |E_D|^2 = (1/4) \sqrt{|E_1|^2 - 2|E_1 E_2| \cos \varphi + |E_2|^2}$$

If the amplitudes  $|E_1|$  and  $|E_2|$  are equal, then

$$(9) \quad |E_s| = (|E_1|/2) \sqrt{2(1 + \cos \varphi)} = |E_1| \cos (\varphi/2)$$

$$(10) \quad |E_b| = (|E_1|/2) \sqrt{2(1 - \cos \varphi)} = |E_1| \sin (\varphi/2)$$

$$(11) \quad |E_s| - |E_b| = |E_1| [\cos (\varphi/2) - \sin (\varphi/2)]$$

$$(12) \quad |E_s| / |E_b| = \cotan (\varphi/2)$$

When  $|E_1| \neq |E_2|$  determination of  $\varphi$  by (11) or (12) is in error by  $\Delta\psi$ . From (7) and (8)

$$(13) \quad \cotan \frac{\varphi + \Delta\psi}{2} = \sqrt{\frac{|E_1|^2 + 2|E_1E_2| \cos \varphi + |E_2|^2}{|E_1|^2 - 2|E_1E_2| \cos \varphi + |E_2|^2}}$$

Hence

$$(14) \quad \left| \frac{E_2}{E_1} \right|^2 + 2 \frac{1 + \cotan^2 [(\varphi + \Delta\psi)/2]}{1 - \cotan^2 [(\varphi + \Delta\psi)/2]} \left| \frac{E_2}{E_1} \right| \cos \varphi + 1 = 0$$

From trigonometry

$$(15) \quad \frac{1 + \cotan^2 [(\varphi + \Delta\psi)/2]}{1 - \cotan^2 [(\varphi + \Delta\psi)/2]} = - \frac{1}{\cos (\varphi + \Delta\psi)}$$

$$(16) \quad |E_2| / |E_1| = \cos \varphi' \cos (\varphi + \Delta\psi) + \sqrt{[\cos \varphi / \cos (\varphi + \Delta\psi)]^2 - 1}$$

#### REFERENCES

1. "Electronic Instruments" (book), *M.I.T. Radiation Laboratory Series*, Volume 21. McGraw Hill Book Company, First Edition, Page 342.
2. "Automatic Frequency Control Systems," A. F. Pomeroy, *United States Patent* 2,288,025.
3. "The Carrier Stabilization of Frequency Modulated Transmitters," *Brown Boveri Review*, Vol. 33, August 1946, Page 193.
4. "Frequency Modulated Broadcast Transmitters for 88-108 Megacycles," Leonard Everett, *Electrical Communication*, Vol. 24, March 1947, Pages 84-86.
5. "Transconductance as a Criterion of Electron Tube Performance," T. Slonczewski: *Bell Sys. Tech. Jour.*, Vol. XVIII, April 1949, Pages 315-328.

# Physical Principles Involved in Transistor Action\*

By J. BARDEEN and W. H. BRATTAIN

The transistor in the form described herein consists of two-point contact electrodes, called emitter and collector, placed in close proximity on the upper face of a small block of germanium. The base electrode, the third element of the triode, is a large area low resistance contact on the lower face. Each point contact has characteristics similar to those of the high-back-voltage rectifier. When suitable d-c. bias potentials are applied, the device may be used to amplify a-c. signals. A signal introduced between the emitter and base appears in amplified form between collector and base. The emitter is biased in the positive direction, which is that of easy flow. A larger negative or reverse voltage is applied to the collector. Transistor action depends on the fact that electrons in semi-conductors can carry current in two different ways: by excess or conduction electrons and by defect "electrons" or holes. The germanium used is n-type, i.e. the carriers are conduction electrons. Current from the emitter is composed in large part of holes, i.e. of carriers of opposite sign to those normally in excess in the body of the block. The holes are attracted by the field of the collector current, so that a large part of the emitter current, introduced at low impedance, flows into the collector circuit and through a high-impedance load. There is a voltage gain and a power gain of an input signal. There may be current amplification as well.

The influence of the emitter current,  $I_e$ , on collector current,  $I_c$ , is expressed in terms of a current multiplication factor,  $\alpha$ , which gives the rate of change of  $I_c$  with respect to  $I_e$  at constant collector voltage. Values of  $\alpha$  in typical units range from about 1 to 3. It is shown in a general way how  $\alpha$  depends on bias voltages, frequency, temperature, and electrode spacing. There is an influence of collector current on emitter current in the nature of a positive feedback which, under some operating conditions, may lead to instability.

The way the concentrations and mobilities of electrons and holes in germanium depend on impurities and on temperature is described briefly. The theory of germanium point contact rectifiers is discussed in terms of the Mott-Schottky theory. The barrier layer is such as to raise the levels of the filled band to a position close to the Fermi level at the surface, giving an inversion layer of p-type or defect conductivity. There is considerable evidence that the barrier layer is intrinsic and occurs at the free surface, independent of a metal contact. Potential probe tests on some surfaces indicate considerable surface conductivity which is attributed to the p-type layer. All surfaces tested show an excess conductivity in the vicinity of the point contact which increases with forward current and is attributed to a flow of holes into the body of the germanium, the space charge of the holes being compensated by electrons. It is shown why such a flow is to be expected for the type of barrier layer which exists in germanium, and that this flow accounts for the large currents observed in the forward direction. In the transistor, holes may flow from the emitter to the collector either in the surface layer or through the body of the germanium. Estimates are made of the field produced by the collector current, of the transit time for holes, of the space charge produced by holes flowing into the collector, and of the feedback resistance which gives the influence of collector current on emitter current. These calculations confirm the general picture given of transistor action.

## I—INTRODUCTION

THE transistor, a semi-conductor triode which in its present form uses a small block of germanium as the basic element, has been described briefly

\* This paper appears also in the *Physical Review*, April 15, 1949.

in the Letters to the Editor columns of the *Physical Review*.<sup>1</sup> Accompanying this letter were two further communications on related subjects.<sup>2, 3</sup> Since these initial publications a number of talks describing the characteristics of the device and the theory of its operation have been given by the authors and by other members of the Bell Telephone Laboratories staff.<sup>4</sup> Several articles have appeared in the technical literature.<sup>5</sup> We plan to give here an outline of the history of the development, to give some further data on the characteristics and to discuss the physical principles involved. Included is a review of the nature of electrical conduction in germanium and of the theory of the germanium point-contact rectifier.

A schematic diagram of one form of transistor is shown in Fig. 1. Two point contacts, similar to those used in point-contact rectifiers, are placed in close proximity ( $\sim .005\text{--}.025$  cm) on the upper surface of a small block of germanium. One of these, biased in the forward direction, is called the emitter. The second, biased in the reverse direction, is called the collector. A large area low resistance contact on the lower surface, called the base electrode, is the third element of the triode. A physical embodiment of the device, as designed in large part by W. G. Pfann, is shown in Fig. 2. The transistor can be used for many functions now performed by vacuum tubes.

During the war, a large amount of research on the properties of germanium and silicon was carried out by a number of university, government, and industrial laboratories in connection with the development of point contact rectifiers for radar. This work is summarized in the book of Torrey and Whitmer.<sup>6</sup> The properties of germanium as a semi-conductor and as a rectifier have been investigated by a group working under the direction of K. Lark-Horovitz at Purdue University. Work at the Bell Telephone Laboratories<sup>7</sup> was initiated by R. S. Ohl before the war in connection with the development of silicon rectifiers for use as detectors at microwave frequencies. Research and development on both germanium and silicon rectifiers during and since the war has been done in large part by a group under J. H. Scaff. The background of information obtained in these various investigations has been invaluable.

The general research program leading to the transistor was initiated and directed by W. Shockley. Work on germanium and silicon was emphasized because they are simpler to understand than most other semi-conductors. One of the investigations undertaken was the study of the modulation of conductance of a thin film of semi-conductor by an electric field applied by an electrode insulated from the film.<sup>3</sup> If, for example, the film is made one plate of a parallel plate condenser, a charge is induced on the surface. If the individual charges which make up the induced charge are mobile, the conductance of the film will depend on the voltage applied to the condenser.

The first experiments performed to measure this effect indicated that most of the induced charge was not mobile. This result, taken along with other unexplained phenomena such as the small contact potential difference between n- and p- type silicon<sup>8</sup> and the independence of the rectifying properties of the point contact rectifier on the work function of the metal point, led one of the authors to an explanation in terms of surface states.<sup>9</sup> This work led to the concept that space charge barrier layers may be present at the free surfaces of semi-conductors such as germanium and silicon, independent of a metal contact. Two experiments immediately suggested were to measure the dependence of contact potential on impurity concentration<sup>10</sup> and to measure the change of contact potential on illuminating the surface with light.<sup>11</sup> Both of these experiments were successful and confirmed the theory. It was while studying the latter effect with a silicon surface immersed in a liquid that it was found that the density of surface charges and the field in the space charge region could be varied by applying a potential across an electrolyte in contact with the silicon surface.<sup>12</sup> While studying the effect of field applied by an electrolyte on the current voltage characteristic of a high-back-voltage germanium rectifier, the authors were led to the concept that a portion of the current was being carried by holes flowing near the surface. Upon replacing the electrolyte with a metal contact transistor action was discovered.

The germanium used in the transistor is an n-type or excess semi-conductor with a resistivity of the order of 10-ohm cm, and is the same as the material used in high-back-voltage germanium rectifiers.<sup>13</sup> All of the material we have used was prepared by J. C. Scaff and H. C. Theuerer of the metallurgical group of the Laboratories.

While different metals may be used for the contact points, most work has been done with phosphor bronze points. The spring contacts are made with wire from .002 to .005" in diameter. The ends are cut in the form of a wedge so that the two contacts can be placed close together. The actual contact area is probably no more than about  $10^{-6}$  cm<sup>2</sup>.

The treatment of the germanium surface is similar to that used in making high-back-voltage rectifiers.<sup>14</sup> The surface is ground flat and then etched. In some cases special additional treatments such as anodizing the surface or oxidation at 500°C have been used. The oxide films formed in these processes wash off easily and contact is made to the germanium surface.

The circuit of Fig. 1 shows how the transistor may be used to amplify a small a-c. signal. The emitter is biased in the forward (positive) direction so that a small d-c. current, of the order of 1 ma, flows into the germanium block. The collector is biased in the reverse (negative) direction with a higher voltage so that a d-c. current of a few milliamperes flows out through the collector point and through the load circuit. It is found

that the current in the collector circuit is sensitive to and may be controlled by changes of current from the emitter. In fact, when the emitter current is varied by changing the emitter voltage, keeping the collector voltage constant, the change in collector current may be larger than the change in emitter current. As the emitter is biased in the direction of easy flow, a small a-c. voltage, and thus a small power input, is sufficient to vary the emitter current. The collector is biased in the direction of high resistance and may be matched to a high resistance load. The a-c. voltage and power in the load circuit are much larger than those in the input. An overall power gain of a factor of 100 (or 20 db) can be obtained in favorable cases.

Terminal characteristics of an experimental transistor<sup>15</sup> are illustrated in Fig. 3, which shows how the current-voltage characteristic of the collector is changed by the current flowing from the emitter. Transistor characteristics, and the way they change with separation between the points, with temperature, and with frequency, are discussed in Section II.

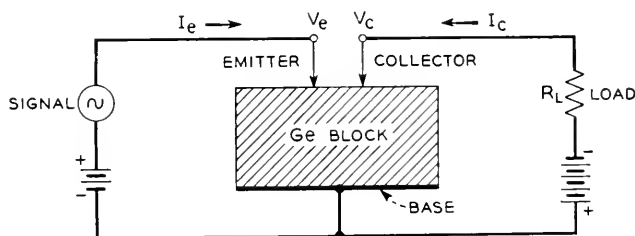


Fig. 1—Schematic of transistor showing circuit for amplification of an a-c. signal and the conventional directions for current flow. Normally  $I_e$  and  $V_e$  are positive,  $I_c$  and  $V_c$  negative.

The explanation of the action of the transistor depends on the nature of the current flowing from the emitter. It is well known that in semi-conductors there are two ways by which the electrons can carry electricity which differ in the signs of the effective mobile charges.<sup>16</sup> The negative carriers are excess electrons which are free to move and are denoted by the term conduction electrons or simply electrons. They have energies in the conduction band of the crystal. The positive carriers are missing or defect "electrons" and are denoted by the term "holes". They represent unoccupied energy states in the uppermost normally filled band of the crystal. The conductivity is called n- or p-type depending on whether the mobile charges normally in excess in the material under equilibrium conditions are electrons (negative carriers) or holes (positive carriers). The germanium used in the transistor is n-type with about  $5 \times 10^{14}$  conduction electrons per c.c.; or about one electron per  $10^8$  atoms. Transistor action depends on the fact that the current from the emitter is composed in

large part of *holes*; that is of carriers of opposite sign to those normally in excess in the body of the semi-conductor.

The collector is biased in the reverse, or negative direction. Current flowing in the germanium toward the collector point provides an electric

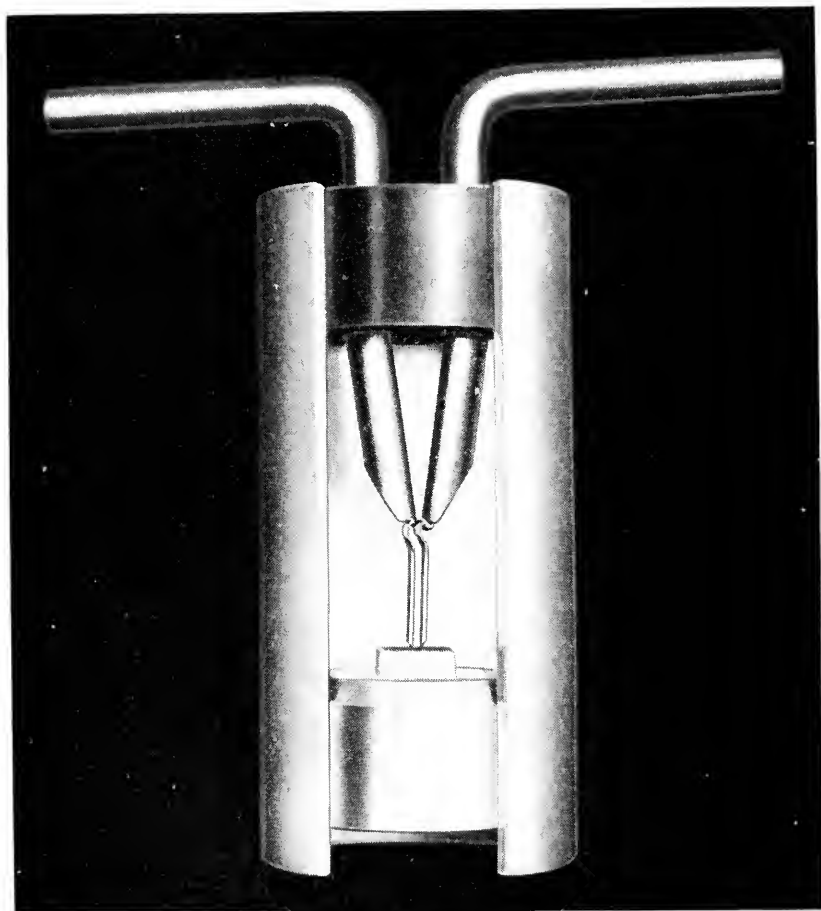


Fig. 2—Microphotograph of a cutaway model of a transistor

field which is in such a direction as to attract the holes flowing from the emitter. When the emitter and collector are placed in close proximity, a large part of the hole current from the emitter will flow to the collector and into the collector circuit. The nature of the collector contact is such as to provide a high resistance barrier to the flow of electrons from the metal to the semi-conductor, but there is little impediment to the flow of holes into

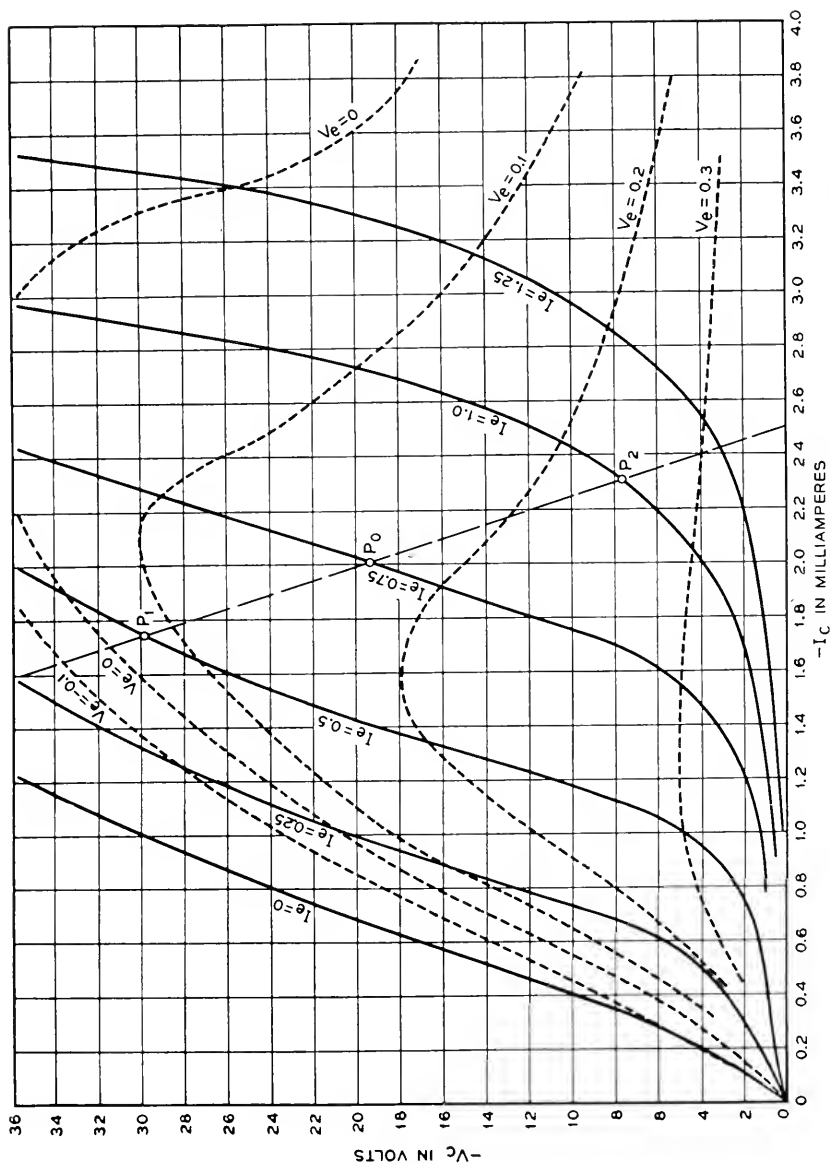


Fig. 3—Characteristics of an experimental transistor.<sup>15</sup> The conventional directions for current and voltage are as in Fig. 1.



the contact. This theory explains how the change in collector current might be as large as but not how it can be larger than the change in emitter current. The fact that the collector current may actually change more than the emitter current is believed to result from an alteration of the space charge in the barrier layer at the collector by the hole current flowing into the junction. The increase in density of space charge and in field strength makes it easier for electrons to flow out from the collector, so that there is an increase in electron current. It is better to think of the hole current from the emitter as modifying the current-voltage characteristic of the collector, rather than as simply adding to the current flowing to the collector.

In Section III we discuss the nature of the conductivity in germanium, and in Section IV the theory of the current-voltage characteristic of a germanium-point contact. In the latter section we attempt to show why the emitter current is composed of carriers of opposite sign to those normally in excess in the body of germanium. Section V is concerned with some aspects of the theory of transistor action. A complete quantitative theory is not yet available.

There is evidence that the rectifying barrier in germanium is internal and occurs at the free surface, independent of the metal contact.<sup>9, 17</sup> The barrier contains what Schottky and Spenke<sup>18</sup> call an inversion region; that is a change of conductivity type. The outermost part of the barrier next to the surface is p-type. The p-type region is very thin, of the order of  $10^{-5}$  cm in thickness. An important question is whether there is a sufficient density of holes in this region to provide appreciable lateral conductivity along the surface. Some evidence bearing on this point is described below.

Transistor action was first discovered on a germanium surface which was subjected to an anodic oxidation treatment in a glycol borate solution after it had been ground and etched in the usual way for diodes. Much of the early work was done on surfaces which were oxidized by heating in air. In both cases the oxide is washed off and plays no direct role. Some of these surfaces were tested for surface conductivity by potential probe tests. Surface conductivities, on a unit area basis, of the order of .0005 to .002 mhos were found.<sup>2</sup> The value of .0005 represents about the lower limit of detection possible by the method used. It is inferred that the observed surface conductivity is that of the p-type layer, although there has been no direct proof of this. In later work it was found that the oxidation treatment is not essential for transistor action. Good transistors can be made with surfaces prepared in the usual way for high-back-voltage rectifiers provided that the collector point is electrically formed. Such surfaces exhibit no measurable surface conductivity.

One question that may be asked is whether the holes flow from the emitter to the collector mainly in the surface layer or whether they flow

through the body of the germanium. The early experiments suggested flow along the surface. W. Shockley proposed a modified arrangement in which in effect the emitter and collector are on opposite sides of a thin slab, so that the holes flow directly across through the semi-conductor. Independently, J. N. Shive made, by grinding and etching, a piece of germanium in the form of a thin flat wedge.<sup>19</sup> Point contacts were placed directly opposite each other on the two opposite faces where the thickness of the wedge was about .01 cm. A third large area contact was made to the base of the wedge. When the two points were connected as emitter and collector, and the collector was electrically formed, transistor action was obtained which was comparable to that found with the original arrangement. There is no doubt that in this case the holes are flowing directly through the n-type germanium from the emitter to the collector. With two points close together on a plane surface holes may flow either through the surface layer or through the body of the semi-conductor.

Still later, at the suggestion of W. Shockley, J. R. Haynes<sup>20</sup> further established that holes flow into the body of the germanium. A block of germanium was made in the form of a thin slab and large area electrodes were placed at the two ends. Emitter and collector electrodes were placed at variable separations on one face of the slab. The field acting between these electrodes could be varied by passing currents along the length of the slab. The collector was biased in the reverse direction so that a small d-c. current was drawn into the collector. A signal introduced at the emitter in the form of a pulse was detected at a slightly later time in the collector circuit. From the way the time interval, of the order of a few microseconds, depends on the field, the mobility and sign of the carriers were determined. It was found that the carriers are positively charged, and that the mobility is the same as that of holes in bulk germanium (1700 cm<sup>2</sup>/volt sec).

These experiments clarify the nature of the excess conductivity observed in the forward direction in high-back-voltage germanium rectifiers which has been investigated by R. Bray, K. Lark-Horovitz, and R. N. Smith<sup>21</sup> and by Bray.<sup>22</sup> These authors attributed the excess conductivity to the strong electric field which exists in the vicinity of the point contact. Bray has made direct experimental tests to observe the relation between conductivity and field strength. We believe that the excess conductivity arises from holes injected into the germanium at the contact. Holes are introduced because of the nature of the barrier layer rather than as a direct result of the electric field. This has been demonstrated by an experiment of E. J. Ryder and W. Shockley.<sup>23</sup> A thin slab of germanium was cut in the form of a pie-shaped wedge and electrodes placed at the narrow and wide boundaries of the wedge. When a current is passed between the electrodes,

the field strength is large at the narrow end of the wedge and small near the opposite electrode. An excess conductivity was observed when the narrow end was made positive; none when the wide end was positive. The magnitude of the current flow was the same in both cases. Holes injected at the narrow end lower the resistivity in the region which contributes most to the over-all resistance. When the current is in the opposite direction, any holes injected enter in a region of low field and do not have sufficient life-time to be drawn down to the narrow end and so do not alter the resistance very much. With some surface treatments, the excess conductivity resulting from hole injection may be enhanced by a surface conductivity as discussed above.

The experimental procedure used during the present investigation is of interest. Current voltage characteristics of a given point contact were displayed on a d-c. oscilloscope.<sup>24</sup> The change or modulation of this characteristic produced by a signal impressed on a neighboring electrode or point contact could be easily observed. Since the input impedance of the scope was 10 megohms and the gain of the amplifiers such that the lower limit of sensitivity was of the order of a millivolt, the oscilloscope was also used as a very high impedance voltmeter for probe measurements. Means were included for matching the potential to be measured with an adjustable d-c. potential the value of which could be read on a meter. A micromanipulator designed by W. L. Bond was used to adjust the positions of the contact points.

## II—SOME TRANSISTOR CHARACTERISTICS

The static characteristics of the transistor are completely specified by four variables which may be taken as the emitter and collector currents,  $I_e$  and  $I_c$ , and the corresponding voltages,  $V_e$  and  $V_c$ . As shown in the schematic diagram of Fig. 1, the conventional directions for current flow are taken as positive into the germanium and the terminal voltages are relative to the base electrode. Thus  $I_e$  and  $V_e$  are normally positive,  $I_c$  and  $V_c$  negative.

There is a functional relation between the four variables such that if two are specified the other two are determined. Any pair may be taken as the independent variables. As the transistor is essentially a current operated device, it is more in accord with the physics involved to choose the currents rather than the voltages. All fields in the semi-conductor outside of the space charge regions immediately surrounding the point contacts are determined by the currents, and it is the current flowing from the emitter which controls the current voltage characteristic of the collector. The voltages are single-valued functions of the currents but, because of inherent feedback, the currents may be double-valued functions of the voltages.

In reference 1, the characteristics of an experimental transistor were shown by giving the constant voltage contours on a plot in which the independent variables  $I_c$  and  $I_e$  are plotted along the coordinate axes.

In the following we give further characteristics, and show in a general way how they depend on the spacing between the points, on the temperature, and on the frequency. The data were taken mainly on experimental setups on a laboratory bench, and are not to be taken as necessarily typical of the characteristics of finished units. They do indicate in a general way the type of results which can be obtained. Characteristics of units made in pilot production have been given elsewhere.<sup>5</sup>

The data plotted in reference 1 were taken on a transistor made with phosphor bronze points on a surface which was oxidized and on which potential probe tests gave evidence for considerable surface conductivity. The collector resistance is small in units prepared in this way. In Fig. 3 are shown the characteristics of a unit<sup>15</sup> in which the surface was prepared in a different manner. The surface was ground and etched in the usual way<sup>14</sup>, but was not subjected to the oxidation treatment. Phosphor bronze contact points made from 5 mil wire were used. The collector was electrically formed by passing large currents in the reverse direction. This reduced the resistance of the collector in the reverse direction, improving the transistor action. However, it remained considerably higher than that of the collector on the oxidized surface.

While there are many ways of plotting the data, we have chosen to give the collector voltage,  $V_c$ , as a function of the collector current,  $I_c$ , with the emitter current,  $I_e$ , taken as a parameter. This plot shows in a direct manner the influence of the emitter current on the current-voltage characteristic of the collector. The curve corresponding to  $I_e = 0$  is just the normal reverse characteristic of the collector as a rectifier. The other curves show how the characteristic shifts to the right, corresponding to larger collector currents, with increase in emitter current. It may be noted that the change in collector current for fixed collector voltage is larger than the change in emitter current. The current amplification factor,  $\alpha$ , defined by

$$\alpha = -(\partial I_c / \partial I_e)_{V_c = \text{const.}} \quad (2.1)$$

is between 2 and 3 throughout most of the plot.

The dotted lines on Fig. 3 correspond to constant values of the emitter voltage,  $V_e$ . By interpolating between the contours, all four variables corresponding to a given operating point may be obtained. The  $V_e$  contours reach a maximum for  $I_e$  about 0.7 ma. and have a negative slope beyond. To the left of the maximum,  $V_e$  increases with  $I_c$  as one follows along a line corresponding to  $V_c = \text{const.}$  To the right,  $V_e$  decreases as

$I_e$  increases, corresponding to a negative input admittance. For given values of  $V_e$  and  $V_c$ , there are two possible operating points. Thus for  $V_e = 0.1$  and  $V_c = -20$  one may have  $I_e = 0.3$  ma,  $I_c = -1.1$  ma or  $I_e = 1.0$ ,  $I_c = -2.7$ .

The negative resistance and instability result from the effect of the collector current on the emitter current.<sup>1</sup> The collector current lowers the potential of the surface in the vicinity of the emitter and increases the effective bias on the emitter by an equivalent amount. This potential drop is  $R_F I_c$ , where  $R_F$  is a feedback resistance which may depend on the currents flowing. The effective bias on the emitter is then  $V_e - R_F I_c$ , and we may write

$$I_e = f(V_e - R_F I_c), \quad (2.2)$$

where the function gives the forward characteristic of the emitter point. In some cases  $R_F$  is approximately constant over the operating range; in other cases  $R_F$  decreases with increasing  $I_c$  as the conductivity of the germanium in the vicinity of the points increases with forward current. Increase of  $I_e$  by a change of  $V_e$  increases the magnitude of  $I_c$ , which by the feedback still further increases  $I_e$ . Instability may result. Some consequences will be discussed further in connection with the a-c. characteristics.

Also shown on Fig. 3 is a load line corresponding to a battery voltage of  $-100$  in the output circuit and a load,  $R_L$ , of 40,000 ohms, the equation of the line being

$$V_c = -100 - 40 \times 10^3 I_c. \quad (2.3)$$

The load is an approximate match to the collector resistance, as given by the slope of the solid lines. If operated between the points  $P_1$  and  $P_2$ , the output voltage is 8.0 volts r.m.s. and the output current is 0.20 ma. The corresponding values at the input are 0.07 and 0.18, so that the overall power gain is

$$\text{Gain} \sim 8 \times 0.20 / (0.07 \times 0.18) \sim 125, \quad (2.4)$$

which is about 21 db. This is the available gain for a generator with an impedance of 400 ohms, which is an approximate match for the input impedance.

We turn next to the equations for the a-c. characteristics. For small deviations from an operating point, we may write

$$\Delta V_c = R_{11} \Delta I_e + R_{12} \Delta I_c, \quad (2.5)$$

$$\Delta V_e = R_{12} \Delta I_e + R_{22} \Delta I_c, \quad (2.6)$$

in which we have taken the currents as the independent variables and the directions of currents and voltages as in Fig. 1. The differentials represent

small changes from the operating point, and may be small a-c. signals. The coefficients are defined by:

$$R_{11} = (\partial V_e / \partial I_e)_{I_c = \text{const.}}, \quad (2.7)$$

$$R_{12} = (\partial V_e / \partial I_c)_{I_e = \text{const.}}, \quad (2.8)$$

$$R_{21} = (\partial V_c / \partial I_e)_{I_c = \text{const.}}, \quad (2.9)$$

$$R_{22} = (\partial V_c / \partial I_c)_{I_e = \text{const.}}, \quad (2.10)$$

These coefficients are all positive and have the dimensions of resistances. They are functions of the d-c. bias currents,  $I_e$  and  $I_c$ , which define the operating point. For  $I_e = 0.75$  ma and  $I_c = -2$  ma the coefficients of the unit of Fig. 3 have the following approximate values:

$$\begin{aligned} R_{11} &= 800 \text{ ohms,} \\ R_{12} &= 300, \\ R_{21} &= 100,000, \\ R_{22} &= 40,000. \end{aligned} \quad (2.11)$$

Equation (2.5) gives the emitter characteristic. The coefficient  $R_{11}$  is the input resistance for a fixed collector current (open circuit for a-c.). To a close approximation,  $R_{11}$  is independent of  $I_c$ , and is just the forward resistance of the emitter point when a current  $I_e$  is flowing. The coefficient  $R_{12}$  is the feedback or base resistance, and is equal to  $R_F$  as defined by Eq. (2.2) in case  $R_F$  is a constant. Both  $R_{11}$  and  $R_{12}$  are of the order of a few hundred ohms,  $R_{12}$  usually being smaller than  $R_{11}$ .

Equation (2.6) depends mainly on the collector and on the flow of holes from the emitter to the collector. The ratio  $R_{21}/R_{22}$  is just the current amplification factor  $\alpha$  as defined by Eq. (2.1). Thus we may write:

$$\Delta V_c = R_{22} (\alpha \Delta I_e + \Delta I_c). \quad (2.12)$$

The coefficient  $R_{22}$  is the collector resistance for fixed emitter current (open circuit for a-c.), and is the order of 10,000–50,000 ohms. Except in the range of large  $I_e$  and small  $I_c$ , the value of  $R_{22}$  is relatively independent of  $I_c$ . The factor  $\alpha$  generally is small when  $I_c$  is small compared with  $I_e$ , and increases with  $I_c$ , approaching a constant value the order of 1 to 4 when  $I_c$  is several times  $I_e$ .

The a-c. power gain with the circuit of Fig. 1 depends on the operating point (the d-c. bias currents) and on the load impedance. The positive feedback represented by  $R_{12}$  increases the available gain, and it is possible to get very large power gains by operating near a point of instability. In giving the gain under such conditions, the impedance of the input generator should be specified. Alternatively, one can give the gain which would exist with no feedback. The maximum available gain neglecting feedback, obtained when the load  $R_L$  is equal to the collector resistance  $R_{22}$ ,

and the impedance of the generator is equal to the emitter resistance,  $R_{11}$ , is:

$$\text{Gain} = \alpha^2 R_{22} / 4R_{11}, \quad (2.13)$$

which is the ratio of the collector to the emitter resistance multiplied by  $1/4$  the square of the current amplification factor. This gives the a-c. power delivered to the load divided by the a-c. power fed into the transistor. Substituting the values listed above (Eqs. (2.11)) for the unit whose characteristics are shown in Fig. 3 gives a gain of about 80 times (or 19 db) for the operating point  $P_0$ . This is to be compared with the gain of 21 db estimated above for operation between  $P_1$  and  $P_2$ . The difference of 2 db represents the increase in gain by feedback, which was omitted in Eq. (2.13).

Equations (2.5) and (2.6) may be solved to express the currents as functions of the voltages, giving

$$\Delta I_e = Y_{11} \Delta V_e + Y_{12} \Delta V_c \quad (2.14)$$

$$\Delta I_c = Y_{21} \Delta V_e + Y_{22} \Delta V_c \quad (2.15)$$

where

$$\begin{aligned} Y_{11} &= R_{22}/D, \quad Y_{12} = -R_{12}/D \\ Y_{12} &= -R_{21}/D, \quad Y_{22} = R_{11}/D \end{aligned} \quad (2.16)$$

and  $D$  is the determinant of the coefficients

$$D = R_{11} R_{22} - R_{12} R_{21}. \quad (2.17)$$

The admittances,  $Y_{11}$  and  $Y_{22}$ , are negative if  $D$  is negative, and the transistor is then unstable if the terminals are short-circuited for a-c. currents. Stability can be attained if there is sufficient impedance in the input and output circuits exterior to the transistor. Feedback and instability are increased by adding resistance in series with the base electrode. Further discussion of this subject would carry us too far into circuit theory and applications. From the standpoint of transistor design, it is desirable to keep the feedback resistance,  $R_{12}$ , as small as possible.

#### VARIAION WITH SPACING

One of the important parameters affecting the operation of the transistor is the spacing between the point electrodes. Measurements to investigate this effect have been made on a number of germanium surfaces. Tests were made with use of a micro-manipulator to adjust the positions of the points. The germanium was generally in the form of a slab from .05 to 0.20 cm thick, the lower surface of which was rhodium plated to form a low resistant contact, and the upper plane surface ground and etched, or other-

wise treated to give a surface suitable for transistor action. The collector point was usually kept fixed, since it is more critical, and the emitter point moved. Measurements were made with formed collector points. Most of the data have been obtained on surfaces oxidized as described below.

As expected, the emitter current has less and less influence on the collector as the separation<sup>26</sup>,  $s$ , is increased. This is shown by a decrease in  $R_{21}$ , or  $\alpha$ , with  $s$ . The effect of the collector current on the emitter, represented by the feedback resistance  $R_{12}$ , also decreases with increase in  $s$ . The other coefficients,  $R_{11}$  and  $R_{22}$ , are but little influenced by spacing. Figures

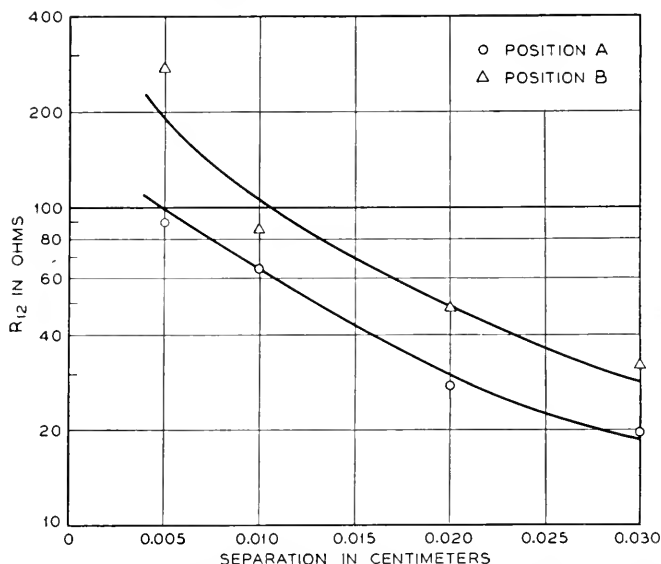


Fig. 4—Dependence of feedback resistance  $R_{12}$  on electrode separation for two different parts A and B, of the same germanium surface. The surface had been oxidized by heating in air.

4, 5 and 6 illustrate the variation of  $R_{12}$  and  $\alpha$  with the separation. Shown are results for two different collector points A and B on different parts of the same germanium surface<sup>25</sup>. In making the measurements, the bias currents were kept fixed as the spacing was varied. For collector A,  $I_e = 1.0$  ma and  $I_c = 3.8$  ma; for collector B,  $I_e = 1.0$  ma and  $I_c = 4.0$  ma. The values of  $R_{11}$  and  $R_{22}$  were about 300 and 10,000, respectively, in both cases.

Figure 5 shows that  $\alpha$  decreases approximately exponentially with  $s$  for separations from .005 cm to .030 cm, the rate of decrease being about the same in all cases. Extrapolating down to  $s = 0$  indicates that a further



increase of only about 25 per cent in  $\alpha$  could be obtained by decreasing the spacing below .005 cm.

Figure 6 shows that the decrease of  $\alpha$  with distance is dependent on the germanium sample used. Curve 1 is similar to the results in Fig. 5. Curve

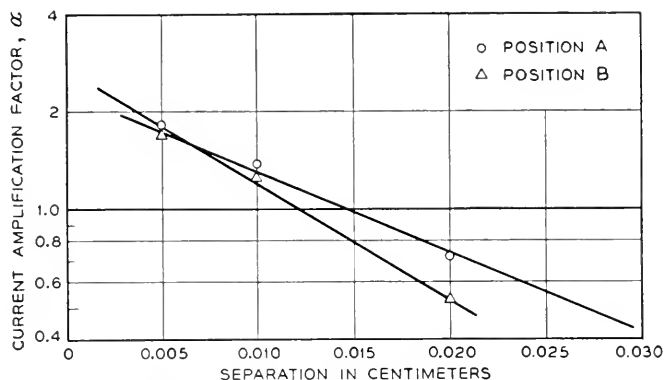


Fig. 5—Dependence of current amplification factor  $\alpha$  on electrode separation. Positions A and B as in Fig. 4.

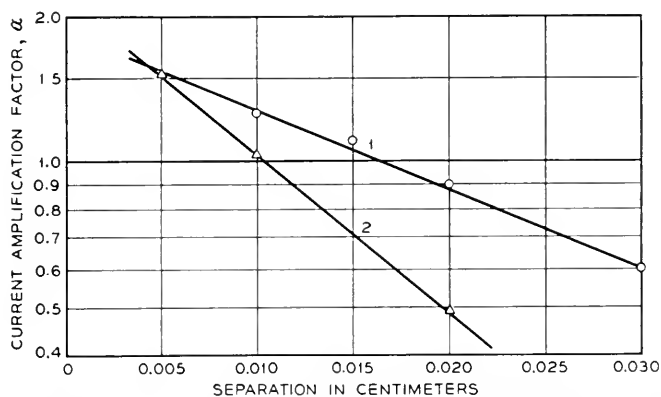


Fig. 6—Dependence of current amplification factor  $\alpha$  on separation for germanium surfaces from two different melts, 1 and 2.

2 is for a germanium slice with the same surface treatment but from a different melt.

Figure 4 shows the corresponding results for  $R_{12}$ . There is an approximate inverse relationship between  $R_{12}$  and  $s$ .

Another way to illustrate the decreased influence of the emitter on the collector with increase in spacing is to plot the collector characteristic for fixed emitter current at different spacings. Figure 7 is such a plot for a

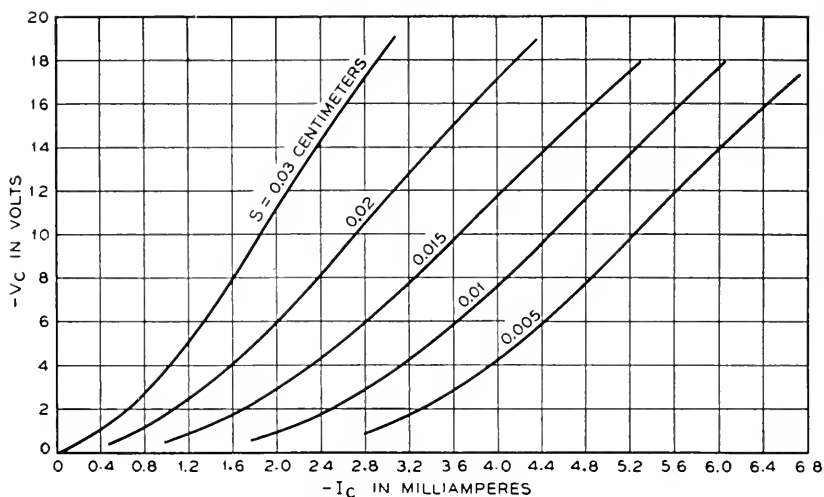


Fig. 7—Collector characteristic  $V_c$  vs  $I_c$  for fixed  $I_s$  but variable distance of separation.

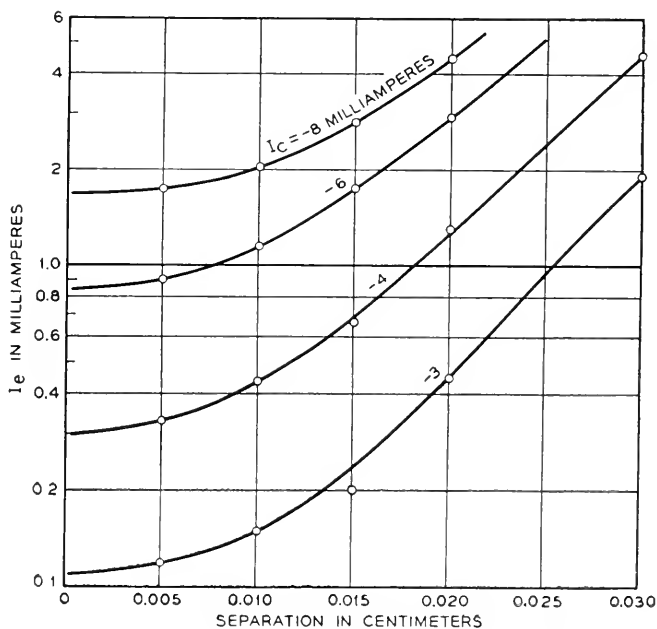


Fig. 8—Emitter current  $I_e$  vs separation for fixed  $I_c$  and  $V_c$ .

different surface which was ground flat, etched, and then oxidized at  $500^\circ\text{C}$  in moist air for one hour. The resultant oxide film was washed off.<sup>27</sup> The emitter current  $I_e$  was kept constant at 1.0 ma.

Data taken on the same surface have been plotted in other ways. As the spacing increases, more emitter current is required to produce the same change in collector current. The fraction of the emitter current which is

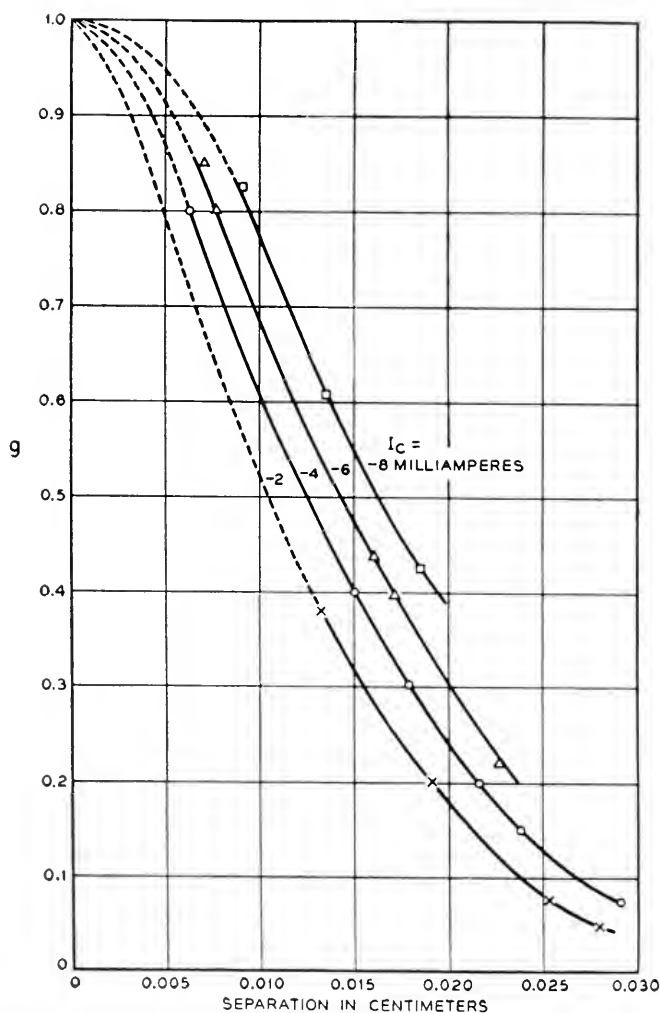


Fig. 9—The factor  $g$  is the ratio of the emitter current extrapolated to  $s = 0$  to that at electrode separation  $s$  required to give the same collector current,  $I_c$  and voltage,  $V_c$ . Plot shows variation of  $g$  with  $s$  for different  $I_c$ . The factor is independent of  $V_c$  over the range plotted.

effective at the collector decreases with spacing. It is of interest to keep  $V_c$  and  $I_c$  fixed by varying  $I_e$  as  $s$  is changed and to plot the values of  $I_e$  so obtained as a function of  $s$ . Such a plot is shown in Fig. 9. The collec-

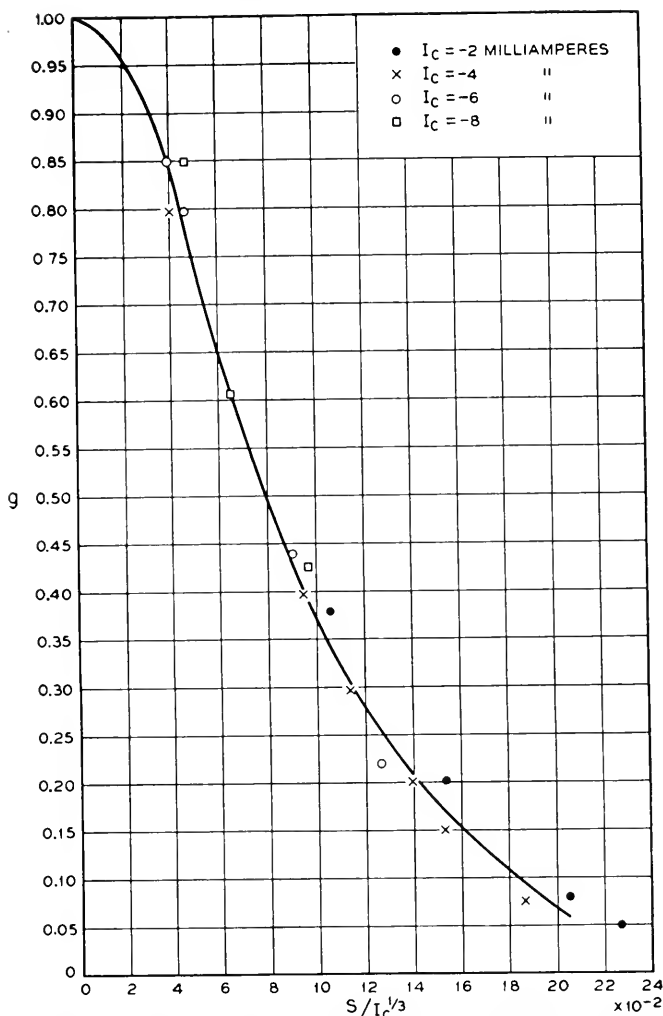


Fig. 10—The factor  $g$  (Fig. 9) plotted as a function of  $s/I_c^{1/3}$ , with  $s$  in cm. and  $I_c$  in amps.

tor voltage,  $V_c$ , is fixed at  $-15$  volts. Curves are shown for  $I_c = -3$ ,  $-4$ ,  $-6$ , and  $-8$  ma. We may define a geometrical factor,  $g$ , as the ratio of  $I_e$  extrapolated to zero spacing to the value of  $I_e$  at the separation  $s$ :

$$g(s) = (I_e(0)/I_e(s))_{V_c, I_c = \text{const.}} \quad (2.18)$$

It is to be expected that  $g(s)$  will depend on  $I_c$ , as it is the collector current which provides the field which draws the holes into the collector. For the

same reason, it is expected that  $g(s)$  will be relatively independent of  $V_c$ . This was indeed found to be true in this particular case and the values  $V_c = -5, -10$ , and  $-15$  were used in Figure 9 which gives a plot of  $g$  versus  $s$  for several values of  $I_c$ . The dotted lines give the extrapolation to  $s = 0$ . As expected,  $g$  increases with  $I_c$  for a fixed  $s$ . The different curves can be brought into approximate agreement by taking  $s/I_c^{1/3}$  as the independent variable, and this is done in Fig. 10. As will be discussed in Section V, such a relation is to be expected if  $g$  depends on the transit time for the holes.

#### VARIATION WITH TEMPERATURE

Only a limited amount of data has been obtained on the variation of transistor characteristics with temperatures. It is known that the reverse

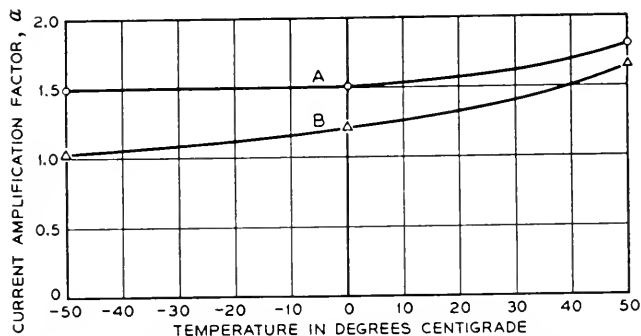


Fig. 11—Current amplification factor  $\alpha$  vs. temperature for two experimental units A and B.

characteristic of the germanium diode varies rapidly with temperature, particularly in the case of units with high reverse resistance. In the transistor the collector is electrically formed in such a way as to have relatively low reverse resistance, and its characteristic is much less dependent on temperature. Both  $R_{22}$  and  $R_{11}$  decrease with increase in  $T$ ,  $R_{22}$  usually decreasing more rapidly than  $R_{11}$ . The feedback resistance,  $R_{12}$ , is relatively independent of temperature. The current multiplication factor,  $\alpha$ , increases with temperature, but the change is not extremely rapid. Figure 11 gives a plot of  $\alpha$  versus  $T$  for two experimental units. The d-c. bias currents are kept fixed as the temperature is varied. The over-all change in  $\alpha$  from  $-50^\circ\text{C}$  to  $+50^\circ\text{C}$  is only about 50 per cent. The increase in  $\alpha$  with  $T$  results in an increase in power gain with temperature. This may be nullified by a decrease in the ratio  $R_{22}/R_{11}$ , so that the over-all gain at fixed bias current may have a negative temperature coefficient.

## VARIATION WITH FREQUENCY

Equations (2.5) and (2.6) may be used to describe the a-c. characteristics at high frequencies if the coefficients are replaced by general impedances. Thus if we use the small letters  $i_e$ ,  $v_e$ ,  $i_c$ ,  $v_c$ , to denote the amplitude and phase of small a-c. signals about a given operating point, we may write

$$v_e = Z_{11} i_e + Z_{12} i_c, \quad (2.19)$$

$$v_c = Z_{21} i_e + Z_{22} i_c. \quad (2.20)$$

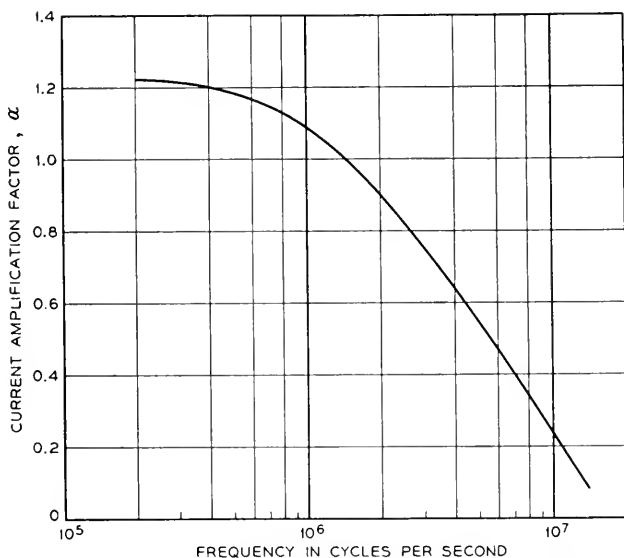


Fig. 12—Current amplification factor  $\alpha$  vs. frequency

Measurements of A. J. Rack and others,<sup>28</sup> have shown that the over-all power gain drops off between 1 and 10 mc/sec and few units have positive gain above 10 mc/sec. The measurements showed further that the frequency variation is confined almost entirely to  $Z_{21}$  or  $\alpha$ . The other coefficients,  $Z_{11}$ ,  $Z_{12}$  and  $Z_{22}$ , are real and independent of frequency, at least up to 10 mc/sec. Figure 12 gives a plot of  $\alpha$  versus frequency for an experimental unit. Associated with the drop in amplitude is a phase shift which varies approximately linearly with the frequency. A phase shift in  $Z_{21}$  of  $90^\circ$  occurs at a frequency of about 4 mc/sec, corresponding to a delay of about  $5 \times 10^{-8}$  seconds. Estimates of transit time for the holes to flow from the emitter to the collector, to be made in Section V, are of the same order. These results suggest that the frequency limitation is associated with transit time rather than electrode capacities. Because of the difference

in transit times for holes following different paths there is a drop in amplitude rather than simply a phase shift.

### III—ELECTRICAL CONDUCTIVITY OF GERMANIUM

Germanium, like carbon and silicon, is an element of the fourth group of the periodic table, with the same crystal structure as diamond. Each germanium atom has four near neighbors in a tetrahedral configuration with which it forms covalent bonds. The specific gravity is about 5.35 and the melting point  $958^{\circ}\text{C}$ .

The conductivity at room temperature may be either n or p type, depending on the nature and concentration of impurities. Scaff, Theuerer, and Schumacher<sup>29</sup> have shown that group III elements, with one less valence electron, give p-type conductivity; group V elements, with one more valence electron, give n-type conductivity. This applies to both germanium

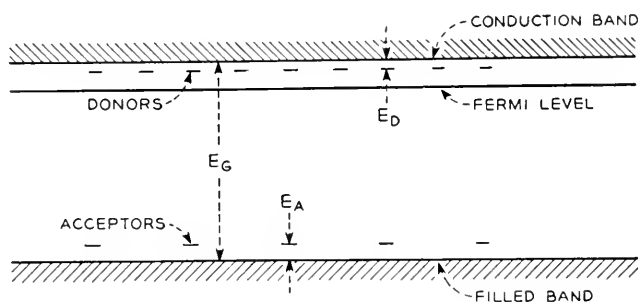


Fig. 13—Schematic energy level diagram for germanium showing filled and conduction bands and donor and acceptor levels.

and silicon. There is evidence that both acceptor (p-type) and donor (n-type) impurities are substitutional<sup>30</sup>.

A schematic energy level diagram<sup>31</sup> which shows the allowed energy levels for the valence electrons in a semi-conductor like germanium is given in Fig. 13. There is a continuous band of levels, the filled band, normally occupied by the electrons in the valence bonds; an energy gap,  $E_G$ , in which there are no levels of the ideal crystal; and then another continuous band of levels, the conduction band, normally unoccupied. There are just sufficient levels in the filled band to accommodate the four valence electrons per atom. The acceptor impurity levels, which lie just above the filled band, and the donor levels, just below the conduction band, correspond to electrons localized about the impurity atoms. Donors are normally neutral, but become positively charged by excitation of an electron to the conduction band, an energy  $E_D$  being required. Acceptors, normally neutral, are negatively ionized by excitation of an electron from the filled band, an energy  $E_A$

being required. Both  $E_D$  and  $E_A$  are so small in germanium that practically all donors and acceptors are ionized at room temperature. If only donors are present, the concentration of conduction electrons is equal to the concentration of donors, and the conductivity is n-type. If only acceptors are present, the concentration of missing electrons, or holes, is equal to that of the acceptors, and the conductivity is p-type.

It is possible to have both donor and acceptor type impurities present in the same crystal. In this case, electrons will be transferred from the donor levels to the lower lying acceptor levels. The conductivity type then depends on which is in excess, and the concentration of carriers is equal to the difference between the concentrations of donors and acceptors. It is probable that impurities of both types are present in high-back-voltage germanium. The relative numbers in solid solution can be changed by heat treatment, thus changing the conductivity and even the conductivity type.<sup>13</sup> The material used in rectifiers and transistors has a concentration of conduction electrons of the order of  $10^{15}/\text{c.c.}$ , which is about one for each  $5 \times 10^7$  atoms.

The conductivity depends on the concentrations and mobilities of the carriers: Let  $\mu_e$  and  $\mu_h$  be the mobilities, expressed in  $\text{cm}^2/\text{volt sec}$ , and  $n_e$  and  $n_h$  the concentrations (number/ $\text{cm}^3$ ) of the electrons and holes respectively. If both types of carriers are present, the conductivity, in mhos/cm, is

$$\sigma = n_e e \mu_e + n_h e \mu_h, \quad (3.1)$$

where  $e$  is the electronic charge in coulombs ( $1.6 \times 10^{-19}$ ).

Except for relatively high concentrations ( $\sim 10^{17}/\text{cm}^3$  or larger), or at low temperatures, the mobilities in germanium are determined mainly by lattice scattering and so should be approximately the same in different samples. Approximate values, estimated from Hall and resistivity data obtained at Purdue University<sup>32</sup> and at the Bell Laboratories<sup>33</sup> are:

$$\mu_h = 5 \times 10^6 T^{-3/2}, \quad (3.2)$$

$$\mu_e = 7.5 \times 10^6 T^{-3/2} (\text{cm}^2/\text{volt sec}), \quad (3.3)$$

in which  $T$  is the absolute temperature. There is a considerable spread among the different measurements, possibly arising from inhomogeneity of the samples. The temperature variation is as indicated by theory. These equations give  $\mu_h \sim 1000$  and  $\mu_e \sim 1500 \text{ cm}^2/\text{volt sec}$  at room temperature. The resistivity of high-back-voltage germanium varies from about 1 to 30 ohm cm, corresponding to values of  $n_e$  between  $1.5 \times 10^{14}$  and  $4 \times 10^{15}/\text{cm}^3$ .

At high temperatures electrons may be thermally excited from the filled band to the conduction band, an energy  $E_g$  being required. Both the ex-



cited electron and the hole left behind contribute to the conductivity. The conductivities of all samples approach the same limiting values, regardless of impurity concentration, given by an equation of the form

$$\sigma = \sigma_{\infty} \exp(-E_G/2kT), \quad (3.4)$$

where  $k$  is Boltzmann's constant. For germanium,  $\sigma_{\infty}$  is about  $3.3 \times 10^4$  mhos/cm and  $E_G$  about 0.75 ev.

The exponential factor comes from the variation of concentration with temperature. Statistical theory<sup>34</sup> indicates that  $n_e$  and  $n_h$  depend on temperature as

$$n_e = C_e T^{3/2} \exp(-\varphi_e/kT) \quad (3.5a)$$

$$n_h = C_h T^{3/2} \exp(-\varphi_h/kT) \quad (3.5b)$$

where  $\varphi_e$  is the energy difference between the bottom of the conduction band and the Fermi level and  $\varphi_h$  is the difference between the Fermi level and the top of the filled band. The position of the Fermi level depends on the impurity concentration and on temperature. The theory gives

$$C_e \sim C_h \sim 2(2\pi mk/h^2)^{3/2} \sim 5 \times 10^{15} \quad (3.6)$$

where  $m$  is an effective mass for the electrons (or holes) and  $h$  is Plank's constant. The numerical value is obtained by using the ordinary electron mass for  $m$ .

The product  $n_e n_h$  is independent of the position of the Fermi level, and thus of impurity concentration, and depends only on the temperature. From Eqs. (3.5a) and (3.5b)

$$n_e n_h = C_e C_h T^3 \exp(-E_G/kT). \quad (3.7)$$

In the intrinsic range, we may set  $n_e = n_h = n$ , and find, using (3.1), (3.2), and (3.3), an expression of the form (3.4) for  $\sigma$  with

$$\sigma_{\infty} = 11.5 \times 10^6 e (C_e C_h)^{1/2}. \quad (3.8)$$

Using the theoretical value (3.6) for  $(C_e C_h)^{1/2}$ , we find

$$\sigma_{\infty} = 0.9 \times 10^4 \text{ mhos/cm},$$

as compared with the empirical value of  $3.3 \times 10^4$ , a difference of a factor of 3.6. A similar discrepancy for silicon appears to be related to a variation of  $E_G$  with temperature. With an empirical value of

$$C_e C_h = 25 \times 10^{30} \times 3.6^2 \sim 3 \times 10^{32}, \quad (3.9)$$

Eq. (3.7) gives

$$n_e n_h \sim 10^{27}/\text{cm}^6 \quad (3.10)$$

when evaluated for room temperature. Thus for  $n_e \sim 10^{15}/\text{cm}^3$ , corresponding to high-back-voltage germanium,  $n_h$  is the order of  $10^{12}$ . The equilibrium concentration of holes is small.

Below the intrinsic temperature range,  $n_e$  is approximately constant and  $n_h$  varies as

$$n_h = (C_e C_h T^3 / n_e) \exp(-E_G/kT). \quad (3.11)$$

#### IV—THEORY OF THE DIODE CHARACTERISTIC

Characteristics of metal point-germanium contacts include high forward currents, as large as 5 to 10 ma at 1 volt, small reverse currents, correspond-

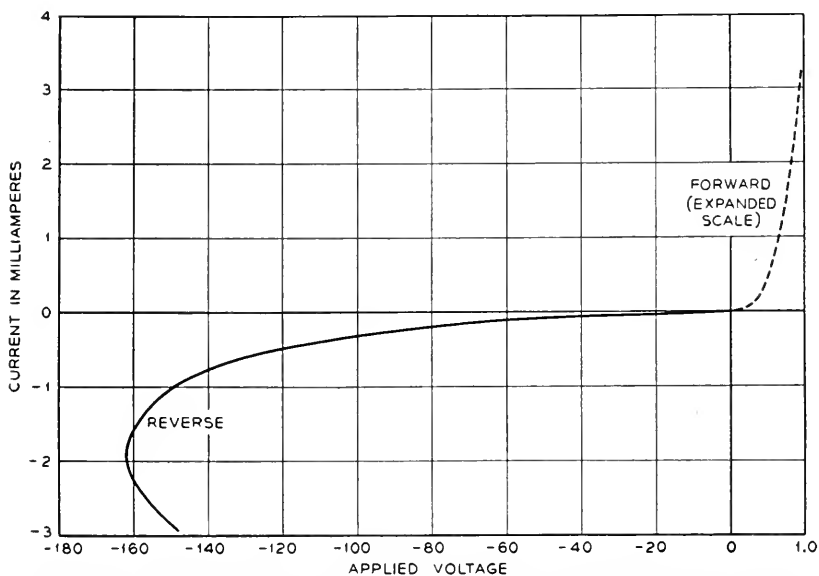


Fig. 14—Current-voltage characteristic of high-back-voltage germanium rectifier. Note that the voltage scale in the forward direction has been expanded by a factor of 20.

ing to resistances as high as one megohm or more at reverse voltages up to 30 volts, and the ability to withstand large voltages in the reverse direction without breakdown. A considerable variation of rectifier characteristics is found with changes in preparation and impurity content of the germanium, surface treatment, electrical power or forming treatment of the contacts, and other factors.

A typical d-c. characteristic of a germanium rectifier<sup>35</sup> is illustrated in Fig. 14. The forward voltages are indicated on an expanded scale. The forward current at one volt bias is about 3.5 ma and the differential resistance is about 200 ohms. The reverse current at 30 volts is about .02 ma

and the differential resistance about  $5 \times 10^5$  ohms. The ratio of the forward to the reverse current at one volt bias is about 500. At a reverse voltage of about 160 the differential resistance drops to zero, and with further increase in current the voltage across the unit drops. The nature of this negative resistance portion of the curve is not completely understood, but it is believed to be associated with thermal effects. Successive points along the curve correspond to increasingly higher temperatures of the contact. The peak value of the reverse voltage varies among different units. Values of more than 100 volts are not difficult to obtain.

Theories of rectification as developed by Mott,<sup>36</sup> Schottky,<sup>37</sup> and others<sup>38</sup> have not been successful in explaining the high-back-voltage characteristic in a quantitative way. In the following we give an outline of the theory and its application to germanium. It is believed that the high forward currents can now be explained in terms of a flow of holes. The type of barrier which gives a flow of carriers of conductivity type opposite to that of the base material is discussed. It is possible that a hole current also plays an important role in the reverse direction.

#### THE SPACE-CHARGE LAYER

According to the Mott-Schottky theory, rectification results from a potential barrier at the contact which impedes the flow of electrons between the metal and the semi-conductor. A schematic energy level diagram of the barrier region, drawn roughly to scale for germanium, is given in Fig. 15. There is a rise in the electrostatic potential energy of an electron at the surface relative to the interior which results from a space charge layer in the semi-conductor next to the metal contact. The space charge arises from positively ionized donors, that is from the same impurity centers which give the conduction electrons in the body of the semi-conductor. In the interior, the space-charge of the donors is neutralized by the space charge of the conduction electrons which are present in equal numbers. Electrons are drained out of the space-charge layer near the surface, leaving the immobile donor ions.

The space charge layer may be a result of the metal-semi-conductor contact, in which case the positive charge in the layer is compensated by an induced charge of opposite sign on the metal surface. Alternatively, the charge in the layer may be compensated by a surface charge density of electrons trapped in surface states on the semi-conductor.<sup>9</sup> It is believed, for reasons to be discussed below, that the latter situation applies to high-back-voltage germanium, and that a space-charge layer exists at the free surface, independent of the metal contact. The height of the conduction band above the Fermi level at the surface,  $\varphi_s$ , is then determined by the distribution in energy of the surface states.

That the space-charge layer which gives the rectifying barrier in germanium arises from surface states, is indicated by the following:

(1) Characteristics of germanium-point contacts do not depend on the work function of the metal, as would be expected if the space-charge layer were determined by the metal contact.

(2) There is little difference in contact potential between different samples of germanium with varying impurity concentration. Benzer<sup>39</sup>

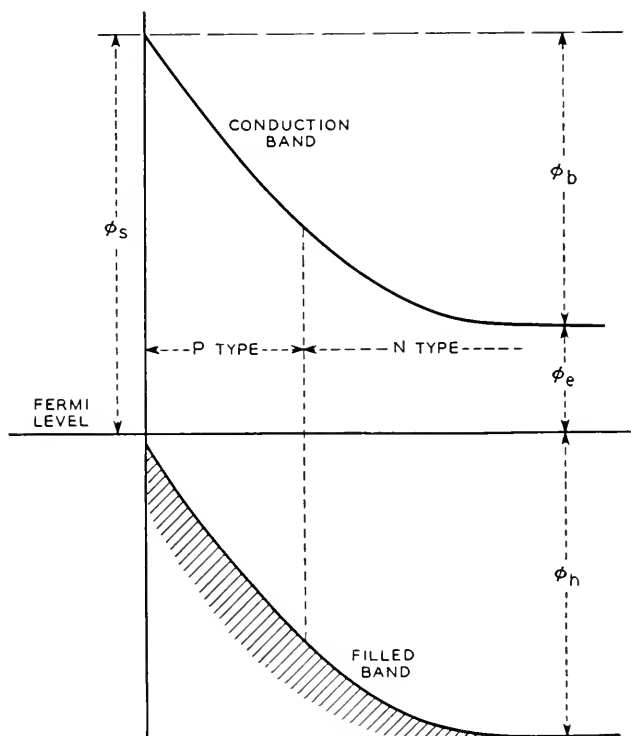


Fig. 15—Schematic energy level diagram of barrier layer at germanium surface showing inversion layer of p-type conductivity.

found less than 0.1-volt difference between samples ranging from n-type with  $2.6 \times 10^{18}$  carriers/cm<sup>3</sup> to p-type with  $6.4 \times 10^{18}$  carriers/cm<sup>3</sup>. This is much less than the difference of the order of the energy gap, 0.75 volts, which would exist if there were no surface effects.

(3) Benzer<sup>40</sup> has observed the characteristics of contacts formed from two crystals of germanium. He finds that in both directions the characteristic is similar to the reverse characteristic of one of the crystals in contact with a highly conducting metal-like germanium crystal.

(4) One of the authors<sup>11</sup> has observed a change in contact potential with light similar to that expected for a barrier layer at the free surface.

Prior to Benzer's experiments, Meyerhof<sup>8</sup> had shown that the contact potential difference measured between different metals and silicon showed little correlation with rectification, and that the contact potential difference between n- and p-type silicon surfaces was small. There is thus evidence that the barrier layers in both germanium and silicon are internal and occur at the free surface<sup>11</sup>.

In the development of the mathematical theory of the space-charge layer at a rectifier contact, Schottky and Spence<sup>18</sup> point out the possibility of a change in conductivity type between the surface and the interior if the potential rise is sufficiently large. The conductivity is p-type if the Fermi level is closest to the filled band, n-type if it is closest to the conduction band. In the illustration (Fig. 15), the potential rise is so large that the filled band is raised up to a position close to the Fermi level at the surface. This situation is believed to apply to germanium. There is then a thin layer near the surface whose conductivity is p-type, superimposed on the n-type conductivity in the interior. Schottky and Spence call the layer of opposite conductivity type an inversion region.

Referring to Eqs. (3.5a and 3.5b) for the concentrations, it can be seen that since  $C_e$  and  $C_h$  are of the same order of magnitude, the conductivity type depends on whether  $\varphi_e$  is larger or smaller than  $\varphi_h$ . The conductivity is n-type when

$$\varphi_e < 1/2 E_G, \quad \varphi_h > 1/2 E_G, \quad (4.1)$$

and is p-type when the reverse situation applies. The maximum resistivity occurs at the position where the conductivity type changes and

$$\varphi_e \sim \varphi_h \sim 1/2 E_G. \quad (4.2)$$

The change from n- to p-type will occur if

$$\varphi_s > 1/2 E_G, \quad (4.3)$$

or if the overall potential rise,  $\varphi_b$ , is greater than

$$1/2 E_G - \varphi_{e0}, \quad (4.4)$$

where  $\varphi_{e0}$  is the value of  $\varphi_e$  in the interior. Since for high-back-voltage germanium,  $E_G \sim 0.75$  e.v. and  $\varphi_{e0} \sim 0.25$  e.v., a rise of more than 0.12 e.v. is sufficient for a change of conductivity type to occur. A rise of 0.50 e.v. will bring the filled band close to the Fermi level at the surface.

Schottky<sup>37</sup> relates the thickness of the space charge layer with a potential rise as follows. Let  $\rho$  be the average charge density, assumed constant for simplicity, in the space charge layer. In the interior  $\rho$  is compensated by

the space charge of the conduction electrons. Thus, if  $n_0$  is the normal concentration of electrons,<sup>42</sup>

$$\rho = en_0 \quad (4.5)$$

Integration of the space charge equations gives a parabolic variation of potential with distance, and the potential rise,  $\varphi_b$ , is given in terms of the thickness of the space charge layer,  $\ell$ , by the equation

$$\varphi_b = 2\pi e\rho\ell^2/\kappa = 2\pi e^2n_0\ell^2/\kappa \quad (4.6)$$

For

$$\varphi_b = \varphi_s - \varphi_{c0} \sim 0.5 \text{ e.v.} \sim 8 \times 10^{-13} \text{ ergs}$$

and

$$n_0 \sim 10^{15}/\text{cm}^3$$

the barrier thickness,  $\ell$ , is about  $10^{-4}$  cm. The dielectric constant,  $\kappa$ , is about 18 in germanium.

When a voltage,  $V_a$ , is applied to a rectifying contact, there will be a drop,  $V_b$ , across the space charge layer itself and an additional drop,  $IR_s$ , in the body of the germanium which results from the spreading resistance,  $R_s$ , so that

$$V_a = V_b + IR_s. \quad (4.7)$$

The potential energy drop,  $-eV_b$ , is superimposed on the drop  $\varphi_b$  which exists under equilibrium conditions. For this case Eq. (4.6) becomes

$$\varphi_b - eV_b = 2\pi e^2n_0\ell^2/\kappa \quad (4.8)$$

The potential  $V_b$  is positive in the forward direction, negative in the reverse. A reverse voltage increases the thickness of the layer, a forward voltage decreases the thickness of the layer. The barrier disappears when  $eV_b = \varphi_b$ , and the current is then limited entirely by the spreading resistance in the body of the semi-conductor.

The electrostatic field at the contact is

$$F = 4\pi en_0\ell/\kappa = (8\pi n_0(\varphi_b - eV_b)/\kappa)^{1/2} \quad (4.9)$$

For  $n_0 \sim 10^{15}$ ,  $\ell \sim 10^{-4}$  and  $\kappa \sim 18$ , the field  $F$  is about 30 e.s.u. or 10,000 volts/cm. The field increases the current flow in much the way the current from a thermionic emitter is enhanced by an external field.

Previous theories of rectification have been based on the flow of only one type of carrier, i.e. electrons in an n-type or holes in a p-type semi-conductor. If the barrier layer has an inversion region, it is necessary to consider the flow of both types of carriers. Some of the hitherto puzzling features

of the germanium diode characteristic can be explained by the hole current. While a complete theoretical treatment has not been carried out, we will give an outline of the factors involved and then give separate discussions for the reverse and forward directions.

The current of holes may be expected to be important if the concentration of holes at the semi-conductor boundary of the space charge layer is as large as the concentration of electrons at the metal-semi-conductor interface. In equilibrium, with no current flow, the former is just the hole concentration in the interior,  $n_{h0}$ , which is given by

$$n_{h0} = C_h T^{3/2} \exp(-\varphi_{h0}/kT), \quad (4.10)$$

where  $\varphi_{h0}$  is the energy difference between the Fermi level in the interior and the top of the filled band. The concentration of electrons at the interface is given by:

$$n_{em} = C_e T^{3/2} \exp(-\varphi_s/kT). \quad (4.11)$$

Since  $C_h$  and  $C_e$  are of the same order,  $n_{h0}$  will be larger than  $n_{em}$  if  $\varphi_s$  is larger than  $\varphi_{h0}$ . This latter condition is met if the hole concentration at the metal interface is larger than the electron concentration in the interior. The concentrations will, of course, be modified when a current is flowing; but the criterion just given is nevertheless a useful guide. The criterion applies to an inversion barrier layer regardless of whether it is formed by the metal contact or is of the surface states type. In the latter case, as discussed in the Introduction, a lateral flow of holes along the surface layer into the contact may contribute to the current.

Two general theories have been developed for the current in a rectifying junction which apply in different limiting cases. The diffusion theory applies if the current is limited by the resistance of the space charge layer. This will be the case if the mean free path is small compared with the thickness of the layer, or, more exactly, small compared with the distance required for the potential energy to drop  $kT$  below the value at the contact. The diode theory applies if the current is limited by the thermionic emission current over the barrier. In germanium, the mean free path ( $10^{-5}$  cm) is of the same order as the barrier thickness. Analysis shows, however, that scattering in the barrier is unimportant and that it is the diode theory which should be used.<sup>43</sup>

#### REVERSE CURRENT

Different parts of the d-c. current-voltage characteristics require separate discussion. We deal first with the reverse direction. The applied voltages are assumed large compared with  $kT/e$  (.025 volts at room temperature), but small compared with the peak reverse voltage, so that ther-

mal effects are unimportant. Electrons flow from the metal point contact to the germanium, and holes flow in the opposite direction.

Benzer<sup>43</sup> has made a study of the variation of the reverse characteristic with temperature. He divides the current into three components whose relative magnitudes vary among different crystals and which vary in different ways with temperature. These are:

(1) A saturation current which arises very rapidly with applied voltage, approaching a constant value at a fraction of a volt.

(2) A component which increases linearly with the voltage.

(3) A component which increases more rapidly than linearly with the voltage.

The first two increase rapidly with increasing temperature, while the third component is more or less independent of ambient temperature. It is the saturation current, and perhaps also the linear component, which are to be identified with the theoretical diode current.

The third component is the largest in units with low reverse resistance. It is probable that in these units the barrier is not uniform. The largest part of the current, composed of electrons, flows through patches in which the height of the barrier is small. The electrically formed collector in the transistor may have a barrier of this sort.

Benzer finds that the saturation current predominates in units with high reverse resistance, and that this component varies with temperature as

$$I_s = -I_0 e^{\epsilon/kT}, \quad (4.12)$$

with  $\epsilon$  nearly 0.7 e.v. The negative sign indicates a reverse current. According to the diode theory,<sup>44</sup> one would expect it to vary as

$$I_s = -BT^2 e^{\epsilon/kT}. \quad (4.13)$$

Since  $\epsilon$  is large, the observed current can be fitted just about as well with the factor  $T^2$  as without. The value of  $\epsilon$  obtained using (4.13) is about 0.6 e.v. The saturation current<sup>43</sup> at room temperature varies from  $10^{-7}$  to  $10^{-6}$  amps, which corresponds to values of  $B$  in the range of 0.01 to 0.1 amps/deg<sup>2</sup>.

The theoretical value of  $B$  is 120 times the contact area,  $A_c$ . Taking  $A_c \sim 10^{-6}$  cm<sup>2</sup> as a typical value for the area of a point contact gives  $B \sim 10^{-4}$  amps/deg<sup>2</sup> which is only about 1/100 to 1/1000 of the observed. It is difficult to reconcile the magnitude of the observed current with the large temperature coefficient, and it is possible that an important part of the total flow is a current of holes into the contact. Such a current particularly is to be expected on surfaces which exhibit an appreciable surface conductivity.

Neglecting surface effects for the moment, an estimate of the saturation



hole current might be obtained as follows: The number of holes entering the space charge region per second is<sup>45</sup>

$$n_{hb}v_a A_c/4,$$

where  $n_{hb}$  is the hole concentration at the semi-conductor boundary of the space-charge layer and  $v_a$  is an average thermal velocity ( $\sim 10^7$  cm/sec.). The hole current,  $I_h$ , is obtained by multiplying by the electronic charge, giving

$$I_h = -n_{hb}ev_a A_c/4 \quad (4.14)$$

If we set  $n_{hb}$  equal to the equilibrium value for the interior, say  $10^{12}/\text{cm}^3$ , we get a current  $I_h \sim 4 \times 10^{-7}$  amps, which is of the observed order of magnitude of the saturation current at room temperature. With this interpretation, the temperature variation of  $I_s$  is attributed to that of  $n_h$ , which, according to Eq. (3.11), varies as  $\exp(-E_g/kT)$ . The observed value of  $\epsilon$  is indeed almost equal to the energy gap.

The difficulty with this picture is to see how  $n_{hb}$  can be as large as  $n_h$  when a current is flowing. Holes must move toward the contact area primarily by diffusion, and the hole current will be limited by a diffusion gradient. The saturation current depends on how rapidly holes are generated, and reasonable estimates based on the mean life time,  $-\tau$ , yield currents which are several orders of magnitude too small. A diffusion velocity,  $v_D$ , of the order

$$v_D \sim (D/\tau)^{1/2}, \quad (4.15)$$

replaces  $v_a/4$  in Eq. (4.14). Setting  $D \sim 25$  cm<sup>2</sup>/sec and  $\tau \sim 10^{-6}$  sec gives  $v_D \sim 5 \times 10^3$ , which would give a current much smaller than the observed. What is needed, then, is some other mechanism which will help maintain the equilibrium concentration near the barrier. Surface effects may be important in this regard.

#### FORWARD CURRENT

The forward characteristic is much less dependent on such factors as surface treatment than the reverse. In the range from 0 to 0.4 volts in the forward direction, the current can be fitted quite closely by a semi-empirical expression<sup>46</sup> of the form:

$$I = I_0(e^{\beta V_b} - 1), \quad (4.16)$$

where  $V_b$  is the drop across the barrier resulting from the applied voltage, as defined by Eq. (4.7). Equation (4.16) is of the general form to be expected from theory, but the measured value of  $\beta$  is generally less than the theoretical value  $e/kT$  (40 volts<sup>-1</sup> at room temperature). Observed values

of  $\beta$  may be as low as 10, and in other units are nearly as high as the theoretical value of 40. The factor  $I_0$  also varies among different units and is of the order  $10^{-7}$  to  $10^{-6}$  amperes. While both experiment and theory indicate that the forward current at large forward voltages is largely composed of holes, the composition of the current at very small forward voltages is uncertain. Small areas of low  $\varphi_s$ , unimportant at large forward voltages, may give most of the current at very small voltages. Currents flowing in these areas will consist largely of electrons.

Above about 0.5 volts in the forward direction, most of the drop occurs across the spreading resistance,  $R_s$ , rather than across the barrier. The theoretical expression for  $R_s$  for a circular contact of diameter  $d$  on the surface of a block of uniform resistivity  $\rho$  is:

$$R_s = \rho/2d \quad (4.17)$$

Taking as typical values for a point contact on high-back-voltage germanium,  $\rho = 10$  ohm cm. and  $d = .0025$  cm, we obtain  $R_s = 2000$  ohms, which is the order of ten times the observed.

As discussed in the Introduction, Bray and others<sup>21, 22</sup> have attempted to account for this discrepancy by assuming that the resistivity decreases with increasing field, and Bray has made tests to observe such an effect. The authors have investigated the nature of the forward current by making potential probe measurements in the vicinity of a point contact.<sup>2</sup> These measurements indicate that there may be two components involved in the excess conductivity. Some surfaces, prepared by oxidation at high temperatures, give evidence for excess conductivity in the vicinity of the point in the reverse as well as in the forward direction. This ohmic component has been attributed to a thin p-type layer on the surface. All surfaces investigated exhibit an excess conductivity in the forward direction which increases with increasing forward current. This second component is attributed to an increase in the concentration of carriers, holes and electrons, in the vicinity of the point with increase in forward current. Holes flow from the point into the germanium and their space charge is compensated by electrons.

The ohmic component is small, if it exists at all, on surfaces treated in the normal way for high-back-voltage rectifiers (i.e., ground and etched). The nature of the second component on such surfaces has been shown by more recent work of Shockley, Haynes<sup>20</sup>, and Ryder<sup>23</sup> who have investigated the flow of holes under the influence of electric fields. These measurements prove that the forward current consists at least in large part of holes flowing into the germanium from the contact.

It is of interest to consider the way the concentrations of holes and electrons vary in the vicinity of the point. An exact calculation, including the

effect of recombination, leads to a non-linear differential equation which must be solved by numerical methods. A simple solution can be obtained, however, if it is assumed that all of the forward current consists of holes and if recombination is neglected.

The electron current then vanishes everywhere, and the electric field is such as to produce a conduction current of electrons which just cancels the current from diffusion, giving

$$n_e F = -(kT/e) \text{grad } n_e. \quad (4.18)$$

This equation may be integrated to give the relation between the electrostatic potential,  $V$ , and  $n_e$ ,

$$V = (kT/e) \log (n_e/n_{e0}). \quad (4.19)$$

The constant of integration has been chosen so that  $V = 0$  when  $n_e$  is equal to the normal electron concentration  $n_{e0}$ . The equation may be solved for  $n_e$  to give:

$$n_e = n_{e0} \exp(eV/kT). \quad (4.20)$$

If trapping is neglected, electrical neutrality requires that

$$n_e = n_h + n_{e0}. \quad (4.21)$$

Using this relation, and taking  $n_{e0}$  a constant, we can express field  $F$  in terms of  $n_h$

$$F = -(kT/e(n_h + n_{e0})) \text{grad } n_h \quad (4.22)$$

The hole current density,  $i_h$ , is the sum of a conduction current resulting from the field  $F$  and a diffusion current:

$$i_h = n_h e \mu_h F - kT \mu_h \text{grad } n_h \quad (4.23)$$

Using Eq. (4.22), we may write this in the form

$$i_h = -kT \mu_h ((2n_h + n_{e0})/(n_h + n_{e0})) \text{grad } n_h \quad (4.24)$$

The current density can be written

$$i_h = - \text{grad } \psi, \quad (4.25)$$

where

$$\psi = kT \mu_h (2n_h - n_{e0} \log ((n_h + n_{e0})/n_{e0})) \quad (4.26)$$

Since  $i_h$  satisfies a conservation equation,

$$\text{div } i_h = 0, \quad (4.27)$$

$\psi$  satisfies Laplace's equation.

If surface effects are neglected and it is assumed that holes flow radially in all directions from the point contact,  $\psi$  may be expressed simply in terms of the total hole current,  $I_h$ , flowing from the contact:

$$\psi = -I_h/2\pi r \quad (4.28)$$

Using (4.26), we may obtain the variation of  $n_h$  with  $r$ . We are interested in the limiting case in which  $n_h$  is large compared with the normal electron concentration,  $n_{e0}$ . The logarithmic term in (4.26) can then be neglected, and we have

$$n_h = I_h/4\pi r\mu_h kT. \quad (4.29)$$

For example, if  $I_h = 10^{-3}$  amps,  $\mu_h = 10^3$  cm<sup>2</sup>/volt sec, and  $kT/e = .025$  volts, we get, approximately,

$$n_h = 2 \times 10^{13}/r. \quad (4.30)$$

For  $r \sim .0005$  cm, the approximate radius of a point contact,

$$n_h \sim 4 \times 10^{16}/\text{cm}^3, \quad (4.31)$$

which is about 40 times the normal electron concentration in high-back-voltage germanium. Thus the assumption that  $n_h$  is large compared with  $n_{e0}$  is valid, and remains valid up to a distance of the order of .005 cm, the approximate distance the points are separated in the transistor.

To the same approximation, the field is

$$F = kT/e r, \quad (4.32)$$

independent of the magnitude of  $I_h$ .

The voltage drop outside of the space-charge region can be obtained by setting  $n_e$  in (4.19) equal to the value at the semi-conductor boundary of the space-charge layer. This result holds generally, and does not depend on the particular geometry we have assumed. It depends only on the assumption that the electron current  $i_e$  is everywhere zero. Actually  $i_h$  will decrease and  $i_e$  increase by recombination, and there will be an additional spreading resistance for the electron current.

If it is assumed that the concentration of holes at the metal-semi-conductor interface is independent of applied voltage and that the resistive drop in the barrier layer itself is negligible, that part of the applied voltage which appears across the barrier layer itself is:

$$V_b = (kT/e) \log (n_{hb}/n_{h0}), \quad (4.33)$$

where  $n_{hb}$  is the hole concentration at the semi-conductor boundary of the space charge layer and  $n_{h0}$  is the normal concentration. For  $n_{hb} \sim 5 \times 10^{16}$  and  $n_{h0} \sim 10^{12}$ ,  $V_b$  is about 0.35 volts.

The increased conductivity caused by hole emission accounts not only for the large forward currents, but also for the relatively small dependence of spreading resistance on contact area. At a small distance from the contact, the concentrations and voltages are independent of contact area. The voltage drop within this small distance is a small part of the total and does not vary rapidly with current.

We have assumed that the electron current,  $I_e$ , at the contact is negligible compared with the hole current,  $I_h$ . An estimate of the electron current can be obtained as follows: From the diode theory,

$$I_e = (en_{eb}v_a A_c/4) \exp(-(\varphi_b - eV_b)/kT), \quad (4.34)$$

since the electron concentration at the semi-conductor boundary of the space-charge layer is  $n_{eb}$  and the height of the barrier with the voltage applied is  $\varphi_b - eV_b$ . For simplicity we assume that both  $n_{eb}$  and  $n_{hb}$  are large compared with  $n_{i0}$  so that we may replace  $n_{eb}$  by  $n_{hb}$  without appreciable error. The latter can be obtained from the value of  $\psi$  at the contact:

$$\psi = I_h/4a \quad (4.35)$$

Expressing  $\psi$  in terms of  $n_{hb}$ , we find

$$n_{hb} = I_h/8kT\mu_h a \quad (4.36)$$

Using (4.33) for  $V_b$ , and (3.5b) for  $n_{i0}$  we find after some reduction,

$$I_e = I_h^2/I_{crit}, \quad (4.37)$$

where

$$I_{crit} = \frac{256 C_h (kT\mu_h)^2 T^{3/2}}{\pi e v_a} \exp(-\varphi_{hm}/kT) \quad (4.38)$$

The energy difference  $\varphi_{hm}$  is the difference between the Fermi level and the filled band at the metal-semi-conductor interface. Evaluated for germanium at room temperature, (4.38) gives

$$I_{crit} = 0.07 \exp(-\varphi_{hm}/kT) \text{ amps,}$$

which is a fairly large current if  $\varphi_{hm}$  is not too large compared with  $kT$ . If  $I_h$  is small compared with  $I_{crit}$ , the electron current will be negligible.

#### V—THEORETICAL CONSIDERATIONS ABOUT TRANSISTOR ACTION

In this section we discuss some of the problems connected with transistor action, such as:

- (1) fields produced by the collector current,
- (2) transit times for the holes to flow from emitter to collector,
- (3) current multiplication in collector,
- (4) feedback resistance.

We do no more than estimate orders of magnitude. An exact calculation, taking into account the change of conductivity introduced by the emitter current, loss of holes by recombination, and effect of surface conductivity, is difficult and is not attempted.

To estimate the field produced by the collector, we assume that the collector current is composed mainly of conduction electrons, and that the electrons flow radially away from the collector. This assumption should be most nearly valid when the collector current is large compared with the emitter current. The field at a distance  $r$  from the collector is,

$$F = \rho I_c / 2\pi r^2 \quad (5.1)$$

For example, if,  $\rho = 10$  ohm cm,  $I_c = .001$  amps, and  $r = .005$  cm,  $F$  is about 100 volts/cm.

The drift velocity of a hole in the field  $F$  is  $u_h F$ . The transit time is

$$T = \int \frac{dr}{\mu_h F} = \frac{2\pi}{\mu_h \rho I_c} \int_0^s r^2 dr, \quad (5.2)$$

where  $s$  is the separation between the emitter and collector. Integration gives,

$$T = \frac{2\pi s^3}{3\mu_{h0} I_c} \quad (5.3)$$

For  $s = .005$  cm,  $\mu_h = 1000$  cm<sup>2</sup>/volt sec,  $\rho = 10$  ohm cm, and  $I_c = .001$  amps,  $T$  is about  $0.25 \times 10^{-7}$  sec. This is of the order of magnitude of the transit times estimated from the phase shift in  $\alpha$  or  $Z_{21}$ .

The hole current,  $I_h$ , is attenuated by recombination in going from the emitter to the collector. If  $\tau$  is the average life time of a hole,  $I_h$  will be decreased by a factor,  $e^{-T/\tau}$ . In Section II it was found that the geometrical factor,  $g$ , which gives the influence of separation on the interaction between emitter and collector, depends on the variable  $s/I_c^{1/3}$ . This suggests that the transit time is the most important factor in determining  $g$ . An estimate<sup>17</sup> of  $\tau$ , obtained from the data of Fig. 10, is  $2 \times 10^{-7}$  sec.

Because of the effect of holes in increasing the conductivity of the germanium in the vicinity of the emitter and collector, it can be expected that the field, the life time, and the geometrical factor will depend on the emitter current. The effective value of  $\rho$  to be used in Eqs. (5.1) and (5.2) will decrease with increase in emitter current. This effect is apparently not serious with the surface used in obtaining the data for Figs. 8 to 10.

Next to be considered is the effect of the space charge of the holes on the barrier layer of the collector. An estimate of the hole concentration can be obtained as follows: The field in the barrier layer is of the order of  $10^4$

volts/cm. Multiplying by the mobility gives a drift velocity,  $V_d$  of  $10^7$  cm/sec, which is approximately thermal velocity.<sup>48</sup> The hole current is

$$I_h = n_h e V_d A_c \quad (5.4)$$

where  $A_c$  is the area of the collector contact, and  $n_h$  the concentration of holes in the barrier. Solving for the latter, we get

$$n_h = I_h / e V_d A_c \quad (5.5)$$

For  $I_h = .001$  amps  $V_d = 10^7$  cm/sec, and  $A_c = 10^{-6}$  cm,  $n_h$  is about  $.6 \times 10^{15}$ , which is of the same order as the concentration of donors. Thus the hole current can be expected to alter the space charge in the barrier by a significant amount, and correspondingly alter the flow of electrons from the collector. It is believed that current multiplication (values of  $\alpha > 1$ ) can be accounted for along these lines.

As discussed in Section II, there is an influence of collector current on emitter current of the nature of a positive feedback. The collector current lowers the potential of the surface in the vicinity of the emitter by an amount

$$V = \rho I_c / 2\pi s \quad (5.6)$$

The feedback resistance  $R_F$  as used in Eq. (2.2) is

$$R_F = \rho / 2\pi s \quad (5.7)$$

For  $\rho = 10$  ohm cm and  $s = .005$  cm, the value of  $R_F$  is about 300 ohms, which is of the observed order of magnitude. It may be expected that  $R_F$  will decrease as  $\rho$  decreases with increase in emitter current.

The calculations made in this section confirm the general picture which has been given of the way the transistor operates.

## VI—CONCLUSIONS

Our discussion has been confined to the transistor in which two point contacts are placed in close proximity on one face of a germanium block. It is apparent that the principles can be applied to other geometrical designs and to other semi-conductors. Some preliminary work has shown that transistor action can be obtained with silicon and undoubtedly other semi-conductors can be used.

Since the initial discovery, many groups in the Bell Laboratories have contributed to the progress that has been made. This work includes investigation of the physical phenomena involved and the properties of the materials used, transistor design, and measurements of characteristics and circuit applications. A number of transistors have been made for experimental use in a pilot production. Obviously no attempt has been made

to describe all of this work, some of which has been reported on in other publications<sup>5</sup>.

In a device as new as the transistor, various problems remain to be solved. A reduction in noise and an increase in the frequency limit are desirable. While much progress has been made toward making units with reproducible characteristics, further improvement in this regard is also desirable.

It is apparent from reading this article that we have received a large amount of aid and assistance from other members of the Laboratories staff, for which we are grateful. We particularly wish to acknowledge our debt to Ralph Bown, Director of Research, who has given us a great deal of encouragement and aid from the inception of the work and to William Shockley, who has made numerous suggestions which have aided in clarifying the phenomena involved.

#### REFERENCES

1. J. Bardeen and W. H. Brattain, *Phys. Rev.*, **74**, 230 (1948).
2. W. H. Brattain and J. Bardeen, *Phys. Rev.*, **74**, 231 (1948).
3. W. Shockley and G. L. Pearson, *Phys. Rev.*, **74**, 232 (1948).
4. This paper was presented in part at the Chicago meeting of the American Physical Society, Nov. 26, 27, 1948. W. Shockley and the authors presented a paper on "The Electronic Theory of the Transistor" at the Berkeley meeting of the National Academy of Sciences, Nov. 15-17, 1948. A talk was given by one of the authors (W. H. B.) at the National Electronics Conference at Chicago, Nov. 4, 1948. A number of talks have been given at local meetings by J. A. Becker and other members of the Bell Laboratories Staff, as well as by the authors.
5. Properties and characteristics of the transistor are given by J. A. Becker and J. N. Shive in *Elec. Eng.* **68**, 215 (1949). A coaxial form of transistor is described by W. E. Kock and R. L. Wallace, Jr. in *Elec. Eng.* **68**, 222 (1949). See also "The Transistor, A Crystal Triode," D. G. F. and F. H. R., *Electronics*, September (1948) and a series of articles by S. Young White in *Audio Eng.*, August through December, (1948).
6. H. C. Torrey and C. A. Whitmer, *Crystal Rectifiers*, McGraw-Hill, New York (1948).
7. J. H. Scaff and R. S. Ohl, *Bell System Tech. Jour.* **26**, 1 (1947).
8. W. E. Meyerhof, *Phys. Rev.*, **71**, 727 (1947).
9. J. Bardeen, *Phys. Rev.*, **71**, 717 (1947).
10. W. H. Brattain and W. Shockley, *Phys. Rev.*, **72**, p. 345(L) (1947).
11. W. H. Brattain, *Phys. Rev.*, **72**, 345(L) (1947).
12. R. B. Gibney, formerly of Bell Telephone Laboratories, now at Los Alamos Scientific Laboratory, worked on chemical problems for the semi-conductor group, and the authors are grateful to him for a number of valuable ideas and for considerable assistance.
13. J. H. Scaff and H. C. Theuerer "Preparation of High Back Voltage Germanium Rectifiers" NDRC 14-555, Oct. 24, 1945—See reference 6, Chap. 12.
14. The surface treatment is described in reference 6, p. 369.
15. The transistor whose characteristics are given in Fig. 3 is one of an experimented pilot production which is under the general direction of J. A. Morton.
16. See, for example, A. H. Wilson *Semi-Conductors and Metals*, Cambridge University Press, London (1939) or F. Seitz, *The Modern Theory of Solids*, McGraw-Hill Book Co., Inc., New York, N.Y., (1940), Sec. 68.
17. The nature of the barrier is discussed in Sec. IV.
18. W. Schottky and E. Spenke, *Wiss. Veroff. Siemens-Werke*, **18**, 225 (1939).
19. J. N. Shive, *Phys. Rev.* **75**, 689 (1949).
20. J. R. Haynes, and W. Shockley, *Phys. Rev.* **75**, 691 (1949).
21. R. Bray, K. Lark-Horovitz and R. N. Smith, *Phys. Rev.*, **72**, 530 (1948).
22. R. Bray, *Phys. Rev.*, **74**, 1218 (1948).
23. E. J. Ryder and W. Shockley, *Phys. Rev.* **75**, 310 (1949).



24. This instrument was designed and built by H. R. Moore, who aided the authors a great deal in connection with instrumentation and circuit problems.
25. The surface had been oxidized, and potential probe measurements (ref. (2)) gave evidence for considerable surface conductivity.
26. Measured between centers of the contact areas.
27. Potential probe measurements on the same surface, given in reference (2), gave evidence of surface conductivity.
28. Unpublished data.
29. J. H. Scaff, H. C. Theuerer, and E. E. Schumacher, "P-type and N-type Silicon and the Formation of the Photovoltaic Barrier in Silicon" (in publication).
30. G. L. Pearson and J. Bardeen, *Phys. Rev.* March 1, 1949.
31. See, for example, reference 6, Chap. 3.
32. K. Lark-Horovitz, A. E. Middleton, E. P. Miller, and I. Walerstein, *Phys. Rev.* 69, 258 (1946).
33. Hall and resistivity data at the Bell Laboratories were obtained by G. L. Pearson on samples furnished by J. H. Scaff and H. C. Theuerer. Recent hall measurements of G. L. Pearson on single crystals of n- and p-type germanium give values of 2600 and 1700 cm<sup>2</sup>/volt sec. for electrons and holes, respectively at room temperature. The latter value has been confirmed by J. R. Haynes by measurements of the drift velocity of holes injected into n-type germanium. These values are higher, particularly for electrons, than earlier measurements on polycrystalline samples. Use of the new values will modify some of the numerical estimates made herein, but the orders of magnitude, which are all that are significant, will not be affected. W. Ringer and H. Welker, *Zeits. f. Naturforschung*, 1, 20 (1948) give a value of 2000 cm<sup>2</sup>/volt sec. for high resistivity n-type germanium.
34. See R. H. Fowler, *Statistical Mechanics*, 2nd ed., Cambridge University Press, London (1936).
35. From unpublished data of K. M. Olsen.
36. N. F. Mott, *Proc. Roy. Soc.*, 171A, 27 (1939).
37. W. Schottky, *Zeits. f. Phys.*, 113, 367 (1939), *Phys. Zeits.*, 41, p. 570 (1940), *Zeits. f. Phys.*, 118, p. 539 (1942). Also see reference 18.
38. See reference 6, Chap. 4.
39. S. Benzer, Progress Report, Contract No. W-36-039-SC-32020, Purdue University, Sept. 1-Nov. 30, 1946.
40. S. Benzer, *Phys. Rev.*, 71, 141 (1947).
41. Further evidence that the barrier is internal comes from some unpublished experiments of J. R. Haynes with the transistor. Using a fixed collector point, and keeping a fixed distance between emitter and collector, he varied the material used for the emitter point. He used semi-conductors as well as metals for the emitter point. While the impedance of the emitter point varied, it was found that equivalent emitter currents give changes in current at the collector of the same order for all materials used. It is believed that in all cases a large part of the forward current consists of holes.
42. The space charge of the holes in the inversion region of the barrier layer is neglected for simplicity.
43. Reference 6, Chap. 4.
44. S. Benzer "Temperature Dependence of High Voltage Germanium Rectifier D.C. Characteristics," *N.D.R.C.* 14-579, Purdue Univ., October 31, 1945. See reference 6, p. 376.
45. See, for example, E. H. Kennard, *Kinetic Theory of Gases*, McGraw-Hill, Inc., New York, N. Y. (1938) p. 63.
46. Reference 6, p. 377.
47. Obtained by plotting  $\log g$  versus  $s^3/I_c$ . This plot is not a straight line, but has an upward curvature corresponding to an increase in  $\tau$  with separation. The value given is a rough average, corresponding to  $s^3/I_c$  the order of  $10^{-3}$  cm<sup>3</sup> amp.
48. One may expect that the mobility will depend on field strength when the drift velocity is as large as or is larger than thermal velocity. Since ours is a borderline case, the calculation using the low field mobility should be correct at least as to order of magnitude.

## Lightning Current Observations in Buried Cable

By H. M. TRUEBLOOD and E. D. SUNDE

Results are given of observations of lightning currents, voltages, and charges in a buried cable over most of three lightning seasons. These are compared with theoretical expectations. Data regarding the incidence of lightning strokes to ground, as observed with automatic recording equipment, are also reported, together with comparisons with similar data published previously.

### INTRODUCTION

LIGHTNING currents in buried telephone cable are of considerable importance in that they may cause excessive voltages between the cable sheath and the conductors with resultant insulation failure, and may also cause severe damage by crushing the cable or fusing holes in the sheath. The incidence of lightning strokes to buried cable, the resulting voltages, and lightning trouble expectancy, have therefore been subjects of theoretical, experimental, and field studies, which, together with operating experience, have pointed the way to improvements in the design of communication cable to minimize its liability to lightning damage, and in the application of remedial measures where excessive lightning trouble has been experienced.<sup>1</sup>

The territory around Atlanta, Georgia, has appeared to be particularly severe with respect to these lightning hazards, because of high earth resistivity and high thunderstorm rate. Buried cables initially installed in this territory were accordingly provided with protective measures in the form of increased core-sheath insulation and shield wires buried with the cable. In spite of these measures, however, a substantially higher rate of lightning damage than anticipated was experienced, as a result of which a new design was adopted for the transcontinental coaxial cable westward from Atlanta. In this cable, the lead sheath was insulated from an outside corrugated 10-mil copper shield by a 100-mil layer of thermoplastic insulation intended to prevent the entrance of lightning currents into the sheath and thereby to minimize voltages between the sheath and the cable conductors.

Simulative tests with surge currents, believed to have a wave shape representative of lightning stroke current, had indicated satisfactory agreement between measured and calculated voltages between sheath and cable conductors. It appeared, therefore, that the departure from predicted

<sup>1</sup> References are listed at end of paper.

lightning trouble expectancy in the earlier cables was due to one or more of the following conditions: a higher rate of occurrence of lightning strokes during thunderstorms, higher stroke currents than in other parts of the country, a longer duration of the lightning currents than assumed, or a higher incidence of strokes to buried cable than predicted theoretically. The observations described here, the larger part of which have extended over a period of three lightning seasons, were intended to secure information on these points. The data forming the principal subject of this paper were obtained from a section of the coaxial cable mentioned above, which for a number of reasons was particularly suitable for the purpose.

## I. THEORETICAL EXPECTATIONS

### 1.0 *General*

As mentioned above, the observations were made on a cable route through territory of high thunderstorm rate and high earth resistivity, both of which facilitate measurements of currents along the cable. As a result of the high thunderstorm rate, the incidence of strokes to ground is high, and because of the high earth resistivity, the number of strokes to ground near the cable which flash to latter is also high. Another result of the high earth resistivity is that the attenuation of current along the cable is relatively low, so that currents and voltages may be observed at appreciable distances along the cable from the points of the lightning strokes. The rate of attenuation is, furthermore, smaller the longer the duration of the lightning current, that is, the longer the time to half-value. Since lightning trouble experience in this territory indicated the possibility of currents of rather long durations, this was an additional factor favorable to the purposes of the tests, although, like the others, it increases the liability of cables to lightning damage.

Though the relationships of the various factors mentioned above to earth resistivity and to lightning current wave shape have been dealt with in detail in the study<sup>1</sup> referred to above, they are briefly reviewed here to facilitate comparisons with and discussions of the observations.

### 1.1 *Incidence of Strokes to Buried Cable*

The current in a lightning stroke to ground spreads in all directions from the point where it enters the earth. If a cable is in the vicinity, it will provide a low resistance path, so that much of the current will flow to the cable and in both directions along the sheath to remote points. The current in the ground between the lightning channel and the cable may give rise to a voltage drop along the surface of the earth sufficient to exceed the breakdown gradient of the soil, particularly when the earth resistivity is

high. The lightning stroke will then arc directly to the cable from the point where it enters the ground, often at the base of a tree. Furrows exceeding 100 feet in length have been found along the ground path of such an arc.

For a crest current  $J$  in the lightning stroke, the arcing distance in meters is given by<sup>1</sup>

$$r = k(J\rho)^{1/2} \quad (1)$$

where  $J$  is in kiloamperes,  $\rho$  is the earth resistivity in meter-ohms and  $k$  is a constant depending on the surface breakdown gradient of the soil. Low resistivity soil, up to  $\rho = 100$  meter-ohms, has an average breakdown gradient of about 2500 volts/cm, and the corresponding value of  $k$  is about .08. For high resistivity soil,  $\rho = 1000$  meter-ohms and up, the average breakdown gradient is about 5000 volts/cm and  $k \cong .047$ . Thus, for an earth resistivity of 2000 meter-ohms, and  $J = 100$  ka,  $r \cong 21$  meters or 70 feet.

The number of strokes arcing to a cable of length  $s$  may conveniently be expressed as

$$N = 2\bar{r}sn \quad (2)$$

where  $n$  is the number of strokes to ground per unit area,  $\bar{r}$  is an equivalent arcing distance, and  $2\bar{r}s$  an equivalent area near the cable within which the cable is assumed to attract all lightning strokes. In obtaining  $\bar{r}$ , the number of strokes arcing to the cable from various distances  $r$  as given by (1), depending on the current in the strokes, must be evaluated. This number and the equivalent arcing distance will thus depend on the crest current distribution of lightning strokes. For the distribution curve shown by Curve 1 in Fig. 1, the effective distance in meters is<sup>1</sup>

$$\begin{aligned} \bar{r} &\cong .36\rho^{1/2} \text{ when } \rho \leq 100 \text{ meter-ohms} \\ &\cong .22\rho^{1/2} \text{ when } \rho \geq 1000 \text{ meter-ohms} \end{aligned} \quad (3)$$

Thus, for soil having an average resistivity near the surface (to a depth of at least 10 meters) of 2000 meter-ohms,  $\bar{r} \cong 10$  meters = 33 feet.

A cable will thus collect direct lightning strokes for an effective distance  $\bar{r}$  to either side of it, and when the incidence of strokes to ground per unit area is known, the number of strokes to a cable of a given length may readily be calculated. The incidence of strokes to ground has been estimated, on the average, as about 2.4 per square mile for each 10 thunderstorm days, and the corresponding expectancy of strokes to a buried cable, per 100 miles of length, is about 2.1 for 10 thunderstorm days when the earth resistivity is 1000 meter-ohms and 3.0 when it is 2000 meter-ohms.

The distribution of the crest currents in direct strokes to a cable may be

obtained by use of Curve 2 in Fig. 1, which is a theoretical curve derived from Curve 1. Thus for a total of 2.1 for 10 thunderstorm days, the incidence of strokes exceeding 60 ka is  $2.1 \cdot 0.2 = 0.42$ . In Fig. 2 are shown crest current distribution curves for cable currents due to direct strokes obtained in this manner, together with distribution curves for currents due to both direct strokes and strokes to ground not arcing to the cable. The latter curves may be obtained by methods similar to those used in evaluating curves for the lightning trouble expectancy of buried cable, which are

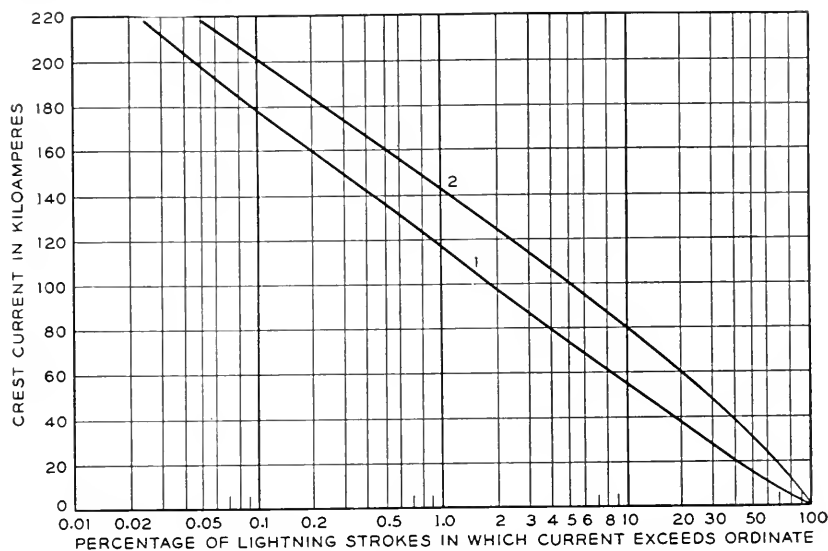


Fig. 1.—Distribution of crest currents in lightning strokes.

Curve 1. Currents in strokes to transmission line ground structures, based on 4410 measurements, 2721 in U. S. and 1689 in Europe.

Curve 2. Currents in strokes to buried structures derived from Curve 1.

shown in Fig. 3 for cable having a dielectric strength of 2 kv between the sheath and the cable conductors.<sup>1</sup> The latter curves may, in fact, be used to find the incidence of cable currents of various crest values due to direct strokes and strokes to ground, by calculating the cable currents required to produce 2 kv between the sheath and the core corresponding to various sheath resistances shown in Fig. 3. Thus for a sheath resistance of 2 ohms per mile and an earth resistivity of 1000 meter-ohms, this current is 14.2 ka (see Section 1.3) and for a sheath resistance of 1 ohm, it is 28.4 ka, etc., as plotted in Fig. 2 for an earth resistivity of 1000 meter-ohms.

From the above it follows that a verification of the distribution curves in Fig. 2 by observations of lightning currents in buried cable would apply

equally well to the curves in Fig. 3, which have been used to evaluate the liability of such cable to lightning damage.

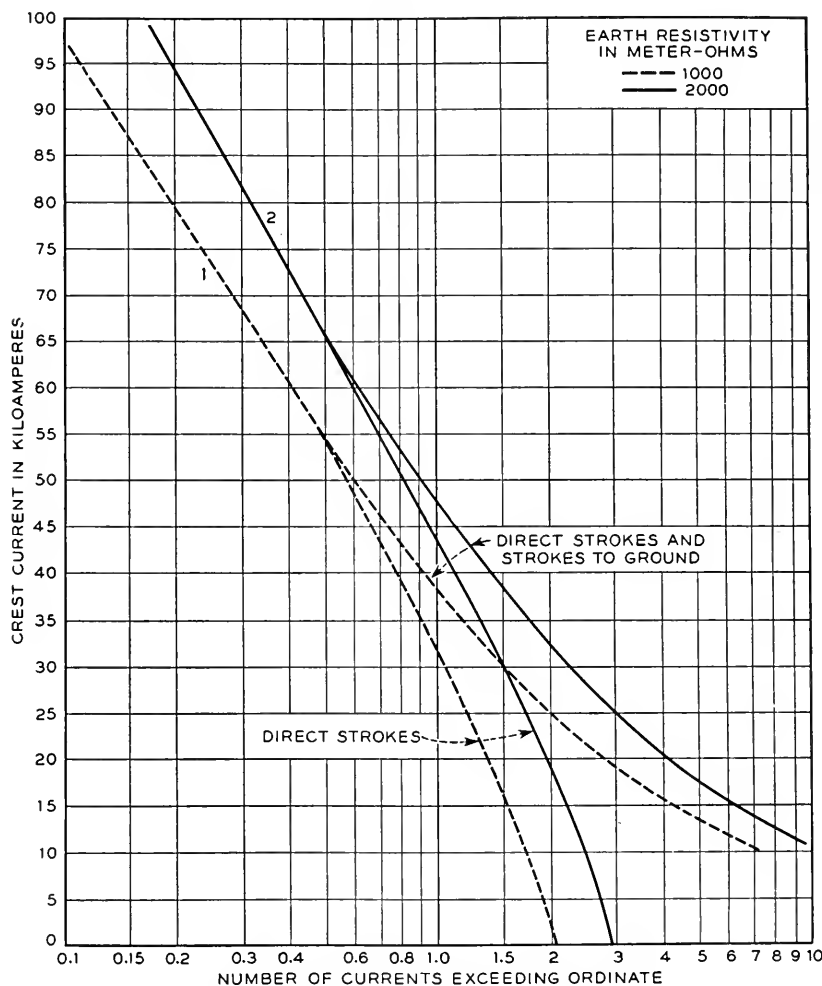


Fig. 2—Incidence of currents exceeding ordinate per 100 miles and 10 thunderstorm days.

### 1.2 Propagation of Currents Along Cable

The current entering the cable at or near the stroke point, depending on whether a direct stroke or a nearby stroke to ground is involved, is attenuated as it travels along the sheath towards remote points. The current leaving the sheath must flow through the adjacent soil, and the leak-

age current is therefore smaller the higher the soil resistivity. Thus the current will travel farther the higher the earth resistivity. It has been shown elsewhere<sup>1, 2</sup> that a sinusoidal current would be propagated as

$$I(x) = I(0) e^{-\Gamma x} \quad (4)$$

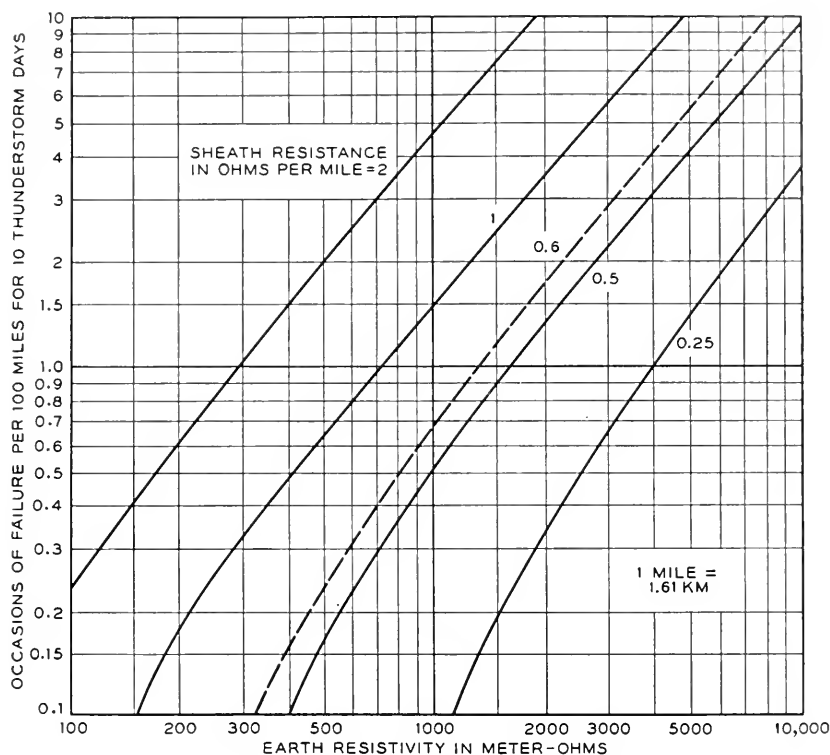


Fig. 3—Theoretical lightning trouble expectancy curves showing number of times insulation failures due to excessive voltages would be expected per 100 miles for 10 thunderstorm days, for cables having sheath resistances as indicated on curves and 2000 volts insulation between core and sheath. Dashed line represents full size cable.

where  $I(0)$  is the current in the sheath in one direction from the stroke point,  $I(x)$  the current at the distance  $x$ , and the propagation constant  $\Gamma$  per meter is given by:

$$\Gamma = \sqrt{i\omega\nu/2\rho} \quad (5)$$

where  $\omega = 2\pi f$ ,  $\nu$  = inductivity of the earth =  $1.257 \cdot 10^{-6}$  henry/meter, and  $\rho$  is the earth resistivity in meter-ohms.

Let it be assumed that the current at the distance  $x$  has been evaluated for a given earth resistivity  $\rho$  and radian frequency  $\omega$ . If the earth re-

sistivity is increased by a factor  $k$ , or if  $\omega$  is decreased by the same factor, it is evident from (4) and (5) that the same current will be obtained at the distance  $x_1 = k^{1/2}x$ . Thus, if the earth resistivity is increased by  $k = 4$ ,  $x_1 = 2x$  and the current attenuation will be half as great as before. This rule applies to surge-currents of a given wave-shape as well, since they may be regarded as composed of sinusoidal components, each of which would

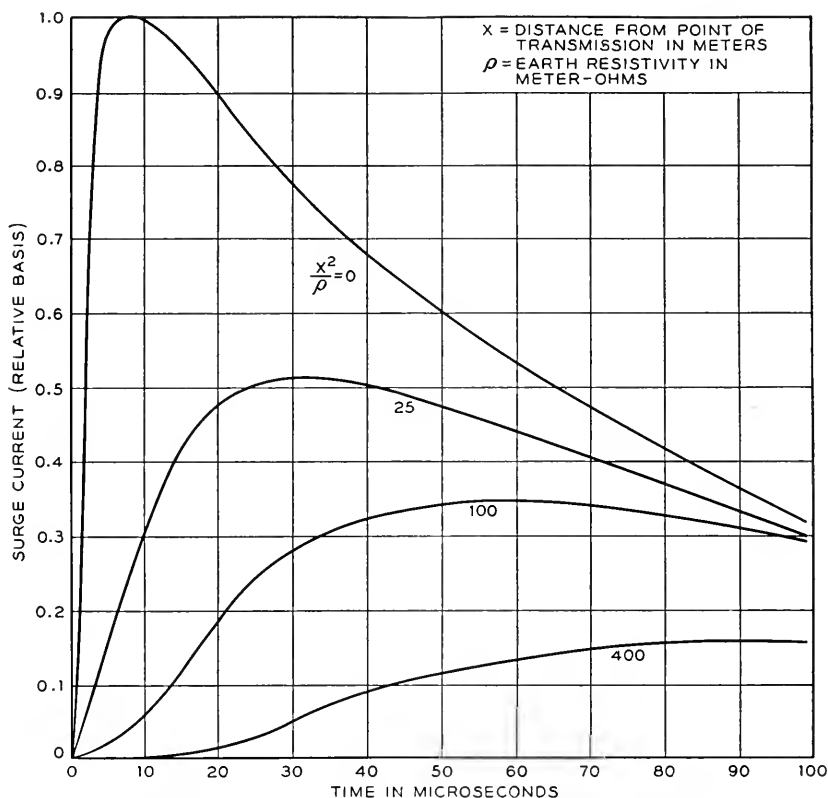


Fig. 4—Attenuation and distortion of surge current transmitted along a buried conductor.

travel farther by the factor  $k^{1/2}$ . Furthermore, it follows by the same reasoning that for surge-currents of congruent wave-shapes, but different durations, the rate of attenuation is inversely proportional to the square root of the duration. That is to say, let in one case the current reach its crest value at the stroke point in 5 microseconds and its half-value in 65 microseconds, and let the crest current at a given distance  $x$  have a certain value. Then, if in another case the current reaches the same stroke-point crest



value in 20 microseconds, with half-value in 260 microseconds, the same crest current as that found before at  $x$  is obtained at twice the distance  $x$ . This follows because all component frequencies of the first surge are related to corresponding components of the second surge by the same factor, viz. 4.

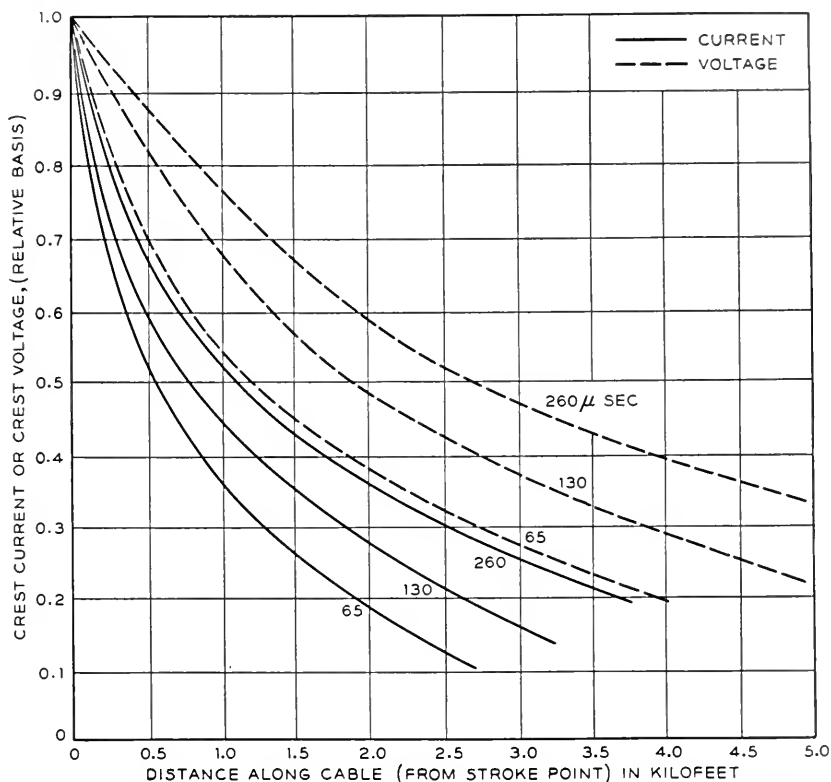


Fig. 5—Variation in crest current in cable and in voltage between sheath and copper shield for stroke currents having various times to half-value as indicated on curves, for an earth resistivity of 1000 meter-ohms.

In Fig. 4 are shown curves<sup>2</sup> from which the attenuation may be obtained for a surge-current reaching its crest value in 5 microseconds and its half-value in 65 microseconds, as shown by the curve for  $x^2/\rho = 0$ . The crest current has attenuated by 50 per cent when  $x^2/\rho = 25$  or  $x = 5\rho^{1/2}$ . Thus, for an earth resistivity of 1000 meter-ohms,  $x = 160$  meters = 525 feet when the time to half-value of the current at the stroke point is 65 microseconds, while  $x = 1050$  feet when the current at the stroke point reaches its half-value in 260 microseconds. In Fig. 5 are shown crest current

attenuation curves obtained in this manner, together with similar curves for the voltage, between the sheath and the core conductor of an ordinary cable, or between the copper shield and the lead sheath of the cable on which these observations were made.

### 1.3 Crest Values and Attenuation of Voltages

The current along the copper shield produces a voltage between this shield and the lead sheath, due to the resistance drop along the shield from the stroke point to a point sufficiently remote for the current in the shield to have become negligible. This voltage is proportional to the unit-length resistance of the copper shield. From the considerations of the preceding section, it follows that the voltage will be proportional to the square root of the earth resistivity and, if the wave-shape remains congruent but the duration of the current is changed, that it will be proportional to the square root of the duration or of the time to half-value. These two propositions follow from the fact that the voltage is proportional to the distance traveled by the current before it is attenuated to a given value.

The crest voltage between the sheath and the cable conductors of an ordinary cable, or between the copper shield and the insulated lead sheath of a cable of the type on which these observations were made, is given by the following expression for a current reaching its half-value in 65 microseconds:

$$V = 2.25 JR\rho^{1/2} \quad (6)$$

where  $V$  is in volts and  $J$  is the crest current in kiloamperes,  $R$  the resistance per mile of the outer envelope (in this case the copper shield), and  $\rho$  the earth resistivity in meter-ohms. This formula follows from expressions given in the paper referred to previously, which also contains curves from which the voltage attenuation along the cable shown in Fig. 5 may be obtained. For a resistance of .7 ohm/mile, which is that of the copper shield, and  $\rho = 1000$  meter-ohms, the crest voltage for a current of 1 ka would thus be 50 volts; and, for a crest current of 200 ka, 10,000 volts. If the dielectric strength of the thermoplastic insulation exceeds 10 kv, the liability of such cable to lightning damage would thus be small, unless the time to half-value of the current substantially exceeds 65 microseconds.

## II. EXPERIMENTAL INSTALLATION

### 2.0 General

From the preceding discussion it is seen that a lightning current dropping to half-value in some 50 to 75 microseconds, which is of the wave-shape ordinarily assumed, would attenuate to half its crest value in 500 to 1000 feet when the earth resistivity is from 1000 to 2000 meter-ohms. With

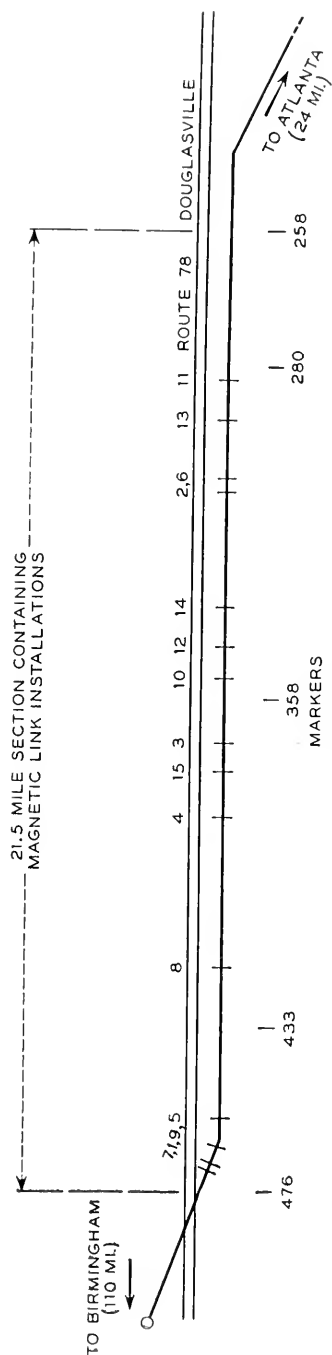


Fig. 6—Location of test section with points of 15 numbered maximum observed cable currents indicated (Table I).

test points along the cable at intervals of about 2300 feet, as employed in the observations, it should thus be possible to secure substantial indications at a number of points along the test section, although closer spacings would of course be desirable.

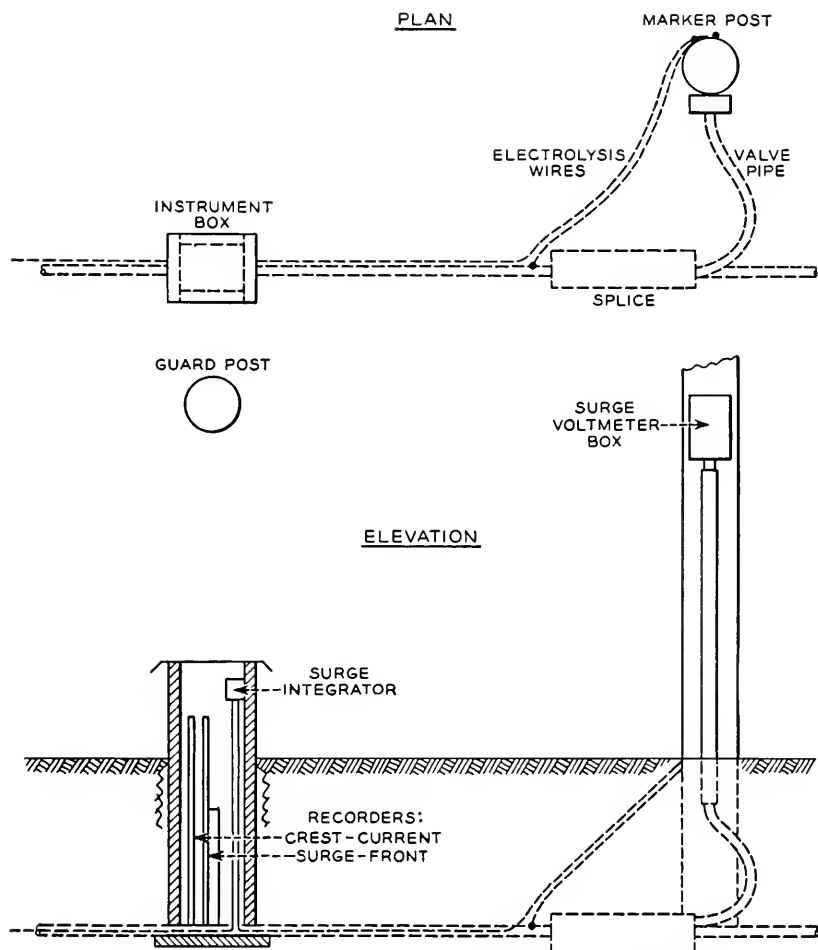


Fig. 7—Typical instrument arrangement at splice points about 2300 feet apart.

In Fig. 6 is shown the 21.5-mile test section and in Fig. 7 a typical installation at every second splice in the cable. At these points the lead sheath is accessible through a lead gas-pressure pipe extending to a marker post, an arrangement which was utilized in making measurements of voltage between the sheath and the outside copper shield. At the same points an

insulated wire is installed along the outside of the copper shield for measurement of voltage drop in the copper jacket, in connection with routine corrosion surveys. This facilitated measurements of the charge transferred along the shield by lightning currents, as described in the following. Magnetic link instruments intended to measure the steepness of the wave front were also employed, but lacked the sensitivity required for accurate measurements and are not discussed further here.

In addition to these measurements of current, charge, and voltage, involving the cable structure, observations were also made of the incidence of strokes to ground as described later in this paper.

### 2.1 Crest Current Measurements

To measure crest currents in the cable, magnetic links<sup>3</sup> were mounted at distances of 1.6, 5.7, 12.7, and 36.4 inches from the center of the cable, to cover a current range from 1 to 220 ka. The readings on these magnetic links indicated the total current in the cable, that is, the sum of the currents in the copper shield, the lead sheath, and inside cable conductors.

### 2.2 Measurements of Charge

These measurements were made by means of *surge integrators*.<sup>4</sup> In principle this instrument consists of a shunt  $R_0$  across which is connected a coil of inductance  $L$ . When a surge current  $I_0(t)$  passes through the shunt, the current  $I(t)$  in the coil is given by:

$$\begin{aligned} L \frac{dI(t)}{dt} &= R_0 I_0(t) \\ I(t) &= \frac{R_0}{L} \int_0^t I_0(t) dt \\ &= \frac{R_0}{L} Q_0(t) \end{aligned}$$

where  $Q_0(t)$  is the charge which has passed through the shunt up to the time  $t$ . By measuring the crest value  $\hat{I}$  of the current  $I(t)$ , the total charge may be obtained from the relation:

$$\hat{Q}_0 = \frac{L}{R_0} \hat{I}$$

This relation is always valid if the surge current rises to a peak value and then decays uniformly. The relation should provide a good approximation to the total charge conveyed by natural lightning strokes, even if there are small oscillations.

The shunt  $R_0$  consisted of about 26 feet of the copper shield over the cable,

which had a resistance of about 3.5 milliohms. The inductance  $L$  consisted of two coils connected in series, each containing a magnetic link. The larger of these coils had 187 turns of copper wire, the smaller 50 turns. The larger coil provided the greater sensitivity, on account of the more intense magnetization of the link. The relation between the current  $\hat{I}$  in the coil and the deflection on the magnetic link meter<sup>3</sup> used to measure the intensity of magnetization was obtained by calibration with direct current.

The inductance of the two coils in series was about 700 microhenries and the d-c resistance about .39 ohms. The time constant of the coils  $L/R$  was thus about 1800 microseconds, which is large compared to the duration of the main surge of a lightning stroke, which may last for 100 to 500 microseconds. The instrument will thus effectively integrate the main surge, but will not record the charge which may be caused by a small tail current of much longer duration.

The measurements of charge were made mainly to determine the time to half-value of the currents. The theoretical curves in Part I and elsewhere in this paper are based on a current of the form:

$$J(t) = 1.15\hat{J} (e^{-at} - e^{-bt})$$

where  $a = .013 \cdot 10^6$ ,  $b = .5 \cdot 10^6$  for a current reaching its crest value  $\hat{J}$  in about 5 microseconds and decaying to its half-value in 65 microseconds. If  $\alpha = R/L = .00056 \cdot 10^6$  for the surge integrator, the total charge recorded for a current of the above wave shape is

$$\hat{Q} = \hat{J} 1.15 \left[ \frac{1}{a + \alpha} - \frac{1}{b + \alpha} \right] = \hat{J} \cdot 83 \cdot 10^{-6}$$

for a current decaying to its half-value in 65 microseconds. The relationship between  $\hat{Q}/\hat{J}$  and the time to half-value,  $t_{1/2}$ , is as follows for currents reaching their half-values in 65, 130, 260, and 520 microseconds:

$\hat{Q}/\hat{J}$ :	83	160	295	540 microseconds
$t_{1/2}$ :	65	130	260	520 microseconds

From a curve of  $\hat{Q}/\hat{J}$  versus  $t_{1/2}$ , the time to half-value may be obtained from the observed ratio of charge to crest current. The values given later on, in Table I, were obtained in this manner. If a triangular wave shape had been assumed, the times to half-value would have been  $\hat{Q}/\hat{J}$  and therefore somewhat longer.

### 2.3 Measurements of Voltage Between Sheath and Copper Shield

These measurements were made by means of a magnetic link voltmeter consisting of a solenoid of inductance  $L$  containing the magnetic link and a

series resistance,  $R$ . When a constant voltage  $E$  is suddenly applied the current through the coil is

$$I = \frac{E}{R} (1 - e^{-(R/L)t})$$

If the time constant  $L/R$  is small in comparison with the time to crest value of a variable voltage to be measured, there will be no material delay between the crest value of the voltage and that of the current in the coil. The applied voltages may therefore be obtained by multiplying the coil current as obtained from the magnetic link reading by the series resistance, provided the latter is much greater than the impedance of the circuit to which the instrument is connected. Since the voltmeter in the present case was designed to measure the voltage between the sheath and the copper shield, and the surge impedance of this test circuit is less than 3 ohms, comparatively low values of series resistance could be used. Three separate solenoids and series resistances were used, to provide three voltage ranges, from 0 to 1.5 kv, 0 to 4 and 0 to 9 kv.

#### 2.4 Magnetic Link Calibrations

When several magnetic links, which have been exposed to the same field, are inserted in the magnetic link meter, considerable differences in the deflections may be observed due to variations in the material of the links. For this reason, all links used in this installation were placed in a magnetic field of 257 gauss and were then classified according to their response in the magnetic link meter. This field was such as to produce deflections in the most useful part of the meter range, centering around mid-scale.

By this method the magnetic links used in the installation were divided into four classes, in accordance with the ratio of the deflection observed on the magnetic link meter for the link in question to the average deflection for all links. The maximum deviation from the average in each class was about  $\pm 3$  per cent. Instruments of the same type at all installations were provided with links of the same class, to minimize inaccuracies.

#### 2.5 Observations of Incidence of Strokes to Ground

To obtain data on the incidence of strokes to ground, observations were made at one location within the test section, by means of an automatically operated magnetic wire recorder arranged to record thunder picked up by a microphone. The recorder was provided with a triggering arrangement which put it in operation on the approach of a thunderstorm, by action of the voltage induced in an antenna by lightning current. The induced voltage from a given lightning stroke was also made to record itself upon the magnetic wire; and, from the delay between this indication and the

recorded thunder, the distance to the lightning stroke could be determined upon play-back of the wire record. In this manner the number of strokes to ground within areas of various radii around the observation point could be ascertained, and thus the incidence of strokes to ground. These observations were made during the 1947 and 1948 lightning seasons.

### III. RESULTS OF OBSERVATIONS

#### 3.0 *General*

From the preceding discussion of theoretical expectations and of the experimental arrangement, it is evident that considerable attenuation would take place between the stroke point and the nearest test points on either side, for a stroke midway between the latter. Accurate evaluation of the maximum current, voltage, and charge, and of the current wave-shape, would thus be rather difficult for strokes nearly midway between test points, since these quantities would have to be evaluated by extrapolation from the observations at the points along the cable. Such extrapolation is rendered more accurate by employing the theoretical attenuation curves given in Fig. 5. This has been done for the currents, by trial and error, until the current wave-shape derived at the stroke point approximately coincided with that assumed for the attenuation curve used in the extrapolation.

These observations involving the cable structure extended over the greater part of three lightning seasons, and included a total of 108 thunderstorm days, 35 in 1946, 38 in 1947 and 35 in 1948. The average number of thunderstorm days per year as recorded by the Atlanta Weather Bureau is 49, which compares with about 60 given on the U. S. Weather Bureau map.<sup>5</sup> The more significant data are tabulated in Table I.

In the following, the observations made of currents, voltages and charges along the cable are discussed for a number of the more important strokes and compared with theoretical expectations. This is followed by a discussion of the observed incidence of cable currents of substantial magnitude and of the incidence of strokes to ground observed at one location along the route and at a second point in the northern part of the country.

#### 3.1 *Wave-Shapes and Attenuation of Currents*

In Fig. 8 is shown the distribution along the cable of the crest currents, the crest voltages, and the charges, for the most severe direct stroke measured, which had a crest value of 70 ka and a total charge of 11 coulombs. This stroke occurred to a 35-foot antenna connected to the cable and used in oscillographic observations of induced voltages due to strokes to ground, as another means of securing data on stroke currents. At this same point



TABLE I  
SUMMARY OF CURRENTS EXCEEDING 10 KA

Stroke No. *	Year	Date	Extrapolated Crest Current (Kiloamperes)	Extrapolated Max. Charge (Coulombs)	Derived Time to Half-value (Microseconds)	Shown In
1	1946	April 7	30	7	430	
2	35	June 21	20	4	170	
3	Thunder-	June 21	15	14	950	
4	storm	Aug. 3	16	3.6	190	Fig. 11
5	Days	Aug. 3	16	4	240	
6		Aug. 25	50	11.2	190	Fig. 9
7	1947	May —	20	12	580	
8	38	July 28	14	4	240	
9	Thunder-	Aug. 5	14	3.8	180	
10	storm	Aug. 18	10	6.4	620	
11	Days					
11	1948	April 19 to 23	20	8	370	
12	35	July 14	15	7.6	530	
13	Thunder-	July 28	70**	11.2	130	Fig. 8
14	storm	July 28	50	8.8	140	Fig. 10
15	Days	Aug. 4	12	12	1000	

\* For location of strokes, see Fig. 6.

\*\* Measured at stroke point.

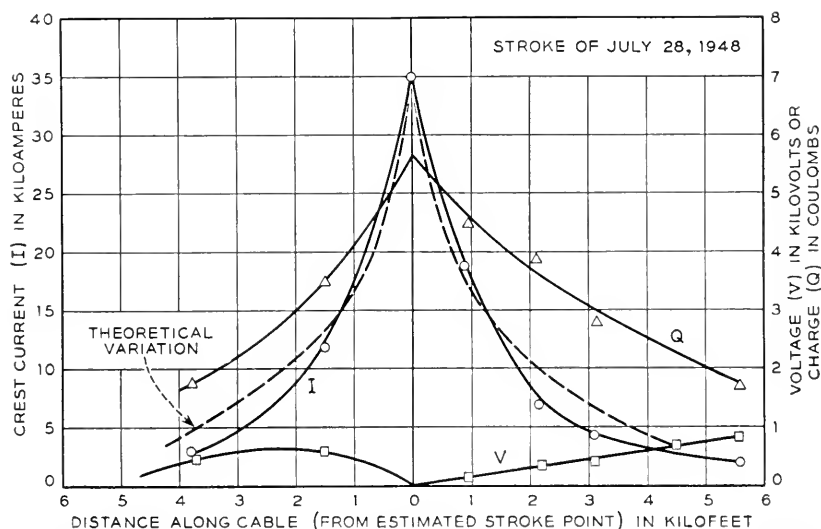


Fig. 8—Variation in crest current, voltage, and charge along cable for max. observed stroke current of 70 ka, having a time to half-value of 130 microseconds. Dashed curve shows theoretical variation of current for this time to half-value and an earth resistivity of 1200 meter-ohms. Variation in voltage between sheath and copper shield indicates breakdown between sheath and copper shield near stroke point.

simulative surge tests had been made three years before to obtain data on voltages in the cable due to surge currents, and tests had also been made of the dielectric strength of the thermoplastic insulation between the sheath and the copper shield. These latter tests disclosed low dielectric strength in the thermoplastic insulation at the location of the antenna referred to above, a defect which was repaired at the time. The voltage curve in Fig.

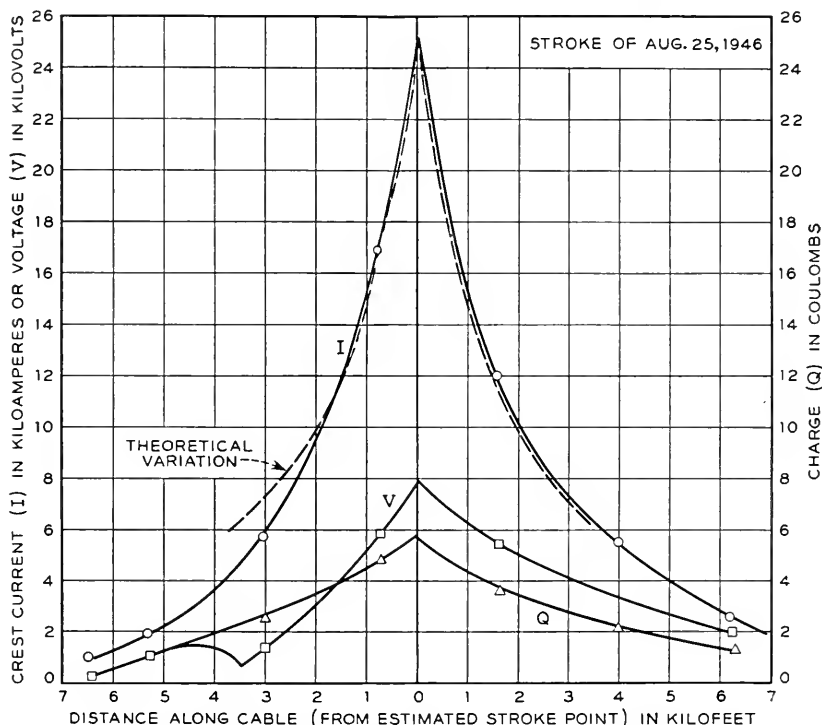


Fig. 9—Variation in crest current, voltage, and charge along cable for an extrapolated stroke current of 50 ka, having an estimated time to half-value of 190 microseconds. Dashed curve shows theoretical variation of current for this time to half-value and an earth resistivity of 1700 meter-ohms.

8 indicates that breakdown of the thermoplastic insulation occurred as a result of excessive voltage between the sheath and the copper jacket, but no other damage to the cable resulted. In Fig. 8 is also shown the theoretical variation in crest current along the cable, for a uniform earth of 1200 meter-ohms resistivity, for a stroke current reaching its half-value in 130 microseconds, as obtained from the crest current and charge at the stroke point.

In Fig. 9 are shown similar curves for an extrapolated stroke current of 50 ka and 190 microseconds to half-value, together with the theoretical

attenuation curve for the current for 1700 meter-ohms, which appears to provide a fairly satisfactory check on the extrapolation. The maximum observed voltage obtained by extrapolation is about 8 kv, which compares with 5.6 calculated as outlined in Section 1.3. The higher observed voltage may be due to a long duration tail current of small value, which may increase the voltage appreciably because of its slow rate of attenuation along the cable.

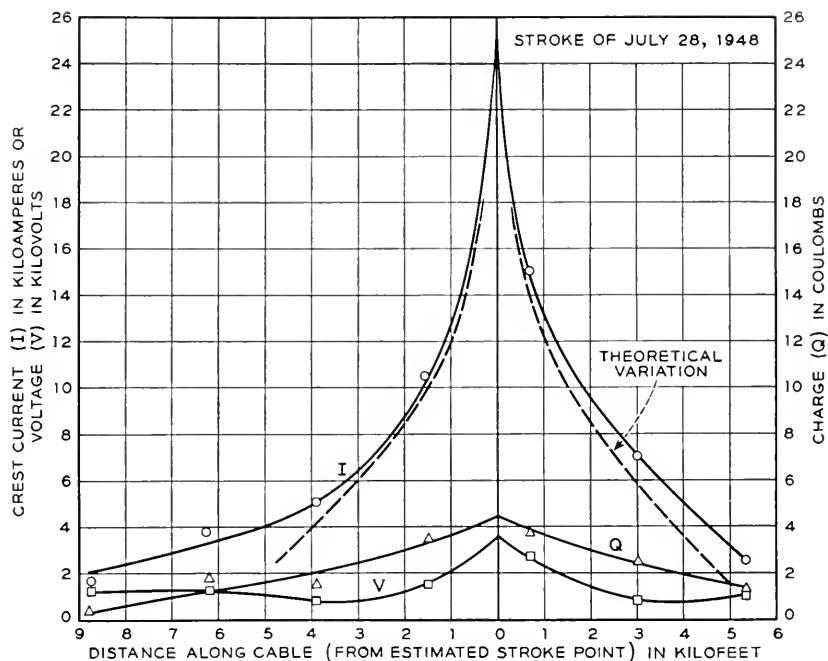


Fig. 10—Variation in crest current, voltage, and charge along cable for an extrapolated stroke current of 50 ka, having a time to half-value of 140 microseconds. Dashed curve shows theoretical variation of current for an earth resistivity of 1200 meter-ohms.

In Fig. 10 are shown similar curves for an extrapolated stroke current of 50 ka, reaching its half-value in 140 microseconds, together with theoretical attenuation curve for the current, for an earth resistivity of 1200 meter-ohms. The maximum extrapolated voltage is in this case about 3.5 kv, as compared with 4.1 calculated for 1200 meter-ohms.

The curves in Fig. 11 are for a fairly low extrapolated current, 16 ka, reaching its half-value in 190 microseconds. Again satisfactory agreement between observed and calculated attenuation is obtained. The maximum observed voltage of 1.5 kv in this case agrees with that calculated for an earth resistivity of 1200 meter-ohms.

Some of the other observations, not reproduced here, were less consistent than those shown, probably due to the combined effects of more than one stroke; but they permitted fairly satisfactory determinations of crest currents and times to half-value.

From Table I it appears that the minimum duration to half-value is about 130 microseconds, the maximum about 1000 and that the average for the three most severe strokes is about 150 microseconds. In general the duration appears to be longer the lower the crest currents, the average for currents of 20 ka and less being about 500 microseconds to half-value.

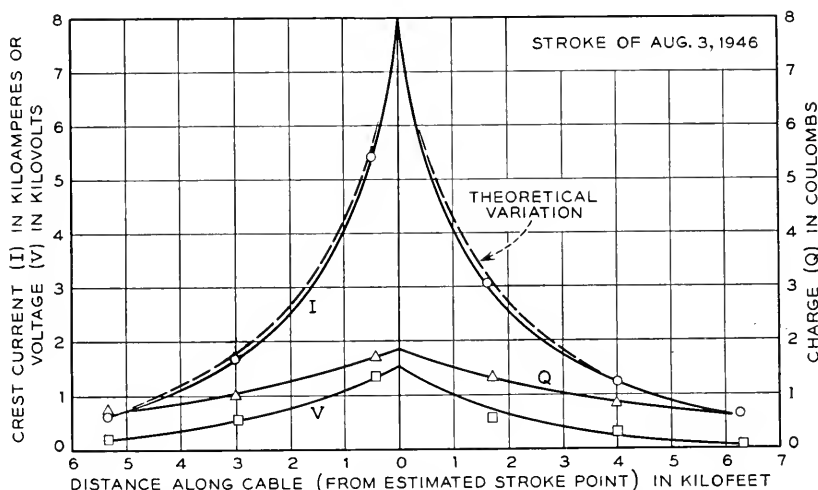


Fig. 11—Variation in crest current, voltage, and charge along cable for an extrapolated stroke current of 16 ka, having a time to half-value of 190 microseconds. Dashed curve shows theoretical variation of current for this time to half-value and an earth resistivity of 1200 meter-ohms.

In the above derivations a simple wave-shape was assumed, although actually it is likely to be rather complex with many fluctuations. The use of an equivalent simple wave-shape is, however, permissible in evaluating the liability to lightning damage, since statistical results rather than the wave-shapes of individual currents are of main importance.

Regarding the cause for the long duration of the currents, it appears to be inherent in meteorological rather than geological conditions, as for the wave-shapes of lightning currents in general. The significance of meteorological conditions is also indicated by the observations discussed in Section 3.3. In the case of strokes to the cable, the latter provides a path of very low impedance compared to that of the lightning channel, so that the wave-shape is determined by the impedance of the lightning channel and the distribution of charge along the leader and in the cloud. This is also true

for strokes to ground not arcing to the cable, at least during the time required for the tip of the channel to propagate from the earth towards the cloud, which may be of the order of 50 to 100 microseconds, depending on the height of the cloud. During this interval ionization of the soil around the base of the channel provides a path in the earth of low impedance compared to that of the channel, as shown in the paper referred to previously. It is possible of course that, during later stages of the discharge, the resistivity of the earth to some extent may limit the current, as the impedance of the completely ionized channel will then be lower and that in the earth higher because of the lower current in the earth with resultant decrease in ionization. This, however, would tend to reduce the current and thereby decrease rather than increase the time to half-value, and at the same time it would tend to cause a long duration tail current of low magnitude.

### 3.2 *Incidence of Cable Currents of Various Crest Values*

In Fig. 12 is shown the number of observed currents exceeding various crest values, together with curves of the crest current distribution expected on the basis of the theoretical curves given in Fig. 2. The latter curves, together with those in Fig. 3, are based on an incidence of strokes to ground of 2.4 per square mile for 10 thunderstorm days, a value derived from the rate of strokes to transmission line ground structures, as outlined in the paper referred to previously. Although the observations appear to be in fairly satisfactory agreement with theoretical expectations, a total of 15 currents is hardly sufficient as a check of the theoretical curves, particularly since the latter presume a uniform earth structure.

The intersections of the theoretical curves (Fig. 12) with the axis of abscissae indicate that from five to seven of the currents were due to direct strokes. Actually, visual evidence of direct strokes was found in but two cases, in which the strokes occurred to and damaged test equipment. This does not preclude the possibility of additional direct strokes, as evidence thereof in the absence of cable damage may easily escape detection.

### 3.3 *Incidence of Strokes to Ground*

In Fig. 13 is shown the incidence of strokes to ground observed during 1947 and 1948 from one point within the test section, by the method described in Section 2.5. In the same figure are shown the results of similar observations by the same method, made at one location in New Jersey during 1948 for purposes of comparison. Published data obtained from direct visual and aural observations at one locality in Massachusetts<sup>6</sup> are also shown in the same figure.

As shown by the curves in Fig. 13, the observed or apparent incidence of strokes to ground diminishes as the radius of the observation area increases,

for the reason that more of the remote than of the near strokes of low intensity escape observation. To find the actual incidence, a curve of the apparent incidence versus the radius of the observation area may be extrapolated to an area of zero radius. On account of the comparatively few observations for small radii, however, such extrapolation is rather inaccurate.

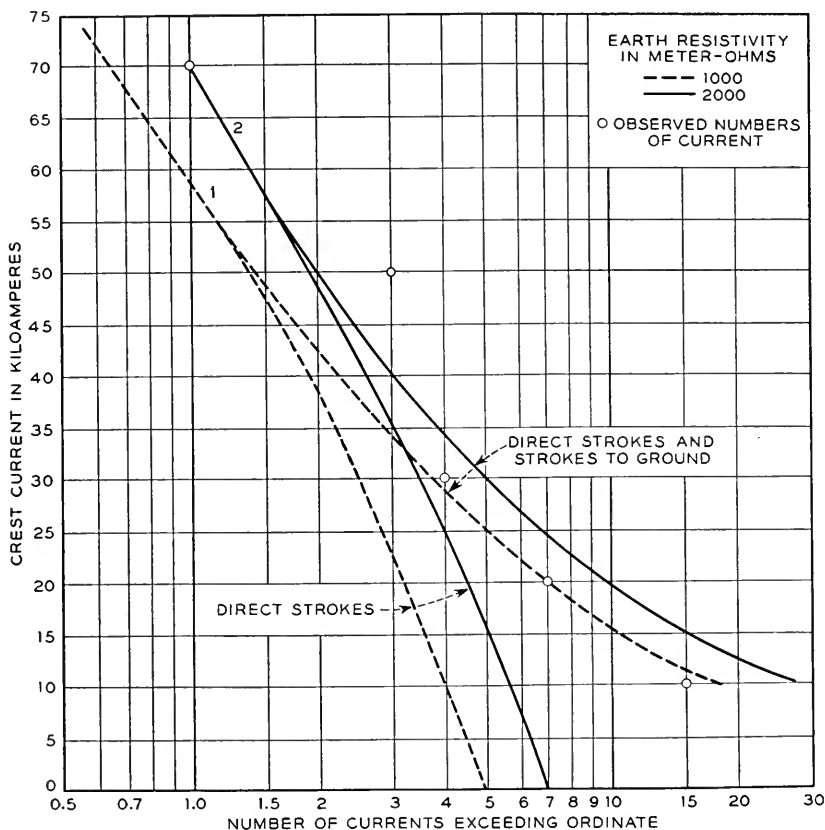


Fig. 12—Comparison between observed and theoretically expected number of currents exceeding given crest values during 108 thunderstorm days in a 21.5-mile section.

rate. Improved accuracy is obtained by using theoretical expectancy curves in the extrapolation as indicated by the curves in the figure. These curves are derived on the assumption that the proportion of currents exceeding a given crest value  $I$  is given by  $P(I) = e^{-kI}$  where  $k$  is a constant—a relation in substantial agreement with observations<sup>1</sup>—and that the energy in the electromagnetic wave from the stroke current, as well as that in the sound wave due to the thunder, is proportional to  $I^2/r^2$ , where  $r$

is the distance to the stroke. If the trigger arrangement in the apparatus mentioned in Section 2.5 is sufficiently sensitive to be operated by strokes so remote that the thunder cannot be distinguished above noise on the wire record, then the energy in the sound wave would be controlling, in the sense that it would determine the making of a usable record. On the other hand if the triggering should occur only for strokes of such substantial intensity

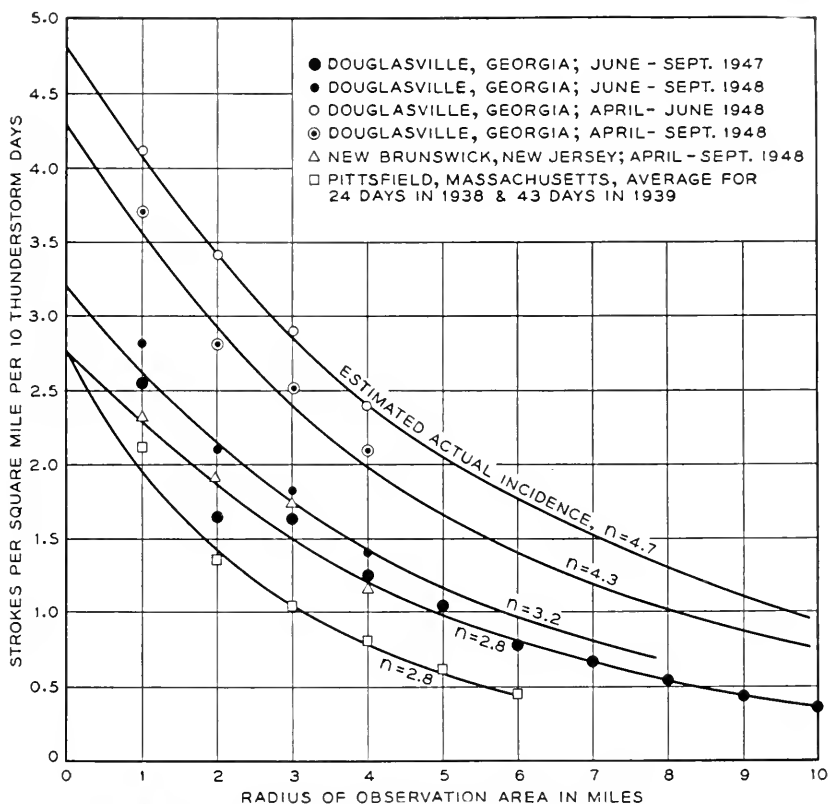


Fig. 13.—Apparent incidence of strokes to ground, per square mile per ten thunder storm days, as a function of radius of observation area.

that some of the more remote strokes of low intensity would not be recorded, then the energy in the electromagnetic wave would be controlling. Similarly, in the case of direct visual-aural observation, the light radiation from the stroke may be assumed proportional to  $I^2/r^2$ . If, for any of these methods the energy density is taken as  $u = cI^2/r^2$  where  $c$  is a constant and the minimum energy required for observation is  $u_0$ , then only stroke currents in excess of  $I = (u_0/c)^{1/2}r$  would be observed. The observed or

apparent number of strokes to ground within an area of radius  $r$  would then be, for an actual incidence  $n$  of strokes to ground and with  $P(I) = e^{-kI}$ :

$$\begin{aligned} N_a &= 2\pi n \int_0^r r e^{-\alpha r} dr \\ &= \frac{2\pi n}{\alpha^2} [1 - e^{-\alpha r} (1 + \alpha r)] \end{aligned}$$

where  $\alpha = k(u_0/c)^{1/2}$ .

The apparent incidence of strokes to ground  $n_a = N_a/\pi r^2$  is accordingly

$$n_a = \frac{2n}{(\alpha r)^2} [1 - e^{-\alpha r} (1 + \alpha r)]$$

By choice of a proper value of  $\alpha$  in the latter expression a theoretical curve, varying in substantially the same manner with  $r$  as a given observed curve, may be obtained. The actual incidence is next obtained by taking a value of  $n$  such that the two curves substantially coincide. This value of  $n$  also corresponds to the incidence given by the theoretical curve for  $r = 0$ , i.e. the value that would be expected if a sufficient number of observations were available for small values of  $r$  to permit extrapolation of the observed curves to  $r = 0$ . The value of  $n$  obtained in the above manner is about 2.8 for the New Jersey and Massachusetts and 1947 Georgia observations. The latter extended over the last half of the lightning season, while the 1948 Georgia observations, which indicate a higher incidence, extended over the entire season. The comparison, shown in the figure, between the observations in Georgia during the first and second halves of the 1948 season, indicates that the incidence during the first half is about 50 per cent greater than during the second half. A similar comparison of the New Jersey observations, not shown in the figure, indicates the opposite trend, i.e. a somewhat smaller incidence during the first half. The difference, however, is less marked than in the Georgia case.

There is reason to believe that this change in Georgia with the advance of the season is due to a change in the character of the lightning storms. During several years the more severe lightning damage on cable routes in this territory has occurred during early-season thunderstorms, which ordinarily are of the "frontal" type extending over fairly wide areas where hot and cold masses of air come together. These storms appear to be of greater extent, duration, and severity than the "convection" type of storm, ordinarily experienced later in the season, which occur more frequently as the result of local air convection currents but are of more limited extent and duration than storms of the frontal type.<sup>7</sup>



As mentioned before, the theoretical expectancy of lightning damage and of strokes to the cable discussed in this paper has been based on an incidence of 2.4 strokes per square mile for 10 thunderstorm days, a value derived from magnetic link observations of the rate of stroke occurrence to the aerial supporting structures of transmission lines, on the assumptions that they attract lightning strokes in accordance with laws established from laboratory observations on small-scale models, and that the average height of the ground wires is 70 feet above the earth or adjacent trees.<sup>1</sup> If this height had been taken as 60 feet instead the incidence would have been 2.8, in substantial agreement with that obtained from our observations for northern territory—in the main the territory traversed by the transmission lines from which the data were obtained.

The curves shown in Fig. 13 include substantial areas and a rather large amount of data and should, therefore, be fairly representative. Thus a radius of four miles corresponds to an observation area of 50 square miles. Within this area a total of 342 strokes was recorded during 1948 at the observation point in the test section near Atlanta. One of the storms during this period, in which the antenna was struck, passed directly over the observation point and provided a considerable amount of the data. However, even if the observations during this storm were omitted, the total for the season would have been reduced by less than 10 per cent, while the observations during July, August, and September would have been reduced about 20 per cent and would have been slightly lower than in the same 1947 period. The data thus indicate that the yearly incidence per square mile of strokes to ground is about 2.8 per 10 thunderstorm days in northern parts of the country, but may be as high as 4.3 in those southern parts where more severe types of thunderstorms occur. Considering, however, both the 1947 and 1948 observations in Georgia, it appears that an incidence of 3.7 would be a reasonable expectation for an entire season. With this incidence, rather than 2.4 as assumed in Fig. 12, Curves 1 and 2 in that figure would approximately correspond to earth resistivities of 500 and 1000 meter-ohms, respectively.

### CONCLUSIONS

The observations indicate that the duration of lightning currents in the southern territory under observation is substantially longer than the average ordinarily assumed. The time to half-value of intense currents, which are of main importance as regards liability to lightning damage, is of the order of 150 microseconds, and for lower currents even larger. This, together with the higher incidence of strokes to ground and the high earth resistivity, would appear to account for the high rate of lightning damage experienced in this territory in cables of earlier design than the copper-

jacketed cable upon which measurements were made. The incidence of cable currents of various intensities, their rate of attenuation, and the resultant voltages appear to be in satisfactory agreement with theoretical expectations.

#### ACKNOWLEDGEMENTS

The field observations were made possible by the cooperation of the Long Lines Department of the A. T. and T. Company, and the Southern Bell Telephone and Telegraph Company, both in the installation and the operation of the equipment. The observations were conducted by our associate Mr. D. W. Bodle, who was also responsible for the design of the automatic recording equipment used to measure the rate of strokes to ground, and who suggested, from some of the observations discussed here, the greater intensity of early-season storms.

#### REFERENCES

1. E. D. Sunde: "Lightning Protection of Buried Toll Cable," *B. S. T. J.*, Vol. 24, April 1945.
2. E. D. Sunde: "Earth Conduction Effects in Transmission Systems," D. Van Nostrand Company, Inc., New York, London, Toronto, 1949.
3. C. M. Foust and H. P. Kuehni: "The Surge-crest Ammeter," *General Electric Review*, Vol. 35, December 1932.
4. C. F. Wagner and G. D. McCann: "New Instruments for Recording Lightning Currents," *Trans. A. I. E. E.*, Vol. 58, 1939.
5. W. H. Alexander: "The Distribution of Thunderstorms in the United States—1904–1933"—*Monthly Weather Review*, Vol. 63, 1935.
6. J. H. Hagenguth: "Photographic Study of Lightning," *Trans. A. I. E. E.*, Vol. 66, 1947.
7. F. A. Berry, E. Bollay and N. R. Beers: "Handbook of Meteorology," McGraw-Hill Book Company, Inc., New York and London, 1945.

## The Electrostatic Field in Vacuum Tubes With Arbitrarily Spaced Elements

By W. R. BENNETT and L. C. PETERSON

VACUUM tubes with close spacing between electrodes have become of increasing importance in recent years. The higher transconductances and lower electron transit times thus obtained combine with other features to raise both the frequency and band width at which the tube may operate satisfactorily as an amplifier. Specific designs have been discussed in papers by E. D. McArthur and E. F. Peterson<sup>1</sup>, and by Fremlin, Hall and Shatford<sup>2</sup>. The important contributions to structural technique made by E. V. Neher have been described in the Radiation Laboratory Series<sup>3</sup>. Further important advances in the art have been recently announced by J. A. Morton and R. M. Ryder of the Bell Laboratories at the recent I.R.E. Electronics Conference held at Cornell University in June, 1948. The material of the present paper represents work done by the authors over a decade ago, and naturally there has been considerable publication on related topics in the intervening years. It has been suggested by our colleagues, however, that some of the results are not available in the technical literature and are of sufficient utility to warrant a belated publication. These results have to do with the variation of the electric intensity, amplification factor, and current density which takes place along the cathode surface because of the nearby grid wires.

We shall deal mainly with the approximate solution which neglects the effect of space charge. The correction required to take account of space charge is in general relatively small as shown by both qualitative argument and experimental data in an early paper by R. W. King<sup>15</sup>. More recent theoretical work<sup>19</sup> extending into the high frequency realm has confirmed the minor nature of the modification needed. The problem is thereby reduced to one of finding solutions of Laplace's equation which reduce to constant values on the cathode, grid, and anode surfaces. The original work on this problem was done by Maxwell<sup>4</sup> who calculated the electrostatic screening effect of a wire grating between conducting planes long before the vacuum tube was invented. All subsequent work has followed the methods outlined by Maxwell. In particular he suggested the replacement of the conducting planes by an infinite series of images of the grid wires and described an appropriate solution in series for the case of finite size wires. The useful approximation obtained when the diameter of the grid wires is

assumed small compared to their spacing was discussed in detail only for the case of large distances between the grating and each of the conducting planes.

Figure 1 shows the assumed geometry of the grid, anode, and cathode. End effects are neglected. The origin is taken at the center of one of the grid wires which have radius  $c$ , and the  $X$ -axis is along the grid plane. The spacing of the wires between centers is  $a$ , the distance from grid to anode is  $d_2$ , and that from grid to cathode is  $d_1$ . No restrictions are placed on the sizes of  $a$ ,  $d_2$ , and  $d_1$ . Above the anode and below the cathode is shown a doubly infinite set of images which may be inserted to replace the conducting planes of the anode and cathode. By symmetry the potential from the

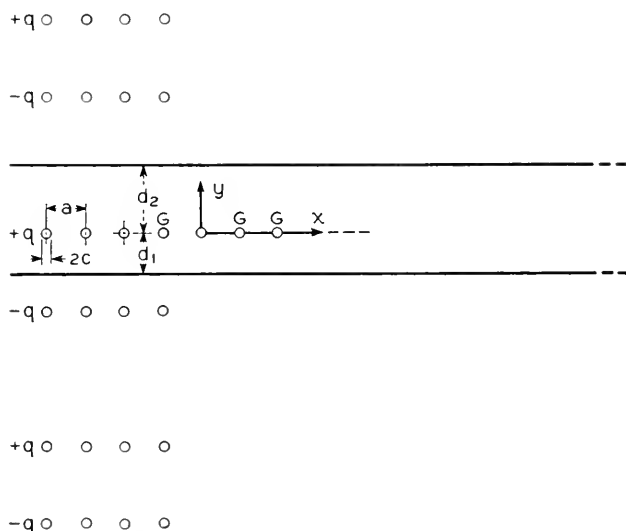


Fig. 1—Array of images for production of equipotential surfaces in planar triode.

array of charges there shown must be constant for all  $x$  when  $y = d_2$  and also for all  $x$  when  $y = -d_1$ . The double periodicity of the array suggests immediately an application of elliptic functions. The solution of the symmetrical case was actually stated in terms of the elliptic function  $\text{sn } z$  by F. Noether<sup>5</sup>. The extension to the non-symmetrical case shown in Fig. 2 is fairly obvious. One of the authors worked out such a solution in terms of Jacobi's Theta functions in 1935, but abandoned any plans for publishing his analysis in view of the excellent treatment appearing shortly after that time in the Proceedings of the Royal Society by Rosenhead and Daymond<sup>6</sup>, who applied Theta functions to both tetrodes and triodes, and both cylindrical and planar tube structures for the case of fine grid wires. Some of their formulas were later included in a book by Strutt<sup>7</sup>. Methods of calculating

the case of thick grid wires in terms of expansions in series of elliptic functions were discussed by Knight, Howland and McMullen<sup>8-10</sup>. The problem of a finite number of grid wires was treated by Barkas<sup>11</sup>. More recently tubes with close spacing between grid and cathode, but with anode and grid assumed far apart, have been analyzed in terms of elementary functions by

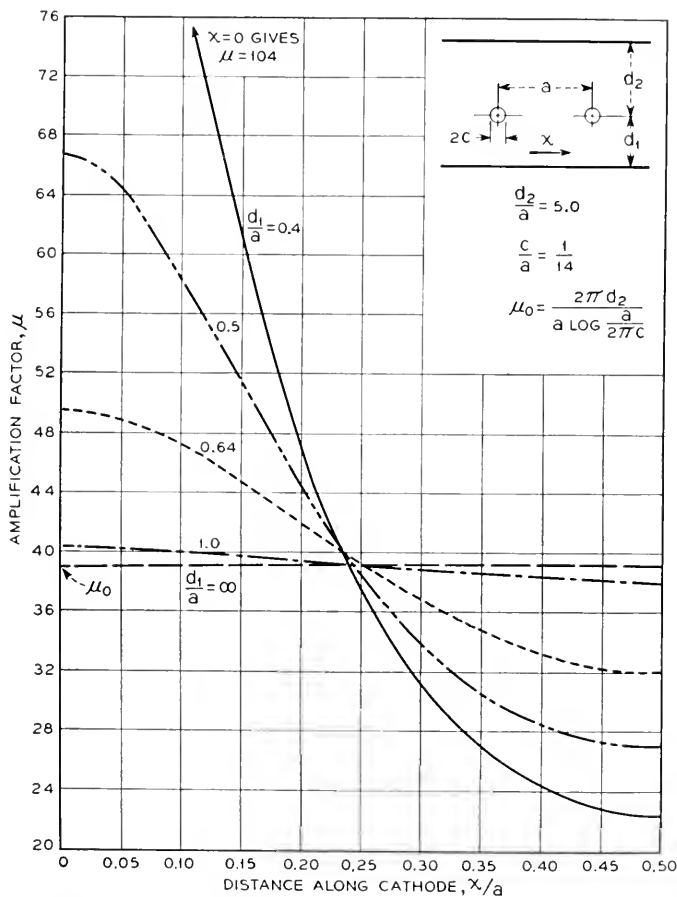


Fig. 2—Variation of amplification factor along the cathode surface of a triode.

Fremlin<sup>12</sup>. A solution based on the Schwartz-Christoffel transformation has been given by Herne<sup>13</sup> for the case of grid wires of finite size and approximately circular in shape.

Since the derivations have been adequately covered in the references cited, we merely state the final formula here and indicate how it may be verified as correct. Let  $V(x, y)$  represent the potential function corresponding to

Fig. 1, the planar triode with fine grid wires. The potential of the cathode is set equal to zero. Then in the space between anode and cathode,

$$AV(x, y) = [2\pi d_2(y - d_2)/a + (d_1 + d_2)f(x, y)]V_g + [B(y + d_1) - 2\pi d_2 y/a - d_1 f(x, y)]V_p, \quad (1)$$

where

$$f(x, y) = \ell n \left| \frac{\vartheta_1[\pi(x + iy - 2i d_2)/a]}{\vartheta_1[\pi(x + iy)/a]} \right| \quad (2)$$

$$A = (d_1 + d_2)B - 2\pi d_2^2/a \quad (3)$$

$$B = \ell n \left| \frac{a\vartheta_1(2\pi i d_2/a)}{\pi i \vartheta_1'(0)} \right| \quad (4)$$

Here we have used Jacobi's notation for the  $\vartheta_1$ -function, as explained by Whittaker and Watson<sup>14</sup>, rather than the Tannery-Molk notation used by Rosenhead and Daymond. We write  $\vartheta_1(\pi z)$  for their  $\vartheta_1(z)$ . In our notation

$$\vartheta_1(z) = 2 \sum_{n=0}^{\infty} (-)^n e^{i(n+1/2)2\tau} \sin(2n+1)z \quad (5)$$

where the parameter  $\tau$  in the above formulas is given by:

$$\tau = 2i(d_1 + d_2)/a \quad (6)$$

By  $\vartheta_1'(z)$  is meant the derivative with respect to  $z$ :

$$\vartheta_1'(z) = 2 \sum_{n=0}^{\infty} (-)^n (2n+1) e^{i(n+1/2)2\tau} \cos(2n+1)z \quad (7)$$

Verification of the solution is straightforward. The resulting  $V(x, y)$  is seen to be the real part of a function which is analytic in the complex variable  $x + iy$  except for logarithmic singularities at the points where the Theta functions vanish. Hence  $V(x, y)$  satisfies Laplace's equation in two dimensions in the region excluding the singular points. Since the zeros of  $\vartheta_1(z)$  occur at  $z = m\pi + n\pi\tau$ , where  $m$  and  $n$  take on all positive and negative values as well as zero, the singular points of the solution are at

$$\left. \begin{aligned} x + iy &= ma + 2in(d_1 + d_2) - 2id_2 \\ \text{and} \quad x + iy &= ma + 2in(d_1 + d_2) \end{aligned} \right\} \quad (8)$$

which coincide with the centers of the image circles of Fig. 1. The logarithmic singularities represent line charges with the first set arising from a  $\vartheta_1$ -function in the numerator, yielding a positive charge, and the second set from the  $\vartheta_1$ -function in the denominator giving a negative sign. The equipotential curves are approximately circular in the neighborhood of the

charges and hence  $V(x, y)$  gives a constant potential on the surface of each grid wire if the radius of the grid wire is small compared with the spacing.

We may show by direct substitution that  $V(x, y)$  becomes equal to  $V_p$  at all points of the anode and equal to zero at all points of the cathode. On the anode we have  $y = d_2$  which, when substituted in the expression for  $f(x, y)$ , gives the logarithm of the absolute value of the ratio of conjugate complex quantities, and hence

$$f(x, d_2) = 0$$

Substituting in (1), we then readily verify that  $V(x, d_2) = V_p$ . On the cathode we make use of the quasi-periodicity of the  $\vartheta_1$ -function, as expressed by

$$\vartheta_1(z) = -e^{i(\pi\tau+2z)} \vartheta_1(z + \pi\tau), \quad (9)$$

to prove

$$f(x, -d_1) = \frac{2\pi d_2}{a}, \quad (10)$$

from which it follows that  $V(x, -d_1) = 0$ . To show that all grid wires are at the same potential, we make use of the other periodicity of the  $\vartheta_1$ -function,

$$\vartheta_1(z + \pi) = -\vartheta_1(z), \quad (11)$$

which shows that

$$f(x \pm ma, y) = f(x, y), \quad m = 0, 1, 2, \dots \quad (12)$$

It remains to prove that  $V$  actually approaches the value  $V_\theta$  in the neighborhood of the typical wire, which may be taken at the origin since the solution repeats periodically with the wire spacing. We let

$$x + iy = ce^{i\theta} \quad (13)$$

and assume  $c/a \ll 1$ . Expanding in power series in  $c/a$ , we find that the first order terms are included in:

$$f(c \cos \theta, c \sin \theta) = \ln \left| \frac{\vartheta_1(-2\pi i d_2/a)}{\vartheta_1'(0) \pi c e^{i\theta/a}} \right| = B \quad (14)$$

The sign of the argument of the  $\vartheta_1$ -function in the numerator is of no consequence since it does not affect the absolute value. Substituting back in (1), we then find

$$\lim_{c/a \rightarrow 0} V(c \cos \theta, c \sin \theta) = V_\theta \quad (15)$$

The solution is thus completely established.

The quantities in which we are specifically interested are electric field, amplification factor, and current density. The electric field is equal to the negative gradient of the potential function. The amplification factor is found by taking the ratio of partial derivatives of the electric field at the cathode with respect to grid and anode voltages. The current density may then be studied for any assumed operating values of grid and plate voltages.

To calculate the gradient we note that since  $V(x, y)$  is the real part of an analytic function  $W(z) = V + iU$ , it follows from the Cauchy-Riemann equations,

$$W'(z) = \frac{\partial V}{\partial x} - i \frac{\partial V}{\partial y} = -E_x + iE_y \quad (16)$$

where  $E_x$  and  $E_y$  are the  $x$ - and  $y$ - components of the electric intensity. From (1),

$$AW(z) = [(d_1 + d_2) F(z) - 2\pi d_2(iz + d_2/a)]V_g + [B(d_1 - iz) + 2\pi i d_2 z/a - d_1 F(z)]V_p \quad (17)$$

where

$$F(z) = \ell n \frac{\partial_1 [\pi(z - 2i d_2)/a]}{\partial_1(\pi z/a)} \quad (18)$$

Calculating the derivative and making use of the relation,

$$\frac{\partial'_1(z - \pi\tau)}{\partial_1(z - \pi\tau)} = \frac{\partial'_1(z)}{\partial_1(z)} + 2i, \quad (19)$$

we find at the cathode surface

$$F'(x - i d_1) = \frac{2\pi i}{a} [1 + C(x)] \quad (20)$$

where

$$C(x) = Im \frac{\partial'_1 [\pi(x + i d_1)/a]}{\partial_1 [\pi(x + i d_1)/a]} \quad (21)$$

It follows that when  $y = -d_1$ , we must have  $E_x = 0$  and

$$aAE_y/2\pi = [d_1 + (d_1 + d_2)C(x)]V_g + [d_2 - d_1 - aB/2\pi - d_1 C(x)]V_p \quad (22)$$

The amplification factor is then given by

$$\mu = \frac{\partial E_y / \partial V_g}{\partial E_y / \partial V_p} = \frac{d_1 + (d_1 + d_2)C(x)}{d_2 - d_1 - aB/2\pi - d_1 C(x)} \quad (23)$$

Numerical calculation from these formulas can be made by means of (5) and (6). When  $d_1$  and  $d_2$  are both large compared with unity, Eq. (23)



reduces to the familiar approximate formula derived, for example, in an early paper by R. W. King<sup>15</sup>,

$$\mu \doteq \frac{2\pi d_2}{a \ln \frac{a}{2\pi c}}, \quad (23a)$$

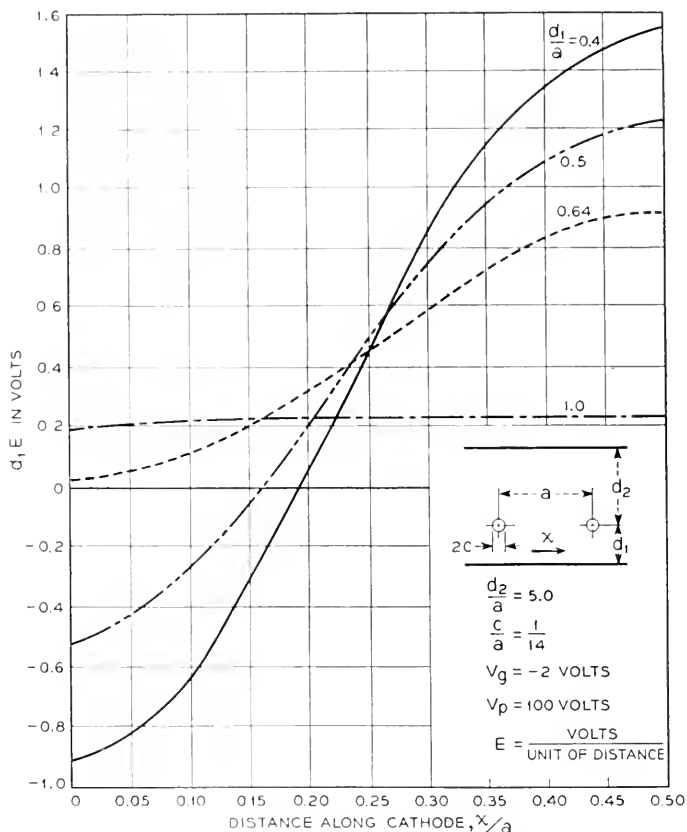


Fig. 3—Variation of cathode field strength in a triode.

Some calculated curves for  $\mu$  and  $E_\theta$  are shown in Figs. 2 and 3. Figure 2 shows the amplification factor as a function of the distance along the cathode with the ratio of grid-cathode separation to grid wire spacing as a parameter. The ratio of grid-anode separation to grid wire spacing is held constant at five. Only half the grid spacing interval is included since the curves are symmetrical. The increase in  $\mu$ -variation as the grid-cathode separation becomes small is clearly demonstrated. For negligible  $\mu$ -variation we must select  $d_1/a$  of the order of 2 or greater.

Figure 3 shows the variation in field strength along the cathode for the typical operating point,  $V_g = -2$  and  $V_p = 100$  volts. It is to be noted that for  $d_1/a$  less than 0.6, the electric field actually changes sign as we move from a point immediately below a grid wire to the midpoint between two grid wires. In other words a part of the cathode will not emit at all in these cases while the remainder emits in a non-uniform manner. In the rather extreme case of  $d_1/a = 0.4$  only about a quarter of the cathode is emitting. It is worth noting how relatively rapid the "shadow" or "island" formation increases between  $d_1/a = 0.64$  and 0.5 as compared to the increase in the interval from 0.5 to 0.4.

If the equation for  $\mu$  is solved for  $C(x)$  and the result substituted back in the expression for  $E_y$  at the cathode we find:

$$-E_y = \frac{V_g + V_p/\mu}{d_1 + (d_1 + d_2)/\mu} \quad (24)$$

where here of course  $\mu$  varies with  $x$ . This is identical with the expression derived by Benham<sup>16</sup> from Maxwell's approximate solution except that in the latter case  $\mu$  was a constant. Our colleague, Mr. L. R. Walker, has pointed out that the equation follows directly from the assumption of small grid wires without explicit solution for the potential function. Since the charge density  $\sigma_c$  on the cathode is proportional to the field strength (the factor of proportionality in MKS units is the dielectric constant  $\epsilon$  of vacuum or  $9.854 \times 10^{-12}$  farads/meter), Maxwell's capacity coefficients  $C_{gc}$  and  $C_{pc}$  may be calculated from

$$\sigma_c = \epsilon E_y = -(C_{gc}V_g + C_{pc}V_p) \quad (25)$$

The minus sign is used here because we are taking the ratio of charge to voltage at the negative plate of the condenser consisting of cathode, grid and anode surfaces. Hence

$$C_{gc} = \frac{\epsilon}{d_1 + (d_1 + d_2)/\mu} \quad (26)$$

$$C_{pc} = \frac{\epsilon/\mu}{d_1 + (d_1 + d_2)/\mu} \quad (27)$$

Since  $\mu$  is variable, an integration is required to determine the total capacitance. From the periodicity of  $\mu$  with grid spacing it is possible to express the result in terms of the average values of  $C_{gc}$  and  $C_{pc}$  over an interval of length  $a$  along a direction parallel to the grid plane and multiply these values by the total area of cathode surface.

Equation (24) may be interpreted in a number of different ways of which we shall mention the following two:

1. The "equivalent voltage"  $V_\theta + V_p/\mu$  does not act at the grid but at a distance  $D$  from the cathode, where

$$D = d_1 + (d_1 + d_2)/\mu \quad (28)$$

Both the equivalent voltage and distance vary along the cathode surface.

2. The "equivalent voltage"

$$V_e = (V_\theta + V_p/\mu)/[1 + (1 + d_2/d_1)/\mu] \quad (29)$$

acts in the grid plane and varies with distance along the cathode surface.

As far as the cold tube is concerned the two formulas are equivalent at the cathode, but not at the grid. When the tube is heated and complete space charge is present, the two formulas also differ at the cathode. The current density in the presence of space charge is, according to (28) and Child's law:

$$I = K(V_\theta + V_p/\mu)^{3/2}/D^2 \quad (30)$$

while, from (29),

$$I = KV_e^{3/2}/d_1^2 \quad (31)$$

In both,  $K^2 = 32 e^2/81 m$ , where  $e/m$  is the ratio of electronic charge to mass. The value of current given by (31) is  $[1 + (1 + d_2/d_1)/\mu]^{1/2}$  times as large as that given by (30). If  $\mu \gg 1 + d_2/d_1$  the two values are nearly the same. In tubes with close grid-to-cathode spacing the inequality may not be fulfilled. As to which viewpoint is more accurate, we note that Ferris and North in their papers<sup>17, 18</sup> on input loading adopted the latter, and that at high frequencies where electron transit time must be considered the second viewpoint is preferable because of the more accurate representation of effects at the grid. For a more complete discussion see Reference 19. Figure 4 shows curves of relative current density as a function of distance along the cathode as computed from Eq. (31). The transconductance for unit area of cathode surface as computed from the same equation is given by:

$$\begin{aligned} d_1^2 g_{mo} &= d_1^2 \frac{\partial I}{\partial V_\theta} = \frac{2}{3} \epsilon \sqrt{\frac{2e}{m} \left( V_\theta + \frac{V_p}{\mu} \right) \left( \frac{d_1}{D} \right)^3} \\ &= 3.512(V_\theta + V_p/\mu)^{1/2} (d_1/D)^{3/2} \text{ micromhos.} \end{aligned} \quad (32)$$

The resulting variation with distance along the cathode is shown in Fig. 5.

Defining the figure of merit  $M$  at a point  $x$  along the cathode as the ratio

between the transconductance  $\partial I/\partial V_g$  and the sum of  $C_{gc}$  and  $C_{pc}$  at this point, we find from (30)

$$M = (4J/3)^{1/3} [d_1 + (d_1 + d_2)/\mu]^{-1/3} \mu/(\mu + 1) \quad (33)$$

where  $J = eI/m\epsilon$ ,  $e/m = 1.77 \times 10^{11}$  coulombs/kg. From (31), we find on the other hand

$$M = (4J/3 d_1)^{1/3} \mu/(\mu + 1) \quad (34)$$

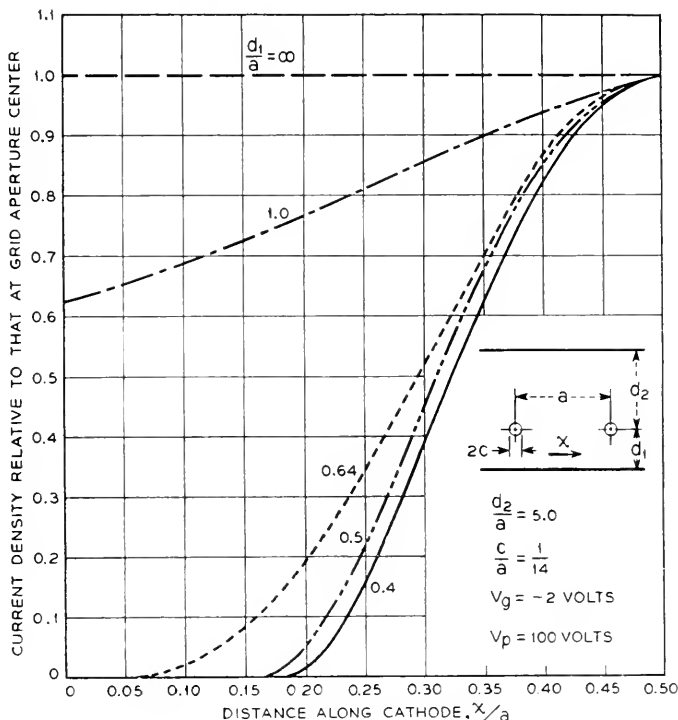


Fig. 4—Variation of current density in a triode.

Both formulas indicate that for a cathode capable of supplying a given current density the only means of improvement lies in decreasing the cathode-grid spacing. The improvement is extremely slow; doubling the figure of merit requires an eight-fold decrease in spacing.

We again emphasize that the calculated current densities and figures of merit are functions of  $x$ , the distance along the cathode. The total current between the two grid wires is found from (30) to be

$$I_T = 2K \int_{x_0}^{a/2} (V_g + V_p/\mu)^{3/2} dx/D^2 \quad (35)$$

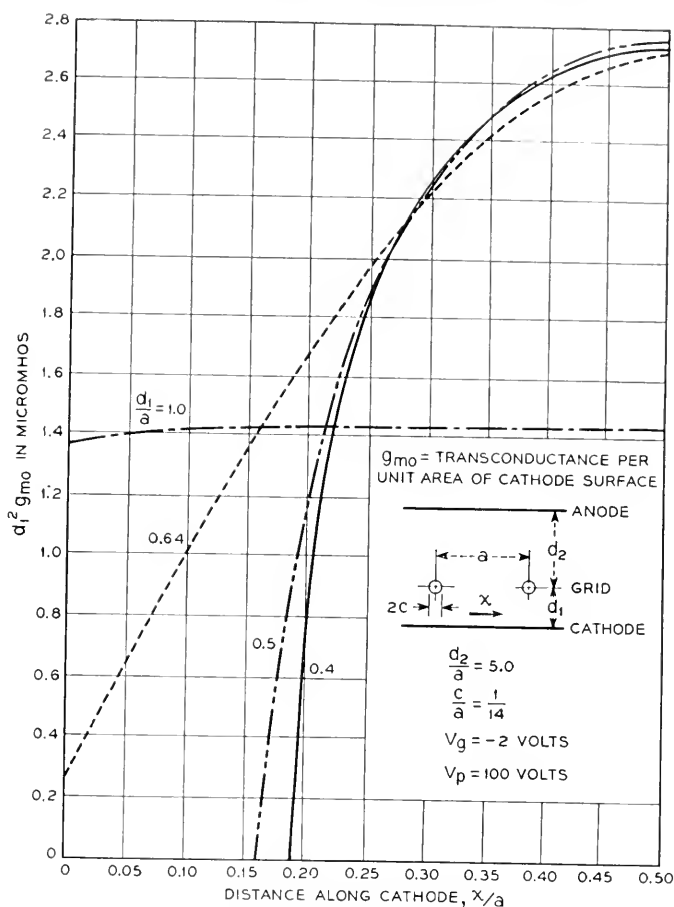


Fig. 5—Variation of transconductance along the cathode surface of a triode.

while, from (31),

$$I_T = \frac{2K}{d_1^2} \int_{x_0}^{a/2} [(\mu V_g + V_p)/(\mu + 1 + d_2/d_1)]^{3/2} dx \quad (36)$$

where  $x_0$  is given by

$$V_g + V_p/\mu(x_0) = 0 \quad (37)$$

On the basis of several reasonable assumptions it may be shown that both (35) and (36) lead to an approximate  $5/2$  power law instead of  $3/2$  power law. Such a law has actually been observed in cases where shadow formation was suspected.

We wish to express our appreciation to Messrs. R. K. Potter, J. A. Morton,

and R. M. Ryder for their encouragement, and to Miss M. C. Packer for aid in the numerical computations.

## REFERENCES

1. E. D. McArthur and E. F. Peterson, "The Lighthouse Tube; A Pioneer Ultra-High-Frequency Development," *Proc. Nat. Electronic Conference*, Chicago, Oct. 1944, Vol. I, pp. 38-47.
2. J. H. Fremlin, R. N. Hall, and P. A. Shatford, "Triode Amplification Factors," *Electr. Comm.*, Vol. 23 (1946), pp. 426-435.
3. Hamilton, Knipp, and Kuper, "Klystrons and Microwave Triodes, Radiation Laboratory Series, New York, 1948, p. 153.
4. J. C. Maxwell, "A Treatise on Electricity and Magnetism," Vol. 1, pp. 310-316.
5. Riemann-Weber, "Differentialgleichungen der Physik," Vol. 2, p. 311.
6. L. Rosenhead and S. D. Daymond, "The Distribution of Potential in Some Thermionic Tubes," *Proc. Roy. Soc.*, Vol. 161 (1937), pp. 382-405.
7. M. J. O. Strutt, "Moderne Mehrgitter-Elektronenröhren," Berlin, 1940, S. 154.
8. R. C. Knight, *Proc. London Math. Soc.* (2) Vol. 39 (1935), pp. 272-281.
9. R. C. J. Howland and B. W. McMullen, "Potential Functions Related to Groups of Circular Cylinders," *Proc. Cambr. Phil. Soc.*, Vol. 32 (1936), pp. 402-415.
10. R. C. Knight and B. W. McMullen, "The Potential of a Screen of Circular Wires between two Conducting Planes," *Phil. Mag. Ser. 7*, Vol. 24, 1937, pp. 35-47.
11. Barkas, "Conjugate Potential Functions and the Problem of the Finite Grid," *Phys. Rev.*, Vol. 49 (1936), pp. 627-630.
12. J. H. Fremlin, "Calculation of Triode Constants," *Phil. Mag. Ser. 7*, Vol. 27 (1939), pp. 709-741; also *Electr. Comm.*, Vol. 18 (1939), pp. 33-49.
13. H. Herne, "Valve Amplification Factor," *Wireless Engineer*, Vol. 21 (1944), pp. 59-64.
14. Whittaker and Watson, "Modern Analysis," Third Edition, Cambridge (1940), Chapter XXI, p. 462.
15. R. W. King, "Thermionic Vacuum Tubes," *Bell System Technical Journal*, Vol. II (1923), pp. 31-100.
16. W. E. Benham, "A Contribution to Tube and Amplifier Theory," *Proc. I. R. E.*, Vol. 26 (1938), pp. 1093-1170.
17. W. R. Ferris, "Input Resistance of Vacuum Tubes at Ultra-High Frequencies," *Proc. I. R. E.*, Vol. 24 (1936), pp. 82-105.
18. D. O. North, "Analysis of the Effects of Space Charge on Grid Impedance," *Proc. I. R. E.*, Vol. 24 (1936), pp. 108-136.
19. F. B. Llewellyn and L. C. Peterson, "Vacuum Tube Networks," *Proc. I. R. E.*, Vol. 32 (1944), pp. 144-166.

## Transconductance as a Criterion of Electron Tube Performance

By T. SLONCZEWSKI

QUANTITATIVE evaluation of electron tube performance has assumed added importance with the increasing extension of electronics into the fields of measurement and control. Simplification of the process of selection of suitable tube types and operating conditions from the general data available is of considerable value to all engineers concerned with electronics circuit design. The conventional procedure involves analysis of the plate current-grid voltage characteristics. The simpler method presented herein supplies the same information from an analysis of the transconductance-grid voltage characteristics. These are usually supplied by the manufacturer or can be obtained readily by measurement<sup>1</sup>.

The method presented herein has been employed successfully for a number of years in the development of electronic measuring apparatus by a group of engineers who attended lectures on the subject given by the author. It applies chiefly to pentodes, where the internal plate impedance is high with respect to the load impedance. Its merit resides in the comparative brevity of the formulae, the ease of computation and the facility in obtaining the data from which the computations are made. It allows one to form a preliminary judgment of the performance of a tube from a brief glance at the characteristics furnished by the manufacturer better and faster than any other method known to the author. It should prove of value to the instructor teaching electron tube theory.

In the interest of simplicity some of the subscripts  $m$ ,  $p$ ,  $c$  and  $g$  appended usually to symbols for transconductance, plate current and grid voltages are deleted below. The scope of the discussion is so limited that no confusion may arise from this omission. The formulae are expressed in terms of amplitudes of voltage and current, capital letters being used for their symbols. All values are in peak volts. Levels are in decibels.

The  $g$ - $e$  characteristic is introduced into the problem by starting with the general expression for the plate current

$$i = i_0 + \frac{\partial i}{\partial e} v + \frac{1}{2!} \frac{\partial^2 i}{\partial e^2} v^2 + \frac{1}{3!} \frac{\partial^3 i}{\partial e^3} v^3 + \dots \quad (1)$$

where  $v$  is the voltage measured from the bias point  $E_c$ , where the derivatives are taken, and utilizing the definition of the transconductance

<sup>1</sup> Radio Engineers' Handbook, F. E. Terman, McGraw-Hill, 1943, p. 961.

$$g = \frac{\partial i}{\partial e} \quad (2)$$

Inserting (2) into (1) and calling  $G$  the value of  $g$  at  $E_c$  we obtain

$$i = \int_{-\infty}^{E_c} g de + Gv + \frac{1}{2} \frac{\partial g}{\partial e} v^2 + \frac{1}{6} \frac{\partial^2 g}{\partial e^2} v^3 + \frac{1}{24} \frac{\partial^3 g}{\partial e^3} v^4 \dots \quad (3)$$

The first term of this expression is the space current of the tube at no load, that is when  $v = 0$ . On the  $g$ - $e$  diagram, Fig. 1, it represents the area under the curve from the tube cut off  $C$  to the tube bias  $E_c$ . The second term represents the function of the tube as an amplifier. The third term represents the second-order modulation current. The latter is responsible for the objectionable generation of a second harmonic in an amplifier and the useful presence of the second harmonic in the frequency doubler, the direct current in a rectifier and the sidebands in a modulator.

The fourth and higher terms represent, in general, undesirable effects of modulation. They are usually smaller than the first two and, since their effects are additive, the first three terms of expression (3) may be studied profitably disregarding the others. If necessary, the effects of the higher-order terms may be added later.

#### THE IDEALIZED PARABOLIC PENTODE

If, over a certain range of grid biases  $e_A$  to  $e_B$ , the effect of the fourth and higher terms of series (3) is negligible the  $g$ - $e$  characteristic will be a straight line. Herein lies one of the advantages of the method, for a straight portion of a curve can be easily selected by inspection and checked with a straight edge. It is thus possible to select easily such a tube and operating point that third and higher-order modulation products are absent in the output. There is no such simple method of verifying whether a current characteristic is parabolic. That there are tubes having approximately straight portions of  $g$ - $e$  characteristics can be verified by inspection of (Fig. 1) where the characteristic of the 6AG7 is given.

Since a portion of the  $g$ - $e$  characteristic is a straight line, the third term coefficient  $\frac{\partial g}{\partial e}$  may be replaced by the ratio  $\frac{\Delta g}{\Delta e}$  where  $\Delta e$  is an arbitrary interval of grid voltage and  $\Delta g$  the corresponding change in  $g$ . In many of the following computations it will be advantageous to use for  $\Delta e$  the total excursion of the grid voltage.

On the basis of the simplifying assumption of a parabolic pentode it is possible to derive the simple formulae given below which cover the performance of the tube as an amplifier, rectifier and modulator.



## THE PARABOLIC PENTODE AMPLIFIER

Over the straight portion of the  $g$ - $e$  curve the following relations hold for an input  $v = P \cos pt$ .

The fundamental current is  $I_p = GP$  where  $P$  is the grid swing.

The second harmonic current is

$$I_{2p} = \frac{1}{4} \frac{\Delta g}{\Delta e} P^2$$

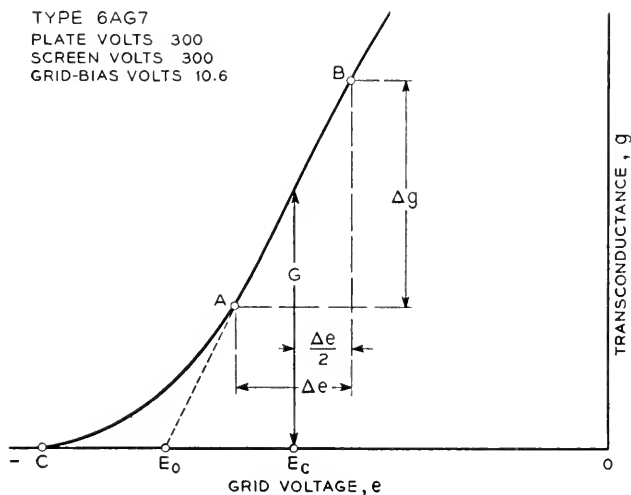


Fig. 1— $g$ - $e$  characteristic having principally second order modulation over part of the range.

To find the level  $H_2$  of the second harmonic below the fundamental, prolong the straight portion of the characteristic down to the virtual cutoff  $E_0$  (Fig. 1). Then

$$H_2 = 20 \log \frac{I_p}{I_{2p}} = 20 \log \frac{E_c - E_0}{P} + 12.$$

For the case when all of the parabolic characteristic is used

$$P = \frac{\Delta e}{2} \quad \text{and} \quad H_2 = 20 \log \frac{G}{\Delta g} + 18.$$

If it is desired to express  $H_2$  in terms of the output current  $i_p$  and the space current  $i_0$  the following approximate formula may be used:

$$H_2 = 20 \log \frac{i_0}{I_p} + 18.$$

This expression neglects the area under the characteristic on the left of the line  $AE_0$ , Fig. 1. The formula is useful in selecting a tube for closer consideration.

When a tube is used as a preamplifier in a wave analyzer an error of measurement may occur if two input frequencies intermodulate in the amplifier to produce a current of the same frequency as the one being measured. For instance, the fundamental  $R \cos rt$  and the second harmonic  $W \cos wt$  may intermodulate to form the third harmonic. If  $I_{r-w}$  is the disturbing current and  $I_p$  the wanted output, then

$$20 \log \frac{I_p}{I_{r-w}} = 20 \log \frac{E_c - E_0}{P} + 6 - 20 \log \frac{R}{P} - 20 \log \frac{W}{P}$$

### THE RECTIFIER

The portion of the plate current resulting from the rectification of a signal  $P \cos pt$  is

$$I_{dc} = \frac{1}{4} \frac{\Delta g}{\Delta e} P^2.$$

If several frequencies were present,  $P_1 \cos pt$ ,  $P_2 \cos p_2t$  and so on,

$$I_{dc} = \frac{1}{4} \frac{\Delta g}{\Delta e} (P_1^2 + P_2^2 + \dots)$$

Thus  $I_{dc}$  is proportional to the square of the root-mean-square voltage input. This property of the parabolic tube of measuring the root-mean-square voltage is often useful in the measurement field.

If  $\Delta e$  is the parabolic range of the tube and  $\Delta g$  the corresponding change in  $g$ , the largest possible rectified current obeying the root-mean-square law will obtain for an amplitude  $P = \frac{\Delta e}{2}$ . Then

$$I_{\max} = \frac{1}{16} \Delta g \Delta e.$$

### THE FREQUENCY DOUBLER

The second harmonic is given, as before, by

$$I_2 = \frac{1}{4} \frac{\Delta g}{\Delta e} P^2.$$

The largest possible output current is

$$I_{\max} = \frac{1}{16} \Delta g \Delta e.$$

In general, the level of the undesirable fundamental will be higher than the harmonic by

$$H_2 = 20 \log \frac{I_p}{I_{2p}} = \log \frac{E_c - E_0}{P} + 12.$$

For the maximum current case this reduces to

$$H_2 = 20 \log \frac{g}{\Delta g} + 18.$$

#### THE MODULATOR

When two inputs  $P \cos pt$  and  $Q \cos qt$  are applied to the grid, the output is

$$\begin{aligned} i = i_0 + \frac{1}{4} \frac{\Delta g}{\Delta e} (P^2 + Q^2) + \frac{1}{4} \frac{\Delta g}{\Delta e} (P^2 \cos 2pt + Q^2 \cos 2qt) \\ + \frac{1}{2} \frac{\Delta g}{\Delta e} PQ \cos (p + q)t + \frac{1}{2} \frac{\Delta g}{\Delta e} PQ \cos (p - q)t \end{aligned}$$

The last two terms represent the sidebands.

In the case of a detector the available supply of the carrier voltage  $Q$  is copious. Putting  $Q = \frac{\Delta e}{2}$  the well known result is obtained

$$I_{p+q} = I_{p-q} = \frac{1}{4} \Delta g P.$$

The conversion transconductance is

$$G_e = \frac{\Delta g}{4}.$$

To formulate filtering requirements the signal and carrier leaks must be found.

The signal leak is

$$20 \log \frac{I_p}{I_{p \pm q}} = 20 \log \frac{G}{\Delta g} + 12.$$

The carrier leak is

$$20 \log \frac{I_q}{I_{p \pm q}} = 20 \log \frac{G}{\Delta e} + 20 \log \frac{\Delta e}{P} + 6.$$

In the design of a heterodyne oscillator a generous supply of both input voltages is easily available and maximum output current is desirable. This occurs when  $P = Q = \frac{\Delta e}{4}$ . Then

$$I_{p-q} = \frac{1}{32} \Delta g \Delta e.$$

Whether  $P$  equals  $Q$  or not, the unwanted products are

$$20 \log \frac{I_q}{I_{p-q}} = 20 \log \frac{E_c - E_0}{Q} + 6$$

$$20 \log \frac{I_p}{I_{p-q}} = 20 \log \frac{E_c - E_0}{P} + 6$$

$$20 \log \frac{I_{2p}}{I_{p-q}} = 20 \log \frac{P}{Q} - 6$$

$$20 \log \frac{I_{2p}}{I_{p-q}} = 20 \log \frac{Q}{P} - 6$$

$$20 \log \frac{I_{r+q}}{I_{p-q}} = 0.$$

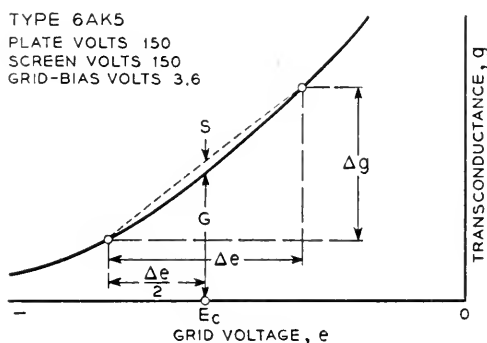


Fig. 2— $g$ - $e$  characteristic exhibiting third order modulation.

### THIRD ORDER MODULATION

When we do take into consideration the fourth term of equation (3), that is  $\frac{1}{6} \frac{\partial^2 g}{\partial e^2} v^3$  the  $g$ - $e$  characteristic will no longer be a straight line but a parabola. It turns out that all of the computations of the second-order effects as shown are so little affected that no corrections are necessary. The presence of third-order modulation caused by the term  $\frac{1}{6} \frac{\partial^2 g}{\partial e^2} v^3$  will, however, add new types of modulation products to the output. These are usually objectionable.

A typical  $g$ - $e$  characteristic with third-order modulation present is shown on Fig. 2. The curvature is usually concave upward. Instead of measuring the derivative  $\frac{\partial^2 g}{\partial e^2}$  needed for the computations, it is more practical to scale

off the amount  $S$  by which the characteristic sags in the middle of the interval  $\Delta e$  (Fig. 2).

The plate current is then given by the expression

$$i = i_0 + Gv + \frac{1}{2} \frac{\Delta g}{\Delta e} v^2 + \frac{4S}{3(\Delta e)^2} v^3. \quad (4)$$

#### SINGLE FREQUENCY INPUT

When the signal input to an amplifier consists of a single frequency  $v = P \cos pt$ , the output current is given by

$$i = i_0 + \frac{\Delta g}{\Delta e} P^2 + \left[ G + \frac{S}{(\Delta e)^2} P^2 \right] P \cos pt \\ + \frac{1}{4} \frac{\Delta g}{\Delta e} P^2 \cos 2pt + \frac{1}{3} \frac{S}{(\Delta e)^2} P^3 \cos 3pt.$$

The second-order effects consisting of the rectified current and second harmonic are seen to be unaffected by the presence of third-order modulation. However, the first-order effect, the fundamental output, ceases to be linear and a new product, the third harmonic, appears.

The change in fundamental output is expressible as a loading effect on transconductance. The effective transconductance of the tube is.

$$G_e = G + S \left( \frac{P}{\Delta e} \right)^2.$$

Expressed in db's the non-linearity effect is approximately

$$20 \log \frac{G_e}{G} = 8.6 \frac{S}{G} \left( \frac{P}{\Delta e} \right)^2.$$

When  $P$  is large it is convenient to select  $\Delta e = 2P$  and get

$$G_e = G + \frac{S}{4}, \quad 20 \log \frac{G_e}{G} = 2.15 \frac{S}{G}.$$

$S$  is positive when the  $g$ - $e$  curve is concave upward.

The third harmonic content of the output is

$$H_3 = 20 \log \frac{I_p}{I_{3p}} = 20 \log \frac{G}{S} + 40 \log \frac{\Delta e}{P} + 10.$$

If we select  $\Delta e = 2P$  the second term drops out

$$H_3 = 20 \log \frac{G}{S} + 22.$$

If the curve is concave upward the third harmonic increases the peak value

of the wave. If it is concave downward the peak value of the wave decreases.

In the case of a two-frequency input  $v = P \cos pt + Q \cos qt$  the second-order products are again unaffected. The third-order products will be:

$$\begin{aligned} I_{3p} &= \frac{1}{3} \frac{S}{(\Delta e)^3} P^3 \\ I_{3q} &= \frac{1}{3} \frac{S}{(\Delta e)^2} Q^3 \\ I_{2p \pm q} &= \frac{S}{(\Delta e)^2} P^2 Q \\ I_{p \pm 2q} &= \frac{S}{(\Delta e)^2} P Q^2. \end{aligned}$$

There are situations in the design of detectors where the  $I_{q \pm 2p}$  current may be disturbing. For example, in a wave analyzer modulation stage when measuring the second harmonic  $P_2 \cos (2p)t$  the desired second-order product is  $I_{q-(2p)}$ . This is, however, of the same frequency as the third-order product  $I_{q-2p}$  generated by the intermodulations of the strong fundamental  $P_1 \cos pt$  and the carrier  $Q \cos qt$ . The level of the wanted product with respect to the unwanted one is given by

$$20 \log \frac{I_{p-(2p)}}{I_{q-2p}} = 20 \log \frac{\Delta g}{S} + 20 \log \frac{\Delta e}{P_1} + 20 \log \frac{P_2}{P_1} - 6.$$

If there are two interfering inputs  $R \cos rt$  and  $W \cos wt$  they may, together with the carrier  $Q \cos qt$ , form an objectionable product  $i_{r \pm w \pm q}$  of the same frequency as the wanted product  $i_{p-q}$ . The level of this disturbing product with respect to the wanted product is then given by

$$20 \log \frac{I_{p-q}}{I_{q \pm r \pm w}} = 20 \log \frac{\Delta g}{S} + 20 \log \frac{\Delta e}{R} + 20 \log \frac{P}{W} - 12.$$

When two input frequencies are present in the input, the effective transconductance of the tube becomes

$$G_e = G + \frac{S}{(\Delta e)^2} (P^2 + 2Q^2).$$

The amplifier gain depends on the level of all of the components of the input.

#### FOURTH ORDER MODULATION

If the fourth term of equation (3) is absent, but the fifth term  $\frac{1}{24} \frac{\partial^3 g}{\partial e^3} v^4$  is present, fourth-order modulation will occur. The  $g$ - $e$  characteristic will be a cubic with an inflection point at  $E_e$ .

TABLE I

If modulation up to the fourth order is present and  $v = P \cos pt + Q \cos qt$ , the plate current is  $i = \sum_{m=0}^{m=4} \sum_{n=0}^{n=4} a_{mn} \cos (mp \pm nq)$ . The values of  $a_{mn}$  are:

$m$	$n$			
	0	1	2	3
0	$\frac{1}{4} \frac{\Delta_g}{\Delta e} (P^2 + Q^2) + \frac{3D}{4(\Delta e)^3} [4Q^2 P^2 + Q^4 + P^4]$	$\left[ G + \frac{S}{(\Delta e)^2} (2P^2 + Q^2) \right] Q$	$\left[ \frac{1}{4} \frac{\Delta_g}{\Delta e} + \frac{3D}{(\Delta e)^3} (P^2 + Q^2) \right] Q^2$	$\frac{1}{3} \frac{S}{(\Delta e)^2} Q^3$
1	$\left[ G + \frac{S}{(\Delta e)^2} (P^2 + 2Q^2) \right] P$	$\left[ \frac{1}{2} \frac{\Delta_g}{\Delta e} + \frac{3D}{(\Delta e)^3} (Q^2 + P^2) \right] PQ$	$\frac{S}{(\Delta e)^2} P^2 Q^2$	$\frac{D}{(\Delta e)^3} P Q^2$
2	$\left[ \frac{1}{4} \frac{\Delta_g}{\Delta e} + \frac{3D}{(\Delta e)^3} (P^2 + Q^2) \right] P^2$	$\frac{S}{(\Delta e)^2} P^2 Q$	$\frac{3}{2} \frac{D}{(\Delta e)^3} P^2 Q^2$	0
3	$\frac{1}{3} \frac{S}{(\Delta e)^2} P^3$	$\frac{D}{(\Delta e)^3} P^3 Q$	0	0
	$\frac{1}{4} \frac{D}{(\Delta e)^3} P^4$	0	0	0

$$g = G + \frac{\partial g}{\partial e} v + \frac{1}{6} \frac{\partial^3 g}{\partial e^3} v^3$$

To compute fourth-order effects a tangent is drawn to the curve in the middle of the range  $\Delta e$  (Fig. 3). It will represent a parabolic pentode over the range  $\Delta e$  and  $\Delta g$ . The departure  $D$  of the actual curve from the parabolic pentode at the extremes of the range  $\Delta e$  is measured. The  $g$ - $e$  curve becomes

$$g = G + \frac{\Delta g}{\Delta e} v + \frac{8DV^3}{(\Delta e)^3}.$$

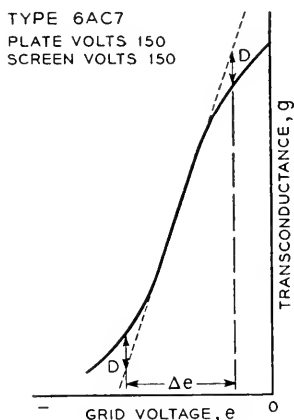


Fig. 3— $g$ - $e$  characteristic exhibiting fourth order modulation.

As a rule  $D$  is negative. It decreases the slope of the curve. The plate current is

$$i = i_0 + Gv + \frac{1}{2} \frac{\Delta g}{\Delta e} v^2 + \frac{2D}{(\Delta e)^3} v^4. \quad (5)$$

From this expression the fourth-order effects may be computed.

#### SINGLE FREQUENCY INPUT

Fourth-order modulation has no effect on the gain of the amplifier. It affects the second-order products, the rectified current and the second harmonic and adds the fourth harmonic.

In an amplifier it is unimportant to correct the value of  $H_2$  for fourth-order modulation. The fourth harmonic is given by

$$H_4 = 20 \log \frac{G}{D} + 60 \log \frac{\Delta e}{P} + 12.$$



In a rectifier, the effect of fourth-order modulation is to destroy the square law of the rectifier. The error is

$$\frac{\Delta I_{dc}}{I_{dc}} = 3 \frac{D}{\Delta g} \cdot \left( \frac{P}{\Delta e} \right)^2.$$

This correction is valid for the case of frequency doublers.

### TWO-FREQUENCY INPUT

In a detector the fourth-order modulation produces an overloading effect; the modulator gain is then a function of the input

$$G = \frac{\Delta g}{4} + \frac{3}{8}D + \frac{3}{2}D \left( \frac{P}{\Delta e} \right)^2.$$

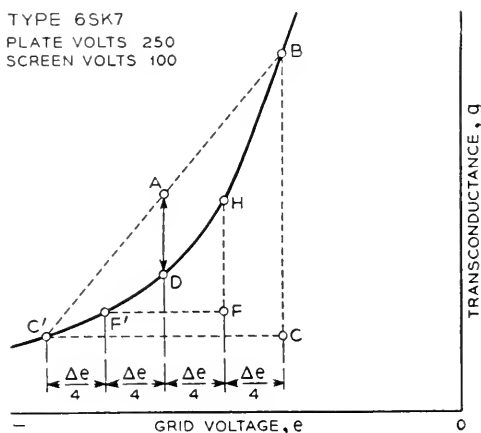


Fig. 4— $g$ - $e$  characteristic with second, third and fourth order modulation present.

$$D = \frac{2}{3}(\overline{CB} - 2\overline{FH}); \Delta g = \overline{CB} - 2D; S = \overline{AD}$$

Neglecting  $\frac{3}{8}D$  in comparison with  $\frac{\Delta g}{4}$ , the error in linearity is

$$\frac{\delta I_{dc}}{G_c} = 6 \frac{D}{\Delta g} \left( \frac{P}{\Delta e} \right)^2.$$

There will be also a cross-loading effect for an interfering signal  $R \cos rt$ .

$$\frac{\delta I_{dc}}{G_c} = 2D \left( \frac{R}{\Delta e} \right)^2$$

In a heterodyne oscillator fourth-order modulation will produce a second harmonic at the output.

$$H_2 = 20 \log \frac{\Delta g}{D} + 20 \log \frac{\Delta e}{P} + 20 \log \frac{\Delta e}{Q} - 10.$$

For the case of maximum output at  $P = Q = \frac{\Delta e}{4}$

$$H_2 = 20 \log \frac{\Delta g}{D} + 14.$$

#### ACCURACY OF COMPUTATIONS

Before closing the subject, let us consider for a moment the accuracy involved. Very careful measurement of the characteristics of samples of some tubes, notably the 310A and 807 has shown that over a large range the fit with a parabola is excellent. On the other hand the electron tube bulletins give characteristics which are avowedly average. The drafting errors must be large and the temptation to use a straight edge instead of a french curve must be great. Probably no two observers will agree as to the extent of the straight part of a conductance curve. Even in the case of the 310A and 807 tubes mentioned above, manufacturing variations may affect the transconductance curve from tube to tube.

With this in mind we may conclude that the results obtained, that is, the values of the current obtained by the methods evolved above, must be approximate in character. The value of the analysis given lies in its simplicity rather than accuracy. Admitting that the situation is not satisfactory from the standpoint of reproducibility of results we must face the fact that there is no method nor the promise of a method for computing performance of a tube that would come within slide rule accuracy. We may console ourselves that in practice accuracy in estimating output levels and unwanted products is not really required. An error of 3 db or in the case of unwanted products an error of 6 db is of small consequence. This is about the variation to be expected to exist between two individual electron tubes and it must be included as a tolerance in determining performance requirements.

In connection with the third-order modulation the question arises whether the transconductance characteristic is really parabolic and not a curve of fourth or sixth degree and, if so, whether the equations derived above still apply.

While no accurate test can be applied conveniently we may compare a parabola with a quartic passing through the same three points. The parabola is characterized by a smooth curvature, while the quartic and the higher-degree curves have a flat middle portion with the ends turned up sharply. An inspection of the transconductance characteristics of tubes reveals that they are of the smoother curvature type—that is, that a square term is the chief contribution to the series representing the curve.

Should this not be the case and should we possibly mistake a quartic for a parabola, we still would obtain all of the phenomena caused by third-order

modulation; that is, we would get a third harmonic, a transconductance increment, a finite detector discrimination, and so on, only their values would be somewhat different. Moreover, a more elaborate analysis reveals that the computations as made above would be in error by relatively small amounts and, what is more important, they would always be on the safe side. The only important error would be the absence of the fifth harmonic, which cannot be produced by third-order modulation.

Experience with computations checked by measurement reveals that the equations apply in a great majority of practical cases. The computations may be used, therefore, as a guide in the selection of tubes, operating parameters, and in experiments, even though we must realize that they may not be fully justified theoretically and are not quite accurate.

### CONCLUSION

The analysis of the transconductance characteristics of tubes could be pushed further to fifth, sixth and higher orders of modulation, but it is hardly worth it. The mathematical treatment becomes burdensome, the results are uninteresting and the applications are rare except in a qualitative way. Thus, having completed the discussion of the fourth-order modulation, we find an extension of the treatment to higher orders of modulation unprofitable.

The material presented in this article has consisted chiefly of a list of formulas which may be applied to practical computations of the transmission and quality of transmission of electron tubes. They will be found to be useful in design of electron tube circuits. The second objective of the analysis is to give the user a mental picture of the tube performance in terms of its conductance characteristic.

Thus in general the quality of transmission of an amplifier, its discrimination against interfering voltages, amplitude distortion, and second harmonic content are measured by the bias cut-off interval. The capacity of the tube to deliver large currents at small distortion is measured by the area under the characteristic. The gain is measured by the transconductance and, in some cases, by the steepness of the characteristic. Freedom from third- and fourth-harmonic distortion and input-output linearity are measured by the linearity of the characteristic.

In a modulator the current capacity of the tube is measured by the area between the characteristic and the lines defining the voltage and the transconductance range used. The conversion transconductance is measured by the transconductance range available. The linearity of the characteristic will measure the discrimination against third-order products. In the case of a rectifier the criteria will be the same as in the case of the modulator.

A tube with a small slope and large transconductance will deliver with

small distortion large currents whether used as an amplifier or modulator or rectifier. It will be a poor voltage amplifier, detector or voltmeter. A tube with a steep characteristic and large transconductance will be a good voltage amplifier, detector or voltmeter, but will carry little current.

Of course there are no rules without exception and special cases will be found in practice where the above recommendations may be violated. Electron tubes are used in many other ways than those discussed above and the present analysis covers only a small part of the field. The methods of computing modulation products shown above can be extended to triodes with little or no modification in cases of modulator or rectifier design where the external plate impedance is very low at the input frequencies.

## Abstracts of Technical Articles by Bell System Authors

*Administration of a Sampling Inspection Plan.*<sup>1</sup> H. F. DODGE. Greatly expanded production during the war brought about extensive use of scientific sampling plans both within manufacturing plants and by procurement agencies. Perhaps most widely used were standard plans involving single sampling, double sampling, and multiple sampling for visual and gaging inspections on a go no-go basis. This paper discusses how a manufacturer may make use of these sampling plans in a manufacturing plant, how he goes about deciding on suitable levels of quality expressed in per cent defective, how he determines whether sampling can be used advantageously in place of 100% inspection, and how he can choose and administer sampling plans that will limit the risks of sampling as well as provide the desired protection with a minimum amount of inspection. Particular attention is given to the operating characteristics and the mode of application of the standard AOQL (average outgoing quality limit) sampling plans published by Dodge and Romig.

*The Bridge Erosion of Electrical Contacts. Part I.*<sup>2</sup> J. J. LANDER and L. H. GERMER. Bridge erosion is the transfer of metal from one electrode to the others, which occurs when an electric current is broken in a low voltage circuit which is essentially purely resistive. It is associated with the bridge of molten metal formed between the electrodes as they are pulled apart, and more specifically with the ultimate boiling of some of the metal of this bridge before the contact is finally broken. This paper is concerned with fundamental studies of this molten bridge and with empirical measurements of the transfer of metal.

*Electron Bombardment Conductivity in Diamond.*<sup>3</sup> KENNETH G. MCKAY. A study has been made of electron bombardment conductivity in diamond using primary electrons of energies up to 14,000 ev. An alternating field method is used which reduces or eliminates the effects of internal space charge fields. Data on internal yields as a function of crystal field are given for both electron and positive hole carriers. Internal yields as high as 600 have been attained. The experimental curves are fitted to a theoretical curve for the space charge free crystal from which are derived reasonable values for the number of electrons produced in the conduction band per incident primary electron, the probable life time of the conduction

<sup>1</sup> *Industrial Quality Control*, November 1948.

<sup>2</sup> *Jour. Applied Physics*, October 1948.

<sup>3</sup> *Phys. Rev.*, December 1, 1948.

electrons and the crystal trap density. Experiments are described which lead to a hypothesis of space charge neutralization. A possible cause of the current fluctuations observed at high crystal fields is discussed.

*The Philosophy of PCM.*<sup>4</sup> B. M. OLIVER, J. R. PIERCE and C. E. SHANNON. Recent papers describe experiments in transmitting speech by PCM (pulse code modulation). This paper shows in a general way some of the advantages of PCM, and distinguishes between what can be achieved with PCM and with other broadband systems, such as large-index FM. The intent is to explain the various points simply, rather than to elaborate them in detail. The paper is for those who want to find out about PCM rather than for those who want to design a system. Many important factors will arise in the design of a system which are not considered in this paper.

*Objectives for Sound Portrayal.*<sup>5</sup> RALPH K. POTTER. Translation of sound into visible patterns is discussed in terms of broad objectives. It is suggested that no single design can be optimum and that perhaps the most useful standard of reference is the human ear. Special interests and complexity generally affect final design requirements.

*A Waveguide Bridge for Measuring Gain at 4000 Mc.*<sup>6</sup> A. L. SAMUEL and C. F. CRANDELL. A bridge has been constructed for measuring the gain and phase delay of amplifiers in the vicinity of 4000 Mc. The equipment is described, and the methods employed to reduce the possible errors are discussed. The general method may be adapted for use in any desired frequency range.

*Video Distribution Facilities for Television Transmission.*<sup>7</sup> ERNEST H. SCHREIBER. This paper describes the Bell System's plans for furnishing network and local video facilities. The Telephone Company is now using broad-band coaxial cable and microwave radio systems to provide regular message telephone service on a number of principal intercity routes throughout the nation. These facilities can be used to provide television transmission channels when properly equipped. Video service between Washington, D. C., New York, and Boston over these two types of facilities has been demonstrated. New facilities are rapidly being extended. Local video channels for pickup and metropolitan-area networks are provided by ordinary paper-insulated cable pairs, special shielded polyethylene-insulated pairs, by microwave radio systems, or by combinations of these systems. Amplifier and equalizing arrangements for providing wide-band transmission over these facilities are described. Present Bell System views of the availability of microwave and coaxial cable facilities on the principal routes,

<sup>4</sup> *Proc. I. R. E.*, November 1948.

<sup>5</sup> *Jour. Acous. Soc. Amer.*, January 1949.

<sup>6</sup> *Proc. I. R. E.—Waves and Electrons Section*—November 1948.

<sup>7</sup> *S. M. P. E. Journal*, December 1948.

types of circuits, bandwidths, bridging and terminating arrangements, and general information concerning the provision of television circuits are covered.

*Communication in the Presence of Noise.*<sup>8</sup> CLAUDE E. SHANNON. A method is developed for representing any communication system geometrically. Messages and the corresponding signals are points in two "function spaces," and the modulation process is a mapping of one space into the other. Using this representation, a number of results in communication theory are deduced concerning expansion and compression of bandwidth and the threshold effect. Formulas are found for the maximum rate of transmission of binary digits over a system when the signal is perturbed by various types of noise. Some of the properties of "ideal" systems which transmit at this maximum rate are discussed. The equivalent number of binary digits per second for certain information sources is calculated.

*Earth Conduction Effects in Transmission Systems*<sup>9</sup> ERLING D. SUNDE. Earth conduction problems are encountered in both communication and power system engineering in connection with investigations of earth resistivity, grounding, corrosion of buried metallic structures, power system impedances and fault currents, inductive interference, lightning disturbances, and in connection with ground-wave radiation fields. Mr. Sunde deals comprehensively with the theory underlying various earth conduction effects and with its engineering applications, and brings together in unified manner many topics that hitherto have received only separate discussion in the literature. The author's purpose throughout has been to tie his discussion to practical considerations and problems.

Beginning with a review of the theory underlying various earth conduction effects and with its engineering applications, the book contains the following chapter headings: basic electromagnetic concepts and equations, earth resistivity testing and analysis, resistance of grounding arrangements, mutual impedance of insulated earth-return conductors, propagation characteristics of earth-return conductors, d-c earth conduction and corrosion protection, power system earth conduction and inductive interference, surge characteristics of earth-return conductors, lightning protection of cable and transmission lines.

A carefully compiled bibliography is included.

<sup>8</sup> *Proc. I. R. E.*, January 1949.

<sup>9</sup> Published by *D. VanNostrand Company, Inc.*, New York, London and Toronto, January, 1949. 373 pages. \$6.00.

## Contributors to This Issue

DIETRICH A. ALSBERG, Technical College of Stuttgart, 1938; Case School of Applied Science, postgraduate in electrical engineering, 1939-40. From 1940-43 Mr. Alsberg was engaged as development engineer by several organizations. From 1943-45 he served in the U. S. Army Ordnance Department at Aberdeen Proving Ground and in the European Theater. In 1945 he joined the Bell Telephone Laboratories where he is concerned with phase and transmission measurement problems.

JOHN BARDEEN, University of Wisconsin, B.S. in E.E., 1929, M.S., 1930; Gulf Research and Development Corporation, 1930-33; Princeton University, 1933-35, Ph.D. in Math. Phys., 1936; Junior Fellow, Society of Fellows, Harvard University, 1935-38; Assistant Professor of Physics, University of Minnesota, 1938-41; Prin. Phys., Naval Ordnance Laboratory, 1941-45. Bell Telephone Laboratories, 1945-. Dr. Bardeen is engaged in theoretical problems related to semiconductors.

W. R. BENNETT, B.S., Oregon State College, 1925; A.M., Columbia University, 1928. Bell Telephone Laboratories, 1925-. Mr. Bennett has been active in the design and testing of multichannel communication systems, particularly with regard to modulation processes and the effects of nonlinear distortion. He is now engaged in research on various transmission problems.

WALTER H. BRATTAIN, B.S., Whitman College, 1924; M.A., University of Oregon, 1926; Ph.D., University of Minnesota, 1929; Major Phys., Bureau of Standards, 1928-29. Bell Telephone Laboratories, 1929-42. Columbia University, N.D.R.C., 1942-44. Bell Telephone Laboratories, 1944-. Dr. Brattain is engaged in the study of semiconductors.

C. H. DAGNALL, S.B., Massachusetts Institute of Technology, 1918; S.B., Harvard University, 1918; M.S., Cornell University, 1922. Signal Corps, U.S.A., 1918; General Electric Company, 1919; Instructor in Electrical Engineering, Cornell University, 1919-25. Bell Telephone Laboratories, 1925-. Mr. Dagnall has been chiefly concerned with the design of transmission networks.

F. S. FARKAS, E. E., 1929, Polytechnic Institute of Brooklyn. Engineer-



ing Department, Western Electric Company, 1920-25; Bell Telephone Laboratories, 1925-. Mr. Farkas was engaged in the development of transmission networks and is now concerned with the development of radio and network switching.

F. J. HALLENBECK, E.E., 1936, Polytechnic Institute of Brooklyn. Engineering Department, Western Electric Company, 1923-25; Bell Telephone Laboratories, 1925-. Mr. Hallenbeck has been concerned chiefly with the development of transmission networks for carrier systems.

R. A. LECONTE, E.E., Electrotechnical Institute, Grenoble University, France, 1908; French Army Corps of Engineers, 1915-20. Mr. Leconte came originally to the United States in 1917 with a French military mission and came back in 1919 to the French purchasing organization in this country. He joined the Engineering Department, Western Electric Company, in 1922; Bell Telephone Laboratories, 1925-. He has been concerned with voice frequency repeater and carrier terminal developments.

DANIEL LEED, B.S., College of the City of New York, 1941; Kollsman Instrument Company, 1941-43. Federal Telephone and Radio Corporation, 1943-44. Corps of Engineers, Los Alamos Laboratories of the Manhattan District, 1944-46. Bell Telephone Laboratories, 1946-. Mr. Leed is engaged in circuit development for phase and transmission measurement systems, particularly in the field of automatic frequency control.

D. B. PENICK, University of Texas, B.S. in Electrical Engineering, 1923, B.A., 1924; Columbia University, M.A., 1927. Engineering Department, Western Electric Company, 1924-25. Bell Telephone Laboratories, 1925-. Mr. Penick has been engaged in the development of carrier telephone systems.

LISS C. PETERSON, Chalmers Technical University, Gothenburg, 1921; Technical Universities of Charlottenburg and Dresden, 1921-23. American Telephone and Telegraph Company, 1925-30; Bell Telephone Laboratories, 1930-. Mr. Peterson has recently been concerned with the theory of hearing.

P. W. ROUNDS, A.B., Harvard University, 1929. Bell Telephone Laboratories, 1929-. Mr. Rounds has been engaged in the design of transmission networks.

C. W. SCHRAMM, B.S. in Electrical Engineering, Armour Institute

(now Illinois Institute) of Technology, 1927. Illinois Bell Telephone Company, 1927-29. Bell Telephone Laboratories, 1929-. Mr. Schramm has been concerned with the development of carrier telephone systems for both message and program use. During the war his attention was directed to the design of radar test equipment.

T. SLONCZEWSKI, B.S. in Electrical Engineering, Cooper Union Institute of Technology, 1926. Bell Telephone Laboratories, 1926-. Mr. Slonczewski has been engaged in the development of electrical measuring apparatus.

F. E. STEHLIK, B.E.E., 1933, M.E.E., 1935, Polytechnic Institute of Brooklyn. Bell Telephone Laboratories, 1936-. Mr. Stehlik was engaged in the design of crystal filters and is now concerned with the development of high-frequency networks.

E. D. SUNDE, B.S., Haugesund, Norway, 1922; E.E., Darmstadt, Germany, 1926. American Telephone and Telegraph Company, 1927-33; Bell Telephone Laboratories, 1933-. Mr. Sunde has been engaged in studies of interference in telephone circuits from power lines and railway electrification and is now concerned with studies of protection of the telephone plant against lightning damage.

H. M. TRUEBLOOD, B.S., Earlham College, 1902; B.S., Haverford College, 1903; Mass. Inst. Technology, 1908-09; Ph.D. (physics), Harvard University, 1913; Field Officer, U. S. Coast and Geodetic Survey, 1903-08; Instructor and Assistant Professor in Electrical Engineering, University of Pennsylvania, 1914-17; U. S. Naval Experimental Station, New London, Connecticut, 1917-19. American Telephone and Telegraph Company, Department of Development and Research, 1919-34; Bell Telephone Laboratories, 1934-. At present, Assistant Director of Transmission Engineering. Most of Dr. Trueblood's work has been on interference with communication systems from natural and other sources, with work on radar and radar testing equipment during World War II.

ANTHONY J. WIER, L.L.B., New Jersey Law School, 1935. New York Telephone Company, Plant Maintenance; and Western Electric Company, Installation and Equipment Engineering; 1914-28. Bell Telephone Laboratories, 1928-. Mr. Wier has been engaged in development work on toll telephone and telegraph equipment since 1928.

# THE BELL SYSTEM TECHNICAL JOURNAL

DEVOTED TO THE SCIENTIFIC AND ENGINEERING ASPECTS  
OF ELECTRICAL COMMUNICATION

Editorial Note regarding Semiconductors.....	335
Hole Injection in Germanium—Quantitative Studies and Filamentary Transistors <i>W. Shockley, G. L. Pearson, J. R. Haynes</i>	344
Some Circuit Aspects of the Transistor <i>R. M. Ryder and R. J. Kircher</i>	367
Theory of Transient Phenomena in the Transport of Holes in an Excess Semiconductor <i>Conyers Herring</i>	401
On the Theory of the A-C. Impedance of a Contact Rectifier <i>J. Bardeen</i>	428
The Theory of p-n Junctions in Semiconductors and p-n Junction Transistors.....	<i>W. Shockley</i> 435
Band Width and Transmission Performance <i>C. B. Feldman and W. R. Bennett</i>	490
Abstracts of Technical Articles by Bell System Authors...	596
Contributors to this Issue.....	599

AMERICAN TELEPHONE AND TELEGRAPH COMPANY  
NEW YORK

# THE BELL SYSTEM TECHNICAL JOURNAL

*Published quarterly by the  
American Telephone and Telegraph Company  
195 Broadway, New York, N. Y.*

---

## EDITORS

R. W. King

J. O. Perrine

## EDITORIAL BOARD

C. F. Craig

O. E. Buckley

O. B. Blackwell

M. J. Kelly

H. S. Osborne

A. B. Clark

J. J. Pilliod

F. J. Feely

---

## SUBSCRIPTIONS

Subscriptions are accepted at \$1.50 per year. Single copies are 50 cents each.  
The foreign postage is 35 cents per year or 9 cents per copy.

---

Copyright, 1949  
American Telephone and Telegraph Company

# The Bell System Technical Journal

Vol. XXVIII

July, 1949

No. 3

---

## Editorial Note regarding Semiconductors

ALL but one of the papers that comprise this issue discuss practical applications of semiconductors and touch upon their properties as employed in rectifying devices, detectors, and in a new amplifying unit—the so-called transistor. These semiconductor papers all relate to one another and present, as a whole, a current but well developed account of the behavior and uses of these very promising additions to today's vast array of electrical appliances.

Because semiconductors are relative newcomers, few engineers have as yet had occasion to become familiar with their characteristics and the reasons for their somewhat unexpected performance. Accordingly, it seems appropriate to preface the present group of papers with a brief introductory note devoted to the nature of the physical phenomena encountered.

The semiconductors of interest in the communications art are electronic rather than ionic conductors, and include copper oxide, various other oxides, selenium, germanium and silicon. Being electronic conductors, the constituent atoms remain in fixed positions. They may lose or gain electrons during the conduction process but the structure of the conductor as a whole and its chemical composition are not affected.

Basic to the theory of these semiconductors is the idea that electrons can carry current in two distinguishable and distinctly different ways: one being called "excess conduction," "conduction by excess electrons," or simply "conduction by electrons;" and the other being called "deficit conduction" or "conduction by holes." The possibility that these two processes may be simultaneously and separably active in a semiconductor affords a basis for explaining transistor action.

We shall confine our attention to the behavior of electrons within the silicon and germanium type of crystal lattice, and especially as it is modified by minute amounts of suitably chosen impurities.<sup>1</sup>

<sup>1</sup> There has been very marked development in the understanding of semiconductors since 1940. This understanding is an outgrowth of the research and development program on crystal rectifiers undertaken in connection with the radar program during the war and continued in several laboratories thereafter. Some of the wartime work was carried out in the Radiation Laboratory of M.I.T., which operated under the supervision of the National Defense Research Committee. The Radiation Laboratories Series volume "Crystal Rectifiers" by H. C. Torrey and C. A. Whitmer reports this program and mentions in particular as chief contributors to crystal research and development in England: the General Electric

Silicon and germanium form what are called "covalent crystals," the atoms being held together by "electron-pair bonds" formed by the valence electrons. The covalent bond in the hydrogen molecule is the simplest electron-pair bond. Figure 1 represents two hydrogen atoms and a hydrogen molecule.<sup>2</sup> Each atom consists of a proton and one electron. The proton weighs approximately 2,000 times as much as the electron and is a relatively immobile particle about which the electron moves in its orbit or quantum mechanical wave function. In an isolated atom, this wave function has spherical symmetry and the electronic charge is distributed on the average as a diffuse sphere centered about the proton. When the two atoms are brought close together, interaction between the wave functions of the two electrons takes place and the electronic cloud of each becomes modified, as suggested in the figure. The result is to produce an extra accumulation of charge between the two protons which acts to bind them together. According to quantum mechanical laws associated with the "Pauli exclusion principle," the bond is especially stable when it contains precisely two electrons. It is weakened considerably by removal of one electron and is not greatly strengthened by the addition of a third electron. This special stability of the electron-pair bond or covalent bond is a fundamental fact of chemistry which is now quite well understood on the basis of wave mechanics.

The elements carbon, silicon and germanium have the common feature of being tetravalent. Although they possess respectively 6, 14 and 32 electrons all together, in each case only four of these are able to enter into chemical reactions. The remaining electrons are closely bound to the nucleus producing a stable "ionic core" having a net charge of  $+4$  units. This core can be regarded as completely inactive so far as electronic processes in chemical reactions and in semiconductors are concerned.

Each of these atoms tends to form covalent or electron-pair bonds with four other atoms. This tendency is completely satisfied in the diamond lattice which is the crystalline form of all three elements. The lattice, shown in Fig. 2, is a cubic arrangement and may be regarded as made up of four interpenetrating simple cubic lattices like the one formed by the atoms on the four corners of the cube shown. In this structure each typical atom is surrounded by four neighbors regularly placed about it, with which it forms four

---

Company, British Thompson-Houston Ltd., Telecommunications Research Establishment and Oxford University; and in the United States: the Bell Telephone Laboratories, Westinghouse Research Laboratory, General Electric Company, Sylvania Electric Products, Inc., and the E.I. duPont de Nemours and Company. It is also pointed out that the crystal groups at the University of Pennsylvania and Purdue University, who operated under N.D.R.C. contracts, were responsible for much fundamental work.

<sup>2</sup>The figures in this introduction and the text associated with them, like the following paper on "Hole Injection in Germanium", follow closely the presentation in a book entitled "Holes and Electrons, an Introduction to the Physics of Transistors" now under preparation by W. Shockley.

covalent bonds. These neighbors are arranged on the corners of a regular tetrahedron in conformity with the known chemical behavior of the tetrahedral carbon atom.<sup>3</sup> For purposes of discussion of conductivity in these crystals, we shall represent the three-dimensional array in two dimensions as is shown in Fig. 3, indicating that each carbon atom forms an electron-pair bond with four neighbors.

On the basis of this valence bond structure we can intuitively see why diamond should be an insulator. Although it contains a large number of

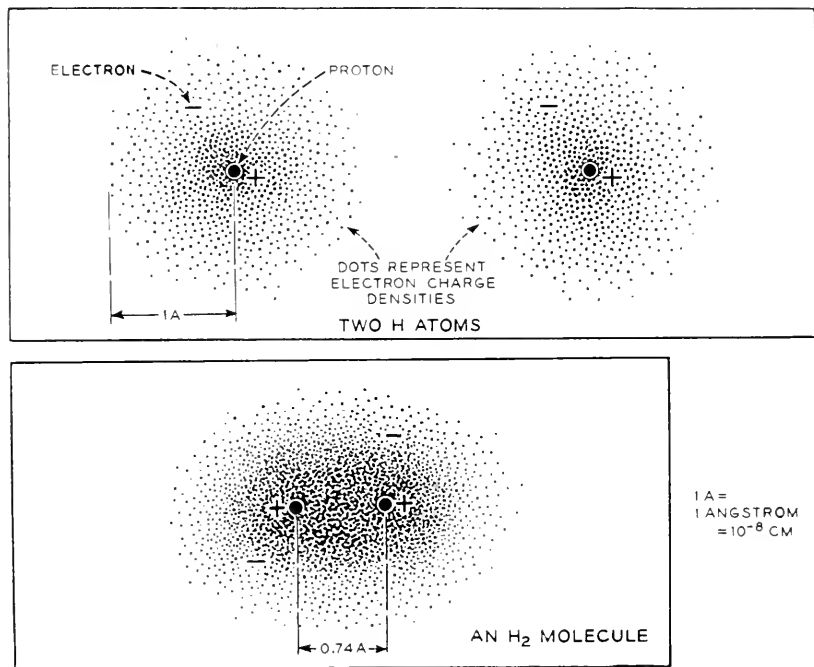


FIG. 1.

electrons, as does a metal, the covalent bond is a quite different structure from the metallic bond. In an ideally perfect diamond crystal, each valence bond would contain its two electrons; therefore, every electron would be tightly bound and thus unable to enter into the conduction process.

Conductivity can be produced in diamond, however, in a number of ways, all of which involve destroying the perfection of the valence bond structure.

<sup>3</sup> Long before the arrangement of atoms in the diamond crystal was established by X-rays, the organic chemists had concluded that carbon formed four bonds at the tetrahedral angles—a truly remarkable result of inductive reasoning based on observations of the optical properties of solutions of organic compounds.

Thus, if high-energy particles or quanta of radiation fall upon the crystal, they can break the bonds. Conductivity in diamond induced by bombardment in this way has recently received considerable prominence in connection with "crystal counters" which have been used to detect nuclear particles and in experiments on conductivity induced by electron bombardment. An electron ejected from a bond constitutes a localized negative charge in the crystal and, since initially the bond structure was electrically neutral, the electron as it departs from its point of liberation leaves behind an equal, localized positive charge. Such a migratory electron, because it represents

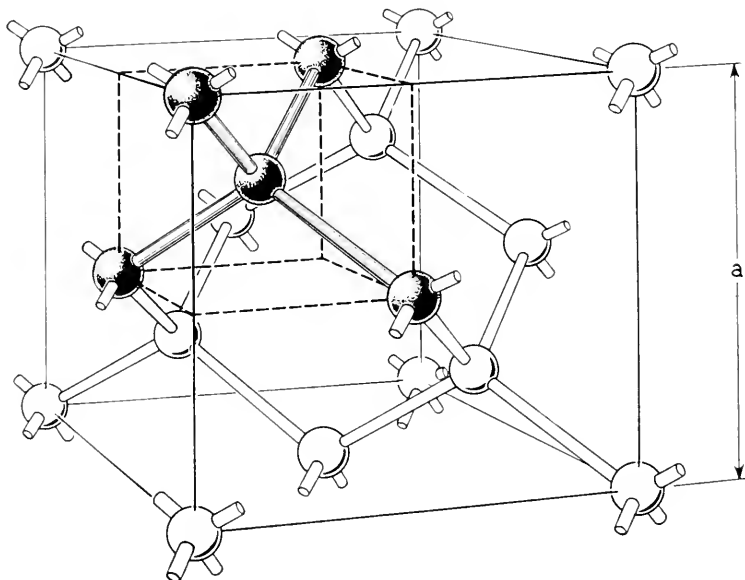


FIG. 2.

an excess over and above that required to complete the bond structure in its neighborhood, is called an "excess electron." Since it cannot enter any of the completed bonds in the lattice, it moves about in the crystal in a random manner under the influence of thermal agitation. If an electric field is applied, it tends to drift in the direction of the applied force and to carry a current. This illustrates conduction by excess electrons (referred to simply as conduction by electrons) and, as we shall see, is to be distinguished from the other process whereby an electron deficit enables conduction to be effected by "holes."

Such a hole, constituting a net, localized, positive charge in the crystal, moves from place to place by a reciprocal motion of electrons in the valence bonds; and, under the influence of an electric field, its random motion ac-



quires a systematic drift. Therefore it also can contribute to the current; in other words, current can flow as well by virtue of a deficit of electrons as by an excess of them.

In an illuminated and bombarded diamond crystal the electrons and holes, produced in pairs by the excitation, will of course drift in opposite directions under the influence of a field; the electron, being negative, drifts in the op-

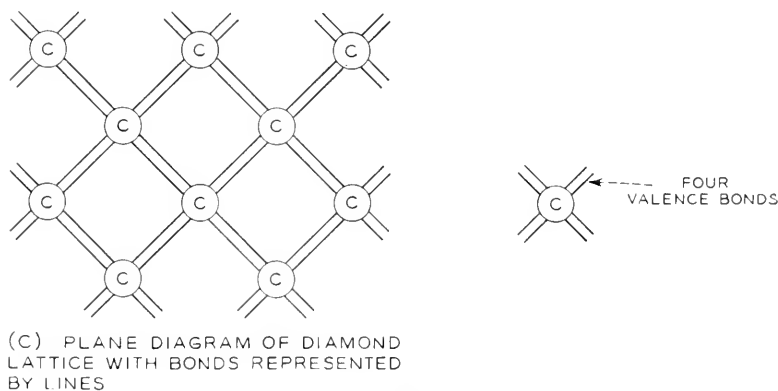
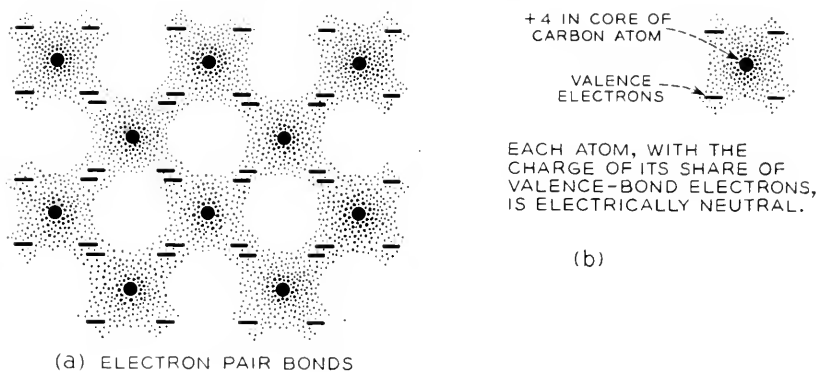


FIG. 3.

posite direction from the applied field, but its current is in the direction of the field. In the case of the hole, the reciprocal electron motions are once more opposite to the direction of the field (on the average). As a consequence, the net result is that the hole drifts in a direction to increase the current represented by the electrons. If the source of bombardment or illumination is removed, the conductivity dies away and the crystal will return to its normal state. This can occur by the recombination of holes and electrons. Whenever an electron drops into a hole, both the hole and the electron dis-

appear and the bond structure becomes complete, the excess energy being given up to the atoms in the form of thermal vibrations.<sup>4</sup>

If the temperature is sufficiently elevated, spontaneous breaking of some fraction of the covalent bonds by agitation will occur producing electrons and holes in equal numbers. In a diamond this effect would occur at such high temperatures that it would not be observed. However, it plays a major role in silicon and germanium at temperatures well within the range of investigation in the laboratory.

On the basis of quantum mechanical theory, it is found that a very high degree of symmetry exists between the behavior of electrons and the behavior

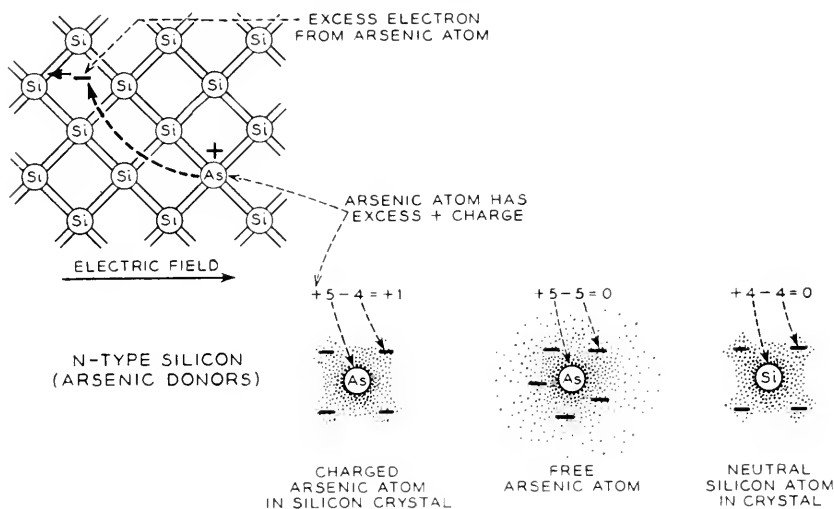


Fig. 4.

of holes. One may think of the hole as moving through the crystal as a positively charged particle with much the same attributes as a free electron except for the sign of its charge.

#### IMPURITY SEMICONDUCTORS: DONORS AND ACCEPTORS

If the only cases of conductivity open to investigation were like those discussed above, for which electrons and holes are present in equal numbers, the problem of interpreting the data would be very difficult. Fortunately, in the semiconductors silicon and germanium, there are cases in which conductivity is due to excess electrons only or to holes only.<sup>5</sup>

<sup>4</sup> The process of recombination may actually be much more complicated and may involve intermediate stages in which the hole or the electron is trapped.

<sup>5</sup> The behavior of silicon with impurities of the sorts discussed here was investigated by Scaff, Theurer, and Schumacher. Their work was stimulated by the development of silicon detectors for microwave use by R. S. Ohl, also of Bell Telephone Laboratories, in the prewar years.

If the conductivity of the sample is due to excess electrons it is called *n-type*, since the current carriers act like negative charges; if due to holes, it is called *p-type*, since the carriers act like positive charges.

Either type of conduction can be produced at will by admixture of a suitable "impurity," a donor such as arsenic yielding an excess of free electrons, while an acceptor like boron causes an electron deficit or a surplus of positive holes. The reason why arsenic and boron serve in these opposite capacities comes readily to hand.

The arsenic atom has five valence electrons surrounding a core having a net charge of  $+5$  units and, when introduced (e.g. in silicon) as a low-fraction impurity, it is believed that each arsenic atom displaces one of the silicon atoms from its regular site and forms four covalent bonds with the neighboring silicon atoms, thus using four of its five valence electrons (see Fig. 4). The extra electron cannot fit into these four bonds and is free to move about the crystal. This excess electron therefore constitutes a mobile localized negative charge. The arsenic atom, on the other hand, is an *immobile* localized positive charge, since its core, with a charge of  $+5$  units, is not neutralized by its share ( $-4$ ) of the charge in the valence bonds. Its net charge, therefore, just balances that of the excess electron it sets free in the crystal. Thus arsenic impurity atoms add excess electrons but do not disturb the over-all electrical neutrality of the crystal. The negative electrons, however, are somewhat attracted by the positive arsenic atoms and at low temperatures become weakly bound to them. At room temperature, thermal agitation shakes them off so that they become free.

To produce a p-type semiconductor we choose an added impurity, such as boron, having three valence electrons and therefore not enough to complete the valence bond structure surrounding it. The hole in one of the bonds to the boron atom can be filled by an electron from an adjacent bond, and when this occurs the hole migrates away to the bond which just gave up one of its electrons. The boron atom thus becomes an *immobile* localized negative charge. Because of the symmetry between the behavior of holes and electrons, we can describe the situation by saying that the negative boron atom attracts the positively charged hole but that thermal agitation shakes the latter off at room temperature so that it is free to wander about and contribute to the conductivity.

Because of their valencies, phosphorous and antimony, as well as arsenic are in the donor class while aluminum, gallium and indium are additional examples of the acceptor class.

It is beyond the scope of this prefatory note to describe how, by measurements of conductivity and the Hall effect as influenced by the amount of added donor or acceptor, it has been possible to determine the concentration of electrons and holes, as well as to fix the energies needed to remove an electron from a donor, a hole from an acceptor, and to break a covalent bond

between lattice atoms. In samples of germanium of such purity that the amount of added donor or acceptor was too small to determine by conventional chemical methods, the conductivity was still controlled by the processes outlined above. And it is interesting to note that a portion of this investigation was carried out with the aid of radioactive antimony alloyed with the germanium, the radioactive property making possible an accurate count of antimony atoms, though present only in extremely attenuated amounts.

The semiconductor papers in this issue of the Journal will explain how these simple facts of electron exchange give rise to rectifying and amplifying properties.

#### SEMICONDUCTOR RECTIFIERS AND AMPLIFIERS

A contact between a metal and semiconductor may act as a rectifier, the contact resistance being high for one direction of current flow and low for the opposite. Rectification results from the presence in the semiconductor adjacent to the interface of a potential barrier or hill which the current carriers, electrons or holes, must surmount in order to flow across the junction. The direction of easy flow is that in which the carriers flow from the semiconductor to the metal. An applied voltage which produces a current flow in this direction reduces the height of the potential hill and allows the carriers to flow more easily to the metal. When the voltage is applied in the opposite direction the height of the barrier which the carriers must surmount in going from the metal into the semiconductor is unchanged, to a first approximation, and the resistance of the contact remains high. A *p*-type semiconductor is positive, an *n*-type negative, relative to the metal, in the direction of easy flow.

Rectifying contacts can also be made between two semiconductors of opposite conductivity types. The direction of easy flow is again that for which the *p*-type is positive, the *n*-type negative. The rectifying boundary may separate two regions with different conductivity characteristics within the same crystal.

In some contact rectifiers it is necessary to consider the flow of both types of carriers, electrons and holes, even though one type is overwhelmingly in excess under equilibrium conditions. An example is the germanium point contact rectifier such as the 400 type varistor. The germanium used is *n*-type and the normal concentration of holes is small compared to the concentration of conduction electrons. Nevertheless, a large part of the current in the forward direction consists of holes flowing away from the contact rather than electrons flowing in. The flow increases the concentration of holes in the vicinity of the contact and there is a corresponding increase in the concentration of electrons to compensate for the space charge of the holes. This increase in concentration of carriers increases the conductivity

of the germanium. The holes introduced in this way gradually combine with electrons and disappear so that at large distances the current consists largely of electrons. Similar effects occur at  $n$ - $p$  boundaries in germanium; the current in the forward direction consists in part of holes flowing from the  $p$ -type region into the  $n$ -type region and electrons flowing from the  $n$ -type region into the  $p$ -type region.

The alteration of concentration of carriers and conductivity by current flow may be used to produce amplification in a number of ways. In the type-A transistor two point contacts are placed in close proximity on the upper face of a small block of  $n$ -type germanium. A large area low resistance contact on the base is the third element of the triode. Each point, when connected separately with the base electrode, has characteristics similar to those of the rectifier. When operated as an amplifier, one point, called the emitter, is biased in the forward direction so that a large part of the current consists of holes flowing away from the contact. The second point, called the collector, is biased in the reverse direction. In the absence of the emitter, the current consists largely of electrons flowing from the collector point to the base electrode. When the two points are in close proximity there is a mutual influence which makes amplification possible. The collector current produces a field which attracts the positively charged holes flowing from the emitter, so that a large part of the emitter current flows to the collector and into the collector circuit.

It has been found that rectifying boundaries between  $n$ - and  $p$ -type germanium may be used both as emitters and collectors, so that it is possible to make transistors without point contacts.

The following five papers are concerned with the behaviors of holes and electrons in semiconductors, with particular emphasis upon rectifying junctions and transistors. The first paper "Hole Injection in Germanium" describes new experiments on the behavior of holes and shows how their numbers and velocities may be measured and how they may be used to modulate the conductivity in the "filamentary transistor." The second paper "Some Circuit Aspects of the Transistor" describes the characteristics and equivalent circuits for the transistor. "Theory of Transient Phenomena in the Transport of Holes in an Excess Semiconductor" describes in mathematical terms a number of the processes encountered in the first paper and brings out interesting features of the nature of an advancing wave front of holes. "The Theory of Rectifier Impedances at High Frequencies" analyzes the behavior of metal-semiconductor rectifiers for high frequencies for the case in which the current is carried by one type of carrier only. As mentioned above, in rectifiers formed from  $p$ - $n$  junctions, currents of both holes and of electrons must be considered. Such rectifiers and related subjects are dealt with in "The Theory of  $p$ - $n$  Junctions in Semiconductors and  $p$ - $n$  Junction Transistors."

# Hole Injection in Germanium—Quantitative Studies and Filamentary Transistors\*

By

W. SHOCKLEY, G. L. PEARSON and J. R. HAYNES

Holes injected by an emitter point into thin single-crystal filaments of germanium can be detected by collector points. From studies of transient phenomena the drift velocity and lifetimes (as long as 140 microseonds) can be directly observed and the mobility measured. Hole concentrations and hole currents are measured in terms of the modulation of the conductivity produced by their presence. Filamentary transistors utilizing this modulation of conductivity are described.

## 1. INTRODUCTION

THE invention of the transistor by J. Bardeen and W. H. Brattain<sup>1, 2, 3</sup> has given great stimulus to research on the interaction of holes and electrons in semiconductors. The techniques discussed in this paper for investigating the behavior of holes in *n*-type germanium were devised in part to aid in analyzing the emitter current in transistors. The early experiments suggested that the hole flow from the emitter to the collector took place in a surface layer.<sup>1, 2</sup> The possibility that transistors could also be produced by hole flow directly through *n*-type material was proposed in connection with the *p-n-p* transistor.<sup>4</sup> Quite independently, J. N. Shive<sup>5</sup> obtained evidence for hole flow through the body of *n*-type germanium by making a transistor with points on opposite sides of a thin germanium specimen. Such hole flow is also involved in the coaxial transistor of W. E. Kock and R. L. Wallace.<sup>6</sup> Further evidence for hole injection into the body of *n*-type germanium under conditions of high fields was obtained by E. J. Ryder.<sup>7</sup>

In keeping with these facts it is concluded<sup>3</sup> that with two points close together on a plane surface, as in the type-A transistor<sup>8</sup>, holes may flow either in a surface layer or through the body of the germanium. For surface flow to be large, special surface treatments appear to be necessary; such treatments were not employed in the experiments described in this paper and the results are consistent with the interpretation that the hole current from the emitter point flows in the interior.

The experiments described in this paper, in addition to any practical implications, serve to put the action of emitter points on a quantitative basis and to open up a new area of research on conduction processes in semicon-

\* It is planned to incorporate this material in a book entitled "Holes and Electrons, an Introduction to the Physics of Transistors" currently being written by W. Shockley. This book is to cover much of the material planned for the "Quantum Physics of Solids" series which was discontinued because of the war.

ductors. It is worth while at the outset to contrast some of the new aspects of these experiments with the earlier experimental status of the bulk properties of semiconductors. Prior to the invention of the transistor, inferences about the behaviors of holes and electrons were made from measurements of conductivity and Hall effect. For both of these effects, under essentially steady state conditions, measurements were made of such quantities as lengths, currents, voltages and magnetic fields. The measurement of time was not involved, except indirectly in the calibration of the instruments. Nevertheless, on the basis of these data, definite mental pictures were formed of the motions of holes and electrons describing in particular their drift velocity in electric fields and the transverse thrust exerted upon them by magnetic fields. The new experiments show that something actually does drift in the semiconductor with the predicted drift velocity and does behave as though it had a plus or minus charge, just as expected for holes and electrons. In addition, experiments described elsewhere<sup>9</sup> show that the effect of sidewise thrust by a magnetic field actually is observed in terms of the concentration of holes and electrons near one side of a filament of germanium.

We shall discuss here evidence that holes are actually introduced into *n*-type germanium by the forward current of an emitter point and show how the numbers and lifetimes of the holes can be inferred from the data. We shall refer to this important process as "hole injection." Discussions of the reasons why an emitter should emit holes are given for point contacts by J. Bardeen and W. H. Brattain<sup>1, 2, 3</sup> and for *p-n* junctions elsewhere in this journal.<sup>4</sup> There are other possible ways in which semiconductor amplifiers can be made without the use of hole injection into *n*-type material or electron injection into *p*-type material.\* In this paper, however, our remarks will be restricted to semiconductors which have only one type of carrier present in appreciable proportions under conditions of thermal equilibrium; for such cases the theoretical considerations are simplified and are apparently in good agreement with the experiments.

## 2. THE MEASUREMENT OF DENSITY AND CURRENT OF INJECTED HOLES

The experiment in its semiquantitative form is relatively simple and is shown in Fig. 1.<sup>10</sup> A rod of *n*-type germanium is subjected to a longitudinal electric field  $E$  applied by a battery  $B_1$ . Collector and emitter point contacts are made to the germanium with the aid of a micromanipulator. The collector point is biased like a collector in a type-A transistor by the battery  $B_2$  and the signal obtained across the load resistor  $R$  is applied to the input of an oscilloscope. At time  $t_1$  the switch in the emitter circuit is closed so that a forward current, produced by the battery  $B_3$ , flows through the emitter point. At  $t_3$  the switch is opened. The voltage wave at the collector, as

\* For example see references 1 and 11.

observed on the oscilloscope, has the wave form shown in part (b) of the figure.

These data are interpreted as follows: When the emitter circuit is closed, the electrons in the emitter wire start to flow away from the germanium (i.e. positive current flows into the germanium). These electrons are furnished by an electron flow in the germanium towards the point of contact. The flow in the germanium may be either by the excess electron process or by the hole process. In Fig. 2 we illustrate these two possibilities. At first

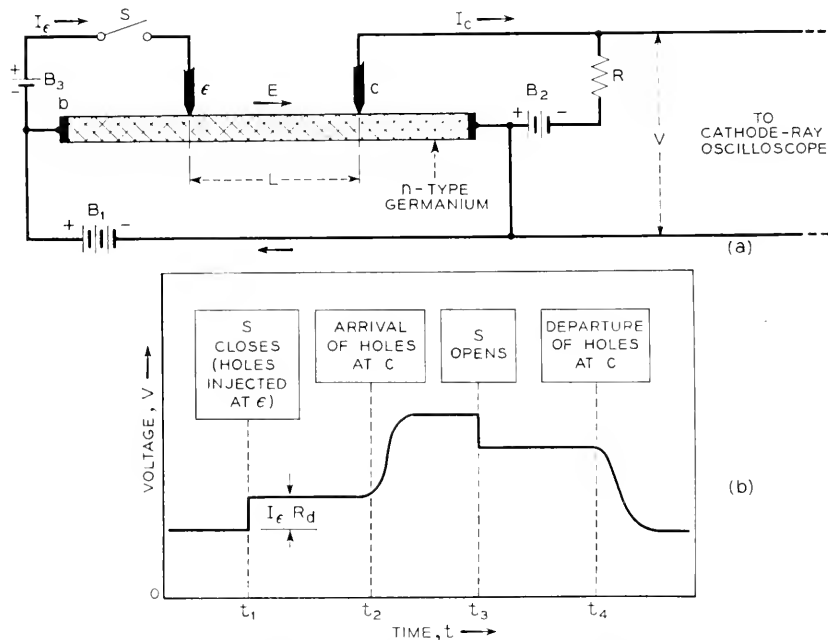


Fig. 1—Experiment to investigate the behavior of holes injected into *n*-type germanium

(a) Experimental arrangement.

(b) Signal on oscilloscope showing delay in hole arrival at  $t_2$  in respect to closing  $S$  at  $t_1$  and delay in hole departure at  $t_4$  in respect to opening  $S$  at  $t_3$ .

glance it might appear that the difference between these two processes is unimportant since the net result in both cases is a transfer of electrons from the germanium to the emitter point. There is, however, an important difference, one which makes several forms of transistor action possible. In the case of the hole process an electron is transferred from the valence band structure to the metal. After this the hole moves deeper into the germanium. As a result the electronic structure of the germanium is modified in the neighborhood of the emitter point by the presence of the injected holes.

Under the influence of the electric field  $E$ , the injected holes drift toward



the collector point with velocity  $\mu_p E$ , where  $\mu_p$  is the mobility of a hole, and thus traverse the distance  $L$  to the collector point in a time  $L/\mu_p E$ . When they arrive at the collector point, they increase its reverse current and produce the signal shown at  $t_2$ .

There are two important differences between the signal produced at  $t_2$  and that produced at  $t_1$ . The signal at  $t_1$ , which is in a sense a pickup signal, would be produced even if no hole injection occurred. We shall illustrate this by considering the case of a piece of ohmic material substituted for the

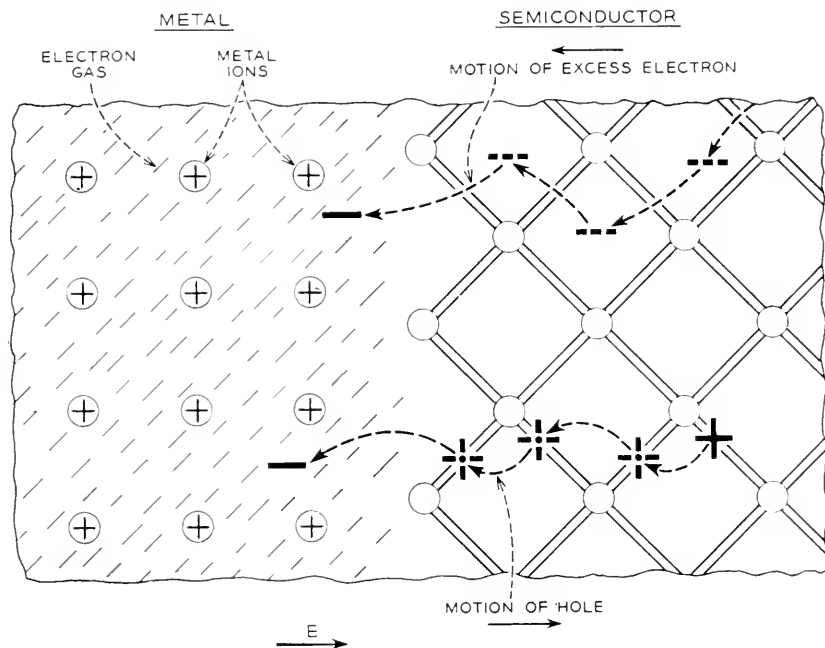


Fig. 2—Electron flow to the metal may be produced by an excess electron moving toward the metal or by bonding electrons jumping (dashed arrows) successively into a hole thus displacing the hole deeper into the semiconductor.

germanium. Conventional circuit theory applies to such a case; however, in order to contrast this purely ohmic case with that of hole injection, we shall also give a description of the conventional theory of signal transmission in terms of the motion of the carriers. According to conventional circuit theory, the addition of the current  $I_e$  would simply produce an added  $IR$  drop due to current flow in the segment of the specimen to the right of the collector. This voltage drop is denoted as  $I_e R_d$  in part (b),  $R_d$  representing the proper combination of resistances to take into account the way in which  $I_e$  divides in the two branches. This signal will be transmitted from the emitter to the collector with practically the speed of light—the ordinary theory of signal

transmission along a conductor being applicable to it. This high speed of transmission does not, of course, imply a correspondingly high velocity of motion of the current carriers. In fact the rapidity of signal transmission has nothing to do with the speed of the carriers and comes about as follows: If the ohmic material is an electronic conductor, then the withdrawal of a few electrons by the emitter current produces a local positive charge. This positive charge produces an electric field which progresses with the speed of light and exerts a force on adjoining electrons so that they move in to neutralize the space charge. The net result is that electrons in all parts of the specimen start to drift practically instantaneously. They flow into the specimen from the end terminals to replace the electrons flowing out at the emitter point and no appreciable change in density of electrons occurs anywhere within the specimen.\*

The distinction between the process just described and that occurring when holes are injected into germanium is of great importance in understanding many effects connected with transistor action. One way of summarizing the situation is as follows: In a sample having carriers of one type only, electrons for example, it is impossible to alter the density of carriers by trying to inject or extract carriers of the same type. The reason is, as described above (or proved in the footnote), that such changes would be accompanied by an unbalanced space charge in the sample and such an unbalance is self-annihilating and does not occur.†

When holes are injected into *n*-type germanium, they also tend to set up a space charge. Once more this space charge is quickly neutralized by an electron flow. In this case, however, the neutralized state is not the normal thermal equilibrium state. Instead the number of current carriers present has been increased by the injected holes and by an equal number of electrons drawn in to neutralize the holes. The total number of electrons in the specimen will thus be increased, the extra electrons coming in from the metal terminals which complete the circuit with the emitter point. The presence of the holes and the neutralizing electrons near the emitter point modify the conductivity. As we shall show below, this modification of conductivity may be so great that it can be used to measure hole densities and also to give power gain in modified forms of the transistor. We shall summarize this situation as follows: *In a semiconductor containing substantially only one type of current carrier, it is impossible to increase the total carrier concentration by*

\* This is a description in words of the result ordinarily expressed in terms of the dielectric relaxation time obtained as follows:  $\nabla \cdot I = -\rho$ ,  $I = \sigma E = -\sigma \nabla \Psi$ ,  $\nabla^2 \Psi = -4\pi\rho/\kappa = \dot{\rho}/\sigma$  so that  $\rho = \rho_0 \exp [-(4\pi\sigma/\kappa)t]$ , where  $I$  = current density,  $\rho$  = charge density,  $\sigma$  = conductivity,  $E$  = electric field,  $\Psi$  = electrostatic potential,  $\kappa$  = dielectric constant.

† In the case of modulation of conductivity by surface charges,<sup>11</sup> a net charge is produced by the field from the condenser plate. The changed charge density extends slightly into the specimen but should not be confused with the true volume effect of hole injection. Such space charge layers are discussed in other articles in this issue.<sup>1, 12</sup>

injecting carriers of the same type; however, such increases can be produced by injecting the opposite type since the space charge of the latter can be neutralized by an increased concentration of the type normally present.

Thus we conclude that the existence of two processes of electronic conduction in semiconductors, corresponding respectively to positive and negative mobile charges, is a major feature in several forms of transistor action.

In terms of the description given above, the experiment of Figure 1 is readily interpreted. The instantaneous rise at  $t_1$  is simply the ohmic contribution due to the changing total currents in the right branch when the emitter current starts to flow. After this, there is a time lag until the holes injected into the germanium drift down the specimen and arrive at the collector. When the current is turned off at  $t_3$ , a similar sequence of events occurs.

The measured values of the time lag of  $t_1 - t_2$ , the field  $E$  and the distance  $L$  can be used to determine the mobility of the holes. The fact that holes, rather than electrons, are involved is at once evident from the polarity of the effect; the disturbance produced by the emitter point flows in the direction of  $E$ , as if it were due to positive charges; if the electric field is reversed, the signal produced at  $t_2$  is entirely lacking. The values obtained by this means are found to be in good agreement with those predicted from the Hall effect and conductivity data. The Hall mobility values obtained on single crystal filaments of  $n$ - and  $p$ -type germanium<sup>13</sup> are

$$\mu_p = 1700 \text{ cm sec per volt/cm}$$

$$\mu_n = 2600 \text{ cm sec per volt/cm}$$

The agreement between Hall effect mobility and drift mobility, as was pointed out at the beginning of this section, is a very gratifying confirmation of the general theoretical picture of holes drifting in the direction of the electric field.

We shall next consider a more quantitative embodiment of the experiment just considered. In Fig. 3, we show the experimental arrangement. In this case it is essential in order to obtain large effects that the cross-section of the germanium filament be small. A thin piece of germanium is cemented to a glass backing plate and is then ground to the desired thickness. After this the undesired portions are removed by sandblasting while the desired portions are protected by suitable jigs consisting of wires, scotch tape, metal plates, etc. After the sandblasting, the surface of the germanium is etched. In this way specimens smaller than  $0.01 \times 0.01$  cm in cross-section have been produced. The ends of the filament are usually made very wide so as to simplify the problem of making contacts.

Under experimental conditions, a battery like  $B_1$ , of Figure 1 applies a "sweeping" field in the filament so that any holes injected by the emitter

current are swept along the filament from left to right. In the small filaments used for these experiments, the resulting concentration of holes is so high that large changes in conductivity are produced to the right of the emitter point and, as we shall describe below, these changes can be measured and the results used to determine the hole current at the emitter point. In order to treat this situation quantitatively, we introduce a quantity  $\gamma$  defined as follows:

$\gamma =$  the fraction of the emitter current carried by holes.

Accordingly, a current  $\gamma I_e$  of holes flows to the right from  $\epsilon$  and produces a hole density, denoted by  $p$ , which is neutralized by an equal added electron density. A fraction  $(1 - \gamma)I_e$  of electrons flows to the left; these electrons do not, however, produce any increased electron density to the left of the emitter since they are of the sign normally present in the  $n$ -type material. The presence of the holes to the right in the filament increases the conductivity  $\sigma$  (as shown in Fig. 3c) both because of their own presence and the presence of the added electrons drawn in to neutralize the space charge of the holes. The mobility of electrons is greater than the mobility of holes, the ratio being<sup>13</sup>

$$b = \mu_n / \mu_p = 1.5 \text{ for germanium}$$

and the electrons are always more numerous than the holes\*

$$n = n_0 + p, \quad (2.1)$$

where  $n_0$  is the concentration of electrons which would be present to neutralize the donors if  $p$  were equal to zero; consequently, the current carried by electrons is greater than the current carried by holes. The concentration of holes diminishes to the right due to the fact that holes may recombine with electrons as they flow along the filament.

From this experiment the value of  $\gamma$  and the lifetime of a hole in the filament can be determined. The measurements are made with the aid of the two probe points  $P_1$  and  $P_2$ . The conductance of the filament between these points is obtained by measuring the voltage difference  $\Delta V$  and dividing it into the current  $I_b + I_e$ , no current being drawn by the probes themselves. The necessary formulae for calculating hole density and hole current,

\* The notation used in the equations is as follows:  $n, p, n_0$  = respectively density of electrons, of holes, of electrons when no holes are injected.  $N_d$  and  $N_a$  are the densities of donors and acceptors, assumed ionized so that  $n_0 = N_d - N_a$ .  $I_e, I_b, I_c$  are as shown on Figs. 3 and 9. ( $I_e$  used for the probe collector in Figures 1 and 8 does not enter the equations.)  $q = |q|$  is the charge on the electron, used to be consistent with Ref. 4, where  $e$  is used for 2.718 ...

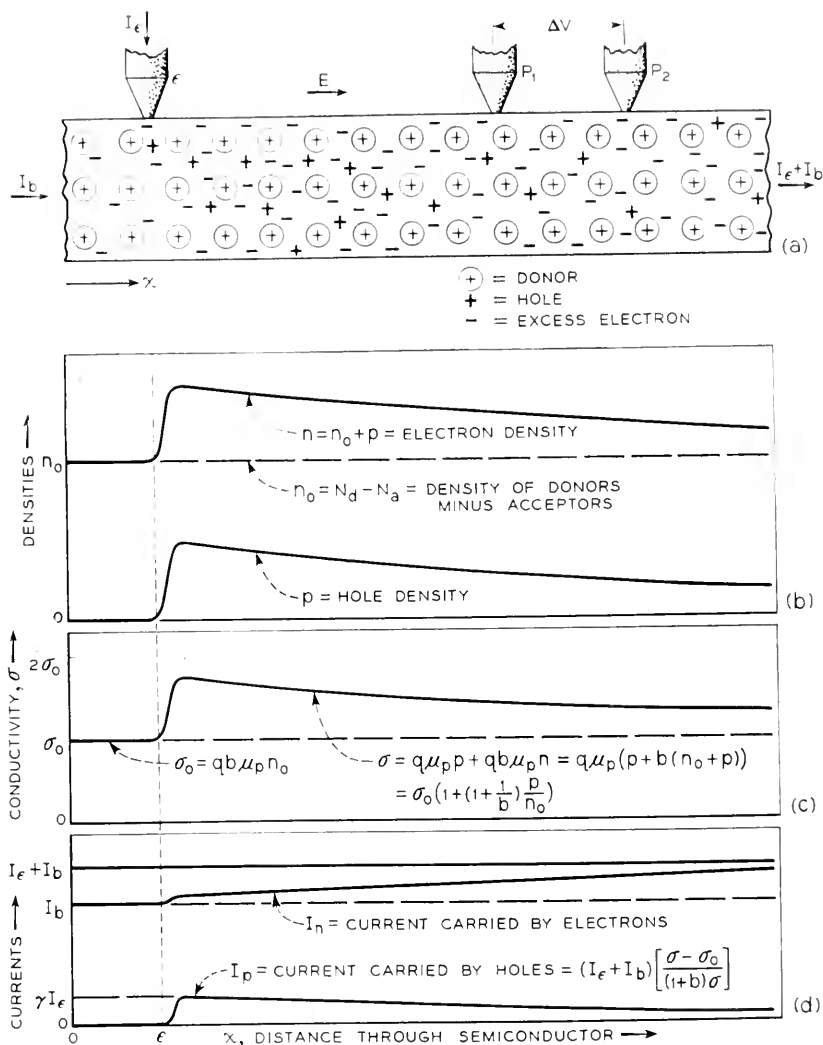


Fig. 3—Method of measuring hole densities and hole currents.

(a) Distribution of holes, electrons and donors. Acceptors, which may be present, are omitted for simplicity, the excess of donor density  $N_d$  over acceptor density  $N_a$  being  $n_0$ .

(b) To the right of the emitter the added hole density  $p$  is compensated by an equal increase in electron concentration.

(c) The conductivity is the sum of hole and electron conductivities.

(d) The total current  $I_b + I_\epsilon$  to the right of the emitter is carried by  $I_p$  and  $I_n$  in the ratio of the hole to the electron conductivity.

shown on the Figure, are derived as follows:

$$\text{Normal conductivity: } \sigma_0 = q\mu_n n_0, \quad (2.2)$$

$$\begin{aligned} \text{conductivity with holes present } \sigma &= q\mu_n n + q\mu_p p \\ &= q\mu_n(n_0 + p) + q\mu_p p = \sigma_0[1 + (1 + b^{-1})(p/n_0)]. \end{aligned} \quad (2.3)$$

The conductance,

$$G = (I_e + I_h)/\Delta V,$$

between  $P_1$  and  $P_2$  is proportional to the local conductivity, and hence to

$$1 + (1 + b^{-1})(p/n_0),$$

so that a measurement of the conductance gives a measurement of  $p/n_0$ . Letting  $G$  and  $G_0$  be the conductances between the points with and without hole injection, we have

$$\frac{G}{G_0} = \frac{\sigma}{\sigma_0} = 1 + (1 + b^{-1})(p/n_0) \quad (2.4)$$

or

$$\frac{p}{n_0} = \frac{\sigma - \sigma_0}{\sigma_0(1 + b^{-1})} = \frac{(G/G_0) - 1}{1 + b^{-1}}. \quad (2.5)$$

The ratio of hole current to electron current is  $q\mu_p p / q\mu_n n$  and the fraction of the current carried by holes is thus

$$\begin{aligned} \frac{I_p}{I_n + I_p} &= \frac{q\mu_p p}{q\mu_n n + q\mu_p p} = \frac{p}{bn_0 + (1 + b)p} \\ &= \frac{p/n_0}{b[1 + (1 + b^{-1})(p/n_0)]} = \frac{1 - (G_0/G)}{1 + b} \end{aligned} \quad (2.6)$$

Hence from the measured values of  $G$ , it is possible to obtain the fraction of the current carried by holes. Multiplying this fraction by  $I_e + I_h$  then gives the actual hole current flowing past the probe points.\* If there were no decay, the current past the probe points would be  $\gamma I_e$  and since  $I_e$  is known,  $\gamma$  could be easily determined. Actually, however, there may be quite an appreciable decay. However, if the current  $I_h$  is increased, the holes will be swept more rapidly from the emitter to the probes and less decay will result. Thus by increasing  $I_h$ , the effect of recombination can be minimized and the value of hole current can be extrapolated to the value it would have in the absence of decay. This value is, of course,  $\gamma I_e$ .

\* In these calculations the formulae  $n = p + n_0$ , corresponding to completely ionized donors and acceptors, has been used. In germanium this is a good approximation. For silicon, however, modifications will be necessary.

In Fig. 4 we show some plots of this sort. The ordinate is  $I_p/I_e$  which should approach  $\gamma$  as the value of  $I_b$  becomes larger. The theory indicates that a logarithmic plot should be used and that the abscissa should be made proportional to transit time so that the case of no decay or zero transit time

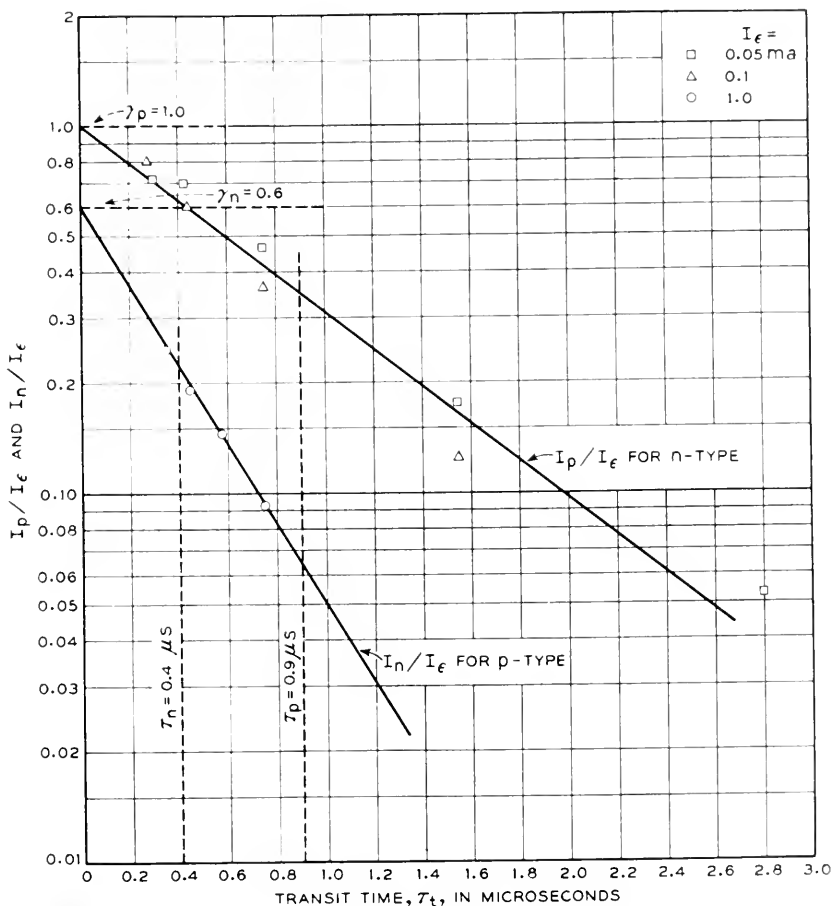


Fig. 4—Extrapolation of measured hole and electron currents to zero transit time in order to determine  $\gamma$ .

comes at the left edge.<sup>†</sup> The conclusion reached from this plot is that for the case of the *n*-type sample, the value of  $\gamma$  is substantially unity,—all the

<sup>†</sup> If the lifetime of a hole is  $\tau$ , then the hole current at the points is  $I_p = \gamma I_e \exp(-t/\tau)$  where  $t$  is the transit time to a point midway between the points, say a distance  $L$  from the emitter. If the electric field is  $E = \Delta V/\Delta L$ , then the transit time  $t = L\Delta L/\mu_p\Delta V$ . Hence if  $\ln I_p$ , as determined from the ratio of conductivities is plotted against  $t = L\Delta L/\mu_p\Delta V$  a straight line with intercept  $\ln \gamma I_e$  and slope  $-1/\tau$  should be obtained.

emitter current is holes. For the opposite case in which electrons are injected into *p*-type material,<sup>14</sup> the corresponding value of  $I_n/I_e$  extrapolates to 0.6 indicating that for this case 60% of the current is carried by electrons and 40% by holes. For these particular specimens the lifetimes are found to be 0.9 and 0.41 microseconds respectively. There is a body of evidence, some of which we discuss below, that holes combine with electrons chiefly on the surface of the filament.

### 3. THE INFLUENCE OF HOLE DENSITY ON POINT CONTACTS

The presence of holes near a collector point causes an increase in its reverse current; in fact the amplification in a type-A transistor is due to the modulation of the collector current by the holes in the emitter current. The influence of hole density upon collector current has been studied in connection with experiments similar to those of Fig. 3. After the hole current and the hole density are measured, a reverse bias of 20 to 40 volts is applied. The reverse current is found to be a linear function of the hole density. Figure 5 shows typical plots of such data. Different collector points, as shown, have quite different resistances. However, once data like that of Fig. 5 have been obtained for a given point, the currents can then be used as a measure of hole density. This experimental procedure for determining hole density is simpler than that involved in using the two points and much better adapted to studies of transient phenomena. It is necessary in employing this technique to keep the current drawn by the collector point somewhat smaller than  $I_b + I_e$ ; otherwise the disturbance in the current flow due to the collector current is too great and the sample of the hole current is not representative. Experiments have shown, however, that this condition is readily achieved and that the collector current may be satisfactorily used as a measure of hole density.

The hole density also affects the resistance of a point at low voltage. Studies of this effect have also been made in connection with the experiment of Fig. 3. After the hole density has been determined from measurements of  $\Delta V$  and  $I_b + I_e$ , a small additional voltage (0.015 volts) was applied between  $P_1$  and  $P_2$  and the current flowing externally between  $P_1$  and  $P_2$  was measured. From these data a differential conductance, for small currents, is obtained for the two points  $P_1$  and  $P_2$  in series. As is shown in Fig. 6, this conductance is seen to be a linear function of the hole concentration. The conductance of a point contact arises in part from electron flow and in part from hole flow. From experiments using magnetic fields<sup>9</sup>, it has been estimated that under equilibrium conditions the two contributions to the conductance may be comparable. In connection with Fig. 6 it should be noted that the hole concentration on the abscissa is the average hole



concentration throughout the entire cross section; the hole concentration may be much less near the surface due to recombination on the surface.

Techniques of the sort described above can be used to measure the properties of collector points. If a collector point is placed between the emitter and  $P_1$  in Fig. 3, then the hole current extracted by the collector can be determined in terms of the hole current past  $P_1$  and  $P_2$ . By these means an "intrinsic  $\alpha$ " for the collector point can be determined. The intrinsic  $\alpha$  is

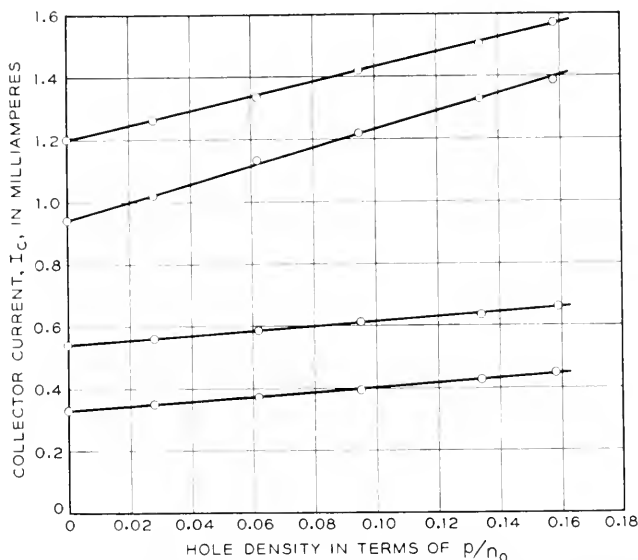


Fig. 5—Dependence of collector current  $I_c$  upon average hole density being swept by collector point. Collector biased 20 volts reverse.

defined as the ratio of change in collector current per unit change in hole current actually arriving at the collector.

#### 4. STUDIES OF TRANSIENT PHENOMENA

The technique of using a collector point to measure hole concentrations has been employed in a number of experiments similar to those described in connection with Fig. 1. These experiments give information concerning hole lifetimes, hole mobilities, diffusion and conductivity modulation.

One of the methods employed to measure hole lifetime involves the measurement of the increase in collector current, produced by the arrival of the leading edge of the hole pulse, as a function of the transit time of the holes from emitter to collector. This time is varied by varying the distance between the emitter and the collector points.

In Fig. 7 we show a plot, obtained in this way, from a sample of germanium having dimensions  $1.0 \times .05 \times .08$  cm. It is seen that the increase in collector current due to hole arrival decays exponentially with a time constant of 18 microseconds. This time constant increases as the dimensions of the germanium sample are increased so that a time constant of 140 microseconds was measured, using a sample having dimensions  $2.5 \times .35 \times .30$

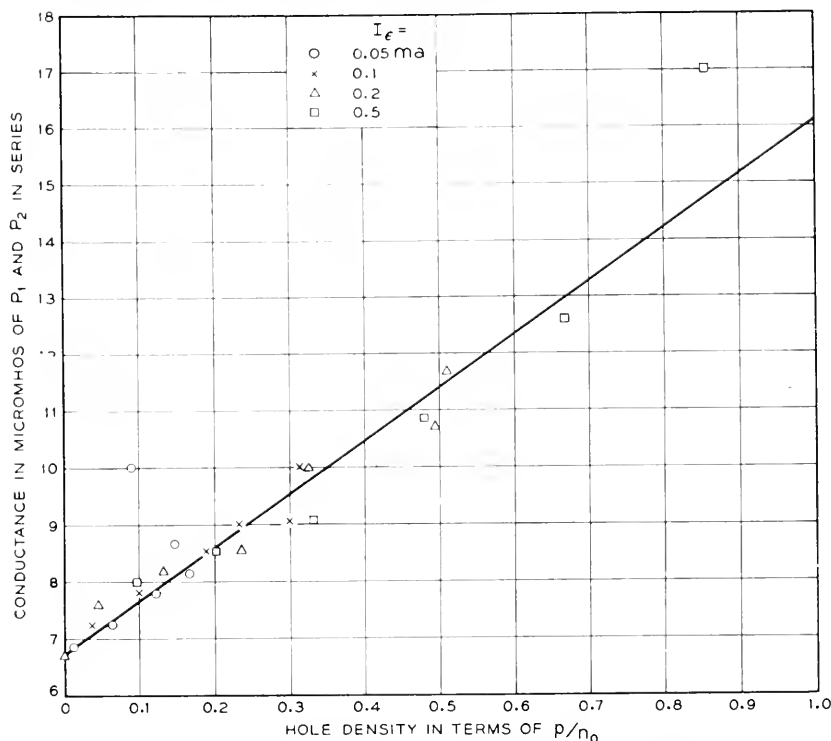


Fig. 6—Conductance of  $P_1$  and  $P_2$  of Fig. 3 in series as a function of  $p/n_0$ , showing that conductance depends on hole concentration but not on currents in filament. For each value of  $I_e$  the hole density was varied by varying  $I_b + I_e$  from .038 to 0.78 ma.

cm. Since the holes injected into the interior of this sample can diffuse to the surface and recombine in about 100 microseconds, the process may still be largely one of surface recombination. In any event, it may be concluded that the lifetime in the bulk material used must be at least 140 microseconds. Making use of the electron density determined from other measurements, we conclude that the recombination cross section must be less than  $10^{-15}$   $\text{cm}^2$ . This cross section, which is less than  $1/400$  the area of a germanium

atom, may be so small because a hole-electron pair has difficulty in satisfying in the crystal the conditions somewhat analogous to conservation of energy and momentum which hinder recombination of electrons and positive ions in a gas discharge. Thus it has been pointed out that a hole-electron pair will have a lowest energy state in which the two current carriers behave something like the proton and electron of a hydrogen atom.<sup>15</sup> Such a bound pair are called an exciton and the energy given up by their recombination is the "exciton energy." In order to recombine they must radiate this energy in

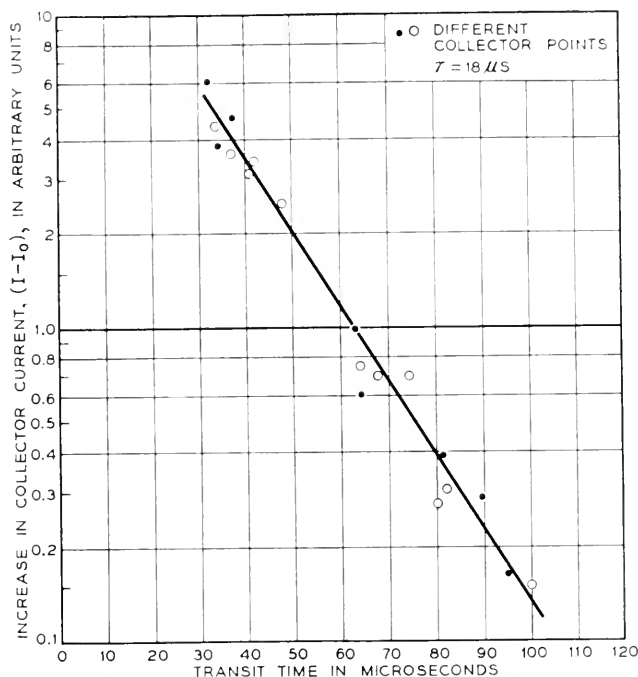


Fig. 7—The decay of injected holes in a sample of *n*-type germanium.

the form of a light quanta (photon) or a quantum of thermal vibration of the crystal lattice (phonon). The recombination time for the photon recombination process can be estimated from the optical constants for germanium and the theory of radiation density using the principle of detailed balancing, which states that under equilibrium conditions the production of hole electron pairs by photon absorption equals the rate of recombination with photon emission; the lifetime obtained in this way is about 1 second at room temperature indicating that the photon process is unimportant.<sup>19</sup> As has been pointed out by A. W. Lawson,<sup>16</sup> the highest energy phonon will have

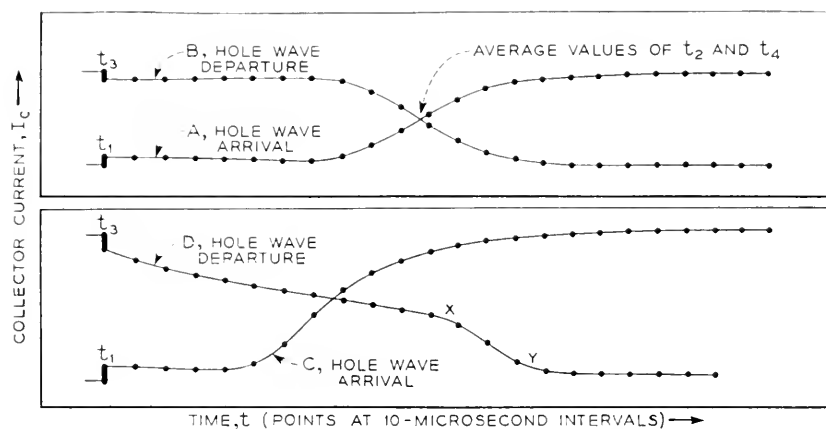
insufficient energy to carry away the "exciton energy" of a hole-electron pair and, therefore, the release of energy will require the cooperation of several phonons with a correspondingly small transition probability.

When a square pulse of holes is injected in an experiment like that of Fig. 1, the leading and trailing edges of the current at the collector point are deformed for several reasons. Due to the high local fields at the emitter point, some of the holes actually start their paths in the wrong direction—i.e. away from the collector; these lines of flow later bend forward so that those holes also pass by the collector point but with a longer transit time than holes which initially started towards the collector. A spread in transit times of this sort is probably largely responsible for the loss of gain at high frequencies in transistors. For the experiments described below, however, this effect is negligible compared to two others which we shall now describe.

On top of the systematic drift of holes in the electric field, there is superimposed a random spreading as a result of their thermal motion. This would cause a sharp pulse of holes to become spread so that after drifting for a time  $t_d$  the hole concentration would extend over a distance proportional to  $\sqrt{Dt_d}$  where  $D$ , the diffusion constant for holes,  $= kT\mu_p/q = 45 \text{ cm}^2/\text{sec}$ . As a result of this effect, the leading and trailing edges of the square wave of emission current become spread out when they arrive at the collector. This is shown in Fig. 8, curve *A* for the leading edge and *B* for the trailing edge. The points are 10 microsecond marker intervals traced from an oscilloscope, the time being measured from the instant at which the emitter current starts. For *A* and *B* the emitter current was so small compared to the current  $I_b$  that the holes produced a negligible modulation of conductivity and each hole moved in essentially the same electric field. It is to be observed that the wave shapes are nearly symmetrical in time about the half rise point and that the *A* and *B* waves are identical except for sign. This is just the result to be expected from diffusion. Furthermore, analysis shows that the spread in arrival time is in good quantitative agreement with the theoretical wave shape using the diffusion constant appropriate for holes. For this case the mid-point of the rise, corresponding to the crossing point of the curves, gives the average arrival time and has been used to obtain an accurate measure of the mobility.

Curves *C* and *D* correspond to conditions in which the emitter current was relatively large—two thirds of the base current. High impedance sources are used so that  $I_b$  is constant and  $I_e$  is a good flat topped wave. For the currents used in this experiment, the conductivity is appreciably modulated by the presence of holes. This accounts for the shape of curve *C*, corresponding to the arrival of holes at the collector. It is seen that this curve is not symmetrical but is much more gradual towards later times. The reason for

this is that the first holes to arrive are those which have diffused somewhat ahead of the rest and move in material of low conductivity. The later holes travel in an environment of relatively high conductivity and, consequently, in a lower electric field. (Since the current is the same at all points between emitter and collector, the field is inversely proportional to the conductivity.) The transit time for the later holes is, therefore, longer and the hole density builds up more slowly for the latter part of the incoming pulse of holes. The wave form obtained from the trailing edge of the emitter pulse, curve *D*, is in striking contrast with the leading edge. The first gradual decay, up to



- A & B EMITTER CURRENT SMALL, ABOUT 4% OF  $I_b$ , SO THAT ALL HOLES MOVE IN THE SAME FIELD.  
 C LEADING EDGE OF PULSE FOR  $I_e = 2/3 I_b$ .  
 D TRAILING EDGE OF HOLE PULSE FOR  $I_e = 2/3 I_b$ , SHOWING SHARPENING FROM X TO Y DUE TO TENDENCY OF LAGGING HOLES TO CATCH UP.

Fig. 8—Collector current characteristics for the circuit shown in Fig. 1.

point X, is due to recombination of holes and electrons; at  $t_3$  the emitter current becomes zero; consequently, the electric field is reduced and the holes arriving at X have taken a longer transit time than the holes arriving at  $t_3$  and a larger fraction of them have recombined with electrons. The true trailing edge, running from X to Y, is appreciably sharper than the leading edge. The reason for this is that holes lagging behind the main body of holes are in a region of relatively low conductivity and high electric field and tend to catch up with the main body. Thus the same effect which lengthens wave C acts to shorten wave D.

C. Herring has been able to obtain mathematical solutions for the appropriate equations bearing on the matters just discussed. His theory is presented elsewhere in this issue.<sup>17</sup>

The delay feature discussed in connection with Figs. 1 and 8 indicates interesting possibilities of using germanium filaments as delay or storage elements.

### 5. THE THEORY OF THE FILAMENTARY TRANSISTOR

In Fig. 9 we show a transistor with a filamentary structure.<sup>15</sup> Modulation is achieved in this case by injecting holes at the emitter point which flow to the right and modulate the resistance in the output branch between emitter and collector. Structures of this sort can be produced by the sand-blasting technique discussed in Section 2. The enlarged ends, which give the

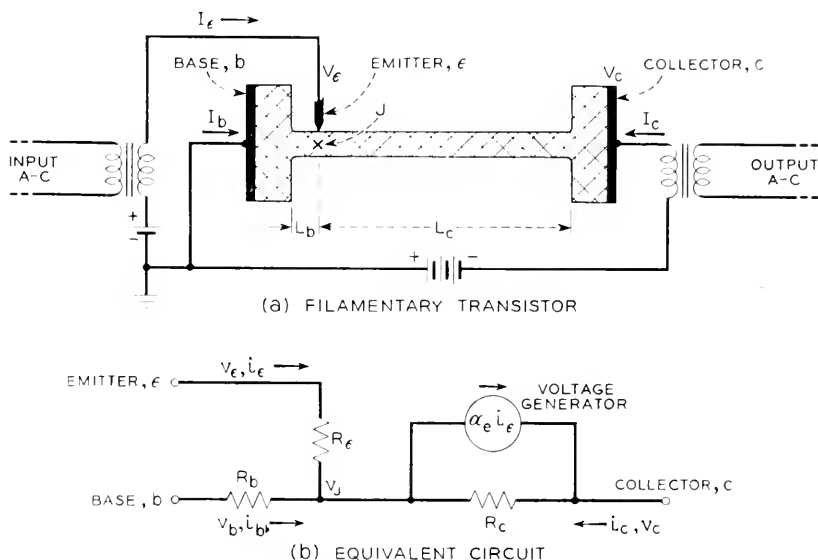


Fig. 9—Filamentary transistor and equivalent circuit.

unit a dumbbell appearance, decrease the problem of making contact to the unit. The large area at the left side serves the additional purpose of reducing unwanted hole emission from the metal electrode and affords an opportunity for any emitted holes to recombine before they enter the narrow part of the unit.

The theory of this transistor is relatively simple and most of the features we shall discuss in connection with it have counterparts in the theory of the type-A transistor. We shall discuss the case for which the injected current is a small fraction of the total current in the filament. Under these conditions we can use a simple linear theory. We shall show that the behavior of the transistor can be given for small a-c signals by the equivalent circuit in

Figure 9(b), which shows the current and voltage relationships in a form equivalent to those used in connection with the type-A transistor.

The point  $J$  in Fig. 9 represents a point in the filament near the emitter point. The current from the emitter point will be determined by the difference between its voltage  $V_e$  and that of the surrounding semiconductor, namely the voltage at  $J$ . Thus we can write

$$I_e = f_e(V_e - V_J). \quad (5.1)$$

For small a-c variations,  $i_e$ ,  $v_e$  and  $v_J$ , this equation leads to the relationship

$$i_e = (v_e - v_J)f'_e, \quad (5.2)$$

where  $f'_e$  is the derivative of  $f_e$  in respect to its argument. Letting  $f'_e = 1/R_e$  this equation becomes

$$v_e - v_J = R_e i_e. \quad (5.3)$$

This relationship is correctly represented by the  $R_e$  branch of the equivalent circuit. The voltage at  $J$ , under the assumed operating conditions with  $I_e$  positive and much less than  $I_c$ , will be  $-I_b R_b$  where  $R_b$  is the resistance from the base to an imaginary equipotential surface passing through  $J$  and  $v_b = 0$ , corresponding to *grounded base* operation. This leads to

$$v_J = -R_b i_b = +R_b i_e + R_b i_c, \quad (5.4)$$

since  $i_b + i_e + i_c = 0$ . This relationship is obviously satisfied by the  $R_b$  branch of the equivalent circuit.

We now come to the collector branch which we have represented as a resistance  $R_c$  and a parallel current generator\*  $\alpha_e i_e$ . (This circuit is equivalent to another in which the parallel current generator is replaced by a series voltage generator  $\alpha_e R_c i_e$ .) We must show that this part of the equivalent circuit represents correctly the effect of injecting holes into the right arm of the filament. We shall suppose that there is negligible recombination so that the hole current injected at the emitter point flows through the entire filament. (We consider recombination in the next section.) The current  $I_c$  in the collector branch thus contains a component  $-\gamma I_e = I_p$  of hole current (minus because of the algebraic convention that positive  $I_c (= -I_b - I_e)$  flows to the left). The added hole and electron concentrations lower the resistance and  $R_c$  changes to  $R_c + \delta R_c$ , where  $\delta R_c$  is negative. The current voltage relationship for this branch of the filament then becomes

$$V_c - V_J = (R_c + \delta R_c) I_c. \quad (5.5)$$

\*  $\alpha_e$  in the equivalent circuit differs from  $\alpha = -(\partial I_c / \partial I_e) v_e$  by the relationship  $\alpha_e = \alpha + (\alpha - 1)(R_b/R_c)$ , equivalent to equation (6.8).

Our problem is to reexpress this relationship in terms of the small a-c components and show that it reduces to the relationship

$$v_c - v_J = R_c(i_e + \alpha_e i_c) \quad (5.6)$$

corresponding to the equivalent circuit. For small emitter current the analysis is carried out conveniently as follows: The ratio of hole current to the total current is  $-\gamma I_c / I_e$ . The ratio  $(R_c + \delta R_c) / R_c$  corresponds to  $G_0 / G$  discussed in connection with Fig. 3. The ratio of hole current to total current is given in (2.6) in terms of  $G_0 / G$  and may be rewritten as

$$-\frac{\gamma I_c}{I_e} = \frac{1 - (G_0 / G)}{1 + b} = \frac{-\delta R_c}{(1 + b)R_c}, \quad (5.6)$$

giving

$$\delta R_c = R_c(1 + b)\gamma I_c / I_e. \quad (5.7)$$

(Since  $I_c$  is negative and  $I_e$  is positive this equation shows that  $\delta R_c$  is negative, i.e., the conductivity has been increased by the hole current.) Putting this value of  $R_c + \delta R_c$  into the equation for  $V_c - V_J$  gives

$$\begin{aligned} V_c - V_J &= (R_c + \delta R_c)I_c \\ &= R_c[I_c + (1 + b)\gamma I_c]. \end{aligned} \quad (5.8)$$

If we consider small a-c variations in the currents and voltages, this reduces to the equation given by the equivalent circuit with

$$\alpha_e = (1 + b)\gamma. \quad (5.9)$$

The data of Section 2 indicate that for holes injected into  $n$ -type germanium  $\gamma = 1$ , and since  $b = 1.5$  we obtain  $\alpha_e = 2.5$ .

The quantity  $v_J$  can be eliminated by using  $v_J = R_b(i_e + i_c)$  in equation (5.3) for  $v_e$  and the small signal form of (5.8) for  $v_c$  leading to the pair of equations

$$v_e = (R_e + R_b)i_e + R_b i_c \quad (5.10)$$

$$v_c = (R_b + \alpha_e R_c)i_e + (R_c + R_b)i_c. \quad (5.11)$$

These equations are formally identical with those for the equivalent circuits of the type-A transistor.

It should be emphasized that although hole injection into  $n$ -type germanium plays a role in both the type-A and the particular form of filamentary transistor shown in Fig. 9, there are differences in the principles of operation. One important feature of the type-A is the high impedance of the rectifying collector contact which, however, does not impede hole flow and another important feature is the current amplification occurring at the collector contact. Neither of these features is present in the filamentary type shown. Instead, the high impedance at the collector terminal arises from the small



cross-section of the filament. The modulation of the output current takes place through the change in body conductivity due to the presence of the added holes, a change which appears to be unimportant in the type-A transistor. In the filamentary type, current amplification is produced by the extra electrons whose presence is required to neutralize the space charge of the holes. Current amplification in the type-A transistor is, probably, also produced by the space charge of the holes<sup>3</sup> but the details of the mechanism are not as easily understood.

## 6. EFFECTS ASSOCIATED WITH TRANSIT TIME

Two important effects arise from the fact that a finite transit time is required for holes to traverse the  $R_c$  side of the filament: during this time the holes recombine with electrons and the modulation effect is attenuated for this reason; also the modulation of the conductivity of the filament at any instant is the result of the emitter current over a previous interval and for this reason there will be a loss of modulation when the period of the a-c signal is comparable with the transit time or less.

For the small signal theory, the effect of transit time is readily worked out in analytic terms. We shall give a derivation based on the assumption that the lifetime of a hole before it combines with an electron is  $\tau_p$ . According to this assumption, the fraction of the holes injected at instant  $t_1$  which are still uncombined at time  $t_2$  is  $\exp[-(t_2 - t_1)/\tau_p]$ . This means that the effect in the filament at any instant  $t_2$  is the average, weighted by this factor, of all the contributions prior to  $t_2$  back to time  $t_2 - \tau_t$  where  $\tau_t$  is the transit time; holes injected prior to  $t_2 - \tau_t$  have passed out of the filament by time  $t_2$ . If the emitter current is represented by  $i_{e0}e^{i\omega t}$ , the effective average emitter current is

$$i_{e\text{ eff}}(t_2) = i_{e0} \int_{t_2 - \tau_t}^{t_2} e^{i\omega t_1 - (t_2 - t_1)/\tau_p} dt_1 / \tau_t. \quad (6.1)$$

The term  $dt_1/\tau_t$  is chosen so that a true average is obtained since the sum of all the  $dt_1$  intervals add up to  $\tau_t$ . The integral is readily evaluated and gives

$$i_{e\text{ eff}}(t_2) = i_{e0} e^{i\omega t_2} \frac{1 - \exp[-i\omega\tau_t - (\tau_t/\tau_p)]}{i\omega\tau_t + (\tau_t/\tau_p)}. \quad (6.2)$$

The result so far as the equivalent circuit is concerned is that obtained by taking  $\alpha_e$  as\*

$$\alpha_e = \gamma(1 + b)\beta, \quad (6.3)$$

\* The derivation of equations (5.10) and (5.11), describing the equivalent circuit, shows that hole injection enters only through the term  $\delta R_c I_c$  in (5.8). This term leads only to  $\alpha_e R_c i_e = (1 + b)\gamma R_c i_e$  in (5.11) and should be replaced by  $(1 + b)\gamma R_c i_{e\text{ eff}} = (1 + b)\gamma\beta R_c i_e$  leading to (6.3).

where

$$\beta = \frac{1 - \exp[-i\omega\tau_t - (\tau_t/\tau_p)]}{i\omega\tau_t + (\tau_t/\tau_p)}. \quad (6.4)$$

$\beta$  represents the effect of recombination and transit angle,  $\omega\tau_t$ , in reducing the gain.

We shall consider two limiting cases of this expression. First if  $\omega\tau_t$  is very small, the new factor becomes

$$\beta = (\tau_p/\tau_t)(1 - e^{-\tau_t/\tau_p}). \quad (6.5)$$

If  $\tau_t$  is much larger than  $\tau_p$ , so that the holes recombine before traversing the filament, then the exponential is negligible and  $\beta$  becomes simply  $\tau_p/\tau_t$ . This means that the effectiveness of the holes is reduced by the ratio of their effective distance of travel to the entire length of the filament, i.e.,  $\tau_p/\tau_t$  is the ratio of distance travelled in one lifetime to the entire length of the filament. Essentially the holes modulate only the fraction of the filament which they penetrate. The transit time depends on the field in the filament which is  $|V_c - V_J|/L_c$ , the absolute value being used since  $V_c$  is negative. The transit time is thus

$$\tau_t = L_c [\mu_p |V_c - V_J|/L_c] = L_c^2 \mu_p |V_c - V_J|. \quad (6.6)$$

For very small emitter currents  $V_c - V_J = R_c V_c$  ( $R_c + R_b$ ) so that

$$\tau_t = L_c^2 (R_c + R_b) \mu_p R_c |V_c| \quad (6.7)$$

and  $\tau_t$  is inversely proportional to  $V_c$ . For large values of  $V_c$ ,  $\tau_t$  approaches zero and  $\beta$  approaches unity. The dependence of  $\beta$  upon  $V_c$  has been investigated by measuring  $\alpha$  and plotting it as a function of  $|1/V_c|$  as shown in Fig. 10. The value of

$$\alpha = -(\partial I_c / \partial I_e)_{V_c} \quad (6.8)$$

is readily found from the equivalent circuit, using equation (5.11), to be

$$\alpha = \frac{R_b}{R_b + R_c} + \frac{\alpha_e R_c}{R_b + R_c}. \quad (6.9)$$

For the particular structure investigated, the values of  $R_b$  and  $R_c$ , obtained at  $I_e = 0$ , were in the ratio 1:4. The value of  $\alpha$  obtained by extrapolating the data to  $|1/V_c| = \infty$  is 2.2; the value given by the formula for this case with  $\beta = 1$ , is

$$\alpha = 0.2 + 0.8 \times 2.5 \times \gamma, \quad (6.10)$$

from which we find  $\gamma = 1.0$ , in agreement with the result of Fig. 4 that

substantially all of the emitter current is carried by holes. The theoretical curve shown on the Figure is

$$\alpha = 0.2 + 0.8 \times 2.5 \times |V_c|^{10} (1 - e^{10|V_c|}). \quad (6.11)$$

This corresponds to

$$\frac{\tau_t}{\tau_p} = \frac{10}{|V_c|} = \frac{I_e^2 (R_c + R_b)}{\tau_p \mu_p R_c |V_c|}, \quad (6.12)$$

from which it was concluded that for the particular bridge studied  $\tau_p$  was 0.2 microseconds.

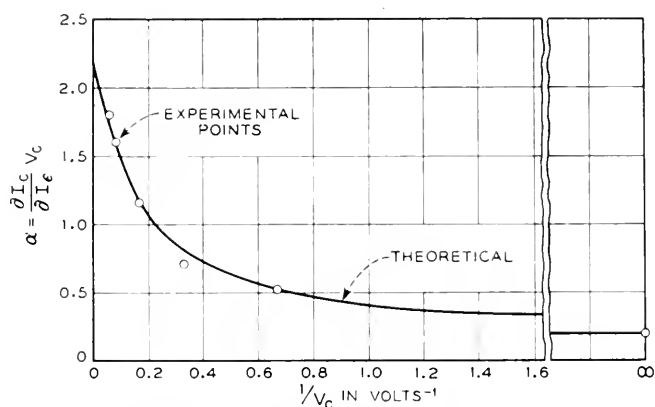


Fig. 10— $\alpha$  versus  $1/V_c$  showing agreement with the theory for the value of  $\beta$ .

If  $\tau_t$  is much shorter than  $\tau_p$ , then the holes penetrate the whole filament and  $\beta$  becomes

$$\beta = \frac{1 - \exp(-i\omega\tau_t)}{i\omega\tau_t} = \frac{e^{-i\omega\tau_t/2} \sin(\omega\tau_t/2)}{(\omega\tau_t/2)}. \quad (6.13)$$

For small values of  $\omega\tau_t$ ,  $\beta$  approaches unity since  $(\sin x)/x$  approaches unity as  $x$  approaches zero. For  $\omega\tau_t/2 = \pi$ , the response is zero. This is the condition that  $\tau_t = 2\pi/\omega = 1/f$ . For this case the filament is just so long that the modulation is averaged over the time of one cycle of the input signal and since this average includes all phases, the modulation vanishes.

Preliminary experiments with filamentary transistors, made in accordance with the principles discussed above, appear to confirm the general aspects of the theory. Power gains of 15 db have been obtained and frequency responses showing a drop of 3 db in  $\alpha$  at  $10^6$  cycles/sec. have been observed. Noise measurements indicate an improvement of 10 to 15 db over the average type-A transistor for comparable conditions of preparation.

## ACKNOWLEDGMENTS

We have been aided and encouraged in these experiments by many of our colleagues in the Research and Apparatus Development Departments. We are particularly indebted to W. H. Brattain and H. R. Moore for help with experimental problems, to J. Bardeen and W. van Roosbroeck for assistance with the theory and to P. W. Foy and W. C. Westphal for their many contributions in connection with fabricating and measuring the filaments.

## REFERENCES

1. J. Bardeen and W. H. Brattain, *Phys. Rev.*, **74**, 230 (1948).
2. W. H. Brattain and J. Bardeen, *Phys. Rev.*, **74**, 231 (1948).
3. J. Bardeen and W. H. Brattain, *Phys. Rev.*, **75**, 1208 (1949).
4. W. Shockley, *Bell Syst. Tech. J.*, July (1949).
5. J. N. Shive, *Phys. Rev.*, **75**, 689 (1949).
6. W. E. Kock and R. L. Wallace, *Electrical Engineering*, **68**, 222 (1949).
7. E. J. Ryder and W. Shockley, *Phys. Rev.*, **75**, 310 (1949).
8. For reviews of the type-A transistor see reference 3, R. M. Ryder, *Bell Laboratories Record*, Mar. 1949, J. A. Becker and J. N. Shive, *Electrical Engineering*, **68**, 215 (1949) and R. M. Ryder, *Bell Syst. Tech. J.*, July (1949).
9. H. Suhl and W. Shockley, *Phys. Rev.*, **75**, 1617 (1949), **76**, 180 (1949).
10. Experiments of this sort were first reported by J. R. Haynes and W. Shockley, *Phys. Rev.*, **75**, 691 (1949).
11. W. Shockley and G. L. Pearson, *Phys. Rev.*, **74**, 232 (1948).
12. John Bardeen, *Bell Syst. Tech. J.*, July (1949).
13. G. L. Pearson, *Phys. Rev.*, **76**, 179 (1949).
14. Transistors using *p*-type germanium have been described by W. G. Pfann and J. H. Scaff, *Phys. Rev.*, **76**, 459 (1949). Electron injection in *p*-type germanium has also been observed by R. Bray, *Phys. Rev.*, **76**, 458 (1949) and *Phys. Rev.*, **76**, 152 (1949).
15. G. Wannier, *Phys. Rev.*, **52**, 191 (1937).
16. Personal communication; a somewhat similar case is treated by B. Goodman, A. W. Lawson and L. I. Schiff, *Phys. Rev.*, **71**, 191 (1947).
17. C. Herring, *Bell Syst. Tech. J.*, July (1949).
18. Transistors of this type, employing *p-n* junctions as well as point contacts as emitters, have been discussed by W. Shockley, G. L. Pearson, M. Sparks, and W. H. Brattain, *Phys. Rev.*, **76**, 459 (1949).
19. Optical constants for germanium have been published by W. H. Brattain and H. B. Briggs, *Phys. Rev.*, **75**, 1705 (1949). The integration over the radiation distribution was carried out by W. van Roosbroeck.

## Some Circuit Aspects of the Transistor

By R. M. RYDER and R. J. KIRCHER

### INTRODUCTION

THE purpose of this note is to discuss in a general way some circuit aspects of the transistor. It is rather interesting that in order to discuss its circuit aspects, little direct reference to the transistor is necessary. One needs only certain properties of the transistor which are empirically obtainable by measurement; these properties then determine behavior in the manner prescribed by the methods of general network theory. In principle, one needs no knowledge of the physics of the transistor in order to treat it circuitwise; any "black box" with the same electrical behavior at its terminals would act the same way.

It is rather fortunate for our purposes that the problem does separate nicely in this way. The operation of the transistor is reasonably well understood; but, for calculations of performance from physical properties, the numerical parameters needed are somewhat inaccessible, numerous and complicated. The paper by Shockley<sup>1</sup> gives some calculations of this kind which are illuminating for theoretical understanding. However, just as with electron tubes, practical engineering calculations often do not need to go back to the ultimate physics. Starting from the electrical properties of the transistor as empirically determined by measurements on its terminals, we need go only to the literature of electrical engineering to find much practically useful information on properties of circuits which could be built around the unit.

This method of characterizing the electrical performance of a device more or less independently of its physical construction has come into wide use in recent years. A considerable amount of work has been done with applications to both electron tubes and transistors at the Bell Telephone Laboratories by L. C. Peterson.<sup>2</sup> The purpose of the present note, however, is not to go deeply into the subject but rather to review it in a general way, indicating applications to some of the simpler transistor circuits and comparisons with electron tubes. For more profound analyses one may refer to Peterson's work.

<sup>1</sup> "The Theory of p-n Junctions in Semiconductors and p-n Junction Transistors," W. Shockley, this issue of *The Bell System Technical Journal*.

<sup>2</sup> "Equivalent Circuits of Linear Active Four-Terminal Networks," L. C. Peterson, *Bell System Technical Journal*, Oct. 1948, pp. 593-622.

The method used for circuit analysis may be grouped under the following headings:

1. Linear problems, like low-level amplifiers or the question of onset of oscillations. Such problems visualize the transistor as making only small excursions from an assumed operating point and are best treated by the method of small-signal analysis. The unit is assigned an equivalent circuit or, in mathematical terms, is dealt with by means of linear equations.
2. Slightly non-linear problems, like Class A power amplifiers. Here the excursions about the operating point are large enough to bring in higher-order effects like harmonic generation or intermodulation, but still small enough so that these effects can be treated by adding to the equivalent circuit certain distortion generators. Mathematically, some terms need to be added to the linear equations but these terms are of the nature of corrections, not big changes.
3. Highly non-linear problems, such as Class B or C amplifiers, oscillators, switches, harmonic generators. Here the excursions about the characteristic are so large as to reduce the linear approximation to the status of a qualitative guide or perhaps to invalidate it entirely; mathematically, the small signal series either require many terms for accuracy or else do not converge at all. These large-signal problems usually have to be treated by methods special for each problem. Frequently one uses graphical constructions from the static characteristics, or analytical methods starting from reasonable approximations to the static characteristics.
4. Finally, in certain highly non-linear problems the non-linear features are in a sense subsidiary; one is really interested in the behavior of a superposed small signal subject to a linear analysis. The non-linear part of the problem may appear in the form of circuit parameters or frequency shifts which may be left for empirical determination. Such problems are exemplified by mixers, modulators, or switches.

The subsequent discussion will emphasize mainly the linear problems where the methods of circuit analysis are most effective, but will touch on some of the other fields occasionally.

### THE TYPE A TRANSISTOR

Perhaps at this point is the place to pay our respects to the physics of the transistor. A view of the Type A transistor<sup>3</sup>, currently being made in small quantities, is shown in Fig. 1. It is about  $\frac{1}{2}$  inch long and  $\frac{3}{16}$  inch in diameter. Two small phosphor bronze "cat-whiskers" make point contacts close together to a block of germanium. A large area ohmic contact to the

<sup>3</sup> "Type A Transistor," R. M. Ryder, *Bell Laboratories Record*, March 1949, pp. 89-93.

germanium constitutes the third electrode, called the base. How it works is shown in a purely descriptive way in Fig. 2. One point, called the collector,

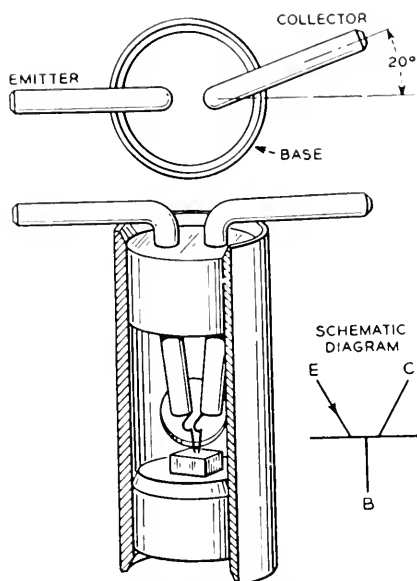


Fig. 1—Cutaway view of transistor.

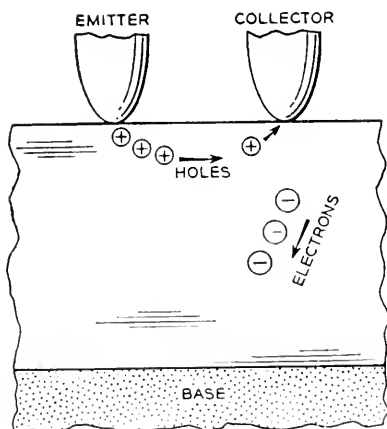


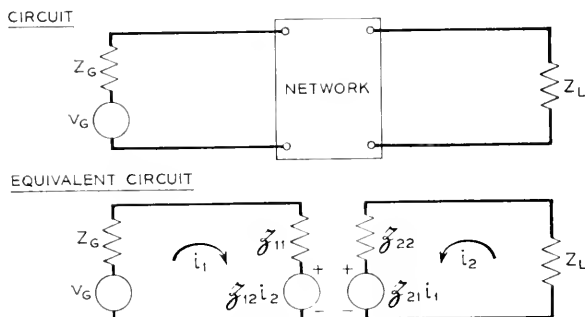
Fig. 2—Transistor mechanism.

is a rectifier biased strongly in the low-conducting direction. It therefore has a rectifying barrier in the germanium near it, which causes the collector impedance to be high. However, the collector can be influenced by the

emitter if the latter is arranged to emit anomalous charge carriers, that is, carriers of the sign not normally present in the interior of the material.

### EQUIVALENT CIRCUITS

As has been explained by Bardeen, Brattain, and Shockley, many features of the transistor are nicely explained by this picture of its action; but, for present purposes of circuit analysis, we shall now take the purely empirical



Equations

$$\begin{aligned} i_1(Z_G + \mathfrak{Z}_{11}) + i_2\mathfrak{Z}_{12} &= v_G \\ i_1\mathfrak{Z}_{21} + i_2(\mathfrak{Z}_{22} + Z_L) &= 0 \end{aligned}$$

Circuit determinant  $\Delta = (\mathfrak{Z}_{11} + Z_G)(\mathfrak{Z}_{22} + Z_L) - \mathfrak{Z}_{12}\mathfrak{Z}_{21}$

Input impedance  $Z_{11} = \mathfrak{Z}_{11} - \frac{\mathfrak{Z}_{12}\mathfrak{Z}_{21}}{\mathfrak{Z}_{22} + Z_L}$

Output impedance  $Z_{22} = \mathfrak{Z}_{22} - \frac{\mathfrak{Z}_{12}\mathfrak{Z}_{21}}{\mathfrak{Z}_{11} + Z_G}$

Operating power gain  $G_0 = 4R_G R_L \left| \frac{-\mathfrak{Z}_{21}}{\Delta} \right|^2$

Insertion power gain  $G_1 = \left| \frac{(Z_G + Z_L)\mathfrak{Z}_{21}}{\Delta} \right|^2$

Fig. 3—Synopsis of general four-pole—impedance analysis.

view and regard the transistor as a *black box* whose performance is to be determined by electrical measurements on its terminals.

A picture of a black box is shown in Fig. 3 along with the equations describing it. The performance is completely characterized if one knows the voltage and current at each of the two pairs of terminals. Now, of these four variables, only two are independent since, if any two are fixed, the other two are determined. One can therefore describe the network in terms of any two variables and, since there are six possible ways to choose a pair of variables from a set of four, there are six ways of describing the network.

To recall what is done for electron tubes is helpful. In the case of a triode



the voltages on grid and plate are usually taken as independent variables; the grid and plate currents are taken as functions of the voltages. It becomes natural, then, to measure tubes with regulated power supplies having low impedances to keep the voltages constant, and one is then naturally led to describe tubes in terms of admittances. Now the trouble with this scheme for transistors is that many of them oscillate when connected to low impedances, that is, many transistors are short-circuit unstable. To avoid this difficulty it is convenient to measure with high impedances in the leads; the analytical counterpart is to regard the currents as independent variables, leading naturally to a description of the transistor in terms of impedances, as shown in the figure.

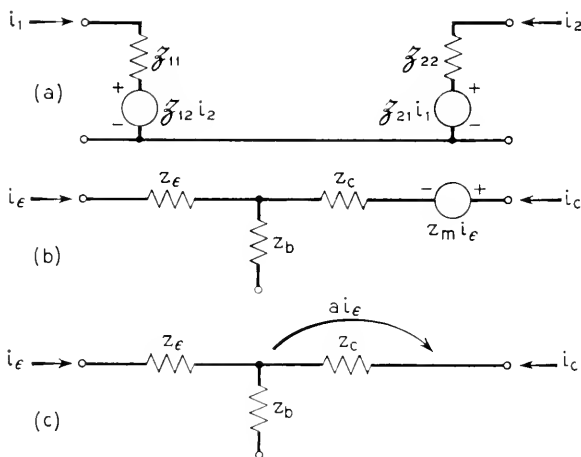
This description by open-circuit impedances happens to be a good one for many purposes, but there is nothing final or unique about it. In fact at high frequencies one of the other descriptions becomes more convenient.

By interpreting the  $\mathcal{Z}$  equations as circuit equations, one is led directly to the first equivalent circuit of Fig. 4. A little consideration shows why the  $\mathcal{Z}$ 's are called open-circuit impedances. For example, if the second mesh is open-circuited, then the equation says that  $\mathcal{Z}_{11}$  is the ratio of input voltage to input current, that is, the input open-circuit impedance; while  $\mathcal{Z}_{21}$  is the ratio of output voltage to input current, that is, the open-circuit forward transimpedance. Similarly  $\mathcal{Z}_{12}$  is the open-circuit feedback transimpedance and  $\mathcal{Z}_{22}$  is the open-circuit output impedance. Most of the subsequent discussion is concerned with low frequencies, where the impedances reduce to resistances.

This equivalent circuit for small signals is only one of many possibilities. Another, which is in fact more frequently used, is shown on Fig. 4. It consists of a T of resistors, each of which is associated with one of the transistor leads, and a voltage generator in series with the collector lead whose ratio to the emitter current is also of the dimensions of a resistance. The elements of this equivalent circuit are related to the former one by a simple subtraction. The other equivalent circuit on Fig. 4 is obtained by converting the series voltage generator to the equivalent shunt current generator, whose ratio to the emitter current is now a dimensionless constant which we shall call  $a$ .

These circuits, as well as all the other numerous possibilities, are equivalent in the sense that they all give exactly the same performance for any external connection of the unit. These three, however, are particularly well-behaved in that usually none of the circuit elements is negative; they are readily accessible to measurement; the association of the various circuit elements with corresponding regions within the transistor appears to have some physical significance; and, finally, the parameters are not too dreadfully dependent on the exact operating point used.

In the choice among various equivalent circuits, it appears that the optimum of convenience is also the one which most closely approaches the underlying physical situation. In agreeing to use the *black box* approach we have resolutely ignored the physical details, but here they are presenting themselves in a new way, having sneaked in the back door after we barred the front. Now, however, having chosen an equivalent circuit, we shall continue pursuing the circuit analysis in resolute ignorance of the physics. In what follows various equivalent circuits may be used, depending on the convenience of the moment.



Figs. 4—Some equivalent circuits.

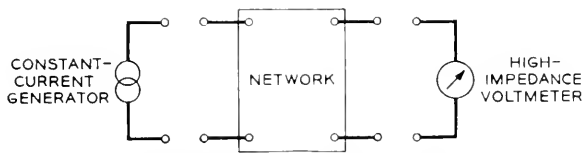


Fig. 5—Principle of measurement method.

The principle of a method used for rapid measurement of the transistor impedances is shown in Fig. 5, illustrating the measurement of forward transimpedance. A pair of terminals of the transistor is driven by a small alternating current of a few thousand cycles from a high impedance generator; the voltage developed is read by a high-impedance voltmeter. By calibrating the meter directly in ohms, one can read off the open circuit resistances of the unit as rapidly as one can switch and read meters.

Average values found by this method for the Type A transistor are shown on Fig. 6, together with data on the direct-current operating point. Since

development is still at an early stage, there are considerable variations between units.

### SINGLE STAGE AMPLIFIERS. STABILITY, ELECTRON TUBE ANALOGY

An amplifier can be built in a straightforward manner by using the emitter as input electrode and collector as output electrode, the base being common to the two circuits. This amplifier is therefore called the grounded base amplifier. Figure 7 shows a schematic circuit using the average parameters just mentioned, working between 500 ohms and 20,000 ohms. The amplifier has an operating power gain of 17 db, power output Class A 10 milliwatts, noise figure at 1000 cycles 60 db with a variation inversely with frequency, and frequency response down 3 db at 5 megacycles.

Type A Transistor			
D.C. Operating Point:		$I_e = 0.6$ ma	$V_e = 0.71$
		$I_c = -2$ ma	$V_c = -40$ V
Circuit Parameters:		$r_e = 240$ ohms	$r_b = 290$ ohms
		$r_c = 19000$ ohms	$r_m = 34000$ ohms
		$Z_{11} = 530$ ohms	$Z_{12} = 290$ ohms
		$Z_{21} = 34000$ ohms	$Z_{22} = 19000$ ohms

Fig. 6—Equivalent circuit parameter values.

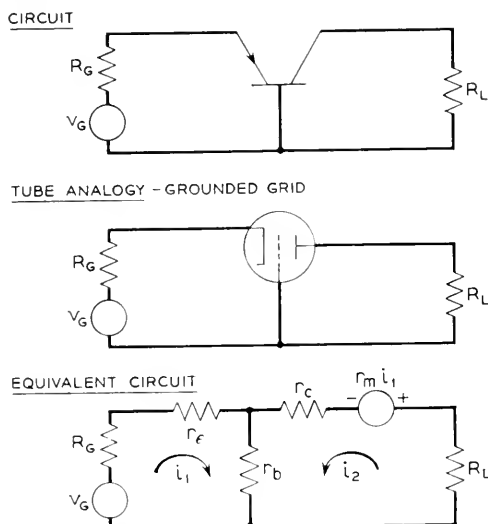
Some comments are in order on how this amplifier compares with an electron tube amplifier. First of all, the amplifying function and the manner of analyzing it from the circuit point of view are very similar, even though the internal mechanisms are markedly different. Secondly, there are qualitative differences in circuit behavior, which are set forth on Fig. 8. The base resistance  $r_b$  acts as a positive feedback element which, under adverse conditions, can cause the circuit to oscillate. A necessary condition for stability is that the circuit determinant shall be positive, and this can be written as follows:

$$\frac{r_m}{R_c} < 1 + \frac{R_E}{R_B} + \frac{R_E}{R_C} \quad (1)$$

Here the quantity  $r_m$  is the net mutual resistance of the transistor, and the capital R's are the total resistances in the corresponding leads, internal and external. One can see several features, as follows:

1. If  $R_B = 0$ , the circuit can be stable.
2. If  $R_B > 0$ , as usual, the circuit can be stable if the emitter and collector lead resistances are large enough or if  $r_m$  is not too large. In other words, resistance in the base lead tends toward instability if  $r_m$  is large; resistance in emitter or collector leads tends toward stability.

In the grounded base circuit the property of low base resistance is important, since the backward transmission depends directly on this property. In circuit terms, the base impedance is the feedback impedance in the grounded base circuit, and its value helps to set a limit on the stable gain which can be realized.



Equations:

$$\begin{aligned} i_1(R_G + r_e + r_b) + i_2 r_b &= v_G \\ i_1(r_b + r_m) + i_2(r_b + r_c + R_L) &= 0 \end{aligned}$$

Circuit determinant  $\Delta = (R_G + r_e + r_b)(R_L + r_c + r_b) - r_b(r_b + r_m) > 0$  for stability

Input impedance  $R_{11} = r_e + r_b - \frac{r_b(r_b + r_m)}{R_L + r_c + r_b}$

Output impedance  $R_{22} = r_c + r_b - \frac{r_b(r_b + r_m)}{R_G + r_e + r_b}$

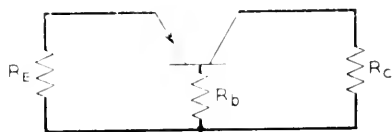
Operating power gain  $G_0 = 4R_G R_L \left( \frac{-(r_b + r_m)}{\Delta} \right)^2$

Typical values: For  $R_G = 500\omega$ ,  $R_L = 20,000\omega$   
Then  $R_{11} = 280\omega$ ,  $R_{22} = 9600\omega$   
 $G_0 = 17^{db}$

Fig. 7—Synopsis of grounded base amplifier.

The grounded base circuit has properties which are strongly reminiscent of the grounded grid electron triode amplifier in that both have low input impedance, high output impedance, and no change of signal polarity in transmission. The analogy was pointed out by Shockley. That this similarity is no coincidence can be seen by comparing the third equivalent circuit

above with the triode equivalent circuit of F. B. Llewellyn and L. C. Peterson<sup>4</sup> in Fig. 9. Both circuits have the same topological form, and have similar impedance levels if the triode is considered to be operating in the frequency range of some tens of megacycles. The most important difference concerns the quantity  $a$ , a current amplification factor which, for the transistor, may be considerably greater than unity; while the analogous quantity



Can be stable if:

$$\frac{r_m}{R_c} < 1 + \frac{R_E}{R_b} + \frac{R_E}{R_c}$$

$R$ 's include resistive elements both internal and external to the transistor.

Fig. 8—Stability

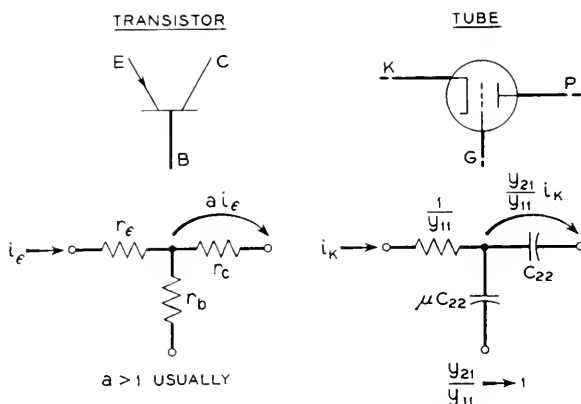


Fig. 9—Transistor-electron tube analogy.

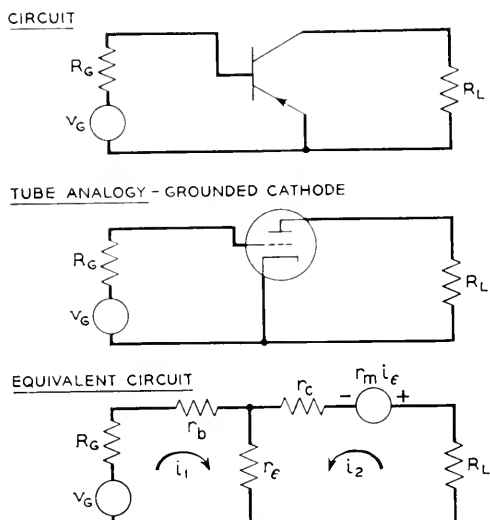
for the triode is close to unity for usual conditions. Another difference, of less importance, is the fact that the tube quantities analogous to  $r_c$  and  $r_b$  are capacitive reactances; their ratio, however, is like the ratio of  $r_c$  to  $r_b$  in magnitude.

One of the first consequences of this transistor-tube analogy is the suggestion that different transistor connections analogous to the different electron triode connections may be interesting.<sup>3</sup> The analogy makes emitter analogous

<sup>4</sup> "Vacuum Tube Networks," F. B. Llewellyn and L. C. Peterson, *Proc. I.R.E.*, March 1944, page 159, Fig. 13.

<sup>3</sup> Loc. cit.

to cathode, base to grid, and collector to plate; the conventional or grounded cathode tube connection is therefore analogous to the grounded emitter connection of a transistor, shown on Fig. 10. It is found that when  $a = 1$  the analogy is fairly close, in that the transistor has comparatively high-



Equations:

$$i_1(R_G + r_b + r_\epsilon) + i_2 r_\epsilon = v_G$$

Circuit determinant:

$$i_1(r_\epsilon - r_m) + i_2(R_L + r_\epsilon + r_c - r_m) = 0$$

$$\Delta = (R_G + r_b + r_\epsilon)(R_L + r_\epsilon + r_c - r_m) + r_\epsilon(r_m - r_\epsilon) > 0 \text{ for stability}$$

Input impedance

$$R_{11} = r_b + r_\epsilon + \frac{r_\epsilon(r_m - r_\epsilon)}{R_L + r_\epsilon + r_c - r_m}$$

Output impedance

$$R_{22} = r_c + r_\epsilon - r_m + \frac{r_\epsilon(r_m - r_\epsilon)}{R_G + r_b + r_\epsilon}$$

Operating Gain

$$G_F = 4 R_G R_L \left( \frac{r_m - r_\epsilon}{\Delta} \right)^2$$

Backward Operating Gain  $G_R = 4 R_G R_L \left( \frac{r_\epsilon}{\Delta} \right)^2$

Typical values: For  $R_G = 500^\circ$ ,  $R_L = 20000^\circ$ . Then  $R_{11} = 2100^\circ$ ,  $R_{22} = -6900^\circ$ ,  $G_F = 24^{db}$ ,  $G_R = -19^{db}$

Fig. 10—Synopsis of grounded emitter amplifier.

input impedance, high-output impedance, and changes signal polarity in transmission. When  $a > 1$ , as is usual, the analogy becomes less close, and feedback effects tend to become large and obnoxious; the open-circuit output impedance is usually negative. This behavior is readily under-

standable from stability considerations, since the base lead is now one of the signal terminals and, as before mentioned, putting resistance in the base lead tends toward instability if  $a$  is enough greater than unity. The effect is so severe that often it is worth while to add resistance in the collector lead, thereby reducing  $a$  to the neighborhood of unity, and simultaneously reducing the amplifier to a state of greater tractability.

Another feature of the grounded emitter amplifier is that the base resistance  $r_b$  is usually negligible, in contrast to its pronounced effect on the reverse transmission of the grounded base amplifier. The role of feedback element is taken over here by the emitter resistance  $r_e$ . These considerations have important effects on the properties of cascaded amplifiers and will be reverted to later.

For numerical comparison we might work the grounded emitter amplifier between the same two terminations as the grounded base amplifier above, namely from 500 into 20,000 ohms. It would then have a gain of about 24 db, an improvement of 7 db over the grounded base, with about the same power output and noise figure. This improvement is obtained at greater risk of oscillation; in fact the output impedance of this amplifier is negative.

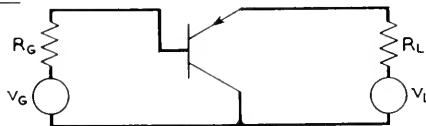
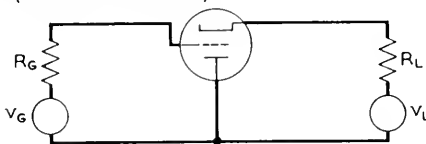
The remaining tube connection — the cathode follower or grounded plate — is analogous to the grounded collector connection (Fig. 11); again, when  $a = 1$  the analogy is fairly close, in that the transistor has high-input impedance, low-output impedance, and no change of polarity in transmission. In fact when  $a = 1$  the device is usable in very much the same manner as the cathode follower. The power output is lower than the other connections because the output electrode (the emitter) does not carry much direct current.

However, when we make  $a$  greater than 1 the effect is even more pronounced than it was in the grounded emitter case. As  $a$  increases from 1, the grounded collector amplifier rapidly loses its resemblance to the cathode follower and begins to transmit in both directions as a bilateral element. When  $a = 2$ , the operating gains in the two directions are the same; and for  $a > 2$  the transmission is actually greater in the "backward" direction. Another curious feature is that, while the "forward" transmission is still without change in signal polarity, the "reverse" transmission inverts the signal polarity.

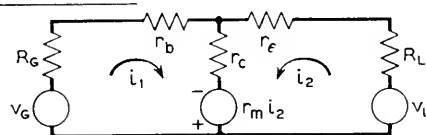
In any device which is supposed to give gain in both directions, naturally stability must be a controlling consideration. This amplifier is of course still subject to the aforementioned stability condition (1) and it is found that with care one can actually get power gains in both directions of transmission without instability, i.e. a simple bilateral amplifier is present. One numerical example may suffice. Assume a transistor having the properties

$r_e = 250$  ohms,  $r_b = 250$  ohms,  $r_c = 20,000$  ohms,  $r_m = 40,000$  ohms, so that  $a = 2$  and both base and emitter resistances  $r_e$  and  $r_b$  are negligible.

CIRCUIT

TUBE ANALOGY - GROUNDED PLATE  
(CATHODE FOLLOWER)

EQUIVALENT CIRCUIT



Equations:

$$\begin{aligned} i_1(R_G + r_b + r_c) + i_2(r_c - r_m) &= v_G \\ i_1 r_c + i_2(R_L + r_e + r_c - r_m) &= v_L \end{aligned}$$

Circuit determinant

$$\Delta = (R_G + r_b + r_c)(R_L + r_e + r_c - r_m) + r_c(r_m - r_e) > 0 \text{ for stability}$$

Input impedance

$$R_{11} = r_b + r_c + \frac{r_c(r_m - r_e)}{R_L + r_e + r_c - r_m}$$

Output impedance

$$R_{22} = r_e + r_c - r_m + \frac{r_c(r_m - r_e)}{R_G + r_b + r_c}$$

Operating Gain

$$G_F = 4 R_G R_L \left( \frac{-r_e}{\Delta} \right)^2$$

Backward Operating Gain  $G_R = 4 R_G R_L \left( \frac{-r_e + r_m}{\Delta} \right)^2 = (1 - a)^2 G_F$

Typical values:

$$\begin{aligned} \text{For } R_G &= 20000^\omega, R_L = 10000^\omega \\ \text{Then } R_{11} &= -4100^\omega \\ R_{22} &= -7600^\omega \\ G_F &= 15^{db} \\ G_R &= 13^{db} \end{aligned}$$

Fig. 11—Synopsis of grounded collector amplifier

Working between 20,000-ohm terminations, such an amplifier should have 6 db power gain in both directions and should still be stable even if one of its terminations changes 50% in the unfavorable direction.



The grounded emitter connection can also exhibit bilateral properties.

Recapitulating these three single-stage amplifiers, we see that when  $a = 1$  their properties are close enough to the analogous electron tube arrangements to be easily remembered; but that, when  $a$  is different from 1, their properties begin to diverge from their tube counterparts. Some of these circuits will perform in a simple manner functions which are impossible to the analogous tube connections, although of course the functions could be accomplished by using more tubes or more complicated circuits.

### FREQUENCY RESPONSE

So far the analysis of transistors has been given only for the resistive case, appropriate at low frequencies. When the frequency is raised, reactive components appear and the situation becomes more complicated, although of course still subject to the same general methods of analysis.

One might expect that since semiconducting diodes work at microwave frequencies, so also would semiconducting triodes. For the Type A transistor, this hope is blasted because of the essentially different nature of the mechanism, involving as it does the physical transport of charge carriers over appreciable distances. For certain features of the transistor, however, the analogy does hold. For example, the emitter by itself is a diode; and, in keeping with this fact, its open-circuit impedance does not change much with frequency in the range in which we shall be interested. For most engineering purposes the open-circuit input impedance of a Type A transistor may be regarded as a resistance independent of frequency. Such deviations as occur are small and entirely similar to what take place in an analogous diode.

The same situation holds with respect to the base resistance  $r_b$  and the collector resistance  $r_c$ , that is, they act as one might expect of a diode. The base resistance is substantially constant with frequency; the collector resistance has associated with it a slight amount of capacitance, mostly due to the case, leads, and wiring external to the unit, which gives a variation of properties with frequency in high-impedance circuits. The analogous capacitance on the emitter side is negligible because of the lower value of emitter impedance. One has, therefore, the T of resistors in the equivalent circuit substantially constant with frequency.

The dominant factor governing frequency response of the transistor is therefore largely expressed as a variation of the net mutual impedance  $r_m$  or, one may say as well, in the factor  $a$  which is the ratio of  $r_m$  to  $r_c$ .

Measurements of  $r_m$  as a function of frequency encounter the practical difficulty that it is impossible to present to the transistor over a wide frequency range an impedance high compared to the collector impedance. It is, however, quite easy to present to the collector a relatively low impedance

(75 ohms), which is constant over the frequency range of interest. Concurrently it is relatively simple to present to the emitter a high impedance,

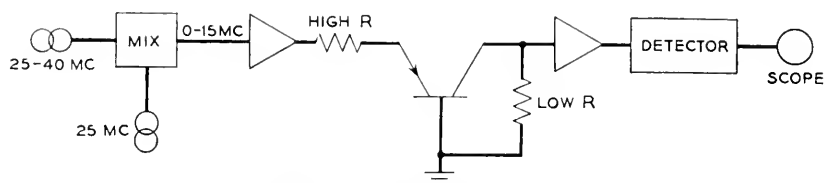


Fig. 12—Sweeper for measuring frequency response.

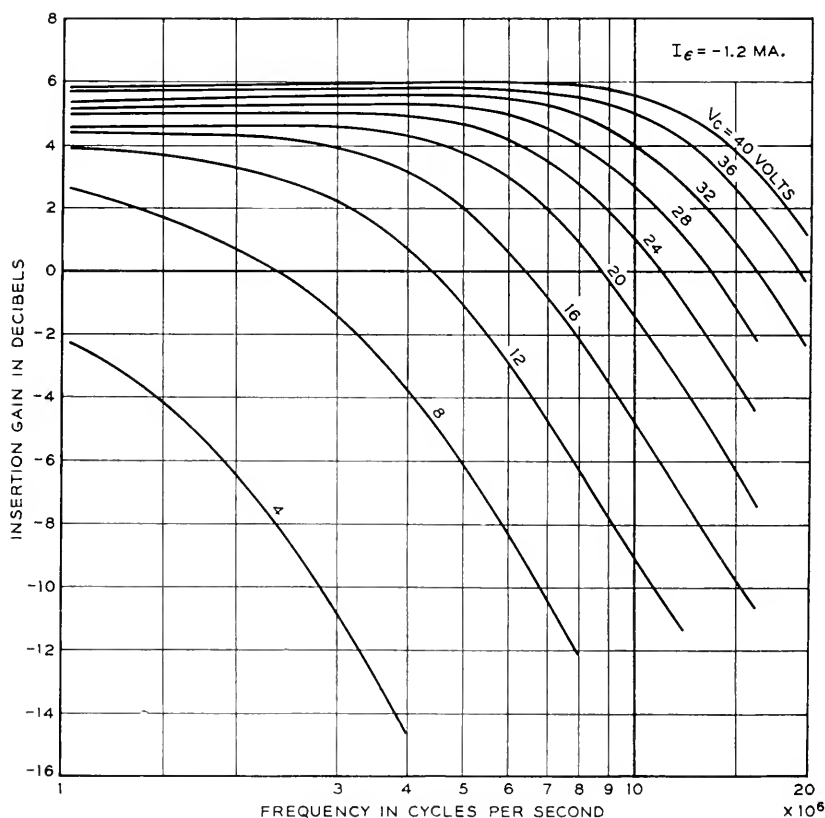


Fig. 13—Alpha versus frequency.

that is, to drive it with a constant current generator. Under these conditions the insertion power gain of the transistor is approximately  $\alpha^2$ , where the current amplification factor  $\alpha$  is the ratio of increment in collector current to

increment in emitter current at constant collector voltage.<sup>5</sup> The quantities  $\alpha$  and  $a$  are usually nearly the same.

An oscilloscopic presentation of  $\alpha$  versus frequency is possible and is a great convenience since many units can be measured quickly and variation with operating point observed directly. The sweep frequency generator built for this purpose is diagrammed in Fig. 12. It presents on an oscilloscope the magnitude of  $\alpha$  as a function of frequency from 0 to 15 megacycles. Means are also available for making point-by-point plots which are more accurate, though much slower.

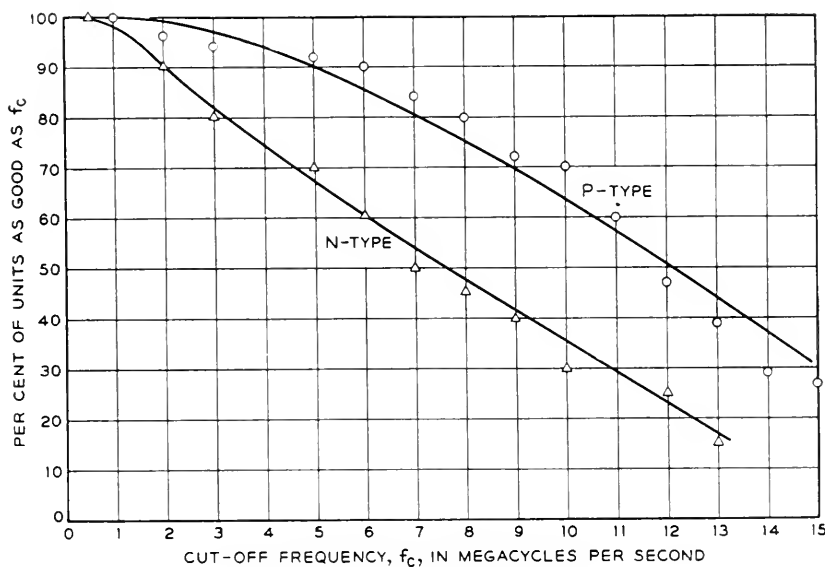


Fig. 14—Cut-off frequency statistics.

A set of curves of current amplification factor  $\alpha$  versus frequency, as obtained with this apparatus, is shown in Fig. 13. The cutoff shape is a little sharper than that of a single R-C circuit but less so than that of a pair, one of which is shunt-peaked enough to make the combination flat. The apparent high-frequency asymptote varies in different units from 7 to 11 db per octave.

The phase shift associated with this curve has been found to be related to the amplitude in the same way as if the characteristic were that of a "mini-

<sup>5</sup> Actually,  $\alpha = (\partial I_c / \partial I_e)_{V_c}$  is only one of a set of four circuit parameters  $h_{ij}$  whose relationship to  $I_e$  and  $V_c$  is the same as that of the  $Z$ 's to  $I_e$  and  $I_c$ , and which furnish an alternative circuit representation of the transistor. The other three  $h$ 's can be measured in a similar manner but are of less interest.

num phase" passive circuit.<sup>6</sup> Accordingly the phase shift, like the amplitude variation, is also intermediate between a single R-C interstage and the flat compensated pair of interstages.

When variations between curve shapes are not too large, the shape can be characterized by a single parameter which we take as the cutoff frequency  $f_c$ . Cutoff is defined as the frequency where the magnitude of  $\alpha^2$  is halved. Some statistical data on cutoff frequency of different units made of N-type and P-type germanium are plotted in Fig. 14. The P-material is somewhat

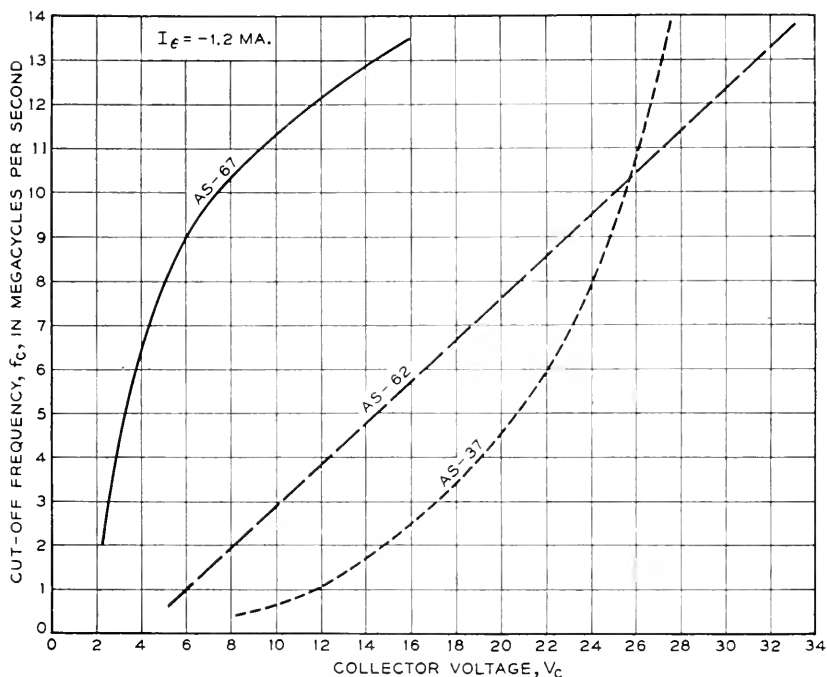


Fig. 15—Cut-off frequency versus collector voltage.

better, in keeping with the fact that the active charge carriers producing the transistor effect in it are electrons having greater mobility than the holes which are active in N-type germanium.

As one changes the operating point of the transistor the frequency response curve changes in such a way that the shape remains sensibly constant on a logarithmic frequency scale, but the scale changes. The cutoff frequency is usually roughly proportional to the collector voltage, with only minor dependence on the other operating parameter, as shown in Fig. 15 unit AS62.

<sup>6</sup> "Network Analysis and Feedback Amplifier Design," H. W. Bode, D. Van Nostrand Publishing Co., 1945.

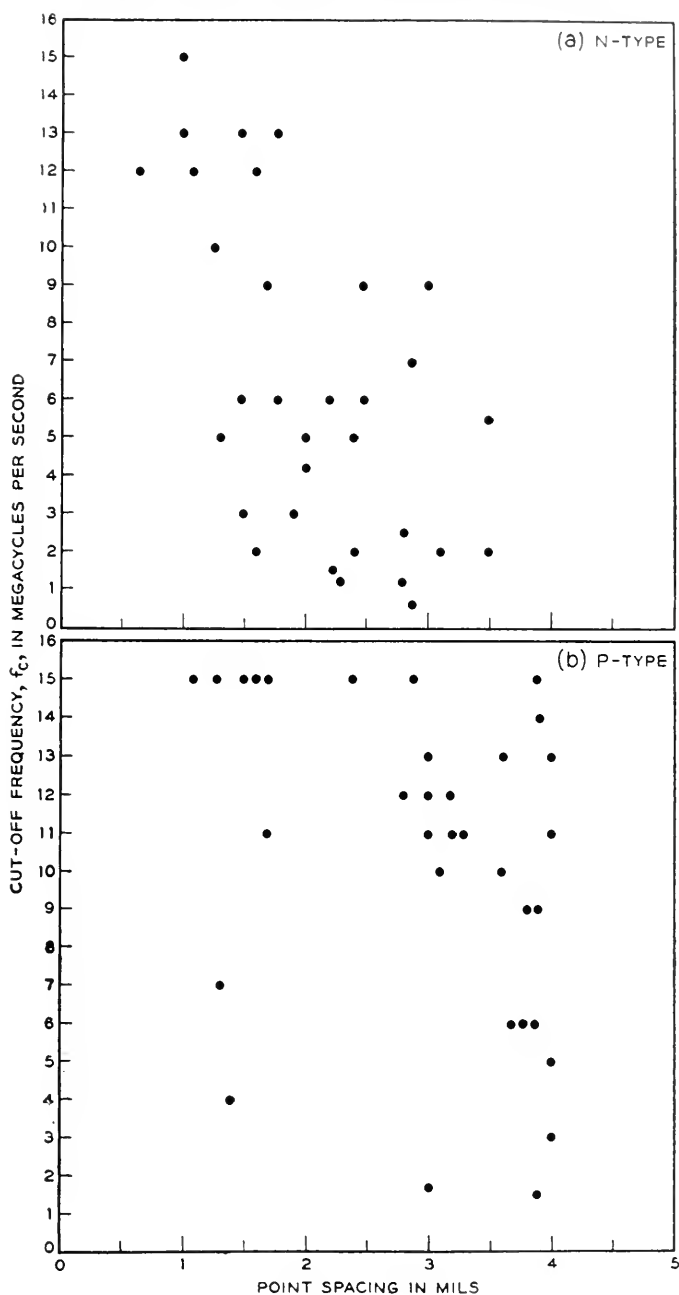


Fig. 16—Cut-off frequency versus point spacing.

Other types of variations of cutoff frequency with collector voltage are exhibited by some transistors.

That frequency cutoff is affected by the spacing between points of the transistor is shown in Fig. 16, which gives some support to the idea that the cutoff frequency might vary inversely as point spacing, other things being equal. However, one has only to look at the graph to see that other things are not equal for, at any given point spacing, the cutoff frequencies of different units vary by almost an order of magnitude. It is, however, clear that point spacing is one of the important factors.

In recapitulation of the measurements of frequency behavior, it appears possible to build Type A transistors with frequency cutoffs well above 10 megacycles. At the present time, the factors determining the frequency behavior are not yet under good control.

#### CASCADE AMPLIFIERS

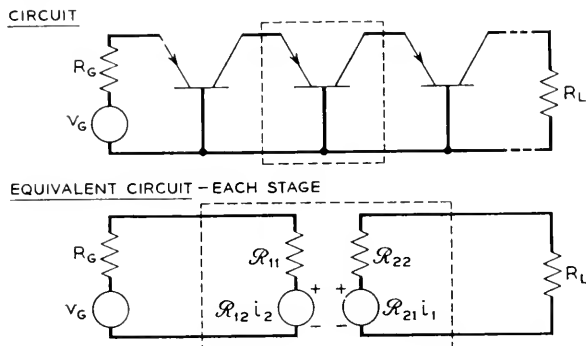
Many cascading possibilities exist, since any connection of the transistor might be used in combination with other connections, as well as involving all the parameter variations which might be made on each single stage. Some of the more elementary possibilities will be mentioned. Since feedback in each unit greatly complicates the situation, the essential features of the amplifiers may become clearer by discussing an idealized case where feedback is absent or greatly reduced. For similar reasons, the preliminary discussion is confined to frequencies low enough so that the equivalent circuits are purely resistive.

Perhaps the most straightforward cascade amplifier is the iterated grounded-base cascade, outlined in Fig. 17. Neglecting feedback, the insertion power gain is nearly equal to the current amplification factor  $\alpha$  squared. For the Type A transistor this amounts to some 5 db per stage. For most uses this could be regarded as impractically low, but it might be pointed out that the tube analog (grounded grid cascade) is even worse; for when  $\alpha = 1$  the maximum insertion gain is 0 db per stage. Both amplifiers of course can be made practical by interstage transformers (Fig. 18). For the Type A transistor, the matched gain without feedback rises to about 15 db per stage, which still compares favorably in magnitude with most grounded-grid tubes.

When feedback is considered by allowing  $r_b$  to return to its usual value of a few hundred ohms, the question of stability becomes important. The nominal Type A transistor is still stable when the cascade interstages are matched, the gain rising to about 21 db per stage. For many units having more than the usual amount of feedback, the interstages cannot be matched without violating the stability condition and therefore encountering os-

cillations; but one can normally count on stable gains of 15 to 20 db per stage, the transformers being perhaps somewhat mismatched.

Interesting possibilities for a good cascade amplifier with more gain than the grounded base cascade are offered by the grounded emitter connection. Incidentally, this gain advantage is also enjoyed by the grounded cathode or conventional tube connection, so that one would expect it to apply here from the electron tube analogy; but in transistors the feature that  $\alpha$  may be greater than 1 brings in complications having no simple analogy for tubes.



Without feed back ( $R_{12} = 0$ ):

Iterative impedance  $R_G = R_{22}$ ,  $R_L = R_{11}$

Circuit determinant  $\Delta = (R_{11} + R_{22})^2$

$$\text{Insertion Power Gain } G_I = \left| \frac{-R_{21}}{R_{11} + R_{22}} \right|^2$$

$$= \left( \frac{\alpha}{1 + R_{11}/R_{22}} \right)^2$$

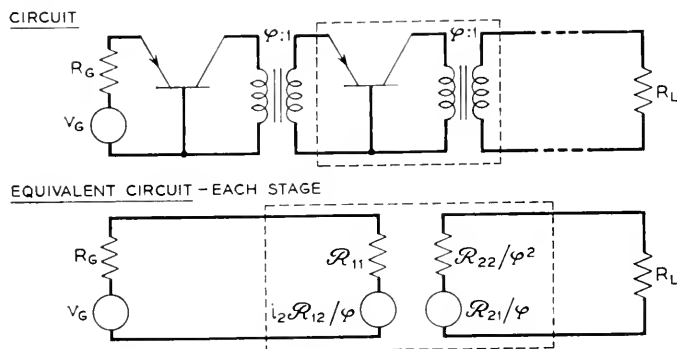
Nominal Type A Gain = 5<sup>db</sup>

Fig. 17—Synopsis of grounded base cascade.

The iterated grounded emitter cascade without feedback (that is, emitter resistance  $r_e = 0$ ) is unstable for the nominal Type A transistor, but can be stabilized in many ways of which we shall mention only one. The equivalent circuit of Fig. 19 shows an added resistor which may be thought of as adjusting the value of the collector resistance, and tends to make the unit more stable. When this resistor is adjusted to make the total collector resistance  $R_c$  about equal to the net mutual resistance  $r_m$ , thus reducing the effective value of  $\alpha$  to the neighborhood of unity, then the cascade amplifier becomes stable, its gain being sensitive to the exact value chosen for the adjusting resistor. A numerical calculation for the grounded emitter

amplifier using the nominal Type A transistor adjusted in this way gives the following results:

Assuming an adjusted value of collector resistance of 36000 ohms to be satisfactory for stability, then the iterative input impedance is 2300 ohms, output impedance 4000 ohms, and insertion gain about 21 db per stage without transformers. Three-stage stable amplifiers having power gains of about 55 db have been operated.



Without feed back ( $\mathcal{R}_{12} = 0$ ):

Iterative impedance  $R_G = \mathcal{R}_{22} / \phi^2$ ,  $R_L = \mathcal{R}_{11}$

Circuit determinant  $\Delta = (\mathcal{R}_{11} + \mathcal{R}_{22} / \phi^2)^2$

Insertion Power Gain  $G_I = \left( \frac{-\mathcal{R}_{21} / \phi}{\mathcal{R}_{11} + \mathcal{R}_{22} / \phi^2} \right)^2$

Maximum when  $\mathcal{R}_{11} = \mathcal{R}_{22} / \phi^2$

$$G_{I \text{ max.}} = \frac{\mathcal{R}_{21}}{4 \mathcal{R}_{11} R_{22}} = \frac{1}{4} \alpha^2 \frac{\mathcal{R}_{22}}{\mathcal{R}_{11}}$$

Nominal Type A Gain: without feed back = 15<sup>db</sup>  
with  $\mathcal{R}_{12}$  normal = 17<sup>db</sup>

Fig. 18—Synopsis of grounded base cascade with transformers.

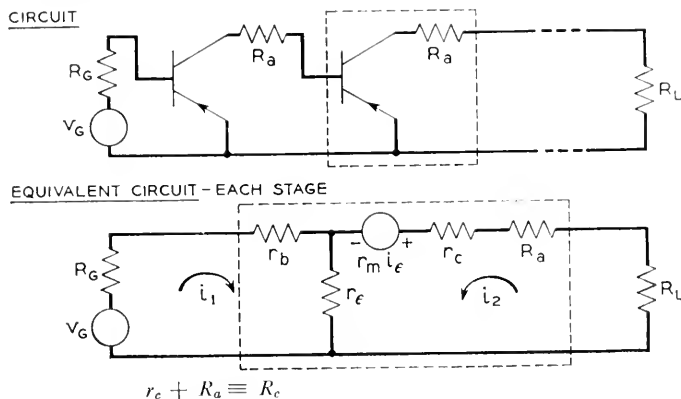
Another interesting feature of the grounded emitter amplifier is the ease with which negative feedback may be applied to it. A resistor inserted in the emitter lead gives local negative feedback analogous to the cathode feedback of tubes, while feedback involving several stages is also obtainable by common-lead methods analogous to common-cathode resistors familiar in the tube art. By such means, as is well known, distortion instability or gain variation may be reduced, or power output increased.

Theoretical study of these and other iterative amplifiers, particularly at higher frequencies, is conveniently carried on with the aid of the formulas



of Figs. 20 and 21 which give some of the iterative properties of a general fourpole and the effect thereon of an interstage matching transformer.

The iterative method of course does not exhaust the possibilities of cascade amplifiers. They can also be designed stage by stage. Even when feedback is large they can be cascaded together in the manner used for filter sections. A particular design of this sort is shown in Fig. 22. It is a grounded



Equations:

$$\begin{aligned} i_1(R_G + r_b + r_e) + i_2 r_e &= v_G \\ i_1(r_e - r_m) + i_2(R_L + r_e + R_e - r_m) &= 0 \end{aligned}$$

Circuit determinant  $\Delta = (R_G + r_b + r_e)(R_L + r_e + R_e - r_m) - r_e(r_e - r_m) > 0$  for stability

Without feed back ( $r_e = 0$ )

Iterative impedance  $R_G = R_e - r_m, R_L = r_b$

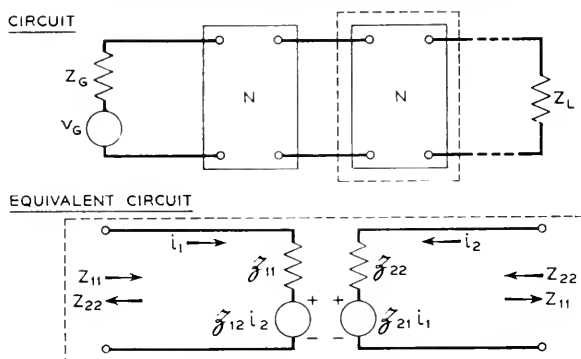
Circuit determinant  $\Delta = (r_b + R_e - r_m)^2$

Insertion Power Gain  $G_I = \left( \frac{r_m}{r_b + R_e - r_m} \right)^2$

Nominal Type A Gain with  $R_e = 3600\Omega$   
 without feed back  $23^{db}$   
 with  $r_e$  normal  $21^{db}$

Fig. 19—Synopsis of grounded emitter cascade.

base stage followed by a grounded collector and accordingly has the tube analog grounded-grid, cathode follower, from which one would expect that the terminating impedances would be low and the interstage impedance high. This amplifier matched a 600-ohm line to better than 10% and had 16 db insertion gain, with a bandwidth of about a megacycle. An adaptation for video purposes was made to obtain over a band from 100 cycles to 3.5 megacycles, an insertion gain of 20 db in a 75-ohm coaxial line.



Equations:

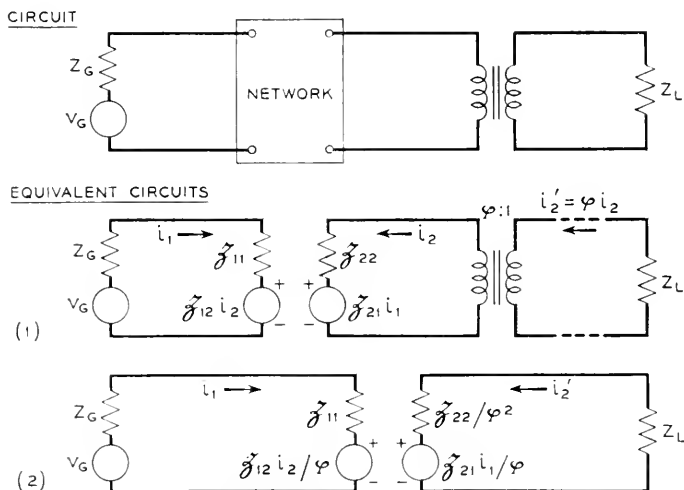
$$\begin{aligned} i_1(\bar{\mathcal{D}}_{11} + Z_{22}) + i_2\bar{\mathcal{D}}_{12} &= v_G \\ i_1\bar{\mathcal{D}}_{21} + i_2(\bar{\mathcal{D}}_{22} + Z_{11}) &= 0 \end{aligned}$$

Terminations:

$$\begin{aligned} Z_{11} &= Z_L = -\bar{\mathcal{D}}_{22} + \frac{1}{2}(\bar{\mathcal{D}}_{11} + \bar{\mathcal{D}}_{22})(1 + \sqrt{1 - y}) \\ Z_{22} &= Z_G = -\bar{\mathcal{D}}_{11} + \frac{1}{2}(\bar{\mathcal{D}}_{11} + \bar{\mathcal{D}}_{22})(1 + \sqrt{1 - y}) \\ y &= 4\bar{\mathcal{D}}_{12}\bar{\mathcal{D}}_{21}/(\bar{\mathcal{D}}_{11} + \bar{\mathcal{D}}_{22})^2 \end{aligned}$$

Circuit determinant  $\Delta = \frac{1}{2}(\bar{\mathcal{D}}_{11} + \bar{\mathcal{D}}_{22})^2(1 - y + \sqrt{1 - y})$ Insertion Power Gain  $G_I = \frac{\bar{\mathcal{D}}_{21}}{\bar{\mathcal{D}}_{11} + \bar{\mathcal{D}}_{22}} \frac{2}{1 + \sqrt{1 - y}}$ 

Fig. 20—Synopsis of iterated cascade of four-poles.

Equations:  $i_1(\bar{\mathcal{D}}_{11} + Z_G) + i_2'\bar{\mathcal{D}}_{12}/\varphi = v_G$ 

$$i_1\bar{\mathcal{D}}_{21}/\varphi + i_2'\left(\frac{\bar{\mathcal{D}}_{22}}{\varphi^2} + Z_L\right) = 0$$

Fig. 21—Four-pole with ideal transformer.

The foregoing amplifiers both have rather low output powers because of the fact that the emitter, a low-current electrode, is the output electrode. A way of improving this situation has been suggested in the second amplifier schematic shown in Fig. 22. The first stage is a grounded emitter and the second a grounded collector transistor, the latter operating in what we have called the "backward" direction so that the output electrode is the base and the power level is improved. This amplifier can be stabilized by negative feedback obtainable by inserting a resistor in the first stage emitter lead.

These examples emphasize that one can cascade unlike stages and that feedback can be used to stabilize performance, just as with electron tubes. These amplifiers can be further cascaded to obtain more gain. Other possibilities worthy of mention include modifying the design of the first stage

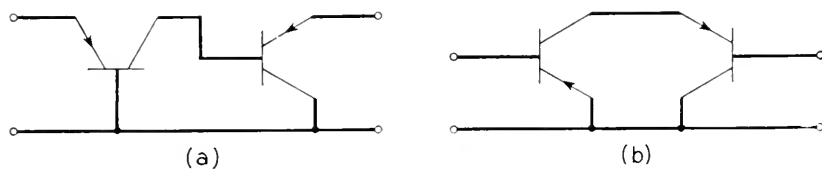


Fig. 22—Non-iterative cascade amplifiers.

of an iterative amplifier to obtain good noise figure, or of the last stage for greater power output.

### BAND PASS AMPLIFIERS

Bandpass amplifiers require a few remarks before concluding the small-signal discussion. The design within the band may be carried out by the methods previously discussed; but frequently attention must also be paid to properties outside the band, to an extent unusual with tubes. The reason, of course, is connected with that Dr. Jekyll and Mr. Hyde of transistors,  $\alpha$  (or  $a$ ) greater than 1. When a transistor may be short-circuit unstable, then oscillations may result from the practise usual with electron tube amplifiers of letting the impedances outside the band fall to low values. For the same reason design of power leads requires more care than usual. The problems encountered are somewhat similar to those of tube amplifiers with feedback in that one must pay attention to characteristics far outside the useful band. In the case of transistors, one may have to exercise design care to avoid oscillations even when the gain of the amplifier is less than unity.

### LARGE SIGNAL ANALYSIS

Large signals are those which involve considerable excursions over the electrical characteristics of the device and cannot be regarded as small

changes near an assumed operating point. For their general study a most convenient tool is provided by the set of static characteristics of the unit.

Since most analyses begin with the static characteristics, perhaps some excuse is needed for the unorthodox approach which has delayed them to this point. Two reasons may be cited: First, the small-signal behavior is in a sense simpler, being capable of discussion by the familiar linear methods of circuit theory. Second, the small-signal behavior has brought out some features, notably short-circuit instability, which have a bearing on certain features of the static characteristics, on the methods of measuring them, and on the particular manner of expressing them.

A set of characteristics representative of Type A transistor performance is shown in Fig. 23, consisting of four plots, one of each of the electrode voltages against each of the currents with the other current as parameter. Contrary to electron tube practise, rather than the voltages we take the currents as the independent variables. This choice avoids the experimental difficulty that the short-circuit unstable transistors might oscillate if we were to attempt to hold the electrode voltages constant, as well as the concomitant analytical trouble that in that case the voltage-dependent characteristics become double-valued.

The relationship of these characteristics to the open-circuit impedances is direct and quickly shown. Suppose the voltages are expressed formally as functions of the currents:

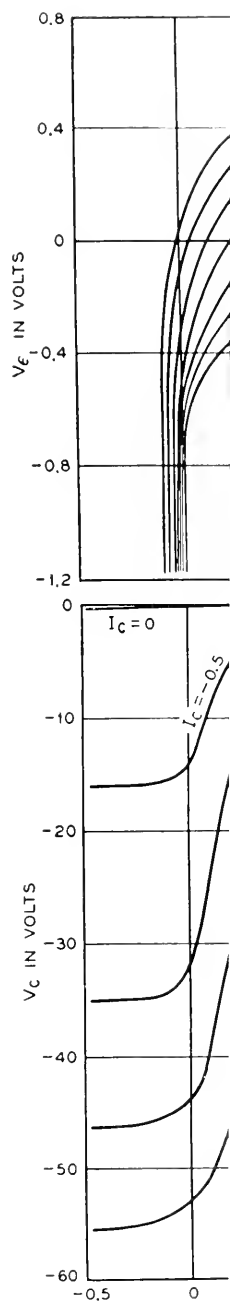
$$\begin{aligned} V_E &= f_1(I_E, I_C) \\ V_C &= f_2(I_E, I_C) \end{aligned} \quad (2)$$

Differentiating, and identifying the differentials as small-signal variables, we get immediately the equations for the open-circuit resistances:

$$\begin{aligned} v_E &= i_E \frac{\partial f_1}{\partial I_E} + i_C \frac{\partial f_1}{\partial I_C} \\ v_C &= i_E \frac{\partial f_2}{\partial I_E} + i_C \frac{\partial f_2}{\partial I_C} \end{aligned} \quad (3)$$

Accordingly, the open-circuit resistances are the slopes of these static characteristics. The reactive components do not appear because our assumptions (2) were not sufficiently general to take them into account or, in other words, the reactive information is not contained in the static characteristics.

Just as there are five other pairs of small signal parameters which could have been chosen, so there are five other ways in which the static characteristics could have been expressed. Often these other ways are convenient for special purposes or are closely connected with particular large signal circuits.



t-by-point  
r has been  
ie six pairs  
y two-pole  
resistance

a thermal  
esults as a  
sual region  
able if the

om a tran-  
by means  
the class of  
illustrated  
f a Type A  
y that part  
slope, and

mpt to get  
distortion,

where the  
correspond-

load region  
emitter im-  
nomenon is  
t is a minor

e it can no  
ter current  
in electron

t overloads  
om heating  
overloading  
ssion.

to overload  
to choosing

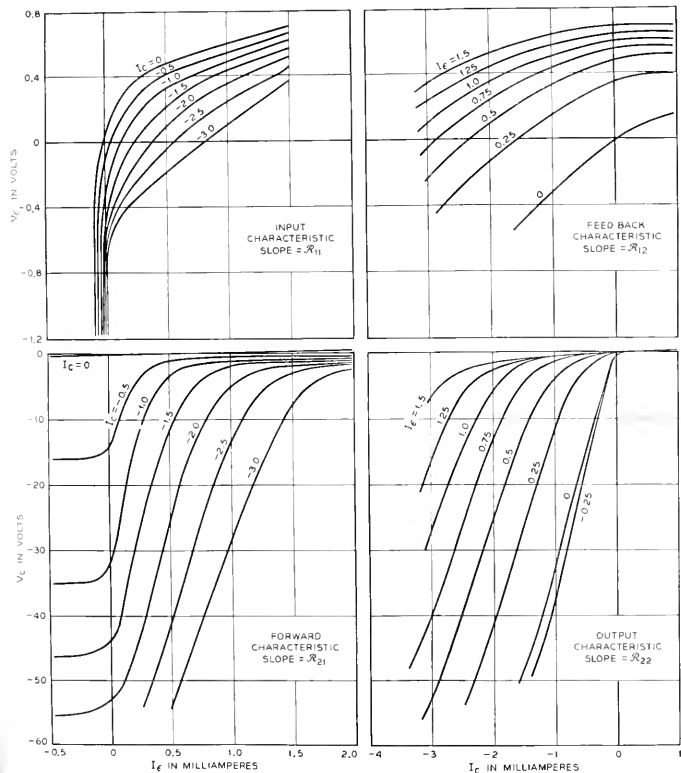


Fig. 23—Static characteristics.

Measurement of the characteristics can be by conventional point-by-point plots or by oscilloscope presentation. An oscilloscopic curve tracer has been built which can show any of the four characteristics for any of the six pairs of independent parameters of the Type A transistor, as well as any two-pole characteristic which might be of interest (such as a negative resistance characteristic).

Occasionally the static characteristics are affected by effects of a thermal nature such that an oscilloscope trace does not give the same results as a slow point-by-point plot. These thermal effects are small in the usual region of operation of the Type A transistor but may become appreciable if the unit is heated by excessive power dissipation in it.

### POWER OUTPUT AND DISTORTION

The problem of obtaining good "undistorted" power output from a transistor at low frequencies is one which is conveniently discussed by means of the static characteristics. Analytically this question belongs to the class of slightly non-linear problems but, for descriptive purposes, it is illustrated by the curves of Fig. 24. The family of collector characteristics of a Type A transistor is shown. The region of linear operation is substantially that part of the plot where the curves are uniformly spaced, have constant slope, and lie within the permitted power dissipation of the unit.

In driving a Type A transistor harder and harder in an attempt to get greater power output, one may encounter four types of overload distortion, analogous to the types found in tubes.

1. One may drive the emitter negative into the cutoff region where the collector current fails to respond to changes in emitter potential, corresponding to grid cut-off in a tube.

2. One may drive the emitter positive into an emitter overload region where non-linear distortion may be encountered because the emitter impedance changes with its voltage. The corresponding tube phenomenon is positive grid distortion. For both tubes and transistors this effect is a minor one which may be actually beneficial in practical cases.

3. The collector may be driven down to low potential where it can no longer draw the current required to follow the impressed emitter current variations. This distortion corresponds to plate "bottoming" in electron tubes.

4. The collector may be driven up to high currents where it overloads because of the non-linear voltage response in that region arising from heating effects. This effect has practical consequences something like the overloading of electron tubes which may arise from insufficient cathode emission.

In other words, either emitter or collector may be driven into overload or cut-off and the problem of getting good power output reduces to choosing

changes ne  
convenient

Since mo  
excuse is n  
this point.  
a sense sim  
of circuit t  
features, ne  
features of  
and on the

A set of  
is shown in  
voltages ag  
Contrary t  
currents as  
difficulty t  
were to att  
comitant a  
acteristics l

The rela  
is direct ar  
as function

Different  
we get inn

Accordin  
characteris  
sumptions  
in other wo  
acteristics.

Just as t  
have been c  
istics coul  
for special  
circuits.



Measurement of the characteristics can be by conventional point-by-point plots or by oscilloscope presentation. An oscilloscopic curve tracer has been built which can show any of the four characteristics for any of the six pairs of independent parameters of the Type A transistor, as well as any two-pole characteristic which might be of interest (such as a negative resistance characteristic).

Occasionally the static characteristics are affected by effects of a thermal nature such that an oscilloscope trace does not give the same results as a slow point-by-point plot. These thermal effects are small in the usual region of operation of the Type A transistor but may become appreciable if the unit is heated by excessive power dissipation in it.

### POWER OUTPUT AND DISTORTION

The problem of obtaining good "undistorted" power output from a transistor at low frequencies is one which is conveniently discussed by means of the static characteristics. Analytically this question belongs to the class of slightly non-linear problems but, for descriptive purposes, it is illustrated by the curves of Fig. 24. The family of collector characteristics of a Type A transistor is shown. The region of linear operation is substantially that part of the plot where the curves are uniformly spaced, have constant slope, and lie within the permitted power dissipation of the unit.

In driving a Type A transistor harder and harder in an attempt to get greater power output, one may encounter four types of overload distortion, analogous to the types found in tubes.

1. One may drive the emitter negative into the cutoff region where the collector current fails to respond to changes in emitter potential, corresponding to grid cut-off in a tube.

2. One may drive the emitter positive into an emitter overload region where non-linear distortion may be encountered because the emitter impedance changes with its voltage. The corresponding tube phenomenon is positive grid distortion. For both tubes and transistors this effect is a minor one which may be actually beneficial in practical cases.

3. The collector may be driven down to low potential where it can no longer draw the current required to follow the impressed emitter current variations. This distortion corresponds to plate "bottoming" in electron tubes.

4. The collector may be driven up to high currents where it overloads because of the non-linear voltage response in that region arising from heating effects. This effect has practical consequences something like the overloading of electron tubes which may arise from insufficient cathode emission.

In other words, either emitter or collector may be driven into overload or cut-off and the problem of getting good power output reduces to choosing

an operating point and load impedance such as to avoid these non-linear effects as long as possible. Reverting to Fig. 24, since one wants as large a product of  $\Delta V \cdot \Delta I$  as possible, the problem may be thought of in geometrical terms as approximately that of constructing the largest possible rectangle such that a load line extending diagonally across the corners of this rectangle

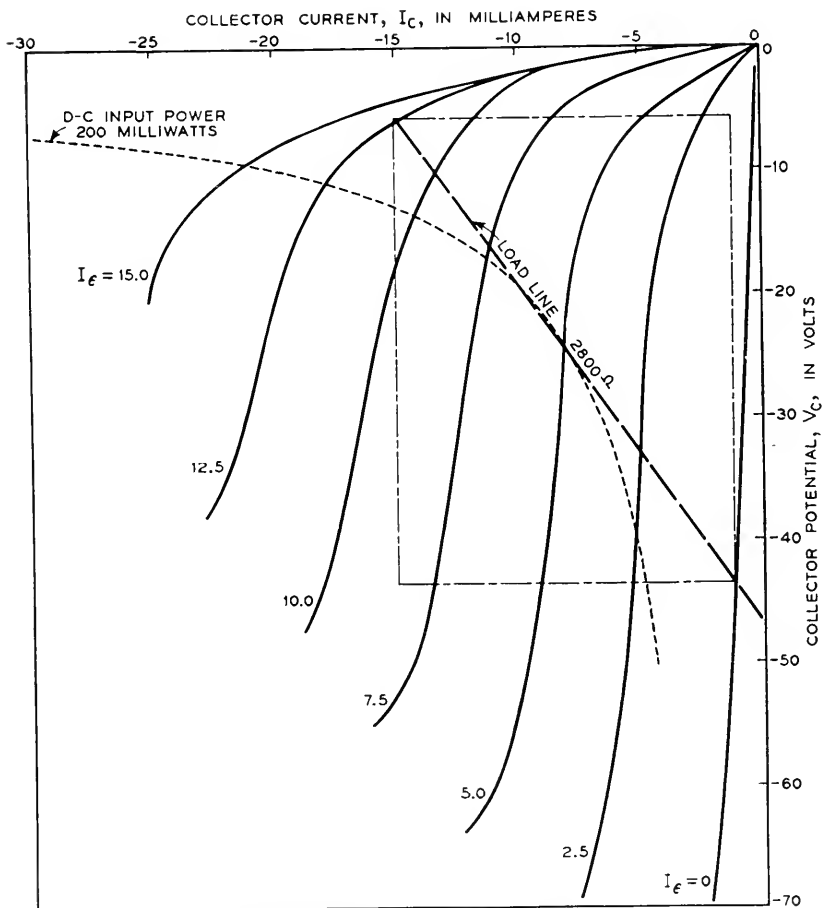


Fig. 24 - Collector power output plot.

lies within the "linear" region of operation. The slope of this line gives the load impedance required, its intercept the collector supply voltage (for resistance coupling), and the sides of the rectangle give the extreme values of voltage and current. The center of the rectangle is approximately the quiescent or small-signal operating point.

Under optimum conditions of load impedance and operating point,

one obtains power efficiencies comparable to Class A electron tube operation, that is, 20 to 35% efficiency with a few percent harmonic distortion. As contrasted to recommendations for good low-level gain for the Type A transistor, the optimum conditions for power output have usually involved lower load impedances and higher currents. Representative values may be: load impedance, 5000 ohms; collector current,  $-8$  milliamperes at  $-35$  volts bias; emitter current, 3 milliamperes; power output, 60 milliwatts, with distortion less than ten percent.

One complication of the power transistor is that, when the optimum load impedance is low, the operating point gets nearer to the region where the transistor may tend to oscillate if it happens to be one of the kind which is short-circuit unstable. A saving circumstance here is available in that

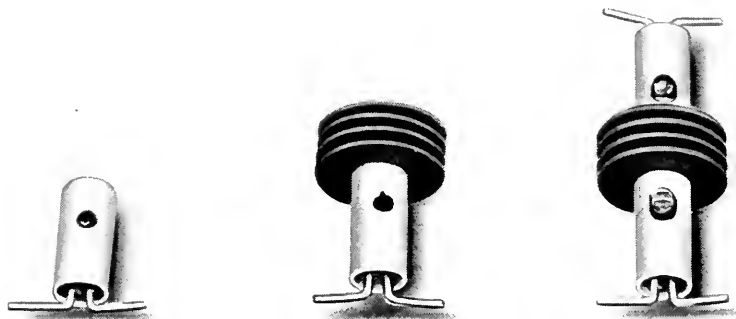


Fig. 25—Some power transistors.

added resistance in the emitter lead tends to promote stability, so that the transistor may be stabilized by operating out of a higher generator impedance, possibly at some cost in reduced gain. A corollary aspect of the same phenomenon is that the input impedance of a high-power transistor may become very low or even negative.

Higher power output from the transistor can also be obtained by increasing the permissible collector dissipation. This has been accomplished by using a thin wafer of germanium directly soldered to a copper base equipped with suitable fins to facilitate the removal of heat generated in the vicinity of the collector point. An increase in allowable dissipation from 200 to 600 milliwatts has been thereby obtained. Output powers of approximately 200 milliwatts at a conversion efficiency of 33% have been realized.

The photograph of Fig. 25 shows on the left the type A transistor, in the center the power version of this unit, and on the right is shown a double

ended type of power transistor using two germanium wafers with a common radiator for push-pull applications.

### OTHER LARGE-SIGNAL APPLICATIONS

The static characteristics can be used for calculations of many large-signal circuits of which only a few examples can be given here. The first is a tickler feedback oscillator of Fig. 26, which uses the grounded-base circuit with a resonant circuit in the collector lead, transformer-coupled back to the emitter.

Other circuits making use of the special possibilities of the transistor include an oscillator with anti-resonant circuit in the base lead, or with a

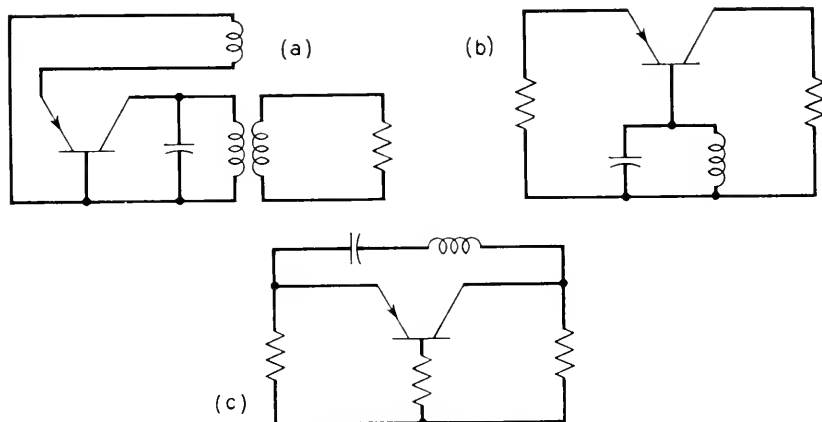


Fig. 26—Transistor oscillators.

series resonant circuit from collector to emitter. Some of these circuits make use of the short-circuit instability peculiar to the transistor and accordingly would not work with electron tubes.

### NOISE

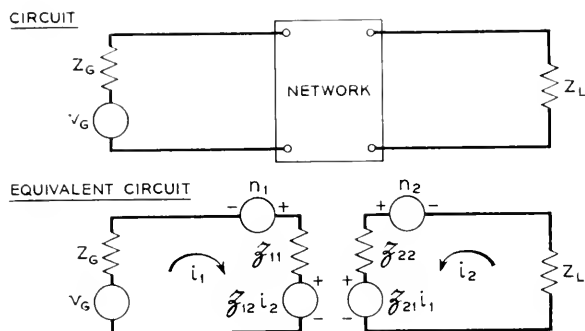
A discussion of small-signal amplifiers would be incomplete without some mention of the limiting factor of noise. The noise has been left to the last, however, because its discussion complicates the circuits slightly, and perhaps because it is not well to present too early an aspect of performance which is at the moment so much inferior to electron tubes.

On the circuit representation of noise as well as signal much work has been done by L. C. Peterson.<sup>7</sup> It turns out that in the general four-terminal network in which we are interested, a complete noise representation for

<sup>7</sup> "Signal and Noise in Microwave Tetrode," *Proc. I.R.E.*, Nov. 1947, pp. 1264-1272.

circuit purposes may be obtained by adding two noise generators to the equivalent circuit of four signal parameters, as shown in Fig. 27.

These noise representations are on an entirely similar basis to the signal representations. Just as four elements in any independent configuration suffice for signal description, so two noise generators in either series or shunt in any convenient independent locations can be added to account for the noise. All these representations give the same signal and noise behavior for any external connections. Still, some may be better than others in corresponding to the actual physics of the transistor; presumably the



$$\begin{aligned} \text{Equations: } i_1(Z_G + \mathfrak{Z}_{11}) + i_2\mathfrak{Z}_{12} &= v_G \oplus N_1 \\ i_1\mathfrak{Z}_{21} + i_2(\mathfrak{Z}_{22} + Z_L) &= \oplus N_2 \end{aligned}$$

Circled  $\oplus$  signs indicate addition with attention to any correlations which may exist between noise generators or mean square additions if no correlation exists.

$$\text{Noise Figure } F = 1 + \frac{1}{4kTBR_G} \left\{ \overline{N_1^2} \oplus \overline{N_2^2} \left( \frac{\mathfrak{Z}_{11} + Z_G}{\mathfrak{Z}_{21}} \right)^2 \right\}$$

Fig. 27—Synopsis of general four-pole, including noise.

better representations will show particularly simple behavior, for example, in their dependence upon the d-c operating point of the transistor. The usual choice puts noise voltage generators in series with the emitter and collector leads, as shown.

If the two noise generators were truly independent physical sources of noise, their outputs would be expected to show no correlation and their noise power contributions would be simply additive. This independence is not usually the case for the Type A transistor. By adding the noise outputs and comparing the power in the sum to that in the separate components, correlation coefficients ranging from  $-.8$  to  $+.4$  have been found. From this the conclusion can be drawn that the physical sources of noise in the network do not act in series with the leads but at least to some extent arise elsewhere

in the transistor and contribute correlated noise output to both the generators of the circuit representation.

The transistor noise is of two types. One is a rushing sound somewhat similar qualitatively to thermal resistance noise; the other is a frying or rough sound which occurs erratically, usually in the noisier units. The noise

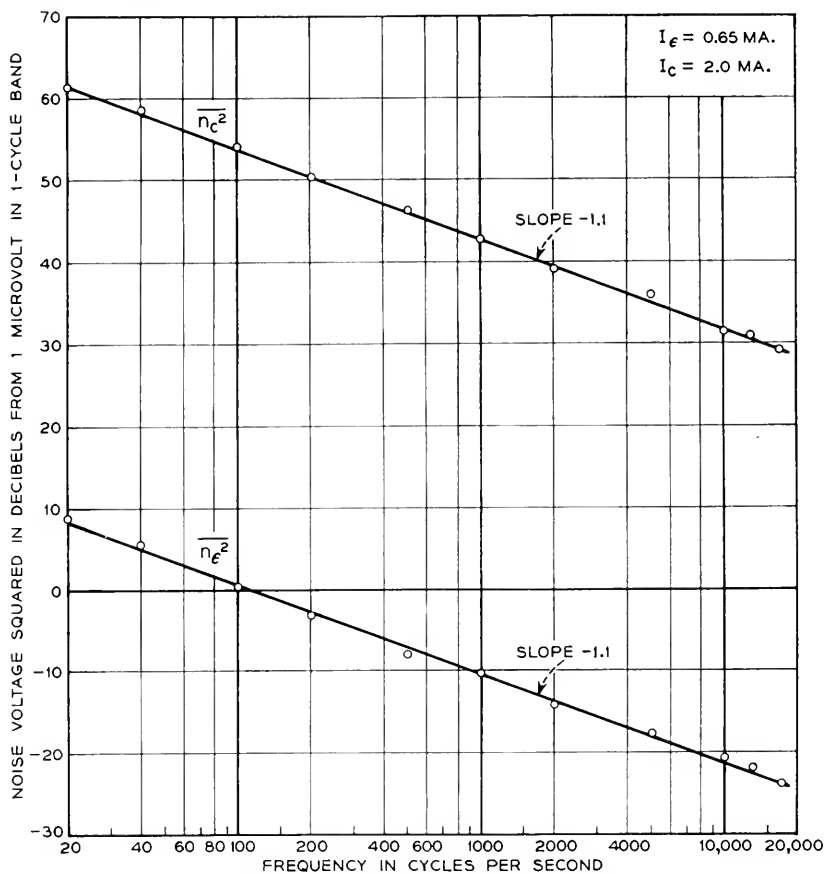


Fig. 28—Transistor noise versus frequency.

power per unit bandwidth varies almost exactly inversely with frequency as shown in Fig. 28, being in this respect reminiscent of contact noise.

Since the noise dependence on frequency is known, its level may be given as noise voltage per unit bandwidth at a reference frequency (1000 cycles). The collector noise usually dominates as far as practical effects on the output are concerned. Representative values are about 100 microvolts per cycle at 1000 cycles for the collector, and one or two microvolts for the emitter.

The noise voltages depend mainly on the collector direct voltage as shown in Fig. 29. While they do vary with the other operating parameter at constant collector voltage, such variations rarely exceed 10 db, which is much less than the variations with collector voltage.

More important than the actual level of the noise is its relation to thermal resistance noise, which is the ultimate limit to amplification. This relationship is conveniently expressed by means of the noise figure, or number of times noisier than amplified thermal noise in the output of the amplifier.

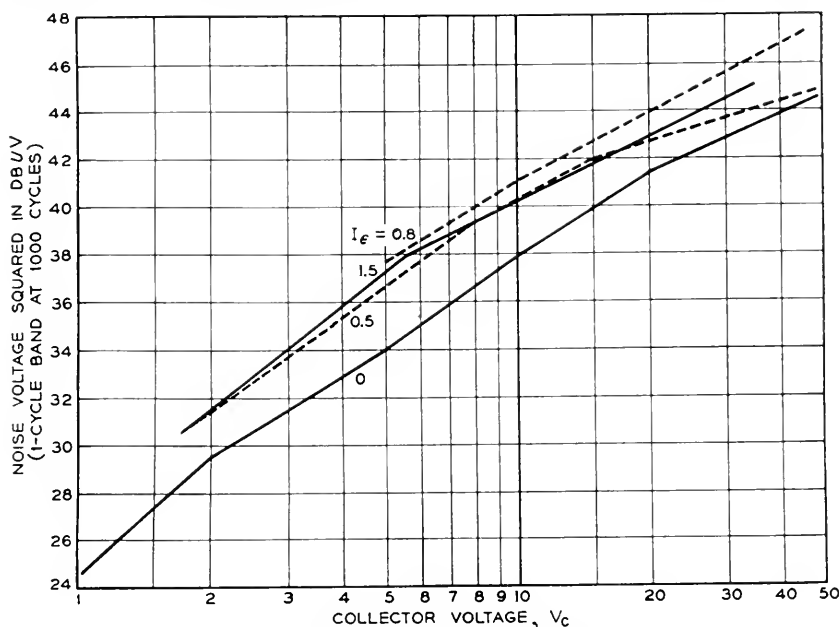


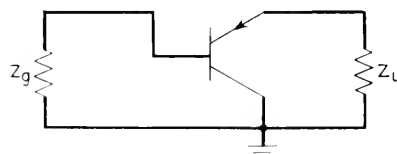
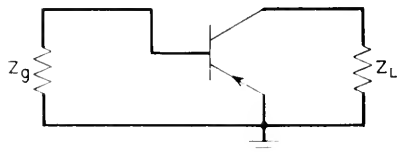
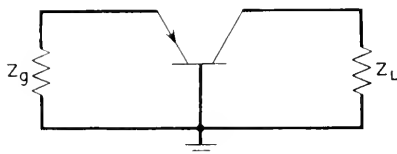
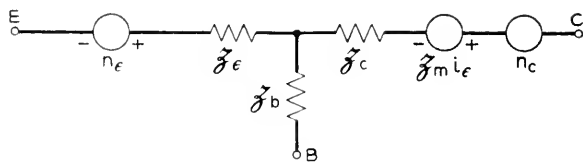
Fig. 29—Transistor noise versus operating point.

A representative noise figure for the Type A transistor at 1000 cycles is 60 db, with individual units ranging from 50 to 70 db.

Noise figure formulas for the three single-stage connections are given in Fig. 30. The noise performance of the three connections would usually not be very different if it were not for stability considerations, which may render unusable the generator impedance which would give optimum performance. Mainly, on account of stability, the grounded base connection may be said to give the best noise performance, with the grounded emitter running a close second.

The noise figure of any device depends upon the generator impedance out of which it works but does not depend upon the load. Accordingly, there exists an optimum generator impedance which gives the best noise

## Equivalent Circuit



Grounded Base

$$F = 1 + \frac{1}{4kTBR_G} \left[ N_\epsilon^2 \oplus N_c^2 \left( \frac{Z_G + z_\epsilon + z_b}{z_m + z_b} \right)^2 \right]$$

Grounded Emitter

$$F = 1 + \frac{1}{4kTBR_G} \left[ N_\epsilon^2 \left( \frac{Z_G + z_m + z_b}{z_m - z_\epsilon} \right)^2 \oplus N_c^2 \left( \frac{Z_G + z_b + z_\epsilon}{z_m - z_\epsilon} \right)^2 \right]$$

Grounded Collector

$$\text{Forward } F = 1 + \frac{1}{4kTBR_G} \left[ N_\epsilon^2 \left( \frac{Z_G + z_c + z_b}{z_c} \right)^2 \oplus N_c^2 \left( \frac{Z_G + z_b}{z_c} \right)^2 \right]$$

$$\text{Backward } F = 1 + \frac{1}{4kTBR_L} \left[ N_\epsilon^2 \oplus N_c^2 \left( \frac{Z_L + z_\epsilon}{z_m - z_c} \right)^2 \right]$$

Fig. 30—Noise figure formulas.



figure of which the unit is capable. This optimum source impedance is best for signal-to-noise performance, not for signal performance alone; hence, as is well known for vacuum tubes, it is usually not a match for the unit, and in general both the resistive and reactive components of impedance may be mismatched to the unit.

For the transistor at low frequencies in the grounded-base connection, reactive effects are negligible and the emitter noise generator may usually be neglected. Under these conditions the optimum noise figure is obtained from a generator of impedance equal to the open-circuit input resistance of the transistor (not the actual working input resistance, which may be quite different).

The best operating point for low noise is usually obtained at a moderate collector voltage (20 volts) and a small emitter current (0.5 ma.).

#### SUMMARY

A tentative evaluation of the Type A transistor may be made on the basis of presently available information. Before making it, we should say that a comparison with the field of electron tubes is obviously unfair — there are many against one, and a little one at that. Furthermore the little one is a baby not only in size but in length of time under development. It is only natural that the full possibilities are not yet apparent. With these reservations, we can make the following statements about the present Type A transistor:

Gain: the transistor figure of about 17 db per stage is somewhat low compared to 30 or 40 db obtainable from audio tubes. When the bandwidth is taken into consideration the gain-band product of the transistor is good but, since the excess bandwidth cannot be exchanged for gain, this number is in this case illusory for narrow-band amplifiers. For video amplifiers the comparison is more favorable.

Stability considerations differ from the electron tube in such a way as to be likely to give more trouble at low frequencies. At video frequencies this difference is less marked if we play fair by comparing with a triode tube instead of a pentode. The latter is of course better shielded than the transistor.

Frequency response appears to be practical up to 10 megacycles or more.

Power output efficiency of around 30%, Class A, seems fully comparable to an electron tube, so that a comparison between the two can be based on input d-c power.

Noise figure of 60 db at 1000 cycles is much worse than that of a good electron tube, which can come close to 0 db. In view of the frequency dependence which brings the transistor noise figure down to 30 db at a megacycle, the comparison at video frequencies is less unfavorable, particularly if some developmental improvement can be made.

So far on most counts the comparison is not too favorable but, as we said before, it isn't fair to the baby. In addition there are a number of other considerations which are secondary from the point of view of pure technique but may be dominant from other points of view. Among favorable factors here are: small size; low power drain; no standby power, but instant response when needed; low heating effect when used in large numbers; and ruggedness.

The life of transistors should be fairly long on the basis of diode performance, but the device is too new to permit definite statement. The mechanical simplicity might well lead one to hope for low cost, but no production figures are as yet available.

In fine, even if Type A transistor performance does not excel all electron tubes, it is still good enough for many applications and will be considerably better in the future.

#### ACKNOWLEDGEMENT

This survey is based on the work of many people, only a few of whom have been mentioned in the text. The examples of circuits have not been numerous or exhaustive, but rather have been used to illustrate the methods adopted; these are general enough to be adapted to the solution of many particular problems.

# Theory of Transient Phenomena in the Transport of Holes in an Excess Semiconductor

By CONYERS HERRING

An analysis is given of the transient behavior of the density of holes  $n_h$  in an excess semiconductor as a function of time  $t$  and of position  $x$  with respect to the electrode from which they are being injected. When the geometry is one-dimensional, an exact solution for the function  $n_h(x, t)$  can be constructed, provided certain simplifying assumptions are fulfilled, of which the most important are that there be no appreciable trapping of holes or electrons and that diffusion be negligible. An attempt is made to estimate the range of conditions over which the neglect of diffusion will be justified. A few applications of the theory to possible experiments are discussed.

A variety of experiments have been performed, and others are planned, which involve measurement of transient or steady-state phenomena due to the drift of positive holes along a specimen of  $n$ -type semiconductor after they have been introduced at an *injection electrode* or *emitter*.<sup>1</sup> These phenomena are presumably a result of the interplay of drift, space-charge, recombination, and diffusion effects. This paper seeks to relate these effects to the phenomena, and its principal contribution is an explicit calculation of the transient phenomena outside the range of small-signal theory, for cases where the geometry is one-dimensional and where certain simplifying assumptions, notably the neglect of diffusion, are justified. Removal of some of these simplifying assumptions and a more careful development of the theory will be necessary in certain applications.

Section 1 discusses the physical assumptions and boundary conditions involved in setting the problem up. Section 2 contains calculations of the distribution of holes along the length of the semiconductor at various times, for the mathematically simplest case where recombination and diffusion are ignored and all currents are held constant after the start of the injection. This simple case illustrates the method of attack to be used in the more general calculations of Section 4, and it is hoped that this sketching of basic ideas will enable the hasty reader to pass on to Section 6 without going

<sup>1</sup> Experiments of this sort have been undertaken with the objective of testing and extending the theoretical interpretation of transistor action proposed by J. Bardeen and W. H. Brattain, *Phys. Rev.*, **75**, 1208 (1949), especially as regards the role of volume transport of holes, a role first suggested by J. N. Shive, *Phys. Rev.*, **75**, 689 (1949). Examples of the type of experiment discussed in the present paper have been described by: J. R. Haynes and W. Shockley, *Phys. Rev.*, **75**, 691 (1949) (transient effects); W. Shockley, G. L. Pearson, M. Sparks and W. H. Brattain, in a paper presented at the Cambridge Meeting of the American Physical Society, June 16-18, 1949 (steady-state transport); W. Shockley, G. L. Pearson, and J. R. Haynes, *Bell Sys. Tech. Jour.*, this issue (steady-state and transient effects).

through the mathematical details of Sections 3, 4, and 5. Section 3 contains the complete differential equations of the problem, including diffusion and recombination, and Section 4 gives the solution when only the diffusion terms are neglected. Section 5 contains some order-of-magnitude estimates regarding diffusion effects. Section 6 summarizes the capabilities of the theory so far developed, presents some obvious generalizations, and discusses an interesting *shock wave* phenomenon which occurs whenever the injected hole current is quickly decreased.

## 1. BASIC ASSUMPTIONS AND BOUNDARY CONDITIONS

Consider the  $n$ -type semiconducting specimen shown in Fig. 1, having electrodes at its two ends,  $x = -a$  and  $x = b$ , respectively, and an injection electrode system at  $x = 0$  somewhere in between. Let a current of density  $j_a$  per unit area enter at the left-hand end, and let a current of density  $j_e$  be injected at  $x = 0$ . To make the problem strictly one-dimensional, it will be

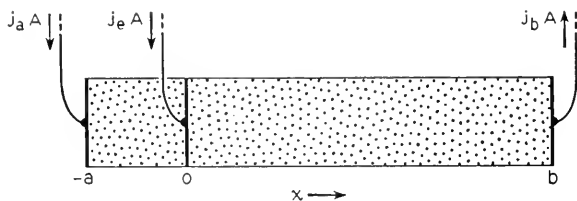


Fig. 1—Idealized experiment on hole transport in one dimension.

supposed that this injection takes place uniformly over the plane cross-section of the specimen at  $x = 0$ , instead of taking place at isolated points of the surface, as is usually the case in experiments. This idealization will presumably be justified if the thickness of the specimen is small compared with lengths in the  $x$ -direction which are significant in the experiment and if the injected positive holes are able to spread themselves uniformly over the cross-section before appreciable recombination has taken place.

Unless otherwise stated, it will be supposed that  $j_e$  consists entirely of positive holes, i.e., that the number of electrons withdrawn from the specimen by the electrode at  $x = 0$  is negligible compared with the number of holes injected. The currents  $j_a$  and  $j_e$  need not be constant in time, although most of the analysis to be given below will assume them constant after the time of initiation of  $j_e$ .

One can set up differential equations for the variation with  $x$  and time of the electron density,  $n_e$ , and the hole density,  $n_h$ . These equations will in the general case involve migration due to electrostatic fields, diffusion, recombination, trapping, and thermal release of electrons and holes from traps. It will be assumed, however, that trapping and thermal release from traps can be neglected, or, more precisely stated, that creation of mobile

holes and electrons occurs only at the electrodes, and that the disappearance of mobile holes and electrons is caused only by mechanisms which cause holes and electrons to disappear in equal numbers at essentially the same time and place. If this assumption is valid, the charge density due to impurity centers will never differ from its equilibrium value by an amount comparable with the density due to free electrons. This assumption can be expected to be reasonably good for an  $n$ -type impurity semiconductor in which the number of donor levels is very much greater than the number of acceptor levels and for which, at the operating temperature, practically all the donor levels have been thermally ionized, while thermal excitation of electrons from the normally full band has not yet become appreciable.

As has just been mentioned, the differential equations for the behavior of the electron and hole densities involve migration under the influence of the local electric field  $E(x, t)$ . This field is in turn influenced by the space charge due to any inequality between the hole density  $n_h$  and the electron excess  $(n_e - n_0)$ , where  $n_0$  is the normal electron density. If the difference  $(n_h - n_e + n_0)$  were comparable with  $n_h$  or  $n_e$ , the problem would be very complicated. Fortunately, however, this difference cannot have an appreciable value over an appreciable range of  $x$ , on the scale of typical experiments. For example, if  $(n_h - n_e + n_0)$  were  $10^{-2}$  of  $n_0$  for a range  $\Delta x$  of  $1\mu$ , and if  $n_0$  is  $10^{15} \text{ cm}^{-3}$ , then the difference in field strength on the two sides of  $\Delta x$  would be about  $2000 \text{ v/cm}$ , a field which would outweigh all other fields in the problem and rapidly neutralize the space charge. Moreover, the time required for the evening out of any such abnormally high space charge would be very short, of the order of magnitude of the resistivity of the specimen expressed in absolute electrostatic units ( $1 \text{ sec.} = 9 \times 10^{11} \Omega \text{ cm}$ ). Thus it will be quite legitimate to assume  $(n_h - n_e + n_0) = 0$  in all equations of the problem except Poisson's equation which determines the field  $E$ , and so  $n_e$  can be eliminated from the conduction-diffusion equations for holes and electrons. These two equations can then be used, as is shown below, to determine the two unknown functions  $n_h$  and  $E$ , Poisson's equation being discarded as unnecessary.

The boundary conditions for these differential equations consist of two parts, the conditions at  $t = 0$  and those at and to the left of  $x = 0$ . In most of the applications to be considered, the injection current  $j_e$  will be assumed to commence at  $t = 0$ . Thus, initially, the specimen will be free of holes and, at  $t = 0^+$ , will have a field  $E_a = j_a/\sigma_0$  in the region  $-a < x < 0$ , and a field  $E_0 = j_b/\sigma_0$  in the region  $0 < x < b$ , where  $\sigma_0$  is the normal conductivity of the specimen and  $j_b = j_a + j_e$  is the total current density to the right of  $x = 0$ . The boundary condition at  $x = 0$  is determined by the magnitudes of the electronic and hole contributions to the injection current  $j_e$ . If no electrons are withdrawn by the electrode at  $x = 0$ , then the electron currents just to the left and just to the right of  $x = 0$  must be equal, and the

hole current densities on the two sides must differ by  $j_c$ ; if a part of  $j_c$  is due to withdrawal of electrons, then the electronic current will have a corresponding discontinuity. If  $j_a$  is positive, i.e., flows from left to right in the specimen, the current can be assumed to be practically entirely electronic over most of the range from  $-a$  to 0; i.e., as  $x$  becomes negative the hole current must rapidly approach zero and the electron current must rapidly approach  $j_a$ . In fact, if diffusion is ignored the electron and hole currents must have these limiting values for any negative  $x$ .

The preceding discussion and the mathematics to follow have been couched in purely one-dimensional language, i.e., have been formulated as if the electron and hole densities were functions of  $x$  alone, independent of  $y$  and  $z$ , and as if the semiconductor extended to infinity in the  $y$ - and  $z$ -directions. However, it is easy to see at each stage that practically the same equations can be written for transport of holes along a narrow filament whose thickness is small compared with the linear scale of the phenomena along its length, even when the density of holes is not uniform over the cross-section of the filament. If the density of holes is uniform over the cross-section, all the equations will of course hold as written. However, recent work<sup>2</sup> has suggested that holes recombine with electrons so rapidly at the surface that the density of holes may be much smaller near the surface than in the center of the cross-section. In such case all the equations of this memorandum must be interpreted as applying to the mean value,  $\bar{n}_h(x)$ , of the density of holes,  $n_h(x, y, z)$ , averaged over the cross-section of the filament; also, the rate of recombination of holes and electrons must be set equal to some function of  $\bar{n}_h$ , as yet not reliably known, instead of to a constant times the product of electron and hole densities. This will of course alter most of the quantitative predictions of Section 4, but will not require any change in the method of calculation.

## 2. FORMULATION AND SOLUTION OF THE PROBLEM WITH NEGLECT OF DIFFUSION AND RECOMBINATION

For this case the electron and hole currents can each be equated to the product of field strength  $E$  by particle density  $n$  by mobility  $\mu$ , and the continuity equations are

$$\frac{\partial n_h}{\partial t} = - \frac{\partial}{\partial x} (E \mu_h n_h) \quad (1)$$

$$\frac{\partial n_e}{\partial t} = \frac{\partial}{\partial x} (E \mu_e n_e). \quad (2)$$

<sup>2</sup> H. Suhl and W. Shockley, paper Q11 presented at the Washington Meeting of the American Physical Society, April 29, 1949; see also Shockley, Pearson, Sparks and Brattain, reference 1.

Since the neutrality condition requires  $\frac{\partial n_h}{\partial t} = \frac{\partial n_e}{\partial t}$ , subtracting (1) and (2) and integrating gives the equation of conservation of total current:

$$E(\mu_e n_e + \mu_h n_h) = j(t) \cdot e = \text{const. indep. of } x$$

where of course  $j = j_b = (j_a + j_e)$  when  $0 < x < b$  and when conditions are such that all currents flow from left to right. Putting the neutrality condition  $n_e = n_h + n_0$ , into the equation gives the following relation between  $E$  and  $n_h$ :

$$E[(\mu_e + \mu_h)n_h + \mu_e n_0] = j \cdot e \quad (3)$$

This can be used to eliminate either  $E$  or  $n_h$  from (1). If  $E$  is eliminated we have

$$\frac{\partial n_h}{\partial t} = - \frac{\mu_e \mu_h n_0 j}{e[(\mu_e + \mu_h)n_h + \mu_e n_0]^2} \frac{\partial n_h}{\partial x} = -V(n_h) \frac{\partial n_h}{\partial x} \quad (4)$$

where  $V(n_h)$  is an abbreviation for the coefficient shown. If, instead,  $n_h$  is eliminated from (1) a similar equation results:

$$\frac{\partial E}{\partial t} = \frac{E}{j} \frac{dj}{dt} - V(E) \frac{\partial E}{\partial x} \quad (5)$$

where

$$V(E) = eE^2 \mu_h \mu_e n_0 / j = E \mu_h (E/E_0) \quad (6)$$

where

$$E_0 = j/\sigma_0 \quad (7)$$

i.e., the field necessary to maintain the total current by electronic conduction in the normal state of the specimen. The velocity  $V(E)$  is of course numerically the same as the  $V(n_h)$  occurring in (4) when  $E$  and  $n_h$  are related by (3).

The solution can be based on either (4) or (5). We shall use (4), as  $n_h$  is the most interesting quantity for direct measurement, and as the differential equation to be given below for the case where diffusion terms are included is simpler when  $n_h$  is chosen as the dependent variable.

Equation (4) (or (5)) describes a wave propagated with the variable velocity  $V$ . If  $j_e \ll j_a$ , so that  $E$  is never greatly different from  $E_0$ , (4) (or (5)) and (6) indicate that  $n_h$  (or  $E$ ) is propagated with the constant velocity  $E_0 \mu_h$ , as is of course to be expected. More interesting is the case where  $j_e$  and  $j_a$  are comparable, so that  $V$  departs significantly from constancy. It is tempting to suppose that, for this case also, the curve of  $n_h$  against  $x$  at any time  $t$  can be constructed by taking the graph of  $n_h$  against  $x$  at  $t = 0$  and moving each point of the curve horizontally to the right a

distance  $V(n_h)t$ . One can, in fact, easily verify that this construction gives a solution of (4), by writing (4) in the form

$$\left(\frac{\partial \lambda}{\partial t}\right)_{n_h} = -\frac{\left(\frac{\partial n_h}{\partial t}\right)_x}{\left(\frac{\partial n_h}{\partial x}\right)_t} = V(n_h)$$

whence it is obvious that the function  $n_h(x, t)$  defined implicitly by

$$x(n_h, t) = x(n_h, 0) + V(n_h)t$$

satisfies (4) for any form of the arbitrary function  $x(n_h, 0)$ , and that, conversely, any solution of (4) must be of this form.

Assuming, as in the preceding, that all currents flow from left to right, the boundary conditions at  $t = 0^+$  are:

$$n_h = 0 \text{ for } x < 0 \text{ and } x > 0 \quad (8)$$

or, equivalently,

$$\left. \begin{aligned} E &= E_a = j_a/\sigma_0 & \text{for } x < 0 \\ E &= E_0 = (j_a + j_e)/\sigma_0 & \text{for } x > 0 \end{aligned} \right\} \quad (9)$$

The boundary conditions at  $x = 0$  are, for  $t > 0$ ,

$$n_h = 0 \text{ or, equivalently, } E = E_a \text{ for } x = 0^- \quad (10)$$

and

$$n_h = n_{h1} \text{ or, equivalently, } E = E_1, \text{ for } x = 0^+ \quad (11)$$

where  $E_1$  and  $n_{h1}$  are given by the requirement of continuity of electronic current, i.e.,

$$E_a n_0 \mu_e = E_1 (n_0 + n_{h1}) \mu_e$$

whence, using the relation (3) between  $E_1$  and  $n_{h1}$  and expressing  $E_a$  as  $j_a/n_0 e \mu_e$

$$n_{h1} = \frac{n_0}{\frac{j_a \mu_h}{j_e \mu_e} - 1} \quad (12)$$

or, alternatively,

$$E_1 = E_0 \left[ 1 - \frac{(\mu_e + \mu_h)}{\mu_h} \frac{j_e}{(j_a + j_e)} \right] \quad (13)$$

According to (12),  $n_{h1}$  is small when  $j_e$  is small; and, by (13),  $E_1$  is only slightly below  $E_0$  for this case. As  $j_e$  increases,  $n_{h1}$  increases and  $E_1$  decreases,



and (12) and (13) would make  $n_{h1}$  infinite and  $E_1$  zero when  $j_e/j_a = \mu_h/\mu_e$ . This merely means that the assumptions made in this section, in particular the neglect of diffusion and recombination or the assumption that no electrons are taken out by the injection electrode, must fail to be valid before  $j_e$  gets as large as  $\mu_h j_a/\mu_e$ . It will, in fact, be shown in Section 5 how the presence of enormous concentration gradients makes it essential to consider the effects of diffusion near  $x = 0$  when  $j_e$  becomes large.

Putting the boundary conditions (8), (9), (10), and (11) into the wave-

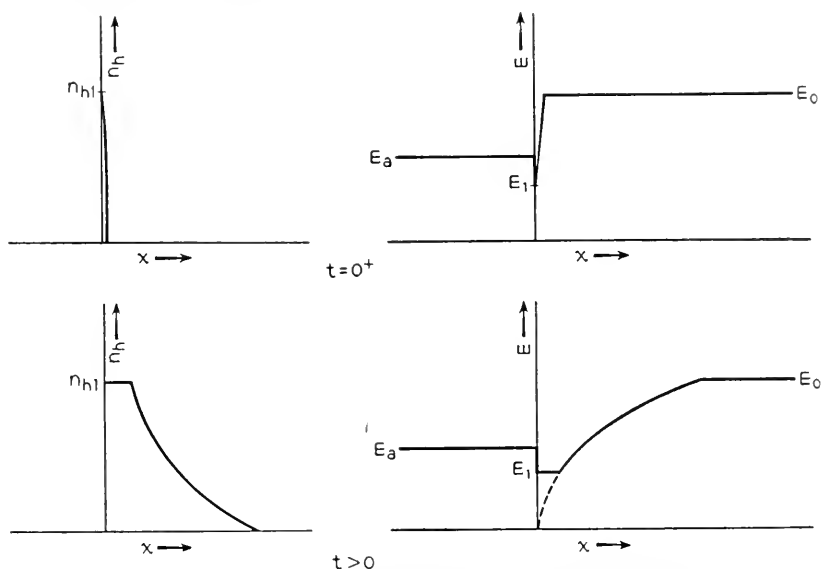


Fig. 2—Schematic variation of hole density  $n_h$  and electric field  $E$  with distance  $x$  from injection electrode and time  $t$  after the start of the injected current, in the approximation neglecting diffusion and recombination.

propagation construction described above gives the solution shown schematically in Fig. 2. An infinitesimal instant after  $t = 0$ ,  $n_h$  is zero everywhere except in an infinitesimal interval at  $x = 0$ , where it rises to a maximum value  $n_{h1}$  given by (12). This is shown schematically in the upper left diagram of Fig. 2. The corresponding plot of  $E$ , shown in the upper right, dips down to  $E_1$ , which is less than either  $E_a$  or  $E_0$ , in this infinitesimal interval. After a finite time has elapsed, the curves of  $n_{h1}$  and  $E$  against  $x$  are simply those obtained by moving each point of the right-hand portions of these  $t = 0^+$  curves a distance  $Vt$  horizontally to the right, as shown in the bottom two sketches. Here  $V$  depends on the ordinate in each diagram, taking on its maximum value  $F_0\mu_h$  when  $n_{h1} = 0$  or  $E = E_0$ . Since  $V$  is proportional to  $E^2$ , the curve in the lower right diagram is a parabola in the range be-

tween the front and the rear of the transient disturbance; this parabola, if continued, would have its vertex at the origin. After a sufficiently long time a steady state will be reached in which the field for positive  $x$  has the uniform value  $E_1$  and the density of holes the uniform value  $n_{h1}$ .

It is possible to measure  $n_h$  as a function of  $t$  for fixed  $x$  by using a closely spaced pair of probes to measure the potential gradient  $E$ , and converting  $E$  to  $n_h$  by (3); alternatively, the current to a single negatively biased probe can be used as a measure of  $n_h$ , if calibrated by the two-probe method. The

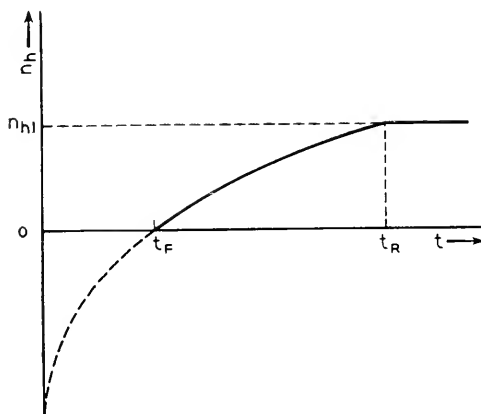


Fig. 3—Schematic variation of hole density  $n_h$  with time  $t$  after the start of the injected current, at some given distance downstream from the injection electrode, in the approximation neglecting diffusion and recombination.

portion of this curve of  $n_h$  against  $t$  for which  $0 < n_h < n_{h1}$  is given, in the present approximation, by

$$\begin{aligned} t = x/V(n_h) &= \frac{x[(\mu_e + \mu_h)n_h + \mu_e n_0]^2 e}{\mu_e \mu_h n_0 (j_a + j_e)} \\ &= t_F [1 + (1 + \mu_h/\mu_e)n_h/n_0]^2 \end{aligned} \quad (14)$$

where

$$t_F = x/E_0 \mu_h \quad (15)$$

is the time of arrival of the front of the disturbance. This curve is a parabola, as shown in Fig. 3; if continued, the parabola would have its vertex on the negative  $n_h$  axis, as shown. The rear of the disturbance, at which  $n_h$  becomes constant and equal to  $n_{h1}$ , arrives at a time  $t_R$  given by inserting  $n_{h1}$  from (12) into (14):

$$t_R = t_F / [1 - (1 + \mu_e/\mu_h)j_e/(j_a + j_e)]^2 \quad (16)$$

Note that the velocity of advance of the rear of the disturbance is less than that with which the holes drift in the steady-state field  $E_1$ . In other words, wave velocity and particle velocity must be distinguished in phenomena of this sort, although they happen to coincide at the front of the disturbance.

The discussion just given has been based on the assumption that  $j_a$  and  $j_c$  are independent of time, and that they both flow from left to right in Fig. 1. Time changes in the currents are easily taken into account in the  $n_h$  construction of Fig. 2: according to (4), it is merely necessary to move the various points of the curve of  $n_h$  against  $x$  to the right with the variable velocity  $V(n_h, t)$  instead of the constant velocity  $V(n_h)$ ; in addition,  $n_{h1}$  will in general not be a constant, so that the part of the curve for small  $x$  will no longer be a horizontal line. As for the restriction that the currents all flow from left to right, only a change of notation is needed to make all formulas apply to the case where all currents flow from right to left; and the case where part of  $j_c$  flows to the right and part to the left can, obviously, occur only under conditions where the assumptions of this section are not fulfilled, i.e., can occur only if electrons are removed at  $x = 0$  or if both diffusion and recombination are important. For, if diffusion is negligible, the existence of a potential maximum at  $x = 0$  implies a convergence of electrons from both sides onto the plane  $x = 0$ , and recombination alone cannot annihilate electrons at a finite rate in an infinitesimal volume.

Mention has already been made of the fact that equations such as (12) and (13) give an infinite density of holes when  $j_c/j_a = \mu_h/\mu_e$ , and are nonsensical for larger values of  $j_c/j_a$ . It is easy to see why any theory which neglects diffusion must break down for values of  $j_c/j_a$  of this size and larger if no electrons are removed by the injection electrode. If  $j_c/j_a$  is too large, any positive field just to the right of the injection plane  $x = 0$  will cause more electrons to flow in the negative  $x$ -direction than can be carried off by the current  $j_a$  which flows in the region of negative  $x$ . This difficulty cannot be eliminated by making the field smaller in the region of small positive  $x$ , since making the field smaller requires a higher density of holes to carry the hole current  $j_c$ ; and this in turn requires a higher density of electrons to preserve electrical neutrality. Thus, though it may be possible to realize experimental conditions under which the approximations of this section are valid for moderate values of  $j_c/j_a$ , increase of  $j_c/j_a$  above the critical value will always result in the building up of an enormously high density of holes and electrons near  $x = 0$ , and one must then consider diffusive transport and possibly other phenomena such as breakdown of the assumption that no electrons are removed by the injection electrode.

It will be shown below that the effect of recombination on the curves of  $n_h$  against  $x$  at various times  $t$  can be taken into account by using a geometrical construction similar to that of Fig. 2 except that, instead of moving the

various points of the curve horizontally to the right with increasing time, one must move them along a family of decreasing curves (cf. Figs. 4, 5, and 6). The effect of diffusion can be described roughly as a migration of each point from one of these curves to another.

### 3. COMPLETE DIFFERENTIAL EQUATIONS OF THE PROBLEM

As was mentioned in Section 1, the transport of electrons and holes along a narrow filament can be described by one-dimensional equations even if recombination at the surface of the filament causes the distribution of electrons and holes to be non-uniform over its cross-section. In the equations to follow,  $n_h$  and  $n_e$  will be understood to refer to averages, over the cross-section, of the hole and electron densities, respectively; the electrostatic field  $E$  can always be assumed uniform over the cross-section of the filament, if the latter is thin. The as yet uncertain influence of the surface on the rate of recombination of electrons and holes can be allowed for by writing the recombination rate as  $n_0 R(n_h/n_0)/\tau$  particles per unit volume per unit time, where  $R$  is a function which is asymptotically  $n_h/n_0$  as its argument  $\rightarrow 0$ , and where  $\tau$  is the recombination time for small hole densities. For pure volume recombination,  $R = n_h n_e / n_0^2 = (n_h/n_0)(1 + n_h/n_0)$ , while a conceivable extreme of surface recombination would be  $R = n_h/n_0$ .

Using this function, the continuity equations for electrons and holes can then be written, with inclusion of recombination and diffusion terms

$$\frac{\partial n_h}{\partial t} = -\frac{\partial}{\partial x} (E \mu_h n_h) - \frac{n_0}{\tau} R\left(\frac{n_h}{n_0}\right) + \frac{\partial}{\partial x} \left( D_h \frac{\partial n_h}{\partial x} \right) \quad (17)$$

$$\frac{\partial n_e}{\partial t} = \frac{\partial}{\partial x} (E \mu_e n_e) - \frac{n_0}{\tau} R\left(\frac{n_h}{n_0}\right) + \frac{\partial}{\partial x} \left( D_e \frac{\partial n_e}{\partial x} \right) \quad (18)$$

where the  $D$ 's are the diffusion constants, related to the mobilities  $\mu$  by the Einstein relation

$$D/\mu = kT/e \quad (19)$$

Using the neutrality condition  $n_e = n_0 + n_h$ , subtracting (17) from (18) and integrating gives the equation of constancy of current, the generalization of (3):

$$E[(\mu_e + \mu_h)n_h + \mu_e n_0] + \frac{kT}{e} (\mu_e - \mu_h) \frac{\partial n_h}{\partial x} = j(t)/e. \quad (20)$$

Solving for  $E$  gives

$$E = \frac{j - kT(\mu_e - \mu_h) \frac{\partial n_h}{\partial x}}{e[(\mu_e + \mu_h)n_h + \mu_e n_0]} \quad (21)$$

which can be substituted into (17) to give a differential equation for  $n_h$  alone:

$$\frac{\partial n_h}{\partial t} = -\frac{j}{e} \frac{\partial}{\partial x} \left[ (\mu_e + \frac{\mu_h n_h}{\mu_e n_0}) n_h + \mu_e n_0 \right] - \frac{n_0}{\tau} R \left( \frac{n_h}{n_0} \right) + \frac{kT}{e} \mu_h \mu_e \frac{\partial}{\partial x} \left[ \frac{(n_0 + 2n_h)}{(\mu_e + \mu_h) n_h + \mu_e n_0} \frac{\partial n_h}{\partial x} \right]. \quad (22)$$

The first term on the right represents drift, the second recombination, and the third diffusion. This holds whether  $j$  is constant in time or not. However, as the remainder of this memorandum will be devoted to the case where the currents involved are held constant after their initiation, it will be convenient to simplify the notation by introducing a current-dependent scale for  $x$  and writing the equation in terms of the dimensionless variables

$$\nu = n_h/n_0, s = t/\tau, \xi = x/E_0\mu_h\tau = xen_0\mu_e/j\mu_h\tau \quad (23)$$

In terms of these (22) becomes simply

$$\frac{\partial \nu}{\partial s} = -\frac{\partial}{\partial \xi} \left[ \frac{\nu}{1 + (1 + \mu_h/\mu_e)\nu} \right] - R(\nu) + \left( \frac{j}{j} \right)^2 \frac{\partial}{\partial \xi} \left[ \frac{(1 + 2\nu) \frac{\partial \nu}{\partial \xi}}{1 + (1 + \mu_h/\mu_e)\nu} \right] \quad (24)$$

where  $R(\nu) = \nu(1 + \nu)$  for pure volume recombination, or  $= \nu$  for a surface recombination uninfluenced by the electron density, and where

$$J = (kTe \mu_e^2 n_0^2 / \mu_h \tau)^{1/2} = \sigma_0 (kT/e \mu_h \tau)^{1/2} \quad (25)$$

Numerically the characteristic field is, at  $300^\circ\text{K}$ , with  $\mu_h = 1700 \text{ cm}^2/\text{v sec}$ ,<sup>3</sup>

$$(kT/e\mu_h\tau)^{1/2} = 3.90 (\tau/1\mu\text{s})^{-1/2} \text{ volts/cm} \quad (26)$$

Note that the importance of the diffusion term in (24) goes down inversely as the *square* of the current density used and inversely as the *square* of the recombination time; this is because an increase in the distance the holes travel decreases the distance they diffuse by decreasing the concentration gradient, and also makes a given diffusion distance less serious by comparison with the total distance traveled. Note also that, if  $\mu_e = \mu_h$ , the last term of (24) reduces simply to  $\left(\frac{j}{j}\right)^2 \frac{\partial^2 \nu}{\partial \xi^2}$ , but that, if  $\mu_e \neq \mu_h$ , the diffusion term is not a simple second derivative.

<sup>3</sup>G. L. Pearson, paper Q9 presented at the Washington Meeting of the American Physical Society, April 29, 1949.

## 4. SOLUTION INCLUDING RECOMBINATION BUT NEGLECTING DIFFUSION

It is plausible to expect by analogy with Fig. 2 that (24) can be solved, neglecting the last term, by a similar construction in which the curve of  $n_h$  against  $x$  at time  $t$  is derived from that at time 0 by moving each point to the right along a descending curve, instead of along a horizontal line as before. To show that this is indeed the case, and at the same time to show that the diffusion term cannot so easily be taken into account, let (24) be written, omitting its last term, as

$$\frac{\partial \nu}{\partial s} = -\Phi(\nu) \frac{\partial \nu}{\partial \xi} - R(\nu)$$

where  $\Phi$  is just the translation into dimensionless variables of the velocity  $V$  encountered in (4). This can be converted into a differential equation for  $\xi$  by writing

$$\left(\frac{\partial \nu}{\partial s}\right)_{\xi} = -\frac{\left(\frac{\partial \xi}{\partial s}\right)_{\nu}}{\left(\frac{\partial \xi}{\partial \nu}\right)_s}$$

and multiplying through by  $\left(\frac{\partial \xi}{\partial \nu}\right)_s$ :

$$\left(\frac{\partial \xi}{\partial s}\right)_{\nu} = R(\nu) \left(\frac{\partial \xi}{\partial \nu}\right)_s + \Phi(\nu) \quad (27)$$

or with  $w = \int \frac{d\nu}{R(\nu)}$ ,

$$\frac{\partial \xi}{\partial s} - \frac{\partial \xi}{\partial w} = \Phi(w)$$

$$\frac{\partial \left( \xi + \int \Phi dw \right)}{\partial s} - \frac{\partial \left( \xi + \int \Phi dw \right)}{\partial w} = 0$$

whence the general solution is

$$\xi = - \int \Phi dw + f(s + w) \quad (28)$$

where  $f$  is an arbitrary function. If the same transformation is tried on (24) with the diffusion term retained, the equation corresponding to (27) has an additional term on the right containing a quotient of second and first derivatives of  $\xi$  with respect to  $\nu$ , and the simple explicit solution fails.

To apply (28) to explicit calculation, or even to visualize it physically, it is necessary to determine the proper form of the arbitrary function  $f$  to fit

the boundary conditions of the problem. This is most conveniently done by introducing a family of curves as suggested by the analogy with Fig. 2. The analogy suggests that we should try to find curves in the  $\nu, \xi$  plane (the full curves of Fig. 4) such that a point can move along any one of them with velocity components

$$\frac{d\xi}{ds} = \Phi, \quad \frac{d\nu}{ds} = -R.$$

The equation of any such curve is

$$\frac{d\xi}{d\nu} = -\Phi/R$$

or

$$\xi(\nu, \nu_0) = \int_{\nu}^{\nu_0} \frac{\Phi}{R} d\nu \quad (29)$$

where  $\nu_0$ , the intercept of the curve on the  $\nu$ -axis, is taken as a parameter distinguishing the curve in question from others of the family. A point which starts at height  $\nu_0$  on the  $\nu$ -axis at time  $s = 0$  will reach height  $\nu$  at time

$$s(\nu, \nu_0) = \int_{\nu}^{\nu_0} \frac{d\nu}{R}. \quad (30)$$

Thus, after time  $s$ , the locus of all points which start at all the various heights  $\nu_0$  will be the curve obtained by eliminating  $\nu_0$  between (29) and (30) (shown dotted in Fig. 4). That this curve is, in fact, of the form (28) and therefore a solution of the differential equation is easily seen by writing (29) and (30) in terms of integrals taken from some arbitrary but fixed lower limit:

$$\begin{aligned} \xi(\nu, \nu_0) &= -\int^{\nu} \frac{\Phi}{R} d\nu + \int^{\nu_0} \frac{\Phi}{R} d\nu \\ s(\nu, \nu_0) &= -\int^{\nu} \frac{d\nu}{R} + \int^{\nu_0} \frac{d\nu}{R}. \end{aligned}$$

As  $\nu_0$  is varied both the integrals with upper limit  $\nu_0$  will vary, and either can be expressed as a function of the other:

$$\int^{\nu_0} \frac{\Phi d\nu}{R} = f\left(\int^{\nu_0} \frac{d\nu}{R}\right)$$

whence

$$\xi = -\int^{\nu} \frac{\Phi}{R} d\nu + f\left(s + \int^{\nu} \frac{d\nu}{R}\right)$$

which is identical with (28).

The equations (29) and (30) of course apply only to the portion of the curve of  $\nu$  against  $\xi$  which is derived from starting points  $\nu_0$  on the  $\nu$  axis which are less than the maximum value  $\nu_1$  corresponding to the value  $n_{h1}$  given by (12): The points for  $\nu_0 < \nu_1$  are merely initiated at time  $s = 0$  and propagated by the differential equation from then on; the point  $\nu = \nu_1$ ,  $\xi = 0$ , on the other hand, remains a source at all times from the initiation of the injection onward. Thus the complete curve of  $\nu$  against  $\xi$  for any positive  $s$  follows the dotted construction of Fig. 4 from the  $\xi$  axis up to where it intersects the full curve corresponding to  $\nu_0 = \nu_1$ , after which it

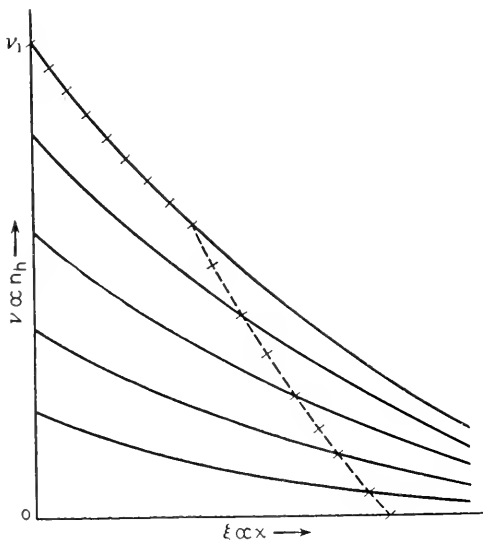


Fig. 4—Schematic illustration of the method of constructing the curve of hole density  $n_h$  against distance  $x$  from the injection electrode at some given time, taking account of recombination but neglecting diffusion.

follows the latter curve, as indicated by the crosses in the figure. The steady-state distribution is thus simply the full curve for  $\nu_0 = \nu_1$ .

For explicit calculation for the case of pure volume recombination one must insert  $\Phi = 1/[1 + (1 + \mu_h/\mu_e)\nu]^2$ ,  $R = \nu(1 + \nu)$  into (29) and (30). The integrations are easily carried out and give

$$\xi = \left[ \frac{1 + \mu_e/\mu_h}{1 + (1 + \mu_h/\mu_e)\nu_0} + \ln \frac{\nu_0}{1 + (1 + \mu_h/\mu_e)\nu_0} + \frac{\mu_e^2}{\mu_h^2} \ln \frac{1 + (1 + \mu_h/\mu_e)\nu_0}{1 + \nu_0} \right] - [\text{same with } \nu \text{ instead of } \nu_0] \quad (31a)$$

$$s = \ln \frac{\nu_0}{1 + \nu_0} - \ln \frac{\nu}{1 + \nu} \quad (32a)$$



For the case of a surface recombination uninfluenced by electron concentration one obtains similarly, with  $R = \nu$ :

$$\xi = \left[ \frac{1}{1 + (1 + \mu_h/\mu_e)\nu_0} - \ln \frac{\nu_0}{1 + (1 + \mu_h/\mu_e)\nu_0} \right] - [\text{same with } \nu \text{ instead of } \nu_0] \quad (31b)$$

$$s = \ln \frac{\nu_0}{\nu} \quad (32b)$$

When  $\mu_e = 3\mu_h$ , 2, as for germanium, (31a) and (31b) become respectively

$$\xi = \left[ \frac{5/2}{1 + 5\nu_0/3} + \ln \frac{\nu_0}{1 + 5\nu_0/3} + \frac{9}{4} \ln \frac{1 + 5\nu_0/3}{1 + \nu_0} \right] - [\text{same with } \nu \text{ instead of } \nu_0] \quad (33a)$$

and

$$\xi = \left[ \frac{1}{1 + 5\nu_0/3} + \ln \frac{\nu_0}{1 + 5\nu_0/3} \right] - [\text{same with } \nu \text{ instead of } \nu_0] \quad (33b)$$

These can also be written, using (32a) and (32b),

$$\xi = s + \frac{5/2}{1 + 5\nu_0/3} - \frac{5/2}{1 + 5\nu/3} + \frac{5}{4} \ln \left[ \frac{(1 + 5\nu_0/3)(1 + \nu)}{(1 + 5\nu/3)(1 + \nu_0)} \right] \quad (34a)$$

and

$$\xi = s + \ln \left( \frac{\nu + 3/5}{\nu_0 + 3/5} \right) - \frac{1}{1 + 5\nu/3} + \frac{1}{1 + 5\nu_0/3} \quad (34b)$$

Figures 5a and 5b show as a full curve the plot of eq. (33a) for the case  $\nu_0 = \infty$ , and the full curve in Fig. 6 shows in the same way the plot of (33b) for  $\nu_0 = \infty$ . Changing  $\nu_0$  of course merely shifts either curve horizontally. Note the very sharp increase of  $\nu$  for small  $\xi$ , which shows up in pronounced manner on the expanded scale of Fig. 5b. The corresponding values of  $s$ , computed from (32a) or (34a), are marked on the curve of Fig. 5; the corresponding marks on the curve of Fig. 6 also represent values of  $s$  at intervals of 0.2, but are not labeled with absolute values because (32b) is infinite for  $\nu_0 = \infty$ .

For large  $\xi$ ,  $\nu$  becomes very small and it becomes legitimate to expand the logarithms. The first few terms of the resulting asymptotic expression for  $\xi$  are, for  $\nu_0 = \infty$  and the recombination function leading to (31a),

$$\xi \sim \left( \frac{\mu_e^2}{\mu_h^2} - 1 \right) \ln (1 + \mu_h/\mu_e) - (1 + \mu_e/\mu_h) - \ln \nu + (3 + 2\mu_h/\mu_e)\nu \quad (35a)$$

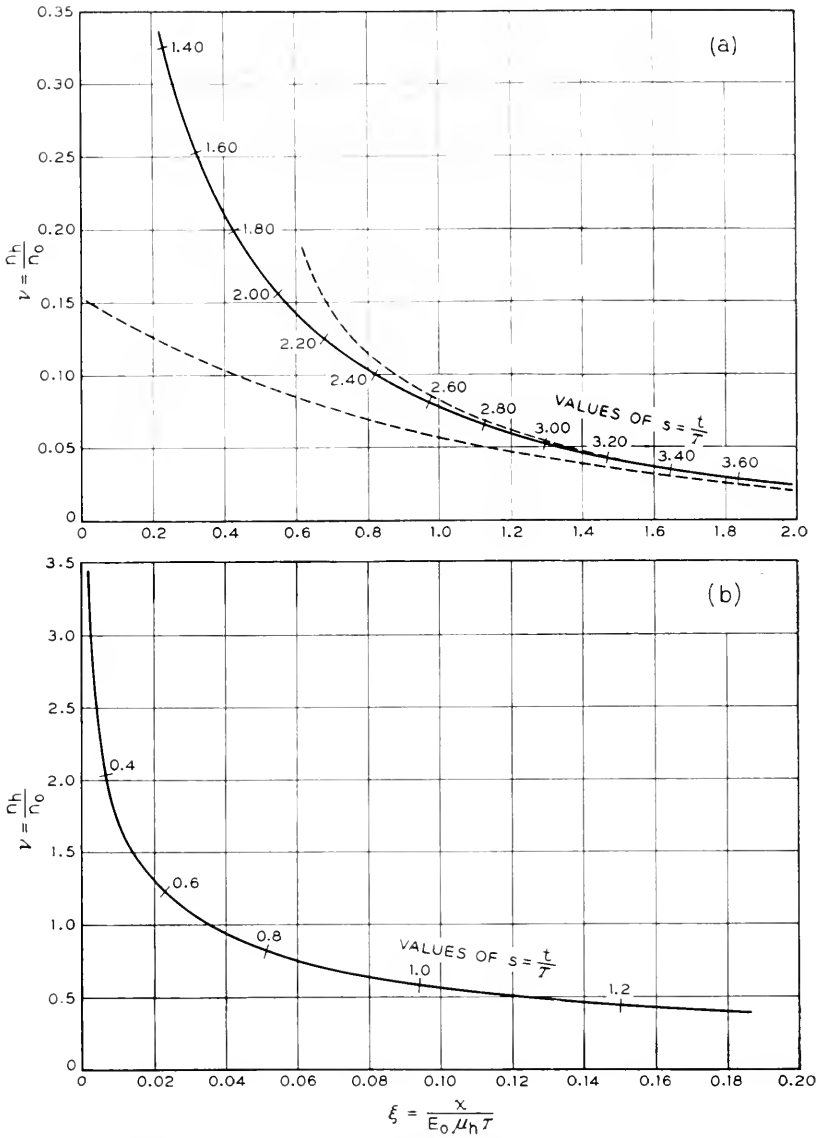


Fig. 5—Steady-state curve of hole density  $n_h$  against distance  $x$ , for the case of ideal volume recombination (recombination rate  $= n_h n_e / \tau n_0$ ), and asymptotic approximations to this curve.

while, for the recombination function leading to (31b),

$$\xi \sim -\ln(1 + \mu_e \mu_v) - 1 - \ln \nu + 2(1 + \mu_e \mu_v)\nu \quad (35b)$$

In Figs. 5a and 6 the lower dotted curve represents the sum of the terms of (35a) or (35b) respectively as far as the term in  $\ln \nu$ ; in this approximation the dependence of  $\nu$  on  $\xi$  is exponential. An exponential behavior of this sort is assumed in the small-signal theory of the modulation of the resistance of a filament of semiconductor by hole injection.<sup>4</sup> The upper dotted curve

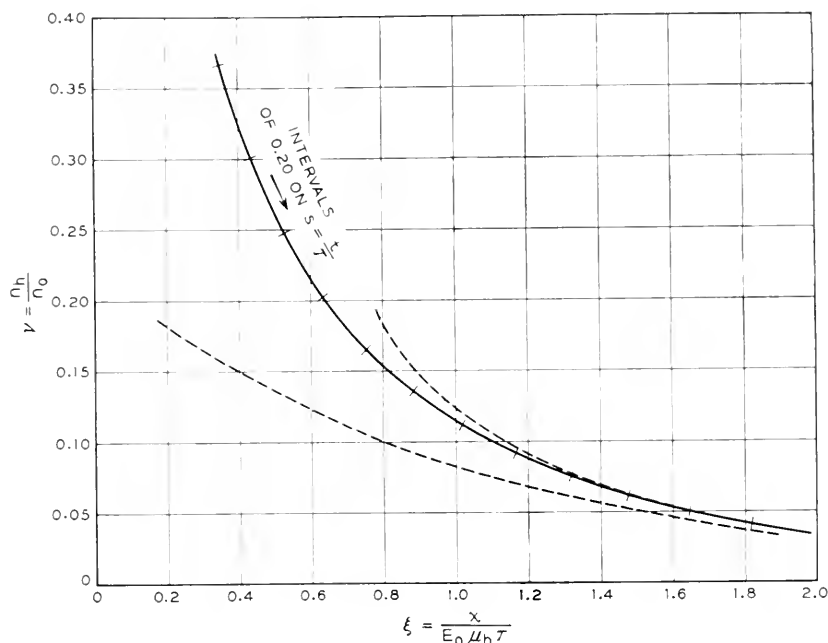


Fig. 6—Steady-state curve of hole density  $n_h$  against distance  $x$ , for the case of ideal surface recombination (recombination rate  $= n_h/\tau$ ), and asymptotic approximations to this curve.

in Figs. 5a and 6 is a plot of (35a) or (35b), respectively, with the linear term included. It will be seen that in both figures the simple exponential approximation is already quite far off when  $\nu = n_h/n_0 = 0.1$ , though it improves rapidly for smaller  $\nu$ .

Figure 7 shows a sample plot of  $\nu$  against  $\xi$  for the case of ideal volume recombination (eqs. (31a) etc.), for the numerical conditions  $s = 1$ ,  $v_1 = 0.3$  (cf Fig. 4). According to (12), whose validity at  $\xi = 0$  is unimpaired by the occurrence of recombination, this value of  $v_1$  implies  $j_a/j_e = 6.5$ . The left-

<sup>4</sup> W. Shockley, G. L. Pearson, and J. R. Haynes, *Bell Sys. Tech. Jour.*, this issue.

hand portion of this curve is simply traced from Fig. 5, with a horizontal shift sufficient to give an intercept at  $\nu = 0.3$ ; the right-hand portion was constructed by placing the paper for Fig. 7 over that for Fig. 5, shifting horizontally until the point corresponding to one of the values of  $s$  marked on Fig. 5 lay on the axis of ordinates of Fig. 7, marking the position of the point labeled with one plus this value of  $s$ , and repeating.

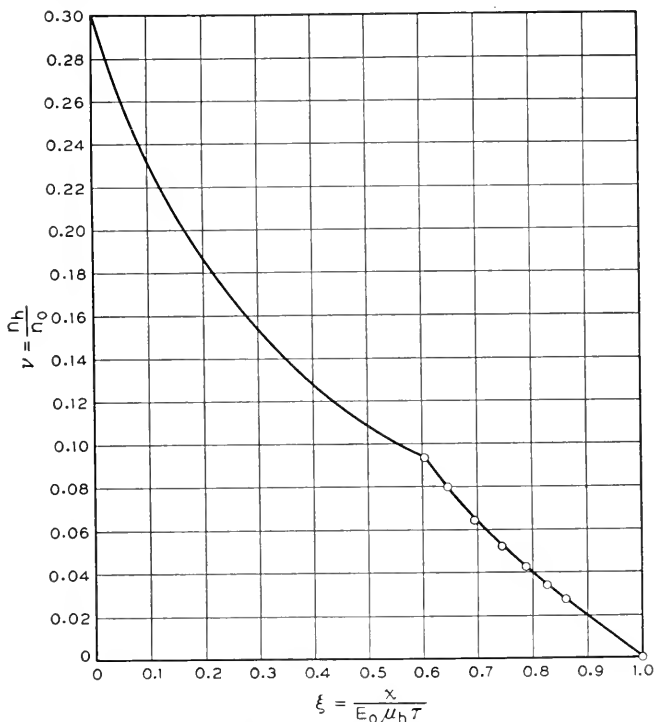


Fig. 7—Variation of hole density  $n_h$  with distance  $x$  at time  $t = \tau$  assuming  $n_{h1} = 0.3 n_0$  recombination rate  $= n_h n_e / \tau n_0$ , and neglecting diffusion.

Figure 8 shows sample plots of  $\nu$  against  $s$  for the same case of ideal volume recombination, with  $\nu_1 = 0.3$ , for  $\xi = 0.5$  and  $\xi = 1.0$ . Curves for a different  $\nu_1$  would start out exactly the same, but rise higher. The rising portion of the curve for  $\xi = 0.5$ , for example, was constructed from the curve of Fig. 5a by locating various points  $(\xi, \nu)$  on the latter curve and associating with the  $\nu$  value of each such point a value of  $s$  equal to the difference of the  $s$  values marked on the curve of Fig. 5a for the two points abscissae  $\xi$  and  $(\xi - 0.5)$ . As Fig. 5a was prepared entirely by slide rule, the accuracy is not all that can be desired; the individual computed points are shown to give an idea of the magnitude of the computational errors.

For convenience in future calculations the equations will be appended which correspond to (31) to (34) when, instead of  $n_h$ , the field  $E$  is used as dependent variable in the differential equations. In terms of the dimensionless variable

$$\epsilon = E/E_0 = \frac{1}{1 + \nu(1 + \mu_h/\mu_e)} \quad (36)$$

and the parameter  $\epsilon_0$  corresponding to  $\nu = \nu_0$ , the equations are, for ideal volume recombination (eqs. (31a) etc.),

$$\xi = \left[ (1 + \mu_e/\mu_h)\epsilon_0 - \frac{\mu_e^2}{\mu_h^2} \ln \left( 1 + \frac{\mu_h}{\mu_e} \epsilon_0 \right) + \ln (1 - \epsilon_0) \right] \quad (37a)$$

— [same with  $\epsilon$  instead of  $\epsilon_0$ ]

$$s = \ln \frac{(1 - \epsilon_0)}{\left( 1 + \frac{\mu_h}{\mu_e} \epsilon_0 \right)} - \ln \frac{(1 - \epsilon)}{\left( 1 + \frac{\mu_h}{\mu_e} \epsilon \right)} \quad (38a)$$

while, for the recombination function leading to eqs. (31b) etc.,

$$\xi = \epsilon_0 - \epsilon + \ln \frac{1 - \epsilon_0}{1 - \epsilon} \quad (37b)$$

$$s = \ln \left[ \frac{\frac{1}{\epsilon_0} - 1}{\frac{1}{\epsilon} - 1} \right]. \quad (38b)$$

The electrostatic potential  $U$  is

$$U = - \int E \, dx = - E_0^2 \mu_h \tau \int \epsilon \, d\xi.$$

In the steady state the relation between  $\epsilon$  and  $\xi$  is given by (37) with  $\epsilon_0$  set equal to  $\epsilon_1$  which, by (13), is  $1 - \frac{(\mu_e + \mu_h)}{\mu_h} \frac{j_e}{(j_a + j_e)}$ . For this case

$$\begin{aligned} U &= -E_0^2 \mu_h \tau \left[ \epsilon \xi - \int \xi \, d\epsilon \right] \\ &= -E_0^2 \mu_h \tau \left[ \epsilon (\mu_e^2/\mu_h^2 - 1) - \epsilon^2 (1 + \mu_e/\mu_h)/2 \right. \\ &\quad \left. - \ln (1 - \epsilon) - \frac{\mu_e^2}{\mu_h^2} \ln \left( 1 + \frac{\mu_h}{\mu_e} \epsilon \right) \right] + \text{const.} \end{aligned} \quad (39a)$$

for ideal volume recombination; while, for the assumptions leading to eqs. (31b), etc. the relation is

$$U = -E_0^2 \mu_h \tau [\epsilon - \epsilon^2/2 - \ln(1 - \epsilon)] + \text{const.} \quad (39b)$$

Thus, in the steady state, the difference in potential between any two points to the right of  $x = 0$  can be obtained by finding the values of  $\epsilon$  for these two points by (37), and then using these to evaluate the difference in the values of (39) at the two points. To the left of  $x = 0$ , of course,  $E$  is constant and equal to  $j_a/\sigma$ .

### 5. DIFFUSION EFFECTS

Diffusion will obviously be very important at small values of  $\xi = x/E_0 \mu_h \tau$  when  $n_{h1}$  is large, because of the tremendous concentration gradients which

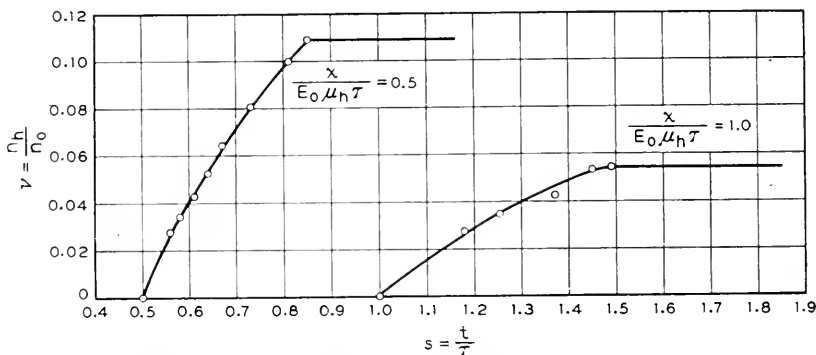


Fig. 8—Transient behavior of  $n_h$  with time at position  $x/E_0 \mu_h \tau = 0.5$  and  $1.0$ , assuming  $n_{h1} = 0.3 n_0$  and recombination rate  $= n_h n_e / \tau n_0$ .

Figs. 5 and 6 predict for such cases. Also, of course, diffusion will round off the discontinuities in slope which appear at the front and rear of the transient disturbance as in Fig. 7 and Fig. 8. At other points the importance of diffusion effects can be roughly estimated either by comparing the diffusion current with the drift current or by comparing the divergences of these two contributions to the current, i.e., the last and first terms on the right of (24). Referring to these terms in (24) we have

$$\left[ \frac{\text{diffusion current}}{\text{drift current}} \right] = \left( \frac{j}{j} \right)^2 \frac{(1 + 2\nu)}{\nu} \left[ \frac{\partial \nu}{\partial \xi} \right] \quad (40)$$

$$\left[ \frac{\text{div. diffusion current}}{\text{div. drift current}} \right] = \left( \frac{j^2}{j} \right) \cdot \left[ [1 + (1 + \mu_h/\mu_e)\nu][1 + 2\nu] \frac{\partial^2 \nu}{\partial \xi^2} / \frac{\partial \nu}{\partial \xi} + (1 - \mu_h/\mu_e) \frac{\partial \nu}{\partial \xi} \right]. \quad (41)$$

For the steady-state curve approximate values of the expressions (40) and (41) can be computed by evaluating the derivatives of  $\xi$  with respect to  $\nu$

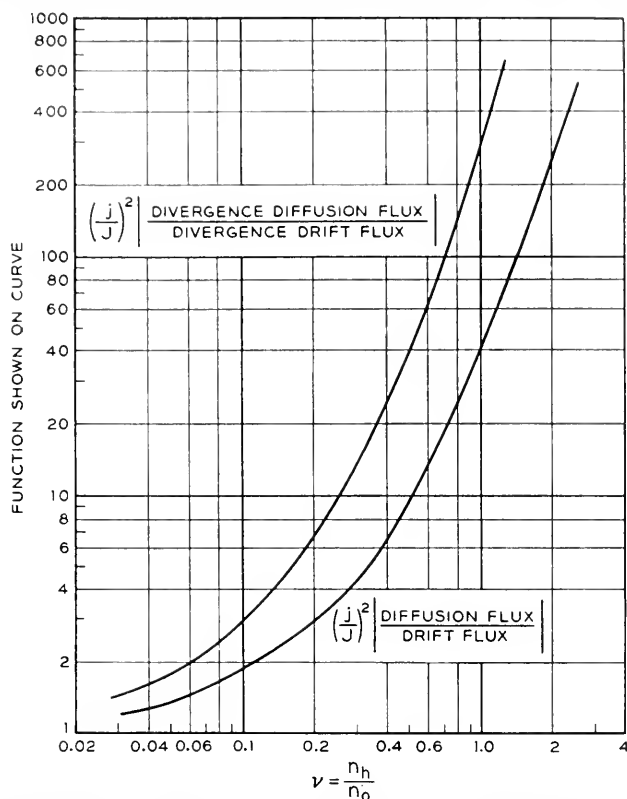


Fig. 9—Asymptotic magnitude of diffusion terms in the steady-state flux of holes, when  $j/J$  is large.

from (29) or (31). For the case of ideal volume recombination with  $\mu_e \mu_h = 3/2$  this gives, if the diffusion effects are not too large,

$$\left[ \frac{\text{diffusion current}}{\text{drift current}} \right] \approx \left( \frac{j}{J} \right)^2 (1 + \nu)(1 + 2\nu)(1 + \frac{5}{3}\nu)^2 \quad (42)$$

$$\left[ \frac{\text{div. diffusion current}}{\text{div. drift current}} \right] \approx \left( \frac{j}{J} \right)^2 (1 + \frac{5}{3}\nu)^2 (1 + \frac{28}{3}\nu + 21\nu^2 + \frac{16}{3}\nu^3). \quad (43)$$

These functions are plotted in Fig. 9. From this figure one can estimate roughly when diffusion will begin to have serious effects other than a slight rounding of the leading and trailing ends of the transient. For example, if

it is desired that the ratio (43) be less than about 0.1 in the steady state for values of  $\nu$  as high as 0.3, the upper curve of Fig. 9 shows that the current density used must be large enough to make  $\left(\frac{j}{j_c}\right)^2 \leq \frac{0.1}{13.6}$ , i.e.,  $j \geq 11.7 J$ , where  $J$  is given by (25) and (26).

An approximate evaluation of (40) and (41) in the transient region can be performed by graphical or numerical differentiation of a curve such as that of Fig. 7. For example, a rough calculation based on Fig. 7 gives, in the middle of the transient portion ( $\xi = 0.75$ ),

$$\left[ \frac{\text{div. diffusion current}}{\text{div. drift current}} \right] \approx 3 \left( \frac{j}{j_c} \right)^2.$$

More important and also more difficult to estimate is the effect of diffusion in rounding off the front and rear edges of the transient. Various ways can be devised to estimate a rough upper limit to the amount of rounding off to be expected. One such is to compute what the diffusive flux just behind the front of the advancing disturbance would be if the distribution of holes were the same as in the absence of diffusion. Under conditions where diffusion is not too serious the time integral of this diffusive flux between any two times can be equated to the increase in rounding of the front, as measured by the area between an ideal curve such as that of Fig. 7 and the actual curve of  $\nu$  against  $\xi$  for the same time  $s$ . The integration cannot be extended back to time zero, however, since the integral of the flux diverges logarithmically. The fact that the diffusive flux is actually finite instead of infinite of course arises from the fact that at small times the concentration gradient a short distance behind the front can no longer be approximated by the gradient which would obtain in the absence of diffusion, but instead is very much less. This suggests that an upper limit to the total diffusive flux passing into the region of the front from time 0 to time  $s$  can be obtained by taking the flux computed as described above between the times  $s_0$  and  $s$ , and adding to it the total number of holes which have left the injection electrode between time 0 and time  $s_0$ . Since this gives an upper limit for any  $s_0$ , one may use the minimum of the resulting sum as  $s_0$  is varied.

The results of some sample calculations of this sort are shown in Fig. 10, which refers to the same time, currents, and recombination function as Fig. 7, viz.,  $s = t/\tau = 1.0$ ,  $j_e/j_a = 2/13$ , ideal volume recombination. The full curve is the transient portion of Fig. 7 replotted on a larger scale. The lower dotted curve is a curve drawn in by hand in such a way as to make the area between it and the full curve equal the upper limit computed in the manner just described, for the case  $j = 100J$ . The upper curve was drawn



similarly for  $j = 31.6J$ . Since the true curve of  $v$  against  $\xi$  must lie between the dotted curve and the full curve in each case, it can be concluded that for times and current ratios of this order the diffusionless theory of Section 4 gives a useful approximation to the transient when  $j \gtrsim 100J$ . At the other end, it seems likely that for  $j \lesssim 10J$  the theory of Section 4 has no quantitative utility at all in the transient region.

When diffusion effects are sufficiently great, account must also be taken of the fact that the boundary conditions at the injection electrode ( $x = 0$ )

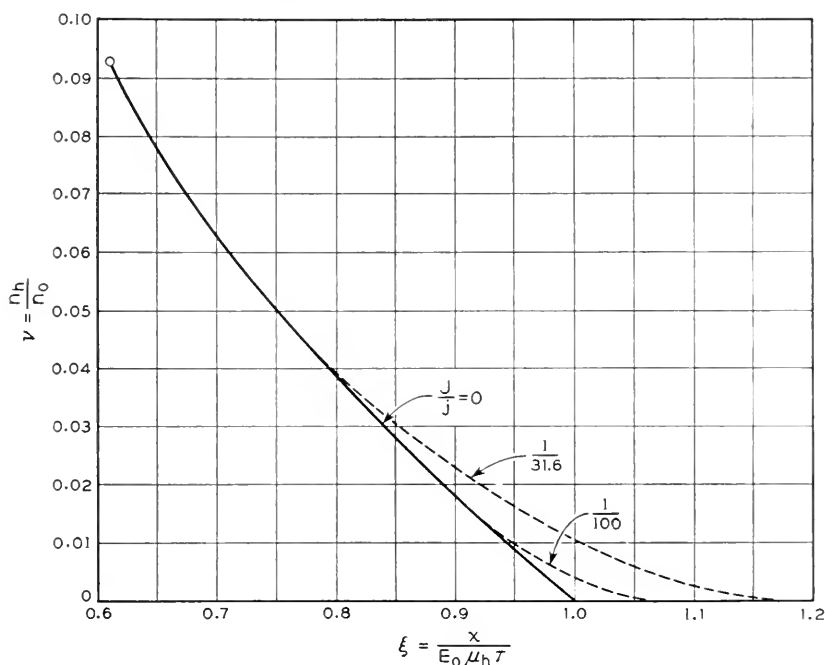


Fig. 10—Approximate magnitudes of the rounding of the front by diffusion for various values of  $j/J$ , for the case  $t = \tau$ ,  $j_e/j_a = 2/13$ , ideal volume recombination. Ordinate is proportional to hole density, abscissa to distance from injection electrode.

take a different form from those in the absence of diffusion. In the absence of diffusion and with the assumption that only holes are injected at  $x = 0$ , the current just to the right of  $x = 0$  must consist of a contribution  $j_e$  from holes and a contribution  $j_a$  from electrons, while the current just to the left of  $x = 0$  is purely electronic and of magnitude  $j_a$ . This implies, as we have seen in Section 2, that the hole density be discontinuous, with the value  $n_{h1}$  given by (12) just to the right of  $x = 0$ , and the value zero just to the left. But if diffusion is allowed, the hole density must be continuous. For the

idealized case where holes are injected on the plane  $x = 0$  and no electrons are removed there, the equations to be satisfied are

$$D_e \left( \frac{\partial n_e}{\partial x} \right)_+ + n_e \mu_e E_+ = D_e \left( \frac{\partial n_e}{\partial x} \right)_- + n_e \mu_e E_- \quad (44)$$

$$-D_h \left( \frac{\partial n_h}{\partial x} \right)_+ + n_h \mu_h E_+ = \frac{j_e}{e} - D_h \left( \frac{\partial n_h}{\partial x} \right)_- + n_h \mu_h E_- \quad (45)$$

$$D_e \left( \frac{\partial n_e}{\partial x} \right)_- - D_h \left( \frac{\partial n_h}{\partial x} \right)_- + (n_e \mu_e + n_h \mu_h) E_- = j_a / e \quad (46)$$

where subscripts  $+$  and  $-$  refer to conditions just to the right of  $x = 0$  and just to the left, respectively. Using the neutrality condition  $n_e = n_0 + n_h$  these are three equations for the five unknowns  $\left( \frac{\partial n_h}{\partial x} \right)_\pm$ ,  $E_\pm$ ,  $n_h$ . To complete the determination of these quantities the differential equation (22) must be solved and the boundary conditions imposed that  $n_h \rightarrow 0$  as  $x \rightarrow \pm \infty$ .

Actually the problem of estimating conditions at  $x = 0$  may not be quite as formidable as the preceding paragraph suggests, at least if the diffusion parameter  $J/j$  is reasonably small and if  $j_e/j_a$  is also not too large. For such cases the "upstream diffusion" of holes into the region of negative  $x$  will probably reach a steady state in a very short time. Solutions of the steady state differential equation in this region have been obtained numerically by W. van Roosbroeck (unpublished). Such solutions will give one relation between  $n_h$  and  $\left( \frac{\partial n_h}{\partial x} \right)_-$ ; another relation, in the form of a fairly narrow range of limits, is provided by the fact that  $\left( \frac{\partial n_e}{\partial x} \right)_+$  will under these conditions be  $\ll \left( \frac{\partial n_e}{\partial x} \right)_-$ , being in fact probably somewhere between zero and the value for the diffusionless case with the same value of  $n_{h1}$ .

Of course, if the mathematical solution for this one-dimensional idealization is to be applied to a case where holes are injected into a filament by a pointed electrode on its boundary, little meaning can be attached to variations in the  $n_h$  of the mathematical solution within a range of  $x$  values smaller than the diameter of the filament.

## 6. SUMMARY AND DISCUSSION

There are three principal factors which limit the range of conditions within which the present theory provides a useful approximation to the transient behavior of  $n_h$  as a function of  $t$  and  $x$ . These are diffusion, trapping, and departure from one-dimensional geometry. If the geometry is sufficiently nearly one-dimensional and trapping is negligible, the discussion

of Section 5 shows that the theory of Section 4, with its neglect of diffusion, will give a useful approximation to the truth whenever the field in which the holes migrate is sufficiently strong —e.g., strong enough to make the current density  $j \gtrsim 100J$ , where  $J$  is given by (25) and (26). The obtaining of "sufficiently strong" fields without excessive heating or other undesirable effects is facilitated by the use of specimens with as long a recombination time  $\tau$  as possible, and by the use of specimens of low conductivity. However, it is hard to say how low the conductivity can be made without danger that the "no trapping" assumption will break down, since for this assumption to be valid the density of hole traps must be  $\ll$  the density of donors.

The numerical predictions of the theory depend upon the way in which the rate of recombination is assumed to depend upon the concentrations of electrons and holes, i.e., upon the form of the function  $R(\nu)$  introduced in (17) and (18). The full curves of Figs. 5 and 6 give the steady-state dependence of  $n_h$  on  $x$  for two simple assumptions regarding  $R(\nu)$ , the dependence corresponding to any given boundary value  $n_{h1}$  at  $x = 0$  being simply obtained by a suitable horizontal shift of the curve plotted. When the currents are held constant after their initiation, the auxiliary time scale in these figures can be used to construct the transient disturbance at any time, by the methods described in connection with the examples of Figs. 7 and 8.

These results should hold for a plane-parallel arrangement of electrodes or, to a good approximation, for electrodes placed along the length of a narrow filament, provided the  $n_h$  appearing in the equations is interpreted as a cross-sectional average of the hole density and provided the other assumptions given in Section 1 are fulfilled. It is easy to see, however, that practically the same equations apply to cases of cylindrical or spherical geometry, in the approximation where diffusion is neglected. For, in these cases, the original equations (17) and (18) merely have  $\frac{\partial}{\partial x}(\cdots)$  replaced by  $\frac{1}{r} \frac{\partial}{\partial r}(r \cdots)$

or  $\frac{1}{r^2} \frac{\partial}{\partial r}(r^2 \cdots)$ ; if the diffusion terms are neglected the solution is the same as before with  $x$  replaced by  $r^2/2$  (cylindrical case) or  $r^3/3$  (spherical case) and with  $j$  replaced by  $I/2\pi d$  (cylindrical case,  $d$  = thickness of sample,  $I$  = total current) or by  $I/4\pi$  (spherical case). However, it may be difficult to realize experimentally conditions approximating cylindrical or spherical geometry which satisfy the requirement that diffusion effects be small.

Another generalization which is easily made is the removal of the assumption that no electrons are withdrawn by the electrode at  $x = 0$ . As far as conditions to the right of  $x = 0$  are concerned (Fig. 1), the only change required in the diffusionless theory is to interpret  $j_e$  as the current density leaving the emitter electrode in the form of holes, rather than as the total current from the emitter electrode, and to interpret  $j_a$  as the sum of the

current leaving the emitter electrode in the form of electrons and any current to the left of  $x = 0$ .

It should also be clear that the entire analysis of this paper, though it has for definiteness been formulated for the case where holes are injected into an excess semiconductor, applies just as well to any case where electrons can be injected into a defect semiconductor. For the latter case it is merely necessary to interchange the subscripts  $e$  and  $h$  in the formulas. Though the types of experiments discussed in this paper have to date only been reported for  $n$ -type germanium, the occurrence of similar phenomena in  $p$ -type specimens is indicated by the successful use of such specimens in transistors.<sup>5</sup>

An interesting and possibly quite useful phenomenon should occur when, after establishment of a steady state, the current  $j_e$  is suddenly turned off. There will result a transient disturbance propagated in the direction of in-

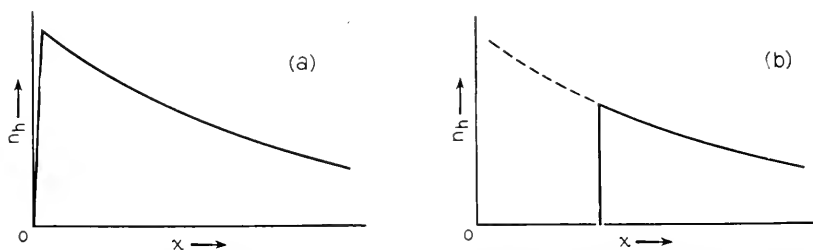


Fig. 11—Schematic variation of hole density  $n_h$  with distance  $x$ , illustrating formation of a shock wave by quickly decreasing  $j_e$  to zero, for the case where  $j = j_e + j_a$  is kept constant.

- (a) Immediately after reduction of  $j_e$  to zero.
- (b) Later time.

creasing  $x$ , which is very much like a shock wave in a gas. This, the most interesting feature of the phenomenon, will occur regardless of whether  $j_a$  remains constant when  $j_e$  is cut off; however, the simplest example for illustrative purposes is the case where  $j_a$  is increased by the amount  $j_e$  at the instant when the latter is cut off, so that  $j$  remains constant. For this case, illustrated in Fig. 11, the values of  $n_h$  ahead of the advancing front will remain the same at each point as in the previous steady state. Just behind the front,  $n_h$  must drop abruptly to zero. If  $j/J$  is large, where  $J$  is given by (25), the drop will be extremely sharp. For the change in the form of the front with time is compounded out of diffusion and propagation with variable velocity along descending curves, as shown schematically in Fig. 4. Since the latter propagation involves a more rapid motion to the right, the smaller  $n_h$ , it tends to steepen the front, and this steepening must continue until

<sup>5</sup> W. G. Pfann and J. H. Scaff, paper presented at the Cambridge Meeting of the American Physical Society, June 16-18, 1949.

the diffusive spreading becomes sufficient to counterbalance it. It is not necessary, for the production of a steep front of this kind, that the decrease of  $j_e$  to zero be brought about with corresponding rapidity; even a gradual decrease of  $j_e$  will lead to a front which becomes steeper as it advances, and if the decrease of  $j_e$  is not too gradual a "shock front" will have developed after a short distance. The order of magnitude of the "shock front thickness" can be estimated by finding the value of the time  $\Delta t$  for which the diffusion distance  $\Delta x_D = (2D \Delta t)^{1/2}$  equals the difference  $\Delta x_V$  between the drift distances of the holes at the top and bottom of the front, i.e.,  $\Delta x_V = [V(0) - V(n_h)]\Delta t$ , where  $V$  is given by (4) and  $n_h$  is the height of the front. For this value of  $\Delta t$ ,

$$\Delta x_D = 2D/[V(0) - V(n_h)] \quad (48)$$

and this is presumably of the order of magnitude of the thickness of the front. If  $D$  is interpreted as  $D_h = kT\mu_h/e$ , which is good enough for the present purpose, this gives

$$\Delta x_D = \frac{2kT}{eE_0} \cdot \left[ 1 - \frac{1}{1 + \nu(1 + \mu_h/\mu_e)} \right]^2. \quad (49)$$

Of course, this extremely sharp front can be realized only when the conditions of one-dimensional geometry are accurately fulfilled. When the geometry is made sufficiently ideal, observation of the thickness of the "shock front" can provide a valuable check on the validity of the basic assumptions of the theory such as the neglect of trapping.<sup>6</sup>

The author would like to express his indebtedness to many of his colleagues, and especially to J. Bardeen, J. R. Haynes, and W. van Roosbroeck, for many illuminating discussions of the topics covered in this paper.

<sup>6</sup> The accompanying paper by W. Shockley, G. L. Pearson and J. R. Haynes describes some observations of this *shock wave* effect, though under conditions where  $\nu \ll 1$ , so that the thickness of the front as given by (49) is still fairly large.

## On the Theory of the A-C. Impedance of a Contact Rectifier

By J. BARDEEN

THE a-c. impedance of the rectifying contact between a metal and a semiconductor is measured by superimposing a small a-c. current on a d-c. bias current. It is generally recognized<sup>1</sup> that an equivalent circuit consists of a parallel resistance and capacitance in series with a resistance as shown in Fig. 1. The parallel components represent the impedance of the barrier layer itself and depend on the d-c. bias current flowing. The series resistance is that of the body of the semiconductor. It has been shown theoretically by Spenke<sup>2</sup> that under quite general conditions the parallel capacitance and resistance are independent of frequency. Unfortunately Spenke's proof is highly mathematical and is also not readily available. The derivation of the impedance relations which is presented here is in some ways more general and gives more physical insight into the problem.

The method of analysis which is used is similar to that employed by Miss C. C. Dilworth<sup>3</sup> for the d-c. case. Except for some obvious differences in sign, the theory is the same for *n*- and *p*-type semiconductors.<sup>4</sup> We give the theory for the latter because the signs are a little simpler for positively charged holes than for negatively charged conduction electrons. Before the discussion of the theory of the a-c. impedance, a brief outline of Schottky's theory of the barrier layer will be given.

A rough schematic energy level diagram, based on Schottky's theory of the barrier layer at a contact between a metal and a *p*-type semiconductor, is illustrated in Fig. 2. The diagram is plotted upside down from the usual one in order to show the energy of holes increasing upward. The energy of electrons increases downward. In a defect or *p*-type semiconductor, such as Cu<sub>2</sub>O, electrons are thermally excited to acceptor levels, charging the acceptors negatively, and leaving missing electrons or holes in the filled band. The holes are mobile and provide the conductivity. Electron states with energies lying above the Fermi level in the diagram, corresponding to lower energies for electrons, have a probability of more than one-half of

<sup>1</sup> For an outline of the theory of contact rectifiers together with references to the earlier literature, see H. C. Torrey and C. A. Whitmer, "Crystal Rectifiers," McGraw-Hill Book Company, Inc., New York, New York (1948).

<sup>2</sup> Eberhard Spenke, *Wiss. Veröff. Siemens's Konzern*, **20**, 40 (1941).

<sup>3</sup> C. C. Dilworth, *Proc. Phys. Soc. London*, **60**, 315 (1947). A similar method was used earlier by H. A. Kramers, *Physica* **1**, 284 (1940), in a discussion of the diffusion of particles over potential barriers.

<sup>4</sup> We suppose that only one type of carrier takes part in conduction.

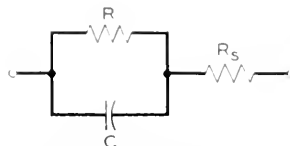


Fig. 1—Equivalent circuit for contact rectifier. The parallel components  $R$  and  $C$  represent the barrier layer itself and  $R_s$  represents the resistance of the body of the semiconductor.

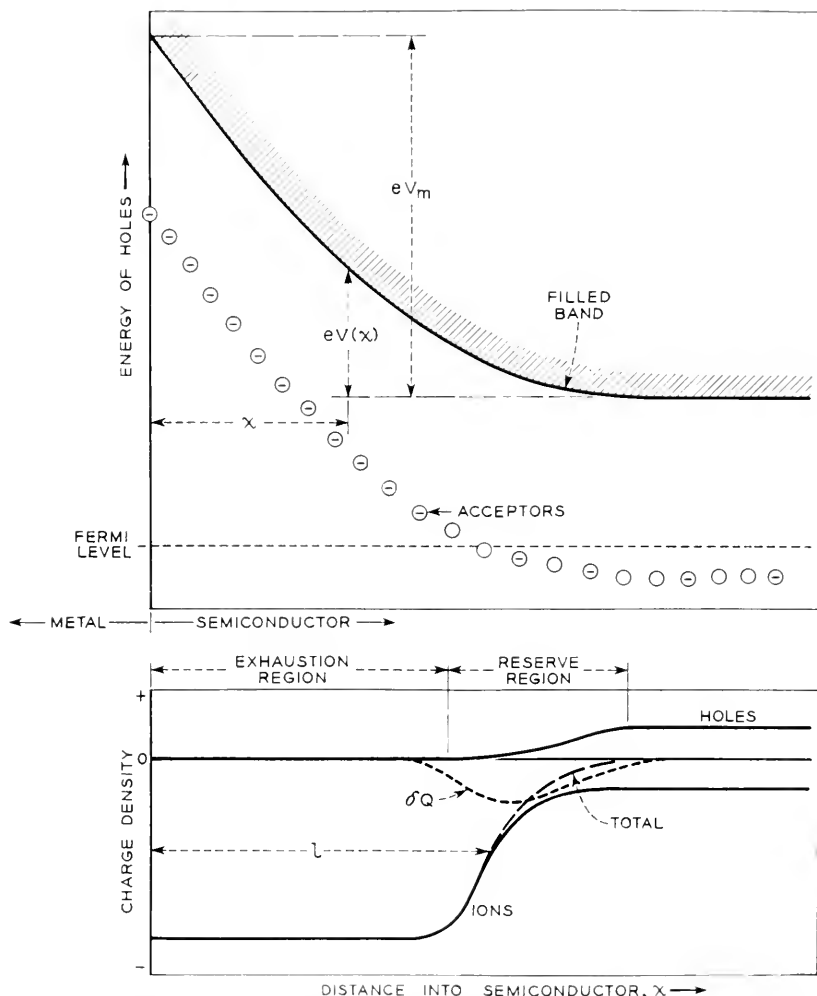


Fig. 2 Schematic energy level diagram of p type semiconductor in contact with a metal. The diagram is plotted upside down from the usual way in order to show the energy of holes increasing upward. The energy of electrons increases downward. The lower diagram gives the density of charge in the barrier layer. In the body of the semiconductor the space charge of the holes is compensated by the space charge of the negatively charged acceptor ions. Holes are drained out of the barrier layer by the electric field, leaving the negative space charge of the acceptors. The rise in electrostatic potential in the barrier region results from this negative space charge together with the compensating positive charge on the metal. The capacitance of the barrier layer is approximately that of a parallel plate condenser with plate separation  $\ell$ .

being occupied by electrons; those below the Fermi level are most likely unoccupied. Holes are depleted from the barrier layer, leaving the negative space charge of the acceptors. This negative space charge, together with the compensating positive charge on the metal, gives the potential energy barrier which impedes the flow of holes from semiconductor to metal. The thickness of the barrier layer may vary from  $10^{-6}$  to  $10^{-4}$  cm, depending on the materials forming the contact.

In drawing the diagram of Fig. 2 it has been assumed for simplicity that the concentration of acceptors is uniform over the region of interest. In the main body of the semiconductor only a few of the acceptors are charged. Throughout a large part of the barrier layer practically all acceptors are negatively charged and there are very few holes in the filled band. This part of the barrier layer has been called by Schottky the exhaustion region and is in our case a region of uniform space charge, as shown in the lower diagram of Fig. 2. The transition zone in which the concentration of holes is decreasing and the concentration of charged acceptors is increasing is called the reserve region.

In thermal equilibrium, with no applied voltage, the potential drop across the barrier layer,  $V_m$ , may be a fraction of a volt. If a voltage is applied in such a direction as to make the semiconductor positive relative to the metal, the effective height of the barrier is reduced and holes flow more easily from the semiconductor to the metal. This is the direction of easy flow. If a voltage is applied in the opposite direction the height of the barrier is increased for holes going from semiconductor to metal and remains unchanged, to a first approximation, for holes going from metal to semiconductor (actually electrons going from the filled band of the semiconductor to the metal). This is the reverse or high resistance direction.

If a voltage is applied in the reverse direction, and equilibrium is established, the thickness of the exhaustion layer increases. The reserve region keeps the same form but moves outward from the metal. A forward voltage decreases the thickness of the space charge layer.

The change in charge density corresponding to a small reverse voltage is shown schematically by the curve marked  $\delta Q$  in the lower diagram of Fig. 2. The maximum of  $\delta Q$  occurs where the total charge density is changing most rapidly with distance. If  $l$  is the distance from the metal to this maximum, the effective capacitance  $C$ , is approximately that of a parallel plate condenser with plate separation  $l$  and with the dielectric constant of the medium equal to that of the semiconductor. The capacitance decreases as  $l$  increases with a d-c. bias applied in the reverse direction and the capacitance increases with forward bias. Schottky<sup>5</sup> has shown that information

<sup>5</sup> Walter Schottky, *Zeits. f. Phys.* **118**, 539 (1942).



about the concentrations of donors and acceptors can be obtained from the variation of capacitance with bias.

In the equivalent circuit of Fig. 1 the capacitance  $C$  is in parallel with the differential resistance,  $R$ , of the contact, and the parallel components are in series with the resistance  $R_s$  of the body of the semiconductor. Spence showed that  $R$  and  $C$  are independent of frequency if the frequency is low enough so that the charge density is in equilibrium during the course of a cycle.

If the applied voltage is suddenly changed, it will take time for the charges to adjust to new equilibrium values. The time constant for the readjustment of charge of the carriers (holes in this case) is  $\kappa\rho/4\pi$ , where  $\rho$  is the resistivity (in e.s.u.) of the body of the semiconductor and  $\kappa$  is the dielectric constant, and is  $\sim 10^{-10}$  sec. for a resistivity of 100 ohm cm. Even if a larger value of  $\rho$  is used, corresponding to a point in the reserve layer, the relaxation time for the carriers is very short.<sup>6</sup> A much longer time may be required for readjustment of charge on the donor or acceptor ions, giving a variation of  $R$  and  $C$  at lower frequencies. If the barrier is nonuniform over the contact area, so that much of the current flows through low-resistance patches, the equivalent circuit may consist of a number of circuits like those of Fig. 1 in parallel. In this case, if an attempt is made to represent the contact by a single circuit of this form, it will be found that  $R$  and  $C$  vary with frequency.

The derivation of the current voltage characteristic for the general case of a time dependent applied voltage follows. The total current per unit area is the sum of contributions from conduction, diffusion, and displacement currents:

$$I(t) = \sigma E - eD(\partial n/\partial x) + (\kappa/4\pi)(\partial E/\partial t), \quad (1)$$

where

$n(x,t)$  = concentration of holes;

$\sigma = n(x,t)e\mu$  is the conductivity;

$e$  = magnitude of electronic charge;

$\mu$  = mobility of holes;

$D = \mu kT/e$  = diffusion coefficient;

$V(x,t)$  = electrical potential;

$E(x,t) = -\partial V(x,t)/\partial x$  = electric field strength.

The coordinate  $x$  extends into the semiconductor from the junction. Equation (1) may be written in the form

$$I(t) = ne\mu(-\partial V/\partial x) - \mu kT(\partial n/\partial x) - (\kappa/4\pi)(\partial^2 V/\partial x \partial t) \quad (1')$$

<sup>6</sup> Another limit is the transit time of carriers through the barrier layer. This time is generally shorter than the relaxation time of the semiconductor.

The potential  $V$  is determined from the charge density,  $q$ , by Poisson's equation

$$\partial^2 V / \partial x^2 = -4\pi q / \kappa. \quad (2)$$

Since the charge density may be expressed in terms of  $n(x, t)$  and the density of fixed charge, these two equations may be used to determine  $n$  and  $V$  when  $I(t)$  is specified. Spenke eliminates the potential  $V$  between (1) and (2) and gets a rather complicated equation for  $n$ . We prefer to deal with Eq. (1) directly, to treat the potential  $V(x, t)$  as a known function, and to solve for the concentration,  $n(x, t)$ .

The plane  $x = 0$  is taken at the interface between metal and semiconductor and the plane  $x = x_1$  just beyond the barrier layer in the semiconductor. It is assumed that  $V = 0$  at  $x = x_1$ . Under thermal equilibrium conditions, with no current flowing, the hole concentration in the barrier layer varies as  $\exp(-eV/kT)$ , taking the values:

$$n = n_0 \text{ at } x = x_1 \quad (3a)$$

$$n = n_m = n_0 \exp(-eV_m/kT) \text{ at } x = 0, \quad (3b)$$

where  $n_0$  is the equilibrium concentration in the body of the semiconductor and  $V_m$  is the height of the potential barrier. We suppose that the boundary conditions (3a) and (3b) also hold when a current is flowing and when there is an additional voltage,  $V_a$ , across the barrier layer. Our procedure is to solve Eq. (1) for  $n(x, t)$ , with  $V(x, t)$  assumed known, and then to determine  $I(t)$  in such a way that the boundary conditions are satisfied. The solution of Eq. (1) which satisfies (3b) is:

$$n(x, t) = n_0 \exp[-e(V - V_a)/kT] - \frac{1}{\mu kT} \int_0^x \left( I + \frac{\kappa}{4\mu} \frac{\partial^2 V'}{\partial x' \partial t} \right) \exp[e(V' - V)/kT] dx' \quad (4)$$

The prime indicates that the variable is  $x'$  rather than  $x$ . At  $x = 0$ ,  $V$  is the sum of  $V_m$  and the applied potential,  $V_a$ :

$$V = V_a + V_m \text{ at } x = 0 \quad (5)$$

The current  $I(t)$  is determined in such a way that (3a) is satisfied. Setting  $x = x_1$ , using (3a), and solving the resulting equation for  $I(t)$ , we get:

$$I(t) = \frac{\mu kT [n_0 \exp(eV_a/kT) - n_0 \exp(eV/kT)] - \int_0^{x_1} \frac{\kappa}{4\pi} \frac{\partial^2 V'}{\partial x' \partial t} \exp(eV'/kT) dx'}{\int_0^{x_1} \exp(eV'/kT) dx'} \quad (6)$$

Provided that the barrier height,  $V_m + V_a$ , is as much as several times  $kT/e$ ,<sup>7</sup> the integrand in both integrals is largest near  $x = 0$  and drops rapidly with increase in  $x$ . Where the integrand is large we may write to a sufficient approximation:

$$V = V_a + V_m - Fx, \quad (7)$$

where  $F$  is the field in the semiconductor at the interface. The approximation (7) may be used if  $kT/eF$  is small compared with the thickness of the barrier layer. The value of  $\partial^2 I / \partial x \partial t$  is nearly constant over the important part of the integration and may be replaced by its value at  $x = 0$  and taken out of the integral. The upper limit  $x_1$  may be replaced by  $\infty$  without appreciable error, so that we get finally:

$$I(t) = I_m(Q)(1 - \exp[-eV_a/kT]) + \partial Q / \partial t, \quad (8)$$

where

$$I_m(Q) = (4\pi e \mu Q n_e / \kappa) \exp[-eV_m/kT] \quad (9)$$

and

$$Q = \kappa F / 4\pi \quad (10)$$

is the surface charge density at the metal interface.

The current  $I_m(Q)$  has a simple interpretation; it is just the conduction current in the semiconductor at the interface resulting from the field  $F$ . In equilibrium, this conduction current is balanced by a diffusion current of equal magnitude and opposite sign. A voltage  $V_a$  applied in the reverse direction reduces the diffusion current at the interface as compared with the conduction current by the factor  $\exp[-eV_a/kT]$ . The current  $\partial Q / \partial t$  is the displacement current at the interface.

Actually, the diffusion theory as given above is not complete. The Schottky effect, the lowering of the barrier by the image force, has been neglected. There may be appreciable tunneling through the barrier. There may be a patch field resulting from nonuniformity of the barrier. If the variations in the patch fields are not too large, the modification of current resulting from these factors depends only on the field at the metal and not on the form of the barrier at some distance from the metal. Thus we may expect the form (8) to be generally valid if  $I_m(Q)$  is considered to be a general function of  $Q$ . Equation (10) is also of the form to be expected from the diode theory.<sup>1</sup> In the latter case,  $I_m(Q)$  is the thermionic emission current from metal to semiconductor.

If the current is varying in time it is the instantaneous value of  $Q$  at

<sup>7</sup> The value of  $kT/e$  at room temperature is .025 volts.

time  $t$  which is to be used in Eq. (10). At high frequencies, the charge at the interface need not be in phase with the applied voltage. If the frequency is low enough so that the charges maintain their equilibrium values during the course of a cycle,  $Q$  will be in phase with  $V$  and the parallel capacitance for unit area is simply:

$$C = dQ/dV. \quad (12)$$

The barrier layer may be represented by this capacitance in parallel with the d-c. differential resistance,  $R$ .

Both  $R$  and  $C$  may depend on the d-c. bias current flowing. Variations of  $R$  and  $C$  with frequency at moderate frequencies may result from large scale nonuniformities of the barrier such that the patch fields extend over a large fraction of the thickness of the barrier layer or from charge relaxation times associated with acceptors, donors or trapped carriers. At low frequencies, drift of ions may be involved.

Attempts which have been made to determine the variation of resistivity in the barrier layer from impedance data are invalid. It is not correct to take the impedance of an element of thickness  $dx$  to be

$$dx [\sigma(x) + (j\omega\kappa/4\pi)]$$

and integrate over  $dx$  to obtain the impedance of the layer. This procedure omits terms arising from diffusion and changes of concentration in time. It is possible to obtain an integral of Eq. (1') if both sides are divided by  $ne\mu$ . Integrating over  $x$  from  $x = 0$  to  $x = x_1$ , and using the boundary conditions (3a), (3b) and (5), we get

$$V_a = \int_0^{x_1} \frac{I(t) + (\kappa/4\pi)(\partial^2 V/\partial x \partial t)}{ne\mu} dx, \quad (13)$$

which means that the integral of the conduction current over the conductivity gives the applied voltage. This is consistent with the representation of the barrier by a resistance and capacitance in parallel.

#### ACKNOWLEDGMENTS

The author is indebted to W. Shockley, W. H. Brattain, and P. Debye for stimulating discussions and suggestions.

# The Theory of $p$ - $n$ Junctions in Semiconductors and $p$ - $n$ Junction Transistors

By W. SHOCKLEY

In a single crystal of semiconductor the impurity concentration may vary from  $p$ -type to  $n$ -type producing a mechanically continuous rectifying junction. The theory of potential distribution and rectification for  $p$ - $n$  junctions is developed with emphasis on germanium. The currents across the junction are carried by the diffusion of holes in  $n$ -type material and electrons in  $p$ -type material, resulting in an admittance for a simple case varying as  $(1 + i\omega\tau_p)^{1/2}$  where  $\tau_p$  is the lifetime of a hole in the  $n$ -region. Contact potentials across  $p$ - $n$  junctions, carrying no current, may develop when hole or electron injection occurs. The principles and theory of a  $p$ - $n$ - $p$  transistor are described.

## TABLE OF CONTENTS

1. Introduction	
2. Potential Distribution and Capacity of Transition Region	
2.1 Introduction and Definitions	
2.2 Potential Distribution in the Transition Region	
2.3 The Transition-Region Capacity	
2.4 The Abrupt Transition	
3. General Conclusions Concerning the Junction Characteristic	
4. Treatment of Particular Models	
4.1 Introduction and Assumptions	
4.2 Solution for Hole Flow into the $n$ -Region	
4.3 D-C. Formulae	
4.4 Total Admittance	
4.5 Admittance Due to Hole Flow in a Retarding Field	
4.6 The Effect of a Region of High Rate of Generation	
4.7 Patch Effect in $p$ - $n$ Junctions	
4.8 Final Comments	
5. Internal Contact Potentials	
6. $p$ - $n$ - $p$ Transistors	
Appendix I A Theorem on Junction Resistance	
Appendix II Admittance in a Retarding Field	
Appendix III Admittance for Two Layers	
Appendix IV Time Constant for the Capacity of the Transition Region	
Appendix V The Effect of Surface Recombination	
Appendix VI The Effect of Trapping upon the Diffusion Process	
Appendix VII Solutions of the Space Charge Equation	
Appendix VIII List of Symbols	

## 1. INTRODUCTION

AS IS well known, silicon and germanium may be either  $n$ -type or  $p$ -type semiconductors, depending on which of the concentrations  $N_d$  of donors or  $N_a$  of acceptors, is the larger. If, in a single sample, there is a transition from one type to the other, a rectifying photosensitive  $p$ - $n$  junction is formed.<sup>1</sup> The theory of such junctions is in contrast to those

<sup>1</sup> For a review of work on silicon and germanium during the war see H. C. Torrey and C. A. Whitmer, *Crystal Rectifiers*, McGraw-Hill Book Company, Inc., New York (1948).  $p$ - $n$  junctions were investigated before the war at Bell Telephone Laboratories by R. S. Ohl. Work on  $p$ - $n$  junctions in germanium has been published by the group at Purdue

of ordinary rectifying junctions because, on both sides of the junction, both electron flow and hole flow must be considered. In fact, a major portion of the hole current may persist into the  $n$ -type region and vice-versa. In later sections we show how this feature has a number of interesting consequences, which we shall describe briefly in this introduction.

A  $p$ - $n$  junction may act as an emitter in the transistor sense, since it can inject hole current into  $n$ -type material. The a-c. impedance of a  $p$ - $n$  junction may exhibit a frequency dependence characterized by this diffusion of holes and of electrons. For high frequencies the admittance varies approximately as  $(i\omega)^{1/2}$  and has comparable real and imaginary parts. When a  $p$ - $n$  junction makes contact to a piece of  $n$ -type material containing a high concentration of injected holes, it acts like a semipermeable membrane and tends to come to a potential which corresponds to the hole concentration.

Although some results can be derived which are valid for all  $p$ - $n$  junctions, the diversity of possible situations is so great and the solution of the equations so involved that it is necessary to illustrate them by using a number of special cases as examples. In general we shall consider cases in which the semiconductor may be classified into three parts, as shown in Fig. 1. The meaning of the transition region will become clearer in later sections; in general it extends far enough to either side of the point at which  $N_d - N_a = 0$  so that the value of  $|N_d - N_a|$  at its boundaries is not much smaller than in the low resistance parts of the specimen. As stated above, appreciable hole currents may flow into the  $n$ -region beyond the transition region. For this reason, the rectification process is not restricted to the transition region alone. We shall use the word *junction* to include all the material near the transition region in which significant contributions to the rectification process occur. It has been found that various techniques may be employed to make nonrectifying metallic contacts to the germanium; when this is properly done, the resistance measured between the metal terminals in a suitably proportioned specimen is due almost entirely to the rectifying junction up to current densities of  $10^{-1}$  amp/cm<sup>2</sup>.

---

directed by K. Lark-Horovitz; S. Benzer, *Phys. Rev.* 72, 1267 (1947); M. Becker and H. Y. Fan, *Phys. Rev.* 75, 1631 (1949); and H. Y. Fan, *Phys. Rev.* 75, 1631 (1949). Similar junctions occur in lead sulfide according to L. Sosnowski, J. Starkiewicz and O. Simpson, *Nature* 159, 818 (1947), L. Sosnowski *Phys. Rev.* 72, 641 (1947), and L. Sosnowski, B. W. Soole and J. Starkiewicz, *Nature* 160, 471 (1947). The theory described here has been discussed in connection with photoelectric effects in  $p$ - $n$  junctions by F. S. Goucher, Meeting of the American Physical Society, Cleveland, March 10-12, 1949 and by W. Shockley, G. L. Pearson and M. Sparks, *Phys. Rev.* 76, 180 (1949). For a general review of conductivity in  $p$ - and  $n$ -type silicon see G. L. Pearson and J. Bardeen, *Phys. Rev.* 75, 865 (1949), and J. H. Scaff, H. C. Theuerer and E. E. Schumacher, *Jl. of Metals*, 185, 383 (1949) and W. G. Pfann and J. H. Scaff, *Jl. of Metals*, 185, 389 (1949). The latter two papers also discuss photo-voltaic barriers. The most recent and thorough theory for frequency effects in metal semiconductor rectifiers is given elsewhere in this issue (J. Bardeen, *Bell Sys. Tech. Jl.*, July 1949).

Even for distributions of impurities as simple as those shown in part (b) there are two distinctly different types of behavior of the electrostatic potential in the transition region, each of which may be either rectifying or nonrectifying. The requirement that the junction be rectifying can be stated in terms of the current distribution, certain cases of which are shown in (c). The total current, from left to right, is  $I$ , the hole and electron currents being

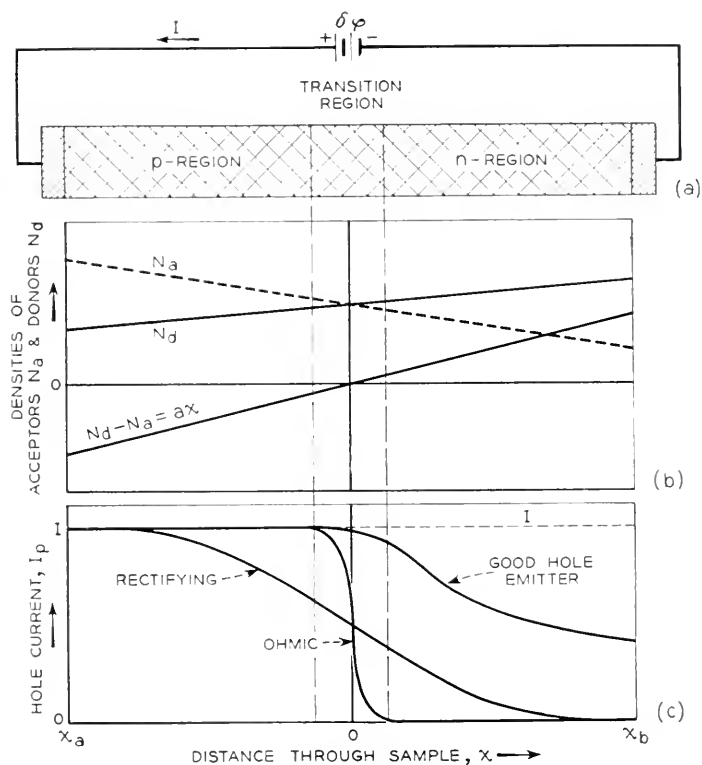


Fig. 1—The  $p$ - $n$  junction.

(a) Schematic view of specimen, showing non-rectifying end contacts and convention for polarities of current and voltage.

(b) Distribution of donors and acceptors.

(c) Three possible current distributions.

$I_p$  and  $I_n$ , with  $I = I_p + I_n$ . Well away from the junction in the  $p$ -type material, substantially all of the current is carried by holes and  $I_p = I$ ; similarly, deep in the  $n$ -type material  $I_n = I$  and  $I_p = 0$ . In general in a nonrectifying junction, the hole current does not penetrate the  $n$ -type material appreciably whereas in the rectifying junction it does. Under some conditions the major flow across the junction will consist of holes; such

cases are advantageous as emitters in transistor applications using  $n$ -type material for the *base*.

Where the hole current flows in relatively low resistance  $n$ -type material, it is governed by the diffusion equation and the concentration falls off as  $\exp(-x/L_p)$  where  $L_p$  is the diffusion length:

$$L = \sqrt{D\tau_p}.$$

Here  $D$  is the diffusion constant for holes and  $\tau_p$  their mean lifetime. The lifetime may be controlled either by surface recombination<sup>2</sup> or volume recombination. Surface recombination is important if the specimen has a narrow cross-section.

Under a-c. conditions, the diffusion current acquires a reactive component corresponding to a capacity. In addition, a capacitive current is required to produce the changing potential distribution in the transition region itself.

In the following sections we shall consider the behavior of the junction analytically, treating first the potential distribution in the transition region and the charges required change the voltage across it in a pseudo-equilibrium case. We shall then consider d-c. rectification and a-c. admittance.

## 2. POTENTIAL DISTRIBUTION AND CAPACITY OF TRANSITION REGION

### 2.1 Introduction and Definitions

We shall suppose in this treatment that all donors and acceptors are ionized (a good approximation for Ge at room temperature) so that we have to deal with four densities as follows:

$n$  = density of electrons in conduction band

$p$  = density of holes in valence-bond band

$N_d$  = density of donors

$N_a$  = density of acceptors

The total charge density is

$$\rho = q(p - n + N_d - N_a), \quad (2.1)$$

where  $q$  is the electronic charge. We shall measure electrostatic potential  $\psi$  in the crystal, as shown in Fig. 2, from such a point, approximately<sup>3</sup> midway in the energy gap, that if the Fermi level  $\varphi$  is equal to  $\psi$ , the concentrations of holes and electrons are equal to the concentration  $n_i = p_i$  char-

<sup>2</sup> H. Suhl and W. Shockley *Phys. Rev.* 75 1617 (1949).

<sup>3</sup> A difference in effective masses for holes and electrons will cause a shift of  $\psi$  from the midpoint between the bands.



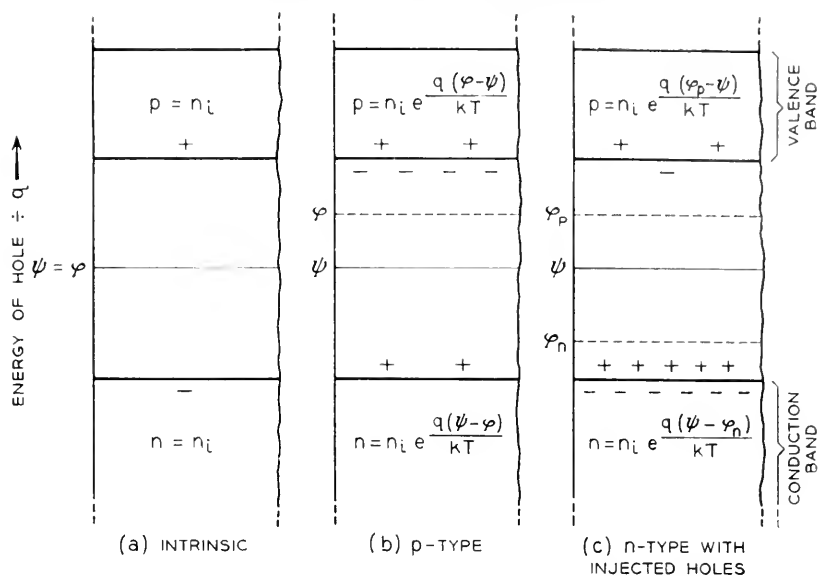


Fig. 2—Electrostatic potential  $\psi$ , Fermi level  $\phi$  and quasi Fermi levels  $\phi_p$  and  $\phi_n$ .  
(In order to show electrostatic potential and energies on the same ordinates, the energies of holes, which are minus the energies of electrons, are plotted upwards in the figures in this paper.)

acteristic of a pure sample. For an impurity semi-conductor we shall have, as shown in (b),

$$p = n_i e^{q(\phi - \psi)/kT} \quad (a) \quad (2.2)$$

$$n = n_i e^{q(\psi - \phi)/kT}, \quad (b)$$

where  $q$  is the electronic charge. Accordingly,

$$p = q\{N_d - N_c + 2n_i \sinh [q(\phi - \psi)/kT]\}. \quad (2.3)$$

When the hole and electron concentrations do not have their equilibrium values, because of hole or electron injection or production of hole-electron pairs by light, etc., it is advantageous to define two non-equilibrium quasi Fermi levels  $\phi_p$  and  $\phi_n$  by the equations

$$p = n_i e^{q(\phi_p - \psi)/kT} \quad (a) \quad (2.4)$$

$$n = n_i e^{q(\psi - \phi_n)/kT} \quad (b)$$

as indicated in Fig. 2 (c). In terms of  $\phi_p$  and  $\phi_n$ , the hole and electron currents take the simple forms:

$$I_p = -q[D\nabla p + \mu p \nabla \psi] = -q\mu p \nabla \phi_p \quad (2.5)$$

$$I_n = bq[D\nabla n - \mu n \nabla \psi] = -qb\mu n \nabla \phi_n \quad (2.6)$$

where the mobility  $\mu$  and diffusion constant  $D$  for holes are related by Einstein's equation

$$\mu = qD/kT \quad (2.7)$$

and  $b$  is the ratio of electron mobility to hole mobility.<sup>4</sup>

Under equilibrium conditions  $\varphi_p = \varphi_n = \varphi$  where  $\varphi$  is independent of position. Under those conditions,  $I_p$  and  $I_n$  are both zero according to equations (2.5) and (2.6). The electrostatic potential  $\psi$ , however, will not in general be constant and there will be unbalanced charge densities throughout the semiconductor. We shall consider the nature of the conditions which determine  $\psi$  for a general case and will later treat in detail the behavior of  $\psi$  for  $p$ - $n$  junctions.

For equilibrium conditions, there is no loss in generality in setting  $\varphi$  arbitrarily equal to zero. The charge density expression (2.3) may then be rewritten as

$$\rho = \rho_d - \rho_i \sinh u \quad (2.8)$$

where

$$u \equiv q\psi/kT, \quad \rho_i \equiv 2n_iq, \quad \rho_d \equiv q(N_d - N_a) \quad (2.9)$$

In equation (2.8)  $\rho_d$  and  $u$  and, consequently,  $\rho$  may be functions of position. The potential  $\psi$  must satisfy Poisson's equation which leads to the equation

$$\nabla^2 \psi = -4\pi\rho/\kappa \quad (2.10)$$

where  $\kappa$  is the dielectric constant, (2.10) can be rewritten as

$$\nabla^2 u = \frac{4\pi q \rho_i}{kT\kappa} \left( \sinh u - \frac{\rho_d}{\rho_i} \right) \quad (2.11)$$

What this equation requires in physical terms is that the electrostatic potential produces through (2.8) just such a total charge density  $\rho$  that this charge density, when used in Poisson's Equation (2.10), in turn produces  $\psi$ . It seems intuitively evident that the equation for  $u$  will always have a physically meaningful solution; no matter how the charge density  $\rho_d$  due to the impurities varies with position, the holes and electrons should be able to distribute themselves so that equilibrium is produced. For a one-dimensional case, it is not difficult to prove that a unique solution exists for  $u(x)$  for any  $\rho_d(x)$  (Appendix VII).

<sup>4</sup> We prefer  $b$  in comparison to  $c$  for this ratio since  $c$  for the speed of light also occurs in formulae involving  $b$ .

The coefficient in (2.11) has the dimensions of  $(\text{length})^{-2}$  leading us to define a quantity

$$\begin{aligned} L_D &= \sqrt{\kappa kT/4\pi q\rho_i} = \sqrt{\kappa kT/8\pi q^2 n_i} \\ &= 2.1 \times 10^{-3} \text{ cm for Si with } \kappa = 12.5,^5 n_i = 2 \times 10^{10} \text{ cm}^{-3} \\ &= 6.8 \times 10^{-5} \text{ cm for Ge with } \kappa = 19,^6 n_i = 3 \times 10^{13} \text{ cm}^{-3} \end{aligned} \quad (2.12)$$

where the subscript  $D$  for Debye emphasizes the similarity of  $L_D$  to the characteristic length in the Debye-Hückel theory of strong electrolytes. The meaning of the Debye length is apparent from the behavior of the solution in a region where  $\rho_d$  is constant, and  $u$  differs only slightly from the value  $u_0$  which gives neutrality, with  $\rho_i \sinh u_0 = \rho_d$ . Under these conditions,

$$\frac{d^2 u}{dx^2} = (L_D^{-2} \cosh u_0)(u - u_0) \quad (2.13)$$

so that  $u - u_0$  varies as  $\exp(\pm x\sqrt{\cosh u_0}/L_D)$ . In general, we shall be interested in cases in which the deviation of  $u$  from  $u_0$  decays to a small value in one direction. It is evident that the distance required to reduce the deviation to  $1/e$  is  $L_D/\sqrt{\cosh u_0}$ . If only small variations in  $\rho_d$  occur within a distance  $L_D/\sqrt{\cosh u_0}$ , then the semiconductor will be substantially neutral. However, if a large variation of  $\rho_d$  occurs in this distance, a region of local space charge will occur. These two cases are illustrated in connection with the potential distribution in a p-n junction.

## 2.2 Potential Distribution in the Transition Region<sup>7</sup>

We shall discuss the case shown in Fig. 1 for which the charge density due to donors and acceptors is given by

$$N_d - N_a = ax \quad (2.14)$$

This relationship defines a characteristic length  $L_a$  given by

$$L_a = n_i/a \quad (2.15)$$

If  $L_a \gg L_D$ , the condition of electrical neutrality is fulfilled (Appendix VII) and  $u$  satisfies the equation

$$\sinh u = \rho_d/\rho_i = ax/2n_i = x/2L_a$$

<sup>5</sup> J. F. Mullaney, *Phys. Rev.* 66, 326 (1944).

<sup>6</sup> H. B. Briggs and W. H. Brattain, *Phys. Rev.*, 75, 1705 (1949).

<sup>7</sup> Potential distributions in rectifying junctions between semiconductors and metals have been discussed by many authors, in particular N. F. Mott, *Proc. Roy. Soc.* 171A, 27 (1939) and W. Schottky *Zeits. f. Physik* 113, 367 (1939) 118, 539 (1942) and elsewhere. A summary in English of Schottky's papers is given by J. Joffe, *Electrical Communications* 22, 217 (1945). All such theories are in principle similar in involving the solution of equations like (2.11). See, for example, H. Y. Fan, *Phys. Rev.* 62, 388 (1942).

On the other hand, if  $L_D \gg L_a$ , a large change in impurity concentration occurs near  $x = 0$  without compensating electron and hole densities occurring. Mathematically, we find that (2.11) can be expressed in the form

$$\frac{d^2 u}{dy^2} = \frac{1}{K^2} (-y + \sinh u) \quad (2.16)$$

and

$$y = x/2L_a, \quad K = L_D/2L_a \quad (2.17)$$

In Appendix VII, it is verified that the appropriate solution for  $K \ll 1$  is that giving local neutrality,  $u = \sinh^{-1} y$ ; while for  $K \gg 1$ , there is space charge as described below.

For  $L_D \gg L_a$ , or  $K \gg 1$ , there is a space charge layer in which  $N_d - N_a$  is uncompensated. To a first approximation, we can neglect the electron and hole space charge in the layer and obtain, by integrating twice,

$$\psi = -\frac{2\pi q a x^3}{3\kappa} + a_2 x, \quad (2.18)$$

where we have chosen the zero of potential as the value at  $x = 0$ , a condition required by the symmetry between  $+x$  and  $-x$  of (2.14). Although the potential rise is steep in the layer,  $d\psi/dx$  should be small at the point  $x_m$  where the neutral  $n$ -type material begins. As an approximation we set  $d\psi/dx = 0$  at  $x = x_m$ :

$$\frac{d\psi}{dx} = -\frac{2\pi q a x_m^2}{\kappa} + a_2 = 0; \quad (2.19)$$

this leads to a value for  $a_2$  which may be inserted in (2.18) to evaluate  $\psi$  at  $x_m$ :

$$\psi_m = \frac{4\pi q a x_m^3}{3\kappa} = \frac{4\pi q}{3\kappa a^2} (a x_m)^3 = \frac{4\pi q}{3\kappa a^2} n_m^3 \quad (2.20)$$

where  $n_m = a x_m$  is the density of electrons required to neutralize  $N_d - N_a = a x_m$  at the edge of the space-charge layer. This value of  $n_m$  must correspond to that associated with  $\psi_m$  by (2.2)

$$n_m = n_i e^{q\psi_m/kT}. \quad (2.21)$$

We thus have two equations relating  $\psi_m$  and  $n_m$  and the parameter " $a$ ." To solve them we plot  $\ln \psi_m$  versus  $\ln n_m$  as shown in Fig. 3. On this figure the relationship

$$\begin{aligned} \psi_m &= \frac{4\pi q}{3\kappa} \frac{n_m^3}{a^2} \\ &= 3.18 \times 10^{-8} \frac{n_m^3}{a^2} \text{ volts for Ge} \\ &= 4.83 \times 10^{-8} \frac{n_m^3}{a^2} \text{ volts for Si} \end{aligned} \quad (2.22)$$

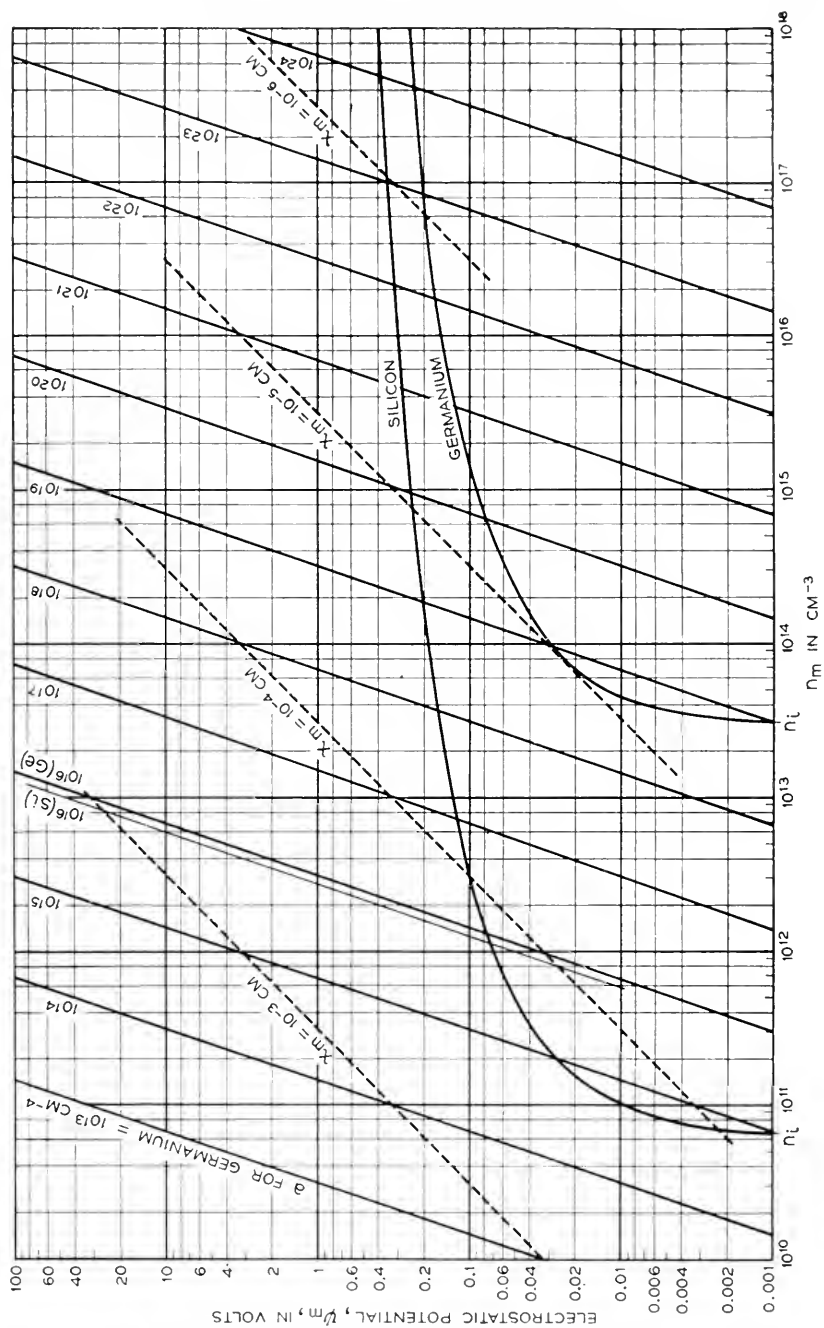


Fig. 3—Solutions for the boundaries of the space-charge region.

becomes a family of straight lines with " $a$ " as a parameter. (Only  $a = 10^{16}$  cm $^{-4}$  is shown for Si, all the other lines being for Ge.) The half thickness  $x_m (= n_m/a)$  of the space-charge region is also shown. Solutions are obtained when these lines cross the curves  $n_m = n_i \exp (q\psi_m/kT)$ , which are shown for room temperature. The condition that the intersection lie well to the right on the curve is equivalent to  $K \gg 1$ . For two Si samples cut from a melt,  $a$  was determined from measurements of conductivity<sup>8</sup> and was about  $10^{15}$  to  $10^{16}$  cm $^{-4}$ . For these, the space charge region has a half-width  $x_m$  of more than  $10^{-4}$  cm. For other temperatures, the curves can be appropriately translated.<sup>9</sup>

In Fig. 4(a) we show the limiting potential shapes:

$$ax = 2n_i \sinh \frac{q\psi}{kT} \quad \text{for } K \ll 1 \quad (2.23)$$

$$\psi = (\psi_m/2)(-(x/x_m)^3 + 3(x/x_m)) \quad \text{for } K \gg 1 \quad (2.24)$$

In Fig. 4(b) the charge densities are shown. For the space-charge case,  $|N_d - N_a|$  is greater than  $n$  or  $p$ . For a higher potential rise, i.e. larger  $\psi_m$ , the discrepancy would be greater and  $N_d - N_a$  would be unneutralized except near  $x_m$ .

### 2.3 The Transition-Region Capacity

When the voltage across the junction is changing, a flow of holes and electrons is required to alter the space charge in the transition region. We shall calculate the charge distribution in the transition region with the aid of a pseudo-equilibrium model in which the following processes are imagined to be prevented: (1) hole and electron recombination, (2) electron flow across the  $p$ -region contact at  $x_a$  (Fig. 1), (3) hole flow across the  $n$ -region boundary at  $x_b$ . Under these conditions holes which flow in across  $x_a$  must remain in the specimen. If a potential  $\delta\varphi$  is applied at the  $p$  end, then holes will flow into the specimen until  $\varphi_p$  has increased by  $\delta\varphi$  so that the holes inside are in equilibrium with the contact which applies the potential. Since the specimen as a whole remains neutral, an equal electron flow will occur at  $x_b$ . When the specimen arrives at its pseudo-equilibrium steady-state, the potential distribution will be modified in the transition region and the number of holes in this region will be different from the number present under conditions of true thermal equilibrium. The added number of holes is proportional to  $\delta\varphi$  for small values of  $\delta\varphi$  and thus acts like the charge on a condenser. Our problem in this section is to calculate how this charge depends

<sup>8</sup> Unpublished data of W. H. Brattain and G. L. Pearson.

<sup>9</sup> The effect of unionized donors and acceptors can also be included by letting  $n_i$  include the properly weighted donor states and  $p_i$ , the acceptor states.

upon  $\delta\phi$  for various types of transition regions and to express the result as a capacity.

The justification for this pseudo-equilibrium treatment is as follows: Under actual a-c. conditions the potential drop in the *p*- and *n*-regions themselves are small because of their high conductivity so that most of the po-

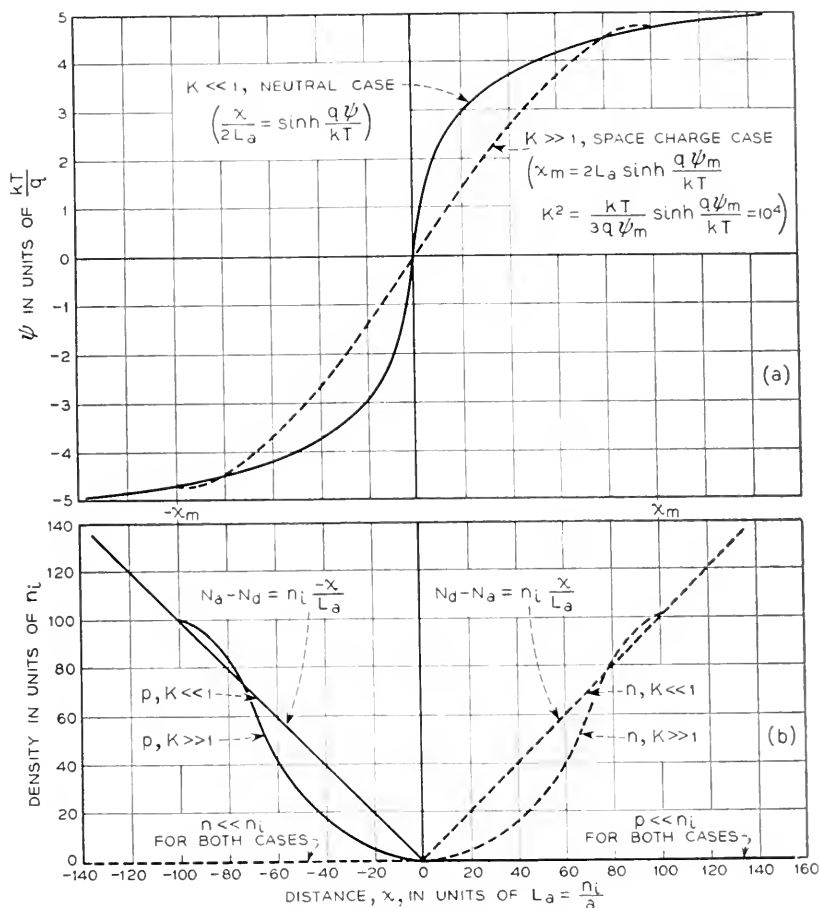


Fig. 4—Electrostatic potential and densities for *p-n* junctions.

tential drop occurs across the transition region. On the *p*-side of the transition region a large supply of holes is available to modify the potential and the fact that a current is flowing across the junction disturbs their concentration negligibly; the electrons on the *n*-side are similarly situated. Hence the distribution of holes and electrons in the transition region will be much the same as for the pseudo-equilibrium case. The question of how the hole

current required to change the potential distribution in the transition region is related to other hole currents is discussed in Section 4.1.

Under our assumptions, after the voltage  $\delta\varphi$  is applied, a steady state is reached involving no current hence  $\nabla\varphi_p = \nabla\varphi_n = 0$ . Consequently, both  $\varphi_p$  and  $\varphi_n$  are constant and

$$\varphi_p - \varphi_n = \delta\varphi \quad (2.25)$$

since the holes are being supplied from a source at a potential  $\delta\varphi$  higher than for the electrons.

We shall then have

$$p = n_i e^{q(\varphi_p - \psi)/kT} = n_1 e^{q(\varphi_1 - \psi)/kT} \quad (2.26)$$

$$n = n_i e^{q(\psi - \varphi_n)/kT} = n_1 e^{q(\psi - \varphi_1)/kT} \quad (2.27)$$

where

$$\varphi_1 = (\varphi_p + \varphi_n)/2, \quad \varphi_p = \varphi_1 + \delta\varphi/2, \quad \varphi_n = \varphi_1 - \delta\varphi/2 \quad (2.28)$$

and

$$n_1 = n_i e^{q\delta\varphi/2kT}. \quad (2.29)$$

Thus the effect of applying the potential  $\delta\varphi$  in the pseudo-equilibrium case is equivalent to changing  $n_i$  to  $n_1$  just as if the energy gap had been reduced by  $q\delta\varphi$ .

In the  $p$ -region,  $n \ll p$  and so that  $p = -ax$  is a good approximation. Similarly, in the  $n$ -region, we set  $n = ax$ . Hence we have in the  $p$ -region

$$\psi = \varphi_1 + (\delta\varphi/2) - (kT/q) \ln(-ax/n_i) \quad (2.30)$$

and in the  $n$ -region

$$\psi = \varphi_1 - (\delta\varphi/2) + (kT/q) \ln(ax/n_i). \quad (2.31)$$

Hence the effect of  $\delta\varphi$  is to shift  $\psi$  in the  $p$ -region upwards by  $\delta\varphi$  compared to  $\psi$  in the  $n$ -region. This is an example of the general result that  $\psi - \varphi_p$  tends to remain constant at a given point in the  $p$ -region no matter what disturbances occur and  $\psi - \varphi_n$  tends to remain constant in the  $n$ -region.

#### *The Capacity for the Neutral Case $K \ll 1$*

For the neutral case, we calculate the total number of holes,  $P$ , between  $x_c$  and  $x_b$  as a function of  $\delta\varphi$ . The charge of these holes is  $qP$  and the effective capacity is  $q dP/d\delta\varphi$ . As explained above, we are really interested in the change in number of holes in the transition region. However, the value of  $P$  is relatively insensitive to the location of the limits  $x_a$  and  $x_b$  so long as they lie in regions where the conductivity approaches the maximum values in the



*p*- and *n*-regions. In the following calculations, we shall consider a unit area of the junction so that values of *P* and of capacity are on a unit area bases.

The value of *P* is obtained by integrating *p dx* making use of the neutrality condition to establish the functional relationship between *p* and *x*. The neutrality condition can be written as

$$ax = 2n_1 \sinh \frac{q(\psi - \varphi_1)}{kT} \equiv 2n_1 \sinh u \quad (2.32)$$

where  $u \equiv q(\psi - \varphi_1)/kT$  and

$$p = n_1 e^{q(\varphi_1 - \psi)/kT} \equiv n_1 e^{-u} \quad (2.33)$$

$$n = n_1 e^{-u} \quad (2.34)$$

so that the value of *P* can be obtained by changing variables from *x* to *u*:

$$\begin{aligned} P &= \int_{x_a}^{x_b} p \, dx = \int_{u_a}^{u_b} p(2n_1/a) \cosh u \, du \\ &= (n_1^2/a) \int_{u_a}^{u_b} [1 + e^{-2u}] \, du = (n_1^2/a)[u_b - u_a + (e^{-2u_a} - e^{-2u_b})/2] \end{aligned} \quad (2.35)$$

For the cases of practical interest, the value of *p* at *x* = *x<sub>a</sub>*, denoted by *p<sub>a</sub>*, and the value of *n* at *x* = *x<sub>b</sub>*, denoted by *n<sub>b</sub>*, will both be large compared to *n<sub>1</sub>*. Consequently, we conclude that

$$u_a = -\ln(p_a/n_1) \text{ and } u_b = \ln(n_b/n_1)$$

are both larger than unity in absolute value but probably less than twenty for a reasonable variation of impurity between *x<sub>a</sub>* and *x<sub>b</sub>*. (For example for a change in potential of 0.2 volts such as would occur between *p*- and *n*-type germanium, *u<sub>a</sub>* and *u<sub>b</sub>* would each be about 4 in magnitude.) Hence we obtain for *P*,

$$\begin{aligned} P &= (n_1^2/2a)(2(u_b - u_a) + (p_a/n_1)^2 - (n_b/n_1)^2) \\ &\cong p_a^2/2a + (n_1^2/a)(u_b - u_a) \end{aligned} \quad (2.36)$$

where we have neglected  $(n_b/n_1)^2$  which is  $\ll 1$  and the negligible compared to *u<sub>b</sub>* - *u<sub>a</sub>*. The term  $p_a^2/2a$  is simply the integrated acceptor-minus-donor density in the *p*-region, as may be seen as follows:

$$\int_{x_a}^0 (N_a - N_d) \, dx = \int_{x_a}^0 (-ax) \, dx = ax_a^2/2 = p_a^2/2a. \quad (2.37)$$

The second term in (2.36) is essentially the sum of the holes of the right of *x* = 0 plus the electrons to the left of *x* = 0, whose charge is also com-

pensated by holes. The total number of holes can be expressed in terms of  $\delta\varphi$  through the dependence of  $n_i$  on  $\delta\varphi$ . The second term is thus

$$\begin{aligned} (n_i^2/a)[\ln(n_b/n_i) + \ln(p_a/n_i)] \\ = (n_i^2/a)e^{q\delta\varphi/kT} \cdot [\ln(n_b p_a/n_i^2) - q\delta\varphi/kT] \end{aligned} \quad (2.38)$$

Hence for a small change  $d\delta\varphi$  in  $\delta\varphi$ , the change in charge  $dQ = q dP$  and the capacity  $C$  are given by

$$C = \frac{dQ}{d\delta\varphi} = \frac{q^2}{kT} \frac{n_i^2}{a} [\ln(n_b p_a/n_i^2) - (q\delta\varphi/kT) - 1]. \quad (2.39)$$

This capacity can be reexpressed in terms of the difference in  $\psi$  between  $x_a$  and  $x_b$ : When  $\delta\varphi = 0$ , corresponding to the thermal equilibrium case, we have

$$p_a n_b = n_i^2 e^{q(\psi_b - \psi_a)/kT} \quad (2.40)$$

Using this together with the definitions of  $L_D$  and  $L_a$  we obtain

$$C = \frac{\kappa[q(\psi_b - \psi_a - \delta\varphi)/kT - 1] e^{q\delta\varphi/kT}}{4\pi(2L_D^2/L_a)} \quad (2.41)$$

In this expression  $\psi_a$  and  $\psi_b$  are the potentials when  $\delta\varphi = 0$ ; so that

$$\psi_b - (\psi_a + \delta\varphi)$$

is thus the increase in potential in going from  $x_a$  to  $x_b$  when  $\delta\varphi$  is applied.

For thermal equilibrium,  $\delta\varphi = 0$  and, as discussed above, the term in  $\psi_b - \psi_a$  will be about 10. Hence, using the definition  $K = L_D/2L_a$ , we have

$$C \cong \kappa/4\pi(4KL_D/10) \quad (2.42)$$

For  $K \ll 1$ , the case for which this formula is valid,  $C$  will be the capacity of a condenser whose dielectric layer is much less than  $L_D$  thick.

#### *Capacity for Space Charge Case, $K \gg 1$*

As discussed in connection with (2.30) and (2.31), the applied potential  $\delta\varphi$  reduces the increase ( $= 2\psi_m$ ) in  $\psi$  between the  $p$ -region and the  $n$ -region by  $\delta\varphi/2$  on each side of  $x = 0$ . This is accomplished by a narrowing of the space charge layer by  $\delta x_m$  on each side where (according to (2.20))

$$\delta\psi_m = -\delta\varphi/2 = 4\pi q a x_m^2 \delta x_m / \kappa \quad (2.43)$$

The decrease in width  $\delta x_m$  brings with it an increase in number of holes  $-ax \delta x_m$  per unit area of the junction on the  $p$ -side and an equal number of electrons on the  $n$ -side. Thus a charge of holes per unit area of  $\delta Q = -q a x_m \delta x_m$  must flow in from the left. The capacity per unit area is, therefore,

$$C = \delta Q / \delta\varphi = q a x_m \delta x_m / \delta\varphi = \kappa / 4\pi 2x_m \quad (2.44)$$

corresponding to a condenser of thickness  $2x_m$ . It is evident that formula (2.44) will hold for a small change  $d\delta\varphi$  superimposed on a large bias  $\delta\varphi$  provided that  $2x_m$  is the thickness of the space charge region under the conditions when  $\delta\varphi$  is applied. If  $\psi_{n,0}$  is the value of  $\psi$  for  $\delta\varphi = 0$ , then  $\psi_m = \psi_{n,0} - \delta\varphi/2$ ; and  $C$  will vary as

$$C = \kappa[4\pi qa/3\kappa(\psi_{n,0} - \delta\varphi/2)]^{1/3}/8\pi \quad (2.45)$$

so that  $1/C^3$  should plot as a straight line versus  $\delta\varphi$  with slope

$$- (8\pi/\kappa)^3(3\kappa/8\pi qa) = - \frac{192\pi^2}{\kappa^2 qa}. \quad (2.46)$$

In addition to the holes which flow to account for the change in  $\psi_m$ , the concentration of holes in the  $n$ -region will be increased by a factor  $\exp(q\delta\varphi/kT)$ . However, this increase does not lie in the transition region; we shall consider it later, in Section 4, in connection with a-c. admittance.

### Comparison of the Two Capacities

It is instructive to compare the two capacities just derived. We suppose that for one value of  $n_i$  we have  $K \gg 1$  so that the space charge solution is good. For this case we choose  $x_a = -x_m$  and  $x_b = +x_m$  so as to bound the space charge layer. We then imagine  $n_i$  to be increased, either by raising the temperature or by applying a potential difference  $\delta\varphi$ . The capacity then changes from

$$C_{\text{sp. chg.}} = \kappa/8\pi x_m \text{ to } C_{\text{neut.}} = 5\kappa/8\pi K L_D \quad (2.47)$$

(i.e., from (2.44) to (2.42)) so that the ratio is

$$\frac{C_{\text{neut.}}}{C_{\text{sp. chg.}}} = \frac{5x_m}{K L_D} \quad (2.48)$$

For  $K < 1$ , this ratio is large, both because of  $K$  in the denominator and because  $x_m > L_a$  so that  $x_m/L_D > L_a/L_D = 1/2 K$ .

In Section 4.4 we shall compare these capacities with that due to diffusion of holes and electrons beyond the transition region.

### 2.4 The Abrupt Transition

For completeness we shall consider the case in which the impurity concentration changes abruptly from  $p_p$  to  $n_n$  at  $x = 0$ . For this case the potential in the space-charge layer will be of the parabolic type discussed by Schottky, the potentials varying as

$$\psi = (2\pi/\kappa)q p_p(x - x_p)^2 + \text{constant}, \quad x < 0 \quad (2.49)$$

$$\psi = -(2\pi/\kappa)q n_n(x - x_n)^2 + \text{constant}, \quad x > 0 \quad (2.50)$$

where  $x_p < 0$  and  $x_n > 0$  are the ends of the space-charge layer in the  $p$ - and  $n$ -regions. The gradient of potential at  $x = 0$  must be equal for the two layers leading to

$$-p_p x_p = n_n x_n \quad (2.51)$$

so that if the total width of the space charge layers is  $W = x_n - x_p$ , it follows that

$$x_p = -n_n W / (n_n + p_p) \text{ and } x_n = p_p W / (n_n + p_p). \quad (2.52)$$

The potential difference across the layer, which is  $\psi_b - \psi_a$  is

$$\psi_b - \psi_a = (2\pi q / \kappa) (p_p x_p^2 + n_n x_n^2) = [2\pi q p_p n_n / \kappa (p_p + n_n)] W^2 \quad (2.53)$$

If  $p_p \gg n_n$  this reduces to

$$\psi_b - \psi_a = 2\pi q n_n W^2 / \kappa \quad (2.54)$$

the formula given by Schottky, which should be appreciable in this case, for which all the voltage drop occurs in the  $n$ -region.

The capacity for the abrupt transition will be

$$C = \kappa / 4\pi W \quad (2.55)$$

where  $W$  is obtained by solving (2.53). For this case  $(1/C)^2$  should plot as a straight line versus  $\psi_b - \psi_a$ :

$$\frac{1}{C^2} = [8\pi(p_p + n_n) / \kappa q p_p n_n] (\psi_b - \psi_a). \quad (2.56)$$

### 3. GENERAL CONCLUSIONS CONCERNING THE JUNCTION CHARACTERISTIC

In this section we shall consider direct current flow through the junction and shall derive the results quoted in Fig. 1 relating the current distribution to the characteristics of the junction. We shall suppose that holes and electrons are thermally generated in pairs at a rate  $g$  and recombine at a rate  $rn p$  so that the net rate of generation per unit volume is

$$(\text{net rate of generation}) = g - rn p, \quad (3.0)$$

which vanishes at equilibrium. Obviously,  $g = rn_i^2$ . If relatively small concentrations  $\delta p$  and  $\delta n$  of holes and electrons are present in excess of the equilibrium values, the net rate of generation is

$$\delta \dot{p} = \delta \dot{n} = g - r(n + \delta n)(p + \delta p) = -rn\delta p - rp\delta n \quad (3.1)$$

This is equivalent to saying that excess holes in an  $n$ -type semiconductor,

and excess electrons in a *p*-type semiconductor, respectively, have lifetimes  $\tau_p$  and  $\tau_n$  given by

$$\delta \dot{p} = -\delta p / \tau_p = -r n \delta p \text{ or } \tau_p = 1 / r n = p / g \quad (3.2)$$

and

$$\delta \dot{n} = -\delta n / \tau_n = -r p \delta n \text{ or } \tau_n = 1 / r p = n / g. \quad (3.3)$$

We shall have occasion to use this interpretation later. (We later consider the modifications required when surface recombination occurs, Section 4.2, Appendix V, and the effect of a localized region of high recombination rate, Section 4.6, Appendix III.)

In principle, the steady-state solution can be obtained in terms of the three potentials  $\psi$ ,  $\varphi_p$  and  $\varphi_n$ . These must satisfy three simultaneous ordinary differential equations, which we shall derive. As discussed in Section 2, we consider all donors and acceptors to be ionized so that Poisson's equation becomes

$$\frac{d^2 \psi}{dx^2} = -\frac{4\pi q}{\kappa} (ax + n_i e^{q(\varphi_p - \psi)/kT} - n_i e^{q(\psi - \varphi_n)/kT}) \quad (3.4)$$

an equation in which the unknowns are the three functions  $\varphi_p$ ,  $\varphi_n$  and  $\psi$ . The total current density, from left to right, is

$$I = I_p + I_n = -q\mu \left[ p \frac{d\varphi_p}{dx} + bn \frac{d\varphi_n}{dx} \right]. \quad (3.5)$$

The elimination of  $p$  and  $n$  by equation (2.4) results in an equation involving the three unknown functions and  $I$ . The divergence of hole current, equal to the net rate of generation of holes, is

$$\begin{aligned} \frac{dI_p}{dx} &= -q\mu p \left[ \frac{q}{kT} \left( \frac{d\varphi_p}{dx} \right)^2 - \frac{q}{kT} \frac{d\psi}{dx} \frac{d\varphi_p}{dx} + \frac{d^2 \varphi_p}{dx^2} \right] \\ &= q(g - rn\dot{p}) = qg(1 - e^{q(\varphi_p - \varphi_n)/kT}), \end{aligned} \quad (3.6)$$

with  $p$  in the second term given by (2.4) so that (3.6) is also an equation for the three unknown functions. The equation for  $dI_n/dx$  can be derived from the last two and adds nothing new. These three equations can be used to solve for  $d^2\psi/dx^2$ ,  $d^2\varphi_p/dx^2$  and  $d\varphi_n/dx$  in terms of lower derivatives and  $I$ . They thus constitute a set of equations sufficient to solve the problem provided that physically meaningful boundary conditions are imposed. We shall not, however, deal directly with these equations; the main reason for deriving them was to show that the problem in question is, in principle, completely formulated. Instead of attempting to solve the equations, we shall discuss certain general features of the solutions for  $\varphi_p$  and  $\varphi_n$ , using

approximate methods, and in this way bring out the essential features of the theory of rectification.

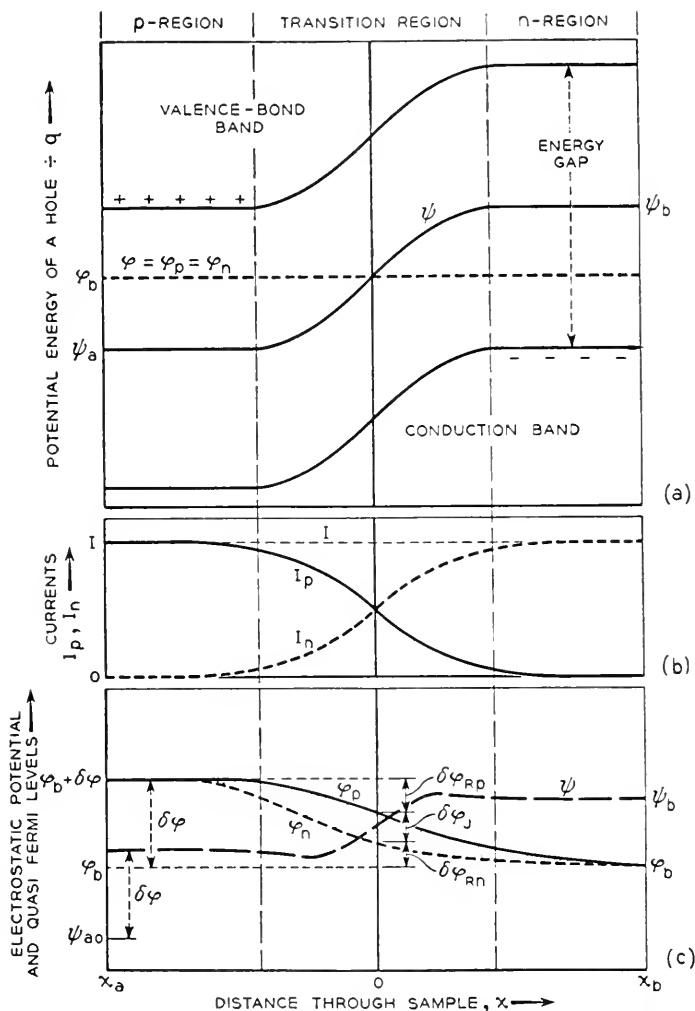


Fig. 5—Potential and current distributions for forward current in  $p$ - $n$  junctions.  
 (a)  $p$ - $n$  junction under equilibrium conditions.  
 (b) Division of current between holes and electrons.  
 (c) Distribution of potentials for forward current flow showing how the potential  $\delta\varphi$  applied at  $x_a$  changes  $\varphi_p$ ,  $\varphi_n$  and  $\psi$ .

In Fig. 5 we represent a general situation which may be used to illustrate the nature of the resistance of the junction. Part (a) corresponds to thermal equilibrium and shows the potential distribution and Fermi level in ac-

cordance with the scheme used in Fig. 2. Part (b) shows the current distribution for a forward current  $I$  from left to right and (c) shows the corresponding potential distribution and values of  $\varphi_n$  and  $\varphi_p$ , the total applied potential being  $\delta\varphi$ . Recombination prevents the hole current from penetrating far into the  $n$ -region, the depth of penetration being described by the diffusion length  $L_p = \sqrt{D\tau_p} = \sqrt{Dp_n/g}$ , where  $p_n$  is the hole concentration in the  $n$ -region. The electron current similarly is limited by  $L_n = \sqrt{bD\tau_n} = \sqrt{bDn_p/g}$ . (Diffusion lengths are evaluated for particular models of the junction in Section 4.) Far from the junction, therefore, the hole and electron concentrations have their normal values and consequently  $\varphi_p = \varphi_n$  and  $\varphi_p - \psi$  has its normal value. This accounts for the equal displacement  $\delta\varphi$  for all three curves at  $x = x_a$ . The curves for  $\varphi_p$  and  $\varphi_n$  have a continuous downward trend which produces the currents

$$I_p = -q\mu p \frac{d\varphi_p}{dx} \quad \text{and} \quad I_n = -qb\mu n \frac{d\varphi_n}{dx}. \quad (3.7)$$

The area between the  $\varphi_p$  and  $\varphi_n$  curves has a special significance: This difference is related to the excess rate of recombination and the integral of this rate over the entire specimen must be sufficient to absorb the hole current  $I_p = I$  entering at  $x_a$  so that the entire current at  $x_b$  is carried by electrons. In terms of  $\varphi_p - \varphi_n$  and equation (3.6) we obtain

$$\begin{aligned} I &= I_p(x_a) - I_p(x_b) = \int_{x_a}^{x_b} -dI_p \\ &= gq \int_{x_a}^{x_b} (e^{q(\varphi_p - \varphi_n)/kT} - 1) dx. \end{aligned} \quad (3.8)$$

From (3.8) we conclude that if  $g$  is increased indefinitely for a specified current  $I$ , then  $\varphi_p - \varphi_n$  must approach zero. For this case, in which the rate of recombination and generation is very high,  $\varphi_p = \varphi_n$  and

$$I = I_p + I_n = -q\mu(p + bn) d\varphi_p/dx \quad (3.9)$$

and

$$\delta\varphi = -\int_{x_a}^{x_b} d\varphi_p = I \int_{x_a}^{x_b} dx/q\mu(p + bn) \equiv IR_0, \quad (3.10)$$

where  $R_0$  is simply the integral of the local resistivity corresponding to densities  $p$  and  $n$ . For smaller values of  $g$ ,  $I$  does not divide in the ratio  $p:bn$  and  $\varphi_p \neq \varphi_n$  and  $\delta\varphi > IR_0$ .<sup>10</sup>

We shall next give an approximate treatment for the case in which  $\delta\varphi_J$  ( $J$  for junction), the value of  $\varphi_p - \varphi_n$  at  $x = 0$ , is an appreciable fraction of

<sup>10</sup> A general proof that  $\delta\varphi > IR_0$  is given in Appendix I.

the total voltage drop. For this purpose we treat  $\varphi_p - \varphi_n$  as constant over a range of integration from  $x = -L_n$  to  $x = +L_p$  obtaining

$$\begin{aligned} I &= gq(L_n + L_p)[e^{(q\delta\varphi_J/kT)} - 1] \\ &= I_s[e^{(q\delta\varphi_J/kT)} - 1] \end{aligned} \quad (3.11)$$

where

$$I_s = gq(L_n + L_p) \quad (3.12)$$

is the current density corresponding to the total rate of generation of hole-electron pairs in a volume  $L_n + L_p$  thick. We next consider  $\delta\varphi_{Rp} + \delta\varphi_{Rn}$  shown in Fig. 5c, where, as the subscript  $R$  implies, these are thought of as resistive terms and are given by the integrals

$$\delta\varphi_{Rp} + \delta\varphi_{Rn} = - \int_{x_a}^0 d\varphi_p - \int_0^{x_b} d\varphi_n = \int_{x_a}^0 I_p dx / q\mu p + \int_0^{x_b} I_n dx / q\mu n.$$

The denominators are both approximately  $q\mu(p + bn)$  which occurs in the integral for  $R_0$ . Furthermore, for most of the first range  $I_p = I$  and for most of the second  $I_n = I$ . Near  $x = 0$ ,  $I_p$  or  $I_n$  must be at least  $I/2$ . Hence it is evident that  $\delta\varphi_{Rp} + \delta\varphi_{Rn}$  cannot be much less than  $IR_0$ . We shall represent it by  $IR_1$  where  $R_0 < 2R_1 < 2R_0$ .

In terms of  $R_1$  and  $I_s$ , the relationship between current and voltage becomes

$$\delta\varphi = \delta\varphi_{Rp} + \delta\varphi_{Rn} + \delta\varphi_J = R_1 I + \frac{kT}{q} \ln \left( 1 + \frac{I}{I_s} \right). \quad (3.13)$$

This corresponds to an ideal rectifier in series with a resistance  $R_1$ . The junction will, therefore, be a good rectifier if the second term represents a much higher resistance.

We shall compare the two resistances for the case corresponding to  $K \ll 1$ . For this case, we have  $p = -ax$  and  $n = +ax$  except in the narrow range  $|x| < L_a = n_i/a$ . The integral  $R_0$  can be approximated by integrating  $dx/\sigma$  for  $x$  outside of the range  $\pm L_a$  using the approximation  $\pm ax$  for  $p$  and  $n$  and approximating the integral from  $-L_a$  to  $+L_a$  by  $2L_a/\sigma$  (intrinsic). This procedure gives

$$\begin{aligned} R_1 &= \int_{L_a}^{-x_a} dx / q\mu ax + \frac{2L_a}{q\mu n_i(1+b)} + \int_{L_a}^{x_b} dx / q\mu bax \\ &= \frac{L_a}{q\mu n_i} \left( 1 + \frac{1}{b} \right) \ln (x_b/L_a) \end{aligned} \quad (3.14)$$

where it is supposed that  $-x_a \doteq x_b$  and that  $\ln (x_b/L_a)$  is large compared to  $2/(b+2+1/b)$ . The evaluation of  $L_p$  and  $L_n$  for use in  $I_s$  is more involved



since  $\tau_p$  and  $\tau_n$  are both functions of  $x$ . We shall obtain an approximate self-consistent diffusion length by assuming that the holes diffuse, on the average, to just such a depth,  $L_p$ , that in uniform material of the type found at  $L_p$ , their diffusion length would also be  $L_p$ . At a depth  $L_p$ , the value of  $n$  is  $aL_p$  so that by (3.2),  $\tau_p$  is  $1/raL_p = n_i^2/gaL_p$ . Thus we write

$$L_p^2 = D\tau_p = Dn_i^2/gaL_p. \quad (3.15)$$

We can solve the equation (3.15) for  $L_p$  and a similar one for  $L_n$  and insert the results in equation (3.13). For small  $I$  this gives

$$\begin{aligned} \delta\varphi/I = R_1 + (kT/qI_s) &= \frac{L_a}{q\mu n_i} \left(1 + \frac{1}{b}\right) \ln(x_b/L_a) \\ &+ kT/(q^2 g^{2/3} (DL_a n_i)^{1/3} (1 + b^{1/3})). \end{aligned} \quad (3.16)$$

It is seen that for  $g$  large, the second term, corresponding to the rectifying resistance, becomes small. For this case, as discussed above,  $\varphi_p = \varphi_n$  and the exact integral for  $R_0$  should be used and the junction will give poor rectification.

It is also instructive to consider  $L_a$  as a variable. Increasing  $L_a$  corresponds to making the transition from  $p$  to  $n$  more gradual. It is evident that varying  $L_a$  changes the two terms of (3.16) in opposite directions so that there will be an intermediate value of  $L_a$  for which the resistance of the junction is a minimum. As  $L_a$  approaches zero, however, the second term should be modified: If we imagine that in the transition region the concentration ( $N_d - N_a$ ) varies only over a finite range, bounded by fixed values  $n_n$  and  $p_p$  in the  $n$ - and  $p$ -regions, then it is clear that the limiting values of  $L_p$  and  $L_n$  should be given not by (3.15) but by  $\sqrt{D\tau_p}$  and  $\sqrt{bD\tau_n}$  where  $\tau_p$  and  $\tau_n$  are evaluated in the  $n$ -region and  $p$ -region. This leads to a limiting value for  $I_s$ , which is given in equation (4.11) of the following section. In the range for which (3.16) applies, however, the interesting result holds that widening the transition region initially decreases the resistance by furnishing a larger volume in which holes and electrons may combine or be generated.

The condition that  $\delta\varphi_J$  dominate the resistance is that the second term of (3.16) be much larger than the first. This leads to the inequality

$$1 \ll \frac{kT}{q^2 g^{2/3} (DL_a n_i)^{1/3}} \cdot \frac{q\mu n_i}{L_a} = (Dn_i/gL_a^2)^{2/3} = (L_{pi}/L_a)^{4/3} \quad (3.17)$$

where we have neglected various factors involving  $b$ , which are nearly unity, and  $\ln(x_b/L_a)$  (which must be about 4 for Ge since the conductivity at  $x_b$  is about  $\exp(4)$  times the intrinsic conductivity). The quantity

$$L_{pi} = (Dn_i/g)^{1/2} \quad (3.18)$$

is the diffusion length for holes in the intrinsic region. The inequality states that the diffusion length must be much larger than  $L_a$ . This is equivalent to the previous statement that the hole current must penetrate the  $n$ -region for the rectifier to have a good characteristic. (If a local region of high recombination is present in the transition region, this result just quoted need not apply. See Section 4.6.)

If the hole current penetrates deeply into the  $n$ -region and  $R_1$  is negligible, then we can conclude that the current-voltage characteristic will fit the ideal formula. For these assumptions  $\delta\varphi_{Rp}$  on Fig. 5 will be small and the principal change in  $\varphi_p$  will occur relatively deep in the  $n$ -region, at least beyond the transition region. So long as the hole concentration introduced in the  $n$ -region is much smaller than  $n_n$ , the hole current into the  $n$ -region will be a linear function of the value of  $p$  at the right edge of the transition region, being zero when  $p$  equals  $p_n$ , the equilibrium value of  $p$ . This leads at once to a hole current proportional to  $p - p_n$  and since the shift of  $\varphi_p$  in respect to  $\psi$  at the edge of transition region is  $\delta\varphi$ ,  $p - p_n$  is equal to  $p_n(\exp(a\delta\varphi/kT) - 1)$ . (These ideas are discussed in detail in Section 4.) A similar relationship will hold for electrons entering the  $p$ -region; hence the total current will vary as  $\exp(q\delta\varphi/kT) - 1$ . This is a theoretical rectification formula<sup>11</sup> giving the maximum rectification for carriers of charge  $q$ .

#### 4. TREATMENT OF PARTICULAR MODELS

##### 4.1 Introduction and Assumptions

In this section we shall deal chiefly with good rectifiers so that the  $IR$  drop, discussed in connection with  $R_1$  in Section 3, is negligible. We shall deal chiefly with the case for which the transition region is narrow compared to the diffusion length; consequently, there is little change in  $I_p$  in traversing the transition region. In Fig. 6(a) we consider a hypothetical junction in which the properties are uniform outside the transition region. The division of the specimen into three parts as shown is seen to be reasonable for germanium: In  $n$ -type germanium, the diffusion constant for holes is about  $40 \text{ cm}^2/\text{sec}$  and the lifetime is greater than  $10^{-6} \text{ sec}$  so that the diffusion distance is  $L_p = \sqrt{D\tau_p} > 6 \times 10^{-3} \text{ cm}$ . This is much greater than most transition regions.

The major drop in  $\varphi_p$  must occur to the right of the transition region. This follows from our assumptions: First, we may neglect the  $IR$  drop in the  $p$ -region; hence  $\varphi_p$  is substantially constant from  $x = x_a$  to  $x = x_{Tp}$ . Second, the decrease in  $\varphi_p$  is much less in the transition region than in the  $n$ -region; this follows from two considerations: the resistance for hole flow is lower in

<sup>11</sup> C. Wagner, *Phys. Zeits.* 32, 641-645 (1931).

the transition region than in the  $n$ -region; the effective length of flow in the  $n$ -region, being  $L_p$ , is greater than the width of the transition region. Consequently, the variation of  $\varphi_p$  shown in Fig. 6(c) is seen to be reasonable. Similar considerations apply to  $\varphi_n$ . As is shown in Fig. 6(c), the application of  $\delta\varphi$  does not alter  $\varphi_p - \psi$  in the  $p$ -region nor  $\varphi_n - \psi$  in the  $n$ -region. The

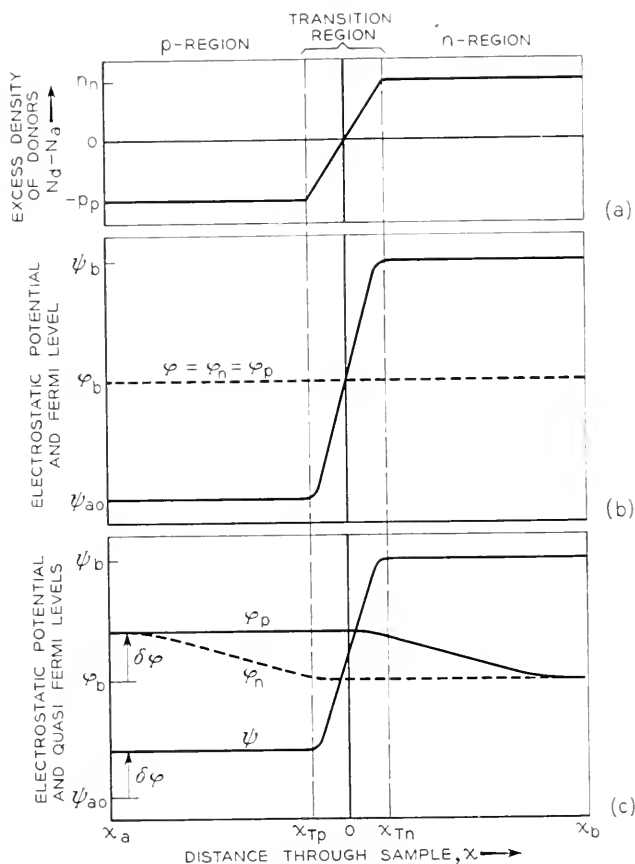


Fig. 6—Simplified model of a  $p$ - $n$  junction.

- (a) Distribution of donors and acceptors.
- (b) Potentials for thermal equilibrium.
- (c) Effect of  $\delta\varphi$  applied potential in forward direction.

reason, as discussed in connection with (2.31), is that in these regions electrical neutrality requires an essentially constant value for the more abundant carrier. Hence the relationships between the  $\varphi$ 's and  $\psi$  follow from (2.4).

The nature of the potential distribution in the transition region has no effect in the considerations just discussed. However, as shown in Section 2,

the capacity of the transition region, which we shall denote by  $C_T$  in this section, does depend on the nature of the transition region and, consequently, on the value of  $K$ .

If the sizes of the  $p$ -region and  $n$ -region are large compared to the diffusion lengths, we may assume the current at  $x_a$  to be substantially  $I_p$  only and that at  $x_b$ ,  $I_n$  only. The total current entering at  $x_a$  can be accounted for as doing three things: (1) neutralizing the electron current flowing into the  $p$ -region across  $x_{Tp}$ , (2) contributing to the charge in the transition region (this corresponds to the capacity discussed in Section 2) and (3) contributing a current flow to the right across  $x_{Tn}$ .

We have selected the hole current for analysis because the hole has a positive charge and the connection between the algebra and the physical picture is simplified. For the same reason, the text emphasizes forward current, although the equations are equally applicable to reverse currents. Nothing essential is left out by this process; since the sample as a whole remains uncharged, the current  $I$  is the same for all values of  $x$  and if  $I_p$  is known, then  $I_n = I - I_p$  is also determined.

#### 4.2 Solution for Hole Flow into the $n$ -region

We shall calculate first the hole current  $I_p(x_{Tn})$  flowing across  $x_{Tn}$ . It is readily evaluated as follows: The value of  $p(x_{Tn})$  is given by

$$\begin{aligned} p(x_{Tn}) &= n_i e^{q(\varphi_b + \delta\varphi - \frac{1}{2}\varphi_b)/kT} \\ &= p_n e^{q\delta\varphi/kT} \end{aligned} \quad (4.1)$$

where  $p_n$  is the hole concentration in the  $n$ -region for thermal equilibrium. If we apply a small a-c. signal superimposed on a d-c. bias so that

$$\delta\varphi = \tau_0 + \tau_1 e^{i\omega t} \quad (4.2)$$

where  $\tau_1$  is an a-c. signal, assumed so small that linear theory may be employed (i.e.  $\tau_1 \ll kT/q$ ), then

$$p(x_{Tn}) = (p_n e^{q\tau_0/kT})(1 + (q\tau_1/kT)e^{i\omega t}).$$

We resolve this density into a d-c. component  $p_0$  and an a-c. component  $p_1 e^{i\omega t}$ :

$$p(x_{Tn}) = p_0 + p_1 e^{i\omega t} \quad (4.3)$$

where

$$p_0 = p_n (e^{q\tau_0/kT} - 1) \quad (4.4)$$

$$p_1 = (qp_n \tau_1/kT) e^{q\tau_0/kT}. \quad (4.5)$$

So long as  $p(x_{Tn}) \ll n_n$ , the normal concentration of electrons in the

*n*-region, the lifetime  $\tau_p$  and diffusion constant  $D$  for a hole will be substantially unaltered by  $\delta\varphi$ . Application of the hole-current equation to the hole density  $p(x, t)$  gives

$$I_p = -qD \frac{\partial p}{\partial x}. \quad (4.6)$$

Combining this with the recombination equation

$$\frac{\partial p}{\partial t} = \frac{p_n - p}{\tau_p} - \frac{1}{q} \frac{\partial I_p}{\partial x} = \frac{p_n - p}{\tau_p} + D \frac{\partial^2 p}{\partial x^2} \quad (4.7)$$

leads to the solution

$$p = p_n + p_0 e^{(x_{Tn}-x)/\sqrt{D\tau_p}} + p_1 e^{i\omega t + (x_{Tn}-x)(1+i\omega\tau_p)^{1/2}/(D\tau_p)^{1/2}}. \quad (4.8)$$

The quantity  $\sqrt{D\tau_p}$  is the diffusion length and is denoted by  $L_p$ . (We shall use subscript  $p$  for holes in the *n*-region and *n* for electrons in the *p*-region for both  $L$  and  $\tau$ .)

When  $p$  is large compared to  $p_n$ , but small compared to  $n_n$ , the expression for  $p$  leads to the following formula for  $\varphi_p$ :

$$\varphi_p = \varphi_n + v_r - (kT/q)(x - x_{Tn})/L_p + i_1 e^{i\omega t - (x-x_{Tn})[(1+i\omega\tau_p)^{1/2}-1]/L_p}. \quad (4.9)$$

This shows that the d-c. part of  $\varphi_p$  varies linearly in the *n*-region, for large forward currents, and decreases by  $(kT/q)$  in each diffusion length  $L_p$ . The transition from this linear dependence to an exponential decay for  $\varphi_p$  comes when  $\varphi_p - \varphi_n = (kT/q)$ . This behavior of the d-c. part of  $\varphi_p$  is useful in connection with diagrams of  $\varphi_p$  versus distance. (See Sections 5 and 6.)

The solution just obtained for  $p$  gives rise to a current at  $x_{Tn}$  of

$$\begin{aligned} I_p(x_{Tn}) &= -qD \frac{\partial p}{\partial x} \\ &= qp_0 D/L_p + qp_1 D e^{i\omega\tau} (1 + i\omega\tau_p)^{1/2}/L_p. \end{aligned} \quad (4.10)$$

The d-c. part is calculated by substituting (4.4) for  $p_0$ :

$$\begin{aligned} I_{p0}(x_{Tn}) &= (qp_n D/L_p)(e^{qv_0/kT} - 1); \\ &\equiv I_{ps}(e^{qv_0/kT} - 1) \end{aligned} \quad (4.11)$$

and the a-c. part is similarly obtained from (4.5) for  $p_1$ :

$$\begin{aligned} I_{p1}(x_{Tn}) &= (qp_n \mu/L_p)[e^{(qv_0/kT)}](1 + i\omega\tau_p)^{1/2} v_1 e^{i\omega t} \\ &\equiv (G_p + iS_p)v_1 e^{i\omega t} \equiv A_p v_1 e^{i\omega t} \end{aligned} \quad (4.12)$$

where  $A_p$  is called the admittance (per unit area) for holes diffusing into the *n*-region; its real and imaginary parts are the conductance and suscept-

ance. For  $\omega\tau_p$  small, the real term  $G_p$  is simply conductance per  $\text{cm}^2$  of a layer  $L_p$  cm thick with hole conduction corresponding to the density  $p_n + p_0$ ; it is also the differential conductance obtained by differentiating (4.11) in respect to  $\tau_0$ . For the case of zero bias this establishes the result quoted in Section 1 that the voltage drop is due to hole flow in the  $n$ -region where the hole conductivity is low.

In this section we have treated  $\tau_p$  as arising from body recombination. In a sample whose  $y$  and  $z$  dimensions are comparable to  $L_p$  or  $L_n$ , surface recombination may play a dominant role. However, as we show in Appendix V, the theory given here may still apply provided appropriate values for  $\tau_p$  and  $\tau_n$  are used.

### 4.3 D-C. Formulae

The total direct hole current flowing in at  $x_a$  is  $I_{x0}$  plus the current required to recombine with electrons in the  $p$ -region. This latter current is, of course, equal to the electron current flowing into the  $p$ -region. This electron current, denoted by  $I_{x0}$  or  $I_{x0}(x_{Tp})$ , is obtained by the same procedure as that leading to (4.11) for  $I_{x0}$  except that  $bD$  replaces  $D$  and the subscripts of  $L$  and  $\tau$  are now  $n$ . Combining the two currents leads to the total direct current:

$$I_0 = I_{p0} + I_{n0} = (qL) \left( \frac{p_n}{L_p} + \frac{tn_p}{L_n} \right) (e^{q\tau_0/kT} - 1) \quad (4.13)$$

for the direct current per unit area for applied potential  $\tau_0$ .<sup>12</sup> The algebraic signs are such that  $I > 0$  corresponds to current from the  $p$ -region to the  $n$ -region in the specimen;  $\tau_0 > 0$  corresponds to a plus potential applied to the  $p$ -end. The ratio of hole current to electron current across the transition region is

$$\begin{aligned} \frac{I_{p0}}{I_{n0}} &= \frac{p_n}{L_p} \cdot \frac{L_n}{bn_p} = \frac{p_p}{bn_n} \cdot \frac{\sqrt{bD\tau_n}}{\sqrt{D\tau_p}} \\ &= \frac{p_p}{bn_n} \sqrt{\frac{bn_n}{p_p}} = \sqrt{\frac{\sigma_p}{\sigma_n}} \end{aligned} \quad (4.14)$$

where we have used the relationships  $n_n p_n = n_p^2$  from (2.2) and  $\tau_p n_n = \tau_n p_p = 1/r$  from (3.2) and (3.3). These results can be summarized by saying that the current flows principally into the material of higher re-

<sup>12</sup> For convenience we repeat the definitions here:  $q \equiv$  magnitude of electronic charge;  $D \equiv$  diffusion constant for holes;  $p_n$  and  $n_n \equiv$  thermal equilibrium value of  $p$  and  $n$ , assumed constant throughout  $n$ -region ( $x > x_{Tp}$ );  $n_p$  and  $p_p \equiv$  similar values for  $x < x_{Tp}$ ;  $L_p \equiv$  diffusion length  $\equiv \sqrt{D\tau_p}$  for holes in  $n$ -region;  $\tau_p \equiv$  lifetime of hole in  $n$ -region before recombination;  $b =$  electron mobility/hole mobility;  $L_n$  and  $\tau_n$  similar in quantities for electrons in  $p$ -region;  $\sigma_n = q\mu n_n$  and  $\sigma_p = q\mu p_p$  are the conductivities of the two regions.

sistivity. We can also say that the hole current depends only on the  $n$ -type material and vice versa. For a  $p$ - $n$  junction emitter in a transistor with an  $n$ -type base, it is thus advantageous to use high conductivity  $p$ -type material so as to suppress an unwanted electron current.

For comparison with experiment, it is advantageous to express the values of  $p_n$  and  $n_p$  in terms of the conductivities  $\sigma_n$  and  $\sigma_p$ . If the conductivity of the intrinsic material is written as

$$\sigma_i = q\mu n_i(1 + b), \quad (4.15)$$

then, if  $p_n \ll n_n$  and  $n_p \ll p_p$ , we find

$$q\mu p_n = b\sigma_i^2/(1 + b)^2\sigma_n \quad (4.16)$$

$$q\mu b n_p = b\sigma_i^2/(1 + b)^2\sigma_p. \quad (4.17)$$

Using these equations, we may rewrite (4.11) and a corresponding equation for electron current into the  $p$ -region so as to express their dependence on d-c. bias  $v_0$  and the properties of the regions:

$$\begin{aligned} I_{p0}(v_0) &= \frac{b\sigma_i^2}{(1 + b)^2\sigma_n L_p} \cdot \frac{kT}{q} (e^{qv_0/kT} - 1) \\ &\equiv G_{p0} \frac{kT}{q} (e^{qv_0/kT} - 1) \\ &\equiv I_{ps}(e^{qv_0/kT} - 1) \end{aligned} \quad (4.18)$$

$$\begin{aligned} I_{n0}(v_0) &= \frac{b\sigma_i^2}{(1 + b)^2\sigma_p L_n} \cdot \frac{kT}{q} (e^{qv_0/kT} - 1) \\ &\equiv G_{n0} \frac{kT}{q} (e^{qv_0/kT} - 1) \\ &\equiv I_{ns}(e^{qv_0/kT} - 1). \end{aligned} \quad (4.19)$$

The values of  $G_{p0}$  and  $G_{n0}$  (which are readily seen to be the values of the low-frequency, low-voltage ( $v_0 < kT/q$ ) conductances) and the saturation reverse currents are given by

$$G_{p0} \equiv \frac{l\sigma_i^2}{(1 + b)^2\sigma_n L_p} \equiv \frac{q}{kT} I_{ps} \quad (4.20)$$

$$G_{n0} \equiv \frac{l\sigma_i^2}{(1 + b)^2\sigma_p L_n} \equiv \frac{q}{kT} I_{ns} \quad (4.21)$$

The expression for direct current then becomes

$$\begin{aligned} I_0(v_0) &= [I_{p0} + I_{n0}] \left( \frac{e^{qv_0/kT}}{q} \right) [e^{qv_0/kT} - 1] \\ &= (I_{ps} + I_{ns}) [e^{qv_0/kT} - 1]. \end{aligned} \quad (4.22)$$

#### 4.4 Total Admittance

In order to calculate the alternating current, we must include the capacity of the transition region, discussed in Section 2. Denoting this by  $C_T$ , we then find for the total alternating current.

$$I_{ac} = (G_p + iS_p + G_n + iS_n + i\omega C_T) v_1 = A v_1 \quad (4.23)$$

where  $G_n$  and  $S_n$  are similar to  $G_p$  and  $S_p$  but apply to electron current into the  $p$ -region. The value of the hole and electron admittances can be expressed as

$$A_p = G_p + iS_p = (1 + i\omega\tau_p)^{1/2} G_{p0} e^{qv_0/kT} \quad (4.24)$$

$$A_n = G_n + iS_n = (1 + i\omega\tau_n)^{1/2} G_{n0} e^{qv_0/kT} \quad (4.25)$$

For low frequencies, such that  $\omega$  is much less than  $1/\tau_p$ , we can expand  $G_p + iS_p$  as follows:

$$G_p + iS_p = G_{p0} e^{qv_0/kT} + i\omega(\tau_p/2)G_{p0} e^{qv_0/kT} \quad (4.26)$$

Hence  $(\tau_p/2)G_{p0} e^{qv_0/kT}$  behaves like a capacity.

It is instructive to interpret this capacity for the case of zero bias,  $v_0 = 0$ , for which we find:

$$C_p = \tau_p G_{p0} / 2 = \tau_p q p_n \mu / 2L_p = q^2 p_n L_p / 2kT. \quad (4.27)$$

The last formula, obtained by noting that  $\tau_p \mu = q\tau_p D / kT = qL_p^2 / kT$ , has a simple interpretation:  $qp_n L_p$  is the total charge of holes in a layer  $L_p$  thick. For a small change in voltage  $v$ , this density should change by a fraction  $qv/kT$  so that the change in charge divided by the change in  $v$  is  $(q/kT)(qp_n L_p)$  which differs from  $C_p$  only by a factor of 2, which arises from the nature of the diffusion equation.

This capacity can be compared with  $C_{T \text{ neut.}}$ , discussed in Section 2, (see equation (2.39) and text for (2.42)) for germanium at room temperature as follows:

$$\frac{C_p}{C_{T \text{ neut.}}} = \frac{q^2 p_n L_p}{2kT} \cdot \frac{kTa}{10q^2 n_i^2} = \frac{p_n L_p a}{20n_i^2}. \quad (4.28)$$

For a structure like Fig. 6(c), the excess of donors over acceptors reaches its maximum value, equal to  $n_n$ , at  $x_{Tn}$  leading to  $n_n = ax_{Tn}$ . Consequently  $a = n_n / x_{Tn}$ . Substituting this value for  $a$  in (4.28) and noting that  $p_n n_n = n_i^2$  gives

$$\frac{C_p}{C_{T \text{ neut.}}} = \frac{L_p}{20x_{Tn}} \quad (4.29)$$

As discussed at the beginning of this section,  $L_p \doteq 6 \times 10^{-3}$  cm for holes



in germanium. Hence if the transition region is  $6 \times 10^{-4}$  cm thick, the diffusion capacity  $C_p$  will dominate the capacitive term in the admittance.

Although  $A_p$  simulates a conductance and capacitance in parallel at low frequencies, its high-frequency behavior is quite different. In Fig. 7 the

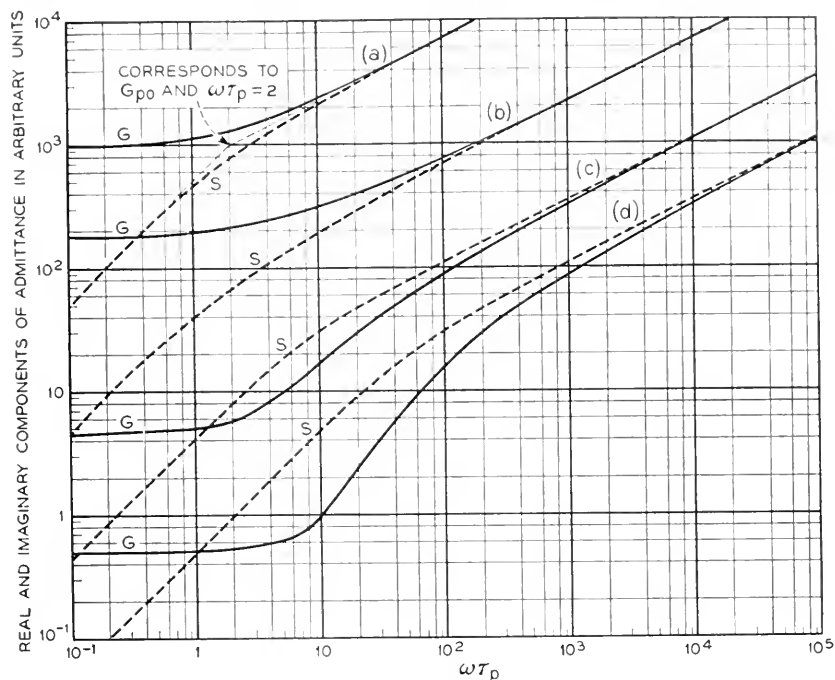


Fig. 7—Real,  $G$ , and imaginary,  $S$ , components of admittance for hole flow into  $n$ -region.

- (a)  $10^3 A_p / G_{p0} = 10^3 (1 + i\omega\tau_p)^{1/2}$  corresponding to uniform  $n$ -region.
- (b)  $10^2 \times$  Formula of Appendix III, corresponding to layer of high recombination rate in front of  $n$ -region. This causes  $G$  to exceed  $S$  at higher frequencies than for (a).
- (c)  $10 \times$  Equation (4.33), corresponding to a retarding field in the  $n$ -region, with  $L_r = L_p / \sqrt{10}$ .
- (d) Equation (4.33) with  $L_r = L_p / 10$ .

behavior of  $(1 + i\omega\tau_p)^{1/2} = A_p / G_{p0}$ , is shown. For high frequencies  $G_p$  and  $S_p$  are equal:

$$G_p = S_p = \sqrt{\tau_p/2} G_{p0} \sqrt{\omega} = \frac{b\sigma_i^2 \sqrt{\omega}}{(1+b)^2 \sigma_n \sqrt{2D}} \quad (4.30)$$

Thus for high frequencies the admittance is independent of  $\tau_p$  and is determined by the diffusion of holes in and out of the  $n$ -region. The three straight asymptotes have a common intersection at the point  $G_{p0}$ ,  $\omega\tau = 2$  on Fig. 7, a fact which is useful in estimating the value of  $\tau$  from such data.

For large  $\omega$ ,  $S_p$  varies as  $\omega^{1/2}$  as shown in (4.30) whereas  $S_T = \omega C_T$ . Hence

at very high frequencies  $C_T$  will dominate the admittance. At very high frequencies  $C_T$  itself will have a frequency dependence; however, for the assumptions on which the treatment of this section is based, the relaxation time for the transition region  $\tau_T$  is much less than  $\tau_p$ . This is a consequence of the fact that, although diffusion of holes into the transition region is required for the charging of  $C_T$ , the distance is relatively short, being in fact only that fraction of the width  $x_{Tn} - x_{Tp}$  of the transition region in which  $\psi$  rises by  $kT/q$ ; in germanium this will be about one-tenth of  $x_{Tn} - x_{Tp}$ . Since diffusion times vary as (distance)<sup>2</sup>, the ratio of the times is

$$\frac{\tau_T}{\tau_p} = \frac{(x_{Tn} - x_{pn})^2}{100L_p^2}. \quad (4.31)$$

Hence if  $L_p > x_{Tn} - x_{pn}$ ,  $\tau_T$  will be much less than  $\tau_p$ .<sup>13</sup>

#### 4.5 Admittance Due to Hole Flow in a Retarding Field

In Appendix II we treat the case in which a potential gradient, due to changing concentration for example, is present in the  $n$ - and  $p$ -regions. This tends to prevent holes from diffusing deep in the  $n$ -region and for this reason the  $n$ -region acts partly like a storage tank for holes under a-c. conditions, thus enhancing  $S_p$  compared to  $G_p$  in  $A_p$ . If the electric field is  $-d\psi/dx = kT/qL_r$ , where  $L_r$  is the distance required for an increase of  $kT/q$  of potential (i.e. a factor of  $e$  increase in  $n_n$ ), then the value of  $A_p$  is

$$A_p = [q\mu p_n/L_p] \frac{(2L_r/L_p)(1 + i\omega\tau_p)}{1 + [1 + (1 + i\omega\tau_p)(2L_r/L_p)^2]^{1/2}} \quad (4.32)$$

For  $\omega\tau_p > 1$ , this admittance is largely reactive provided  $2L_r/L_p$  is sufficiently small.

The dependence of  $A_p$  upon  $\omega$  is shown in Fig. 7 for two values of  $L_r/L_p$ . The plot shows the real and imaginary parts of

$$A_p/[2q\mu p_n L_r/L_p^2] = \frac{(1 + i\omega\tau_p)}{1 + [1 + (1 + i\omega\tau_p)(2L_r/L_p)^2]^{1/2}} \quad (4.33)$$

for  $L_p/L_r = 10^{1/2}$  and  $L_p/L_r = 10$ , the two curves being relatively displaced vertically by one decade. The second value implies that the field keeps the holes back so that they penetrate only  $1/10$  their possible diffusion length in no field. It is seen that for this case the storage effect is very pronounced and the susceptance  $S$  is much larger than  $G$  for high frequencies.

The function  $(1 + i\omega\tau_p)^{1/2}$ , discussed earlier, corresponds to the limiting case of (4.32) for  $L_r = \infty$ .

<sup>13</sup> In Appendix IV an analytic treatment of  $C_T$  is given.

#### 4.6 The Effect of a Region of High Rate of Generation

There is evidence that imperfections, such as surfaces and cracks, add materially to the rate of generation and recombination of holes and electrons. If there is a localized region of high recombination rate in the transition region, there will be a pronounced modification of the admittance characteristics. In Fig. 8(a) such a layer is represented at  $x = 0$ . In Fig. 8(b) the customary plot of  $\varphi_p$  and  $\varphi_n$  versus  $x$  is shown. If we neglect the effect of the series resistance terms denoted by  $R_1$  in Section 3, the change  $\delta\varphi$  will

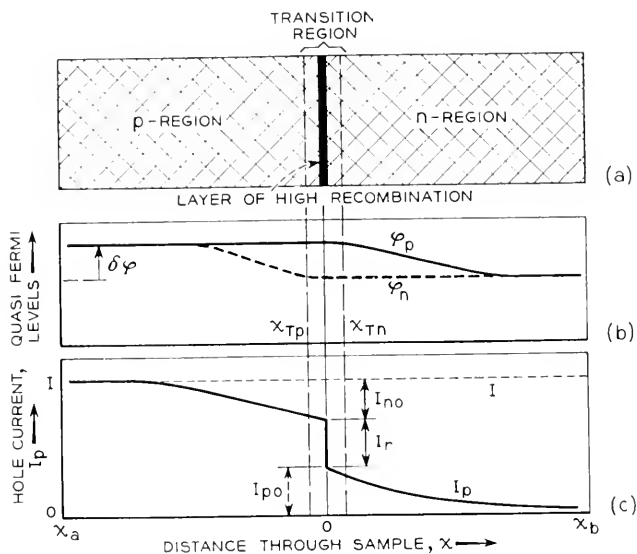


Fig. 8—The effect of a localized layer of high recombination rate on the junction characteristic.

(a) Location of layer of high recombination rate.

(b) Quasi Fermi levels.

(c) Distribution of hole current showing rapid change at layer of high recombination rate.

occur in the  $p$ -region for  $\varphi_n$  and in the  $n$ -region for  $\varphi_p$ . The hole current flowing into the  $n$ -region will thus be the same as before and will be given by equation (4.11) or (4.18) and denoted by  $I_{p0}(\delta\varphi)$ . Similarly, the electron current will be  $I_{n0}(\delta\varphi)$ . In the layer we shall suppose that there is a rate of generation of hole electron pairs equal to  $g_a$  per unit area of the layer and a rate of recombination proportional to  $r_a n p$  per unit area. We suppose, furthermore, that the layer is so thin that  $n$  and  $p$  are uniform throughout the layer. The net rate of generation is thus

$$g_a - r_a n p = g_a [1 - e^{q(\varphi_p - \varphi_n)/kT}] \quad (4.34)$$

since for equilibrium conditions the rates balance so that  $r_a n_i^2 = g_a$ . The net hole current recombining in the layer per unit area is thus

$$I_r(\varphi_p - \varphi_n) = qg_a [e^{q(\varphi_p - \varphi_n)/kT} - 1] \quad (4.35)$$

There must, therefore, be a discontinuous decrease of hole current across the layer. The total hole current flowing in at  $x = x_a$ , which is also the total current  $I$ , thus does three things: for  $x < x_{Tp}$ , it combines with  $I_{n0}(\delta\varphi)$ ; for  $x_{Tp} < x < x_{Tn}$ , it combines with electrons at rate  $I_r(\delta\varphi)$ ; for  $x > x_{Tn}$ , it flows into the  $n$ -region in amount  $I_{p0}(\delta\varphi)$ . This leads to

$$I = I_{n0}(\delta\varphi) + I_{p0}(\delta\varphi) + I_r(\delta\varphi). \quad (4.36)$$

In other words the layer of high recombination acts like a rectifier in parallel with  $I_{n0}(\delta\varphi) + I_{p0}(\delta\varphi)$ . The frequency characteristic of  $I_r(\delta\varphi)$ , however, will be independent of frequency and will contribute a pure conductance to the admittance of the junction.

If the layer is considered to have finite width, however, it will exhibit frequency effects just as does  $I_p$  in the  $n$ -region. In Appendix III, we treat a case in which the layer is a part of the  $n$ -region itself but has a recombination time different from the main layer. If the time is shorter, a large amount of the hole current may recombine in this layer. For high frequencies, the current may not penetrate the layer, in which case the admittance for hole current is determined by the thin layer rather than by the whole  $n$ -type region. A case of this sort is shown in Fig. 7. In this case the thickness of the layer is  $\frac{1}{3}$  of its diffusion length and in it the lifetime of a hole  $\tau_l$  is  $\frac{1}{9}$  the value  $\tau_p$  in the main body of the  $n$ -region. The hole current will thus be restricted to this layer when the diffusion distance  $\sqrt{D/\omega}$  is less than the layer thickness ( $\frac{1}{3}$ )  $\sqrt{D\tau_l}$ ; this corresponds to  $\omega\tau_l > 9$  or  $\omega\tau_p > 81$ . The presence of the high rate of combination in the layer is evidenced by the tendency of  $G$  to be greater than  $S$  at high frequencies. If the layer were infinitely thin, as discussed above, it would simply add a constant conductance to the admittance.

#### 4.7 Patch Effect in $p$ - $n$ Junctions

If there are localized regions of high recombination rate, a "patch effect" may be produced in an  $n$ - $p$  junction. As an extreme example, suppose the value of  $g_a$  for the layer just considered is allowed to become very large; then the recombination resistance may become small compared to  $R_1$  in Section 3 and the junction will become substantially ohmic. If the region of high rate of recombination is relatively small compared to the area of the rest of the junction, then the behavior of the junction as a whole may be regarded as being that due to two junctions in parallel. Over most of the area,

the currents will flow as if the patch were not present so that one component of the current will be that due to the uniform junction. In addition there will be current due to recombination and generation in the patch. The series resistance to the patch will be relatively high due to the constriction of the current paths. On the other hand, the value of  $I_r(\delta\phi)$  associated with the patch may be very high. Hence the current due to the patch will be that of a low impedance ideal rectifier in series with a high resistance; and if the ratio of impedances is high enough, such a series combination amounts essentially to an ohmic leakage path. Thus patches in the *p-n* junction will tend to introduce leakage paths and destroy saturation in the reverse direction.

An extreme example of a region of high rate of recombination would be a particle of metal making a non-rectifying contact to both *p*- and *n*-type germanium. Since holes and electrons are essentially instantly combined in a metal, the boundary condition at the metal surface would be equality of  $\varphi_p$  and  $\varphi_n$ . This would mean that near the metal particle,  $\varphi_p$  and  $\sigma_n$  could not differ by  $\delta\varphi$ , the condition required, over some parts of the junction at least, in order for ideal rectification to occur.

A common source of imperfection in *p-n* junctions arises from dirt or fragments on the surface which overlap the junction. Even if these do not actually constitute a short circuit across the junction, they may furnish patches of the sort discussed here and modify the junction characteristic.

#### 4.8 Final Comments

Another possible cause for frequency effects may be found in the trapping of holes or electrons.<sup>14</sup> When an added hole concentration is introduced into an *n*-region, a certain fraction of the holes will be captured by acceptors and later re-emitted or else recombined with electrons while trapped. Investigation of this process is given in Appendix VI. One interesting result is that the trapping of holes in a uniform *n*-region cannot produce an effective susceptance (i.e.  $i\omega C$ ) in excess of the conductance, as can a retarding field.

Finally it should be remarked that important and significant variations of the conductivity in the *p*- and *n*-regions may be produced by hole or electron injection. Under these conditions, when the hole concentration approaches  $n_n$ ,  $\psi - \varphi_n$  will vary. Under these conditions  $R_1$  may be appreciably altered. These factors favor the *p-n* junction as a rectifier since they lead to a reduction of series resistance under conditions of forward bias and thus tend to improve the rectification ratio.

<sup>14</sup> Frequency dependent effects in  $\text{Cu}_2\text{O}$  rectifiers have been explained in this way by J. Bardeen and W. H. Brattain, personal communication.

## 5. INTERNAL CONTACT POTENTIALS

The theory of  $p$ - $n$  junctions presented above has interesting consequences when applied to the distribution of potential between two semiconductors

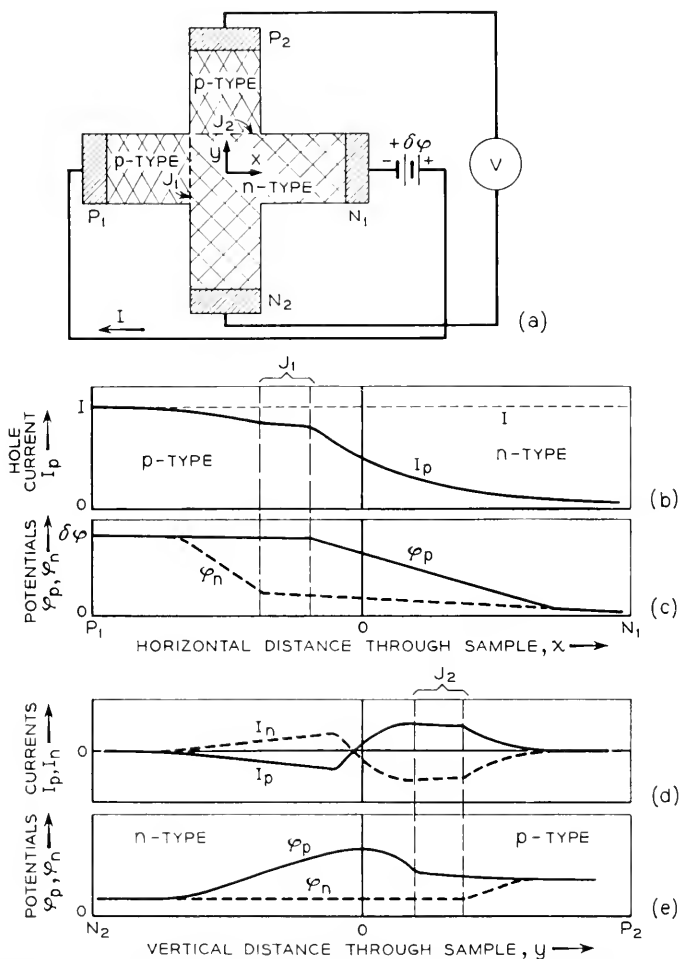


Fig 9--Internal contact potentials showing how presence of injected holes produces a contact potential across  $J_2$ .

under conditions of hole or electron injection. In Fig. 9 we illustrate an X-shaped structure. A forward current flows across the junction  $P_1$  and out of branch  $N_1$ . If the distance across the intersection is comparable with or small compared to the diffusion length for holes, a potential difference should be measured between  $P_2$  and  $N_2$ . The reason for this is that holes

flow easily into  $P_2$  since the potential distribution there favors their entrance. Since, however,  $P_2$  is open-circuited this hole flow biases  $J_2$  in the forward direction; since  $J_2$  is high resistance, an appreciable bias is developed before the counter current equals the inward hole flow and a steady state is reached. No similar effect occurs in the branch  $N_2$ ; consequently  $P_2$  will be found to be floating (open-circuited) at a more positive potential than  $N_2$ .

Parts (b) to (e) describe this reasoning in more complete terms. We suppose that the  $p$ -regions are more highly conducting than the  $n$ -regions so that the current across  $J_1$ , shown in (b), is mainly holes. The potentials  $\varphi_p$  and  $\varphi_n$  along the  $x$ -axis will be similar to those of Figs. 5 and 6; (c) shows this situation and indicates that the diffusion length for electrons in the  $p$ -region is less than for holes in the  $n$ -region. Along the  $y$  axis  $\varphi_p$  and  $\varphi_n$  vary as shown in (e), the reasoning being as follows: At the origin of coordinates  $\varphi_p$  and  $\varphi_n$  have the same values as for (c). The transverse hole current (d) has a small positive component at  $y = 0$  since, as mentioned above,  $P_2$  tends to absorb holes and thus increase diffusion along the plus  $y$ -axis. Since the net transverse current is zero,  $I_n = -I_p$  in (d). The  $\varphi$  curves of (e) have been drawn to conform to the currents in (d);  $\varphi_n$  is nearly constant in the  $n$ -region and  $\varphi_p$  is nearly constant in the  $p$ -region. As concluded in connection with Figs. 5 and 6,  $\varphi_n$  and  $\varphi_p$  are also nearly constant across the transition region. These conclusions lead to the shape of  $\varphi_n$  and  $\varphi_p$  for  $y > 0$  in (e). For  $y < 0$ , the reasoning is the same as that used in Sections 3 and 4 and we conclude that  $\varphi_n$  is essentially constant. Hence, a difference in the Fermi levels at  $P_2$  and  $N_2$  will result.

In Fig. 10 we show a structure for which we can make quantitative calculations of the variations of  $\varphi_p$  and  $\varphi_n$ . We assume for this case that the forward current from  $P_1$  to  $N$  does not produce an appreciable voltage drop, i.e. change in  $\psi$  and  $\varphi_n$ , in region  $N$ . This will be a good approximation if the dimensions are suitably proportioned. We shall next solve for the steady-state distribution of  $p$  subject to the indicated boundary conditions assuming that  $p$  is a function of  $x$  only. As we have discussed in Section 4.1, when  $p$  is small compared to  $n$  in the  $n$ -region, we can write

$$p = p_n e^{q(\varphi_p - \varphi_n)/kT} \quad (5.1)$$

In keeping with the treatment in the next section of this structure as a transistor, the terminals are designated emitter, collector and base, the potentials with respect to the base being  $\varphi_e$  and  $\varphi_c$ . The contact to  $N$  or the base is such that  $\varphi_b = \varphi_n$  in this region. Hence, the boundary conditions at  $J_1$  and  $J_2$  are

$$p_1 = p_n e^{q\varphi_e/kT} \quad x = -w \quad (5.2)$$

$$p_2 = p_n e^{q\varphi_c/kT} \quad x = +w \quad (5.3)$$

The function  $p(x)$  which satisfies these boundary conditions and the equation

$$D \frac{d^2 p}{dx^2} - \frac{p - p_n}{\tau_p} = 0 \quad (5.4)$$

is

$$p(x) = p_n + \frac{p_1 + p_2 - 2p_n}{2 \cosh(w/L_p)} \cosh(x/L_p) + \frac{p_2 - p_1}{2 \sinh(w/L_p)} \sinh(x/L_p) \quad (5.5)$$

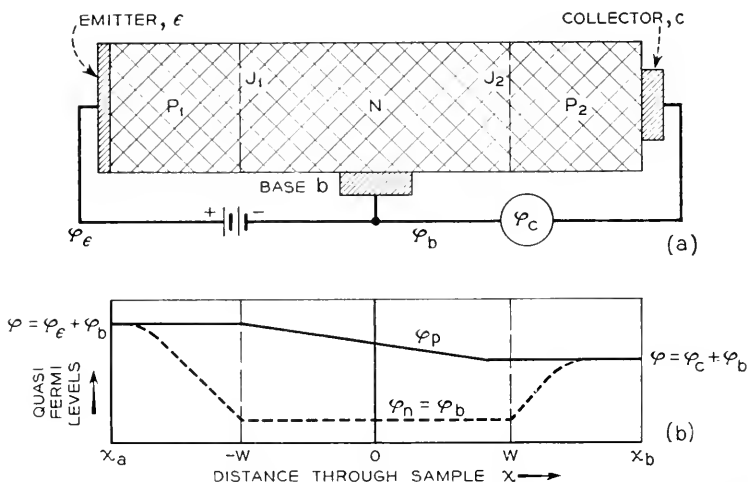


Fig. 10—Model used for calculation of internal contact potential and to illustrate  $p$ - $n$ - $p$  transistor.

- (a) Semiconductor with two  $p$ - $n$  junctions and ohmic metal contacts.  
 (b) Quasi Fermi levels showing internal contact potential between  $b$  and  $c$ .

which gives rise to a hole current across  $J_2$  into  $P_2$  of amount

$$\begin{aligned} I_p &= -qD \left. \frac{dp}{dx} \right|_{x=w} \\ &= \frac{qD}{2L_p} \left[ (p_1 - p_2) \coth \frac{w}{L_p} + (2p_n - p_1 - p_2) \tanh \frac{w}{L_p} \right] \\ &= \frac{qD}{2L_p} \left[ (p_1 - p_n) \left( \coth \frac{w}{L_p} - \tanh \frac{w}{L_p} \right) \right. \\ &\quad \left. - (p_2 - p_n) \left( \coth \frac{w}{L_p} + \tanh \frac{w}{L_p} \right) \right] \\ &= + \frac{p_n qD}{L_p} \left[ \frac{[e^{q\varphi_c/kT} - 1]}{\sinh(2w/L_p)} - \frac{(e^{q\varphi_c/kT} - 1)}{\tanh(2w/L_p)} \right] \\ &= \operatorname{csch}(2w/L_p) I_{p0}(\varphi_c) - \coth(2w/L_p) I_{p0}(\varphi_c) \end{aligned} \quad (5.6)$$



where, by  $I_{j0}(\varphi)$ , we mean the hole current which would flow in the forward direction across either  $J_1$  or  $J_2$  if uninfluenced by the other (i.e. the function of (4.11) or (4.18) and (4.20).) The equation shows that a fraction  $\text{csch}(2w/L_p)$  of the current  $I_{p0}(\varphi_c)$ , which would be injected by  $\varphi_c$  on  $P_1$  in the absence of  $J_2$ , flows into  $P_2$ . The conductance of  $P_2$  across  $J_2$  is increased by the factor  $\coth(2w/L_p)$ .

The current *into*  $P_2$  carried by electrons will be unaffected by  $J_1$  and can be denoted by  $-I_{n0}(\varphi_c)$  the minus sign resulting from the fact that currents *into*  $P_2$  are in the reverse direction. The total current flowing *into*  $P_2$  contains the  $-I_{n0}(\varphi_c)$  and  $-I_{p0}(\varphi_c)$  terms and must cancel the  $+I_{j0}(\varphi_c)$  term for equilibrium. Hence:

$$I_{n0}(\varphi_c) + \coth(2w/L_p) I_{p0}(\varphi_c) = \text{csch}(2w/L_p) I_{j0}(\varphi_c) \quad (5.7)$$

If  $p_n \gg n_p$ , the  $I_{n0}$  term can be neglected compared to  $\coth(2w/L_p) I_{j0}$ . Hence the value of  $\varphi_c$  must satisfy

$$I_{j0}(\varphi_c) = \text{sech}(2w/L_p) I_{j0}(\varphi_c). \quad (5.8)$$

For  $\varphi_c > kT/q$ , the exponential approximation may be used for  $I_{j0}$  in both terms:

$$\varphi_c = \varphi_c - (kT/q) \ln \cosh(2w/L_p), \quad (5.9)$$

so that, if  $(2w/L_p)$  is the order of unity,  $\varphi_c$  should be only about  $(kT/q)$  less than  $\varphi_c$ . For  $(2w/L_p)$  large, we get

$$\varphi_c = \varphi_c - (kT/q) (2w/L_p) \quad (5.10)$$

corresponding to the linear drop of  $\varphi_p$ , discussed in connection with equation (4.9), across the distance  $2w$ .

When  $\varphi_c$  is negative, so that we have to deal with reverse current,  $\varphi_c$  will not decrease indefinitely but will reach a minimum value given by

$$[\exp q\varphi_c/kT] - 1 = -\text{sech}(2w/L_p) \quad (5.11)$$

and corresponding to saturation reverse current across  $J_1$ , so that

$$\varphi_c = -(kT/q) \ln [1 + (1/2) \text{csch}^2(w/L_p)]. \quad (5.12)$$

The floating potentials of *p*-type contacts to *n*-type material into which holes have been injected (or *n*-type contacts to *p*-type material with injected electrons) are reminiscent of probes in gas discharges which tend to become charged negative in respect to the space around them because they catch electrons more easily than positive ions. The situation may also be compared with that producing thermal e.m.f.'s; in fact a "concentration temperature" of the semiconductor with injected holes can be defined by finding the temperature for which  $n_p = n_i^2(T)$ . We conclude that, in the

absence of thermal equilibrium, different potentials depending on the nature of the contact are, in general, the rule rather than the exception.

The bias developed on  $P_2$  or  $c$  will change its conductance. If we suppose that  $\varphi_e$  and  $\varphi_b$  are held constant, then the current flowing into  $c$  is obtained by the same reasoning that led to (5.7) and is

$$I_c(\varphi_c, \varphi_e) = I_{n0}(\varphi_c) + \coth \frac{2\tilde{w}}{L_p} I_{p0}(\varphi_c) - \operatorname{csch} \frac{2\tilde{w}}{L_p} I_{p0}(\varphi_e). \quad (5.13)$$

For an infinitesimal change in  $\varphi_c$  from the value which makes  $I_c(\varphi_c, \varphi_e)$  vanish, the admittance to  $c$  is readily found from (4.18) and (4.19) to be

$$\begin{aligned} \left( \frac{\partial I_c}{\partial \varphi_c} \right)_{\varphi_e} &= I'_{n0}(\varphi_c) + \coth \frac{2\tilde{w}}{L_p} I'_{p0}(\varphi_c) \\ &= \left[ G_{n0} + \coth \frac{2\tilde{w}}{L_p} G_{p0} \right] e^{q\varphi_c/kT} \end{aligned} \quad (5.14)$$

which shows that pronounced variations in admittance should be associated with variations in hole density in  $N$  in Fig. 10.<sup>15</sup>

## 6. $p$ - $n$ - $p$ TRANSISTORS

The structure shown in Fig. 10 is a transistor with power gain provided the distance  $w$  is not too great. As a first approximation, we shall neglect the drop due to currents in the  $N$  region. If we use  $P_2$  as the collector and call the collector current,  $I_c$ , positive when it flows into  $P_2$  from outside, we shall have from (5.13)

$$I_c = -\operatorname{csch} \frac{2\tilde{w}}{L_p} I_{p0}(\varphi_e) + \coth \frac{2\tilde{w}}{L_p} I_{p0}(\varphi_c) + I_{n0}(\varphi_c). \quad (6.1)$$

The emitter current is similarly

$$I_e = \coth \frac{2\tilde{w}}{L_p} I_{p0}(\varphi_e) - \operatorname{csch} \frac{2\tilde{w}}{L_p} I_{p0}(\varphi_c) + I_{n0}(\varphi_e). \quad (6.2)$$

If  $p_n \gg n_p$ , then the  $I_{n0}$  terms can be neglected. However, the base current will not vanish but will be

$$\begin{aligned} I_b &= -I_e - I_c = \left[ \operatorname{csch} \frac{2\tilde{w}}{L_p} - \coth \frac{2\tilde{w}}{L_p} \right] [I_{p0}(\varphi_e) + I_{p0}(\varphi_c)] \\ &= \frac{2 \sinh^2 \tilde{w}/L_p}{\sinh 2\tilde{w}/L_p} [I_{p0}(\varphi_e) + I_{p0}(\varphi_c)]. \end{aligned} \quad (6.3)$$

<sup>15</sup> The variations in admittance discussed in connection with metal point contacts in an accompanying paper in this issue (W. Shockley, G. L. Pearson and J. R. Haynes, *Bell Sys. Tech. J.*, July, 1949), arise from this cause; however, the nature of the contact is not as simple as here.

For  $w/L_p$  large, the junctions do not interact and the hyperbolic coefficient becomes unity and  $I_b = -[I_{p0}(\varphi_e) + I_{p0}(\varphi_c)]$ .

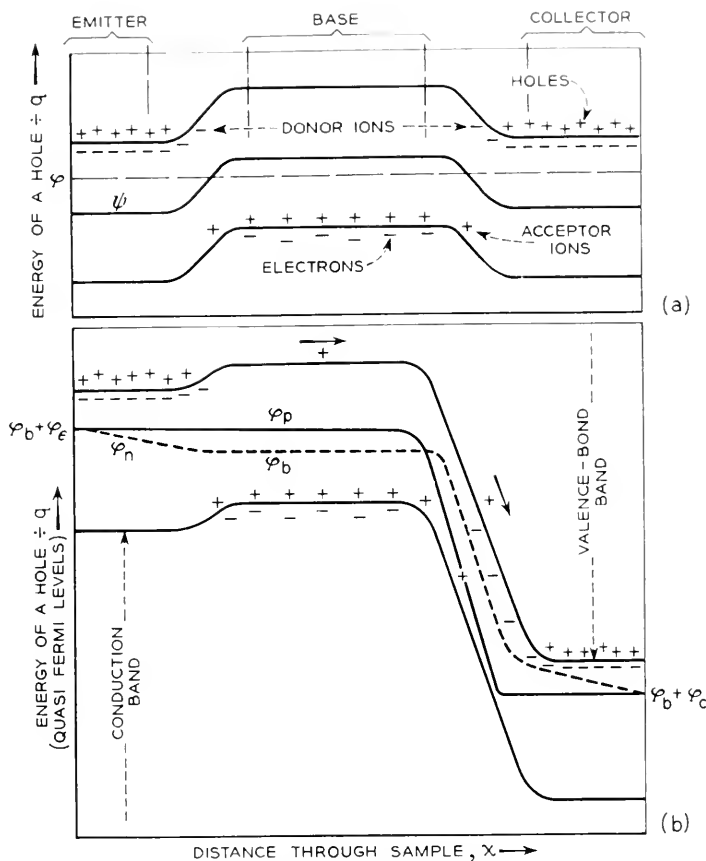


Fig. 11—*p-n-p* transistor.

(a) Thermal equilibrium.

(b) Operating condition.

If  $\varphi_c$  is several volts negative, so that  $I_{p0}(\varphi_c)$  has its saturation value  $I_{ps}$  (see (4.11) and (4.20)), then the ratio  $-\delta I_c / \delta I_e \equiv \alpha$  has the value

$$\alpha = -\frac{\delta I_c}{\delta I_e} = \frac{\operatorname{csch} \frac{2w}{L_p}}{\coth \frac{2w}{L_p}} = \operatorname{sech} \frac{2w}{L_p}. \quad (6.4)$$

For  $(2w/L_p) = 0.5, 1, 2$  respectively,  $\alpha = 0.89, 0.65, 0.27$ . Since the output impedance  $R_{22}$  will be very high when  $\varphi_c$  is in the reverse direction, and the

input impedance will be low, the power gain formula<sup>16</sup>  $\alpha^2 R_{22}/R_{11}$  will yield power gain even when  $\alpha$  is less than unity.

In certain ways the structure of Fig. 10 resembles a vacuum tube. In Fig. 11, we show the energy band diagram, with energies of holes plotted upwards so as to be in accord with the convention for voltages. (a) shows the thermal equilibrium distribution and (b) the distribution under operating conditions. It is seen that the potential hill, which holes must climb in reaching the collector, has been reduced by  $\varphi_e$ . The  $n$ -region represents in a sense the grid region in a vacuum tube, in which the potential and hence plate current, is varied by the charge on the grid wires. Here the potential in the  $n$ -region is varied by the voltage applied between base and emitter. In both cases one current is controlled by another. In the vacuum tube the current which charges the grid wires controls the space current. Because the grid is negative to the cathode, the electrons involved in the space current are kept away from the grid while at the same time the electrons in the grid are kept out of the space by the work function of the grid (provided that the grid does not become overheated.) In Fig. 11, the electrons flowing into the base control the hole current from emitter to collector. In this case the controlled and controlling currents flow in the same space but in different directions because of the opposite signs of their charges.

As this discussion suggests, it may be advantageous to operate the  $p$ - $n$ - $p$  transistor like a grounded cathode vacuum tube, with the emitter grounded and the input applied to the base.

The  $p$ - $n$ - $p$  transistor has the interesting feature of being calculable to a high degree. One can consider such questions as the relative ratios of width to length of the  $n$ -region and the effect of altering impurity contents and scaling the structure to operate in different frequency ranges. However, we shall not pursue these questions of possible applications further here.

#### ACKNOWLEDGMENT

The writer is indebted to a number of his colleagues for stimulating discussions and encouragement, in particular to H. R. Moore, G. L. Pearson and M. Sparks, whose experimental work, to be described in later publications, suggested development of the theory along the lines presented above. He is also indebted to J. Bardeen, P. Debye, G. Wannier and W. van Roosbroeck for theoretical comments and suggestions and especially to the last and to Mrs. G. V. Smith for valuable assistance in preparing the manuscript.

<sup>16</sup> Physical Principles Involved in Transistor Action, J. Bardeen and W. H. Brattain, *Phys. Rev.* 75, 1208 (1949).

# APPENDIX I

## A THEOREM ON JUNCTION RESISTANCE

We shall here prove that the junction resistance is never less than the value obtained by integrating the local resistivity  $1/q\mu(p + bn)$ . This is accomplished by analyzing the following equation which we shall discuss before giving the derivation:

$$I\delta\varphi = \frac{1}{q\mu} \int_{x_a}^{x_b} \left( \frac{I_p^2}{p} + \frac{I_n^2}{bn} \right) dx + qg \int_{x_a}^{x_b} (\varphi_p - \varphi_n) (e^{q(\varphi_p - \varphi_n)/kT} - 1) dx,$$

the meaning of the symbols being that shown in Fig. 5. This expression is valid even if large disturbances in  $p$  and  $n$  from their equilibrium values occur. The second integral is positive since the integrand is never negative. It may be very large if  $\varphi_p - \varphi_n \gg kT/q$  in some regions. If, in the first integral, we consider that  $I_p$  and  $I_n$  may be varied subject to the restraint  $I_p + I_n = I$ , we may readily prove that the first integrand takes on a minimum value when

$$I_p = \frac{pI}{p + bn} \quad \text{and} \quad I_n = \frac{bnI}{p + bn}.$$

For this minimum condition, the first integral becomes

$$I^2 \int_{x_a}^{x_b} dx/q\mu(p + bn) = I^2 R_0$$

where  $R_0$  is simply the integrated local resistivity. If  $I$  does divide in this way, the second integral is zero, a result which we can see as follows:

$$I_p = -q\mu p \, d\varphi_p/dx$$

$$I_n = -q\mu bn \, d\varphi_n/dx$$

$$\frac{d\varphi_p/dx}{d\varphi_n/dx} = \frac{I_p/p}{I_n/bn}$$

Hence, if the current divides in the ratio of  $p$  to  $bn$ , then  $d\varphi_p = d\varphi_n$  and, since  $\varphi_p = \varphi_n$  at  $x_a$ ,  $\varphi_p = \varphi_n$  everywhere and the second integral vanishes.

In general, of course, the conditions governing recombination prevent current division in the ratio  $p:bn$  and then  $\delta\varphi/I > R_0$ .

The equation discussed above is derived as follows: We suppose that

$$\varphi_p(x_a) = \varphi_n(x_a) = \varphi_a$$

$$\varphi_p(x_b) = \varphi_n(x_b) = \varphi_b$$

Then

$$\begin{aligned}
 I\delta\varphi &= -(I_p\varphi_p + I_n\varphi_n) \Big|_{x_a}^{x_b} \\
 &= -\int_{x_a}^{x_b} \frac{d}{dx} (I_p\varphi_p + I_n\varphi_n) dx \\
 &= -\int_{x_a}^{x_b} \left( \frac{dI_p}{dx} \varphi_p + \frac{dI_n}{dx} \varphi_n \right) dx - \int_{x_a}^{x_b} \left( I_p \frac{d\varphi_p}{dx} + I_n \frac{d\varphi_n}{dx} \right) dx.
 \end{aligned}$$

Since

$$\frac{dI_p}{dx} = -\frac{dI_n}{dx} = qg(1 - e^{q(\varphi_p - \varphi_n)/kT})$$

and

$$\frac{d\varphi_p}{dx} = -I_p/q\mu p, \quad \frac{d\varphi_n}{dx} = -I_n/q\mu n$$

these two integrals are readily transformed into the ones previously discussed.

## APPENDIX II

### ADMITTANCE IN A RETARDING FIELD

We shall here derive the admittance equation for holes diffusing into a retarding potential  $\psi = kTx/L_r$  in which the potential increases by  $kT$  in each distance  $L_r$ . The differential equation for the a-c. component of  $p$  is

$$i\omega p = -\frac{p}{\tau_p} - \frac{\partial}{\partial x} \left[ -D \frac{\partial p}{\partial x} - \mu p \frac{\partial \psi}{\partial x} \right].$$

This equation may be solved by letting  $p = p_1 \exp(i\omega t - \gamma x)$  as may be seen by rewriting the equation and substituting this expression for  $p$ :

$$\begin{aligned}
 D \left[ \frac{\partial^2 p}{\partial x^2} + \frac{1}{L_r} \frac{\partial p}{\partial x} \right] - \frac{1}{\tau_p} (1 + i\omega\tau_p) p \\
 = -\gamma D \left[ -\gamma + \frac{1}{L_r} \right] p - \frac{1}{\tau_p} (1 + i\omega\tau_p) p = 0
 \end{aligned}$$

leading to

$$\gamma = \frac{1 + [1 + (2L_r/L_p)^2(1 + i\omega\tau_p)]^{1/2}}{2L_r}.$$

The corresponding current evaluated at  $x = 0$  where  $p = p_1 \exp(i\omega t) = (p_n q \tau_1 / kT) \exp(i\omega t)$  is given by

$$\begin{aligned} I &= -q \left[ D \frac{\partial p}{\partial x} + \mu p \frac{\partial \psi}{\partial x} \right] \\ &= -qD \left[ -\gamma + \frac{1}{L_r} \right] p \\ &= \frac{q(1 + i\omega\tau_p)}{\gamma\tau_p} p \\ &= \frac{p_n q^2 (1 + i\omega\tau_1)}{kT\tau_p} \cdot \frac{2L_r}{1 + [1 + (2L_r/L_p)^2 (1 + i\omega\tau_p)]^{1/2}} \cdot \tau_1 e^{i\omega t} \\ &= \frac{q\mu p_n 2L_r}{L_p^2} \cdot \frac{(1 + i\omega\tau_p)}{1 + [1 + (2L_r/L_p)^2 (1 + i\omega\tau_p)]^{1/2}} \cdot \tau_1 e^{i\omega t} \\ &= A_p \tau_1 e^{i\omega t}. \end{aligned}$$

This is equivalent to (4.32) in Section 4.

### APPENDIX III

#### ADMITTANCE FOR TWO LAYERS

We shall here treat a case in which there is a thin layer on the  $n$ -side of the transition region in which recombination occurs much more readily than deeper in the  $n$ -layer. The case of an infinitely thin plane, discussed in Section 4, is a limiting case of this model. We shall suppose that the layer extends from  $x = -c$  to  $x = 0$  while  $x > 0$  corresponds to the  $n$ -region. We shall suppose that the potential in the layer is uniform with value  $\psi_1$  whereas in the  $n$ -region it has value  $\psi_2$ . The lifetimes of holes will be taken  $\tau_1$  and  $\tau_2$  in the two layers. The solutions for  $p_1$  and  $p_2$  are evidently

$$\begin{aligned} p_1 &= p_{10} + (A e^{-\alpha x} + B e^{+\alpha x}) e^{i\omega t} & x < 0 \\ p_2 &= p_{20} + C e^{-\beta x + i\omega t} & x > 0 \end{aligned}$$

where

$$\begin{aligned} \alpha &= (1 + i\omega\tau_1)^{1/2} / \sqrt{D\tau_1} \equiv (1 + i\omega\tau_1)^{1/2} / L_1 \\ \beta &= (1 + i\omega\tau_2)^{1/2} / \sqrt{D\tau_2} \equiv (1 + i\omega\tau_2)^{1/2} / L_2. \end{aligned}$$

The boundary condition for continuity of  $\varphi_p$ , required to avoid singularity in  $\partial\varphi_p/\partial x$ , is

$$p_2 e^{q\psi_2/kT} = p_1 e^{q\psi_1/kT}$$

and, for continuity of hole current, is  $\partial p_1/\partial x = \partial p_2/\partial x$ . Expressing these in terms of  $A$ ,  $B$ ,  $C$ ,  $\alpha$  and  $\beta$  for the a-c. components yields:

$$A + B = C e^{q(\psi_1 - \psi_2)/kT} \equiv CF$$

$$\alpha(A - B) = \beta C$$

so that

$$A = (F + \beta/\alpha)C/2.$$

$$B = (F - \beta/\alpha)C/2.$$

Hence the ratio  $-\partial p/\partial x/p$  at  $x = -c$  is

$$-\frac{\partial \ln p}{\partial x} = \frac{\alpha(A e^{+\alpha c} - B e^{-\alpha c})}{(A e^{+\alpha c} + B e^{-\alpha c})} = \frac{\alpha(F\alpha \sinh \alpha c + \beta \cosh \alpha c)}{F\alpha \cosh \alpha c + \beta \sinh \alpha c}.$$

Since at  $x = -c$ , the a-c. component of  $p_1$  is  $(q\tau_1/kT)p_{10}e^{i\omega t}$ , the admittance is

$$\begin{aligned} A_p &= \frac{-qD\partial p/\partial x}{v_1 e^{i\omega t}} = (q^2 D p_{10}/kT)(-\partial \ln p/\partial x) \\ &= (q\mu p_{10}/L_1)(1 + i\omega\tau_1)^{1/2} \frac{F\alpha \sinh \alpha c + \beta \cosh \alpha c}{F\alpha \cosh \alpha c + \beta \sinh \alpha c}. \end{aligned}$$

For  $c \rightarrow 0$ , this transforms into

$$(q\mu p_{10}/L_1)(1 + i\omega\tau_1)^{1/2}\beta/F\alpha = (q\mu(p_{10}/F)/L_2)(1 + i\omega\tau_2)^{1/2}$$

which agrees with Section 4, since  $p_{10}/F$  then corresponds to  $p_n$ .

If  $c/L_1$  and  $F$  are not large, an appreciable amount of recombination takes place for  $x > 0$  for low frequencies. Dispersive effects will then occur corresponding to  $\tau_2$ . The a-c. will not penetrate to  $x = 0$ , however, if  $c(\omega/D)^{1/2} \gg 1$  and the dispersive effects will then be determined by  $\tau_1$ .

The frequency-dependent part of the admittance,

$$(1 + i\omega\tau_1) \frac{F\alpha \sinh \alpha c + \beta \cosh \alpha c}{F\alpha \cosh \alpha c + \beta \sinh \alpha c},$$

has been computed and is shown in Fig. 7 for  $\tau_p = \tau_2$ ,  $F = 1$ ,  $\tau_1 = \tau_2/9$  and  $c/L_1 = \frac{1}{3}$ . For these values about half the hole current reaches  $x = 0$  for low frequencies. As the time constant for diffusion through the layer is  $\tau_p/81$ , as discussed in Section 4.6, the layer will act as a largely frequency-independent admittance well above the point for  $\omega\tau_p = 1$ . This is reflected in the behavior of the curves of Fig. 7 and, for frequencies in the  $\sqrt{\omega t}$  range, it is seen that  $G$  is larger than  $S$  by about 50% of the low-frequency value of  $G$ ; this split of  $G + iS$  into  $(\frac{1}{2})G_0$  plus approximately  $(\frac{1}{2})G_0(1 + i\omega\tau_p)^{1/2}$  corresponds to the fact that about half the holes are absorbed in layer 1 for the assumed conditions.



## APPENDIX IV

### TIME CONSTANT FOR THE CAPACITY OF THE TRANSITION REGION

For this case we shall consider the case of holes in an a-c. field with potential

$$\psi = \frac{kT}{q} \left( \frac{x}{L_r} + \frac{x e^{i\omega t}}{L_1} \right)$$

where the d-c. retarding field is  $kT/qL_r$  and the a-c. field is  $kT/qL_1$  where  $1/L_1$  is considered small for the linear theory presented here. The expression for the current of holes is

$$-D \frac{\partial p}{\partial x} - \mu p \frac{\partial \psi}{\partial x} = -D \left[ \frac{\partial p}{\partial x} + p \left( \frac{1}{L_r} + \frac{e^{i\omega t}}{L_1} \right) \right]$$

We shall obtain a solution for  $p$  by letting

$$p = p_0 e^{-x/L_r} + p_1 [e^{-x/L_r} - e^{-\gamma x}] e^{i\omega t},$$

while neglecting recombination in this region so that  $p$  must satisfy the condition  $\dot{p} = -\partial$  (hole current)/ $\partial x$  leading to the differential equation

$$D \left[ \frac{\partial^2 p}{\partial x^2} + \frac{\partial p}{\partial x} \left( \frac{1}{L_r} + \frac{e^{i\omega t}}{L_1} \right) \right] - \dot{p} = 0$$

There are three separate exponential dependencies of the variables leading to three equations (neglecting terms of order  $(1/L_1)^2$ )

$$\begin{aligned} e^{-x/L_r}: \quad & D \left[ p_0 \frac{1}{L_r^2} - p_0 \frac{1}{L_r^2} \right] = 0 \\ e^{-x/L_r + i\omega t}: \quad & D \left[ p_1 \frac{1}{L_r^2} - p_1 \frac{1}{L_r^2} - \frac{1}{L_r L_1} p_0 \right] - i\omega p_1 = 0 \\ e^{-\gamma x + i\omega t}: \quad & D[\gamma^2 - \gamma/L_r] p_1 - i\omega p_1 = 0 \end{aligned}$$

The first equation is satisfied by the equilibrium distribution and the second by

$$p_1 = -p_0 D i\omega L_1 L_r$$

and the last by

$$\gamma = \frac{1 + \sqrt{1 + 4i\omega L_r^2/D}}{2L_r}$$

It is evident that dispersive effects set in when

$$\omega = D/4L_r^2$$

This corresponds to the result used in (4.31) in which  $(x_{Tn} - x_{Tp})/10$  was used for  $L_r$ . For smaller values of  $\omega$  the current may be calculated and put in simple form by expanding  $\gamma$  up to terms including  $\omega^2$ . The resulting expression for the current is

$$I = -i\omega q p_0 L_r (L_r + L_1) e^{i\omega t}$$

This is interpreted as follows: The a-c. voltage across a layer  $L_r$  thick is

$$\delta\psi = (kT/q) (L_r + L_1) e^{i\omega t}$$

and, if we consider plus voltage as producing a field from left to right, then the a-c. voltage across  $L_r$  is  $V = -\delta\psi$ . Substituting this for  $(L_r + L_1)\exp(i\omega t)$  gives

$$I = i\omega q p_0 L_r (q/kT) V$$

Here  $qp_0L_r$  is the total charge in the layer  $L_r$ ,  $(qV/kT)$  is an average fractional change in this charge for  $V$  so that  $(qp_0L_r)(qV/kT) \div V$  is a capacity.

## APPENDIX V

### THE EFFECT OF SURFACE RECOMBINATION

In this appendix we shall consider the effect of surface recombination upon the characteristics of the  $p$ - $n$  junction. As for Section 4 we shall illustrate the theory for the case of holes diffusing into  $n$ -type material. For simplicity we shall treat a square cross-section bounded by  $y = \pm w$ ,  $z = \pm w$ , the current flow being along  $+x$ .

We shall denote the a-c. component of  $p$  as

$$p_1 \equiv p_1(x, y, z, t)$$

At  $x = 0$ , the edge of the  $n$ -region, we shall suppose that  $\varphi_p$  and  $\psi$  are independent of  $y$  and  $z$  so that we shall have

$$p_1(0, y, z, t) = p_{10} e^{i\omega t} = (p_n q\tau_1/kT) e^{i\omega t}$$

by reasoning similar to that used for equation (4.5). The boundary condition at the surface will be

$$-D \frac{\partial p_1}{\partial y} = sp_1 \quad \text{for } y = +w$$

This states that the recombination per unit area is  $sp_1$  and is equal to the diffusion to the surface  $-D\partial p_1/\partial y$ . Similar boundary conditions hold for the other surfaces. By standard procedures involving separation of variables we may verify that the solution satisfying the boundary conditions is

$$p_1 = \sum_{i,j=0}^{\infty} a_{ij} e^{-\alpha_{ij}x + i\omega t} \cos \beta_i y \cos \beta_j z$$

where the eigenvalues  $\beta_i$  are determined by the boundary condition

$$\beta_i w \tan \beta_i w = sb'/D \equiv \chi.$$

We use  $\theta_i = \beta_i w$  for brevity later. Because of the symmetry of the boundary conditions it is not necessary to include sine functions in the sum. The value of  $\alpha_{ij}$  is given by

$$\alpha_{ij} = (1 + i\omega\tau_{ij})^{1/2}/(D\tau_{ij})^{1/2}$$

where  $\tau_{ij}$  is the lifetime of a hole in the eigenfunction  $\cos \beta_i y \cos \beta_j z$ ; i.e.  $\tau_{ij}$  is the lifetime which makes

$$p = \exp(-l/\tau_{ij}) \cos \beta_i y \cos \beta_j z,$$

a function which satisfies the surface boundary conditions, a solution of the equation

$$\partial p_i / \partial t = D \nabla^2 p - p_i / \tau = -D(\beta_i^2 + \beta_j^2)p - p_i / \tau$$

where to simplify the subsequent expressions we have omitted the subscript  $p$  from  $\tau$ . This equation leads to

$$\frac{1}{\tau_{ij}} = D(\beta_i^2 + \beta_j^2) + \frac{1}{\tau}.$$

The coefficients  $a_{ij}$  are readily found since the  $\cos \beta_i y$  functions form an orthogonal set (as may be verified by integrating by parts and using the boundary conditions). The values are

$$a_{ij}/p_{10} = 4[\sin \theta_i \sin \theta_j]^{-1} \theta_j [1 + (1/2\theta_i) \sin 2\theta_i] \cdot [1 + (1/2\theta_j) \sin 2\theta_j]$$

The current corresponding to this solution is

$$I_1 = -qD \iint (\partial p_i / \partial x) dy dz$$

integrated over the cross section at  $x = 0$ . This gives

$$I_1 = qDp_{10}e^{i\omega t} \sum \alpha_{ij}(a_{ij}/p_{10})(4w^2 \theta_i \theta_j) \sin \theta_i \sin \theta_j$$

Substituting for  $a_{ij}$  and inserting  $p_{10} = p_n q v_1 / kT$ , we obtain an expression for the admittance  $A_p = I_1/V_1 \exp(i\omega t)$ :

$$A_p = 4w^2 q \mu p_n \sum_{ij} \alpha_{ij} \frac{4 \sin^2 \theta_i \sin^2 \theta_j}{\theta_i^2 \theta_j^2} \left[ 1 + \left( \frac{1}{2\theta_i} \right) \sin 2\theta_i \right] \left[ 1 + \left( \frac{1}{2\theta_j} \right) \sin 2\theta_j \right]$$

where the sum plays the role formerly taken by  $(1 + i\omega\tau)^{1/2}/\sqrt{D\tau}$  in equation (4.12); the factor  $4w^2$  is the area of the junction.

We shall analyze the formula for the case in which recombination on the

surface is smaller than diffusion to the surface so that  $\chi$  is not large. The values of  $\theta_i$ , over which the sum is to be taken, may be estimated as follows: in each interval of  $\theta_i$  of the form  $n\pi$  to  $(n + (\frac{1}{2}))\pi$ ,  $\theta_i \tan \theta_i$  varies from 0 to  $\infty$ , giving one solution to  $\theta_i \tan \theta_i = \chi$ . For  $\chi$  small, the solutions are approximately

$$\begin{aligned}\theta_0 &\doteq \sin \theta_0 \doteq \tan \theta_0 \doteq \sqrt{\chi} \\ \theta_1 &\doteq \pi + \chi/\pi; \quad -\sin \theta_1 \doteq \tan \theta_1 \doteq \chi/\pi \\ &\quad \dots \quad \dots \quad \dots \\ \theta_n &\doteq n\pi + \chi/n\pi; \quad (-1)^n \sin \theta_n \doteq \tan \theta_n \doteq \chi/n\pi\end{aligned}$$

From this we see that the terms in the sum are as follows:

$$\begin{aligned}\alpha_{00} \cdot 4\chi^2/\chi^2 &= \alpha_{00} \\ \alpha_{n0} \cdot 2(\chi/n\pi)^2/(n\pi)^2 &= \alpha_{n0} 2\chi^2/n^4\pi^4 \\ \alpha_{nm} \cdot 4\chi^4/n^4m^4\pi^8\end{aligned}$$

From this it is evident that unless  $\chi$  is large, the series converges very rapidly. (This conclusion is not altered when the increase in  $\alpha_{nm}$  with  $\beta_n\beta_m$  is considered.) Thus the dominant term in the admittance is

$$4\omega^2 q\mu f_0 (1 + i\omega\tau_{00})^{1/2}/\sqrt{D\tau_{00}}$$

where

$$\begin{aligned}1/\tau_{00} &= 2 \left( \frac{L}{\omega^2} \right) (\theta_0^2) + 1/\tau \\ &\doteq 2 \left( \frac{L}{\omega^2} \right) \frac{s\omega}{D} + 1/\tau \\ &= 2 \left( \frac{s}{\omega} \right) + 1/\tau\end{aligned}$$

This expression is valid only for  $s\omega/D$  small so that  $\theta_0^2 \doteq s\omega/D$ . The term  $s/(\omega/2)$  represents the rate of decay due to holes recombining on the surface,  $s$  having the dimensions of velocity. For  $\omega \gg 1/\tau_{00}$ , the admittance becomes  $4\omega^2 q\mu f_0 (i\omega/D)^{1/2}$ , the same value as given in equation (4.12) for large  $\omega$  and an area  $4\omega^2$ .

The conclusion from this appendix is that for  $\chi$  small, the effect of surface recombination is simply to modify the effective value of  $\tau$  and otherwise leave the theory of Section 4 unaltered.

For very large values of  $\chi$ , it is necessary to consider higher terms in the sum and several values of  $\tau$  will be important. Under these conditions the

approximation is that, at  $x = 0$ ,  $p_1$  is independent of  $x$  and  $y$  may become a poor one, especially for forward currents, because the transverse currents to the edges will be important. Under these conditions the role of surface recombination will give rise to patch effects of the sort discussed in Section 4.

## APPENDIX VI

### THE EFFECT OF TRAPPING UPON THE DIFFUSION PROCESS

In this appendix we shall investigate the effect of the trapping of holes upon the impedance. We denote the density of mobile holes in the valence-band band by  $p$  and the density of holes trapped in acceptors by  $p_a$ . For thermal equilibrium at room temperature there will be an equilibrium ratio, called  $\alpha$ , for  $p_a/p$ . For germanium  $\alpha \doteq 10^{-4}$  and for silicon  $\alpha \doteq 0.1$  to  $0.2$ .

We shall consider four processes which occur at rates (per particle per unit time) as follows:

$\nu_r$  direct recombination of a hole with an electron (free or bound to a donor)

$\nu_t$  trapping of a hole by an acceptor

$\nu_{ra}$  recombination of a hole trapped on an acceptor

$\nu_e$  excitation of a trapped hole into the valence-band band.

Under equilibrium conditions as many holes are being trapped (rate  $p\nu_t$ ) as are being excited ( $p_a\nu_e$ ): hence  $\nu_t = \alpha\nu_e$ .

We shall study solutions of the customary form for the a-c. components:

$$p_1 = p_{10} e^{i\omega t - \gamma x}$$

$$p_{1a} = p_{1a0} e^{i\omega t - \gamma x}$$

These must satisfy the equations

$$\dot{p}_1 = D\nabla^2 p_1 - (\nu_t + \nu_r)p_1 + \nu_e p_{1a}$$

$$\dot{p}_{1a} = \nu_t p_1 - (\nu_e + \nu_{ra})p_{1a}$$

These lead readily to the equation for  $\gamma$ :

$$D\gamma^2 = i\omega + \nu_r + \nu_t - \nu_e \nu_t / (i\omega + \nu_e + \nu_{ra}) = i\omega \cdot \left[ 1 + \frac{\nu_e \nu_t}{(\nu_e + \nu_{ra})^2 + \omega^2} \right] + \nu_r + \nu_t \left[ 1 - \frac{\nu_e}{(\nu_e + \nu_{ra}) + \omega^2 / (\nu_e + \nu_{ra})} \right]$$

From this equation we can directly reach the important conclusion that the trapping process can never lead to a capacitive term larger than the resistive term. This result is obtained by analyzing the complex phase of  $\gamma$ , the admittance being proportional to  $\gamma$ . In particular, we find that the real term in  $D\gamma^2$  is always positive, as may be seen from inspection, so that the complex phase angle of  $\gamma$  is less than  $45^\circ$ .

The form reduces to a simple expression if  $\nu_e$  and  $\nu_t$  are very large com-

pared to  $\nu_r$ ,  $\nu_{ra}$  and  $\omega$ , a situation which insures local equilibrium between  $p$  and  $p_a$ . Under these conditions we obtain

$$D\gamma^2 = i\omega[1 + \alpha] + \nu_r + \alpha\nu_{ra}$$

Dividing by  $(1 + \alpha)$  gives

$$[D/(1 + \alpha)]\gamma^2 = [Dp/(p + p_a)]\gamma^2 = i\omega + \frac{p\nu_r + p_a\nu_{ra}}{p + p_a}$$

The interpretation is that the holes diffuse as if their diffusion constant were reduced by the fraction of the time  $p/(p + p_a)$  they are free to move and recombine with a properly weighted average of  $\nu_r$  and  $\nu_{ra}$ .

## APPENDIX VII

### SOLUTIONS OF THE SPACE CHARGE EQUATION

We shall first show that the space charge equation (2.11) has a unique solution for the one dimensional case. For simplicity we write (2.11) in the form

$$\frac{d^2u}{dx^2} = \sinh u - f(x) \quad (\text{A7.1})$$

to which it can be readily reduced. We shall deal with the case for which

$$f = f_a \text{ for } x < x_a \quad (\text{A7.2})$$

$$f = f_b \text{ for } x > x_b > x_a \quad (\text{A7.3})$$

so that the interval  $(x_a, x_b)$  is bounded by semi-infinite blocks of uniform semiconductor. We shall require that  $u$  be finite at  $x = \pm \infty$ . This boundary condition requires that for large values of  $|x|$

$$u = u_a + A_a e^{+\gamma_a x} \quad x \rightarrow -\infty \quad (\text{A7.4})$$

$$u = u_b + A_b e^{-\gamma_b x} \quad x \rightarrow +\infty \quad (\text{A7.5})$$

where

$$\sinh u_a = f_a, \quad \sinh u_b = f_b$$

$$\gamma_a = [(\cosh u_a)^{1/2}]^2, \quad \gamma_b = [(\cosh u_b)^{1/2}]^2$$

(If the opposite signs of the  $\gamma$ 's were present, the boundary conditions would not be satisfied.) The exponential solutions are valid for  $|u - u_a|$  or  $|u - u_b| \ll 1$ . For larger values, however, solutions exist which are obtained by integrating (A7.1) to larger or smaller values of  $x$ .

For these extended solutions the values of  $u(x, A_a)$  and  $u'(x, A_a) (= du/dx)$

are monotonically increasing functions of  $A_a$ . This may be seen by considering  $x = x_a$ . For  $A_a$  sufficiently small, the value of  $u(x_a, A_a)$  and  $u'(x_a, A_a)$  are given simply by (A7.4). For larger values of  $A_a$ , an exact integral will be required. It is evident, however, that all solutions of the form (A7.4) are related simply by translation for  $x < x_a$ . Hence increasing  $A_a$  is simply equivalent to integrating (A7.1) to larger values of  $x$  and it is evident that this increases  $u$  and  $u'$  monotonically. It may be verified that for a sufficiently large  $A_a$  the solution becomes infinite at  $x_a$  so that  $u(x_a, A_a)$  and  $u'(x_a, A_a)$  both vary monotonically and continuously from  $-\infty$  to  $+\infty$  as  $A_a$  varies from negative to positive values. We shall refer to this property of  $u(x_a, A_a)$ ,  $u'(x_a, A_a)$  as  $P_1$ .

We next wish to show that  $u(x_1, A_a)$ ,  $u'(x_1, A_a)$  has the property  $P_1$  for values of  $x_1 > x_a$ . To prove this we note that if for any  $x_1$ ,  $u(x_1, A_a)$  and  $u'(x_1, A_a)$  are finite, the solution may be integrated somewhat further to obtain  $u(x_2, A_a)$ ,  $u'(x_2, A_a)$  for  $x_2 > x_1$ . From equation (A7.1) it is evident that an increase in either  $u(x_1, a)$  or  $u'(x_1, a)$  will result in an increase in  $d^2u/dx^2$  in the interval  $x_1 < x < x_2$  so that  $u$  and  $u'$  at  $x_2$  are monotonically increasing functions of  $u$  and  $u'$  at  $x_1$ . Hence if  $u$  and  $u'$  at  $x_1$  have the property  $P_1$ , so do  $u$  and  $u'$  at  $x_2$ . By extending this argument we conclude that  $u$  and  $u'$  at any value of  $x$  have the property  $P_1$ . (A rigorous proof can easily be completed along these lines provided that  $|f(x)|$  is finite.)

Similarly it may be shown, starting from (A7.5), that  $u(x, A_b)$  is a monotonically increasing function of  $A_b$  and  $u'(x, A_b)$  is a monotonically decreasing function of  $A_b$ .

In order to have a solution satisfying (A7.4) and (A7.5) we must have, for any selected point  $x$ ,

$$u(x, A_a) = u(x, A_b) \quad (\text{A7.6})$$

$$u'(x, A_a) = u'(x, A_b) \quad (\text{A7.7})$$

Now as the equation  $u(x, A_a) = u(x, A_b)$  varies from  $-\infty$  to  $+\infty$ ,  $u'(x, A_a)$  varies from  $-\infty$  to  $+\infty$  and  $u'(x, A_b)$  varies from  $+\infty$  to  $-\infty$ , monotonically and continuously. Hence there is one and only one solution of (A7.1) satisfying (A7.4) and (A7.5).

In order to verify that the solutions discussed in Section 2 are correct for large and for small  $K$ , we show schematically in Fig. A1 the solution for a representative  $K$  as a dashed line together with the curve  $u = u_0(y) = \sinh^{-1} y$ . In terms of  $u_0$ , equation (2.16) becomes

$$\frac{d^2u}{dy^2} = \frac{1}{K^2} (\sinh u - \sinh u_0). \quad (\text{A7.8})$$

From the symmetry of the equation, it is evident that  $u$  must be an odd function of  $y$  and hence that the solution must pass through the origin. The boundary condition in this case will be that  $u \rightarrow u_0$  for  $y \rightarrow \pm \infty$  so that there will be no space charge far from the junction. We can conveniently use the origin as the point at which the solution from  $y = +\infty$  joins that from  $y = -\infty$ ; from symmetry, this requires merely that  $u = 0$  when  $y = 0$ .

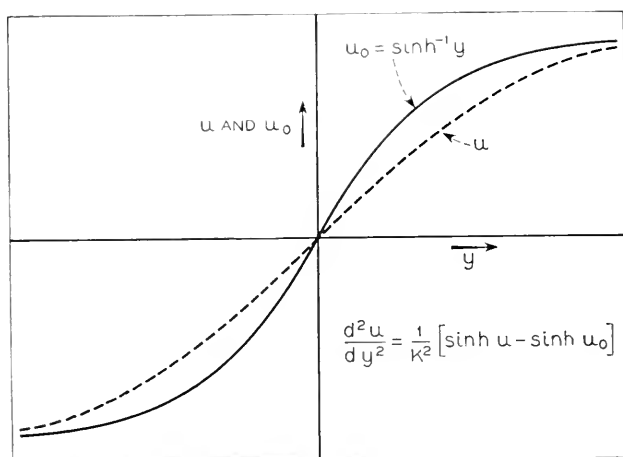


Fig. A1—Behavior of the solution of Equation (2.16) or (A7.8).

For large negative  $y$ ,  $u = \sinh^{-1} y$  and  $du/dy = 1/\cosh u_0$  so that  $du/dy$  is small. It is at once evident that, for large values of  $K$ ,  $u$  must lie above  $u_0$  so that the integral

$$(1/K^2) \int_{-\infty}^y (\sinh u - \sinh u_0) dy = \frac{du}{dy} \quad (\text{A7.9})$$

will be large enough to make the solution  $u(y)$  pass through the origin. If  $u - u_0 > 2$  over the region of largest difference, the space charge will be largely uncompensated and the solution will correspond to that used in equation (2.18). On the other hand, as  $K \rightarrow 0$ , the requirement that  $u(y)$  pass through the origin leads to the conclusion that  $u - u_0$  must be small for all values of  $y$ . The possibility that  $u$  oscillates about  $u_0$  need not be considered since it may readily be seen that, if for any negative value of  $y$ , say  $y_1$ , both  $u(y_1)$  and  $u'(y_1)$  are less than  $u_0(y_1)$  and  $u'_0(y_1)$ , then  $u(y)$  and  $u'(y)$  are progressively less than  $u_0(y)$  and  $u'_0(y)$  as  $y$  increases from  $y_1$  to 0. Hence, if for negative  $y$  the  $u$  curve goes below the  $u_0$  curve, it cannot pass through the origin.



# APPENDIX VIII

## LIST OF SYMBOLS

(Numbers in parentheses refer to equations)

- $a = (N_d - N_a)/x$  (2.14)
- $A$  = admittance per unit area of junction (4.23)
- $A_p$  = component of  $A$  due to hole flow into  $n$ -region (4.12) (4.24)
- $A_n$  = component of  $A$  due to electron flow into  $p$ -region (4.25)
- $A_T$  = component of  $A$  due to varying charge distribution in transition region
- $A$  also used as a constant coefficient in various appendices
- $b$  = ratio of electron mobility to hole mobility
- $b$  = symbol for base in Sections 5 and 6
- $B$  constant coefficient in various expansions in appendices
- $c$  = symbol for collector in Section 6; a length in Appendix III
- $C$  = capacity per unit area
- $C_n, C_p$  (4.25) (4.27) as for  $A_n, A_p$
- $C_T$  (2.42) (2.45) (2.56) as for  $A_T$
- $D$  = diffusion constant for holes ( $bD$  is the diffusion constant for electrons)
- $e = 2.718 \dots$
- $f$  see Appendix 7
- $g$  = rate of generation of hole-electron pairs per unit volume (3.1)
- $G$  = conductance per unit area of junction
- $G_n, G_p$  as for  $A$ 's
- $i = \sqrt{-1}$
- $I$  = current density
- $I_n, I_p$  = current densities due to electrons and holes (2.5) (2.6) (4.10)
- $I_{n0}, I_{p0}, I_{p1}$  (4.11) (4.12) (4.18) (4.19)
- $I_s, I_{ns}, I_{ps}$  saturation reverse current densities (4.11) (4.18) (4.21)
- $I_r$  see text with (4.35)
- $J$  = subscript in Section 3 for junction Fig. 5 equation (3.11)
- $k$  = Boltzmann's constant
- $K$  = space charge parameter (2.17)
- $L$  = length
- $L_a = n_i/a$  (2.15)
- $L_D$  = Debye length (2.12)
- $L_n, L_p$  = diffusion lengths for electron in  $p$ -region and holes in  $n$ -region (4.8)
- $L_r$  = length required for potential increase of  $kT/q$  in region of constant field (4.32) Appendices II and IV
- $L_1$  corresponds to a-c. field, Appendix IV
- $n$  = density of electrons

$n_n, n_p$  = equilibrium densities of electrons in  $n$ - and  $p$ -regions

$p$  = density of holes

$p_n, p_p$  = equilibrium densities of holes in  $n$ - and  $p$ -regions

$p_0$  = d-c. component of non-equilibrium hole density (4.3)

$p_1 \exp(i\omega t)$  = a-c. component of non-equilibrium hole density (4.3)

$P$  = total number per unit area of holes in specimen (2.35)

$q$  = electronic charge ( $q = |q|$ )

$Q = qP$  = total charge per unit area (2.39)

$r$  = recombination coefficient for holes and electrons (3.1)

$R$  = resistance of unit area

$R_0$  = resistance of unit area obtained by integrating conductivity (3.10),  
Appendix I

$R_1$  = effective series resistance, discussed in connection with (3.13)

$s$  = rate of recombination per unit area of surface per unit hole density,  
Appendix V

$S$  = susceptance per unit area (imaginary part of admittance)

$S_p, S_n, S_T$  as for  $I$ 's.

$t$  = time

$T$  = temperature in  $^{\circ}K$

$T$  = subscript for transition region

$u = q\psi/kT$  (2.9),  $q(\psi - \varphi_1)/kT$  (2.32), Appendix VII

$v_0$  and  $v_1 e^{i\omega t}$  = d-c. and a-c. components of voltage applied in forward direction (4.2)

$W$  = width of space charge region in abrupt junction, Section 2.4

$w$  = half thickness of  $n$ -region or transistor base of Sections 5 and 6.

$\bar{w}$  = half width of square rod in Appendix V.

$x$  = coordinate perpendicular to plane of junction

$y, z$  = transverse coordinates, Appendix V

$y$  = reduced length (2.17), Appendix VII

$\alpha$  = current gain factor in transistor (6.4)

$\alpha$  = parameter in Appendix III and VI

$\alpha_{ij}$  = parameter in Appendix V

$\beta_i$  = parameter in Appendix V

$\gamma$  = parameter in Appendices II, IV and VII

$\epsilon$  = symbol for emitter Section 6

$\theta_i = \beta_i w$  Appendix V

$\kappa$  = dielectric constant

$\mu$  = mobility of a hole ( $b\mu$  = mobility of electron)

$\nu$  = rates of recombination etc., Appendix VI

$\rho$  = charge density (2.1)

$\sigma$  = conductivity

$\sigma_i$  = conductivity of intrinsic material (4.15)

$\sigma_n$  = conductivity of  $n$ -region  $\doteq qb\mu n_n$

$\sigma_p$  = conductivity of  $p$ -region  $\doteq q\mu p_p$

$\tau$  = time

$\tau_n, \tau_p$  = life times of electrons in  $p$ -region and holes in  $n$ -region (3.2) (3.3)  
(4.7)

$\tau_T$  = relaxation time of transition region, Appendix IV

$\varphi, \varphi_p, \varphi_n$  = Fermi level and quasi Fermi levels (2.2) (2.4)

$\delta\varphi$  = applied voltage across specimen in forward direction, Section 2.3,  
(4.2)

$\chi = s\omega, D$  in Appendix V

$\psi$  = electrostatic potential (2.2)

$\omega$  = circular frequency of a-c. (4.2)

# Band Width and Transmission Performance

By C. B. FELDMAN and W. R. BENNETT

In modern communication theory band width plays an important role as a transmission parameter. The authors discuss the significance of signal band width and frequency occupancy in relation to other transmission factors such as power, noise, interference, and overall performance for certain specific multiplex systems under assumed operating conditions. The intent of the paper is to show how such problems may be attacked rather than to find an unequivocally best system.

The scope of the paper is described by the following table of Headings and Captions.

## I. INTRODUCTION

- Fig. 1. Outline of multiplex transmission methods
- 1. Non-simultaneous Load Advantage in FDM
- Table I. Non-Simultaneous Multiplex Load Advantage
- 2. Instantaneous Companding Advantage in Time Division
- Fig. 2. Performance of an experimental instantaneous compander
- 3. Non-simultaneous Load Advantage in Pulse Transmission
- Fig. 3. Quantizing noise in each channel when PCM is applied to an FDM group
- 4. Signal Band Width and Frequency Occupancy
- 5. Regeneration and Re-Shaping
- 6. The Radio Repeater
- Fig. 4. Arrangement of two-way two-frequency repeater of television type showing spacing of bands and antenna discrimination
- Fig. 5. Discrimination of I.F. and R.F. circuits in television type repeater

## II. BAND WIDTH CHARACTERISTICS

- Fig. 6. Basic pulse shape and its spectrum
- Fig. 7. Marginal condition in reception of AM pulses and an FM wave in presence of noise.
- Fig. 8. Time allotments in Pulse Position Modulation
- Fig. 9. PPM-AM; fluctuation noise. Relations between band width, power, and signal-to-noise ratio.
- Fig. 10. PPM-AM; CW and similar system interference. Relations between band width and signal-to-interference ratio.
- Fig. 11. PPM-FM; fluctuation noise
- Fig. 12. PPM-FM; CW and similar system interference
- Fig. 13. PAM-FM; fluctuation noise
- Fig. 14. PAM-FM; CW and similar system interference
- Fig. 15. PCM-AM; peak interference
- Fig. 16. PCM-FM; fluctuation noise
- Fig. 17. PCM-FM; CW and similar system interference
- Quantized PPM
- Fig. 18. Comparison of quantized PAM with quantized PPM
- Fig. 19. FDM-FM; fluctuation noise
- Fig. 20. FDM-FM; CW interference

## III. BAND WIDTH AND POWER TABLES

- Table II. Optimum Band Widths for Minimum Power for Message Type Circuits
- Table III. Optimum Band Widths for Minimum Power for Program Type Circuits

Table IV. Minimum Band Widths and Corresponding Power Requirements for Message Type Circuits

Table V. Minimum Band Widths and Corresponding Power Requirements for Program Type Circuits

#### IV. FREQUENCY OCCUPANCY TABLES FOR RADIO RELAY

1. Antenna Characteristics

Fig. 21. Directional selectivity of microwave antenna

Fig. 22. Simplified route patterns for study of selectivity required in congested localities

Table VI. True Frequency Occupancy of Various Message Grade Radio Relay Systems for Congested Routes

Table VII. True Frequency Occupancy of Various Program Type Radio Relay Systems for Congested Routes

2. Conclusions as to Radio

Table VIII. Comparisons of Band Width and Frequency Occupancy for Systems of Equal Ruggedness

#### V. MORE ABOUT THE NON-SIMULTANEOUS LOAD ADVANTAGE

Fig. 23. Theoretical possibilities of exploiting non-simultaneous load advantage by an elastic PLM-AM system

#### VI. OVERLOAD DISTORTION AND NOISE THRESHOLD

Fig. 24. Noise threshold and overload ceiling in frequency divided PCM groups

Fig. 25. Overload characteristics of multirepeater systems

#### VII. PULSES, SPECTRA, AND FILTERS

Fig. 26. Typical pulses and their spectra

1. Pulses for PPM

2. Pulses for PAM

3. Pulses for PCM

4. Optimum Distribution of Selectivity Between Transmitting and Receiving Filters

Fig. 27. Crossfire between frequency divided pulse groups

5. Delay Line Balancing

#### VIII. TRANSMISSION OVER METALLIC CIRCUITS

Fig. 28. Variation of circuit length with number of repeater sections in an AM system with fixed power capacity and noise figure

Fig. 29. Optimum number of repeater sections and maximum circuit length for metallic AM system with fixed power capacity and noise figure

Fig. 30. Optimum number of repeater sections and maximum circuit length for metallic FM system with limiting only at end of system

Fig. 31. Optimum number of repeater sections and maximum circuit length for metallic PPM-AM system with reshaping at every repeater

Fig. 32. Optimum number of repeater sections and maximum circuit length for metallic FM system with limiting at every repeater

Fig. 33. Relation between circuit length, power, and number of repeaters in radio relay systems

#### IX. CONCLUSIONS

#### X. APPENDICES

##### Appendix I. Noise in PCM Circuits

Fig. 34. Stepping and sampling an audio wave

Fig. 35. Variation of quantizing noise with sampling frequency

##### Appendix II. Interference Between Two Frequency Modulated Waves

Fig. 36. Geometric solution for resultant phase of two frequency modulated waves

##### Appendix III. PCM for Band Width Reduction

Appendix IV. Supplementary Details of Derivation of Band Width Curves

Appendix V. Sampling a Band of Frequencies Displaced from Zero

Fig. 37. Minimum sampling frequency for band of width  $W$ 

## LIST OF FREQUENTLY USED SYMBOLS

- $B$  = radio signal band width in megacycles. (Not to be confused with frequency occupancy).  
 $b$  = base or radix of PCM system.  
 $\beta$  = peak-to-peak frequency swing of FM systems in megacycles.  
 $F_b$  = width of baseband (video band) in megacycles.  
 $f_r$  = repetition or sampling frequency in megacycles.  
 $K$  = load rating factor (amplitude ratio).  
 $\log$  = logarithm to base 10.  
 $\ln$  = logarithm to base  $e$ .  
 $N$  = number of channels in a multiplex system.  
 $n$  = number of digits in a PCM system or number of spans in a multirepeater system.  
 $P$  = wanted carrier amplitude.  
 $P_n$  = mean fluctuation noise power per megacycle.  
 $Q$  = interfering carrier amplitude.  
 $S$  = span length in miles.  
 $U$  = band spacing factor.

## I. INTRODUCTION

CARRIER systems for the transmission of many telephone channels on a single metallic circuit have grown to be very important in the telephone network. Since the development of the coaxial cable system in which 480 channels are transmitted in a 2-mc baseband, advances in high frequency techniques, including the war-accelerated microwave art, have inspired efforts to utilize the broad band capabilities of high transmission frequencies. Some of the efforts have related to the wave-guide conductor but mainly they relate to radio relay transmission. As a consequence of these efforts a considerable number of new multiplex methods for use at microwave frequencies have been devised. All of these methods employ bandwidth more liberally than the 4 kc per channel rate associated with single sideband carrier systems, in return for which various transmission advantages are obtained. Theoretically, transmission advantages can be sacrificed to permit bandwidth reduction but the transmission requirements then become very severe. Bandwidth as a transmission parameter has grown to a prominent position in modern communication theory as set forth by Shannon et al.<sup>1, 2, 3</sup>

The liberal use of bandwidth, employed in an effective way, operates to permit higher noise and distortion within a system and, in the case of radio relay systems, operates to permit higher interfering signals from other radio systems. When all the frequency space necessary to avoid mutual inter-

<sup>1</sup> C. E. Shannon, "A Mathematical Theory of Communication," *Bell Sys. Tech. J.*, Vol. 27, pp. 379-423, 623-654, July-Oct. 1948.

<sup>2</sup> B. M. Oliver, J. R. Pierce and C. E. Shannon, "The Philosophy of PCM," *Proc. I. R. E.*, Vol. 36 (1948), pp. 1324-1331.

<sup>3</sup> C. E. Shannon, "Communication in the Presence of Noise," *Proc. I.R.E.*, Vol. 37 (1949), pp 10-21.

ference between systems in a congested area is taken into account, certain wide-band methods, less vulnerable to interference, may be as or more efficient in the use of frequency space than other narrower band multiplex methods.

The principal purpose of this paper is to examine, for various systems, the relations governing the exchange between frequency space and transmission advantages.

It will be shown that the preferred multiplex method depends in part upon:

1. The grade of facility required; low-grade and high-grade channels lead to different preferences. These preferences also are influenced by the length of circuit.
2. The nature of the transmission obstacle over which advantage is sought. These obstacles may be: (a) intrasystem distortion (phase distortion, overload distortion, etc.) and noise; (b) intersystem interference as between similar radio systems or between different types of radio systems, operating on the same frequency.

Other factors beside the transmission considerations discussed here are likely to be involved in a practical multiplex application; hence the system preferences arrived at in this study may not be the controlling factors in practice.

Before a detailed analysis is undertaken, it may be helpful to examine and comment upon the chart shown in Fig. 1. All of the multiplex methods shown here have been studied sufficiently to permit their approximate evaluation with the aid of some theoretical considerations and subject to certain qualifications as pointed out from time to time. Variations and combinations of these are possible,<sup>4</sup> some of which will be discussed later.

In addition to the two general classifications of frequency and time division there is a third type based on carrier phase discrimination. A familiar example is the quadrature carrier system,<sup>5</sup> which is capable of yielding two channels for each double sideband width. In another form<sup>6</sup> each of  $N$  channels is modulated simultaneously on  $N/2$  carriers with a different set of carrier phases provided for each channel. Time division multiplex may be regarded as a kind of phase discrimination in which the signal is modulated on harmonic carriers so phased as to balance out except during the channel sampling time intervals. In true phase discrimination,

<sup>4</sup>A comprehensive listing and discussion of various combinations will be found in a recent paper by V. D. Landon, "Theoretical Analysis of Various Systems of Multiplex Transmission" *R.C.A. Review*, vol. IX, numbers 2 and 3, June-Sept. 1948, pp. 287-351, 438-482.

<sup>5</sup>H. Nyquist, "Certain Topics in Telegraph Transmission Theory," *A.I.E.E. Trans.*, April, 1928, pp. 617-644.

<sup>6</sup>W. R. Bennett, "Time Division Multiplex Systems," *Bell Sys. Tech. J.*, Vol. 20, pp. 199-221, April, 1941.

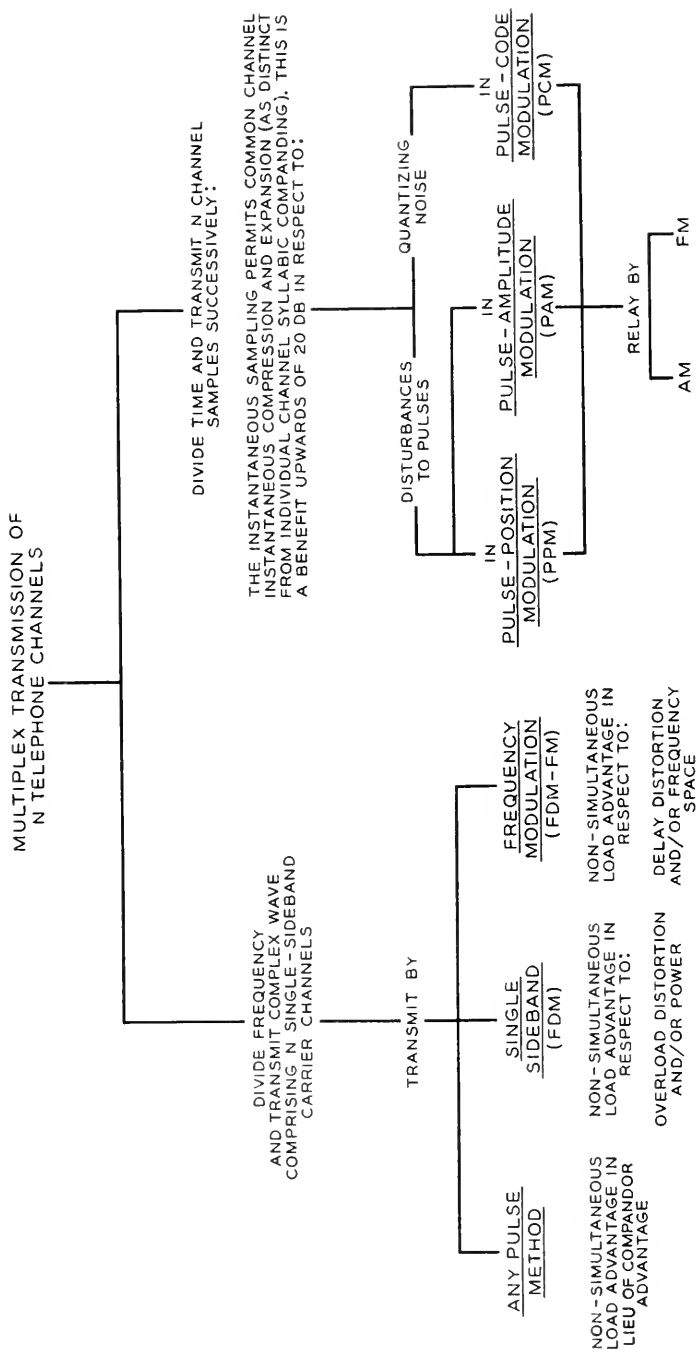


Fig. 1—Outline of multiplex transmission methods.



however, there need be no separation of channels in either time or frequency, and a homodyne detection process is required at the receiver for channel selection. The necessary precision of instrumentation seems in general more difficult to achieve than with either frequency or time division, and only minor prospects appear for exchange of bandwidth for transmission advantage.

Of the systems tabulated, the frequency division method (FDM) with single-sideband suppressed-carrier transmission is the only method in which bandwidth cannot be traded for some transmission advantage.<sup>7</sup> This system will be used as a standard of comparison. The PAM method, with transmission by AM pulses, can trade upon bandwidth only as a means for reducing interchannel crosstalk. In the other pulse systems, as well as all systems using FM, bandwidth may be expended to gain advantage over noise, intersystem interference, and, generally speaking, intrasystem distortion and noise.

#### NON-SIMULTANEOUS LOAD ADVANTAGE IN FDM

The *non-simultaneous load advantage* pertaining to frequency division multiplex refers to the fact that the channel sidebands rarely add to an instantaneous value even approaching the value  $N$  times the peak value for one channel. This means that the required peak capacity of a relay system transmitting the  $N$  channels increases slowly with  $N$ . Current toll transmission practice provides for relative power capacity roughly as follows.<sup>8</sup>

TABLE I  
NON-SIMULTANEOUS MULTIPLEX LOAD ADVANTAGE

N	Required Relative Power Capacity	Advantage
1	0 db	0
10	+6 db	20 - 6 = 14 db
100	+9 db	40 - 9 = 31 db
500	+13 db	54 - 13 = 41 db
1000	+16 db	60 - 16 = 44 db

To emphasize the strikingly large non-simultaneous load advantage statistically obtainable with conversational speech we may examine Table I and note, for instance, that the capacity of a 1000-channel system is completely

<sup>7</sup> We have in mind here a system such as Type K or L in which a minimum separation of adjacent channels in frequency is used. It is true that by spreading the channels far apart in frequency, a reduction in cross-modulation falling in individual channels could be obtained, but the resulting amount of improvement is minor compared with that offered by a corresponding band increase in the other systems.

<sup>8</sup> B. D. Hollbrook and J. T. Dixon, "Load Rating Theory for Multichannel Amplifiers," *Bell Sys. Tech. J.*, Vol. 18, pp. 624-644, October, 1939. The values in the table come from curve C, Fig. 7, taking the single channel sine wave power capacity as +9.5 dbm.

used up by peak instantaneous voltage when 994 channels are disconnected and 6 carry full-load tones.

If a group of carrier channels in frequency-division multiplex were translated to microwave frequencies, the overload distortion affecting the transmission would be predominantly of the third-order class. To a first approximation the third order distortion follows a cube law and may be predicted from the single-frequency compression. We assume here that the power capacity of the repeater is the output at which the single frequency compression occurring through the complete system does not exceed 1 db.<sup>9</sup> This criterion applies roughly to systems of several hundred channels capacity, and to present transmission standards.

#### INSTANTANEOUS COMPANDING ADVANTAGE IN TIME DIVISION

In time-division systems, as ordinarily understood and known in the current literature, each channel successively is provided with its full-load capacity, and thus a non-simultaneous load advantage does not accrue. However, because of the sampling process, instantaneous compression may be applied at the transmitting terminal before noise and distortion are encountered; when complementary expansion is applied at the receiving terminal the noise is suppressed. The expanded samples derived at the receiving terminal then bear an improved relation to noise, particularly in the case of weak samples. Such an instantaneous companding process applied without sampling to a continuous speech wave requires a greatly increased transmission band between compressor and expander but, in a time division system, no more bandwidth is needed to transmit the speech *samples* after they have been compressed than before. An instantaneous compander currently being used experimentally to handle 12 channels in time division has the noise performance characteristics shown<sup>10</sup> in Fig. 2. It is shown as applied to a telephone system in which the channel noise power (unweighted) would be 45 db down from the power of a sine wave which employs the full load capacity provided for the "loudest talker". Abrupt overloading is assumed to take place when peak amplitudes exceed that of the full-load tone. The location, at  $-7.5$  on the load scale, for the power representing the very loud talker (one in a thousand) conforms approximately to current practice. The speech volumes, referred to the point of zero db transmission level, are shown for the sake of completeness.

<sup>9</sup> In a multi-repeater system the compression accumulates. This means that each repeater must be restricted to operate approximately  $10 \log n$  db below the 1 db compression point of one repeater. ( $n$  denotes the number of repeaters.) See Section VI.

<sup>10</sup> Use of the same curve to represent the performance with tone or speech implies an independence of wave form which is not rigorously valid. Calculations based on speech-like signals have indicated that the curve for tone loading is a good approximation when average power is used as the criterion in the manner shown.

The compression and expansion result in a uniform improvement of 26 db for weak signals including the "very weak talker" and a lesser improvement for stronger signals. The noise power in the absence of speech is 71 db

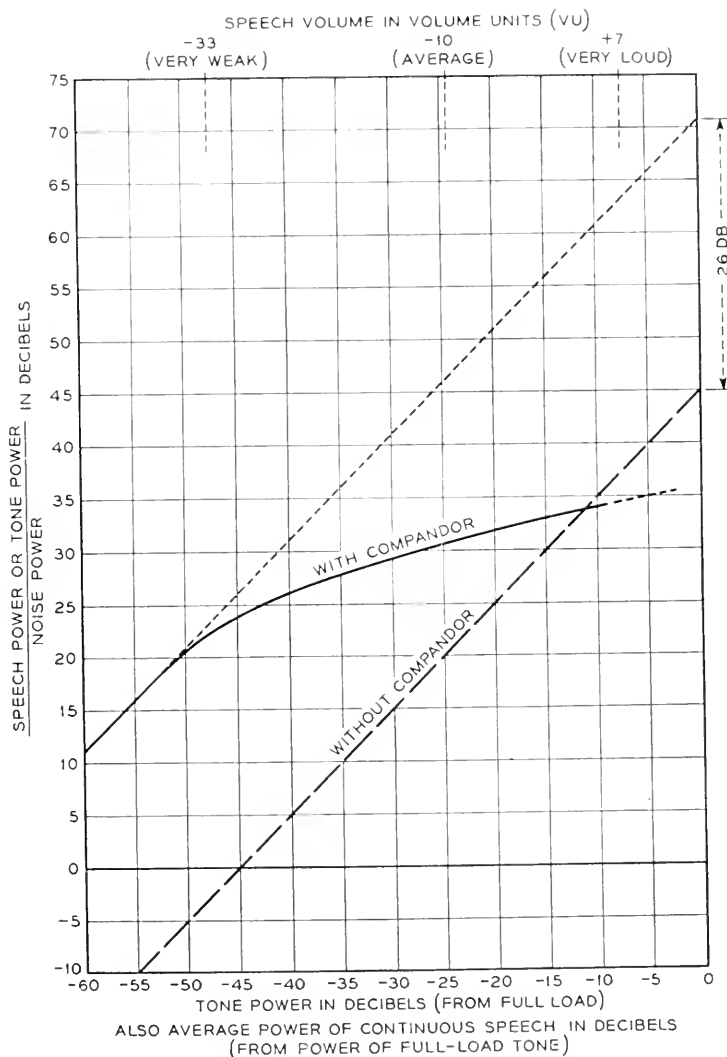


Fig. 2—Performance of an experimental instantaneous compandor.

below the power of the full load sine wave which the channel is designed to handle. The performance is substantially equivalent for telephone purposes to a 71-db circuit without companding, in spite of the fact that for all except the very weak talkers the average noise is greater than with the 71-db circuit.

The noise is increased (over the 71-db value) by the compandor only in the presence of speech and then only in proportion (roughly) to the amplitude, and so becomes masked by the speech. The masking is sufficient to make impairment of medium and loud speech imperceptible provided that the ratio of speech power to noise power is greater than about 22 db. Under these conditions we are justified in defining the equivalent signal-to-noise ratio in terms of the low level noise.

For compandors with a more drastic characteristic, yielding more low-level improvement, the high-level noise increase is enhanced and the limit to this enhancement is controlled by the "uncompanded" signal-to-noise ratio (the ratio without companding.) Thus the amount of low-level improvement that is permissible from the standpoint of high-level performance is determined by the uncompanded signal-to-noise ratio. Experiments have shown that the permissible low-level improvement increases several db for each db increase in uncompanded signal-to-noise ratio. Another way of putting it is that the value of the equivalent signal-to-noise ratio in the speech channel determines the amount of compandor advantage which may be invoked to attain that ratio, and that the permissible compandor contribution increases nearly as fast as the equivalent signal-to-noise ratio. The uncompanded signal-to-noise ratio is thus required to increase only slightly.

For the 45 db uncompanded signal-to-noise ratio of Fig. 2 the compandor could have been designed to yield more than the 26 db low-level improvement shown without impairing high-level performance. In the time-division systems of message grade with which we will deal later, a 22 db compandor advantage is assumed.<sup>11</sup>

In the quantized systems included in the PCM heading the instantaneous compandor advantage applies to the granularity, or quantizing, noise in the same way as to the common kinds of noise which plague other systems. The compandor of Fig. 2 was actually used in an experimental PCM system.<sup>12</sup> A discussion of quantizing noise appears in Appendix I and a more comprehensive treatment appeared in the Bell System Technical Journal recently.<sup>13</sup>

In transmitting frequency divided groups of channels by pulse methods<sup>14</sup>

<sup>11</sup> This is the maximum compandor advantage permissible for a circuit equivalent to 57 db signal-to-noise ratio. We will use this figure in connection with power requirements for circuits whose signal-to-noise ratio is intended to be equivalent to 60 db but since we presume that interference or crosstalk may be present in an amount equal to noise and since the compandor acts on interference as on noise we must protect against high level impairment on the basis that the noise is 3 db greater.

<sup>12</sup> L. A. Meacham and E. Peterson, "An Experimental Multichannel Pulse Code Modulation System of Toll Quality", *Bell Sys. Tech. Jl.*, Vol. 27, pp. 1-43, Jan. 1948.

<sup>13</sup> W. R. Bennett, "Spectra of Quantized Signals," *Bell Sys. Tech. Jl.* Vol. 27, pp. 446-472, July, 1948.

<sup>14</sup> If the group occupies a frequency range extending from zero to  $F_b$ , the minimum sampling rate is well known to be  $2F_b$ . If the group range does not start at zero frequency the minimum sampling rate is not twice the highest frequency of the group but lies between two and four times the width of the band depending on the location of the band. This matter is treated in Appendix V.

the instantaneous compandor advantage is substantially zero because, at full system load, companding actually increases the total noise. In time division the noise is increased at full load by companding but, as discussed earlier, this is permissible because full load occurs only with loud talkers who mask the noise. In a frequency divided group transmitted by pulse methods nearly full load may be produced when a number of loud talkers are momentarily active; the weak talkers then enjoy no improvement due to companding but may, on the contrary, suffer some degradation.

#### NON-SIMULTANEOUS LOAD ADVANTAGE IN PULSE TRANSMISSION

Transmission of a frequency-divided group by pulse methods does, however, permit the realization of a portion of the non-simultaneous load ad-

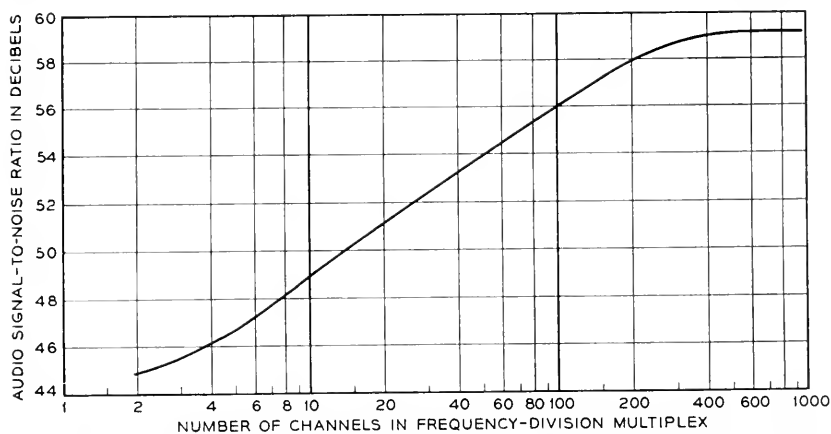


Fig. 3—Quantizing noise in each channel when PCM (128 equal steps) is applied to an FDM group.

vantage in lieu of the instantaneous compandor advantage realizable in time division. A pulse system, designed to carry  $N$  channels in time-division with a certain full load signal-to-noise ratio (without companding) may also be used to carry  $N$  channels in frequency division. These  $N$  channels in frequency division may be treated as a single channel  $N$  times wider than the time-divided channels and sampled  $N$  times faster. The ratio of the full-load signal in this wide band to the noise in the wide band turns out to be the same as the corresponding ratio in each of the narrow, time-divided channels. This fact makes the transmission of large groups of frequency-divided channels advantageous compared to small groups. For instance, in a 100-channel frequency-divided group, a single channel would have available a total load capacity which is 9 db less than that for the multiplex group. This comes from Table I, which shows that 100 channels require

9 db more range than one channel. This makes the signal-to-noise ratio in a channel 9 db lower than if all of the entire load capacity were devoted to that channel. However, in the 100-channel group a single channel receives only 1% of the noise power in the entire band, so a 20 db improvement accrues on this score. The net improvement is  $20 - 9 = 11$  db. Applied to a 128 step PCM system in which the full-load signal-to-noise ratio is 45 db<sup>15</sup> (7 digits binary PCM), the full-load signal-to-noise ratio in one channel of a 100-channel group thus becomes  $45 + 11 = 56$  db. With smaller groups than 100 channels the signal-to-noise ratio falls to 45 db while for larger it reaches 59 db, as shown in Fig. 3. Better results than these are obtainable with time division and instantaneous companding, as shown in Fig. 2, but these results may have significance in relation to the transmission of television by a pulse method, such as PCM. If a 128-step system were used, a large frequency-divided group of telephone channels filling the television band could be substituted for television when desired.

A more powerful application of the non-simultaneous load advantage in time division will be discussed later in Section V.

#### SIGNAL BAND WIDTH AND FREQUENCY OCCUPANCY

We define *signal band width* as the width of the signal spectrum (or more realistically as that portion of the signal spectrum which must be preserved in order to make the signal sufficiently undistorted). *Frequency occupancy* is greater than signal bandwidth in two respects:

First, the frequency range accepted by the receiving filter at the end of each span must be greater than the signal band for reasons of filter imperfection. In all of the pulse or FM systems it would be advantageous from the circuit point of view to make the receiving filter much wider in order thereby to reduce the phase distortion over a small central frequency range occupied by the signal band. The assigned frequency space must include the entire band accepted by the receiving filter. Our comparisons will assume that the filters make use of an appropriate amount of refinement to conserve frequency space.

Second, frequency occupancy must include the multiplication of assignments made necessary to avoid interference between converging or intersecting radio relay routes, between the two directions of a single route, or between a main route and a spur.

Our procedure in evaluating these systems will be to plot for each system certain curves relating power, signal bandwidth and channel signal-to-noise ratio or signal-to-interference ratio for various associated transmission

<sup>15</sup> Appendix I shows that the quantizing noise power at the minimum sampling frequency is the same for wide and narrow signal bands. This illustrates the general principle used here.

conditions. From these curves and other pertinent data we will prepare tables which show the significant frequency occupancy for various radio relay conditions. Such tables will be made for two grades of transmission facilities and for the extremes of signal bandwidth, one corresponding to minimum power and the other to minimum bandwidth. The minimum power condition prevails when the bandwidth has been increased, and the power reduced, to the point where any further increase of bandwidth would require an increase of power to prevent noise from "breaking" either the pulse slicer or the FM limiters.<sup>16</sup> The minimum bandwidth condition occurs when any further band limitation operates to impair the signal too much, assuming that the power is ample to override noise.

#### REGENERATION AND RE-SHAPING

Two distinct classes of relay operation exist, one applying to the quantized systems (PCM) and the other applying to non-quantized systems. When the transmitted signal is intended to convey a continuous range of values (amplitude, time or frequency) noise and distortion accumulate as the signal progresses from repeater to repeater over a relay route. If, however, a range of values is represented by a discrete (quantized) value, a signal may suffer displacement within the boundaries of that range without altering the information conveyed by the signal. If, therefore, in one span of the relay route the displacement is confined to those boundaries the signal may be regenerated and re-transmitted as good as new. No accumulation of noise and distortion need occur, therefore, as the signal traverses span after span. The most common application of regenerative repeater is in printing telegraphy where the signal is either a mark or space and, if correctly determined, may be re-transmitted afresh.

In all of the non-quantized systems the repeaters must have low distortion so that a signal may be conveyed through a large number of them (say 133 for a 4000-mile circuit made up of 30-mile spans) without too much mutilation. In spite of good repeater design a signal passing through such a large number of repeaters will accumulate considerable noise, interference from other systems, and distortion characterizing the repeater design limitations. In non-quantized systems there is no escaping accumulation of this sort. In pulse systems, for instance, phase distortion, common in flat band repeaters, may result in tails and the like, while cumulative frequency discrimination (band narrowing), characterizing simple forms of linear phase repeaters, results in cumulative broadening of the pulses. In the former case the tails

<sup>16</sup> In this connection it is of interest to mention that if the objective were a *very low grade* circuit the power required to prevent breaking might be higher than that required by a method having no improvement threshold, and no power saving could be accomplished by the bandwidth exchange principle. For circuits of telephone grade this situation does not occur.

may eventually grow large enough to break the slicer (if the system employs such a device) while in the latter case the reduced pulse slope and the spreading out of time bounds may also bring about transmission disaster. In both cases these growing distortions successively reduce the margin that it is necessary to provide for noise and interference. To circumvent such effects, the pulses may be reshaped at all or some repeaters. Reshaping consists of measuring the information conveyed by the pulse (in the time or amplitude dimension) and sending out a new pulse of standard shape possessing that measured characteristic in time or amplitude. This process is distinctly different from regeneration as practiced in quantized systems; in general, reshaping can only be counted upon to confine the rate of accumulation of noise, interference and crosstalk to that of power addition from span to span.

In FM systems any distortion which results in amplitude "modulation" of the FM wave may be treated with limiting at each repeater to prevent such amplitude variation from accumulating and breaking the limiter. Like pulse reshaping, this measure does not stop the accumulation of disturbance to the intelligence. Certain kinds of distortion may be combated by double FM.<sup>17</sup>

Reshaping (or, in the case of FM, limiting) may be employed to conserve power in the systems having an improvement threshold. Without reshaping, the minimum repeater power is the marginal<sup>18</sup> value for the total noise accumulated from all spans. If reshaping is practiced at each repeater the power need be marginal for the noise from only one span. More bandwidth must be used, then, in exchange for the lower power; and, while this in turn increases the marginal power, the result is a net power saving. Tables II and III of Section III illustrate this point and Section VIII illustrates its application to metallic circuits.

### THE RADIO REPEATER

Repeaters for relaying television signals must achieve low distortion and we will take a current design and assume that such a repeater represents a basis for discussing the transmission of multiplex telephony by non-quantizing methods. This repeater employs, in the two-way application, four antennas and two frequencies as shown in Fig. 4. It is proposed to transmit 5-mc video television signals by FM in bands spaced 40 mc. The repeater employs double detection and the band separation is effected mainly by the

<sup>17</sup> Leland E. Thompson, "A Microwave Relay System," *Proc. I.R.E.*, Vol. 34, December, 1946, pp. 936-942.

<sup>18</sup> By marginal power is meant that power which just safely exceeds the improvement threshold power. For a given noise level, minimum power is achieved when the bandwidth improvement factor yields the required signal-to-noise ratio in the channel with the power that is marginal for that bandwidth.



selectivity following conversion to intermediate frequency. Microwave receiving filters afford enough selectivity to divert alternate bands into their correct frequency-converting units without disturbing the other bands; and microwave combining filters serve in the transmitting side of the repeater to

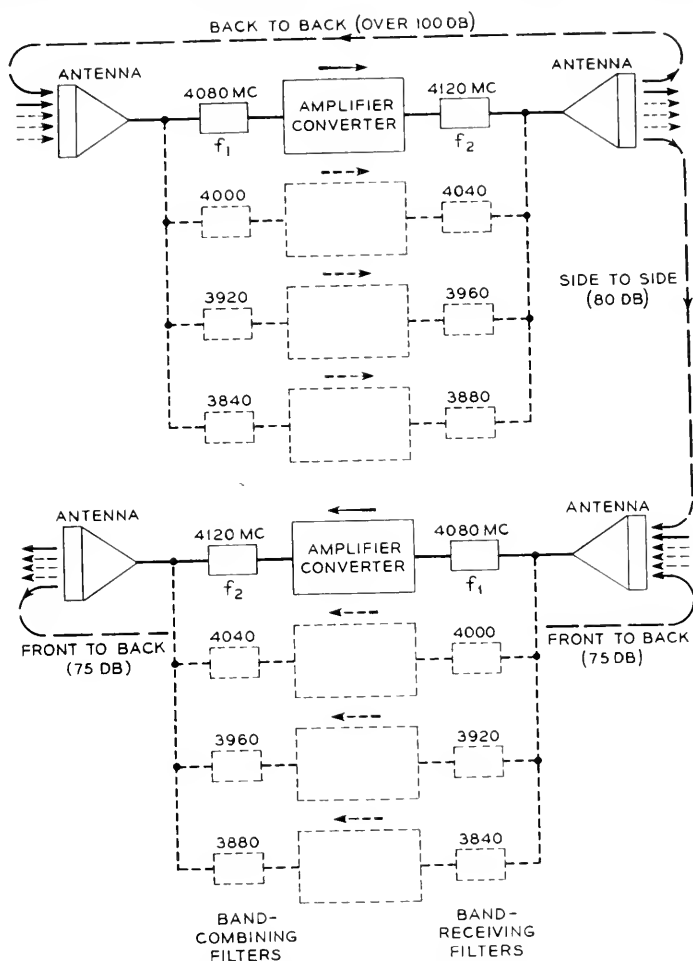


Fig. 4—Arrangement of two-way two frequency repeater of television type showing spacing of bands and antenna discrimination.

bring the bands into the common antenna with small loss and small mutual disturbance.<sup>19</sup> The combining and separating processes are made easier by the interleaving of transmitting with receiving frequencies. Interleaving

<sup>19</sup> W. D. Lewis and L. C. Tillotson, "A Non-reflecting Branching Filter for Microwaves," *Bell Sys. Tech. J.*, Vol. 27, pp. 83-95, January, 1948.

also eases the intermediate-frequency selectivity requirement when the side-to-side antenna loss is greater than the span loss (repeater gain). The stagger between input and output frequencies in one direction is employed to permit frequency selectivity to augment the back-to-back ratio in separating the high-power output from the low-power input.

Figure 5 further describes the repeater in relation to the frequency plan of Fig. 4, showing how the three kinds of antenna discrimination are employed. The back-to-back (BB) and side-to-side (SS) antenna ratios attenuate the high-power transmitted band adjacent to a low-power received

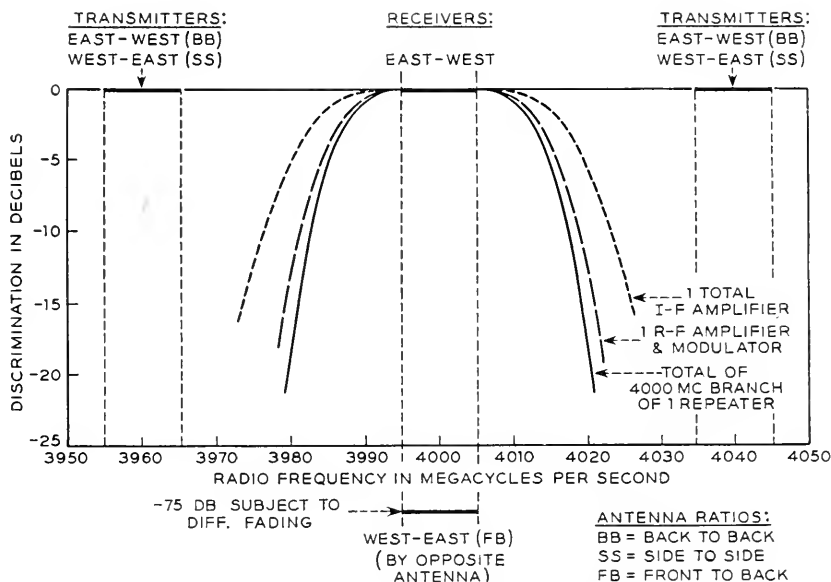


Fig. 5—Discrimination of I.F. and R.F. circuits in television type repeater.

band to a level comparable with the receiving level. The front-to-back ratio (FB) separates bands at the same frequency (which are always similar in power level except for the disparity produced by differential fading of the signals received from the two directions).

For systems in which the signal is highly susceptible to adjacent band crossfire and phase distortion, the signal band must be confined to a certain fraction of the 40-mc band spacing in order to be carried through many such repeaters. With signals of more rugged characteristics, frequency occupancy can be reduced because a larger segment of the pass-band shown in Fig. 5 can be utilized by the signal and/or because the bands can be more closely spaced. With quantized systems and particularly with binary PCM

this reduction of frequency occupancy can be carried very much further when regeneration is practiced.

We will later assign, for each modulation method, a value for the fraction of the band spacing to which the signal bandwidth must be confined. The frequency occupancy is then given by the product of the following three factors:

1. The reciprocal of the above factor, to be called  $U$ .
2. The signal bandwidth for the specified number of channels.
3. The number of frequencies required to operate in the assumed radio situation.

Inspection of Fig. 4 shows two sources of common frequency interference between East- and Westbound signals: (1) backward radiation from one transmitter into the beam of the other and (2) backward reception of the signal intended for the oppositely directed receiving antenna. Both kinds of interference are suppressed by the front-to-back ratio (assumed as 75 db) compared with the desired signal. The effects occur at every repeater and in a 4000-mi. system with 30-mi. spans, addition of the interfering power contributed by the individual repeaters gives two "equivalent" single sources  $75 - 10 \log 133 = 54$  db down. With no fading the two effects combine to form one source 51 db down. The receiver crosstalk is, however, subject to differential fading in adjacent spans. On the assumption that simultaneous deep differential fades on more than one pair of such spans are extremely rare, we base our estimates on a severe fading condition at only one repeater (or a number of less severe differential fades distributed simultaneously over the system having an equivalent effect.) The total interference from the other repeaters is then virtually the same as for 133 non-fading repeaters, while the fading repeater contributes an amount greater than the receiver crosstalk at one non-fading repeater by the depth of the fade expressed in db. We take this differential fade to be 30 db. The total interference from repeater crosstalk is, then, the result of a source 51 db down together with another source  $75 - 30 = 45$  db down. The combined interference is accordingly 44 db down. It is thus necessary that any long distance system using the repeater plan of Fig. 4 must be operable in the continuous presence of interference 44 db down. Under these assumptions, systems in which bandwidth is not or cannot be expended to gain tolerance to interference 44 db down do not allow any frequency to be used more than once in one repeater and therefore a repeater plan must be used which employs four frequencies.

The four-frequency plan would be necessary in the case of conventional frequency division multiplex because such a system cannot tolerate crosstalk only 44 db down.

In all of the systems in which bandwidth may be exchanged for tolerance to interference we restrict, in our comparison tables, the minimum bandwidths to those which provide at least the 44 db tolerance demanded in the two-frequency plan.

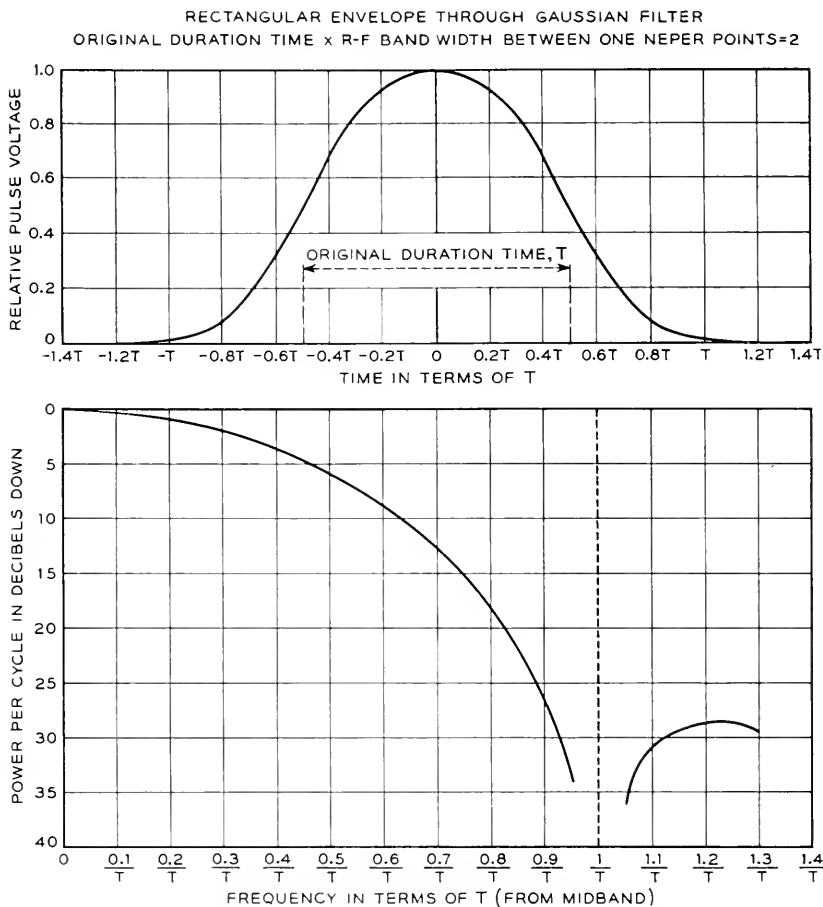


Fig. 6—Basic pulse shape (approximately sinusoidal) and its spectrum.

## II. BAND WIDTH CHARACTERISTICS

The type of pulse assumed in the various pulse transmission systems is shown on Fig. 6. As pulse 4 of Fig. 26, it is further discussed in Section VII. The spectral density or distribution of energy vs. frequency associated with such a pulse is also shown. It is evident from this curve that omission of frequencies beyond a baseband width  $1/T$  can result in distortion or tails of

only a few per cent of the pulse height. We define signal bandwidth for the pulse systems studied here as  $1/T$ , or  $2/T$  in the  $r$ - $f$  medium, i.e., double sideband is assumed in all of the AM pulse cases. In assuming double sideband, we bow to the obvious difficulty of dealing circuit-wise with single sideband and its pulse demodulation problem.

In the FM systems we define the radio signal bandwidth as the peak-to-peak frequency swing,  $\beta$ , plus two times the baseband width,  $2F_b$ .

We shall consider individually the following types of systems where the meaning of the symbols is explained in Fig. 1.

- |           |           |           |           |
|-----------|-----------|-----------|-----------|
| 1. PPM-AM | 3. PAM-AM | 5. PCM-AM | 7. FDM    |
| 2. PPM-FM | 4. PAM-FM | 6. PCM-FM | 8. FDM-FM |

The source of disturbance may be either fluctuation noise, a constant-frequency interfering wave (CW), or a similar but independent system operating on the same frequency allocation. CW interference may fall anywhere within the radio signal band. Interference from echoes, which is a special case of similar system interference, is not treated. In certain cases echoes such as might be produced by multiple reflections in waveguide connections to the top of radio towers may be more detrimental than independent system interference of the same amplitude. We assume that such echoes are suppressed sufficiently by good design.

Our first set of curves, Figs. 9-20, exhibits quantitatively the audio signal-to-noise and audio signal-to-interference ratios which can be obtained with increased radio bandwidth in the various systems. Audio signal is taken to be the power of a test tone which fully loads one channel. Audio noise is expressed as the total noise power in the channel. Audio interference is expressed as the power of all of the extraneous frequencies produced in a channel by the assumed interfering signal. The term "radio bandwidth" is intended to mean double-sideband width and does not imply that the transmission is necessarily by radio. Two of the systems, PAM-AM and FDM, are omitted from this study because, as has been pointed out earlier, they do not provide a significant basis of exchange of bandwidth for suppression of noise and interference. The other systems possess this trading property in varying degree as illustrated by the curves. The FDM and PAM-AM systems are entered in Table IV and discussed under Section III. For comparison with the following curves it may be of interest to note here that for 1000 4-kc message channels in FDM, the bandwidth (single sideband) is 4 mc., and the received power for a 60-db audio signal-to-noise ratio must be  $-77$  dbw.<sup>20</sup> This is the power in a sine wave which employs

<sup>20</sup> Throughout this paper we shall use the abbreviation "dbw" for power expressed in decibels relative to one watt.

the full load capacity in accordance with Table I, at a point where the noise power is  $-189$  dbw per cycle of bandwidth (15 db noise figure, NF).

In most of these curves, plotted for 1000 message channels, the bandwidth scale runs to hundreds of megacycles. We do not mean to imply that the microwave transmission medium can be relied upon to transmit faithfully such wide-band signals or that circuit techniques for producing them are available. As suggested by Fig. 4, the 1000-channel system might be divided into several groups of fewer channels to avoid frequency selective transmission difficulties or circuit limitations. The total frequency occupancy is not altered by such a division, while the required power per group is reduced in proportion to the number of channels.<sup>21</sup>

Curves are shown of audio signal-to-noise ratio as a function of radio signal bandwidth at constant power and at marginal power. Audio signal-to-interference ratios are plotted against radio bandwidth for marginal ratio of radio signal power to interfering signal power. By "marginal power", we mean the radio signal power which just safely exceeds the threshold below which noise or interference causes system failure. In the case of fluctuation noise, any further increment of bandwidth from this point is untenable without an increase in radio signal power. Points on the marginal power curves show as abscissa the bandwidth at which minimum radio power is required to obtain the audio signal-to-noise ratio given by the ordinate. In calculating these curves, we have specified the marginal condition as occurring when the peak disturbance is actually 3 db below the theoretical value which just breaks the system. These relations are shown graphically in Fig. 7. We have in this paper followed the accepted practice of ignoring all fluctuation noise peaks exceeding the rms voltage by more than 12 db. *Radio signal power* is taken as the power averaged over a cycle of the high frequency in the FM wave, or, in the AM pulse case, over a cycle of the high frequency when the pulse is maximum. A curve is included in Fig. 9 showing marginal AM radio pulse power values for various bandwidths of fluctuation noise and a similar curve for FM is shown in Fig. 13. A noise figure of 15 db<sup>22</sup> is assumed for the receiver. We have taken the noise bandwidth as equal to the signal bandwidth throughout. This equality cannot be quite attained in actual systems because of the departure of physical filters from ideal characteristics. In practice an allowance for frequency instability would also have to be included.

The relation of the PPM pulse to channel allotment time is shown in Fig. 8. Pulses in channels adjacent in time can just touch when full load signals are impressed on each. The slicer operates at half the pulse height which, for the assumed pulse shape, is also the point of maximum slope. The width of the

<sup>21</sup> These statements are not exactly true for FDM and FDM-FM, where multiplex load rating is used in the design.

<sup>22</sup> This means that the noise power is 189 db below a watt per cycle of bandwidth.

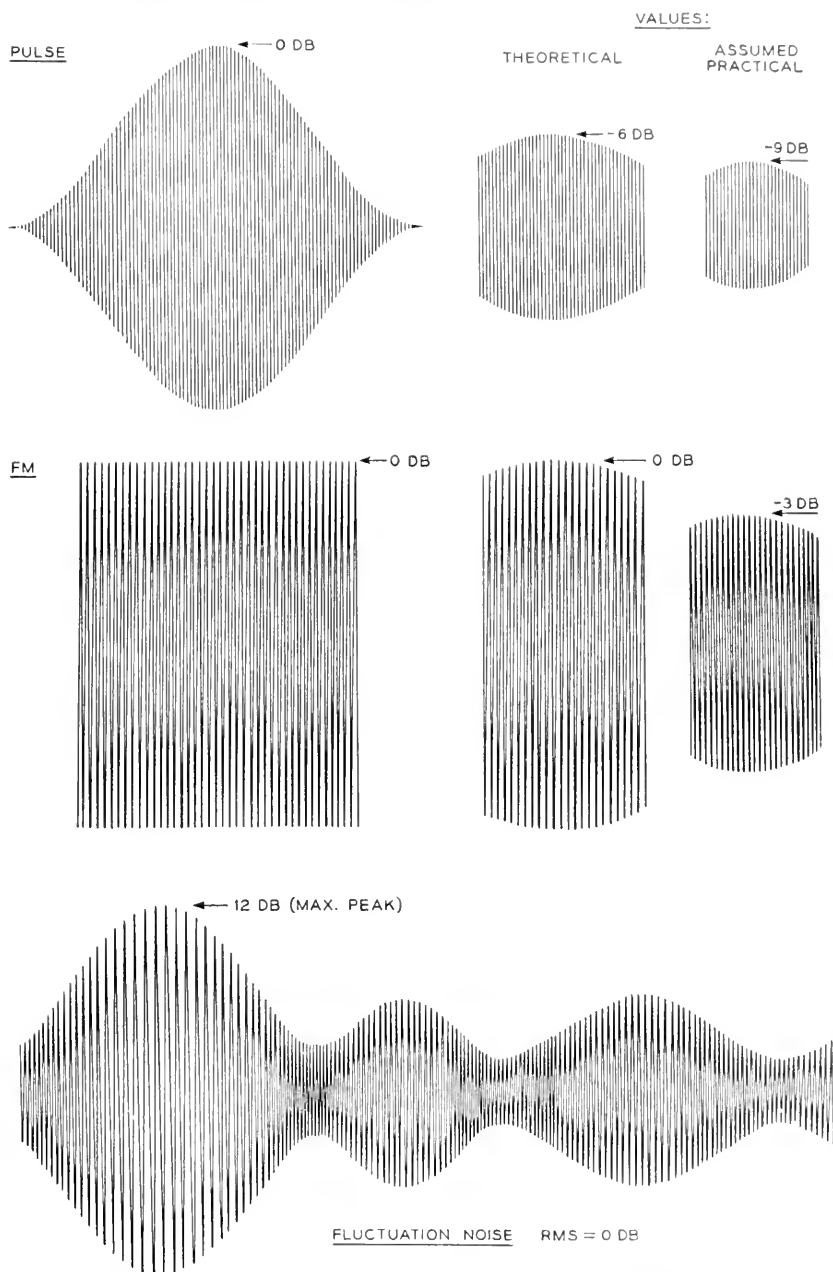


Fig. 7—Marginal condition in reception of AM pulses and an FM wave in presence of noise. Pulse case applies to PCM only if binary.

pulse is inversely proportional to the signal bandwidth. The time available for modulating the pulse position is equal to the channel time minus the pulse duration. The combination of these factors leads to the PPM "slicer

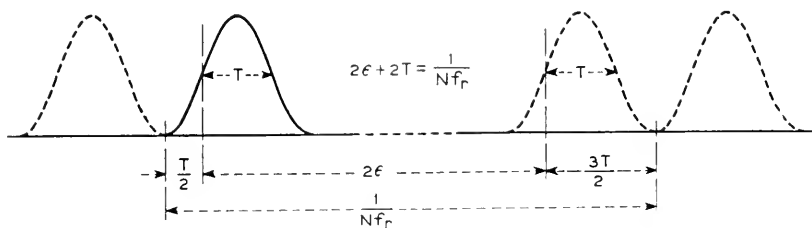


Fig. 8—Time allotments in pulse position modulation.

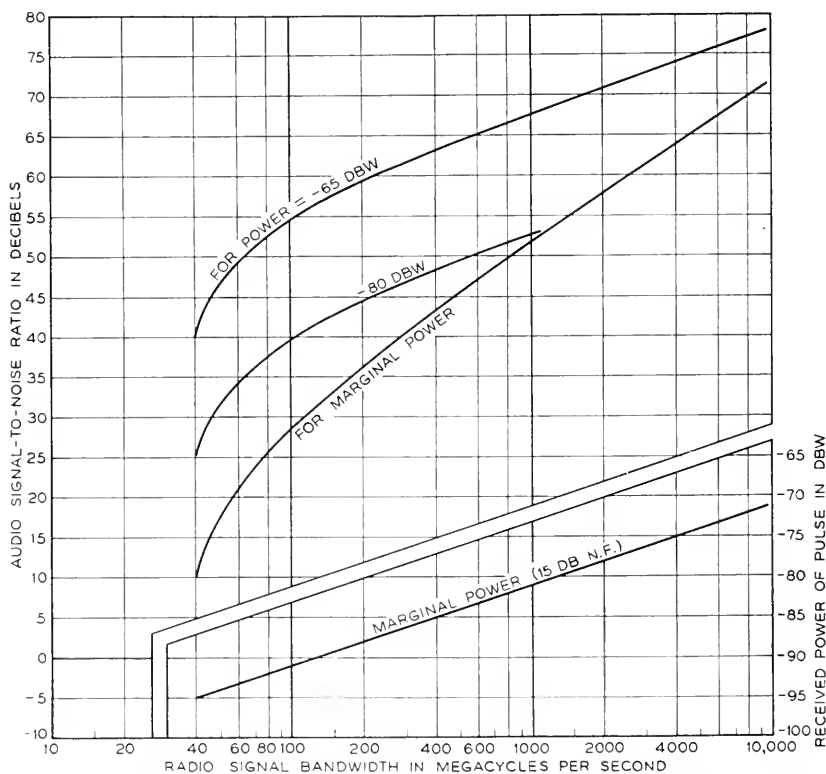


Fig. 9—PPM-AM; performance with respect to fluctuation noise. Relations between bandwidth, power, and audio signal-to-noise ratio for 1000 4-kc channels.

advantage" which, when applied to the  $r$ - $f$  pulse-to-noise ratio, gives the full load audio tone-to-noise ratio in each channel. Details of this calculation and others pertaining to various pulse systems are included in Appendix IV.



FIG. 9 -PPM-AM, FLUCTUATION NOISE

The curves of Fig. 9 were computed from the slicer advantage derived in Appendix IV. The asymptotic slope of the constant power curves of 3 db per octave of bandwidth reflects the 6 db advantage due to the two-fold greater pulse slope (slicer advantage) diminished by the 3 db increase of noise accepted by the two-fold wider band. In the marginal power case

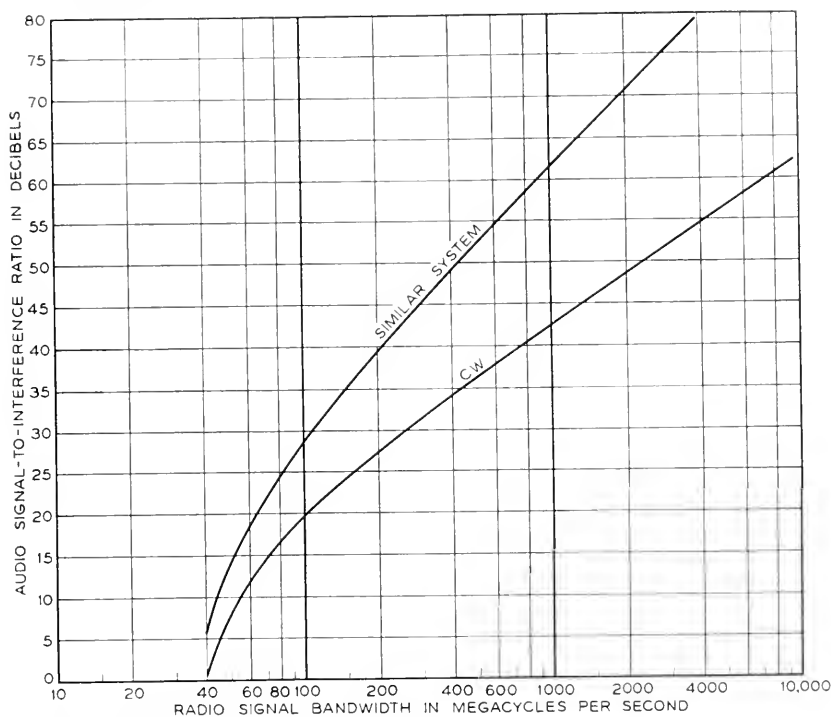


Fig. 10—PPM-AM; performance with respect to CW and similar system interference for 1000 4-kc channels with ratio of pulse to interference marginal. Relations between bandwidth and audio signal-to-interference ratio.

the power is increased with bandwidth so the slicer advantage is preserved and the slope is 6 db per octave.

The sharp reduction of signal-to-noise ratio with reduced bandwidth appearing at the left end of the curves arises from immobilizing the pulse position as the widened pulse uses up more of the total channel time allotment. According to the definition of bandwidth used here and the plan of Fig. 8, no modulation is possible when the bandwidth is  $2/T$  and  $T$  is half of the channel time. For 1000 channels the channel time is 0.125 microseconds and  $T = 0.0625$ , which makes the audio signal-to-noise ratio zero at 32 mc.

FIG. 10—PPM-AM, CW AND SIMILAR SYSTEM INTERFERENCE

The curve of Fig. 10 for marginal ratio of pulse power to CW interfering power has the same shape as the corresponding curve of Fig. 9 for marginal power over fluctuation noise. There is a shift of 9 db in ordinates, however, because the peak factor of the CW interference is 9 db less than that of fluctuation noise. The interference from similar systems follows a different law because of the "exposure factor" arising from the finite probability that the interfering pulse does not overlap the wanted pulse. A straightforward probability calculation taking into account the distribution of pulse voltages in an interfering system occupying the same radio frequency band yields the curve shown on the assumption that the repetition frequencies are asynchronous. As the bandwidth is increased the pulses become shorter and their coincidences less frequent, leading asymptotically to a 9 db per octave slope instead of the 6 db per octave of the CW interference.

FIG. 11—PPM-FM, FLUCTUATION NOISE

In the transmission of PPM by FM there are two sources of advantage over noise. One is the ordinary FM advantage and the other is the slicer advantage of PPM acting on the noise remaining in the FM output. There are, likewise, two separate conditions for system failure; one a breaking of the limiter and the other a breaking of the slicer. A certain amount of radio power will result in marginal operation of the limiter for a certain frequency swing. The corresponding deviation ratio is the quotient of the frequency swing and the baseband width; this ratio is maximum when the baseband is least. Except in the region near the minimum PPM band, advantage accrues faster with bandwidth in FM than in PPM. It is apparent, therefore, that most of the radio bandwidth should be devoted to FM advantage. The optimum proportioning occurs when the baseband width has a small value but not so small as to invoke an unsurmountable penalty by not providing for any position modulation. Mathematical analysis given in Appendix IV shows that the optimum baseband for the pulse position modulation varies with radio bandwidth in the manner shown in Fig. 11 by curve 1. Curve 2 shows the audio signal-to-noise ratio vs. radio bandwidth when the baseband width follows curve 1 and the FM limiter is marginal. It is of interest to compare curve 2 with the poorer performance of the dashed curve 3 which is calculated for the case in which both the FM limiter and the PPM slicer are marginal. The baseband width for the double marginal condition follows curve 4. Curves 5 and 6 show audio signal-to-noise ratio vs. bandwidth for constant radio power and optimum baseband. The curve of marginal amount of radio power is not given in Fig. 11, but is the same as the one given later in Fig. 13.

FIG. 12—PPM-FM, CW AND SIMILAR SYSTEM INTERFERENCE

The curve showing interference from a similar system of lower power was based on a calculation of the beat spectrum between two FM waves, both frequency modulated over the same  $r$ - $f$  range ( $\beta$  mc) by 8 mc. The phase difference between the 8-mc modulating frequencies was assumed to vary, giving rise to various beat spectra. The power in those beat components accepted by a band zero to  $F_b$  was averaged over all 8-mc phase differences

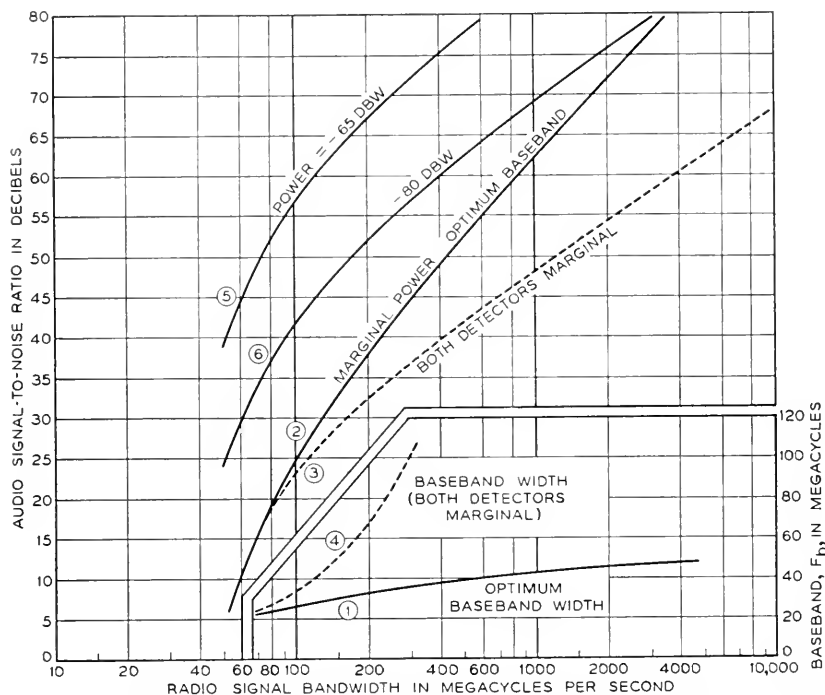


Fig. 11—PPM-FM; performance with respect to fluctuation noise. Relations between bandwidth, power, and audio signal-to-noise ratio for 1000 4-kc channels.

and this average power was taken as a measure of the interference to which the baseband signal is subjected. As outlined here, this procedure is valid for interference between idle PAM-FM systems in which the FM waves are frequency modulated as assumed above. For the PPM-FM case in which we are here interested, we take the position suggested by the transient viewpoint that the effect of interference from spaced pulses will not be much different because of their spacing and so we apply the slicer advantage possessed by the wanted system to the total interference calculated above and obtain the curve shown. At the left hand end where the pulse spacing is only slight

and the sinusoidal frequency modulation is nearly the correct representation, the above procedure is not subject to much suspicion. The validity of the right-hand portion of the curve is upheld by the fact that it is about 12 db lower than the marginal fluctuation noise curve of Fig. 11. If the wide swing FM interfering wave had a spectrum much like fluctuation noise of the same power as the FM wave the difference would be 9 db.

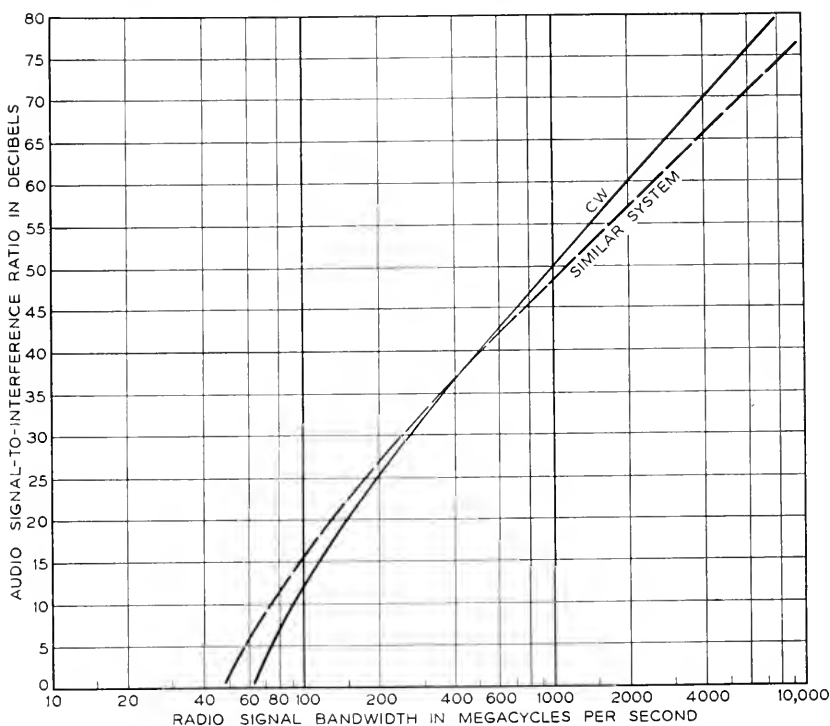


Fig. 12—PPM-FM; performance with respect to CW and similar system interference for 1000 4-kc channels with ratio of FM wave to interference marginal. Relations between bandwidth and audio signal-to-interference ratio when baseband is optimum for suppression of fluctuation noise.

It has been explicitly assumed that both systems are idle, but we see no reason to believe that if either or both were normally active the interference would be significantly different for our purposes.

Audible interference from a CW wave is caused by a disturbance to the frequency of the FM wave. Let us first assume that the CW frequency lies near the middle of the frequency swing range. No disturbance to the FM wave occurs as its frequency passes through coincidence with that of the CW but, as the frequencies diverge, the magnitude of the disturbance as well as

the frequency of the disturbance increases linearly. The baseband filter is excited only during the time the difference is less than  $F_b$ . Thus, the disturbance results from a series of perturbations to the otherwise smooth frequency variation of the FM wave. The time during which these perturbations can affect the baseband filter is short compared with the shortest pulse the baseband filter can pass, except when the baseband width is greater than half of the swing. This occurs at the extreme left-hand end of the curve. We have not attempted to calculate the response to these transients except to note that the response is a pulse which extends roughly  $2T$  from its point of origin, peaking somewhere near the center of this interval. If we assume that the PPM pulses are closely spaced ( $\epsilon = 0$ ) so that they result in a wave frequency modulated by 8 mc, there are two such evenly spaced disturbance pulses per cycle of modulation (two per  $2T$  interval) and therefore there is an almost continuous disturbance wave in the base band filter output whose amplitude does not greatly exceed its RMS value. We have accordingly calculated the power sum of all the extraneous frequencies passed by the baseband filter, assuming the FM wave to be sinusoidally modulated. The location of the CW frequency giving greatest interference power was used in these calculations except in the wide band cases where the worst frequency appeared to be near the edge of the band. Here the transient viewpoint indicated that the resulting interference in the baseband would be greater if the CW frequency were nearer the center.

If the trailing edge is used to measure the time of the pulse, the principal disturbance of this time arises from the perturbation produced at the leading edge of the same pulse, and so the calculation for close-spaced pulses is not greatly in error when applied to wider-spaced pulses. If the leading edge were used the worst CW frequency for widely spaced pulses would be one differing from the rest frequency by  $F_b$  and the interference would be worse, we think, than that arising from the frequency worst for trailing edge operation.

It has been explicitly assumed that the system is idle, but we see no reason to believe that the interference would be significantly different with normal activity.

#### FIG. 13—PAM-FM, FLUCTUATION NOISE

Fluctuation noise in a PAM-FM system produces the sloped noise spectrum characteristic of FM in the output of the frequency detector. The noise power per cycle is zero at zero frequency and increases with the square of the frequency. The baseband filter accepts only the portion of the spectrum between zero and  $F_b$ . If instantaneous sampling of the signal values is used, all noise frequencies in this range are equally effective as causes of errors. Use of a channel gate of maximum permissible duration

consistent with a satisfactory margin over crosstalk from adjacent channels furnishes a practical method of discriminating against the influence of noise components near the top of the baseband where the noise spectrum is strongest. The exact shape of the gate is not very critical. The curves have been calculated for a rectangular gate coincident with the channel allotment time, which is just possible without crosstalk in the case of non-

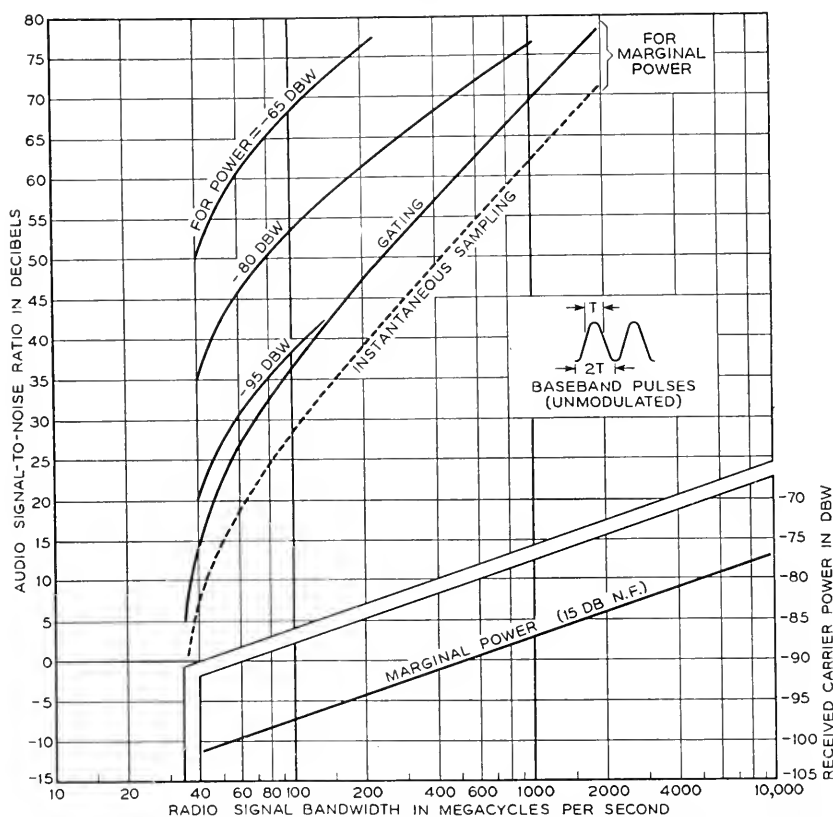


Fig. 13—PAM-FM; performance with respect to fluctuation noise. Relations between bandwidth, power, and audio signal-to-noise ratio for 1000 4-kc channels.

overlapping sinusoidal pulses. A somewhat shorter rectangular gate or a gate of sinusoidal shape leads to very nearly the same results. The advantage of gating as compared to instantaneous sampling is approximately 8 db. Calculation of the gated noise is a straightforward process if based on the concept of the FM noise spectrum acting as signal on a product demodulator in which the carrier consists of the harmonics of the gating function. Each harmonic demodulates the spectrum centered about the harmonic

frequency and contributes audio power proportional to the product of harmonic power and spectral density. The channel filter accepts only the demodulated noise falling in the audio signal range.

The marginal power curve has been drawn for a 3 db ratio of peak carrier to peak interference or 12 db ratio of mean carrier power to mean fluctuation noise power. Curves for specific amounts of received power are included as

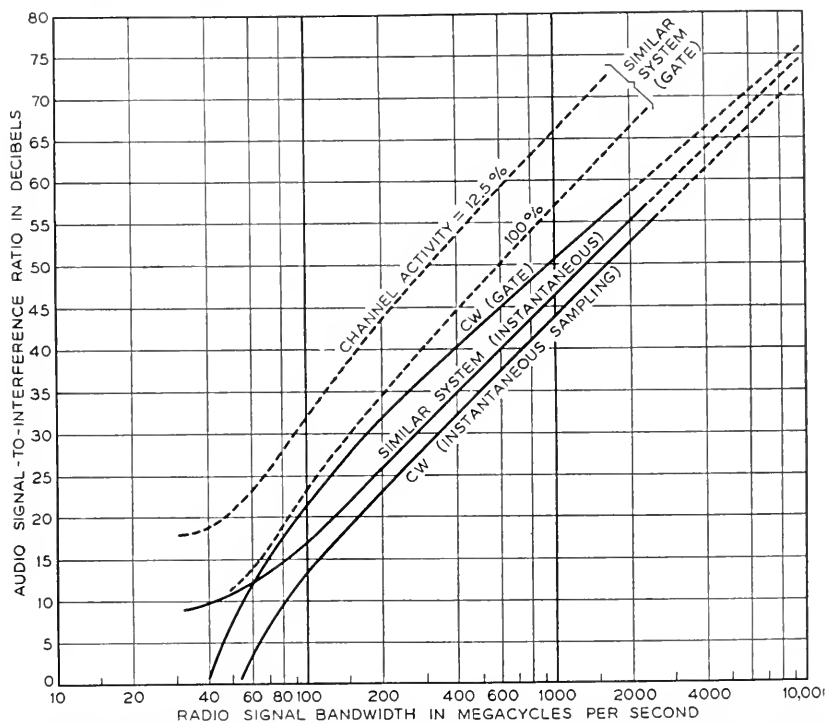


Fig. 14—PAM-FM; performance with respect to CW and similar system interference for 1000 4 kc channels with ratio of FM wave to interference marginal. Relations between bandwidth and audio signal-to-interference ratio.

well as the curve of marginal received power vs. radio signal bandwidth for a receiver with 15 db noise figure.

FIG. 14—PAM-FM, CW AND SIMILAR SYSTEM INTERFERENCE

CW interference can be calculated conveniently by assuming all channels idle and determining at what frequency within the radio signal band a CW component of fixed power produces maximum disturbance of an audio channel. This worst possible amount of disturbance is then assumed not to be much affected by the various channel loading conditions existing during normal operation of the system. When all channels are idle, the transmitted

carrier of a PAM-FM system using sinusoidal pulses assumes the particularly simple form of an FM wave modulated by a sinusoidal signal having frequency  $Nf_r$  (8 mc for 1000 channels) and total frequency swing  $\beta/2$ . Hence the rigorous steady state solution for interference between CW and sinusoidally modulated FM was calculated and the interfering components falling in the baseband range selected. The gating function was then applied to these components in the same way as described above for fluctuation noise, and the resulting products falling in the audio channel range evaluated. The signal-to-interference ratio was expressed as the ratio of rms signal power received from a full-load channel test tone to the rms value of the audio interference. A range of frequency locations for the CW interference was investigated for each radio signal bandwidth and the one giving maximum audio interference used for the point on the curve. The worst position of the CW was usually found to be near the extremities of the idle channel frequency swing. Curves are shown for a rectangular gate of maximum duration and for instantaneous sampling.

When the source of interference is a similar system, we assume that the midband frequencies differ only slightly. With both systems idle, we have two sinusoidally modulated FM waves which are identical except for (1) a small variable difference between mean carrier frequencies and (2) a variable phase shift between the two modulating frequencies. The interference falling in the baseband consists of steady state components which are approximately harmonics of the channel slot frequency  $Nf_r$ . As is characteristic of FM interference, the amplitude at the  $m$ th harmonic contains a factor proportional to  $m$ ; and the component near zero frequency, the approximate zeroth harmonic, is very small. If we gate this interference with a rectangular gate of duration  $1/Nf_r$ , we find that the gated output vanishes for input components at  $Nf_r, 2Nf_r, \dots$ , because these frequencies are located at the infinite loss points of the aperture admittance. The gate would transmit the zeroth harmonic, but this component tends toward zero amplitude. Our conclusion is that two idle PAM-FM systems accurately lined up to occupy the same frequency range are balanced against interference from each other when a rectangular channel gate of full channel allotment time is used. The balance tends to disappear as the channels are loaded because the interference then spreads throughout the base band instead of being concentrated at the blind spots of the aperture. Thus, for the first time in our consideration of pulsed systems, we are obliged to take account of channel loading conditions.<sup>23</sup>

<sup>23</sup> A wave could be frequency modulated about a central frequency by PAM pulses of plus and minus sign and an idle system would thus consist of a wave of constant frequency. The weaker of two such idle systems aligned in frequency would produce no (or very little) interference in the other, using either channel gating or instantaneous sampling. The susceptibility to CW interference would be greater than in the biased modulation assumed above, however.



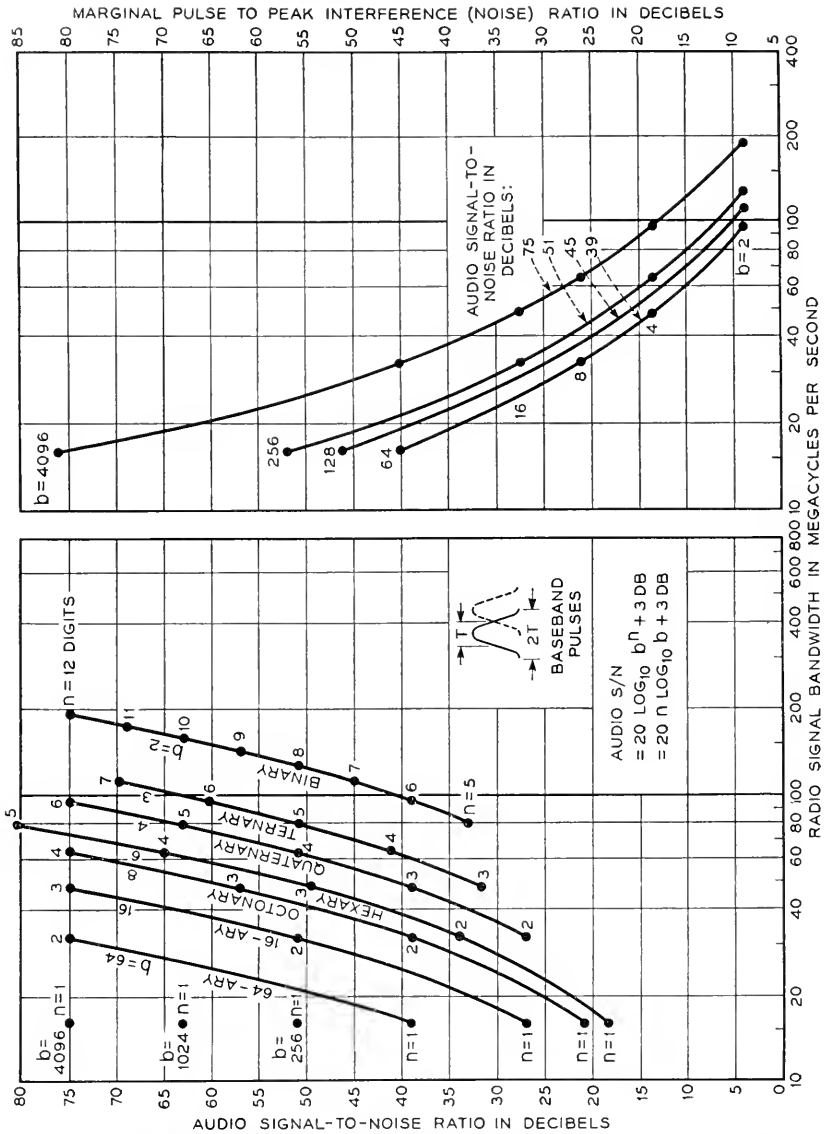
We note that the balance disappears if instantaneous sampling is used instead of gating because there is no longer any aperture discrimination. The curve for instantaneous sampling is plotted on Fig. 14. Calculation of this curve brings out the fact that the amplitude of the interfering components also depend on the framing phase difference between the two systems. When the framing frequencies are in phase, the two waves have a constant frequency difference, and the interference vanishes. We assume the phase difference as equally likely to fall anywhere within a complete cycle and average the received interference power over all phases. The curve is found to approach an asymptotic ordinate of 9 db at minimum band width as the frequency swings on the two systems approach zero together. The 9 db limit is compounded of 3 db from the marginal ratio between the two carriers, 3 db from averaging over the carrier phase difference, and 3 db from averaging over the framing phase difference. When wide bands and large swings are used, the curve approaches parallelism with the dashed one of Fig. 13 for fluctuation noise but about 15 db lower. Of this difference 9 db is accounted for by the higher marginal mean power level. The remainder is assignable to differences in spectral distribution; in particular the *r-f* spectrum of idle similar system interference is concentrated in half of the band instead of being uniformly spread as in fluctuation noise.

The curve for gated similar system interference has been estimated by assuming that, with all channels loaded and a wide frequency swing, the performance is like that with fluctuation noise except for a 3 db correction allowed for the more concentrated spectrum. This gives an asymptote on the right parallel to the solid marginal curve of Fig. 13 and 12 db lower. At the left the curve must approach the same asymptote as the one for instantaneous sampling. It then seems reasonable to assume that the interference power is directly proportional to the number of active channels and the curve for an average of one eighth of the channels loaded is obtained by raising the full load curve 9 db.

FIG. 15—PCM-AM

The curves on the left show how the audio signal-to-noise ratio varies with bandwidth, the audio noise being quantizing, or granularity, noise as discussed in Appendix I. The number of digits per code symbol is  $n$  and the number of digit values (including zero), i.e., the base, is  $b$ . Bandwidth is  $2/T$  where  $T$  is the time per pulse and is therefore 16 mc per digit. The curves are, of course, a set of discrete points rather than continuous as shown. The steep rise is to be contrasted with the 3 to 9 db per octave slopes of the curves previously presented.

The curves on the right plot the maximum values (with a 3 db allowance included) of peak noise or interference, referred to the highest pulse value,



quantized PAM having the number of steps necessary to yield the specified signal-to-noise ratio. The quantized PAM bandwidth of 16 mc assumes the use of overlapping sinusoidal pulses as in binary PCM. Actually, such an overlap would be hazardous in the higher base systems; and quantized PAM, like unquantized PAM, should perhaps be assigned more time per pulse but not as much as  $2T$  because regeneration could be employed to prevent accumulation of interchannel crosstalk. The tables presented later do not include the bandwidth increase that would follow such an increase in time per channel.

The curves at the right in Fig. 15 are terminated at 16 mc corresponding to one pulse per channel. In accordance with the principles of Appendix III more than one channel per pulse can be transmitted, theoretically. To include such a hypothetical case of less than one digit per channel, the curves could have been extended upward to the left. The 39 db signal-to-noise ratio curve would have reached an ordinate of 81 db at 8 mc on the bandwidth axis.

It is of interest to compare the audio signal-to-noise ratio of unquantized PAM with that of quantized PAM for the interference ratios demanded by quantized PAM. In the case of marginal CW interference the audio noise (evaluating the audio disturbance as noise of equivalent power) turns out to be the same as the quantizing noise and so, in a circuit of more than one span, quantized PAM is advantageous from a transmission point of view. With fluctuation noise the unquantized PAM audio noise would be 9 db lower than the quantizing noise and so, in a circuit of more than 9 spans of equal loss, the quantized PAM would be preferred.

#### FIG. 16—PCM-FM, FLUCTUATION NOISE

Here FM advantage is employed to permit operation in the presence of more noise than is possible with AM. It seems more illuminating to explain these curves by checking their correctness rather than by deriving them.

In all cases, a baseband signal-to-noise ratio giving the same margin over noise peaks as for AM (Fig. 15) is obtained by FM advantage. For the solid curves the FM limiter is assumed to be marginal (12 db radio signal-to-noise ratio), and for the dashed curves the radio signal-to-noise ratio is assumed to be the same as the marginal requirement for binary PCM-AM (18 db). The FM advantage with respect to an FM wave of the same power as in the peak AM pulse is, in db

$$20 \log \frac{\beta}{F_b} + 4.8 = 20 \log \left( \frac{B}{F_b} - 2 \right) + 4.8$$

However, the FM power is greater than the peak AM pulse power by 10

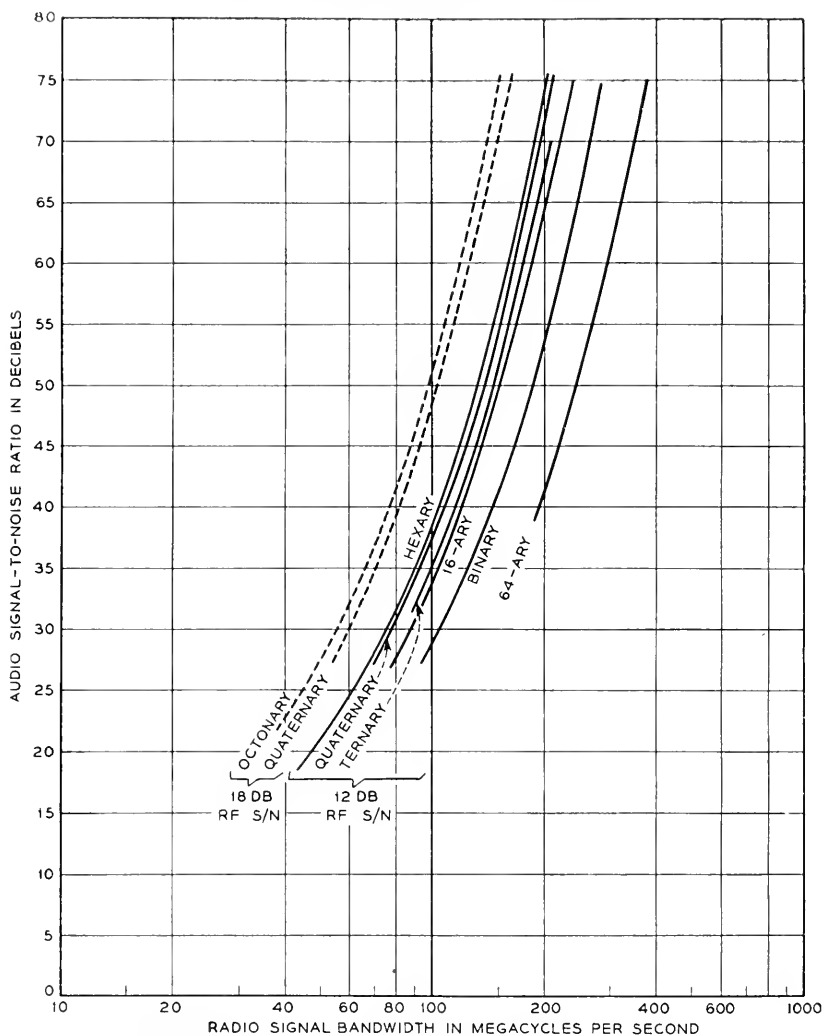


Fig. 16—PCM-FM; performance with respect to fluctuation noise. Relations between bandwidth, power, and audio signal-to-noise for 1000 4-kc channels, showing optimum bases for different ratios of FM wave to noise.

$\log \frac{B}{2F_b}$  because the FM power-to-noise ratio is maintained regardless of bandwidth. The total advantage of the FM case is therefore

$$20 \log \left( \frac{B}{F_b} - 2 \right) + 4.8 + 10 \log \frac{B}{2F_b}$$

and this must just make up for the difference between the 12 db (or 18 db) FM wave-to-noise ratio and the pulse-to-noise ratios of 18 db + 20 log  $(b - 1)$  required in the AM case. Substituting values from the curves will show that this is so.

These curves show a minimum bandwidth for an optimum PCM base. This is to be expected since two different rates of exchange between bandwidth and advantage are involved. One is the advantage growing out of PCM of reduced base while the other is the conventional FM advantage. An analogous situation was found in PPM-FM.

It is of interest to examine the PCM-FM situation when the FM circuit is as tolerant of noise as the most tolerant AM case, namely when the  $r$ - $f$  signal-to-noise ratio is 18 db. The optimum PCM base is octonary and the corresponding minimum bandwidth (as we define it) is actually 20% less than for binary AM. This apparent advantage of PCM-FM is not obtained when tolerance to CW and similar systems is considered. Figure 17, which follows, shows that when allowance is made for a 9 db  $r$ - $f$  signal-to-interference ratio (as in binary PCM-AM), the minimum FM bandwidth is greater by about 30% than for binary AM and the optimum base is ternary or quaternary. If the 3 db interference tolerance possible in FM is required, it is obtained, as shown in Fig. 17, with ternary PCM-FM, at a cost of approximately twice the bandwidth required in binary PCM-AM, which has a tolerance of 9 db. We should point out here that binary PCM transmitted by single sideband and detected by a local carrier has a tolerance of 3 db and requires half the bandwidth shown in Fig. 16. PCM-FM requires a bandwidth 3.8 times that of single sideband binary PCM for the same 3 db tolerance.

FIG. 17—PCM-FM, CW AND SIMILAR SYSTEM INTERFERENCE

In PCM, sequences of several pulses of the same amplitude may occur. The FM signal then consists of a steady frequency. A steady beat frequency persisting for several pulse periods will be produced by CW interference.<sup>24</sup> If this beat frequency is  $F_b$  the maximum interfering amplitude will be produced. The amplitude is  $(Q/P) F_b$  while the step interval is  $\beta/(b - 1)$ . To confine the interference to a half step (with 3 db margin) requires that

$$\beta/(b - 1) \geq 2(Q/P) \sqrt{2} F_b$$

For  $Q/P = 0.707$ ,

$$\beta \geq 2(b - 1) F_b$$

<sup>24</sup> The general solution of the problem of frequency error produced by superimposing a sine wave on an unmodulated carrier is given in Appendix II.

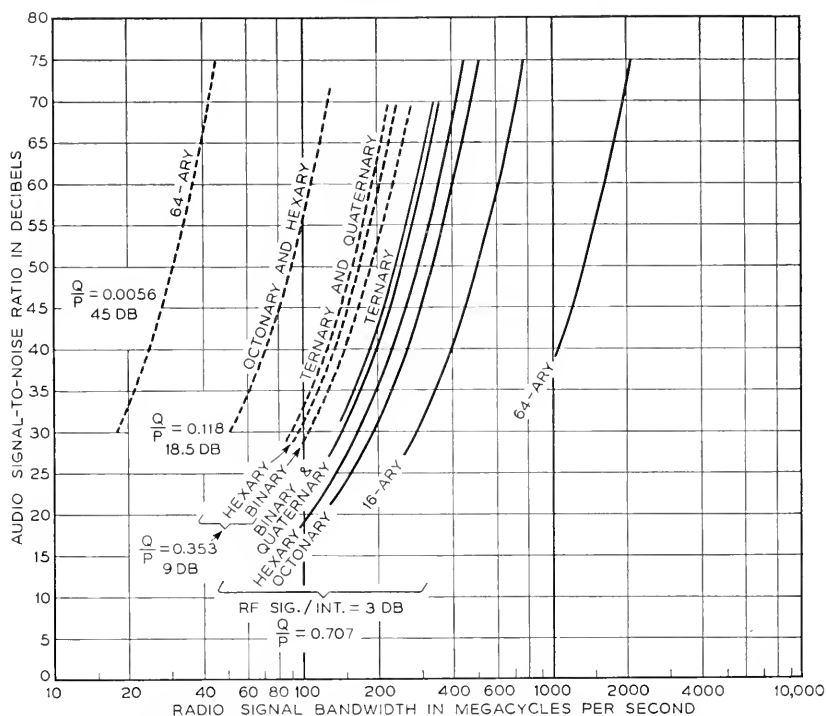


Fig. 17—PCM FM; performance with respect to CW and similar system interference for 1000 4-kc channels. Relations between bandwidth and audio signal-to-noise ratio showing optimum bases for different ratios of FM wave to interference.

and the minimum band width becomes

$$B = \beta + 2 F_b = 2bF_b$$

For  $Q/P = 0.3535$  (9 db) the minimum required value of  $\beta$  is halved so that

$$B = (b + 1) F_b$$

For  $Q/P = 0.118$  (18.5 db) the minimum required value of  $\beta$  is further reduced threefold so that

$$B = \frac{b + 5}{3} F_b$$

The curves of Fig. 17 are calculated from these relations.

With interference from a similar system a number of necessary conditions must be met. If the systems are similar in PCM base and in radio frequency, the sustained beat frequencies that may occur are  $\beta/(b - 1)$  and

multiples thereof. The amplitude of the lowest of these frequencies is  $(Q/P)\beta/(b-1)$ . For  $Q/P = 0.707$ , this frequency must be suppressed by the baseband filter since otherwise the threshold would be exceeded. Thus,

$$\begin{aligned}\beta &\geq (b-1) F_b \\ B &= \beta + 2F_b = (b+1) F_b\end{aligned}$$

For  $Q/P = 0.353$ , the lowest beat frequency need not be suppressed but the  $2\beta/(b-1)$  frequency must be suppressed; thus  $2\beta/(b-1) \geq F_b$ .

$$\begin{aligned}\beta &\geq \frac{b-1}{2} F_b \\ B &= \beta + 2F_b = \frac{b+3}{2} F_b\end{aligned}$$

Comparing these bandwidth values with those required for CW shows that the above requirements are more lenient than for the corresponding CW cases, particularly for the higher values of  $b$  where the above bandwidth values approach one-half of those obtained for CW.

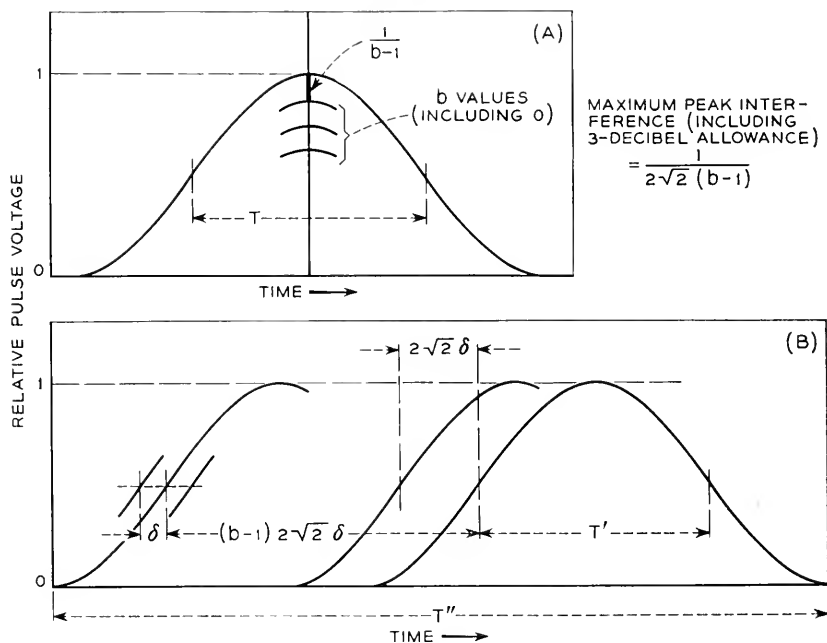
However, the above requirements are not quite sufficient. Transitions between adjacent frequency values, occurring in one system, will produce varying beat frequencies which pass through all values. This case differs from the CW case in that the beat frequency is not sustained and that the baseband filter output will not be as high as in the CW case. Calculations show that the bandwidth requirements are intermediate between those for the CW case and the similar system case considered previously.

When we remember that for low base systems (binary) the requirements for similar system and CW interference are nearly alike, while for high base systems a small frequency difference in frequency alignment can produce similar system interference completely equivalent to CW interference, we may regard Fig. 17 as applying to both, practically. Such a conclusion also makes the curves apply to interference between systems of different base.

### QUANTIZED PPM

PCM pulses, including the limiting case of quantized PAM pulses, may be transmitted by time modulation instead of frequency modulation, i.e., by "quantized PPM." In this case, as in PCM-FM, bandwidth may be used to increase the tolerance to noise and interference. Figure 18 illustrates this case. At (A) is shown a PCM pulse having  $b$  values including zero, the highest amplitude being unity. The maximum tolerable peak interference is  $1/2\sqrt{2}(b-1)$  and the time per pulse is taken as  $T$ . (For high base systems the time per pulse should be greater, perhaps  $2T$  as pointed out in the discussion of PCM-AM). At (B) is shown the quantized PPM

pulse of the same amplitude. The time per pulse is taken to be  $T''$  and the duration of the pulse at half height is  $T'$ . If  $T''$  is put equal to  $T$  the ratio of the PPM bandwidth to the PCM bandwidth is  $T/T'$ . The time shift



$$\delta = \frac{\text{INTERFERENCE}}{\text{SLOPE OF PULSE}}; \quad \text{SLOPE} = \frac{\pi}{2T'}$$

#### CASE 1

$$\text{INTERFERENCE} = \frac{1}{2\sqrt{2}(b-1)}$$

$$\delta = \frac{2T'}{2\pi\sqrt{2}(b-1)}$$

$$T'' = T' \left( 2 + \frac{2}{\pi} \right)$$

#### CASE 2

$$\text{INTERFERENCE} = 0.353 \text{ (9 DB)}$$

$$\delta = \frac{2T' \times 0.353}{\pi} = \frac{T'}{\sqrt{2}\pi}$$

$$T'' = T' \left[ 2 + \frac{2(b-1)}{\pi} \right]$$

IF WE TAKE THE TIME PER PULSE TO BE  $T$  AND  $T''$  AND MAKE THEM EQUAL, THE BANDWIDTH RATIOS BECOME

$$2 + \frac{2}{\pi} = 2.64$$

$$2 + \frac{2(b-1)}{\pi}$$

Fig. 18—Comparison of quantized PAM with quantized PPM.

produced by peak interference is represented by  $\delta$ . Our system is marginal when the smallest quantized step produces a shift of  $2\sqrt{2}\delta$ . The peak time shift produced by a signal is then  $(b-1)2\sqrt{2}\delta$ . Two cases are considered. In one the PPM system operates in the presence of the same peak interference as in the PCM case. The bandwidth ratio is 2.64. The other case



assumes that the peak interference is marginal for all bandwidths (9 db down). The bandwidth ratio is then  $2\left(1 + \frac{b-1}{\pi}\right)$ . It was previously found that in PCM-FM, with peak interference 9 db down, the radio bandwidth must be  $(b+1)F_b$ . Since the radio bandwidth of PCM-AM is  $2F_b$ , the bandwidth ratio is  $(b+1)/2$ . Comparing these bandwidth ratios we see that the PPM bandwidth required to operate in the presence of marginal interference is nearly two times that required in PCM-FM. Furthermore, this PPM bandwidth ratio applies to marginal fluctuation noise whereas in PCM-FM a more favorable result was obtained.

FIG. 19 FDM-FM, FLUCTUATION NOISE

When a group of channels in frequency division is transmitted by frequency modulation, the addition of channel voltages is translated to an addition of instantaneous frequency shift. The non-simultaneous load advantage applicable to a multichannel amplifier for frequency divided channels thus becomes an advantage in reduction of total frequency swing as compared to the sum of the individual peak frequency swings of the channels. The numerical db increments versus number of channels listed in Table I should, however, be modified for the following reason: The fluctuation noise spectrum in the output of an FM detector is not uniform with frequency, and hence the noise is unequally distributed among the channels. In order to obtain the same noise in all channels it is necessary to taper the signal levels in such a way that the full load frequency swing produced by one channel is proportional to the frequency of the channel. The frequency swing corresponding to full load in the top channel is therefore a larger part of the maximum instantaneous swing required for the group than the swings corresponding to lower channels. The result is, in effect, phase modulation. The multiplex addition factors for tapered level channels have not been determined experimentally. We have assumed here a 3 db reduction in the power capacity values listed in Table I. These reduced values then give the incremental capacity referred to *full load on the top channel*. Curves are shown for 100, 500 and 1000 channels. On account of the multiplex addition factor, it is not possible to obtain results for other numbers of channels from one curve by simply changing the frequency scale.

The derivation of these curves is straightforward but leads to an expression for the required bandwidth as a root of a cubic equation. As in the case of Fig. 16 we shall discuss the FDM-FM curves by checking them numerically. We have assumed that the channels are tapered in level and that we have, in fact, phase modulation with its consequent flat base-band noise distribution. To check the 60-db point on the 1000-channel

curve, we calculate that the noise in the entire baseband must be 43 db below the power in a sine wave which employs the full system load capacity. This figure comes from reducing the 60 db full load *channel* ratio by 30 db because of the 1000-fold greater baseband width and increasing it by the amount,  $16 - 3 = 13$  db, by which the full system load must exceed full load in the top channel. Thus  $60 - 30 + 13 = 43$  db. An FM advantage of 31 db must be obtained to permit the marginal *r-f* signal-

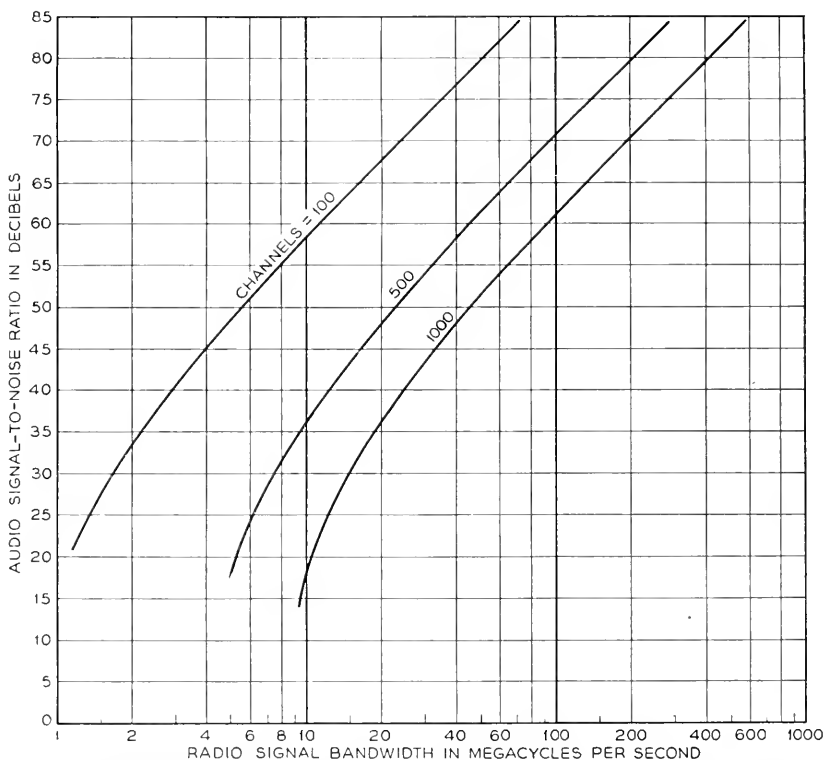


Fig. 19—FDM-FM; performance with respect to fluctuation noise. Relations between bandwidth and audio signal-to-noise ratio for marginal power; 4-kc channels.

to-noise ratio of 12 db to satisfy the above requirement,  $(43 - 12 = 31)$ . We get this advantage in part by phase modulation gain given by  $20 \log \frac{\beta}{F_b} - 6$  db. This gain is referred to 100% modulation AM whose unmodulated carrier power is the same as the FM wave power. This means that the reference is a system in which the FDM baseband appears as upper and lower sidebands which, when demodulated, yield a baseband

signal-to-noise ratio equal to the ratio of unmodulated carrier power to the noise power in the double width radio band. Since we keep the FM power marginal for all bandwidths an additional bandwidth improvement of  $10 \log \frac{B}{2F_b}$  accrues. Substituting  $B = 92$  mc,  $F_b = 4$  mc, and  $\beta = 92 - 8 = 84$  mc, will show that the above gains total 31 db.

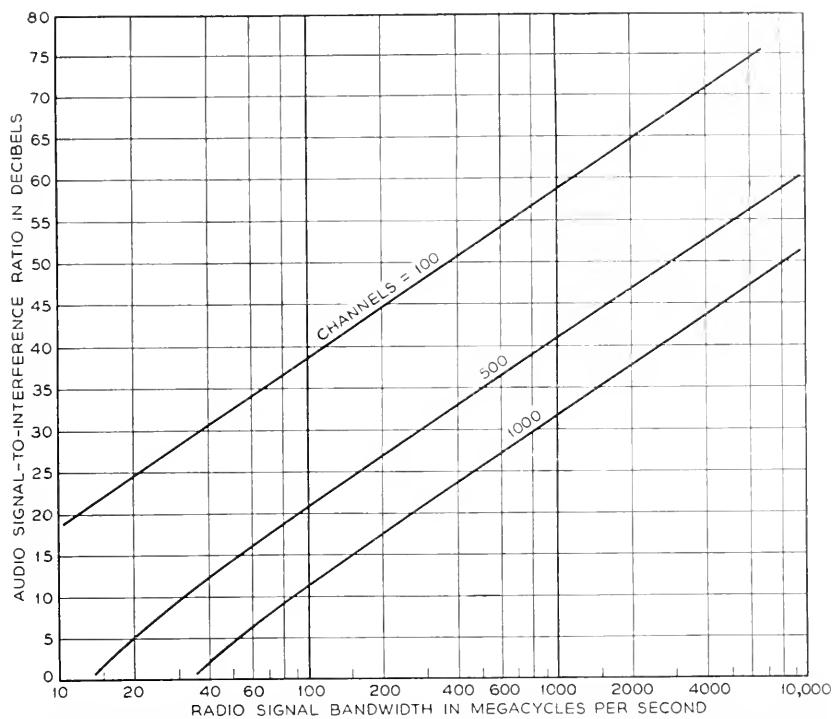


Fig. 20—FDM-FM; performance with respect to CW interference. Relations between bandwidth and audio signal-to-interference ratio for marginal ratio of FM wave to interference; 4-kc channels.

FIG. 20 — FDM-FM, CW INTERFERENCE

The disturbance produced by CW is most readily evaluated when all channels are idle for then we have only the frequency error produced by a sine wave of relatively small amplitude superimposed on the steady sinusoidal carrier wave. To a first approximation (see Appendix II) the error has a frequency equal to the difference between the carrier and CW frequencies and an amplitude equal to this frequency difference multiplied by the ratio of the CW to the carrier amplitude. The error thus increases linearly with the frequency of the channel in which it falls but, since the channel levels

are also tapered in the same way, the signal-to-interference ratio is independent of the frequency of the disturbing CW. Varying the CW frequency only changes the number of the channel into which the interference falls. Loading the channels distributes the interference over several channels instead of concentrating it in one, but we have plotted in Fig. 20 the more severe case in which all channels are idle.

We have not undertaken to compute curves for similar system interference in the case of FDM-FM, but estimates for two extreme conditions can be made. In the case of low index FM systems the carrier frequency component of the spectrum is not affected by the modulating signal and the FM wave is, in fact, like an AM wave with the carrier displaced 90 degrees in phase. A similar interfering FM wave combines with the wanted FM to produce frequency or amplitude variations and does this cyclically as the  $r$ - $f$  phase between the systems varies. When the phases are appropriate for the production of frequency variation, crosstalk appears in the wanted reception at a level lower by the ratio of FM wave amplitude. Averaging over all  $r$ - $f$  phases should reduce the crosstalk by 3 db. The actual amount of interference received in a channel is less than would be predicted from replacement of the interfering FM wave by fluctuation noise of the same mean power spread over the  $r$ - $f$  band, because the bulk of the interfering power is contained in the carrier component located at a frequency which does no harm. Increase of the frequency swing in both systems produces significant reduction in crosstalk when the carrier amplitude diminishes appreciably and important higher order sidebands appear, i.e. when the interfering system has its spectrum spread out more or less uniformly, like noise. Systems designed for wide swings under full load may, however, operate with only a few channels active; in such cases the low index situation may exist and the received interference will be down approximately by the ratio of the FM waves, without the benefit of FM advantage. While in this situation the bulk of the interfering power is again contained in the harmless carrier, the received interference is concentrated in a few channels and is greater than if the interfering wave power were spread, like noise, thinly over the  $r$ - $f$  band, which in this case is many times wider than the band occupied by the low index signal. For such adverse loading conditions, the curve for similar system interference, while starting at the left above the corresponding noise curve of Fig. 19, may actually cross over and finally approach it from the lower side.

In the case of systems of very wide swing such as are involved in Table II we regard the interfering system as equivalent, under all common load conditions, to noise spread uniformly over the bandwidth and having the same power as the interfering wave. The entry in Table II is obtained by reading

the curve of Fig. 19 at 69 db audio signal-to-noise ratio which would be appropriate to yield 60 db when the "noise" is marginal at 3 db below the FM wave power instead of 12 db. A different procedure is required for the narrow band entries of Table IV. Here the emphasis on conservation of bandwidth leads to a two-frequency repeater plan with tolerance of similar system interference 44 db down. A 60 db audio signal-to-interference ratio can be met under these conditions with moderate swings for which the equivalent noise representation of the interference is not valid. The result is considerably influenced by the channel loading and we have no impeccable method of calculating the necessary bandwidth. We estimate that a bandwidth of 22.5 mc., with  $\beta = 14.5$  mc., will satisfy the requirements for all except unusually adverse loading conditions.

### III. BAND WIDTH AND POWER TABLES

The information contained in the curves of Fig. 9-20 has been used in preparing Tables II and III, which show what can be done with the various systems when bandwidth is used freely. The prime objective studied here is the conservation of peak transmitted power. In Table II the audio channel must meet message circuit requirements<sup>25</sup> while, in Table III, a much better grade of performance—more than sufficient for transmission of high fidelity musical programs—is stipulated. We have prepared Table III (as well as Table V) on the basis of replacing the 1000 4-kc. message channels of Table II with 250 16-kc. channels. Since we have available established load rating theory only for message circuits, we have omitted FDM and FDM-FM from Table III (and Table V). The values of Table II are based on a nominal 60 db ratio of signal-to-noise, but it is assumed permissible to meet this in the pulse systems by using 22 db of instantaneous companding so that only 38 db signal-to-noise ratio is actually required within the compandor. The PCM systems provide for a 39 db circuit within the compandor, corresponding to 6 binary digits, 3 quaternary digits, 2 octonary digits or one 64-ary digit. No allowance is made for the accumulation of quantizing noise arising when several PCM links are connected in tandem at voice frequency. In practice, 7 binary digits might be used. This would provide for several links and would permit slightly more companding. Table III assumes a 75 db signal-to-noise ratio and no companding and is referred to here as a "program" circuit. We use such a high-grade circuit to illustrate more emphatically how the system preferences depend

<sup>25</sup> We do not pretend to deal fully with the involved matter of system requirements distinguishing between kinds of noise and interference or crosstalk that appear in message channels. We merely assume that the power of the separate types of disturbances considered must be individually 60 db below that of a full load test tone under the worst specified transmission condition.

TABLE II  
OPTIMUM BAND WIDTHS FOR MINIMUM POWER FOR MESSAGE TYPE CIRCUITS  
133 30-mi spans, 1000 4-kc channels, 15 db NF, 75 db span loss.

SYSTEM	$S/N(1)$ IN DB	NUMBER OF RESHAPINGS: (4)						ONE EXPOSURE TO MARGINAL INTERFERENCE		MARGINAL PEAK INTERFERENCE IN DB
		133		5(2)		1(3)		CW	SIMILAR SYSTEM	
		BAND WIDTH IN MC	POWER IN WATTS	BAND WIDTH IN MC	POWER IN WATTS	BAND WIDTH IN MC	POWER IN WATTS			
PPM-AM	38									-9
PPM-FM	38									-3
PAM-FM	38									-3
FDM-FM	60									-3

(1) AUDIO SIGNAL TO NOISE (OR INTERFERENCE) RATIO

(2) RESHAPING EVERY 27 SPANS

(3) ASSUMES 12.5% ACTIVITY

(4) REGENERATION IN THE CASE OF PCM, LIMITING IN THE CASE OF FM

(5) ASSUMES 12.5% ACTIVITY

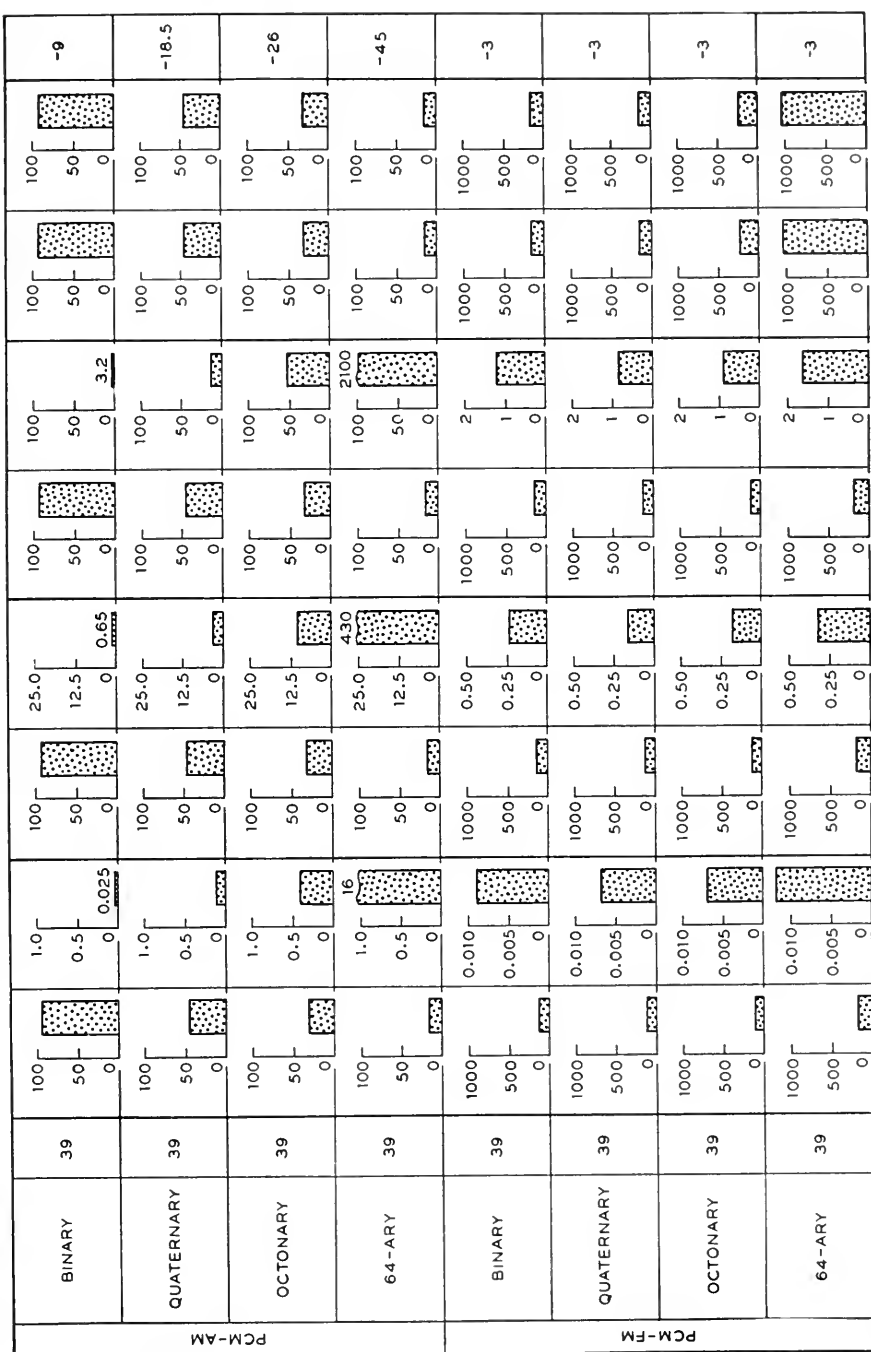
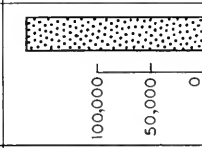
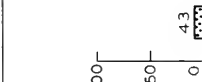
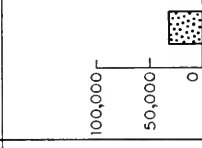
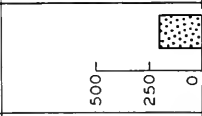
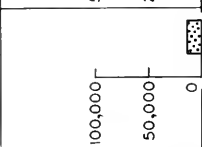
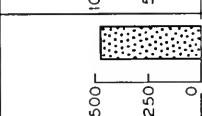
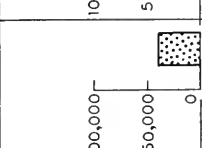
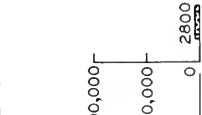
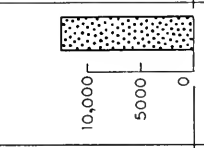
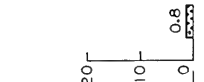
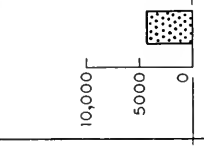
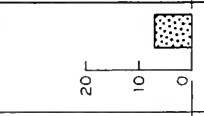
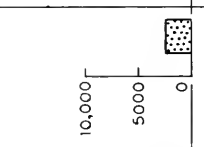
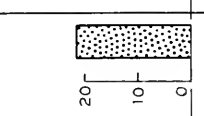
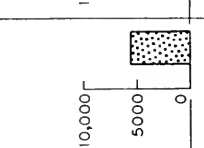
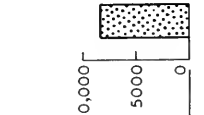
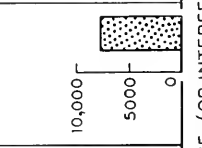
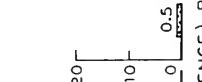
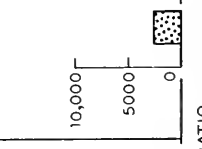
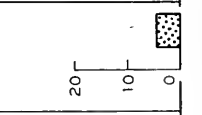
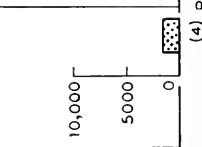
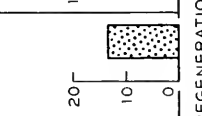
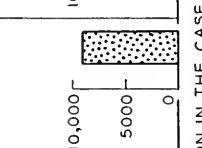
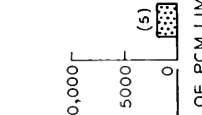


TABLE III  
OPTIMUM BAND WIDTHS FOR MINIMUM POWER FOR PROGRAM TYPE CIRCUITS  
133 30-mi spans, 250 16-kc channels, 15 db NF, 75 db span loss.

SYSTEM	S/N(1) IN DB	NUMBER OF RESHAPINGS: (4)						ONE EXPOSURE TO MARGINAL INTERFERENCE		MARGINAL PEAK INTERFERENCE IN DB
		133		5(2)		1(3)		CW	SIMILAR SYSTEM	
		BAND WIDTH IN MC	POWER IN WATTS	BAND WIDTH IN MC	POWER IN WATTS	BAND WIDTH IN MC	POWER IN WATTS			
PPM-AM	75									-9
										-3
PAM-FM	75									-3

(1) AUDIO SIGNAL TO NOISE (OR INTERFERENCE) RATIO

(2) RESHAPING EVERY 27 SPANS

(3) RESHAPING AT END OF 133 SPANS

(4) REGENERATION IN THE CASE OF PCM LIMITING IN  
THE CASE OF FM

(5) ASSUMES 12.5% ACTIVITY





upon signal-to-noise ratio. Both tables apply to long systems comprising 133 repeaters spaced 30 miles apart. The span loss is 75 db. Three reshaping or regeneration plans are shown: reshaping at every repeater, reshaping five times in the complete system, and no reshaping within the system.

In the case of PCM, reshaping becomes a true regeneration which completely removes noise accumulated in the transmission link; while, in the non-quantized pulse systems, reshaping restores the original pulse shape but retains timing or amplitude errors. In the case of FM systems, reshaping is accomplished by the amplitude limiter which removes envelope variations arising from noise, but does not suppress the accompanying frequency shifts. Reshaping, in contrast to regeneration, is only a partial prevention of cumulative effects but, as shown by the tables, it has definite value in enabling the use of wider transmission bands with corresponding smaller amounts of power than permissible without reshaping. Regeneration completely removes errors in both the amplitude and in the time. The maximum bandwidth which can be used is independent of the number of regenerations, but the signal power must be increased in proportion to the number of spans covered before regeneration.

In the case of non-regenerative radio transmission systems, we may regard the 75 db span loss as 60 db free space loss plus a fading allowance of 15 db. This allowance is intended to cover the increment of noise caused by fading in the entire system. Available data on distribution of fading are too meager to permit generalization, but indicate that on some routes, at least, the total degradation suffered would rarely be worse than that produced by 15 db simultaneous fades on all spans; and hence a design based on 75 db span loss should satisfy the noise requirements except for an extremely small fraction of the time. In other words a few spans of the non-regenerative system may fade deeply but, in regard to total accumulated noise, the system is credited with the higher signal-to-noise ratio occurring on spans which are not simultaneously in fading minima. In regenerative PCM systems no credit accrues from a higher signal-to-noise ratio occurring between points of regeneration, and protection must be provided against the worst condition that is likely to occur in any section included between regeneration points.

However, the values of minimum power obtained by lavish use of bandwidth exhibited in Tables II and III may be particularly significant for wave guide transmission systems; and hence the assumption that all spans have the same loss is appropriate here.

The outstanding features of Tables II and III are the extremely small amounts of power needed in the PCM systems with only moderate expenditures of bandwidth as compared with the non-quantized system. These

results illustrate the properties of PCM as a means of converting bandwidth into transmission advantage.

The PCM-FM entries are taken from the curves of Fig. 16 plotted for noise 12 db down. Curves are also given in Fig. 16 for noise 18 db down. It will be noted that the bandwidths indicated become smaller when the noise is required to be farther down, but that the power requirements become greater because the bandwidth reduction factor is less than the factor multiplying the  $r$ - $f$  signal-to-noise ratio.

The columns at the right in Tables II and III show the bandwidths which must be employed in order to attain a 60 db signal-to-interference ratio in the presence of one source of interference whose amplitude is just marginal for the type of system concerned.

Tables IV and V are prepared from another point of view—that of conserving bandwidth<sup>26</sup> instead of power. The systems particularly suited for narrow bands such as FDM and PAM-AM have been added to the list. The actual minimum bandwidths are, in many cases, determined by engineering judgment; smaller values than those tabulated may be possible at the expense of greatly increased power and precision requirements. Thus in the case of PPM-AM we have arbitrarily chosen 40 mc as necessary for 1000 4-kc channels. According to our initial postulate the audio signal-to-noise ratio vanishes at 32 mc, and indefinitely great signal power would be required as we approach this limit. In PAM-AM we have assumed that pulses in adjacent channels just touch, thereby setting the bandwidth at 32 mc. Smaller bandwidths could be used if the pulses were allowed to overlap. This would reduce the allowable duration of the channel gate and deprive the system of some of its tolerance to similar system interference as well as noise. The maximum pulse power required for 100% modulation is tabulated. If instantaneous sampling were used this would be 6 db above the unmodulated pulse power which is, in turn, 38 db above the mean total fluctuation power accumulated in a 32-mc band from 133 spans. We have reduced the value of power thus computed by 1.7 db to allow for a calculated improvement in signal-to-noise ratio obtainable by gating at the channel input with a time function of the same shape as the signal pulse.

The FM systems listed are of two kinds. The first is a relatively narrow-band type in which advantages such as relative immunity to gain fluctuation and amplitude non-linearity are sought with small increment in bandwidth over AM. Since these objectives are not sufficient in themselves to fix the actual bandwidth needed, an arbitrary additional requirement has

<sup>26</sup> We do not here entertain the idea of using certain exchange methods to permit use of less band width than the conventional minimum of 4 kc per channel, but rather to use modest amounts of additional band width. Appendix III discusses briefly a band reduction principle.

TABLE IV  
MINIMUM BAND WIDTHS AND CORRESPONDING POWER REQUIREMENTS FOR MESSAGE TYPE  
CIRCUITS

133 30-mi spans, 1000 4-kc channels, 15 db NF.

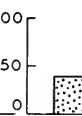
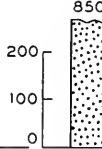
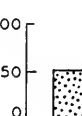
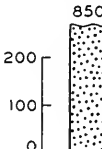
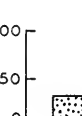
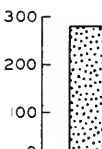
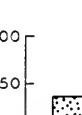
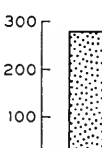
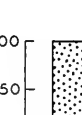
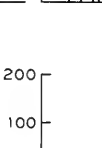
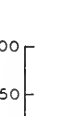
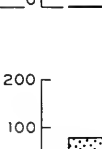
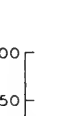

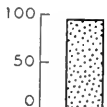
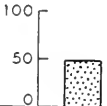
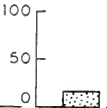
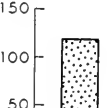
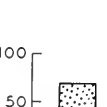
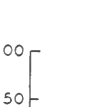
SYSTEM		S/N IN DB	BAND WIDTH IN MC	POWER IN WATTS	TOLERABLE INTERFERENCE RATIO IN DB		SPAN LOSS IN DB
					CW	SIMILAR SYSTEM	
PPM-AM		38			46	41 <sup>(1)</sup>	75
PPM-FM		38			49	39 <sup>(1)</sup>	75
PAM-AM		38			44	40 <sup>(1)</sup>	75
PAM-FM	NARROW BAND	38			46	23 <sup>(2)</sup>	75
	WIDE BAND	38			20	9 <sup>(2)</sup>	75
FDM		60			76	60	75
FDM-FM		60			68	44	75

TABLE IV—Concluded

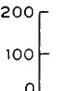
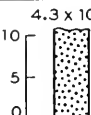
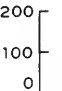
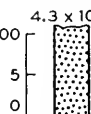
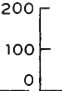
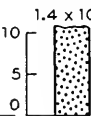
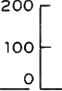
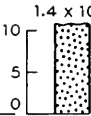
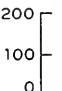
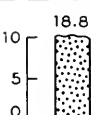
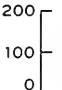
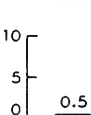
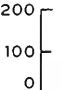
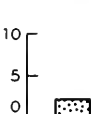
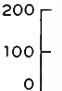
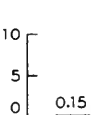
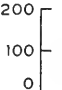
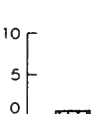
SYSTEM		S/N IN DB	BAND WIDTH IN MC	POWER IN WATTS	TOLERABLE INTERFERENCE RATIO IN DB		SPAN LOSS IN DB
					CW	SIMILAR SYSTEM	
PCM-AM	BINARY	39		0.25	9	9	85
	QUATERNARY	39		1.1	18.5	18.5	85
	64-ARY	39			45	45	85
PCM-FM	QUATERNARY	39		0.076	9	9	85
	OCTONARY	39		0.25	18.5	18.5	85
	64-ARY	39			45	45	85

REGENERATE AT EVERY REPEATER IN PCM

- (1) INTERFERING SYSTEM IDLE; ACTIVITY HAS SMALL EFFECT.  
 (2) ASSUMING 12.5% CHANNEL ACTIVITY.

TABLE V  
MINIMUM BAND WIDTHS AND CORRESPONDING POWER REQUIREMENTS FOR PROGRAM TYPE  
CIRCUITS

133 30-mi spans, 250 16-kc channels, 15 db NF.

SYSTEM		S/N IN DB	BAND WIDTH IN MC	POWER IN WATTS	TOLERABLE INTERFERENCE RATIO IN DB		SPAN LOSS IN DB
					CW	SIMILAR SYSTEM	
PPM-AM		75			83	78 <sup>(1)</sup>	75
PPM-FM		75			86	76 <sup>(1)</sup>	75
PAM-AM		75			81	77 <sup>(1)</sup>	75
PAM-FM	NARROW BAND	75			83	60 <sup>(2)</sup>	75
	WIDE BAND	75			25	9 <sup>(2)</sup>	75
PCM-AM	BINARY	75			9	9	85
	QUATERNARY	75			18.5	18.5	85
PCM-FM	QUATERNARY	75			9	9	85
	OCTONARY	75			18.5	18.5	85

REGENERATE AT EVERY REPEATER IN PCM

(1) INTERFERING SYSTEM IDLE; ACTIVITY HAS SMALL EFFECT.

(2) ASSUMING 12.5% CHANNEL ACTIVITY.

been imposed that the transmitted power in the FM system should be equal to that required in the corresponding AM system. The resulting values of bandwidth are found to be reasonable ones for low index FM. An exception is made in the case of FDM-FM systems of message type where it is found that a net economy of frequency occupancy can be obtained by increasing the frequency swing sufficiently to tolerate similar system interference 44 db down. This enables the two-frequency repeater plan of Fig. 4, as discussed in Section I, to be used and substantially reduces the frequency occupancy over that of a lower index FM system more vulnerable to antenna crosstalk and therefore requiring more frequency assignments. We have estimated that a radio signal bandwidth of 22.5 mc achieves the required 44 db tolerance. The second type of FM is a wide-band system designed for specified tolerances of interference from similar systems. Data on this second type will be used later in our study of inter-route interference, where it will appear that ruggedness is a more important criterion of frequency occupancy than the minimum bandwidth needed for transmission.

No curves have been furnished to determine the FDM entries, since there is no variation with radio bandwidth to consider. The band required is merely the number of channels multiplied by the width of a channel. The power required for message channels is determined by calculating the amount of power in one channel to give a 60 db margin over mean fluctuation noise power in a 4-kc band and applying the multiplex addition factor of Table I. Similar system interference is simply linear crosstalk and must be, we say, 60 db down. CW interference referred to maximum system power must be down an additional amount equal to the multiplex addition factor of Table I in order to meet 60 db suppression in the disturbed channel. Since the two-frequency plan of Fig. 4 does not suppress interference between the two directions of a single route by 60 db, we must use twice as many frequency assignments as there shown. This duplication will appear in Table VI. FDM is the only system of Table IV for which such duplication is necessary, since the others do not require more than 44 db suppression. In the program type systems of Table V, however, the first four listed would need duplicated frequency assignments.

The PCM-AM systems of course do not use any smaller bandwidths than those given in Tables II and III and would, therefore, be expected to show disadvantageously in a bandwidth comparison with the other systems. On the other hand they make, relatively, a good showing in power requirements and in tolerance to CW and similar system interference.

In the next section we shall show that economy of bandwidth may, in fact, be illusory because of the greater susceptibility to intra- and inter-system interference associated with narrow band methods. It is not the bandwidth actually needed for transmission that is important, but the

tightness with which the bands may be packed into the frequency range without mutual interference. Because of the ruggedness of low-base PCM, neighboring frequency bands can actually be allowed to overlap. Introduction of the proper spacing factors for satisfactory separation in frequency between adjacent bands causes the PCM system to overtake the other methods in effective utilization of frequency space, especially when intersecting routes are involved.

The PCM-FM systems listed in Tables IV and V are of the second class listed above, in which equivalent ruggedness rather than equivalent power as compared to AM is the criterion. Thus, binary PCM-AM is compared with a PCM-FM system having the same 9-db tolerance of interference. The curves of Fig. 17 show that, with such a tolerance, the minimum PCM-FM bandwidth is secured when the base is either three or four. We choose the quaternary case here because the signal-to-noise ratios obtainable coincide with those of the binary. Likewise, either octonary or hexary PCM-FM furnishes the optimum base for the 18.5 db tolerance possessed by quaternary PCM-AM and, of the two, octonary is more suitable for our tabulation. In determining the power required to override fluctuation noise in a PCM-FM system designed for a specified tolerance of similar system interference, we must make sure that both the limiter and slicer are protected against breaking.

The values of repeater power capacity shown in Tables IV and V will satisfy the noise requirements on a 133-span non-regenerated circuit with 75 db loss on all spans. For spans of 60 db free space loss the tabulated power thus provides for 15 db fades simultaneously on all spans, or for 13 db simultaneous fades of 25 db, or for a single fade of 36 db. PCM systems employing regeneration on every span must be powered for the deepest fade that is likely to be encountered. We have arbitrarily taken this to be 25 db making the span loss 85 db. This is probably not a sufficient allowance for some situations but will serve for illustrative purposes. If regeneration were not practiced the power would be  $25 - 15 = 10$  db lower from the fading allowance standpoint but would have to be increased  $10 \log 133 = 21$  db for noise accumulation, so regeneration results in a power saving of 11 db. If, with regeneration, we were to protect each span against the deepest single fade (36 db) permitted by the power provided for non-regenerative operation, the power advantage of regeneration would disappear ( $36 - 15 - 21 = 0$  db).

In general, when the power without regeneration protects against simultaneous fades upwards of just a few db there is little or no power advantage in regeneration if we then protect each span against the deepest single fade permitted when regeneration is not practiced. This is true even for large numbers of spans. There remain, however, important advantages for



regeneration in preventing accumulation of disturbances that are not much affected by the distribution of fading.

#### IV. FREQUENCY OCCUPANCY TABLES FOR RADIO RELAY

The frequency space occupancy for a single two-way route is, according to principles laid down in the introduction, a frequency block  $2U$  times the signal bandwidth.<sup>27</sup> Our problem, as stated in the introduction, is to examine the situations arising when a number of 1000-channel routes converge toward a terminal city, assuming all of the routes to be of the same kind. We will determine the number of times the above frequency blocks must be repeated in the spectrum in order to keep interference within tolerable bounds. The sum of these blocks then really defines the frequency occupancy and determines the space which must be allocated or, conversely, determines the number of routes a given allocation will accommodate. We will use the tolerable ratios of similar system interference taken from Tables IV and V, together with appropriate antenna directivity, to determine the number of these blocks.

#### ANTENNA CHARACTERISTICS

The directional discrimination afforded by the antennas is obviously an important factor in frequency economy. For our present study, we employ an antenna having a directional pattern slightly superior to that of the 4000-mc shielded lens antenna in use on the New York-Boston radio relay circuit. Figure 21 shows the assumed directional characteristic omitting "nulls" between the minor lobes. Of importance also are the nearby discrimination characteristics of the antennas as given in Fig. 4.

The situations arising at a point where a number of routes converge (or cross) or where a route is equipped with a spur connection are variations of that occurring at a single repeater point. In fact, the situation in which two routes converge from approximately opposite directions occurs at every repeater point in a straight route, while a repeater point at which the route bends sharply is like a terminal point at which two routes converge at a small angle.

The crosstalk in our assumed two-frequency long distance repeater system has been estimated in Section I (under "The Radio Repeater") and was found equivalent to a single source of similar system interference 44 db down. A system which possesses just enough tolerance to withstand the accumulated crosstalk on a long straight repeater system is not capable of meeting another such system at an angle unless additional frequencies are

<sup>27</sup> In the case of very tender systems, such as FDM, the factor  $2U$  is replaced by  $4U$  because a four-frequency plan is needed for a two-way repeater.  $U$  is the band spacing factor discussed under "The Radio Repeater."

invoked. The FDM-FM system of "minimum band width" listed in Table IV is intended to possess this 44 db tolerance. To illustrate the requirement of new frequencies let us take the case of several FDM-FM routes

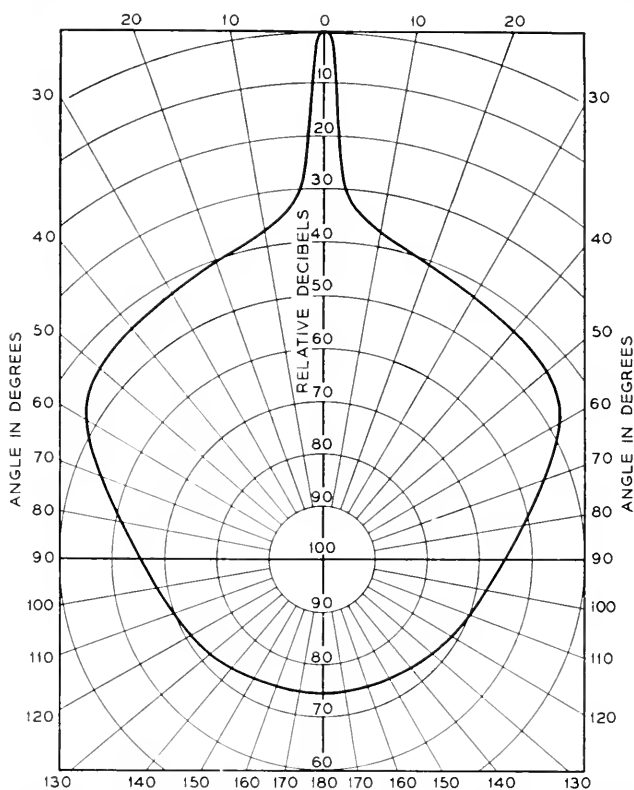


Fig. 21—Assumed directional selectivity of 10 ft. x 10 ft. antenna at 4000 mc.

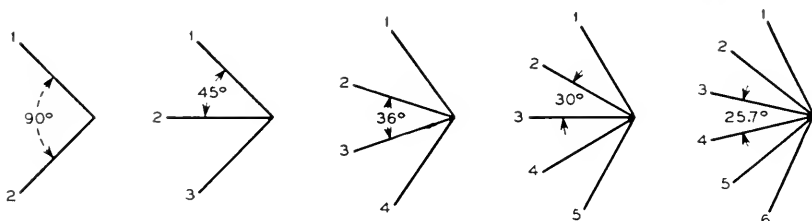


Fig. 22—Simplified route pattern for study of selectivity required in congested localities.

converging in the manner suggested by any of the diagrams of Fig. 22. A critical situation occurs in regard to the frequencies used for receiving at the point toward which the systems converge. If the same receiving

frequency were to be used on two or more routes, receiving directional discrimination amounting to 75 db would have to be secured:

1. Required interference ratio	44 db from Table IV FDM-FM
2. Allowance for repeater crosstalk	1 (51 db down)
3. Differential fading allowance <sup>28</sup>	30
	—
	75 db

The repeater crosstalk is here taken to be equivalent to one source 51 db down which is the value corresponding to no differential fading on adjacent spans as calculated in Section I. It will be remembered that allowance was made for a single differential fade of 30 db occurring somewhere along the route. Here we assume that this differential fade may occur between two of the converging paths and we demand that the receiving directional discrimination shall protect the system against such an occurrence. In this case the required directional discrimination turns out to be equal to the 75 db front-back ratio from which the 44 db figure was obtained. This is manifestly impossible with the assumed directivity characteristic<sup>29</sup> and the angles involved. Therefore, different receiving frequencies are required on each route. These same frequencies may be used for transmitting at the junction, provided the disposition of terminals is such as to provide enough directional discrimination and physical separation to permit operation at the low received level in the face of the high transmitted level on the same frequency. The interference path loss plus antenna discrimination must be, for the case involving the longest span:

1. Required interference ratio	44 db (FDM-FM, Table IV)
2. Allowance for repeater crosstalk	1
3. Free space span loss	60
4. Fading allowance	25
	—
	130 db

We continue our discussion of the converging routes of Fig. 22 by assuming that:

1. Conditions encountered elsewhere on the routes do not restrict the freedom to switch the frequencies among the routes.

2. The disposition of terminals at the junction is such that inter-terminal interference is not a controlling factor.

Under the above assumptions the directional discrimination of the terminal

<sup>28</sup> This differential fading allowance corresponds to a fade of 25 db below free space on one route and a 5 db increase over free space on the other.

<sup>29</sup> The use of perpendicular polarizations cannot, we assume, be counted on to give further discrimination when the directional discrimination is already 40 or more decibels.

antennas alone determines the number of different frequencies. The same receiving frequency may be used at the junction on two routes separated by an angle sufficient to yield the required antenna discrimination. All intervening routes must employ different frequencies. The frequencies so determined may be used for transmitting from the junction if they are staggered with respect to the receiving frequencies. Take, for instance, the five-route plan shown in Fig. 22. Suppose the directional discrimination needs to be 60 db for a particular system. The directional pattern shows that this requirement is met at 85 degrees. Thus, routes 1 and 4 may use frequency A, say. Routes 2 and 3 then must use different frequencies, B and C. Thus, we have:

Route	1	2	3	4	5
Trans. Freq.	A	B	C	A	B
Rec. Freq.	B	C	A	B	C
or	(C	A	B	C	A)

While the treatment of the route congestion problem outlined above is oversimplified it enables us to make a broad survey having some significance.

Table VI for 1000 4-kc message channels and Table VII for 250 16-kc "program" channels were derived on the above basis. The decibel figures at the head of each column are the allowable interference ratios from Tables IV and V increased by 30 db for differential fading.<sup>30</sup> A single source of interference of the values given in the table is supposed to degrade the circuit to the minimum requirements for a long circuit. In regenerative PCM there is no accumulation of degradation due to interference occurring on various spans. In non-quantized systems such degradations are cumulative. However, when protection to the above values is provided, with no allowance of 30 db for differential fading of the desired and interfering signals, the occurrence of *simultaneous* additional degradations is extremely unlikely. Protection against this severe fading at one point alternately protects against the simultaneous occurrence of several less severe fades.

The values of repeater power capacity shown in the table will satisfy the noise requirements on a 133-span transcontinental nonregenerated circuit with 15 db fades simultaneously on all spans. This is equivalent to providing for 13 simultaneous fades of 25 db or, statistically, for the fading that is not likely to be exceeded except during a small fraction of the time. The PCM systems employing regeneration are powered for 25 db fades on any or all spans.<sup>31</sup> The free space span loss is 60 db.

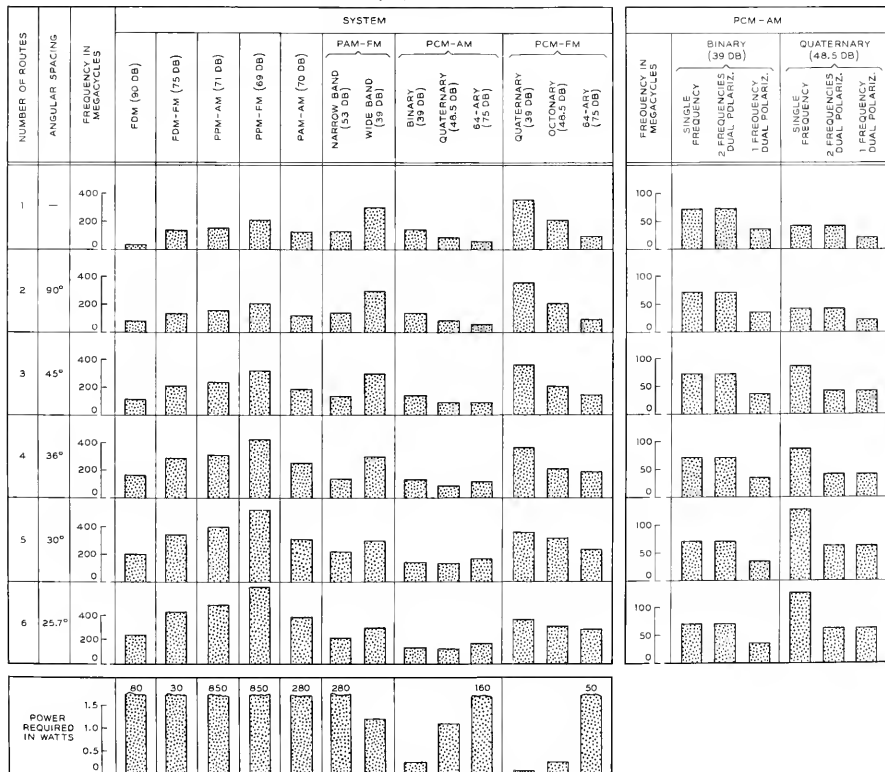
In computing the frequency occupancy we take cognizance of the fact

<sup>30</sup> The FDM-FM entry provides 1 db additional allowance for repeater crosstalk as mentioned before. Repeater crosstalk is negligible in the other systems.

<sup>31</sup> No such distinction was made in Tables II and III. There, provision was made for 75 db span loss in all cases.



TABLE VI  
TRUE FREQUENCY OCCUPANCY OF VARIOUS MESSAGE GRADE RADIO RELAY SYSTEMS FOR CONGESTED ROUTES  
133 30-mi spans, 1000 4-kc channels, 15 db NF



that systems of different vulnerability require different guard space to protect against adjacent-band crosstalk. In Section VII it is concluded that with binary PCM-AM the band spacing could perhaps be as small as  $1.5/T_0$  with realizable filters and gates.  $T_0$  is the time allotted to one pulse. Underlying the meaning of  $B$  as used heretofore in connection with PCM-AM, is the relation  $T_0 = 2/B$ . If the band spacing is to be taken as  $1.5/T_0$ , the band spacing may be expressed in terms of  $B$  as  $0.75 B$ . In other words, the band spacing factor  $U$  may be reduced to 0.75.

In the case of ideal *FM* systems the receiving frequency discrimination need not suppress adjacent radio signal bands to anywhere near the degree required of co-channel interference, provided the near edges of the adjacent signal bands differ by more than the width of the baseband filter. We do not, of course, assume ideal apparatus and have been rather liberal in guard space allowance.

The following band spacing factors, to be used with the bandwidths of Tables IV and V, are considered realizable and consistent with the shape of the spectrum to be transmitted. A reduction to practice would likely lead to somewhat different factors but these will suffice for our illustrative Tables VI and VII. In the non-regenerative systems, the spacing factor required to protect against interference from new frequencies required at a junction is, perhaps, less than is required to protect against interference at every repeater on a long route. A small economy in occupancy could properly be invoked on this account in some cases but, in the interest of simplicity, this has been neglected, and the same factor  $U$  will be associated with every frequency required.

SYSTEM OF TABLE VI	FACTOR $U$
FDM	2.5
FDM-FM	3
PPM-AM	2
PPM-FM	2
PAM-AM	2
PAM-FM (narrow band)	2
PAM-FM (wide band)	1.5
PCM-AM (64-ary)	2
PCM-AM (quaternary)	0.9
PCM-AM (binary) <sup>12</sup>	0.75
PCM-FM (64-ary)	2
PCM-FM (octonary)	1.5
PCM-FM (quaternary)	1.5

<sup>12</sup> The experimental system described by Meacham and Peterson (loc. cit.) employs a spacing factor of 1.12.





that systems of different vulnerability require different guard space to protect against adjacent-band crosstalk. In Section VII it is concluded that with binary PCM-AM the band spacing could perhaps be as small as  $1.5/T_0$  with realizable filters and gates.  $T_0$  is the time allotted to one pulse. Underlying the meaning of  $B$  as used heretofore in connection with PCM-AM, is the relation  $T_0 = 2/B$ . If the band spacing is to be taken as  $1.5/T_0$ , the band spacing may be expressed in terms of  $B$  as  $0.75 B$ . In other words, the band spacing factor  $U$  may be reduced to 0.75.

In the case of ideal *FM* systems the receiving frequency discrimination need not suppress adjacent radio signal bands to anywhere near the degree required of co-channel interference, provided the near edges of the adjacent signal bands differ by more than the width of the baseband filter. We do not, of course, assume ideal apparatus and have been rather liberal in guard space allowance.

The following band spacing factors, to be used with the bandwidths of Tables IV and V, are considered realizable and consistent with the shape of the spectrum to be transmitted. A reduction to practice would likely lead to somewhat different factors but these will suffice for our illustrative Tables VI and VII. In the non-regenerative systems, the spacing factor required to protect against interference from new frequencies required at a junction is, perhaps, less than is required to protect against interference at every repeater on a long route. A small economy in occupancy could properly be invoked on this account in some cases but, in the interest of simplicity, this has been neglected, and the same factor  $U$  will be associated with every frequency required.

SYSTEM OF TABLE VI	FACTOR $U$
FDM	2.5
FDM-FM	3
PPM-AM	2
PPM-FM	2
PAM-AM	2
PAM-FM (narrow band)	2
PAM-FM (wide band)	1.5
PCM-AM (64-ary)	2
PCM-AM (quaternary)	0.9
PCM-AM (binary) <sup>12</sup>	0.75
PCM-FM (64-ary)	2
PCM-FM (octonary)	1.5
PCM-FM (quaternary)	1.5

<sup>12</sup> The experimental system described by Meacham and Peterson (loc. cit.) employs a spacing factor of 1.12.

TABLE VII  
TRUE FREQUENCY OCCUPANCY OF VARIOUS PROGRAM TYPE RADIO RELAY SYSTEMS FOR  
CONGESTED ROUTES

133 30-mi spans, 250 16-kc channels, 15 db NF.

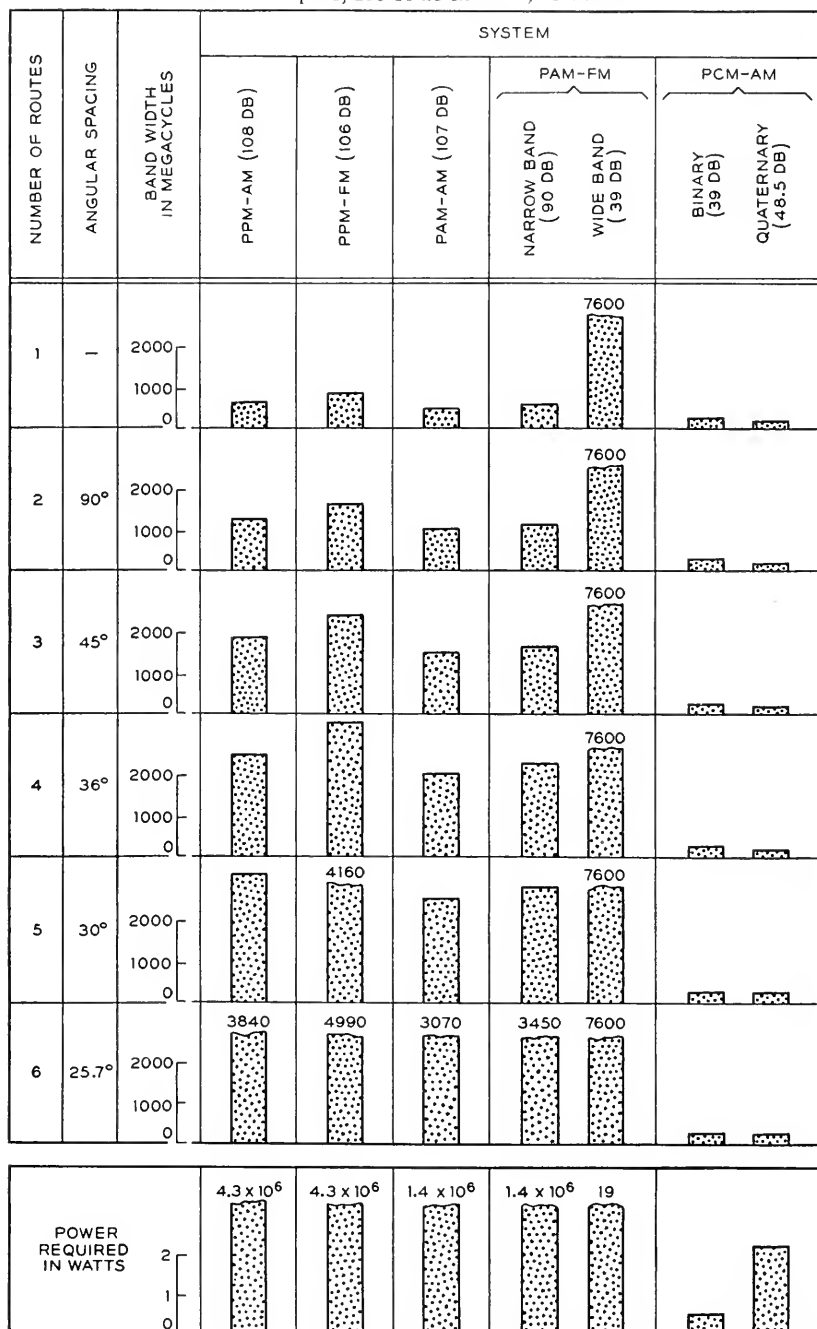


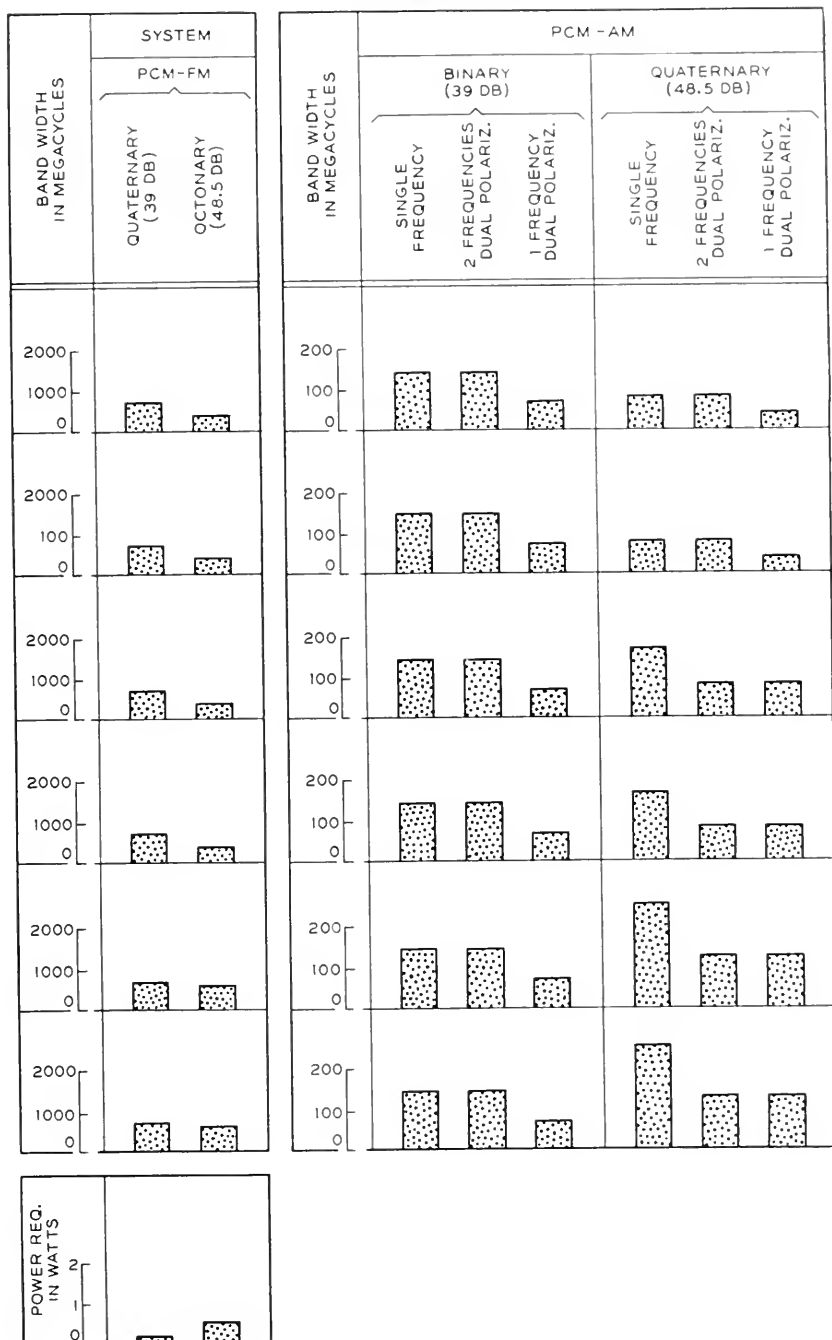
TABLE VII—*Concluded*

TABLE VIII  
COMPARISONS OF BAND WIDTH AND FREQUENCY OCCUPANCY FOR SYSTEMS OF EQUAL RUGEDNESS  
Dotted bars show bandwidth; crosshatched bars show relative frequency occupancy.

SIMILAR SYSTEM INTERFERENCE RATIO IN DB	BAND WIDTH IN MC	1000 MESSAGE-TYPE CHANNELS						250 PROGRAM- TYPE CHANNELS	
		PCM-AM	PCM-FM	PPM-AM	PPM-FM	PAM-FM (12.5% ACTIVITY)	FDM-FM**	PCM-AM	PCM-FM
18.5									
				OCCUPANCY RATIO, U					
9									
				OCCUPANCY RATIO, U					
3									
				OCCUPANCY RATIO, U					

\* SUPPRESSED CARRIER, HOMODYNE DETECTION

\*\* INTERFERENCE CALCULATED AS NOISE OF SAME POWER

These factors were multiplied by the product of bandwidth and number of frequencies to obtain the dotted bars in Table VI.

In regard to the "program grade" of circuit we must be more liberal in our allowance for guard space. Our estimates for the band spacing factor are:

SYSTEM OF TABLE VII	FACTOR U
PPM-AM	4
PPM-FM	4
PAM-AM	4
PAM-FM (narrow band)	4
PAM-FM (wide band)	3
PCM-AM (quaternary)	0.9
PCM-AM (binary)	0.75
PCM-FM (octonary)	1.5
PCM-FM (quaternary)	1.5

These factors were used to compute the dotted bars in Table VII.

If transmission on two polarizations can be accomplished with mutual cross-fire suppressed to a sufficient degree, half of the channels could be transmitted by each polarization, on the same frequency, thus halving the frequency occupancy. A probably unattainable cross-fire ratio seems necessary to meet the requirements in the non-regenerative systems, if we remember that the interference produced by cross-fire accumulates from span to span; but a suppression likely to be attainable, of the order of 15-20 db, makes this frequency saving feasible in the rugged systems such as binary PCM-AM or PCM-FM. The tables show entries for binary and quaternary PCM-AM, assuming dual polarization transmission.

If antennas could be improved to insure nearby discrimination ratios adequate to allow use of the same frequency in and out and west and east, the single-route occupancy would be halved again; with such a one-frequency repeater plan the occupancy in a congested area is not, however, always halved. Whenever the frequency requirements, as determined by the terminal antenna directivity, result in two or more frequencies, A, B, C . . . etc., there is no saving accruing from a one-frequency repeater plan, because two-frequency routes can be accommodated with no additional frequencies by suitably switching frequencies. It is only in the case of a system so rugged that the terminal antenna directivity permits a single frequency, A, to be used that the occupancy is reduced and it is then halved. With PCM of low base this is a possibility and the tables include entries for this case.

As to achieving antenna characteristics suitable for one-frequency operation, it may be noted that reflection from a heavy rainfall in front of the

antennas limits the attainable side-to-side ratio.<sup>32</sup> Reflection from aircraft may also impose a practical limitation. Spacing the antennas laterally (on two towers) would achieve freedom from these limitations. Another way of coping with the antenna discrimination obstacle is to use short spans in congested areas. This reduces the discrimination requirements particularly because fading is reduced by shortening the spans.

#### CONCLUSIONS AS TO RADIO

Of the systems included in Table VI we find that, for six routes, binary PCM-AM, even without the potential frequency economy of dual polarization and/or single-frequency repeaters, has come close to being the most economical of frequency space; quaternary PCM-AM shows a slight advantage (which would be lost if the route spacing were less than fifteen degrees). Even without dual polarization or single-frequency repeaters, the binary PCM-AM occupancy is less, for more than 3 routes, than the *occupancy* required by FDM whose *band width* is 4 kc per channel. There is here an excellent illustration of the possibility of a net saving in frequency space through the use of tough wide-band systems.

The power requirements also favor the low-base PCM systems. It should be noted, in particular, that the linearity requirements with FDM demand that the tabulated power of 80 watts be a very light load on the repeaters.

Inspection of Table VII brings out the effectiveness of the coding principle if very high-grade channels are required. Only with PCM (of low base, as shown) are the occupancy and power requirements both within the practical realm. The non-PCM methods that achieve small occupancy, comparable with that of low-base PCM, all require colossal amounts of power. When the power requirement is reduced and the ruggedness increased by use of band width, the occupancy becomes, in turn, colossal. This is illustrated by the two entries for PAM-FM.

As route congestion increases without limit, any type of system that permits exchange between bandwidth and ruggedness will always achieve the minimum occupancy when bandwidth has been used to secure the degree of ruggedness that avoids multiplying the frequency assignments. Our studies have shown that, with the assumptions made, this result is valid for channels of message grade when the congestion has reached a degree that is by no means fantastic. We have accordingly prepared Table VIII in which the dotted bars show the bandwidths (taken from Fig. 9-19) of the various systems when their interference tolerances are alike and have values of 18.5, 9, and 3 db.<sup>33</sup> While these systems, having the same tolerance, all

<sup>32</sup> Measurements made at the BTL radio laboratory at Holmdel, N. J. indicate that this limit to side-to-side ratio is of the order of 85 to 90 db.

<sup>33</sup> The AM pulse systems are here assumed to achieve the 6 db increase in tolerance by suppressing the carrier.

fare alike in respect to frequency requirements imposed by antenna directivity, the bandwidth figures do not adequately reflect the merits of the systems. This is because the band-spacing factors are different and, in addition, only the regenerative systems can be expected to achieve the halving of occupancy accruing from dual polarization and from one-frequency routes. The crosshatched bars of Table VIII include the effect of multiplying by the estimated band-spacing factors shown beneath the bars. These band spacing factors are in some cases smaller than those previously tabulated for the less rugged systems of Tables IV and V. Only the PCM methods are shown for the case of very high-grade channels, since the non-PCM methods are so strikingly less effective here.

These conclusions depend for validity on the assumptions made and particularly on those concerning antennas, route disposition and fading, and apply when the converging systems *are of the same kind*. In a real situation, departures from the assumed conditions could markedly affect the conclusions. For instance, the meritorious showing of PCM in respect to efficient utilization of frequency space in the face of route congestion depends heavily on the assumption that all routes in the occupied space employ PCM. Any routes employing a modulation method that is highly vulnerable to interference like some of the narrower bandwidth methods would have to employ higher power to operate in the face of interference from the PCM routes. This higher power, concentrated in a narrower band, could destroy the PCM routes. In some cases it would obviously be impossible to assign values of power which permit the two kinds of routes to share the same frequency band.

Our calculations should be taken to illustrate the factors involved and the philosophy by which such problems may be approached rather than to find an unequivocally best system.

## V. MORE ABOUT THE NON-SIMULTANEOUS LOAD ADVANTAGE

The transmission advantage enjoyed by multiplexing many single sideband telephone channels in frequency division, discussed in the introduction, stems from several factors:

1. During the busiest period, only a small percentage (of the order of 12 to 15%) of the channels are actually transmitting speech ("talk spurts") at one time, on the average.
2. There are only a few *loud* talkers; the remaining ones range downward to a volume 35 to 40 db lower.
3. In the addition of the sideband voltages representing the talkers actually producing talk spurts, only a fraction of the grand maximum occurs often enough to be significant.

With frequency division all of these factors jointly contribute in a natural

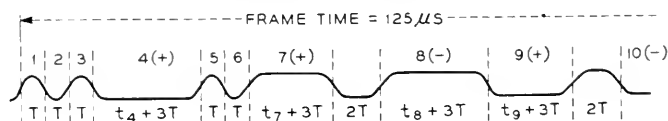
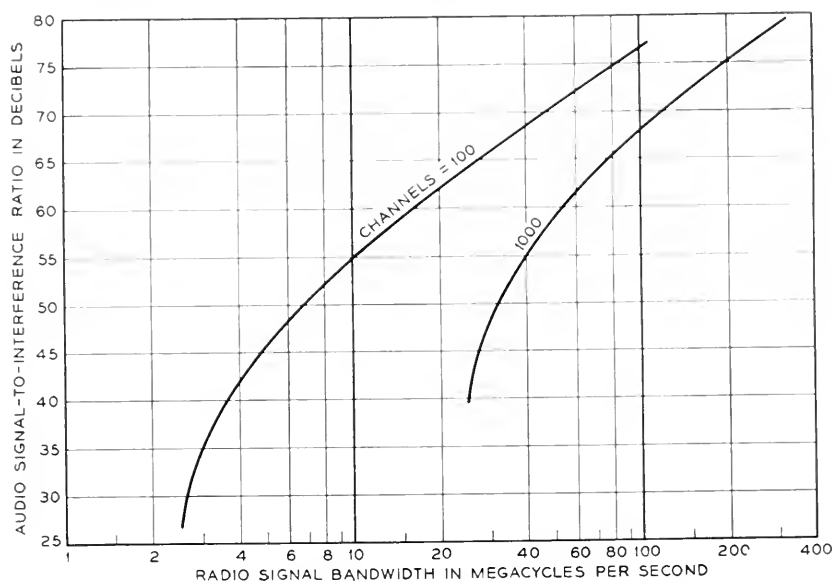
and automatic manner to the low peak load ratings given in Table I. In time division, complicated instrumentation is needed to obtain such a low load rating (in time, now, not power capacity) and the saving is in bandwidth (time). Savings accruing from item (1) above are theoretically obtainable in all time-division systems (and, in fact, in nonmultiplexed multipair cable transmission systems) by having automatic devices which skip the channels that are momentarily inactive and which advise the receiver of the skipping. It is possible also to benefit from items (2) and (3) above in systems which transmit a time interval to represent an amplitude. The amplitudes may be sent as absolute magnitudes together with a polarity indication. If this is done the channel time allotments actually required in a given multiplex frame appear piled up end to end, and many more channels can be handled than if provision were made for full amplitude on all. PPM is one such system, and PCM is another if the code symbols containing fewest digits are used to represent the smallest absolute magnitudes.

The use of instantaneous companding, which tends to make all talkers contribute equally to the system load, reduces the advantage represented by (2) above, but does not basically affect (1) which represents a substantial part of the total multiplex advantage.

It is illuminating to compute the performance of a pulse length modulation system (PLM) employing the elastic time allotment and assuming that the load ratings of Table I apply. We imagine a system working on the principles illustrated in Fig. 23. There we assign a time  $T (= 2/B)$  to each inactive channel. Active channels whose absolute amplitudes are described by  $t$ , are assigned  $t + 3T$  and those that are negative are preceded by a  $2T$  pulse to designate that they are negative. If the interference is no greater than marginal (9 db down) the receiver can distinguish between (a), the  $T$  intervals which count off the channels that are skipped and (b), the  $2T$  polarity indications and (c), the  $3T$  minimum signal intervals. The frame time of 125 microseconds must include the sum of these intervals plus  $Kt_0$  where  $t_0$  is the time shift for a full-load tone in a single channel which gives the required signal-to-noise ratio for the bandwidth  $B (= 2/T)$ . The load rating factor is  $K$ , expressed as an amplitude ratio. The relations used to plot the two curves of Fig. 23 are shown in the insert. Little or no instantaneous companding could be used to advantage so that a signal-to-interference ratio of 50 to 60 db would be required and for 1000 channels the bandwidth would be between 30 and 50 mc, which is some two or three-fold less than in binary PCM-AM, both systems being equally tolerant to a single source of CW interference. The elastic principle could presumably be applied to PCM also to achieve a several-fold bandwidth reduction, but no experience has been obtained with any of these elastic systems. While this paper has avoided for the most part questions of instru-



mentation, it should be pointed out that the elastic schemes tend to become complex apparatus-wise. If one chooses to discount this on the grounds



$N$  = NUMBER OF CHANNELS

$a$  = NUMBER OF ACTIVE CHANNELS

$$125 = N \left( 1 - \frac{a}{N} \right) T + N \frac{a}{N} 3T + \frac{1}{2} N \frac{a}{N} 2T + t_0 K = \frac{2N}{B} \left( 1 + 3 \frac{a}{N} \right) + t_0 K$$

$$t_0 = \frac{125 - \frac{N}{B} \left( 2 + \frac{6a}{N} \right)}{K}$$

$$\text{SLICER ADVANTAGE} = 20 \log_{10} \frac{\pi}{2} \frac{t_0}{T} - 3 \text{ DB}$$

$$\frac{S}{I} = \text{RF PULSE TO INTERFERENCE RATIO} + 20 \log_{10} \frac{\pi}{2} \frac{t_0}{T} - 3$$

CALCULATED FOR: RF RATIO = 9 DB (MARGINAL)

$N = 1000$   $K = 6.3$  (16 DB)

$N = 100$   $K = 2.83$  (9 DB)

$$\frac{a}{N} = \frac{1}{8}$$

Fig. 23—Theoretical possibilities of exploiting non-simultaneous load advantage by an elastic PLM-AM system.

that future developments may resolve the complexity, there remains the objection that any system designed to take advantage of the multiplex load rating counts heavily on being used almost exclusively for conversational

speech under present operating procedures. The extensive use of telephone channels for nontelephone purposes is thus curtailed.

## VI. OVERLOAD DISTORTION AND NOISE THRESHOLD

In designing a microwave system for a large number of channels the power required to override noise may exceed the power capacity of available amplifiers. Also, the bandwidth may exceed the limit imposed by microwave transmission phenomena or circuit techniques. In either case, the remedy is to divide the channels into several groups of fewer channels and transmit the groups in adjacent narrower bands spaced by the proper factor  $U$ , and separable with filters for individual amplification, reshaping or regeneration. The power requirement falls off linearly with bandwidth. The filter problem for AM pulse transmission is considered in Section VII. The total frequency occupancy is no greater for this division since the same percentage "guard band" is involved if, in both cases, the neighboring, foreign signals are of the same kind as the wanted signals. In case the neighboring signals are of a different kind, the multiple band arrangement is in fact likely to represent a smaller occupancy because the occupancy is in general more sharply defined when made up of several narrower bands.

When considering a multiple group arrangement, it may be economical to provide for a substantial amount of common amplification prior to separation into the several bands which receive individual treatment. The non-linearity of the common amplifier then sets a limit to the common amplification. Experiments bearing on this overload limit were made with the PCM equipment described by Meacham and Peterson.<sup>12</sup> Two- and eight-frequency groups were employed and the amplifier load was increased until the effects of distortion began to appear. The distortion was measured in terms of the maximum amount of CW interference which, when added to the amplifier output, resulted in no audible effect in the PCM channels. The right-hand part of Fig. 24 plots the results. For eight bands (six of which were not pulsed but were left on as unmodulated carriers) it is seen that the margin provided against CW interference begins to shrink rapidly when the single group load is 20 db below the output at which 1 db compression occurs. The margin is completely used up (the channels begin to show noise) when the load is 13 db higher. The left-hand part of Fig. 24 plots the manner in which the low level limitation (noise) was found to appear. Margin against CW interference shows a reduction for a pulse-to-noise ratio of 28 db and is completely used up at a ratio of 18 db.

The overload occurred in the 4000-mc power amplifier associated with the repeater, and the noise originated in the receiver.

In non-reshaping amplitude-modulated systems, the effect of compression

<sup>12</sup> Loc. cit.

occurring in the repeaters is cumulative. In microwave repeaters second-order distortion products fall outside the band and third-order distortion is likely to be predominant. We assume in what follows that the distortion arises solely from a cubic term. When the low-level gains of the repeaters are maintained equal to the preceding span losses, it can be shown that the single-frequency compression characteristic at the end of  $n$  spans is approxi-

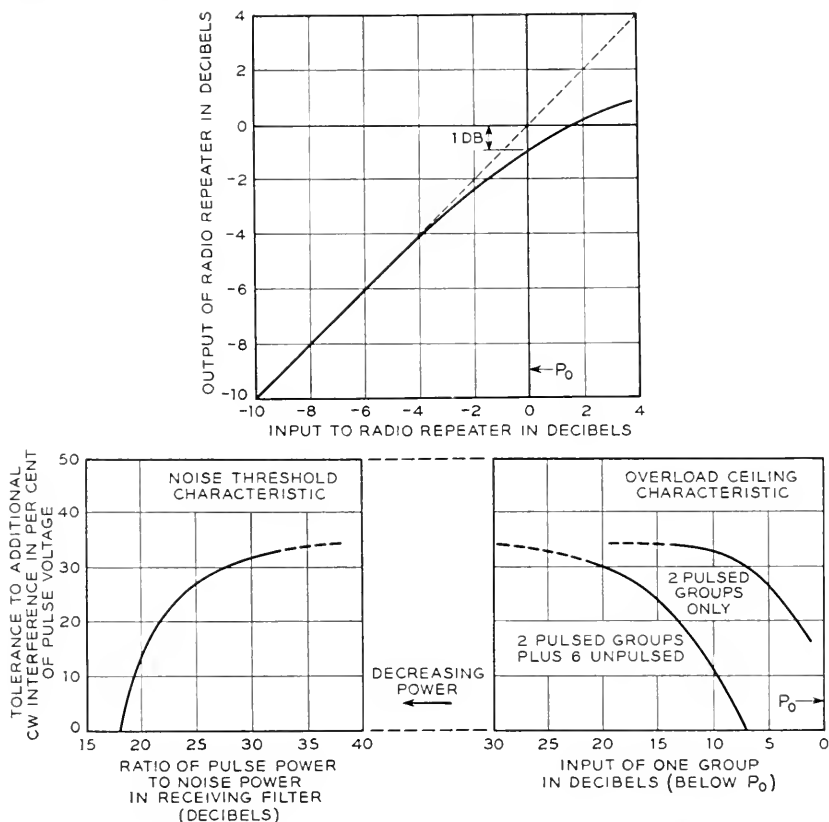


Fig. 24—Noise threshold and overload ceiling in frequency divided PCM groups.

mately the same as for one span but occurs at a power level  $10 \log n$  db lower. This approximation becomes more exact as the over-all distortion involved becomes less (as by lower input power). Fig. 25 shows a third order compression curve for one span and the resulting curves, obtained graphically, for 2, 4 and 10 spans. Examination of these curves shows that the curves are substantially the same as for the single span but displaced, 3, 6 and 10 db respectively. This is illustrated by line A, which intersects all of the curves at the same compression value (1.7 db). The points

marking the intersections are seen to be displaced from the intersection with the curve for one span by approximately 3, 6 and 10 db. If the phase of the repeaters is as linear as it must be in pulse systems, this single frequency characteristic can be applied for the entire signal band as if it resulted from a single source of third-order distortion. The effect of this distortion is

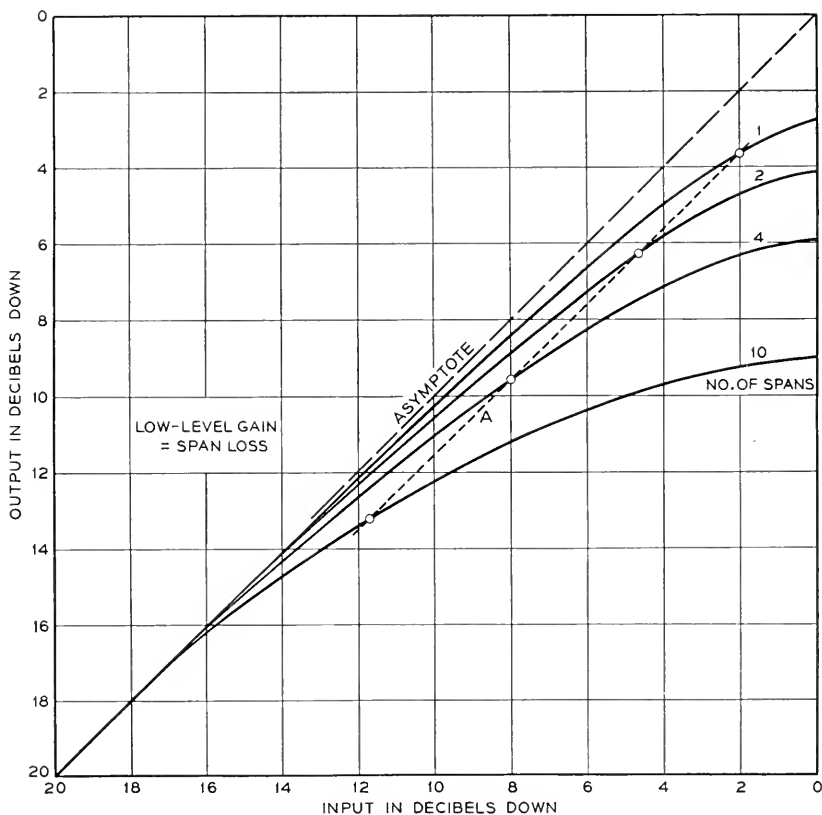


Fig. 25—Overload characteristics of multi-repeater systems.

serious in multiband PCM repeaters, as illustrated by the measurements on Fig. 24, but is, generally speaking, less important in single band pulse repeaters. For instance<sup>34</sup> PPM-AM pulses and binary PCM-AM pulses might operate on the flat part of curve 10 (Fig. 25). With PCM of higher

<sup>34</sup> On the grounds that pulse slicers themselves include the compression function to a high degree, one might not see the harm of compression in repeaters. If all of the compression occurred *after* the noise had been acquired there would be no fundamental compression penalty in slicing pulse systems. The penalty comes about because as the pulses progress from span to span they shrink and become more vulnerable to noise.

base as well as with PAM, the repeater loading would have to be sharply reduced, however.

More power on all spans could be obtained by making the repeater gain greater than the span loss. This very quickly defeats its purpose, however, because the excess low-level gain raises low-level noise between pulses to a high level status as it progresses from span to span.

Reshaping of AM pulses (and of course regeneration in PCM-AM) at all repeaters avoids the cumulative effect of compression by permitting the repeater gain to be greater than the span loss by the amount of compression on one span.

When a signal is transmitted by FM, the phase curve of the transmission circuit plays a role somewhat analogous to the amplitude characteristic of an AM system. The correspondence is not complete, however, for we find that modulation products arising from even-order phase distortion as well as from odd fall in the signal band even though the FM band is located in a frequency range very high compared with the baseband width. For amplitude modulated signals in the baseband, we can replace the FM phase distortion effects by an equivalent non-linear baseband amplifier characteristic which has the same shape with respect to zero voltage input as the phase characteristic has with respect to the midband frequency of the FM range. If the distortion is small, the square and cube law approximations obtained by expanding the phase-shift function about the mid frequency may be applied as in conventional multichannel cross-modulation theory.<sup>35</sup> We shall not here attempt to discuss the accumulation of phase distortion in a multi-repeater FM system.

## VII. PULSES, SPECTRA, AND FILTERS

In this section, we will consider: (1) pulse shapes in relation to the particular pulse modulation method employing them, (2) the shaping filters by which they may be obtained and (3) the transmitting and receiving filters employed in systems comprising a multiplicity of adjacent frequency bands each carrying pulse signals.

Column A of Fig. 26 shows various pulse shapes which can be approximated (with the exception of shapes 8 and 9) by fairly simple circuits, both in the baseband and radio spectrum. Pulse 1 is an "unshaped" rectangular pulse. A good approximation to it can be obtained in wide-band circuits accommodating the extensive spectrum it possesses, i.e., in circuits having rise and decay times short compared with the duration  $T_0$ . Such a pulse when transmitted through Gaussian filters of the various widths shown in

<sup>35</sup> W. R. Bennett, "Cross-Modulation in Multichannel Amplifiers" *Bell System Technical Journal*, Vol. 19, pp. 587-610, October, 1940.

column C emerges with smooth transitions as shown in 2, 3 and 4. These pulses rise and fall in a nearly sinusoidal manner. The width between half-amplitude points is  $T_0$ . Shortening the rectangular pulse ("curbing") and narrowing the shaping filter can be made to result in pulses 5 and 6 which have the same width between, say, 3% points (at  $t_1$ ) as pulse 4.

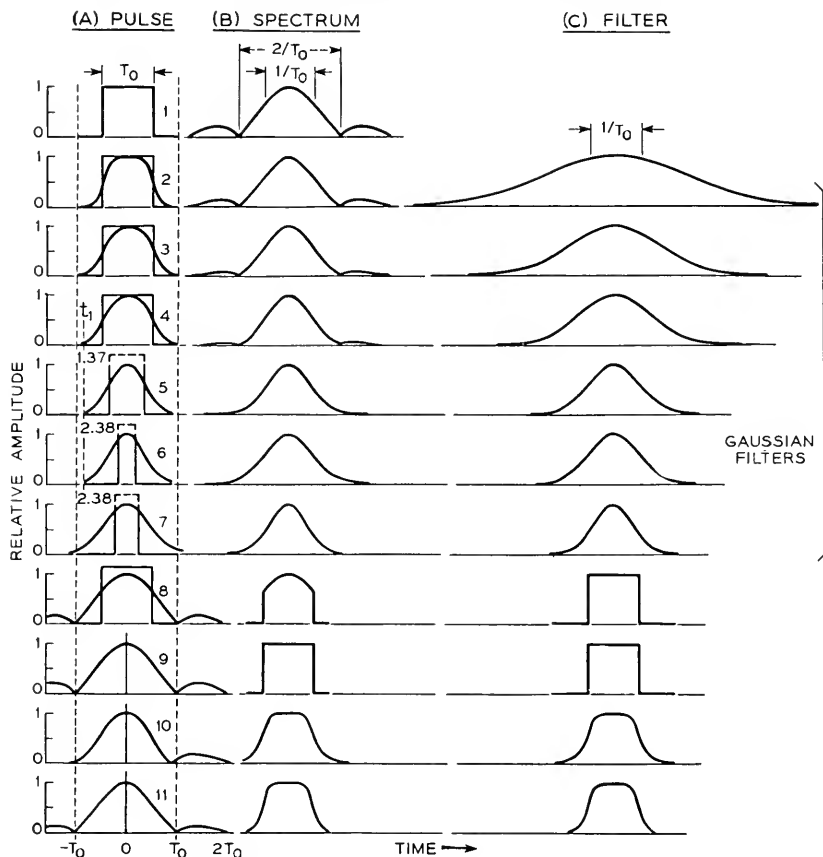


Fig. 26—Typical pulses and their spectra.

Pulses 5 and 6 are then shorter than 4 between half-amplitude points. If the half-amplitude width is made the same as in pulse 4 the width between lower amplitude points is greater than in pulse 4. This is illustrated in pulse 7.

Gaussian filters<sup>36</sup> as defined here are naturally linear phase networks

<sup>36</sup> Gaussian filters are networks whose transfer admittance follows the error law as a function of frequency. A decibel plot of a bandpass Gaussian filter is accordingly a parabola in shape.

and we have assumed linear phase in computing pulses 2 to 7. A good approximation to the Gaussian filter can be obtained both as to phase and amplitude with a number of tuned circuits in tandem, coupled through buffers. A fair approximation can also be obtained by combining a 3- or 4-section maximally flat filter<sup>37</sup> with a tuned circuit through a buffer.

Rectangular or near-rectangular shaping filters produce pulses with overshoot as shown by pulses 8 to 11. The filter corresponding to pulses 8 and 9 is assumed to have rectangular shape and linear phase. Filters of this sort have no simple approximation in practice and are included for comparison with filters 10 and 11 which are made up of simple maximally flat networks. In pulses 9, 10 and 11 the "unshaped pulse" is assumed to be very narrow and of amplitude sufficient to yield pulses of the heights shown.

Let us now regard these pulses as received pulses and compare them in respect to shape for use in various kinds of pulse systems.

**PPM.** In PPM the pulses may occupy any time position in the assigned interval and so the tails of pulses 8 to 11 may "crosstalk" into time assigned to an adjacent channel. To allow guard time for the train of tails or to design for satisfactory operation in the presence of the tails is uneconomical of frequency space. It follows that pulses which are more definitely bounded in time such as those obtained with Gaussian filters are more desirable and likely to be more economical of frequency space in general despite their wider spectrum.

In PPM where the trailing (or leading) edge of a pulse is used to convey the information a flat top pulse such as pulse 2 is no better than one in which the flat portion is absent and the two transitions brought together.<sup>38</sup> The latter pulse would, in fact, be superior since more time would then be available for additional channels or for greater swing.

We are thus led to conclude that one of the pulses in the 4 to 6 group is the preferred shape for PPM. We chose pulse 4 in our illustrative calculations and defined bandwidth as  $2/T_0$ , but pulses 5 or 6 would have given substantially the same results.

**PAM.** In PAM the pulses occur at standardized, regular times so that if pulse 9 were used the accompanying tails, which disappear completely at instants  $T_0$ ,  $2T_0$ , etc., from the pulse peak, need not theoretically produce crosstalk between channels if the channels are spaced  $T_0$  and the pulse amplitudes are measured *instantaneously* at the time the nulls occur. As a practical matter both the precise pulse shape and the instantaneous measure-

<sup>37</sup> W. W. Mumford, "Maximally-Flat Filters in Wave Guide," *Bell Sys. Tech. J.*, Vol. 27, October, 1948, pp. 684-713.

<sup>38</sup> Such a pulse would look like pulse 4 if the latter were shrunk to occupy 0.6 of the time shown in the plot. The spectrum would accordingly be that of pulse 4 expanded by the factor 1.7 but would not include more significant band width than is necessary to form pulse 2 as shown. This deduction follows from the fact that the rise time of pulse 2 is the same with or without the flat top.

ments at precise instants are probably not realizable to a degree which would keep the crosstalk within tolerable limits, so that one of the smooth pulse shapes is preferred. Pulse 4 with a spacing of  $T_0$  is feasible from the sampling precision point of view but a spacing of  $2T_0$  provides margin against crosstalk arising from small imperfections in any realizable approximation to the theoretical pulse.

It is to be noted that, if an instantaneous sample is taken of a PAM pulse, the measured magnitude is affected directly by the instantaneous value of noise present in the entire band occupied by the pulse. No frequency selectivity can be applied afterward to remove the influence of any part of the noise band because the error, even though caused by wide-band components, is exactly the same as could have been produced by a uniquely determined wave wholly confined to the signal band itself. The best signal-to-noise ratio obtainable with instantaneous sampling is that associated with minimum bandwidth for the pulse (i.e., pulse 9) and the corresponding maximum stringency of synchronization requirements on the sampling and pulse distortion. The same signal-to-noise ratio can, however, be approached with a wider band provided that we allow a finite segment of the received pulse to enter the channel filter. An averaging out of higher-frequency disturbances produced by wide-band noise is thus attained.

*PCM.* In PCM a short sample taken near the center of a pulse serves to determine correctly the presence or absence of a pulse even in the presence of interference at or near the breaking point of the slicer. Thus, pulse 4 may be used with a spacing of  $T_0$ , and if a gate pulse 25% of  $T_0$  is used, it need not be aligned with an inordinate precision to obtain good operation.<sup>39</sup> Greater tolerance in the matter of sampling would be obtained with pulse 2 but the frequency extravagance could scarcely be countenanced. As stated we assume pulse 4 in our PCM bandwidth curves but employ pulse 11 in Tables VI-VIII. Use of pulse 11 is a frequency conservation measure that seems feasible only with PCM and is attractive only with binary PCM.

#### OPTIMUM DISTRIBUTION OF SELECTIVITY BETWEEN TRANSMITTING AND RECEIVING FILTERS

In a regenerative repeater system both the receiving and transmitting filters may be Gaussian without suffering cumulative narrowing of the system bandwidth since each span commences with a freshly shaped pulse. In this case, the transmitting filter of one repeater and the receiving filter of the succeeding repeater combine, as Gaussian filters do, to make another Gaussian filter. The resulting pulse may be one of the series 2 to 6 of Fig. 26. On the assumption that one of these shapes is desired and that the trans-

<sup>39</sup> This is the pulse shape approximated in the experimental system described by Meacham and Peterson (*loc. cit.*).



mitting and receiving filters are to be Gaussian, a problem arises as to how to divide the total selectivity (in column C) between them. If most of the pulse shaping is done at the transmitter, the Gaussian receiving filter must be extremely broad, with the result that discrimination between pulses in adjacent bands is poor and the bands must be spaced widely in order to keep cross-fire down. If, on the other hand, all of the shaping is done at the receiver the wide spectrum of the unshaped transmitted pulse spills over into neighboring bands unless the bands are widely spaced. Clearly, an optimum proportioning of selectivity exists and it is interesting and enlightening to analyze this problem. Such an analysis was made for pulses 4, 5 and 6. This analysis pertains only to crossfire and not to signal-to-noise ratio as influenced by curbing (shortening of the rectangular pulses) and by the division of selectivity between transmitting and receiving filters. Wide receiving filters accept more noise and narrow ones may prevent the transmitted pulse from attaining full height in the receiving filter output if curbing is used. If the curbing is pronounced, as in pulses 6 to 11, amplification may have to follow the transmitting filter to establish the desired transmitted power level. For divisions of selectivity close to the optimum, the receiving filter selectivity appreciably reduces the transmitted pulse height in the case of pulse 5 and seriously reduces it in the case of pulse 6.

Crossfire from a pulse in an unwanted band appears as a transient in the wanted band. In some circumstances, this transient has peaks which occur while the crossfiring pulse is rising and falling and has a minimum between which sometimes dips below the level fixed with the steady-state discrimination to the crossfiring carrier. If the pulses in the crossfiring band are synchronized with those in the wanted band as they might be in PAM and PCM only the minimum, central, crossfire might be significant. If, as in PPM, the pulses cannot be synchronized, the peak crossfire is significant. Curves for two values of band separation are shown in Fig. 27, one appropriate to yield minimum crossfire in the 25 to 35 db range and the other to yield peak crossfire in that range. This is the range that is sufficient for binary PCM. The steady state discrimination is also shown. We conclude from this study that pulses 4 or 5 are about equally good in respect to minimum central crossfire and that pulse 4 is slightly preferable in that the trough and the crest are more symmetrical. For PCM in which the pulse spacing is made equal to  $T_0$  this symmetry means that there is the same margin for misalignment of the gating pulse, as regards correctly interpreting a space or a mark. Pulses 5 and 6 appear to be about equally good in respect to peak crossfire but both (and particularly pulse 6) incur a signal-to-noise penalty because the receiving filter does not permit the transmitted pulse to attain full height.

In practice, the approximations to Gaussian filters have shown worse

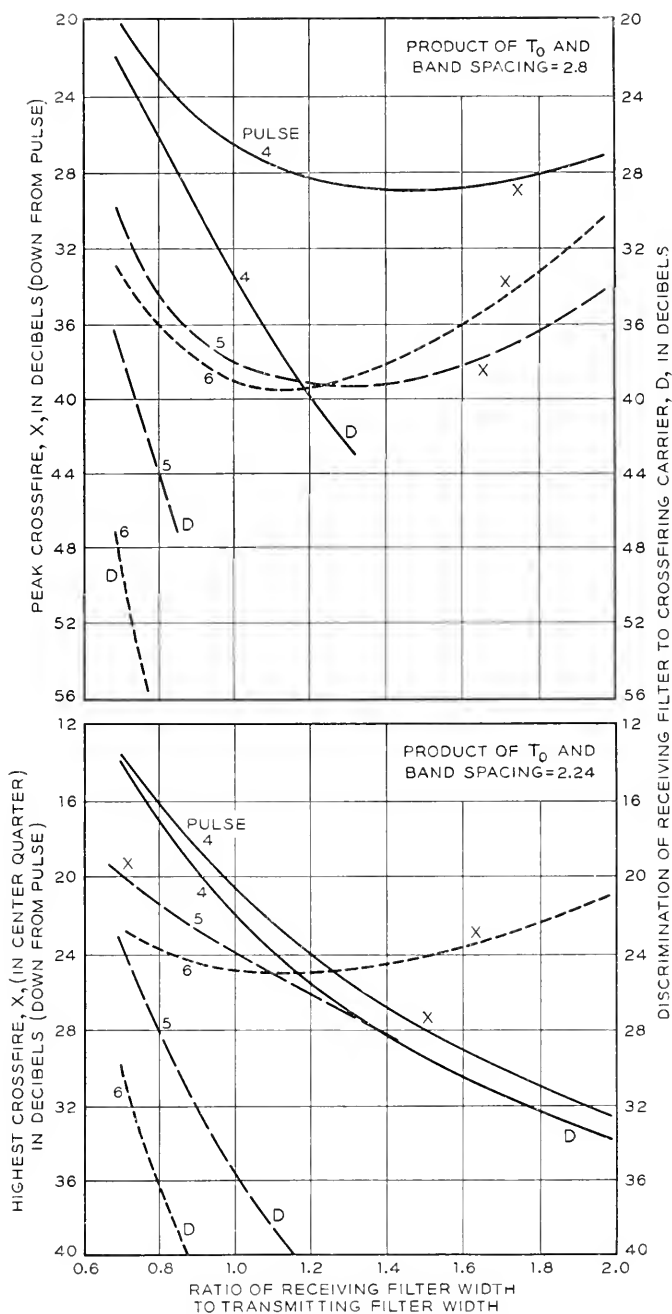


Fig. 27—Crossfire between frequency divided pulse groups.

pulse crossfire than the curves predict. This is particularly so for cases in which the curves show crossfire 30 or more decibels down. Approximations usually possess less rapidly falling attenuation skirts and possess phase distortion, both of which prevent realization of the calculated crossfire values.

Because regeneration (or reshaping) *permits* the use of Gaussian receiving filters, it does not follow that *flat-topped* filters are inferior as receiving filters. Calculations were made for maximally flat receiving filters of about the same overall complexity as was involved in the Gaussian approximations. They showed that when the transmitted pulse has the shape 4 and the flat filter is scaled to transmit such a pulse without much distortion, values of peak crossfire of the order of 30 db can be obtained when the product of band spacing and  $T_0$  is 2.8. It was also found that the crossfire in that case consists of a single peak (not unlike the main pulse) nearly coincident in time with the crossfiring pulse. Our Gaussian approximations gave peak crossfire of this same order, for band spacing times  $T_0 = 2.8$ . The maximally flat receiving filter accepts roughly twice the noise power accepted by the optimum Gaussian filter, so the favor remains with the Gaussian filter and pulses 4 or 5.

The main conclusion from all of this is that, if smooth pulses, like numbers 4 or 5, are employed, band spacings of the order of  $2.8/T_0$  (perhaps  $2.5/T_0$ ) can be used with crossfire entirely suitable for binary PCM, as well as for PPM systems with sufficient swing ratio. Larger spacings would be required for PCM using multi-valued digits, and for PAM.

As mentioned earlier, the use of pulses 10 or 11 spaced by  $T_0$  is possible in binary PCM, with small penalty, if very short accurately aligned gate pulses are used. The spectrum of these pulses is more sharply defined and includes a band only slightly wider than  $1/T_0$ . Rectangular receiving filters of that width could be used side-by-side so that the band spacing would be only slightly greater than  $1/T_0$ . This is the "theoretical minimum" and in telegraph parlance would be specified as a band spacing of twice the dot frequency.

Pulse 10 results from transmitting a very short pulse through a 4-section maximally flat filter whose response is shown in Column C. The phase distortion characteristics of such a filter produces asymmetry in the pulse. Pulse 11 is produced by the filter shown, assuming that the distortion is corrected. Most of the pulse shaping is assumed to reside in the transmitting filter. The assumed receiving filter is a 4-section maximally flat filter, and therefore has the shape of the filter shown for pulse 10, but is about 30% wider than shown. When two such bands are spaced  $1.5/T_0$  the maximum crossfire is about 26 db down.

With shaping and receiving filters of reasonable complexity a band spacing

of  $1.5/T_0$  to  $1.7/T_0$  can be expected to have satisfactorily small crossfire for binary PCM. Pulse 11 and a spacing of  $1.5/T_0$  were assumed for binary PCM-AM in Tables VI to VIII.

Figure 26 shows the envelopes of r.f. pulses produced by passing flat-topped r.f. pulses or r.f. *spikes* through r.f. filters. These envelopes are the baseband shapes produced by wide-band envelope detectors. If baseband pulses are shaped by baseband filters the resulting pulses are the same as shown for pulses 1 to 7, but for pulses 8 to 11 the tails turn out to be overshoots passing smoothly through zero instead of reaching zero cusp-wise. If these pulses are used to modulate the amplitude of a carrier in a product modulator, the cusps in the envelope are produced as shown, but if they are used to modulate the frequency of a carrier the baseband pulses produced by frequency detection retain their smooth transition through zero. In PAM-FM relatively wide gate pulses could be centered at time zero,  $T_0$ ,  $2T_0$ , etc., and the inter-pulse crosstalk would be partially balanced out by partial cancellation of positive and negative contributions. By the use of biases in the AM case a similar result could be obtained. Our tables, assuming pulse 4 spaced  $2T_0$ , do not reflect this possibility of operation.

#### DELAY LINE BALANCING

Techniques have been developed<sup>41, 40</sup> in which the received pulse train is split into two or more branches, after detection to the baseband, and recombined with suitable delays, attenuations and polarity reversals. Such a procedure is effective in reducing the pulse tails or hangover and its use has been especially valuable in experimental PAM and PAM-FM systems. While this device may be regarded as a kind of phase and amplitude equalizer (comprising as it does only linear, passive elements) the result may be a pulse shape slightly more desirable than those obtained from simple but "ideal" networks, shown in Fig. 26. Our judgment that pulses of shape 4, spaced  $2T_0$ , should be used in PAM-FM may be slightly pessimistic if this kind of balancing is used.

More significant reductions of inter-pulse interference may be sought by the method suggested by MacColl<sup>41</sup> (which is more than "equalizing") but this method, like the PCM method of Appendix III soon makes preposterous demands on the transmission medium and upon the transmitted power.

#### VIII. TRANSMISSION OVER METALLIC CIRCUITS

In radio relay transmission we have assumed a span length of 30 miles and have assumed span losses in keeping with the microwave antenna art

<sup>41</sup> V. D. Landon, loc. cit.

<sup>40</sup> W. D. Boothroyd and E. M. Creamer, Jr., "A Time Division Multiplexing System," Paper presented at winter general meeting, A.I.E.E., New York, Jan. 31, 1949.

<sup>41</sup> U. S. Patent No. 2,056, 284 Oct. 6, 1936 issued to L. A. MacColl.

and the relatively meager propagation experience now available. The high cost of the towers, power facilities and access roads involved in repeaters as we know them points to the desirability of few repeaters and long spans. Topography usually permits spans of a few tens of miles without requiring towers of excessive height. Very much longer spans can rarely be had without tremendous towers and are questionable because of the increase of fading depth with distance.

In wave guide (or other metallic conductor) transmission entirely different considerations apply and we will discuss some electrical relationships which seem significant in this case.

Let us consider a microwave repeater having a noise figure NF and a power capacity PC. The overload characteristic, together with the amount of nonlinear distortion that the signal can stand, determines the maximum output power. This maximum power is the power capacity. These two characteristics, PC and NF, thus determine the amount of attenuation that may be introduced between the transmitting half of a repeater regarded now as a transmitting terminal and the receiving half regarded as a receiving terminal. This amount of attenuation expressed in decibels, which we will designate as  $M$ , is available to be used up by the loss of one span plus accumulation of noise from  $n$  repeaters and may be regarded as a figure of merit of the repeater.

Five different relationships apply as follows:

$$\text{AM Systems: } M = \text{span loss}_{db} + 20 \log n \quad (1)$$

$$\text{FM Systems: } M = \text{span loss}_{db} + 10 \log n \quad (2)$$

PPM-AM Systems with

$$\begin{aligned} \text{reshaping repeaters: } M &= \text{span loss}_{db} + 5 \log n \quad (3) \\ \text{Band increased } {}^2\sqrt{n} &\text{ referred to (1)} \end{aligned}$$

FM Systems with

$$\begin{aligned} \text{limiting repeaters: } M &= \text{span loss}_{db} + 3.33 \log n \quad (4) \\ \text{Band increased } {}^3\sqrt{n} &\text{ referred to (2)} \end{aligned}$$

PCM Transmission with

$$\text{regenerative repeaters: } M = \text{span loss}_{db} + \text{zero} \quad (5)$$

In (1) the  $20 \log n$  term includes  $10 \log n$  for noise accumulation plus  $10 \log n$  for cumulative compression. In microwave amplifiers only odd-order terms contribute to the distortion and the third order term predominates for moderate degrees of overload. This results in the well-known compression characteristic such as appears in Figs. 24 and 25 previously discussed. A significant approximation for the over-all compression when

$n$  such amplifiers are connected in tandem is that the compression characteristic is the same as with one amplifier but occurs at outputs  $10 \log n$  db lower. Thus, the power level must be reduced  $10 \log n$  db and this penalty accrues over and above the noise accumulation penalty.

In (2) only noise accumulation occurs.

In (3) and (4) it is assumed that minimum power conditions are attained and the operation has reached the straight part of the minimum (marginal) power curves. Without reshaping, the system must be powered so that, at the final repeater, the accumulation of noise does not exceed the marginal value. With reshaping at each of the  $n$  repeaters each span may be marginal. Making each span marginal with the same bandwidth would be accomplished with  $10 \log n$  db less power and would make the signal-to-noise ratio  $10 \log n$  db lower. This can be made up by using more bandwidth. In marginal PPM-AM the signal-to-noise ratio improvement occurs at the rate of 20 db per decade of bandwidth and thus the bandwidth must be increased by  $^2\sqrt{n}$ . This requires, to keep the operation marginal, an increase in power of  $10 \log n^{1/2} = 5 \log n$  db. In the case of marginal FM, signal-to-noise ratio is improved at the rate of 30 db per decade, and the bandwidth must accordingly be increased by  $^3\sqrt{n}$ . To keep the operation marginal, the power must be increased  $10 \log n^{1/3} = 3.33 \log n$  db. The entries in Tables II and III invoke these relationships. There,  $n$  may be thought of as having values 1, 5 or 133.

Equation (5) reflects the fact that where PCM regenerative repeaters are employed no accumulation of noise occurs with number of spans.

With metallic conductors, the span loss in decibels is proportional to the length of span. If  $A$  denotes the span loss in decibels per mile and  $S$  denotes span length in miles, the circuit length  $L = nS$  and

$$M = \frac{AL}{n} + x \log n \quad (6)$$

or,

$$L = \frac{n}{A} M - \frac{nx}{A} \log n \quad (7)$$

where  $x$  is the appropriate coefficient, 20, 10, 5 or 3.33. In this expression there is an optimum value of  $n$  corresponding to a maximum value of circuit length  $L$ . Figure 28 is a plot of circuit length for  $x = 20$  (Eq. 1), showing the maxima. Figures 29 to 32 show the optimum values of  $n$  and the resulting maximum circuit lengths for each of the relations expressed in equations (1), (2), (3), (4).

Considerations affecting transmission over metallic circuits are different from those affecting radio relay in at least the following four ways:

1. Interference from other routes substantially vanishes with coaxial and

wave-guide conductors. This diminishes the premium on ruggedness provided sufficient power is available so that ruggedness with respect to noise is not critical.

2. Since there is no fading and all spans can be of approximately equal length, all spans will possess the same loss, approximately. This situation

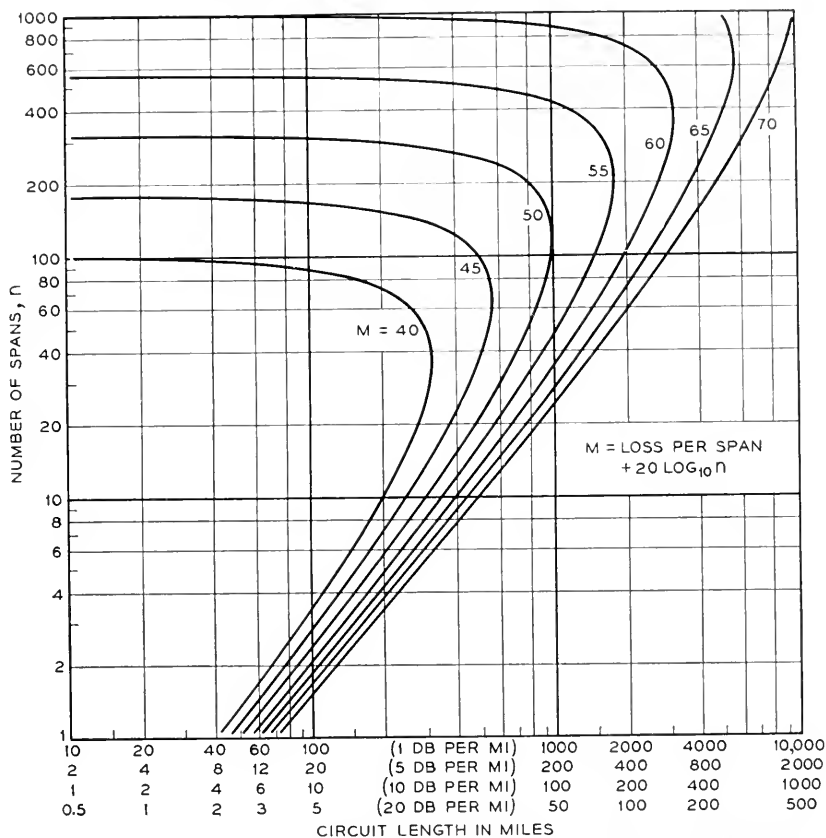


Fig. 28—Variation of circuit length with number of repeater sections in an AM system with fixed power capacity and noise figure.

is favorable to all systems but is most favorable to PCM, which gets no credit for low loss spans.

3. In the case of wave guide, frequency space may be much less precious than in coaxial or radio relay transmission.

4. There is a possibility that many small repeaters should replace the few higher powered repeaters used in radio relay.

These different considerations may lead to a different evaluation of the

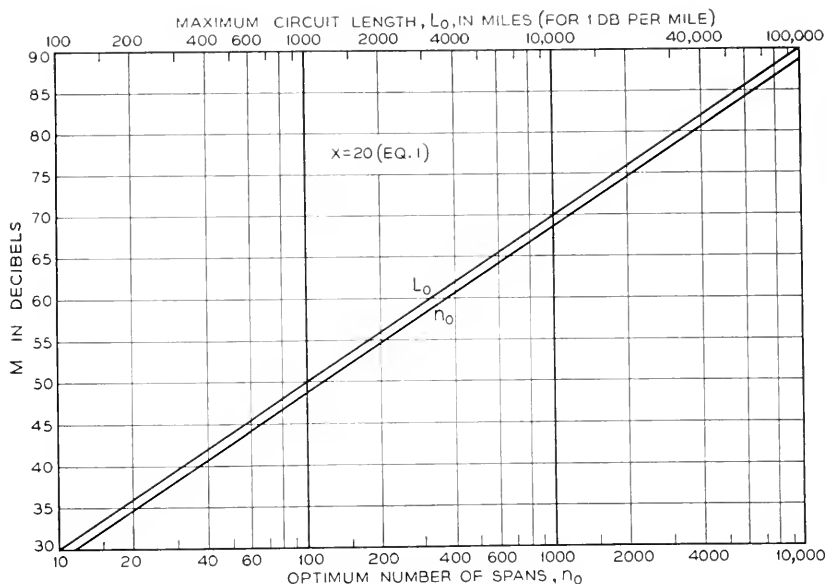


Fig. 29—Optimum number of repeater sections and maximum circuit length for metallic AM system with fixed power capacity and noise figure.

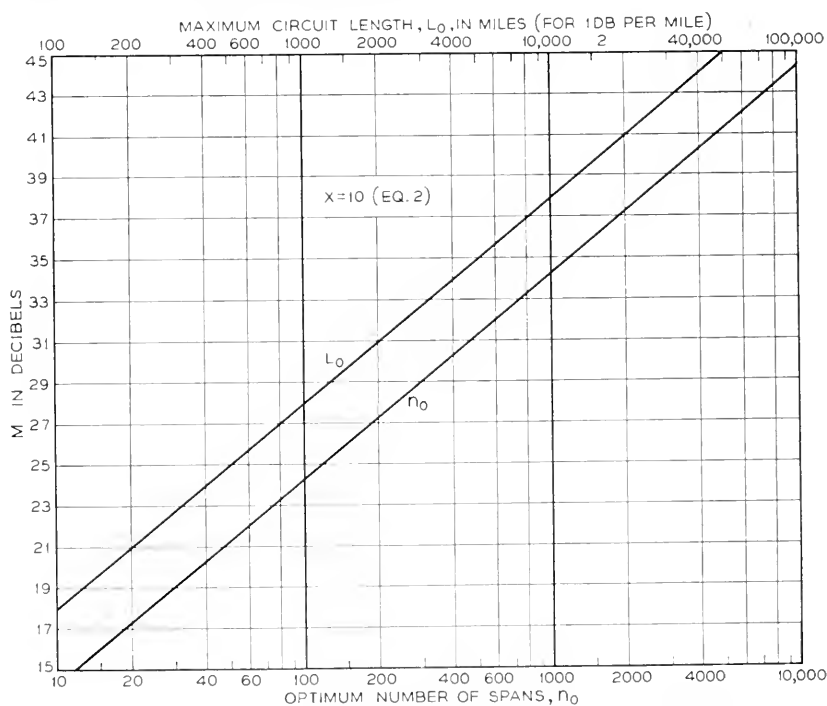


Fig. 30—Optimum number of repeater sections and maximum circuit length for metallic FM system with limiting only at end of system.



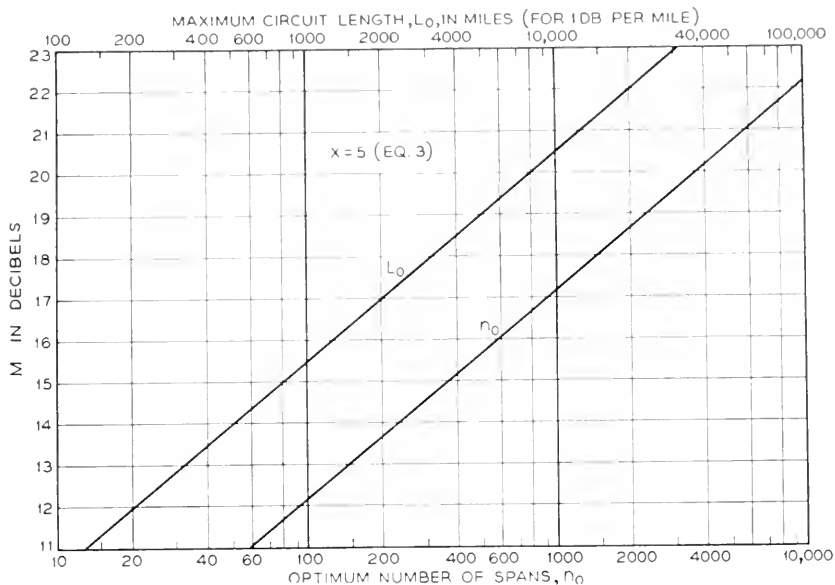


Fig. 31—Optimum number of repeater sections and maximum circuit length for metallic PPM-AM system with reshaping at every repeater.

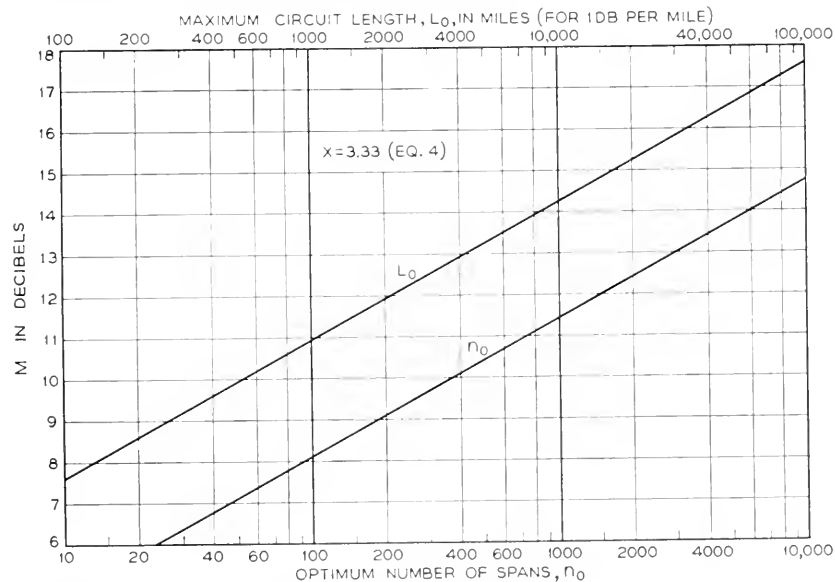


Fig. 32—Optimum number of repeater sections and maximum circuit length for metallic FM system with limiting at every repeater.

modulation methods discussed in this paper. We will not attempt to make such a re-evaluation here.

It is of interest now to return to radio relay transmission and examine the relations derived for metallic conductors, but now assuming that the span attenuation is that associated with an inverse  $k$ -power of distance law ( $k = 2$  for free space attenuation). If we use the symbol  $E$  to denote the excess power capacity (in decibels) of the repeater over that required for a unit span of, say, one mile, we get the relation

$$10k \log L = E + (10k - x) \log n \quad (8)$$

where  $x = 20, 10, 5, 3.33, 0$  for the cases described by equations (1), (2), (3), (4), (5) respectively. The equation shows no optimum number of spans

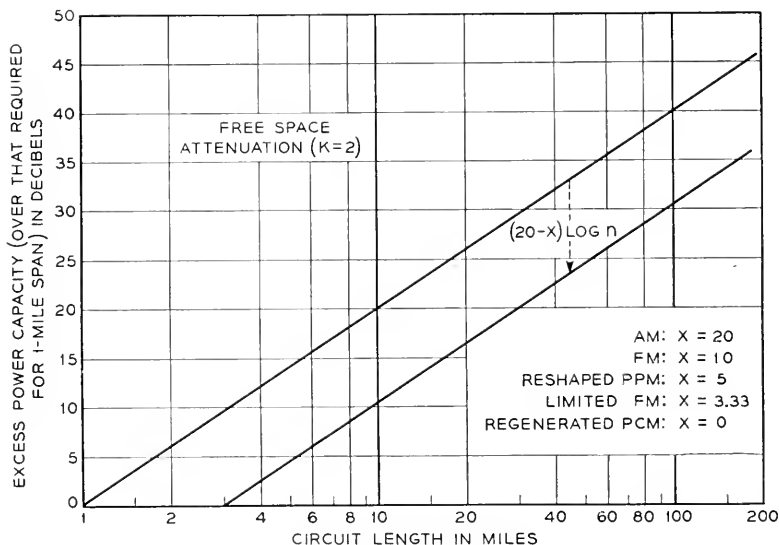


Fig. 33—Relation between circuit length, power, and number of repeaters in radio relay systems.

corresponding to a maximum circuit length. It also shows that when  $x$  is less than  $10k$  the circuit length can be increased indefinitely by adding spans although the spans become shorter with increased circuit length. When  $x = 10k$  the circuit length can not be increased beyond the maximum single span, i.e., it depends solely upon  $E$  and is not affected by the number of spans. If  $x$  is greater than  $10k$  the circuit length again cannot be increased beyond the maximum single span and is reduced by employing more than one span. This last case does not occur for free space attenuation. In Fig. 33 is plotted the relationship between  $L$ ,  $E$  and  $n$  for the free space attenuation law ( $k = 2$ ). The curve passing through zero decibels excess power capacity at one mile circuit length applies to one span for any value

of  $x$  or to any number of spans when  $x = 20$ . In other words the maximum circuit length for  $x = 20$  is the length of span corresponding to the excess power capacity as noted above for  $x = 10k$ . For all smaller values of  $x$  any circuit length can be achieved with any value of excess power capacity if a sufficient number of spans is employed. The number of spans required for a given circuit length is obtained by moving the curve downward until it intersects the desired length at the appropriate excess power ordinate, and equating  $(20 - x) \log n$  to the downward shift in decibels.

Notwithstanding the present radio outlook in which large towers and antennas seem indicated, it is of interest to imagine small repeaters powered for a one-mile span, say. Using FM with limiting at every repeater, a 100-mile circuit could be obtained with 250 repeaters spaced 0.4 miles. This result comes from Fig. 33 with excess power = zero db and  $x = 3.33$ . A difficulty with such a case might be multiple paths produced by one repeater output overreaching into other spans.

The inverse  $k$  power attenuation does not accurately describe propagation over long spans; fading then occurs and is greater for long spans than short spans. This introduces a term in the span loss similar to that of the metallic conductor case in which the span loss is proportional to span length.

## IX. CONCLUSIONS

We have, in this paper, examined some of the relations governing the exchange of bandwidth for advantages in transmission that grow out of the liberal use of bandwidth. While we have not dealt specifically with the instrumentation involved in the application of the various exchange methods, we have taken cognizance of certain basic obstacles in circuit design such as overload distortion, phase distortion and discrimination characteristics of selective networks and the limitations of microwave antennas. Not having, in most cases, a wealth of experience bearing on the manner in which these obstacles affect the transmission problem, we have been obliged to estimate their effect in many cases. Considerable unreliability in these estimates would not, however, much affect the broad purpose of the paper. The economic factor that is involved in achieving reliable operation of apparatus has been largely ignored, although methods that seem to lead to fantastic instrumentation have not been given much attention.

Ruggedness of the transmitted signal, which is obtained at the cost of increased *bandwidth* can, properly handled, be made to conserve *frequency occupancy* in two ways: (a) ruggedness reduces the required "guard space" between one band and neighboring bands carrying other signals; (b) ruggedness reduces the multiplication of frequency assignments necessary in congested radio route situations.

For wave guide systems, the inter-route interference problem arising from

route congestion disappears but ruggedness is still a valuable feature. As to PCM, regeneration is an outstanding asset applicable also in wave guide transmission. In the case of very high-grade channels the unique advantage of PCM that stems from the coding principle is presumably valuable in any transmission medium. We have shown that, theoretically, PCM methods can achieve lower power requirements than any of the other methods considered and can do so with considerably less frequency space.

While this paper is primarily concerned with the transmission of multiplex telephony, it seems appropriate to dwell briefly on the transmission of television signals by radio relay. The repeater plan of Fig. 4 is capable of handling long distance transmission of a 5-mc (video) television signal (by FM). The frequency occupancy of a single two-way route is 80 mc. The occupancy for 1000 4-kc telephone channels is 72 mc from Table VI for binary PCM-AM with dual polarization. At this rate a 5-mc video television band would require 90 mc assuming that the 39 db signal-to-quantizing noise ratio is satisfactory for television.<sup>42</sup> Remembering that route congestion can lead to a greater occupancy than 80 mc in the FM case and perhaps to no increase over 90 mc in the PCM case, we conclude that on these assumptions PCM might be a desirable method for long television relay routes. In the event that a better signal-to-noise ratio is found necessary, binary PCM provides 6 db improvement for each additional digit.

These conclusions relate to the transmission problem under the assumed conditions, and do not reflect the impact of many factors that may grow out of an application to a real situation. As has been said before, this paper should be taken to illustrate the way in which the transmission factors are interrelated, and the philosophy by which the problem is approached, rather than to find an unequivocally best system.

In preparing this paper the authors have, of course, drawn on the general transmission background of the Bell Telephone Laboratories. Nourishment has come particularly from W. M. Goodall, A. L. Durkee, H. S. Black, D. H. Ring, J. C. Schelleng and F. B. Llewellyn in addition to those mentioned specifically in the paper.

We wish specifically to thank Mr. R. K. Potter, whose broad transmission concepts were responsible for initiating the work.

## APPENDIX I

### NOISE IN PCM CIRCUITS

In the transmission of speech by PCM the kinds of noise and distortion which are acquired by other systems in transmission are completely missing.

<sup>42</sup> W. M. Goodall, "Television by Pulse-Code Modulation." Paper presented at 1949 IRE National Convention, New York, March 9, 1949.

Instead, a special kind of impairment is incurred at the terminals, because of the fact that the speech wave is transmitted by quantized amplitude samples of the wave. Transmitting samples of a wave results in a received wave having no impairment, provided the samples are not subjected to time or amplitude distortion. In PCM, since the samples are telegraphed, their reception is inaccurate by the quantization imposed by the code. These errors in the samples constitute the sole inherent impairment in transmission.

Strictly speaking, the transmission impairment in PCM is manifested only when a signal is being transmitted. An imaginary telephone circuit with the transmitting side completely devoid of any kind of signal, except that from the talker, could be transmitted by PCM from coast to coast and would sound completely silent if the talker were silent. In any real situation, however, some background noise (room noise, breath noise or line noise) is always present in the subscriber's circuit. This background noise is usually comparable to or greater than the weak parts of weak speech. In order to transmit the speech of weak talkers the size of the discrete amplitude steps must be small with the result that at least a few steps are always brought into play by background noise.

Being thus enabled to rule out the case of no *signal* we are able to ascribe a basic signal impairment to a PCM system. This impairment is, strictly speaking, a result of non-linear distortion inherent in the quantizing, but because of its very complex nature it behaves, and sounds, much like thermal noise and we have accordingly called it *quantizing noise*. A PCM circuit can be regarded as a source of noise whose rms value is simply related to the size of the quantizing step and the sampling frequency, as follows:

In a low-pass band extending to approximately 40% of the sampling frequency the basic noise power is related to the power of a sine wave signal by

$$\frac{\text{Signal power}}{\text{Noise power}} = 20 \log_{10} \frac{\text{peak-to-peak signal voltage}}{\text{step voltage}} + 3 \text{ db}$$

This band of noise has an amplitude distribution somewhat different from thermal noise, and a spectral distribution which depends somewhat upon the spectral distribution of the signal and upon its amplitude and disposition with respect to the step boundaries.

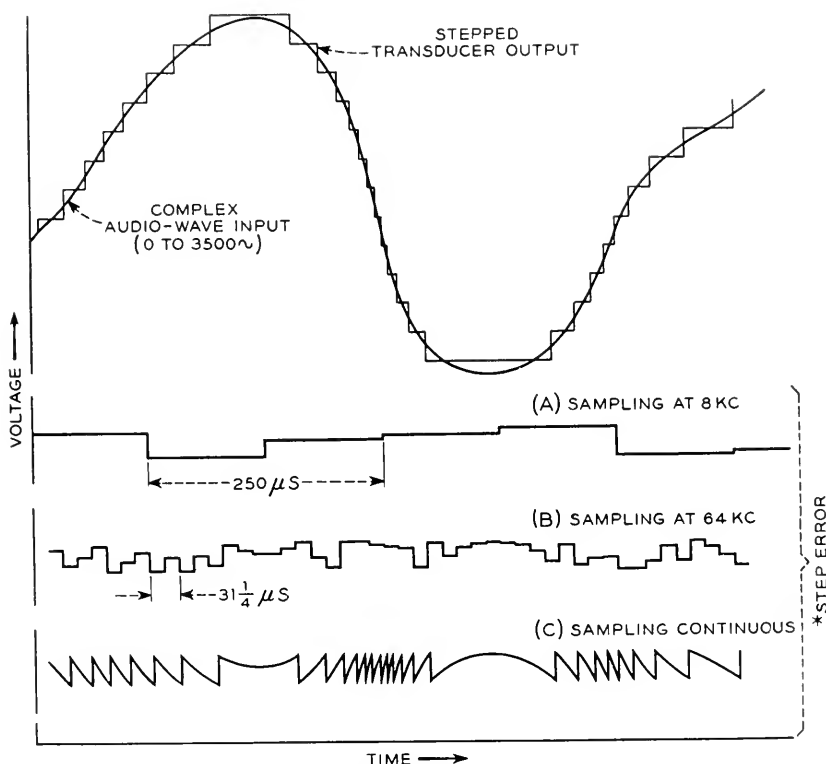
For a sine wave signal the noise spectrum is characterized by a number of prominent components rising above a diffuse background of numerous smaller components. The outstanding components may be either harmonics of the signal frequency or differences between harmonics of the sampling frequency and harmonics of the signal frequency. The background thus consists of an array of various orders of cross-products between the signal and the sampling rate. When the amplitude of the signal is comparable to one step in the quantizing process, a few components may contain a substan-

tial portion of the total power in the distortion spectrum. If the signal is not only weak but has its frequency near the low edge of the band, the distortion spectrum has a decided downward slope on the frequency scale with a major part of the distortion power concentrated in the lower harmonics of the signal frequency. Similarly, a weak signal at the upper edge of the band may cause a few scattered difference products to be outstanding. Stronger signals with more centrally located frequencies give practically a uniform distribution of distortion power throughout the signal band. For all except the extreme cases of low amplitudes and frequencies near the edges of the band, the weighting network used to evaluate the telephonic interfering effect of noise gives a reading equal to that obtained with a flat band of thermal noise of the same mean power. The exceptional cases show a spread in the readings which are sensitive to amplitude, frequency and disposition with respect to step boundaries. The spread is reduced when complex signal waves are applied. An operationally significant case is that in which the noise is produced by residual power hum in the equipment. In such a case, weighted noise readings range from approximately the value obtained for flat noise of the same mean power, to several db lower. Connecting even a short subscriber's loop to the input usually adds enough miscellaneous noise, if the steps are as small as they need to be, to remove the variability and to yield a reading within one db of the equivalent flat noise case.

Thus, a PCM system, like any other transmission system, possesses a noise source and experiments show that this noise combines by power addition with that from another system connected to the input or output of the PCM system. In tandem connections of PCM systems in which successive quantizations may occur, the quantizing noise also adds like power, from system to system, and soon becomes almost indistinguishable from thermal noise.

The quantizing noise consists of distortion products which may be classified as two kinds. One class includes those products which would be produced by transmitting the wave through a transducer whose input-output characteristic is stepped like a staircase. If such a transducer were actually used the PCM process would be equivalent to sampling its output at a regular rate and transmitting the step designations by code. This sampling process, applied to the stepped transducer output, produces the other class of distortion (or noise) and is illustrated in Fig. 34. Let us consider the sampled value as the sum of the true value plus the step error, and focus attention on the step error which is responsible for the distortion. At minimum permissible sampling frequency (twice the highest signal frequency), the step errors in consecutive samples are practically unrelated to each other. The low-pass output filter passes most of the power in this sequence of random errors

when they occur at a frequency only twice the filter cutoff frequency. See A in Fig. 34. If the sampling frequency were increased from the minimum permissible value, the consecutive step errors would still be unrelated to each other, and more and more of the step error spectrum (noise) would fall above the low-pass filter. This is shown in B.



\*THE QUANTIZING NOISE CONSISTS OF THE RESPONSE OF A 3500-CYCLE LOW-PASS FILTER TO THE STEP ERROR

Fig. 34—Stepping and sampling an audio wave.

Reduction of noise would occur in this way until the sampling frequency became so high that a considerable number of samples are taken while the wave crosses a step interval. Correlation between successive step errors then begins to be apparent. When the interval between samples becomes vanishingly small, the process is equivalent to transmitting the stepped transducer output directly. This case appears in C.

In an alternate line of thinking, one may regard the stepped transducer

output as the signal wave plus a wide spectrum of distortion frequencies representing the effect of the steps. From this point of view, it is clear that only a high sampling frequency prevents lower sidebands associated with the sampling frequency and its harmonics from overlapping the signal band.

Quantizing noise decreases with increase of sampling frequency at an initial rate of approximately 3 db per octave and continues until correlation of successive errors becomes appreciable. This occurs at a sampling frequency which is dependent upon the spectral distribution of the signal, being lower for signals having a predominately low-frequency spectral density. An increase of step size also reduces the lowest sampling frequency at which effects of correlation are observed. Figure 35 shows curves calculated for an

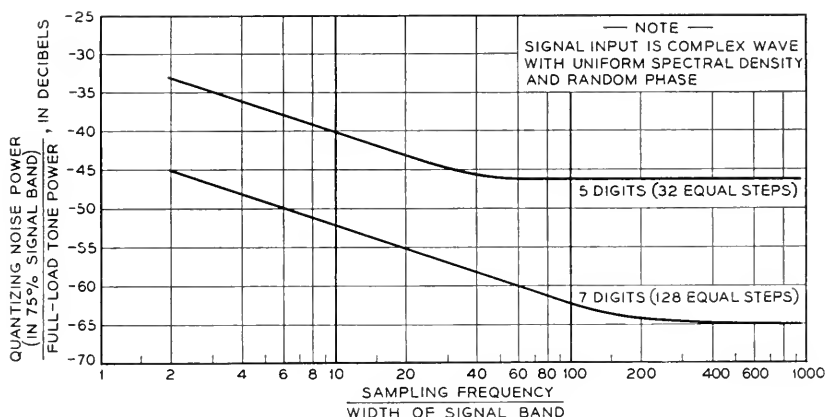


Fig. 35—Variation of quantizing noise with sampling frequency.

input consisting, in fact, of thermal noise. Such an input is a rough approximation to a speech wave.

The asymptotic values shown for five and seven digits represent the quantizing noise corresponding to transmission of the thermal noise signal through stepped transducers having 32 and 128 steps, respectively. The curves suggest that sampling is a penalty such that 32-step granularity without sampling is about equivalent<sup>43</sup> to 128-step granularity with sampling at the minimum rate. However, sending information which designates the irregular instants of time at which the signal enters and leaves each step interval is far less efficient than designating the steps at the regular instants of the minimum sampling rate.

<sup>43</sup> The equivalence would be in terms of total noise power; the properties of the asymptotic noise are different than were described earlier in this appendix, for sampling at the minimum rate.



## APPENDIX II

## INTERFERENCE BETWEEN TWO FREQUENCY MODULATED WAVES

This problem occurs so frequently in the present paper that its solution is appended here for reference. Figure 36 shows a geometric figure from which the phase of a two-component wave can be calculated. We write

$$P \cos \theta + Q \cos \varphi = R \cos \psi$$

where

$$R^2 = P^2 + Q^2 + 2PQ \cos (\theta - \varphi)$$

$$\tan \psi = \frac{P \sin \theta + Q \sin \varphi}{P \cos \theta + Q \cos \varphi}$$

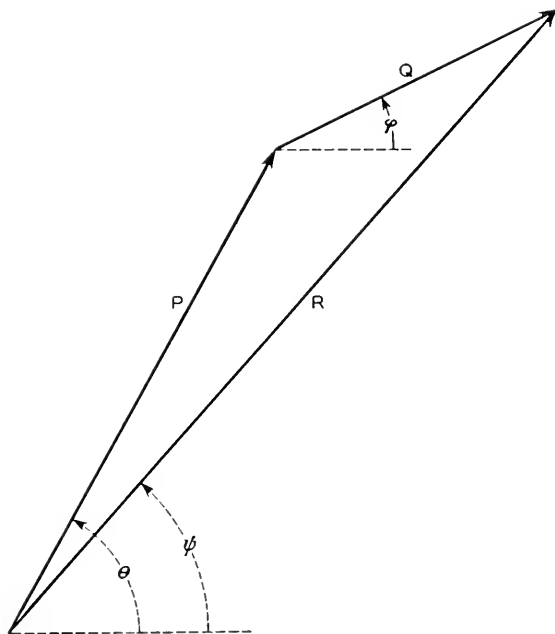


Fig36. —Geometric solution for resultant phase of two frequency modulated waves.

The response of a perfect frequency detector in radians/sec. is given by

$$\begin{aligned} \Omega &= d\psi/dt = \frac{d}{dt} \left( \arctan \frac{P \sin \theta + Q \sin \varphi}{P \cos \theta + Q \cos \varphi} \right) \\ &= \frac{1}{2}(\theta' + \varphi') + \frac{\theta' - \varphi'}{2} \frac{P^2 - Q^2}{P^2 + Q^2 + 2PQ \cos (\theta - \varphi)} \end{aligned}$$

In the above expression, the primes represent derivatives with respect to time. If  $Q/P < 1$ , we expand in Fourier series, obtaining

$$\Omega = \theta' + (\theta' - \varphi') \sum_{m=1}^{\infty} \left(-\frac{Q}{P}\right)^m \cos m(\theta - \varphi).$$

When  $Q/P$  is small, we retain only the term proportional to  $Q/P$  as the error, which may be written in the compact form:

$$\Omega - \theta' \doteq \frac{Q}{P} \frac{d}{dt} \sin(\varphi - \theta)$$

If the waves are unmodulated,  $\theta = pt$  and  $\varphi = qt$ , giving

$$\Omega - \theta' \doteq \frac{Q}{P} (q - p) \cos(q - p)t$$

### APPENDIX III

#### PCM FOR BANDWIDTH REDUCTION

We have treated PCM as a means of increasing bandwidth beyond the value corresponding to one pulse per sample per channel (quantized PAM) and have studied the transmission advantages that accrue therefrom. The PCM method can, in principle, serve to reduce bandwidth. An example of bandwidth reduction,<sup>44, 45</sup> suggested to the writers by C. E. Shannon, is as follows:

Any number, say  $N$ , of 4 kc telephone channels can be transmitted in the form of one quantized pulse per 125 microseconds, by sampling all channels in the usual way, encoding each sample into a code symbol having, say, 64 possible values, assembling all code pulses into one new group and decoding this group at the transmitter. If only one channel were to be transmitted the decoded signal would have 64 possible amplitudes; for two channels it would have  $64^2$  possible amplitudes, and for  $N$  channels,  $64^N$ . Now, if a single quantized pulse conveying these amplitudes could be transmitted without an error as large as one step, the receiver could encode the quantized pulse, disassemble the resulting code pulses into groups according to channels and decode the groups to obtain the  $N$  channel samples. The requirements on transmission circuits capable of the precision required to transmit even two channels in place of one are very severe, however.

In the event the signals to be transmitted were not speech signals but a very elemental kind of signal such as a black and white pattern requiring for

<sup>44</sup> A paper "Reducing Transmission Bandwidth" by Bailey and Singleton *Electronics*, Aug. 1948 gives a somewhat different example of reduction.

<sup>45</sup> An early disclosure of a system theoretically capable of any desired amount of bandwidth reduction is contained in U. S. Patent No. 2,056,284, Oct. 6, 1936, issued to L. A. MacColl. As in the current proposals, the decreased band is obtained at the expense of a vastly greater signal-to-noise ratio requirement and the necessity for precise synchronism between transmitter and receiver.

its description not 64 values but only 2, the number of possible amplitudes would be  $2^N$ . With some of the better transmission circuits in existence, as many as 10 such channels could be multiplexed in the same bandwidth required by one channel, by this adaptation of the PCM method.

The above considerations show that PCM offers the means of matching the transmission signal to the capabilities of the transmission circuit in order to transmit the maximum amount of information. As has been shown, with microwave telephone systems the economical balance seems to come well over on the wide band side, permitting operation with low transmitted power through relatively strong interference.

## APPENDIX IV

### SUPPLEMENTARY DETAILS OF DERIVATION OF BANDWIDTH-CURVES

#### PPM-AM

The diagram of Fig. 8 shows that the maximum time deviation is assumed to be

$$\epsilon = \frac{1}{2Nf_r} - T = \frac{1}{2Nf_r} - \frac{1}{F_b}. \quad (1)$$

The shift in time produced by an interfering voltage of magnitude  $E_n$  at the slicing instant is

$$\Delta t = E_n/s \quad (2)$$

where  $s$  is the slope of the signal pulse at the slicing instant. For small noise the slicing instant occurs near half the peak,  $E$ , of the pulse and the slope of the assumed sinusoidal pulse (Fig. 6) is:

$$s = \frac{\pi}{2T} E = \frac{\pi F_b E}{2} \quad (3)$$

Hence

$$\Delta t = \frac{2E_n}{\pi F_b E}. \quad (4)$$

The signal-to-noise power ratio in the channel is the ratio of mean square values of signal deviation  $\sigma$  and  $\Delta t$ . For thermal noise we assume that the root mean square value is one fourth the peak and place the peak at  $1/\sqrt{2}$  times  $E/2$  for marginal operation. We write, therefore,

$$E_n = E/2\sqrt{2}, \quad \overline{\Delta t^2} = (4E_n^2/\pi^2 F_b^2 E^2)/16 \quad (5)$$

$$\overline{\sigma^2} = \frac{\epsilon^2}{2} = \frac{1}{2} \left( \frac{1}{2Nf_r} - \frac{1}{F_b} \right)^2 = \frac{1}{2F_b^2} \left( \frac{F_b}{2Nf_r} - 1 \right)^2 \quad (6)$$

$$S/N = 4\pi \left( \frac{F_b}{2Nf_r} - 1 \right) = 4\pi \left( \frac{B}{4Nf_r} - 1 \right). \quad (7)$$

Here  $S/N$  is the ratio of root mean square audio signal and noise voltages. The formula illustrates a general principle common to all the pulse systems in that the marginal signal-to-noise ratio is a function of  $B/Nf_r$ . The axes of the curves have been labeled for  $N = 1000$  and  $f_r = 8$  kc, but can be read for any other values of  $N$  and  $f_r$  by changing  $B$  accordingly. Equation (7) was used to plot the marginal power curve of Fig. 9. We note that the ratio of rms pulse voltage at the top of the pulse to the rms noise voltage is  $E/\sqrt{2}$  divided by  $E_n/4$  which leads to a value of eight when (5) is substituted. The "slicer advantage" is thus the right-hand member of (7) divided by eight.

For CW interference in a PPM-AM system the procedure used above applies except that the root mean square interference is now  $1/\sqrt{2}$  times the peak instead of one fourth. The marginal ratio of rms audio signal to rms audio interference ratio is therefore poorer by a factor of  $2\sqrt{2}$ , or

$$S/I = \pi \sqrt{2} \left( \frac{B}{4Nf_r} - 1 \right). \quad (8)$$

When the interference is from a similar system, we calculate the distribution of the disturbance as follows. The probability that there is an interfering pulse present during slicing is the ratio of the pulse duration to the channel allotment, or

$$p_0 = 2Nf_r \tau = \frac{2Nf_r}{F_b}. \quad (9)$$

The interfering carrier will not, in general, be exactly synchronous with the wanted carrier, and hence the actual interference is a beat frequency with envelope having a voltage distribution calculable from the pulse shape. For a sinusoidal pulse of height  $A$ , the probability  $p(y) dy$  that the instantaneous magnitude of the interfering envelope is in the interval  $dy$  at  $y$  is

$$p(y) dy = \frac{p_0 dy}{\pi \sqrt{y(A-y)}}, \quad 0 < y < A. \quad (10)$$

Since the relative phase of the two carriers drifts with time, the mean square interfering voltage is half the mean square interfering envelope, or

$$E_n^2 = \frac{1}{2} \int_0^A y^2 p(y) dy = \frac{3Nf_r A^2}{9F_b} = \frac{3Nf_r A^2}{4B}. \quad (11)$$

Hence

$$\overline{\Delta t^2} = \frac{12Nf_r A^2}{\pi^2 B^3 E^2} \quad (12)$$

and

$$\frac{S}{I} = \frac{\pi E}{A} \left( \frac{B}{4Nf_r} - 1 \right) \sqrt{\frac{B}{6Nf_r}}. \quad (13)$$

For marginal interference  $E = 2\sqrt{2}A$  and

$$\frac{S}{I} = 2\pi \left( \frac{B}{4Nf_r} - 1 \right) \sqrt{\frac{B}{3Nf_r}}. \quad (14)$$

This equation shows that  $S/I$  varies as  $(B/Nf_r)^{3/2}$  for large bandwidths giving 9 db improvement per octave of bandwidth. The curves of Fig. 10 were plotted from equations (8) and (14).

### PPM-FM

The pulse here is transmitted by a change in frequency from  $f_1$  to  $f_1 + \beta$  and back again. The total frequency swing  $\beta$  corresponds to the pulse height  $E$  in the AM case. The frequency detector delivers a pulse of height  $\beta$  to the baseband filter. Associated with the pulse is the error caused by noise or interference in the rf-band. In the case of fluctuation noise having mean power  $P_n$  per cycle in the rf-medium, a baseband filter of width  $F_b$  accepts the familiar triangular voltage distribution of noise with frequency resulting<sup>46</sup> in a mean square integrated magnitude expressed on a frequency scale as:

$$E_n^2 = P_n F_b^3 / 3W_c \quad (15)$$

where  $W_c$  is the mean carrier power. Then, on substituting  $\beta$  for  $E$ , and the above expression for  $\overline{E_n^2}$  in the equation for  $\Delta t$ :

$$\overline{\Delta t^2} = \frac{4P_n F_b}{3\pi^2 \beta^2 W_c} \quad (16)$$

Taking the ratio of  $\overline{\epsilon^2}$  to  $\overline{\Delta t^2}$ ,

$$(S/N)^2 = \frac{3\pi^2 \beta^2 W_c}{8P_n F_b^3} \left( \frac{F_b}{2Nf_r} - 1 \right)^2. \quad (17)$$

The radio signal bandwidth  $B$  is approximately equal to the frequency swing plus a sideband at each end or

$$B = \beta + 2F_b \quad (18)$$

Using this relation to eliminate  $\beta$ , we have

$$(S/N)^2 = \frac{3\pi^2 (B - 2F_b)^2 W_c}{8P_n F_b^3} \left( \frac{F_b}{2Nf_r} - 1 \right)^2. \quad (19)$$

For marginal operation of the FM limiter:

$$W_c = kP_n B \quad (20)$$

where we shall assume  $k = 16$  in numerical calculations.

<sup>46</sup> An elementary component of interference  $Q \cos qt$  produces a frequency error  $(Q/P)f \cos 2\pi ft$  where  $f$  is the difference between the interfering and carrier frequencies. The corresponding mean square frequency error is  $f^2 Q^2 / 2P^2$ . But  $Q^2 / 2 = P_n df$  and there are equal contributions from upper and lower sidebands centered around the carrier. Also replacing  $P^2 / 2$  by  $W_c$ , we get a mean square frequency error in band  $df$  at  $f$  equal to  $P_n f^2 df / W_c$ . Integrating over frequencies from 0 to  $F_b$  gives the above result.

Then

$$(S/N)^2 = \frac{3k\pi^2}{8} \left(\frac{B}{F_b}\right)^3 \left(1 - 2\frac{F_b}{B}\right)^2 \left(\frac{F_b}{2Nf_r} - 1\right)^2. \quad (21)$$

The signal-to-noise ratio is found to be maximum when

$$\frac{F_b}{Nf_r} = \sqrt{\left(\frac{B}{4Nf_r} + 1\right)^2 + \frac{3B}{Nf_r}} - \frac{B}{4Nf_r} - 1. \quad (22)$$

To calculate the CW interference with an idle channel we assume that the carrier wave of the system is represented by

$$V_1(t) = P \cos [2\pi f_1 t + \phi(t)] \quad (23)$$

where

$$\phi(t) = \begin{cases} \pi\beta \left(t + \frac{1}{\pi F_b} \sin \pi F_b t\right), & 0 < t < \frac{1}{F_b} \\ \pi\beta/F_b, & \frac{1}{F_b} < t < \frac{1}{2Nf_r} \end{cases} \quad (24)$$

$$\phi(-t) = -\phi(t), \quad \phi\left(t \pm \frac{2m}{F_b}\right) = \phi(t), \quad m = 1, 2, \dots \quad (25)$$

We have chosen  $\phi(t)$  so that the phase is a continuous function of time with a derivative representing the correct frequency. This gives a sinusoidal change in the instantaneous frequency  $\phi'(t)/2\pi$  starting with the value  $f_1$  at  $t = -\frac{1}{F_b}$ , reaching the peak  $f_1 + \beta$  at  $t = 0$ , and subsiding to  $f_1$  at  $t = \frac{1}{F_b}$ . By making the wave repeat with frequency  $Nf_r$ , we assume all channels of the system are idle since all pulses are at their central positions. It seems reasonable to neglect the effect of variations in adjacent channel loading on CW interference in one channel. The interfering CW wave is represented by

$$V_2(t) = Q \cos (2\pi f_2 t + \theta) \quad (26)$$

To a first approximation the resulting error in frequency at the output of the frequency detector is:

$$\delta(t) = \frac{Q}{2\pi P} \frac{d}{dt} \sin [2\pi(f_1 - f_2)t + \phi(t) - \theta] \quad (27)$$

By straightforward Fourier series expansion and differentiation:

$$\delta(t) = \frac{Q}{P} F_b \sum_{n=-\infty}^{\infty} (c + n\lambda) A_n \cos [2\pi F(c + n\lambda)t - \theta] \quad (28)$$

where:

$$c = (f_1 - f_2)/F_b, \quad \lambda = Nf_r/F_b, \quad y = \beta/F_b, \quad (29)$$

$$A_n = 2\lambda \mathcal{J}_{2n\lambda - y}(y) - \frac{1}{n\pi} [(-)^n + \sin(2n\lambda - y)\pi], \quad (30)$$

$$A_0 = 2\lambda \mathcal{J}_{-y}(y) + (1 - 2\lambda) \cos \pi y. \quad (31)$$

The function  $\mathcal{J}_\nu(y)$  is Anger's function:<sup>47</sup>

$$\mathcal{J}_\nu(y) = \frac{1}{\pi} \int_0^\pi \cos(\nu\theta - y \sin \theta) d\theta \quad (32)$$

It is equal to  $J_\nu(y)$ , the more familiar Bessel function of the first kind, only when  $\nu$  is an integer. The values of  $\nu = 2n\lambda - y$  appearing in this solution are in general not integers and hence the ordinary tables of Bessel functions are inapplicable.

The baseband filter accepts the components of the error which have frequencies in the range:

$$-F_b \leq F_b(c + n\lambda) \leq F_b \quad (33)$$

or

$$-\frac{1+c}{\lambda} \leq n \leq \frac{1-c}{\lambda}. \quad (34)$$

The interfering wave in the baseband filter output is then

$$\delta_0(t) = \frac{Q}{P} F_b \sum_{n=n_1}^{n_2} (c + n\lambda) A_n \cos[2\pi F_b(c + n\lambda)t - \theta] \quad (35)$$

where  $n_1$  is the smallest integer not less than  $-(1+c)/\lambda$  and  $n_2$  is the largest integer not greater than  $(1-c)/\lambda$ . It would be convenient at this point to assume that  $\overline{\Delta^2}$  is expressible directly in terms of  $\delta_0^2(t)$ . However, there is reason to believe that such an assumption is pessimistic especially at the higher bandwidths where the disturbance  $\delta_0(t)$  may never reach its maximum values in the neighborhood of the actual slicing instant. A complete investigation requires a study of the instantaneous wave form of  $\delta_0(t)$  in the neighborhood of the slicing instant. We note that if the slicer operates at the trailing edge, the unperturbed slicing instant is  $t = \frac{1}{2F_b} + m/f_r$ , and the value of the disturbance at that instant is:

$$\delta_0\left(\frac{1}{2F_b} + m/f_r\right) = \frac{Q}{P} F_b \sum_{n=n_1}^{n_2} (c + n\lambda) A_n$$

<sup>47</sup> Watson, Theory of Bessel Functions, Chapter X.

$$\cos \left[ 2\pi(c + n\lambda) \left( \frac{1}{2} + m \frac{F_b}{f_r} \right) - \theta \right], \quad m = 0, \pm 1, \pm 2, \dots \quad (36)$$

Averaging the square over all values of  $\left[ 2m\pi \frac{F_b}{f_r} - \theta + c\pi \right]$ , which may be treated as a randomly distributed angle, we find an expression for  $\delta_0^2$  averaged over the values at the slicing instants and not over all time, viz.:

$$\bar{\delta}_0^2 = \frac{Q^2}{2P^2} F_b^2 (R^2 + X^2) \quad (37)$$

$$\text{where} \quad R = \sum_{n=n_1}^{\infty} (c + n\lambda) A_n \cos \left[ n\pi\lambda \left( 1 + \frac{2mF_b}{f_r} \right) \right] \quad (38)$$

$$X = \sum_{n=n_1}^{\infty} (c + n\lambda) A_n \sin \left[ n\pi\lambda \left( 1 + \frac{2mF_b}{f_r} \right) \right] \quad (39)$$

Then

$$\overline{\Delta t^2} = \frac{2Q^2(R^2 + X^2)}{\pi^2 P^2 \beta^2} \quad (40)$$

and

$$\frac{S}{I} = \frac{\pi P}{Q} \left( \frac{B}{2F_b} - 1 \right) \left( \frac{F_r}{2Nf_r} - 1 \right) (R^2 + X^2)^{-1/2} \quad (41)$$

For each value of  $B$ , the value of  $S/I$  should be computed over a range of values of  $c$ ; and the lowest value of  $S/I$ , corresponding to the most unfavorable allocation of the CW frequency, plotted as a point on the curve. The curve of Fig. 12 was not calculated in this way but estimated from the simpler solution existing when the pulses are contiguous.

When the interference is from a similar system, we substitute for the interfering wave:

$$V_2(t) = Q \cos [2\pi f_1 t + \phi(t - \tau) + \theta] \quad (42)$$

This gives

$$\delta(t) = \frac{Q}{2\pi P} \frac{d}{dt} \sin [\phi(t) - \phi(t - \tau) - \theta + 2\pi(f_1 - f_2)t] \quad (43)$$

We distinguish between the cases of overlapping and non-overlapping pulses.



If the pulses do not overlap, we take the origin of time midway between pulses and write

$$\frac{\phi(t) - \phi(t - \tau)}{\pi\beta} = \begin{cases} -\frac{1}{F_b}, -\frac{1}{2Nf_r} < t < -\frac{\tau}{2} - \frac{1}{F_b} \\ t + \frac{\tau}{2} + \frac{1}{\pi F_b} \sin \pi F_b \left( t + \frac{\tau}{2} \right), -\frac{1}{F_b} < t + \frac{\tau}{2} < \frac{1}{F_b} \\ \frac{1}{F_b}, \frac{1}{F_b} - \frac{\tau}{2} < t < \frac{\tau}{2} - \frac{1}{F_b} \\ -t + \frac{\tau}{2} - \frac{1}{\pi F_b} \sin \pi F_b \left( t - \frac{\tau}{2} \right), -\frac{1}{F_b} < t - \frac{\tau}{2} < \frac{1}{F_b} \\ -\frac{1}{F_b}, \frac{1}{F_b} + \frac{\tau}{2} < t < \frac{1}{2Nf_r} \end{cases} \quad (44)$$

If the pulses overlap, we also take the origin midway between pulses, but we then obtain

$$\frac{\phi(t) - \phi(t - \tau)}{\pi\beta} = \begin{cases} -\frac{1}{F_b}, -\frac{1}{2Nf_r} < t < -\frac{\tau}{2} - \frac{1}{F_b} \\ t + \frac{\tau}{2} + \frac{1}{\pi F_b} \sin \pi F_b \left( t + \frac{\tau}{2} \right), -\frac{1}{F_b} - \frac{\tau}{2} < t < \frac{\tau}{2} - \frac{1}{F_b} \\ t - \frac{1}{F_b} + \frac{2}{\pi F_b} \sin \pi \frac{F_b \tau}{2} \cos \pi F_b t, \frac{\tau}{2} - \frac{1}{F_b} < t < \frac{1}{F_b} - \frac{\tau}{2} \\ -t + \frac{\tau}{2} - \frac{1}{\pi F_b} \sin \pi F_b \left( t - \frac{\tau}{2} \right), \frac{1}{F_b} - \frac{\tau}{2} < t < \frac{1}{F_b} + \frac{\tau}{2} \\ -\frac{1}{F_b}, \frac{1}{F_b} + \frac{\tau}{2} < t < \frac{1}{2Nf_r} \end{cases} \quad (45)$$

In both cases the right-hand members are even functions of  $t$ .

Hence

$$\sin [\phi(t) - \phi(t - \tau) - \theta] = \sum_{m=1}^{\infty} B_m \cos 2m\pi Nf_r t \quad (46)$$

$$\cos [\phi(t) - \phi(t - \tau) - \theta] = \frac{A_0}{2} + \sum_{m=1}^{\infty} A_m \cos 2m\pi N f_r t \quad (47)$$

The coefficients  $A_m$  and  $B_m$  are considerably more complicated than in the corresponding CW case.

### PAM-FM

An idle  $N$ -channel system sends sinusoidal pulses of duration  $2/F_b = 1/Nf_r$  which merge into a continuous sinusoidal variation of frequency expressible by

$$f = f_1 + \frac{\beta}{4} \cos \pi F_b t \quad (48)$$

where  $\beta$  is the peak-to-peak frequency swing and  $f_1$  is the mid-frequency. A full load audio tone frequency  $\frac{q}{2\pi}$  impressed on one channel produces a series of sinusoidal pulses of varying heights expressed with sufficient accuracy for a large number of channels by

$$F = f_1 + \frac{\beta}{2} g_0(t) \cos qt \quad (49)$$

where  $g_0(t)$  represents a pulse of unit height and duration  $\frac{2}{F_b}$  repeated periodically at the frame frequency  $f_r$ . Aperture effect is neglected in this approximation. We may expand  $g_0(t)$  in a Fourier series:

$$g_0(t) = \frac{G_0}{2} + \sum_{m=1}^{\infty} G_m \cos 2m\pi f_r t \quad (50)$$

where

$$G_m = 2f_r \int_{-1/2Nf_r}^{1/2Nf_r} g_0(t) \cos 2m\pi f_r t \, dt \quad (51)$$

When a rectangular gate of full-channel duration  $1/Nf_r$  is used between the baseband filter and the audio output filter for the channel,  $F$  represents the input to the channel filter. The only term passed by the latter is

$$F_q = \frac{\beta}{4} G_0 \cos qt \quad (52)$$

$$G_0 = 2f_r \int_{-1/2Nf_r}^{1/2Nf_r} \frac{1}{2}(1 + \cos 2\pi N f_r t) \, dt = \frac{1}{N} \quad (53)$$

Therefore the peak sine wave channel output is  $\beta/4N$ , and the mean square value is  $\beta^2/32N^2$ . If a gating function  $g_1(t)$  is used instead of a rectangular gate, we replace  $g_0(t)$  by  $g_0(t)g_1(t)$  in the calculation of  $G_0$ .

When the interference is fluctuation noise of mean power  $P_n df$  in bandwidth  $df$ , the mean square frequency error in the output of the frequency detector is  $w_n(f)df$  at frequency  $f$ , where

$$w_n(f) = P_n f^2 / W_c \quad (54)$$

The baseband filter accepts the portion of this spectrum between  $f = 0$  and  $f = F_b$ .

The action of the rectangular gate on this spectrum may be calculated by multiplication of the typical spectral component by the gating function:

$$G(t) = \frac{a_0}{2} + \sum_{m=1}^{\infty} a_m \cos 2\pi m f_r t \quad (55)$$

where for  $G(t) = 1$  throughout the channel allotment time,

$$a_m = 2f_r \int_{-1/2Nf_r}^{1/2Nf_r} \cos 2\pi m f_r t \, dt = \frac{2 \sin \frac{m\pi}{N}}{m\pi} \quad (56)$$

Each harmonic of  $G(t)$  beats with the noise spectrum on either side to produce audio components which sum up to total mean square audio noise:

$$W_n = \frac{1}{4} \int_0^{f_r/2} \left[ a_0^2 w_n(f) + \sum_{m=1}^{2N} a_m^2 w_n(mf_r + f) + \sum_{m=1}^{2N} a_m^2 w_n(mf_r - f) \right] df \quad (57)$$

The summations stop at  $2N$  because the baseband filter cuts off at  $f = F_b = 2Nf_r$ . The contribution of the  $a_0$  term is negligible. Then

$$\begin{aligned} W_n &= \frac{P_n}{\pi^2 W_c} \sum_{m=1}^{2N} \frac{\sin^2 \frac{m\pi}{N}}{m^2} \int_0^{f_r/2} [(mf_r + f)^2 + (mf_r - f)^2] df \\ &= \frac{P_n f_r^3}{\pi^2 W_c} \sum_{m=1}^{2N} \left( 1 + \frac{1}{12m^2} \right) \sin^2 \frac{m\pi}{N}. \end{aligned} \quad (58)$$

When  $N$  is large, the sum approaches

$$W_n \cong \frac{NP_n f_r^3}{\pi^2 W_c} \quad (59)$$

and

$$(S/N)^2 = \frac{\pi^2 W_c}{32N^3 P_n f_r} \left( \frac{\beta}{f_r} \right)^2 \quad (60)$$

$$S/N = \frac{\pi}{4} \left( \frac{B}{Nf_r} - 4 \right) \sqrt{\frac{kB}{2Nf_r}} \quad (61)$$

on substituting  $W_c = kP_n B$ ,  $\beta = B - 2F_b$ , and  $F_b = 2Nf_r$ . Equation (61) with  $k = 16$  was used to obtain the marginal power curve of Fig. 13. The result may be compared with that given by Rauch<sup>48</sup> (See also Landon<sup>4</sup>) for a rectangular pulse and rectangular gate, which requires a higher value for  $F_b$ . The two systems give the same signal-to-noise ratio when the rectangular pulse and gate of Rauch's system endure for one half of the total channel allotment time. The value of  $F_b$  necessary for such a case was estimated by Rauch to be  $3.5Nf_r$ . A calculation made as above, except that the gate was assumed sinusoidal instead of rectangular, showed very nearly the same signal-to-noise ratio.

The case of CW interference with all channels idle is represented by the r.f. wave:

$$V(t) = P \cos \left( 2\pi f_1 t + \frac{\beta}{2F_b} \sin \pi F_b t \right) + Q \cos 2\pi f_2 t. \quad (62)$$

When  $Q/P$  is small, the detected frequency is

$$\begin{aligned} f &= f_1 + \frac{\beta}{4} \cos \pi F_b t - \frac{Q}{2\pi P} \frac{d}{dt} \sin \left[ 2\pi(f_1 - f_2)t + \frac{\beta}{2F_b} \sin \pi F_b t \right] \\ &= f_1 + \frac{\beta}{4} \cos \pi F_b t - \delta(t). \end{aligned} \quad (63)$$

By Fourier series expansion followed by differentiation, the error  $\delta(t)$  may be written as:

$$\delta(t) = \frac{Q}{P} \sum_{m=-\infty}^{\infty} \left( f_1 - f_2 + \frac{mF_b}{2} \right) J_m(x) \cos 2\pi \left( f_1 - f_2 + \frac{mF_b}{2} \right) t, \quad (64)$$

where  $x = \beta/2F_b$ . The baseband filter passes only those components of  $\delta(t)$  which have frequencies in the range  $-F_b$  to  $F_b$ . Writing  $c = (f_1 - f_2)F_b$ , we find:

$$\delta_0(t) = \frac{QF_b}{P} \sum_{m=m_1}^{m_2} \left( c + \frac{m}{2} \right) J_m(x) \cos 2\pi F_b \left( c + \frac{m}{2} \right) t \quad (65)$$

where  $m_2$  is the largest integer which does not exceed  $2(1 - c)$  and  $m_1$  is the smallest integer which is not exceeded by  $-2(1 + c)$ . The term integer is here understood to include zero and both positive and negative integers. The wave  $\delta_0(t)$  is next multiplied by the gating function  $G(t)$  and the components falling in the audio band  $-f_r/2$  to  $f_r/2$  selected. We find:

$$G(t)\delta_0(t) = \frac{F_b Q}{2P} \sum_{m=m_1}^{m_2} \sum_{n=-\infty}^{\infty} a_n \left( c + \frac{m}{2} \right) J_m(x) \cos 2\pi[(2c + m)N + n]f_r t \quad (66)$$

with  $a_n = a_{-n}$ .

<sup>4</sup> Loc. cit.

<sup>48</sup> L. L. Rauch, Fluctuation Noise in Pulse-Height Multiplex Radio Links, Proc. I.R.E., Vol. 35, Nov. 1947, pp. 1192-1197.

For each value of  $m$ , there is only one value of  $n$  satisfying the audio filter inequality, which may be written:

$$-\frac{1}{2} - (2c + m)N < n < \frac{1}{2} - (2c + m)N \quad (67)$$

Hence interference accepted by the channel filter is:

$$I(t) = \frac{F_b Q}{2P} \sum_{m=m_1}^{m_2} a_n \left( c + \frac{m}{2} \right) J_m(x) \cos 2\pi[(2c + m)N + n]f_r t \quad (68)$$

The mean square value of interference is

$$I^2(t) = \frac{F_b^2 Q^2}{8P^2} \sum_{m=m_1}^{m_2} a_n^2 \left( c + \frac{m}{2} \right)^2 J_m^2(x). \quad (69)$$

The signal-to-interference ratio is

$$(S/I)^2 = \frac{G_0^2 \beta}{32} [I^2(t)]^{-1} \quad (70)$$

or

$$S/I = \frac{G_0 \beta P}{2F_b Q} \left[ \sum_{m=m_1}^{m_2} a_n^2 \left( c + \frac{m}{2} \right)^2 J_m^2(x) \right]^{-1/2}. \quad (71)$$

When a rectangular gate of duration equal to the full channel allotment is used, we substitute  $a_n = 2(\sin n\pi/N)/n\pi$ . We then find that the largest values of mean square interference occur when  $c$  is an odd multiple of one fourth. If we set

$$c = -(2r + 1)/4, r = 0, \pm 1, \pm 2, \dots \quad (72)$$

it follows that if  $N$  is an even integer,

$$n = (r + \frac{1}{2} - m)N, \quad (73)$$

$$\sin \frac{n\pi}{N} = \sin (r + \frac{1}{2} - m)\pi, \quad (74)$$

$$\left| \sin \frac{n\pi}{N} \right| = 1. \quad (75)$$

Substituting these values in the expression for  $S/I$ , we find

$$S/I = \frac{\pi \beta P}{2F_b Q} \left[ \sum_{m=r-1}^{r+2} J_m^2(x) \right]^{-1/2}. \quad (76)$$

The value of  $r$  is to be chosen as the integer which makes  $S/I$  a minimum; i.e., we place the CW frequency at that part of the band where it does the most damage. The curve marked CW(Gate) of Fig. 14 was obtained in this way.

When instantaneous sampling is used instead of a gate, the value of  $a_n$  becomes a constant for all values of  $n$  of interest and is equal to  $a_0$ . We then find:

$$S/I = \frac{\beta P}{2F_b Q} \left[ \sum_{m \geq -2(1+c)}^{\leq 2(1-c)} \left( c + \frac{m}{2} \right)^2 J_m^2(x) \right]^{-1/2}. \quad (77)$$

Here  $c$  is to be selected to make  $S/I$  minimum for each value of  $x$ . The poorest values of  $S/I$  occur when Bessel functions of comparable order and argument appear in the summation, which means that  $c$  is in the neighborhood of  $-x/2$ . The corresponding difference between the CW and mid-carrier frequencies is one-fourth the peak-to-peak swing.

To calculate the interference between two similar idle systems, we set

$$V(t) = P \cos \left( 2\pi f_1 t + \frac{\beta}{2F_b} \sin \pi F_b t \right) + Q \cos \left[ 2\pi f_2 t + \frac{\beta}{2F_b} \sin (\pi F_b t - \theta) \right]. \quad (78)$$

The frequency error registered in the first system is then

$$\begin{aligned} \delta(t) &= \frac{Q}{2\pi P} \frac{d}{dt} \sin [2\pi(f_1 - f_2)t + x \sin \pi F_b t - x \sin (\pi F_b t - \theta)] \\ &= \frac{Q}{2\pi P} \frac{d}{dt} \sin \left[ 2\pi(f_1 - f_2)t + 2x \sin \frac{\theta}{2} \cos \left( \pi F_b t - \frac{\theta}{2} \right) \right] \\ &= \frac{Q}{P} \sum_{m=-\infty}^{\infty} \left( f_1 - f_2 + \frac{mF_b}{2} \right) J_m \left( 2x \sin \frac{\theta}{2} \right) \\ &\quad \cdot \cos \left[ 2\pi \left( f_1 - f_2 + \frac{mF_b}{2} \right) t - \frac{m\theta}{2} \right]. \end{aligned} \quad (79)$$

It follows that the response of the baseband filter is

$$\delta_0(t) = \frac{QF_b}{P} \sum_{m=m_1}^{m_2} \left( c + \frac{m}{2} \right) J_m \left( 2x \sin \frac{\theta}{2} \right) \cos \left[ 2\pi F_b \left( c + \frac{m}{2} \right) t - m \frac{\theta}{2} \right]. \quad (80)$$

The effects of the channel gate and filter are computed in the same way as for CW, giving the audio interference:

$$\begin{aligned} I(t) &= \frac{F_b Q}{2P} \sum_{m=m_1}^{m_2} a_n \left( c + \frac{m}{2} \right) J_m \left( 2x \sin \frac{\theta}{2} \right) \\ &\quad \cdot \cos \left( 2\pi[(2c + m)N + n]f_r t - m \frac{\theta}{2} \right) \end{aligned} \quad (81)$$

Since the two systems occupy the same frequency assignment, we assume that  $c$  is not greatly different from zero. Then for fixed  $\theta$ :

$$\overline{I^2(l)} = \frac{F_b^2 Q^2}{32P^2} \sum_{m=m_1}^{m_2} m^2 a_n^2 J_m^2 \left( 2x \sin \frac{\theta}{2} \right) \quad (82)$$

Since  $\theta$ , the frame phase difference, is a random angle we average over its possible values by setting:

$$\begin{aligned} A_m(x) &= \frac{1}{2\pi} \int_0^{2\pi} J_m^2 \left( 2x \sin \frac{\theta}{2} \right) d\theta = \frac{1}{\pi} \int_0^\pi J_m^2(2x \sin \phi) d\phi \\ &= \frac{\Gamma^2(m + \frac{1}{2})(2x)^{2m}}{\pi(2m)!(m!)^2} \\ &\quad \cdot {}_2F_3(m + \frac{1}{2}, m + \frac{1}{2}; 2m + 1, m + 1, m + 1; -4x^2), \\ &\quad m \geq 0 \end{aligned} \quad (83)$$

$$A_{-m}(x) = A_m(x)$$

Noting further that for  $c = 0$ ,  $m_1 = -2$ ,  $m_2 = 2$ , and  $n = -mN$ , we have then:

$$I^2(l) = \frac{F_b^2 Q^2}{16P^2} [a_N^2 A_1(x) + 4a_{2N}^2 A_2(x)] \quad (84)$$

and

$$S/I = \frac{G_0 \beta P}{F_b Q \sqrt{2}} [a_N^2 A_1(x) + 4a_{2N}^2 A_2(x)]^{-1/2}. \quad (85)$$

For a sinusoidal pulse and rectangular gate of full channel allotment time in duration,  $a_N = a_{2N} = 0$ ,  $I^2(l) = 0$ , and  $S/I$  is infinite. If instantaneous sampling is used,

$$G_0 = a_N = a_{2N} \quad (86)$$

and

$$S/I = \frac{\beta P}{\sqrt{2} F_b Q} [A_1(x) + 4A_2(x)]^{-1/2} \quad (87)$$

The curve for similar system interference with instantaneous sampling, Fig. 14, was calculated from Eq. (87).

For small values of  $x$ , we may use the ascending power series:

$$A_1(x) = \frac{x^2}{2} \left[ 1 - \frac{3^2}{3 \cdot 2^2 \cdot 1!} x^2 + \frac{3^2 \cdot 5^2}{3 \cdot 4 \cdot 2^2 \cdot 3^2 \cdot 2!} x^4 - \dots \right] \quad (88)$$

$$A_2(x) = \frac{3x^4}{32} \left[ 1 - \frac{5^2}{5 \cdot 3^2 \cdot 1!} x^2 + \frac{5^2 \cdot 7^2}{5 \cdot 6 \cdot 3^2 \cdot 4^2 \cdot 2!} x^4 - \dots \right] \quad (89)$$

For large values of  $x$ , the following asymptotic formula has been derived by Mr. S. O. Rice by use of the Mellin-Barnes contour integral representation and the method of steepest descents:

$$\pi^2 x A_m(x) \sim \ln x + \ln 32 + \gamma - 2 \left( 1 + \frac{1}{3} + \frac{1}{5} + \cdots + \frac{1}{2m-1} \right) \\ - (-)^m \frac{\pi^2}{4} \sqrt{\frac{\pi}{2x}} \cos \left( 4x + \frac{\pi}{4} \right) + \cdots \quad (90)$$

$\gamma = \text{Euler's constant} = 0.5772 \dots$

As  $x$  approaches zero,  $S/I$  approaches  $2P/Q$ , which is to be expected because the frequency deviation of the unwanted carrier is represented by a pair of first order sidebands  $P/Q$  times as great as those on the wanted carrier. Averaging over the random carrier phase difference brings in a factor  $\sqrt{2}$ , and averaging over all frame phases accounts for another.

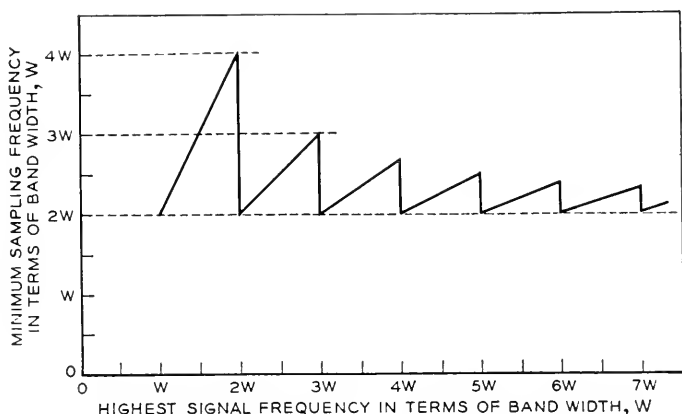


Fig. 37—Minimum sampling frequency for band of width  $W$ .

## APPENDIX V

### SAMPLING A BAND OF FREQUENCIES DISPLACED FROM ZERO

It is often necessary to transmit a signal band which does not extend all the way down to zero frequency. For example, a group of channels in FDM may be based on a set of carrier frequencies remote from zero. When we consider the application of pulse methods to transmit such a signal, the question of what sampling rate is needed immediately arises. A band extending from  $f_1$  to  $f_1 + W$  could of course be translated to the range 0 to  $W$  by standard modulation techniques, sampled at a rate  $2W$ , and restored to the original range by an inverse translation at the receiver. The frequency shifting apparatus required includes modulators, carrier generators, band separating filters, and possibly amplifiers to make up the inevitable losses.



A direct sampling process which avoids shifting the band may therefore be preferred. A useful theorem for uniformly spaced samples is that the minimum sampling frequency is not in general twice the highest frequency in the band but is given by the formula:

$$f_r = 2W \left( 1 + \frac{k}{m} \right), \quad (1)$$

where:

$f_r$  = minimum sampling frequency

$W$  = width of band

$f_2$  = highest frequency in band

$m$  = largest integer not exceeding  $f_2/W$

$$k = \frac{f_2}{W} - m$$

The value of  $k$  in (1) varies between zero and unity. When the band is located between adjacent multiples of  $W$ , we have  $k = 0$  and it follows that  $f_r = 2W$  no matter how high the frequency range of the signal may be. As  $k$  increases from zero to unity the sampling rate increases from  $2W$  to  $2W \left( 1 + \frac{1}{m} \right)$ . The curve of minimum sampling rate versus the highest frequency in a band of constant width thus becomes a series of sawteeth of successively decreasing height as shown in Fig. 37. The highest sampling rate is required when  $m = 1$  and  $k$  approaches unity. This is the case of a signal band lying between  $W - \Delta f$  and  $2W - \Delta f$  with  $\Delta f$  small. The sampling rate needed is  $2(2W - \Delta f)$  which approaches the value  $4W$  as  $\Delta f$  approaches zero. Actually when  $\Delta f = 0$ , we change to the case of  $m = 2$ ,  $k = 0$ , and  $f_r = 2W$ . The next maximum on the curve is  $3W$ , which is approached when  $f_2$  nears  $3W$ . The successive maxima decrease toward the limit  $2W$  as  $f_2$  increases. The sampling theorem contained in Eq. (1) may be verified from steady state modulation theory by noting that the first order sidebands on harmonics of  $2W$  do not overlap the signal when the equation is satisfied.

## Abstracts of Technical Articles by Bell System Authors

*The Transistor—A New Semiconductor Amplifier.*<sup>1</sup> J. A. BECKER and J. N. SHRIVE. This article describes the construction, characteristics, and behavior of the newly discovered device, the transistor. Used as a semiconductor amplifier, it works on an entirely different principle and is capable of performing the same tasks now done by the vacuum tube triode.

*A Review of Magnetic Materials.*<sup>2</sup> R. A. CIEGWIDEN. Significant advances have been made within recent years in the development of new and better magnetic materials, and in the theories of magnetism. High permeability materials that may be classed as non-conductors, materials with greatly improved initial permeabilities, and permanent magnet alloys capable of storing four or five times as much energy as those obtainable ten years ago are now available. Descriptions of some of these developments are given. The paper gives compilations of data and curve sheets showing some of the typical characteristics of many of these materials.

*Ratio of Frequency Swing to Phase Swing in Phase- and Frequency-Modulation Systems Transmitting Speech.*<sup>3</sup> D. K. GANNETT and W. R. YOUNG. Computed and measured data are presented bearing on the relation between the phase and the frequency swing in phase- and frequency-modulation systems when transmitting speech. The results were found to vary with different voices, with the microphone and circuit characteristics, and with the kind of volume regulation used. With a particular carbon microphone, it was found that a phase deviation of 10 radians corresponds to a frequency deviation of between 11 and 15 kc in a phase-modulation system, and between 6 and 12 kc in a frequency-modulation system, depending on conditions.

*Design and Performance of Ethylene Diamine Tartrate Crystal Units.*<sup>4</sup> J. P. GRIFFIN and E. S. PENNELL. A research program on synthetic crystals has resulted in the development and adoption of EDT for carrier telephone filters. Some unusual physical properties of the crystalline material give rise to novelty in the processing methods and mechanical design of the units. These properties include anisotropic expansion coefficients, fragility, natural cleavages and water solubility. The electrical properties of EDT result in filters with wider pass bands and lower impedance levels than commercially obtainable with quartz.

<sup>1</sup> *Electrical Engineering*, v. 68, pp. 215-221, March 1949.

<sup>2</sup> *Metal Progress*, November 1948.

<sup>3</sup> *Proc. I. R. E.*, v. 37, pp. 258-263, March 1949.

<sup>4</sup> *A. I. E. E. Transactions*, v. 67, pt. 1, pp. 557-561, 1948.

*Recent Improvements in Loading Apparatus for Telephone Cables.*<sup>5</sup> S. G. HALE, A. L. QUINLAN, and J. E. RANGES. Through the use of improved materials, manufacturing techniques, and designs, a series of exchange-area loading coils has been provided which is equivalent electrically to the superseded types but requires one-third less copper and has considerably smaller overall dimensions. Similarly, 3-coil toll cable loading units have been provided with a saving of one-half in both copper and core material, with a small sacrifice in electrical behavior as compared with superseded types. The reduced size of the new coils and units, together with improved assembly arrangements, made possible a 65 per cent saving in the volume and weight of the cases housing them.

*The Coaxial Transistor.*<sup>6</sup> WINSTON E. KOCK and R. L. WALLACE, JR. The success of the earlier types of transistors led to the exploration of other forms of similar amplifiers, one of which is the coaxial transistor. A description of its construction, characteristics, and many advantages is contained in this article.

*Paralleled-Resonator Filters.*<sup>7</sup> J. R. PIERCE. This paper describes a class of microwave filters in which input and output waveguides are connected by a number of resonators, each coupled directly to both guides. Signal components of different frequencies can pass from the input to the output largely through different resonators. This type of filter is a realization of a lattice network. An experimental filter is described.

*A Broad-Band Microwave Relay System between New York and Boston.*<sup>8</sup> G. N. THAYER, A. A. ROETKEN, R. W. FRIIS, and A. L. DURKEE. This paper describes the principal features of a broad-band microwave relay system which has recently been installed between New York and Boston. The system operates at frequencies around 4,000 Mc and provides two two-way channels, each accommodating a signal-frequency band extending from 30 cps to 4.5 Mc. Noise and distortion characteristics are satisfactory for the transmission of several hundred simultaneous telephone conversations or a standard black-and-white television program.

*Growing Crystals of Ethylene Diamine Tartrate.*<sup>9</sup> A. C. WALKER and G. T. KOHMAN. The need for a synthetic piezoelectric crystal to relieve the critical quartz supply situation has resulted in the development by the Bell Telephone Laboratories of a new organic salt crystal, ethylene diamine tartrate, which is being used in place of quartz in telephone circuits.

This crystal is grown from a supersaturated aqueous solution of its salt by an entirely new method known as the constant temperature process. It

<sup>5</sup> *A. I. E. E. Transactions*, v. 67, pt. 1, pp. 385-392, 1948.

<sup>6</sup> *Electrical Engineering*, v. 68, pp. 222-223, March 1949.

<sup>7</sup> *Proc. I. R. E.*, v. 37, pp. 152-155, February 1949.

<sup>8</sup> *Proc. I. R. E.—Waves and Electrons Section*, v. 37, pp. 183-188, February 1949.

<sup>9</sup> *A. I. E. E. Transactions*, v. 67, pt. 1, pp. 565-570, 1948.

differs from previous methods used for growing large single crystals from solution, in that the solution saturated at one temperature is continuously fed into a crystallizer tank maintained at a slightly lower temperature, thus providing the supersaturation condition necessary for crystal growth. Further, the solution is circulated in such a manner that the partially impoverished mother liquor overflows from the growing tank back into the saturator where it is refortified and filtered. It is then heated and returned to the growing tank in such a way as to avoid the formation of undesirable crystal nuclei.

The paper contains a description of the new method which is now in commercial operation, together with a general discussion of some of the important principles involved in the successful growth of large single crystals of water soluble salts.

*Crystal Filters Using Ethylene Diamine Tartrate in Place of Quartz.*<sup>10</sup> E. S. WILLIS. Ethylene diamine tartrate (EDT) crystal filters were developed to replace the earlier quartz type channel filters in the broad-band carrier telephone systems, because of the threatened scarcity of quartz. These new filters give performance comparable to that of the earlier design. The growth of the EDT crystals from seeds and their fabrication into crystal units for use in filters are covered in companion papers on "Design and Performance of Ethylene Diamine Tartrate Crystal Units" and "Growing Crystals of Ethylene Diamine Tartrate" in this same volume of the *Transactions*

<sup>10</sup> *A. I. E. E. Transactions*, v. 67, pt. 1, pp. 552-556, 1948

## Contributors to This Issue

JOHN BARDEEN, University of Wisconsin, B.S. in E.E., 1928; M.S., 1930. Gulf Research and Development Corporation, 1930-33; Princeton University, 1933-35, Ph.D. in Math. Phys., 1936; Junior Fellow, Society of Fellows, Harvard University, 1935-38; Assistant Professor of Physics, University of Minnesota, 1938-41; Prin. Phys., Naval Ordnance Laboratory, 1941-45. Bell Telephone Laboratories, 1945-. Dr. Bardeen is engaged in theoretical problems related to semiconductors.

W. R. BENNETT, B.S., Oregon State College, 1925; A.M., Columbia University, 1928. Bell Telephone Laboratories, 1925-. Mr. Bennett has been active in the design and testing of multichannel communication systems, particularly with regard to modulation processes and the effects of nonlinear distortion. He is now engaged in research on various transmission problems.

C. B. FELDMAN, University of Minnesota, B.S. in Electrical Engineering, 1926; M.S., 1928. Bell Telephone Laboratories, 1928-. As Transmission Research Engineer, Mr. Feldman has charge of a group studying new transmission methods. He is a Fellow of the Institute of Radio Engineers.

J. R. HAYNES, B.S. in Physics, University of Kentucky, 1930. Bell Telephone Laboratories, 1930-. Mr. Haynes is in the Physical Research Department, engaged in solid state studies.

CONYERS HERRING, A.B., University of Kansas, 1933; Ph.D., Princeton University, 1937; National Research Fellow, Massachusetts Institute of Technology, 1937-39; Instructor in Mathematics and Research Associate in Mathematical Physics, Princeton University, 1939-40; Instructor in Physics, University of Missouri, 1940-41; Columbia University Division of War Research, 1941-45; Professor of Applied Mathematics, University of Texas, 1946. Bell Telephone Laboratories, 1945-. Dr. Herring has been engaged in theoretical problems in the fields of solid state physics and electron emission.

R. J. KIRCHER, B.S. in E.E., California Institute of Technology, 1929; M.S., Stevens Institute of Technology, 1941. Bell Telephone Laboratories,

1929-. Mr. Kircher was engaged in radar and counter measures projects during the war. Electronic Apparatus Development Department since 1944. Transistor Development Group since 1948.

G. L. PEARSON, A.B., Willamette University, 1926; M.A. in Physics, Stanford University, 1929. Bell Telephone Laboratories, 1929-. Mr. Pearson is in the Physical Research Department where he has been engaged in the study of noise in electric circuits and the properties of electronic semi-conductors.

ROBERT M. RYDER, Yale University, B.S. in Physics, 1937; Ph.D., 1940. Bell Telephone Laboratories, 1940-. Dr. Ryder joined the Laboratories to work on microwave amplifier circuits, and during most of the war was a member of a group engaged in studying the signal-to-noise performance of radars. In 1945 he transferred to the Electronic Development Department to work on microwave oscillator and amplifier tubes for radar and radio relay applications. He is now in a group engaged in the development of transistors.

W. SHOCKLEY, B.Sc., California Institute of Technology, 1932; Ph.D., Massachusetts Institute of Technology, 1936. Bell Telephone Laboratories, 1936-. Dr. Shockley's work in the Laboratories has been concerned with problems in solid state physics.

# THE BELL SYSTEM TECHNICAL JOURNAL

DEVOTED TO THE SCIENTIFIC AND ENGINEERING ASPECTS  
OF ELECTRICAL COMMUNICATION

Reactance Tube Modulation of Phase Shift Oscillators  
*F. R. Dennis and E. P. Felch* 601

A Broad-Band Microwave Noise Source  
*W. W. Mumford* 608

Electronic Admittances of Parallel-Plane Electron Tubes  
at 4000 Megacycles..... *Sloan D. Robertson* 619

Passive Four-Pole Admittances of Microwave Triodes  
*Sloan D. Robertson* 647

Communication Theory of Secrecy Systems  
*C. E. Shannon* 656

The Design of Reactive Equalizers..... *A. P. Brogle, Jr.* 716

Abstracts of Technical Articles by Bell System Authors... 751

Contributors to this Issue..... 753

AMERICAN TELEPHONE AND TELEGRAPH COMPANY  
NEW YORK

# THE BELL SYSTEM TECHNICAL JOURNAL

*Published quarterly by the  
American Telephone and Telegraph Company  
195 Broadway, New York, N. Y.*



## EDITORS

R. W. King

J. O. Perrine

## EDITORIAL BOARD

C. F. Craig

O. E. Buckley

H. S. Osborne

M. J. Kelly

J. J. Pilliod

A. B. Clark

F. J. Feely



## SUBSCRIPTIONS

Subscriptions are accepted at \$1.50 per year. Single copies are 50 cents each.  
The foreign postage is 35 cents per year or 9 cents per copy.



Copyright, 1949  
American Telephone and Telegraph Company

PRINTED IN U. S. A.



# The Bell System Technical Journal

Vol. XXVIII

October, 1949

No. 4

---

## Reactance Tube Modulation of Phase Shift Oscillators

By F. R. DENNIS and E. P. FELCH

This paper describes a basic circuit for reactance tube modulation of phase shift oscillators. The design of suitable phase shift oscillators for frequencies from audio through the ultra-high frequencies is discussed. Experimental performance data derived from several types of frequency modulated phase shift oscillators are presented.

### INTRODUCTION

**F**REQUENCY modulation of oscillators is finding wide-spread use in such diverse fields as FM broadcasting, telemetering systems for guided missiles and measuring apparatus for observing transmission frequency characteristics on cathode ray tubes. Design objectives for such oscillators may be listed briefly as:

1. A wide range of frequency modulation or, alternatively, high modulation sensitivity.
2. A linear relationship between instantaneous values of modulation input voltage and frequency deviation.
3. Freedom from accompanying amplitude modulation.
4. Inherent center frequency stability.
5. Ease and stability of adjustment.
6. A minimum number of components, none of which should be critical.
7. Modulation by dc, audio, or video inputs.
8. Operation anywhere in the frequency spectrum from low audio frequencies through the ultra-high frequency region.

The circuits described in this paper were developed in the course of an investigation of various frequency modulation circuits for use in visual transmission measuring systems. The oscillators had to be capable of linear modulation at 60 cycles over a  $\pm 3$  megacycle band at 25 megacycles and over a  $\pm 9$  megacycle band at 80 megacycles. Existing designs fell short of meeting the requirements with respect to several of the characteristics listed above. The reactance tube modulated phase shift oscillator circuit was found to perform satisfactorily in the transmission set and proved superior in many respects to all the other circuits tried. Tests of the circuit at other frequencies disclosed that the advantages were not peculiar to the frequency range and the following description is presented with the expectation that it may prove useful to others.

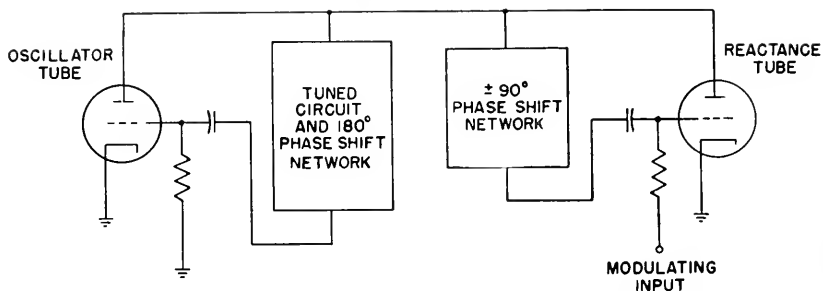


Fig. 1—Simplified schematic of conventional reactance tube modulated oscillator.

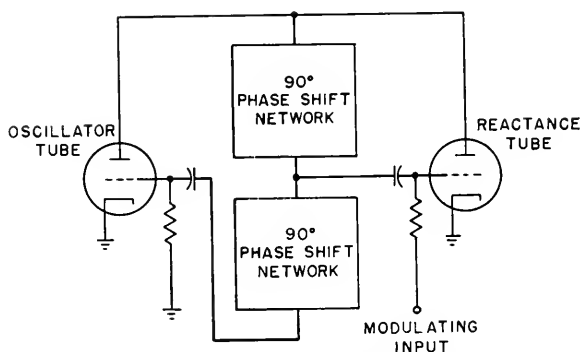
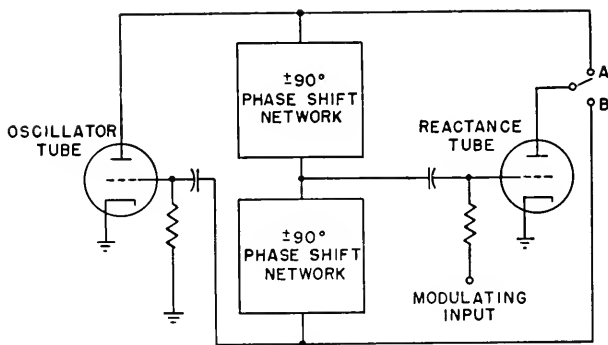


Fig. 2—Simplified schematic of phase shift reactance tube modulated oscillator.



TUBE CONNECTION	A		B	
NETWORKS	LEADING (+90°)	LAGGING (-90°)	LEADING (+90°)	LAGGING (-90°)
OSCILLATION FREQ.	DECREASES	INCREASES	DECREASES	INCREASES

Fig. 3—Direction of frequency deviation for increasing  $G_M$  of reactance tube.



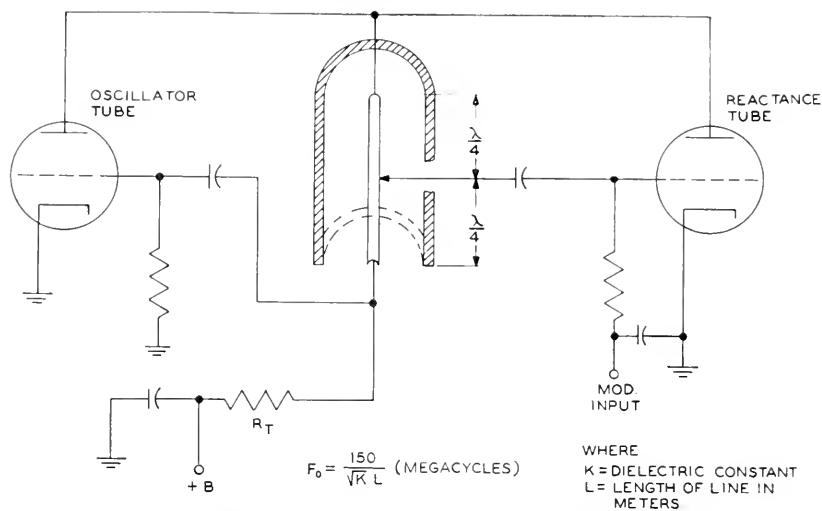


Fig. 6—Transmission line reactance tube modulated oscillator.

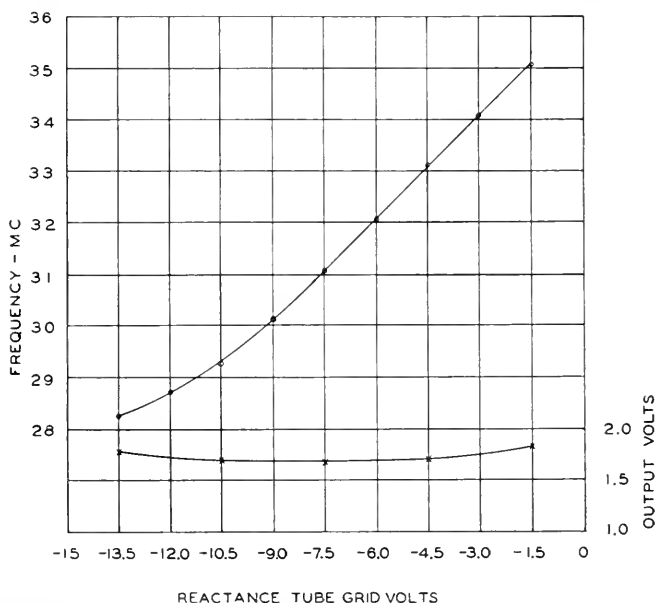


Fig. 7 Performance curves of typical LC reactance tube modulated phase shift oscillator.

simplified form is shown in Fig. 1. The input and output of a vacuum tube amplifier are connected together by a tuned circuit and feedback network which introduces  $180^\circ$  phase shift at the undeviated frequency  $F_0$ .

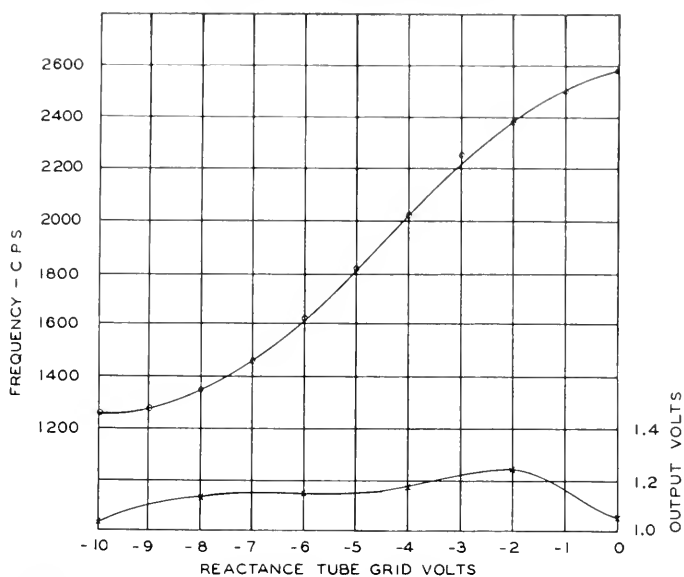


Fig. 8—Performance curves of typical RC reactance tube modulated phase shift oscillator.

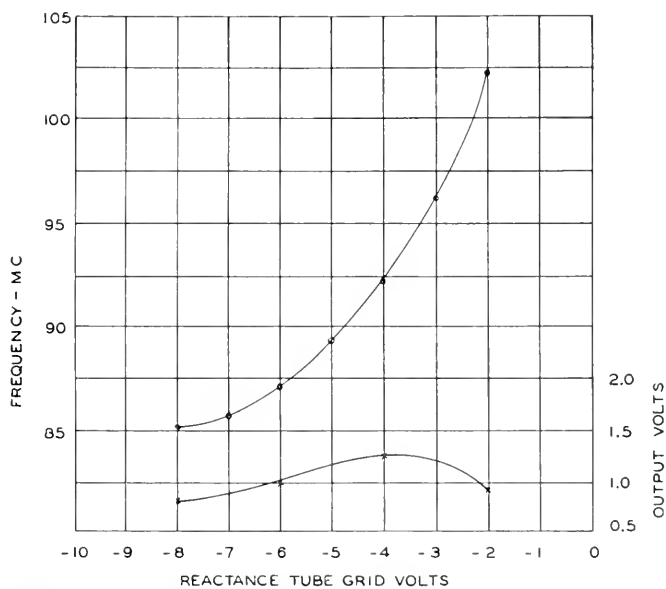


Fig. 9—Performance curves of typical transmission line reactance tube modulated oscillator.

An auxiliary path contains the reactance tube fed from a  $90^\circ$  phase shift network connected as shown. The direction of frequency deviation is determined by the sign of the  $90^\circ$  phase shift. The amount of the deviation is

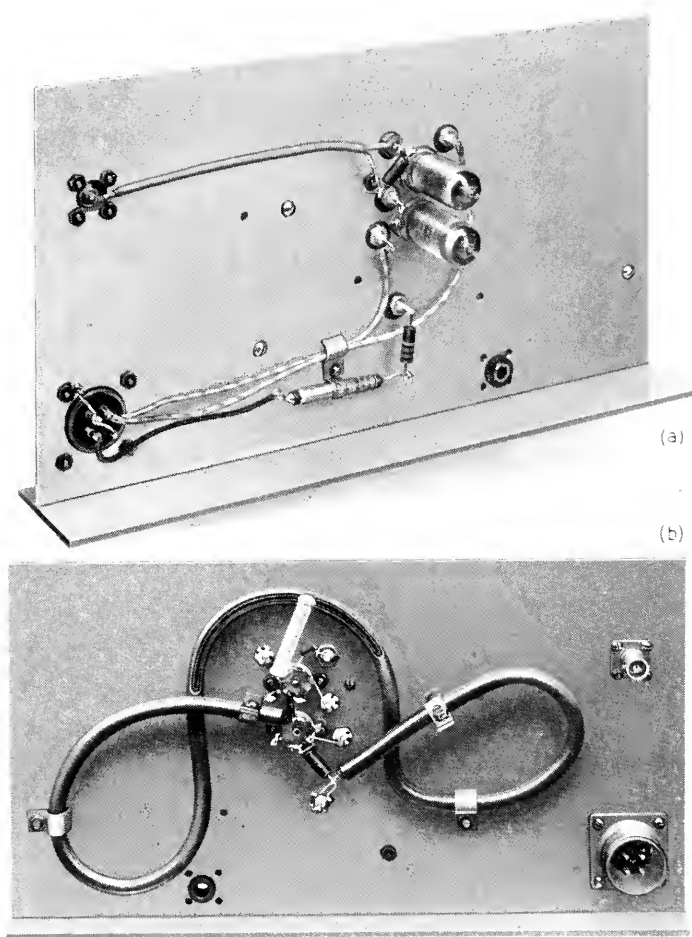


Fig. 10—Construction of transmission line reactance tube modulated oscillator.  
(a) Tube side. (b) Line side.

determined by the transconductance variation of the reactance tube, by the impedance across which the reactance tube is connected and by the loss in the  $90^\circ$  phase shift network. The linearity is a function of all of these factors. In general the frequency deviation may be increased by increasing

the  $L/C$  ratio in the oscillator tuned circuit, but only at the expense of frequency stability.

A simplified schematic of the reactance tube modulated phase shift oscillator is shown in Fig. 2. The mathematical theory of operation is analogous to that of the conventional reactance tube modulated oscillator, and the same methods of analysis may be applied. The  $90^\circ$  phase shift network required in the reactance tube grid circuit is a portion of the feedback network and provides half of the  $180^\circ$  phase shift required for oscillation. In this circuit the reactance tube is tightly coupled into the oscillating circuit with minimum loss in the  $90^\circ$  phase shift network. Hence small values of  $L/C$  ratio may be employed with a consequent increase in the inherent frequency stability. In practice, oscillators comparable in stability to good nonmodulated oscillators may be realized. The direction of deviation is determined by whether the phase of the reactance tube grid voltage leads or lags the reactance tube plate current. The permutations of connections and signs of the  $90^\circ$  phase shift networks are shown on Fig. 3 with the corresponding directions of frequency deviation.

The phase shift networks need not be of the LC lumped constant variety. For example, RC networks or sections of transmission line may be employed to particular advantage at the lower and higher frequencies respectively. A few of the many possible circuit configurations are shown in Figs. 4, 5, 6.

#### EXPERIMENTAL DATA

Frequency deviation and output variation curves for some typical oscillators are shown in Figs. 7, 8, and 9.

The oscillator of Fig. 9 which was built by Mr. D. Leed, is shown in Fig. 10. The transmission line is a section of RG59U cable with the shield removed, encased in a copper tube with a slot for bringing out the center tap of the line to the reactance tube grid. The tubes are 6J6's with both sections connected in parallel.

#### CONCLUSION

Frequency modulated phase shift oscillators of several types have been described. These offer interesting possibilities for applications over a wide range of frequencies wherever stable, simple frequency modulated oscillators are required. With respect to range, linearity, and freedom from amplitude modulation their performance, as shown, is superior to that of conventional circuits and is at least equal to that of the complex circuits employed in the most critical applications.

## A Broad-Band Microwave Noise Source

By W. W. MUMFORD

Measurements of the microwave noise power available from gaseous discharges, such as in an ordinary fluorescent lamp, show remarkable uniformity and stability. Such tubes are therefore suitable for a new type of standard noise source.

### INTRODUCTION

A STANDARD noise source, such as a hot resistance or a temperature limited diode, has been used advantageously for making measurements of the noise figure of radio receivers in the short-wave and the ultra-short wave region. The use of such a tool eliminates the possible errors which are practically inescapable when using the large amounts of attenuation which are needed for the determination of the ratio of power levels encountered in measuring noise figures with a standard signal generator. For example, the power from a standard signal generator might be measurable and known accurately at a level of 40 db below a watt, whereas the noise power available from a resistance might be 141 db below one watt.<sup>1</sup> It is difficult to ascertain accurately power ratios of this magnitude,  $10^{10}$ .

Another advantage of using a standard noise source arises from the fact that ordinarily the bandwidth of the receiver need not be considered, thereby eliminating a time consuming measurement. This assumes, of course, that the bandwidth of the noise source is much greater than that of the amplifier under test.

In the microwave region it is possible to match a resistive element to the waveguide over a wide enough band, but ordinary resistive materials will not stand the high temperatures (5000 degrees or more) needed to measure the noise figures encountered in practice. The noise diode is capable of furnishing adequate noise power, but one with wide bandwidth has yet to be developed. A good, stable, broadband microwave noise generator is needed.

Another possible source of noise power consists of a gaseous discharge.<sup>2</sup> Before we examine the data which have led us to conclude that the gaseous discharge is a good, broad-band, stable microwave noise generator and possibly a calculable noise standard, we review our definitions of noise figure

<sup>1</sup> This figure, 141 db below one watt, assumes that the effective bandwidth is 2 mc. The resistance noise power available from a generator at 290° Kelvin is 204 db below one watt per cycle.

<sup>2</sup> G. C. Southworth, *Journal of the Franklin Institute*, Vol. 239, # 14, pp. 285-298, April 1945.



and gain,<sup>3</sup> and discuss the factors involved in making noise figure measurements by means of a noise source.

### NOTES ON NOISE FIGURE

*Definition:* The NOISE FIGURE of a network, with a generator connected to its input terminals, is the ratio of the available signal-to-noise power ratio at the signal generator terminals (weighted by the network bandwidth) to the available signal-to-noise power ratio at its output terminals.

*Definition:* The GAIN of a network is the ratio of the available signal power at the output terminals of the network to the available signal power at the output terminals of the signal generator.

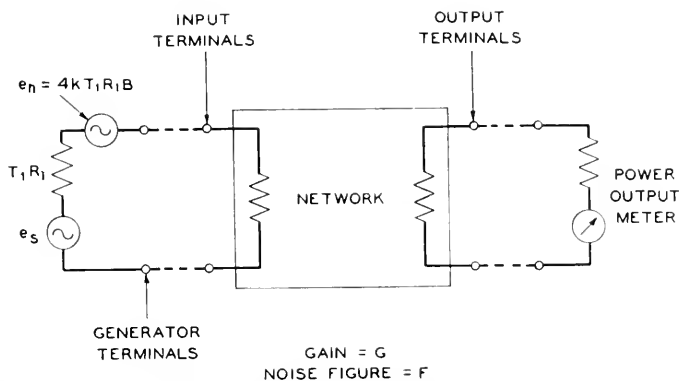


Fig. 1—Schematic diagram of generator, network and output power meter.

These definitions apply to a circuit consisting of a generator, a network and an output power meter as shown schematically in Fig. 1. The signal power available from the generator, having an open circuit voltage  $e$  and an internal resistance  $R_1$ , is:

$$P_{SA} = \frac{e^2}{4R_1} \quad (1)$$

The noise power available from the signal generator resistance,  $R_1$ , at absolute temperature  $T_1$ , is

$$P_{NA} = \frac{4KT_1 R_1 B}{4R_1} = kT_1 B \quad (2)$$

where  $B$  is the effective bandwidth of the network, by which the generator noise is weighted in this case.

<sup>3</sup> H. T. Friis, *Proc. I. R. E.*, Vol. 32, # 17, pp. 419-422, July, 1944.

The weighted available signal-to-noise ratio at the generator terminals is:

$$\frac{P_{SA}}{P_{NA}} = \frac{\frac{e^2}{4R_1}}{KT_1B} \quad (3)$$

The network amplifies (or attenuates) the generator's signal power by the factor  $G$ , the gain of the network, so that the available signal power at the output terminals of the network is:

$$P_{so} = G \frac{e^2}{4R_1} \quad (4)$$

The network amplifies (or attenuates) the generator noise power by the same factor  $G$ , and also delivers noise power which originates within itself,  $N_N$ , so that the total available noise power at the output terminals of the network is:

$$P_{No} = GkT_1B + N_N \quad (5)$$

The available signal-to-noise ratio at the output terminals of the network is then:

$$\frac{P_{so}}{P_{No}} = \frac{G \frac{e^2}{4R_1}}{GkT_1B + N_N} \quad (6)$$

We now express the noise figure of the network,  $F$ , which by definition is the ratio of equation (3) to equation (6), thus,

$$F = \frac{GkT_1B + N_N}{GkT_1B} \quad (7)$$

We should pause at this point to consider this equation further, for it leads us to a simpler definition of noise figure.

*Definition:* The noise figure of a network is the ratio of the noise power output of that network to the noise power output which would exist if the network were noiseless. The temperature of the signal generator resistance is 290 degrees Kelvin.

The choice of generator temperature of 290 degrees is an arbitrary one, which makes  $kT_1 = 4(10)^{-21}$  watts per cycle bandwidth;  $-10 \log kT_1 = 204$  db below one watt per cycle. Putting  $T_1 = 290$  in equation (7) gives:

$$F = \frac{Gk \ 290 \ B + N_N}{Gk \ 290 \ B} \quad (8)$$

Rearranging (8) we have:

$$N_N = (F - 1)Gk \ 290 \ B \quad (9)$$

Equation (9) will now be used to illustrate one method of measuring noise figures. In this method, the network output noise power is measured for two known values of the temperature of the generator resistance,  $T_2$  and  $T_1$ . When the generator is hot, the output noise power is, by equation (5):

$$P_{NOH} = GkT_2B + N_N \quad (10)$$

When the generator is cool, the output noise power is:

$$P_{NOC} = GkT_1B + N_N \quad (11)$$

Calling the ratio of these two noise powers  $F$ :

$$F = \frac{P_{NOH}}{P_{NOC}} = \frac{GkT_2B + N_N}{GkT_1B + N_N} \quad (12)$$

Substituting for  $N_N$  the value given in equation (9), we have for the noise figure:

$$F = \frac{\left(\frac{T_2}{290} - 1\right) - F\left(\frac{T_1}{290} - 1\right)}{F - 1} \quad (13)$$

In practice  $T_1$  is often near enough to 290 degrees so that the second term in the numerator of equation (13) is negligible. Setting  $T_1$  equal to 290 degrees, equation (13) becomes:

$$F = \frac{\frac{T_2}{290} - 1}{F - 1} \quad (14)$$

The determination of noise figure by this method is independent of the gain of the network, the degree of mismatch and the bandwidth, provided that the band of the noise source is broad compared with the overall RF band of the network and the output power meter.

#### THE NOISE SOURCE

The limitations at microwaves of a noise source such as a heated wire will now be discussed. In particular we are interested in measuring amplifiers which have noise figures between 10 and 100 (10 db to 20 db) and bandwidths up to 200 mc. If a hot wire could be matched to the impedance of a waveguide over a wide enough band, and raised to a temperature of  $10 \times 290$  degrees our  $F$  factor would be (rearranging eq. 14):

$$F = \frac{\frac{T_2}{290} - 1}{F} + 1 \quad (15)$$

and setting  $T_2 = 2900$  degrees Kelvin

$$Y = 1.9 \text{ for } F = 10$$

$$Y = 1.09 \text{ for } F = 100$$

Assuming that  $Y$  can be read to within  $\pm 1\%$  our accuracy in determining  $F$  would be within about  $\pm 1\%$  for  $F = 10$  but only within about  $\pm 10\%$  for  $F = 100$ . If the noise source had a temperature of  $40 \times 290$  degrees, our experimental errors would be reduced accordingly to about  $\pm 1/4\%$  for  $F = 10$  and  $\pm 2.5\%$  for  $F = 100$ . Since metal wires will not stand such temperatures, we must look to something different for the noise source if these accuracies are to be achieved.

In view of the foregoing considerations, the nonoscillating reflex klystron presented one possibility of a suitable microwave noise source. This, however, was not exploited because the bandwidth was not wide enough.

Another possibility was found to be an electrical gas discharge. This type of source was determined to generate noise at microwave lengths when the open end of the input-waveguide of a sensitive microwave receiver was directed toward various gaseous discharge tubes, including a 721A TR tube containing water vapor and hydrogen, a neon light in a stroboscope, a mercury vapor rectifier and an ordinary fluorescent desk lamp. Of these, the commercial fluorescent lamp appeared to lend itself most readily to mounting in a waveguide without the complication of the effects of the internal metal electrodes, so further tests were performed on it.

### MICROWAVE MEASUREMENTS

A T-5, 6-watt, daylight fluorescent lamp,<sup>4</sup> lighted from a d-c. source, was mounted with its axis parallel to the magnetic vector in a waveguide as illustrated in Fig. 2. The lamp itself was 9" long, with cathodes at each end. These could be isolated from the field in the 1" x 2" waveguide by enclosing the portion of the lamp which extended beyond the walls of the waveguide in cylindrical metal shields which formed waveguides beyond cutoff. Thus, energy was kept from reaching the cathodes, and the noise source was effectively confined to that part of the discharge which appeared inside the main waveguide. A piston in back of the gaseous discharge tube served to tune out the susceptance and a trimming screw provided an additional adjustment. The conductance could be adjusted by varying the direct current.

The admittance of the combination could be adjusted for an impedance

<sup>4</sup> A commercial fluorescent lamp contains about two mm. of argon and six to ten microns of mercury gas. The argon merely facilitates the initiation of the discharge; the mercury furnishes the radiation which excites the fluorescent material.

match at any operating frequency from 3700 mc to 4500 mc. The admittance diagram when the circuit was adjusted for match at 3960 mc is shown in Fig. 3; the standing wave ratio was less than 2.9 db from 3700 to 4240 mc.

At 3960 mc the conductance of the gaseous discharge varied directly with the direct current, while the negative susceptance had a broad maximum of  $-j.62 Y_0$  mhos at a current of 65 to 100 milliamperes, as shown in Fig. 4. These values are for the gaseous discharge; the susceptances of the enclosing glass tubing, the back piston and the holes in the sidewalls have been subtracted from the measured results. It is interesting to note that the discharge appears to be inductive.

The waveguide circuit containing the gaseous discharge tube was connected to the input waveguide of a sensitive microwave receiver which was used as a relative noise power meter. The noise power available from the

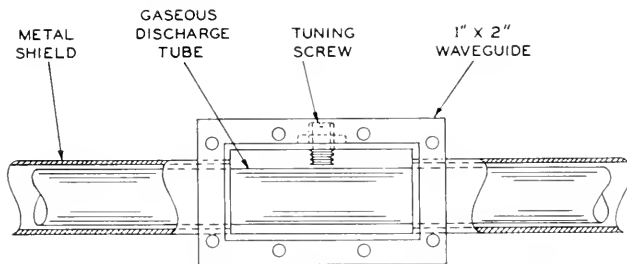


Fig. 2—Waveguide circuit for microwave noise generator using a gaseous discharge tube.

gaseous discharge was substantially independent of the direct current from 40 ma to 140 ma. These data are plotted in Fig. 5, which gives  $10 \log \left( \frac{T}{290} - 1 \right)$  versus direct current in milliamperes. The ordinate has been chosen so as to conform with absolute measurements made subsequently. The r.m.s. deviation from the straight line which represents a probable coefficient of only  $-.003$  db per milliampere was about  $\pm .05$  db. We do not claim to be able to achieve even this degree of accuracy with our present measuring equipment and hence do not place much confidence in the numerical value of this coefficient. Actually the decrease in noise with increasing current may have been associated with a change in the ambient temperature rather than with the increased current density. At least it is in the right direction for this to be the case.

The temperature coefficient of the noise from the discharge was found to be negative; when a piece of dry ice was held on the tubular shield of the circuit for a few minutes (long enough for frost to form on the brass) the output noise power of the discharge increased 0.6 db. The circuit was heated

on a hot plate and allowed to return to room temperature gradually, then cooled with an air stream and allowed to warm up gradually while the output noise and the temperature of the waveguide were being recorded. This revealed the temperature coefficient of  $-.055$  db per degree centigrade. The data (plotted in Fig. 6) show an r.m.s. deviation of  $\pm .114$  db from this coefficient.

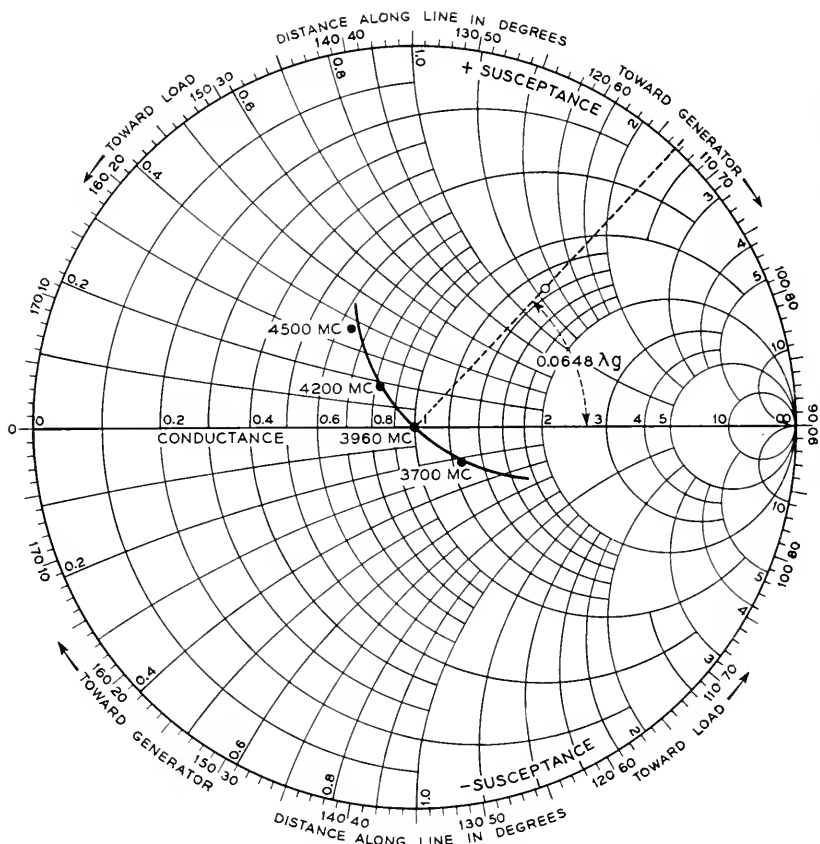


Fig. 3—Admittance diagram of microwave noise generator.

The ambient temperature of the waveguide circuit had very little effect on the admittance of the gaseous discharge.

As a check on variability with respect to time, two of these noise sources were compared, one against the other, at five-minute intervals for 65 minutes. During this time the waveguide temperature of source #1 rose from  $34^\circ$  to  $35.2^\circ$  C and that of source #2 rose from  $33.7^\circ$  to  $36.1^\circ$ . Each comparison was corrected, according to the coefficient of  $-.055$  db per degree C

and the observed temperature, to a common temperature of  $34^{\circ}\text{C}$ . Assuming that the noise figure of the microwave receiver was constant, source #1

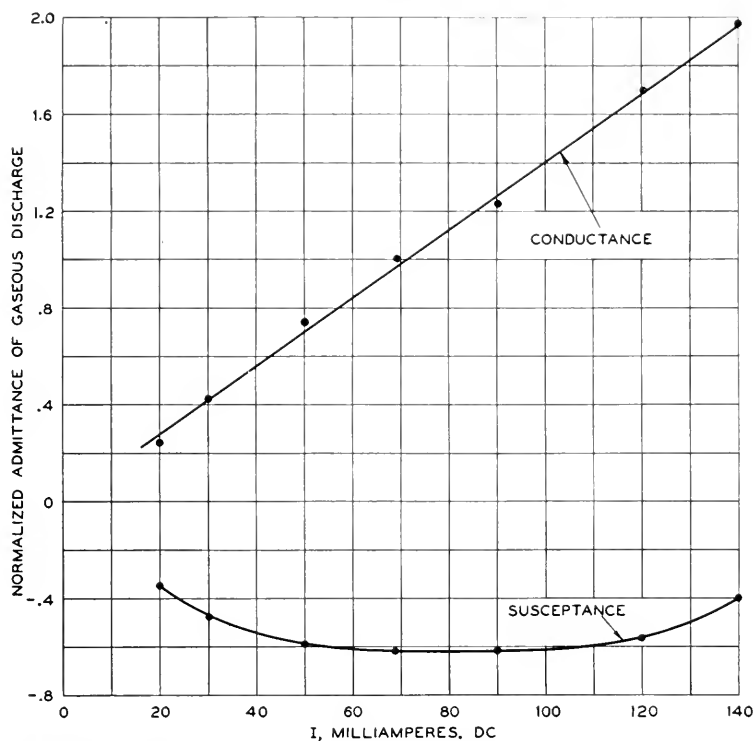


Fig. 4—Admittance of the gaseous discharge at 3960 mc as a function of the direct current in the discharge.

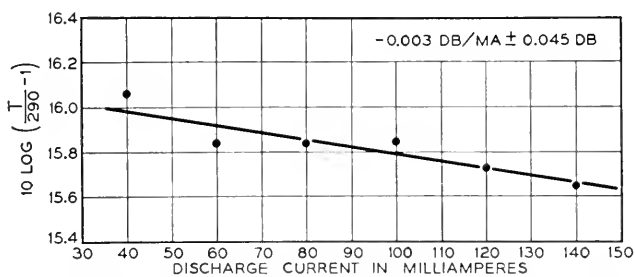


Fig. 5—The microwave noise power is practically independent of the discharge current.

showed variations whose r.m.s. deviation was  $\pm 0.11$  db, while source # 2 had similar deviations of  $\pm 0.092$  db. Assuming on the other hand that source #1 held constant and that the microwave measuring set varied with time,

source #2 displayed r.m.s. deviations of  $\pm 0.088$  db. These variations are in fact comparable with the probable experimental error, and the proof that they actually exist at all still remains to be demonstrated.

Of thirty-two different lamps, including 10 different types of fluorescent coatings such as used in the pink, red, gold, soft white, daylight, green, white, 4500° white, black light and blue, thirty-one<sup>5</sup> were all within  $\pm 0.25$  db of each other as was also a germicidal lamp with no fluorescent coating. Thus it appears that the source of the microwave noise energy lies chiefly in the gaseous discharge rather than in the fluorescent coating.

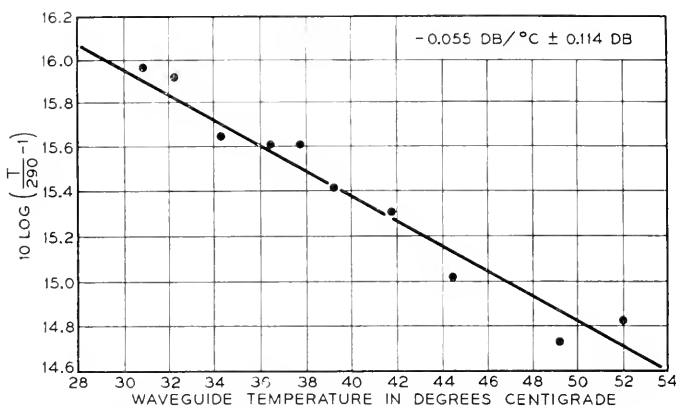


Fig. 6—The microwave noise power depends slightly upon the temperature of the waveguide circuit.

If this noise is tied up with the electron temperature of the discharge, we should expect the noise to be flat, or "white" noise. Corroborative evidence of this was observed when the spectrum of the noise was examined over the band from 3700 to 4500 mc at points 20 mc apart and no irregularities were found. The nature of the experiment was such that frequency bands of excessive noise power would have been observed had they been present. Further tests should indicate whether or not a gradual change in noise with frequency exists. It appears, however, unlikely that such a slope exists at 4000 mc.

Furthermore, since the level of the noise energy is so constant with respect to time, reproducible from tube to tube, practically independent of the current and only slightly affected by the ambient temperature, we might expect that it is being controlled or limited by some invariant physical property of the atoms and ions within the gaseous discharge. If this is the case, an absolute measurement of the noise power might lead us to some

<sup>5</sup> One of the 32 lamps flickered erratically. At times its noise was  $\frac{1}{2}$  db higher than the average.



theoretical explanation which, when applied to the case in hand, would explain the observed results qualitatively and quantitatively, thereby establishing a new absolute standard noise source for microwave measurements.

The microwave noise power from such a discharge tube was measured at 3950 mc in cooperation with Mr. C. F. Edwards on his calibrated measuring set on two different occasions, 16 days apart. The values obtained were 15.86 db and 15.80 db respectively for  $10 \log \left( \frac{T}{290} - 1 \right)$ .<sup>6</sup> This places the temperature,  $T$ , in the neighborhood of 11,400 degrees Kelvin. It is believed that the absolute measurements are correct to within  $\pm .25$  db or better.

Having determined the temperature of this noise source, we might ask, "If we should terminate our waveguide in a black body at 11,400 degrees, how much microwave noise power would we get from it?" The black body radiates with three polarizations, only one of which is propagated along the waveguide, and this available power is given by Nyquist:<sup>7</sup>

$$P_{NA} = \frac{hfB}{e^{hf/kT} - 1} \quad (16)$$

where  $h = 6.61 (10)^{-34}$  joule sec.

$k = 1.381 (10)^{-23}$  joule/deg.

$f$  = frequency in cycles per sec.

$B$  = bandwidth in cycles per sec.

At 4000 mc,  $\frac{hf}{kT}$  is, for  $T = 290$  degrees,  $6.6 (10)^{-4}$  which is so small that the

denominator of (16) can be replaced by  $\frac{hf}{kT}$ . This gives us the familiar expression for thermal noise:

$$P_{NA} = kTB \text{ watts} \quad (17)$$

In other words, thermal noise is black body radiation with but one polarization.

Going one step further we might also ask the question, "If we should examine the radiation from this black body with an optical spectroscope, at what wavelength would we find its maximum radiated energy?" The spectroscope detects radiation having three polarizations, and Planck's radiation law applies. From Wien's displacement law, the wavelength of maximum radiation is given by the relation:

$$\lambda_m T = 0.289 \text{ cm deg.} \quad (18)$$

<sup>6</sup> The temperature of the waveguide was 32°C when these values were measured.

<sup>7</sup> H. Nyquist, *Phys. Rev.*, Second Series, Vol. 32, pp. 110-113, July 1928.

Substituting  $T = 11,400$  degrees,

$$\lambda_m = 2535 (10)^{-8} \text{ cm} \quad (19)$$

This is indeed an interesting result, since the mercury vapor discharge in the fluorescent lamp radiates most of its energy at  $\lambda = 2536.52 (10)^{-8} \text{ cm}$ . The design of the lamp was guided by the effort to accentuate the radiation at this wavelength, and the manufacturers state that this has been achieved so that no other spectral line is excited to radiate more than two percent of the input power.<sup>8</sup> The conversion loss from dc to  $2536 (10)^{-8} \text{ cm}$  is only 2 or 3 db.

The striking similarity between the black body and the mercury vapor discharge at these two wavelengths, 7.6 cm and  $2536 (10)^{-8} \text{ cm}$ , suggests the following hypothesis:

*Hypothesis:* In a gaseous discharge which is radiating light energy substantially monochromatically at a particular wavelength,  $\lambda_m$ , the microwave noise energy is the same as that available from a black body which radiates its maximum energy at that wavelength.

Applying this hypothesis to the case in hand, where  $\lambda_m$  is  $2536.52 (10)^{-8} \text{ cm}$ , and using Wien's displacement law (eq. 18) we calculate the temperature to be

$$T = \frac{0.289}{2536.52} = 11,394^\circ \quad (21)$$

$$\frac{T}{290} = 39.29$$

$$\left( \frac{T}{290} - 1 \right) = 38.29 \quad (22)$$

$$10 \log \left( \frac{T}{290-1} \right) = 15.84 \text{ db} \quad (23)$$

Since this calculated value is so close to the measured values of 15.8 db and 15.86 db, it will be assumed to be correct until proved otherwise.

#### CONCLUSIONS

A commercial fluorescent lamp is a reliable source of microwave noise energy. At 4000 mc its effective temperature is 11,394 degrees Kelvin which is convenient for measuring noise figures of 20 db or less. The noise power is practically independent of the fluorescent coating, the current density and only slightly affected by the room temperature. The lamp lends itself readily to a broad-band impedance match in the waveguide.

<sup>8</sup> G. E. Inman and R. N. Thayer, *A. I. E. E. Transactions*, Vol. 57, pp. 723-726, Dec. 1938.

## Electronic Admittances of Parallel-Plane Electron Tubes at 4000 Megacycles

By SLOAN D. ROBERTSON

This paper reports the results of some measurements of the electronic admittances of close-spaced parallel-plane diodes and "1553" triodes at a frequency of 4000 megacycles. These results reveal that the diode admittance and the input short-circuit admittance of the triode depart considerably from the values predicted by single-velocity theory. The triode transadmittance, however, is only slightly lower in magnitude than the low-frequency value.

THE high-frequency admittances of electron streams flowing between parallel-plane electrodes have stimulated considerable theoretical interest. Llewellyn<sup>1,2,3,5</sup> has given an analysis of the particular case in which all electrons in any plane perpendicular to the direction of flow are assumed to have identical velocities. In practice, this approximation gives a reasonably accurate expression for electron stream admittances if the electrode spacing is relatively large, and if the frequency is not so high that the actual spread in electron velocities represents an appreciable fraction of the transit time. Others have treated various aspects of the general problem<sup>4,5,6,7,8,9,10</sup>. Theoretical consideration has also been given to the problem of electron flow in which the electrons possess a Maxwellian velocity distribution<sup>11,12,13,14</sup>. There has been, however, no complete analysis of the microwave-frequency case which takes account of the Maxwellian velocities.

In order to orient the present work properly with previous work let us consider briefly the parallel plane diode shown in Fig. 1, which shows three representative potential distribution curves. If only a relatively few electrons are available at the cathode, the potential distribution between electrodes will be approximately equal to the space-charge-free distribution indicated by curve *a*. If an ample supply of electrons is provided by the cathode and if all electrons leave the cathode with zero velocity, then the space charge is complete in accordance with Child's law, and the potential distribution follows curve *b*. If, on the other hand, the cathode is capable of supplying an ample supply of electrons, the electrons being emitted with a Maxwellian velocity distribution, the potential distribution will be represented by a curve of the type shown by *c*. The cases shown by curves *a* and *b* can be treated by the Llewellyn analysis. With wide spacings and at lower frequencies the admittances obtained with distributions of the *c* type may be approximated by the results obtained by analysis of distributions of the *b* type. With the very close spacings encountered in the Bell

Laboratories 1553 triode<sup>15</sup> the theoretical analysis no longer represents a valid approximation.

Let us consider curve *c* in greater detail. The fact that electrons are emitted with a Maxwellian velocity distribution, instead of being emitted at zero velocity as in the Child's law or complete space charge case, means that more electrons are introduced in the space between the electrodes than can flow to the anode in accordance with Child's law. The surplus electrons depress the potential in front of the cathode to a value below that of the cathode. This potential minimum is indicated by  $V_m$  in the figure. Electrons which have insufficient energy to cross this barrier return to the cathode.

In the space between the cathode and the potential minimum, electrons are found traveling with various velocities in both directions. Between the potential minimum and the anode, electrons travel in one direction only,

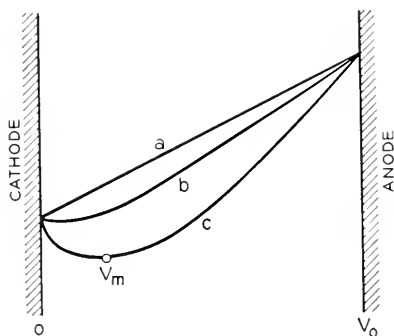


Fig 1—Potential distributions in a diode

toward the anode, but with multiple velocities. With close spacings and higher frequencies the distance between the cathode and the potential minimum may be an appreciable part of the total cathode-anode spacing, with the result that the electrons returning to the cathode may absorb a substantial amount of power from the high-frequency field.

This argument also applies to the cathode-grid region of a microwave triode such as the 1553. In order to increase the transconductance of the triode, it is desirable to locate the grid as close to the cathode as possible. The close spacing, however, leads to a greater loss of power to the returning electrons, which prevents a realization of the full benefits expected from the reduced spacing. All of these difficulties are a result of the Maxwellian velocity distribution of the emitted electrons.

In view of the importance of electron stream admittances in the design of microwave amplifiers and of the need for a better understanding of the performance of the 1553, a program was initiated to investigate some of

these effects experimentally. It seemed best to start this work with a study of the electron stream admittances of simple diodes, with the object of extending the measurements to the triode as the work progressed.

### DIODES

The diodes used in this work were identical in construction with the 1553 triode, but for the substitution of a solid copper anode in place of the grid. In all cases the cathode-anode spacing was approximately 0.65 mil, and the area of the cathode was 0.164 square centimeters. With this spacing one would expect the potential minimum to be relatively close to the anode such that a considerable portion of the cathode-anode region would contain electrons moving in both directions. The potential distribution then would be something like that shown in Fig. 2.

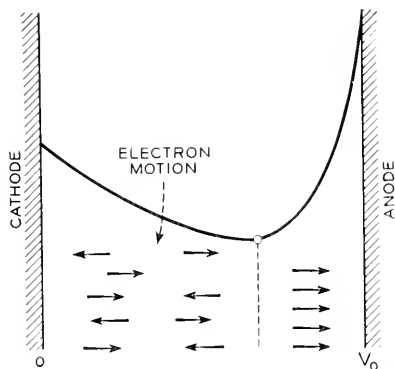


Fig. 2—Electron motion in a close-spaced diode.

The method used in measuring the microwave-frequency input admittances of diodes was based largely on a technique used by Mr. J. A. Morton, and will be described in some detail.

In a typical amplifier, radio-frequency power is fed from a waveguide source to the cathode-grid input region of a 1553 triode through a waveguide-cavity transformer. A similar circuit can be used for measuring diode admittances. The fundamental problem is to learn how to relate admittances measured with a standing wave detector located in the waveguide supply line to the equivalent two-terminal admittances located at the cathode-anode gap of the diode itself. In other words, we have to know the transformation-ratio between an admittance across the cathode-anode gap of the diode and the corresponding admittance which will be measured in the waveguide.

Let us refer to the circuit in Fig. 3. The circuit shows an input trans-

mission line which, for example, may be a waveguide having a characteristic impedance  $Z_{0y}$ , connected through an ideal transformer to an output line having a characteristic impedance  $Z_{0x}$ . The output line is connected to the transformer at the point  $x_0$ , where  $x_0$  represents the gap terminals of the diode. Suppose for the moment that provision has been made for connecting the output line at the point in the circuit normally occupied by the cathode-anode planes of the diode. This can be done by means of the special testers shown in Fig. 4. In these testers the anode has been omitted and provision has been made for attaching a coaxial line across the gap between the cathode and anode planes. The diodes used in later tests were identical with the device of Fig. 4, except that the coaxial output fitting was replaced by a sheet copper anode.

Referring again to Fig. 3, assume that the output line is shorted at point  $x_0$ . If power is introduced in the input line at the left, a standing wave pattern in the input line will pass through a minimum at some point  $y_0$ .

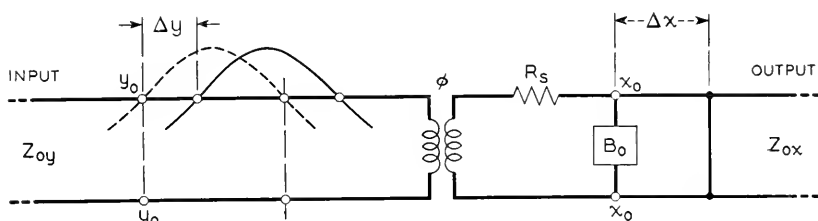


Fig. 3—Equivalent circuit of diode measuring equipment.

If the short circuit is now moved to the right by an increment  $\Delta x$ , the standing wave minimum will move by an increment  $\Delta y$ . The relation between  $\Delta x$  and  $\Delta y$  is given by the following equation:

$$\frac{1}{Z_{0y}} \cot \frac{2\pi\Delta y}{\lambda_y} = \frac{\phi}{Z_{0x}} \cot \frac{2\pi\Delta x}{\lambda_x} - \phi B_0 \quad (1)$$

where  $\lambda_y$  and  $\lambda_x$  are the respective wavelengths in the two lines (which may not be equal if, for example, one is a coaxial and the other is a waveguide).  $\phi$  is the transformation ratio of the ideal transformer, and  $B_0$  is the effective leakage susceptance of the tube and transformer referred to the terminals at  $x_0$ . If  $\frac{2\pi\Delta y}{\lambda_y}$  is plotted as a function of  $\frac{2\pi\Delta x}{\lambda_x}$  on cot-cot coordinate paper, a straight line is obtained whose slope  $m$  is

$$m = \phi \frac{Z_{0y}}{Z_{0x}} \quad (2)$$

and whose ordinate intercept  $\rho$  is

$$\rho = -\phi B_0 Z_{0y} \quad (3)$$

A typical cot-cot plot is shown in Fig. 5.

Now, assume that the right-hand transmission line is removed and that the diode gap is connected at the transformer terminals  $x_0$ . The normalized admittance referred to the point  $y_0$  on the input line can be measured by a simple standing wave measurement. Represent this admittance by  $\bar{Y}_{wg}$ .

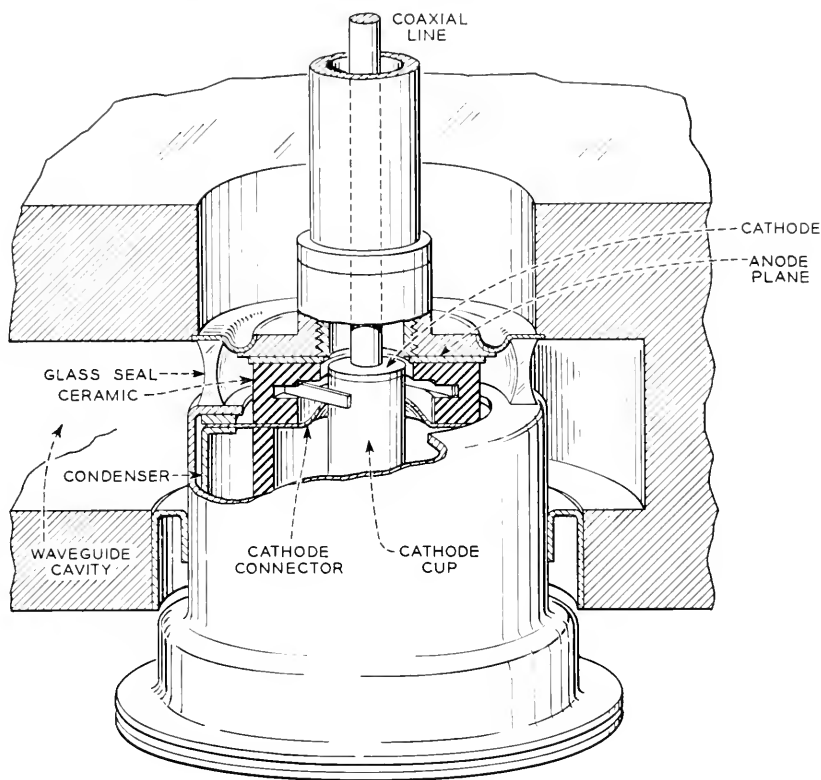


Fig. 4—Coaxial tester.

Let the unknown diode admittance be represented by  $\Gamma_x$ .  $\Gamma_x$  is then given by the following relation:

$$\Gamma_x = \frac{1}{Z_{0x}m} [\bar{Y}_{wg} + j\rho] \quad (4)$$

Hence, having determined  $y_0$ , it is only necessary to measure the slope  $m$  and the intercept  $\rho$  on the cot-cot curve in order to relate  $\Gamma_x$  to  $\bar{Y}_{wg}$ . The characteristic impedance of the output line  $Z_{0x}$  used in obtaining the cot-cot plot must also be known. Since a coaxial is used for this line, its characteristic impedance is easily calculated.

If no losses were associated with the transformer or the parts of the diode external to the actual cathode-anode region, such as the metal vacuum

envelope and certain ceramic details of the tube, the above measurements would give complete information regarding the circuit. Certain losses have been found, however. These are measured as follows: At the time when terminals  $x_0$  are shorted a standing wave measurement is made in the wave-

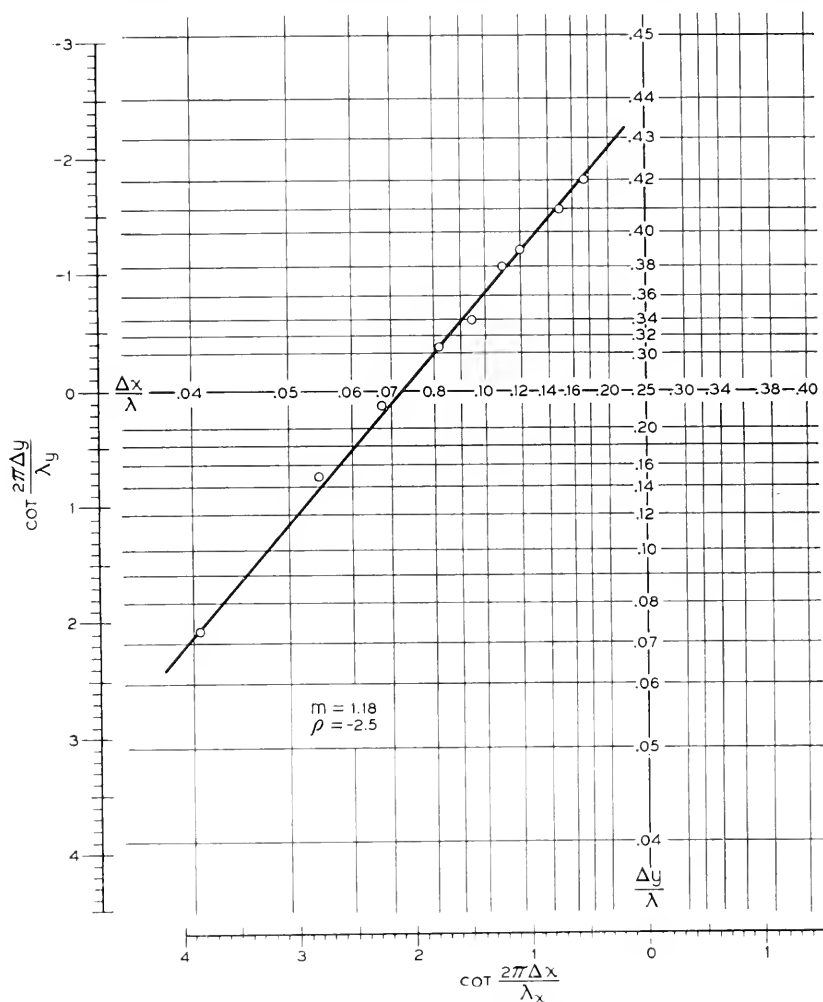


Fig. 5—Typical cotangent-cotangent plot.

guide line at the left. From this measurement and the cot-cot data it is possible to compute an equivalent resistance in series with the gap caused by losses present in the circuit. This equivalent series resistance is given by

$$R_s = \frac{Z_{0x}m}{SWR} \quad (5)$$



where  $SWR$  is the voltage standing wave ratio mentioned above. The determination of a series loss resistance in this manner is quite analogous to the short-circuit test used in determining the losses in a power transformer.

There is one other factor in the cot-cot technique which is worthy of mention. If, at the very beginning, the output line is terminated in  $Z_{0L}$  and if the transformer is adjusted so that the input line is matched, then the value of  $m$  will be unity and  $\rho$  will equal zero. It is then unnecessary to take a cot-cot curve. It is, however, still necessary to locate  $y_0$  by shorting the terminals at  $x_0$ .

#### DIODE ADMITTANCE AT 4060 MEGACYCLES

Electron stream admittance measurements with diodes were made in the following way: A coaxial tester was installed and the circuit was adjusted for a slope  $m$  of about one. This coaxial tester was then removed and replaced by another in order to learn whether the slope obtained with one tester would be the same with another, supposedly identical, tester. This process was repeated several times, and the slope was found to vary no more than about 10% from one tester to the other.

The procedure was then to replace the coaxial tester with a diode and make admittance measurements with the assumption that the slope would be the same for the diode as for the tester. This assumption was believed to be reasonable since the structure of the diode was identical with that of the tester except that an anode was substituted for the coaxial output connector. In either case all elements that were located inside the waveguide cavity were presumably identical.

Electron stream measurements were made at a frequency of 4060 megacycles with a number of diodes over a wide range of anode and heater voltages. In making these measurements, the radio-frequency power was kept at a relatively low level (0.2 milliwatt) in order that the measured admittances would be independent of the radio frequency voltage.

Results for several diodes are shown in Figs. 6 through 13. The various symbols used in the figures are defined as follows:

$V_H$  = heater voltage

$I_H$  = heater current

$V_0$  = anode voltage (neglecting contact potentials)

$I_0$  = anode current in ma

$J_0$  = anode current density in  $\text{ma}/\text{cm}^2$

$g_0$  = low-frequency diode conductance measured with an audio frequency bridge

$g$  = high-frequency diode conductance measured as described above

$b$  = high-frequency diode susceptance

$R_s$  = equivalent resistance in series with diode

In computing the admittance of the electron stream it was necessary to

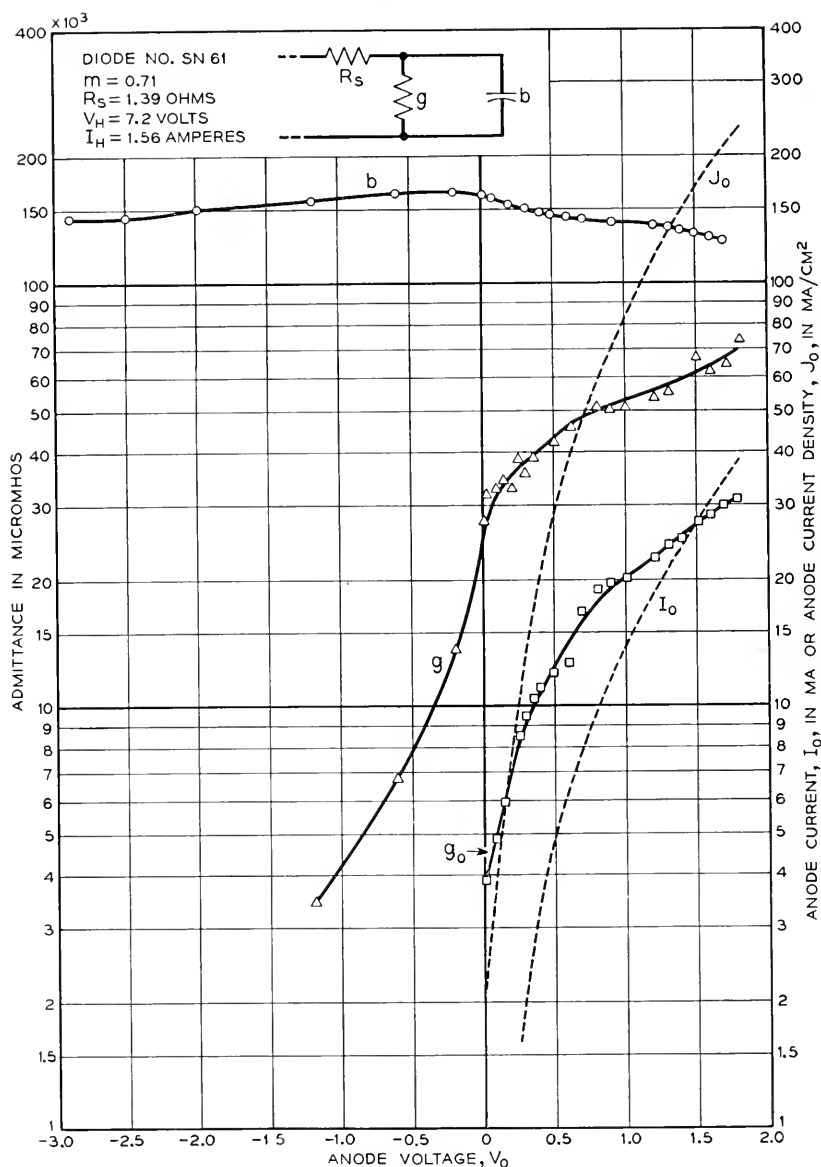


Fig. 6—Admittance of a diode.

allow for the circuit and tube losses previously discussed. The equivalent series resistance  $R_s$  of the diode circuit was determined by biasing the tube negatively to the point where a further increase in bias failed to produce a

perceptible change in the waveguide standing wave ratio. Under such conditions the electrons experienced a large retarding field at the cathode and did not emerge an appreciable distance into the cathode-anode region. Any resistance measured at this time was due to the series loss and was not

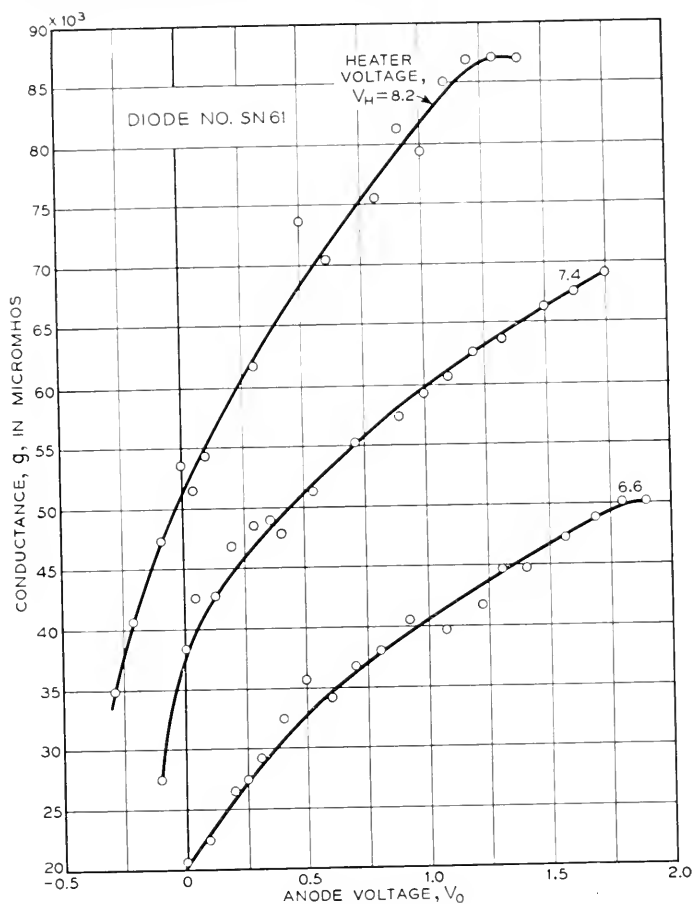


Fig. 7—Effect of heater voltage upon diode conductance.

produced electronically. The diode series resistances varied from about 1.3 to 5.0 ohms with an average value around 3 ohms.

Figure 6 shows the results of admittance measurements of a diode. As expected, the high-frequency conductance is considerably greater than the low-frequency value  $g_0$ . In fact  $g$  is seen to have a value of several thousand micromhos when the negative bias of the tube is such that no perceptible anode current flows. The susceptance  $b$  for large negative anode potentials

has a value of 150,000 micromhos, which agrees fairly well with the value computed from the geometrical capacitance. As anode current is drawn and a space charge condition prevails,  $b$  drops to a value of 125,000 micromhos. Theoretical considerations would predict a drop of about 40% in the case of a single-velocity electron stream. This is somewhat greater than the drop exhibited in Fig. 6.

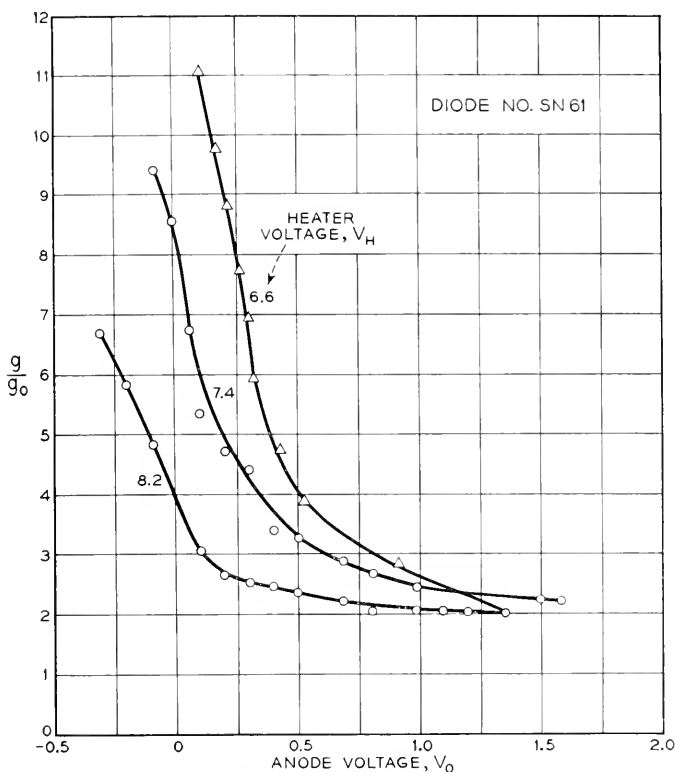


Fig. 8—Effect of heater voltage upon  $g/g_0$ .

Figures 7 and 8 show the effect of cathode temperature on  $g_0$  and the ratio  $g/g_0$ . The parameter used to represent the cathode temperature is the heater voltage  $V_H$ . As the heater voltage is raised the total conductance  $g$  increases. The ratio  $g/g_0$ , however, decreases, particularly for low or negative anode voltages. This means that, with a given anode voltage, as the cathode temperature is raised,  $g_0$  increases more rapidly than  $g$ . If the curves of Fig. 8 are replotted in terms of  $J_0$  rather than  $V_0$ , the ratio  $g/g_0$  is relatively independent of  $V_H$ . This is shown in Fig. 9.

The results of measurements on another diode are shown in Fig. 10.

These are very similar in all respects to those of the preceding figure. It is probable that the cathode-anode spacings of the two diodes of Figs. 6 and 10 were somewhat greater than the 0.65 mil for which they were designed. In both cases the capacitances measured at low frequency were somewhat low.

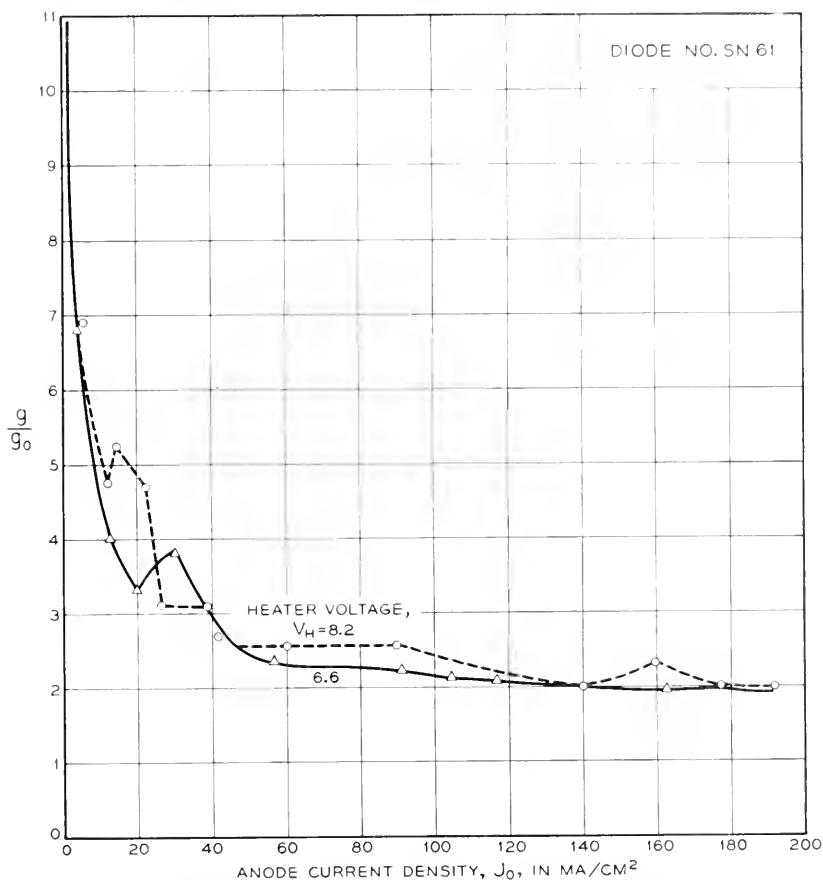


Fig. 9—Variation of  $g/g_0$  with current density and heater voltage.

In Fig. 11, results are shown for a third diode. In this case the susceptance at a large negative bias is in almost exact agreement with the value to be expected with the intended diode spacing of 0.65 mil. It is interesting to observe that, with this tube,  $b$  drops a greater amount as the current increases. Moreover, the ratio  $g/g_0$  is greater than that found with earlier diodes.

In Fig. 12 data are shown for a diode having a very high value of  $g_0$ . From the standpoint of cathode activity this was the best tube that was

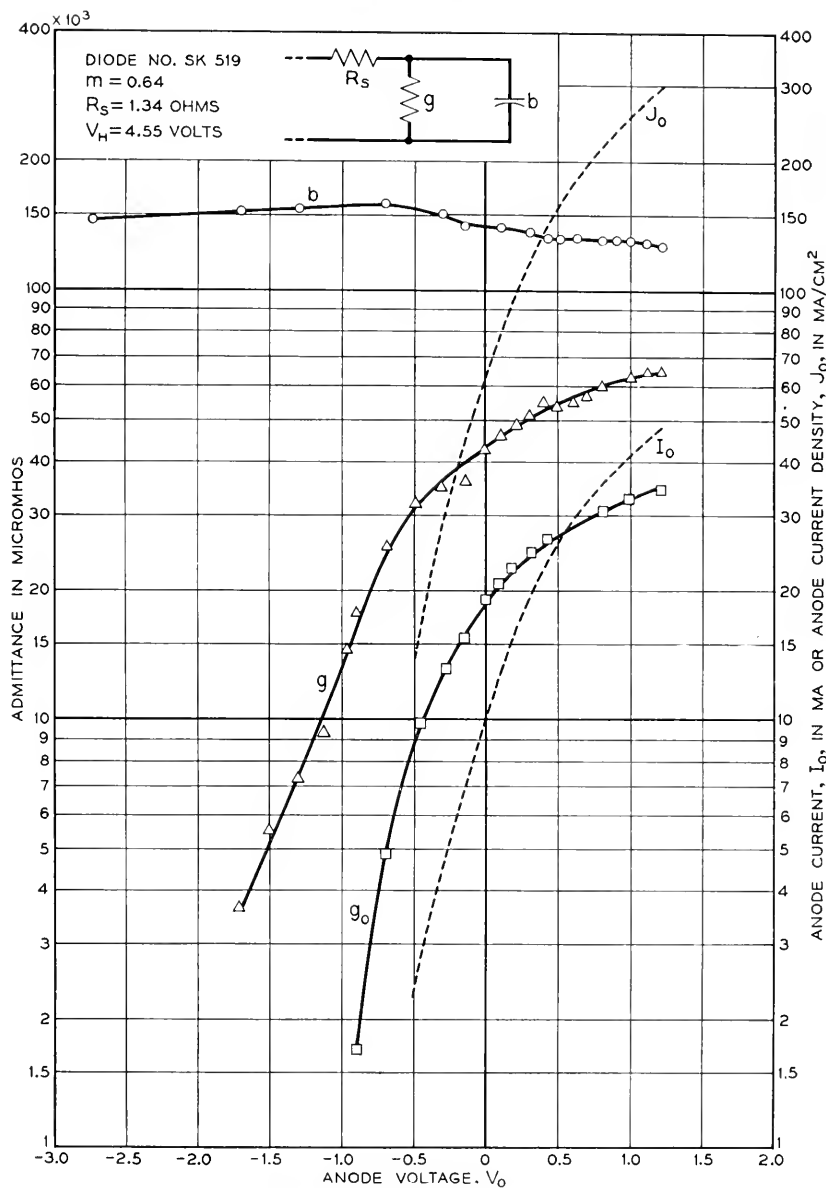


Fig. 10—Admittance of a diode.

tried. At maximum current the susceptance  $b$  dropped to 50% of the initial value. The data of Fig. 12 have been replotted in Fig. 13 in terms of the variable  $126x^{\frac{2}{3}}/\lambda J_0^{\frac{2}{3}}$ , where  $x$  is the cathode-anode spacing. In the Llewellyn

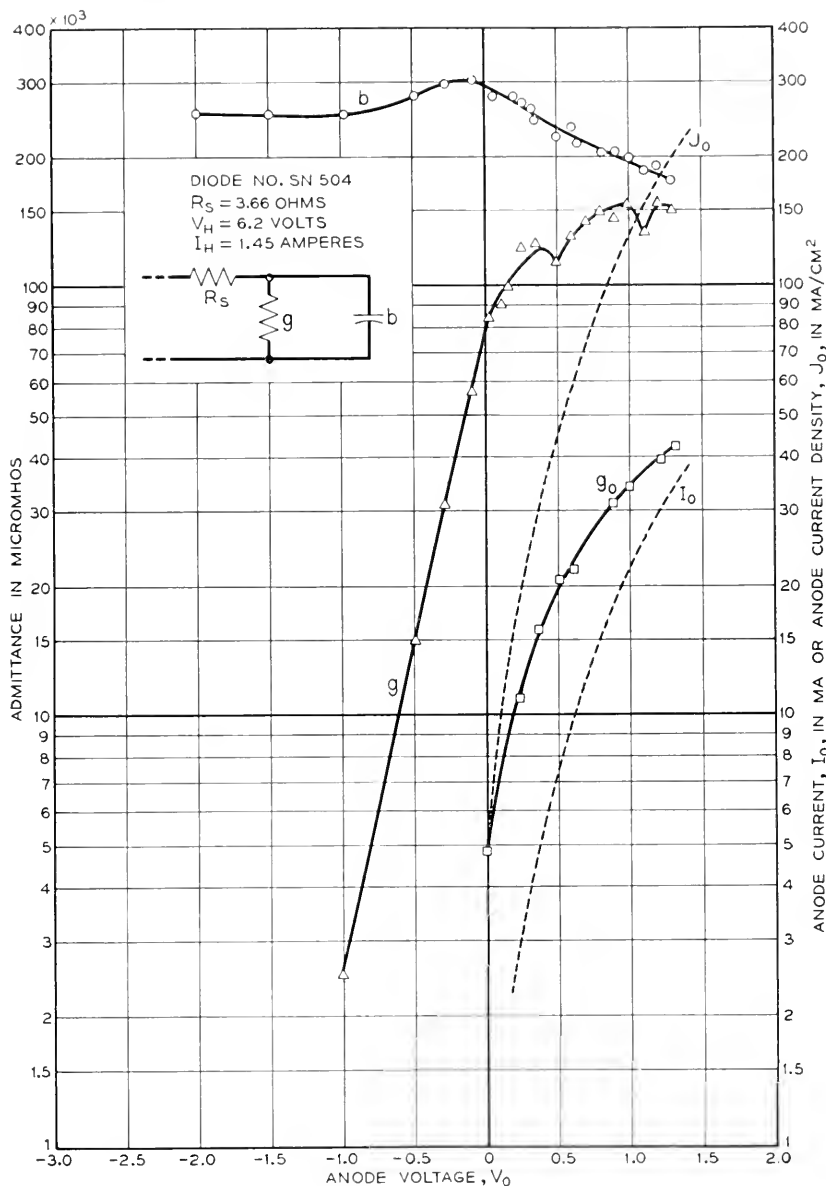


Fig. 11—Admittance of a diode.

theory this variable is equal to the transit time. The solid curves in the figure are the theoretical results of the Llewellyn theory, whereas the broken curves present the corresponding experimental values. In the latter it should

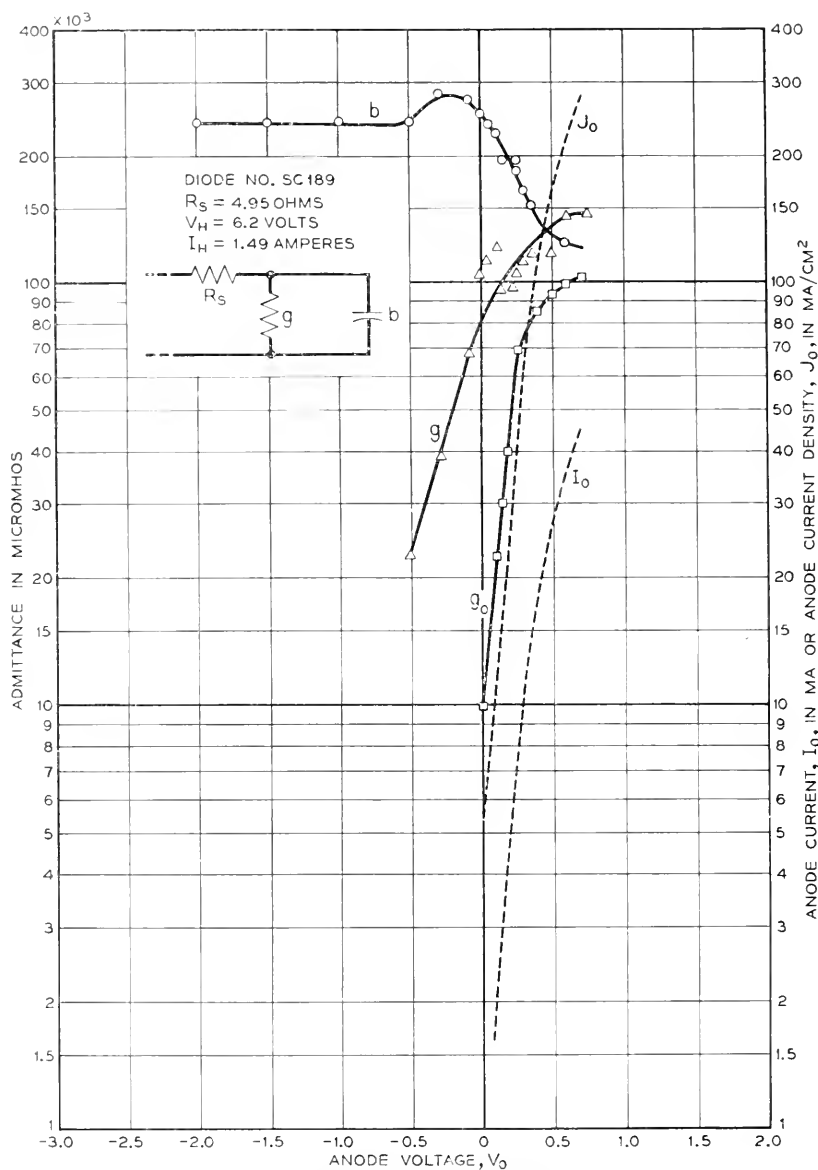


Fig. 12--Admittance of a diode.

be understood that the abscissa do not represent transit time. The curves do serve, however, to compare the theoretical diode resulting from a single-valued electron velocity assumption with the actual diode in which a Max-



wellian velocity distribution prevails. In the experimental case it is probable that, for values of the abscissa greater than 6 or 7, the actual transit time is considerably greater than in the theoretical case. In fact, at a value of 11.4 the anode voltage was zero, the anode current being maintained by the thermal energy of the electrons.

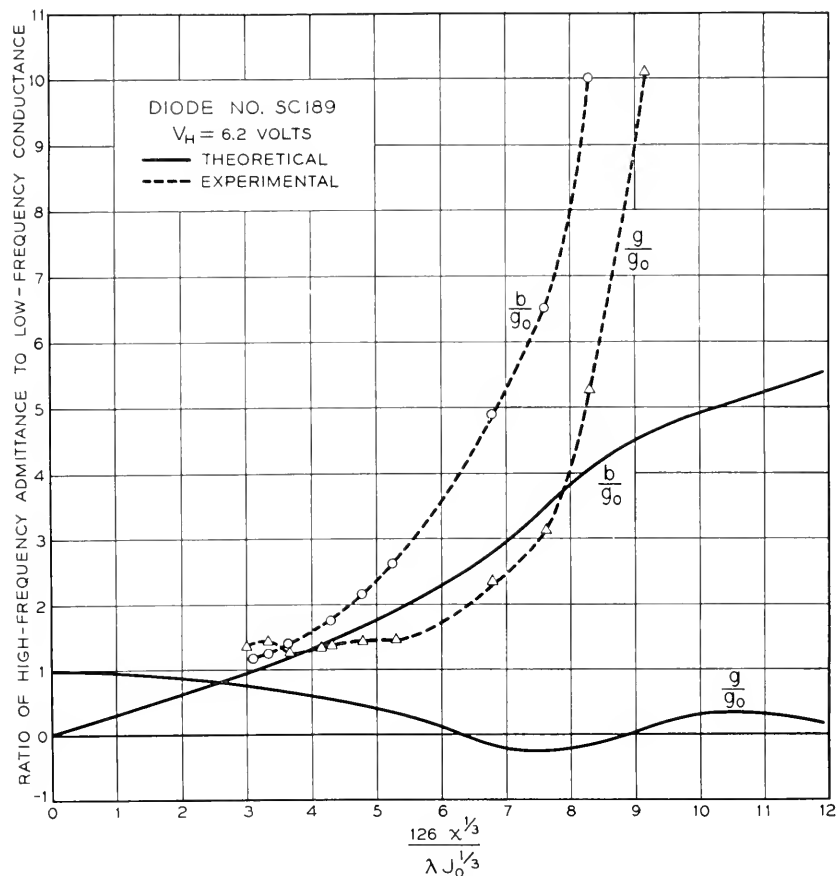


Fig. 13—Comparison of theoretical and experimental values of diode conductance and susceptance.

Other diodes were tested, but they exhibited results substantially equivalent to those already disclosed. In a few cases anomalous results were obtained. With some diodes the capacitance with no electron flow did not approach the low-frequency value. These were rejected on the assumption that there was some mechanical imperfection in the tube which changed the calibration of the measuring equipment.

With the realization that sufficient data are not available to define the phenomena in all detail, it is believed that certain general conclusions can be drawn. From the present work and that of Lavoo<sup>16</sup> and others<sup>17,18,19</sup>, it is apparent that the microwave conductance of a close-spaced diode is substantially greater than the low-frequency value. The ratio  $g/g_0$  appears to increase as the spacing decreases. This increase will probably continue until the position of the potential minimum approaches the anode plane. The susceptance decreases with increasing current and appears to level off at high-current densities. The final value at a current density of  $240 \text{ ma/cm}^2$  varied between 0.5 and 0.9 of the initial value.

For a given current density, the ratio  $g/g_0$  does not appear to vary appreciably as the cathode temperature is changed.

An attempt was made to study the available diodes at 10,000 megacycles. It was found, however, that the value of  $R_s$  was so high at this frequency and that variations in tube conductance were so small in comparison with  $R_s$  that accurate results could not be obtained.

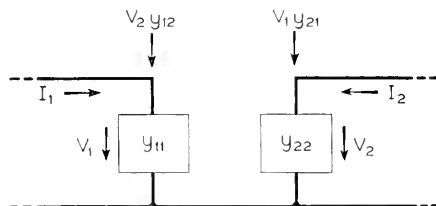


Fig. 14—Equivalent circuit of a triode.

#### FOUR-POLE ADMITTANCES OF A TRIODE

A triode may be considered as an active linear four-pole transducer, and may be defined by the network of Fig. 14. It is apparent that

- $y_{11}$  is the input admittance with the output shorted,
- $y_{22}$  is the output admittance with the input shorted,
- $y_{12}$  is the feedback admittance with the input shorted,
- $y_{21}$  is the transadmittance with the output shorted.

The values of the parameters  $y_{11}$ ,  $y_{22}$ ,  $y_{12}$ , and  $y_{21}$  to be measured at the grid, cathode, and anode terminals differ from the values of the  $y$  admittance coefficients given by Llewellyn and Peterson<sup>5</sup> who define  $y_{11}$  as the admittance of the diode coinciding with the cathode and the fictitious equivalent grid plane, and  $y_{22}$  as the admittance between the equivalent grid plane and the anode, and finally  $y_{21}$  as the transadmittance between the two. The relations between the  $y$  admittance coefficients of Llewellyn and Peterson and the coefficients measured by the author are given by Peterson.<sup>6</sup> It turns out that, with a high- $\mu$  tube, such as the 1553 triode, the two sets of

coefficients differ in the order of 10–20% over the useful operating range of current densities; so, for practical considerations, the measure coefficients may be regarded as substantially equivalent to the coefficients referred to the fictitious grid plane. Not that they will be equal to the theoretical values, but they may be regarded as being associated with the same geometry and will serve at least as a qualitative test of the validity of the theoretical values for the physical tube.

In order to measure the four-pole parameters, the 1553 triode was mounted in a coaxial circuit of the type shown in Fig. 15. The grid-anode output circuit of the tube is seen to connect directly with the coaxial output line. The input circuit required a more careful design. Due to the size of the base of the tube it was necessary to taper the input coaxial as shown. In the early stages of this work, difficulty was experienced with higher order modes in the large diameter section of the input coaxial. It was believed that these modes were generated by the action of the parallel wire grid which lacked the

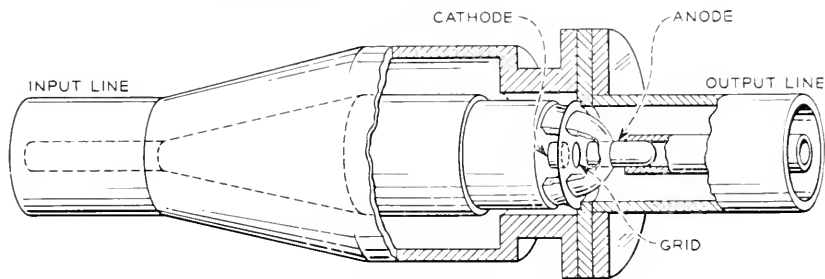


Fig. 15—Detail of coaxial mount for measuring four-pole admittances of a triode.

radial symmetry appropriate to coaxial transmission. The difficulty was overcome by constricting the outer diameter of the coaxial line in the immediate vicinity of the grid of the tube, thus inhibiting generation of the higher order mode.

Before measurements could be made it was necessary first to calibrate both the input and the output circuits in a manner similar to that used and described in connection with the diode measurements. The coaxial tester used for calibrating the input circuit was identical with that used for the diode work. For the output circuit a similar tester was used. As one might expect, the value of the cot-cot slope of the output circuit was close to unity. The value actually turned out to be 0.9. In the input circuit the slope was so great that it was difficult to measure, so that it was necessary to introduce a transformer in the coaxial input circuit to permit tuning.

The complete apparatus necessary to measure  $y_{11}$  and  $y_{22}$  is shown in Fig. 16. This equipment, save for the details already discussed, is quite conventional in every respect.

In order to measure  $y_{11}$ , the output coaxial line was short-circuited at a point an integral number of half-wave-lengths from the grid-anode terminals of the tube. The admittance measured in the input line could then be used in computing  $y_{11}$ . To measure  $y_{22}$ , the procedure was reversed, the input line being shorted, and the corresponding admittance being measured in the output line. In either case the normalized line admittances were measured by the standard procedure of determining the standing wave ratio in the line and locating the position of the standing wave minimum with respect to the equivalent terminals of the tube.

The transfer admittances were measured with the equipment shown in Fig. 17. The equipment shown here has been fully described in a recent

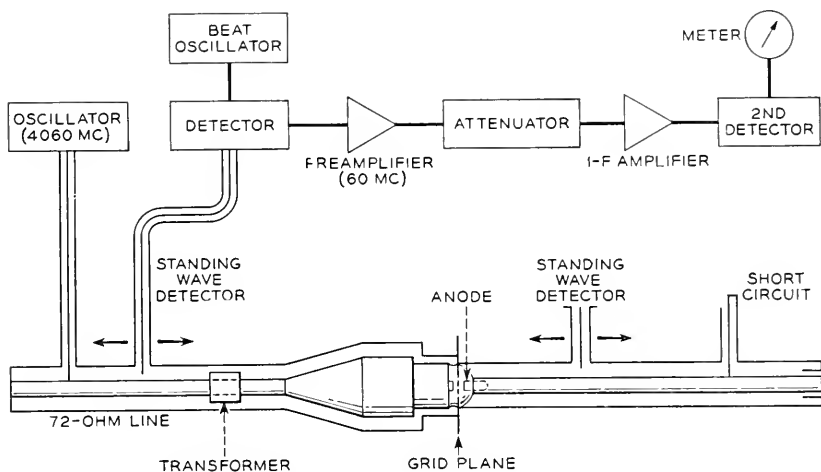


Fig. 16—Circuit connected for measuring input short-circuit admittance of a triode.

paper<sup>20</sup> and will be described only briefly here. The output of a signal oscillator is divided into two portions. One portion is applied to a balanced modulator where it is modulated by an audio-frequency signal. The suppressed-carrier, double-sideband signal from the modulator is applied to the input circuit of the triode. Probes are provided for sampling the voltages  $V_1''$  and  $V_2''$  at points an integral number of half wavelengths from the input and output gaps of the tube respectively. The other portion of the oscillator power is fed through a calibrated phase shifter and is applied to a crystal detector in the manner of a local oscillator of a double-detection receiver. The signal samples at  $V_1''$  and  $V_2''$  are then alternately applied to the crystal detector where they are demodulated by the action of the homodyne carrier. In each case the phase shifter is adjusted so that the audio signal disappears in the detector output. This occurs when the phase of the homodyne carrier

is in quadrature with the signal sidebands. The difference in phase between the two adjustments of the phase shifter is equal to the phase between  $V''_1$  and  $V''_2$ . In measuring the transfer phase from  $V''_1$  to  $V''_2$  the output coaxial line is terminated in its characteristic impedance. By reversing this procedure it is possible, of course, to measure the ratio of  $V''_2$  to  $V''_1$  with the input circuit terminated in  $Z_0$ . The ratio of the magnitudes of  $V''_1$  and  $V''_2$  may be measured either with the equipment shown in Fig. 17 by adjusting the phase of the homodyne carrier to maximize the signals in each case and

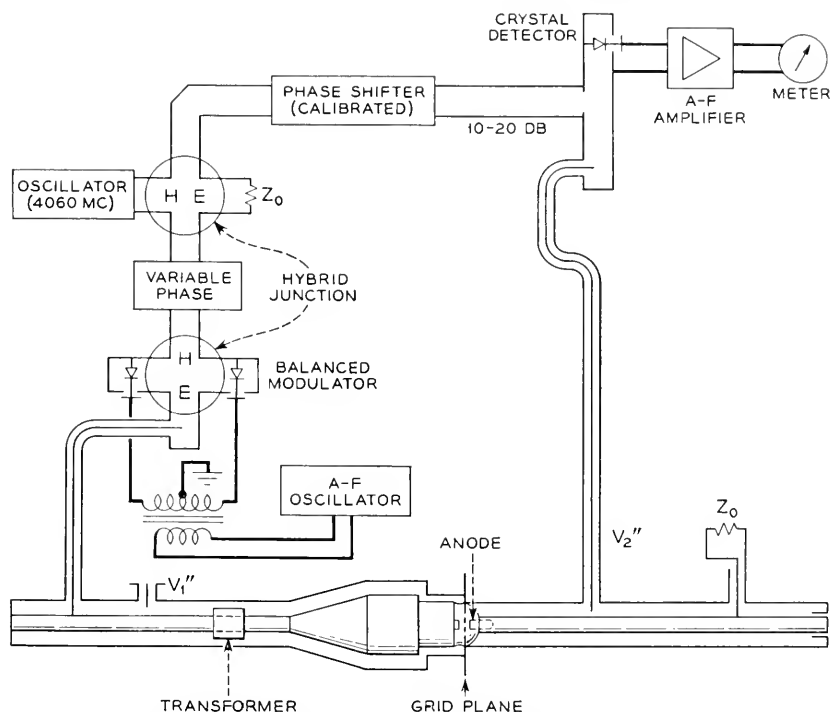


Fig. 17—Circuit for measuring transfer phase of a triode.

comparing the levels, or by using the equipment in Fig. 16 in the conventional way.

Figure 18 is a photograph of the triode circuit which shows the input and output coaxial standing-wave detectors with the triode mounted in the enlarged section at the center.

As in the case of the diode it was found that, with the tube biased negatively such that no electrons could leave the immediate vicinity of the cathode, the input circuit exhibited an equivalent series resistance  $R_s$ . The latter had to be allowed for in reducing the experimental data.

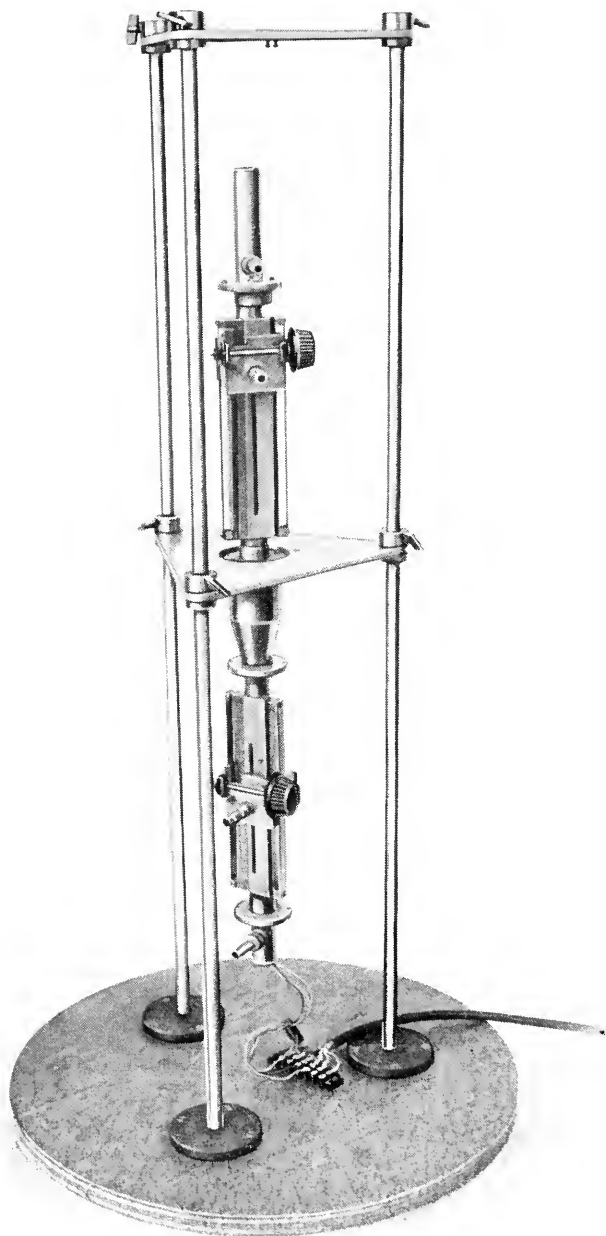


Fig. 18—Coaxial mount for measuring triode admittances.

The experimental data obtained as described above were sufficient for computing the four-pole parameters. The calculations necessary for the reduction of the data can best be understood by referring to Fig. 19. The various symbols used in connection with the figure are defined as follows:

$\bar{Y}_1$  = Normalized admittance measured at 1-1 with 2-2 shorted

$\bar{Y}_2$  = Normalized admittance measured at 2-2 with 1-1 shorted

$V_1''$  =  $\gamma_{21}$  (measured with output line terminated in  $Z_0$ )

$I_2''$  =  $\gamma_{21}$  (measured with output line terminated in  $Z_0$ )

The above parameters represent those obtained by the measurements described above.

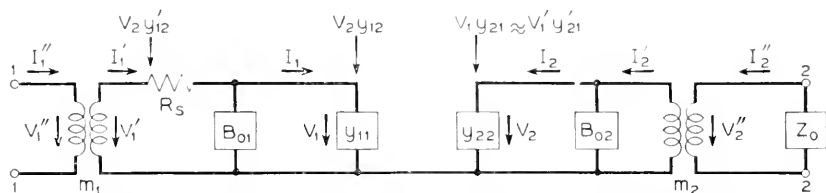


Fig. 19--Equivalent circuit of triode and associated measuring equipment.

In calibrating the circuit the following parameters were obtained:

$\rho_1$  = ordinate intercept of input cot-cot curve

$\rho_2$  = ordinate intercept of output cot-cot curve

$m_1$  = slope of input cot-cot curve

$m_2$  = slope of output cot-cot curve

$$B_{01} = -\frac{\rho_1}{66m_1} \quad B_{02} = -\frac{\rho_2}{66m_2}$$

$Z_0$  = characteristic impedance of input and output coaxial lines.

$R_s$  was measured by shorting the output line, placing a large negative bias on the tube, and measuring the admittance of the input line. Then

$$R_s = 66m_1 Re(\bar{Y}_1) \quad (6)$$

where the number 66 represents the characteristic impedance of the coaxial line used in calibrating the input circuit, corresponding to  $Z_{0x}$  in Equation 4.

Fortunately for simplicity, the series resistance in the output circuit was negligible.

The computations are then as follows:

$$y'_{11} = \frac{\bar{Y}_1}{66m_1} \quad y'_{22} = \frac{\bar{Y}_2}{66m_2} \quad (7)$$

$$y_{11} = \frac{\bar{Y}_1}{66m_1 - \bar{Y}_1 R_s} + \frac{j\rho_1}{66m_1} \quad (8)$$

$$y_{22} = \frac{1}{66m_2} [\bar{V}_2 + jp_2] \quad (9)$$

In order to compute  $y_{21}$ , the following four-pole equations are used:

$$V_1' = \frac{I_1'}{y_{11}} + \frac{V_2 y_{12}'}{y_{11}} \quad (10)$$

$$V_1 = \frac{I_1}{y_{11}} + \frac{V_2 y_{12}}{y_{11}} \quad (11)$$

$$V_2 = \frac{I_2}{y_{22}} + \frac{V_1 y_{21}}{y_{22}} \approx \frac{I_2}{y_{22}} + \frac{V_1' y_{21}'}{y_{22}} \quad (12)$$

It follows that

$$V_1 y_{21} \approx V_1' y_{21}' \quad (13)$$

$$y_{21} \approx y_{21}' \frac{V_1'}{V_1} \quad (14)$$

Referring to Fig. 19, one may write

$$V_1 = V_1' - (I_1' + V_2 y_{12}') R_s \quad (15)$$

Combining (10) and (15)

$$\frac{V_1'}{V_1} = \frac{1}{1 - y_{11}' R_s} \quad (16)$$

$y_{21}'$  can be evaluated by making use of the relation

$$V_2 \approx \frac{I_2'}{y_{22}'} + \frac{V_1' y_{21}'}{y_{22}'} \quad (17)$$

Dividing (17) by  $V_2$  and rearranging terms

$$y_{21}' \approx \left( \frac{y_{22}'}{V_1'} \right) \left[ 1 - \frac{I_2'}{V_2 y_{22}'} \right] \quad (18)$$

where  $I_2'/V_2$  can be expressed as

$$\frac{I_2'}{V_2} = \frac{1}{66m_2 \bar{Z}_0} = \frac{1}{66m_2} \quad (19)$$

where  $\bar{Z}_0 = 1$ .

$V_1'/V_2$  can be expressed in terms of  $\gamma_{21}$ ,  $m_1$ , and  $m_2$  by using the relations:

$$\frac{V_1'}{V_1''} = \sqrt{\frac{66m_1}{Z_0}} \quad \frac{V_2}{V_2''} = \sqrt{\frac{66m_2}{Z_0}} \quad (20)$$



Solving (20) for  $V_1'/V_2'$  and remembering that  $V_1''/V_2'' = \gamma_{21}$ ,

$$\frac{V_1'}{V_2'} = \gamma_{21} \sqrt{\frac{m_1}{m_2}} \quad (21)$$

If (19) and (21) are substituted in (18), one finds

$$y_{21}' \approx \frac{y_{22}'}{\gamma_{21}} \sqrt{\frac{m_2}{m_1}} \left[ 1 + \frac{1}{66m_2 y_{22}'} \right] \quad (22)$$

By using (14) and (16),  $y_{21}$  can then be written as

$$y_{21} \approx \frac{y_{22}'}{\gamma_{21}} \sqrt{\frac{m_2}{m_1}} \left[ 1 + \frac{1}{66m_2 y_{22}'} \right] \left[ \frac{1}{1 - y_{11}' R_s} \right] \quad (23)$$

Several 1553 triodes were available for study. Typical experimental results obtained with two of them are shown in Figs. 20, 21, and 22. The triode used in obtaining the data of Fig. 20 had input and output spacings of 0.65 and 12 mils, respectively. The cathode and anode diameters were 180 mils. The grid opening was 250 mils and was wound with 0.3 mil tungsten wire at 1000 strands per inch. In the figures,  $V_g$  and  $V_p$  represent the d-c. grid and plate potentials, respectively.

There are a number of interesting things to observe in Fig. 20. As with the diode,  $b_{11}$  for a large negative bias approaches the "cold" value computed from the capacitance. However, as anode current is drawn,  $b_{11}$  drops rapidly to a much lower value than was the case for the diodes. The conductance  $g_{11}$  behaves somewhat like  $g$  for the diode.  $b_{22}$  is equal to the value computed from the grid-anode capacitance and is not appreciably influenced by the electron stream.  $g_{22}$  was very low with a magnitude of slightly less than 1000 micromhos at maximum anode current. It is not shown in the figure. The transadmittance  $y_{21}$  is worth considering. When the bias is several volts negative,  $y_{21}$  has a value of about 9000 micromhos. This is about 50 times as high as one would expect from a consideration of the electrostatic capacitance between the cathode and anode of the tube. This effect has been investigated more fully and is discussed in another paper.<sup>21</sup> As the tube starts to draw plate current,  $y_{21}$  rises and reaches a maximum of about 40,000 micromhos. The low-frequency transconductance was measured and is plotted in the figure. It will be observed that the high-frequency transadmittance is only slightly lower than  $g_m$ . This is in agreement with the theories of Llewellyn.<sup>5</sup> The agreement appears reasonable when one remembers that, in the theoretical analysis, the magnitude of the ratio  $y_{21}/g_0$  is relatively independent of the transit time in the input space.

Figure 21 shows the results of measurements on a triode identical with that of Fig. 20 except that the grid consists of a mesh of 0.3 mil tungsten wires wound at 550 strands per inch in both directions. It will be noted

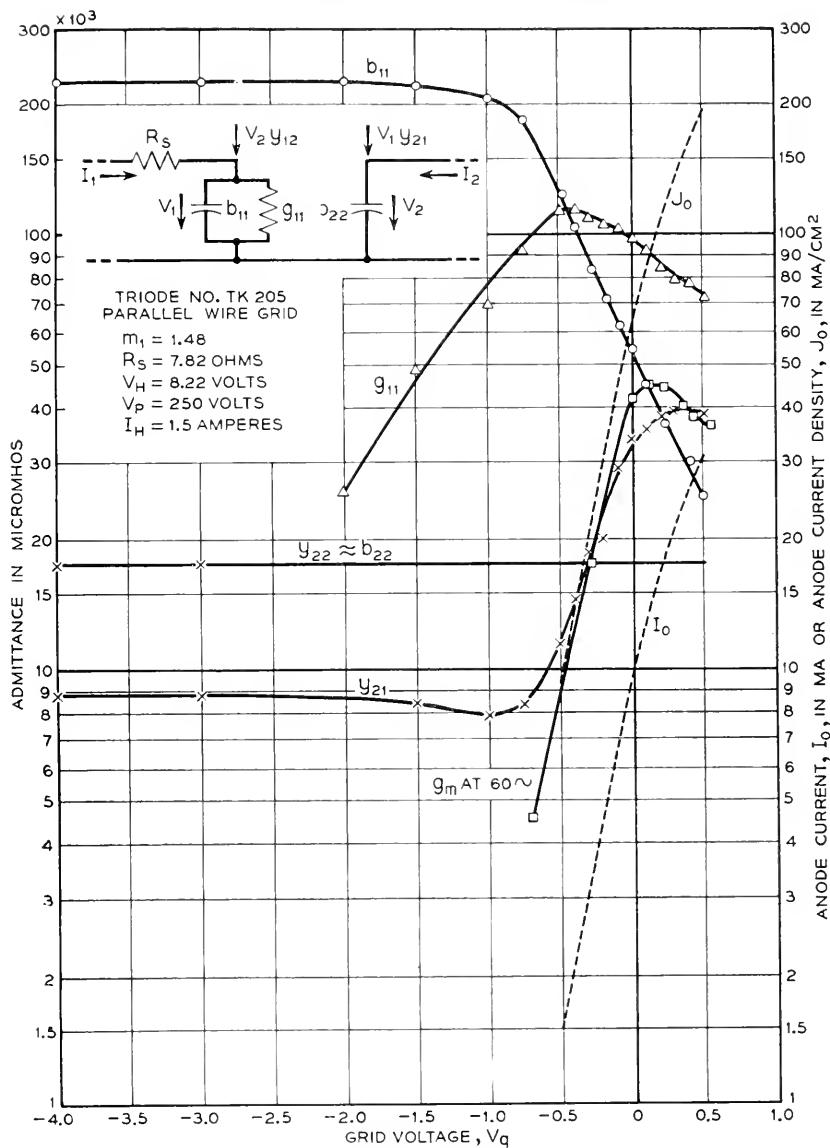


Fig. 20—Four-pole admittances of a triode having a parallel-wire grid.

that  $y_{21}$  is much lower when this tube is biased beyond cutoff than in the previous case. The electromagnetic coupling is therefore much less for the mesh grid. This has also been treated in the above reference.<sup>21</sup> With high negative bias the feedback admittance  $y_{12}$  was substantially equal to  $y_{21}$

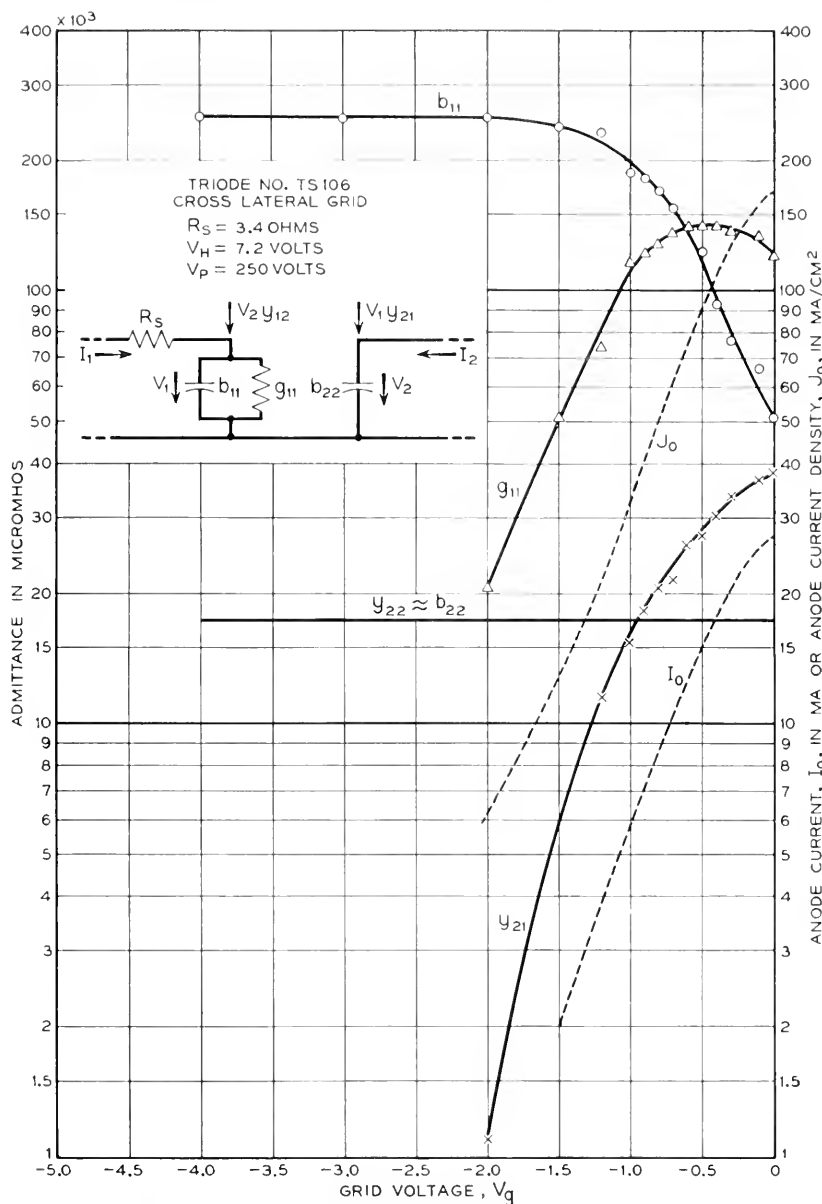


Fig. 21—Four-pole admittances of a triode having a cross-lateral grid.

but, as the current density increased,  $y_{12}$  tended to decrease. The feedback admittance was always lower for the mesh grid than for the parallel-wire grid.

The remaining parameters for the triode of Fig. 21 are very similar to those of Fig. 20.

Figure 22 shows the variation of the phase of the transadmittances  $y_{21}$  for the two triodes. The figure also shows the theoretical curve of the Llewellyn analysis for purposes of comparison. As in the case of Fig. 13 the abscissa do not represent transit time for the experimental values. The quantity  $x$  is equal to the cathode-grid spacing.

It is of interest to compare the triode measurements with those of the diode. It was expected that  $g_{11}$  for the triode should correspond with  $g$  for the diode. Within the limits of reasonable experimental accuracy this appears to be the case. For the triode at low frequencies  $g_0 \approx g_m$ . The triode

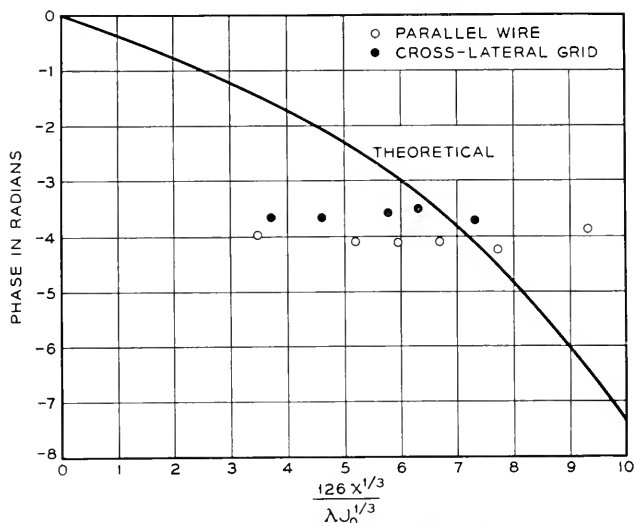


Fig. 22—Phase of triode transadmittance.

results indicate that the ratio  $g_{11}/g_m$  is quite comparable in magnitude with the corresponding ratio  $g/g_0$  for the diode. This was expected. The behavior of  $b_{11}$  for the triode was unexpected. It was thought that, as the grid voltage was varied so that the input space changed from a condition of zero space charge to one of maximum space charge,  $b_{11}$  would vary from its initial "cold" value to a value approaching 60% of the latter. This was not so. In the figures one observes that it drops to a much lower value. This effect has not been explained from a theoretical standpoint. There are several qualitative interpretations, but as yet no way of determining which of them is correct in a quantitative sense has been found. The observed phenomenon could, for example, be explained by an increase in the effective series resistance of the tube caused perhaps by an increase in the resistance of the

cathode coating.<sup>14</sup> Since the effect was not observed to such a marked degree in the case of the diodes, it seems probable that this is not the correct explanation.

It is probable that the observed variation in  $b_{11}$  is a space charge effect. It is evident in examining the diode curves that tubes which possessed the higher values for  $g_0$  exhibited a greater variation in  $b$ . If maximum  $g_0$  can be taken as a measure of the cathode activity, we can then perhaps relate the variation in susceptance with cathode activity and hence with the location of the potential minimum. A shift in the position of the potential minimum, however, may produce two effects. It varies the transit time of the electrons and changes the degree of space charge in the input space. Either effect might account for the variation of  $b_{11}$ . A clue to this effect might be discovered by making measurements on structures with different cathode-grid spacings.

The following experiments were performed to determine the effect of plate voltage on the input admittance of the triode of Fig. 20. The plate and grid voltages were varied simultaneously in such a way that the sum of the direct currents to the grid and plate remained constant at 30 milliamperes corresponding to a current density of 184 ma/cm<sup>2</sup>. The input admittance did not vary from the value shown for this same current density in Fig. 20 even though the plate voltage was varied from 250 volts to 40 volts. In a second experiment the plate potential was maintained at -90 volts with respect to the cathode and the grid potential was varied such that the direct grid current varied over a range of 0 to 10 milliamperes. Again the admittances were found to be equal to those of Fig. 20 for the corresponding total currents. These two experiments suggest that, for a given geometry, the value of  $b_{11}$  is primarily a function of the total current density in the input circuit.

#### ACKNOWLEDGEMENT

The author wishes to acknowledge his indebtedness to the late Mr. A. E. Bowen who contributed valuable advice during the course of these experiments, to Messrs. J. A. Morton and M. E. Hines who provided the necessary tubes and testers which made this work possible, and to Mr. F. A. Braun who played an indispensable role in the taking and reduction of data.

#### REFERENCES

1. "Electron Inertia Effects," F. B. Llewellyn, Cambridge University Press.
2. "Equivalent Networks of Negative Grid Vacuum Tubes at Ultra-High Frequencies," F. B. Llewellyn, *B. S. T. J.*, Vol. 15, pp. 565-586, October 1936.
3. "Operation of Ultra-High Frequency Vacuum Tubes," F. B. Llewellyn, *B. S. T. J.*, Vol. 14, pp. 632-665, October 1935.
4. "Theory of the Internal Action of Thermionic Systems at Moderately High Frequencies," W. E. Benham, *Phil. Mag.*, Vol. 5, pp. 641-662, March 1928; and Vol. 11 pp. 457-517, Feb. 1931.

5. "Vacuum-Tube Networks," F. B. Llewellyn and L. C. Peterson, *Proc. I. R. E.*, Vol. 32, no. 3, pp. 144-166, March 1944.
6. "Equivalent Circuits of Linear Active Four-Terminal Networks," L. C. Peterson, *B. S. T. J.*, Vol. XXVII, No. 4, pp. 593-622, October 1948.
7. "Impedance Properties of Electron Streams," L. C. Peterson, *B. S. T. J.*, Vol. 18, pp. 465-481, July 1939.
8. "Klystron and Microwave Triodes," Hamilton, Knipp and Kuper, pp. 97-169, *Radiation Laboratory Series*, Vol. 7, McGraw-Hill, 1948.
9. "High-Frequency Total Emission Loading in Diodes," Nicholas A. Begovich, *Journal Applied Physics*, Vol. 20, No. 5, pp. 457-461, May 1949.
10. "On the Velocity-Dependent Characteristics of High-Frequency Tubes," Julian K. Knipp, *Journal Applied Physics*, Vol. 20, No. 5, pp. 425-431, May 1949.
11. I. Langmuir, *Phys. Rev.*, 21, pp. 419-435, 1923.
12. "Extension and Application of Langmuir's Calculations on a Phase Diode with Maxwellian Velocity Distribution of the Electrons," A. Van Der Ziel, *Philips Research Reports*, Vol. 1, No. 2, pp. 97-118, January 1946.
13. "Extension of Langmuir's ( $\xi, \eta$ ) Tables for a Plane Diode with a Maxwellian Distribution of the Electrons," P. H. J. A. Klegmen, *Philips Research Reports*, Vol. 1, No. 2, January 1946, pp. 81-96.
14. "Some Characteristics of Diodes with Oxide-Coated Cathodes," W. R. Ferris, *R. C. A. Review*, Vol. X, No. 1, pp. 134-149, March 1949.
15. "A Microwave Triode for Radio Relay," J. A. Morton, *Bell Laboratories Record*, Vol. XXVII, No. 5, May 1949.
16. "Transadmittance and Input Conductance of a Lighthouse Triode at 3000 Megacycles," Norman T. Lavoo, *Proc. I. R. E.*, Vol. 35, No. 11, pp. 1248-1251, November 1947.
17. "Total Emission Damping in Diodes," A. Van Der Ziel, *Nature*, Vol. 159, No. 4046, May 17, 1947, pp. 675-676, (52 mc).
18. "Total Emission Damping," J. Thomson, *Nature*, Vol. 161, No. 4100, pp. 847, May 29, 1948.
19. "Total Emission Damping with Space-Charge Limited Cathodes," C. N. Smyth, *Nature*, 157, 841, June 22, 1946.
20. "A Method of Measuring Phase at Microwave Frequencies," S. D. Robertson, *B. S. T. J.*, Vol. XXVIII, No. 1, pp. 99-103, January 1949.
21. "Passive Four-Pole Admittance of Microwave Triodes," S. D. Robertson, this issue of the *B. S. T. J.*
22. "Total Emission Noise in Diodes," A. Van Der Ziel and A. Versnel, *Nature*, Vol. 159, No. 4045, pp. 640-641, May 10, 1947.
23. "Ultra-High-Frequency Oscillations by Means of Diodes," F. B. Llewellyn and A. E. Bowen, *B. S. T. J.*, Vol. 18, pp. 280-291, April 1939.

## Passive Four-Pole Admittances of Microwave Triodes

By SLOAN D. ROBERTSON

Measurements have been made of the passive, four-pole admittances of parallel-plane triodes over a wide range of cathode-to-grid and grid-to-plate spacings at a frequency of 4060 megacycles. Results are given for a parallel wire grid and a cross-lateral grid. The microwave transadmittances are found to be much higher than the values measured at low frequencies.

**D**URING the course of an experimental study of the active four-pole admittances<sup>1</sup> of the 1553 close-spaced triode,<sup>2</sup> a question arose as to whether the grid wires were introducing any appreciable inductance or resistance in the circuit used for measurement. It appeared necessary, therefore, to learn something of the passive four-pole parameters of the triode in order to separate the electronic from the passive admittances. It was generally believed that the electrostatic analyses of the passive admittances which have been successfully applied at the lower frequencies would no longer be valid with close-spaced structures at microwave frequencies. For example, it was considered possible that the grid wires themselves might possess an effective inductive reactance, so that the admittances between the grid and cathode or between the grid and anode might not be equal to the values computed from the electrostatic capacitances. Moreover, it was thought likely that energy might be transmitted from the cathode-grid region to the cathode-plate region or vice versa, not only by the medium of the electrostatic coupling, but also by means of an electromagnetic coupling through the grid. The measurements to be reported below indicate that the first of these conjectures was false, but that the second was true.

In view of the lack of available information on these questions in general, it seemed highly desirable to employ the available measuring equipment, not only to determine the passive parameters of a triode having electrode spacings corresponding with those of the 1553, but to extend the scope of the measurements to include a wide range of electrode spacings in order that the results would be of more general interest.

Although these measurements were in principle very simple, in practice the mechanical problem of achieving the desired degree of accuracy proved rather difficult. It was required that the cathode, grid, and anode planes be almost perfectly parallel and that the spacings between them be adjustable

<sup>1</sup> S. D. Robertson, "Electronic Admittances of Parallel-Plane Electron Tubes at 4000 Megacycles," this issue of the *B. S. T. J.*

<sup>2</sup> J. A. Morton, "A Microwave Triode for Radio Relay," *Bell Laboratories Record*, Vol. XXVII, No. 5, pp. 166-170, May 1949.

to specific values with a high degree of precision. In order to equal the dimensional tolerances of the 1553 it was necessary that parallelism and spacing be accurate to 0.1 mil.

A schematic diagram of the apparatus is shown in Fig. 1. A flat, circular disc having a 250-mil diameter aperture, across which the grid was stretched, was mounted upon the face of the hollow micrometer screw #1. The latter was mounted so that its face was accurately parallel with the end face of the central conductor of the input coaxial line in the upper part of the figure. By means of the micrometer #1 the input spacing  $S_1$ , which we shall consider as representing the cathode-grid spacing, could be adjusted. The central conductor of the coaxial line was insulated at d.c. from the outer conductor; hence it was possible to use an ohmmeter to indicate when the grid was just touching the coaxial face. The micrometer could then be backed away from the grid by any desired amount. The input coaxial was fitted with a standing wave detector in the form of a probe which could be moved along the line and placed at any arbitrary distance  $h$  from the grid.

On the output side of the circuit, in the lower part of the figure, there was another coaxial line arranged so that its center conductor could be driven by micrometer #2. The latter was insulated from the outer conductor of the coaxial by means of a condenser in order that an ohmmeter could be used to determine the position of the micrometer which caused the central conductor to just touch the grid. Spacing  $S_2$  could then be adjusted. The output coaxial line was terminated in its characteristic impedance of 62 ohms. At a distance of  $\lambda/2$  from the grid a probe was located for sampling the power in the output line.

The diameter of the input coaxial conductor was 180 mils at the end. In the figure it will be noted that at a short distance from the end the diameter increased to a larger diameter (250 mils). Because of the required length of the central conductor, it was necessary to increase its size in this way for mechanical rigidity. The effect of this change in cross-section was computed and allowed for in the final results. The output coaxial conductor was relatively short, so that it was possible to assign a diameter of 180 mils for its entire length. The 180-mil diameter was selected to correspond with the diameters of the cathode and anode in the 1553 triode.

The procedure for making the measurements was as follows: With a particular set of spacings  $S_1$  and  $S_2$  the standing wave ratio in the input line was measured. This ratio, together with the measurement of the position of a standing wave minimum, permitted the calculation of an input admittance  $Y$  to be made. Then with the standing wave detector probe placed at a distance  $h = \lambda/2$  from the grid, the ratio of the voltage at the input terminals of the triode to the voltage appearing at the output probe was measured both as to magnitude and phase as described in a recent



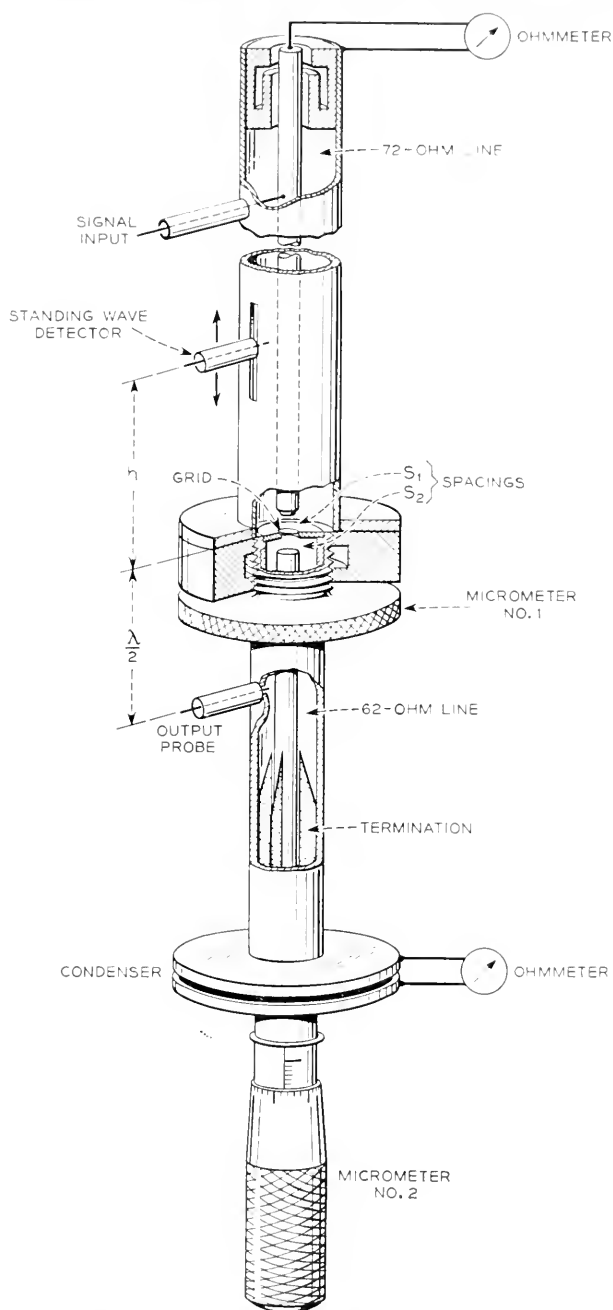


Fig. 1—Apparatus for measuring passive admittances of triode.

paper.<sup>3</sup> This quantity will be called  $\gamma$ . These measurements were sufficient for an evaluation of the four-pole parameters of the structure. All measurements were made at a frequency of 4060 megacycles.

The equivalent circuit of the passive triode structure is shown in Fig. 2. The desired parameters are  $y_{11}$ ,  $y_{12}$ , and  $y_{22}$ . The following equations indi-

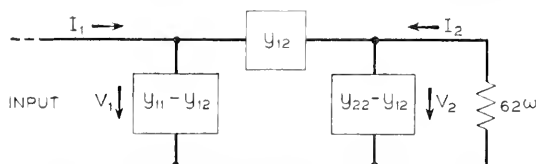


Fig. 2—Equivalent passive circuit of a triode.

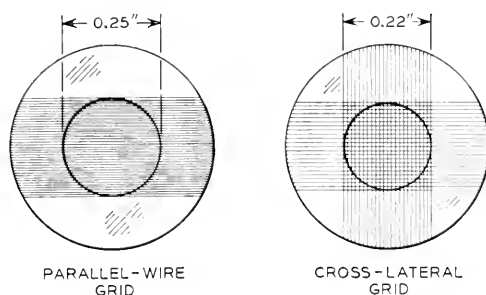


Fig. 3—Types of grids used in the measurements.

cate the relation between these parameters and the measured quantities  $Y$  and  $\gamma$ :

$$y_{11} = Y + \frac{62y_{12}^2}{62y_{22} + 1} \approx Y \quad (1)$$

$$y_{12} = \frac{y_{22}}{\gamma} \left[ 1 + \frac{1}{62y_{22}} \right] \quad (2)$$

where the number 62 represents the output terminating impedance. For all cases to be described here the second term on the right side of Equation 1 is small in comparison with  $Y$ . This is a result of the small values encountered for  $y_{12}$ . To a good approximation  $y_{11}$  is equal to the measured input admittance  $Y$ . This was verified by observing the variation in input admittance as the output spacing was varied while keeping the input spacing fixed. Only a slight variation in admittance was observed, which indicated that the fractional term in Equation 1 was small in comparison with  $Y$ .

Suppose, then, that for a given input and output spacing  $S_1$  and  $S_2$ ,

<sup>3</sup> "A Method of Measuring Phase at Microwave Frequencies," S. D. Robertson, *Bell System Technical Journal*, Vol. XXVIII, No. 1, pp. 99-103, January 1949.

$Y$  and  $\gamma$  are known.  $y_{22}$  can readily be determined by readjusting the input spacing to equal the output spacing and measuring a second admittance  $Y'$ .  $y_{22}$  will be approximately equal to this value. There is, then, sufficient information to compute  $y_{12}$ .

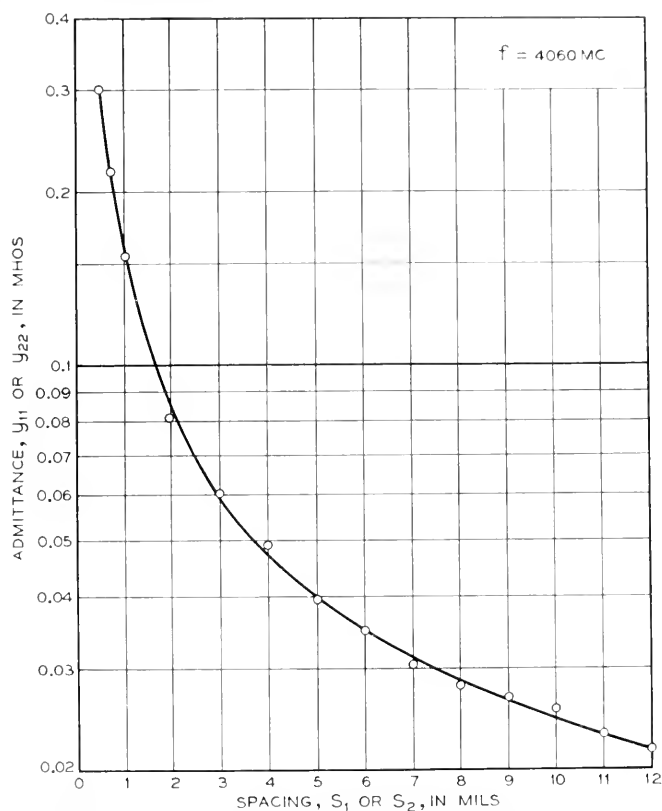


Fig. 4—Variation of passive input and output admittances with spacing.

Two grids were used in this work. The first was a parallel wire grid of 0.3 mil tungsten wire wound at 1000 turns per inch. The second was also of 0.3 mil tungsten wound in a crisscross fashion at 550 turns per inch. Both grids are shown in Fig. 3. It will be noted that the cross-lateral grid has an aperture 220 mils in diameter.

The values of  $y_{11}$  and  $y_{22}$  were found to be almost purely capacitive and were the same for both types of grid. These values are shown in Fig. 4.  $y_{11}$  and  $y_{22}$  correspond to capacitances  $C_{11}$  and  $C_{22}$ , which agree surprisingly well with the calculated capacitances between the grid and cathode, and grid and plate planes, respectively. Figure 5 shows the experimentally

determined values of  $C_{11}$  and  $C_{22}$  plotted as a dashed curve. The theoretical values (neglecting fringing capacitance) are shown by the solid curve. Since fringing was neglected, it is not surprising that the measured capacitances should exceed the calculated values by the amount shown.

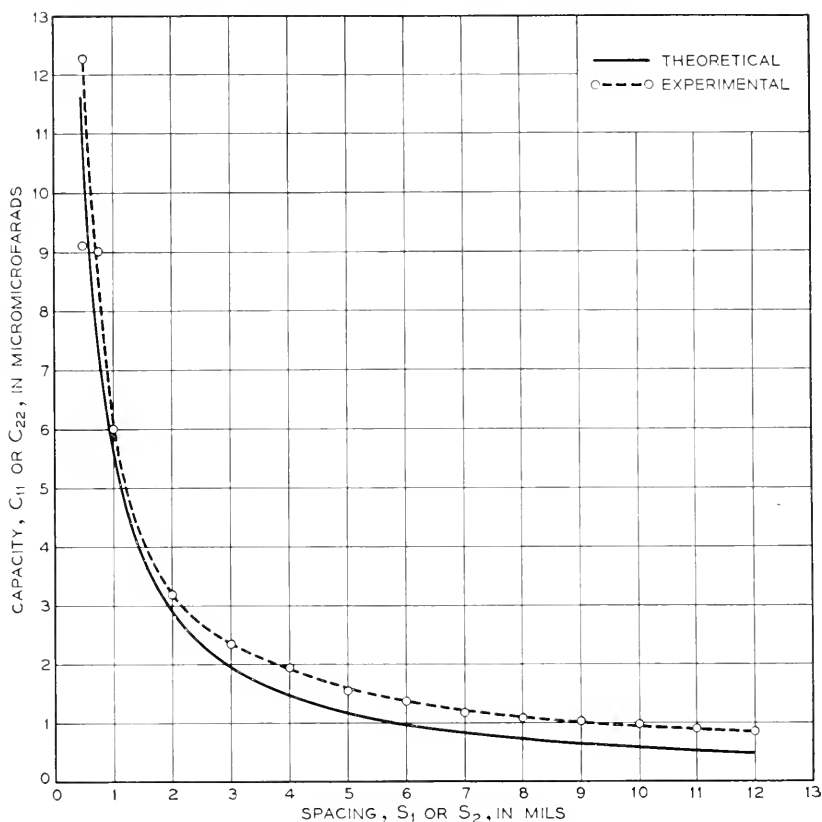


Fig. 5—Comparison of theoretical and experimental values of input and output capacitances.

The magnitudes of  $y_{12}$  for each grid over a range of values of  $S_1$  and  $S_2$  are shown in Figs. 6 and 7. It will be noted that, for a given set of spacings  $S_1$  and  $S_2$ ,  $y_{12}$  is much greater for the parallel wire grid than for the cross-lateral. This is the sort of result one would expect if  $y_{12}$  resulted from electromagnetic coupling through the grid, since the parallel wire grid would be expected to offer a better transmission path than the cross-lateral grid. It was not practicable with the equipment used in these experiments to measure the values of  $y_{12}$  at low frequencies where  $y_{12}$  would be determined by the cathode-plate capacitance. Data were available, however, for the low-frequency, cathode-plate capacitance of the standard, parallel-wire

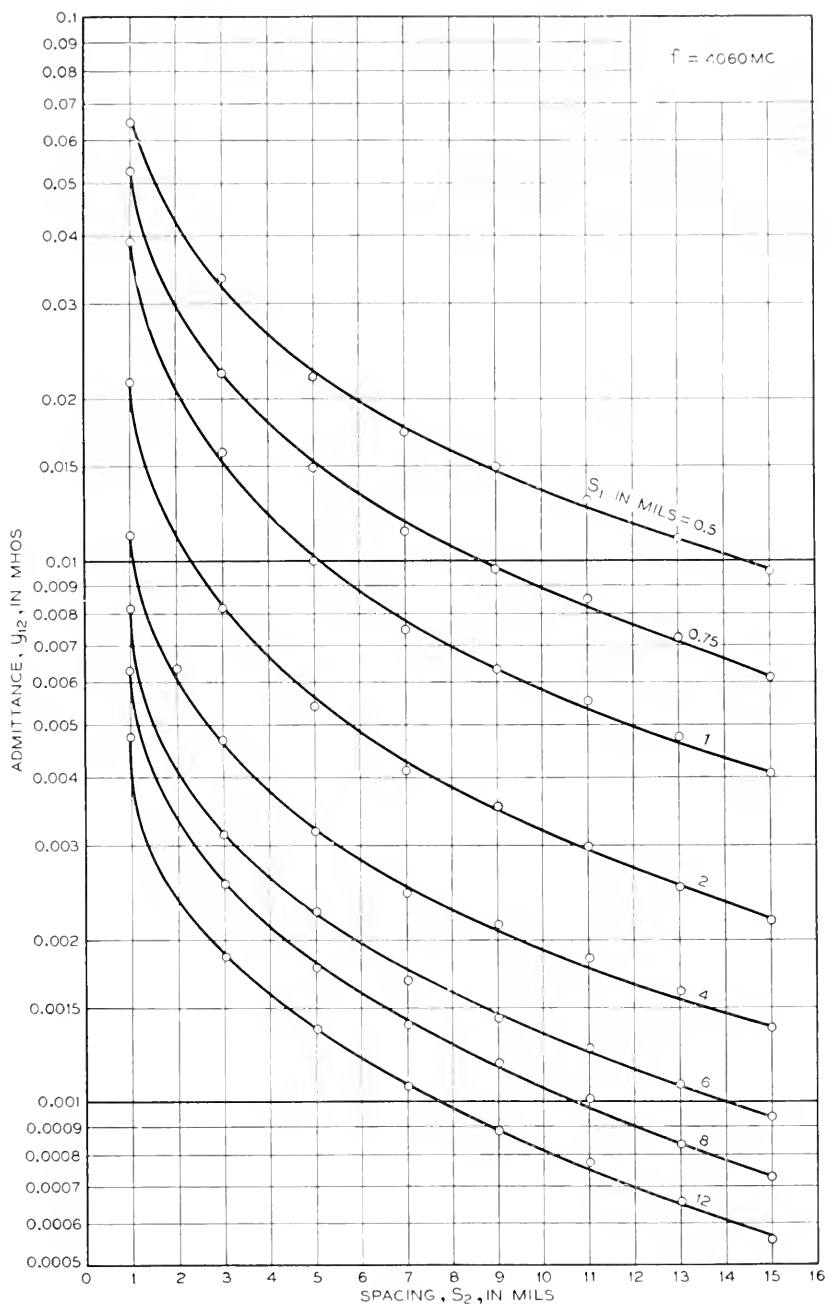


Fig. 6—Passive transadmittances of a triode having a parallel wire grid of 0.3 mil wire wound at 1000 turns per inch.

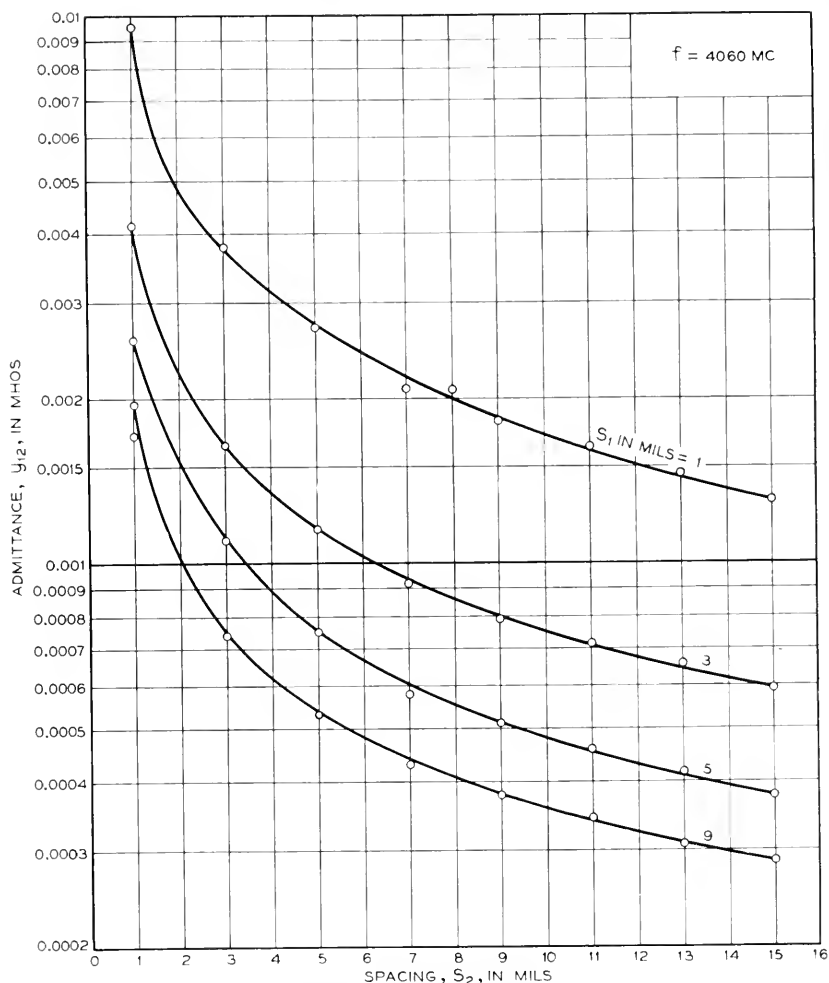


Fig. 7—Passive transmittances of a triode having a cross-lateral grid of 0.3 mil wire wound at 550 turns per inch.

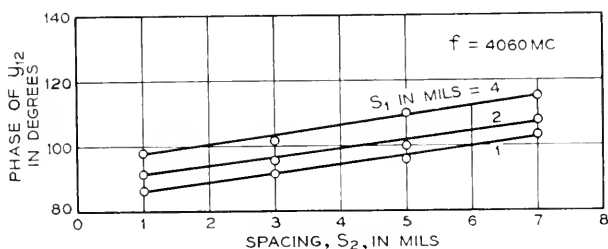


Fig. 8—Phase of the transmittance of the parallel-wire grid.

grid, 1553 triode having input and output spacings of 0.5 and 12 mils respectively. The capacitances averaged about  $0.008 \mu\mu\text{f}$ , which would correspond to a value of  $y_{12}$  of 0.0002 mho at 4060 megacycles. The latter is about 50 times lower than the measured 4060 megacycle value. Evidently, therefore, electromagnetic coupling plays a dominant role.

Reciprocity should give a reasonable idea of the accuracy of these measurements. Thus, for  $S_1 = 0.001''$  and  $S_2 = 0.012''$ , one would expect the same  $y_{12}$  as for the case where  $S_1 = 0.012''$  and  $S_2 = 0.001''$ . An examination of the data will indicate that the reciprocal differences are of the order of 10% in some cases. These differences may be partly the result of the change in line cross section encountered in going from the input to the output. That is to say, the two cases being compared are not quite reciprocal in geometry.

Figure 8 shows the phase of  $y_{12}$  for the parallel wire grid. Because of the low transmission through the grids there was not sufficient energy to determine the transfer phases with any very great accuracy, particularly for wide spacings in the case of the parallel wire grid and for all spacings in the case of the cross-lateral. Consequently, Fig. 8 shows only those results which are believed to be reasonably accurate.

The author wishes to acknowledge the contribution of Mr. F. A. Braun who ably assisted in this work.

# Communication Theory of Secrecy Systems\*

By C. E. SHANNON

## 1. INTRODUCTION AND SUMMARY

THE problems of cryptography and secrecy systems furnish an interesting application of communication theory.<sup>1</sup> In this paper a theory of secrecy systems is developed. The approach is on a theoretical level and is intended to complement the treatment found in standard works on cryptography.<sup>2</sup> There, a detailed study is made of the many standard types of codes and ciphers, and of the ways of breaking them. We will be more concerned with the general mathematical structure and properties of secrecy systems.

The treatment is limited in certain ways. First, there are three general types of secrecy system: (1) concealment systems, including such methods as invisible ink, concealing a message in an innocent text, or in a fake covering cryptogram, or other methods in which the existence of the message is concealed from the enemy; (2) privacy systems, for example speech inversion, in which special equipment is required to recover the message; (3) "true" secrecy systems where the meaning of the message is concealed by cipher, code, etc., although its existence is not hidden, and the enemy is assumed to have any special equipment necessary to intercept and record the transmitted signal. We consider only the third type—concealment systems are primarily a psychological problem, and privacy systems a technological one.

Secondly, the treatment is limited to the case of discrete information, where the message to be enciphered consists of a sequence of discrete symbols, each chosen from a finite set. These symbols may be letters in a language, words of a language, amplitude levels of a "quantized" speech or video signal, etc., but the main emphasis and thinking has been concerned with the case of letters.

The paper is divided into three parts. The main results will now be briefly summarized. The first part deals with the basic mathematical structure of secrecy systems. As in communication theory a language is considered to

\* The material in this paper appeared originally in a confidential report "A Mathematical Theory of Cryptography" dated Sept. 1, 1945, which has now been declassified.

<sup>1</sup> Shannon, C. E., "A Mathematical Theory of Communication," *Bell System Technical Journal*, July 1948, p. 379; Oct. 1948, p. 623.

<sup>2</sup> See, for example, H. F. Gaines, "Elementary Cryptanalysis," or M. Givierge, "Cours de Cryptographie."



be represented by a stochastic process which produces a discrete sequence of symbols in accordance with some system of probabilities. Associated with a language there is a certain parameter  $D$  which we call the redundancy of the language.  $D$  measures, in a sense, how much a text in the language can be reduced in length without losing any information. As a simple example, since  $u$  always follows  $q$  in English words, the  $u$  may be omitted without loss. Considerable reductions are possible in English due to the statistical structure of the language, the high frequencies of certain letters or words, etc. Redundancy is of central importance in the study of secrecy systems.

A secrecy system is defined abstractly as a set of transformations of one space (the set of possible messages) into a second space (the set of possible cryptograms). Each particular transformation of the set corresponds to enciphering with a particular key. The transformations are supposed reversible (non-singular) so that unique deciphering is possible when the key is known.

Each key and therefore each transformation is assumed to have an *a priori* probability associated with it—the probability of choosing that key. Similarly each possible message is assumed to have an associated *a priori* probability, determined by the underlying stochastic process. These probabilities for the various keys and messages are actually the enemy cryptanalyst's *a priori* probabilities for the choices in question, and represent his *a priori* knowledge of the situation.

To use the system a key is first selected and sent to the receiving point. The choice of a key determines a particular transformation in the set forming the system. Then a message is selected and the particular transformation corresponding to the selected key applied to this message to produce a cryptogram. This cryptogram is transmitted to the receiving point by a channel and may be intercepted by the "enemy\*." At the receiving end the inverse of the particular transformation is applied to the cryptogram to recover the original message.

If the enemy intercepts the cryptogram he can calculate from it the *a posteriori* probabilities of the various possible messages and keys which might have produced this cryptogram. This set of *a posteriori* probabilities constitutes his knowledge of the key and message after the interception. "Knowledge" is thus identified with a set of propositions having associated probabilities. The calculation of the *a posteriori* probabilities is the generalized problem of cryptanalysis.

As an example of these notions, in a simple substitution cipher with random key there are  $26!$  transformations, corresponding to the  $26!$  ways we

\*The word "enemy," stemming from military applications, is commonly used in cryptographic work to denote anyone who may intercept a cryptogram.

can substitute for 26 different letters. These are all equally likely and each therefore has an *a priori* probability  $1/26!$ . If this is applied to "normal English" the cryptanalyst being assumed to have no knowledge of the message source other than that it is producing English text, the *a priori* probabilities of various messages of  $N$  letters are merely their relative frequencies in normal English text.

If the enemy intercepts  $N$  letters of cryptogram in this system his probabilities change. If  $N$  is large enough (say 50 letters) there is usually a single message of *a posteriori* probability nearly unity, while all others have a total probability nearly zero. Thus there is an essentially unique "solution" to the cryptogram. For  $N$  smaller (say  $N = 15$ ) there will usually be many messages and keys of comparable probability, with no single one nearly unity. In this case there are multiple "solutions" to the cryptogram.

Considering a secrecy system to be represented in this way, as a set of transformations of one set of elements into another, there are two natural combining operations which produce a third system from two given systems. The first combining operation is called the product operation and corresponds to enciphering the message with the first secrecy system  $R$  and enciphering the resulting cryptogram with the second system  $S$ , the keys for  $R$  and  $S$  being chosen independently. This total operation is a secrecy system whose transformations consist of all the products (in the usual sense of products of transformations) of transformations in  $S$  with transformations in  $R$ . The probabilities are the products of the probabilities for the two transformations.

The second combining operation is "weighted addition."

$$T = pR + qS \qquad p + q = 1$$

It corresponds to making a preliminary choice as to whether system  $R$  or  $S$  is to be used with probabilities  $p$  and  $q$ , respectively. When this is done  $R$  or  $S$  is used as originally defined.

It is shown that secrecy systems with these two combining operations form essentially a "linear associative algebra" with a unit element, an algebraic variety that has been extensively studied by mathematicians.

Among the many possible secrecy systems there is one type with many special properties. This type we call a "pure" system. A system is pure if all keys are equally likely and if for any three transformations  $T_i$ ,  $T_j$ ,  $T_k$  in the set the product

$$T_i T_j^{-1} T_k$$

is also a transformation in the set. That is enciphering, deciphering, and enciphering with any three keys must be equivalent to enciphering with some key.

With a pure cipher it is shown that all keys are essentially equivalent—they all lead to the same set of *a posteriori* probabilities. Furthermore, when a given cryptogram is intercepted there is a set of messages that might have produced this cryptogram (a “residue class”) and the *a posteriori* probabilities of messages in this class are proportional to the *a priori* probabilities. All the information the enemy has obtained by intercepting the cryptogram is a specification of the residue class. Many of the common ciphers are pure systems, including simple substitution with random key. In this case the residue class consists of all messages with the same pattern of letter repetitions as the intercepted cryptogram.

Two systems  $R$  and  $S$  are defined to be “similar” if there exists a fixed transformation  $A$  with an inverse,  $A^{-1}$ , such that

$$R = AS.$$

If  $R$  and  $S$  are similar, a one-to-one correspondence between the resulting cryptograms can be set up leading to the same *a posteriori* probabilities. The two systems are crypt analytically the same.

The second part of the paper deals with the problem of “theoretical secrecy.” How secure is a system against cryptanalysis when the enemy has unlimited time and manpower available for the analysis of intercepted cryptograms? The problem is closely related to questions of communication in the presence of noise, and the concepts of entropy and equivocation developed for the communication problem find a direct application in this part of cryptography.

“Perfect Secrecy” is defined by requiring of a system that after a cryptogram is intercepted by the enemy the *a posteriori* probabilities of this cryptogram representing various messages be identically the same as the *a priori* probabilities of the same messages before the interception. It is shown that perfect secrecy is possible but requires, if the number of messages is finite, the same number of possible keys. If the message is thought of as being constantly generated at a given “rate”  $R$  (to be defined later), key must be generated at the same or a greater rate.

If a secrecy system with a finite key is used, and  $N$  letters of cryptogram intercepted, there will be, for the enemy, a certain set of messages with certain probabilities, that this cryptogram could represent. As  $N$  increases the field usually narrows down until eventually there is a unique “solution” to the cryptogram; one message with probability essentially unity while all others are practically zero. A quantity  $H(N)$  is defined, called the equivocation, which measures in a statistical way how near the average cryptogram of  $N$  letters is to a unique solution; that is, how uncertain the enemy is of the original message after intercepting a cryptogram of  $N$  letters. Various properties of the equivocation are deduced—for example, the equivocation

of the key never increases with increasing  $N$ . This equivocation is a theoretical secrecy index—theoretical in that it allows the enemy unlimited time to analyse the cryptogram.

The function  $H(N)$  for a certain idealized type of cipher called the random cipher is determined. With certain modifications this function can be applied to many cases of practical interest. This gives a way of calculating approximately how much intercepted material is required to obtain a solution to a secrecy system. It appears from this analysis that with ordinary languages and the usual types of ciphers (not codes) this “unicity distance” is approximately  $H(K)/D$ . Here  $H(K)$  is a number measuring the “size” of the key space. If all keys are *a priori* equally likely  $H(K)$  is the logarithm of the number of possible keys.  $D$  is the redundancy of the language and measures the amount of “statistical constraint” imposed by the language. In simple substitution with random key  $H(K)$  is  $\log_{10} 26!$  or about 20 and  $D$  (in decimal digits per letter) is about .7 for English. Thus unicity occurs at about 30 letters.

It is possible to construct secrecy systems with a finite key for certain “languages” in which the equivocation does not approach zero as  $N \rightarrow \infty$ . In this case, no matter how much material is intercepted, the enemy still does not obtain a unique solution to the cipher but is left with many alternatives, all of reasonable probability. Such systems we call *ideal* systems. It is possible in any language to approximate such behavior—i.e., to make the approach to zero of  $H(N)$  recede out to arbitrarily large  $N$ . However, such systems have a number of drawbacks, such as complexity and sensitivity to errors in transmission of the cryptogram.

The third part of the paper is concerned with “practical secrecy.” Two systems with the same key size may both be uniquely solvable when  $N$  letters have been intercepted, but differ greatly in the amount of labor required to effect this solution. An analysis of the basic weaknesses of secrecy systems is made. This leads to methods for constructing systems which will require a large amount of work to solve. Finally, a certain incompatibility among the various desirable qualities of secrecy systems is discussed.

## PART I

### MATHEMATICAL STRUCTURE OF SECRECY SYSTEMS

#### 2. SECRECY SYSTEMS

As a first step in the mathematical analysis of cryptography, it is necessary to idealize the situation suitably, and to define in a mathematically acceptable way what we shall mean by a secrecy system. A “schematic” diagram of a general secrecy system is shown in Fig. 1. At the transmitting

end there are two information sources—a message source and a key source. The key source produces a particular key from among those which are possible in the system. This key is transmitted by some means, supposedly not interceptible, for example by messenger, to the receiving end. The message source produces a message (the “clear”) which is enciphered and the resulting cryptogram sent to the receiving end by a possibly interceptible means, for example radio. At the receiving end the cryptogram and key are combined in the decipherer to recover the message.

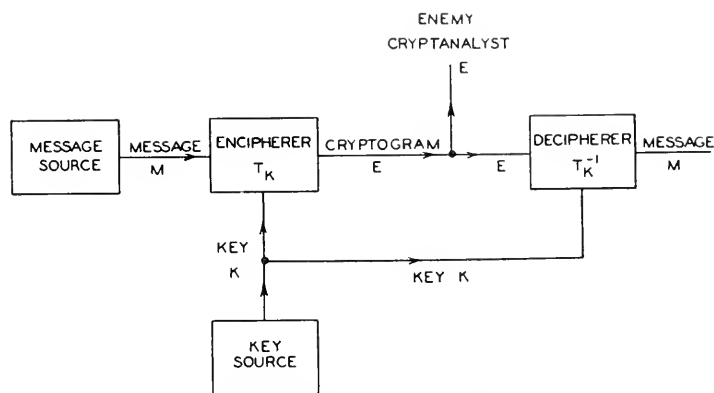


Fig. 1—Schematic of a general secrecy system.

Evidently the encipherer performs a functional operation. If  $M$  is the message,  $K$  the key, and  $E$  the enciphered message, or cryptogram, we have

$$E = f(M, K)$$

that is  $E$  is a function of  $M$  and  $K$ . It is preferable to think of this, however, not as a function of two variables but as a (one parameter) family of operations or transformations, and to write it

$$E = T_i M.$$

The transformation  $T_i$  applied to message  $M$  produces cryptogram  $E$ . The index  $i$  corresponds to the particular key being used.

We will assume, in general, that there are only a finite number of possible keys, and that each has an associated probability  $p_i$ . Thus the key source is represented by a statistical process or device which chooses one from the set of transformations  $T_1, T_2, \dots, T_m$  with the respective probabilities  $p_1, p_2, \dots, p_m$ . Similarly we will generally assume a finite number of possible messages  $M_1, M_2, \dots, M_n$  with associated *a priori* probabilities  $q_1, q_2, \dots, q_n$ . The possible messages, for example, might be the possible sequences of English letters all of length  $N$ , and the associated probabilities are then

the relative frequencies of occurrence of these sequences in normal English text.

At the receiving end it must be possible to recover  $M$ , knowing  $E$  and  $K$ . Thus the transformations  $T_i$  in the family must have unique inverses  $T_i^{-1}$  such that  $T_i T_i^{-1} = I$ , the identity transformation. Thus:

$$M = T_i^{-1}E.$$

At any rate this inverse must exist uniquely for every  $E$  which can be obtained from an  $M$  with key  $i$ . Hence we arrive at the definition: A secrecy system is a family of uniquely reversible transformations  $T_i$  of a set of possible messages into a set of cryptograms, the transformation  $T_i$  having an associated probability  $p_i$ . Conversely any set of entities of this type will be called a "secrecy system." The set of possible messages will be called, for convenience, the "message space" and the set of possible cryptograms the "cryptogram space."

Two secrecy systems will be the same if they consist of the same set of transformations  $T_i$ , with the same message and cryptogram space (range and domain) and the same probabilities for the keys.

A secrecy system can be visualized mechanically as a machine with one or more controls on it. A sequence of letters, the message, is fed into the input of the machine and a second series emerges at the output. The particular setting of the controls corresponds to the particular key being used. Some statistical method must be prescribed for choosing the key from all the possible ones.

To make the problem mathematically tractable we shall assume that *the enemy knows the system being used*. That is, he knows the family of transformations  $T_i$ , and the probabilities of choosing various keys. It might be objected that this assumption is unrealistic, in that the cryptanalyst often does not know what system was used or the probabilities in question. There are two answers to this objection:

1. The restriction is much weaker than appears at first, due to our broad definition of what constitutes a secrecy system. Suppose a cryptographer intercepts a message and does not know whether a substitution, transposition, or Vigenère type cipher was used. He can consider the message as being enciphered by a system in which part of the key is the specification of which of these types was used, the next part being the particular key for that type. These three different possibilities are assigned probabilities according to his best estimates of the *a priori* probabilities of the encipherer using the respective types of cipher.
2. The assumption is actually the one ordinarily used in cryptographic studies. It is pessimistic and hence safe, but in the long run realistic, since one must expect his system to be found out eventually. Thus,

even when an entirely new system is devised, so that the enemy cannot assign any *a priori* probability to it without discovering it himself, one must still live with the expectation of his eventual knowledge.

The situation is similar to that occurring in the theory of games<sup>3</sup> where it is assumed that the opponent "finds out" the strategy of play being used. In both cases the assumption serves to delineate sharply the opponent's knowledge.

A second possible objection to our definition of secrecy systems is that no account is taken of the common practice of inserting nulls in a message and the use of multiple substitutes. In such cases there is not a unique cryptogram for a given message and key, but the encipherer can choose at will from among a number of different cryptograms. This situation could be handled, but would only add complexity at the present stage, without substantially altering any of the basic results.

If the messages are produced by a Markoff process of the type described in (1) to represent an information source, the probabilities of various messages are determined by the structure of the Markoff process. For the present, however, we wish to take a more general view of the situation and regard the messages as merely an abstract set of entities with associated probabilities, not necessarily composed of a sequence of letters and not necessarily produced by a Markoff process.

It should be emphasized that throughout the paper a secrecy system means not one, but a set of many transformations. After the key is chosen only one of these transformations is used and one might be led from this to define a secrecy system as a single transformation on a language. The enemy, however, does not know what key was chosen and the "might have been" keys are as important for him as the actual one. Indeed it is only the existence of these other possibilities that gives the system any secrecy. Since the secrecy is our primary interest, we are forced to the rather elaborate concept of a secrecy system defined above. This type of situation, where possibilities are as important as actualities, occurs frequently in games of strategy. The course of a chess game is largely controlled by threats which are *not* carried out. Somewhat similar is the "virtual existence" of unrealized imputations in the theory of games.

It may be noted that a single operation on a language forms a degenerate type of secrecy system under our definition—a system with only one key of unit probability. Such a system has no secrecy—the cryptanalyst finds the message by applying the inverse of this transformation, the only one in the system, to the intercepted cryptogram. The decipherer and cryptanalyst in this case possess the same information. In general, the only difference between the decipherer's knowledge and the enemy cryptanalyst's knowledge

<sup>3</sup> See von Neumann and Morgenstern "The Theory of Games," Princeton 1947.

is that the decipherer knows the particular key being used, while the cryptanalyst knows only the *a priori* probabilities of the various keys in the set. The process of deciphering is that of applying the inverse of the particular transformation used in enciphering to the cryptogram. The process of cryptanalysis is that of attempting to determine the message (or the particular key) given only the cryptogram and the *a priori* probabilities of various keys and messages.

There are a number of difficult epistemological questions connected with the theory of secrecy, or in fact with any theory which involves questions of probability (particularly *a priori* probabilities, Bayes' theorem, etc.) when applied to a physical situation. Treated abstractly, probability theory can be put on a rigorous logical basis with the modern measure theory approach.<sup>4,5</sup> As applied to a physical situation, however, especially when "subjective" probabilities and unrepeatable experiments are concerned, there are many questions of logical validity. For example, in the approach to secrecy made here, *a priori* probabilities of various keys and messages are assumed known by the enemy cryptographer—how can one determine operationally if his estimates are correct, on the basis of his knowledge of the situation?

One can construct artificial cryptographic situations of the "urn and die" type in which the *a priori* probabilities have a definite unambiguous meaning and the idealization used here is certainly appropriate. In other situations that one can imagine, for example an intercepted communication between Martian invaders, the *a priori* probabilities would probably be so uncertain as to be devoid of significance. Most practical cryptographic situations lie somewhere between these limits. A cryptanalyst might be willing to classify the possible messages into the categories "reasonable," "possible but unlikely" and "unreasonable," but feel that finer subdivision was meaningless.

Fortunately, in practical situations, only extreme errors in *a priori* probabilities of keys and messages cause significant errors in the important parameters. This is because of the exponential behavior of the number of messages and cryptograms, and the logarithmic measures employed.

### 3. REPRESENTATION OF SYSTEMS

A secrecy system as defined above can be represented in various ways. One which is convenient for illustrative purposes is a line diagram, as in Figs. 2 and 4. The possible messages are represented by points at the left and the possible cryptograms by points at the right. If a certain key, say key 1, transforms message  $M_2$  into cryptogram  $E_4$  then  $M_2$  and  $E_4$  are connected

<sup>4</sup> See J. L. Doob, "Probability as Measure," *Annals of Math. Stat.*, v. 12, 1941, pp. 206-214.

<sup>5</sup> A. Kolmogoroff, "Grundbegriffe der Wahrscheinlichkeitsrechnung," *Ergebnisse der Mathematik*, v. 2, No. 3 (Berlin 1933).



by a line labeled 1, etc. From each possible message there must be exactly one line emerging for each different key. If the same is true for each cryptogram, we will say that the system is *closed*.

A more common way of describing a system is by stating the operation one performs on the message for an arbitrary key to obtain the cryptogram. Similarly, one defines implicitly the probabilities for various keys by describing how a key is chosen or what we know of the enemy's habits of key choice. The probabilities for messages are implicitly determined by stating our *a priori* knowledge of the enemy's language habits, the tactical situation (which will influence the probable content of the message) and any special information we may have regarding the cryptogram.

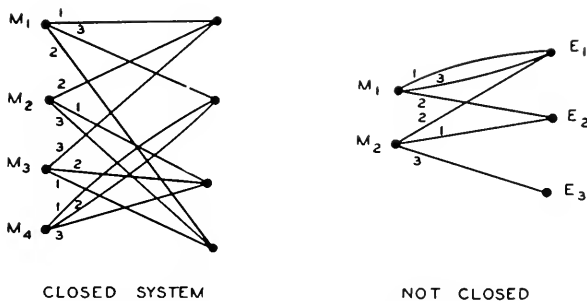


Fig. 2—Line drawings for simple systems.

#### 4. SOME EXAMPLES OF SECRECY SYSTEMS

In this section a number of examples of ciphers will be given. These will often be referred to in the remainder of the paper for illustrative purposes.

##### 1. Simple Substitution Cipher.

In this cipher each letter of the message is replaced by a fixed substitute, usually also a letter. Thus the message,

$$M = m_1 m_2 m_3 m_4 \dots$$

where  $m_1, m_2, \dots$  are the successive letters becomes:

$$\begin{aligned} E &= e_1 e_2 e_3 e_4 \dots \\ &= f(m_1) f(m_2) f(m_3) f(m_4) \dots \end{aligned}$$

where the function  $f(m)$  is a function with an inverse. The key is a permutation of the alphabet (when the substitutes are letters) e.g.  $X G U A C D T B F H R S L M Q V Y Z W I E J O K N P$ . The first letter  $X$  is the substitute for  $A$ ,  $G$  is the substitute for  $B$ , etc.

## 2. Transposition (Fixed Period $d$ ).

The message is divided into groups of length  $d$  and a permutation applied to the first group, the same permutation to the second group, etc. The permutation is the key and can be represented by a permutation of the first  $d$  integers. Thus, for  $d = 5$ , we might have 2 3 1 5 4 as the permutation. This means that:

$$\begin{array}{cccccccccccc} m_1 & m_2 & m_3 & m_4 & m_5 & m_6 & m_7 & m_8 & m_9 & m_{10} & \cdots & \text{becomes} \\ m_2 & m_3 & m_1 & m_5 & m_4 & m_7 & m_8 & m_6 & m_{10} & m_9 & \cdots & \end{array}$$

Sequential application of two or more transpositions will be called compound transposition. If the periods are  $d_1, d_2, \dots, d_s$  it is clear that the result is a transposition of period  $d$ , where  $d$  is the least common multiple of  $d_1, d_2, \dots, d_s$ .

## 3. Vigenère, and Variations.

In the Vigenère cipher the key consists of a series of  $d$  letters. These are written repeatedly below the message and the two added modulo 26 (considering the alphabet numbered from  $A = 0$  to  $Z = 25$ ). Thus

$$e_i = m_i + k_i \pmod{26}$$

where  $k_i$  is of period  $d$  in the index  $i$ . For example, with the key  $G A H$ , we obtain

message	$N O W I S T H E \cdots$
repeated key	$G A H G A H G A \cdots$
cryptogram	$T O D O S A N E \cdots$

The Vigenère of period 1 is called the Caesar cipher. It is a simple substitution in which each letter of  $M$  is advanced a fixed amount in the alphabet. This amount is the key, which may be any number from 0 to 25. The so-called Beaufort and Variant Beaufort are similar to the Vigenère, and encipher by the equations

$$e_i = k_i - m_i \pmod{26}$$

and

$$e_i = m_i - k_i \pmod{26}$$

respectively. The Beaufort of period one is called the reversed Caesar cipher.

The application of two or more Vigenères in sequence will be called the compound Vigenère. It has the equation

$$e_i = m_i + k_i + l_i + \cdots + s_i \pmod{26}$$

where  $k_i, l_i, \dots, s_i$  in general have different periods. The period of their sum,

$$k_i + l_i + \dots + s_i$$

as in compound transposition, is the least common multiple of the individual periods.

When the Vigenère is used with an unlimited key, never repeating, we have the Vernam system,<sup>6</sup> with

$$e_i = m_i + k_i \pmod{26}$$

the  $k_i$  being chosen at random and independently among 0, 1,  $\dots$ , 25. If the key is a meaningful text we have the "running key" cipher.

#### 4. Digram, Trigram, and $N$ -gram substitution.

Rather than substitute for letters one can substitute for digrams, tri-grams, etc. General digram substitution requires a key consisting of a permutation of the  $26^2$  digrams. It can be represented by a table in which the row corresponds to the first letter of the digram and the column to the second letter, entries in the table being the substitutes (usually also digrams).

#### 5. Single Mixed Alphabet Vigenère.

This is a simple substitution followed by a Vigenère.

$$\begin{aligned} e_i &= f(m_i) + k_i \\ m_i &= f^{-1}(e_i - k_i) \end{aligned}$$

The "inverse" of this system is a Vigenère followed by simple substitution

$$\begin{aligned} e_i &= g(m_i + k_i) \\ m_i &= g^{-1}(e_i) - k_i \end{aligned}$$

#### 6. Matrix System.<sup>7</sup>

One method of  $n$ -gram substitution is to operate on successive  $n$ -grams with a matrix having an inverse. The letters are assumed numbered from 0 to 25, making them elements of an algebraic ring. From the  $n$ -gram  $m_1 m_2 \dots m_n$  of message, the matrix  $a_{ij}$  gives an  $n$ -gram of cryptogram

$$e_i = \sum_{j=1}^n a_{ij} m_j \quad i = 1, \dots, n$$

<sup>6</sup> G. S. Vernam, "Cipher Printing Telegraph Systems for Secret Wire and Radio Telegraphic Communications," *Journal American Institute of Electrical Engineers*, v. XLV pp. 109-115, 1926.

<sup>7</sup> See L. S. Hill, "Cryptography in an Algebraic Alphabet," *American Math. Monthly*, v. 36, No. 6, 1, 1929, pp. 306-312; also "Concerning Certain Linear Transformation Apparatus of Cryptography," v. 38, No. 3, 1931, pp. 135-154.

The matrix  $a_{ij}$  is the key, and deciphering is performed with the inverse matrix. The inverse matrix will exist if and only if the determinant  $|a_{ij}|$  has an inverse element in the ring.

### 7. The Playfair Cipher.

This is a particular type of digram substitution governed by a mixed 25 letter alphabet written in a 5 x 5 square. (The letter *J* is often dropped in cryptographic work—it is very infrequent, and when it occurs can be replaced by *I*.) Suppose the key square is as shown below:

<i>L</i>	<i>Z</i>	<i>Q</i>	<i>C</i>	<i>P</i>
<i>A</i>	<i>G</i>	<i>N</i>	<i>O</i>	<i>U</i>
<i>R</i>	<i>D</i>	<i>M</i>	<i>I</i>	<i>F</i>
<i>K</i>	<i>Y</i>	<i>H</i>	<i>V</i>	<i>S</i>
<i>X</i>	<i>B</i>	<i>T</i>	<i>E</i>	<i>W</i>

The substitute for a digram *AC*, for example, is the pair of letters at the other corners of the rectangle defined by *A* and *C*, i.e., *LO*, the *L* taken first since it is above *A*. If the digram letters are on a horizontal line as *RI*, one uses the letters to their right *DF*; *RI* becomes *DR*. If the letters are on a vertical line, the letters below them are used. Thus *PS* becomes *UV*. If the letters are the same nulls may be used to separate them or one may be omitted, etc.

### 8. Multiple Mixed Alphabet Substitution.

In this cipher there are a set of  $d$  simple substitutions which are used in sequence. If the period  $d$  is four

$$m_1 m_2 m_3 m_4 m_5 m_6 \cdots$$

becomes

$$f_1(m_1) f_2(m_2) f_3(m_3) f_4(m_4) f_1(m_5) f_2(m_6) \cdots$$

### 9. Autokey Cipher.

A Vigenère type system in which either the message itself or the resulting cryptogram is used for the “key” is called an autokey cipher. The encipherment is started with a “priming key” (which is the entire key in our sense) and continued with the message or cryptogram displaced by the length of the priming key as indicated below, where the priming key is COMET. The message used as “key”:

Message	<i>S E N D S U P P L I E S</i> . . .
Key	<i>C O M E T S E N D S U P</i> . . .
Cryptogram	<i>U S Z H L M T C O A Y H</i>

The cryptogram used as "key":<sup>8</sup>

Message	<i>S E X D S U P P L I E S . . .</i>
Key	<i>C O M E T U S Z H L O H . . .</i>
Cryptogram	<i>U S Z H L O H O S T S . . .</i>

#### 10. *Fractional Ciphers.*

In these, each letter is first enciphered into two or more letters or numbers and these symbols are somehow mixed (e.g. by transposition). The result may then be retranslated into the original alphabet. Thus, using a mixed 25-letter alphabet for the key, we may translate letters into two-digit quinary numbers by the table:

0	1	2	3	4
0	<i>L</i>	<i>Z</i>	<i>Q</i>	<i>C P</i>
1	<i>A</i>	<i>G</i>	<i>N</i>	<i>O U</i>
2	<i>R</i>	<i>D</i>	<i>M</i>	<i>I F</i>
3	<i>K</i>	<i>Y</i>	<i>H</i>	<i>V S</i>
4	<i>X</i>	<i>B</i>	<i>T</i>	<i>E W</i>

Thus *B* becomes 41. After the resulting series of numbers is transposed in some way they are taken in pairs and translated back into letters.

#### 11. *Codes.*

In codes words (or sometimes syllables) are replaced by substitute letter groups. Sometimes a cipher of one kind or another is applied to the result.

### 5. VALUATIONS OF SECRECY SYSTEMS

There are a number of different criteria that should be applied in estimating the value of a proposed secrecy system. The most important of these are:

#### 1. *Amount of Secrecy.*

There are some systems that are perfect—the enemy is no better off after intercepting any amount of material than before. Other systems, although giving him some information, do not yield a unique "solution" to intercepted cryptograms. Among the uniquely solvable systems, there are wide variations in the amount of labor required to effect this solution and in the amount of material that must be intercepted to make the solution unique.

<sup>8</sup>This system is trivial from the secrecy standpoint since, with the exception of the first *d* letters, the enemy is in possession of the entire "key."

## 2. *Size of Key.*

The key must be transmitted by non-interceptible means from transmitting to receiving points. Sometimes it must be memorized. It is therefore desirable to have the key as small as possible.

## 3. *Complexity of Enciphering and Deciphering Operations.*

Enciphering and deciphering should, of course, be as simple as possible. If they are done manually, complexity leads to loss of time, errors, etc. If done mechanically, complexity leads to large expensive machines.

## 4. *Propagation of Errors.*

In certain types of ciphers an error of one letter in enciphering or transmission leads to a large number of errors in the deciphered text. The errors are spread out by the deciphering operation, causing the loss of much information and frequent need for repetition of the cryptogram. It is naturally desirable to minimize this error expansion.

## 5. *Expansion of Message.*

In some types of secrecy systems the size of the message is increased by the enciphering process. This undesirable effect may be seen in systems where one attempts to swamp out message statistics by the addition of many nulls, or where multiple substitutes are used. It also occurs in many "concealment" types of systems (which are not usually secrecy systems in the sense of our definition).

# 6. THE ALGEBRA OF SECRECY SYSTEMS

If we have two secrecy systems  $T$  and  $R$  we can often combine them in various ways to form a new secrecy system  $S$ . If  $T$  and  $R$  have the same domain (message space) we may form a kind of "weighted sum."

$$S = pT + qR$$

where  $p + q = 1$ . This operation consists of first making a preliminary choice with probabilities  $p$  and  $q$  determining which of  $T$  and  $R$  is used. This choice is part of the key of  $S$ . After this is determined  $T$  or  $R$  is used as originally defined. The total key of  $S$  must specify which of  $T$  and  $R$  is used and which key of  $T$  (or  $R$ ) is used.

If  $T$  consists of the transformations  $T_1, \dots, T_m$  with probabilities  $p_1, \dots, p_m$  and  $R$  consists of  $R_1, \dots, R_k$  with probabilities  $q_1, \dots, q_k$  then  $S = pT + qR$  consists of the transformations  $T_1, T_2, \dots, T_m, R_1, \dots, R_k$  with probabilities  $pp_1, pp_2, \dots, pp_m, qq_1, qq_2, \dots, qq_k$  respectively.

More generally we can form the sum of a number of systems.

$$S = p_1T + p_2R + \cdots + p_mT^r \quad \sum p_i = 1$$

We note that any system  $T$  can be written as a sum of fixed operations

$$T = p_1T_1 + p_2T_2 + \cdots + p_mT_m$$

$T_i$  being a definite enciphering operation of  $T$  corresponding to key choice  $i$ , which has probability  $p_i$ .

A second way of combining two secrecy systems is by taking the "product," shown schematically in Fig. 3. Suppose  $T$  and  $R$  are two systems and the domain (language space) of  $R$  can be identified with the range (cryptogram space) of  $T$ . Then we can apply first  $T$  to our language and then  $R$

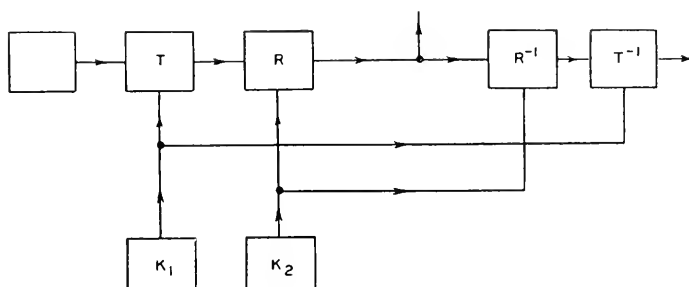


Fig. 3—Product of two systems  $S = RT$ .

to the result of this enciphering process. This gives a resultant operation  $S$  which we write as a product

$$S = RT$$

The key for  $S$  consists of both keys of  $T$  and  $R$  which are assumed chosen according to their original probabilities and independently. Thus, if the  $m$  keys of  $T$  are chosen with probabilities

$$p_1 p_2 \cdots p_m$$

and the  $n$  keys of  $R$  have probabilities

$$p'_1 p'_2 \cdots p'_n,$$

then  $S$  has at most  $mn$  keys with probabilities  $p_i p'_j$ . In many cases some of the product transformations  $R_i T_j$  will be the same and can be grouped together, adding their probabilities.

Product encipherment is often used; for example, one follows a substitution by a transposition or a transposition by a Vigenère, or applies a code to the text and enciphers the result by substitution, transposition, fractionation, etc.

It may be noted that multiplication is not in general commutative, (we do not always have  $RS = SR$ ), although in special cases, such as substitution and transposition, it is. Since it represents an operation it is definitionally associative. That is  $R(ST) = (RS)T = RST$ . Furthermore we have the laws

$$p(p'T + q'R) + qS = pp'T + pq'R + qS$$

(weighted associative law for addition)

$$T(pR + qS) = pTR + qTS$$

$$(pR + qS)T = pRT + qST$$

(right and left hand distributive laws)

and

$$p_1T + p_2T + p_3R = (p_1 + p_2)T + p_3R$$

It should be emphasized that these combining operations of addition and multiplication apply to secrecy systems as a whole. The product of two systems  $TR$  should not be confused with the product of the transformations in the systems  $T_iR_j$ , which also appears often in this work. The former  $TR$  is a secrecy system, i.e., a set of transformations with associated probabilities; the latter is a particular transformation. Further the sum of two systems  $pR + qT$  is a system—the sum of two transformations is not defined. The systems  $T$  and  $R$  may commute without the individual  $T_i$  and  $R_j$  commuting, e.g., if  $R$  is a Beaufort system of a given period, all keys equally likely,

$$R_iR_j \neq R_jR_i$$

in general, but of course  $RR$  does not depend on its order; actually

$$RR = I$$

the Vigenère of the same period with random key. On the other hand, if the individual  $T_i$  and  $R_j$  of two systems  $T$  and  $R$  commute, then the systems commute.

A system whose  $M$  and  $E$  spaces can be identified, a very common case as when letter sequences are transformed into letter sequences, may be termed *endomorphie*. An endomorphic system  $T$  may be raised to a power  $T^n$ .

A secrecy system  $T$  whose product with itself is equal to  $T$ , i.e., for which

$$TT = T,$$

will be called idempotent. For example, simple substitution, transposition of period  $p$ , Vigenère of period  $p$  (all with each key equally likely) are idempotent.



The set of all endomorphic secrecy systems defined in a fixed message space constitutes an "algebraic variety," that is, a kind of algebra, using the operations of addition and multiplication. In fact, the properties of addition and multiplication which we have discussed may be summarized as follows:

*The set of endomorphic ciphers with the same message space and the two combining operations of weighted addition and multiplication form a linear associative algebra with a unit element, apart from the fact that the coefficients in a weighted addition must be non-negative and sum to unity.*

The combining operations give us ways of constructing many new types of secrecy systems from certain ones, such as the examples given. We may also use them to describe the situation facing a cryptanalyst when attempting to solve a cryptogram of unknown type. He is, in fact, solving a secrecy system of the type

$$T = p_1A + p_2B + \cdots + p_rS + p'X \quad \sum p = 1$$

where the  $A, B, \cdots, S$  are known types of ciphers, with the  $p_i$  their *a priori* probabilities in this situation, and  $p'X$  corresponds to the possibility of a completely new unknown type of cipher.

## 7. PURE AND MIXED CIPHERS

Certain types of ciphers, such as the simple substitution, the transposition of a given period, the Vigenère of a given period, the mixed alphabet Vigenère, etc. (all with each key equally likely) have a certain homogeneity with respect to key. Whatever the key, the enciphering, deciphering and decrypting processes are essentially the same. This may be contrasted with the cipher

$$pS + qT$$

where  $S$  is a simple substitution and  $T$  a transposition of a given period. In this case the entire system changes for enciphering, deciphering and decryptment, depending on whether the substitution or transposition is used.

The cause of the homogeneity in these systems stems from the group property—we notice that, in the above examples of homogeneous ciphers, the product  $T_iT_j$  of any two transformations in the set is equal to a third transformation  $T_k$  in the set. On the other hand  $T_iS_j$  does not equal any transformation in the cipher

$$pS + qT$$

which contains only substitutions and transpositions, no products.

We might define a "pure" cipher, then, as one whose  $T_i$  form a group. This, however, would be too restrictive since it requires that the  $E$  space

be the same as the  $M$  space, i.e. that the system be endomorphic. The fractional transposition is as homogeneous as the ordinary transposition without being endomorphic. The proper definition is the following: A cipher  $T$  is *pure* if for every  $T_i, T_j, T_k$  there is a  $T_s$  such that

$$T_i T_j^{-1} T_k = T_s$$

and every key is equally likely. Otherwise the cipher is mixed. The systems of Fig. 2 are mixed. Fig. 4 is pure if all keys are equally likely.

*Theorem 1: In a pure cipher the operations  $T_i^{-1} T_j$  which transform the message space into itself form a group whose order is  $m$ , the number of different keys.*

For

$$T_i^{-1} T_k T_k^{-1} T_j = I$$

so that each element has an inverse. The associative law is true since these are operations, and the group property follows from

$$T_i^{-1} T_j T_k^{-1} T_l = T_s^{-1} T_k T_k^{-1} T_l = T_s^{-1} T_l$$

using our assumption that  $T_i^{-1} T_j = T_s^{-1} T_k$  for some  $s$ .

The operation  $T_i^{-1} T_j$  means, of course, enciphering the message with key  $j$  and then deciphering with key  $i$  which brings us back to the message space. If  $T$  is endomorphic, i.e. the  $T_i$  themselves transform the space  $\Omega_M$  into itself (as is the case with most ciphers, where both the message space and the cryptogram space consist of sequences of letters), and the  $T_i$  are a group and equally likely, then  $T$  is pure, since

$$T_i T_j^{-1} T_k = T_i T_r = T_s.$$

*Theorem 2: The product of two pure ciphers which commute is pure.*

For if  $T$  and  $R$  commute  $T_i R_j = R_l T_m$  for every  $i, j$  with suitable  $l, m$ , and

$$\begin{aligned} T_i R_j (T_k R_l)^{-1} T_m R_n &= T_i R_j R_l^{-1} T_k^{-1} T_m R_n \\ &= R_u R_v^{-1} R_w T_r T_s^{-1} T_t \\ &= R_h T_\theta. \end{aligned}$$

The commutation condition is not necessary, however, for the product to be a pure cipher.

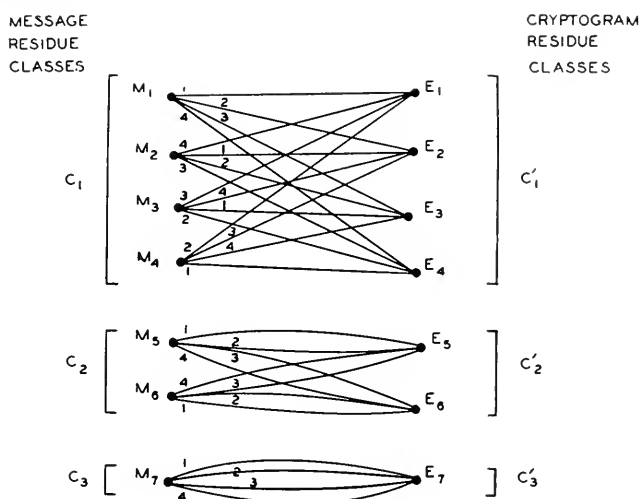
A system with only one key, i.e., a single definite operation  $T_1$ , is pure since the only choice of indices is

$$T_1 T_1^{-1} T_1 = T_1.$$

Thus the expansion of a general cipher into a sum of such simple transformations also exhibits it as a sum of pure ciphers.

An examination of the example of a pure cipher shown in Fig. 4 discloses

certain properties. The messages fall into certain subsets which we will call *residue classes*, and the possible cryptograms are divided into corresponding residue classes. There is at least one line from each message in a class to each cryptogram in the corresponding class, and no line between classes which do not correspond. The number of messages in a class is a divisor of the total number of keys. The number of lines "in parallel" from a message  $M$  to a cryptogram in the corresponding class is equal to the number of keys divided by the number of messages in the class containing the message (or cryptogram). It is shown in the appendix that these hold in general for pure ciphers. Summarized formally, we have:



PURE SYSTEM  
Fig. 4—Pure system.

*Theorem 3: In a pure system the messages can be divided into a set of "residue classes"  $C_1, C_2, \dots, C_s$  and the cryptograms into a corresponding set of residue classes  $C'_1, C'_2, \dots, C'_s$  with the following properties:*

- (1) *The message residue classes are mutually exclusive and collectively contain all possible messages. Similarly for the cryptogram residue classes.*
- (2) *Enciphering any message in  $C_i$  with any key produces a cryptogram in  $C'_i$ . Deciphering any cryptogram in  $C'_i$  with any key leads to a message in  $C_i$ .*
- (3) *The number of messages in  $C_i$ , say  $\varphi_i$ , is equal to the number of cryptograms in  $C'_i$  and is a divisor of  $k$  the number of keys.*

- (4) Each message in  $C_i$  can be enciphered into each cryptogram in  $C'_i$  by exactly  $k/\varphi_i$  different keys. Similarly for decipherment.

The importance of the concept of a pure cipher (and the reason for the name) lies in the fact that in a pure cipher all keys are essentially the same. Whatever key is used for a particular message, the *a posteriori* probabilities of all messages are identical. To see this, note that two different keys applied to the same message lead to two cryptograms in the same residue class, say  $C'_i$ . The two cryptograms therefore could each be deciphered by  $\frac{k}{\varphi_i}$  keys into each message in  $C_i$  and into no other possible messages. All keys being equally likely the *a posteriori* probabilities of various messages are thus

$$P_E(M) = \frac{P(M)P_M(E)}{P(E)} = \frac{P(M)P_M(E)}{\sum_M P(M)P_M(E)} = \frac{P(M)}{P(C_i)}$$

where  $M$  is in  $C_i$ ,  $E$  is in  $C'_i$  and the sum is over all messages in  $C_i$ . If  $E$  and  $M$  are not in corresponding residue classes,  $P_E(M) = 0$ . Similarly it can be shown that the *a posteriori* probabilities of the different keys are the same in value but these values are associated with different keys when a different key is used. The same set of values of  $P_E(K)$  have undergone a permutation among the keys. Thus we have the result

*Theorem 4: In a pure system the a posteriori probabilities of various messages  $P_E(M)$  are independent of the key that is chosen. The a posteriori probabilities of the keys  $P_E(K)$  are the same in value but undergo a permutation with a different key choice.*

Roughly we may say that any key choice leads to the same cryptanalytic problem in a pure cipher. Since the different keys all result in cryptograms in the same residue class this means that all cryptograms in the same residue class are cryptanalytically equivalent—they lead to the same *a posteriori* probabilities of messages and, apart from a permutation, the same probabilities of keys.

As an example of this, simple substitution with all keys equally likely is a pure cipher. The residue class corresponding to a given cryptogram  $E$  is the set of all cryptograms that may be obtained from  $E$  by operations  $T_j T_k^{-1} E$ . In this case  $T_j T_k^{-1}$  is itself a substitution and hence any substitution on  $E$  gives another member of the same residue class. Thus, if the cryptogram is

$$E = X \ C \ P \ P \ G \ C \ F \ Q,$$

then

$$E_1 = R \ D \ H \ H \ G \ D \ S \ N$$

$$E_2 = A \ B \ C \ C \ D \ B \ E \ F$$

etc. are in the same residue class. It is obvious in this case that these cryptograms are essentially equivalent. All that is of importance in a simple substitution with random key is the *pattern* of letter repetitions, the actual letters being dummy variables. Indeed we might dispense with them entirely, indicating the pattern of repetitions in  $E$  as follows:



This notation describes the residue class but eliminates all information as to the specific member of the class. Thus it leaves precisely that information which is cryptanalytically pertinent. This is related to one method of attacking simple substitution ciphers—the method of pattern words.

In the Caesar type cipher only the first differences mod 26 of the cryptogram are significant. Two cryptograms with the same  $\Delta e_i$  are in the same residue class. One breaks this cipher by the simple process of writing down the 26 members of the message residue class and picking out the one which makes sense.

The Vigenère of period  $d$  with random key is another example of a pure cipher. Here the message residue class consists of all sequences with the same first differences as the cryptogram, for letters separated by distance  $d$ . For  $d = 3$  the residue class is defined by

$$\begin{aligned} m_1 - m_4 &= e_1 - e_4 \\ m_2 - m_5 &= e_2 - e_5 \\ m_3 - m_6 &= e_3 - e_6 \\ m_4 - m_7 &= e_4 - e_7 \\ &\vdots \\ &\vdots \\ &\vdots \end{aligned}$$

where  $E = e_1, e_2, \dots$  is the cryptogram and  $m_1, m_2, \dots$  is any  $M$  in the corresponding residue class.

In the transposition cipher of period  $d$  with random key, the residue class consists of all arrangements of the  $e_i$  in which no  $e_i$  is moved out of its block of length  $d$ , and any two  $e_i$  at a distance  $d$  remain at this distance. This is used in breaking these ciphers as follows: The cryptogram is written in successive blocks of length  $d$ , one under another as below ( $d = 5$ ):

$$\begin{array}{ccccc} e_1 & e_2 & e_3 & e_4 & e_5 \\ e_6 & e_7 & e_8 & e_9 & e_{10} \\ e_{11} & e_{12} & \cdot & \cdot & \cdot \\ \cdot & \cdot & \cdot & \cdot & \cdot \end{array}$$

The columns are then cut apart and rearranged to make meaningful text. When the columns are cut apart, the only information remaining is the residue class of the cryptogram.

*Theorem 5: If  $T$  is pure then  $T_i T_j^{-1} T = T$  where  $T_i T_j$  are any two transformations of  $T$ . Conversely if this is true for any  $T_i T_j$  in a system  $T$  then  $T$  is pure.*

The first part of this theorem is obvious from the definition of a pure system. To prove the second part we note first that, if  $T_i T_j^{-1} T = T$ , then  $T_i T_j^{-1} T_s$  is a transformation of  $T$ . It remains to show that all keys are equiprobable. We have  $T = \sum_s p_s T_s$  and

$$\sum_s p_s T_i T_j^{-1} T_s = \sum_s p_s T_s.$$

The term in the left hand sum with  $s = j$  yields  $p_j T_i$ . The only term in  $T_i$  on the right is  $p_i T_i$ . Since all coefficients are nonnegative it follows that

$$p_j \leq p_i.$$

The same argument holds with  $i$  and  $j$  interchanged and consequently

$$p_j = p_i$$

and  $T$  is pure. Thus the condition that  $T_i T_j^{-1} T = T$  might be used as an alternative definition of a pure system.

## 8. SIMILAR SYSTEMS

Two secrecy systems  $R$  and  $S$  will be said to be *similar* if there exists a transformation  $A$  having an inverse  $A^{-1}$  such that

$$R = AS$$

This means that enciphering with  $R$  is the same as enciphering with  $S$  and then operating on the result with the transformation  $A$ . If we write  $R \approx S$  to mean  $R$  is similar to  $S$  then it is clear that  $R \approx S$  implies  $S \approx R$ . Also  $R \approx S$  and  $S \approx T$  imply  $R \approx T$  and finally  $R \approx R$ . These are summarized by saying that similarity is an equivalence relation.

The cryptographic significance of similarity is that if  $R \approx S$  then  $R$  and  $S$  are equivalent from the cryptanalytic point of view. Indeed if a cryptanalyst intercepts a cryptogram in system  $S$  he can transform it to one in system  $R$  by merely applying the transformation  $A$  to it. A cryptogram in system  $R$  is transformed to one in  $S$  by applying  $A^{-1}$ . If  $R$  and  $S$  are applied to the same language or message space, there is a one-to-one correspondence between the resulting cryptograms. Corresponding cryptograms give the same distribution of *a posteriori* probabilities for all messages.

If one has a method of breaking the system  $R$  then any system  $S$  similar

to  $R$  can be broken by reducing to  $R$  through application of the operation  $A$ . This is a device that is frequently used in practical cryptanalysis.

As a trivial example, simple substitution where the substitutes are not letters but arbitrary symbols is similar to simple substitution using letter substitutes. A second example is the Caesar and the reversed Caesar type ciphers. The latter is sometimes broken by first transforming into a Caesar type. This can be done by reversing the alphabet in the cryptogram. The Vigenère, Beaufort and Variant Beaufort are all similar, when the key is random. The "autokey" cipher (with the message used as "key") primed with the key  $K_1 K_2 \cdots K_d$  is similar to a Vigenère type with the key alternately added and subtracted Mod 26. The transformation  $A$  in this case is that of "deciphering" the autokey with a series of  $d$   $A$ 's for the priming key.

## PART II

### THEORETICAL SECRECY

#### 9. INTRODUCTION

We now consider problems connected with the "theoretical secrecy" of a system. How immune is a system to cryptanalysis when the cryptanalyst has unlimited time and manpower available for the analysis of cryptograms? Does a cryptogram *have* a unique solution (even though it may require an impractical amount of work to find it) and if not how many reasonable solutions does it have? How much text in a given system must be intercepted before the solution becomes unique? Are there systems which never become unique in solution no matter how much enciphered text is intercepted? Are there systems for which no information whatever is given to the enemy no matter how much text is intercepted? In the analysis of these problems the concepts of entropy, redundancy and the like developed in "A Mathematical Theory of Communication" (hereafter referred to as MTC) will find a wide application.

#### 10. PERFECT SECRECY

Let us suppose the possible messages are finite in number  $M_1, \cdots, M_n$  and have *a priori* probabilities  $P(M_1), \cdots, P(M_n)$ , and that these are enciphered into the possible cryptograms  $E_1, \cdots, E_m$  by

$$E = T_i M.$$

The cryptanalyst intercepts a particular  $E$  and can then calculate, in principle at least, the *a posteriori* probabilities for the various messages,  $P_E(M)$ . It is natural to define *perfect secrecy* by the condition that, for all  $E$  the *a posteriori* probabilities are equal to the *a priori* probabilities independently of the values of these. In this case, intercepting the message has

given the cryptanalyst no information.<sup>9</sup> Any action of his which depends on the information contained in the cryptogram cannot be altered, for all of his probabilities as to what the cryptogram contains remain unchanged. On the other hand, if the condition is *not* satisfied there will exist situations in which the enemy has certain *a priori* probabilities, and certain key and message choices may occur for which the enemy's probabilities do change. This in turn may affect his actions and thus perfect secrecy has not been obtained. Hence the definition given is necessarily required by our intuitive ideas of what perfect secrecy should mean.

A necessary and sufficient condition for perfect secrecy can be found as follows: We have by Bayes' theorem

$$P_E(M) = \frac{P(M)P_M(E)}{P(E)}$$

in which:

$P(M)$  = *a priori* probability of message  $M$ .

$P_M(E)$  = conditional probability of cryptogram  $E$  if message  $M$  is chosen, i.e. the sum of the probabilities of all keys which produce cryptogram  $E$  from message  $M$ .

$P(E)$  = probability of obtaining cryptogram  $E$  from any cause.

$P_E(M)$  = *a posteriori* probability of message  $M$  if cryptogram  $E$  is intercepted.

For perfect secrecy  $P_E(M)$  must equal  $P(M)$  for all  $E$  and all  $M$ . Hence either  $P(M) = 0$ , a solution that must be excluded since we demand the equality independent of the values of  $P(M)$ , or

$$P_M(E) = P(E)$$

for every  $M$  and  $E$ . Conversely if  $P_M(E) = P(E)$  then

$$P_E(M) = P(M)$$

and we have perfect secrecy. Thus we have the result:

*Theorem 6: A necessary and sufficient condition for perfect secrecy is that*

$$P_M(E) = P(E)$$

*for all  $M$  and  $E$ . That is,  $P_M(E)$  must be independent of  $M$ .*

Stated another way, the total probability of all keys that transform  $M_i$

<sup>9</sup> A purist might object that the enemy has obtained some information in that he knows a message was sent. This may be answered by having among the messages a "blank" corresponding to "no message." If no message is originated the blank is enciphered and sent as a cryptogram. Then even this modicum of remaining information is eliminated.



into a given cryptogram  $E$  is equal to that of all keys transforming  $M_j$  into the same  $E$ , for all  $M_i$ ,  $M_j$  and  $E$ .

Now there must be as many  $E$ 's as there are  $M$ 's since, for a fixed  $i$ ,  $T_i$  gives a one-to-one correspondence between all the  $M$ 's and some of the  $E$ 's. For perfect secrecy  $P_M(E) = P(E) \neq 0$  for any of these  $E$ 's and any  $M$ . Hence there is at least one key transforming any  $M$  into any of these  $E$ 's. But all the keys from a fixed  $M$  to different  $E$ 's must be different, and therefore *the number of different keys is at least as great as the number of  $M$ 's*. It is possible to obtain perfect secrecy with only this number of keys, as

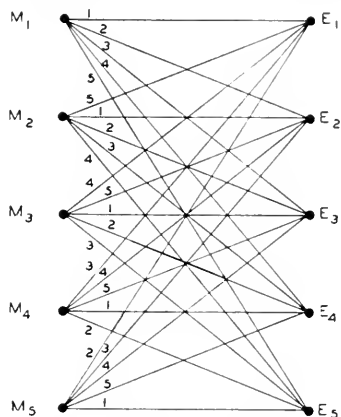


Fig. 5—Perfect system.

one shows by the following example: Let the  $M_i$  be numbered 1 to  $n$  and the  $E_i$  the same, and using  $n$  keys let

$$T_i M_j = E_s$$

where  $s = i + j \pmod{n}$ . In this case we see that  $P_E(M) = \frac{1}{n} = P(E)$  and we have perfect secrecy. An example is shown in Fig. 5 with  $s = i + j - 1 \pmod{5}$ .

Perfect systems in which the number of cryptograms, the number of messages, and the number of keys are all equal are characterized by the properties that (1) each  $M$  is connected to each  $E$  by exactly one line, (2) all keys are equally likely. Thus the matrix representation of the system is a "Latin square."

In MTC it was shown that information may be conveniently measured by means of entropy. If we have a set of possibilities with probabilities  $p_1, p_2, \dots, p_n$ , the entropy  $H$  is given by:

$$H = - \sum p_i \log p_i.$$

In a secrecy system there are two statistical choices involved, that of the message and of the key. We may measure the amount of information produced when a message is chosen by  $H(M)$ :

$$H(M) = - \sum P(M) \log P(M),$$

the summation being over all possible messages. Similarly, there is an uncertainty associated with the choice of key given by:

$$H(K) = - \sum P(K) \log P(K).$$

In perfect systems of the type described above, the amount of information in the message is at most  $\log n$  (occurring when all messages are equiprobable). This information can be concealed completely only if the key uncertainty is at least  $\log n$ . This is the first example of a general principle which will appear frequently: that there is a limit to what we can obtain with a given uncertainty in key—the amount of uncertainty we can introduce into the solution cannot be greater than the key uncertainty.

The situation is somewhat more complicated if the number of messages is infinite. Suppose, for example, that they are generated as infinite sequences of letters by a suitable Markoff process. It is clear that no finite key will give perfect secrecy. We suppose, then, that the key source generates key in the same manner, that is, as an infinite sequence of symbols. Suppose further that only a certain length of key  $L_K$  is needed to encipher and decipher a length  $L_M$  of message. Let the logarithm of the number of letters in the message alphabet be  $R_M$  and that for the key alphabet be  $R_K$ . Then, from the finite case, it is evident that perfect secrecy requires

$$R_M L_M \leq R_K L_K.$$

This type of perfect secrecy is realized by the Vernam system.

These results have been deduced on the basis of unknown or arbitrary *a priori* probabilities for the messages. The key required for perfect secrecy depends then on the total number of possible messages.

One would expect that, if the message space has fixed known statistics, so that it has a definite mean rate  $R$  of generating information, in the sense of MTC, then the amount of key needed could be reduced on the average in just this ratio  $\frac{R}{R_M}$ , and this is indeed true. In fact the message can be passed through a transducer which eliminates the redundancy and reduces the expected length in just this ratio, and then a Vernam system may be applied to the result. Evidently the amount of key used per letter of message is statistically reduced by a factor  $\frac{R}{R_M}$  and in this case the key source and information source are just matched—a bit of key completely conceals a

bit of message information. It is easily shown also, by the methods used in MTC, that this is the best that can be done.

Perfect secrecy systems have a place in the practical picture—they may be used either where the greatest importance is attached to complete secrecy—e.g., correspondence between the highest levels of command, or in cases where the number of possible messages is small. Thus, to take an extreme example, if only two messages “yes” or “no” were anticipated, a perfect system would be in order, with perhaps the transformation table:

$M$	$K$	$A$	$B$
	yes	0	1
	no	1	0

The disadvantage of perfect systems for large correspondence systems is, of course, the equivalent amount of key that must be sent. In succeeding sections we consider what can be achieved with smaller key size, in particular with finite keys.

## 11. EQUIVOCATION

Let us suppose that a simple substitution cipher has been used on English text and that we intercept a certain amount,  $N$  letters, of the enciphered text. For  $N$  fairly large, more than say 50 letters, there is nearly always a unique solution to the cipher; i.e., a single good English sequence which transforms into the intercepted material by a simple substitution. With a smaller  $N$ , however, the chance of more than one solution is greater; with  $N = 15$  there will generally be quite a number of possible fragments of text that would fit, while with  $N = 8$  a good fraction (of the order of  $1/8$ ) of all reasonable English sequences of that length are possible, since there is seldom more than one repeated letter in the 8. With  $N = 1$  any letter is clearly possible and has the same *a posteriori* probability as its *a priori* probability. For one letter the system is perfect.

This happens generally with solvable ciphers. Before any material is intercepted we can imagine the *a priori* probabilities attached to the various possible messages, and also to the various keys. As material is intercepted, the cryptanalyst calculates the *a posteriori* probabilities; and as  $N$  increases the probabilities of certain messages increase, and, of most, decrease, until finally only one is left, which has a probability nearly one, while the total probability of all others is nearly zero.

This calculation can actually be carried out for very simple systems. Table I shows the *a posteriori* probabilities for a Caesar type cipher applied to English text, with the key chosen at random from the 26 possibilities. To enable the use of standard letter, digram and trigram frequency tables, the

text has been started at a random point (by opening a book and putting a pencil down at random on the page). The message selected in this way begins "creases to . . ." starting inside the word increases. If the message were known to start a sentence a different set of probabilities must be used, corresponding to the frequencies of letters, digrams, etc., at the beginning of sentences.

TABLE I

<i>A Posteriori</i> Probabilities for a Caesar Type Cryptogram					
Decipherments	<i>N</i> = 1	<i>N</i> = 2	<i>N</i> = 3	<i>N</i> = 4	<i>N</i> = 5
<i>C R E A S</i>	.028	.0377	.1111	.3673	1
<i>D S F B T</i>	.038	.0314			
<i>E T G C U</i>	.131	.0881			
<i>F U H D V</i>	.029	.0189			
<i>G V I E W</i>	.020				
<i>H W J F X</i>	.053	.0063			
<i>I X K G Y</i>	.063	.0126			
<i>J Y L H Z</i>	.001				
<i>K Z M I A</i>	.004				
<i>L A N J B</i>	.034	.1321	.2500		
<i>M B O K C</i>	.025		.0222		
<i>N C P L D</i>	.071	.1195			
<i>O D Q M E</i>	.080	.0377			
<i>P E R N F</i>	.020	.0818	.4389	.6327	
<i>Q F S O G</i>	.001				
<i>R G T P H</i>	.068	.0126			
<i>S H U Q I</i>	.061	.0881	.0056		
<i>T I V R J</i>	.105	.2830	.1667		
<i>U J W S K</i>	.025				
<i>V K X T L</i>	.009				
<i>W L Y U M</i>	.015		.0056		
<i>X M Z V N</i>	.002				
<i>Y N A W O</i>	.020				
<i>Z O B X P</i>	.001				
<i>A P C Y Q</i>	.082	.0503			
<i>B Q D Z R</i>	.014				
<i>H</i> (decimal digits)	1.2425	.9686	.6034	.285	0

The Caesar with random key is a pure cipher and the particular key chosen does not affect the *a posteriori* probabilities. To determine these we need merely list the possible decipherments by all keys and calculate their *a priori* probabilities. The *a posteriori* probabilities are these divided by their sum. These possible decipherments are found by the standard process of "running down the alphabet" from the message and are listed at the left. These form the residue class for the message. For one intercepted letter the *a posteriori* probabilities are equal to the *a priori* probabilities for letters<sup>10</sup> and are shown in the column headed *N* = 1. For two intercepted letters the probabilities are those for digrams adjusted to sum to unity and these are shown in the column *N* = 2.

<sup>10</sup> The probabilities for this table were taken from frequency tables given by Fletcher Pratt in a book "Secret and Urgent" published by Blue Ribbon Books, New York, 1939. Although not complete, they are sufficient for present purposes.

Trigram frequencies have also been tabulated and these are shown in the column  $N = 3$ . For four- and five-letter sequences probabilities were obtained by multiplication from trigram frequencies since, roughly,

$$p(ijkl) = p(ijk)p_{jk}(l).$$

Note that at three letters the field has narrowed down to four messages of fairly high probability, the others being small in comparison. At four there are two possibilities and at five just one, the correct decipherment.

In principle this could be carried out with any system but, unless the key is very small, the number of possibilities is so large that the work involved prohibits the actual calculation.

This set of *a posteriori* probabilities describes how the cryptanalyst's knowledge of the message and key gradually becomes more precise as enciphered material is obtained. This description, however, is much too involved and difficult to obtain for our purposes. What is desired is a simplified description of this approach to uniqueness of the possible solutions.

A similar situation arises in communication theory when a transmitted signal is perturbed by noise. It is necessary to set up a suitable measure of the uncertainty of what was actually transmitted knowing only the perturbed version given by the received signal. In MTC it was shown that a natural mathematical measure of this uncertainty is the conditional entropy of the transmitted signal when the received signal is known. This conditional entropy was called, for convenience, the equivocation.

From the point of view of the cryptanalyst, a secrecy system is almost identical with a noisy communication system. The message (transmitted signal) is operated on by a statistical element, the enciphering system, with its statistically chosen key. The result of this operation is the cryptogram (analogous to the perturbed signal) which is available for analysis. The chief differences in the two cases are: first, that the operation of the enciphering transformation is generally of a more complex nature than the perturbing noise in a channel; and, second, the key for a secrecy system is usually chosen from a finite set of possibilities while the noise in a channel is more often continually introduced, in effect chosen from an infinite set.

With these considerations in mind it is natural to use the equivocation as a theoretical secrecy index. It may be noted that there are two significant equivocations, that of the key and that of the message. These will be denoted by  $H_E(K)$  and  $H_E(M)$  respectively. They are given by:

$$H_E(K) = \sum_{E, K} P(E, K) \log P_E(K)$$

$$H_E(M) = \sum_{E, M} P(E, M) \log P_E(M)$$

in which  $E$ ,  $M$  and  $K$  are the cryptogram, message and key and

$P(E, K)$  is the probability of key  $K$  and cryptogram  $E$

$P_E(K)$  is the *a posteriori* probability of key  $K$  if cryptogram  $E$  is intercepted

$P(E, M)$  and  $P_E(M)$  are the similar probabilities for message instead of key.

The summation in  $H_E(K)$  is over all possible cryptograms of a certain length (say  $N$  letters) and over all keys. For  $H_E(M)$  the summation is over all messages and cryptograms of length  $N$ . Thus  $H_E(K)$  and  $H_E(M)$  are both functions of  $N$ , the number of intercepted letters. This will sometimes be indicated explicitly by writing  $H_E(K, N)$  and  $H_E(M, N)$ . Note that these are "total" equivocations; i.e., we do not divide by  $N$  to obtain the equivocation rate which was used in *MTC*.

The same general arguments used to justify the equivocation as a measure of uncertainty in communication theory apply here as well. We note that zero equivocation requires that one message (or key) have unit probability, all others zero, corresponding to complete knowledge. Considered as a function of  $N$ , the gradual decrease of equivocation corresponds to increasing knowledge of the original key or message. The two equivocation curves, plotted as functions of  $N$ , will be called the equivocation characteristics of the secrecy system in question.

The values of  $H_E(K, N)$  and  $H_E(M, N)$  for the Caesar type cryptogram considered above have been calculated and are given in the last row of Table I.  $H_E(K, N)$  and  $H_E(M, N)$  are equal in this case and are given in decimal digits (i.e. the logarithmic base 10 is used in the calculation). It should be noted that the equivocation here is for a particular cryptogram, the summation being only over  $M$  (or  $K$ ), not over  $E$ . In general the summation would be over all possible intercepted cryptograms of length  $N$  and would give the average uncertainty. The computational difficulties are prohibitive for this general calculation.

## 12. PROPERTIES OF EQUIVOCATION

Equivocation may be shown to have a number of interesting properties, most of which fit into our intuitive picture of how such a quantity should behave. We will first show that the equivocation of key or of a fixed part of a message decreases when more enciphered material is intercepted.

*Theorem 7: The equivocation of key  $H_E(K, N)$  is a non-increasing function of  $N$ . The equivocation of the first  $A$  letters of the message is a non-increasing function of the number  $N$  which have been intercepted. If  $N$  letters have been intercepted, the equivocation of the first  $N$  letters of message is less than or equal to that of the key. These may be written:*

$$\begin{aligned}
H_E(K, S) &\leq H_E(K, N) & S &\geq N, \\
H_E(M, S) &\leq H_E(M, N) & S &\geq N \text{ (if for first } A \text{ letters of text)} \\
H_E(M, N) &\leq H_E(K, N)
\end{aligned}$$

The qualification regarding  $A$  letters in the second result of the theorem is so that the equivocation will not be calculated with respect to the amount of message that has been intercepted. If it is, the message equivocation may (and usually does) increase for a time, due merely to the fact that more letters stand for a larger possible range of messages. The results of the theorem are what we might hope from a good secrecy index, since we would hardly expect to be worse off on the average after intercepting additional material than before. The fact that they can be proved gives further justification to our use of the equivocation measure.

The results of this theorem are a consequence of certain properties of conditional entropy proved in MTC. Thus, to show the first or second statements of Theorem 7, we have for any chance events  $A$  and  $B$

$$H(B) \geq H_A(B).$$

If we identify  $B$  with the key (knowing the first  $S$  letters of cryptogram) and  $A$  with the remaining  $N - S$  letters we obtain the first result. Similarly identifying  $B$  with the message gives the second result. The last result follows from

$$H_E(M) \leq H_E(K, M) = H_E(K) + H_{E,K}(M)$$

and the fact that  $H_{E,K}(M) = 0$  since  $K$  and  $E$  uniquely determine  $M$ .

Since the message and key are chosen independently we have:

$$H(M, K) = H(M) + H(K).$$

Furthermore,

$$H(M, K) = H(E, K) = H(E) + H_E(K),$$

the first equality resulting from the fact that knowledge of  $M$  and  $K$  or of  $E$  and  $K$  is equivalent to knowledge of all three. Combining these two we obtain a formula for the equivocation of key:

$$H_E(K) = H(M) + H(K) - H(E).$$

In particular, if  $H(M) = H(E)$  then the equivocation of key,  $H_E(K)$ , is equal to the *a priori* uncertainty of key,  $H(K)$ . This occurs in the perfect systems described above.

A formula for the equivocation of message can be found by similar means. We have:

$$H(M, E) = H(E) + H_E(M) = H(M) + H_M(E)$$

$$H_E(M) = H(M) + H_M(E) - H(E).$$

If we have a product system  $S = TR$ , it is to be expected that the second enciphering process will not decrease the equivocation of message. That this is actually true can be shown as follows: Let  $M$ ,  $E_1$ ,  $E_2$  be the message and the first and second encipherments, respectively. Then

$$P_{E_1 E_2}(M) = P_{E_1}(M).$$

Consequently

$$H_{E_1 E_2}(M) = H_{E_1}(M).$$

Since, for any chance variables,  $x$ ,  $y$ ,  $z$ ,  $H_{xy}(z) \leq H_y(z)$ , we have the desired result,  $H_{E_2}(M) \geq H_{E_1}(M)$ .

*Theorem 8: The equivocation in message of a product system  $S = TR$  is not less than that when only  $R$  is used.*

Suppose now we have a system  $T$  which can be written as a weighted sum of several systems  $R$ ,  $S$ ,  $\dots$ ,  $U$

$$T = p_1 R + p_2 S + \dots + p_m U \quad \sum p_i = 1$$

and that systems  $R$ ,  $S$ ,  $\dots$ ,  $U$  have equivocations  $H_1$ ,  $H_2$ ,  $H_3$ ,  $\dots$ ,  $H_m$ .

*Theorem 9: The equivocation  $H$  of a weighted sum of systems is bounded by the inequalities*

$$\sum p_i H_i \leq H \leq \sum p_i H_i - \sum p_i \log p_i.$$

*These are best limits possible. The  $H$ 's may be equivocations either of key or message.*

The upper limit is achieved, for example, in strongly ideal systems (to be described later) where the decomposition is into the simple transformations of the system. The lower limit is achieved if all the systems  $R$ ,  $S$ ,  $\dots$ ,  $U$  go to completely different cryptogram spaces. This theorem is also proved by the general inequalities governing equivocation,

$$H_A(B) \leq H(B) \leq H(A) + H_A(B).$$

We identify  $A$  with the particular system being used and  $B$  with the key or message.

There is a similar theorem for weighted sums of languages. For this we identify  $A$  with the particular language.

*Theorem 10: Suppose a system can be applied to languages  $L_1$ ,  $L_2$ ,  $\dots$ ,  $L_m$  and has equivocation characteristics  $H_1$ ,  $H_2$ ,  $\dots$ ,  $H_m$ . When applied to the weighted sum  $\sum p_i L_i$ , the equivocation  $H$  is bounded by*

$$\sum p_i H_i \leq H \leq \sum p_i H_i - \sum p_i \log p_i.$$



*These limits are the best possible and the equivocations in question can be either for key or message.*

The total redundancy  $D_N$  for  $N$  letters of message is defined by

$$D_N = \log G - H(M)$$

where  $G$  is the total number of messages of length  $N$  and  $H(M)$  is the uncertainty in choosing one of these. In a secrecy system where the total number of possible cryptograms is equal to the number of possible messages of length  $N$ ,  $H(E) \leq \log G$ . Consequently

$$\begin{aligned} H_E(K) &= H(K) + H(M) - H(E) \\ &\geq H(K) - [\log G - H(M)]. \end{aligned}$$

Hence

$$H(K) - H_E(K) \leq D_N.$$

This shows that, in a closed system, for example, the decrease in equivocation of key after  $N$  letters have been intercepted is not greater than the redundancy of  $N$  letters of the language. In such systems, which comprise the majority of ciphers, it is only the existence of redundancy in the original messages that makes a solution possible.

Now suppose we have a pure system. Let the different residue classes of messages be  $C_1, C_2, C_3, \dots, C_r$ , and the corresponding set of residue classes of cryptograms be  $C'_1, C'_2, \dots, C'_r$ . The probability of each  $E$  in  $C'_1$  is the same:

$$P(E) = \frac{P(C_i)}{\varphi_i} \quad E \text{ a member of } C_i$$

where  $\varphi_i$  is the number of different messages in  $C_i$ . Thus we have

$$\begin{aligned} H(E) &= - \sum_i \varphi_i \frac{P(C_i)}{\varphi_i} \log \frac{P(C_i)}{\varphi_i} \\ &= - \sum_i P(C_i) \log \frac{P(C_i)}{\varphi_i} \end{aligned}$$

Substituting in our equation for  $H_E(K)$  we obtain:

*Theorem 11: For a pure cipher*

$$H_E(K) = H(K) + H(M) + \sum_i P(C_i) \log \frac{P(C_i)}{\varphi_i}.$$

This result can be used to compute  $H_E(K)$  in certain cases of interest.

## 13. EQUIVOCATION FOR SIMPLE SUBSTITUTION ON A TWO LETTER LANGUAGE

We will now calculate the equivocation in key or message when simple substitution is applied to a two letter language, with probabilities  $p$  and  $q$  for 0 and 1, and successive letters chosen independently. We have

$$H_E(M) = H_E(K) = -\sum P(E) P_E(K) \log P_E(K)$$

The probability that  $E$  contains exactly  $s$  0's in a particular permutation is:

$$\frac{1}{2}(p^s q^{N-s} + q^s p^{N-s})$$

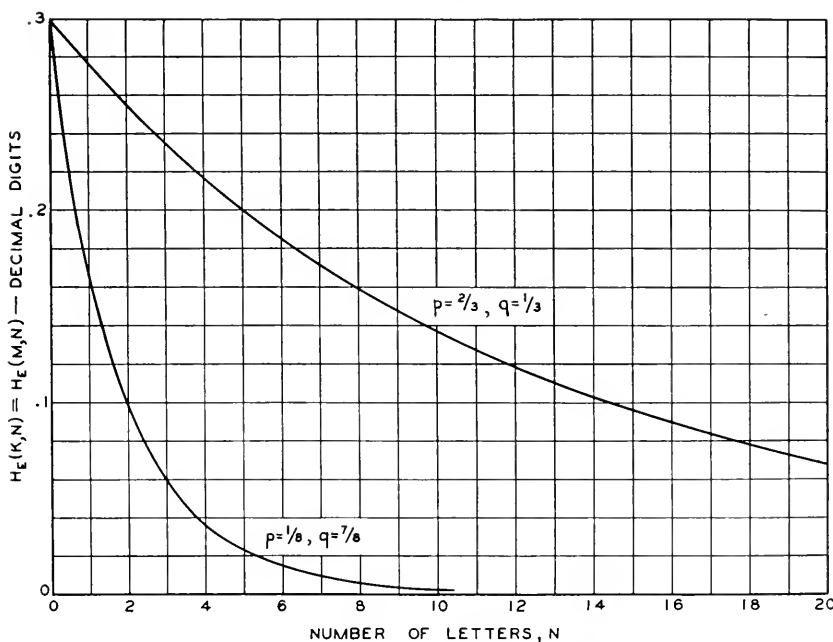


Fig. 6—Equivocation for simple substitution on two-letter language.

and the *a posteriori* probabilities of the identity and inverting substitutions (the only two in the system) are respectively:

$$P_E(0) = \frac{p^s q^{N-s}}{(p^s q^{N-s} + q^s p^{N-s})} \quad P_E(1) = \frac{p^{N-s} q^s}{(p^s q^{N-s} + q^s p^{N-s})}.$$

There are  $\binom{N}{s}$  terms for each  $s$  and hence

$$H_E(K, N) = -\sum_s \binom{N}{s} p^s q^{N-s} \log \frac{p^s q^{N-s}}{(p^s q^{N-s} + q^s p^{N-s})}.$$

For  $p = \frac{1}{3}$ ,  $q = \frac{2}{3}$ , and for  $p = \frac{1}{8}$ ,  $q = \frac{7}{8}$ ,  $H_E(K, N)$  has been calculated and is shown in Fig. 6.

#### 14. THE EQUIVOCATION CHARACTERISTIC FOR A "RANDOM" CIPHER

In the preceding section we have calculated the equivocation characteristic for a simple substitution applied to a two-letter language. This is about the simplest type of cipher and the simplest language structure possible, yet already the formulas are so involved as to be nearly useless. What are we to do with cases of practical interest, say the involved transformations of a fractional transposition system applied to English with its extremely complex statistical structure? This complexity itself suggests a method of approach. Sufficiently complicated problems can frequently be solved statistically. To facilitate this we define the notion of a "random" cipher.

We make the following assumptions:

1. The number of possible messages of length  $N$  is  $T = 2^{R_0 N}$ , thus  $R_0 = \log_2 G$ , where  $G$  is the number of letters in the alphabet. The number of possible cryptograms of length  $N$  is also assumed to be  $T$ .
2. The possible messages of length  $N$  can be divided into two groups: one group of high and fairly uniform *a priori* probability, the second group of negligibly small total probability. The high probability group will contain  $S = 2^{RN}$  messages, where  $R = H(M)/N$ , that is,  $R$  is the entropy of the message source per letter.
3. The deciphering operation can be thought of as a series of lines, as in Figs. 2 and 4, leading back from each  $E$  to various  $M$ 's. We assume  $k$  different equiprobable keys so there will be  $k$  lines leading back from each  $E$ . For the random cipher we suppose that the lines from each  $E$  go back to a random selection of the possible messages. Actually, then, a random cipher is a whole ensemble of ciphers and the equivocation is the average equivocation for this ensemble.

The equivocation of key is defined by

$$H_E(K) = \sum P(E)P_E(K) \log P_E(K).$$

The probability that exactly  $m$  lines go back from a particular  $E$  to the high probability group of messages is

$$\binom{k}{m} \left(\frac{S}{T}\right)^m \left(1 - \frac{S}{T}\right)^{k-m}$$

If a cryptogram with  $m$  such lines is intercepted the equivocation is  $\log m$ .

The probability of such a cryptogram is  $\frac{mT}{SK}$ , since it can be produced by

$m$  keys from high probability messages each with probability  $\frac{T}{S}$ . Hence the equivocation is:

$$H_E(K) = \frac{T}{Sk} \sum_{m=1}^k \binom{k}{m} \left(\frac{S}{T}\right)^m \left(1 - \frac{S}{T}\right)^{k-m} m \log m$$

We wish to find a simple approximation to this when  $k$  is large. If the expected value of  $m$ , namely  $\bar{m} = Sk/T$ , is  $\gg 1$ , the variation of  $\log m$  over the range where the binomial distribution assumes large values will be small, and we can replace  $\log m$  by  $\log \bar{m}$ . This can now be factored out of the summation, which then reduces to  $\bar{m}$ . Hence, in this condition,

$$H_E(K) \doteq \log \frac{Sk}{T} = \log S - \log T + \log k$$

$$H_E(K) \doteq H(K) - DN,$$

where  $D$  is the redundancy per letter of the original language ( $D = D_N/N$ ).

If  $\bar{m}$  is small compared to the large  $k$ , the binomial distribution can be approximated by a Poisson distribution:

$$\binom{k}{m} p^m q^{k-m} \doteq \frac{e^{-\lambda} \lambda^m}{m!}$$

where  $\lambda = \frac{Sk}{T}$ . Hence

$$H_E(K) \doteq \frac{1}{\lambda} e^{-\lambda} \sum_2^{\infty} \frac{\lambda^m}{m!} m \log m.$$

If we replace  $m$  by  $m + 1$ , we obtain:

$$H_E(K) \doteq e^{-\lambda} \sum_1^{\infty} \frac{\lambda^m}{m!} \log (m + 1).$$

This may be used in the region where  $\lambda$  is near unity. For  $\lambda \ll 1$ , the only important term in the series is that for  $m = 1$ ; omitting the others we have:

$$\begin{aligned} H_E(K) &\doteq e^{-\lambda} \lambda \log 2 \\ &\doteq \lambda \log 2 \\ &\doteq 2^{-ND} k \log 2. \end{aligned}$$

To summarize:  $H_E(K)$ , considered as a function of  $N$ , the number of intercepted letters, starts off at  $H(K)$  when  $N = 0$ . It decreases linearly with a slope  $-D$  out to the neighborhood of  $N = \frac{H(K)}{D}$ . After a short transition region,  $H_E(K)$  follows an exponential with "half life" distance

$\frac{1}{D}$  if  $D$  is measured in bits per letter. This behavior is shown in Fig. 7, together with the approximating curves.

By a similar argument the equivocation of message can be calculated. It is

$$H_E(M) = R_0 N \text{ for } R_0 N \ll H_E(K)$$

$$H_E(M) = H_E(K) \text{ for } R_0 N \gg H_E(K)$$

$$H_E(M) = H_E(K) - \varphi(N) \text{ for } R_0 N \sim H_E(K)$$

where  $\varphi(N)$  is the function shown in Fig. 7 with  $N$  scale reduced by factor of  $\frac{D}{R_0}$ . Thus,  $H_E(M)$  rises linearly with slope  $R_0$ , until it nearly intersects

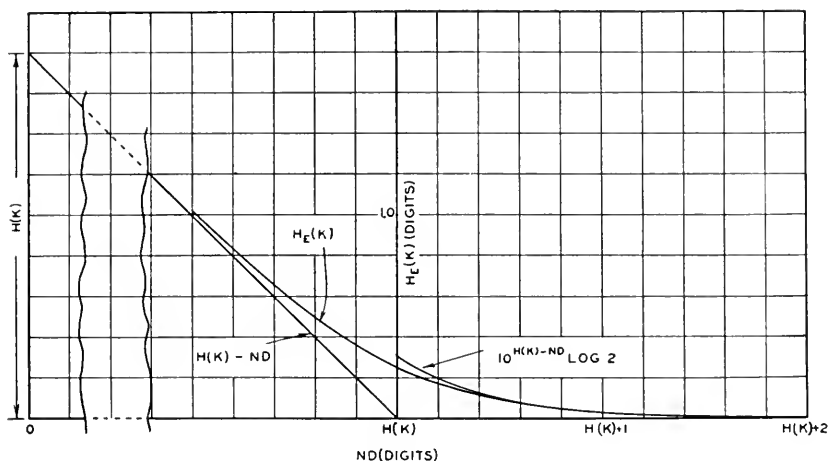


Fig. 7—Equivocation for random cipher.

the  $H_E(K)$  line. After a rounded transition it follows the  $H_E(K)$  curve down.

It will be seen from Fig. 7 that the equivocation curves approach zero rather sharply. Thus we may, with but little ambiguity, speak of a point at which the solution becomes unique. This number of letters will be called the unicity distance. For the random cipher it is approximately  $H(K)/D$ .

## 15. APPLICATION TO STANDARD CIPHERS

Most of the standard ciphers involve rather complicated enciphering and deciphering operations. Furthermore, the statistical structure of natural languages is extremely involved. It is therefore reasonable to assume that the formulas derived for the random cipher may be applied in such cases. It is necessary, however, to apply certain corrections in some cases. The main points to be observed are the following:

1. We assumed for the random cipher that the possible decipherments of a cryptogram are a random selection from the possible messages. While not strictly true in ordinary systems, this becomes more nearly the case as the complexity of the enciphering operations and of the language structure increases. With a transposition cipher it is clear that letter frequencies are preserved under decipherment operations. This means that the possible decipherments are chosen from a more limited group, not the entire message space, and the formula should be changed. In place of  $R_0$  one uses  $R_1$  the entropy rate for a language with independent letters but with the regular letter frequencies. In some other cases a definite tendency toward returning the decipherments to high probability messages can be seen. If there is no clear tendency of this sort, and the system is fairly complicated, then it is reasonable to use the random cipher analysis.

2. In many cases the complete key is not used in enciphering short messages. For example, in a simple substitution, only fairly long messages will contain all letters of the alphabet and thus involve the complete key. Obviously the random assumption does not hold for small  $N$  in such a case, since all the keys which differ only in the letters not yet appearing in the cryptogram lead back to the same message and are not randomly distributed. This error is easily corrected to a good approximation by the use of a "key appearance characteristic." One uses, at a particular  $N$ , the effective amount of key that may be expected with that length of cryptogram. For most ciphers, this is easily estimated.

3. There are certain "end effects" due to the definite starting of the message which produce a discrepancy from the random characteristics. If we take a random starting point in English text, the first letter (when we do not observe the preceding letters) has a possibility of being any letter with the ordinary letter probabilities. The next letter is more completely specified since we then have digram frequencies. This decrease in choice value continues for some time. The effect of this on the curve is that the straight line part is displaced, and approached by a curve depending on how much the statistical structure of the language is spread out over adjacent letters. As a first approximation the curve can be corrected by shifting the line over to the half redundancy point—i.e., the number of letters where the language redundancy is half its final value.

If account is taken of these three effects, reasonable estimates of the equivocation characteristic and unicity point can be made. The calculation can be done graphically as indicated in Fig. 8. One draws the key appearance characteristic and the total redundancy curve  $D_N$  (which is usually sufficiently well represented by the line  $ND_\infty$ ). The difference between these out to the neighborhood of their intersection is  $H_E(M)$ . With a simple substitution cipher applied to English, this calculation gave the

curves shown in Fig. 9. The key appearance characteristic in this case was estimated by counting the number of different letters appearing in typical English passages of  $N$  letters. In so far as experimental data on the simple substitution could be found, they agree very well with the curves of Fig. 9, considering the various idealizations and approximations which have been made. For example, the unicity point, at about 27 letters, can be shown experimentally to lie between the limits 20 and 30. With 30 letters there is

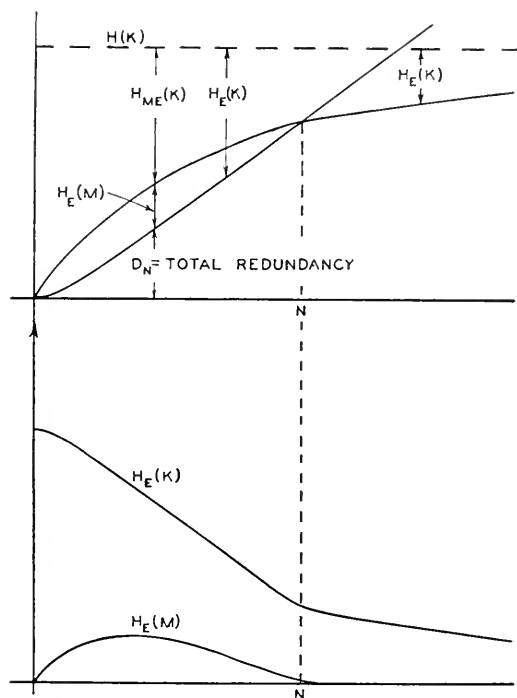


Fig. 8—Graphical calculation of equivocation.

nearly always a unique solution to a cryptogram of this type and with 20 it is usually easy to find a number of solutions.

With transposition of period  $d$  (random key),  $H(K) = \log d!$ , or about  $d \log d/e$  (using a Stirling approximation for  $d!$ ). If we take .6 decimal digits per letter as the appropriate redundancy, remembering the preservation of letter frequencies, we obtain about  $1.7d \log d/e$  as the unicity distance. This also checks fairly well experimentally. Note that in this case  $H_E(M)$  is defined only for integral multiples of  $d$ .

With the Vigenère the unicity point will occur at about  $2d$  letters, and this too is about right. The Vigenère characteristic with the same key size

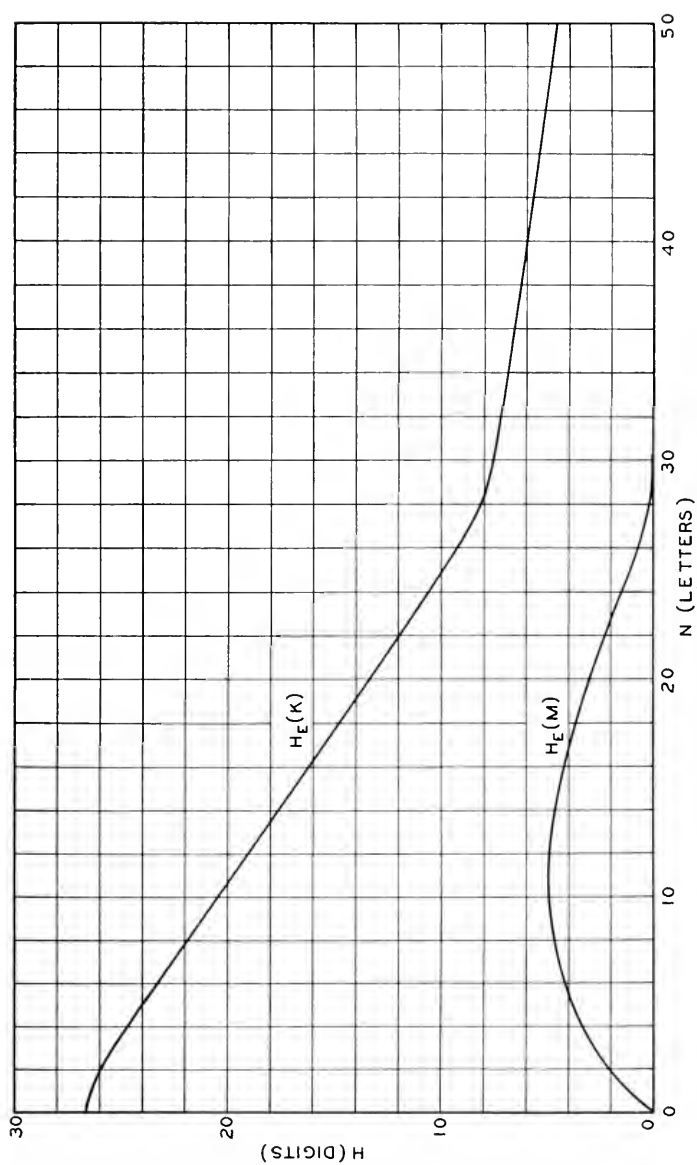


Fig. 9—Equivocation for simple substitution on English.



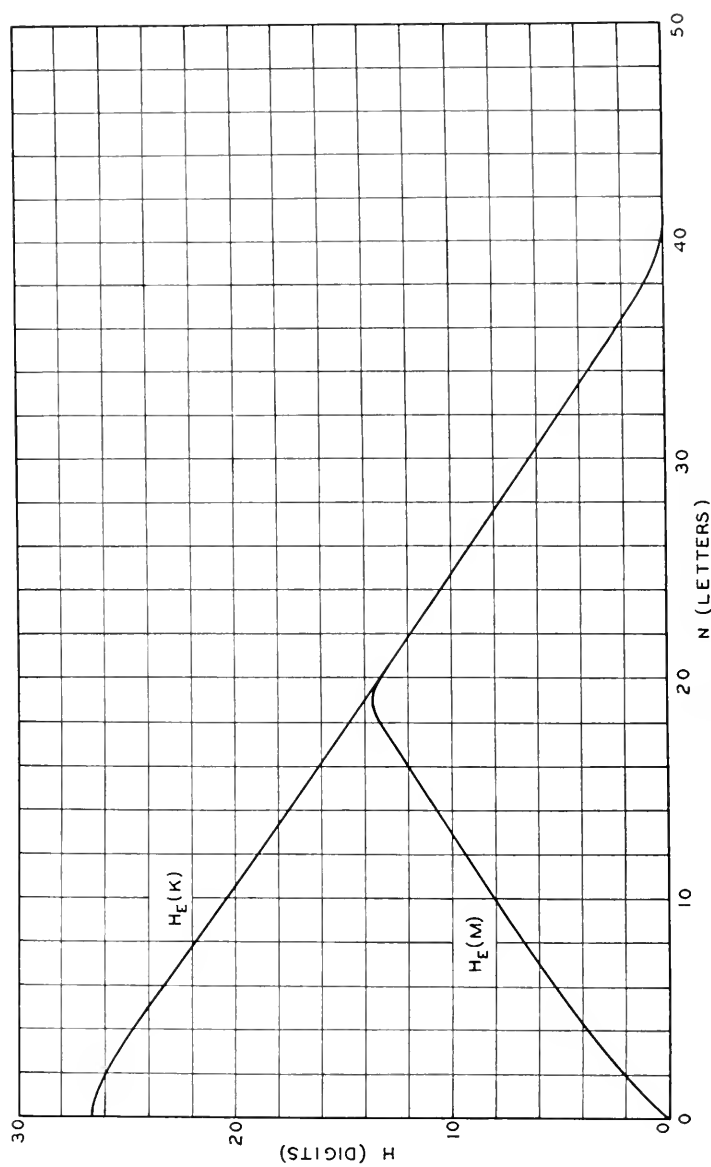


Fig. 10—Equivocation for Vigenère on English.

as simple substitution will be approximately as shown in Fig. 10. The Vigenère, Playfair and Fractional cases are more likely to follow the theoretical formulas for random ciphers than simple substitution and transposition. The reason for this is that they are more complex and give better mixing characteristics to the messages on which they operate.

The mixed alphabet Vigenère (each of  $d$  alphabets mixed independently and used sequentially) has a key size,

$$H(K) = d \log 26! = 26.3d$$

and its unicity point should be at about  $53d$  letters.

These conclusions can also be put to a rough experimental test with the Caesar type cipher. In the particular cryptogram analyzed in Table I, section 11, the function ( $H_E(K, N)$ ) has been calculated and is given below, together with the values for a random cipher.

$N$	<u>0</u>	<u>1</u>	<u>2</u>	<u>3</u>	<u>4</u>	<u>5</u>
$H$ (observed)	1.41	1.24	.97	.60	.28	0
$H$ (calculated)	1.41	1.25	.98	.54	.15	.03

The agreement is seen to be quite good, especially when we remember that the observed  $H$  should actually be the average of many different cryptograms, and that  $D$  for the larger values of  $N$  is only roughly estimated.

It appears then that the random cipher analysis can be used to estimate equivocation characteristics and the unicity distance for the ordinary types of ciphers.

## 16. VALIDITY OF A CRYPTOGRAM SOLUTION

The equivocation formulas are relevant to questions which sometimes arise in cryptographic work regarding the validity of an alleged solution to a cryptogram. In the history of cryptography there have been many cryptograms, or possible cryptograms, where clever analysts have found a "solution." It involved, however, such a complex process, or the material was so meager that the question arose as to whether the cryptanalyst had "read a solution" into the cryptogram. See, for example, the Bacon-Shakespeare ciphers and the "Roger Bacon" manuscript.<sup>10</sup>

In general we may say that if a proposed system and key solves a cryptogram for a length of material considerably greater than the unicity distance the solution is trustworthy. If the material is of the same order or shorter than the unicity distance the solution is highly suspicious.

This effect of redundancy in gradually producing a unique solution to a cipher can be thought of in another way which is helpful. The redundancy is essentially a series of conditions on the letters of the message, which

<sup>10</sup> See Fletcher Pratt, *loc. cit.*

insure that it be statistically reasonable. These consistency conditions produce corresponding consistency conditions in the cryptogram. The key gives a certain amount of freedom to the cryptogram but, as more and more letters are intercepted, the consistency conditions use up the freedom allowed by the key. Eventually there is only one message and key which satisfies all the conditions and we have a unique solution. In the random cipher the consistency conditions are, in a sense "orthogonal" to the "grain of the key" and have their full effect in eliminating messages and keys as rapidly as possible. This is the usual case. However, by proper design it is possible to "line up" the redundancy of the language with the "grain of the key" in such a way that the consistency conditions are automatically satisfied and  $H_E(K)$  does not approach zero. These "ideal" systems, which will be considered in the next section, are of such a nature that the transformations  $T_i$  all induce the same probabilities in the  $E$  space.

### 17. IDEAL SECRECY SYSTEMS.

We have seen that perfect secrecy requires an infinite amount of key if we allow messages of unlimited length. With a finite key size, the equivocation of key and message generally approaches zero, but not necessarily so. In fact it is possible for  $H_E(K)$  to remain constant at its initial value  $H(K)$ . Then, no matter how much material is intercepted, there is not a unique solution but many of comparable probability. We will define an "ideal" system as one in which  $H_E(K)$  and  $H_E(M)$  do not approach zero as  $N \rightarrow \infty$ . A "strongly ideal" system is one in which  $H_E(K)$  remains constant at  $H(K)$ .

An example is a simple substitution on an artificial language in which all letters are equiprobable and successive letters independently chosen. It is easily seen that  $H_E(K) = H(K)$  and  $H_E(M)$  rises linearly along a line of slope  $\log G$  (where  $G$  is the number of letters in the alphabet) until it strikes the line  $H(K)$ , after which it remains constant at this value.

With natural languages it is in general possible to approximate the ideal characteristic—the unicity point can be made to occur for as large  $N$  as is desired. The complexity of the system needed usually goes up rapidly when we attempt to do this, however. It is not always possible to attain actually the ideal characteristic with any system of finite complexity.

To approximate the ideal equivocation, one may first operate on the message with a transducer which removes all redundancies. After this almost any simple ciphering system—substitution, transposition, Vigenère, etc., is satisfactory. The more elaborate the transducer and the nearer the output is to the desired form, the more closely will the secrecy system approximate the ideal characteristic.

*Theorem 12: A necessary and sufficient condition that  $T$  be strongly ideal is that, for any two keys,  $T_i^{-1}T_j$  is a measure preserving transformation of the message space into itself.*

This is true since the *a posteriori* probability of each key is equal to its *a priori* probability if and only if this condition is satisfied.

## 18. EXAMPLES OF IDEAL SECRECY SYSTEMS

Suppose our language consists of a sequence of letters all chosen independently and with equal probabilities. Then the redundancy is zero, and from a result of section 12,  $H_E(K) = H(K)$ . We obtain the result

*Theorem 13: If all letters are equally likely and independent any closed cipher is strongly ideal.*

The equivocation of message will rise along the key appearance characteristic which will usually approach  $H(K)$ , although in some cases it does not. In the cases of  $n$ -gram substitution, transposition, Vigenère, and variations, fractional, etc., we have strongly ideal systems for this simple language with  $H_E(M) \rightarrow H(K)$  as  $N \rightarrow \infty$ .

Ideal secrecy systems suffer from a number of disadvantages.

1. The system must be closely matched to the language. This requires an extensive study of the structure of the language by the designer. Also a change in statistical structure or a selection from the set of possible messages, as in the case of probable words (words expected in this particular cryptogram), renders the system vulnerable to analysis.

2. The structure of natural languages is extremely complicated, and this implies a complexity of the transformations required to eliminate redundancy. Thus any machine to perform this operation must necessarily be quite involved, at least in the direction of information storage, since a "dictionary" of magnitude greater than that of an ordinary dictionary is to be expected.

3. In general, the transformations required introduce a bad propagation of error characteristic. Error in transmission of a single letter produces a region of changes near it of size comparable to the length of statistical effects in the original language.

## 19. FURTHER REMARKS ON EQUIVOCATION AND REDUNDANCY

We have taken the redundancy of "normal English" to be about .7 decimal digits per letter or a redundancy of 50%. This is on the assumption that word divisions were omitted. It is an approximate figure based on statistical structure extending over about 8 letters, and assumes the text to be of an ordinary type, such as newspaper writing, literary work, etc. We may note here a method of roughly estimating this number that is of some cryptographic interest.

A running key cipher is a Vernam type system where, in place of a random sequence of letters, the key is a meaningful text. Now it is known that running key ciphers can usually be solved uniquely. This shows that English can be reduced by a factor of two to one and implies a redundancy of at least 50%. This figure cannot be increased very much, however, for a number of reasons, unless long range "meaning" structure of English is considered.

The running key cipher can be easily improved to lead to ciphering systems which could not be solved without the key. If one uses in place of one English text, about 4 different texts as key, adding them all to the message, a sufficient amount of key has been introduced to produce a high positive equivocation. Another method would be to use, say, every 10th letter of the text as key. The intermediate letters are omitted and cannot be used at any other point of the message. This has much the same effect, since these spaced letters are nearly independent.

The fact that the vowels in a passage can be omitted without essential loss suggests a simple way of greatly improving almost any ciphering system. First delete all vowels, or as much of the message as possible without running the risk of multiple reconstructions, and then encipher the residue. Since this reduces the redundancy by a factor of perhaps 3 or 4 to 1, the unicity point will be moved out by this factor. This is one way of approaching ideal systems—using the decipherer's knowledge of English as part of the deciphering system.

## 20. DISTRIBUTION OF EQUIVOCATION

A more complete description of a secrecy system applied to a language than is afforded by the equivocation characteristics can be found by giving the *distribution of equivocation*. For  $N$  intercepted letters we consider the fraction of cryptograms for which the equivocation (for these particular  $E$ 's, not the mean  $H_E(M)$ ) lies between certain limits. This gives a density distribution function

$$P(H_E(M), N) dH_E(M)$$

for the probability that for  $N$  letters  $H$  lies between the limits  $H$  and  $H + dH$ . The mean equivocation we have previously studied is the mean of this distribution. The function  $P(H_E(M), N)$  can be thought of as plotted along a third dimension, normal to the paper, on the  $H_E(M), N$  plane. If the language is pure, with a small influence range, and the cipher is pure, the function will usually be a ridge in this plane whose highest point follows approximately the mean  $H_E(M)$ , at least until near the unicity point. In this case, or when the conditions are nearly verified, the mean curve gives a reasonably complete picture of the system.

On the other hand, if the language is not pure, but made up of a set of pure components

$$L = \sum p_i L_i$$

having different equivocation curves with the system, then the total distribution will usually be made up of a series of ridges. There will be one for each  $L_i$  weighted in accordance with its  $p_i$ . The mean equivocation characteristic will be a line somewhere in the midst of these ridges and may not give a very complete picture of the situation. This is shown in Fig. 11. A similar effect occurs if the system is not pure but made up of several systems with different  $H$  curves.

The effect of mixing pure languages which are near to one another in statistical structure is to increase the width of the ridge. Near the unicity

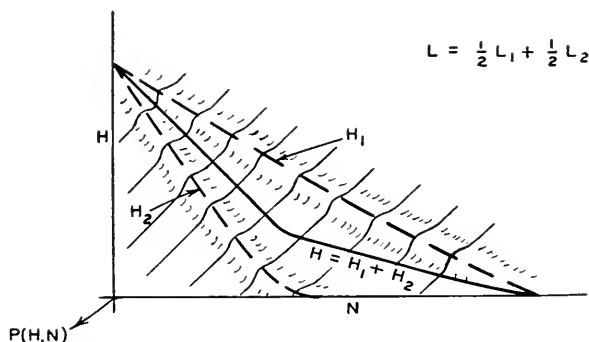


Fig. 11—Distribution of equivocation with a mixed language  $L = \frac{1}{2}L_1 + \frac{1}{2}L_2$ .

point this tends to raise the mean equivocation, since equivocation cannot become negative and the spreading is chiefly in the positive direction. We expect, therefore, that in this region the calculations based on the random cipher should be somewhat low.

### PART III

#### PRACTICAL SECRECY

##### 21. THE WORK CHARACTERISTIC

After the unicity point has been passed in intercepted material there will usually be a unique solution to the cryptogram. The problem of isolating this single solution of high probability is the problem of cryptanalysis. In the region before the unicity point we may say that the problem of cryptanalysis is that of isolating all the possible solutions of high probability (compared to the remainder) and determining their various probabilities.

Although it is always possible in principle to determine these solutions (by trial of each possible key for example), different enciphering systems show a wide variation in the amount of work required. The average amount of work to determine the key for a cryptogram of  $N$  letters,  $W(N)$ , measured say in man hours, may be called the work characteristic of the system. This average is taken over all messages and all keys with their appropriate probabilities. The function  $W(N)$  is a measure of the amount of "practical secrecy" afforded by the system.

For a simple substitution on English the work and equivocation characteristics would be somewhat as shown in Fig. 12. The dotted portion of

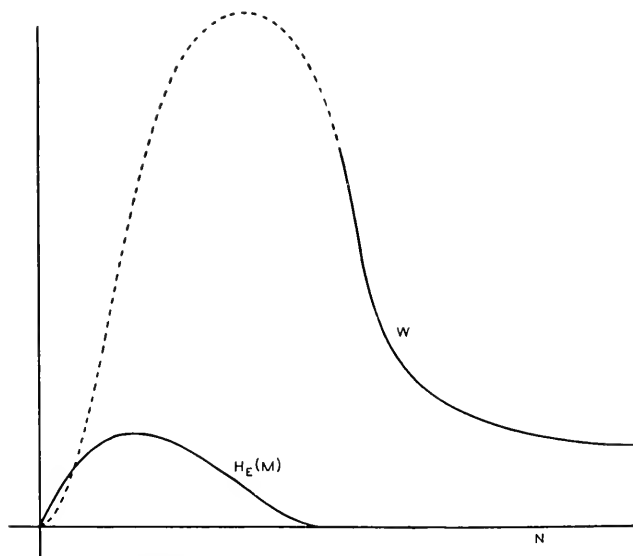


Fig. 12—Typical work and equivocation characteristics.

the curve is in the range where there are numerous possible solutions and these must all be determined. In the solid portion after the unicity point only one solution exists in general, but if only the minimum necessary data are given a great deal of work must be done to isolate it. As more material is available the work rapidly decreases toward some asymptotic value—where the additional data no longer reduces the labor.

Essentially the behavior shown in Fig. 12 can be expected with any type of secrecy system where the equivocation approaches zero. The scale of man hours required, however, will differ greatly with different types of ciphers, even when the  $H_E(M)$  curves are about the same. A Vigenère or compound Vigenère, for example, with the same key size would have a

much better (i.e., much higher) work characteristic. A good practical secrecy system is one in which the  $W(N)$  curve remains sufficiently high, out to the number of letters one expects to transmit with the key, to prevent the enemy from actually carrying out the solution, or to delay it to such an extent that the information is then obsolete.

We will consider in the following sections ways of keeping the function  $W(N)$  large, even though  $H_E(K)$  may be practically zero. This is essentially a "max min" type of problem as is always the case when we have a battle of wits.<sup>11</sup> In designing a good cipher we must maximize the minimum amount of work the enemy must do to break it. It is not enough merely to be sure none of the standard methods of cryptanalysis work—we must be sure that no method whatever will break the system easily. This, in fact, has been the weakness of many systems; designed to resist all the known methods of solution, they later gave rise to new cryptanalytic techniques which rendered them vulnerable to analysis.

The problem of good cipher design is essentially one of finding difficult problems, subject to certain other conditions. This is a rather unusual situation, since one is ordinarily seeking the simple and easily soluble problems in a field.

How can we ever be sure that a system which is not ideal and therefore *has* a unique solution for sufficiently large  $N$  will require a large amount of work to break with *every* method of analysis? There are two approaches to this problem; (1) We can study the possible methods of solution available to the cryptanalyst and attempt to describe them in sufficiently general terms to cover any methods he might use. We then construct our system to resist this "general" method of solution. (2) We may construct our cipher in such a way that breaking it is equivalent to (or requires at some point in the process) the solution of some problem known to be laborious. Thus, if we could show that solving a certain system requires at least as much work as solving a system of simultaneous equations in a large number of unknowns, of a complex type, then we would have a lower bound of sorts for the work characteristic.

The next three sections are aimed at these general problems. It is difficult to define the pertinent ideas involved with sufficient precision to obtain results in the form of mathematical theorems, but it is believed that the conclusions, in the form of general principles, are correct.

<sup>11</sup> See von Neumann and Morgenstern, *loc. cit.* The situation between the cipher designer and cryptanalyst can be thought of as a "game" of a very simple structure; a zero-sum two-person game with complete information, and just two "moves." The cipher designer chooses a system for his "move." Then the cryptanalyst is informed of this choice and chooses a method of analysis. The "value" of the play is the average work required to break a cryptogram in the system by the method chosen.



## 22. GENERALITIES ON THE SOLUTION OF CRYPTOGRAMS

After the unicity distance has been exceeded in intercepted material, any system can be solved in principle by merely trying each possible key until the unique solution is obtained—i.e., a deciphered message which “makes sense” in the original language. A simple calculation shows that this method of solution (which we may call *complete trial and error*) is totally impractical except when the key is absurdly small.

Suppose, for example, we have a key of  $26!$  possibilities or about 26.3 decimal digits, the same size as in simple substitution on English. This is, by any significant measure, a small key. It can be written on a small slip of paper, or memorized in a few minutes. It could be registered on 27 switches, each having ten positions, or on 88 two-position switches.

Suppose further, to give the cryptanalyst every possible advantage, that he constructs an electronic device to try keys at the rate of one each micro-second (perhaps automatically selecting from the results by a  $\chi^2$  test for statistical significance). He may expect to reach the right key about half way through, and after an elapsed time of about  $2 \times 10^{26} / 2 \times 60^2 \times 24 \times 365 \times 10^6$  or  $3 \times 10^{12}$  years.

In other words, even with a small key complete trial and error will never be used in solving cryptograms, except in the trivial case where the key is extremely small, e.g., the Caesar with only 26 possibilities, or 1.4 digits. The trial and error which is used so commonly in cryptography is of a different sort, or is augmented by other means. If one had a secrecy system which required complete trial and error it would be extremely safe. Such a system would result, it appears, if the meaningful original messages, all say of 1000 letters, were a random selection from the set of all sequences of 1000 letters. If any of the simple ciphers were applied to this type of language it seems that little improvement over complete trial and error would be possible.

The methods of cryptanalysis actually used often involve a great deal of trial and error, but in a different way. First, the trials progress from more probable to less probable hypotheses, and, second, each trial disposes of a large group of keys, not a single one. Thus the key space may be divided into say 10 subsets, each containing about the same number of keys. By at most 10 trials one determines which subset is the correct one. This subset is then divided into several secondary subsets and the process repeated. With the same key size ( $26! \doteq 2 \times 10^{26}$ ) we would expect about  $26 \times 5$  or 130 trials as compared to  $10^{26}$  by complete trial and error. The possibility of choosing the most likely of the subsets first for test would improve this result even more. If the divisions were into two compartments (the best way to

minimize the number of trials) only 88 trials would be required. Whereas complete trial and error requires trials to the order of the number of keys, this subdividing trial and error requires only trials to the order of the key size in bits.

This remains true even when the different keys have different probabilities. The proper procedure, then, to minimize the expected number of trials is to divide the key space into subsets of equiprobability. When the proper subset is determined, this is again subdivided into equiprobability subsets. If this process can be continued the number of trials expected when each division is into two subsets will be

$$h = \frac{H(K)}{\log 2}$$

If each test has  $S$  possible results and each of these corresponds to the key being in one of  $S$  equiprobability subsets, then

$$h = \frac{H(K)}{\log S}$$

trials will be expected. The intuitive significance of these results should be noted. In the two-compartment test with equiprobability, each test yields one bit of information as to the key. If the subsets have very different probabilities, as in testing a single key in complete trial and error, only a small amount of information is obtained from the test. Thus with  $26!$  equiprobable keys, a test of one yields only

$$- \left[ \frac{26! - 1}{26!} \log \frac{26! - 1}{26!} + \frac{1}{26!} \log \frac{1}{26!} \right]$$

or about  $10^{-25}$  bits of information. Dividing into  $S$  equiprobability subsets maximizes the information obtained from each trial at  $\log S$ , and the expected number of trials is the total information to be obtained, that is  $H(K)$ , divided by this amount.

The question here is similar to various coin weighing problems that have been circulated recently. A typical example is the following: It is known that one coin in 27 is counterfeit, and slightly lighter than the rest. A chemist's balance is available and the counterfeit coin is to be isolated by a series of weighings. What is the least number of weighings required to do this? The correct answer is 3, obtained by first dividing the coins into three groups of 9 each. Two of these are compared on the balance. The three possible results determine the set of 9 containing the counterfeit. This set is then divided into 3 subsets of 3 each and the process continued. The set of coins corresponds to the set of keys, the counterfeit coin to the correct key, and the weighing procedure to a trial or test. The original uncertainty is  $\log_3 27$

bits, and each trial yields  $\log_2 3$  bits of information; thus, when there is no "diophantine trouble,"  $\log_2 27/\log_2 3$  or 3 trials are sufficient.

This method of solution is feasible only if the key space can be divided into a small number of subsets, with a simple method of determining the subset to which the correct key belongs. One does not need to assume a complete key in order to apply a consistency test and determine if the assumption is justified—an assumption on a part of the key (or as to whether the key is in some large section of the key space) can be tested. In other words it is possible to solve for the key bit by bit.

The possibility of this method of analysis is the crucial weakness of most ciphering systems. For example, in simple substitution, an assumption on a single letter can be checked against its frequency, variety of contact, doubles or reversals, etc. In determining a single letter the key space is reduced by 1.4 decimal digits from the original 26. The same effect is seen in all the elementary types of ciphers. In the Vigenère, the assumption of two or three letters of the key is easily checked by deciphering at other points with this fragment and noting whether clear emerges. The compound Vigenère is much better from this point of view, if we assume a fairly large number of component periods, producing a repetition rate larger than will be intercepted. In this case as many key letters are used in enciphering each letter as there are periods. Although this is only a fraction of the entire key, at least a fair number of letters must be assumed before a consistency check can be applied.

Our first conclusion then, regarding practical small key cipher design, is that a considerable amount of key should be used in enciphering each small element of the message.

### 23. STATISTICAL METHODS

It is possible to solve many kinds of ciphers by statistical analysis. Consider again simple substitution. The first thing a cryptanalyst does with an intercepted cryptogram is to make a frequency count. If the cryptogram contains, say, 200 letters it is safe to assume that few, if any, of the letters are out of their frequency groups, this being a division into 4 sets of well defined frequency limits. The logarithm of the number of keys within this limitation may be calculated as

$$\log 2! 9! 9! 6! = 14.28$$

and the simple frequency count thus reduces the key uncertainty by 12 decimal digits, a tremendous gain.

In general, a statistical attack proceeds as follows: A certain statistic is measured on the intercepted cryptogram  $E$ . This statistic is such that for all reasonable messages  $M$  it assumes about the same value,  $S_K$ , the value

depending only on the particular key  $K$  that was used. The value thus obtained serves to limit the possible keys to those which would give values of  $S$  in the neighborhood of that observed. A statistic which does not depend on  $K$  or which varies as much with  $M$  as with  $K$  is not of value in limiting  $K$ . Thus, in transposition ciphers, the frequency count of letters gives no information about  $K$ —every  $K$  leaves this statistic the same. Hence one can make no use of a frequency count in breaking transposition ciphers.

More precisely one can ascribe a “*solving power*” to a given statistic  $S$ . For each value of  $S$  there will be a conditional equivocation of the key  $H_s(K)$ , the equivocation when  $S$  has its particular value, and that is all that is known concerning the key. The weighted mean of these values

$$\sum P(S) H_s(K)$$

gives the mean equivocation of the key when  $S$  is known,  $P(S)$  being the *a priori* probability of the particular value  $S$ . The key size  $H(K)$ , less this mean equivocation, measures the “*solving power*” of the statistic  $S$ .

In a strongly ideal cipher *all* statistics of the cryptogram are independent of the particular key used. This is the measure preserving property of  $T_j T_k^{-1}$  on the  $E$  space or  $T_j^{-1} T_k$  on the  $M$  space mentioned above.

There are good and poor statistics, just as there are good and poor methods of trial and error. Indeed the trial and error testing of an hypothesis *is* a type of statistic, and what was said above regarding the best types of trials holds generally. A good statistic for solving a system must have the following properties:

1. It must be simple to measure.
2. It must depend more on the key than on the message if it is meant to solve for the key. The variation with  $M$  should not mask its variation with  $K$ .
3. The values of the statistic that can be “resolved” in spite of the “fuzziness” produced by variation in  $M$  should divide the key space into a number of subsets of comparable probability, with the statistic specifying the one in which the correct key lies. The statistic should give us sizeable information about the key, not a tiny fraction of a bit.
4. The information it gives must be simple and usable. Thus the subsets in which the statistic locates the key must be of a simple nature in the key space.

Frequency count for simple substitution is an example of a very good statistic.

Two methods (other than recourse to ideal systems) suggest themselves for frustrating a statistical analysis. These we may call the methods of *diffusion* and *confusion*. In the method of diffusion the statistical structure of  $M$  which leads to its redundancy is “dissipated” into long range sta-

tistics—i.e., into statistical structure involving long combinations of letters in the cryptogram. The effect here is that the enemy must intercept a tremendous amount of material to tie down this structure, since the structure is evident only in blocks of very small individual probability. Furthermore, even when he has sufficient material, the analytical work required is much greater since the redundancy has been diffused over a large number of individual statistics. An example of diffusion of statistics is operating on a message  $M = m_1, m_2, m_3, \dots$  with an “averaging” operation, e.g.

$$y_n = \sum_{i=1}^s m_{n+i} \pmod{26},$$

adding  $s$  successive letters of the message to get a letter  $y_n$ . One can show that the redundancy of the  $y$  sequence is the same as that of the  $m$  sequence, but the structure has been dissipated. Thus the letter frequencies in  $y$  will be more nearly equal than in  $m$ , the digram frequencies also more nearly equal, etc. Indeed any reversible operation which produces one letter out for each letter in and does not have an infinite “memory” has an output with the same redundancy as the input. The statistics can never be eliminated without compression, but they can be spread out.

The method of *confusion* is to make the relation between the simple statistics of  $E$  and the simple description of  $K$  a very complex and involved one. In the case of simple substitution, it is easy to describe the limitation of  $K$  imposed by the letter frequencies of  $E$ . If the connection is very involved and confused the enemy may still be able to evaluate a statistic  $S_1$ , say, which limits the key to a region of the key space. This limitation, however, is to some complex region  $R$  in the space, perhaps “folded over” many times, and he has a difficult time making use of it. A second statistic  $S_2$  limits  $K$  still further to  $R_2$ , hence it lies in the intersection region; but this does not help much because it is so difficult to determine just what the intersection is.

To be more precise let us suppose the key space has certain “natural coordinates”  $k_1, k_2, \dots, k_p$  which he wishes to determine. He measures, let us say, a set of statistics  $s_1, s_2, \dots, s_n$  and these are sufficient to determine the  $k_i$ . However, in the method of confusion, the equations connecting these sets of variables are involved and complex. We have, say,

$$\begin{aligned} f_1(k_1, k_2, \dots, k_p) &= s_1 \\ f_2(k_1, k_2, \dots, k_p) &= s_2 \\ &\vdots \\ f_n(k_1, k_2, \dots, k_p) &= s_n, \end{aligned}$$

and all the  $f_i$  involve all the  $k_i$ . The cryptographer must solve this system simultaneously—a difficult job. In the simple (not confused) cases the functions involve only a small number of the  $k_i$ —or at least some of these do. One first solves the simpler equations, evaluating some of the  $k_i$  and substitutes these in the more complicated equations.

The conclusion here is that for a good ciphering system steps should be taken either to diffuse or confuse the redundancy (or both).

#### 24. THE PROBABLE WORD METHOD

One of the most powerful tools for breaking ciphers is the use of probable words. The probable words may be words or phrases expected in the particular message due to its source, or they may merely be common words or syllables which occur in any text in the language, such as *the*, *and*, *tion*, *that*, and the like in English.

In general, the probable word method is used as follows: Assuming a probable word to be at some point in the clear, the key or a part of the key is determined. This is used to decipher other parts of the cryptogram and provide a consistency test. If the other parts come out in the clear, the assumption is justified.

There are few of the classical type ciphers that use a small key and can resist long under a probable word analysis. From a consideration of this method we can frame a test of ciphers which might be called the acid test. It applies only to ciphers with a small key (less than, say, 50 decimal digits), applied to natural languages, and not using the ideal method of gaining secrecy. The acid test is this: How difficult is it to determine the key or a part of the key knowing a small sample of message and corresponding cryptogram? Any system in which this is easy cannot be very resistant, for the cryptanalyst can always make use of probable words, combined with trial and error, until a consistent solution is obtained.

The conditions on the size of the key make the amount of trial and error small, and the condition about ideal systems is necessary, since these automatically give consistency checks. The existence of probable words and phrases is implied by the assumption of natural languages.

Note that the requirement of difficult solution under these conditions is not, by itself, contradictory to the requirements that enciphering and deciphering be simple processes. Using functional notation we have for enciphering

$$E = f(K, M)$$

and for deciphering

$$M = g(K, E).$$

Both of these may be simple operations on their arguments without the third equation

$$K = h(M, E)$$

being simple.

We may also point out that in investigating a new type of ciphering system one of the best methods of attack is to consider how the key could be determined if a sufficient amount of  $M$  and  $E$  were given.

The principle of confusion can be (and must be) used to create difficulties for the cryptanalyst using probable word techniques. Given (or assuming)  $M = m_1, m_2, \dots, m_s$  and  $E = e_1, e_2, \dots, e_s$  the cryptanalyst can set up equations for the different key elements  $k_1, k_2, \dots, k_r$  (namely the enciphering equations).

$$\begin{aligned} e_1 &= f_1(m_1, m_2, \dots, m_s; k_1, \dots, k_r) \\ e_2 &= f_2(m_1, m_2, \dots, m_s; k_1, \dots, k_r) \\ &\cdot \\ &\cdot \\ &\cdot \\ &\cdot \\ e_s &= f_s(m_1, m_2, \dots, m_s; k_1, \dots, k_r) \end{aligned}$$

All is known, we assume, except the  $k_i$ . Each of these equations should therefore be complex in the  $k_i$ , and involve many of them. Otherwise the enemy can solve the simple ones and then the more complex ones by substitution.

From the point of view of increasing confusion, it is desirable to have the  $f_i$  involve several  $m_i$ , especially if these are not adjacent and hence less correlated. This introduces the undesirable feature of error propagation, however, for then each  $e_i$  will generally affect several  $m_i$  in deciphering, and an error will spread to all these.

We conclude that much of the key should be used in an involved manner in obtaining any cryptogram letter from the message to keep the work characteristic high. Further a dependence on several uncorrelated  $m_i$  is desirable, if some propagation of error can be tolerated. We are led by all three of the arguments of these sections to consider "mixing transformations."

## 25. MIXING TRANSFORMATIONS

A notion that has proved valuable in certain branches of probability theory is the concept of a *mixing transformation*. Suppose we have a probability or measure space  $\Omega$  and a measure preserving transformation  $F$  of the space into itself, that is, a transformation such that the measure of a

transformed region  $FR$  is equal to the measure of the initial region  $R$ . The transformation is called mixing if for any function defined over the space and any region  $R$  the integral of the function over the region  $F^n R$  approaches, as  $n \rightarrow \infty$ , the integral of the function over the entire space  $\Omega$  multiplied by the volume of  $R$ . This means that any initial region  $R$  is mixed with uniform density throughout the entire space if  $F$  is applied a large number of times. In general,  $F^n R$  becomes a region consisting of a large number of thin filaments spread throughout  $\Omega$ . As  $n$  increases the filaments become finer and their density more constant.

A mixing transformation in this precise sense can occur only in a space with an infinite number of points, for in a finite point space the transformation must be periodic. Speaking loosely, however, we can think of a mixing transformation as one which distributes any reasonably cohesive region in the space fairly uniformly over the entire space. If the first region could be described in simple terms, the second would require very complex ones.

In cryptography we can think of all the possible messages of length  $N$  as the space  $\Omega$  and the high probability messages as the region  $R$ . This latter group has a certain fairly simple statistical structure. If a mixing transformation were applied, the high probability messages would be scattered evenly throughout the space.

Good mixing transformations are often formed by repeated products of two simple non-commuting operations. Hopf<sup>12</sup> has shown, for example, that pastry dough can be mixed by such a sequence of operations. The dough is first rolled out into a thin slab, then folded over, then rolled, and then folded again, etc.

In a good mixing transformation of a space with natural coordinates  $X_1, X_2, \dots, X_s$  the point  $X_i$  is carried by the transformation into a point  $X'_i$ , with

$$X'_i = f_i(X_1, X_2, \dots, X_s) \quad i = 1, 2, \dots, S$$

and the functions  $f_i$  are complicated, involving all the variables in a "sensitive" way. A small variation of any one,  $X_s$ , say, changes all the  $X'_i$  considerably. If  $X_s$  passes through its range of possible variation the point  $X'_i$  traces a long winding path around the space.

Various methods of mixing applicable to statistical sequences of the type found in natural languages can be devised. One which looks fairly good is to follow a preliminary transposition by a sequence of alternating substitutions and simple linear operations, adding adjacent letters mod 26 for example. Thus we might take

<sup>12</sup> E. Hopf, "On Causality, Statistics and Probability," *Journal of Math. and Physics*, v. 13, pp. 51-102, 1934.



$$F = LSLSLT$$

where  $T$  is a transposition,  $L$  is a linear operation, and  $S$  is a substitution.

## 26. CIPHERS OF THE TYPE $T_kFS_j$

Suppose that  $F$  is a good mixing transformation that can be applied to sequences of letters, and that  $T_k$  and  $S_j$  are any two simple families of transformations, i.e., two simple ciphers, which may be the same. For concreteness we may think of them as both simple substitutions.

It appears that the cipher  $TFS$  will be a very good secrecy system from the standpoint of its work characteristic. In the first place it is clear on reviewing our arguments about statistical methods that no simple statistics will give information about the key—any significant statistics derived from  $E$  must be of a highly involved and very sensitive type—the redundancy has been both diffused and confused by the mixing transformation  $F$ . Also probable words lead to a complex system of equations involving all parts of the key (when the mix is good), which must be solved simultaneously.

It is interesting to note that if the cipher  $T$  is omitted the remaining system is similar to  $S$  and thus no stronger. The enemy merely “unmixes” the cryptogram by application of  $F^{-1}$  and then solves. If  $S$  is omitted the remaining system is much stronger than  $T$  alone when the mix is good, but still not comparable to  $TFS$ .

The basic principle here of simple ciphers separated by a mixing transformation can of course be extended. For example one could use

$$T_kF_1S_jF_2R_i$$

with two mixes and three simple ciphers. One can also simplify by using the same ciphers, and even the same keys as well as the same mixing transformations. This might well simplify the mechanization of such systems.

The mixing transformation which separates the two (or more) appearances of the key acts as a kind of barrier for the enemy—it is easy to carry a known element over this barrier but an unknown (the key) does not go easily.

By supplying two sets of unknowns, the key for  $S$  and the key for  $T$ , and separating them by the mixing transformation  $F$  we have “entangled” the unknowns together in a way that makes solution very difficult.

Although systems constructed on this principle would be extremely safe they possess one grave disadvantage. If the mix is good then the propagation of errors is bad. A transmission error of one letter will affect several letters on deciphering.

## 27. INCOMPATIBILITY OF THE CRITERIA FOR GOOD SYSTEMS

The five criteria for good secrecy systems given in section 5 appear to have a certain incompatibility when applied to a natural language with its complicated statistical structure. With artificial languages having a simple statistical structure it is possible to satisfy all requirements simultaneously, by means of the ideal type ciphers. In natural languages a compromise must be made and the valuations balanced against one another with a view toward the particular application.

If any one of the five criteria is dropped, the other four can be satisfied fairly well, as the following examples show:

1. If we omit the first requirement (amount of secrecy) any simple cipher such as simple substitution will do. In the extreme case of omitting this condition completely, no cipher at all is required and one sends the clear!
2. If the size of the key is not limited the Vernam system can be used.
3. If complexity of operation is not limited, various extremely complicated types of enciphering process can be used.
4. If we omit the propagation of error condition, systems of the type *TFS* would be very good, although somewhat complicated.
5. If we allow large expansion of message, various systems are easily devised where the "correct" message is mixed with many "incorrect" ones (misinformation). The key determines which of these is correct.

A very rough argument for the incompatibility of the five conditions may be given as follows: From condition 5, secrecy systems essentially as studied in this paper must be used; i.e., no great use of nulls, etc. Perfect and ideal systems are excluded by condition 2 and by 3 and 4, respectively. The high secrecy required by 1 must then come from a high work characteristic, not from a high equivocation characteristic. If the key is small, the system simple, and the errors do not propagate, probable word methods will generally solve the system fairly easily, since we then have a fairly simple system of equations for the key.

This reasoning is too vague to be conclusive, but the general idea seems quite reasonable. Perhaps if the various criteria could be given quantitative significance, some sort of an exchange equation could be found involving them and giving the best physically compatible sets of values. The two most difficult to measure numerically are the complexity of operations, and the complexity of statistical structure of the language.

## APPENDIX

*Proof of Theorem 3*

Select any message  $M_1$  and group together all cryptograms that can be obtained from  $M_1$  by any enciphering operation  $T_i$ . Let this class of crypto-

grams be  $C_1'$ . Group with  $M_1$  all messages that can be obtained from  $M_1$  by  $T_i^{-1}T_jM_1$ , and call this class  $C_1$ . The same  $C_1'$  would be obtained if we started with any other  $M$  in  $C_1$  since

$$T_sT_j^{-1}T_iM_1 = T_iM_1.$$

Similarly the same  $C_1$  would be obtained.

Choosing an  $M$  not in  $C_1$  (if any such exist) we construct  $C_2$  and  $C_2'$  in the same way. Continuing in this manner we obtain the residue classes with properties (1) and (2). Let  $M_1$  and  $M_2$  be in  $C_1$  and suppose

$$M_2 = T_1T_2^{-1}M_1.$$

If  $E_1$  is in  $C_1'$  and can be obtained from  $M_1$  by

$$E_1 = T_\alpha M_1 = T_\beta M_1 = \cdots = T_\eta M_1,$$

then

$$\begin{aligned} E_1 &= T_\alpha T_2^{-1}T_1M_2 \Rightarrow T_\beta T_2^{-1}T_1M_2 = \cdots \\ &= T_\lambda M_2 = T_\mu M_2 \cdots \end{aligned}$$

Thus each  $M_i$  in  $C_1$  transforms into  $E_1$  by the same number of keys. Similarly each  $E_i$  in  $C_1'$  is obtained from any  $M$  in  $C_1$  by the same number of keys. It follows that this number of keys is a divisor of the total number of keys and hence we have properties (3) and (4).

# The Design of Reactive Equalizers\*

By A. P. BROGLE, Jr.

This paper describes a systematic method of approximating with a finite number of network elements a transfer characteristic which is a prescribed function of frequency, rather than a constant, over the useful frequency band. Although applied here only to input and output coupling networks as reactive equalizers and where loss equalization to an extremely high degree of precision over a wide frequency band is desired, the mathematical expressions which form the basis for the design are applicable to any 4-terminal network whose transfer characteristic is specified in a similar manner over the real frequency range.

The selection of the appropriate form of the transfer function for equalization purposes is the fundamental consideration. A squared Tchebycheff polynomial is found to be particularly suitable to produce a desired cut-off characteristic without impairing the precision of equalization in the useful band.

A method of polynomial approximation based on the transformation  $\omega = \tan \varphi/2$  is used to obtain the coefficients of the in-band approximating function. Predistorting the transfer specification and minimizing the mean-square error, the coefficients become the Fourier cosine coefficients for an infinite frequency range; and are the solutions of a linear set for a finite range,  $0 \leq \varphi \leq \pi/2$ .

## 1. INTRODUCTION

IN MOST broad-band communication systems, the problems of loss equalization and distortion correction are fundamental. Of the various types of electrical networks which are found useful as equalizers and compensators, the most frequently employed are the so-called constant resistance networks. In particular, they are of three usual types, as indicated in Fig. 1.

In all cases, the relationship  $Z_1 Z_2 = R^2$ , which is always possible to fulfill if  $Z_1$  and  $Z_2$  are built up of resistive and reactive components in the well-known manner, provides the means of altering the transmission properties of the circuit without affecting its impedance.<sup>1</sup> Methods are also available which extend the problem to more complicated configurations having these constant resistance properties. However, in some applications, where signal-to-noise ratio considerations are of importance, the resistive elements included as components of  $Z_1$  and  $Z_2$  in these circuits place a limitation on the final performance of the system. Hence, the satisfactory transmission and *impedance matching* properties of these circuits are purchased at the expense of a substantially increased noise level. As a consequence of this limitation on the performance of standard constant resistance equalizers, recent work

\* The work presented in this paper is part of a thesis, "Design of Reactive Equalizers with Prescribed Parasitic Capacitance," submitted by the author in partial fulfillment of the requirements for the degree of Master of Science at the Massachusetts Institute of Technology (Feb. 1949).

<sup>1</sup> Ref. 5, pp. 1-2.

has indicated the advantage of adapting reactive input and output coupling networks, ordinarily employed solely as impedance matching devices, to the additional role of partial distortion equalization.<sup>2</sup>

As a reactive equalizer, a lossless input or output coupling network partially equalizes the loss characteristic of a transmission line or cable by providing an insertion gain characteristic to compensate for the line loss characteristic. However, before the rigorous formulation of the problem is undertaken in the following section, it is necessary to discuss briefly the role of input and output coupling networks as equalizers in communications

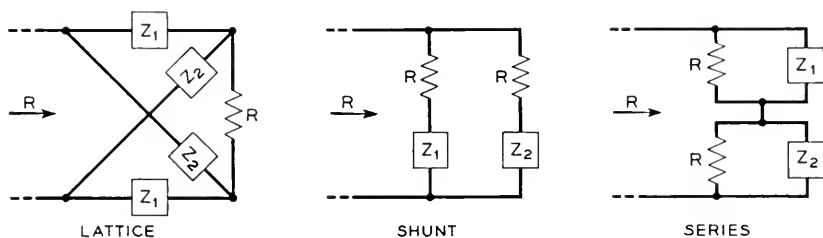


Fig. 1—Constant resistance networks.

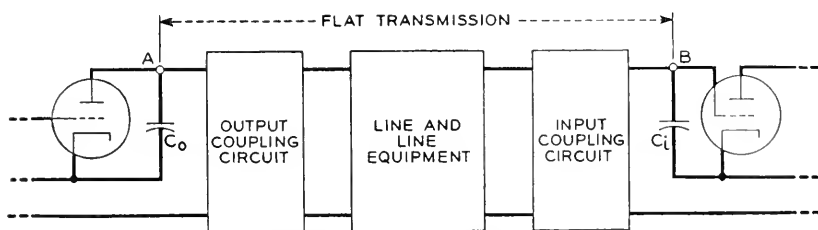


Fig. 2—Simplified section of a broad-band transmission system.

systems, and to outline the external requirements and limitations imposed by the system itself on these networks.

The characteristics of input and output coupling networks which are of engineering interest are:

- (1) The contribution of the coupling circuits to the transmission performance of the system as a whole.
- (2) The impedance matching requirements between the coupling networks and the transmission line.
- (3) The limitation on the maximum performance of a coupling network imposed by the parasitic capacitance usually present in the termination.

These characteristics are perhaps best illustrated by a somewhat idealized section of a broad-band transmission system. Figure 2 represents the output

<sup>2</sup> Ref. 1, pp. 383-392.

stage of a repeater, a section of the associated transmission line, and the first stage of the succeeding repeater of a simplified system.

The specification of a flat transmission characteristic over the useful frequency band between A and B in the figure indicates that equalization for the line loss of the section must occur in either or both coupling circuits, in the line equipment, or in all three of these circuits. For feedback amplifiers, the most desirable type, a flat characteristic between A and B can be specified only if the feedback circuits, or  $\beta$  circuits, of the amplifiers are designed to have no transmission variation with frequency. In general, it is possible to suppose the feedback factor,  $\beta$ , of the amplifiers to be the appropriately varying function of frequency to equalize a part of the line loss, thus altering the transmission specification from A to B. However, the  $\beta$  circuits must include regulation of other types in most cases. Hence, it is impractical to include much loss equalization in these circuits.

Since satisfactory performance of the section is dependent also on the maintenance of a large signal-to-noise ratio, it is important that the line contain no sources of additional loss. It is clear, then, that the best transmission performance is obtained (1) without the use of equalization in the line<sup>3</sup> and (2) when the reactive input and output coupling circuits equalize as large a percentage as possible of the total line loss.

Physically, the coupling circuits will be transformers, plus any number of tuning and shaping elements. In addition to the primary function of metal-lically separating the line from the repeater amplifiers, it will be seen later that the transformers provide the means of adjusting, independent of the value of the prescribed line impedance, the final impedance level of the network to conform with the value of the parasitic capacitance present.

Besides the contribution of the various networks in the system to the overall transmission performance, there is the problem of matching the coupling circuits to the line. For constant-resistance equalization, this problem is immediately solved by the relationship  $Z_1 Z_2 = R^2$ . Well-established techniques make it a relatively simple matter to design for a specified attenuation variation with frequency at the same time that the impedance of the equalizer is matched to the line. This same procedure, with certain modifications, can be carried over to the design of reactive equalizers. In Fig. 2, the transformers of the input and output coupling circuits are un-terminated. That is, the input of the output circuit and the output of the input circuit are terminated in substantially open circuits. In order to prevent the reflection of power at the junctions of the coupling circuits and the line, the impedances of the input and output circuits as viewed from the line must be made equal to the impedance of the line. This impedance re-

<sup>3</sup> In practice, the  $\beta$  circuits and constant resistance networks associated with the line actually equalize a certain percentage of the total line loss characteristic.

quirement is fulfilled by providing both coupling circuits with a balancing network connected as shown in Fig. 3. By accepting a small constant transmission loss,<sup>4</sup> the relationship  $Z_1 Z_2 = R^2$  is satisfied if the impedance  $Z_2$  of the balancing network is made the inverse of the transmission circuit impedance  $Z_1$ . Because of the relative ease of designing an inverse impedance  $Z_2$ , once  $Z_1$  is known in the final stages of a particular design, it is appropriate to omit from further discussion the presence of the balancing networks.

The fundamental theoretical limitation in the maximum transmission performance of these coupling networks is due directly to the presence of the parasitic tube capacitances  $C_0$  and  $C_i$ . If the parasitic capacitances were not present, the turns ratios of the transformers in the coupling circuits could quite evidently be made extremely high in order to produce over any specified frequency band as large a transmission response as desired. However, even though these capacitances are usually small, they always tend to short circuit the coupling networks whenever the impedance ratios of the

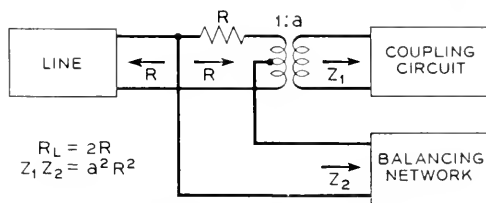


Fig. 3—Balancing network arrangement.

transformers are made too high. The determination of the maximum response of these networks over a prescribed frequency range is thus a basic problem in the design of reactive equalizers.

The fundamental limitation on the response of these networks is expressed in terms of the total area available under the transfer characteristic.<sup>5</sup> When this characteristic is a desired function over a finite frequency band, the maximum utilization of the area available is obviously attained when all the area is included in the useful band. This condition is described as a *resistance efficiency* of 100 per cent. A smaller resistance efficiency, 75 per cent for example, means that three-fourths of the total area under the characteristic is available in the useful frequency region, while the remainder of the area may be utilized to decrease the rate at which the characteristic is *cut-off*. Hence, the realization of a prescribed resistance efficiency in the

<sup>4</sup> The effective impedance of the line as viewed from the coupling circuit is equal to twice the actual line impedance. Thus, a penalty of  $10 \log \frac{R_L}{R} = 3\text{db}$  is imposed by the presence of the balancing network.

<sup>5</sup> See eq. (4) and discussion in the following section.

design of a reactive equalizer places a definite requirement on the behavior of the transfer characteristic outside the useful frequency band.

Although the precision of equalization as a design requirement actually is inclusive in the term *transmission performance* as used previously, it is included here as a separate requirement to emphasize its importance in this problem. The specification of a flat transmission from A to B in Fig. 2 provides the means of assigning to the tolerance of equalization a quantitative meaning. Hence, the tolerance per repeater section of the system may be expressed as the maximum allowable db deviation from the flat transmission characteristic, A to B, over the useful frequency band. For extremely broad-band systems, such as a coaxial system for simultaneous long-distance telephone and television transmission, many repeater sections appear in tandem between terminals. Thus, the deviations in each of these sections contribute to the system as a whole. In addition to the distances usually involved, repeater spacing becomes closer as the effective transmission band of these systems is increased. In order to design new systems with increasingly better overall tolerances, at the same time that the broad-banding requirements call for a greatly increased number of repeater sections per system, the tolerances imposed on the individual sections become exceedingly small. As a consequence, the maximum tolerance for an individual section must be specified as perhaps less than  $\pm 0.05$  db deviation.

## 2. THE PROBLEM OF REACTIVE EQUALIZATION

In this section the problem of reactive equalization will be formulated in terms of the special problems of input and output coupling circuit design. Broadly speaking, the general characteristics of input and output coupling networks, as outlined in the introduction to establish the practical basis for reactive equalization, will be further developed in order to give them a quantitative meaning. Because of the complexity of some derivations and their extensive treatment elsewhere, detailed proofs in general will be merely outlined. The method of analysis follows Bode's treatment of the problem while the principal results taken from network theory are Guillemin's.

As previously stated, the unterminated case for input and output coupling circuits arises whenever the terminating resistance is infinite in comparison with the other impedances of the network.<sup>6</sup> Figures 4 and 5 represent, respectively, an output and an input coupling network of the type illustrated in Fig. 2 with infinite terminations. In each figure,  $R_L$  represents the line,  $N$  is the lossless coupling network, and  $C_n$  is the parasitic shunt capacitance

<sup>6</sup> The so-called *terminated case* exists when the parasitic capacitance  $C_0$  or  $C_i$  in Fig. 2 is shunted by a finite resistance. Since no essential differences exist between the two cases with respect to the approximation problem, an analysis for the unterminated case alone is sufficient to clarify the more important design considerations.



which limits the response over any specified frequency band. For purposes of analysis and design, it is convenient to represent the coupling transformers in the manner indicated. By adopting this equivalent representation of a physical transformer, the so-called high-side equivalent circuit of the transformer, which includes the leakage reactance, the magnetizing inductance, and the input and output winding capacitances, is incorporated as part of the coupling network itself.

By excluding the ideal transformer portion of the equivalent representation of the physical transformer from the network itself, a simplification is possible. As shown in Figs. 6 and 7, the combination of the resistance  $R_L$

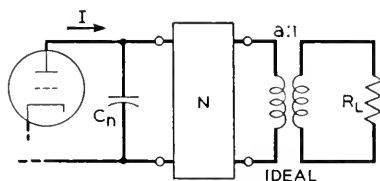


Fig. 4—Output coupling circuit.

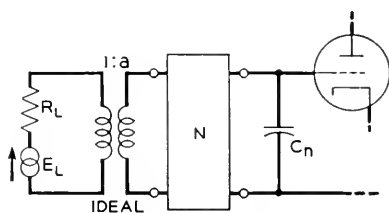


Fig. 5—Input coupling circuit.

and the ideal transformer may, in each case, be replaced by a resistance  $R_0 = a^2 R_L$ , where “ $a$ ” is the step-up turns ratio of the ideal transformer.  $R_L$  is the specified resistance, and  $R_0$  and “ $a$ ” are determined in the design procedure from the maximum response obtainable with the prescribed capacitance  $C_n$  in the termination.

The starting point for the study of these circuits is a consideration of the limitation on the amplitude response of these networks with frequency due to the presence of  $C_n$  in the terminations. Since the current ratio  $\frac{I_L}{I}$  in Fig. 6

and the voltage ratio  $\frac{E}{E_L}$  in Fig. 7 might be as large as desired if it were not

for the presence of  $C_n$ , the immediate problem is that of relating the magnitude of these ratios, as functions of the real frequency, to the capacitance  $C_n$ . This relationship is dependent on a necessary condition for the physical

realizability of a driving-point impedance function. If this function is chosen as the  $Z = R + jX$  in the figures, the necessary condition of interest is that  $Z$ , as an analytic function, have no poles in the right half of the complex frequency plane and that  $Z$  approach  $\frac{1}{\omega C_n}$  as  $\omega$  approaches infinity. By integrating this function over the appropriate path in the right half of the  $\lambda$  (complex frequency) plane and setting the result equal to zero, the desired expression becomes

$$\int_0^\infty R d\omega = \frac{\pi}{2C_n}. \quad (1)$$

To show that the resistance  $R$  is related to the ratios  $\left| \frac{I_L}{I} \right|$  and  $\left| \frac{E}{E_L} \right|$  it is

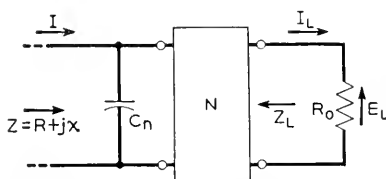


Fig. 6—Modified output coupling circuit of Fig. 4.

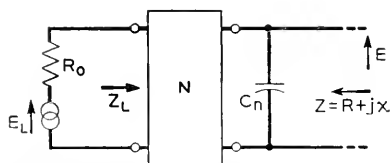


Fig. 7—Modified input coupling circuit of Fig. 5.

necessary to examine the transfer of power through the output circuit of Fig. 6. The power driven into this circuit is  $|I|^2 R$ . Since the network  $N$  is lossless, this is the same power,  $|I_L|^2 R_0$ , which reaches the line. In addition, if the transfer impedance of the circuit is defined as  $Z_{12}(j\omega) = \frac{E_L}{I} = R_0 \frac{I_L}{I}$ , the relationship sought is

$$\left| \frac{I_L}{I} \right|^2 = \left| \frac{Z_{12}(j\omega)}{R_0} \right|^2 = \frac{R}{R_0}. \quad (2)$$

For the input coupling circuit, the ratio  $\left| \frac{E}{E_L} \right|$  is related to the transfer impedance and  $R$  in a similar manner.

<sup>7</sup>Ref. 1, pp. 278-281,

$$\left| \frac{E}{E_L} \right|^2 = \left| \frac{Z_{12}(j\omega)}{R_0} \right|^2 = \frac{R}{R_0} \quad (3)$$

Finally, the transmission gain  $\alpha$  (in nepers) is related to the current ratio  $\left| \frac{I_L}{I} \right|$ , or the voltage ratio  $\left| \frac{E}{E_L} \right|$ , by  $e^\alpha$ . Hence, the quantitative statement for the limitation on the response of these coupling circuits becomes

$$\int_0^\infty e^{2\alpha} d\omega = \int_0^\infty \left| \frac{Z_{12}(j\omega)}{R_0} \right|^2 d\omega = \frac{\pi}{2C_n R_0} \quad (4)$$

Equation (4) is the general formula which relates the response characteristic over the complete frequency range to the prescribed capacitance  $C_n$  and the resistance  $R_0$ . This formula is especially helpful in attaching an analytical meaning to the term partial reactive equalization. If  $\alpha' = f(\omega)$  is used to describe the attenuation characteristic of a line or cable over a specified finite frequency band,  $\alpha = kf(\omega)$  will be the transmission response, in nepers, which is required to equalize a stated fraction of this loss at every frequency in the specified range.  $k$  is then the constant ( $k \leq 1$ ) which numerically expresses the degree of equalization.<sup>9</sup>

Thus, the  $\alpha = kf(\omega)$  in eq. (4) is the desired insertion gain characteristic to compensate partially for the line loss characteristic, and is directly related to this loss over a specified frequency range by a constant  $k$ . The limitation on the response expressed by eq. (4) will be clear if the transmission  $\alpha$  is now defined as  $\alpha = \alpha_0 + kf(\omega)$ , where  $\alpha_0$  represents the general response level. Before this expression is substituted in eq. (4), however, it is necessary to change the limits of integration. Thus, the specification of a maximum response over a finite frequency band requires that the limits become  $\omega_1$  and  $\omega_2$ , the extreme frequencies of the useful band. Since  $R$  must be positive, this condition requires that  $e^{2\alpha}$  be zero everywhere outside the useful range. Carrying out the integration, the result becomes

$$\alpha_0 \leq \frac{1}{2} \ln \left[ \frac{\pi}{2C_n R_0 \int_{\omega_1}^{\omega_2} e^{2kf(\omega)} d\omega} \right] \quad (5)$$

Since  $kf(\omega)$  is always prescribed,  $\alpha_0$  is readily computed.

So far, the equations have considered only the ideal case when the transfer characteristic  $e^{2\alpha}$  is zero outside the useful band. As previously stated, this condition specifies a resistance efficiency of 100 per cent. In practical applications, where a finite number of network elements are employed to approxi-

<sup>8</sup> By (1) substituting the equivalent current source for  $E$ , (2) applying the principle of reciprocity to the input circuit, and (3) writing the relations for the transfer of power through the circuit, eq. (3) is readily derived.

<sup>9</sup> In practice, this constant is called the "slope" of equalization.

mate a transfer characteristic to a specified degree of precision over the useful band, it is not possible for the transfer function chosen to represent the transfer characteristic to approximate zero outside the useful band in a manner to produce a resistance efficiency of 100 per cent. This limitation is then the prerequisite for modifying the performance which the coupling networks are required to achieve. The usual range of resistance efficiencies specified for input and output coupling network applications is approximately 45 to 80 per cent.

This modification of the final performance of the coupling networks may be examined quantitatively by referring to eqs. (1), (4), and (5). In the first two of these equations the integral may be taken only over the useful frequency range,  $\omega_1$  to  $\omega_2$ , provided that the right-hand side of each of these equations is multiplied by the specified resistance efficiency expressed as a fraction.<sup>10</sup> In eq. (5) the equal sign holds only in the limiting case when the resistance efficiency is 100 per cent. If these equations are modified in the manner indicated, the variation of the transfer characteristic outside the useful frequency range may be chosen in any way which satisfies the total area requirements in eqs. (1) and (4) as they stand.

Following the choice of a satisfactory transfer characteristic, the next general problem is the realization of a physical network which will approximate this specified characteristic to the required degree of precision over the complete frequency spectrum. The solution of this problem is the main purpose of this paper.

As is well-known in network theory, the general form of the squared magnitude of the transfer impedance of any physical two-terminal-pair reactive network terminated in resistance may be expressed as the quotient of two polynomials in  $\omega^2$ .

$$\left| \frac{Z_{12}(j\omega)}{R_0} \right|^2 = \frac{A_0 + A_1 \omega^2 + A_2 \omega^4 + \cdots + A_n \omega^{2n}}{B_0 + B_1 \omega^2 + B_2 \omega^4 + \cdots + B_n \omega^{2n}}. \quad (6)$$

Before the necessary and sufficient conditions that the  $\frac{Z_{12}(\lambda)}{R_0}$  derived from eq. (6) be the transfer impedance of a lossless network terminated in resistance are stated, it is appropriate to develop the modifications which must be made in eq. (6) if  $\left| \frac{Z_{12}(j\omega)}{R_0} \right|^2$  is to approximate the transfer characteristic,  $e^{2\alpha}$ , in this problem. This requires that a closer examination be made of the physical limitation that the coupling networks correspond, in part, in structure to the equivalent circuit of the coupling transformer to be used. Figure 8 shows the high-side equivalent circuit of either coupling transformer of Figs. 4 and 5.

<sup>10</sup>  $\omega_1$  is usually chosen as zero.

In the figure,  $L_m$  represents the magnetizing inductance,  $L_2$  represents the leakage reactance, and  $C_1$  and  $C_3$  represent, respectively, the low-side and high-side parasitic winding capacitances. The magnetizing inductance  $L_m$ , since it is usually large so that its impedance is substantially infinite compared with the other impedances of the circuit at high frequencies, affects the response of the transformer at low frequencies only. Since the useful band ordinarily specified does not include the range of frequencies where the effects of  $L_m$  are noticeable, its presence may be omitted from further consideration. In addition, it is never practical to retain  $C_3$  as the final element of the reactive coupling network  $N$ . In this case, the parallel combination of  $C_3$  and  $C_n$  would, of course, seriously limit the final response of the network. Thus, the least number of shaping elements is a series inductance  $L_4$  which splits the high-side winding capacitance  $C_3$  from the prescribed terminating capacitance  $C_n$ . Hence, in general, the reactive coupling network  $N$  is an  $(n - 1)$  element unbalanced ladder structure of alternating series inductances and shunt capacitances beginning with a shunt capacitance

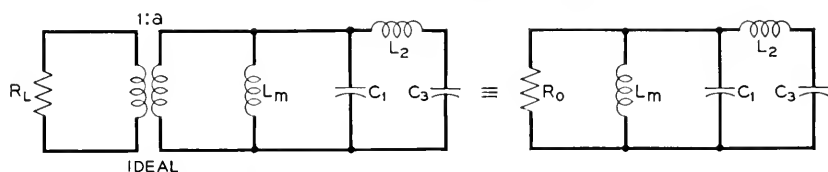


Fig. 8—High-side equivalent circuit of either coupling transformer of Figs. 4 and 5.

and ending with a series inductance. Figure 9, then, indicates the general form of the coupling network to be realized by the function chosen to approximate  $e^{2\alpha}$  in this problem.

Without loss of generality, it is convenient at this point to modify Figs. 6 and 7 in the manner indicated in Figs. 10 and 11. By including  $C_n$  as part of  $N'$  the problem has not been altered. However, it is necessary to recognize that the final adjustment of the impedance level, i.e., the choice of  $R_0$ , must be made in such a manner that the total area requirement, as specified in eq. (4), is still met. In each figure  $z'_{11}$ ,  $z'_{22}$ , and  $z'_{12}$  are the open-circuit driving-point and transfer impedances of the network  $N'$ .

With the element configuration specified and the reactive coupling network  $N'$  defined, it is now appropriate to carry out the modification in the form of  $\left| \frac{Z_{12}(j\omega)}{R_0} \right|^2$  indicated previously. Thus, the fact that  $\frac{R}{R_0} = 1$  at  $\omega = 0$ , and that an  $n$  element unbalanced ladder structure of alternating series inductances and shunt capacitances terminated in a resistance has only an  $n$ th order zero of the transfer impedance,  $\frac{Z_{12}(\lambda)}{R_0}$ , at infinity, allows the

squared magnitude of the transfer impedance in this problem to be written as

$$\left| \frac{Z_{12}(j\omega)}{R_0} \right|^2 = \frac{1}{1 + B_1 \omega^2 + B_2 \omega^4 + \cdots + B_n \omega^{2n}}, \quad (7)$$

where the  $n$  constants  $B_1 \cdots B_n$  are related to the  $n$  elements of the network by the relation

$$\frac{Z_{12}(j\omega)}{R_0} = \frac{\varepsilon'_{12}/R_0}{1 + \varepsilon'_{22}/R_0}. \quad (8)$$

Since the desired transfer characteristic  $\varepsilon'^{\alpha}$  determines the variation of the polynomial  $B(\omega^2) = 1 + B_1 \omega^2 + \cdots + B_n \omega^{2n}$ , a major factor in the design

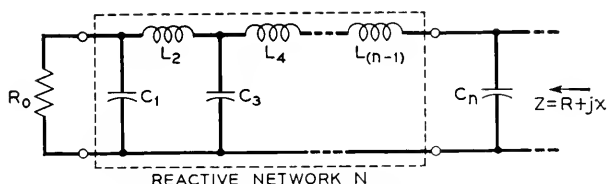


Fig. 9—General form of the coupling networks of Figs. 6 and 7.

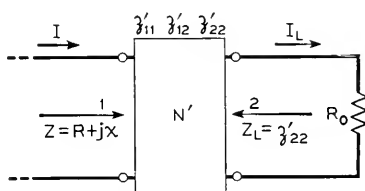


Fig. 10—Output circuit of Fig. 6 with  $C_n$  included as part of  $N'$ .

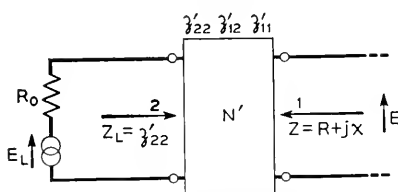


Fig. 11—Input circuit of Fig. 7 with  $C_n$  included as part of  $N'$ .

is the choice of the real coefficients,  $B_1 \cdots B_n$ , by a suitable method of polynomial approximation.

The necessary and sufficient conditions for physical realizability place a restriction on the  $B$ 's of eq. (7). The sufficient condition that  $\left| \frac{Z_{12}(j\omega)}{R_0} \right|^2$  represent the squared magnitude of the transfer impedance of a physical

network of the type described is that  $\left| \frac{Z_{12}(j\omega)}{R_0} \right|^2 \geq 0$  for  $\omega \geq 0$ . This condition will be insured if the polynomial,  $1 + B_1\omega^2 + \dots + B_n\omega^{2n}$ , has no negative real  $\lambda^2$  roots of odd multiplicity.<sup>11</sup> In addition to the sufficiency of eq. (7), if the  $\frac{Z_{12}(\lambda)}{R_0} = \frac{g(\lambda)}{h(\lambda)}$  derived from  $\left| \frac{Z_{12}(\lambda)}{R_0} \right|^2$  in the usual manner is to be the transfer impedance of a lossless network terminated in resistance, it is necessary that  $g(\lambda)$  be either even or odd and that  $h(\lambda)$  be a Hurwitz polynomial.<sup>12</sup> In this problem  $g(\lambda) = 1$  is surely even since all zeros of  $\left| \frac{Z_{12}(\lambda)}{R_0} \right|^2$  occur at infinity; and the method of forming  $\frac{Z_{12}(\lambda)}{R_0}$  always insures that  $h(\lambda) = m + n$ , where  $m$  is the even part and  $n$  is the odd part of  $h(\lambda)$ , is a Hurwitz polynomial. Thus, the fulfillment of the sufficient condition that there be no negative real  $\lambda^2$  roots of odd multiplicity of  $B(\omega^2)$  is the assurance that the  $B$ 's of eq. (7) will always produce a physical network of the configuration of Fig. 9.

Once the conditions for physical realizability have been fulfilled, and a  $\frac{Z_{12}(\lambda)}{R_0}$  has been found in the final stages of a particular design, the network elements are easily calculated from a partial fraction expansion of  $z'_{22} = \frac{m}{n}$  according to the following relation:

$$\frac{Z_{12}(\lambda)}{R_0} = \frac{z'_{12}(\lambda)/R_0}{1 + z'_{22}(\lambda)/R_0} = \frac{g(\lambda)}{m + n} = \frac{g(\lambda)/n}{1 + m/n}, \quad (9)$$

where  $z'_{12}(\lambda) = \frac{g(\lambda)}{n}$  and  $z'_{22}(\lambda) = \frac{m}{n}$ .

The previous discussion of the special problems of input and output coupling circuit design has been based, broadly, on (1) a consideration of the terminating or load impedance, (2) a consideration of the shape of the transfer characteristic, and (3) a consideration of the conditions for physical realizability. A major problem in the design is the choice of an approximating function which satisfactorily matches the stated transfer characteristic over the useful frequency band and, at the same time, sharply changes slope near the cut-off frequency so that it approximates zero outside the useful band in a prescribed manner. When the transfer characteristic is a constant over the useful frequency band, e.g., the impedance matching and low-pass filter cases, techniques which employ Tchebycheff polynomials as the ap-

<sup>11</sup> Ref. 4.

<sup>12</sup> A Hurwitz polynomial is defined as a polynomial in  $\lambda$  which has the property that the quotient of its even and odd parts,  $\varphi(\lambda) = \frac{m}{n}$ , yields a reactance function.

proximating functions are available which make it a relatively simple matter to design physically realizable networks exhibiting this property of a sharp cut-off to zero outside the useful band.<sup>13</sup> However, a similar method of applying Tchebycheff polynomials to transfer characteristics which vary with frequency in a prescribed manner over a finite band has not been evolved. In order to illustrate the preceding statements, Figs. 12 and 13 have been included as representative of typical transfer characteristics.

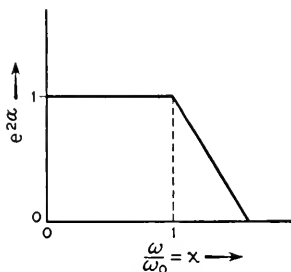


Fig. 12—Transfer characteristic for impedance matching or low-pass filter case.

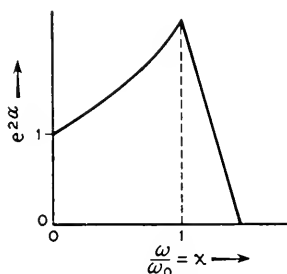


Fig. 13—Transfer characteristic for reactive equalizer case.

### 3. DERIVATION OF SPECIAL TRANSFER FUNCTION

In accordance with the brief discussion at the conclusion of the previous chapter, it is now appropriate to state that it is the purpose of this paper (1) to derive a transfer function which is especially suited to the problem of reactive equalization, and (2) to develop a systematic method which utilizes this special transfer function to approximate satisfactorily, with a finite number of network elements, a specified transfer characteristic over the entire frequency spectrum. This section will consider in detail the first of these two main tasks in the formulation of a design method for reactive equalizers.

With reference to Fig. 13, it is convenient to divide the complete transfer

<sup>13</sup> Ref. 4. Also Ref. 2, pp. 53-79.



characteristic into two separate regions. The specification over the useful band,  $0 \leq \omega \leq \omega_0$ , may be called the in-band region while the specification outside the useful band,  $\omega_0 < \omega \leq \infty$ , may be called the out-band region. Thus, it is seen that the transfer characteristic over the in-band region depends exclusively on the  $\alpha = kf(\omega)$  which is required to equalize a stated fraction of the power loss between repeaters while the transfer characteristic in the out-band region depends only on the specified resistance efficiency.

The first step in the derivation of the special transfer function for equalization purposes is a normalization of the transfer characteristic of Fig. 13 in terms of eq. (7). As indicated in Fig. 14, a constant,  $K$ , is chosen so that  $Ke^{2\alpha}$  ( $K < 1$ ) is equal to unity at  $\frac{\omega}{\omega_0} = x = 1$ . This choice of the transfer characteristic is convenient since the transfer characteristic is now expressed in a form similar to the familiar form of the transfer characteristic of a low-

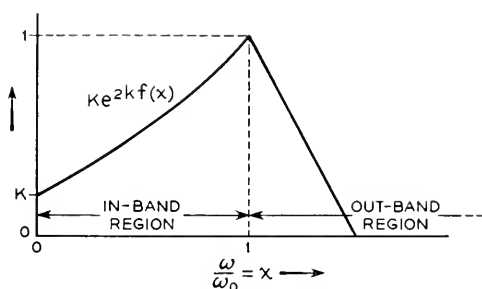


Fig. 14—Normalized transfer characteristic of Fig. 13.

pass filter and, hence, suitable for the addition of a Tchebycheff polynomial.<sup>14</sup>

With the transfer characteristic appropriately specified, the next step is to show the manner in which the denominator  $B(x^2)$  of eq. (7), where this equation is multiplied by the factor  $K$ , can be broken up into two functions of  $x^2$  so that one of these functions approximates the reciprocal of the in-band region of the transfer characteristic while the other produces the desired cut-off characteristic.

The derivation of the desired denominator,  $B(x^2)$ , begins by writing the transfer characteristic of Fig. 14 for the in-band region as

$$\frac{1}{B(x^2)} = Ke^{2kf(x)} \quad (10)$$

<sup>14</sup> In order to make the following derivation clear, it is suggested that the discussion of Tchebycheff polynomials, pp. 733-734, be examined at this time.

<sup>15</sup> The transmission  $\alpha = \alpha_0 + kf(x)$  will be written as  $kf(x)$  for the remainder of this analysis. The general transmission level  $\alpha_0$  may be found in the final stages of a particular design when the impedance level is adjusted to conform with the prescribed  $C_n$ .

In terms of  $B(x^2)$  directly and a desired transmission  $\alpha'_0$  at the angular cut-off frequency  $\omega_0$ , equation (10) becomes

$$B(x^2) = e^{2\alpha'_0} e^{-2kf(x)}, \quad (11)$$

where  $K = e^{-2\alpha'_0}$ . Equation (11) now represents the characteristic that is to be approximated over the useful frequency band while Fig. 15 shows a plot of this function.

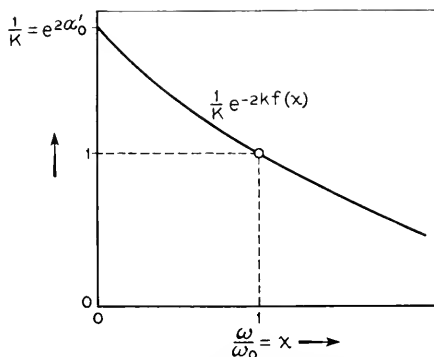


Fig. 15—Specification for  $B(x^2)$  over useful frequency band.

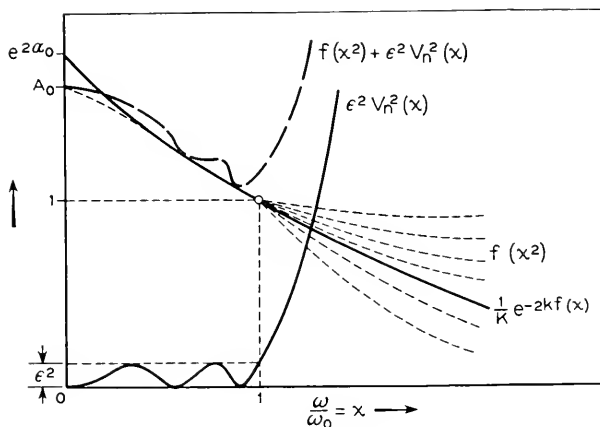


Fig. 16—Combined approximating function for  $B(x^2)$  over entire frequency band.

Now, if  $B(x^2)$  is broken up into two parts and represented as

$$B(x^2) = f(x^2) + \epsilon^2 I_n^2(x),^{16} \quad (12)$$

<sup>16</sup> It is important to note that eq. (12) now represents the approximating function over the entire frequency range as compared to eq. (11) which represents the function to be approximated only over the useful range.

where  $f(x^2)$  is the rational function which approximates  $e^{2\alpha'_0} e^{-2kf(x)}$  over the useful band,  $V_n(x)$  is a Tchebycheff polynomial of order  $n$  (odd), and  $\epsilon$  is the coefficient of the Tchebycheff polynomial,  $B(x^2)$  in Fig. 15 will be modified as shown in Fig. 16. In this figure it is to be noted that  $f(x^2)$ , the in-band approximating function, is represented as having a variety of variations outside the useful band. The function has been indicated in this manner to emphasize that a fairly wide latitude in the choice of the behavior of  $f(x^2)$  outside the useful is permitted since  $\epsilon^2 V_n^2(x)$ , the out-band approximating function, is the predominant function in this region. In addition, the variations of  $\epsilon^2 V_n^2(x)$  in the in-band region have been exaggerated in order to demonstrate their effect on the combined approximating function,  $f(x^2) + \epsilon^2 V_n^2(x)$ , over the useful frequency band.

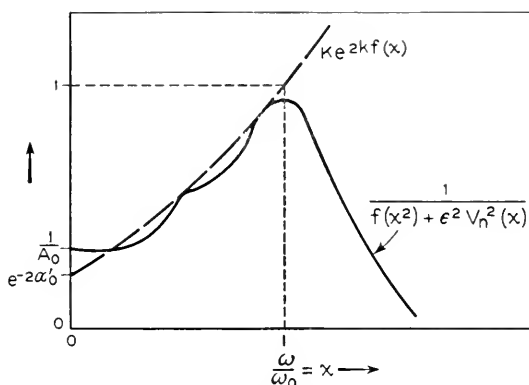


Fig. 17—Resultant transfer function for equalization purposes.

Finally, when the relation expressed by eq. (12) is reciprocated and re-plotted in terms of  $K \left| \frac{Z_{12}(jx)}{R_0} \right|^2$ , the result shown in eq. (13) and Fig. 17 is obtained.

$$K \left| \frac{Z_{12}(jx)}{R_0} \right|^2 = \frac{1}{f(x^2) + \epsilon^2 V_n^2(x)}. \quad (13)$$

Comparing the resultant special transfer function shown in Fig. 17 with the transfer characteristic shown in Fig. 14, and assuming that  $f(x^2)$  and the coefficient of the Tchebycheff polynomial have been suitably chosen, it is established contingently that the combination of functions chosen to represent  $B(x^2)$  produces the desired result.

This brief derivation serves as a guide to the main problem of choosing a particular  $f(x^2)$  and a particular  $\epsilon^2 V_n^2(x)$  which, when added together and

reciprocated, approximate the transfer characteristic to the specified degree of precision.

The choice of these approximating functions begins by finding a polynomial

$$f(x^2) = A_0 + A_1x^2 + A_2x^4 + \cdots + A_nx^{2n} \quad (14)$$

which approximates  $e^{2\alpha'_0} e^{-2kf(x)}$  to the required degree of precision throughout the useful band and has an out-band variation subject to the initial requirements that  $f(x^2)$  be positive and that the slope of  $f(x^2)$  not vary rapidly in the immediate out-band region (approximately  $1 \leq x \leq 1.5$ ). For values of  $x$  greater than about 1.5, the Tchebycheff polynomial is the determining function, and variations in  $f(x^2)$  are no longer of importance. A precise statement of these conditions and the exact frequency range in which they are valid depend on the degree of equalization and the desired resistance efficiency in a particular design. However, a more critical examination of Figs. 16 and 17 indicates that the generalized conditions stated above are a reasonable guide in the choice of  $f(x^2)$  for most applications.

The main criteria for judging the acceptability of a particular out-band variation which accompanies the choice of in-band variation of  $f(x^2)$  to produce optimum precision are physical realizability and the attainment of a desired resistance efficiency. Considering first the condition for physical realizability,  $\frac{1}{f(x^2) + \epsilon^2 V_n^2(x)} \geq 0$  for  $0 \leq x \leq \infty$ , and referring to Fig. 16, a negative value of  $f(x^2)$  in the immediate out-band region might be of sufficient magnitude to cancel the positive effect of  $\epsilon^2 V_n^2(x)$  and, hence, produce a negative value of  $f(x^2) + \epsilon^2 V_n^2(x)$ . However, at higher frequencies, the squared Tchebycheff polynomial takes on very large positive values. Thus, negative values and variations in  $f(x^2)$  are effectively reduced in the magnitude of their effect on

$$K \left| \frac{Z_{12}(jx)}{R_0} \right|^2 = \frac{1}{f(x^2) + \epsilon^2 V_n^2(x)}$$

in direct relation to the increase in the magnitude of  $\epsilon^2 V_n^2(x)$ .

In order that an accurate prediction of the resistance efficiency may be made, it is necessary that the slope of  $f(x^2) + \epsilon^2 V_n^2(x)$  increase in a uniform manner in the immediate out-band region. Since variations in the slope of  $f(x^2)$  have their largest effect in the region just outside the useful band, it is, of course, best to prevent rapid variations in this region.

The remaining condition on the form of  $f(x^2)$  is that  $A_0$  should be adjusted so that  $A_0 < e^{2\alpha'_0}$ . By providing the transfer specification with a less steep slope requirement at low frequencies it is possible to obtain over the valuable

portion of the useful band an increased precision of equalization.<sup>17</sup> This adjustment represents an increased transmission at low frequencies. Thus, it is sometimes necessary to employ an equalizer of the constant resistance type when additional equalization is desired at low frequencies. Figures 16 and 17 have been drawn to reflect this condition on  $A_0$ .

After an  $f(x^2)$  which conforms with the requirements outlined above has been found, it is necessary to find a

$$\epsilon^2 V_n^2(x) = A_1' x^2 + A_2' x^4 + \cdots + A_n' x^{2n} \quad (15)$$

which, when added to  $f(x^2)$ , produces the desired  $B(x^2)$ . This procedure is greatly facilitated by the known properties of Tchebycheff polynomials:

A Tchebycheff polynomial of order  $n$  is defined by

$$V_n(x) = \cos(n \cos^{-1} x). \quad (16)$$

This function oscillates between plus one and minus one for  $|x| < 1$  and approaches  $\pm \infty$  for  $|x| > 1$ . Tabulated below are the expanded analytical expressions for the polynomials for  $n = 1$  through  $n = 8$ .

$$\begin{aligned} V_1(x) &= x & V_5(x) &= 16x^5 - 20x^3 + 5x \\ V_2(x) &= 2x^2 - 1 & V_6(x) &= 32x^6 - 48x^4 + 18x^2 - 1 \\ V_3(x) &= 4x^3 - 3x & V_7(x) &= 64x^7 - 112x^5 + 56x^3 - 7x \\ V_4(x) &= 8x^4 - 8x^2 + 1 & V_8(x) &= 128x^8 - 256x^6 + 160x^4 - 32x^2 + 1 \end{aligned}$$

With the help of the recursion formula,

$$xV_n(x) = \frac{1}{2}[V_{n+1}(x) + V_{n-1}(x)], \quad (17)$$

the corresponding expressions for  $n > 8$  may be systematically calculated. Figure 18 shows a plot of the Tchebycheff polynomial for  $n = 5$ .

In the case of low-pass filters<sup>18</sup> and impedance matching networks,<sup>19</sup> Tchebycheff polynomials are often used for the solution of the approximation problem. The function  $|Z_{12}(jx)|^2$  in these cases has an oscillatory behavior which approximates unity in the useful band, and has all its zeros at infinity so that the network consists of  $n$  elements of an unbalanced ladder structure of alternating series inductances and shunt capacitances. The appropriate function for  $|Z_{12}(jx)|^2$  is

$$|Z_{12}(jx)|^2 = \frac{1}{1 + \epsilon^2 V_n^2(x)}, \quad (18)$$

<sup>17</sup> There is a practical limit to the reduction of  $A_0$  below  $\epsilon^2 \alpha_0^2$ . Referring to Figs. 13 and 14, it is apparent that  $K = \frac{1}{A_0}$ . Thus,  $A_0$  is a direct measure of the impedance level over the useful band, and must not be made too small if the highest practical level of response is to be attained.

<sup>18</sup> Ref. 2, pp. 53-79.

<sup>19</sup> Ref. 3, pp. 26-34.

where  $\epsilon$  is an arbitrary constant. Figure 19 shows the plot of the squared Tchebycheff polynomial,  $\epsilon^2 V_n^2(x)$ , for the values of  $n = 5$ , and  $\epsilon = 0.5$  and  $\epsilon = 0.1$ , while Fig. 20 shows a plot of the transfer function expressed in eq. (18).

It is to be noted that the oscillatory behavior with equal maxima and minima of squared Tchebycheff polynomials for values of  $x < 1$  and the rapid approach to  $+\infty$  for values of  $x > 1$  make their use particularly suitable as the solution of the approximation problem for low-pass filters and impedance matching networks. It is now apparent that these same

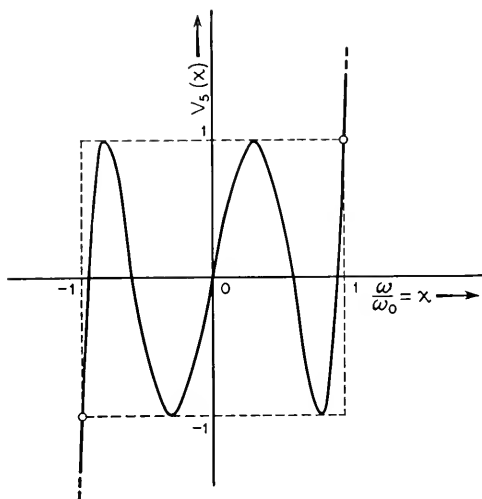


Fig. 18—Tchebycheff polynomial,  $V_n(x)$ , for  $n = 5$ .

properties validate their use as the out-band approximating function for reactive equalizers.<sup>20</sup>

Another useful property of squared Tchebycheff polynomials as approximating functions for low-pass filters and impedance matching networks is the inclusion of the specification of the tolerance as a factor in the transfer function. The allowable db deviation over the useful band is related to  $\epsilon$  by

$$\epsilon^2 = e^{2\alpha_p} - 1,$$

where  $\alpha_p$  is the maximum pass-band loss in nepers. Thus, the appropriate choice of  $\epsilon$  always realizes the specified tolerance over the useful band.

<sup>20</sup> When better tolerances are required and when the network configuration is not rigidly specified, Jacobian elliptic functions, rather than Tchebycheff polynomials, might be employed.

However, it is important to observe that a given value of  $\epsilon$  automatically determines both the pass-band tolerance and the rate of cut-off in the out-band region. Hence, if a specified tolerance is to be realized in the useful band, no control exists over the determination of the resistance efficiency. Also, it is apparent from Figs. 19 and 20 that small in-band deviations are always obtained at the expense of lower resistance efficiencies, and vice versa.

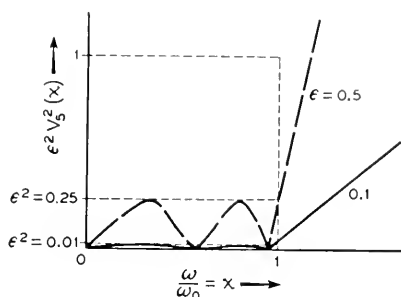


Fig. 19—Squared Tchebycheff polynomials,  $\epsilon^2 V_n^2(x)$ , for  $n = 5$ , and  $\epsilon = 0.5$  and  $\epsilon = 0.1$ .

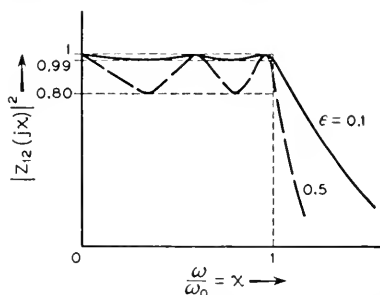


Fig. 20—Transfer function expressed in eq. (18) for the values of  $n$  and  $\epsilon$  shown in Fig. 19.

Returning to the problem of reactive equalization, for  $n$  odd,  $\epsilon^2 V_n^2(x)$  may be expressed as

$$\epsilon^2 V_n^2(x) = \epsilon^2 (C_1 x^2 + C_2 x^4 + \cdots + C_n x^{2n}). \quad (19)$$

Thus, any  $A'_\nu$  of eq. (15) is given by  $A'_\nu = \epsilon^2 C_\nu$ . By using the expressions for  $V_1(x)$  through  $V_8(x)$  tabulated previously, or eq. (17), it is a very simple task to find the  $C_\nu$  for any desired  $n$ . Thus,  $V_n^2(x) = C_1 x^2 + C_2 x^4 + \cdots + C_n x^{2n}$  is readily ascertained, and the only real problem is the choice of  $\epsilon^2$ . If  $f(x^2)$  has already been chosen, this is accomplished by an addition of  $f(x^2)$  and  $\epsilon^2 V_n^2(x)$  for several values of  $\epsilon^2$ . When a  $\epsilon^2$  is found such that the combination, when reciprocated, very closely approximates the specified resistance efficiency,  $B(x^2)$  is completely defined.

The final expression for  $B(x^2)$  may now be written as

$$B(x^2) = f(x^2) + \epsilon^2 V_n^2(x) = (A_0 + A_1 x^2 + \cdots + A_n x^{2n}) + (A'_1 x^2 + \cdots + A'_n x^{2n}). \quad (20)$$

In terms of eq. (20), the corresponding expression for the special transfer function for equalization purposes becomes

$$K \left| \frac{Z_{12}(jx)}{R_0} \right|^2 = \frac{1}{A_0 + (A_1 + A'_1)x^2 + (A_2 + A'_2)x^4 + \cdots + (A_n + A'_n)x^{2n}}. \quad (21)$$

When all the  $A_\nu$  and  $A'_\nu$  are known in a particular design, the coefficients  $B_1 \cdots B_n$  of eq. (7) may be readily determined. Hence, the elements of the network may be found by using the appropriate equations of Section 2.

#### 4. APPROXIMATION METHOD

This section will consider the second of the two main tasks in the formulation of the design method. Broadly speaking, the special transfer function derived in the previous section, eq. (13), provides the approximating functions to be used in this problem while this section develops the systematic method of determining the coefficients of these functions for a finite number of network elements. The function of most interest in the approximation problem is the in-band approximating function  $f(x^2)$ . Thus, the development of the approximation method for reactive equalizers is concerned specifically with the determination, consistent with the previous limitations and requirements, of the coefficients,  $A_0 \cdots A_n$ , of the polynomial  $f(x^2)$ .

The Fourier method of polynomial approximation, first introduced by Wiener,<sup>21</sup> is characterized by a transformation of the independent variable to make the approximating function in the new frequency domain a periodic function. Thus, the well-known method of Fourier analysis is available as a general polynomial approximation method. This method has not been applied extensively in practical applications. However, the uniform nature of  $B(x^2)$  over the useful frequency range makes its application to the design of reactive equalizers of the type described here seem feasible.

By the transformation  $x = \tan \varphi/2$  the frequency domain,  $0 \leq x \leq \infty$ , is transformed to a corresponding  $\varphi$  domain,  $0 \leq \varphi \leq \pi$ . Since the range of interest is 0 to  $\pi$  in the  $\varphi$  domain, all functions may be assumed to be either even or odd with a period  $2\pi$ . Thus, any amplitude approximating function

<sup>21</sup> Ref. 4.



may be written in the  $\varphi$  domain as a Fourier cosine series,

$$f_1(\varphi) = a_0 + a_1 \cos \varphi + a_2 \cos 2\varphi + \cdots + a_n \cos n\varphi = \sum_{k=0}^n a_k \cos k\varphi. \quad (22)$$

In particular, the correspondence of the  $x$  domain and  $\varphi$  domain may be conveniently illustrated as in Fig. 21. It is to be noted that the comparatively limited region of the useful band,  $0 \leq x \leq 1$ , in the  $x$  domain goes into half of the available range,  $0 \leq \varphi \leq \frac{\pi}{2}$ , in the  $\varphi$  domain. It is apparent, then, that some advantage has already been gained by this transformation.

Before attention can be confined to the evaluation of the coefficients,  $a_k$ , it is necessary to establish the form of the approximating function in the  $\varphi$  domain which corresponds to  $f(x^2)$  in the frequency domain, and to relate

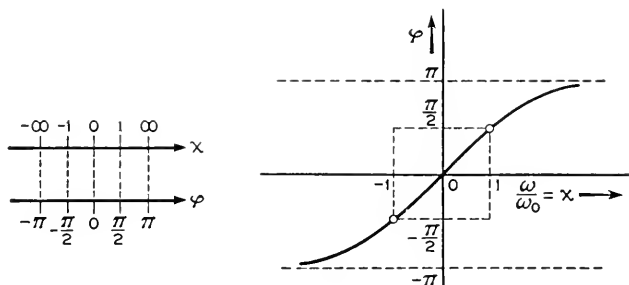


Fig. 21—Graphical representation of the transformation  $x = \tan \frac{\varphi}{2}$ .

the  $A_k$  in eq. (14) to the  $a_k$  in eq. (22). This is accomplished by means of the following relationships:

$$x = \tan \frac{\varphi}{2} = \sqrt{\frac{1 - \cos \varphi}{1 + \cos \varphi}}$$

$$\cos \varphi = \frac{1 - x^2}{1 + x^2}$$

$$\cos n\varphi = V_n(\cos \varphi).$$

Thus, the corresponding expression for eq. (22) in the frequency domain becomes

$$f_1(\varphi) = a_0 + a_1 V_1(\cos \varphi) + a_2 V_2(\cos \varphi) \\ + a_3 V_3(\cos \varphi) + \cdots + a_n V_n(\cos \varphi)$$

$$f_1(\cos \varphi) = b_0 + b_1 \cos \varphi + b_2 \cos^2 \varphi + b_3 \cos^3 \varphi + \cdots + b_n \cos^n \varphi$$

$$f_1(x^2) = b_0 + b_1 \left( \frac{1-x^2}{1+x^2} \right) + b_2 \left( \frac{1-x^2}{1+x^2} \right)^2 + b_3 \left( \frac{1-x^2}{1+x^2} \right)^3 + \cdots + b_n \left( \frac{1-x^2}{1+x^2} \right)^n$$

$$f_1(x^2) = \frac{A_0 + A_1 x^2 + A_2 x^4 + A_3 x^6 + \cdots + A_n x^{2n}}{(1+x^2)^n} = f(x^2) f_2(x^2),$$

$$\text{where } f_2(x^2) = \frac{1}{(1+x^2)^n}.$$

Therefore, it is necessary to predistort the approximated function  $B(x^2)$  by redefining the  $f(\varphi)$  corresponding to  $f(x^2)$  as

$$f(\varphi) = \frac{f_1(\varphi)}{f_2(\varphi)} \rightarrow \sum_{k=0}^n A_k x^{2k} = f(x^2), \quad (22)'$$

where

$$f_1(\varphi) = \sum_{k=0}^n a_k \cos k\varphi \rightarrow \frac{\sum_{k=0}^n A_k x^{2k}}{(1+x^2)^n} = f_1(x^2),$$

and

$$f_2(\varphi) = \cos^{2n} \frac{\varphi}{2} \rightarrow \frac{1}{(1+x^2)^n} = f_2(x^2).$$

Hence,  $f_1(\varphi)$ , which corresponds to the approximating function  $f(x^2)$  multiplied by  $\frac{1}{(1+x^2)^n}$  in the frequency domain, is the approximating function in the  $\varphi$  domain. In practice, the indicated predistortion of  $B(x^2)$  may be carried out either before or after the specification has been transformed to the  $\varphi$  domain. Table I shows the relation of the  $A_k$  to the  $a_k$  for  $n = 3$  and  $n = 5$ .

TABLE I  
RELATION OF THE  $A_k$  OF  $f(x^2)$  TO THE  $a_k$  OF  $f_1(\varphi)$  FOR  $n = 3$  AND  $n = 5$

$n = 3$	$n = 5$
$A_0 = a_0 + a_1 + a_2 + a_3$	$A_0 = a_0 + a_1 + a_2 + a_3 + a_4 + a_5$
$A_1 = 3a_0 + a_1 - 5a_2 - 15a_3$	$A_1 = 5a_0 + 3a_1 - 3a_2 - 13a_3 - 27a_4 - 45a_5$
$A_2 = 3a_0 - a_1 - 5a_2 + 15a_3$	$A_2 = 10a_0 + 2a_1 - 14a_2 - 14a_3 + 42a_4 + 210a_5$
$A_3 = a_0 - a_1 + a_2 - a_3$	$A_3 = 10a_0 - 2a_1 - 14a_2 + 14a_3 + 42a_4 - 210a_5$
	$A_4 = 5a_0 - 3a_1 - 3a_2 + 13a_3 - 27a_4 + 45a_5$
	$A_5 = a_0 - a_1 + a_2 - a_3 + a_4 - a_5$

It is to be recognized in the following derivation and procedure that  $f_1(\varphi)$  represents the actual response of the network while  $B(\varphi) \cos^{2n} \frac{\varphi}{2}$ , the pre-distorted specification for  $B(x^2)$  in the  $\varphi$  domain, represents the desired response. For convenience,  $B(\varphi) \cos^{2n} \frac{\varphi}{2}$  may be called the amplitude function  $a(\varphi)$ . In addition, it is important to note that  $a(\varphi)$  is specified only over the range  $0 \leq \varphi \leq \frac{\pi}{2}$ , and the restrictions on the behavior of the approximating function  $f_1(\varphi)$  outside this range are related to the restrictions on  $f(x^2)$  in the out-band region of the  $x$  domain. The general problem is thus one of approximating the amplitude function  $a(\varphi)$  by a Fourier cosine series, 
$$\sum_{k=0}^n a_k \cos k\varphi.$$

The first step towards a systematic method of obtaining the Fourier cosine coefficients,  $a_0 \cdots a_n$ , is the specification of the manner in which the tolerance of match is to be minimized. In this case, the approximation is always specified in the mean-square sense, i.e., the optimum coefficients are obtained by solving the set of linear equations which are determined when the integral of the error squared,

$$I = \int \left[ a(\varphi) - \sum_{k=0}^n a_k \cos k\varphi \right]^2 d\varphi, \quad (23)$$

is minimized.

The set of linear equations which relates the  $a_k$  of the approximating function  $f_1(\varphi)$  to the approximated function  $a(\varphi)$  is derived for a range 0 to  $s$  in the  $\varphi$  domain with  $s \leq \pi$  by minimizing eq. (23).<sup>22</sup> The minimum condition is specified when the derivative with respect to each coefficient  $a_j$  is zero. Thus,

$$\frac{\partial I}{\partial a_j} = \int_0^s 2 \left[ a(\varphi) - \sum_{k=0}^n a_k \cos k\varphi \right] [-\cos j\varphi] d\varphi = 0 \quad (24)$$

is the analytical expression for this condition. Collecting terms,

$$\begin{aligned} \frac{\partial I}{\partial a_j} &= -2 \int_0^s [a(\varphi) \cos j\varphi] d\varphi + 2 \int_0^s \left[ \sum_{k=0}^n a_k \cos k\varphi \right] [\cos j\varphi] d\varphi \\ &= -2 \int_0^s [a(\varphi) \cos j\varphi] d\varphi + 2a_j \int_0^s \cos j\varphi \cos k\varphi d\varphi = 0, \end{aligned}$$

and letting  $P_{jk} = \int_0^s \cos j\varphi \cos k\varphi d\varphi$  and  $C_k = \int_0^s [a(\varphi) \cos j\varphi] d\varphi$ , the set of

<sup>22</sup> This derivation is similar to one given by R. M. Redheffer in Ref. 6, pp. 8-10.

linear equations becomes

$$\sum_{j=0}^n P_{jk} a_j = C_k. \quad (j = 0, 1, 2, \dots, n) \quad (25)$$

Therefore, the procedure for determining the optimum coefficients for the range 0 to  $s$  in the  $\varphi$  domain is as follows: First, compute the  $C_k$  which depend on the approximated function  $a(\varphi)$ .

$$C_k = \int_0^s [a(\varphi) \cos k\varphi] d\varphi. \quad (26)$$

Next, compute the elements of  $P_{jk}$  given by

$$P_{jk} = \frac{\sin(j-k)s}{2(j-k)} + \frac{\sin(j+k)s}{2(j+k)} \quad (k \neq j);$$

$$P_{jj} = \frac{s}{2}; \quad P_{00} = s. \quad (27)$$

These elements depend only on the range  $s$  and terminate with the desired  $n$  in any design. For convenience, these numbers may be arranged in the form of a symmetrical matrix  $[P_{jk}]$ . Hence, the optimum coefficients are found by solving the matrix equation,

$$[P_{jk}] \times [a_j] = [C_k]. \quad (j, k = 0, 1, 2, \dots, n) \quad (28)$$

In this problem of approximating  $B(x^2)$  to a high degree of precision over the useful frequency range, the range in the  $\varphi$  domain of most interest is 0 to  $\frac{\pi}{2}$ . However, before the approximation over only part of the frequency range is considered, it is helpful to set down the relations which apply when  $a(\varphi)$  is approximated over the whole frequency range,  $s = \pi$ . In this case, the matrix  $[P_{jk}]$  takes on a form in which all non-diagonal entries are zero. Thus,

$$[P_{jk}] = \begin{bmatrix} P_{00} & P_{01} & \cdot & \cdot & P_{0n} \\ P_{10} & P_{11} & \cdot & \cdot & P_{1n} \\ \cdot & \cdot & \cdot & \cdot & \cdot \\ \cdot & \cdot & \cdot & \cdot & \cdot \\ \cdot & \cdot & \cdot & \cdot & \cdot \\ P_{n0} & \cdot & \cdot & \cdot & P_{nn} \end{bmatrix} = \begin{bmatrix} \pi & 0 & 0 & 0 & \cdot & \cdot & \cdot \\ 0 & \frac{\pi}{2} & 0 & 0 & \cdot & \cdot & \cdot \\ 0 & 0 & \frac{\pi}{2} & 0 & \cdot & \cdot & \cdot \\ 0 & 0 & 0 & \frac{\pi}{2} & \cdot & \cdot & \cdot \\ \cdot & \cdot & \cdot & \cdot & \frac{\pi}{2} & \cdot & \cdot \\ \cdot & \cdot & \cdot & \cdot & \cdot & \cdot & \cdot \\ \cdot & \cdot & \cdot & \cdot & \cdot & \cdot & \cdot \end{bmatrix}.$$

The solution in this case is particularly simple, and gives the well-known Fourier coefficients,

$$a_0 = \frac{1}{\pi} \int_0^\pi a(\varphi) d\varphi \quad (j = 0),$$

$$a_j = \frac{2}{\pi} \int_0^\pi a(\varphi) \cos j\varphi d\varphi \quad (j \neq 0).$$

Hence, each coefficient  $a_j$  is dependent only on the area under the corresponding function  $a(\varphi) \cos j\varphi$ .

This result, even though it simplifies the procedure of calculating the  $a_j$  in eq. (28), has only limited usefulness in this problem. As mentioned above, the range of direct interest extends only to  $s = \frac{\pi}{2}$ . Thus, an approximation over the whole range requires that an  $f(x^2)$  be arbitrarily specified in the out-band region. Such a procedure, in this case, is an unnecessary restriction on the form of  $f(x^2)$  outside the useful frequency range. Thus, an approximation over a finite range 0 to  $\frac{\pi}{2}$  is the procedure to be considered in detail.

Starting as before, the system of equations in matrix notation which corresponds to eq. (28) is

$$\begin{bmatrix} \frac{\pi}{2} & 1 & 0 & -\frac{1}{3} & 0 & \frac{1}{5} & \cdot & \cdot \\ 1 & \frac{\pi}{4} & \frac{1}{3} & 0 & -\frac{1}{15} & 0 & \cdot & \cdot \\ 0 & \frac{1}{3} & \frac{\pi}{4} & \frac{3}{5} & 0 & -\frac{5}{21} & \cdot & \cdot \\ -\frac{1}{3} & 0 & \frac{3}{5} & \frac{\pi}{4} & \frac{3}{7} & 0 & \cdot & \cdot \\ 0 & -\frac{1}{15} & 0 & \frac{3}{7} & \frac{\pi}{4} & \frac{5}{9} & \cdot & \cdot \\ \frac{1}{5} & 0 & -\frac{5}{21} & 0 & \frac{5}{9} & \frac{\pi}{4} & \cdot & \cdot \\ \cdot & \cdot & \cdot & \cdot & \cdot & \cdot & \cdot & \cdot \\ \cdot & \cdot & \cdot & \cdot & \cdot & \cdot & \cdot & \cdot \\ \cdot & \cdot & \cdot & \cdot & \cdot & \cdot & \cdot & \cdot \end{bmatrix} \times \begin{bmatrix} a_0 \\ a_1 \\ a_2 \\ a_3 \\ a_4 \\ a_5 \\ \cdot \\ \cdot \\ \cdot \end{bmatrix} = \begin{bmatrix} C_0 \\ C_1 \\ C_2 \\ C_3 \\ C_4 \\ C_5 \\ \cdot \\ \cdot \\ \cdot \end{bmatrix},$$

where the elements of  $[P_{jk}]$  up to and including  $P_{55}$  have been evaluated. Hence, the problem is the solution of the first  $(n + 1)$  of these equations for the coefficients  $a_0 \cdots a_n$ . In practice, this solution may be simplified for a desired  $n$  by computing once and for all the elements of the inverse matrix  $[P_{jk}]^{-1}$ . This matrix is formed by replacing each element of the determinant  $\|P_{jk}\|$  by its minor, dividing each minor by this determinant,

and interchanging rows and columns. Thus, the solution of the  $a_j$  is expressed directly in terms of the  $C_k$  and becomes

$$[a_j] = [P_{jk}]^{-1} \times [C_k] \text{ or } a_j = \sum_{k=0}^n P_{jk}^{-1} C_k. \quad (29)$$

The sufficiency of this procedure is established when it is proved that the determinant  $\|P_{jk}\|$  is different from zero for the particular value of  $s$  considered. Since  $s$  is a rational multiple of  $\pi$  in this case and all non-diagonal entries are algebraic numbers,  $\pi$  cannot satisfy an equation with algebraic coefficients to make  $\|P_{jk}\| = 0$ . Thus, the system of eq. (29) is a unique solution, and this solution gives the absolute minimum in the sense that no other set of  $a_j$  will produce a smaller mean-square error over the range 0 to  $\frac{\pi}{2}$ .

However, for some values of  $n$  the determinant of coefficients becomes extremely small. This condition produces very large numerical values of the elements of  $[P_{jk}]^{-1}$ . Since the  $a_j$  and  $C_k$  are usually small compared with these elements, the accuracy of the solution is impaired. Hence, the system of eq. (29) in some cases represents a set of nearly dependent equations with a fairly wide range of solution. This practical limitation on the uniqueness of these equations may be overcome quite readily by arbitrarily changing one of these equations to produce, for calculation purposes, a dependent set of equations. It turns out that the most expedient choice of this change is to replace the  $P_{00} = \frac{\pi}{2}$  of  $[P_{jk}]$  by  $P_{00} = \frac{\pi}{4}$ . This, in effect, modifies the weighting of  $a_0$  in these equations and does not, in general, limit the usefulness of the result. Hence, the system of eq. (28) with  $\frac{\pi}{2}$  replaced by  $\frac{\pi}{4}$  determines a set of coefficients,  $a_0 \cdots a_n$ , which are reasonably close to the optimum for  $s = \frac{\pi}{2}$ .

It is appropriate at this point to indicate a practical modification in the approximation method which serves, incidentally, to clarify the reasons for accepting as suitable a set of coefficients that are not the optimum  $a_j$  over the useful band in the  $\varphi$  domain.

This modification arises since the foregoing method has considered only the average error over the range 0 to  $\frac{\pi}{2}$ . However, an analysis of the percentage error in  $f(x^2)$ , and of the corresponding deviation in  $\alpha$  over this range, shows that the approximation to  $a(\varphi)$  is most critical at high frequencies and becomes decreasingly critical as lower frequencies are reached. Thus, in any design, it is necessary to make a slight adjustment of the

coefficients  $a_0 \cdots a_n$  after they have been obtained from eq. (29) in order to compensate for this decreased tolerance of  $\sum_{j=0}^n a_j \cos j\varphi$  at high frequencies in the useful band. The exact method of accomplishing this modification depends on the particular design and the ingenuity of the designer. Nevertheless, no more than a few trials are necessary, in general, to produce the desired precision at all frequencies in the useful band.

In practice, then, it is not appropriate that the Fourier cosine coefficients finally chosen represent the optimum coefficients in the mean-square sense. However, the important result established is that a systematic method which realizes a satisfactory set of coefficients  $A_0 \cdots A_n$  of  $f(x^2)$  has been developed.

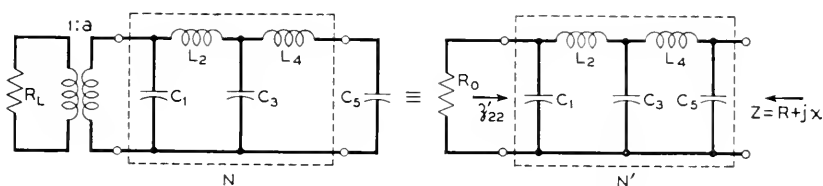


Fig. 22—Input coupling network configuration.

## 5. ILLUSTRATIVE DESIGN

The numerical example which will be considered is the design of an input coupling network to equalize partially the loss characteristic of a coaxial line. On the basis of the previous discussion of the design method it is advantageous to break down the procedure into four general operations:

- (1) Network Specifications
- (2) Transfer Specifications
- (3) Solution of Approximation Problem
- (4) Realization of Non-dissipative Network

The first two of these operations are the choice of the appropriate form of the design requirements while the last two represent the major divisions in the procedure for designing the network to meet these requirements.

In this design, a set of network requirements which are consistent with the requirements indicated in Section 2 may be chosen as indicated in Fig. 22. Thus, in order that the network  $N'$  correspond to the high-side equivalent circuit of the coupling transformer and, at the same time, have a final capacitance  $C_n$ , the least number of elements which may be chosen in a practical design is  $n = 5$ . The specified elements of Fig. 22 are the parasitic terminating capacitance  $C_5$  and the effective impedance of the line,  $R_L$ .<sup>23</sup>

<sup>23</sup> See footnote 4.

Practical values for these elements may be chosen as  $C_5 = 20 \mu\mu f$  and  $R_L = 150$  ohms.

Next, the transfer specifications for this illustration may be summarized as

- (a) Degree of equalization— $k = 0.25$
- (b) Useful band—2.5 to 8.0 mc
- (c) Useful band distortion— $< \pm 0.10$  db
- (d) Resistance efficiency—65%

The computation of the desired transfer characteristic  $Ke^{2kf(x)}$  begins with the consideration of the degree of equalization. In order to equalize one-quarter of the power loss between coaxial repeaters, the transfer characteristic over the useful band must vary as  $Ke^{\alpha'/12}$  where  $\alpha'$  represents the complete line loss between repeaters. If it is assumed that  $\alpha'$  is 4 nepers (34.7 db)<sup>24</sup> at 8.0 mc ( $x = 1$ ) and varies as  $\alpha' = f(x) = 4\sqrt{x}$ , the transfer characteristic over the range,  $0 \leq x \leq 1$ , according to eq. (10), becomes

$$Ke^{2kf(x)} = e^{-2\alpha'_0(1-\sqrt{x})} = e^{-2(1-\sqrt{x})},$$

where  $\alpha = kf(x) = \sqrt{x}$  and  $\alpha'_0 = kf(1) = 1$ .

The specification of a useful band from 2.5 to 8.0 mc (or  $x = 0.3$  to  $x = 1.0$ ) in this example is chosen to illustrate the practical limitation on the precision of equalization at low frequencies. The dashed curve of Fig. 23 indicates a low-frequency response which seems realistic for this illustration.

The computation of the desired transfer characteristic is completed when the out-band portion of the characteristic is chosen to satisfy the specified resistance efficiency. The assumption of a linear cut-off characteristic is suitable as an initial requirement. Hence, the transfer characteristic may be summarized as shown in Fig. 23. The solid curve of this figure represents the transfer characteristic which would be required for equalization over the range,  $0 \leq x \leq 1$ , while the dashed curve indicates the modification in this curve resulting from the choice of a conservative low-frequency response and the specification of a useful band of  $0.3 \leq x \leq 1$ .

The solution of the approximation problem consists of three main operations. First, is the determination of the amplitude function  $a(\varphi)$  from the transfer characteristic specified in Fig. 23. Second, is the determination of the Fourier cosine coefficients,  $a_0 \cdots a_n$ , of the approximating function  $f_1(\varphi)$  and the calculation of the coefficients,  $A_0 \cdots A_n$ , of  $f(x^2)$ . Third, is the choice of the coefficient  $\epsilon^2$  of the squared Tchebycheff polynomial.

The amplitude function  $a(\varphi)$  is calculated from the specified transfer characteristic by using the relations expressed by eq. (22)'. According to eq. (11) of Section 3, the specification for  $B(x^2)$  over the useful band,

<sup>24</sup> This discrimination is correct for 4 or 5 miles of coaxial cable. The attenuation on a coaxial line varies as the square root of frequency.



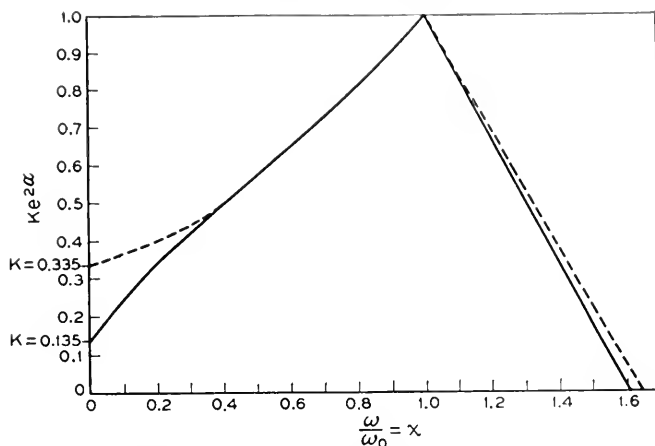


Fig. 23—Transfer characteristic for the network of Fig. 22. The dashed curve indicates the modification which results from the choice of a conservative low-frequency response.

TABLE II

RESULTS OF CALCULATIONS IN THE  $x$  DOMAIN AND IN THE  $\varphi$  DOMAIN

$x$	$B(x^2)$	$f(x^2)$	$\varphi$	$B(\varphi)$	$B(\varphi) \cos^2 \frac{\varphi}{2}$	$f_1(\varphi)$	$f(\varphi)$
0	3.00	2.98	0°	3.00	3.00	2.98	2.98
0.1	2.87	2.91	10°	2.88	2.80	2.77	2.87
0.2	2.69	2.74	20°	2.74	2.49	2.48	2.73
0.3	2.49	2.48	30°	2.56	2.09	2.09	2.57
0.4	2.09	2.17	40°	2.21	1.54	1.58	2.28
0.5	1.80	1.85	50°	1.87	1.05	1.07	1.95
0.6	1.57	1.57	60°	1.60	0.68	0.70	1.65
0.7	1.37	1.39	70°	1.37	0.42	0.43	1.39
0.8	1.22	1.23	80°	1.17	0.24	0.24	1.17
0.9	1.11	1.13	90°	1.00	0.13	0.13	1.00
1.0	1.00	1.00					
1.1	—	0.56					
1.2	—	-0.32					
1.3	—	-2.12					
1.5	—	-11.4					
2.0	—	-115.0					

$0.3 \leq x \leq 1$ , becomes

$$B(x^2) = e^{2\alpha_0'} e^{-2kf(x)} = e^{2(1-x)}.$$

In addition, the specification for  $B(x^2)$  may be extended to zero frequency by reciprocating the dashed portion of the curve of Fig. 23 in the range  $0 \leq x < 0.3$ .

In this illustration a simplified  $f(x^2) = A_0 + A_1x^2 + A_2x^4 + A_3x^6$  of order  $(n - 2)$  may be chosen such that the transfer characteristic is matched within the specified tolerance over the useful band.<sup>25</sup> The specification  $a(\varphi)$  is determined from  $B(x^2)$  by (1) calculating the  $B(\varphi)$  which corresponds to  $B(x^2)$  in the  $\varphi$  domain, and (2) multiplying  $B(\varphi)$  by  $\cos^{2n} \frac{\varphi}{2}$  to obtain  $a(\varphi) = B(\varphi) \cos^{2n} \frac{\varphi}{2}$ . The results of these calculations in the  $\varphi$  domain are indicated by the fifth and sixth columns of Table II.

The Fourier cosine coefficients,  $a_0 \cdots a_n$ , are found by solving the set of linear equations expressed by eq. (25) for  $n = 3$  and  $s = \frac{\pi}{2}$ . The  $C_k$  which depend on the approximated function  $a(\varphi)$  are computed from eq. (26). After the indicated graphical integration is carried out, these constants have the following values in this illustration:

$$C_0 = 2.323$$

$$C_1 = 1.964$$

$$C_2 = 1.148$$

$$C_3 = 0.452$$

The matrix  $[P_{jk}]$  for  $n = 3$  according to eq. (27) is

$$[P_{jk}] = \begin{bmatrix} \frac{\pi}{2} & 1 & 0 & -\frac{1}{3} \\ 1 & \frac{\pi}{4} & \frac{1}{3} & 0 \\ 0 & \frac{1}{3} & \frac{\pi}{4} & \frac{3}{5} \\ -\frac{1}{3} & 0 & \frac{3}{5} & \frac{\pi}{4} \end{bmatrix}.$$

The existence of a solution of eq. (28) depends on  $\|P_{jk}\| \neq 0$ . In this case this determinant becomes

$$\|P_{jk}\| \cong 0.00009.$$

Thus, for all practical purposes, the linear equations for  $n = 3$  represent a dependent set. However, when  $P_{00} = \frac{\pi}{4}$  is substituted for  $\frac{\pi}{2}$  above,<sup>26</sup> the

<sup>25</sup> For the value of the tolerance specified in this illustration, an  $f(x^2)$  of order 3 turns out to be satisfactory. In the general case, where a higher degree of precision is desired, it is, of course, expedient to choose an  $f(x^2)$  of order  $n$ .

<sup>26</sup> See discussion on p. 742.

solution for the  $a_j$  according to eq. (29) is

$$\begin{bmatrix} a_0 \\ a_1 \\ a_2 \\ a_3 \end{bmatrix} = \begin{bmatrix} -1.273 & 2.117 & -1.166 & 0.350 \\ 2.117 & -1.273 & -0.350 & 1.166 \\ -1.166 & -0.350 & 4.320 & -3.798 \\ 0.350 & -1.166 & -3.798 & 4.320 \end{bmatrix} \times \begin{bmatrix} 2.323 \\ 1.964 \\ 1.148 \\ 0.452 \end{bmatrix} = \begin{bmatrix} 0.016 \\ 2.527 \\ -0.150 \\ 0.698 \end{bmatrix}$$

As previously stated, these coefficients represent the practical minimum of the average error in the mean-square sense over the range 0 to  $\frac{\pi}{2}$  in the  $\varphi$  domain. However, they do not represent the best match over the useful band for this illustration. The adjustment of these coefficients to produce a more satisfactory match at high frequencies in the useful band begins by changing the value of  $a_0$  to make  $f_1\left(\frac{\pi}{2}\right) = a_0 - a_2 = 0.125$ . This condition is satisfied when the general level of response is lowered so that  $a_0 = -0.025$ . The only further adjustment that is necessary in order to compensate for the decreased tolerance of  $f_1(\varphi) = \sum_{j=0}^3 a_j \cos j\varphi$  at high frequencies in the useful band is a change in the value of  $a_3$ . When  $a_3$  is adjusted to  $a_3 = 0.623$  a suitable approximating function for  $a(\varphi)$  in this illustration is

$$f_1(\varphi) = \sum_{j=0}^3 a_j \cos j\varphi = -0.025 + 2.527 \cos \varphi - 0.150 \cos 2\varphi + 0.623 \cos 3\varphi.$$

Hence, the approximating function for  $B(\varphi)$  is

$$f(\varphi) = \frac{f_1(\varphi)}{f_2(\varphi)} = \frac{-0.025 + 2.527 \cos \varphi - 0.150 \cos 2\varphi + 0.623 \cos 3\varphi}{\cos^6 \frac{\varphi}{2}}.$$

These functions are tabulated in the last two columns of Table II.

The coefficients  $A_0 \cdots A_3$  of  $f(x^2)$  are easily calculated from the  $f_1(\varphi)$  and  $f(\varphi)$  above by the relation of the  $A_k$  to the  $a_j$  expressed in Table I. Thus,

$$f(x^2) = 2.975 - 6.143x^2 + 7.493x^4 - 3.325x^6.$$

The final operation in the solution of the approximation problem is the choice of the squared Tchebycheff polynomial,  $\epsilon^2 T_n^2(x)$ , which satisfies a resistance efficiency of 65 per cent. The Tchebycheff polynomial for  $n = 5$  is

$$V_5(x) = 5x - 20x^3 + 16x^5.$$

Thus,  $V_5^2(x)$  becomes

$$V_5^2(x) = 25x^2 - 200x^4 + 560x^6 - 640x^8 + 256x^{10}.$$

A  $\epsilon^2 = 0.01$  is easily found such that the resistance efficiency calculated from a graphical integration of  $\frac{1}{f(x^2) + \epsilon^2 V_5^2(x)}$  equals 65 per cent. Hence, the analytical expression for  $K \left| \frac{Z_{12}(jx)}{R_0} \right|^2$  becomes

$$\frac{1}{f(x^2) + \epsilon^2 V_5^2(x)} = \frac{1}{(2.975 - 6.143x^2 + 7.493x^4 - 3.325x^6) + (0.25x^2 - 2.00x^4 + 5.60x^6 - 6.40x^8 + 2.56x^{10})}.$$

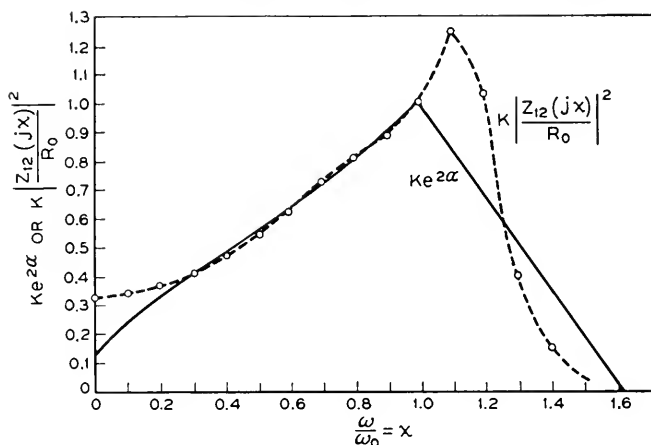


Fig. 24—Comparison of the resultant special transfer function with the transfer characteristic of Fig. 23.

This expression is the resultant special transfer function which satisfactorily approximates the transfer characteristic of Fig. 23. Fig. 24 shows a plot of these functions for comparison purposes.

The squared magnitude of the transfer impedance of the network  $N'$  is found from the analytical expression for the special transfer function by adjusting the value of  $K$  so that  $KA_0 = 1$ . Therefore,

$$\left| \frac{Z_{12}(jx)}{R_0} \right|^2 = \frac{1}{1 - 1.981x^2 + 1.846x^4 + 0.765x^6 - 2.157x^8 + 0.861x^{10}}.$$

The elements of the network  $N'$  are found from the squared magnitude of the transfer impedance by methods standard in circuit theory.<sup>27</sup> The network elements of Fig. 22 in terms of unit impedance and unit radian

<sup>27</sup> Ref. 2, pp. 25-53.

frequency turn out to be

$$C_1 = 0.470 \text{ farads} \quad L_2 = 1.250 \text{ henrys}$$

$$C_3 = 1.201 \text{ farads} \quad L_3 = 2.220 \text{ henrys.}$$

$$C_5 = 0.594 \text{ farads}$$

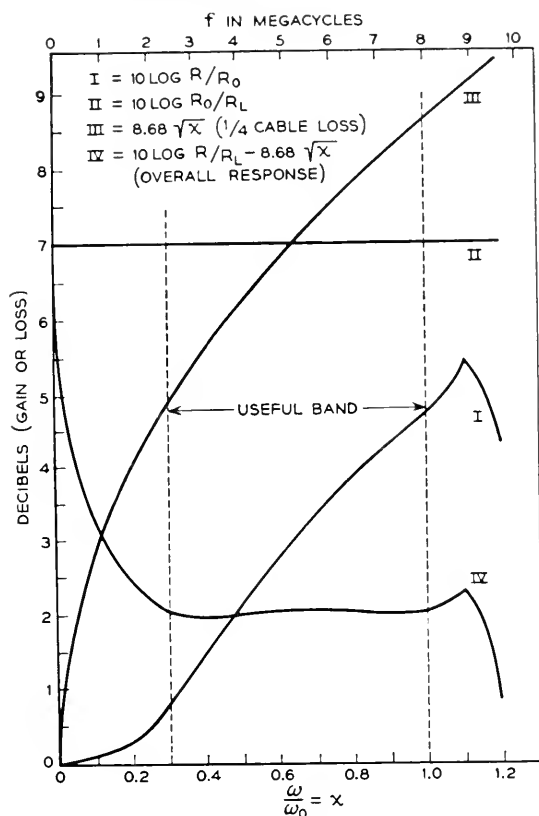


Fig. 25—Computed gain characteristic of the input coupling circuit of Fig. 22.

$R_0$  is calculated from the equation which relates to normalized value of  $C_5$  above to  $\omega_0$  and the actual value of  $C_5 = 20 \times 10^{-12}$  farads. Thus

$$\frac{0.594}{R_0 \omega_0} = 20 \times 10^{-12} \text{ farads,}$$

and  $R_0 = 591$  ohms.

The actual values of the network elements of Fig. 22 are found as

$$C_1 = 15.8 \mu\mu f \quad L_2 = 14.7 \text{ mh}$$

$$C_3 = 40.5 \mu\mu f \quad L_4 = 26.2 \text{ mh,}$$

$$C_5 = 20.0 \mu\mu f$$

and the step-up turns ratio,  $a$ , of the ideal transformer is

$$a = \sqrt{\frac{R_0}{R_L}} = 1.98.$$

These values then represent the input coupling network which theoretically equalizes to the specified degree of precision one-quarter of the power loss between coaxial repeaters over a frequency band from 2.5 to 8.0 mc. The computed gain characteristic of this network is plotted in Fig. 25, Curve I. The presence of the ideal transformer represents an added constant gain, Curve II, given by  $\text{db} = 10 \log \frac{R_0}{R_L} = 5.96$ . The total gain inserted by

the network, the sum of Curves I and II, is  $\text{db} = 10 \log \frac{R}{R_L} = 10 \log \frac{R}{R_0} + 5.96$ .

Since Curve III represents one-quarter of the power loss between repeaters, Curve IV is the overall transmission gain of the line and equalizer.<sup>28</sup> The deviation of Curve IV from a constant transmission over the useful band is less than  $\pm 0.08$  db. It may be concluded, then, that a satisfactory non-dissipative design has been obtained.

#### REFERENCES

1. H. W. Bode, "Network Analysis and Feedback Amplifier Design," Chap. 16, Van Nostrand, New York, 1945.
2. S. Darlington, "Synthesis of Reactance 4-Poles," *Journal of Mathematics and Physics*, Vol. XVIII, pp. 275-353, September, 1939, Also *Bell System Monograph* B-1186.
3. R. M. Fano, "Theoretical Limitations on the Broadband Matching of Arbitrary Impedances," *Report No. 41, M. I. T. Research Laboratory of Electronics*, January, 1948.
4. E. A. Guillemin, "Classroom Notes on Network Synthesis" (Notes dictated at M. I. T., course 6.561 and 6.562—as yet unpublished).
5. E. L. Norton, "Constant Resistance Networks with Applications to Filter Groups," *B. S. T. J.*, Vol. XVI, pp. 178-193, April, 1937. Also *Bell System Monograph* B-991.
6. R. M. Redheffer, "Design of a Circuit to Approximate a Prescribed Amplitude and Phase," *Report No. 54, M. I. T. Research Laboratory of Electronics*, November, 1947.

<sup>28</sup> Criticism may well be directed at the gain peak above the useful band. However, this condition is somewhat exceptional and probably would not occur with an in-band approximating function of order  $n$  rather than  $(n - 2)$ .

## Abstracts of Technical Articles by Bell System Authors

*Testing Cathode Materials in Factory Production.*<sup>1</sup> J. T. ACKER. The paper deals with the methods of testing radio-tube cathode materials in factory production, and especially with a comparison of several specific lots of materials of variable content. It is believed that this is the first time the electron-tube industry has made mass tests on a well-controlled engineering basis of cathode materials which vary in single component elements.

*Advances in the Theory of Ferromagnetism.*<sup>2</sup> R. M. BOZORTH. This article presents the results of the most recent investigations in the field of ferromagnetism. There have been a number of new ideas brought forth through research along these lines, of which three of the most outstanding ones are explained and illustrated.

*On Magnetic Remanence.*<sup>3</sup> R. M. BOZORTH. The magnetic retentivity of many materials is about half of the magnetization at saturation, a fact accounted for by simple domain theory. In some materials, however, the retentivity is only a small fraction of saturation, sometimes less than 10 per cent. The explanation of this fact is discussed. It is suggested that in materials with almost zero magnetic anisotropy the Bloch walls between domains increase in thickness until they envelop the whole specimen and the domain structure disappears.

*Multifrequency Pulsing in Switching.*<sup>4</sup> C. A. DAHLBOM, A. W. HORTON, JR., and D. L. MOODY. Applications of multifrequency pulsing in switching are described in this article. Today, many installations of this type are being made in cities throughout the nation. This system permits operators or senders to complete calls to crossbar offices without the aid of other operators.

*Circuits for Cold Cathode Glow Tubes.*<sup>5</sup> W. A. DEPP and W. H. T. HOLDEN. This paper discusses fundamental operating characteristics and typical circuits using cold cathode glow tubes for relays, impulse generators, pulse counting and interlocking functions.

*The Substitution Method of Measuring the Open Circuit Voltage Generated by a Microphone.*<sup>6</sup> M. S. HAWLEY. An analysis of the substitution method of measuring the open circuit voltage generated by a microphone is given

<sup>1</sup> *Proc. I.R.E.—Waves and Electrons Section*, v. 37, pp. 688-690, June 1949.

<sup>2</sup> *Elec. Engg.*, v. 68, pp. 471-476, June 1949.

<sup>3</sup> *Zeits. f. Physik*, v. 124, 7/12, pp. 519-527, 1948.

<sup>4</sup> *Elec. Engg.*, v. 68, pp. 505-510, June 1949.

<sup>5</sup> *Elec. Mfg.*, v. 44, pp. 92-97, July 1949.

<sup>6</sup> *Jour. Acous. Soc. Amer.*, v. 21, pp. 183-189, May 1949.

which shows that the "normal" substitution voltage equals the open circuit voltage for all types of acoustic measurements and for any value of electric impedance loading the microphone. It is shown that the method recently proposed by some authors of removing the acoustic load from the microphone when applying the substitution voltage results in a substitution voltage which does not equal the open circuit voltage. It is also shown that a formula for the response of a transducer derived for a system in which the microphones are open-circuited may be used when the microphones are terminated by finite electrical impedances, by replacing the generated open circuit voltages in the formula by the corresponding "normal" substitution voltages.

Consideration is given to the restriction in the definition of the pressure response of a transducer made necessary by the fact that the pressure on a microphone diaphragm is a function of the electrical impedance terminating the microphone.

An experiment is described which involves a microphone coupled to a chamber, the acoustical impedance of which is high relative to that of the microphone. The results of this experiment agree with the conclusions of the analysis.

*A Note on Filter-Type Traveling-Wave Amplifiers.*<sup>7</sup> J. R. PIERCE\* and NELSON WAX. A small-signal analysis of systems in which an electron beam interacts with a circuit composed of discrete filter elements is given here. The effects of a line beam interacting with a series of gaps, which are capacitive elements of a filter structure, are calculated, and it is shown that an admittance can be introduced which arises from the presence of the electrons. This admittance is in parallel with the gap capacitance, and thus will alter the propagation factor of the filter circuit. It is shown that traveling-wave solutions exist for the combination of electron beam and filter circuit, and that there is a solution which has a positive real part, indicating that gain will be exhibited.

<sup>7</sup> *Proc. I.R.E.*, v. 37, pp. 622-625, June 1949.

\* Of Bell Tel. Labs.



## Contributors to This Issue

A. P. BROGLE, JR., S.B. and S.M. in Electrical Engineering, Massachusetts Institute of Technology, 1949; Signal Corps, U. S. Army, 1942-46; Bell Telephone Laboratories, 1948. While at the Bell Telephone Laboratories, Mr. Brogle worked on the development of high-frequency networks as part of the M.I.T. Cooperative Course in Electrical Engineering. He is now engaged in Facsimile development at the Signal Corps Engineering Laboratories, Red Bank, New Jersey.

F. R. DENNIS, State College of Washington, B.S. in E.E., 1929. Bell Telephone Laboratories, 1929-. Mr. Dennis has been engaged in the design of electronic measuring apparatus, particularly of the type providing visual display of transmission characteristics. During the war he was engaged in Application Engineering of Airborne Magnetometers in this country and overseas.

E. P. FELCH, Dartmouth College, A.B. in Physics, 1929. Bell Telephone Laboratories, 1929-. Mr. Felch has been concerned with the development of electronic measuring apparatus. During the war he was engaged in the development of Airborne Magnetometers and other magnetic detectors.

WILLIAM W. MUMFORD, B.A., Willamette University, 1930. Bell Telephone Laboratories, 1930-. Mr. Mumford has been engaged in work that is chiefly concerned with ultra-short-wave and microwave radio communication.

SLOAN D. ROBERTSON, B.E.E., University of Dayton, 1936; M.Sc., Ohio State University, 1938, Ph.D., 1941; Instructor of Electrical Engineering, University of Dayton, 1940. Bell Telephone Laboratories, 1940-. Dr. Robertson was engaged in microwave radar work in the Radio Research Department during the war. He is now engaged in fundamental microwave radio research.

CLAUDE E. SHANNON, B.S. in Electrical Engineering, University of Michigan, 1936; S.M. in Electrical Engineering and Ph.D. in Mathematics, M.I.T., 1940. National Research Fellow, 1940. Bell Telephone Laboratories, 1941-. Dr. Shannon has been engaged in mathematical research principally in the use of Boolean Algebra in switching, the theory of communication, and cryptography.

